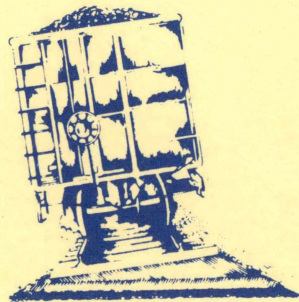


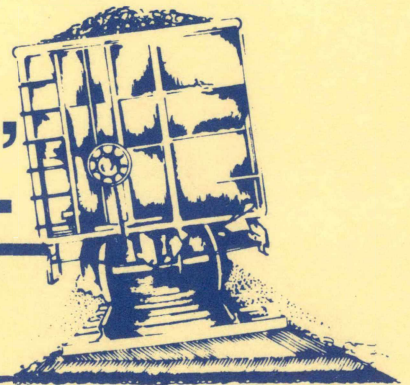
The Second International Heavy Haul Railway Conference

Pre-Conference Proceedings

Colorado Springs, Colorado, U.S.A.
September 25 - September 30, 1982



Co-Sponsored by A.A.R., F.R.A.,
R.P.I., A.R.E.A. & A.S.M.E.



Development of Mineral Railways in Queenstown, Australia: The Goonyella Railway

P. J. Goldston

M.I.E. (Australia)
Chartered Engineer
F.C.I.T., F.A.I.M.
Commissioner for
Railways, Queenstown

The Goonyella Railway in Queenstown, Australia, has now operated for ten years as a Heavy Haul Railway. This paper outlines the approach to financing the railway and the freight pricing mechanism. The various changes to track structure, signal design and wagon design required as a result of operating experience are described.

1. INTRODUCTION

The Goonyella Line is a heavy haulage railway constructed specifically for unit train operation, and was opened in 1971 with the construction of a 124 miles (198 km) link from the Goonyella Mine to the port at Hay Point to haul initially 4.1 million tonnes of coking coal annually.

The Peak Downs Mine was subsequently opened in 1972 and required the construction of 40 mile (48 km) branch for the transport of 5.1 million tonnes annually. A further 17 mile (27 km) of track was constructed to a mine site at Saraji in 1974 for the transport of 4.6 million tonnes annually.

The Norwich Park Mine commenced operations in 1980, and required a 30 mile (49 km) extension from Saraji. This mine added a further 4.3 million tonnes of coal for export annually.

Additional rail links to the existing Goonyella system of lines are now under construction as new mines commence production. Currently, committed projects in the advanced stages are the Blair Athol, Riverside, Oaky Creek and German Creek projects. Figure 1 shows the Goonyella system as it relates to railways and ports in the Central Queensland area of Australia. Figure 2 illustrates a schematic diagram of the existing line and current construction.

It is expected that, with the current upgrading, the Goonyella Line will have to carry a total of 32.5 million net tonnes of coal by 1985, anticipated to increase to a level of 48.4 million net tonnes by 1990.

The following sections in the paper will discuss financial arrangements and operational developments which have occurred since the construction of the Goonyella Line.

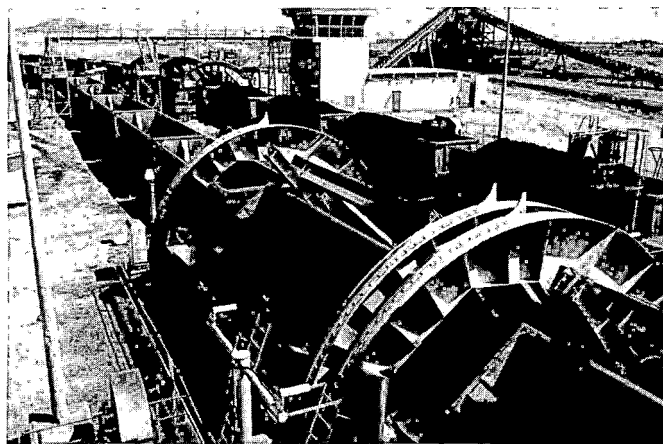


Photo. No. 1. Hay Point Tippler

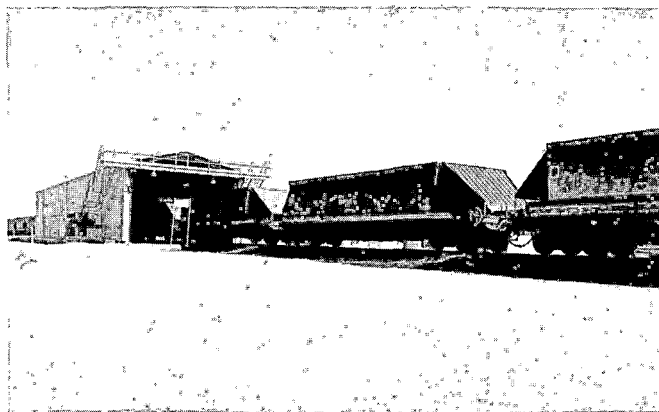
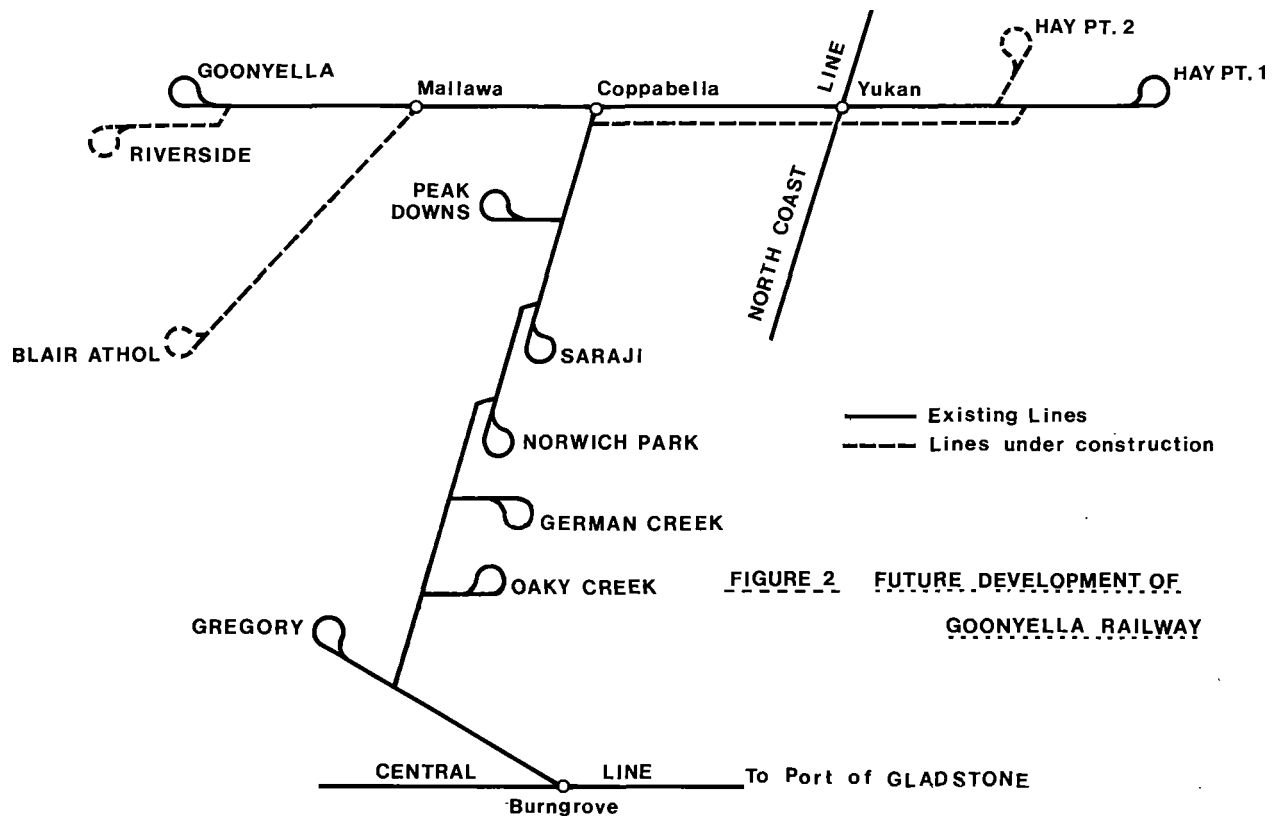


Photo. No. 2. Golding Bottom Discharge Facility



2. FINANCIAL ARRANGEMENTS

The Queensland Railways is a state owned instrumentality operated as a Statutory Corporation with a single Commissioner as its Chief Executive. Notwithstanding the degree of autonomy possessed by the Railway in its day to day operations, the Railway has to vie with other government departments and functions for its share of Loan Funds for construction and development works. Hence, at the outset, it was realised that development and upgrading of new and old railways in Queensland was beyond the financial resources of the State Government.

It should be remembered that many of the mineral fields in this State lie on Government Leasehold property. Hence, one avenue which could be adopted was to allow private enterprise to develop mines and construct private railways and ports. Initially, the Moura Railway Line was to be constructed as a standard gauge, electric railway. The State Government was to have generated its profits by way of mineral royalties.

This method of development was used in one Australian State, and accounts for the fact that private railways exist in north-western Australia. However, in Queensland, the Government of the day, recognising the need to sustain its own rail transport system as a viable alternative to road transport, elected to introduce an innovative and novel approach to the financing of heavy haul railways.

The funds to purchase rollingstock and locomotives, construct new railways and update established facilities are provided by the development company by way of security deposits. The ownership of these items is vested in the Commissioner for Railways. The funds, together with interest, are re-imbursed to the Company over a period of 10 - 15 years, by way of a freight rebate. The developer, of course, in order to qualify for the rebate, has to ensure that the mine produces

pre-determined quantities of the product for transport.

In this way, the State has retained ownership of the heavy haul railways and has been able to enjoy a reasonably good profit level from these operations. Perhaps the most important feature is that the development of the heavy haul railways has allowed the introduction of the latest technology into the system.

This includes C.T.C., Locotrol Equipment, aluminium wagons, continuous welded rail, microwave communications, the latest equipment for track maintenance, and total prestressed concrete bridging.

2.1 The Freight Components

The freight rate comprises three separate components:

- (a) operating costs;
- (b) profit component;
- (c) capital rebate amortisation component.

Of these, the first two are subject to annual escalation. The escalation formula, based on the yearly price movements of fuel oil, steel and labour takes the general form:-

$$F_1 = F + KF \left(K_w \frac{(W_1 - W)}{W} + K_s \frac{(S_1 - S)}{S} + K_d \frac{(d_1 - d)}{d} \right)$$

F and F₁ are freight rates Year 0 and Year 1.

W/W₁ = average hourly wage rate (Year 0/Year 1)

S/S₁ = price of heavy steel rail per tonne landed Brisbane

d/d₁ = price paid by Railways for distillate

K_w, K_s and K_d are factors expressed as decimals, totalling to 1.0. The factors demonstrate the expenditure each component represents of the total operating costs.

The KF factor is the proportion of the whole of the freight rate represented by the operating costs and profit and hence varies from project to project. In periods of low inflation, the relationship between the weightings, K_w, K_s and K_d of the components has been fairly static.

However, in high inflation periods, as experienced in the last decade in Australia, the relationship has fluctuated quite dramatically. For instance, a recent analysis of the weightings in 1981 judged the range of the weighting costs to be:-

$$K_w = 0.70 \text{ (wages are often variable)}$$

$$K_s = 0.23 \text{ to } 0.18$$

$$K_d = 0.07 \text{ to } 0.12$$

$$\frac{\quad}{1.00}$$

Until recently, the escalation equation could not be varied throughout the Agreement Life. But now, because of the variations in the weighting factors, consideration is being given to the reassessment of the weighting factors during the life of the project, say every three years.

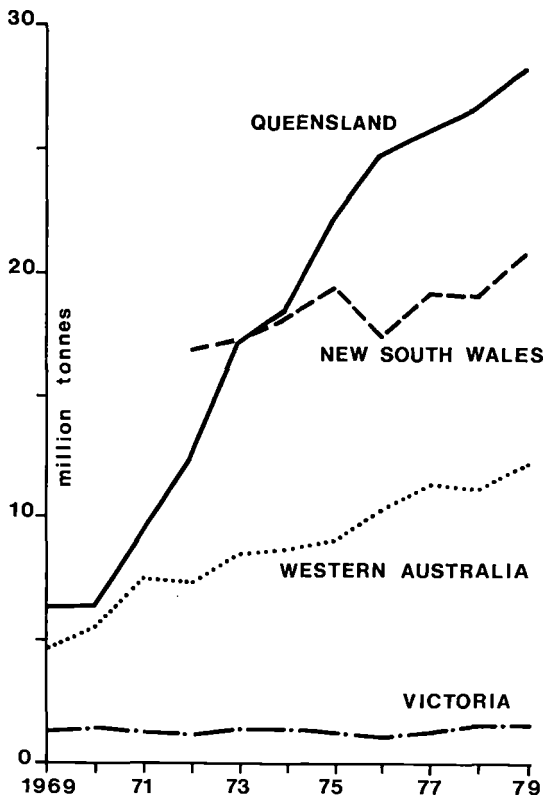


FIGURE 3 COMPARISON OF GROWTH RATES MINERAL TRAFFIC AUSTRALIAN STATE RAILWAYS (SOURCE AUSTRALIAN BUREAU OF STATISTICS)

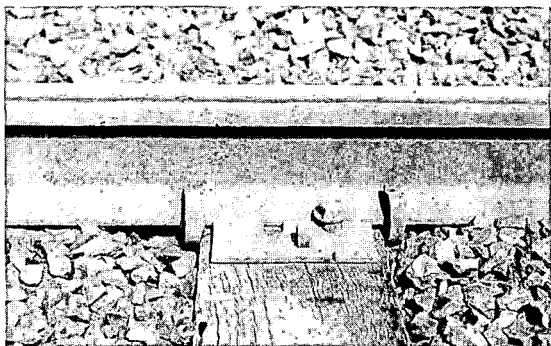


Photo. No. 3. The Old Track Specification

3. TRACK STRUCTURE SPECIFICATION

The following table indicates the original track structure specification together with the modifications, either incorporated now or planned for introduction in the near future.

Item	Old Specification	Modification
Rails	107 lbs/yd (53 kg)	120 lb/yard (60 kg)
Welded Lengths	40 ft (12.2 m) to 200 ft (61 m) and then continuous welding.	40 ft (12.2 m) to 360 ft (110 m) and then continuous welding.
Sleepers	Timber 9" x 6" x 7'0". (230 mm x 150 mm x 2.15 m).	Concrete sleepers 9½" x 8½" x 7'0" (2.45 mm x 215 mm x 2.15m). These are average dimensions.
Spacing	Timber 2624 per mile. (1640 per km)	Concrete 2336 per mile. (1460 per km)
Sleeper Plates	Flat base plate on all curves and straights with no insulation pads.	Cambered 1 in 20 base plate on all curves and straights with high density polyethylene pads.
Ballast	Crushed stone 10" (255 mm) under timber sleeper.	Crushed stone 9 7/8" (250 mm) under concrete sleepers.
Dog-Spikes	7" x 3/4" plain shank (178 mm x 19 mm)	Indirect spring clip type fastening.
Rail Anchors	Heavy Pattern Fair Rail Anchor	Nil.
Lock Spikes	4 per sleeper	Nil.
Grades	Maximum against loaded train 1 in 100 (1%) maximum against empty train 1 in 50 (2%).	No alteration.
Curves	Minimum radius 990 ft (300 m).	No alteration.

4. WAGONS BOTTOM DISCHARGE VS. ROTARY DUMP WAGONS

There is considerable room for argument when comparing the relative merits of bottom discharge and rotary dump wagons. Queensland has both types of wagons operating. Essentially, the selection of the wagon type is a "Horses for Courses" decision. Each type has certain advantages and disadvantages. The rotary dump, or Gondola wagon, has a monocoque body type and thus the advantage of a stronger body, lighter tare weight, and lower capital cost.

On the other hand, the bottom dump wagon has the advantage of a faster discharge rate. In addition, the comparison of capital cost of construction and subsequent maintenance of the unloading facility favours the bottom dump arrangement. The general availability of the bottom discharge structure is higher than the corresponding rotary tippler.

Summarising the relative merits of the two types:-

Gondola Open Type Advantages

Simpler and less costly construction.
 Low tare weight.
 Low maintenance and repair cost of wagon body.

Hopper or Bottom Discharge Type Advantages

Fast unloading rate.
 Lower capital cost of unloading facilities.
 Greater interchangeability of wagons between our ports.
 Wagon lengths can be varied.
 Lower cost of coupling maintenance.
 Larger wagons can be used as our unit train rotary dumpers have been standardised.
 Greater availability of unloading facility.

Disadvantages

Slower unloading rates.
 Lower availability of unloading tippler.
 Higher cost of unloading facilities (usually rotary tippler) both capital and maintenance.
 Wagons generally not interchangeable unless rotary dumpers standardised.
 Wagon length cannot be varied in a particular system, specifically if rotary couplings used.
 Higher cost of rotary couplings maintenance.
 Wagons length generally restricted by dumper.

Disadvantages

Higher unit capital cost.
 Higher tare weight.
 Higher maintenance and repair costs of body.



Photo. No. 4. Typical Q.R. aluminium rotary dumper wagon.

One measure of wagon efficiency is the ratio of total tonnage hauled to move one net tonne of material as shown in the following table.

This table sums the gross wagon tonnage plus the tare of the empty wagon dividing by the net tonnage contained.

Wagon Type	1067 mm - 3'6" gauge		1435 mm - 4'8½" gauge	
	Material Operation	Ratio*	Material Operation	Ratio*
<u>Steel</u>				
Bottom Discharge	Coal Moura	1.75	Iron Ore Goldsworthy	1.57
	Nickel Greenvale		1.60	
Tippler	Iron Ore S. Africa	1.70	Iron Ore Hammersley	1.47
	Coal Blackwater		1.61	
Tippler	Coal Goonyella Blair Athol	1.61		
	Coal Goonyella		1.51	

*Ratio = $\frac{\text{Trailing Loaded} + \text{Trailing Empty Wagons}}{\text{Net Carry}}$

In conclusion, there is an inherently complex decision to be made in selecting the type of wagon, rotary tippler or bottom discharge for a particular project. The overall economics of the project itself will tend to dictate the final selection.

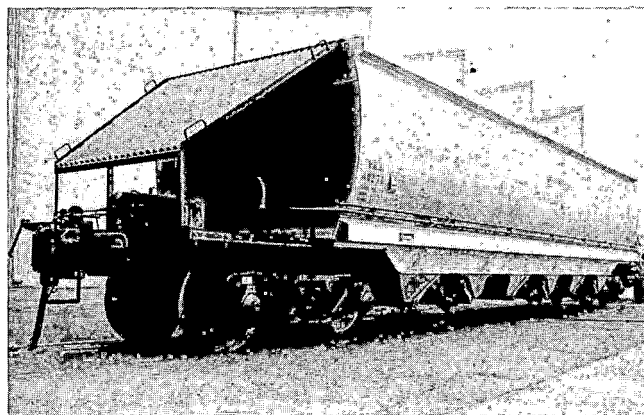


Photo. No. 5. Typical Q.R. aluminium bottom discharge wagon.

5. PERFORMANCE OF 'G' WAGONS - ALUMINIUM GONDOLA TYPE

There were seven hundred and seventy-seven (777) 'G' class wagons purchased for operation of the Goonyella, Peak Downs, Saraji to Hay Point Coal Traffic. These have been supplemented by 'GH' class wagons, and some 'GO' wagons, which represent modification of the original

design. The 'G' wagon is a 71 tonne gross, 'Gondola' type wagon, built of Aluminium Alloy. The wagons are fitted with three (3) piece cast steel bogies, Auscopac type brake equipment, empty/load changeover valves, and a rotary coupler at the leading end of each wagon. Wagons first entered service in October, 1970, and have always operated in block trains of seventy-four (74) wagons pulled by three (3) locomotives, or in locotrol controlled trains which essentially consist of two (2) seventy-four (74) wagon trains coupled together.

As has been our experience with all aluminium wagons, fatigue cracking has occurred. The worst of this occurs at the critical joint area at the end of the shear plate, as shown on the diagram. Cracks commence at the end of a weld and propagate up along the edge of the gusset, eventually resulting in a transverse crack in the side sill, thus destroying the structural integrity of the wagon. Routine inspection enables wagons to be withdrawn for repairs before cracking becomes serious. Repairs involve re-welding, or removing and replacing gusset plates.

Cracking has occurred in other places such as at the end of gussets at the upper corners of the wagon, and the end pillar. These have been less serious, and are more often than not attended to when wagons are in Workshops for other attention, such as brakes or wheels.

The 'G' class wagon has an internal pillar member above the draft gear pocket and extending up the end wall. This resists the draft and buff loads, and transmits forces to the transverse member on top of the end wall, and hence to the cant rail. Apart from causing the cracking in the top corners, this results in the formation of several internal pockets in the wagon. It was subsequently observed that upwards of 3 tonne of coal was not being discharged from the wagons because it became solidly packed into these pockets.

The 'GO' class wagon has an external pillar, and cracking problems at the top corners are less, but coal still packs into corners, and wagons do not empty cleanly. The 'GH' design reverts to a small torsion box type construction and more flexible end wall to cant rail connection. No top corner cracking has been encountered, and the incorporation of radius plates in the corners has resulted in much cleaner discharging. The problem of cracking in the critical joint area has not been overcome on later designs, despite changes to the design detail in this area.

Wear on the mating faces of the collar and yoke of the rotary coupler has been minimal, as opposed to the very heavy wear of identical components in other traffic. The heavy wear was experienced where tipping of wagons occurred while the train was stretched out, and the wearing faces were in contact. This was caused by the empty wagons proceeding down an incline after discharging, and hence the problem was more severe towards the rear of the train, as more wagons proceeded down the slope. At Hay Point the track ahead of the unloading point is level, and wagons are pushed by an indexing arm. The train remains "bunched up", and the load on the wearing faces is minimal, and wear after ten (10) years is similarly well below expectations.

Wear on the Aluminium sides of the wagons, even where coal is discharging, is not measurable.

Corrosion of steel brake pipes has been a problem caused by water from the washed coal, and all pipework is being replaced by galvanised pipes. The high corrosion rate of steel components has also necessitated the re-arrangement of drainage outlets. Drainage outlets are provided to allow water to drain from the wet coal, and to allow rain water to drain off. These wagons operate in the Tropics and the water falling in the wagon during a severe storm could easily result in an additional one (1) tonne of water in the wagon. This makes handling of the coal at the Port much more difficult. Coal does not release as easily from

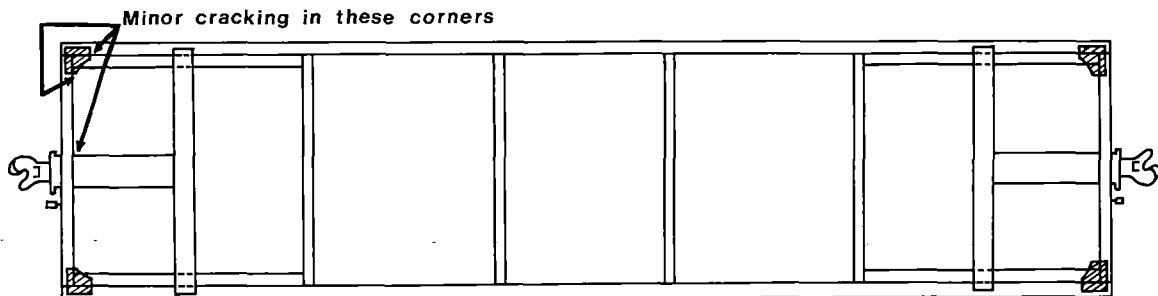
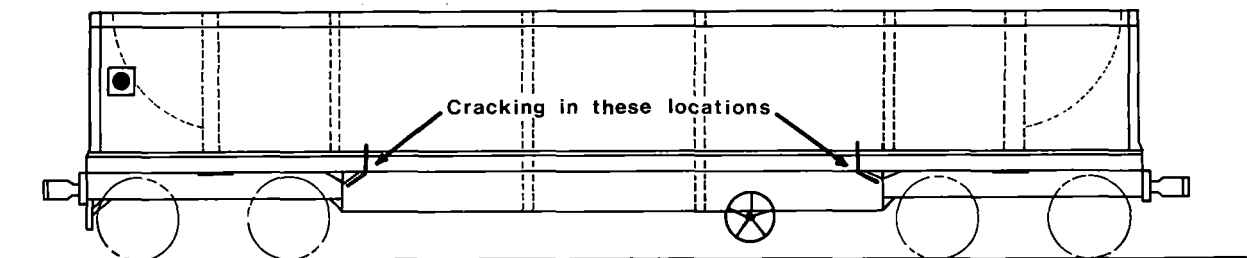


FIGURE 4. TYPICAL CRACKING G TYPE WAGONS

the wagon, and poses problems on conveyor belts. The absence of corrosion on the Aluminium Alloys is justification in itself for choosing Aluminium in preference to steel; this is apart from the benefits of reduced tare, and hence increased capacity, etc.

6. LOCOTROL OPERATIONS

The Goonyella Line was originally planned for 3 multi-unit (2200 HP) D.E.L.s hauling 74 wagons each of 71 tons gross weight with 57 tonnes net of coal for 4,200 tonnes net. As the tonnage rose it became necessary to increase train size to reduce track congestion, or to duplicate track or insert more crossing loops.

The first course was chosen. Queensland Railways officers visiting the United States had found that remote multiple unit operation by radio control, trade name 'Locotrol', in the United States was far past the experimental stage there. It had become an accepted operating technique and the failure-free records of the systems inspected were excellent.

Locotrol operation also provided the advantages of permitting the use of wagons with lower tare weight. With the trailing set of locomotives located in the centre of the train, control of the train became more manageable, specifically braking.

Locotrol operation with 3 locomotives at the head end, then 74 wagons, then 3 more locomotives with a special wagon (LRC) containing remote control equipment, then another 74 wagons was chosen. This gave a train consist of 6 locomotives and 148 wagons for a gross train load of 10,500 tonnes carrying 8,500 tonnes of coal. The number of trains required to carry a given quantity of coal was thus halved.

With Goonyella, Peak Downs and Saraji Mines operating there were 5 such 148 wagon Locotrol trains. With increased production and the opening of Norwich Park this has been increased to 7 such trains.

The annual haulage requirement of these 7 trains is 18.2 million tonnes.

Locotrol which does not operate on any other Australian railway system, has given excellent reliable performance in this area.

Its great advantage, we believe, is that it has negated the perennial argument that trains on 3'6" (1067 mm) gauge, cannot haul tonneages equal to those on the standard gauge (1435 mm). The Goonyella train is the longest and heaviest operating on the State owned systems in Australia. The maximum operating speed is 37.5 m.p.h. (60 k.p.h.).

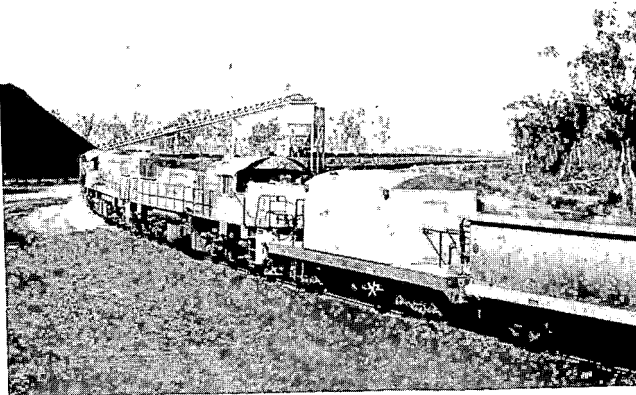


Photo.No. 6. The Locotrol Train.

The second advance is that there are no guards van on these trains. The train is still manned with a three man crew, the train guard being located on the third engine of the first consist.

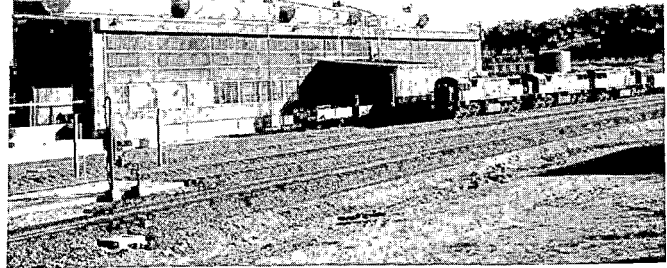


Photo No. 7 Jilalan Diesel Servicing Depot.

7. RAIL-WHEEL INTERACTION

The Goonyella Railway track was initially laid with a vertical rail profile, that is the rail was laid on flat sleeper plates. In addition, the vehicle wheel profile was originally of cylindrical form. This design is in conformity with the existing 10,000 km (6,000 miles) of Q.R. track. It was soon realized that this rail wheel interface was producing:-

- (a) a very severe wear pattern on the wheel flanges,
- (b) a severe form of rail shelling on the gauge lip of curved and tangent rails.

Detailed investigation was undertaken to remedy this situation. To counteract this problem, four possible solutions were considered:-

- (i) Design of a new wheel profile for use on the existing track.
- (ii) Application of cant to the rails, probably in conjunction with the introduction of a new wheel profile.
- (iii) Increasing the strength of the rails to a level at which they can withstand the stresses applied without shelling.
- (iv) Grinding of the rail head to remove the shelled areas and/or provide a restored or new rail profile.

On an operating railway, only (i) and (iv) are relatively practical solutions.

Hence it was decided on the existing route to plane the rail head to produce a surrogate camber of 1 in 20, falling towards the gauge lip. A rail planing machine has recently been purchased to carry out this task. In addition, a modified wheel flange profile has been introduced on wheels requiring turning as a normal maintenance procedure.

In the future, the duplication of the railway will take place. The new track will be constructed with cambered sleeper base plates on concrete sleepers holding 60 kg rails. The wheel flange profile adopted for the current situation is a compromise which has effectively

reduced the rate of rail shelling. It has improved the life of the wheel flange three fold.

Once the old rail has been modified by planing and the new cambered track constructed, it will be necessary to introduce a greater conicity into the wheel flange profile to account for the new conditions.

8. TRACK MAINTENANCE PROCEDURES

Like all major heavy haul Railways, Queensland Railways has difficulty in dividing track occupancy between operational and maintenance requirements. The present track, now nearing its eleventh full year of operation, has carried an estimated tonnage of 220 million gross tonnes by June 1982. The current annual gross tonnage rate of 31.75 million is set to rise to 54.4 million gross tonnes when four new mines reach full production around 1984/85.

In order to cope with this immediate increment, it is proposed to duplicate the existing railway from the Port to the junction town of Coppabella, a distance of 145 km (90 miles). On the present single line, passing loops are located approximately 24 km (15 miles) apart. Maintenance work must be carried out, at present, between train movements. However, once duplication is achieved, the two tracks will be bi-directionally signalled. In addition, dual crossovers will be inserted between the existing passing loop locations. This will allow track maintenance forces to occupy 12 km (7½ miles) sections, for extended periods, free from operational interruptions.

The methods of track renewal operation have had to be revised as time has progressed. To date, very little track renewal, on a face, has been carried out on the Goonyella Line, apart from curve renewal and isolated shelled rails. However, the rate of deterioration of timber sleepers and rail surface wear is increasing and complete track renewal of the existing line will have to be carried out in the near future. Allied to this, of course, is the decision, recently taken to replace timber sleepers with concrete sleepers, on main line, heavy haul tracks.

Other heavy haul lines in Queensland, notably the Moura Railway, terminating at Gladstone, and the Collinsville Railway, connecting to the New Port at Abbot Point, will have to be relaid completely to accommodate increased coal haulages. Hence, there is a considerable amount of track renewal work required within the system.

We believe the most economical way to do this work is to use the Track Renewal Machine (T.R.M.) technique. We are now in a position to order concrete sleepers in sufficient quantities to generate economies of scale, and maintain the rate of supply necessary to keep the T.R.M. fully employed. The experiences to be derived from using the T.R.M. on heavy haul lines will also benefit us greatly in future years when the need to refurbish the other main lines in the State is required.

The other important feature in relation to the track structure has been the introduction of continuously welded rail. Initially, rails are welded in the depot to 61 m. (200 ft) and 110 m. (360 ft) lengths. Field welding of these sections has continued throughout the intervening years to the stage where the line is virtually C.W.R.

Another track innovation is the use of glued joints for track circuit blocks and signalling sections. In the original installation of C.T.C., mechanical joints with end post insulation were used. However, it was found that the end posts were

failing, causing circuit problems. This led to experiments with glued joints around 1975.

The success of this form of joint was such that the whole Goonyella Railway is now fitted with glued joints. So far the failures recorded are less than one percent of the installed joints.

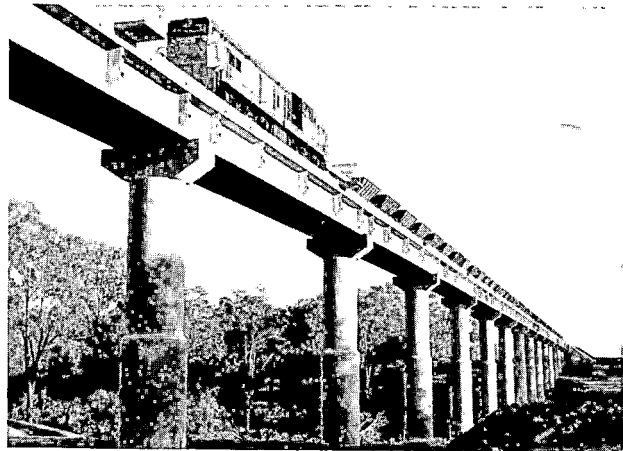


Photo.No. 8. Pre-Stressed Concrete Bridge.



Photo. No. 9. Goonyella Line.

9. BALLOON LOOPS

In order to avoid the significant shunting delays associated with disconnecting locomotives, running around the train, shifting the guards van from one end of the train to the other and recharging the train brakes, for any significant annual tonnage, a balloon loop at the loading and unloading terminals is essential.

The traffic flow advantage of balloon loops for unit trains had been fully demonstrated at the mines supplying coal to Gladstone. Unfortunately, the port layout at Barney Point, Gladstone had not lent itself to a balloon loop installation and the disadvantages of this had become evident in operation.

This became one of the basic design factors of the Goonyella system, and the main criteria in design of balloon loops for such operations are described

in the following sections.

The balloon loop should be shaped so that the loaded train is kept on straight track during the loading operation. This is because wagons have no differential in their axles, and as the outer wheel on a curve has to travel further than the inside wheel, it is necessary for the difference in distance travelled to be made up by slipping. This is readily achieved when a train is travelling at normal speed, but at the very slow speed while unloading, slippage will only occur when the torsion in the axle exceeds UTF, the friction coefficient of wheel on rail, times the wheel radius, times the wheel load.

The twist or torsion in the axle in this situation is referred to as axle windup, and as the wheel load of a loaded wagon is some five times greater than an empty wagon, the large torsional stresses in a loaded wagon over a period of time can lead to fatigue problems in the wagon axles. In addition, the sudden slipping of the wheel on the rail results in a rapid wear rate of rail and wheel.

It is also undesirable because of rail and wheel wear problems to have any of the train on curves which are too sharp. A radius of curvature of 300 m has been adopted in Queensland as the minimum.

The shape of the ideal loop thus becomes:-

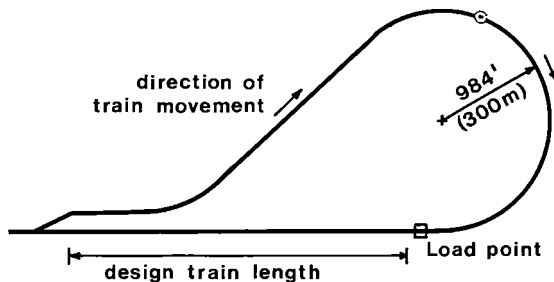


FIGURE 5. DESIRABLE ALIGNMENT FOR BALLOON LOOP AT MINE.

The turnout at the entrance to the loop should be set up so that the loaded train passes through the straight leg.

Having established the alignment of the balloon loop we must now consider the grading. If the locomotives are used to move the train under the loading point, it is generally necessary to move the train forward at a predetermined slow and constant speed. With train lengths of 1 or 2 km, this is a most difficult task to achieve unless the balloon loop is designed to assist the locomotive driver.

The aim is to maintain a constant train resistance through the entire loading cycle, and a resistance which is not so high that it will cause overheating of the traction motors at the very slow speed of loading, (0.3 to 1.3 ft. per second) (0.1 to 0.4 metres per second), nor too low that the locomotive is not working or is required to use its brakes.

A varying train resistance will make it very difficult to maintain a constant speed, particularly where it is necessary to apply and release brakes to achieve the correct loading speed. It is possible to adjust the curvature and grade on each side of the loading point to achieve as far as possible, a constant train resistance through the entire loading cycle.

In order to avoid overheating of the traction

motors at the very slow loading speed and to ensure that the train resistance is sufficient to maintain a load on the locomotives, it is desirable that the train resistance is kept between 10% and 30% of the maximum continuous tractive effort of the locomotives. On the Goonyella trains, the remotely controlled locomotives are positioned half way through the train. The remote locomotives are idle and only the front locomotives are used for loading.

Most of the features of balloon loop design at the loading terminal are also applicable at the unloading terminal. A balloon loop is necessary to avoid the long delays of shunting, and for the same reasons indicated previously, the loaded train should be kept on the straight while unloading.

At Hay Point One, there are two concentric balloon loops constructed with a tandem rotary dumper on each loop. The train is split into two halves, each half being unloaded on one of the loops. In this way, the time to unload the six engine train almost equals the time to unload the three engine train.

10. CONCRETE SLEEPERS

The sleepers used in the initial construction of the Goonyella System were untreated hardwood timber sleepers 2.15 m x 230 mm x 150 mm, installed with a maximum spacing of 620 mm (24.5 in). Timber for sleepers was relatively plentiful at the time of construction of the Line and the low capital cost of timber sleepers rendered them the most economical choice, at the time. However, the quality of the timber offered for sleepers has deteriorated over time. The economic life of timber sleepers has reduced by several years as a consequence.

The following developments since the initial construction have required a reappraisal of the sleeper type for use in the Goonyella System:-

- (a) An increasing shortage of timber for sleeper manufacture, resulting in timber of lower quality and consequently a lower sleeper life expectancy.
- (b) Research and development in concrete sleeper technology, particularly in improved fastening design, which have largely overcome previous problems.
- (c) A reduction in the price differential between timber and concrete sleepers, making concrete sleepers more competitive with timber sleepers for heavy-haul applications.
- (d) The increasing level of traffic on the system, which has decreased the amount of time available for track maintenance work.

These factors, together with the much longer life of the concrete sleeper, have indicated that for the future operation of the Goonyella Line, the use of concrete sleepers would be more economical.

The major advantages of the concrete sleeper track are better resistance to buckling, the improved restraint of creep, the positive gauge control, better retention of top and line, increases in time between resurfacing cycles, better ride quality and the primary obvious advantage of eliminating sleeper and fastening maintenance.

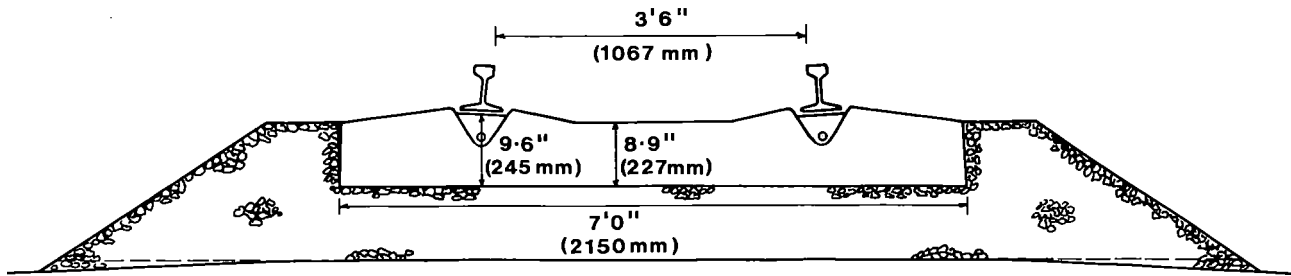


FIGURE 6. TYPICAL CROSS SECTION NEW CONCRETE SLEEPER.

11. CENTRALISED TRAFFIC CONTROL

The introduction of long heavy trains into the system also brought with it the need for operating methods different from the old "Staff and Ticket" or "Electric Staff" systems formerly used. These systems involved an officer at the station handling up a token, in the form of a staff, a ticket, or an electric staff, to the driver of the train as an authority for him to pass on to the next section.

When the very long (2 kilometre) trains have to cross at a station, the procedure for handling the staff, etc. becomes too difficult and time consuming when an officer has to move from one end of the station yard to another.

Initially, low density traffic on the line between Hay Point and Goonyella and the branch from Coppabella to Peak Downs was operated under the Train Order System. Train Order had never been used in Queensland Railways although it had been a feature of South Australian Railways and the Transcontinental Route from Port Pirie to Kalgoorlie. The decision to break from what had been the traditional Queensland safe working system of Staff and Ticket Working was taken because of the advantages of Train Order Working in low density traffic where long heavy trains operated.

Train Orders transmitted from the Central Control point at Mackay over a telephone pole route, allowed the big trains to travel long distances without stopping. The elimination of the necessity to halt the big trains to exchange staffs brought resultant faster schedules and less wear and tear on the rollingstock because of the elimination of many stops.

As train density increased the Train Order system lost these advantages as trains stopped for crossings and fresh orders. This led to the introduction of Centralised Traffic Control (C.T.C.).

C.T.C. was first installed on the Moura Mine to South Gladstone line which had been suffering from delays because of increased densities and then to the Goonyella - Hay Point System. Subsequently all lines used by coal traffic have been converted to Centralised Traffic Control.

C.T.C. has been used for over thirty years in European and American Railway operations and was a tried and proven system when first introduced in Queensland in 1971. It provides for a central control point in a main centre, operating signals and points in the field, perhaps 200 kilometres away.

By operating a push button in the control centre, a signal can be changed in the field, or an electric motor energised to wind over a set of points to the required setting.

The system is fool-proof in that:-

- (a) It prevents an unsafe signalling or points movement being made (this depends on human memory

factors in the old system).

- (b) If there is a failure of the system it always fails to "red", i.e. "Stop".

The Goonyella operation provided the first 'full' C.T.C. operation in Queensland Railways. All signals and points over the whole system are completely controlled from the Mackay Control Centre. The system has proved entirely successful.

A further refinement of C.T.C. recently introduced in certain other sections of the Queensland Railways system is the Train Descriptor. On the ordinary C.T.C. the panel in the Controller's office shows that a particular section of his track is occupied by a train. The Controller must deduce from his diagram which train it is.

With the Train Descriptor, once a train enters a C.T.C. territory the Controller types its number into the computer and thereafter whenever it appears, it is designated by its number.

The Controller can also call for the position of that train and it will immediately come up on the V.T.U. diagram.

In the future, as double track is introduced on the Central Line, North Coast Line and Coppabella - Hay Point Section to handle increased traffic, bi-directional C.T.C. type signalling will be installed on each track. This will allow sections of the heavily used permanent way to be taken out for maintenance without serious delays occurring to traffic.

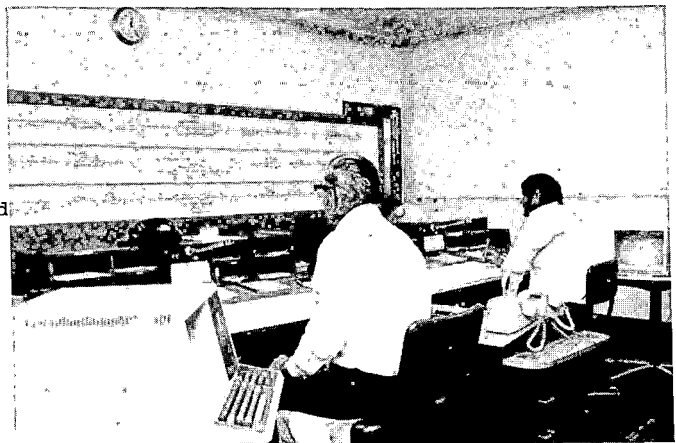


Photo. No. 10. C.T.C. Board and Train Descriptor.

LOCATION \ TYPE	CURRENT		ADDITIONAL		TOTAL	
	HOUSES	QUARTERS	HOUSES	QUARTERS	HOUSES	QUARTERS
SARINA	63	20	50	48	113	68
COPPABELLA	38	85	26	36	64	121
DYSART	3	0	13	31	16	31
MORANBAH	-	-	20	29	20	29
CLERMONT	-	-	7	19	7	19
NEBO	-	-	1	0	1	0
TOTAL	104	105	117	163	221	268

TABLE 1. STAFF HOUSING AND ACCOMMODATION GOONYELLA RAILWAY

12. STAFF HOUSING AND ACCOMMODATION

As a general policy, the Railway administration has traditionally provided some family housing and single person barracks at its depot locations. The heavy haul railways are no exception.

The Diesel Servicing and Wagon Repair facilities on the Goonyella area are located on the Pacific Coast near the town of Sarina. This area is a pleasant location, close to aquatic recreational activities. However, the inland depot sites are much less comfortable.

In remote areas, the Railway has sought to provide facilities well beyond its traditional policy on housing. At the junction town of Coppabella, the community comprises essentially Railway families. The town itself had no recreational facilities or community hall for social functions. Hence, part of the upgrading of existing facilities has been the provision of such necessary items like:- Tennis Courts, Basketball Courts, a Swimming Pool, a Caravan Park, and a Community hall, equipped with catering and bar facilities.

The provision of these latter amenities is a logical progression which seeks firstly to ensure adequate recreational activities for families and

others in lay-off periods. The outcome of this policy then is to provide a harmonious industrial environment and a staffing level adequate to operate the Railway itself.

Table 1 indicates the housing currently provided and planned for the future of the Goonyella system.

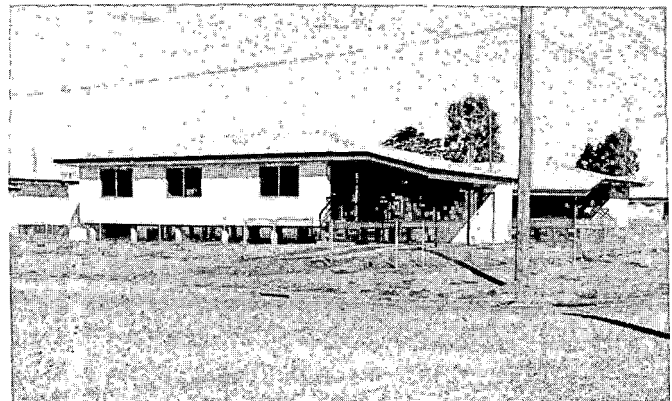


Photo. No. 11. Q.R. New Housing.

13. CONCLUSIONS

This paper has attempted to set out Queensland Railways' experience in heavy haul operations. The decision to undertake the construction and operation of these projects as a State system has had a dramatic impact on both the productivity and technology of the whole Rail System. A dynamic approach has produced many innovative refinements and improvements in every aspect of the heavy haul operation in Queensland.

There is tremendous confidence in the future of the Rail transport industry in Queensland because of the important part Railways have to play in the industrial development of the State.

P.C. Lombard

Pr. Eng., MSAIC
Systems Manager
South African Transport
Services
North Western Cape
System

Sishen-Saldanha : First Six Years

During the period 1976 to 1981, 70 million tonnes of iron ore were transported from Sishen to Saldanha. It was the first time South African Railways operated 26 tonne axle loads. Other firsts for the organization were the UIC 60 chrome-manganese rails, a fleet of cars fully equipped with HS self-steering trucks and 50 kV AC electric traction. Problems and solutions are accounted in a general performance overview.

INTRODUCTION

In May 1976 the first train load of iron ore arrived in Saldanha. Today, more than five years later (September 1981), a nett total of 70 Mt of iron ore has been conveyed.

During the first half of 1977, ownership of the railway line and port changed from the South African Iron and Steel Corporation (ISCOR) to the South African Railways. At that stage the operation of a 26 ton axle load was a new experience to us. For the first time also, all ore cars were equipped with the HS self-steering truck. The UIC 60 kg/m rail profile with chrome-manganese quality was another newcomer on the South African scene.

The change-over from diesel to 50 kV AC traction took place in April 1979. Of the 110 Mt gross traffic conveyed over the line to date, just over 50% was by means of electric traction.

Details of the Sishen-Saldanha layout and various other design parameters were covered by Le Roux (1) in 1978.

A number of serious problems were encountered that had to be solved quickly. This paper reports on how we managed to solve most of them as part of an account of the performance of various elements in the transport chain. Statistical information is included which could be of interest to other heavy haul operators.

TRACK

The overall performance of the track has been very satisfactory to date. Normal mechanised tamping takes place on a cycle of eight months. Apart from repairing derailment damage, no maintenance whatsoever was required on the concrete sleepers and fastenings.

Track maintenance is performed with only two tamping machines over the entire 861 km. Apart from these tampers and one ballast regulator, no other major on-track machines are used. The track maintenance manpower factor is one unit for every 3,44 km.

Wheel load distribution is kept within narrow margins as illustrated by the fact that the standard deviation is less than 5% of the average axle load. A permanent installation for the measurement of wheel loads at the loading station is presently under consideration.

Rail defects

Rail defect inspection at a rate of 300 km per month is conducted by two gangs equipped with hand operated flaw detectors using 0° and 70° probes. Virtually all breaks occur during the cold months, especially when the temperature drops below 0°C.

During the first 100 million gross tons actual transverse rail breaks (excluding weld failures) totalled 3,2/100 km. Thermit and flash-butt welds added 3,4 and 2,8 breaks respectively to push the total to 9,4/100 km.

The corresponding figures for defects removed as a result of ultrasonic inspections are 8,5/100 km (preventing transverse breaks), 11,9/100 km (thermit welds), 2,8/100 km (flash-butt welds) and 4,4/100 km

(piping) for a total of 27,6/100 km.

The total defect rate of only 37/100 km for the first 100 million gross tons, reinforced the confidence that excellent rail life could be expected.

Head checks and rail profile

The appearance of head checks in the 80 mm crown radius region of the UIC 60 rail caused much concern in 1978/79. It was feared that these cracks could turn down into the rail and lead to rail fractures.

A wheel profile was developed which would avoid contact on the 80 mm radius and on the gauge corner of the rail. As described by Scheffel et al (2), this eliminated the high contact stresses and the occurrence of spin creep on that portion of the rail. As a result of this new wheel profile in conjunction with the self-steering trucks and top class track geometry, the incidence of head checks is decreasing noticeably. To date no rail fractures have occurred as a result of head checks.

A new 60 kg/m chrome-manganese rail is now in production in South Africa. It's profile is very similar to that of the UIC 60. It will be used for the new coal line as well as for future rail requirements on Sishen-Saldanha. The main difference in profile is the extension of the width of the 300 mm primary crown radius from 21 mm to 35 mm. This will allow adequate contact area whilst still protecting the gauge corner (2).

Dipped flash-butt joints

The main cause of dipped flash-butt joints is the length of the heat affected zone and the large variation in hardness in the immediate vicinity of the weld. 50 mm on either side of the weld the Brinell hardness is ± 300 while hardness at the joint and of the parent rail is ± 350 and 325 respectively.

TABLE NO. 1

DEVELOPMENT OF DIPPED FLASH-BUTT JOINTS

	AUG '77	MARCH '78	SEPT '78	JAN '79	DEC '79	AUG '80	AUG '81
MEDIUM	14,1	33,7	35,8	32,0	18,1	24,0	24,7
BAD	1,4	17,0	9,8	2,5	1,3	1,3	1,6
TOTAL	15,5	50,7	45,6	34,5	19,4	25,3	26,3
GROSS Mt	15	25	36	40	70	86	108

(% of all joints)

MEDIUM : Depth of dips of up to 2,5 mm measured below a 1 m straight edge.
 BAD : Depth of dips exceeds 2,5 mm.

Several tests were conducted to arrive at an economical solution. It was established that grinding in conjunction with normal tamping (8 month cycle at present) would reduce rail stresses by as much as 83% at the worst joints. Strain gauge tests showed that before grinding the dynamic wheel loads are $\pm 18\%$ above normal and with grinding it is reduced to only 3% above normal. Grinding started during May 1978. As grinding could (at best) be classified a temporary solution, further tests with a vertical jimcrow with a lifting capacity of 1 000 kN were conducted to remove the dip caused by grinding as well as any deformation caused by wheel hammer.

The rail is heated at the joint to a temperature of 350 - 400° C over a distance of 100 mm on either side of the weld. The joint is then lifted by a vertical jimcrow imposing a vertical three point bend. After slow cooling only the high spots (hard spots) are ground and the "low" workhardened spots are not touched to ensure a longer maintenance free period. Practical tests showed that joints treated this way will stand up for three tamping cycles without further attention. Lifting and grinding are presently being done at a rate of 250 joints per month with very good results.

Points and crossings

The original 1 : 12 X 60 kg/m forged chrome-manganese rail crossing required frequent maintenance. Grinding was virtually a weekly requirement. Every three months (intervals of 5 to 6 million gross tons), the crossings had to be removed from track for workshop repairs. The excessive wear can be attributed to the relatively soft material and large throat width.

A South African Railway designed ramped railbound crossing in 14% manganese steel became available in 1978. All crossings were replaced with this new type. Apart from using a much harder material, the crossings had a narrower throat and the wings were ramped. These crossings are giving excellent service. The first ones are now in track for about three years (70 Mt gross).

SIDE WEAR ON RAILS

A form of alternating or intermittent side wear on the rails became evident after the introduction of electric traction in April 1979. Gouging of the high- and metal flow on the low legs of curves is more prominent on maximum gradients where curve radius is less than 2 500 m.

Gouging is also found on straight sections at maximum gradient but without any discernable pattern or wave length. The side wear is measurable but less than 2 mm intermittently over a length of 600 km of the line. A further 70 km has side wear patterns of 2 to 4 mm and it measures 4 to 7,5 mm on about 30 km. This 700 km represents about 80% of the line.

It was established that the class 9E electric locomotives were causing the problem

A high rate of wheel wear was taking place. On average, wheels had to be reprofiled for the first time after 168 000 km. A further 136 000 km (average) followed before the second reprofiling became necessary. Thereafter the wheels lasted a further 80 000 km. The average total wheel life before it had to be retired was approximately 400 000 km.

One of the locomotives was equipped with an inter bogie control gear similar to that used on the class 34 diesel locomotive (U26C). Test recordings showed a marked reduction in bogie rotation. Bogie rotation was also reduced by oiling the horn-guides as this resulted in more freedom for the axle to move laterally.

Due to the fact that the track gauge is generally about 3 mm tighter than the nominal 1 065 mm, the distance between wheel flanges was reduced by 4 mm.

A second locomotive has now been equipped with suitably designed inter bogie control gear (IBC). It is the intention to equip the whole fleet of 25 locomotives with IBC once tests with this one prove to be satisfactory. Horn-guides will also be replaced with a low friction material.

At present however the causes for the incidence of gouging of the rails are still present and therefore remain a very definite threat to the life expectancy of the rails.

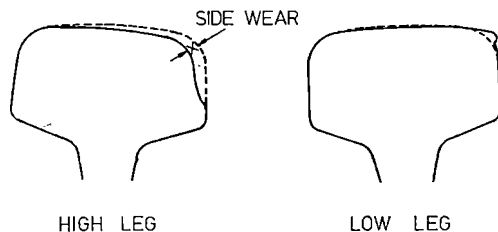


Fig. 1 Intermittent side wear on curves
ROLLING STOCK

Cars

A total of 1 750 type SS10 cars were available in 1976. These had solid cast steel wheels, F-type Timken bearings and mark II HS cross-anchor trucks. A further 500 CR-5 cars were received in 1980 fitted with mark V HS trucks. Except for a few small modifications to components of these trucks the design is the same as on the original SS10.

Couplers and knuckles. During the first 5 years, 72 couplers developed cracks. The crack started on the inside just behind the top pull lug and extended to the top back portion of the coupler head.

Investigation showed that there was an uneven pull due to a slight misfit between the top and bottom lugs and the knuckle. Adding 1,5 mm of material to the knuckle by welding followed by grinding which reprofiled the relative positions between the

contact faces ensured even load distribution.

The 72 couplers were replaced by new ones which incorporated a stronger lug design. Two did however break completely causing the parting of trains.

Broken knuckles occur on average about once for every 60 trains. At the moment this represents about one broken knuckle per month.

Unwanted emergency brake applications (UEBA). An average of about 1,3 UEBA's occur on the Sishen-Saldanha line per month. This correlates well with the incidence of broken knuckles which is a direct result of UEBA's. Although it happens somewhat more frequently in winter, the frequency of UEBA's is decreasing. This is attributed to a proper maintenance programme for brake valves and brake gear in general.

UEBA's often cause unnecessary delays to trains. This prompted the development of a system whereby the faulty car can be detected. Basically the apparatus consists of very accurate time measuring instruments which determines the time difference for the brake application to be propagated to the front and to the rear end of the train. A timer is attached to the port of the brake valves at each end of the train. When an unwanted emergency brake application takes place, the timers are activated the moment they are reached by the waves propagated in both directions from the faulty car. With the propagation speed taken as 282,065 m/s, the exact position of the faulty car can be determined using the time difference.

It is foreseen that all trains will be so equipped in future with an indication in the driver's cab of the position of the faulty car. The existing apparatus still has to be refined however.

Removal of stiffening bars. All the SS10 and CR-5 cars were cross braced with 5 stiffening bars each (75 mm angle iron). These angle irons were welded onto the inside of the car sides. However after a few years in service the angle irons tended to vibrate loose. Within a period of 3 years, 20 vibrated loose completely and fell into the tippler (car dumper) causing damage to the conveyor belt in some cases.

According to the designers of the cars these braces were put in to prevent "bulging" of the body during rough shunting. Test cars were chosen at random and the sides accurately measured for straightness. The stiffening bars were then removed and the sides measured again. Movement of the sides immediately after removal varied between 0 and 8 mm inwards or outwards.

At regular intervals the abovementioned measurements were repeated and after six months in service (\pm 100 000 km) no deformation of the car sides was noticeable. There has been no sign of fatigue cracking between the sidewall and the floor of the car.

During 1980 a start was made to remove the bars. By August 1981 the bars of 1 030 wagons were removed and it is anticipated

that all would be removed by the end of 1981.

Trucks

It was soon realised that the pin-jointed adaptor frame of the mark II HS truck had insufficient strength for the relatively high forces. These forces in the diagonal suspension frame are a direct result of momentary flange contact when negotiating geometric discontinuities such as in turn-outs (3). Due to this the adaptor frames were inclined to crack either at the locating pin or in the region of the portion that fits over the bearing adaptor.

Repairs were carried out on the workshop floor by welding in a strengthening plate on the inside of the adaptor frame and a second one in front in the area where the cracks developed. The cracks were first gouged out and welded. None of the adaptor frames so strengthened have shown any further cracks to date. The adaptor frame for the mark V truck was redesigned. It is also a welded construction and free of stress concentrations. The 500 CR-5 cars are equipped with this new design and have given no problems in service to date. It is also used to replace the adaptor frames on the mark II trucks.

Wheels

Radial fractures and temperature tests.

Soon after operations started on this line, it was realised that wheels were running too hot. Infrared readings were taken to prove the suspicion. As a first step to reduce the high energy inputs into the wheels, train speeds were reduced to 70 km/h for both loaded and empty trains. (The original speeds were 80 km/h for both types of train). Loaded trains were also limited to 50 km/h on down gradients of 1 in 100 (originally 60 km/h).

One of the causes of the problem was "sticking" slack adjusters (universal type) as they were mounted at an angle causing the shaft to jam. This was eliminated by increasing the length of the sleeve.

Portable ultrasonic equipment indicated that as many as 37% of the wheels were cracked to various degrees of seriousness.

To ensure brake release after application, the pressure reduction in the brake pipe during a minimum brake application was increased from 35 kPa to 45 kPa.

Leak-on of brakes was caused by the quick release limiting valve in the ABD valve. In about 600 valves an O-ring was damaged by a small burr. This was rectified by using a small air driven tool with small floating grindstones to hone the hole.

After all these modifications, tests were done to determine the temperature of wheels at the bottom of a 28 km long 1% gradient. The average speed of 11 trains tested was 51 km/h at the measuring point. The average wheel temperature varied between 147° and 264° C. On average only about 0,5% of the cars in each train had wheels with temperatures above 300° C, 5% were above 200° C and 7% between 100° and 200° C. The

maximum was 400° C.

Nowadays most wheels run cooler than 200° C. Using temperature sensitive paint on approximately 500 wheels, yard operating staff are enabled to note any wheels running hot. Recent tests indicated that very few wheels reach a running surface temperature of 350° C. The last annual ultrasonic wheel crack test showed only 1,3% of the wheels to have slight surface cracks. This is considered normal.

Radial fractures due to these cracks caused four derailments during the first two years of operations. Jointly these incidences resulted in damage to almost 70 km of track. Since August 1978 no further radial fractures have occurred.

Wheel life

Up to now the average life for a wheel set before machining was about 300 000 km. The maximum distance recorded to date for a wheelset is 550 000 km.

The reason why wheels have to be re-machined is normally a combination of "hollow wheel" and "high flange". The problems with wheel surface cracks and rail head checking during the first two to three years also necessitated a lot of machining to eliminate the cracks and to achieve the best wheel profile to match the rail profile.

Experience has shown that between two and three reprofilings are possible on a wheel before the minimum wheel diameter is reached. If wheels have to be reprofiled only due to wear, it is estimated that a wheel life of 500 000 km could be expected.

Bearings

At the end of June 1981, after noticing excessive pit marks on the inside of bearing cups taken out after a derailment, it was decided to immediately start on a repair program during which a major overhaul (A-repair) would be effected to all bearings. Initially the expected life of the bearings was 2 million km.

The A-repairs will be done in accordance with our roller bearing code of practice. (This code includes certain important requirements as laid down in the AAR specifications for design, fitting, lubrication and maintenance). Stripping, cleaning, examining and replacing or repairing of certain damaged parts are included.

After 5 years and 750 000 km, 17% of the bearing cups and 99% of seal assemblies must be scrapped. Pit marks, brinell pitting and spall marks are the main causes for rejecting the bearing cups, while the seal assemblies do not conform to the specified tolerances on their inside diameters.

As the danger of a derailment caused by bearing failure now exists it has been decided to work through the fleet as soon as possible to eliminate such bearings. Depending on the availability of spares this programme will consist of a 24 hour shift changing out and repairing 160 bearings per day.

As this problem was only discovered recently, investigations to establish the

cause are still in progress.

DERAILMENTS

To date (September 1981) 15 derailments have occurred which damaged a total of 104 km of track. Four were caused by broken rails, four by broken wheels (radial fractures), six by broken axles and one by a washaway.

One locomotive and 63 cars were damaged in these derailments which also necessitated the replacement of about 45 000 concrete sleepers and more than 56 000 m of rails.

Since the high incidence of derailments in the first years we have had only one each in 1979 and 1980. The figure to date in 1981 is two derailments.

Limiting the number of derailments due to broken rails includes a system of daily patrolling of the line by trolley. When the rail temperature drops below 0° C, patrolling also precedes each train. For this purpose rail temperature alarms were installed at each loop. The 0° C alarm message is transmitted to the control centre at Saldanha via the microwave repeater station. The CTC operator can then arrange for the necessary patrolling.

Two hot box detectors are available. These are situated at Loop 2 and Loop 18. Alarms from these detectors are also transmitted to the control centre at Saldanha.

As described earlier, everything possible was done to correct the causes of the broken wheels. But after three very costly derailments it was evident that some form of alarm should be provided as it was impossible for a driver of a 2,2 km train with powerful locomotives to determine when a car has derailed. The alarm system chosen is fully described in the next paragraph.

Dragging equipment detectors

Various types of alarms were looked at, such as ontrain alarms with automatic brake application, or alternatively, with purely an audible and visual indication to the driver.

These were discarded due to past experience with derailments where trains, that probably otherwise would not have derailed, derailed due to panic application of brakes. Alarms in the cab could distract a driver's attention from his legitimate duties. It was also considered that ontrain alarms, particularly the continuous circuit type, would lead to train delays should the alarm become defective and repairs had to be undertaken before the train could proceed.

Statistics of previous derailments on this line showed that for the first few kilometres after derailment the damage, particularly to sleepers, were not as severe as subsequent damage. On this basis an on-track alarm system was selected with a spacing of 10 km and operated over a radio system.

Dragging equipment detectors were therefore installed at ten kilometre intervals along the Sishen-Saldanha railway line. The purpose of the detectors is to detect

the unwanted dragging of equipment hanging from cars and locomotives and to detect derailed wheels.

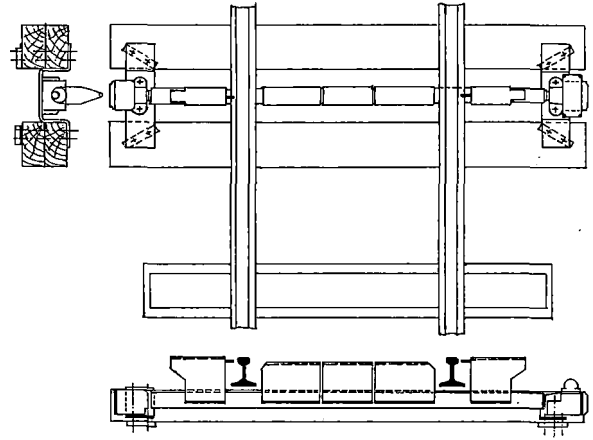


Fig. 2 Dragging equipment detector

A dragging equipment detector consists of vertical metal plates between the two rails and on either side of the rail. The plates are mounted on a horizontal torsion bar underneath the two rails. If the metal plates are deflected out of the vertical position, a contact at the end of the torsion bar will open and indicate an alarm status to the electronic equipment which is associated with the dragging equipment detector.

The electronic equipment at each detector consists of a radio transmitter and receiver with its associated alarm decoder and encoder circuitry. When the electronic equipment detects an alarm status at the detector, a message is transmitted to the control centre at Saldanha via the nearest microwave repeater station. At the control centre the alarm message will be decoded and an alarm will be displayed on the video screen, logged on a hard copy printout and an audible alarm given, to indicate the kilometre distance along the line where a dragging equipment detector has been triggered.

The CTC operator's action is to advise the train driver in the vicinity of the specific detector in order that he may stop as soon as possible.

To ensure that the alarm message does not get lost at the CTC centre, an electronic simulated voice message, indicating the kilometre distance, will be transmitted on the ontrack radio system to all drivers if the CTC operator does not acknowledge the alarm within 15 seconds after its occurrence.

The electronic equipment at the dragging equipment detectors are powered by 12 volt sealed lead acid batteries, which are charged by solar panels. Only dragging equipment detectors situated approximately 5 km outside the home signals at each passing loop and yard (20 in total) are

interlocked with the signalling system. When these dragging equipment detectors are triggered the intermediate home signal ahead of the train will go to yellow while the home signal go to danger. In this instance no voice synthesized alarm is given but it is logged on a printout and displayed on the CTC video screen.

The other dragging equipment detectors in the block sections between loops are not interlocked with the signalling system and will only give the alarm at the CTC centre as previously described.

To date the equipment has minimised three major derailments and detected about 12 instances of equipment hanging from trains thereby completely justifying its cost of R500 000.

ELECTRIFICATION

The performance of the overhead track equipment has been excellent since it was commissioned in April 1979. To date a total of 6 pantograph hookups were caused by the failure of counterweight pulley bearings, isolators and mast anchors (corrosion).

The high creep rate of the very pure local copper is a problem on the 2,5 km tension lengths resulting in the overhead equipment having to be realigned every two years.

Locomotive reliability

The performance of the electric traction service is depicted in figure 3. Any disruption of the service which exceeds 5 minutes or the loss of load (dropping of cars) is classified as a failure.

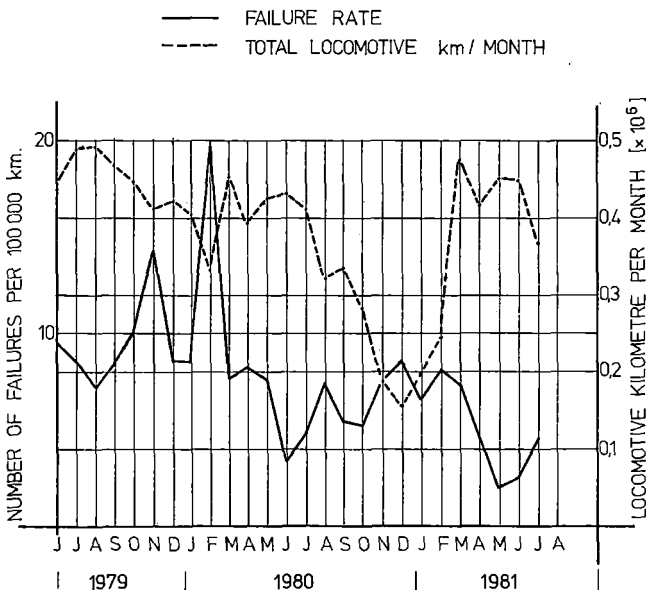


Fig.3 Reliability of electric traction service.

The major factors contributing to these failures (which seldom affects the empty

trains) were false wheelslip operations, the effect of excessive temperatures on electronic frames and compressors, traction motor bearing failures and the generation of harmonics by the locomotives on the 86 km long overhead sections.

The improvement in the reliability can be attributed to the modification programme which eliminated design weaknesses and manufacturing errors in these class 9E 50 kV AC locomotives. The supplier made a total of 181 modifications (104 major ones) on each locomotive. A total of 65 makers defects were declared which included the rebuilding of all the traction motors.

After the successful completion of the harmonic filter modification it will be possible to restore the no load line voltage from 45 to 55 kV and remove the 463 amp current restriction during acceleration. This will allow for an increase of 4,7% in load from 210 to 220 cars for a three locomotive consist.

OPERATIONS

When the South African Railways and Harbours took over the Sishen-Saldanha Railway line in 1977, trains in both directions were scheduled at 8 hour intervals. Trains consisting of 202 cars, conveying 17 170 tons of ore per train were hauled by 6 class 34 diesel electric locomotives (U26C).

After completion of initial test runs with the 50 kV AC class 9E locomotives, a full electric train service for iron ore (on the same schedule used by diesel) was introduced during April 1979. Train loads consisting of 210 cars conveying 17 850 tons per trip were hauled by 3 class 9E locomotives.

By switching over to electric traction we were able to increase our weekly capacity by nearly 4% from 360 570 tons to 374 850 tons per week for the same number of trains (21 per week).

The international iron ore market being a buyer's market presents exporters with the challenge to effect spot sales over and above sales on long term contracts. During August 1979 Iscor, the major exporter through Saldanha Bay Harbour was able to effect such sales of ore when other foreign suppliers were unable to deliver according to contract due to washaways and labour unrest. The resulting unexpected increase in export volumes rather depleted the ore stocks available in Saldanha Bay Harbour with the exporting rate being higher than the transporting capacity from the mine - the 374 850 tons per week already mentioned.

To meet the shipping demand seemed almost impossible. Several suggestions were put forward to augment the situation i.e. increase the number of cars per train to 220 and gain an additional 17 850 ton or one train load per week. This however proved to be impossible at that time with the electric locomotives still undergoing tests. This prohibited the increase in loads prior to certain modifications being made as previously described.

On further investigation by the trains operations research section which included inter alia the drawing of numerous train charts by hand and experimenting with increased speeds where possible over certain sections, it was found that the eight hour intervals between trains in both directions which was up to then considered to be the optimum capacity for existing rolling stock and motive power, could actually be pushed even higher with only a minor change in the intervals between trains.

It was found that by shortening the intervals between trains to 7 hours 10 minutes on day 1, increasing it by 10 minutes per day for day 2 and day 3 i.e. 7 hours 20 minutes intervals on day 2 and 7 hours 30 minutes intervals on day 3 and again returning to 7 hours 10 minutes on day 4 etc., the capacity could actually be increased to 23 trains per week with an additional 24th train every third week.

The varying intervals from day to day was necessary in order to minimize crossing delays to both loaded and empty trains. The shorter turn-around times for locomotives were easily accommodated at both terminals.

The resulting capacity of 410 550 tons with 23 trains per week represented an increase of 9,52% over what we at first believed to be the optimum capacity for the existing car and locomotive fleet. The additional 24th train every third week gave us a further bonus of 17 850 tons or 0,5%. Without any additional capacity outlay and with only minimal extra operating costs we increased our line capacity by 10%.

After the switch-over to electric motive power and with the introduction of maximum demand control on a continuous basis as mentioned hereafter, it was found that the transport capacity cannot economically be fixed at any random volume along the capacity scale. With analysis of the demands per train per metering section for the different train compositions i.e. 3 locomotives and 210 cars or 2 locomotives and 140 cars, certain optimum volumes along the total capacity scale were identified as economically transportable volumes per week.

Table no. 2 shows four such economically transportable volumes which are possible at present (and extend over the full metering month).

TABLE NO. 2
ECONOMICALLY TRANSPORTABLE VOLUMES

A	B	C	D	E
23	210	410 550	72	R391 000
21	210	374 850	72	R391 000
21	140	249 900	60	R326 000
11	210	196 350	52	R283 000
11	140	130 900	36	R196 000

A : TRAINS/WEEK
B : CARS/TRAIN
C : TONS/WEEK
D : TOTAL MVA
E : EFFECTIVE MVA COST/MONTH

Experience has also shown that on average approximately 4% of the theoretical capacity of any of the different economically transportable volumes possible is lost due to locomotive failures or car defects necessitating the reduction in loads, etc. en route.

The promised usable capacity available to the clients is therefore given at 96% of the theoretical capacity.

A further measure engaged in the process of optimizing the benefit derived from the monthly predetermined maximum demand levels was to request the clients to keep their rate of tonnage railed per week as constant as possible for any particular month.

MAXIMUM DEMAND CONTROL

Energy costs which are proportional to tonnage hauled, comprise only 17% of the total electricity costs. The fixed service and extension charges comprise approximately 33%. The highest contributor which can be controlled by the user is maximum demand cost (50%). It therefore receives the maximum management effort in the process of optimizing the cost of electrical power for the tonnage hauled.

The results are achieved with the aid of a flexible time schedule, telemetering of power consumption at each feeder station, computer facilities to process data and to display maximum demand, radio contact between traffic controller and driver, results plotted and evaluated weekly by management, planning tonnage to be hauled on a monthly basis within the supply authority metering period and a lot of team spirit.

It is not possible to indicate the real cost saving since the system was never allowed to run out of control with respect to maximum demand when we have had a severe disruption of the train service. Since the maximum demand is established over only one half hour in the meter month of the supply authority, it is very possible that one disruption in the train service with a bundling of trains in one meter section can result in very high maximum demand readings. The levels laid down thus do not interfere with the normal train service as decided for that month, but is primarily to limit the maximum demand when the train service is disrupted. There are normally two trains in a metered section but the traffic controllers have successfully handled five trains in a metered section with utmost skill, bringing the train service back to normal without exceeding the allowable maximum demand levels. During the initial period of electric traction the locomotive failures were high and resulted in numerous disruptions of the service which tested the skill of the controllers to the utmost. The levels established thus also have to take into consideration

the urgency with which the ore has to be transported and the train service restored back to normal. With the stockpiles near full and a low export rate, the allowable maximum demand levels are set as tight as possible.

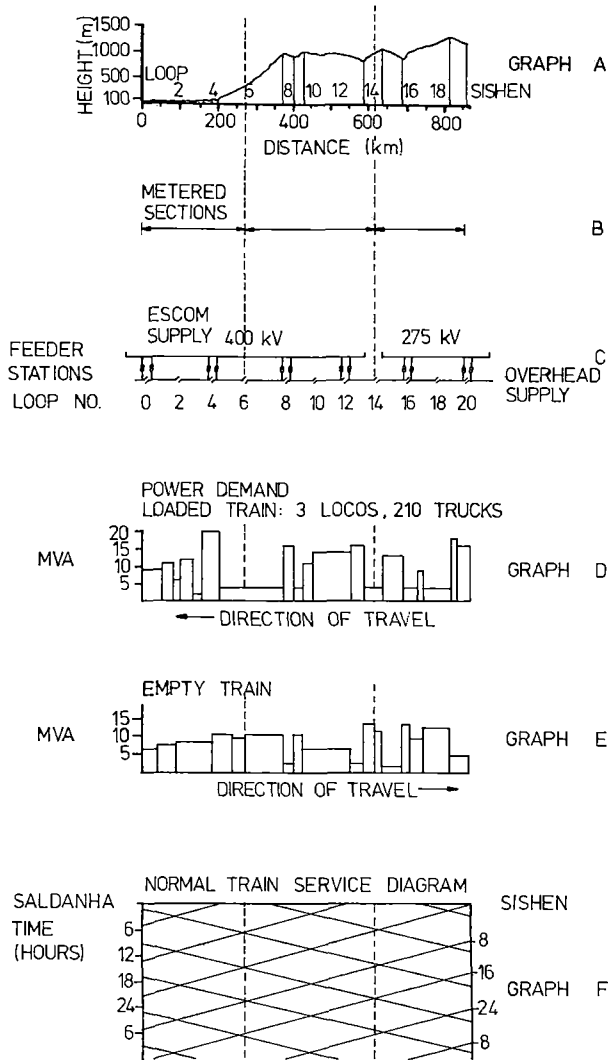


Fig. 4 Power demand of loaded and empty trains.

When the trains negotiate the profile through the three metering sections (figure 4), the power demand for the loaded train is as per graph D and for the empty train as per graph E. Graph F indicate a simplified normal train diagram. The maximum demand is established by the supply authority on a half hourly basis on the half hour. To assist the traffic controller the instantaneous power demand and the integrated average demand from the end of the last half hour to that point in time is indicated on a video screen. The traffic controller must ensure that at the end of the half hour the maximum demand over that half hour is less than the levels laid down. An alarm light

also flashes when the demand up to that point in time exceeds the alarm level. By means of radio contact with the driver he can request empty trains to slow down or stop whilst a loaded train negotiates a gradient. When the traffic controller sees that the one train is going to wait for the next train at a crossing, the earliest train will be slowed down. When the train service is disrupted the controller estimates the demand required and judiciously instructs drivers to proceed according to his revised planning.

COST PROPORTIONS

Figure 5 shows how the different elements of operating costs contribute proportionately to the total transportation and shipping cost.

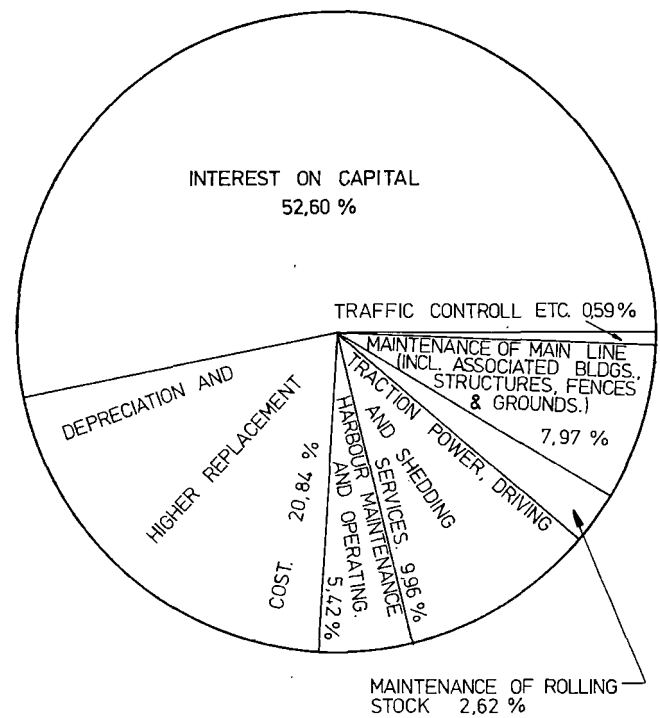


Fig. 5 Average annual cost proportions for the period 1978.04.01 to 1981.03.31.

ACKNOWLEDGEMENTS

Invaluable cooperation and contributions from various sub-sections are gratefully acknowledged. The General Manager of the South African Transport Services is thanked for permission to publish this paper.

REFERENCES

1. le Roux A.S., "Ore transport in South Africa : Sishen-Saldanha," Proceedings of the Heavy Haul Railways Conference, The Institution of Engineers, Australia, September 1978, Session 501, Paper A.5.
2. Scheffel, H. and Tournay, H., "The

development of an optimum wheel profile for self-steering trucks under heavy axle load conditions," Transactions of the ASME, November 1980, 80-WA/RT-5.

3. Scheffel, H. "Experience gained by South African Railways with diagonally stabilised (cross-anchor) bogies having self-steering wheelwets," Proceedings of the Heavy Haul Railways Conference. The Institution of Engineers, Australia, September 1978, Session 311, Paper E.1.

Rationalization Measures Taken Jointly by the Swedish State Railways, The Norwegian State Railways and Swedish Iron Ore Company

Per Eije

Manager
Luleå Operating Region
Swedish State Railways
Luleå, Sweden

The fact that the operation of this railway involved the Swedish State Railways, Norwegian State Railways and The Swedish Iron Ore Company created a unique set of problems. This paper reviews the steps jointly agreed by the three organizations to improve the overall performance of this railway.

RATIONALIZATION MEASURES TAKEN JOINTLY BY THE SWEDISH STATE RAILWAYS, THE NORWEGIAN STATE RAILWAYS AND THE SWEDISH IRON ORE COMPANY

by Per Eije

The purpose of these joint rationalization measures is to reduce the costs for ore transports on the ore line.

PRESENTATION OF ORE LINE BETWEEN LULEÅ AND NARVIK

Ore line

The ore line has a length of 472 km. It runs from Luleå in the Gulf of Bothnia to Narvik on the North Atlantic coast, past the mining areas in Gällivare (Vitåfors) and Kiruna, with a branch-line to the mine in Svappavaara.



Work was started on constructing the line from Luleå towards Gällivare in 1884. Not until 1892 could the Gällivare-Luleå line be opened to traffic. By 1903 the line had reached Narvik and thus has an age of between 80 and 100 years. It was designed and constructed in accordance with the technology available at the time.

The ore line is owned by the Swedish State Railways (SJ) with the exception of the 39 km long section from the Swedish-Norwegian border to Narvik, which is

owned by the Norwegian State Railways (NSB). The Swedish Iron Ore Company (LKAB) owns railway stations for terminal handling in Vitåfors, Svappavaara, Kiruna and Narvik as well as the unloading plants in Luleå and Narvik. Workshops for maintaining locomotives and wagons are located in Luleå, Kiruna and Narvik.

The maximum gradient for goods trains is 10⁰/oo.

The line is a single track line with a standard gauge. The rail weight is 50 kg/m on the Swedish side and 54 kg/m on the Norwegian side. The maximum permissible load per axle is 25 tonnes between Kiruna and Narvik, including the branch-line to Svappavaara, and 20 tonnes elsewhere. The sleeper spacing is 500 mm. The maximum permissible speed is for loaded ore trains 50 km/h and for empty trains 60 km/h. The line is equipped with CTC which is controlled from Narvik (NSB) and Kiruna and Boden (SJ).

Electric operation was introduced on part of the line in 1915 and on the entire line from Luleå to Narvik in 1922.

Rolling stock

Two different types of wagons are used for transporting ore. One is an older three-axle wagon which can take 42 tonnes with a tare of 11 tonnes and the other is a more modern bogie wagon which can take a load of 80 tonnes with a tare of 20 tonnes. Both wagon types are self-discharging (bottom-dumping) but only the latter type is fitted with central coupling. The reason why the wagons are self-discharging is the design of the unloading plant. The wagons are jointly owned by SJ and LKAB. There are 1 500 bogie wagons and 2 100 three-axle wagons.

19 Swedish and 5 Norwegian electric locomotives are used for the ore traffic between Kiruna and Narvik and 20 Swedish locomotives are used for the Vitåfors-Luleå and Vitåfors-Kiruna traffic. In addition to these, LKAB has shunting engines in Narvik and both SJ and LKAB have shunting locomotives in Kiruna and Vitåfors. Shunting is dealt with by SJ locomotives only in Luleå.

Administration and work organization

Traffic, maintenance of rolling stock and fixed installations are administered and executed by SJ and NSB, each for their own part of the line and their own rolling stock. LKAB is responsible for loading and unloading and for maintaining the fixed installations owned by the company. Locomotives and wagons are jointly run by NSB and SJ but a personnel change-over takes place at the border.

The ore line is included as part of Luleå region, which embrace the two most northern counties in Sweden. The SJ regional administration is located in Luleå and NSB has its administration in Narvik. SJ also has local administrative units in Kiruna, Gällivare, Boden and Luleå. LKAB has administrative units in Narvik, Kiruna, Malmerget (Vitåfors) and Luleå.

The number of persons employed in the actual transport operations amounts to 1 100 for SJ, 420 for NSB and 215 for LKAB.

Transport capacity

The ore transport flow can be subdivided into two main sections: the northern consisting of Kiruna (Vitåfors, Svappavaara) - Narvik and southern consisting of Vitåfors-Luleå.

The transport capacity per year, depending on the line and the access to locomotives and wagons, amounts to 31 million tonnes on the northern section and 12 million tonnes on the southern. The maximum permissible train weight for the Kiruna-Narvik section is 5 200 tonnes and for the Vitåfors-Luleå section 3 600 tonnes. The following table illustrates the transport trend.

Ore transports per year, thousands of tonnes

Year	Northern section	Southern section	Total
1902	26		26
1910	2114	1365	3479
1920	1097	1271	2368
1930	5520	2630	8150
1939	6046	3356	9402
1950	7335	3136	10471
1960	12590	3892	16482
1970	19902	6684	26586
1975	15527	7344	22871
1980	19673	4305	23978

Rationalization agreement

Negotiations between LKAB and SJ on a new agreement for the ore transport were carried on throughout practically all of 1978. In connection with these negotiations, both companies agreed to carry out a joint investigation of the possibilities available for reducing the transport costs. The third party involved in the ore transports, NSB, also participated in this investigation. Their participation was, of course, essential. The closed system which the ore transports constitute cannot be changed to any noteworthy degree unless all the parties involved are in agreement. Consequently, measures carried out by the Norwegians must be taken into account on the Swedish side and vice versa.

Inventory of possible actions

The rationalization work began with an inventory, jointly drawn up by LKAB and SJ, of possible cost-reducing actions in the short term. A criterion applied to this inventory was that it should be possible to carry out the actions without any major investments.

The inventory was drawn up by interviewing those who encountered problems in their practical daily work and who had ideas and proposals for solutions. Old reports were studied and those responsible for the inventory also made a study trip to other ore lines.

The Director General reached the following decisions, based on the inventory:

~~all of the actions listed and proposed in the inventory were to be more closely investigated.~~

- this work was to be carried out in a steering group with members from the senior management and the trade unions.
- the Manager of the Operating Region in Luleå was appointed to lead the steering group and also to negotiate a rationalization agreement with the trade unions.
- all of the investigations were to be carried out on a purely business economic basis without consideration of any regional or personal policy viewpoints.

LKAB and NSB also appointed a steering group somewhat later.

The investigation work thus came to be carried out by three steering groups which had to be coordinated from the time and area aspects. This was done by making the chairman of each steering group a member of the two other steering groups.

The investigation

The number of objects to be investigated was large. This meant that the primary investigations could not be carried out in the steering group. The negotiations with the trade unions concerning a rationalization agreement led to an agreement permitting SJ to carry out the remainder of the investigation work in four working groups under the steering group. The working groups included members from SJ, NSB, LKAB and representatives of the Swedish trade unions. As a result, the investigation work was led by three steering groups, SJ, NSB, LKAB, while the actual investigation work was carried out by a number of working groups.

SJ had four working groups

- administration
- traffic
- maintenance, fixed installations
- maintenance, rolling stock

NSB had the same working groups except administration. LKAB had no working groups.

Despite the fact that the work was carried out in accordance with the same pattern at SJ and NSB, certain issues were processed differently.

Results

The following is confined to a brief outline of the investigations made by SJ. An outline is provided for each working group.

Administration

SJ has a functional organization throughout the company, with three main levels. Consequently, the number of managers within an area on the regional and local levels is large. The responsibility for the ore line is shared on the regional level by the Manager of the Operating Region, the Manager of the Fixed Installations Region and the Manager of the Workshop Region. The number of managers on the local level amounts to 12. This state of affairs naturally made collaboration between SJ - LKAB - NSB more difficult. Consequently, one of the main tasks for the working group for administration was to propose a crossorga-

nization in SJ for the ore line with one manager. This organization was to be located in Kiruna.

As has been mentioned above, the ore traffic can be subdivided into two sections, the south section between Vitåfors and Luleå and the northern section between (Vitåfors) Kiruna and Narvik. The northern section carries the completely dominating share of the ore flow.

Consequently, the working group soon decided that the proposed ore line administration be limited to the northern section, in other words the Vitåfors-Vassijaure-Swedish border section for SJ. The working group also proposed that the ore traffic in the southern section should be dealt with by the regular organization, on a contract basis on behalf of the Kiruna administration. The group has now submitted its proposal and is completely unanimous in suggesting that an SJ administration based on Kiruna and with one common manager should be established for the ore line, regardless of the organization which SJ has in other respects. This would not only create a cheaper organization but would also simplify command paths considerably. It should be possible in a somewhat longer term to create a total coordination between LKAB-NSB-SJ with this administration as a basis. The fact that the ore line runs through two countries, with all the concomitant problems arising from national interests, constitutes a difficulty in this regard as in other traffic contexts.

A total integration would provide further coordination gains both in the utilization of personnel and in the utilization of premises.

Traffic

This working group had two types of problem to solve:

- 1) increased utilization of rolling stock so as to be able to reduce the capital service costs
- 2) increased operational efficiency so as to be able to reduce operating costs, particularly staff costs.

Since the turn-round time for both wagons and locomotives is dependent on the terminal handling and on the design of the time table, extensive give-and-take is required between LKAB-SJ-NSB before an optimum result can be achieved.

The work carried out by the group has led to extensive savings in wagons and locomotives. These savings have been achieved by shortening the terminal times and by changing the design of the time table with hourly intervals between the ore trains. The latter has entailed certain alterations and extra costs in the terminal work but the overall gain is significant and amounts to 2 locomotives and 250 wagons. As a result of this, a planned acquisition of locomotives by NSB could be cancelled. Another advantageous result is that the Vitåfors-Narvik traffic can be run with bogie wagons (Uad), thus obtaining a uniform wagon type between Kiruna and Narvik.

In 1976 an agreement was reached between SJ and SF (State Employees' Union) on manning all locomotives with driver only. An exception was, however, made for the ore line during the period November-April when the

ore train locomotives would have a driver and an assistant. This arrangement is expensive and it has been agreed that negotiations shall be started with a view to changing over to one-man operation during the winter season as well. The introduction of ATC is probably a prerequisite for an arrangement of this type.

Coordinating the SJ-LKAB terminal service was considered to be another means of reducing costs. The investigation work confirmed this. Considerable overall savings could be achieved if SJ took over all the work directly connected with the railway, particularly shunting, in the terminal. This would, however, entail a cost increase for SJ while LKAB would have its costs reduced. Negotiations on the distribution of the rationalization gain between SJ and LKAB must be carried out in line with the objectives which apply to both companies.

The working group has also investigated the business economic value of the passenger and goods (non-ore) traffic between Kiruna and Narvik. The result was rather discouraging since this traffic proved to be a far from profitable affair. The revenues did not come anywhere near covering the costs. A further negative factor was that the ore traffic had to bear considerable extra costs due to the fact that the passenger and goods trains, which run at a higher speed, prevented the ore trains from being scheduled in a uniform pattern, thus giving rise to increased turn-round times with concomitant increases in the need for locomotives, wagons and personnel.

Maintenance of fixed installations

Previously there was no road between Kiruna and Narvik. As a result, maintenance personnel had to be transported to and from their work places by means of railway vehicles. The dense train traffic reduces accessibility for these vehicles, and the fact that the vehicles are rail-bound makes it difficult to coordinate and improvise transports etc. A road is now being built and has almost reached the Swedish border. This provides possibilities for basing the transport requirements for maintenance work on road vehicles. A far more efficient transport system than that in use today can be created with the aid of two-way radio communications and a transport centre in Kiruna.

The ore railway stations in Vitåfors and Svappa-vaara are owned by LKAB as is the Sjöbangården station in Kiruna. Like the other tracks located within LKAB's area, these stations are maintained by LKAB. If SJ took over this work and used its machinery and equipment for it, considerable coordination gains could be achieved. The border between Sweden and Norway constitutes an undesirable but nevertheless existing obstacle for routine maintenance work. The group has, however, already proposed certain ideas for increasing the utilization of machinery and equipment etc across the border. National interests play an important part here, as they do in other contexts concerning the possibilities of coordinating work across the border. Political decisions at a high level are required in both countries if these problems are to be solved.

Maintenance of rolling stock

In addition to the normal safety inspection, a particularly careful inspection is carried out at present of the wagons, both when loaded trains and empty trains depart. As a result, repair stations have been located not only in Narvik and Luleå but also in Vitåfors (Gällivare) and Kiruna. The investigation shows that the special wagon inspection need only be carried out once per round trip. This inspection should, in the opinion of the majority within the steering group, be located in Luleå and Narvik respectively, one of the reasons being that the climate is milder in these towns.

In conjunction with this, repair activities should be concentrated to Kiruna and Luleå. Kiruna has been chosen rather than Narvik mainly due to the fact that the building facilities in Kiruna are better. The overall costs can be reduced by taking over the maintenance of LKAB shunting locomotives in Kiruna and Vitåfors. The Uad wagons, one third of which are owned by LKAB and two thirds by SJ, are overhauled at present by SJ in Kiruna and by LKAB in Narvik. Carrying out all overhaul work in Kiruna would mean that considerable savings could be made.

The subdivision of the ore line amongst two countries has entailed irrational solutions in this respect as it has with regard to the maintenance of the ore train locomotives. Since SJ owns most of the rolling stock, concentrating the ore train locomotive maintenance to Kiruna would appear to be a highly rational action, particularly if the building facilities available in Kiruna are also taken into consideration.

Conclusion

During the period when the investigation of the short-term actions which could be taken for reducing the costs on the ore line was in progress, a joint plan was also drawn up for investigating more long-term solutions for reducing costs.

One of the aims here was to investigate the consequences of a complete integration between SJ-LKAB-NSB for the ore transports so that the transports would be dealt with by one company which was jointly owned in some way.

Another objective was to investigate which investments are profitable for reducing operating costs, bearing in mind LKAB's forecasts for mining volume, product mix and the assessed future life of the mines.

Unfortunately this investigation will not be completed before the turn of the 1981/82 year at the earliest. Consequently, no report can be provided on it for the time being.

However, the first stage, which aimed at utilizing possible coordination gains in a simple manner without major investments and to the extent possible with regard to national boundaries, has had a marked effect.

Gains of an order of sek 40 million/year on the Swedish side could be shown to be available if it were not necessary to take into consideration certain staff and regional policy factors. This amount will however probably be reduced somewhat after negotiations with

the trade unions. But the gain per year which can still be achieved is, by no means insignificant.

Another effect of the first stage of the investigation is that, during the work carried out in the various groups, a steady increase could be noted in the understanding between SJ-LKAB-NSB for the necessity of extended integration.

The Railways of Australia Technical Research Programme

H.N. Walker

Chief Engineer
Queensland Railways
Brisbane, Australia

Chairman
Railways of Australia
Vehicle/Track Studies
Co-ordinating Committee

This paper briefly describes the Railways of Australia Research Programme which had its modest beginning in 1977. The integration of four discrete projects has resulted in an extensive multi-disciplinary research programme which has and will continue to be of immense assistance to Australian railway engineers. These projects are supplying valuable data on vehicle and track performance under Australian conditions and developing powerful technical tools for railway management in Australia.

INTRODUCTION:

Historically, the parochialism of railway systems in Australia meant that research was confined to low key internal investigations with limited resources and frequently without positive results being achieved.

With the advent of unit trains, heavier axle load vehicles and demands for higher operating speeds, it was imperative that more information be made available to civil and mechanical engineers regarding track and vehicle characteristics and their inter-relationship. The technical and fiscal demands of acquiring this knowledge was beyond the resources of the individual railway systems in Australia, and a collective approach was made by all Chief Civil Engineers and Chief Mechanical Engineers to have a joint research programme instituted.

In 1977 the Commissioners of the Government Railway Systems in Australia approved a national research programme which represented a momentous occasion in the history of technical research into railway operation in Australia.

The research programme is funded and controlled under the auspices of Railways of Australia (R.O.A.), a national body comprised of the five Government Railway Systems in Australia. There were significant problems to be overcome, not the least of which was the multiplicity of gauges represented by the various Government Systems :-

1) Queensland	-	1067mm	-	10,091 route kms
2) New South Wales	-	1435mm	-	9,756 route kms
3) Victoria	-	1600mm	-	6,647 route kms
		1435mm	-	332 route kms
4) Western Australia	-	1067mm	-	4,393 route kms
		1435mm	-	1,229 route kms
5) Australian National	-	1435mm	-	2,140 route kms
		1067mm	-	869 route kms
		1600mm	-	511 route kms

However, all were drawn together in the need to contend with rising maintenance costs and the common view was shared that this could be best achieved by increased knowledge of Australian track and vehicles and how they interacted.

The primary objective of the Railways of Australia (R.O.A.) research programme was to investigate the optimisation of track and vehicle design for Australian conditions.

R.O.A. RESEARCH PROGRAMME-OUTLINE

CONTROL AND ORGANIZATION

The R.O.A. research programme is directed by a Vehicle/Track Studies Co-ordinating Committee under the present Chairmanship of the Chief Engineer for Queensland Railways, who is the Author of this paper, with representations from all other Government Railways in Australia.

Because of the relative inexperience of Australian railway engineers in the research field, and complexity of management of the programme, the Broken Hill Proprietary Company Limited, Melbourne Research Laboratories

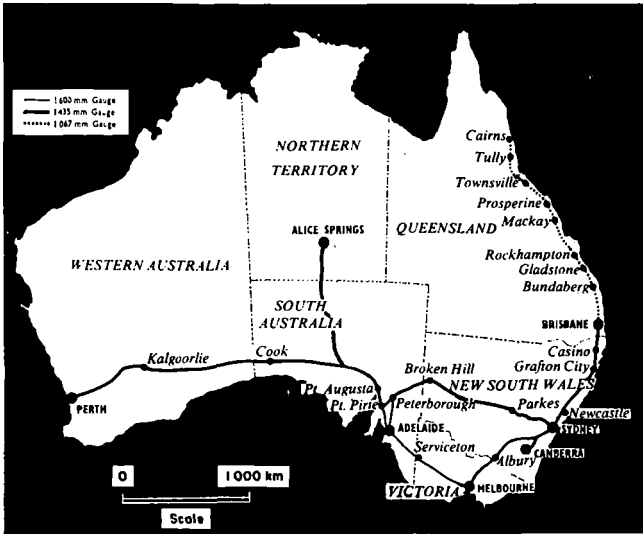


FIGURE 1 Australian Interstate Railway Network.

(B.H.P., M.R.L.), an organisation skilled in railway engineering research was engaged to manage the programme.

The detailed definition and execution of the studies and the associated budgeting and costing is organized by Working Committees comprising specialist engineers from the various railway systems.

Funds are contributed by the Systems on a basis proportional to tonne-kilometres carried. It is estimated that in excess of \$1M (Aust.) has been spent so far on the programme with a proportion of this sustained by the host organisations.

The Bureau of Transport Economics, a Federal Government research body, commissioned B.H.P. M.R.L., to assist in the development of a computer based track design model, the Interactive Track Design Model (I.T.D.M.).

R.O.A. funds were allocated to expedite the development of the Vehicle Simulation Model at the University of Adelaide. This Model had been initiated some years earlier by the former South Australian Railways in conjunction with the University of Adelaide.

These computer based simulation models were to be enhanced and validated by the findings of two research studies, one of which was conducted in New South Wales and the other is continuing in Western Australia. The studies are referred to as "R.O.A. Study No. 1" and "R.O.A. Study No. 2" respectively. The Vehicle Simulation Study was subsequently developed as "Study No. 3".

R.O.A. STUDY NO. 1

Study No. 1, now fully completed, was a Vehicle / Track Interaction Study with the basic aim of providing railway engineers with technical data concerning vehicle and track forces applicable to Australian operating conditions, which could be used to quantify the

relationships between track structure, traffic load, traffic operating conditions, and those factors which cause degradation of materials, track geometry and rollingstock.

The experimental procedures adopted in the Study together with some of the results obtained have been reported previously (1 to 3). The test programme entailed the running of special test trains composed of instrumented freight vehicles over sections of instrumented track containing specific test features (see Table 1) at a range of speeds up to 110 km/h. A total of 596 test train runs were conducted resulting in over 2,000,000 wheel load measurements. There were four (4) full time Engineers on the project team for a period of 18 months with a vast number of part time technical and ancillary staff.

LOCATION	FEATURE	MAGNITUDE OF FEATURE
Tangent site No. 1	Good track	No built in feature
Tangent site No. 1	Dip in both rails (hole)	25mm dip effective over 6 m
Tangent site No. 1	Dip in one rail (twist)	25mm effective over 6 m
Tangent site No. 1	Misalignment	25mm effective over 6 m
Curve site No. 2	Curve	Nom. Radius 1600 m
Curve site No. 2	Change in curve feature	Rail pulled 25mm outward effective over 10m
Tangent site No. 1	Mechanical Square Joint P2	Nom. 20 mm dip at joint.

Table 1 - Details of track features tested.

The test site was chosen on the basis of maximum track possession, adequate mechanical back-up facilities and availability of locomotives and crews. Track gauge was 1435mm and structure comprised of 53 kg/m rail with hardwood sleepers, steel sleeper plates with dogspikes and crushed rock ballast.

Track Load Measurement

Lateral and vertical track forces were measured by rail strain gauging methods

developed by O.R.E. of U.I.C. Strain gauged base plates were also used to measure rail to sleeper vertical forces.

A data acquisition system was set up to record a maximum of 46 channels simultaneously, each with a sampling rate of 1000 Hz. The Computer with 9 track magnetic tape drive for storage was enhanced by a multiplexed 48 channel A/D converter along with floppy disc drives for programme storage.

Measurements were taken over a 12 month period on seven discrete track features likely to be encountered. These appear in Table 1.

Vehicle Instrumentation

Accelerometers and displacement transducers were placed strategically on the vehicle bodies and bogies.

During the course of the testing, twenty freight wagons were run in four different consists called rakes. In addition, two mechanical test vehicles were utilized in 35 unique arrangements of sixteen bogies and variations to these bogies.

Of the twenty rake vehicles, there were ten (10) different classes represented by one loaded and one empty of each class.

Data was recorded on a 14 channel analogue tape enhanced by a 32 channel multiplexer.

Data Analysis Procedures

Vehicles. The analogue recordings of vehicle accelerometers and displacement transducers were reproduced in hard copy by an 8 channel pen recorder and a large proportion of the analysis was performed manually.

A spectral analysis was performed on selected transducer outputs in order to obtain a detailed study of the frequency variations of certain parameters.

Track. The procedure used for the analysis of track data was understandably much more complex. Digitized data recorded by the trackside mini-computer was transferred to a much more powerful computer owned by the State Rail Authority in Sydney, New South Wales.

Manipulation of the data was conducted by sophisticated Fortran programmes developed by the project team.

A number of variations of data presentation were available but the principal ones involved maximum and minimum vertical and lateral force variations with speed for each vehicle, L/V ratio (Lateral load/vertical load) variation with speed and average vertical and lateral load variation along the track.

R.O.A. STUDY NO. 2

The concept of Study No. 2 was the starting point of what was to eventually become the

R.O.A. research programme. This concept entailed quantifying the relationship between the track degradation, time and traffic volumes.

An integral part of achieving this objective was to quantify the vehicle and track forces and Study No. 1 was subsequently sanctioned to give the required input.

Study No. 2 is underway in Western Australia and has a time schedule of ten years.

The primary objectives are:-

1) To quantify the relationship between induced track forces and track degradation as a function of time and amount of traffic.

2) To determine the influence of several different track structure forms and track component types on both capital and track maintenance costs.

COMPUTER SIMULATION MODELS

Interactive Track Design Model (ITDM)

This model was developed independently by B.H.P., M.R.L. under a commission from the B.T.E. and was made available to R.O.A. which is now funding the continuation of the study.

The model is flexible and allows the user to choose from a number of design procedures based on various theories. A comparison can be readily made of various track structure component stresses using different components or arrangements of components with varying design methods.

Costs of track componentry are also incorporated and a "least capital cost" design can be established.

The results of Study No. 1 form part of the input required by the model, while the data obtained from Study No. 2 will be used to calibrate and validate the model for Australian conditions.

Procedures for the incorporation of a track maintenance component have been developed further enhancing the model as a powerful track management tool by designing a "Minimum Total Cost" track structure.

Vehicle Simulation Model

This model presently being developed at the University of Adelaide is an integral part of the overall research programme.

The objective of this project is the development of a digital computer based model that simulates the dynamic response of railway vehicles under varying track geometry and stiffness at various speeds.

Experimental data collected from Study No. 1 is being used in the development of this model.

Features of this model will be:-

- 1) Inclusion of the most up-to-date treatment of wheel rail contact forces especially longitudinal, lateral and spin creep.
- 2) Inclusion of bogie lozenging effects together with other improved mechanical idealizations.
- 3) Improved treatment of wheel and rail geometry and stiffness to handle worn rail profiles as well as varying track geometry.

R.O.A. RESEARCH PROGRAMME-DETAILS

It is not possible to comprehensively cover all of the work embraced by the R.O.A. Research Programme in this paper, however some of the more interesting and important aspects of Study No. 1 and Study No. 2 will now be detailed.

STUDY NO. 1 TEST RESULTS

As mentioned previously the primary objective was to investigate the optimisation of track and vehicle design for Australian conditions and as such the findings should be viewed in this context.

The major findings of Study No. 1 are listed below:-

Vehicles

- . The length and type of vehicle tested did not appear to significantly alter the performance characteristics of the bogies, that is, a poor performing bogie would perform poorly under all vehicles.
- . Empty vehicles with worn wheel profiles had an inherent critical speed for hunting being virtually independent of track type and condition which, in cases, was as low as 70 km/h.
- . On good tangent track all empty vehicles with three piece bogies having worn wheels hunted at speeds in excess of 75-80 km/h. (See Figure 2) The empty vehicles generated lateral forces of around 30 kN which was significantly greater than the 20 kN lateral loads for loaded vehicles.³

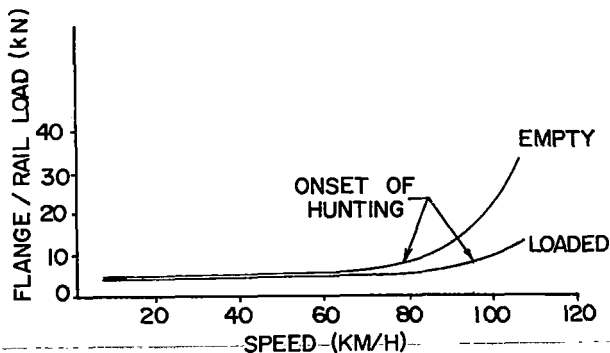


FIGURE 2 Lateral Flange/Rail Loads for typical vehicles with bogies in worn condition traversing good tangent track.

. Empty vehicles were far more susceptible to hunting than loaded vehicles.

. On good track, loaded vehicle hunting was virtually non-existent at speeds less than 200 km/h, even for badly worn wheel profiles.

. Track faults on occasions caused empty hunting vehicles to become temporarily stable.

. Track faults on occasions caused loaded vehicles to begin hunting but generally at speeds above 90 km/h.

. The Derailment Potential (L/V Ratio) rapidly increased above 80 km/h for most empty vehicles, particularly if bogie hunting was occurring. See figure 3.

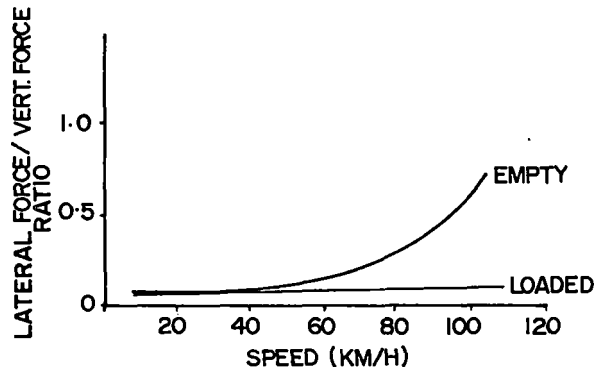


FIGURE 3 Derailment potential for typical vehicles traversing good tangent track.

. For loaded vehicles the Derailment Potential remained constant throughout the speed range tested.

. Vertical loads imposed on the track increased with speed over all features. Maximum wheel loads of 175 kN for 100t vehicle and 150 kN for 76t vehicle were recorded for the 80 km/h speed runs over tangent test track.

. Due to their lighter axle loads the empty vehicles did not deflect the track as much as the loaded vehicles, hence an entirely different track top profile was experienced by the former. This is especially the case for the dip in one rail and the dip in both rails features tested.

. Maximum lateral forces imposed on the track increased with the speed over all features. The maximum lateral force recorded at the misalignment at 80 km/h was 75 kN for a loaded vehicle and 40 kN for an empty vehicle.

. The tests suggest that for maximum economic and safe operation, the three-piece bogie should not be operated above 75 km/h. It is expected that generally the Australian Railway Systems will adopt 80 km/h as a more practical speed limit because at this speed the deterioration in performance was not found to be greatly increased. The bogie and the damping System should basically be in a well maintained condition.

. At speeds lower than 80 km/h the overall performance of the rigid frame primary sprung bogie was very similar to that of other bogies tested. At higher speeds the bogie showed improved lateral stability, lower vertical maximum loads and less wheel unloading compared with the other bogies. The hunting motion of this bogie was significantly different from that of a three piece bogie in that the angle of attack of the wheels to rail was lower.

. In general, the lateral performance of the three-piece bogie with lozenging restraint was better than the ordinary three piece type bogie and under many conditions equivalent to the rigid frame primary sprung bogie. The vertical performance was generally no better than the three piece bogies.

. The importance of damping on the three piece bogies was emphasised in that small variations in the friction wedge components caused major variations in bogie performance. The bogies with the friction wedges inoperative gave the poorest performance of any bogie tested. Of major concern during the tests was the incidence of wheel unloading on empty wagons when negotiating various track features, and some instances of this are shown on graphs (Figures 4 and 5).

On loaded wagons, this condition rarely occurred.

. The condition of the wheels was critical relative to bogie hunting. Bogies with new wheels exhibited less hunting than those with worn wheels. The critical features of the wheel relative to bogie performance appeared to be the flange thickness and the effective root radius of the profile.

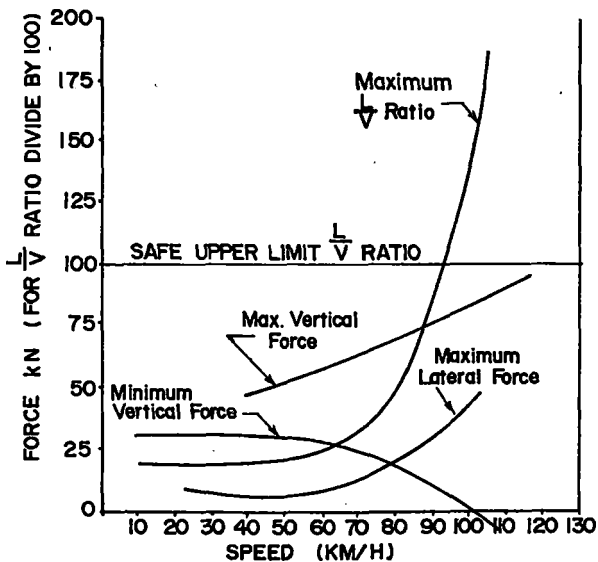


FIGURE 4 VFX Class vehicle empty - track feature-dip in both rails.

Track

. Wheel load patterns generated by the different features were observed. The results gave some striking comparisons. For example, the dip in both rails (hole) generated a predictable bounce in the vehicle from which wheel loading was essentially vertical. The dip in one rail (twist) resulted in small or negligible vehicle response but with track forces which were equal or worse than those measured at the dip in both rails including a significant lateral load. Clearly, by measuring only vehicle ride performance, one is not able to infer track loading values.

. The misalignment of the tangent track caused much higher lateral wheel loadings and significantly more wheel unloading than the other tangent track features, but results also showed that outward lateral forces simultaneously occurred on both rails through the exit of the misalignment.

. The change in radius or more aptly, the curve with an introduced misalignment was clearly the most difficult feature for vehicles to negotiate. It results in the greatest range of loads especially for the loaded vehicles and predictably very high lateral loads. It was, however, quite difficult to pick up the actual peak of lateral loading in the instrumented section particularly for speeds in the order of 100 km/h.

. In addition to the measurement of wheel loads, the work included monitoring the track condition and establishing in quantitative terms the type of track the tests were carried out on. Aspects examined were track deterioration, track stiffness and subgrade soils condition. Some of the results from this are as follows :-

a) High track modulus values were, to a great extent, affected by the rainfall pattern and the amount of voids present in the track structure resulting from support conditions induced by test methods.

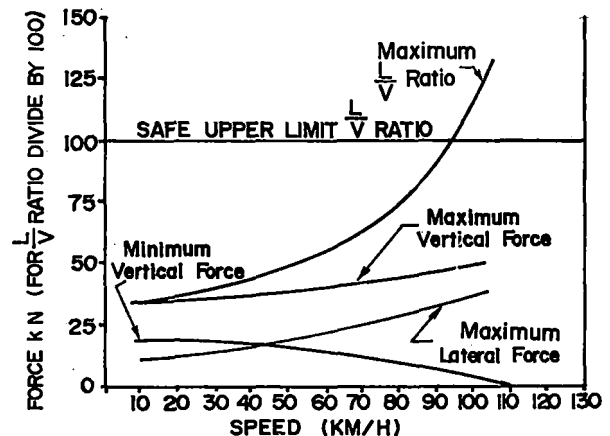


FIGURE 5 CSX Class vehicle empty - track feature lateral misalignment.

- b) By far, the worst track modulus values were recorded near rail joints, underlining their detrimental effects on track, e.g. 3MPa per rail as compared with 15 MPa per rail for good track.
 - c) Simulated rail dips using varying thickness base-plates produced low modulus results similar to a rail joint because of the sleeper to rail void produced.
 - d) By the use of energy loss methods at the mechanical square joint produced low modulus results similar to a rail joint because of the sleeper to rail void produced.
 - e) By the use of energy loss methods at the mechanical square joint permanent reference feature, it was found that, with time, the ballast layer had consolidated, reducing voids.
 - f) The lateral resistance of the track for zero vertical load was found to be 18.0 kN.
 - g) The deterioration of track quality with time at the permanent reference features was not measurable from the track modulus values within the relatively short duration of the test.
 - h) The track recording car (41 kN axle load) did not measure the track as experienced by vehicles with heavy axle loads (235 kN). The data also indicated the rail temperature can have a considerable effect on the magnitude of track misalignment measured by the track recording car.
- As described by Broadley et al (3) use has already been made of the track data to develop a dynamic impact factor applicable to Australian operating conditions, which can be used in the design of new track structures and the upgrading of established track structures.

STUDY NO. 2 DETAILS

The programme has been divided into two phases. The first phase of the programme (1978 - 1980) was devoted to planning and establishing the sections of track for testing (4). The second phase (1980 - 1990) of the programme involves the instrumentation of the sections of track established earlier with recording, processing and analysis of ensuing data.

This section briefly describes the second phase, concentrating on some of the more interesting areas of the work.

In general, the CWR test tracks involve the use of two different rail profiles, three types of sleepers, seven types of fastenings, three different types of ballast and three different ballast depths. Figure 6 is a line diagram giving the location of the test sections on the standard gauge mainline between Perth and Kalgoorlie (refer to Figure 1) and the variable features in each test section.

Each of the 1 km test sections have undergone considerable track instrumentation so as to obtain data of a nature to allow a detailed analysis of observed differences in track degradation, track geometry retention and therefore track maintenance costs.

Therefore an essential part of Study No. 2 is currently the measurement and analysis of data particularly wheel/rail loads, rail/sleeper loads and sleeper support condition, needed to provide a statistical description of the loading environment for each track structure form.

Signals from the track side instrumentation are recorded on an analogue tape system with 16

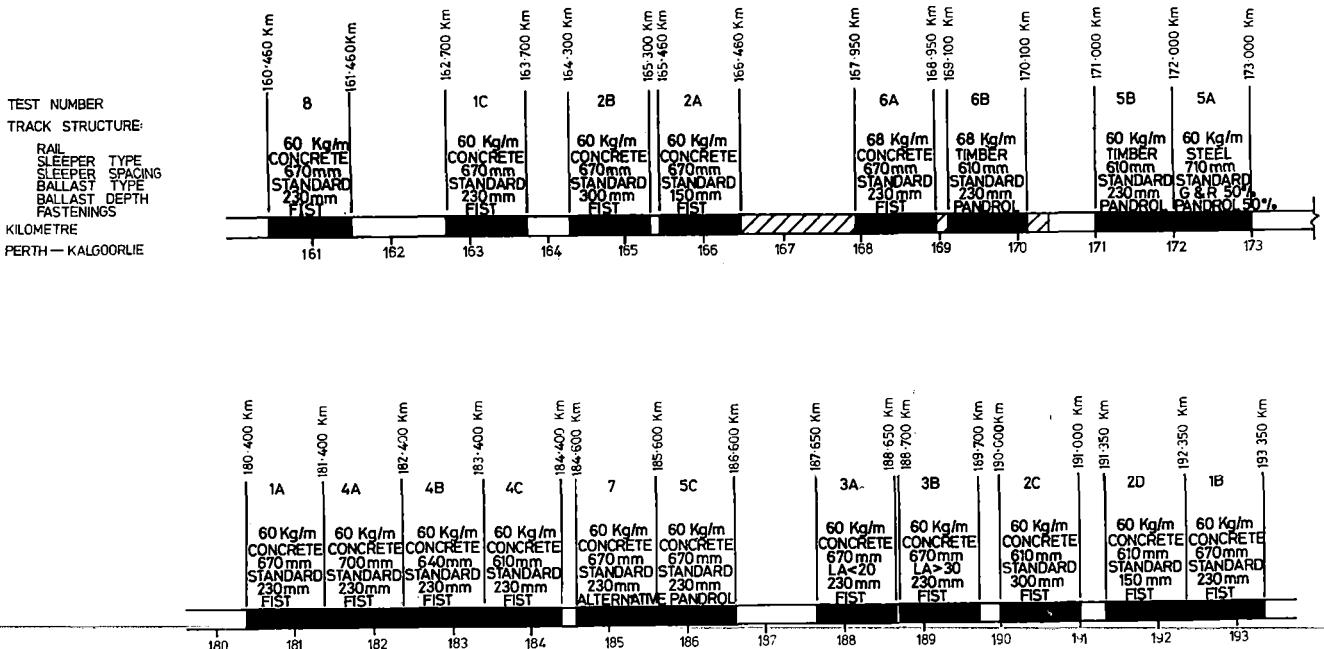


FIGURE 6 Schematic of Study No. 2 test sections.

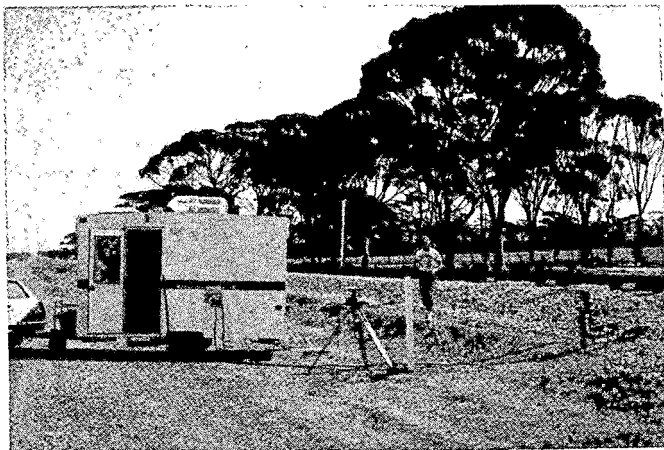


FIGURE 7 Mobile Instrumentation Unit located at an Instrumentation Post.

channel capacity housed in a mobile instrumentation vehicle (Figure 7). The data collected is then stored on magnetic tape on Westrail's IBM-370/138 main frame computer, after having been digitised, for extraction of peak loads, etc.

Amplitude statistics, including mean value, standard deviation, probability distribution, and probability density functions, have been adopted for analysing the track loading and response parameters for this programme.

The track maintenance cost as depicted by the deterioration of track geometry, because of the variation in ballast and formation support, the weather conditions, the difficulty of changing circumstances in traffic carried and even the history of maintenance and rehabilitation of track, is responsible for a major portion of the lifetime cost of track.

Hence, a Matisa PV 6 track recorder car is used to monitor the track geometry on a regular basis. Data from the various channels measuring track parameters such as track top, alignment, twist, etc., is recorded on magnetic tape and analysed using statistical methods and power spectral density (PSD) routines, which reveal the frequency spectrum of line and level deviations.

A sample PSD graph for rail alignment is shown in Figure 8. Examination of this figure shows a significant drop in power at values of frequency corresponding to wave lengths of 5 metres, 2.5 metres, 1.67 metres, etc. Bearing in mind that the Matisa PV 6 car measures alignment using a mid-chord offset system (with a chord length of 10 metres) and calculating the transfer function for this system as $(1 - \cos fL)$ where "L" is the system chord length and "f" is the frequency of waveforms representing track alignment, the drop in power is due to the null response of this measuring system at these wavelengths.

The frequency response of the Matisa PV 6 mid-chord offset system based on the above transfer function, and for that matter for any track recorder car utilising this System of measurement, is variable. It has been shown (5) that the response is ZERO at wavelengths $L/(2n)$ ($n=1,2,..$) i.e. information corresponding to these wavelengths is not recorded. Also the response is DOUBLE at wavelengths of $L/(2n-1)$ ($n=1,2,.....$). At wavelengths equal to $2L/(n-1)$ ($n = 1,2,...$) the response is equal to UNITY i.e. the true wave form of the track is faithfully represented.

The limitations presented by the variable response of the measuring system for rail top and alignment, must therefore be born in mind, so as to avoid wrong conclusions as to the severity or otherwise of the track irregularities measured.

The influence of such factors as speed of recording, direction of travel and temperature during recording, have also been studied with the result that significant variations in measurements can be expected for changes in temperature during recording or between successive recording runs.

Further work is being done in this area to develop factors to account for temperature variations.

As part of the main test programme, dynamic track deflections are being measured under normal traffic conditions in all test sections using the remote laser system developed at the BHP Melbourne Research Laboratories. Since track

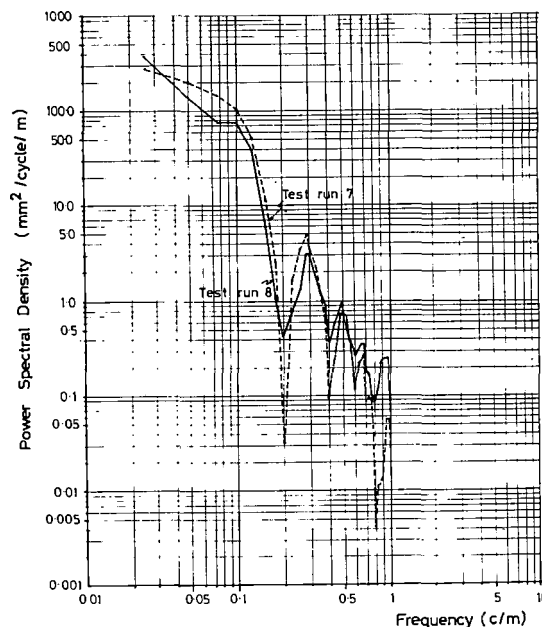


FIGURE 8 Power Spectral Density plot for rail alignment as measured by Matisa PV 6 recording car.

deflection and/or track modulus may be regarded as an overall indicator, in the structural sense, of the track state, their measurement together with the track geometry data obtained will establish allowable track deflection limits for Australian conditions.

In addition to the measurement of track deflection to determine track modulus, procedures for evaluating the separate properties of the ballast and subgrade are required for the layered representation of the track structure. As part of this requirement, a procedure for determining in-situ density of ballast below sleepers without involving track disturbance by their (sleepers) removal, is currently being developed (6).

The approach is based on the "air-permeability" of ballast under the sleeper, and does not require the removal of the sleeper to obtain a density measurement below the sleeper in contrast with the method of YOO, CHEN AND SELIG. (7).

Traffic Data, including number of axles and corresponding axle loads for different traffic types for each direction of travel, is also being collected to provide statistical data on a broad range of vehicle types.

Also, as the programme aims at determining the maintenance costs as a function of time and amount of traffic for specified track quality limits, the various activities that come under maintenance of track are being categorised and all cost associated with each activity for each of the test sections is being recorded. From all the measurements, and a knowledge of the cost of maintaining each test section during the test period, conclusions will be drawn about track structure which is most suitable for a particular operating condition.

The section of track containing the test sections has been declared a restricted area. Maintenance personnel enter under authority only, thus ensuring the proper recording of maintenance costs, both of spot maintenance (the day-to-day basic maintenance of track) and cyclic maintenance (periodic maintenance).

Because of the long time span involved a great deal of planning effort has gone into the setting up of this research programme, and it is considered flexible and able to incorporate changes which may be necessary.

FUTURE OF R.O.A. TECHNICAL RESEARCH

The Co-ordinating Committee is well aware that technical research must ultimately be justified on a cost/benefit basis. Such economic analyses are being fostered by the Committee and we are now examining worthwhile research projects on this basis. At this stage we are only considering applied research and no pure research projects are envisaged.

From the results of the programme completed so far, indications are that further research is required into :-

- a) the effects of cyclic track geometry.
- b) the long term performance of new bogie types.
- c) the effect of vehicle geometry on vehicle performance and track loading.
- d) the performance of different wheel profiles.

There are other important topics under review and some of these will be the subject of economic studies also.

CONCLUSIONS

The R.O.A. research programme has provided an excellent training ground for railway engineers working in multi-disciplinary teams. This programme has highlighted the need to adopt a total system approach to railway engineering problems and for many Australian railway systems was the first time both Mechanical and Civil disciplines worked jointly in this way.

High quality technical data and specific and general guidelines have been produced, and these are enhancing the development of computer models which can be used to economically simulate track and vehicle behaviour. However the need for a great deal more research effort is evident.

To maintain advantage over other modes of transport, research into railway engineering is essential and must continue to ensure a safe, reliable, minimum cost service.

The Railways of Australia Vehicle/Track Studies may be viewed in this light. A programme initiated from a clear need for well planned and co-ordinated research into the vehicle/track system; a programme to provide railway engineers with a factual base to design cost efficient vehicle/track systems for the particular operating conditions so enabling the railways to perform their transportation tasks with greatest efficiency.

.....

ACKNOWLEDGEMENTS

The Author wishes to thank Mr. A. Holme former Chief Civil Engineer of Westrail and former Chairman of the Vehicle/Track Studies Co-ordinating Committee for his contribution to the preparation of this paper.

Mr. Heales of Queensland Railways and Mr. Notte of Westrail also made a major contribution to the preparation of this paper and their assistance is gratefully acknowledged.

REFERENCES:

- 1) Sismey, B.G. 1981, "Railways of Australia Vehicle/Track Interaction Study No. 1" Proc. Railway Engineering Conference, Institution of Engineers Australia, Sydney 7th-10th September, 1981.
- 2) KIMPTON, R.W. "Bogie Performance ROA Tests 80" Proc. Railway Engineering Conference, Institution of Engineers Australia, Sydney 7th-10th September, 1981.
- 3) Broadley, J.R., Johnston, G.D., Pond, B. "The Dynamic Impact Factor" Proc. Railway Engineering Conference, Institution of Engineers Australia, 7th-10th September, 1981.
- 4) Railways of Australia (1978). Vehicle/Track Studies. "Study No. 1 - Vehicle/Track Interaction." Report No. 1.
- 5) Notte, A. (1981). Some Problems Associated with Track Geometry Measurement. Proc. of Railway Engineering Conference, The Institution of Engineers, Australia, Sydney, 7th-10th September.
- 6) Clegg, B. and Moffat, N.A. (1981). Development of a Procedure for In-Situ Ballast Density Determination Below Sleepers. Department of Civil Engineering. The University Western Australia (Not Published).
- 7) Yoo, T.S. Chen, H.M. and Selig, E.T. (1978) Railroad Ballast Density Measurements. Geotechnical Testing Journal Vol. 1 No. 1 March 1978. pp 41-54.
- 8) Railways of Australia (1979). Vehicle/Track Studies. "Study No. 2 - Westrail Track Studies Test Programme"
- 9) Railways of Australia Report. "Vehicle/Track Interaction Study No. 1 Volume 1 and 2 April 1981.

Capacity Planning for Continuous Growth of High Tonnage Trains

C.D. Kloer

Assistant Director
Industrial Engineering
Burlington Northern
Railroad, St. Paul
Minnesota

The approach to line capacity planning in use at Burlington Northern today began in 1973 with the development of the first of a series of line capacity simulation models. These models were developed to analyze track and signal requirements for a rapidly growing commitment to moving western coal in unit trains. In fact the growth in coal traffic was so rapid that, for several years, line capacity studies concentrated on determining minimum requirements for keeping the coal routes fluid. Capital requirements and physical ability to accomplish the necessary construction precluded capacity expansion beyond the minimum level. Track reconstruction and maintenance planning was equally restricted, due to the massive commitment required to convert light secondary lines to heavy tonnage main lines. Growth still exists on these lines today, but at a rate that allows capacity expansion and maintenance planning to be based more directly on economic trade-offs. General rules have been established for long-range planning, but the uniqueness of each line segment mandates detailed analysis before final commitment to any plan. Graphical displays of simulation results, augmented by occasional studies to address unique situations, allow flexible planning that accommodates changing traffic forecasts.

INTRODUCTION

Burlington Northern's long-range planning study of improvements necessary to haul large volumes of western coal started in February, 1973. The Marketing Department, recognizing that the small tonnages we were hauling in unit trains could grow to enormous proportions in the years ahead, requested a major study of our capability to haul western coal. Marketing asked that Industrial Engineering determine the necessary capital improvements to move up to 250 million short tons of coal a year.

The analytical techniques that were available to us in 1973 for a study of this type were limited both in number and scope. We had at our disposal the Train Performance Calculator (TPC) which was a computer model which deals with the performance of a single train alone on a particular line segment. It operates the train over the segment by continuously solving the physics problem resulting from the interaction of the train and the profile of trackage over which it is operating.

We also had at our disposal manual redispatch, or string lining techniques. These, of course, have been used in the railroad industry for years to make new timetables, as well as to make line capacity studies. Running times can be obtained from either a model like the Train Performance Calculator or from dispatchers' train sheets. Information concerning train delays can also be obtained from the dispatchers' train sheets.

Another technique available to us at that time was the Train Meet Delay Model. This was a mathematical model that was originally designed by the

Denver and Rio Grande Western and later modified by the Great Northern Railway. It was designed to calculate meet delay on single track lines with CTC. The model was not a simulation model; it used mathematical equations to develop the likelihood that delays would occur at specific sidings along the line and to calculate the probable amount of delay at each siding.

The Marketing Department's request was for a study of line capacity on 6,833 miles (10,997 km) of track. The line capacity studies we had done prior to this were small, involving line segments less than 50 miles (80 km) long and dealing with just 2 or 3 sidings. We had never done anything of this magnitude before and, frankly, at this point the project was overwhelming. We didn't even have a good definition of line capacity so we started by developing the following: We said that "Line capacity is the volume of a given mix of traffic which a railroad line segment can handle with acceptable delay." The ultimate measure of capacity is revenue ton miles or passenger miles. The definition we use emphasizes that capacity is dependent on the nature of the train, as well as the number of trains. For this massive new coal study it was obvious that many of the line segments were going to become dominated by unit coal trains. Under these changed circumstances, the definition of line capacity could be simplified to: Line capacity is the maximum number of trains that can be run over a line segment without exceeding acceptable standards of train delay.

There are many factors that determine line capacity. The length of the list usually depends on who is writing it. For the purposes of our study, we chose to deal with the following factors:

- A. Acceptable Delay
- B. Traffic Operating Standards
- C. Running Time
- D. Track Configuration
- E. Train Control System
- F. Terminal Characteristics
- G. Track Outages and Equipment Failures

H. Compounding of Delays

Acceptable Delay

We defined acceptable delay as the difference between planned time and the minimum transit time. The planned time is a management decision resulting from a specification of a detailed schedule. In other words, it is a target or goal for the movement of a train over a given line segment. Minimum transit time is the pure running time as developed by the Train Performance Calculator. This is the time that it would take the train to operate over the line segment under ideal conditions with no delays or failures.

Also included in planned time is any time the train is not in motion due to activities such as crew changes, adding helper units, etc. Acceptable delay is broken down into two components: allowable meet delay and allowable contingency delay. We have defined each as 50 percent of acceptable delay. Contingency delay is miscellaneous delay caused by mechanical problems, weather, etc. Meet delay is delay caused by other traffic on the line.

Traffic Operating Standards

Traffic operating standards reflect the type of service a railroad will offer on a line segment in order to satisfy customer demand. Application of these standards to a particular type of train results in the planned time mentioned above. Development of the standards includes specifications for acceptable delay, planned times or train schedules, train priorities, and horsepower per ton or train length and train make-up specifications.

Running Time

Running time is significant because it is a principal factor in determining acceptable delay and because it is a measure of the length of time when a train uses the resources of a line segment. It summarizes many of the determinants of line capacity. It includes:

1. Train Characteristics - horsepower per ton ratio, train length, rolling resistance characteristics, and braking capabilities.
2. Track Characteristics - grades, curvature, track surface conditions affecting adhesion, track quality characteristics affecting speed limits.
3. Signal Characteristics which affect speed limits.
4. Safety Regulations and Work Rules which affect train operating methods.
5. Distance.

Track Configuration

The track configuration includes the number and location of tracks and number and location of usable sidings. The location of multiple tracks and sidings is one of the most important considerations in determining line capacity.

Train Control Systems

The characteristics of the train control system on the line segment being studied affect the quality of the control decisions and the speed with which they can be implemented. The major factors affecting these decisions are the type of signal system, the type and location of turnouts, and the operating rules in effect on the line segment being studied. On the Burlington Northern system we are primarily concerned with the following three basic types of signal and control systems:

1. Timetable and Train Order
2. Automatic Block Signals (ABS)
3. Centralized Traffic Control (CTC)

From a line capacity standpoint, the first two systems are characterized by the fact that train meets must be anticipated well in advance and accommodated in train orders. ABS does allow trains to operate safely at higher speeds. To the extent that this advantage can be exploited, Automatic Block Signals increase line capacity. CTC is characterized by flexibility to change decisions when unforeseen circumstances occur.

Terminal Characteristics

While unit trains are not switched at terminals in the manner of general freight trains, operations such as fueling, inspection and crew changes consume a portion of each train's cycle time. To the extent that time in terminals can be minimized, acceptable delays on line can be increased. If the acceptable delay is increased, the capacity of the line segment is increased.

Terminals generate trains for and absorb trains from the railroad network. The ability of terminals to perform these functions directly affects line capacity. If a train must be held outside a terminal because of overcrowding, the resources of the line segment are reduced and, therefore, the capacity of the segment is reduced. Similarly, if a train must be moved out of a terminal at an otherwise inopportune time, the capacity of the adjoining line segment will be reduced.

Track Outages and Equipment Failures

Programmed maintenance, emergency maintenance, derailments, break-in-tuos, and other occurrences can completely tie up a particular section of track, preventing movement of trains over that section. Unless trains can be routed over other track during these outages, they must wait for the line to reopen. This affects capacity in two ways. First, trains incurring delay while waiting for the line to open have less time available in their schedule for delays while meeting other trains. Second, trains waiting for the line to open get bunched with trains arriving shortly after the line is open, increasing the number of meets in that section.

Compounding of Delays

The "bunching" delay mentioned above can be generalized as follows: Any time a train is delayed on any line segment, its total time on that segment increases, thereby increasing the probability for further delay at some point on the segment.

LINE CAPACITY MODELS

Once the factors affecting line capacity were identified, we proceeded to develop a series of simulation models. These included a Yard Capacity Model, a new Train Performance Simulator, and three line capacity models.

The Yard Capacity Model is used to determine the number of tracks required for fueling, inspection, and crew change at main line service facilities. The Train Performance Simulator is a derivative of the original Canadian National model. Our version was obtained from the Southern Pacific and modified for our timesharing computer system. By using documentation written by the SP we also were able to improve some of the code and logic in the model.

Three line capacity models were developed. The first was suitable for analyzing only single track

with sidings. The second was designed to analyze only alternating segments of double and single track without sidings. The third model, called the Line Capacity Model, replaced the first two.

The Line Capacity Model can be used to analyze single track with sidings or combinations of double track and single track with sidings. It was not designed for analysis of pure double track where use of crossovers for meets and overtakes is integral to operation of the trains.

Limited look-ahead capability allows the model to look far enough ahead to guarantee that space exists for each train it wants to move across the line. This feature provides the ability to simulate high volumes of traffic without locking up the model.

CTC, Train Order Territory, or combinations of the two can be analyzed in a single simulation run.

Trains can enter the simulation randomly or on a schedule. Most BN analyses have used random generation of trains into the system because they have been primarily concerned with coal trains that operate on the basis of a planned number of trips per year rather than on a specific schedule for each trip.

Junction traffic can be accommodated, i.e., trains can enter and leave at any point on the line being simulated.

Site-specific parameters such as acceleration, deceleration, and switch clearance times are generated internally by the model. This is accomplished in a head-end routine that accesses Train Performance Simulator output and extracts information required for the specific line capacity analysis being performed. It then runs the Line Capacity Model using this information.

Scheduled and random outages can also be simulated. Examples of random outages would be locomotive failures, broken knuckles, hot boxes, broken rails, etc. Scheduled outages are generally programmed maintenance. They can be simulated statically, as would be the case with bridge work or, they can move down the track a specified distance each day, as would a tie renewal program. Appropriate slow orders are also accommodated for both types of maintenance.

Output from the Line Capacity Model includes statistics on train delay, queuing of trains within or entering the system, and running time over the line segment. Some statistics are provided in the form of frequency distributions. The main output is the average overall train delay within a user-specified confidence interval. This confidence interval triggers a convergence routine that terminates the simulation when the average overall train delay reaches a steady state. Prior to development of the convergence routine, a typical simulation analyzed one year of operation. Now a typical simulation terminates after two months.

THE YEARS OF RAPID GROWTH

Unit coal trains traverse a large portion of the Burlington Northern system from branch lines to heavily used main lines. Some of these lines were already major freight routes and were able to absorb initial traffic increases without undue effort. Other lines had capacity for regular freight but virtually no capacity to handle any significant volume of unit coal trains, most of which exceed 14,000 short tons in gross weight and 6,000 feet (1,830 m) in length.

The main thrust of line capacity improvements has been on the lines that were destined to have the greatest increase in traffic due to the growth of

unit coal trains; the lines in eastern Wyoming, southwestern South Dakota, and Nebraska. For example, in 1974, when Burlington Northern coal traffic was in its infancy, the lines south and west of Alliance, Nebraska, to Sterling, Colorado, and to Sheridan and Orin, Wyoming, were secondary main lines handling four to six regular freight trains per day and an occasional coal train. The coal trains were shorter than desired for efficient and profitable service because in this entire 580 miles (933 km) of route destined to become the center of Burlington Northern coal operations, there were only three locations where loaded and empty 110-car unit coal trains could meet without one of the trains being split and put on two different side tracks, and two of these locations were available only part of the time. The entire 580 miles (933 km) were operated by train order, and 569 miles (916 km) had no signals whatsoever. In addition, the track through a large portion of this territory while well-suited to regular freight traffic, required the imposition of restricted speeds for loaded coal trains.

To convert the secondary lines to major coal routes, a massive program was undertaken to upgrade existing trackage and signal systems and to construct new passing tracks, second main tracks, yard tracks, and CTC signaling systems. The same philosophy of upgrading and expansion was applied, to a lesser degree, on lines handling lower volumes of coal trains. In addition, the new Orin line, 127 miles (204 km) long, was constructed to provide another route for coal traffic, thereby greatly increasing both the immediate capacity and the ability to expand future capacity to handle coal trains.

The capital requirements for a program of this magnitude, combined with the physical ability to accomplish the work, restricted the amount of construction that could be scheduled each year. As a result, for several years line capacity analyses concentrated on determining minimum requirements for keeping the coal routes fluid. Completion of the basic upgrading to coal train standards coincided with a decline in the rate of growth in coal traffic. At that point, both capacity expansion and maintenance planning were able to shift emphasis. Economic evaluation of alternative projects and project schedules could now become a focal point for future planning efforts.

We have defined a very specific environment in which to plan, and execute plans for, capacity expansion and track upgrading and maintenance. Since this environment set the pattern for the planning process, a quick review may be helpful before we continue.

The capacity and maintenance planning we are concerned with can be characterized as follows:

A. Light duty lines with negligible capacity for meeting unit trains.

B. Four to six regular freights per day, including locals, with no priority trains.

C. Long term growth forecast, with quantum jumps in traffic (5 to 10 trains per day) each year for about 5 years, followed by significant but less rapid continuous growth.

D. Virtually all of the growth consists of unit trains exceeding 14,000 gross short tons and 6,000 feet (1,830 m) in length. These trains operate on the basis of contracts between shipper and receiver for specified annual tonnages.

E. Planned improvements have to meet restrictions imposed by availability of capital and physical ability to accomplish the work.

These characteristics imply the following conditions:

1. Upgrading and expansion of capacity must occur under traffic.

2. Train movement must be such that each train achieves a predetermined average transit time over the line each year. This is equivalent to maintaining a specific average delay for each train operating over the line. Each train makes many trips per year and each trip begins at a different time of day and day of the week. This produces a completely random schedule for trains operating over any given line. As a result, delays will be distributed randomly among the trains. A train incurring major delays on one trip will receive insignificant delays on another trip. This leads us to the realization that we need not concern ourselves with individual trains. Therefore, planning can focus on maintaining a specific average delay for all trains operating over the line in any given year.

3. Capacity expansion projects selected for construction each year must be those that will keep the lines fluid even if this approach will produce a higher total cost than would be possible under other schemes. The result is a piecemeal construction plan that begins with a scattering of small projects and progresses with larger projects at the same locations. Concentration of some of the work each year might be more efficient but would allow traffic in some areas to exceed the capacity far enough to bring operations to a halt.

The rapid growth period was also characterized by "growth pains". For example, as traffic grew, the number of different shippers using their own cars also grew. The resultant growth in spare cars to be used as replacements for cars in need of repair was astronomical. Since most of the spare cars had to be put into the trains at the same terminal, the capacity of the terminal was rapidly exceeded. Some of the spares were then kept at sidings or small yards on line. Trains had to stop at these locations to pick up cars needed to replace those that had been bad ordered. This created so much congestion that a simulation was run to determine how much delay was directly attributable to this operation. Results of the simulation changed the priorities for capacity expansion projects. Terminal capacity that eliminates switching on line was found to be much more beneficial than additional capacity at the on-line switching location. In addition, the terminal capacity usually costs less and is less expensive to maintain.

A capacity expansion policy that cannot be simulated directly with the Line Capacity Model in most cases is that of providing double track for some minimum distance, say 5 to 10 miles (8 to 16 km), on each side of terminals where the majority of trains stop, regardless of the duration of the stop. The value of this policy has been simulated for small terminals where trains stay on the main line. Intuitive extrapolation to larger terminals indicates that this is one of the most significant line capacity policies that could be adopted. Burlington Northern's before-and-after experiences during the rapid growth years underscore this philosophy.

During the major growth period, the Line Capacity Model did not have the ability to simulate track outages. This meant that other means had to be adopted to account for programmed maintenance and track and equipment failures. We decided that capacity planning should allow for the line being out of service 6 hours per day, every day, for maintenance or other reasons. This means that the line must be able to handle 24 hours worth of trains

in 18 hours with acceptable delay. Since the model had to simulate 24 hours per day, we simply used a 24 hour traffic volume that was 33 percent greater than the forecast volume that the line would actually have to handle in 18 hours. Except for any differences in the way trains are bunched throughout the day, this method creates the same train meet delay as an analysis that takes the line out of service. Experience showed this method to be quite accurate for the conditions that existed during the major growth years.

Another phenomenon of rapid growth was the alteration of standard construction methods to accommodate the volume of work and the alteration of maintenance policies to accommodate trains that did not operate on a fixed schedule and therefore could not be a direct input to the daily maintenance schedule. The change in construction methods was one to specialized gangs that moved from one work location to another doing only one job, such as preplating ties. Track renewal (maintenance) policies were changed by limiting the use of sleds to locations with double track or passing sidings. Less mechanized methods were used on single track. This was slower and more costly but allowed the gangs to clear the track for train movements during lunch breaks. Neither of these revised policies is new to the industry, or even to Burlington Northern, but having tried other methods that are fine in most normal situations, we can state unequivocally that anyone faced with a similar growth situation should consider the revised policies.

The planning process was quite lengthy during the rapid growth years. Each year when the new coal forecast was issued by the Coal Division, a detailed analysis was made of every line segment for the second year of the forecast (the first year being already determined by the current capital budget). Various line configurations were tested for each segment; some were developed by the Division Superintendent, others by the Industrial Engineering Department and/or other officers of the railroad. The detailed results were reviewed with the division and the regional officers and the results formed the basis for the budget submission for the following year's capital budget. For the long-range plan we relied on a general line capacity table that will be discussed later in this paper, on early simulations of alternating single/double track and, more recently, on graphs of simulation results, also to be discussed later.

Today's planning process, although unchanged in principle, is much less involved because it employs graphs of simulation results and information developed during earlier analyses.

RULES-OF-THUMB

Various rules-of-thumb have been developed from the vast number of line capacity simulations that have been run since mid-1974. Some of these rules were developed expressly to aid long-range planning, where time constraints on the planning process or uncertainty of the forecast growth make extensive analysis impractical. Other rules were developed from specific studies that were made to assess the impact of local phenomenon on line capacity expansion and establish priorities for improvements. Most of these generalizations were developed for situations in which the majority of the traffic is unit trains. The extent to which they can be used in other situations depends on the situations to which they are being applied and the experience of the person applying them.

1. The most frequently used general rules are in the form of a table of line capacities which is reproduced in Table 1.

As well as implying a sequence for new track and signal construction, Table 1 implies that track upgrading, to provide speed limits approaching 50 mph,

TABLE 1 ESTIMATED TRACK CAPACITIES

<u>Type of Track</u>	<u>Average No. Trains/Day*</u>
Single Track	
2½ mile (4 km) sidings 11 miles (18 km) apart-Timetable and Train Order	10-15
2½ mile (4 km) sidings 11 miles (18 km) apart - CTC	20-25
2½ mile (4 km) sidings 7 miles (11 km) apart - CTC	30-35
5 mile (8 km) sidings 7 miles (11 km) apart - CTC	40-45
Alternating Single/Double Track	
10 mile (16 km) double 30 mile (48 km) single with two 2½ mile (4 km) sidings - CTC	50-55
10 mile (16 km) double 10 mile (16 km) single - CTC	60-70
Double Track - CTC	75-125

***Assumptions:**

- . 50 mph (80 kph) speed limit
- . Average rolling terrain
- . No priorities
- . 50% of the trains have a HP/TT close to 1.0 and 50% have a HP/TT close to 4.0
- . No overtakes
- . Daily average number of trains allows for line out of service six hours per day for maintenance of way or other contingencies.
- . Allowable meet delay 50" - 60"/100 miles (161 km)

The capacity table is used for long-range planning and for rough estimates of capacity requirements on any line that has not been simulated. Since it is directly applicable only under the conditions stated in the table and even then is only an estimate, considerable interpretation and knowledge of local conditions are required when applying it in any specific situation. However, when used with full knowledge of its limitations, it has proven to be the single, most valuable tool to come out of our line capacity work, except for the Line Capacity Model itself.

It should be noted that ABS signaling systems do not appear in the capacity table. This is a phenomenon of the 50 mph (80 kmp) speed limit assumption. From a pure line capacity standpoint, the only advantage to ABS is that it allows trains to operate at speeds above 49 mph (79 kph). Therefore, although it may have other value, ABS does not affect line capacity under the conditions imposed in Table 1. Since Burlington Northern unit coal trains are restricted to 45 mph (72 kph) loaded and 50 mph (80 kph) empty, ABS has not been considered when planning capacity improvements on the coal routes.

The table implies a definite sequence of improvements for capacity expansion. For example, if you begin with a single track line that is dark and has only a few or no sidings, the first major level of increased capacity would be obtained by constructing sidings at reasonable intervals, say 11 miles apart. CTC would be wasted if installed prior to obtaining this reasonable siding spacing. Once this capacity is achieved, however, the next quantum jump in capacity can be attained merely by installing CTC. To obtain the same capacity increase through track construction would be much more expensive than CTC.

should be completed before trying to operate volumes much higher than 10 trains per day over the line. Of course this is not an absolute number and lines with more track already in place can accommodate higher volumes. However, long stretches of low speed limits can severely limit your ability to increase capacity significantly through moderate increases in passing tracks. We have made no particular effort to generalize conclusions on this subject. In practice the economics are governed by the individual situation.

When you begin with a very low capacity line and know that it will gradually have to become a very high capacity line, you can omit consideration of many suitable track configurations for low and intermediate volumes and concentrate on those that can be expanded to obtain the desired configuration for high traffic volumes. An example of such a construction sequence is shown in Figure 1. As traffic begins to grow from an initial level of a few trains per day, sidings are added until the entire line has sidings approximately 10 miles (16 km) apart, as in Configuration A of Figure 1. Track upgrading to increase speed limits can be done concurrently to prepare for volumes in excess of 10 trains per day. The next step is to install CTC and then, as traffic continues to grow, convert pairs of sidings to sections of double track until the entire line has alternating segments of 30 miles (48 km) of single track with sidings and 10 miles (16 km) of double track, as in Configuration B. We call this a 30/10 configuration. The next phase creates more double track sections until Configuration C is attained. Further volume increases require filling in the gaps until full double track is achieved.

Another construction sequence that might be considered would also build to a 10/10 configuration, but

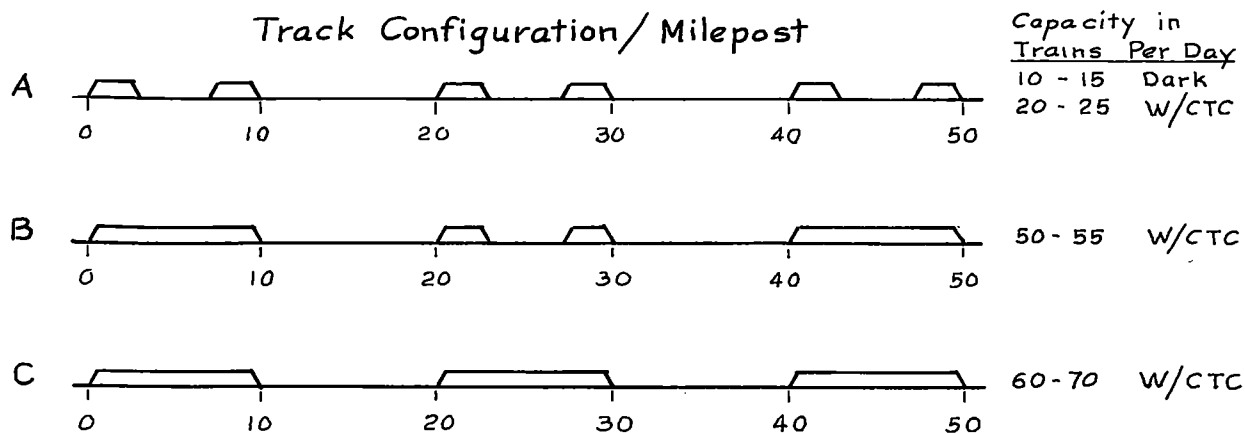


Fig. 1 Construction Sequence

would require less construction to achieve the same capacity increases in the early phases and more construction in the later phases. This sequence would begin with sidings located at the midpoints of planned double track sections. Once sidings are in place for each planned double track section, they would be lengthened gradually until the 10/10 configuration exists. Our analyses have shown that this construction sequence puts the capital expenditures as far into the future as possible. However, this approach is not likely to become popular. A major objection is the fact that you continually return to the same work locations to move the same turnouts. In addition, you have to work at more locations each year than would be necessary under the previously discussed plan. The resulting economics are not what they first appear to be. Also, the locations of existing sidings may encourage a decision to adopt the first plan.

I have just introduced the subject of distance between sidings. Throughout the discussion I will characterize this distance in terms of miles in order to aid conceptualization of the principles being discussed. In reality it is the time in minutes between sidings or double track sections that matters. Unless otherwise stated, the distances referred to are applicable to the case of typical rolling terrain with a 50 mph (80 kph) speed limit and horsepower per trailing ton close to 1.0 for approximately half the trains and close to 4.0 for the other half.

Maximum capacity is achieved through equal spacing of sidings. This theory has been substantiated by an endless number of simulations but was actually applied in another form by many railroads long before development of current simulation techniques through application of the "longest link" approach to capacity planning. That methodology assumed the longest track segment between passing sidings determined the capacity of the entire line. Capacity analyses then examined only a single link. Equal spacing is, of course, only a goal since in practice there are many overriding considerations, such as existing siding locations, grade crossings, tunnels, bridges, and numerous other obstacles and economic considerations.

When applying the equal spacing principle, we should recognize that (a) minor variations have no noticeable effect, and (b) for volumes up to 10-12 trains per day specific siding location/spacing is not critical. Simulations in non-coal territory have shown that variations of as much as 40 miles

(64 km) in new siding location produce essentially the same result when existing spacing is 60 miles (97 km) and traffic volumes are low.

Since Table 1 and Figure 1 both emphasize track configurations that can be expanded to alternating single/double track, we should take a few minutes to examine this configuration. Our experience indicates that traffic levels which overload siding configurations, and would therefore normally necessitate double track, may be handled by alternating single/double configurations, thus avoiding the large investment in complete double track. The benefits of single/double configurations are derived from the following characteristics:

1. Long double track segments allow running meets with no delay to the trains involved in the meet.
2. A long double track segment provides capacity for holding a large number of trains. It is analogous to having terminals scattered throughout a line segment. This capacity allows a dispatcher to advance a larger number of trains further along a line segment in anticipation of a meet or in anticipation of the clearing of a service interruption.
3. The large holding capacity also provides for fleeting trains at minimum headway intervals. This increases the length of delay caused by each meet. But, since fleeting decreases the number of times a train is delayed for meets, the net result is a lower total delay per train over the line segment.

Because of the unique characteristics of any line segment, general results should not be applied to specific line segments. However, the results in Figures 2 and 3 can be used to gain a qualitative feel for the capabilities and basic characteristics of the single/double configuration. These general results were obtained with highly idealized line characteristics: constant 50 mph (80 kph) speed, evenly spaced alternating single track-double track sections (links), no priorities, and homogenous traffic.

Figure 2 shows the performance of a 10 mile (16 km) link length configuration at different traffic levels. Of particular interest is the "fail soft" nature of the configuration. The configuration retains the ability to move trains long after delays have become unacceptable.

Figure 3 shows the effect of varying the link length. Alternating links of less than 8 miles (13 km or 10 minutes) or more than 17 miles (27 km or 20 minutes) appear to result in degraded performance. On the other hand, any link length between 8 and 17

miles (13 and 27 km) is equally desirable as long as all links are the same length.

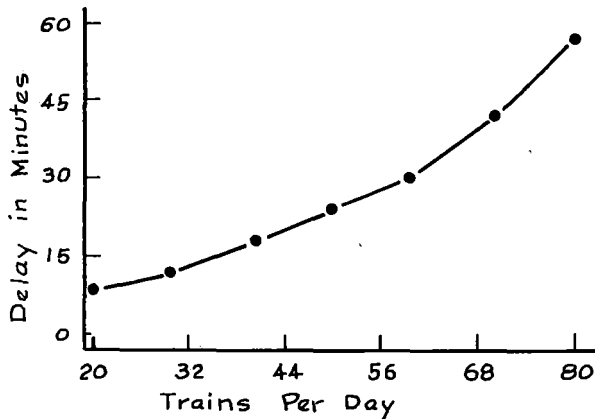


Fig. 2 Alternating Single/Double Track Delay vs. Traffic Volume
(Based on alternating single track, double track links 12 minutes long)

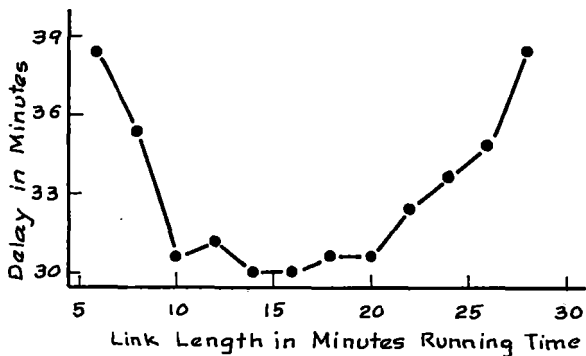


Fig. 3 Alternating Single/Double Track Delay vs. Link Length
(Based on 60 trains per day and homogeneous link lengths)

Figure 4 shows the relationship between delay

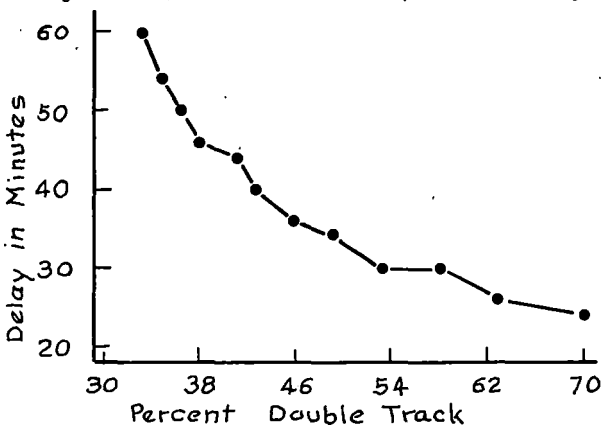


Fig. 4 Alternating Single/Double Track Delay vs. Percent Double Track
(Based on 60 trains per day and 12 minute long double track sections. Single track varied to yield change in percent of double track.)

and single track length. This result was obtained us-

ing a constant 10 mile (16 km) double track length and varying the length of the single track section. Interesting observations here include the flatness of the curve above 50 percent double track and the still adequate performance at 35 percent double track for the high traffic volume used in the example (60 trains per day).

Alternating single/double track also allows both programmed and emergency maintenance to be carried out without a catastrophic effect on train operations. By constructing a double crossover midway between the end points of each double track section, maintenance work need tie up only one-half of one track of one double track segment at a time. The other half of that track continues to provide double track capacity through that section. We have merely shortened one double track link and lengthened one single track link. Train delays are greater than in the non-maintenance case but traffic keeps moving, and at a reasonable pace. Single track links, which still require traffic interruptions for maintenance, represent only one-half of the route miles and only one-third of the track miles.

Burlington Northern has included one double crossover in each 10-mile (16 km) double track segment constructed for growth in coal traffic.

2. A simple rule that has major economic impact is the fact that a very short single track "gap" in a very long double track segment has little impact on the capacity of that double track segment except at extremely high volumes. The only constraint is that the "gap" should not be close to the end of the double track segment. If this rule is used too often for decision making, too many "gaps" will appear on a single line segment and the rule will no longer apply. If used judiciously, however, it can prevent unnecessary expense for such items as major bridges.

3. Consider the steady state case of an established line with an existing track configuration and traffic volume. If the basic running time over the line is increased through imposition of a temporary slow order or any other means, train meet delay will also increase. In general, each minute of additional base running time generates one minute of additional meet delay.

4. Earlier I mentioned that one benefit of alternating single/double track configurations is the ability to fleet trains. Unfortunately, whether there is a full single/double track configuration or there are just a few segments of double track on a line that is essentially single track, some dispatchers tend to overemphasize fleeting to the point where they hold trains just to collect a fleet, when those trains could have advanced unopposed to some distant siding. This is counterproductive. Fleeting should be considered a phenomenon that is merely helpful in some situations and can be accommodated on lines having some double track. The minimum overall delay is achieved with dispatching policies that advance each train as far as possible before making a meet.

GRAPHS

General rules are helpful for long range planning and for generating a practical number of alternative plans for analysis. Final commitment to any detailed capacity expansion plan, however, requires in-depth analysis of each line being considered for expansion. Trade-offs must be examined among various means for increasing capacity. For example, should we upgrade tracks to increase speed limits, add passing tracks, add signals, or increase the horsepower per trailing ton, thereby increasing the performance of some or all

of the trains operated over the line in question.

When traffic growth is to continue for several years and/or the amount of growth is not known with a great degree of accuracy or is subject to changing conditions, graphical displays of simulation results can provide the key to orderly planning. The graphs we have used the most display Meet Delay Curves such as those in Figure 5.

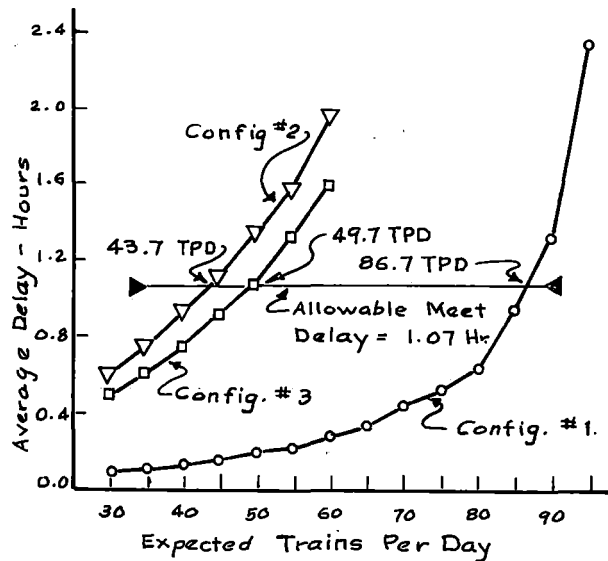


Fig. 5 Meet Delay Curves

The major coal routes have been split into line segments that are sufficiently independent that they can be analyzed individually most of the time. The end points of these segments are terminals or major junctions for traffic taking different routes. A typical segment would be one subdivision. At least one graph of meet delay curves is drawn for each line segment. Average delay per train is plotted against traffic volume in trains per day. A horizontal line is drawn to represent the allowable meet delay over that line segment for each speed limit being considered. Each curve on the graph displays the simulation results for a specific track and signal configuration and speed limit. Normally only one speed limit is associated with any particular graph. "Signal configuration" is used in the broadest terms, i.e., CTC, train order territory, CTC with one power switch and one spring switch per siding, or a specific combination of these systems. All points on these curves that are at or above the allowable delay line represent adequate or excess capacity for the desired level of service.

Each graph provides information required for a decision on what specific investment should be made to raise the capacity of the line to accommodate a particular traffic volume. It can also be used to determine what delay level can be attained if funds are insufficient to support construction producing the desired capacity level. Finally, the desired sequence of construction can be determined from the graph.

Risks associated with uncertain traffic volumes can be assessed by examining the sensitivity of the particular track configuration to changes in volume. In addition, construction plans to which you are not fully committed can be changed if the traffic forecast changes.

By comparing graphs for two or more line segments, it is possible to make traffic routing decisions or decisions on which route should be emphasized for expansion of capacity.

Each unit coal train operates on a planned round trip time, as explained earlier. For internal planning purposes only, this round trip time is split into plan times for each line segment. The segment times can be changed as long as the total does not increase for any train. Since the plan time sets the allowable delay for the line segment, increasing plan time for one segment while decreasing it for another shifts the burden for capacity expansion. This technique permits capacity planning to seek out the lowest cost means for providing capacity. Since BN's coal routes overlap in a complex pattern, meet delay graphs have been indispensable for determining capacity expansion trade-offs among several line segments that would keep the overall network in balance.

Another type of graph we have used is illustrated in Figure 6. The Line Capacity Model does not take

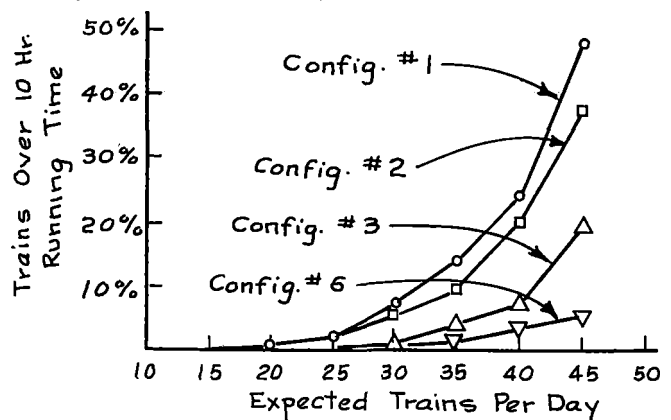


Fig. 6 Hours-Of-Service Curves

hours-of-service limitations into account, but it does keep track of the hours of service consumed by each train. Hours-of-Service Curves are used to supplement the standard meet delay analysis on line segments with long enough planned running times that crews could exceed 12 hours of service frequently. As with the meet delay curves, we have traffic volume on the horizontal axis. However, on the vertical axis we now have percentage of trains exceeding 10 hours of running time. A 10 hour level was selected in this case in order to allow 2 hours for on-duty-to-departure time not included within the bounds of the simulation. Again, each curve on the graph represents a specific track and signal configuration and speed limit.

Hours-of-Service Curves indicate the frequency with which crews will die on line and the sensitivity or stability of each configuration within the neighborhood of the expected traffic volume. It is quite possible for the average delay on a line to be within acceptable limits, while the number of trains able to complete their runs within the 12 hours of service limit is not acceptable. When this occurs, capacity planning is based on hours of service rather than average delay.

MAINTENANCE PLANNING

Double crossovers in double track sections ease the impact of maintenance programs on the capacity of lines with alternating sections of single and double track. On single track lines, however, and on single

track sections of single/double track lines, maintenance planning without careful consideration of the impact on train operations can be disastrous. Traffic disruptions for maintenance cannot be avoided, but with careful planning track occupancy for maintenance and track availability for train operation can be balanced in a manner that allows both the Engineering and Operations personnel to do their jobs. A balance can be struck on the basis of extra cost for compromising the efficiency of the maintenance work versus tangible and intangible costs of delaying trains for long periods of time.

The problem of studying maintenance of way effects on line capacity is complex due to the variable nature of these activities. The bulk of BN maintenance of way is performed during summer months and remains subject to weather conditions and manpower availability.

To illustrate the types of analyses that can be performed with the Line Capacity Model, we will review a study that was made in 1980 to assist Alliance Division personnel in their planning for that year's maintenance activities on the first subdivision. This subdivision is 238 miles (383 km) long and at that time consisted of 4 sections of double track totaling 36 miles (58 km) and 3 sections of single track with a total of 15 passing sidings. The study was made with four purposes in mind: to investigate the effects upon delay and transit time of various work block (maintenance track time) durations; to investigate the effects of splitting work blocks so that congestion could be partially relieved midway through the work day; to investigate restrictions on reworking locations for trains held while the track is out of service; and to compare "reasonable" maintenance plans.

Review of the 1980 trackwork program timetable for the Alliance 1st Subdivision revealed two periods during the year when maintenance activities could be expected to have maximum impact upon line capacity. These periods were singled out for simulation rather than attempting to simulate the entire year. The steady state nature of these periods is desirable for statistical validity of the delay estimates.

The first period selected for study was the month of July 1980. The program for July included a mechanized tie gang, surfacing, and construction of second main track at four locations. The traffic volume was 30 trains per day.

The second period selected was the month of October 1980. The program for October included rail grinding, curve relay, bridge work, and construction of second main track at two locations. This period was simulated using the projected October track configuration which included an additional 32 miles of double track and the same traffic volume as the July simulations. Since rail grinding track time is generally fixed by contract, the majority of the October simulations were performed with rail grinding held constant at 10 hours/day, 6 days/week. The effects of varying track time for curve relaying and bridge work were investigated.

The July maintenance program was used to analyze the impact of increases in the duration of work blocks. The base (non-maintenance) case produced an average delay of 2.0 hours per train, a transit time in excess of 10 hours for 0.6 trains per day, and a transit time in excess of 8 hours for 8.2 trains per day. Each 2 hour increment in the duration of work blocks created a 27 percent increase in average delay, a 9 percent increase in number of trains exceeding 10 hours transit time, and an 11 percent increase in the number of

trains exceeding 8 hours transit time.

Maintenance plans from both study periods were used to investigate the effects of inserting a 2-hour break midway through each work block, and permitting traffic to move during the break. The reductions in average delay gained through splitting work blocks were on the order of 15 percent. The reduction in trains exceeding 10 hours of transit time averaged 9 percent.

Simulations of the July maintenance plan were performed to analyze the effects of differing policies regarding the locations at which trains are held during maintenance periods. Comparable runs were made allowing trains to be held on any link, and limiting available train holding links to the double track segments. The superiority of the "any link" policy appears to be significant when lengthy work blocks are imposed and congestion is at a very high level.

In addition to these somewhat general analyses, comparisons were made of specific track time policies that Alliance Division personnel might reasonably be expected to use. Results of these comparisons provided information previously unavailable for detailed planning of maintenance work.

FUTURE RESEARCH AND APPLICATIONS

Further work is needed to extend these concepts to railroad lines having a broader traffic mix. Additional analysis of trade-offs among factors affecting line capacity also promises to be very rewarding. With sufficient additional research, graphs illustrating basic relationships among various factors may be replaceable by graphs displaying costs directly.

ACKNOWLEDGEMENTS

Portions of this paper were extracted from Industrial Engineering study reports written by W. R. Stockton, B. J. Ryan, and C. L. Kehr. Graphics were provided by R. C. Gilbert.

Planning for Traffic Growth on Rail Lines

N.A.R. Hanks

Assistant Chief
Transportation Planning
CN Rail
Montreal, Canada

J.F.R. Gussow

Transportation Research
Engineer
CN Rail
Montreal, Canada

Recent growth in rail traffic, largely stemming from booming resource development, with added impetus gained from changes in energy use and supply, has led to high density railroad operations. This has created many maintenance and operating challenges for the industry. Questions of how to handle the growth, how to cope with the problems of increasing traffic, and accentuated by an ever-growing proportion of heavy axle cars, have to be addressed. CN Rail has experienced these problems and is managing to find solutions in what appears to be a successful manner. This paper reviews these problems, analyses the solutions, and discusses the actions that CN has taken to effectively meet the demands and expectations placed on it by a growing economy.

PLANNING FOR TRAFFIC GROWTH ON RAIL LINES

INTRODUCTION

What should a railroad do when faced with continuously expanding tonnage, what are the problems of high density railroad operations, and what are the options available for increasing capacity of existing lines and coping with the problems of growth?

Rail traffic in Canada has grown in leaps and bounds in the past twenty years and the

outlook for this decade is further sustained galloping growth -- perhaps something can be learned from how they have coped and are planning to handle their traffic increases. CN Rail, for example, has grown from roughly 80 BGTMs (Billion gross ton miles) in 1962 to 120 in 1972, to 160 in 1980, and is looking towards 230 BGTMs by 1990.

**CN Rail Growth Perspective
(Billion GTM's)**

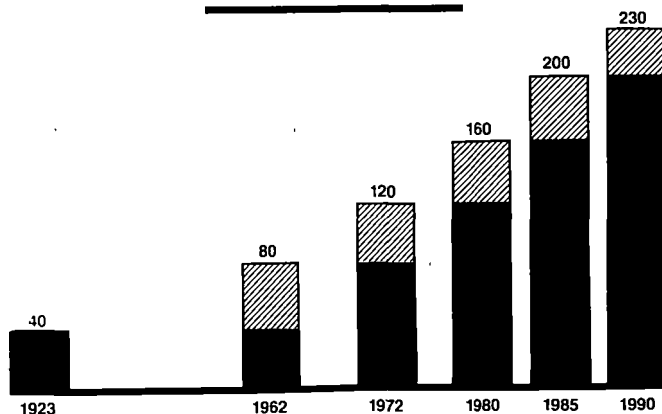


Chart 1

As most of this traffic is handled on their single transcontinental route, and most of the growth is in Western Canada, individual rail lines have had to cope with very large tonnage growths. Individual subdivisions have grown from handlings of less than 15

million tons annually to 40 or 50 million tons. Looking ahead, major route segments of 750 to 1,000 miles in length will be handling average tonnages of 60 to 75 million tons annually by 1990, with individual subdivisions peaking much higher.

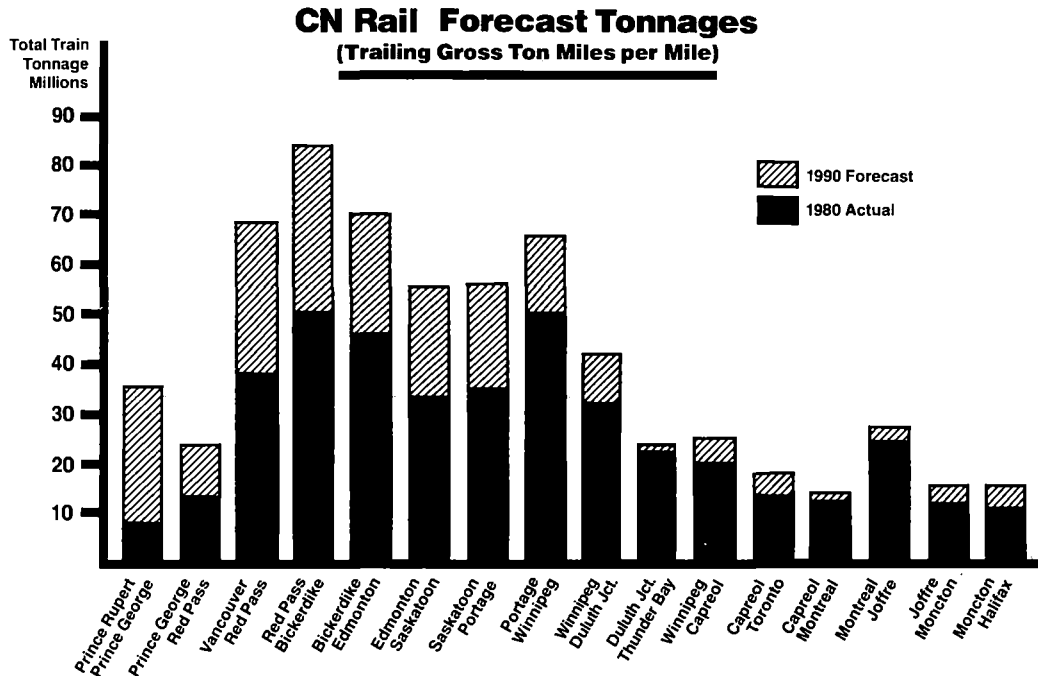


Chart 2

Prior to its Plant Improvement Program in the 1970s, CN Rail's transcontinental route was basically a light to medium traffic route, handling 15 to 20 million gross tons annually, and followed suitable operating and maintenance policies. These have been changed significantly with the necessity to handle heavier traffic levels.

CN Rail has found that the fundamental problems that have to be faced as traffic grows are:

- 1) increased traffic interference and lack of capacity
- 2) accelerated track deterioration
- 3) increased track renewal programs and track maintenance
- 4) growing mutual interference between train operation needs and track renewal/maintenance needs.

Eventually a dilemma is reached where the demand for capacity for track maintenance and track component renewals is as great or greater than that required for the operation of trains and the two demands on track time, are greater than the 24-hour day, (ie. the capacity of the rail line is insufficient to meet the two demands of train operation and track maintenance.) If track maintenance is

let go, the track condition suffers and the train operation cannot be handled. The increase in track maintenance is, of course, necessitated in turn by the increased train operations.

This dilemma is compounded by necessary actions to cope with two other factors

- 1) problems due to train mix (speed & priority)
- 2) accelerated track deterioration due to higher axle loads.

In general, these problems are resolved by embarking on several strategies in concert,

1. improving the standard of the track structure itself
 - deeper, higher quality ballast section
 - heavier rail, continuously welded
 - improved roadbed, drainage and bankwidening
 - concrete ties
2. altered track maintenance methods, to sustain the new standard
 - gang organization & mechanization
 - rail-grinders
 - high miler tampers & rail renewal machines

3. changed operations strategies
 - train lengths
 - reduced variation in train mix
 - altered power/weight ratios
 - altered priorities and speeds of different train classes
 - maximum use of large unit trains
4. improved geometry of track layout
 - siding spacing
 - siding lengths
 - yard track lengths
 - improved entry/exit throats to yards
 - selected application of double track sections
5. improved train control
 - advanced signalling & CTC
 - computer-aided dispatching system.

Railway capacity is a complex issue. Measures of capacity are not easy to define or to quantify. Definitions are, at best, controversial and elusive. Nonetheless, hard measures are often demanded, and, quantification of some kind is necessary to make operating, marketing and financial decisions. There are so many factors that affect the capacity of a railroad, it is not possible to demonstrate with precise numbers the specific capacity of a railroad. However, an examination of the factors affecting capacity does allow some logical ranges on capacity limits at staged intervals of plant and control system configuration. These stages can be broadly grouped into three classes 1) operating procedures and policies 2) geometric layout and control system design 3) track standards and integrity. These will be discussed later.

To add to the confusion of this complex situation, railway capacity can be defined in terms of Physical Capacity, Productive Capacity or Performance Capacity.

Physical Capacity of railways generally refers to the theoretical number of trains that can be handled regardless of running time.

Performance Capacity is a measure of the number of trains that can be handled within consistently acceptable running times.

Productive Capacity is a measure of the maximum amount of ton mile production that can be produced on the rail line, within a given cost and time constraint.

To address the question, of how to cope with high density operations and expanding rail tonnage, we should examine how the basic factors affecting railway capacity impact on these definitions and of particular importance, how track maintenance activities interact on each.

FACTORS AFFECTING LINE CAPACITY

While Productive Capacity is perhaps the

most all-encompassing definition, it is also the most difficult to measure because of the complex interrelationship of the factors that affect the movement of trains and their relative costs. It is easiest to begin by describing the principles that affect the physical capacity of railroad lines, as these principles provide a basis for discussion of the other more complex measures of capacity when the related operating realities are introduced.

This discussion emphasizes the main line capacity issues, since of all of the elements which bear on the productive capacity of a rail system, a deficiency in the main line track capacity is perhaps the most costly and time consuming to remedy. It should be kept in mind, though, that the main track is only one element of a railway system, and upgrading the capacity of the track portion usually requires that the capacities of the related parts of the system such as yards, maintenance facilities and customer loading and unloading facilities will also have to be augmented as components of a full rail system.

Single Track Capacity

Single track is a system of train operation that must allow trains to operate in two directions on just one track. Train length sidings are spaced at regular intervals along the route to allow opposing trains to meet each other. The theoretical capacity of such a line is reached when every train meets an opposing train at each siding along the route, or described another way, when the number of trains on the line equals the number of sidings at any given time. This ideally assumes that the trains have uniform speed characteristics and equal priorities.

The layout of a single track line is usually arranged to provide sufficient sidings to more than handle the expected traffic, and their spacing is ideally established by equalizing the train running times between sidings using the average of the speeds in each direction. A simple indicator of the capacity of such a line is the maximum time spacing between two adjacent usable sidings, often called the controlling grid. Anything that reduces the controlling grid of the line will result in an increase in the physical capacity of the line.

Factors that affect the physical capacity of a rail line are allowable train speed, siding spacing, type of signal or control system, and any imposed schedule that could result in trains running unnecessarily slowly. All of these factors in one way or other could affect the controlling grid of the line and thus the capacity.

The everyday operating realities of a railroad introduce further complications which have to be taken into consideration, and which usually result in a reduction in the train carrying capability of a line. Trains do not all operate at the same speed or with the same priority, and track maintenance is

part of the everyday operating reality. Where a variation of train speeds exists, all trains are forced to conform to the speed of the slowest train resulting in an increased controlling grid. Where faster trains are given a higher priority to allow them to overtake slower trains, the resulting disruption in the uniform train pattern on the line serves to further reduce the number of trains that can be handled.

Track maintenance affects the line capacity in two ways. One, any track outages result in the line or sidings being unavailable for the movement of traffic, and two, the associated temporary slow orders can affect the controlling grid on the line. Where there are scheduled trains operating, the maintenance has to be planned around those trains, which often reduces the productivity of the maintenance gangs, which in turn results in an extension in the number of days that the maintenance program would otherwise take.

Even though track maintenance programs may only be in effect for a portion of the year, they compete with trains for the use of track capacity during that period. It is not unusual, for example, for 50% of available capacity to be used by track maintenance operations throughout the construction season. This is, of course, an essential activity, and any attempt to curtail it in order to reserve capacity for train operations would be counterproductive. Sufficient capacity must therefore be provided to perform track maintenance in addition to that just required to move trains. This means, of course, that during the portion of the year that no maintenance activity exists, there is latent capacity which may not be used.

To recap, the factors affecting the physical capacity of a route include the siding spacing and layout, the train mix considering allowable speeds and priorities, and the method of train control used to handle the traffic. The physical capacity to move trains is significantly reduced by the amount and intensity of maintenance activity and when a wide variation in train mix or priority is present.

Analysis of these factors shows that the best use of available plant capacity is achieved when:

- Trains are operated at a common speed
- Trains have equal priority
- Trains are operated at the fastest average speed
- Trains are paced at regular intervals
- Trains are operated at siding length
- Track outage times are minimized
- Slow order lengths and speed reductions are minimized.

Fulfilling all of the above measures is, of course, unrealistic; however, maximization of capacity can be achieved by aiming to get

the best out of each.

As a practical matter, this theoretical capacity limit can never be achieved in actual operation. The delays incurred by individual trains would be unacceptable long before the line's saturation limit is reached. As a result, it is insufficient to consider only the physical number of trains that can be moved, so a refinement to the definition is required to include a limit to the over-the-road running time of trains.

Performance Capacity

At lower traffic levels, each train's total delay due to meets enroute increases in simple proportion to the number of trains operated. At higher traffic levels, however, the delays incurred as trains meet each other at sidings accumulate very rapidly in a compounding fashion. Every time one new train is added it must meet every other train already on the line plus those that enter while the train moves across the route. Each of these opposing trains is further delayed by the additional meet which increases the chances that other trains will enter the line before they reach their destination terminal. Delay compounds on delay as shown in the following chart.

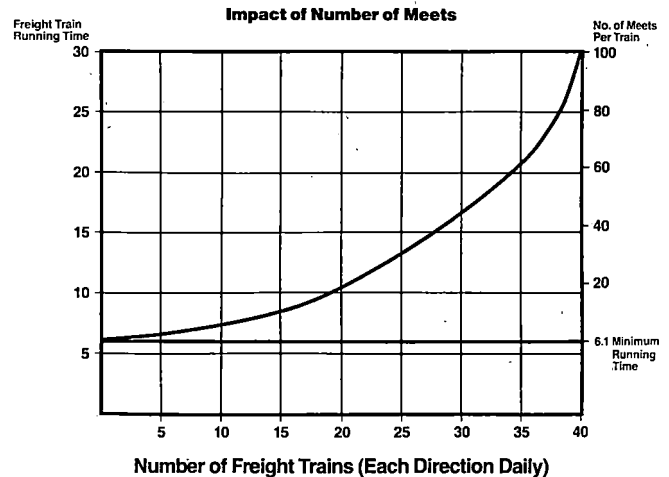


Chart 3

Even though this graph is a theoretical representation, the effect on the average running time of an increasing number of trains is typical of what would happen on an actual rail route. While the number of trains and the average delay go to very high levels toward the right-hand side of the chart, the practical limitations of crew on-duty times constrain the allowable running times of trains to a maximum of eight to ten hours. Physical capacity, as previously defined is still available above, say, a ten-hour limit, but using that capacity would be a tremendous cost in over-the-road time. Thus, realisti-

cally, only the left-hand portion of the graph need be considered as representative of an actual operation.

The position and shape of the curve in the above graph is very sensitive to changes in any of the previously discussed factors that reduce physical capacity, and in particular to increases in the average running time. The ultimate result of this is that the number of trains that can be run while remaining within an acceptable time threshold is extremely sensitive to these outside influences. This can be dramatically demonstrated by considering a rail route where ten hours is the maximum allowable running time. If the running time of each train were extended for whatever reason by only two hours, from the above graph, the feasible number of trains that could be run would drop roughly in half from almost twenty to little over ten. In this case, a 20% increase in running time has resulted in a reduction in the practical capacity of the line of almost 50%.

While this example used simple running times to demonstrate the sensitivity of performance capacity as a measure, other factors such as train mix, relative priorities, and equipment failures will produce further increased running times. These result in similar drops in capacity individually, and in a compounding manner when several factors influence a route at the same time. This effect is important, and should be kept in mind when considering major maintenance programs or when planning for capacity-related changes to the plant.

Productive Capacity

Physical Capacity has been shown to be too idealistic and optimistic a measure to be of any real value in the planning process, but the lessons learned in trying to affect the physical capacity of a line can be effectively applied when deciding what has to be done to handle increasing traffic. Performance Capacity comes closer to describing the limits to the number of trains that a line can handle, but this again does not adequately describe what a railway is trying to accomplish as a business, which is to move products from one location to another. This is what railways are paid to do, and how well a railway accomplishes this function dictates the effectiveness and efficiency of the operation. The amount of production, or work performed by a railway is usually measured in Gross Ton Miles. The measure of its capacity then, is its capability to produce GTMs per day. Neither of the previously discussed capacity measures adequately reflect this reality.

The significance of using Productive Capacity as a measure is demonstrated in Chart 4. The shape of this curve is as a result of the increasing congestion on a line when the number of trains is increased. Each additional train results in a diminishing return, and can reach a point where no additional work is being performed. At this

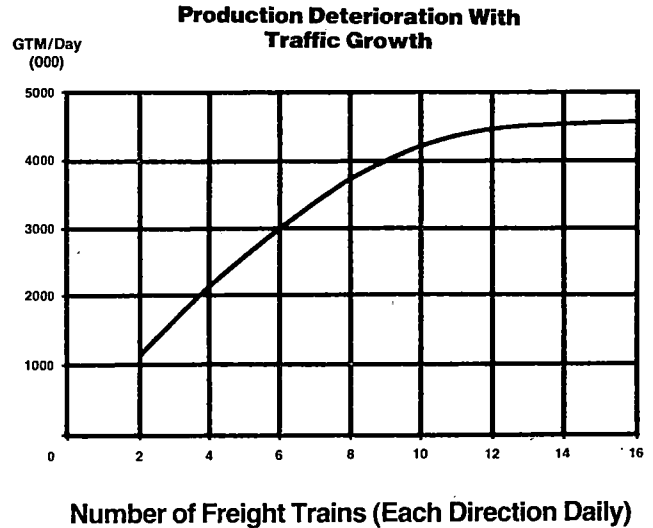


Chart 4

point, there is still plenty of physical space to add trains, and the running time of each train could still be below acceptable limits, but the commitment of more equipment and manpower to run trains would bring no increase in production, and would not be a solution to capacity problems.

Implications

The previous discussion has demonstrated that capacity is not simply the number of trains that can be handled past a given point in a day. Capacity is more a measure of the limits of traffic that a railroad can effectively move from one point to another. It is not unusual that capacity problems are only perceived when over-the-road times become unacceptably high, which could already be beyond the point of efficiency in the operation.

The planning process to correct a capacity deficiency usually begins by calculating the physical capacity of a route and considers the possible factors that affect it, resulting in a series of potential solutions. To evaluate the capability of any plant alterations to handle the expected traffic, and to assess the relative value of any proposed solutions, the performance capacity measure is the most appropriate. The average delay per train can be compared using computer simulations of alternatives, to give a relative ranking, and to compare proposed solutions with past operations to decide how much need be done. To indicate the need for plant alterations, however, and the potential effectiveness of any changes, the productive capacity of the route has to be assessed. The most meaningful indicator of reduced productive capacity is a drop in the overall average speed of train movements.

The series of capacity studies undertaken considering our present traffic mix, maintenance practices, and operating speeds, indicate that the effective capacity limits under various methods of train control on single track range as follows: Train Order -- up to 15 million trailing gross tons; with modified CTC (spring-power switch combination) -- 15 to 25 MGTs; and Full CTC -- 30 to 43 MGTs. It is anticipated that we will handle as much as 52 to 55 million gross tons with double tracked terminal entrance/exit portals and closely spaced intermediate (following) signals applied throughout the route.

These are considered the practical, sustainable levels of single track operations, but they can be exceeded for short periods of time. Specific capacity limits have not been quantified for double track.

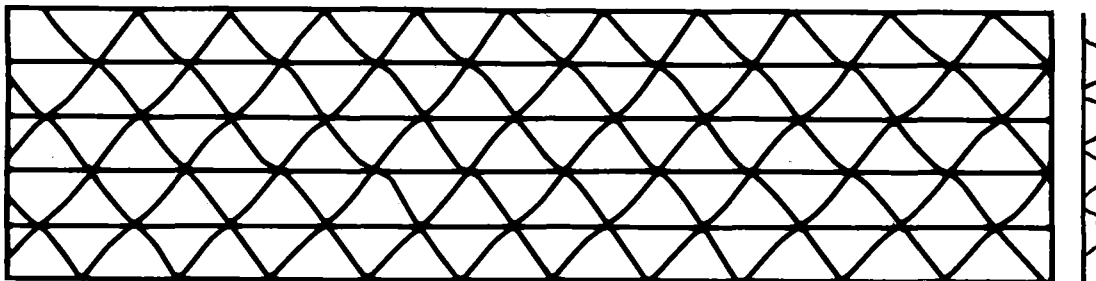
TRACK MAINTENANCE & RENEWAL ACTIVITIES

The extent to which track maintenance and track renewal programs use up line capacity and interfere with train operations is dramatically brought home as a railroad tries to learn to live with growing traffic demands. In its earlier years CN Rail, handl-

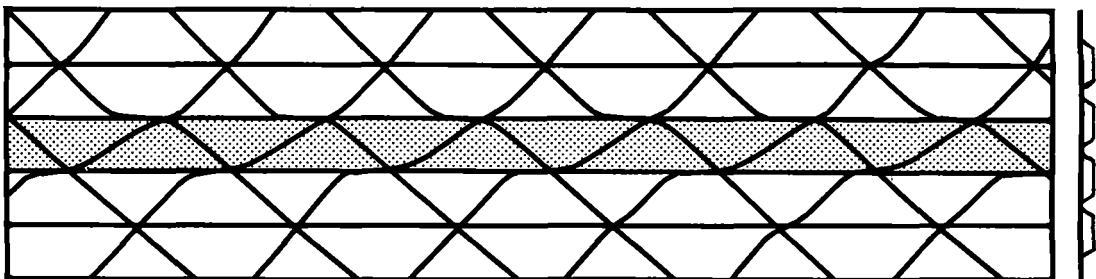
ing roughly 15 million tons annually on its transcontinental lines, managed to live with track maintenance-oriented interference problems relatively straightforwardly. As traffic grew, the amount of time available for track work naturally diminished and yet the track handled more traffic and thus required more work on it. This situation extended itself into an eventual conundrum where train operations and track work activities were vying for track time and collectively demanding more capacity than available. (This was exacerbated by the increase in number of heavy loads but this aspect is left to another paper.)

This dramatic absorption of capacity by track work activities that occurs under heavy traffic conditions is depicted by the following time-distance diagrams. Diagram one depicts a theoretical segment of single track with four passing sidings, showing a saturated situation of all trains having a meet at every siding. In diagram two, the effects of a temporary slow order placed on the central portion of the theoretical subdivision are displayed. This slow order adds about 15% to the overall running time of the trains but capacity for handling trains is reduced by 30%.

Time Distance Diagram #1
Fully Saturated Single Track Segment



Time Distance Diagram #2
Capacity Deterioration by Temporary Slow Order



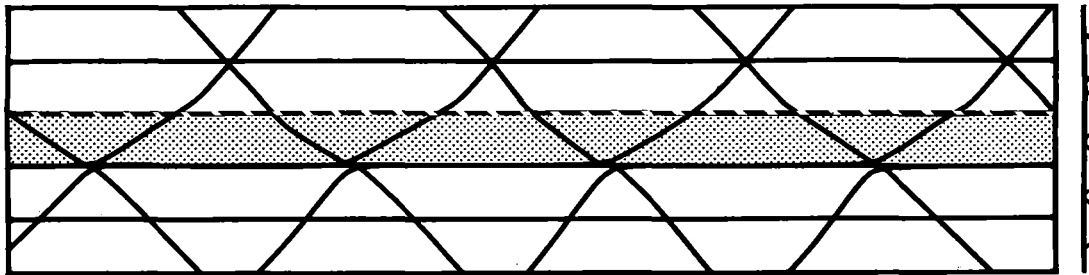
In diagram three, one siding is indicated as out of service, as might be expected when a track gang or work train is occupying it. This feature added to the T.S.O. creates the effect of a further diminution in the capacity of the route, as is demonstrated by the "stringlines" shown.

In diagram four, a further complication is

added, namely an exclusive work block for use of track work gangs. This work block is equal to about 25% of the time shown, (say a 6-hour work block in a 24-hour day). The combined effects of these three typical track work activity requirements reduces the train handling capability (the capacity) of this track segment to 30% of its original capability.

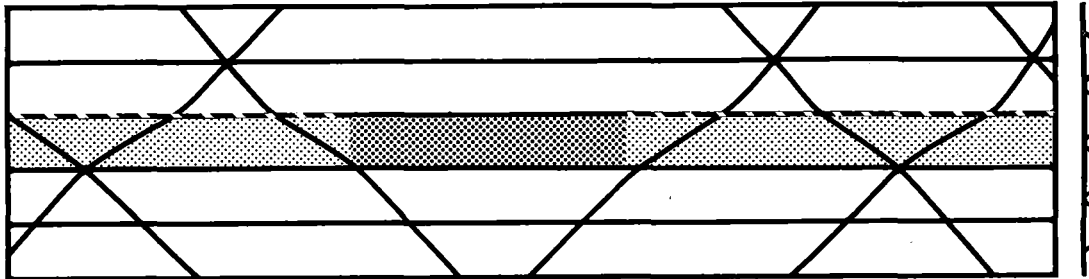
Time Distance Diagram #3

Capacity Deterioration of TSO and Siding Out of Service



Time Distance Diagram #4

TSO, Siding Out of Service and Work Block



In this theoretical example of a short segment of single track operating under saturated traffic conditions, one temporary slow order of 15% of running time, one siding out of service and one simulated 6-hour work block have used 70% of the available capacity.

The effect of this capacity utilization on whole route segments of extended length is depicted in diagram number 5. This is a time distance diagram of train movements on CN Rail between Toronto and Winnipeg, a distance of greater than 1,000 miles. Roughly three day's train movements are covered in this capsulized view, with the track work blocks shown as solid horizontal bars at the location and for the time they were in effect. Note the large effects both upstream and downstream from the work locations of not being able to run trains by them on this single track network, and the heavy bunching of trains in between, even at this relatively light traffic level. The "time windows" created affect train operations and effective line capacity four and five hundred miles distant from the actual work location.

It is clear that all three measures of capacity, numbers of trains, service level, and ton mile production per day are all seriously affected by the amount of track work activity that is done, much in the same manner as all three are affected by increased traffic as described earlier.

EFFECTS OF TRAFFIC GROWTH & COPING WITH THE DEMAND

CN Rail has taken a three-pronged approach to resolving its capacity problems as growth occurs.

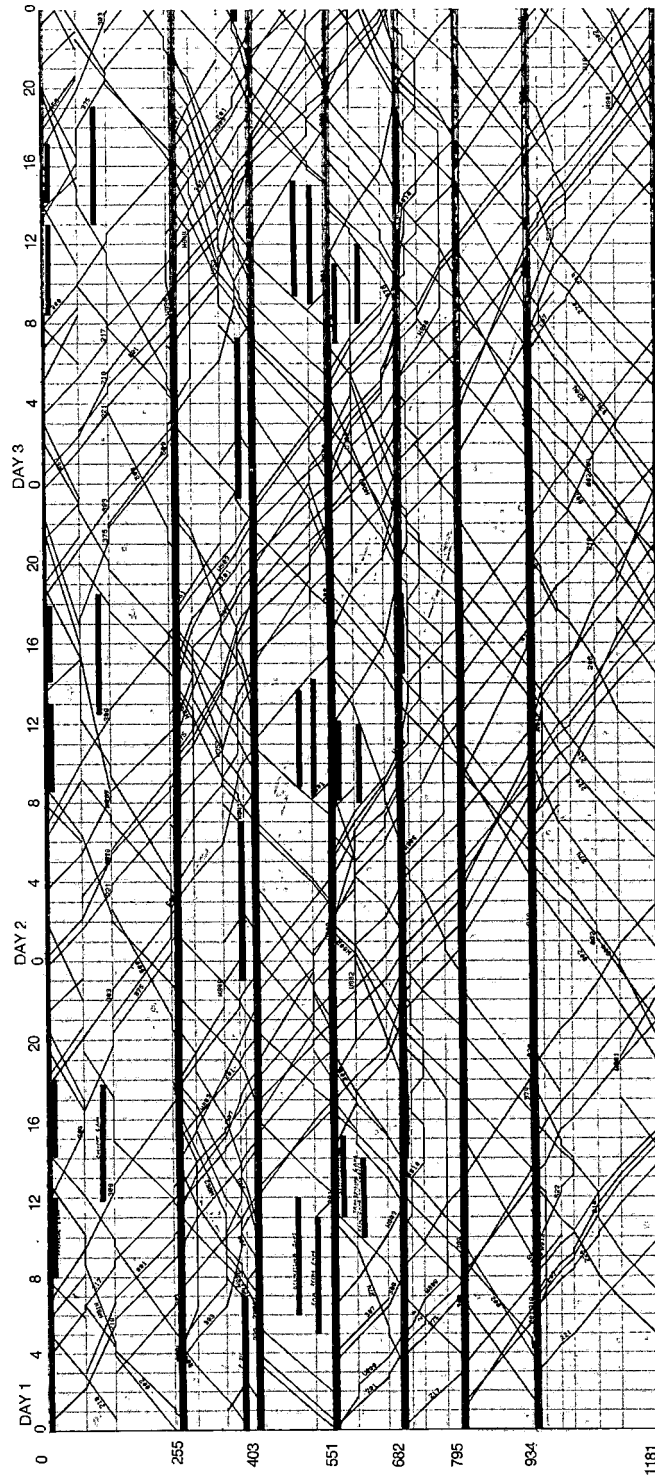
- 1) improved track standards and integrity
- 2) changes in operating procedures and policies
- 3) changes in the control system and plant configuration.

1) Track Standards & Integrity

As traffic grows the need for track maintenance grows and the periodic renewal of track components increases in intensity. The effects, as described above, eventually become paramount to the capacity demand of running trains. The simple answer is to provide more capacity but the options are widened because the capacity measures added can be directed at the trackwork demand in addition to being directed at the train operation demand. Thus much can be done to alleviate the situation by improving the standard of the track structure itself and in altering the track maintenance methods to sustain this new standard.

Much has been accomplished on CN Rail by upgrading their main tracks to a new standard of 12" of best quality crushed stone or slag ballast, 136-lb. continuously welded rail, concrete ties, and improved roadbed, drainage and bank widening. Significant improvements in rail

Time Distance Diagram #5



life have been made by the use of alloy steels in curves. CN Rail has also been in the forefront of North America in the development of maintenance-of-way production machines, the thrust being to get as much track work accomplished as possible once the track is given over to the work gang and

thus reducing the amount of track time in total required. It is now common practice to replace the whole track bed from sub ballast up in one pass, installing new rail, concrete ties and ballast; and, a similar machine replaces both rails at once when only rail replacement is needed. Both these machines

have astounding production rates compared to previous more standard program gang methods.

2) Operating Procedures & Policies

One of the more obvious and most successful actions taken by CN Rail to accommodate growth over the past few years was to move to a standard 6,000-ft. train length. Prior to this, the longest trains were designed around 100-car lengths of the old standard 45-ft. car. Thus a capacity increase of some 30% was obtained without increasing the number of trains.

Beyond this, and not quite as obvious, was a problem of capacity utilization due to the variation in speeds and priorities of different classes of trains. Coincident with the increase in train length, policies on power to weight ratios and priorities were significantly altered to minimize the variation in speed and priority of the different train classes. Express train lengths were increased but their locomotive power was not. Unit trains were increased in power concurrently with their size. The use of direct point to point trains was maximized to avoid terminal congestion, improve throughput and provide some freedom in priority setting and handling. Much of the traffic growth has been in resource products (coal, sulphur, potash, lumber, etc.) which lends itself to unit train movements, commonly handled in 10,000 tons of commodity per train. This has allowed a lot of the gross ton mile growth to be accommodated with proportionately fewer trains. It has, of course, increased the number of slow heavy trains and accentuated the problems stemming from mix of speed with the manifest and express freight trains.

A steady and continuing thrust is being followed to move towards a common speed and avoid mutual interference between train classes as much as possible. Immediate or large steps in this direction cannot, of course, be taken, without impacting the service reliability, but taken as a target, and concentrating on terminal handling, it can lead to significant steps over time without impacting service. In times of severe congestion when traffic peaks and track work seasons coincide, there is little alternative but to submerge priorities and speeds and live with the problem of utter saturation. The trick is to build in enough capacity to keep these situations liveable and of reasonably short duration.

3) Changes In Control Systems & Plant Configuration

Although everything possible is done in all other avenues, as previously described, by and large, the main thrust in coping with major increases in traffic volume comes from changes in plant. In

addition, changes in plant are largely ineffective unless corresponding improvements are made in the signals and control systems.

Clearly, longer trains could not be handled without longer sidings and similar increases in yard tracks to make them compatible. Beyond that, a review of siding spacings was made and additional sidings were added to create as even a grid spacing of sidings as physically feasible. On CN Rail, many of the siding switches were spring operated and all these were replaced with power operated switches. In addition, several bottlenecks at junctions and on ruling grades were alleviated by building small pieces of double track.

Between 1975 and 1980 CN Rail extended 192 sidings, built 14 new sidings, installed 227 power switches and built (collectively), 108 miles of double track, and extended or altered 21 yards, at a cost of some \$272 million dollars.

They are now embarked on a Plant Expansion Program for the 1980-90 decade that will see roughly 50% of the transcontinental route between Winnipeg and Vancouver double tracked, and major revisions to almost all yards on that roughly 2,000-mile route. The planning and implementation of a program of this magnitude is a formidable task in itself. Obviously, it would not do to simply start at one end building double track until finally reaching the other end. The general thrust has been to highlight problem areas by simulation techniques and attacking these in sequential priority order within the limit of funds available and annual construction programs.

In broad terms, a decision was made to move ahead with 100% D.T. in the central section, roughly 310 miles from Edmonton to the junction with our B.C. north line; to build towards 50% D.T. from there 440 miles to Vancouver at the west coast; and, to build roughly 40% D.T. across the Prairies from Edmonton to Winnipeg, (800 miles). In addition, the whole of the B.C. north line to the northerly port on the west coast at Prince Rupert (650 miles) will be upgraded from a secondary track under light traffic and train order operation, into high quality main line single track standards under C.T.C. operation.

Each of these three line segments, Vancouver-Valemount, Valemount-Edmonton, Edmonton-Winnipeg, the B.C. north line, and each of the terminals has been analyzed, and the requirements of individual portions staged into priority sequence, hitting the worst bottlenecks first or those that give the greatest benefit for dollars spent. There will be at any one time throughout the ten years at least 50

individual projects being constructed, either a 5 to 15-mile stretch of double track, or a sequential stage or portion of a terminal. An attempt is being made to avoid "big ticket" items like tunnels and major bridge structures in the initial years, although curve realignment, bridges and tunnels are all part of the overall picture. One of the first projects is a ten-mile connection through the mountains between the B.C. north line and the Vancouver main route which creates an effective 32-mile stretch of D.T. track by using the two routes and new connection unidirectionally.

Critical to the operating effectiveness and growth assimilation will be the upgrading, alteration and improvement of the terminals and yards. Major yard projects will be involved at Vancouver, Edmonton and Winnipeg with fairly large changes also involved at the intermediate yards at Kamloops, Jasper, Saskatoon and Melville, plus B.C. north line yards at Prince George and Prince Rupert. Additional through train handling capability will be provided at all the line terminals along the routes. The estimated cost is in the order of \$1700 million for line improvements, an additional \$500 million for yards and terminals, and another \$750 million for the B.C. north line upgrading in total.

COMPUTER APPLICATIONS

As a result of the planning and analytical workload involved a series of "state of the art" computer analytical tools and simulation models have been developed. A long range (10-year) transportation workload forecast model which works in conjunction with marketing forecasts and econometric models has been developed and is used to get the base traffic demand. This is turned into terminal and line workloads by CANAT, a computer assisted network analysis tool, which basically performs the train service design function. These workloads are then applied and analyzed on a macro basis with a Route Capacity Model, which quantifies alternative solutions on a first cut basis and can be used to investigate a myriad of trials in a very short time. Specific analysis is then done by a detailed computer simulation, and final design is done on a detail basis with a Line Interactive Model, which closely simulates the actual train dispatcher's environment.

One of the first steps to capacity upgrading that has emerged from our analysis is the effectiveness of intermediate signals and short double track stretches at entrance/exit throats to yards and terminals. This one-two punch of closely spaced following signals and double tracked yard portals appears to provide an effective interim stage between single and double track. This allows fleeting around work blocks and an ability to surge traffic. Other sections can then be applied in stages across the subdivisions, in the course of time, in those locations that appear to best enhance the movement as established by detailed simulation of expected traffic levels.

A major stride was recently made in the development of an interactive terminal simulation model that can be used effectively and easily for any yard, regardless of physical and traffic configuration differences. Heretofore, all terminal models were cumbersome and very much "location specific", not generalized application tools.

Almost all of CN Rail's capacity analysis and design models are interactive. This serves two purposes. It simplifies the programming and systems design process by reducing the necessity of simulating the decision process. It also gives more realistic results in that the analytical team makes the decisions and judgement calls and the computer only does the calculations, recording and displaying. Analytical teams are composed of both competent technical people, (transportation engineers and computer specialists) and practical railroaders (Chief Dispatchers, General Yard Masters, etc.).

Complementary to the Plant Expansion Program is the development by CN of a computerized dispatching process that will automate the paper and information flow to the dispatcher, simplify the dispatcher's voice and non-train movement workload, and largely automate the setting of meets and control of train movements. All CTC dispatching control consoles throughout the country will be replaced by this computerized system by 1987. In addition, CN is embarked on a major investigation into the use of micro-electronics and programmable semi-conductors in its signal system which may lead to fundamental changes in both the design and operations capabilities of its signal and control system.

Project Analysis : Doubling the Capacity of the Heavy Haul Coal Line to Richards Bay

W.P. Burger

Pr.Eng., BScBEng. (Civil)
MSAICE
Senior Planning Engineer
South African Transport
Services

Due to the ever increasing demand for thermal coal as an energy source the Government decided during 1978 that the coal export ceiling could be gradually increased from the then authorized 20Mt/a to a maximum of 44Mt/a by 1986. This decision forced the South African Transport Services to analyze the problem critically to find the most economical solution that would also satisfy the very testing technical parameters required in the design and operation of a heavy haul line of this nature. This paper deals with the historical background of this line and also describes the planned improvements which will practically double the present capacity of this busy line within approximately six years.

NOMENCLATURE

a.c.	-	alternating current
B.M.A.	-	Bluff Mechanical Appliance
c	-	grade compensated for curve resistance
C.T.C.	-	centralised traffic control system
Cr Mn	-	Chrome Manganese (Rails)
d.c	-	direct current
D.E.D.	-	Dragging Equipment Detector
H.S.	-	High stability (bogies)
Hz	-	hertz
kV	-	kilovolt
L.W.O.S.T.	-	Low water ordinary Spring Tide
Mt/a	-	Million tons per annum
R.B.C.T.	-	Richards Bay Coal Terminal Company
R-m	-	Million Rands (S.A. currency) (R1=\$1,0561 at 13 October 1981)
T.C.O.A.	-	Transvaal Coal Owners Association
15,15°/∞ etc	-	15,15 units of vertical rise in 1000 units of horizontal distance, i.e. 1 in 66, etc.

1. HISTORIC BACKGROUND

For many years it had been known that the capacity of the Natal main line linking Durban to the interior had inherent capacity limitations, especially for the bulk transport of ore or coal.

In order to meet the challenge of normal traffic growth and also to cater for coal exports that emerged as a reality in the middle sixties, the following developments took place:-

(a) Railway Construction Act No. 17 of 1966 was passed by Parliament for the construction of a new line between Vryheid and Empangeni (see

Figures 1 and 2).

(b) For the construction of the link line between the new Vryheid - Empangeni line and the proposed harbour at Richards Bay, Railway Construction Act No. 38 of 1968 was promulgated.

(c) Meanwhile investigations for a new deep water harbour was carried out at Kosi Bay, Sordwana Bay and Richards Bay. Richards Bay was decided upon as being the most suitable and Harbour Construction Act No. 28 of 1972 was passed.

(d) The remaining link line to be built, the 93km stretch between Broodsnyersplaas and Ermelo was authorised by Railway Construction Act No. 83 of 1971.

(e) At the same time authority was also granted for the upgrading of the line already existing between Ermelo and Vryheid. As the line was of fairly low standard this meant virtually rebuilding this 203km stretch.

1.2 Original Design and Planning Standards

The line between Broodsnyersplaas and Ermelo was constructed to a ruling grade of 10°/∞ c. and that between Ermelo and Richards Bay at 15,15°/∞ c, due to the more mountainous nature of the route.

It was also decided that trains would consist of 76 type CCR1-trucks specially designed to convey payloads of 52,8t each at 18,5t axle loads.

Motive power was to be electric locomotives (d.c.) between Broodsnyersplaas and Ermelo and, in order to save on initial capital outlay on electrification, diesel traction between Ermelo and Richards Bay.

Due to the rapid growth in coal traffic as well as the increase in fuel prices economic evaluations based on capital and operating costs, led to the electrification of the Ermelo - Richards Bay section of the line at 25kV alternating current.

The main features of the lines described above and built in the early seventies, together with the line then existing between Blackhill and Broodsnyersplaas can be summarised as follows:-

TABLE 1

MAIN DESIGN FEATURES OF COAL LINE AS ORIGINALLY CONSTRUCTED

Total Route Length	585,5km
Total Track Length	809,4km
Total No. of Crossing Places	49
Total Length of Twinned Sections	112,2km
Longest Single Line Section	11km
Total number of Curves	386
Combined Length of Curves	212,7km
Percentage Curvature	36,3%
Total Number of Tunnels	25
Combined Tunnel Length	18,25km
Longest Tunnel (Overvaal)	3,93km
Longest Ruling Grade Sections) 10°/∞c	4,15km
) 15,15°/∞c	9,70km

1.3 Initial Phases In Export Programme

In December 1970 the Transvaal Coal Owners Association (TCOA) was granted authority to export 108Mt of coal from the Transvaal coal fields at a rate not exceeding 9Mt/a.

The world-wide energy crisis at the end of 1973 led to an unparalleled interest in South Africa's vast thermal coal reserves by foreign interests. The Government therefore increased the export authority in the following manner:-

(a) An export figure of 12Mt/a from 1 April 1976. (The target date for the opening of the harbour and new line which was met). This comprised an allocation of 10Mt/a to T.C.O.A. and 2Mt/a of anthracite to Natal-based companies. This was termed the Phase One project by the Richards Bay Coal Terminal Company (R.B.C.T.) - a company formed to plan, construct and operate the export terminal at Richards Bay and of which the main exporters became members.

(b) A total figure of 20Mt/a to be exported from 1 April 1979. The additional 8Mt/a was granted to Transvaal based companies not represented by T.C.O.A. as exporter. (This was defined as Phase Two by R.B.C.T.).

During the planning stages it had always been recognised that this line would not be a single purpose coal export line but would also cater for other commodities such as phosphate rock, phosphoric acid, chrome, ferro alloys, granite, timber, etc.

Relatively minor alterations to the original planning enabled the line to be constructed to convey the following traffic:-

- (i) 18Mt/a coal from the Transvaal coal fields;
- (ii) 2Mt/a anthracite from Natal coal fields;
- (iii) 2,5Mt/a of other traffic

TOTAL = 22,5 Mt/a

1.4 Increased Axle Loads

Due to a sustained demand for South African coal, annual export tonnages increased consistently. After careful deliberation the permissible axle loading for coal trucks was raised from 18,5t to 20t in May 1979. This was considered safe on the predominantly 57kg/m rails laid on concrete sleepers at 700mm spacing on a 1200m³/km ballast bed.

This step permitted a further increase in export tonnages, but a predictable increase in track

defects, especially rail-breaks occurred. An analysis, however, showed that rail-breaks increased in direct proportion to the increase in annual gross tonnage and were not specifically linked to the higher axle loading. This aspect will be dealt with more fully in a separate paper.

1.5 Increase In Train Lengths

Over the years train lengths have also increased to the extent where recently a load of 88-CCR1-trucks was introduced. This length is very near the optimum of 90 trucks that can be hauled by 4-7E1 locomotives against a ruling grade of 15,15°/∞c. Limited crossing facilities precludes any further increase in train lengths.

TABLE 2 shows the cumulative totals of net coal exports and gross tonnages (all traffic) for the period 1976/77 to 1980/81.

TABLE 2

FINANCIAL YEAR (1 APRIL-31 MARCH)	TOTAL CUMULATIVE NET COAL EXPORTS (Mt)	TOTAL CUMULATIVE GROSS TONNAGES - ALL TRAFFIC (Mt)
1976/77	5,50	14,31
1977/78	16,94	39,06
1978/79	31,07	72,80
1979/80	53,04	121,03
1980/81	79,05	175,98

The equivalent various tonnages exported at different stages since the line came into operation, as well as the methods employed to convey these tonnages over the a.c. section Ermelo - Richards Bay are reflected in TABLE 3:-

TABLE 3

DATE	APRIL '76	APRIL '79	APRIL '80	APRIL '81
Equivalent Export tonnages Mt/a	12	20	24	26
Axle Loads (t)	18,5	18,5	20	20
Ruling Grade °/∞	15,15(c)	15,15(c)	15,15(c)	15,15(c)
Motive Power	6 Class 34 Diesel	3 Class 7E a.c.	4 Class 7E a.c.	4 Class 7E a.c.
Length of Trains	80-CCR1 Trucks	76-CCR1 Trucks	84-CCR1 Trucks	88-CCR1 Trucks
No. trains per day (coal)	8	14	15	16
Other Long Trains (phosphates etc.)	1	1	1	1
General Short Trains per day	9	9	10	12
TOTAL NO OF TRAINS PER DIRECTION PER DAY	18	24	26	29

2. EXISTING LINE CAPACITY

The determination of capacity on a single line of this nature is dependent on a number of factors, viz., train mass, length, motive power, ruling grades, curvature, speed restrictions, etc. These factors have been incorporated in the train performance graphs produced by means of a computer programme. Using the running times so obtained, train diagrams were prepared which revealed that with the existing facilities the present theoretical line capacity is limited to 24 long coal trains and 12 other, shorter trains per direction per day.

As described in paragraph 1.4 and illustrated in TABLE 3 the equivalent of 26Mt/a of coal is being transported over this line at present (1981). This is achieved by means of 16 coal trains per direction per day, the majority of which consist of 88 trucks each.

A total of 350 annual railing days has been adopted as being a realistic figure. This allows for closures due to unscheduled maintenance, derailments and other unplanned events. Furthermore, an operating efficiency level of 90% is accepted. The balance of 10% provides for solely operating delays e.g. waiting for staff and motive power, differences in train handling techniques varying from driver to driver, delays caused by train controllers, etc. One 88 truck train per day at 20 ton/axle with a 58,38 ton payload per truck will therefore transport a total of :-

$$88 \times 58,38 \times 350 \times 0,9 = 1,618 \text{ Mt/a of coal.}$$

Apart from the 16 coal trains being run another long train conveying phosphate rock, phosphoric acid and chrome is also run daily.

The other commodities mentioned in paragraph 1.3 (b) as well as a fair volume of coal for export through the B.M.A. at Durban, are also being transported in shorter vacuum braked trains over this line. This traffic presently amounts to an average of 12 trains per direction per day.

If the 17 long trains and the abovementioned 12 are compared with the available line capacity of $24 + 12 = 36$ trains, then it becomes clear that at present this line already operates at a practical occupancy level of 81% which is appreciably in excess of the norm of 70% adopted by South African Transport Services for a line of this nature.

3. OPERATING METHOD AND EXISTING FACILITIES

The following is a brief description of the methods of operation, and of certain existing facilities on the various sections of line.

The coal line is at present operated by the advanced centralised traffic control (C.T.C.) method. The main advantages of this method of train control are the significant saving in manpower, and the improved overall control of traffic flow. Three operators at a control centre can for instance replace approximately 30 operators along the line. The services of highly skilled technical staff are however required for the installation and maintenance of a system of this nature.

Centralised traffic control centres for this line are situated at Ogies, Ermelo, Vryheid East and Insele (refer Figure 2).

The C.T.C. system is computer aided and amongst the resulting operating advantages are train number displays, route selection and setting, train graph plotting and train progress monitoring. The latter aspect informs the controller of the

estimated running time left in a section for a train approaching a crossing place thus enabling him to arrange crossings in a more efficient manner. Advance warning is given of special classes of trains (e.g. heavy coal trains) approaching "critical" signals which are not displaying proceed aspects. A "critical" signal is defined as one unavoidably sited on a steep gradient such that a special train having stopped at it, would not be able to depart without resorting to either reversing (unacceptable with long heavy loads) or load splitting.

3.1 Radio Communication

An advanced UHF Radio System between Brood-snyersplaas and Richards Bay has been introduced. This system, provides for voice/data communication over approximately 515km. of route length between the various control centres and trains. A high degree of coverage is achieved by means of 57 trackside radio stations spaced according to the topography.

Communication through tunnels is made possible by means of radiating co-axial cables. Each radio has three independent channels and most locomotives have already been fitted.

The train service requires a high standard of control, and together with the C.T.C. system the direct radio communication between driver and control centre is considered an indispensable aid. A good communication link also exists between the control centres and the mines and the harbour terminal.

3.2 Electrification

The decision to electrify the section of line between Ermelo and Richards Bay at 25kV. a.c. 50 Hz as opposed to the conventional 3kV. d.c. system mainly in use in South Africa was influenced by a variety of factors. Consideration and economic evaluation of parameters such as physical clearances, lighter catenary and contact wires with resultant lighter electrification structures, the long heavy loads envisaged, and the tonnages hauled per locomotive, lead to this decision. Subsequently a decision was taken to electrify a number of main lines in South Africa at this voltage. More detail of the electrification aspects of the coal line will be covered in another paper.

3.3 Motive Power

Over the section between the most northerly coal fields (near Blackhill) and Ermelo, the present 88-truck trains are being worked by five class 6E1 d.c. locomotives.

From Ermelo where a signal switched d.c./a.c. changeover yard has been provided, four class 7E a.c. locomotives take over the task of hauling these 88-truck loads down to Richards Bay.

As a back-up facility in case of electrical supply disruptions, a number of 34-class diesel electric locomotives are also in use on the coal line and the abovementioned loads are at times hauled by six of these as head-end power.

3.4 Trucks

Most of the trucks presently in use for exporting coal are the CCR-1 and CCR-3 types with an overall buffer centre length of 12,07 meters. Most of these have as part of a replacement programme been fitted with the now wellknown high-stability cross anchor bogies. The gross mass of these trucks is limited to 80t (axle loading 20t) and with a tare

of 21,62t, a payload of 58,38t of coal can be achieved. These trucks are fitted with rotary type couplers and are offloaded in pairs by tandem tipplers at the coal terminal without having to be uncoupled from the rest of the load.

A large number of CCL-2 and CCL-4 type trucks are also in use on the coal line, mainly to cater for the export of Natal anthracite from mines at Hlobane, Utrecht and Zungwini. These trucks can also convey coal at 20 ton per axle but at 14,88m each are longer than the CCR's. They are fitted with conventional type fixed couplers and after being uncoupled from the rest of the load at the harbour terminal each car is unloaded individually by a "random" type tippler. It is clear that unloading a load of CCL trucks is more time consuming than is the case with CCR trucks.

4. CHANGED CIRCUMSTANCES

During 1978 and before the 20Mt/a level of exports scheduled for Phase Two as described in paragraph 1.3 (b) had materialised, government authorised an increase in coal exports to a rate not exceeding 40Mt/a from the Transvaal and a further 4Mt/a from Natal. This level of 44Mt/a is known as Phase Three. The run-up dates set for this revised level were 31Mt/a by 1983 and the full 44Mt/a by 1986. Due to the growth pattern of existing and potential overseas coal markets it was considered essential that the increase in exports should as far as possible grow steadily. The additional coal authorised has been allocated to members of T.C.O.A. and to certain oil companies all of whom are now members of R.B.C.T.

The South African Transport Services was thus placed in the challenging position of having to increase by more than 100% the capacity of an already over-taxed line within a matter of six years. The need for a steady growth in exports and much higher demands from technical departments for on-track time for essential work had to be satisfied simultaneously.

5. PLANNING FOR INCREASED EXPORTS

In order to execute the planned improvements to satisfy the needs as described above, a solution had to be found that not only allowed for the short term export requirements, but that could also cater for substantial longer term increased exports - all within the framework of an existing intensive service as previously described.

5.1 Alternative Solutions

In order to find the most economical solution satisfying technical, operating and export requirements, various alternatives were considered. Each alternative was evaluated using the present value method to determine cost advantages/disadvantages based on a 30 year life expectancy. All capital, operating and maintenance costs were incorporated in the studies. Some of the alternatives were:-

5.1.1 Completely double existing line on existing 15,15°/o.c location. Retain 18,5t axle load.

~~(a) Main advantages:-~~

- (i) Lower annual gross tonnage over track (load sharing);

- (ii) Track and other occupations could be granted more readily;
- (iii) Disruption risks smaller due to alternative line being available;
- (iv) No load-adjustments required en route.

(b) Main disadvantages:-

- (i) Complete doubling would require a very large capital investment;
- (ii) A large complement of locomotives and associated train crews would be required to work more shorter trains;
- (iii) Restrictions imposed by the ruling grade of 15,15°/o.c and limitations imposed by existing track standards would prohibit any substantial future increase in export figures in consequence of restricted train lengths.

5.1.2 Double the train lengths to 168 trucks over the a.c. section (Ermelo - Richards Bay) by utilising helper locomotives. Retain existing grades but provide crossing and train make up facilities for double train lengths. Retain 18,5t axle loads.

(a) Main advantages:-

- (i) Compared with alternative 5.1.1 fewer trains for the same annual coal tonnages would be required;
- (ii) Complete doubling would be unnecessary from a capacity point of view;

(b) Main disadvantages:-

- (i) Except for guards, no saving in train crews would be achieved;
- (ii) The very close liaison between two sets of train crews working the same train was not favoured as a permanent measure;
- (iii) No locomotive savings would be achieved;
- (iv) Large yards to make up and break up double train lengths would be required at Ermelo and Richards Bay.

5.1.3 Run trains of 200 trucks at 18,5t axle loads with head end motive power only between Ermelo and Richards Bay and 100 truck trains between the mines and Ermelo. Due to the limitations inherent in the frames of the locomotives and in drawgear the motive power would be limited to a maximum of four locomotives. To haul the envisaged tonnages the ruling grade of 15,15°/o.c would have to be eased to 7,4°/o.c (1 in 140). This implied some 12 deviations with a combined length of approximately 68km.

(a) Main advantages:-

- (i) An appreciable saving on train crews and locomotives would be achieved;
- (ii) The annual coal tonnages could be moved with far less trains leaving ample track time for maintenance crews.
- (iii) With the necessary deviated portions plus long crossing places and some doubled sections, ample spare capacity for future growth could be built into the system.

(b) Main disadvantages:-

- (i) Initial capital investment would be high and a large volume of physical work would have to be done in a relatively short period;
- (ii) The yards at Ermelo, Vryheid East and Richards Bay would have to be enlarged substantially to cater for the 100/200 truck trains;
- (iii) Similar to alternative 5.1.2 gross annual tonnages over the remaining single line portions would be very high, requiring an intensified track maintenance effort.

5.1.4 Conclusion. These as well as other alternatives were evaluated and the present values of costs over a 30 year period were calculated at R1 705m, R1 620m and R1 550m respectively for the above alternatives. The alternative described in paragraph 5.1.3 was thus chosen not only for being the most economical from a cost point of view but because it also allowed for substantial future expansion.

5.2 The Case for Higher Axle Loads

At this time (1978/79) a study group was appointed to investigate the feasibility of introducing a higher axle load on the coal line. The study group's approach was largely influenced by actual results obtained from the Sishen-Saldanha line then already operating at 26t axle load, and secondly, the availability of a wide spectrum of international knowledge on this subject, made possible through the first Heavy Haul Conference, (Perth - September 1978) which was attended by representatives of this study group. The group's mandate was to establish the most economical axle load for the coal line cognisance being taken of the effect of such decision on the whole system viz locomotive and truck design, mines and terminal layouts and track structure.

The study group concluded that full optimisation of all relevant parameters such as axle load, coupler strength, brake system capability, ruling grade and utilisation and availability of adhesion, required a train of 200 x 104t trucks (26t axle load) of 12,07m over coupler centres hauled by four a.c. locomotives of 28t axle loads with a configuration and output similar to the class 9E's 50kV locomotives operating on the Sishen-Saldanha line. (A 28t axle load is the maximum that can be accommodated on the bridges and structures of the coal line).

Such a train would require the ruling grade of the line to be eased to 6,25°/∞ (1 in 160) against loaded trains. However, as the proposed 104 ton trucks would all be fitted with HS-bogies no compensation for curve resistance would be required. Because of the large amount of curvature encountered on the deviations, there would be very little difference in the cost between deviations at 6,25°/∞ (uncompensated) and 7,4°/∞ (compensated) ruling grades - refer alternative paragraph 5.1.3.

Economic studies also showed a clear advantage of this optimum load over the alternative described in paragraph 5.1.3. For example the saving in operating costs alone over a 30 year period was calculated to be of the order of R124m in present value terms.

Early in 1980 the management of South African Transport Services accepted the recommendation, and the final planning of all the facilities to cater

for 200 truck, 26t axle load trains by means of which 44Mt/a coal could be exported by 1986, was put under way.

6. PLANNING ASPECTS TO EXPORT 44Mt/a BY 1986 : (PHASE 3 - R.B.C.T.)

6.1 Planning Standards

In order to create the necessary capacity in time to enable the coal figure to increase gradually from 24Mt/a (at time of planning) to 44Mt/a by 1986 the following steps were decided on:-

(a) As an interim measure, double length trains at 20t axle load with front-end and helper locomotives at the middle will be run between Ermelo and Richards Bay from January 1983. This will allow the export figure to be increased from the present 26Mt/a (refer TABLE 3) to approximately 37Mt/a. This arrangement will continue until approximately mid 1985. Double train lengths could vary from 164 trucks to 176 trucks depending on the type and combination of main and helper locomotives. Possible arrangements could for example be 2-7E main and 5-7E helper locomotives, or 3-7E main and 4-37D helpers, etc.

(b) After this date 100 truck trains will be run between the coal fields and Ermelo (10°/∞ ruling grade) at 20t axle load. Due to the intensity of the train service over this section, the line is to be doubled completely and bi-directionally signalled.

(c) A large yard to make up 100-truck trains into 200-truck trains, and vice-versa, and also to switch between d.c. and a.c. traction will be required at Ermelo.

(d) Between Ermelo and Richards Bay 200-truck trains will be run on a ruling grade (against full loads) of 6,25°/∞. This requires crossing and yard facilities to cater for trains of this length as well as the construction of some 11 deviations with a combined length of approximately 114 km, including a total tunnel length of 14,2km. (trains to run at 20t axle load initially).

(e) Stengthening of the existing running lines to accommodate 26t axle load by 1987, as well as formation improvements will be required. A 200-truck train at this axle load will convey 16 800t of coal, compared with 5137t in 88 trucks at 20t axle per train at present. The new track structure will consist of 60 kg/m Cr-Mn rails, new design FY or PY concrete sleepers at 650mm centres and stone ballast at 1630 m³/km. The new rail profile will be more closely matched to that of the wheels of the HS-bogies to ensure increased wheel-rail contact.

(f) New types of locomotives to eventually haul the loads mentioned are to be designed and acquired, gradually releasing the present 6E1 and 7E fleet on the coal line. The locomotives will be classified as 10E at 21t axle loads for the d.c. section, and 11E at 28t axle load over the a.c. section. In both instances comprehensive performance analysis and economic evaluations proved the Co-Co type of design to be superior to that of the Bo-Bo design for these particularly heavy loads.

(g) A new fleet of gondola type trucks classified the CCL-5 with an all up mass of 104t and fitted with HS-bogies is to be acquired. Prototypes were recently manufactured and tested with promising results. Important dimensions are length 12,07m over buffer centres, height 3,493m and inside width 2,800m. With a tare of only 20t this truck has a

very good 1 : 4,2 tare to payload ratio. This type of truck will be dealt with more comprehensively in another paper.

(h) For the haulage of other types of traffic as well as to serve as a standby in case of major power supply failures a support fleet of 37-class diesel electric locomotives will be in operation on the coal line or on neighbouring lines.

(j) The starting grade for 200-truck trains on the 6,25°/∞ ruling grade line has been determined at 4,0°/∞ (1 in 250). Planning of deviations was done with this in mind as stopping at a critical (non-starting grade) signal would result in a long train having to be split with resultant substantial delays.

(k) For planning purposes the maximum speed of loaded coal trains was taken as 60km/h whilst the empty trains are to return at speeds of 75km/h. The speed differences will compensate for crossing delays as the empty trains will have to wait for the higher priority full trains.

(l) Apart from the hot-box detectors already in operation on the line, the provision of dragging equipment detectors (D.E.D.) is also considered essential. These detectors will be located at strategic points and at regular intervals and when activated will give immediate visual and audible warning to the C.T.C. controller who will immediately establish radio contact with the driver concerned. False alarms e.g. tampering can be identified by combining the activating requirement with the occupation of the track circuit concerned.

(m) Because of the long distances and resultant long running times between the remanning yards at Ermelo, Vryheid East and Richards Bay, routine yard duties such as making up loads, brake tests, etc. will be performed by local drivers to provide mainline drivers with a quicker turn-around time or a longer rest-period. Due to the strain involved in handling a long heavy train of this nature for many hours, it was proposed that the locomotives be manned by two drivers who could take turns at the controls instead of by a driver and an assistant. This proposal has, however, not yet been accepted.

(n) It is estimated that at a coal export level of 44Mt/a combined with all other traffic single line portions of this line will carry approximately 95Mt/a gross traffic. Due to a lack of adequate statistics on SAR type 60kg Cr.Mn. rails, especially non-work hardened, a frequent replacement cycle may be required. With this in mind the planners allowed for daily four-hour occupation periods on various sections of the line. It is also considered essential that the maintenance efforts of all technical departments should be combined as far as practicable. However, the systems approach to track maintenance has subsequently been the subject of further study and the results may have an effect on the previous planning. Details of this approach will be presented in another paper.

(o) The overhead track equipment will have to be strengthened by means of a parallel feeding system and the existing C.T.C. system of train control will be extended to all deviations and alterations to existing layouts. Both these aspects will be covered in more detail in other papers.

6.2 Tabular Presentation of Envisaged Improvements

TABLE 4 combines variables such as train lengths, axle loads, etc. at different stages to give a clear indication of the capacities created by means of the improvements to be undertaken. The total annual coal

exports shown are in line with those envisaged by R.B.C.T. with due regard to governing factors such as tippler capacities, available berths and shiploaders at the terminal.

TABLE 4

METHODS OF SATISFYING EXPORT REQUIREMENTS AT VARIOUS STAGES.

DATE ASPECT	JAN. 1983	JUNE 1984	JAN. 1986	JAN. 1987
EXPORT TONNAGES Mt/a	31	37	44	44
AXLE LOADING t	20	20	20	26
RULING GRADE COALFIELDS - ERMELO (d.c.)	10°/∞ c	10°/∞ c	10°/∞ c	10°/∞ c
RULING GRADE RICHARDS BAY ERMELO (a.c.)	15,15°/∞ c	15,15°/∞ c	6,25°/∞	6,25°/∞
MOTIVE POWER (d.c. section)	5x6E1	5x6E1	6x6E1	4x10E
MOTIVE POWER (a.c. section)	Main + helper locomotives 7E and/or 37D	Main + helper locomotives 7E and/or 37D	3 or 4x11E	4x11E
TRAIN CONSIST (d.c. section)	82-88 x CCR1	82-88 x CCR1	100 x CCL-5	100 x CCL-5
TRAIN CONSIST (a.c. section)	164-176 CCR1	164-176 CCR1	200 x CCL-5	200 x CCL-5
TRAINS PER DAY (COAL) (a.c. section)	10	12	12	9
OTHER LONG TRAINS/DAY (a.c. section)	1	1	1	2
ALL OTHER TRAINS (a.c.)	12	13	13	12
TOTAL a.c. section	23	26	26	23
% OCCUPANCY OF CAPACITY	64%	72%	72%	64%

6.3 Certain Design Details

6.3.1 Improvements at mines. Practically all the export mines will of necessity have to upgrade their existing tracks to cater for the planned 26t axle load. Furthermore, if not already in existence, rapid loading terminals capable of loading a 100-truck train (8 400t of coal) in three hours are

are to be designed and constructed. Silos with capacities of up to 10 000t are being provided and loading is achieved by means of rapid discharging flasks. The trucks are propelled by means of hydraulic ram pushers while compressor cars provide the required air pressure to keep the brakes off during loading. After the loading operation is complete another one and a half hours are required for coupling up locomotives, testing and departure.

6.3.2 Ermelo yard. The new yard that has been designed at Ermelo (Figure 3) will fulfil three main functions, viz. (a) switching over from d.c. to a.c. traction, (b) permitting loads of 100-trucks to be combined into 200-truck loads and vice-versa, and (c) remanning of trains. The various arrivals and departure yards for 100 and 200-truck trains (fulls and empties) are shown on Figure 3 and the arrows indicate the direction of travel and sequence of operations. Local diesel electric locomotives will haul train loads over the balloon tracks between the a.c. and d.c. areas. The yard design allows for substantial expansion beyond 44Mt/a.

6.3.3 Vryheid East yard. Approximately 4Mt/a of coal will eventually originate in the Natal coal fields. Most of this coal will be brought into Vryheid East yard in 50-truck train lengths over branch lines not capable of accommodating longer loads. To make up these trains into 200-truck lengths, a herringbone yard comprising three tracks divided by means of cross-overs into four sections of 50-truck lengths each is to be built here. As remanning as well as certain brake tests of through trains are to be undertaken here a large arrival/departure yard comprising eight roads for 200-truck trains is to be constructed as well. This yard will also act as a reservoir to absorb fluctuations in traffic density.

6.3.4 Richards Bay Coal Terminal. In order to cater for the increased coal export figure of 44Mt/a by 1986 the existing layout of the terminal at Richards Bay which at present allows for a maximum of 28Mt/a has to be altered substantially. The revised layout is depicted on Figure 4 and contains the following features:-

- (a) Various yards for different train lengths are to be constructed as shown.
- (b) A further two berths are to be added to the existing two. Water depth will be minus 19 meters (L.W.O.S.T.) initially but the quay structure will permit of subsequent dredging to minus 23 meters.
- (c) The existing two tandem tippers are to be replaced by three capable of handling 26t axle load trucks in pairs. Tippler capacity will be 15Mt/a each.
- (d) Additional stacking areas for the increased volume of stockpiled coal catering for some 30 different grades are to be provided together with additional stacker/reclaimers and shiploaders.

The terminal working with a throughput time of a train ranging from 10 to 16 hours can briefly be described as follows (refer Figure 4):-

Full 200-truck trains arrive in Yard A where they are split into two 100-truck sections. After the necessary carriage and wagon inspections the 100-truck sections are hauled into the pre-tipping

yard B. The loads are then indexed through the tippers (J) and reach yard C unloaded. Any defective vehicles are shunted out in yard D, and the same number of good order trucks attached. The 100-truck loads are then hauled to departure yard F, combined with another 100-truck load and after the necessary tests have been performed, the 200-truck empty train departs for the coal fields. It is interesting that this yard will have a total length of approximately 9km, and also allow for substantial expansions beyond 44Mt/a.

7. COSTS

To date (October 1981) the total expenditure on the line and harbour amounts to R907,5m, whilst the total estimate including the requirements for the Phase 3 work (44Mt/a) is of the order of R1525m. The expected expenditure for the Phase 3 work only is of the order of R480m on the line and R70m for harbour works. These figures exclude the cost of any rolling stock, as well as the cost of improvements and alterations at the various export mines and at the coal terminal.

8. FUTURE EXPANSIONS

Due to the favourable overseas market a re-appraisal of South Africa's vast extractable coal reserves was made. As this indicated that previous figures had been too low, Government recently announced a further increase in the maximum annual coal export figure. The ceiling has now been raised to 80Mt/a and although no time-scale has been set, it can be assumed that a gradual annual increase beyond 44Mt/a after 1986 will be aimed for.

No detail planning has yet been done but complete doubling of the whole coal line is envisaged. The larger yards and the terminal will have to be modified as well. Presumably some of the existing mines will be expanded and new mines commissioned. The locality of these will to a certain extent determine the need to upgrade existing link lines or even to build new lines.

However, as in the past the South African Transport Services is well set to plan and provide an efficient and economic transport system for conveying this coal so enabling the coal industry to compete successfully in the world market.

9. ACKNOWLEDGEMENTS

In conclusion I would like to thank the South African Transport Services and the Richards Bay Coal Terminal Company for permission to publish this paper. I am also indebted to my colleagues who assisted me in the preparation thereof.

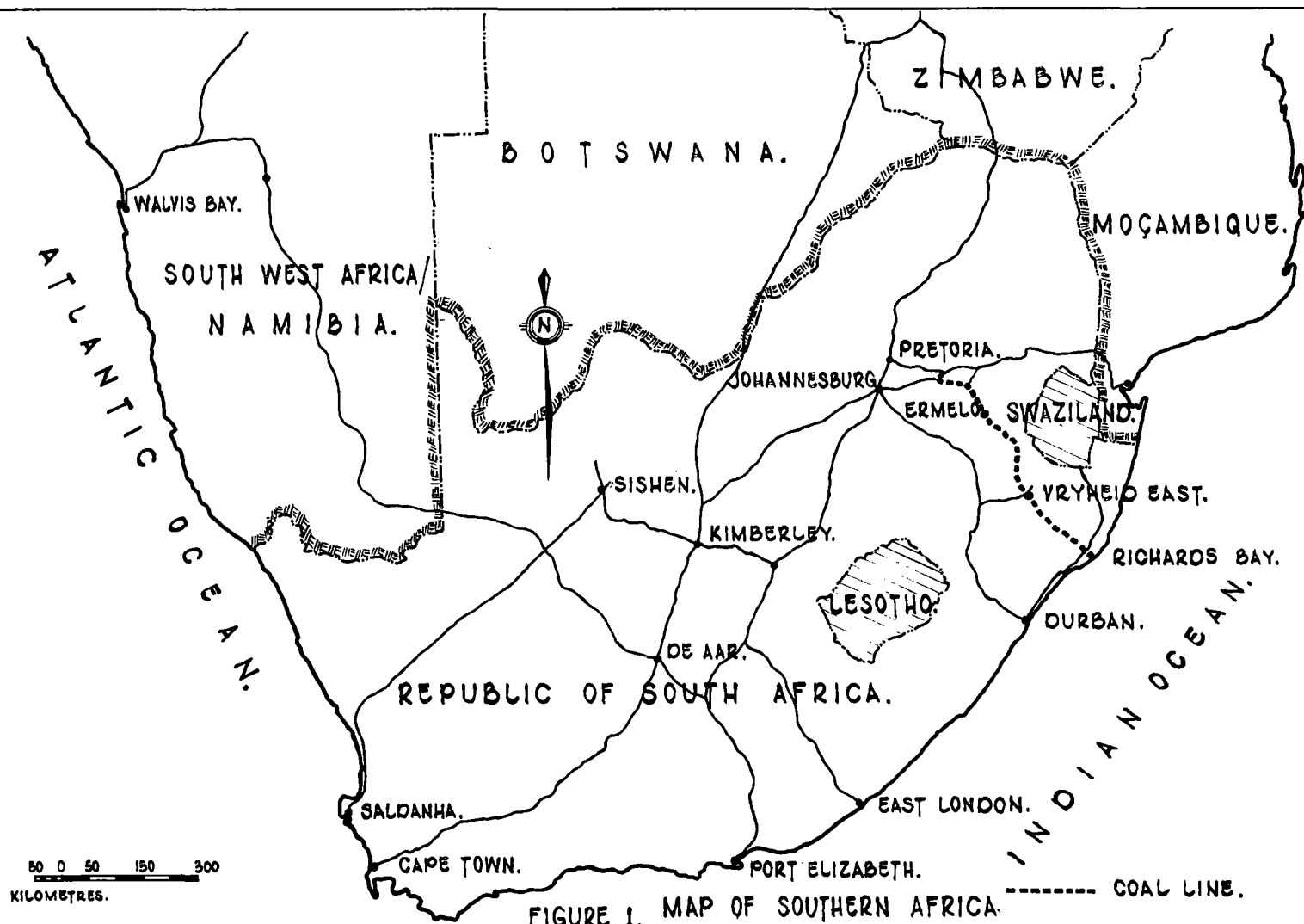
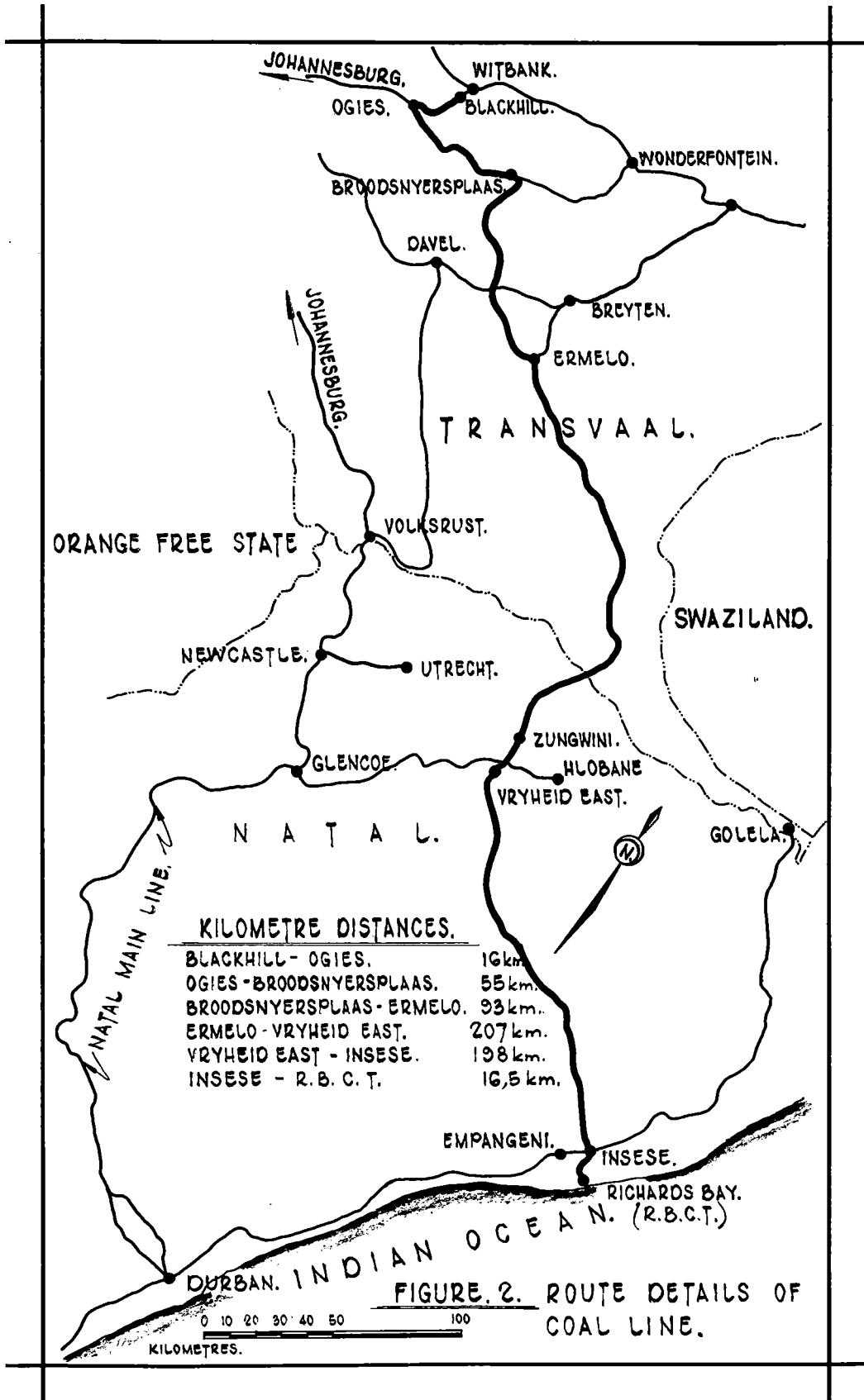


FIGURE 1. MAP OF SOUTHERN AFRICA. DEPICTING LOCATION OF COAL LINE.



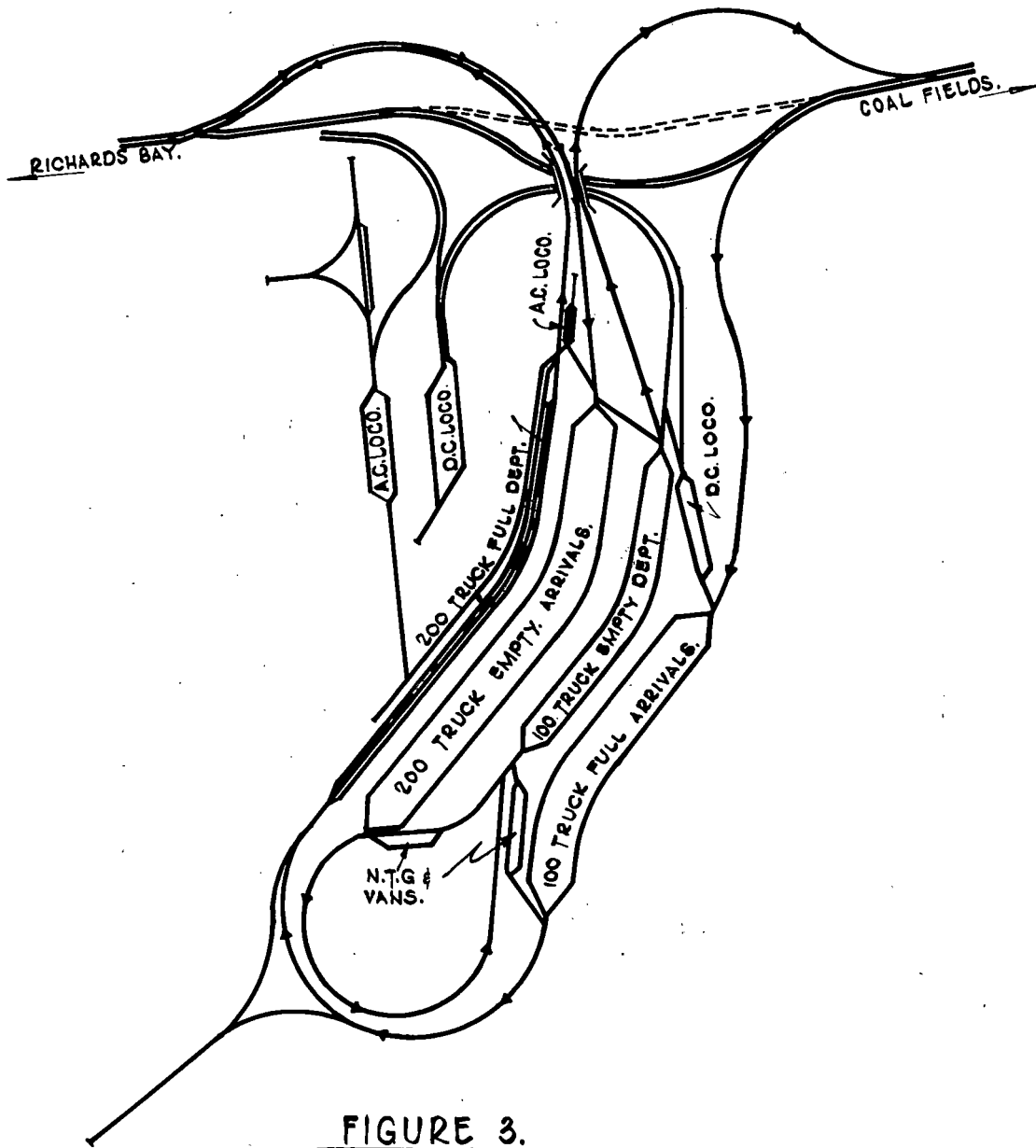
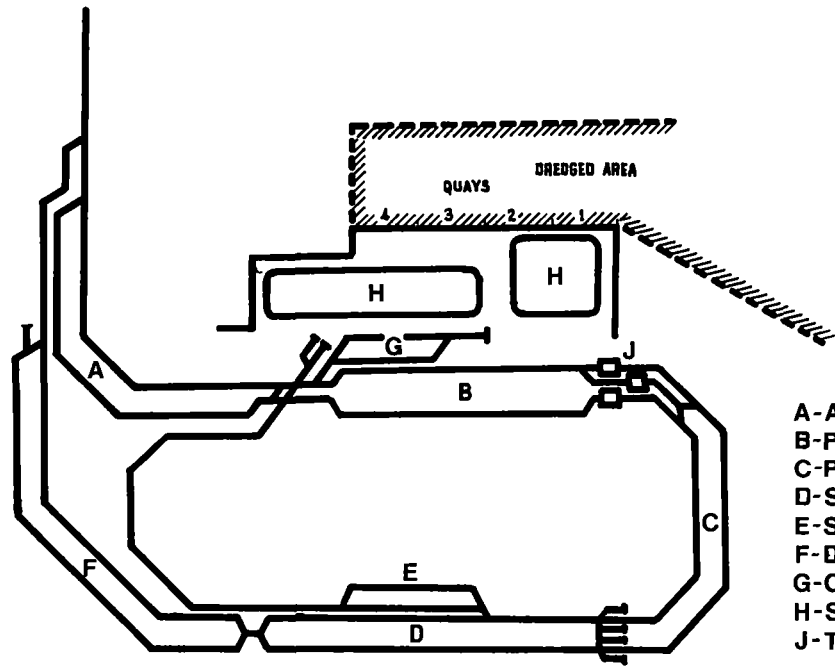


FIGURE 3.
ERMELO - YARD FOR COMPILATION OF
200 TRUCK TRAINS.



- A-Arrivals yard (200 trucks full)
- B-Pre-Tipling yard (100 trucks)
- C-Post-Tipling yard (100 trucks)
- D-Shunting yard. N.T.G. & G.O.W.(100 trucks)
- E-Staging yard
- F-Departure yard (200 trucks)
- G-C.&W. Yard
- H-Stacking area
- J-Tiplers

RICHARDS BAY COAL TERMINAL. PLANNED LAYOUT FOR PHASE 3

figure 4

W.R. Fahey

B.C.E. (Melb)
 M.B.A. (McGill)
 Manager, Engineering
 Hamersley Iron Pty., Ltd.

The Economics of Capacity Expansion

The development of a mining enterprise is necessarily capital intensive. Consequently, the economics of the enterprise turn critically on maximizing use of capital assets. In the Hamersley railway context, the track is the dominant element. The initial project scope required a haulage of 5 million tons and envisaged an ultimate rate of perhaps 10 million. In fact, the haulage required to meet market demand increased for several years, reaching a maximum to date of 40 million tons in 1980. To meet this growth, major capital investments have been necessary to increase the capacity of the system. In the railway, this investment has concentrated on preserving the ability to use single track, by minimizing track occupancy for maintenance while, at the same time, operating the longest and heaviest train possible. Achievement of these targets favours low transportation cost and high capacity.

NOMENCLATURE

A.B.S.	automatic block signal
A.T.C.	automatic train operation
C.T.C.	centralised traffic control
kg/m	kilogramme/metric
km/hr	kilometres/hour
\$M	million Australian dollars (\$1A = \$1.15 US approx)
Mgt/y	million gross tonnes/year
Mnt/y	million net tonnes/year (payload)
p.a.	per annum
t	tonne
t km	tonne kilometre

INTRODUCTION

A comprehensive outline of the economics of a heavy haul railway, as applied to Hamersley Iron, was presented at the First International Heavy Haul Railways Conference(1). In particular, it was concluded that the economics depended on capital utilisation. Because the track is the dominant element in this capital (Table I), it follows that economy will improve with intensive use of the track. This paper will therefore focus in more detail on steps taken in Hamersley to improve track utilisation, with reference also to other strategic issues like locomotives and rolling stock.

What is economic can only be judged within a particular framework. The economic decisions at Hamersley are taken in the circumstances that apply specifically to Hamersley and will not be applicable generally. For purposes of this presentation, therefore, it is more meaningful to express economics not in terms of conventional rates of return or net present values, but rather in investment costs (at present value) and corresponding benefits in terms of savings in time or increases in availability of track or equipment. These measures are more likely to be transferable to other contexts in which their impacts on capacity can be assessed.

BACKGROUND

In 1966, Hamersley railway began with the modest expectation of hauling 5 million tonnes of ore annually. In due course, the growth projection envisaged perhaps 10 million. In the event, there was a compound growth rate of 20% p.a. for a number of years, reaching 35 million in 1975. In 1980, the railway hauled 40 million tonnes of ore (Fig 1).

It is ironical that a capacity constraint was met even before the railway started. Just as the first ore was due to be hauled the 288km from the mine

TABLE I
ANALYSIS OF FREIGHT RATE

% of Cost/t km	At 65 Mgt/y			At 80 Mgt/y		
	CAPITAL CHARGES	OPERATING COST	TOTAL FREIGHT	CAPITAL CHARGES	OPERATING COST	TOTAL FREIGHT
<u>Permanent Way</u>						
Track	49	9	58	37	7	44
Signals	2	1	3	2	1	3
<u>Stock</u>						
Locomotive	5	5	10	5	4	9
Rolling Stock	10	5	15	9	4	13
Workshop	2	-	2	2	-	2
<u>Operating</u>						
Administration	-	2	2	-	2	2
Fuel	-	5	5	-	5	5
Traffic Operating	-	5	5	-	4	4
	68	32	100	55	27	82

at Tom Price to the port at Dampier, a cyclone washed out some 30km of track in April 1966 - a consequence of the meagre or non-existent rainfall and runoff data available for the design of water ways in this remote area.

This hard lesson was one of a number to come, emphasising the inadequacy of the initial design to cope with the continuous and increasingly intensive unit train operations which were, by the early 70's, causing rates of deterioration in the track which were unprecedented. The track had been strengthened by widening (and sometimes rebuilding) embankments, installing replacement 2740mm (9ft) instead of 2400mm (8ft) sleepers, increasing ballast depth to 300mm and increasing the shoulder width. Nevertheless, at an aggregate 200 Mgt, the number of rail failures and the consequent train delays forced the decision to change out the rail entirely. 68kg/m rail was substituted for the previous 59kg/m section. Elastic fastenings were also installed throughout to minimise interruption to train operations due to rail changeouts in curves, occurring as often as every 9 months in the sharpest curve of 400m radius.

In 1972, Hamersley's required haulage capacity increased markedly with the opening of a second mine at Paraburdoo served by a 100km extension to the main line. Based on the lessons of previous experience, this extension was built to very high standards (and after 200 Mgt, has required minimal maintenance).

Concurrently, CTC was commissioned throughout to extend capacity, at a cost equivalent to two 180 car train consists, or less than one tenth of duplicating the main line. Running times were cut significantly. Since then, control of intermediate signals has been implemented to reduce headway and allow longer track occupancies by maintenance forces before clearing for trains.

With the extensive improvements in the fixed plant, the emphasis changed. The potential capacity constraint became the trains themselves, particularly the motive power. With increasing age and very hard service the mechanical availability and reliability of the loco fleet was falling. As an alternative to a replacement investment (and since a 2% improvement would save the purchase of 1 locomotive) the decision was made to upgrade the workshop and set target improvements on availabilities of locos and ore cars

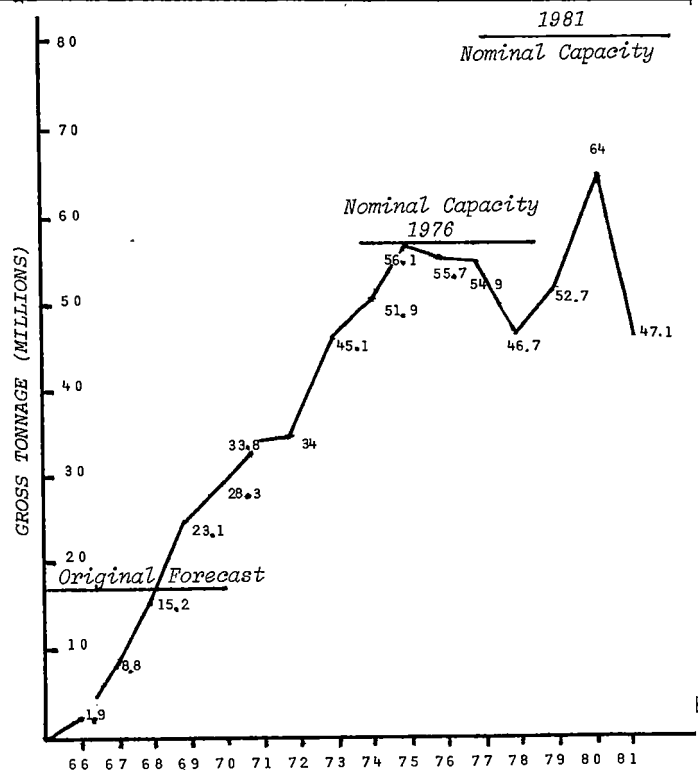


FIGURE 1. RAIL TRAFFIC GROWTH

respectively. The utilisation of equipment was examined critically and the decision made to increase the power/weight ratio by 20%. Trains became 3 locos and 180 cars, with a gross weight of about 22,000 tonnes, necessitating a major thrust in the area of train handling to gain a better understanding of the behaviour of these trains on Hamersley's track. The benefits were realised quickly in reduced running times (see Table II), more reliable performance, and a reduction in derailments.

The present nominal capacity of Hamersley's iron ore production and handling system is about 46 Mnt/y. This is determined by factors other than the railway, though this has not always been so.

At Hamersley there is considerable incentive to push the limit of the single track higher. The costs of doing so are judged in relation to the alternative of double track. This would represent an investment now of about \$M300.

TABLE II
RUNNING TIMES BETWEEN TOM PRICE & DAMPIER

YEAR	RUNNING TIME	
	AVERAGE	MINIMUM
1976	5hr 58m	4hr 12m
1977	5hr 26m	4hr 18m
1978	5hr 27m	4hr 08m
1979	5hr 18m	4hr 08m
1980	5hr 30m	4hr 08m
1981	5hr 09m	3hr 58m

THE IMPACT OF INVESTMENT ON CAPACITY

To assess the investments made by Hamersley with the objective of ensuring that railway capacity has remained adequate to meet haulage demand, it is proposed to examine briefly a selection of representative projects covering a number of aspects of the operation. In particular:

- . Research (joint project with Mount Newman Mining)
- . Installation of C.T.C. (and control of intermediate signals)
- . Concrete sleepers
- . Workshop upgrade

In each case it is intended to focus on the economics, in terms of options available, costs and benefits, and the decisions made.

RESEARCH

Investment: \$M3 (to date)
The Experience at Hamersley

The combination of heavy axle loads and high tonnage, together with the inadequate initial standard of track construction, condemned Hamersley to extremely high levels of track maintenance expenditure annually, particularly on the main line between Dampier and Tom Price.

As tonnage continued to rise, damage increased and available track time diminished because of the need for more trains. Faced with heavy programmes of rail and sleeper renewal, the approach was to work between trains with labour intensive gangs using relatively small and light machines which could quickly take and release occupancy. This proved to be an extremely costly tactic which was not readily achieving the track geometry desired. Moreover, it became painfully apparent at about the 55Mgt/y level that the effective capacity of the Hamersley system would be constrained by the railway at a level below the haulage commitment of about 65Mgt/y. The maintenance approach then current could not cope with the unprecedented tonnages and constantly high axle loads.

In these circumstances Hamersley perceived that the desired capacity could only be achieved by a

maintenance strategy based on prevention, not cure. Consequently, it became a necessity to understand cause and effect in terms of track/train dynamics and, in particular, the ramifications of the wheel/rail interface. To do so, Hamersley made the decision to embark on a major research programme.

Initially, the programme was structured according to areas experiencing the most severe and pressing problems, as follows:

- . rail performance
- . track design
- . vehicle performance
- . train performance

Rail Performance. It is not surprising that immediate emphasis should have been placed on rail, because Hamersley had already gone through the experience of replacing the rail entirely after only some 200Mgt of service.

Gradually, the severe problems of corrugation, material flow, local fatigue effects and inadequate welding techniques yielded to systematic analysis, experimentation and field testing. The technical and economic advantages of high strength rail are clearly established and their use in curves is standard. Furthermore, a strong argument can be put forward in favour of the use of this rail in tangents also.

Track Design. This area concentrated largely on the response to imposed loading of track elements other than rail. Largely through field testing in the form of instrumented track and vehicles and subsequent analysis of force and displacement characteristics, a better understanding of the dynamics emerged. This in turn formed the basis on which the relationships between initial design standards, types and rates of deterioration and effects of maintenance operations, such as tamping and lining, were established.

The objective of defining track standards and geometrical tolerances which will optimise overall maintenance cost is largely achieved.

Vehicle Performance. The understanding of the characteristics of bogies, cars and trains and, in particular, their dynamic response to forcing inputs from track geometry defects is fundamental to minimising wear of components. The development of a computer based model to simulate bogie behaviour on the Hamersley track has been invaluable in the control of vehicle tracking. In this respect, the profile of both wheel and rail is known to be critical to the wear of both. Progress in this area achieved through observation and field trials initially, followed by further refinement using the model, has been marked. The reduction in wear rates has been nothing short of dramatic.

Train Performance. Again it is not surprising that Hamersley would initiate research in this area. In fifteen years of operations, 26 major derailments have occurred. Though not a high rate in relation to train kilometres (at more than 500,000 train km/derailment), the cost at over \$1 million per accident, and the obvious impact on haulage capacity, prompted the research aimed at assessing the degree to which Hamersley was prone to derailment from certain causes, e.g. wheel climb. The investigation provided reassurance in respect to certain derailments which were largely unexplained - and therefore charged to "train dynamics". Of more importance than the primary purpose however, was the secondary effect of leading to an improved appreciation of the importance of the

forces at the wheel/rail interface induced by train behaviour. This in turn led to an expanded effort in the area of longitudinal train forces and effective driving techniques. Along the way a simulator was developed and is now in use for driver training as well as the study of engineering problems associated with train dynamics during loading, dumping and mainline transit.

Impact of Research

At Hamersley, the annual expenditure on railway research is about 1% of the operating budget. This expenditure is spread over a number of defined projects each of which has an objective and is judged in terms of its cost and the probability of its achieving its objective. Each is expected to be positive in a cost/benefit sense where both are measured in dollars.

Equally importantly, there is little doubt that the impact on haulage capacity has been major. Consider the following:

Rails. There have been two important thrusts:

Rail Type and Metallurgy. For a premium of perhaps 25% on cost, rail life has at least doubled in curves which means that the track occupancy by maintenance forces for the purpose of changing rails has been cut in half on about 30% of Hamersley's track. This translates into a net benefit of an addition of some 340 hours of track time available for ore trains annually.

Rail Profile. Much has now been said about the virtues of well matched rail and wheel profiles in reducing interactive forces and hence rail and wheel wear. Until relatively recently, Hamersley was experiencing rapid wear rates in both curves and tangents. The curve wear was not unexpected but the side cutting akin to curve wear on tangent track caused by lateral excursions of trains with a kind of sinusoidal motion was cause for alarm. Conditioned by earlier disastrous rail experience, the outlook was for a tangent rail life perhaps as low as 500 Mgt. This limit has already been exceeded, and better control of vehicle tracking through design of rail and wheel profiles (particularly the former) has changed the outlook to a much more optimistic figure of perhaps 1,000 Mgt. Again, the projected benefit is double the rail life and half the change-out frequency on 70% of the track.

TABLE III
INCREASE IN RAIL LIFE IN CURVES DUE TO GRINDING

Radius of Curve (metres)	Rail Life Increase (%)	
396	10	
610	23	
762	31	
915	38	
1 220	50	
1 524	60	
1 830	68	
		Weighted average increase in rail life for all curves = 48.7%

Note: The larger rail life increases are realised in the curves of higher radius because of the ability to achieve curving without flange contact.

When considered as an increment, the profiling is estimated to add about 50% to the overall life of rails in curves.

In the case of profiling, however, the benefit is not net because of the need for track occupancy to grind. Once the desired rail profiles have been achieved, however, it becomes a question of dressing the rail and the grinding requirement might not be much more than it would otherwise be to combat corrugation.

The net effect of profiling then is estimated to add 525 hours of track time available for trains annually.

Track Condition. It will be apparent that the original Hamersley track has been virtually rebuilt. This arose essentially from two basic factors:

- . The scope of the project as first envisaged, i.e. an ultimate haulage of 10 Mnt/y and construction standards thought to be appropriate
- . Lack of appreciation of the relationship between initial track standards and subsequent maintenance requirements in the context of a heavy haul operation.

The two are interrelated, of course, and both were influenced by the market opportunities and strategic requirements which then prevailed. Decisions made, though proper in the circumstances, condemned the company to very high expenditures in order to cope with track degradation in the face of rapidly rising tonnage. This experience was most convincing in delivering a practical demonstration of the value of high track standards. The research confirms this and is identifying the standards and tolerances which optimise the cost effectiveness of track maintenance-by machines in particular.

Track Maintenance. The impact of the changes can be put into perspective by considering the trends in machines and man hours devoted to track maintenance. Some years ago, the machine fleet consisted of 7 tampers and 4 ballast regulators. There are now 3 tampers and 2 ballast regulators, albeit all large (and expensive) machines with high travelling speed and output capability.

A similar illustration emerges from man hours of labour. In 1975, 953,000 man hours were expended. Since then, the trend line has been steadily downwards to a value of 468,000 man hours in 1981 - a reduction of more than 50%. Expressed another way, there were 7.5 men/Mgt in 1975 vs 5.4/Mgt in 1981, including supervision and administration.

Apart from straight economics, the implications for track occupancy, and hence track haulage capacity, are clear.

Wheels. The rail profiling activity has now been going on for some three years and its effects on rails have been quantified reasonably precisely. The effect on wheels of the rail profiles are not yet quantified but are readily apparent qualitatively in the workshops. From the computer matching of wheel and rail profiles, an improved wheel profile has emerged and is now under test in the car fleet. Preliminary indications are that the relatively high initial wear rates previously experienced with the conical profile have been reduced considerably.

Because wheel condition is a major reason for cutting out cars for shopping, it follows that any

increase in the machining cycle of wheels will lead to an increase in the availability of the car fleet. Some 2% improvement is expected which, in Hamersley's case, is equivalent in capacity to putting an extra 50 cars in the fleet.

Train Dynamics. To start a train operation on the scale of Hamersley's, at a time when the relevant accumulated experience and expertise in the country were just about zero, was no mean feat.

Economics and haulage capacity are favoured by the maximum payload per train. This means operating the longest and heaviest trains possible in the circumstances. The 30t axle load prompted by a general desire for a large scale operation, is now seen to be a fortuitous choice, despite the problems it caused over a period of time. Indeed, it is no longer regarded as the upper limit(2).

The train consist has gone through a series of changes, from one loco and 76 cars initially (1/76) to 2/160 and 3/180, which has been the standard for some years and thought to be about the upper limit for head end power only. There too, the view is changing and a recent test programme of 3/210 has proven quite successful.

Through the process of development, maximum operating speed has increased from 55km/hr, not only because it is desirable in its own right, but as a means of improving train handling at critical locations.

A measure of this progress is perhaps the number of train brake applications in the passage of a loaded train from Tom Price to Dampier, where a reduction of about 50% has been achieved. (A direct cost saving consequence has been a reduction of 30% in brake shoe usage per million tonnes in the last 5 years). It is most likely that decisions of this sort would not even be considered were it not for the contribution of research to the state of knowledge regarding such matters as track condition, in-train forces, fatigue effects, driving techniques, and train behaviour. Some measure of the benefits derived in relation to haulage capacity can be gauged from the history of pull aparts, and consequent delays, on the main line.

TABLE IV
DELAYS DUE TO BROKEN DRAWGEAR

Year	Hours/train
1976	0.13
1977	0.17
1978	0.18
1979	0.13
1980	0.10
1981	0.01

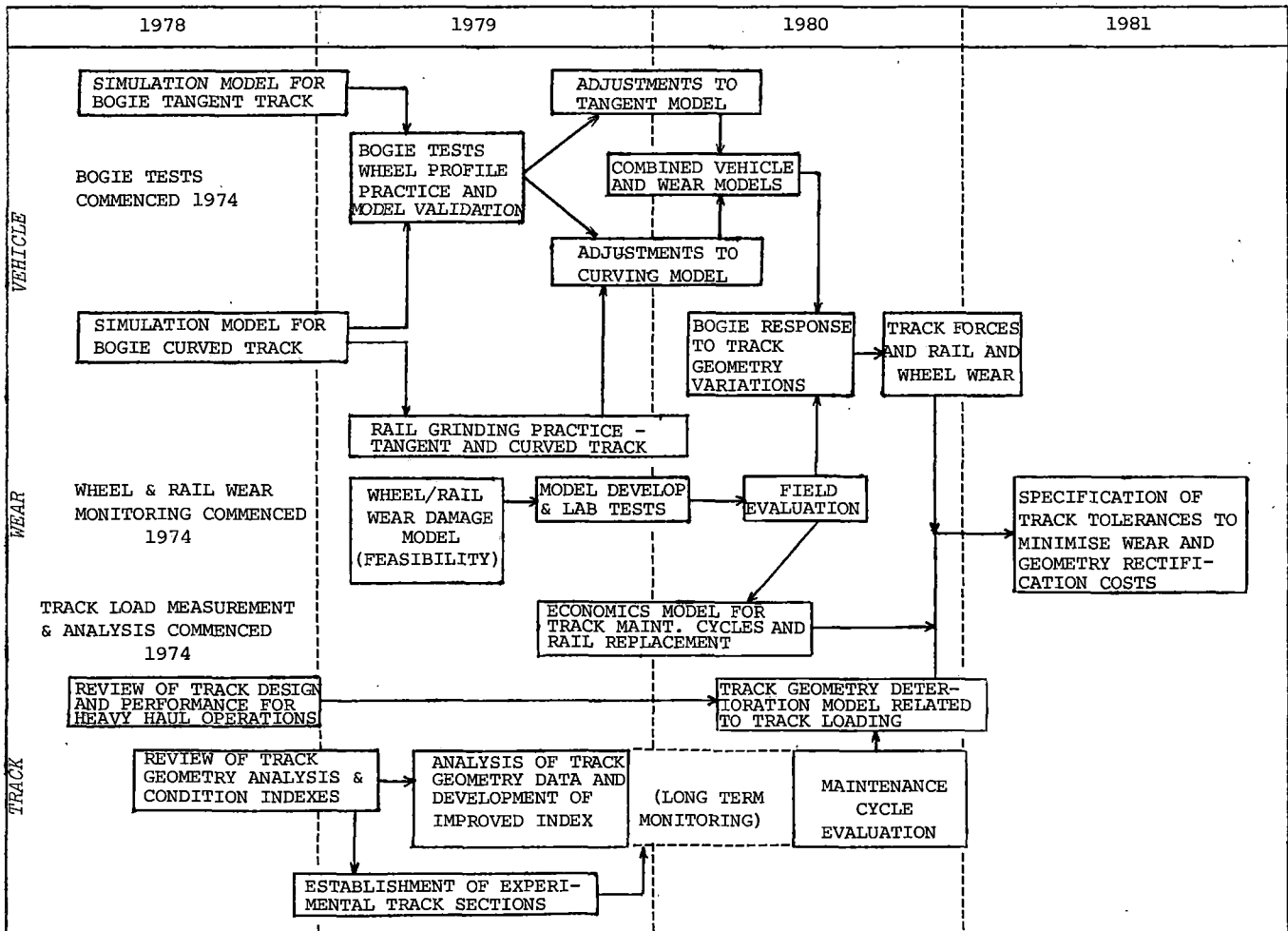


FIGURE 2. SUMMARY OF RESEARCH

The downward trend of recent years, and the big reduction in 1981 in particular, are attributable to the research work on data acquisition and analysis of train dynamics. This identified the driving techniques necessary to reduce in-train forces at locations found to be critical.

Directions For The Future

A summary of the research which has as its focus the wheel/rail interface is well illustrated by Fig 2.

Data Acquisition. Data acquisition on track is largely via conventional EM80 hardware, though what is not so conventional is that it is mounted in a research car ballasted to 30t axle load. This will shortly be supplemented by an optically based head wear gauge capable of reading, at track speed (80km/hr) both the head loss and the existing rail head configuration with high precision.

The other end of the car is devoted to train dynamics data acquisition. Processing of course, is via computers. A suite of programmes makes up a reasonably sophisticated and comprehensive Track Information System. Less progress has been made towards a Vehicle Information System though some of the elements are in place. Apart from the well known Hot Box Detectors and Dragging Equipment Detectors, consideration is being given to an in-motion wheel monitoring system which will acquire and process information on the wheel profile, diameter and tread condition externally and the state of stress and defect condition internally.

Economic Maintenance. Coupled with the appropriate cost information, such systems will enable maintenance operations on track and vehicles to be optimal in an economic sense. For example, in relation to track, the near term probability is shown by the simplistic block diagram of Fig 3 which leads to the kind of track maintenance planning illustrated by Fig 4 where cost effectiveness is almost automatic.

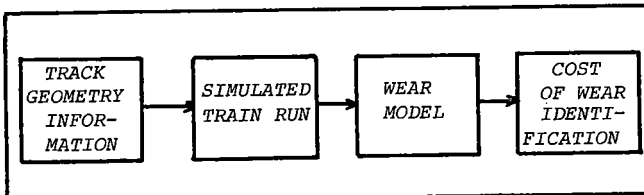


FIGURE 3. STEPS IN MAINTENANCE PLANNING

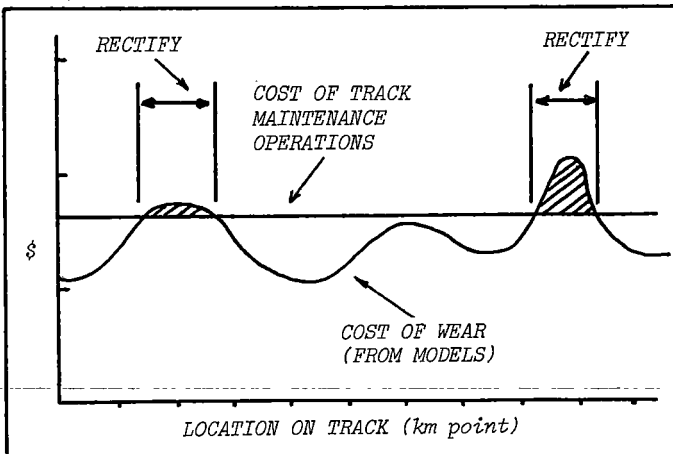


FIGURE 4. COST EFFECTIVE MAINTENANCE

This approach is based on the simple premise that a maintenance or rectification operation is executed when the cost of not doing it is greater. It is an idea that has wide application in heavy haul operations and acts as a considerable stimulus to continuing research.

INSTALLATION OF C.T.C.

Investment: \$M29

Initially, the railway configuration, consisting of the 288km main line with seven crossing loops, provided a theoretical headway of 1hr 50 mins between following trains at the operating speeds then current. (4) With the commissioning of a second mine at Paraburdoo in prospect (a 100km extension of the main line further from the port), provision had to be made for the corresponding increment in railway capacity. Various alternatives were examined including the provision of additional numbers of crossing loops, double track sections, control systems of varying sophistication (e.g. A.B.S., C.T.C., A.T.O) all the way to complete double tracking. The outcome consisted of a combination of crossing loops, double track at critical points and the installation of C.T.C. systems, one for the main line and a second for control of the 7 Mile Yard and the Dampier terminal (port end).

Prior to the introduction of these changes, the running time from Dampier to Tom Price was about 6 hours 40 mins at the 6 train/day level. Afterwards, running times fell rather dramatically by about 1 hr 20 mins in each direction. Since then further reductions have been introduced gradually and the present running time stands at 5 hr 10min. It should be mentioned that many factors have contributed to this subsequent fall, such as better condition of track and equipment, improved power/weight ratios for acceleration and braking, better knowledge of driving techniques/train behaviour, all of which have gradually led to higher operating speeds. There is little doubt, however, that the introduction of the CTC system played a major role in reducing cycle times and, as such, translated directly into savings in the investment in equipment necessary to meet any given tonnage. The immediate benefit represented an increase in capacity in excess of 10%, other things remaining equal. At the much higher haulage rates made possible (and since realised) however, the overall impact is much greater than 10%. Incidentally, in the Hamersley context, running times on the main line constitute approximately one third of train cycle time, with the remainder spent in terminals at the mines and port.

Typically, the fixed signal arrangements between crossing loops are shown in Fig 3.

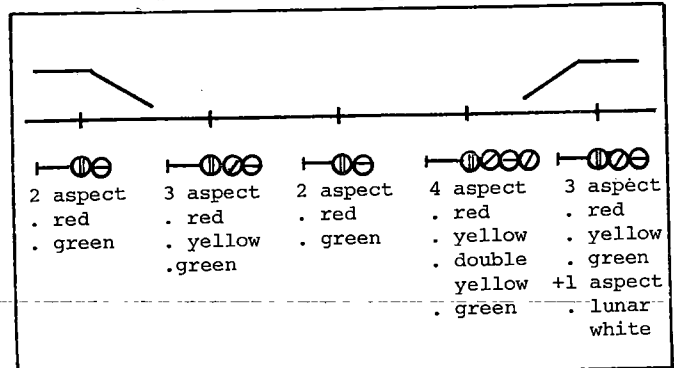


FIGURE 5. FIXED SIGNAL ARRANGEMENT

The installation of the CTC in the configuration shown made possible further incremental steps in the search for added capacity. An example follows.

Control of the Intermediate Signals.

Investment: \$M1

Traffic continued to grow at a rapid rate, at the same time as the track maintenance strategy emphasised the use of small track machinery and labour intensity. In the light of the decision to increase the railway's haulage requirement to 46 Mnt/y, it was clear that a choice would have to be made between more available time on track and more track gangs.

With the signalling arrangements as they stood, an increase in traffic would have reduced the track time available and left no option other than to increase track gang numbers. However, if control of intermediate signals were available, unused periods of track time could be extended to a point where occupancy became feasible in many cases.

Intermediate signals throughout were controlled by the signals at each end of the section and not operated by the Train Controller (Dispatcher) who therefore imposed a requirement that the section be clear between the signals at both ends before allowing a train to enter. As running times through the sections were in the region of 25 mins and gangs were required to clear track 5 mins before a train entered, the implications were:

- . track gangs working close to the end of a section were required to clear track 30 mins before a train reached their work location. As it was possible to have perhaps 5 trains during a work day, they could be stood down for 2.5 hours in an extreme case
- . mechanical gangs, requiring 10 to 15 mins to on and off track machines, would not have enough time to accomplish useful work with trains at close to 25 min intervals and would choose to stay off track with any break less than about 45 mins or more

Control of the intermediate signals would give the Train Controller the flexibility to extend track time availability by half the section running time, thus allowing a surfacing machine, for example, to gain up to 25 mins on each track occupancy period when trains enter from the opposite half of the section.

A careful analysis of the economics indicate that a maintenance cost saving equivalent to the purchase of 10 ore cars annually could be realised, as well as the significant benefit of lessening competition between track forces and trains for track occupancy - in effect, an increase in capacity.

THE CONCRETE DECISION AT HAMERSLEY

Investment: \$M20 (not including installation)

Because the overall profitability of the operation will depend critically on continued use of a single track, it follows that those strategies are favourable which permit the track to be maintained in appropriate condition with minimum need for occupancy. Since sleeper changeout programmes were major users of track occupancy, it was inevitable that attention would focus on the sleeper itself.

On the assumption that the well known properties

of concrete would be beneficial to Hamersley in the long term, a test programme was instituted in 1973 and continued for a number of years. In all, three different types were used at spacings from 610 to 690mm. Close monitoring confirmed the technical performance and increased stability, with a much reduced need for tamping and lining operations. The subsequent fullscale investigation of the comparative economics of timber and concrete(3) was decisive in favour of concrete and the installation programme began in 1980 at the economic rate of 80,000/year.

The major decision having been made, it remained to determine the appropriate values of the control variables: gauge, cant and spacing. Gauge and cant are interrelated in important ways and it is the combination of their values which should be optimised. Because of their lasting effects on subsequent wear rates, a significant research effort was put in the search for the best combination covering such factors as:

- . axle loads and speeds
- . accommodation of lateral excursions
- . flanging forces
- . wheel/rail contact points and band width
- . rolling stock characteristics
- . track configuration

This has led to the adoption of the following:

- | | | |
|---------|---------|--|
| . gauge | 1435mm | +5
-2 |
| . cant | 1 in 40 | (which represented a change from the existing 1 in 20) |

Unlike gauge and cant which are based on technical factors relating to wear, spacing is largely economic, within technical limits imposed by material properties. The conflict between capital cost (which tends to dictate a large spacing) and cost of maintenance (which does the opposite) suggests the existence of a value or range of values which will optimise overall cost. Again, extensive research, explained in some detail elsewhere(5), led to the adoption of 610mm (24in).

Experience on concrete to date indicates the virtual elimination of sleeper replacement and a sharp reduction - of the order of 50% - in routine tamping and lining operations. This translates into a saving of 400 track occupancy hours annually which is an important contribution to the objective of eliminating competition with ore trains.

WORKSHOP UPGRADE

Investment: \$M6

To replace primitive facilities which existed beforehand, a 12,500m² workshop for locomotive and ore car maintenance was built in the early 70's as a consequence of the Paraburdoo mine. It was designed with the far sighted objective of supporting a haulage of 79Mnt/y. By the mid 70's, however, inefficiencies in area utilisation would probably have limited the output capacity to not much more than half of the target value.

The 1976 decision to raise system capacity to 46Mnt/y from the level then current of about 35Mnt/y meant that the Railway would have to have increased locomotive and rolling stock availability. This was achievable in two ways: acquiring more fleet units, or raising the availability of the present fleet. In

the event, the decision was made to proceed with a combination of the two alternatives, as total dependence on the former was uneconomic, while the latter by itself, could not achieve the desired result. The increase was therefore to be achieved by purchasing 7 locomotives and 350 ore cars (bringing the total fleet to 47 locomotives and 2476 ore cars) and by increasing the existing availabilities.

To haul the commitment of 46Mnt/y the mechanical availabilities would have to be 87% for locomotives and 99% for ore cars, compared with historical averages of 73% and 92% respectively.

A study to eliminate the bottlenecks which had developed in the workshops concentrated on the following:

- . the access problem involving such matters as materials receipt, handling and availability, and work practice limited by the number of pits installed
- . low productivity, caused by the condition of existing cranes, movement patterns of locos and ore cars, and fuelling and sanding locations
- . environmental aspects, in terms of lighting, noise and fume levels, and "house-keeping"

The necessary remedial work was carried out under a three stage programme and subsequent experience indicates that the target availabilities are realistic. Values of 85% for locomotives (with 5 replacements due in '82), and 97% for ore cars are achieved fairly regularly at the present time.

The alternative, a fleet increase to 56 locomotives, and about 275 more ore cars (assuming mechanical availabilities at historical levels), would have cost about four times as much.

CONCLUSION

Dealing in a low value, high volume commodity like iron ore brings its own imperatives. The "low value" implies close attention to cost margins in a competitive industry. This suggests the relative importance of economic transportation, achievable only by maximum use of highly capital intensive plant and equipment. The "high volume" suggests a pre-occupation with capacity.

The projects outlined here indicate some of the steps taken by Hamersley in response to these imperatives. The techniques may change over time; the end objective does not. It is minimum transportation cost per tonne of ore at any level of haulage. Individually and collectively, the investments described have contributed to that objective. Besides being economic in their own right, they have increased capacity by:

- . reducing the competition between track maintenance forces and ore trains for track time
- . reducing the interruptions to train operations arising from premature wear and failure of components
- . facilitating the operation of longer and heavier trains at higher speeds (and therefore lower overall cycle times)

Additionally, what is clear is that, without the

change in strategy from cure to prevention, through the application of technology based on research, Hamersley would probably not have reached its present haulage capacity, let alone postured itself for future increases.

REFERENCES

- 1 Purcell, M.S. "Economics of a Heavy Haul Railway", Heavy Haul Railways Conference Proceedings, Sept 1978.
- 2 Mair, R.I. and Marich, S, "Heavy Haul Tracks May Accept 35 tonne Axle Loads", Railway Gazette International, August 1981.
- 3 Fahey, W.R. and Perkins, N.D., "Track Upgrading Cost and Benefit". 3rd International Rail Sleeper Conference Proceedings, Brisbane, September 1979
- 4 Curlewis, W.P.C., "18,000 Tonne Ore Trains in Australia" Railway Engineering Journal, May 1974
- 5 O'Rourke, M.D. "Methodology for Selecting Sleeper Spacing" B.H.P. Melbourne Research Laboratories Report No. MRL/C77/78/27(1), May 1978.

Optimising Operational Modes on the Mt. Newman Mining Company Railroad

D.N. Brown

Operations Planner/
Analyst, Railroad Technical Dept., Mt. Newman Mining Co. Pty. Ltd.
Port Hedland, Australia

Dr. J.H. Brown

Superintendent
Railroad Technical Dept.
Mt. Newman Mining Co. Pty. Ltd. Port Hedland
Australia

Increasing costs have led to an ongoing review of the operating strategies of the Mt. Newman Mining Company Railroad. A number of unit train operations have been examined using a computer simulation, (TRAINOPS) and a costing model developed to enable financial evaluations of alternative expansion paths to be carried out. A preferred strategy for a limited capacity increase has been determined and variations to the existing operation such as banking of trains and increased axle load on ore cars investigated.

INTRODUCTION

The Mt Newman Mining Co operates a single track railroad over 420kms between the iron ore mine at Newman and the ore handling and shiploading facilities at Port Hedland. Unit trains of 3 locomotives and 144 ore cars are operated on a basic 10 train per day timetable. Continuing increases in railroad operating costs, particularly fuel, operating labour, track and rolling stock maintenance costs have resulted in an ongoing review of operating procedures to determine possible alternatives likely to reduce, or at least contain, operating expenditure. The work carried out to reduce track maintenance costs, particularly through the use of high strength rails and steel sleepers has been described elsewhere (1). In the operations area, studies have been carried out into a number of limited expansion strategies to determine the preferred (cost optimum) expansion path and also to examine the effectiveness, in terms of total operating cost, of some possible changes to the method of operating the Railroad.

EXPANSION PATHS

In the thirteen years since its commissioning, the Mt Newman project has increased from an initial capacity of 5 million tonnes per year (mtpy) to 40mtpy today. Railroad capacity was increased primarily by increasing the number of passing sidings (or loops) to allow for 16 train paths in each direction per day and the installation of centralized train control (CTC).

Since then, a variety of expansion alternatives have been considered. These have been mainly, an increase in train length due to the operation of "locotrol" trains, up to 270 cars in length with remote controlled locomotives approximately two thirds the way along the train or alternatively, allowing the use of longer trains with headend only power by reducing the ruling grade; the Chichester Regrade. Increasing the number of trains per day was not seen to be a viable option because of congestion effects and reduced availability of the track for maintenance. Duplication of the track, either wholly or partially was seen to be desirable at very large tonnages if maintenance requirements were to be met.

In the long term, the staging of these expansions has significant financial effects on the Mt Newman Project. Figure 1 shows a simplified decision tree that describes graphically the alternatives open to the Railroad. The tree is simplified because each branch requires the evaluation of further alternatives to obtain the optimum strategy for each branch.

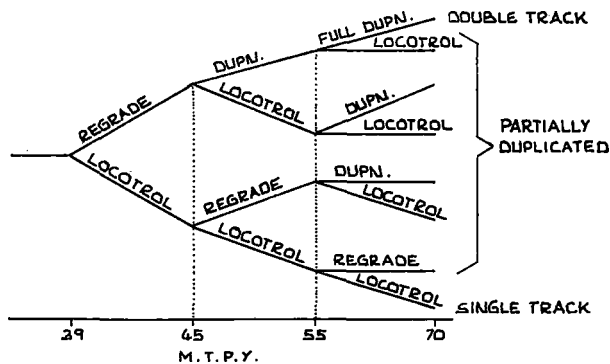


FIG 1 - DECISION TREE FOR EXPANSION

Rama Rao (2) and Pearce (3) described those engineering and economic factors which influence the design of a unit train railway for a specific tonnage to be hauled. The Mt Newman problem is different in that an initial investment has been made and the existing operating system is taken as a starting point. Thus, while microeconomic theory states that the optimum plant capacity is that for which total costs are at a minimum, it is possible that a limited time horizon for a financial evaluation may result in the chosen strategy not necessarily being the theoretical cost optimum. For example, an alternative operating scheme might result in operating costs being significantly lower than the existing case, however, the large capital input required might not be recouped within the given time horizon defined by investors expectations. The financial analysis would then show this project not to be viable. Considerable care is therefore required in selecting the period over which the project is to be evaluated.

Computer Modelling of Operations

The effect of increased congestion, due to the running of additional trains on a single track railway, indicates a realistic maximum number of trains to be less than the design capacity of the line. A number of methods using either queueing theory or simulation have been developed to predict the effect on overall capacity of increasing train numbers (4), (5) and (6).

Purdon, et al (7) described the development of a computer simulation of the Mt Newman Railroad used to assess a number of investment alternatives. One of the major benefits of the simulation approach is the relative ease with which small changes in the track regime can be studied. This also applies to changes in any other of the input variables such as section running time, delay probability and duration, timetabling, variations in loading and dumping times, availability of loadout and dumping facilities and alterations to the train consist (ie. the number of locomotives and cars in a train).

Purdon's model has since been upgraded and is now known as TRAINOPS. Table 1 shows the results of some recent simulations investigating the effect of increasing the number of trains per day within the existing maximum sixteen train paths (or slots) per day in each direction. Examples of the actual printout are given in Appendix I.

TABLE 1
COMPUTER SIMULATION RESULTS

	10tpd	11tpd	12tpd
Loaded Travel Time	7:47	7:47	7:52
Empty Travel Time	8:55	9:02	9:19
Loco Turnaround Time	23:59	23:51	24:31
Ore Car Turnaround Time	31:51	31:31	31:02
Trains Scheduled	276	288	316
Trains Run	265	271	282
% Run/Sched (effic)	94.5%	92.6%	87.6%

Note: Fleetsize constant - 44 locos, 1975 cars.

These results show that for the present fleet size, attempts to increase the number of trains run per day does not achieve the desired objective fully. The model indicates two possible solutions. The first is to purchase more rolling stock to overcome the shortfall in available cars. The second, and obviously preferable solution is to improve the utilization of the existing fleet by reducing queueing times at the terminals. This could be achieved only by improvements to part of the ore handling plant, an area outside the concern of this paper but not necessarily Railroad planners.

The Operations Study

A study of some operating alternatives for the Mount Newman Railroad based on the decision tree shown in Figure 1 has been carried out (8).

The methodology for the study is shown schematically in Figure 2. Tonnage levels for the expansion can be assumed but are usually based on a marketing assessment that is used for planning purposes throughout the Company. It was seen that three separate models would be necessary to complete the study: TRAINOPS, a Costing Model and an Evaluation Model. A limited number of operating strategies were formulated for each specified tonnage level and each strategy was simulated by TRAINOPS to obtain the various fleet requirements, i.e. the number of locomotives and ore cars required to actually operate the railroad for each scenario. The results for the chosen strategies are shown in Table 2.

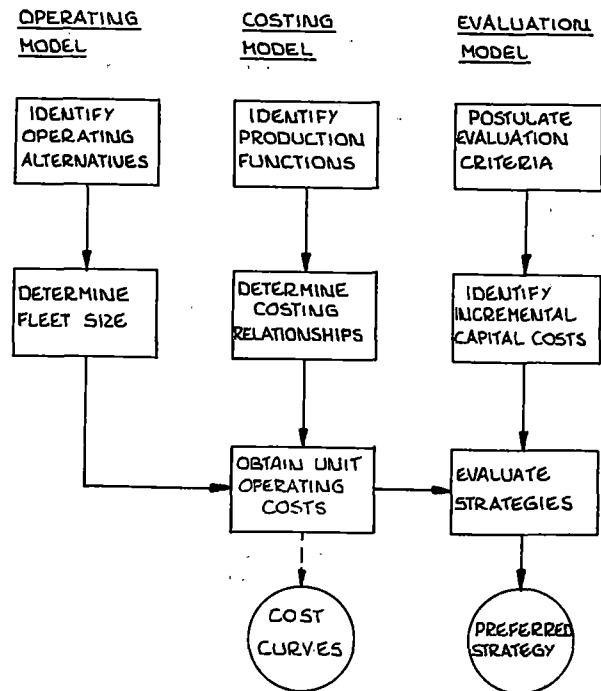


FIG 2 - STUDY METHODOLOGY

TABLE 2

OPERATIONS STUDY SIMULATIONS

	STRATEGY										
	1	2	3	4	5	6	7	8	9	10	11(4)
Tonnage (mtpy)	38.0	38.0	38.0	40.0	40.0	40.0	42.5	42.5	42.5	42.5	42.5
No of std trains/ day (1)	9/10	10/11	11	8/9	10/11	9/10	7/8	10/11	8/9	10/11	13
No of locotrols/ day (2)	1	-	-	2	-	1	3	-	-	1	-
Standard consist(3)	3/144	3/152	3/144	3/144	3/156	3/144	3/144	3/168	3/146	3/144	3/138
Locotrol consist	5/240	-	-	5/240	-	5/230	5/240	-	-	5/230	-
Empty Time	9:31	9:11	9:12	9:39	9:17	9:33	9:19	9:25	9:07	9:57	9:57
Loaded Time	7:47	7:54	7:49	7:46	8:00	7:49	7:47	8:10	7:51	7:57	7:54
Loco Turnaround	24:48	24:59	24:22	24:32	25:08	24:56	24:59	26:18	25:04	26:22	24:49
Car Turnaround	37:30	37:01	32:53	37:41	34:23	35:22	37:55	37:42	38:58	40:50	36:51

- Note: (1) 9/10 and 10/11 refers to existing 69 train per week timetable ie.
10 trains on 3 days, 11 trains on 3 days, 6 trains on track
maintenance day
(2) 1, 2 or 3 locotrol trains per day for 6 days of the week
(3) No of locos/no of ore cars
(4) Two loadout tunnels required

The Costing Model

A rudimentary costing model was developed using actual financial data to predict total operating costs based on production parameters. The output (or production function) of the railroad was defined as:

$$O = D \times T \times C_T \times P$$

where O = the output or capacity (mtpy)
D = the number of railroad operating days per year
T = the number of trains per day
C_T = the number of ore cars per train
and P = the payload or tonnes of ore per car

For the theoretical capacity, D is fixed at 363 days per year (the plant is shut down for Christmas Day and Boxing Day) but T, C_T and P vary according to the strategy under consideration. The actual operating capacity or output will be less than this figure due to such factors as production losses from industrial disputes, effects of cyclones, manning shortages and interaction effects with the Mine and Port areas.

The special case of changes in P or payload is discussed below. Relationships were developed for the major cost accounting areas in the Railroad, eg. Locomotive Overhauls, Fuel, Train Operations that expressed total costs in terms of the production function above. As an example, Loco Overhaul Costs are a function of the number of locomotive kilometres run per year, these are in turn directly proportional to the number of locomotives per train and the total trains run per year. The number of locomotives per train depends on the train length and payload and the total number of trains is dependent on train length, payload and required output.

The total costs comprised fixed and variable cost elements. Fixed costs included administration and supervision, maintenance of fixed plant and some non controllable costs such as annual leave pay loadings. Variable costs comprised those expenditures that varied directly with the output of the accounting areas. Diesel fuel usage was calculated separately as a wholly variable cost. The operation of the Signals and Communications Department, on the other hand, was treated virtually as a fixed cost. In contrast to normal economic explanations of fixed and variable costs, operating labour for the Mt Newman Railroad is essentially a fixed cost because the major part of the workforce is in the track and rolling stock maintenance areas.

At present, the Costing model calculates track maintenance costs on the basis of the incremental gross tonnage over the track. If, as is proposed, the opportunity is taken of reduced ore demand to upgrade the standard of the track even further by rerailling with high strength rails and installing steel sleepers, actual costs will be significantly higher than those predicted by the model. It is proposed to modify the model to account for such planned replacements. Similarly, the additional costs of upgrading rollingstock to a higher standard is not incorporated in the present model. This is also to be rectified.

It is anticipated that the changeover of the Mt Newman accounting system to Responsibility Costing techniques will allow actual operating costs to be accurately determined. Equipment and Job Costing will permit the model to predict more closely cost performance. In its present form, the model can be used for evaluating the relative changes in operating costs faster and more easily than has been possible in the past.

Results of the Costing Model

Use of the model to date indicates that changes in operating strategies have a relatively small effect on the cost of raiiling a tonne of ore however it must be remembered that even small changes in unit costs can mean large absolute changes. This finding is in accord with other investigations into the economics of heavy haul rail transportation, (9), and implies a near horizontal long run cost curve, at least over the output range studied. This is shown graphically in Figure 3.

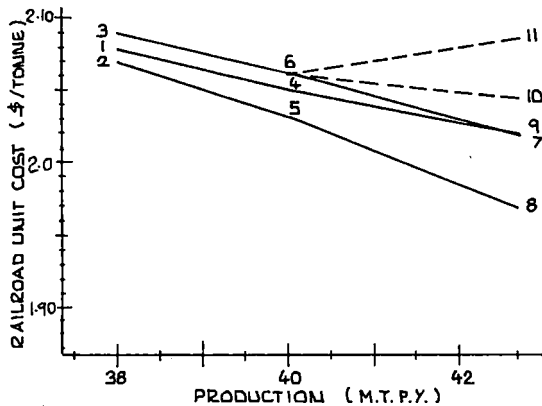


FIGURE 3 - UNIT COST VS TONNAGE

Financial Assessment

Once the operating costs had been obtained for each strategy, a Discounted Cash flow (DCF) Analysis was performed to evaluate the overall performance of the alternatives. Capital inputs, such as additional rollingstock and track work, were costed and the total discounted cost of each alternative over 15 years was obtained.

The Evaluation Model used for this exercise was a computer package developed in house for Mt Newman Mining Co applications (10). This model applies different inflation factors to capital, operating, maintenance, fuel and salvage costs, allows a choice of depreciation methods for capital, assesses taxable savings and discounts the cash flow at a chosen rate to obtain the Net Present Value (NPV) of the cash flow. Alternatives are ranked according to their NPV's; internal rates of return can also be calculated.

Table 3 shows the ranking of the alternatives for both annual operating cost and NPV of total costs (including capital) over a 15 year project life. Internal rates of return on investment have yet to be determined.

TABLE 3

RANKING OF ALTERNATIVES

STRATEGY(1)	TONNAGE (mtpy)	ANNUAL COST (2)	NPV OF TOTAL COSTS(2)
1	38.0	1.0000	-
2	38.0	0.9955	-26.2
3	38.0	1.0030	+13.9*

4	40.0	1.0382	-21.6
5	40.0	1.0272	-33.4
6	40.0	1.0413	-11.2*

7	42.5	1.0866	-52.6
8	42.5	1.0806	-61.4
9	42.5	1.0869	-47.7
10	42.5	1.0972	-42.5*
11	42.5	1.1139	-53.0

- (1) See Table 2 for explanation.
- (2) Both relative to alternative 1.

From Table 3, the preferred expansion path can be seen to be through alternatives 3, 6 and 10 since this path minimises the NPV of costs at each tonnage level. For the Mt Newman Railroad this indicates the preferred path to be one of increasing the number of trains to a maximum of twelve per day and limiting locotrol operation to only one train per day.

As noted above, the choice of the time span of the evaluation can have a marked effect on the ranking of the alternatives. If the period is not long enough, capital costs cannot be offset by increasing operating cost differentials due to inflation. The result is an expansion path that might unnecessarily defer capital inputs. It is believed that an evaluation period of 25-30 years is more suited to projects such as capacity increases for heavy haul railroads. This could possibly alter the ranking indicated above and will be the basis for further investigation.

VARIATIONS TO EXISTING OPERATIONAL MODE

As a result of increasing costs and other economic factors, the MNM Railroad is investigating two major changes to its existing operating practices. The first of these involves the introduction of "banking" locomotives to assist loaded trains over the ruling grade in the Chichester Ranges and the running of two locomotives, instead of three, at the head of each train. The second is increasing axle load by approximately 10%.

Banking

Banking had previously been thought not viable due to maintenance problems with locos stationed halfway down the line and lack of control prior to the installation of CTC.

Preliminary investigations using the Operating and Costing Models indicated substantial savings in the number of locomotives required and hence maintenance savings and fuel usage. Calculations indicate that between 12-18 locomotives are effectively redundant with a consequent 25-30% saving in loco maintenance and 10-11% savings in fuel usage. It is estimated that in the order of \$3-6 million per year could be saved by operating Mt Newman trains in this way.

Increased Axle Load

The second alternative under consideration is to increase the axle load on the Railroad from 30 tonnes to 32.5 tonnes and perhaps ultimately to 35 tonnes. Mair and Marich (11) give an overview of the research that has led to this proposal being considered.

By increasing axle load by 2.5 tonnes the payload of each car can be increased by approximately 8-10%. Due to the constraint of the locomotive's tractive effort on the ruling grade, gross trailing load can not be increased, thus train length has to be reduced. However, due to the increased car loading, the total payload of the shorter train is still 2-3% greater than the original train. Ore cars are then being used more efficiently, reducing the need for replacement or additional cars and the total number of trains required to haul a specified tonnage per year is reduced. This results in fuel and maintenance savings.

Studies by the BHP Melbourne Research Laboratories (MRL) have estimated the impact of the higher axle load on the track and rollingstock (12). Based on this work, internal evaluations (13) have shown that despite increased track maintenance costs (due to increased transverse defect rates and reduced fatigue life of rail necessitating replacement) the proposal is financially viable provided optimistic assessments of defect rates eventuate. The evaluation shows net operating cost savings of 1-2% for the optimistic set of assumptions regarding rail and car bearing life. It is proposed to increase axle load to 32.5 tonnes and closely monitor the effects. One of the other major determinants in this proposal is the fact that all Mt Newman rail is to be replaced with head hardened rail which has a significantly longer fatigue life and is more defect resistant than standard carbon rail.

CONCLUSION

Some of the efforts to optimise the Mt Newman Railroad operation and minimise operating costs have been described. A working computer simulation of the Railroad's operation and the first operating cost model have been developed. The use of these and the evaluation cost model in determining a preferred expansion path has been shown.

Future efforts will be directed towards developing the Operating and Costing Models to more accurately reflect the actual operation of the Railroad in physical and financial terms. A long term goal of this development process is the incorporation of all these models into a planning package suitable for determining the optimum strategy using operations research techniques (14).

The development of such models and techniques is seen to be essential if management is to make well informed decisions regarding the long term development and operation of the Railroad in an increasingly uncertain economic environment.

References

1. Brown, J.H., and Baggott, M.G., "Track Maintenance Management on the Mt Newman Mining Railroad", Proceedings of Second International Heavy Haul Railway Conference, Puetelo, Colorado, September, 1982.
2. Rama Rao, B.V., "Optimisation Analysis for Economic Generation of Transport Capacity on Heavy Haul Railways", Proceedings of Heavy Haul Railways Conference, Inst. of Eng, Aust and Aust. Inst of Mining and Metallurgy, Perth, Australia, September, 1978.
3. Pearce, J.F., "System Design Concepts for Modern Unit Train Operations", Proceedings of Heavy Haul Railways Conference, Perth, Australia, 1978.
4. Kehr, C.L. Kloer, C.D. and Pai, A.N., "Estimating Railroad Line Capacity", Proceedings of SMR Computer Simulation Conference, Newport Beach, California, 1978.
5. Elbrond, J., "A Method for the Calculation of the Capacity of a Single Track Railroad System", Proceedings of Heavy Haul Railways Conference, Perth, Australia, 1978.
6. Petersen, E.R. "A Line Capacity Model", The Eighties: A New Rail Era, Canadian Institute of Guided Ground Transport, 1978.
7. Purdon, R.L., Elbrond, J., and Clark, J.M., "A Comparison of Theoretical and Actual Traffic Schedules on the Mt Newman Railroad", Proceedings of Heavy Haul Railways Conference, Perth, Australia, 1978.
8. Brown, D.N., "Computer Simulation of Mt Newman Mining Company Railroad Operations", RR/80/81/07, March, 1981 Mt Newman Mining Company Pty Ltd., Australia.
9. Rieber, M. and Shao, L.S., "Comparative Coal Transportation Costs: An Economic and Engineering Analysis of Truck, Belt, Rail, Barge and Coal Slurry and Pneumatic Pipelines", PB273 380, August, 1977, U.S. Dept. of the Interior.

- 10 - , "An Introduction to Discounted Cash Flow Techniques Using the Data General Computer", Mt Newman Mining Co Pty Ltd., 1980.
- 11 Mair, R.I. and Marich, S., "Heavy Haul Tracks May Accept 35 tonne Axle Loads", Railway Gazette International, August 1981, pp637-641.
- 12 O'Rourke, M. "Effects of Increasing Axle Load", MRL/CB/8/81/(draft), BHP Melbourne Research Laboratories, April 1981.
- 13 Brown, D.N.. "The Effect of Increasing Axle Load on the Mt Newman Mining Railroad", RR/80/81/15, December 1981 (draft), Mt Newman Mining Co Pty Ltd., Australia.
- 14 Anderson, E.P., "Development and Use of Computer Models for Analysis of Long range Planning Decisions at Southern Pacific Company", Proceedings of Fall Joint Computer Conference on Development and Use of Computer Models, 1968.
- 15 Koutsoyiannis, A., Modern Microeconomics, 1st edn, Macmillan, London, 1975, pp105-150.

APPENDIX I

1.1 TRAINOPS OUTPUT (SUMMARY)

RAILROAD SIMULATION OUTPUT

DURATION IN WEEKS : 4
 TRAINS SCHEDULED PER DAY : 11
 CAPACITY OF MINE LOOP : 3
 NUMBER OF LOADOUTS : 1
 NUMBER OF DUMPERS : 1
 DUMPING FACTOR FOR DUMPER 1 : .00
 DUMPING FACTOR FOR DUMPER 2 : 1.21
DIESEL
 LOADED TRAVEL TIME : 7.44 HH.MM
 EMPTY TRAVEL TIME : 8.24 HH.MM
LOCOMOTIVE DETAILS
 FLEET SIZE : 44
 SYSTEM AVAIL : 38
 SCHEDULE AVAIL : 16
 SICK LOCOS : 0
 TURNAROUND(STD) : 23.09 HH.MM
 TURNAROUND(LTRL) : .00 HH.MM
ORE TRAINS
 EFFICIENCY FACTOR : 73.1 %
 TRAINS SCHEDULED : 276
 TRAINS RAILED : 206
 STANDARDS : 206
 LOCOTROLS : 0
 LATE FROM HEDLAND : 133
 LATE FROM NEWMAN : 76
 TRAINS CANCELLED : 69
 EQUIPMENT TRAFFIC : 0
ORE CAR DETAILS
 FLEET SIZE : 1975
 SYSTEM AVAIL : 100.0%
 SCHEDULE AVAIL : 67
 CARS SCHEDULED : 39744
 CARS RAILED : 29049
 RAKE TURNAROUND : 44.23 HH.MM
SUPPLY TRAINS
 SCHEDULED : 8
 LATE FROM HEDLAND : 2

RAIL DEFECTS
 NUMBER : 8
 AVERAGE DURATION : 1.27 HH.MM
 NO. TRAINS DELAYED : 7
 AVERAGE DELAY : .53 HH.MM

1.2 COSTING MODEL OUTPUT

RAILROAD OPERATING COST MODEL
 D N BROWN NOVEMBER 1981

RUN TITLE OY14 - ANTICIPATED 30MTPY

**** TARGET TONNAGE = 30.00 MTPY(DRY) - PRODN
 **** PRODUCTION = 29.99 MTPY(DRY)
 RAILINGS
 **** NOMINAL RAILINGS = 40.00 MTPY(DRY)
 **** MAX. ACHIEVABLE = 45.21 MTPY-NOM * %EFF
 RAILINGS
 **** SIMULATED = 45.74 MTPY
 RAILINGS

STANDARD TRAINS/YEAR = 2214
 LOCOTROL TRAINS/YEAR = 0

TRAIN SCHEDULE
 10.0 STANDARD TPD - 3 LOCOS, 144 CARS
 0.0 LOCOTROL TPD - 0 0

TRACK CONFIGURATION
 REGRADE - N
 DUPLICATION - N
 DUPLICATE KMS = 0.00
 ADDITIONAL SIDINGS = 0

ROLLINGSTOCK FLEET SIZE
 LOCOS - SIMN INPUT 44, CALCULATED 31
 - TOTAL FLEET REQUIRED = 49
 - AVAILABILITY = 76.0%
 CARS - SIMN INPUT 1975, CALCULATED 1913
 - TOTAL FLEET REQUIRED 1993
 - AVAILABILITY = 96.0%

RAILROAD EFFICIENCE
 - SIMULATED = 94.4%
 - OBS. OPNS = 97.5%

OPERATING COST

I AREA	COST
1 2453	*.****
2 2454	*.****
3 2455	*.****
4 FUEL	**.*
5 2456	*.****
6 246-	**.*
7 2471	*.****
8 2472	*.****
9 2473	*.****
10 2474-6	*.****
11 2489	*.****
TOTAL	**.*

AVERAGE COST/TONNE = \$ *.****
 AVERAGE COST/T.KM = \$ *.*****

An Engineering Statistical Study of The Impact of Axle Weight on Roadway Maintenance Expense

W.G. Hanks

Canadian National
Railways, Montreal
Quebec, Canada

M.D. Roney

Canadian Institute of
Guided Ground Transport
Kingston, Ontario
Canada

Manager
Engineering Systems
Office of Chief Engineer
CP Rail, Montreal
Quebec

In response to current costing procedure's inability to reflect the effect of heavy axle equipment on maintenance-of-way expenses, Canadian National undertook a major effort to introduce these effects into cost estimating. An engineering model of rail life was constructed to develop equivalence weightings for gross ton-miles of traffic with various axle loads and speeds moving over tracks of differing design and curvature. Weighted gross ton-miles produced a substantial improvement in the regression model's ability to explain variations in recorded maintenance-of-way expenses. This method also enabled testing other factors of cost causality, most notably line density. This revised cost function combined deterministic and probabilistic models. This highly specific costing tool can quantify influences of main causal variables affecting roadway maintenance costs, previously hidden within system averages. The paper reviews the evolution of the costing model, presenting sample results.

INTRODUCTION

In the spring of 1977 the Canadian National Railways costing department turned its attention to the inadequacies in the way it was allocating Roadway Maintenance expenses in variable cost estimates of point to point traffic moves. This was principally brought about by the growing awareness of the effect that heavy axle equipment was having on maintenance-of-way expenses, an effect that was not being reflected in these estimates. This was exemplified in the historical expenditures in the western Mountain Region, which represented perennial outliers in statistical analyses of costs using conventional workload measures.

An investigation was therefore launched to provide, in general terms, an improved estimate of the variable roadway maintenance expenses, specifically allowing for the effects of different axle loadings. In fact, since the Canadian National mainland division on which the study was conducted comprises some 31,700 miles of standard gauge track with wide ranges of terrain, density, rail weight, curvature and speed, the study, not surprisingly, uncovered such a range of different and interactive influences on costs that it has only recently been brought to a useful conclusion. This paper reports on both the success and pitfalls of this study, with the view that both contain important inferences about roadway maintenance cost behaviour.

Cost Complex Definition

The expenses grouped under the heading of *Roadway Maintenance* expenses, and analyzed in the study, are collected at the Area level and include expenses

recorded in the following U.C.A. accounts¹:

202 Track and Roadway Maintenance
212 Ties
214 Rails
216 Other Track Material
218 Ballast
229 Repairing Roadway Buildings
269 Repairing Roadway Machines
271 Small Tools and Supplies
273 Maintenance of Public Improvements
281 Right-of-way Expenses

To provide some perspective on the magnitude of dollars analyzed, expenses within this group totalled \$110,463,000 in 1978, 48% of the total CN Roadway Maintenance expenses²:

¹ Equivalent to the regulatory accounting system prescribed in the U.S. by the Interstate Commerce Commission. It should be noted that there is a significant difference between the U.S. accounts and the Canadian accounts for Ties, Rail and Ballast. The Canadian accounts include material for spot renewals only, but include the labour for periodic maintenance and replacement.

² The balance of the Road Maintenance expense accounts covering items such as system and regional headquarters expenses, superintendence, tunnels, bridges, culverts, elevated structures, and building and structure (other than roadway building) maintenance, depreciation, communication systems, signals, removing snow, ice and sand, insurance, injuries and other miscellaneous items were not analyzed in this study. Some of them are in fact affected by this analysis since they are assigned in the costing system in direct proportion to roadway maintenance expenses.

PREVIOUS COSTING MODEL

For the past number of years the extent of variability of this group of costs with traffic has been ascertained through multiple regression analysis. The observations for the dependent variable are the total expenses recorded in these accounts for each of CN's 15 mainland administrative areas. The explanatory variables used are the corresponding five year totals within each area of *Miles of Roadway (MOR)*, *Grade And Curve Index (G&C INDEX)*, *Yard And Train Switching Minutes (YTSM)* and *Gross Ton Miles (GTM)*, i.e.

$$Y = a + b(MOR) + c(G&C INDEX) + d(YTSM) + e(GTM) \quad (1)$$

where Y is the 5 year total of expenditures for each accounting area and a,b,c,d and e are unit cost parameters estimated by the regression procedure.

According to this formulation, fixed costs, as captured by the first two variables and the constant term in the equation, are estimated to be some 18% of the total expense. The variable *terminal maintenance* costs, which are not separated from line expenses in the accounts, are estimated at 20.6% of variable cost, based upon the parameter estimate for *Yard and Train Switching Minutes*. Variable *line* costs, as discerned through the explanatory power of *Gross Ton-Miles*, are 61.4% of total expense. These results are based upon separate regression analysis of *Labour* and *Other* expense, a practice that was adopted to facilitate the indexing of the historically based costs to current year or future year levels.

Critique of Previous Model

Figure 1 shows the statistical significance of the previous model (Eq. 1) for *Labour* and *Other* expenses. A 't' statistic larger than a value of 2 is generally regarded as being a necessary requirement for the coefficients of the workload variables that are used as variable unit costs, i.e. yard and train switching minutes and gross ton-miles. Note that only the gross ton-mile component meets this requirement in these analyses. This indicates that the other variables did not contribute significantly to the ability of the overall regression model to explain variations in expense totals between the fifteen areas. Overall, the fit is statistically valid, but has clearly not demonstrated a high predictive capability. This is reinforced by disturbing patterns in the residuals.

The existence of a negative intercept parameter in the equation for *Other* expenses, as indicated by the negative 't' statistic on the constant term, is of further concern to the railway. This is because the negative intercept must be allocated over the remaining four values in order to conform to the interpretation of the Canadian regulatory body. The result is that a lower unit variable cost than is actually inferred by the regression is assigned as the basis for subsidy claims and abandonment applications submitted to government.

There are two possible causes for a poor fit of the model to the data. Firstly, the assumption of a linear model, i.e. a linear increase in costs with total traffic activity within a region, is a poor one. Of greater potential significance, however, is the possibility that the explanatory variables selected do not adequately reflect maintenance workloads.

Current Analysis

Labour Expenses	=	Constant	t = 0.6
	+	Cost/MOR X MOR	t = 1.83
	+	Cost/IU X G&C Index	t = 0.63
	+	Cost/YTSM X YTSM	t = 1.62
R² = .74	+	Cost/GTM X GTM	t = 3.59

Other Expenses	=	Constant	t = -1.26
	+	Cost/MOR X MOR	t = 0.97
	+	Cost/IU X G&C Index	t = 0.75
	+	Cost/YTSM X YTSM	t = 1.44
R² = .54	+	Cost/GTM X GTM	t = 2.53

Fig. 1: Statistical Results Using Current CN Roadway Maintenance Cost Model

Review of Explanatory Variables

In a multiple regression analysis it is critical to postulate a relationship between the dependent and independent variables that has some meaningful cost causal interpretation. A review of the existing equation immediately uncovered some shortcomings in the existing formulation when measured critically against this criterion.

Firstly, the constant term in the equation has little meaning. It implies that a constant amount of expense would be incurred in each area regardless of the size of the area, such expense being incurred, in the extreme, even if there were no traffic nor miles of roadway. It was concluded that it should be left out of the equation.

The *Miles of Roadway* variable passed the test of rationality, as it is reasonable to assume that expenses not variable with traffic activity are related to the amount of relevant property to be maintained. *Miles of Track* is not an acceptable alternative due to an inherent relationship between traffic activity and miles of track, specifically more or less terminal switching tracks, sidings, double track, etc.

The *Grade and Curve Index* as formulated in the former model is a component of fixed cost. This does not reflect railway experience which shows that cost differentials on lines traversing severe terrain are exacerbated by traffic.

Yard and Train Switching Minutes is clearly not an ideal variable to describe the roadway cost impact of traffic movement within a terminal area. However, it was acknowledged that it is virtually the only workable measure of this activity and hence must be used.

Gross ton-miles has valid physical meaning as a unit of work as it appropriately combines the accumulated weight sustained by the track structure and the number of miles of track that is subject to the wearing effect. Returning to the prime problem of axle load specificity, however, it was clear that the assumption of this formulation that all gross ton-miles are essentially equal in their cost impact was an unacceptable one, and was a major cause of the general

dissatisfaction with the model.

EVOLUTION OF AN IMPROVED MODEL FOR MAINTENANCE-OF-WAY UNIT COST ESTIMATION

Following the foregoing review of the previous model and resulting analysis, the study commenced with an investigation of explanatory variables that would both expand the specificity of the model and increase its accuracy, (i.e. explanatory power), with particular emphasis on the split between fixed, terminal variable and line variable costs. The revised model was of the form:

$$Y = a(\text{MOR}) + b(\text{YTSM}) + c(\text{WGTM}) \quad (2)$$

where WGTM is the number of gross ton-miles, weighted or segregated by considerations of engineering causality to provide a reliable measure of the relative line maintenance workload.

Selection of an Approach to the Estimation of the Specific Unit Costs

The simplest approach to an estimation of the impact of axle load would be to substitute *Gross ton-miles* segregated by axle load groups in place of undifferentiated gross ton-miles, leaving the regression to statistically estimate the appropriate unit cost coefficients. This approach would, however, require a significant increase in the number of data points, i.e. geographical accounting units, beyond the present fifteen. It was consequently abandoned for possible future consideration in conjunction with necessary account disaggregation.

At the other extreme was the potential use of engineering (deterministic) models. These attempt to build up output cost levels by relating them through engineering cause and effect relationships to the unit costs of the basic resources consumed. It was judged, however, that the complexity of the full engineering costing approach would make its implementation impractical, given the large number of individual cost categories that must be considered. Nor was it deemed to be possible to quantify deterministically the breakdown between fixed and variable cost, the separation of variable costs of track deterioration between line-haul and terminal activities or the complex influences of traffic density.

The approach that was adopted as the rational solution ultimately combined the best features of the above options. It involved retention of the regression approach, with its inherent ability to estimate uncertainty, but substitution of an equivalence weighting for the critical gross ton-mile variable that would result in an homogeneous workload measure. This would weight the variable for differences in the maintenance workload for track structures of different categories carrying similar gross ton-mile densities but with different axle load and curvature characteristics.

Development of a Gross Ton-Mile Equivalence Weighting

Conceptually, an equivalence weighting for track wear would account for the variation in the proportion of energy imparted to the track by a given gross ton of traffic that is not dissipated as elastic rebound. This quantity is known from fundamental engineering concepts to be a joint function of the track stresses and track strength. Therefore axle load, speed and track construction were identified as prime variables. The observation that 'heavy axle load' effects were

most serious on curved track that is additionally stressed by lateral loads was logical within this definition and curvature was identified as a further dimension to an equivalence weighting.

Two potential sources for such a weighting were reviewed. One was the weightings contained in the U.S. Federal Railroad Administration report entitled 'Procedures for Analyzing the Economic Costs of Railroad Roadway for Pricing Purposes'(1). The second was a computerized rail life model that was at that time under development by the Canadian Institute of Guided Ground Transport under CN sponsorship. The two were reviewed critically and it was determined that the latter held a stronger scientific basis in the physics of track deterioration, the former having been built up largely from an extrapolation of a relatively small body of factual data. As a confirmation of this approach, the weightings based upon the CIGGT model gave better statistical results than those obtained when FRA weightings were used in the regression of account totals.

The CIGGT Rail Life Model (2) was developed to specifically estimate the consumption of the rail assets from fundamental mechanics. The objective was to arrive at as true a reflection of the true causality relationships as was possible given the state of the art in the sciences of track/train dynamics, wheel/rail interaction and wear. Of particular interest to the study was the potential of this model for an unbiased prediction of parametric sensitivities. In this regard it was significant that the model had actually been calibrated to rail wear and life experience on both the Canadian National and the Quebec North Shore and Labrador Railway. The specific thrust of this calibration had been towards capturing axle load and curvature sensitivities. Therefore, it could be reasonably assured that Canadian main line conditions and CN operating practices, which were a specific input, were being reflected. The ability of the model to capture the interactive nature of wear causality was a conceptual advantage over the engineering costing models. The inherent inclusion of all original formulae and its multivariate nature were further advantages inasmuch as it would ultimately be necessary to update such formulae to reflect changing railway technologies, eg. concrete ties and steerable trucks.

The fact that the CIGGT model has been constructed as a rail life model was not judged to be a serious deterrent to its ability to model variability in all maintenance-of-way costs. Upon review of the basic model, it was surmised that many of the general mechanisms of mechanical rail deterioration are remarkably similar to those at work on the ties and ballast, i.e. on the whole track structure. Thus, for example, abrasion of rail is analogous to plate cutting of ties and abrasion of ballast particles. Similarly, plastic flow of metal at the wheel/rail contact locations is equivalent to the cumulative shear failure occurring when wood fibres are crushed or ballast is displaced. Rail fatigue, on the other hand, appears to be more sensitive to axle load than failure of tie and ballast, which have an important interaction with natural modes of deterioration. Therefore, the module of the rail life model dealing with rail fatigue life was not used in developing a weighting for variable maintenance-of-way costs.

Similarly, the loadings experienced by the various components of the track in the lateral and vertical

plane vary in direct proportion to those sustained by the rail, and as calculated with the model. The function of the track structure is to spread the load down through progressively weaker strata. Therefore the deterioration response of the various track components is also in proportion to the wear of rail in mature track. In current practice, timbering and surfacing programs are fairly consistently a multiple of the rail renewal cycle and, with increasing mechanization, are frequently scheduled in conjunction with rail changeout activity. Similarly, it was assumed that the attention paid to variable maintenance activities by basic forces are more closely related to the rate at which rail is being deteriorated than to simply the total gross tons moving over the track.

It was therefore decided that the most accurate equivalence weighting that could be developed would be the normalized reciprocals of relative rail lives measured in gross ton-miles as predicted with the CIGGT model suitably modified.³

Categorization of Traffic and Track into Homogeneous Groupings

It was estimated that roadway cost variability due to rail load could be captured initially by separating freight, passenger and fast freight gross ton-miles into a total of 19 categories of relatively homogeneous traffic, based upon significant variations in axle weight and average speed. Similarly, 11 curve classes were assumed, running in 1 degree increments from a 'tangent to 0.5 degrees' category up to a last one covering track curvature over 9.5 degrees. Thus the actual table of equivalence weightings was initially an 11 by 19 matrix of 209 different relative cost factors that could result from any given gross ton-mile moving on the system. Their range is illustrated in Figures 2 and 3.

Axle Load/Curvature Weighting

Axle Load Classes	Curvature Classes					
	Tangent	1°	2°	8°	9°	>9.5°
1) Frt. 0-32 Tons	1.000	-	-	-	-	5.437
	-	-	-	-	-	-
	-	-	-	-	-	-
9) Frt. over 130 Tons	3.846	-	-	-	-	27.581
10) Frt. 6 Axle	5.744	-	-	-	-	36.480
	-	-	-	-	-	-
	-	-	-	-	-	-
19) Exp. 50-78 Tons	1.905	-	-	-	-	12.926

Fig. 2: Sample Range of Axle Load/Curvature Weightings for jointed 115 lb rail and a speed of 30 mph.

³ A number of modifications to the original rail life model, in addition to deletion of the fatigue module, were nonetheless required. Therefore, it was specified that variation in characteristic wheel diameter between different axle load classes would be excluded as wheel diameter has a far greater effect on rail, through the wheel rail contact stresses, than on ties or ballast. Similarly, calculations made for different rail types did not specify different crown radii.

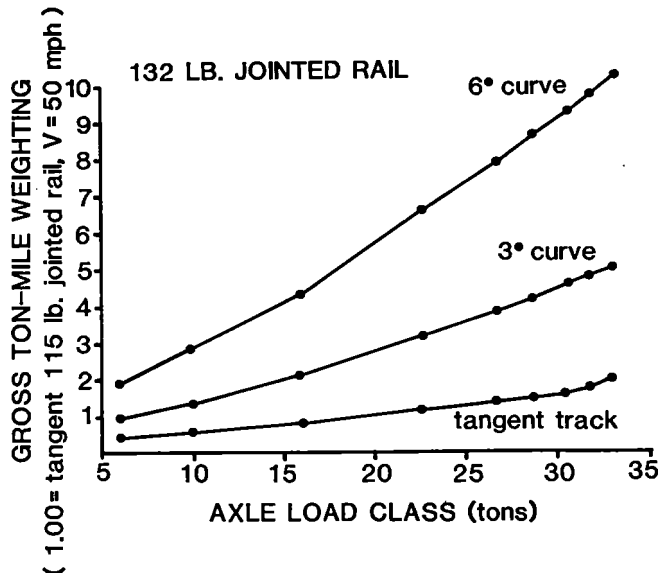


Fig. 3: CIGGT Weighting Factors for Axle Load and Sample Curvatures assuming 132 lb rail and a speed of 30 mph.

As the base assumption of 115 lb/yd jointed track was clearly not representative of all CN rail, additional matrices were calculated to estimate the specific sensitivity of track consumption on both lighter and heavier rail of both jointed and continuously welded construction. The differences were sufficient to result in the inclusion of rail weight as an additional weighting variable. In particular, a large difference was calculated between jointed and welded rail in tangent and low degrees of curvature, reflecting the unfavourable influence of joint impacts. Therefore, tables of equivalence weightings for axle load and curvature classes were produced for track laid with seven different types of rail.

Adjustment for Speed Effects

The seven tables of equivalence weightings were originally developed assuming a system average speed of 30 mph. At the same time, the Train Performance Calculator runs used to determine speeds on all main links showed that a considerable variation from system average speed exists. A review of the deterioration mechanisms led to the prediction that this would have an effect on maintenance-of-way costs that would be both significant and not accurately predicted with the rail model due to the interaction of speed and maintenance tolerance. Due to the intractability of adding a further dimension to the weighting tables (now containing 1463 weightings), it was desired to adjust the tables for speed differences by a relatively simple formula.

It has been the concurrence of the literature sources (1)(3) that speed effects can be applied in a form such as:

$$\text{Speed weighting} = 1 + \frac{V}{A} + \frac{V^2}{B} \quad (3)$$

where V is the average train speed in mph.

The above formula with A = 600 and B = 6000 produced a reasonable approximation of the speed effect

in the range of the system average speed of 30 mph, where the speed component of the weighting tables is estimated to about 17% of the total weightings. Following an evaluation of the ability of a number of equations of this form to explain statistically the variation in normalized roadway expenditures between areas, the above formula was adjusted downward by a speed-specific reduction ratio. Even this was not judged to be sufficient to correctly characterize speed effects on roadway maintenance costs and further refinements were applied.

Firstly, a threshold level of 25 mph, below which changes in speed would have no appreciable effect on maintenance requirements was instituted on the advice of track personnel and following statistical verification that this particular threshold level produced the best improvement in the regression analysis of accounting data.

Secondly, it was estimated that this formula would underestimate the speed effect for lightly loaded cars travelling at from 45-55 mph, as these cars were seen to frequently go into a hunting mode, thus imposing an incremental track damage. To compensate for the contribution of hunting, gross ton-miles in the three lightest axle load classes over tangent track were assigned the weightings of a suitable low curvature if the prespecified speed thresholds were exceeded.

Finally, it was recognized that costs are augmented if the traffic mix is characterized by a large speed range, a common occurrence on CN, which has a significant proportion of lines with both passenger and freight service. This effect stems from the following realities of mixed service:

- both the investment level in track structure and maintenance standards are higher for passenger lines due to the need to maintain a higher level of safety and a certain minimum ride quality.
- superelevation on curves is set closer to the higher speed service.
- design and maintenance standards are a compromise between the requirements of high and low speed service.

It was therefore established that, as a general rule, the wear and tear on track would be nonlinearly proportional to the difference between design speed and operating speed and that this differential could be directly related to the characteristic speed difference between the fastest and slowest traffic classes using the line. Subjective engineering estimates of the effect of speed differentials typically ranged between a 4% to 12% increase in costs with some estimates in the 20% range.

Given these considerations, but a lack of specific data to verify or to even construct a precise representation of this complex effect, a simple adjustment was established. If the speed difference calculated by the Train Performance Calculator exceeded 5 mph, the weighting factor for all gross ton-miles for all traffic on the link was increased by 0.8% for each 1 mph of differential. Both figures were selected from within the range of subjective estimates tested as the combination that produced the best explanatory power in the regression of expenditures.

Multiple Track Effect

There are economies in the maintenance of multiple track as accessibility is improved and maintenance windows are less restricted. Within CN there has been some difference of opinion as to whether the weighting to be applied to additional main track should be 0.7 or 0.8. Following experimentation with the various values in the regression equation, a weighting variable that varies with density of traffic was established. Thus, for example, a second track carrying 30 million gross ton-miles/mile (MGTM) was given a weighting of 0.6, while a second track with up to 5 MGTM was weighted at 0.9.

Effect of Density on Maintenance Expenses

The last influence that the study came to grips with was the effect of line density on variable maintenance expenses. When the study first started, the expectation had been that, with the proper engineering weighting, the cost per weighted gross ton-mile derived from the regression would be reasonably uniform. However, as weightings were added to account for various factors, the statistics consistently inferred that the unit variable cost/GTM was high on low density lines, declined towards a minimum in the medium range densities and started to climb again in the higher densities. This cost behaviour is reflected in Figure 4, which was derived from the regression coefficients resulting when weighted gross ton-miles were segregated according to line density.

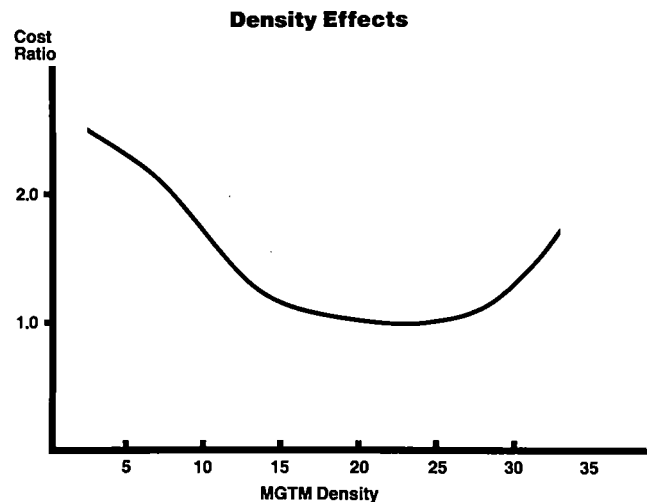


Fig. 4: Effect of Traffic Density on Variable Maintenance Expenses.

This functional form met with the approval of Engineering personnel. They offered the explanation that while on very light density lines the variable portion of maintenance work is a very small proportion of the maintenance effort, it is very high on a per gross ton-mile basis. This was reported to be due to inefficiencies introduced by the small scale of activities, which precluded most opportunities for mechanization, large travel distances between work sites, and was also the result of a significant interaction of environmental and mechanical deterioration (e.g. tie splitting). As traffic densities increase, economies of scale in maintenance can be realized and environmental and mechanical deterioration tend to uncouple (e.g. tieplate cutting).

This efficiency improvement progresses to about 20-25 MGTM/yr. level, at which point there is a

feedback mechanism whereby traffic restricts track time availability. This increases the unit production cost of the maintenance at a rate that outpaces the economies of scale. In fact, the relatively low traffic threshold at which the inflection in the curve occurs may be specific to the CN situation where the highest density lines are found in the least accessible territories.

One Year Lag

As noted earlier, the previous analyses of maintenance-of-way expenses have related traffic volume in a time period to expenditures in the same period. Because of the almost macro nature of these analyses (e.g. cross-section regression over large administrative areas), the simple relationships postulated, and the inherent year to year stability of such aggregate statistics, useable results have been obtained in the past. However, when weightings for a variety of traffic and route specific factors are introduced, it could be expected that the data would become sensitive to the reality of not only a time lag between the cause of maintenance and the act of maintenance but the cumulative nature of the traffic causal factors.

Thus a one year time lag between traffic volume and maintenance expenses was introduced and found to consistently produce a statistically more significant result (higher R^2 , t and F values). The data available did not allow for testing a time lag of more than one year.

Normalization for Cyclic Nature of Capital Expenditures

As a further by-product of the disaggregation of data, the use of 3 or 5 year aggregate (or average) statistics does not adequately compensate for the cyclical nature of a significant portion of the programmed maintenance expenditures. A normalization procedure was therefore instituted to adjust for the fact that 3 year data used in the study would introduce variations between area expenses that were related to these programmed maintenance activities rather than the annual variations in the independent variables used in the analysis. Ideally, under normalization, the expense data itself would be adjusted directly. However, in this study that was not possible since the data to do so were not available and in any event, to do so would have presupposed to some degree the findings of the study.

The only reliable data that were available to work with consisted of a record of the miles of main line rail relayed, by location and by type, for several years before, during, and after the three year study period. The normalization procedure was postulated on the basis that periodic maintenance activity is usually centered around a rail relay, the procedure generally being to ballast and surface 2 years before a relay and timber and surface the year before a relay. This is typically followed by 3 years of considerably reduced costs of spot rail and tie replacements. This assumption means that a periodic rail relay will result in a significant deviation from 'average' maintenance expenses for approximately a six year period.

Estimates were subsequently made of the proportion of the track that would fall within the timing of each of the six years preceding and following rail renewal for each density class within each area. These were based upon the number of miles of new rail laid each year. These estimates were then used in conjunction with a profile of relative expenditures over

a six year period for hypothetical track section undergoing rail renewal to adjust the analysis for distortions due to the timing of maintenance programs.

RESULTS OBTAINED WITH REVISED MODEL

With the application of all the above factors, the roadway maintenance costing model was complete. When the same three year period of data as that analyzed with the current model (Fig. 1) was tested with the new model, the result was a dramatic increase in R^2 , F and t statistics indicating a far greater ability of the model to explain variations in costs between areas. Most importantly, all explanatory variables in the regression became significant and produced estimates of unit costs that were deemed reasonable by both Engineering and Costing personnel. The statistical results obtained with the new analysis (Labour and Other expenses combined) are shown in Figure 5 along with the current Labour and Other analyses, the latter being combined for purposes of the comparison.

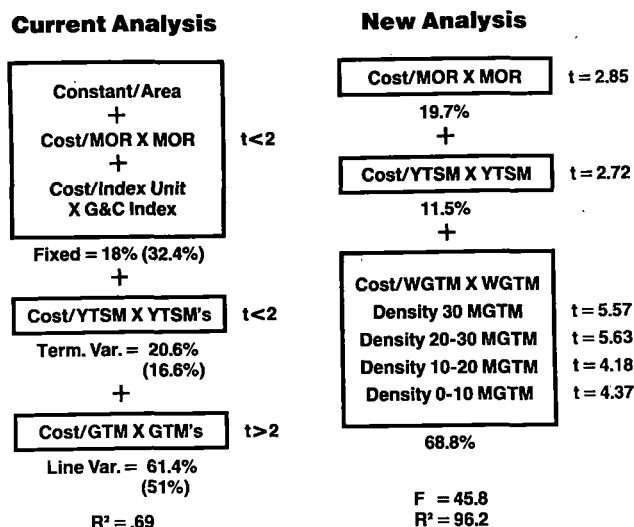


Fig. 5: Comparison of Statistical Results Obtained from Analysis with Current Model and with new Weighted Model

Note that the estimated fixed portion of costs has increased slightly to 19.7%; the linehaul portion has increased somewhat more markedly to 68.8%. The terminal portion, which previously had included cost variability that had not been captured by an unspecific GTM variable, dropped to 11.5% of total Roadway Maintenance expenses. As a sidelight, the bracketed percentages shown under Current Analyses are the percentages obtained when the negative constant value in the Other portion of the analysis is prorated amongst the remaining four variables. These differ from the New Analysis results much more dramatically.

APPLICATION OF RESULTS

The useful output of the analysis is eight unit variable costs for roadway maintenance activities: a variable unit cost per year and train switching minute and seven unit variable costs per weighted gross ton-mile for each of the seven density ranges.

The unit cost per yard and train switching minute could be applied directly in costing applications. There was no change from the way this was being handled in previous procedures. However, to apply the seven weighted gross ton-mile unit costs in cost estimating

required a significant change from the existing procedure of applying a single unit cost to a total gross ton-miles.

The cost analyst had to be provided with a process which could be applied with some facility. This was achieved by producing a set of 16 'Costs per 1000 Gross Tons' for each of the 800 odd segments of the running track used in the analysis. This set of costs was as follows:

- 9 costs by axle loading range for freight traffic
- 3 costs by axle loading range for express or fast freight traffic
- 3 costs for motive power, one each for freight, express and passenger train service
- 1 cost for passenger cars

To compile a variable cost using these tables over a fairly long move is somewhat onerous. To aid this process some aggregated tables were provided for the more frequently used routes.

Examples of the implications of this highly specific costing model to common CN main line movements are given in Figures 6 and 7. These figures report roadway variable costs in the nondimensional form of a percentage of total variable costs of movements in these corridors.

The predictions of the new model are shown as a solid line, while the estimates of the previously accepted model appear as a dashed line. On the Winnipeg-Edmonton run (Fig. 6), over prairie terrain characterized by a largely tangent alignment and a high quality track, variable costs are lower than previously predicted for all but the heaviest cars. Over a more severe terrain and higher density track (Fig. 7), the unit cost of providing track for most cars, and particularly heavy cars, is substantially higher than previously estimated.

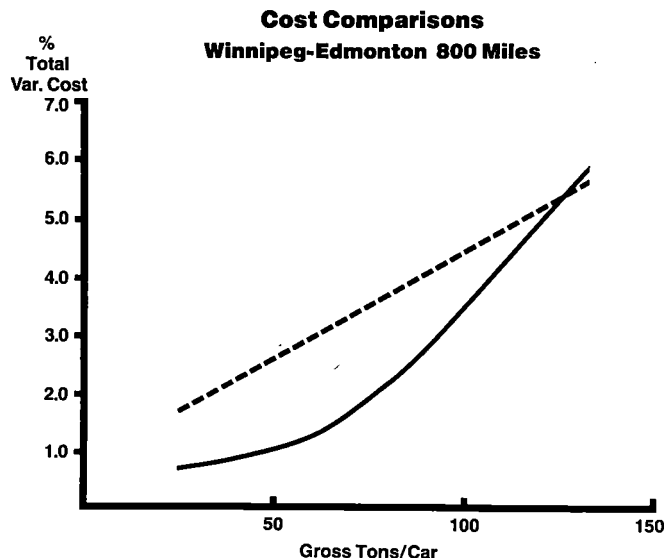


Fig. 6: Comparison of Roadway Cost Predictions of New versus Current Model for Largely Tangent Alignment.

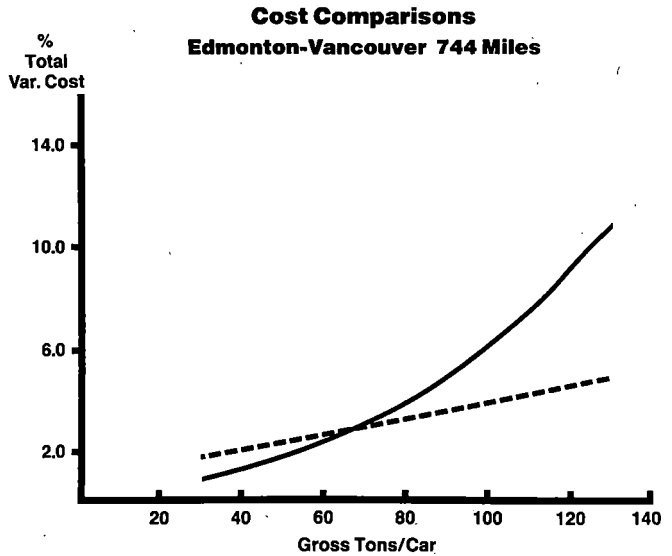


Fig. 7: Comparison of Roadway Cost Predictions of New versus Current Model for High Curvature Alignment.

These results indicate the importance of a proper accounting of the heavy axle load increment. Of perhaps more importance, however, is the consideration of the interaction of axle load and curvature. Separate costing of different traffic density classes is also seen to be paramount.

The revised model is now used for internal roadway maintenance costing by CN Rail and is currently being estimated against current account totals in preparation for introducing it into costing for regulatory purposes. A useful feature of the variable costs that were developed in this study that was not anticipated when the study was undertaken was the ability to predict the effect on the unit costs of proposed or planned changes in speed, different weights of rail, changeovers from jointed to welded rail, discontinuance of passenger trains or reduction in speed differentials, curve reduction, density changes, etc.

PROSPECTS FOR THE FUTURE

While the foregoing is a significant improvement over the simpler model used previously, it cannot be said to be the final model. In terms of applicability the use of the combined engineering/statistical approach would seem to have a long useful life ahead of it. As the basic engineering model from which the GTM weightings were derived is still intact and contains a comprehensive representation of wheel/rail loadings and wear processes, it is conceivable that weightings can be extended to encompass new technology (e.g. premium rail, steerable trucks, concrete ties).

Many areas of improvement in its use are still open for future researchers. Some of these relate to better data, such as better recording of traffic by axle load for each segment of track, better records of average speed while moving over these segments and perhaps most important, a smaller geographical area for recording of expenses to provide a larger 'sample' of expenditures. Others relate to improvements in the basic track force model from which the weightings were

derived, a feature that will probably be a more or less continuous event as research into and understanding of these forces progresses. Still others relate to better understanding and formulation of such items as the adjustments for hunting, for multiple track effects, for speed differential effects.

Lastly, from the researcher and cost analysts point of view, the development of more sophisticated computer use will undoubtedly lead to easier research paths and greatly facilitated application in the area of cost estimating.

REFERENCES

1 Tops On-Line Services, Inc., 'Procedures for Analyzing the Economic Costs of Roadway for Pricing Purposes,' FRA Report No. 16, RPD-11-CM-R, Vol. 1, January 1976.

2 Roney, M.D., Turcot, M.C., and Lake, R.W., 'A model of the Physical and Economic Performance of Rail in Main Line Track,' Proceedings of the First International Heavy Haul Railways Conference, Perth, Western Australia, September, 1978.

3 Peabody, L.E. & Assoc., and Rail Systems Research Associates 'Analysis of Track and Roadbed Maintenance Cost Variability,' 2nd Edition, June, 1977.

M.D. O'Rourke

Senior Research Officer
BHP Melbourne Research
Laboratories, Melbourne
Australia

Engineering Effects of Increasing Axle Load

An in-depth engineering study has been undertaken to determine the effectiveness of higher axle loads in reducing railway costs. The elements of the study consist of detailed technical evaluations of rail, track and vehicle performance, which are utilized to provide cost estimates at higher axle loads. Based on the results, railways adopting high maintenance standards and the latest technological improvements will benefit by increasing axle loads to 33 tons.

INTRODUCTION

Increased productivity in existing railways may be obtained by:

- (i) more intensive utilization of capital resources, e.g. increasing traffic usage of the same line, and
- (ii) reductions in operating costs, e.g. improved maintenance procedures such as rail grinding.

These cost reductions may be obtained in two ways. Firstly, incremental improvements to particular facets of the operation may be implemented. An example of this technique is the introduction of head hardened rails into curves. Alternatively, changes to the major operational variables of the railroad, axle load and speed, which provide limitations to a railway's capacity and efficiency, may be undertaken.

Until recently, 30 tonne axle loads appeared to be the technical economic limit on heavy haul railroads. However, a series of incremental technological improvements, including the introduction of high strength rails, manufactured sleepers and new maintenance procedures such as rail profile grinding, have significantly reduced potential track costs and made feasible higher axle loads. This was particularly the case at Mt. Newman Mining Co. (MNM) where, based on average payloads, ore cars were operating below nominal design capacity (Table 1). In comparison Hamersley Iron (HI) were achieving close to maximum utilization of their cars.

A study was therefore implemented in 1980 to assess the engineering effects of higher axle loads. Three prime areas of engineering concern were delineated, namely;

- track - technical limitations and costs,
- vehicle - technical limitations and costs, and
- rail - technical limitations and costs.

Fifteen cost categories were then developed within this framework. The assessment of the primary factors and their implications upon a decision to increase axle loads forms the basis for this paper.

TABLE 1: ORE CAR AND LOADING CHARACTERISTICS

ORE CAR CHARACTERISTICS	MNM		HI	
	CURRENT* OPERATIONS	35 TONNE AXLE LOAD OPERATION	U.S.A. CARS	JAPANESE CARS
TARE (tonnes)	24.9	24.9	19.0	20.1
PAYLOAD (tonnes)	95.1	115.1	96.1**	94.9**
AXLE LOAD (tonnes)	30.0	35.0	28.8**	28.8**
VOLUME (m ³)	57.3	57.3	45.3	45.3
EST. VOLUME FILLED (%)	75	91**	95	95

* Australian cars only (95% fleet).

** MRL measurements indicate that at times HI load beyond this level.

*** Different loading systems at MNM and HI.

TRACK COSTS TECHNICAL LIMITATIONS

It is frequently suggested that track costs; sleepers, ballast, surfacing, increase with increasing axle load. Certainly the structural requirements are greater with,

- (i) sleepers of larger dimensions,
- (ii) increased ballast depths, and
- (iii) reduced sleeper spacings,

being used. In this sense higher axle loads require a more expensive track structure. At the same time, however, this stronger track structure has the ability to handle more traffic at higher speeds for the same maintenance cost.

To resolve this conflict track maintenance costs in the following categories were examined;

- (i) track degradation rates; surfacing/lining,
- (ii) ballast requirements/subgrade deformation,

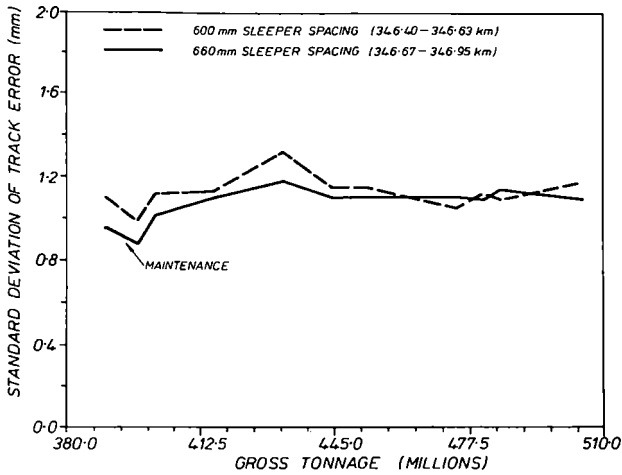


FIG. 1 MT. NEWMAN MINING RAILROAD- STEEL SLEEPERS RIGHT SURFACE.

- (iii) sleeper life,
- (iv) other factors;
 - (a) vertical track buckling,
 - (b) track lateral strength,
 - (c) bridge design, structures.

Of these items (i) track degradation rates, and (iii) sleeper life will be discussed in greater depth although in the analysis no category showed an increase in costs with increasing axle load.

Track Degradation Rates

A major objective of the track studies programme at MRL has been the provision of relationships between track structure (capital) costs and future track maintenance costs.

To obtain these relationships six instrumented locations were established throughout the Hamersley Iron and Mt. Newman Mining tracks. In each of the locations rails were strain gauged to obtain wheel loads, and a newly developed laser system¹ was utilized to make dynamic track deflection measurements.

These data were combined with track deterioration rates measured by a Plasser EM80. The track geometry measurements were carefully adjusted to take account of possible errors in the measurement technique². A typical output for surface degradation with steel sleepers at the 345.9 km to 347.4 km at MNM is shown in Fig. 1.

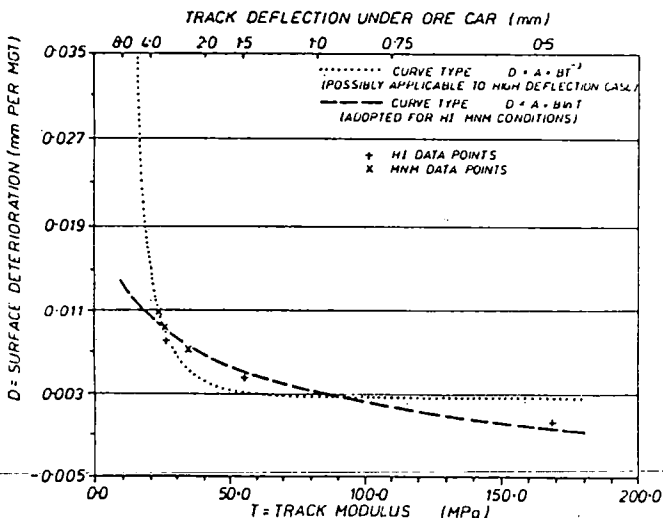


FIG. 2 RELATIONSHIP BETWEEN TRACK DEFLECTION, TRACK MODULUS AND TRACK DEGRADATION RATES.

The combined output from the instrumentation and track geometry is shown in Fig. 2. For deflections of less than 4.5 mm the track deterioration rate increases less than proportionately with deflection. Both steel sleepers at MNM and concrete sleepers at HI exhibit deflections in this range.

As well the deflection measurements indicated that deflection increased less than proportionately with axle load due to the existence of small voids (typically 0.5 mm) beneath the rail seat. This combined with the improved gross/tare ratio, obtained at higher axle loads, led to the conclusion that surfacing costs rather than increasing with axle load would decrease.

Sleeper Life

Timber sleepers are currently being replaced by steel sleepers at MNM. The development work for these sleepers was carried out at MRL³⁻⁶ and a significant part of the development was the assessment of the fatigue characteristics in the critical fastening area. Accordingly, a design method is available which enables changes in load levels to be related directly to the sleeper life.

As the design approach adopted to prevent fatigue in steel sleepers has been dealt with in some detail in previous papers, the technique will only be summarized here.

The basic steps in the design procedure are;

- (i) the determination of the sleeper section properties making an appropriate allowance for corrosion,
- (ii) an assessment of the design environment (load-cycle relationships) to which the sleeper is subjected. This assessment was previously based on AREA experimentation but as a result of extensive in-track testing is now based on field data, pertinent to steel sleeper performance.
- (iii) the calculation of longitudinal bending stresses due to bending along the length of the sleeper. The beam on elastic foundation analysis⁷ is used in this analysis. The theory is documented by Brown and Skinner³.
- (iv) the calculation of transverse stresses in the sleeper section. Due to the trough shape of the sleeper bending occurs in two planes. To determine the stresses in the transverse plane an experimentally determined ratio between longitudinal and transverse stress is used.
- (v) fatigue analysis of the rail fastening.

The sleeper section is deemed to be satisfactory if in accordance with the Miner Palmgren relationship;

$$\sum_{i=1}^m \frac{n_i}{N_i} \leq 1 \tag{1}$$

where n_i = the number of stress cycles at stress level i , and N_i = the number of stress cycles required to cause failure at stress level i .

Values of N_i have been experimentally determined for the two fastening types (Pandrol, Traklok 2) currently considered suitable for use in heavy haul tracks. These values are illustrated in Fig. 3. To ensure that manufacturing quality is sufficient to meet these standards, specifications have been developed for allowable defect sizes using fracture mechanics techniques.

Output from the analysis is shown in Fig. 4 for heavy haul steel sleepers at MNM.

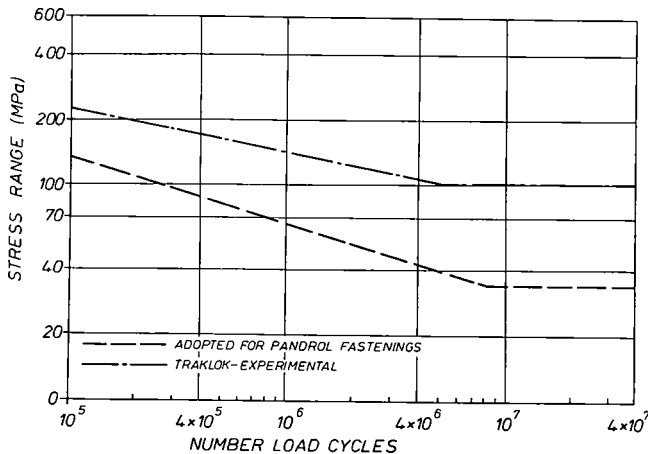


FIG.3. S-N CURVES FOR CALCULATION OF ALLOWABLE STRESSES

The present design will achieve fifty years life with 35 tonne axle loads at current operating conditions (600-660 mm sleeper spacing). The cost penalty associated with increasing axle loads is the discounted future costs of replacement. Because of the time-span involved for discounting the present value of the life reduction is not significant.

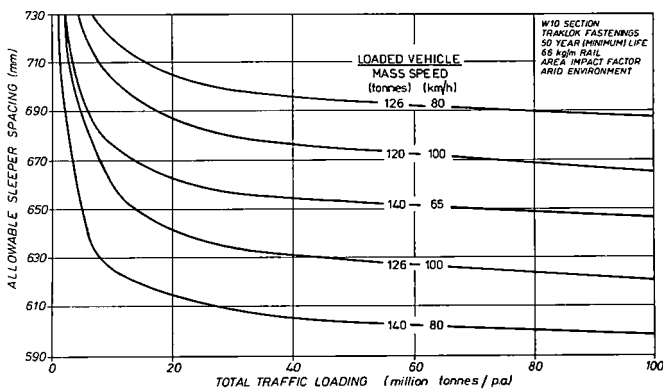


FIG.4. RELATIONSHIP BETWEEN ALLOWABLE SLEEPER SPACING AND TRAFFIC.

VEHICLE COSTS/TECHNICAL LIMITATIONS

The examination of vehicle performance consisted of two stages. Firstly the tangent and curving vehicle models developed by BHP Melbourne Research Laboratories were utilized to assess vehicle behaviour at higher axle loads. The derived data provided significant inputs to the estimation of rail defect occurrences, rail wear and wheel wear.

Secondly estimates of likely trends, with increasing axle load in the following categories;

- (i) wheel wear,
- (ii) bearings,
- (iii) couplers,
- (iv) fuel costs,
- (v) car ownership costs, and
- (vi) inspection costs

were determined. Wheel wear (60%), bearings (11%) and draft gear (12%) constitute 83% of costs in ore car maintenance⁸, while fuel costs, now exceeding \$10m/year are of obvious significance. The last items, car ownership costs and inspection costs, reflect the advantages of having fewer ore cars in operation at higher axle loads.

Of the above factors, wheel wear was the least sensitive to changes in axle load, partially because of the higher gross/tare ratio obtained and partially because of the decreased lateral to vertical (L/V) ratios expected during curving. The costs associated with bearings and couplers, being fatigue related, increased significantly at higher axle loads. However by adopting a strategy of constant train mass (i.e. fewer cars hauled at higher axle loads) it is possible to reduce the number of coupler (draft gear) breakages. Fuel costs, which will be considered in more detail, were found to decrease at higher axle loads.

Vehicle Model Output

Tangent Vehicle Behaviour. Modelling analyses in the United States have shown that increasing axle load will have a definite stabilizing effect on vehicle behaviour in the lateral direction⁹. This effect is, however, significantly influenced by wheel profiles.

The tangent vehicle model was therefore utilized to examine a number of wheel profiles. A typical output is given in Fig. 5. Points of significance are:

- (i) axle load does not appear to have a large influence on vehicle response,
- (ii) the effect of axle load on vehicle response is variable. With the stabilizing profile the peak response is slightly higher with the higher axle loading. The effect of increased axle load with the MNM worn profile is to reduce vehicle response.

Curving Vehicle Behaviour. A bogie curving model was utilized in the analysis of curving behaviour. The model itself has been calibrated by the use of wheel/rail interaction forces, recorded by an instrumented wheelset in four Hamersley Iron and two Mt. Newman Mining curves. These curves cover the most significant curve radii at HI and MNM, namely from 391 m to 1746 m.

Fig. 6 shows the response of lateral wheel-rail interaction forces to changes in car mass. In general these forces increase steadily with car mass but at a low rate. A 10% increase in car gross mass from the present mass causes less than a 1.5 kN increase in rail steady state forces. Dynamic

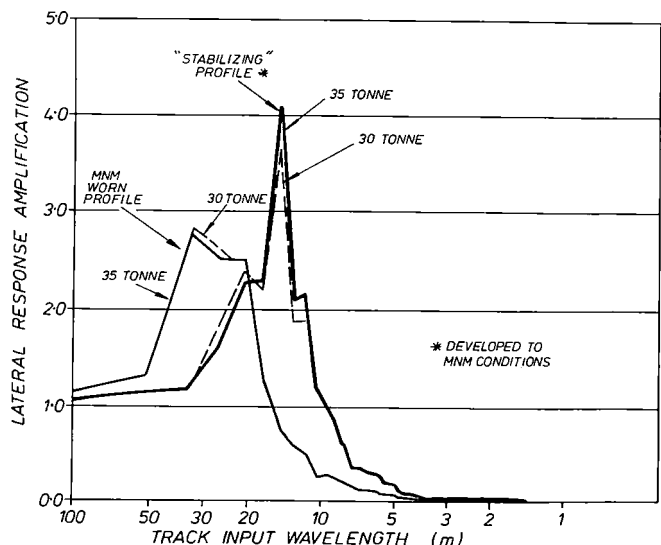


FIG.5. EFFECT OF AXLE LOAD ON LATERAL RESPONSE.

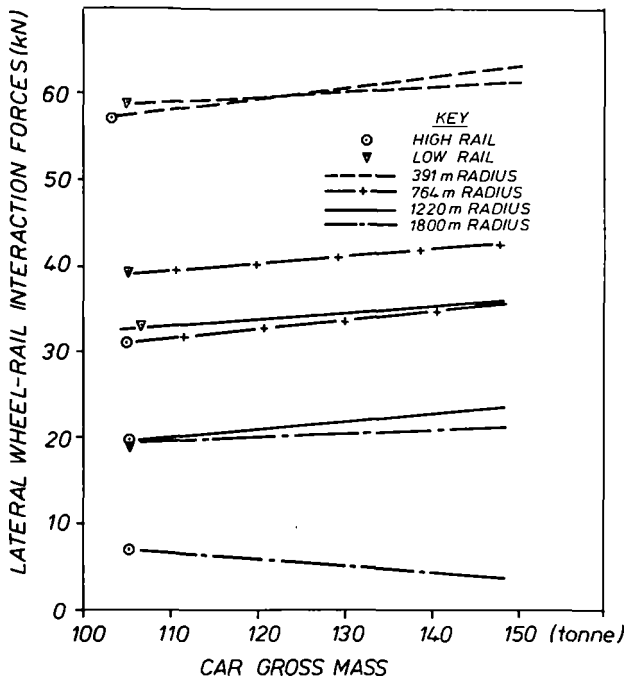


FIG. 6. SENSITIVITY TEST-EFFECTS OF CAR GROSS MASS ON LATERAL WHEEL FORCES.

response is expected to be more sensitive to car load. Based on recorded lateral wheel rail interaction forces at Hamersley Iron and Mt. Newman Mining the dynamic force is expected to be approximately 50% greater than the steady state force, and to be proportional to car mass. That is;

$$F_d = F_s + k \cdot A \quad (2)$$

where F_d = the dynamic wheel rail interaction force,
 F_s = the steady state wheel rail interaction force,
 A = axle load, and
 k = an empirical coefficient.

As an example of this effect, the 113 km (2°) curve at Mt. Newman Mining is considered. Measured values of F_d and F_s were 43.5 kN and 25.5 kN respectively. With a nominal axle load of 300 kN a value of k equal to 0.06 is obtained in Eq. 2. Increasing the axle load to 340 kN gives;

$$\begin{aligned} F_d &= 27.0 + (0.06 \times 340) \\ &= 27.0 + 20.4 = 47.4 \text{ kN} \end{aligned}$$

That is, a 13.3% increase in axle load causes a 9.0% increase in the dynamic force. This is a less than proportional increase. The analysis is also conservative in that the estimate of the transient (dynamic) response of wheel loading to track geometry errors assumes infinite stiffness for the track/car interaction. Lower L/V ratios can therefore be expected in the steady state and dynamic conditions in curved track.

Fuel Costs

Locomotive fuel usage may be related to the drawbar force exerted which is the sum of several resistance forces which are dependent on the

operating conditions of each railroad. The resistance forces encountered include:

- (i) grade resistance
- (ii) curve resistance
- (iii) train rolling resistance
- (iv) bearing (wheel) resistance
- (v) aerodynamic resistance
- (vi) acceleration (starting) resistance
- (vii) track wave resistance.

Of these factors some such as aerodynamic resistance and track wave resistance have traditionally been considered to be influenced by axle load according to the formula (a modification by Muhlenberg¹⁰ of the original Davis¹¹ equation);

$$R = 2.94 + \frac{89.2}{A} + 0.03V + \frac{0.121V^2}{An} \quad (3)$$

where R = resistance (N/tonne),
 A = axle load (tonnes),
 V = speed (km/h), and
 n = the number of axles,

while other factors such as grade resistance and curve resistance are generally considered to be independent of axle load. Data from the curving model (Fig. 6) have shown, however, that decreased lateral curving forces per unit of vertical force are obtained. Reductions in curve resistance may therefore be obtained at higher axle loads. This effect is shown in Fig. 7.

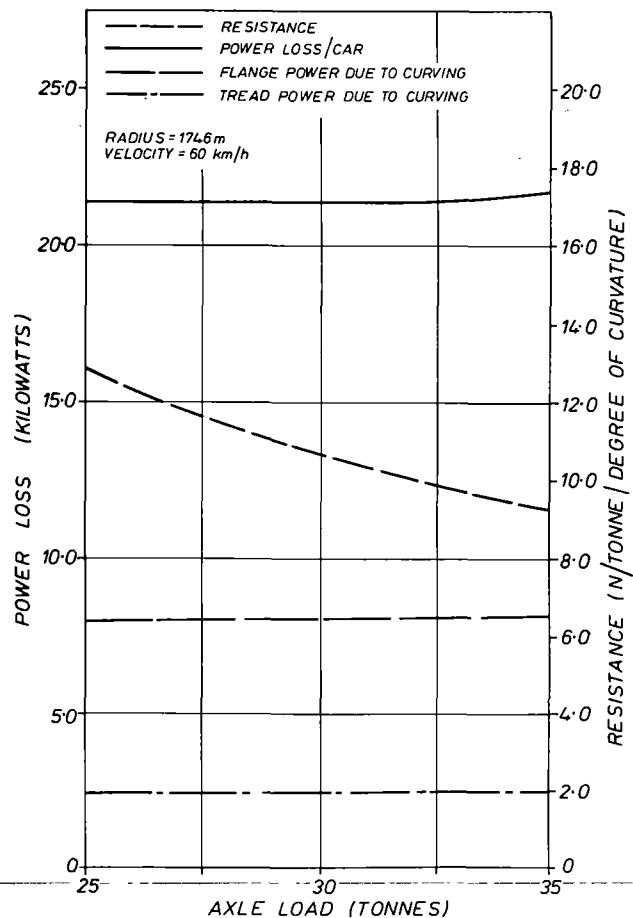


FIG. 7. EFFECT OF AXLE LOAD ON TREAD AND FLANGE POWER LOSSES IN CURVED TRACK.

An improved analysis, modelling the track as a beam on a continuous damped elastic foundation, was therefore undertaken. The analysis used outputs from track instrumentation, track geometry car recordings and the MRL vehicle models, to establish improved theoretical estimates of power (fuel) requirements in track.

For the following base case

- velocity = 60 km/h
- alignment condition factor = 1.0
- car mass = 125 tonnes
- track modulus = 25 MPa

a sensitivity analysis was conducted to examine the importance of operational parameters on fuel usage. The results given in Table 2 indicate that considerable fuel savings may be obtained with high axle load, low speed operations on a well maintained track.

TABLE 2: EFFECT OF ALTERING PARAMETERS ON TRAIN RESISTANCE

PARAMETER	% CHANGE IN PARAMETER	RESULTANT % CHANGE IN TOTAL TRAIN RESISTANCE PER GROSS TONNE
VELOCITY	+ 20	+ 6.6
	- 20	- 1.0
ALIGNMENT - TRACK QUALITY	+ 20	+ 1.5
	- 20	- 3.1
AXLE LOAD	+ 20	- 10.8
	- 20	+ 21.6
TRACK MODULUS	+ 20	- 0.6
	- 20	+ 0.7

RAIL COSTS - TECHNICAL LIMITATIONS

There are a number of failure mechanisms which control the life of rail. For instance, in tangent track at MNM, transverse defects provide an effective limitation to rail life, while in curves excessive wear, principally between the wheel flange and the side of the rail head, causes rail replacement. In tighter curves (<600m radius) plastic flow is a contributing factor, while corrugation formation in curves may considerably reduce effective rail life.

Of these mechanisms plastic flow and corrugations were determined not to have a significant influence, when higher strength rails are used in curves. At higher axle loads the occurrence of transverse defects increases markedly, while rail wear remains a significant replacement criterion in curves, although results from testing indicate the rail wear will not vary significantly with increasing axle load.

Rail Head Wear Limits

Rail has traditionally been replaced in mainline track when wear has approached 25-30% of the head area. The reasons for continuing with this approach, particularly on continuously welded heavy haul track, are however obscure. Intuitively though, replacement criteria would be expected to be related to loading levels imposed on the rail.

The determination of allowable stress levels in rails requires close consideration of the static strength (i.e. yield and ultimate strength) as well as the fatigue and fracture properties of the rail steel.

The stress system which develops in the rail due to wheel loads is highly complex and three dimensional. Four specific locations were therefore chosen for study (Fig. 8) namely the head outer lower corner,

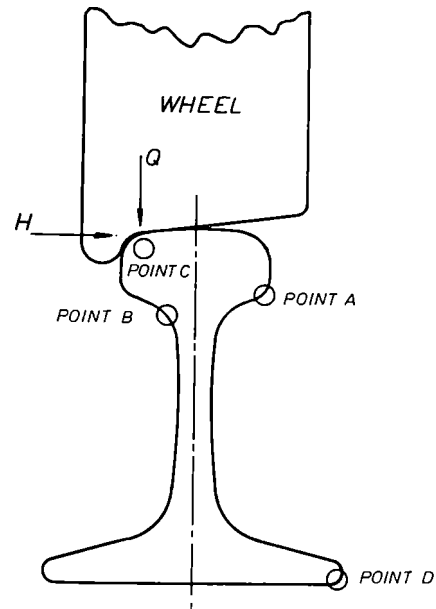


FIG. 8. LOADS APPLIED TO THE RAIL AND THE POINTS EXAMINED IN RAIL WEAR LIMITS STUDY.

head to web transition radius, wheel contact point and outer edge of the foot. Of these the most critical was found to be point A at the outer lower corner of the rail head.

Stresses at this point were calculated according to the guidelines set out by the O.R.E.¹² and also described by Eisenmann¹³. The following five components were added to determine the maximum stress.

(a) The stress due to rail bending in the vertical plane, $\sigma_{Q,x}$ which is related to the peak vertical bending moment, M.

(b) The stress due to the head bending as a beam on elastic foundation (the web is acting as an elastic foundation for the rail head).

(c) The stress contribution due to the application of rail torsion moment.

(d) The stress due to the lateral load acting at the centre of rail twist.

(e) Thermal stresses. A temperature of 45°C below the stress free temperature is representative of the harshest fatigue environment feasible in the Pilbara region. This corresponds to a thermal stress of 109 MPa.

Stresses were calculated for different ratios of lateral to vertical load (L/V), and for five different conditions of actual rail head wear, typical of that experienced by rails in a 391 m curve. A typical result shown in Fig. 9 is indicative that the calculated stresses are linearly related to the applied load, with allowable head wear limits being in inverse proportion to the axle load. The slightly different L/V ratios at the two axle load levels were derived from the curving model and include a dynamic increment.

Transverse Defect Occurrence

The dominant criteria for rail replacement in tangent track experiencing heavy axle load traffic (30 tonnes and greater) is likely to be the rate of transverse defect occurrence.

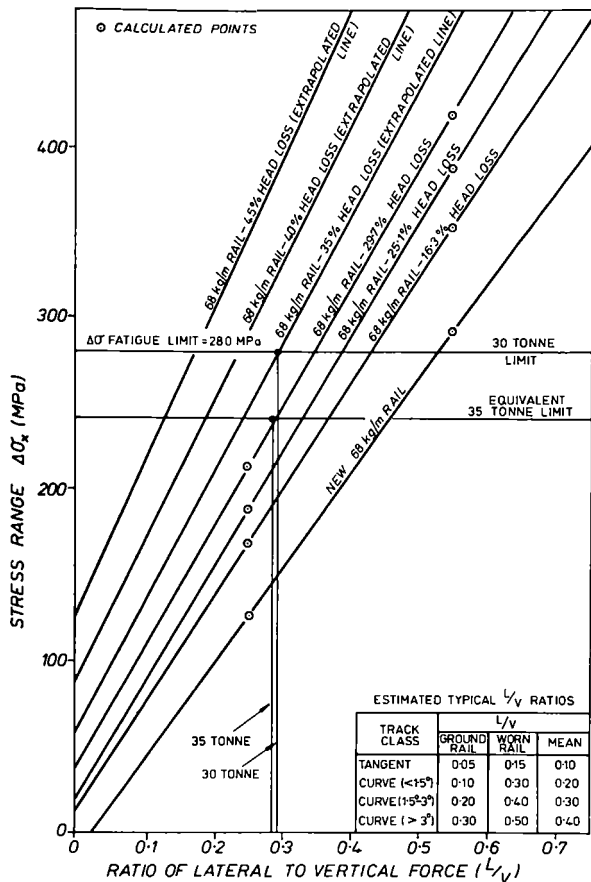


FIG. 9. HEAD WEAR LIMITS.

The literature regarding this aspect of rail performance does however give differing predictions. The results of Zaremski and Abbott¹⁴ indicate that increasing axle loads will substantially increase the occurrence rate of transverse defects. Depending on the particular characteristics proposed the results indicate that the transverse defect occurrence rate is;

$$D_r = A^f \quad (4)$$

where D_r = defect rate,

A = axle load, and

f = exponent approximately equal to 3.

This result is in agreement with predictions using the roller bearing analogy ($f = 3$) suggested by Guins¹⁵.

An alternative analysis¹⁶ indicates that the value of f is 4. This estimate is based on the comparison of bending stresses and fatigue lives with different rail weights. Transverse defects, are however, initiated primarily by contact stresses, rather than bending stresses although bending stresses do play a role.

Field data obtained in Europe¹⁷ support the values of f obtained above with values of f between 3 and 4 being considered to occur in practice. Larger values are obtained by analysing data from Sunnygard¹⁸ where values of between 4.1 and 4.7 for f have been found. (It is likely that these values

may be underestimated as they are rail life assessments and wear contributes to failure at lower axle loads).

In this analysis a value of $f = 4.0$ will be considered as typical of the empirical data. However, due to the possible error associated with this 'f' term a new transverse defect modelling programme¹⁹ is being developed. The programme simulates defect initiation and growth primarily in the shelling-pre transverse defect stage.

The essential differences between this model and formulations such as that of Zaremski and Abbott¹⁴ is that;

- (i) a fracture mechanics mechanism is postulated,
- (ii) contacts in the gauge corner (and the percentage of contacts) control the growth of defects,
- (iii) a loading distribution (or load spectrum) is considered with the mean load and standard deviation creating separate effects, and
- (iv) an inclusion distribution is included.

In comparison with the $f = 4$ empirical result, the model predicts a much greater increase in transverse defect rates, and particularly rapid decreases in rail life with relatively small increases in axle load.

The results also indicate that with small increases in axle load transverse defects may become the rail replacement criterion in curves, instead of rail wear. To obtain an estimate of the magnitude of this effect, values for rail lives due to transverse defects in curves, were estimated (Fig. 10), by adjusting empirical transverse defect rates by a life reduction factor calculated in the model.

Assuming a rail wear life of 300 MGT (with grinding) in curves it can be seen that at higher axle loads (say 32 tonnes) rail lives may begin to be controlled by transverse defect occurrences, particularly on the high rail.

The use of standard carbon rail in curves, particularly sharper curves, is however, being phased out in favour of high strength rails with better wear characteristics. The fatigue performance of these rails would therefore need to be considerably better than that of standard carbon rails if wear life was to be matched to transverse defect life particularly at higher axle loads.

Data on the fatigue characteristics of head hardened rail are quite limited, particularly concerning the threshold stress intensity factor (K_{th}) which has a pronounced effect on fatigue performance. Further studies were therefore conducted at MRL to examine this aspect. These results (Fig. 11) showed

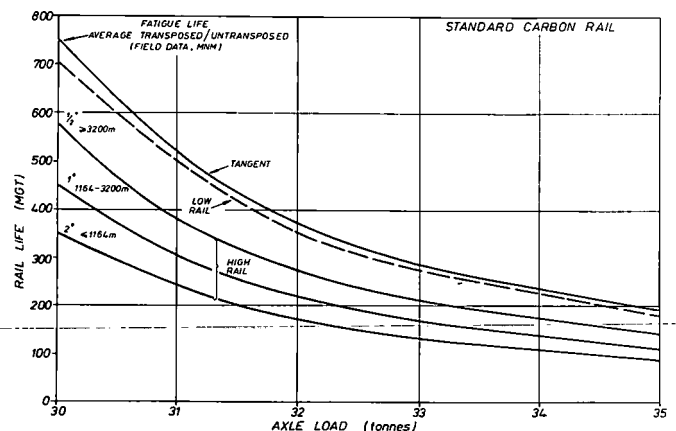


FIG. 10. RAIL REPLACEMENT CRITERIA FOR TRANSVERSE DEFECTS.

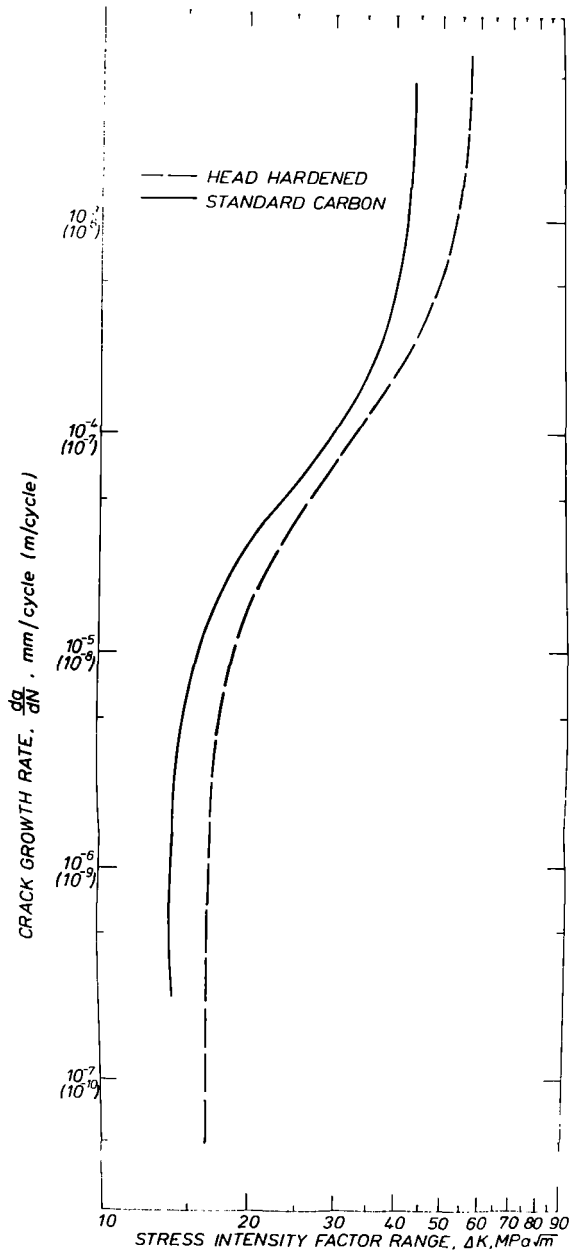


FIG.11 AVERAGE CRACK GROWTH CHARACTERISTICS FOR STANDARD CARBON AND HEAD HARDENED RAIL

that head hardened rail in the critical location exhibited improved crack initiation propagation and fracture characteristics leading to a projected, 2.7 times, increase in rail life.

ASSESSMENT OF INCREASING AXLE LOAD

The previous sections have dealt with some of the more pertinent technical considerations associated with developing the required engineering understanding of the influence of axle load on overall operational performance.

These engineering "factors" must be translated to cost variations to provide estimates of the benefits (costs) associated with increasing axle load. Table 3 summarizes the analysis conducted for the case of a 10% increase in axle load at MNM.

Present costs are "factored" by the engineering change in damage to obtain estimates of future costs at higher axle loads.

With higher loadings increased costs are expected to repair transverse defects, replace rails (curved and tangent) and from wheel bearing fatigue. These increases are however more than balanced by reductions in car and locomotive ownership costs, fuel usage and wheel wear amongst other factors. Further cost advantages appear possible from the use of head hardened rail in tangent track. As such a prima facie case exists at MNM to increase axle load, given that existing rollingstock may be utilized in this changeover.

These effects will vary from one railroad to another dependent on;

- track maintenance standards,
- bogie/vehicle characteristics,
- rail type/profile, and
- sleeper type,

and the application of analyses must be tailored to suit these particular situations. For instance with timber sleepers the effect of increasing axle load may be to significantly reduce sleeper life, while on a track with a poor support condition (low track modulus) significantly increased track maintenance charges may result. This is in contrast to the situation at MNM where steel sleepers are used on track offering excellent support and maintained to a high standard.

As such the overview results summarized in Table 3, must be considered typical of the MNM situation alone. For other railways the cost implications of increasing axle load may be negative. As well, other operational implications involving the capacity of loaders, bridges, dumpers and locomotives must be jointly considered before a decision can be finally made²⁰.

CONCLUSION

Using appropriate analytical techniques it is possible to determine reasonably accurately the effectiveness of increasing axle load in reducing overall railroad costs. The elements of the analysis consist of detailed examinations of individual railway components to assess the engineering outcome of higher axle loads.

Due to the differences in operational practices between even very similar railroads these analyses must be tailor-made to examine individual railway practices. However, based on this analyses it appears that railways having

- high maintenance standards,
- using higher strength rails, and
- good subgrade condition,

can achieve an operational benefit from increasing axle load from 30 tonnes to 33 tonnes.

ACKNOWLEDGEMENT

This study was conducted as part of the joint Mt. Newman Mining and Hamersley Iron research programme. Information was also drawn from separate studies funded directly by Broken Hill Pty. Ltd.

REFERENCES

- 1 Van Hoek, H.C. (1979), "Lasertrak A Dynamic Displacement Measuring System", BHP Melb. Res. Labs. Rep. No. MRL/PS414/79/002, October.

TABLE 3: COST VARIATION PER TONNE OF ORE (MNM)*

ACTIVITY AREA	TANGENT RAIL	STANDARD CARBON RAIL		HEAD HARDENED RAIL	
	PERCENTAGE OF PRESENT COST (HYPOTHETICAL)	FACTORED INCREASE	PERCENTAGE OF PRESENT COST (HYPOTHETICAL)	FACTORED INCREASE	PERCENTAGE OF PRESENT COST (HYPOTHETICAL)
<u>TRACK RELATED COSTS</u>					
Surfacing Costs	5.5	.956	5.3	.956	5.3
Ballast Degradation	0.4	1.00	0.4	1.00	0.4
Sleepers	5.5	1.00	5.5	1.00	5.5
Subgrade Condition	-	1.00	-	1.00	-
<u>VEHICLE RELATED COSTS</u>					
Wheel Wear	8.8	.955	8.4	.925	8.1
Coupler - Fatigue	1.5	.977	1.5	.977	1.5
Bearing - Fatigue	1.8	1.22	2.2	1.22	2.2
Inspection	4.4	.888	3.4	.888	3.9
Fuel Costs	22.1	.957	21.1	.957	21.1
Ownership Costs					
- Ore Cars	33.2	.888	29.5	.888	29.5
- Locomotives	4.4	.981	4.3	.981	4.3
<u>RAIL RELATED COSTS</u>					
Transverse Defects	1.1	1.46	1.6	0.54	0.6
Tangent Rail Replacement	3.3	1.46	4.8	0.70	2.3
Curved Rail Replacement	4.4	1.05	4.6	1.05	4.6
Grinding	2.2	0.955	2.1	0.955	2.1
Switches/Crossings etc.	1.1	1.21	1.3	1.21	1.3
	99.9		96.5		92.7

* Costs not variable with axle load excluded

2 O'Rourke, M.D. and Groenhout, R. (1981), "The Use of Track Geometry Data for Maintenance Planning", Fourth International Rail Track and Sleeper Conference, Adelaide, September.

3 Brown, J.H. and Skinner, D.H. (1978), "The Development of a Steel Sleeper System for Heavy Haul Railways", The Institution of Engineers, Australia, Heavy Haul Railways Conference, Perth, September.

4 Brown, J.H. (1979), "Design Refinements Make the Steel Sleeper Viable", Railway Gazette International, pp. 902-906, October.

5 Wilson, P.K. and O'Rourke, M.D. (1981), "Steel Sleepered Track Systems", Fourth International Rail Track and Sleeper Conference, Adelaide, Sept.

6 O'Rourke, M.D. (1981), "Resume of BHP Insulation Pad Development", BHP Melb. Res. Labs. Rep. No. MRL/PS4/81/009, September.

7 Hetenyi, M. (1946), "Beams on Elastic Foundation", Ann Arbor: The University of Michigan Press.

8 Walker, W.D. (1980), "Unit Train Operation Demands Preventative Maintenance of Wagons", Railway Gazette International, September.

9 Hannebrink, D.N., Lee, H.S.H., Weinstock, H. and Hedrick, J.K. (1976), "Influence of Axle Load, Track Gauge and Wheel Profile on Rail Vehicle Hunting", A.S.M.E. Paper 76-WA/RT-3.

10 Muhlenberg, J.D. (1978), "Resistance of a Freight Train to Forward Motion", Vol. 1, Methodology and Evaluation, Report No. FRA/ORD-78/04.I, April.

11 Davis, W.J. (1926), "The Tractive Resistance

of Electric Locomotives and Cars", General Electric Review, October, pp. 685-700.

12 O.R.E. (1966), "Stress Distribution in the Rails", Question D17, Interim Report No. 2, June.

13 Eisenmann, J. (1970), "Stress Distribution in the Permanent Way Due to Heavy Axle Loads and High Speeds", Proceedings AREA Vol. 71, pp. 24-59.

14 Zaremski, A.M. and Abbott, R.A. (1978), "Fatigue Analysis of Rails Subject to Traffic and Temperature Loading", I.E. Aust. Heavy Haul Railways Conference, Perth, W.A.

15 Guins, S. (1977), "Estimating the Effect of Heavy Axle Loads on Rail Life: Roller Bearing Analogy", ASME Paper 77-RT-9, March.

16 Stone, D.H. (1980), "Comparison of Rail Behaviour With 125 ton and 100 ton Cars", AAR Research and Test Department.

17 O.R.E. (1979), "Effect on the Track of Raising the Axle Load from 20 t to 22 t", Question D141, Report No. 1.

18 Sunnycard, J.R. (1977), "Effect of Heavy Cars on Rail", AREA Bulletin 603, pp. 611-635.

19 Chipperfield C.G. and Skinner, D.H. (1981), "A Study of Subsurface Fatigue in Rails", I.E. Aust. Railway Engineering Conference, Sydney, 7-10th September.

20 Brown, D.N. and Brown, J.H. (1982), "Optimizing Operational Modes on the Mt. Newman Mining Co. Railroad", Prepared for publication at the Second International Heavy Haul Conference, Colorado Springs, September.

Rail Fatigue Resistance— Increased Tonnage and Other Factors of Consequence

B.N. Leis

Transportation &
Structures Department
Battelle Columbus Labs
Columbus, Ohio

R.C. Rice

Transportation &
Structures Department
Battelle Columbus Labs
Columbus, Ohio

Fatigue failure from crack initiation in the rail head is postulated to depend on cyclic octahedral shear, flow induced residual, and thermally induced mean stresses in the rail. The sensitivity of rail life to operational parameters such as vertical and lateral wheel loads, wheel eccentricity, foundation modulus, rail weight versus wheel load, train make-up, and speed and class of track are examined in light of the conference theme of increased tonnage. The results of this study suggest that rail fatigue failure is largely controlled by flow induced residual stresses and thermally induced mean stress. The results are discussed with respect to optimizing rail metallurgies and operating conditions to maximize rail life, subject to the constraints of wear. It is shown that fatigue induced cracking in rail depends strongly on operational characteristics so care must be taken in pooling service experience.

INTRODUCTION

Analysis of rail failure data clearly point to the fact that flaw growth in railroad rail in the United States is a widespread problem [1]. In the short-term it is likely that increased tonnage per track can be achieved through increased wheel loads and increased speed without undue increases in the frequency of rail cracking. Field experience reported by Steele and Reiff [2] as well as by Stone [3], however, suggests that cracking incidence tends to increase exponentially as a function of millions of gross tons (MGT). Thus, there is a limit to the economically useful life of rail. Replacement becomes more economical than repair so that the benefits of increased tonnage per track in the short-term may be offset by higher long-term replacement costs. An alternative to higher tonnage per track is double tracking the line, but again, economics controls the decision. Other alternatives also exist. However, in every case, one is faced with formulating a rail failure model which facilitates near-term economic analyses.

As is evident in Reference 4, the dependence of rail fatigue resistance on various operational parameters (wheel load, speed, etc.) is an important input to economic models of rail systems. Models of rail fatigue behavior therefore have a pivotal role in such studies. Unfortunately, predicting rail fatigue resistance is difficult. As shown recently by Perlman et al., [5], simpler uniaxial models of rail fatigue resistance (e.g., [6,7]) may yield a wide variety of answers, depending on how material and rail stress parameters are selected. ♦

The purpose of this paper is to explore the next level of model complexity. To that end, results of stress analyses that characterize the multiaxial stress field in the rail are coupled with a fatigue analyses procedure sensitive to multiaxial and mean/residual stress effects. In view of the conference theme, the model is used to explore the dependence of life on operational parameters including tonnage. Specifically, the paper uses sensitivity analyses to establish the factors controlling rail life. Because rail life is dominated by initiation [8], the focus is on that phase of the total cracking process.

Although the model presented is general, its use is illustrated here only for situations which culminate in failure across the transverse plane of the rail. That is, the paper addresses detail fractures (DF), transverse fractures or defects (TD), and compound fissures (CF). The paper begins with a review of the relevant phenomenology from which the failure process is postulated. Thereafter, a model framework is advanced and the results of sensitivity analyses related to rail metallurgy and operational parameters are introduced and discussed. Operational parameters examined include maintenance (foundation modulus), curving (lateral) loads, wheel load level, rail weight, speed and class of track, and train make-up. Also considered are flow-induced residual stresses and thermally-induced mean stresses. Finally, the implications of this model regarding trends in flaw character are developed and related to models of rail failure experience, including that based on Weibull analysis.

ALTERNATIVE FAILURE HYPOTHESIS

One approach to develop a failure hypothesis is to assemble what is known about the loading and stress distribution in a component where crack initiation occurs, and develop a failure process consistent with fractographic observations [9]. That is, mechanics considerations and fractographic evidence should be taken together to form a consistent failure

hypothesis. Each of the loading, the stress distribution, the plastic flow and wear process, and rail failure phenomenology, have been reviewed in detail in Reference 10. For the sake of brevity, only the salient features, including the failure hypothesis, are presented here.

Loads and Stresses

The external mechanical loading on a rail derives from many sources. Significantly, certain of these load components occur essentially in phase, whereas others are nonproportional (that is, various components of the loading do not change in direct proportion to each other). Some of them are essentially deterministic, while others are random in nature. These external components act in conjunction with internal stresses that are due to processing and service.

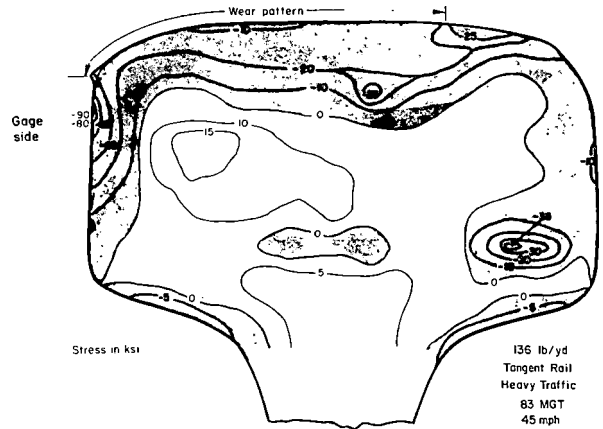
Recent analyses suggest that a beam on elastic foundation (BOEF) model reasonably characterizes the stress field due to vertical external loading away from the contact patch [11]. Because the stresses that exist at the initiation site involve contact stresses, head on web bending, and BOEF bending, all three must be considered. While superposition of stresses in the head could be used, the results of recent finite element analyses (FEA) are available and thus are employed.

Stresses due to external vertical and lateral loads develop the cyclic portion of the loading as trains pass by. These cyclic stresses act in conjunction with residual stresses that vary as a function of cumulative MGT. Residual stresses are observed to increase with MGT [12], being driven by the continued plastic flow process. Initially changes in residual stresses may be large. However, data indicated that the rate of increase levels off with continued usage. Residual stresses are seemingly greater in curved track as compared to tangent track [13]. Figure 1(a), reproduced from Reference 14, shows that axial residual stresses for tangent track are quite large, the maximum being 119 MPa (17.3 ksi) tension for the example shown. Other samples tested show values as high as 152 MPa (22 ksi) [12]. However, there is no distinct pattern in the location of the maximum tensile residual stress across the rail head, save for its lying about 0.4 to 0.6 inch (10 to 15 mm) below the running surface. For curved track, similar patterns develop, however, the maximum axial residual stresses are now about 40 ksi (276 MPa) [13].

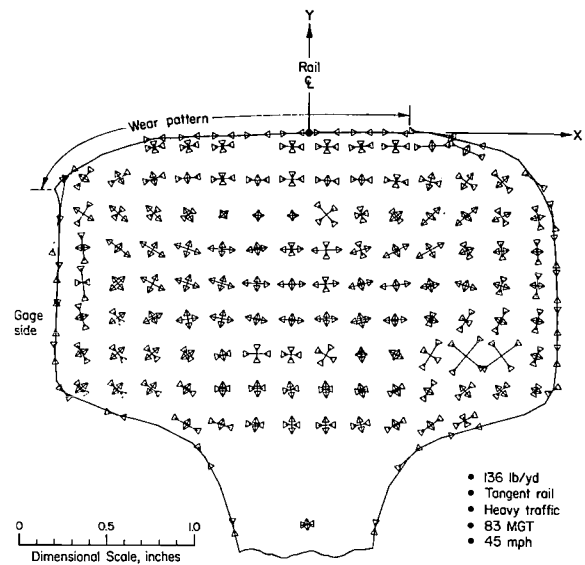
Substantial inplane residual stresses also develop in rails, as is evident in Figure 1(b). Large inplane tensile residual stresses lie toward the gage and field sides of the rails about 0.4 to 0.6 inch (10 to 15 mm) below the running surface, for both tangent and curved track. The tensile residual stresses have values on the order of the yield strength of the material. Tensile peaks of that magnitude again lie 0.4 to 0.6 inch (10 to 15 mm) below the running surface toward the gage or field sides. Compressive peaks often exceed the yield strength indicating heavy work hardening, and tend to occur near the running surface on the gage side.

Residual stresses and service stresses due to wheel loads act in conjunction with thermally induced mean stresses. The magnitude of these stresses depends on the laying temperature. Assuming that track is typically laid at temperatures between 27 and 35°C (80 and 95°F), peak tensile stresses from 103 to 131 MPa (15 to 19 ksi) may develop during

winter, while compression mean stresses may develop during summer extremes.



(a) Contours of constant axial residual stress



(b) Distribution of inplane residual stresses

Fig.1 Residual stress distribution in 136 lb/yd (68.6 kg/m) rail at 42.5 MGT/rail (83 MOT/track)

Wear and Plastic Flow

Wear and plastic flow are driven by the same external forces--tractions along, across, and normal to the running surface. A direct effect of both wear and plastic flow is to reduce the flexural rigidity as compared to new rail. Plastic flow also introduces residual stresses. Suffice it to state here that the effects of wear and flow on life have not been uncoupled, leading to some confusion in data trends [8].¹ For this reason, explicit wear and flow induced failure criteria remain to be developed. Finally, it should be noted that results of limited FEA suggest that octahedral stresses at the same distance below the running surface are comparable in new rail and rail worn 0.3 inch (7.5 mm). This is perhaps due to the dominance of the contact field. In any event, this suggests wear may not be a dominant factor in terms of failure controlled by octahedral shear stresses.

A general model for rail failure prediction must address failure independently by excess wear or flow,¹ as well as by fatigue aggravated by wear and flow. At least three failure scenarios must be addressed. In the first, failure is dominated by excessive wear/flow--failure is said to occur once the intact rail is no longer serviceable at turnouts, etc. The second and third involve fatigue, and wear and/or flow, and both lead to fracture. On the one hand, fatigue initiation occurs in the usual way except plastic flow changes both material hardness and the residual stress field. In the second case, flow or wear may ultimately reduce the section sufficiently to increase stresses such that initiation may occur earlier than expected on the basis of the original rail section.² Of these scenarios, the latter two are dealt with here. The first could be easily added given that independent physically realistic failure criteria exist for both wear and flow.

Consider now the effects of wear and plastic flow on the distribution of the stresses, rather than their magnitudes. Plastic flow means that stresses redistribute as compared to the equilibrium stress field developed during hot rolling. Continued flow means continued redistribution, particularly in situations such as railroad rail where nonproportional action essentially precludes developing a "shakedown"

¹ That they have not been uncoupled in past studies does not mean that they cannot be uncoupled for purposes of future modelling.

² Wear will not be significant in terms of octahedral stresses until its influence on BOEF and head-on-web bending causes these stresses to approach those of the contact field. Given the distance of the rail head from the neutral axis of the rail, BOEF stresses will require significant amounts of wear before this occurs, whereas head-on-web bending will be more sensitive. Limited results for 136 lb/yd (68.6 kg/m) rail suggest that 0.3 inch (7.5 mm) uniform wear does not appreciably alter the magnitude and distribution of octahedral stress. Obviously, further analyses are necessary before the significance of wear to the stress field is adequately characterized.

condition.³ As such, rail residual stresses are anticipated to continue to change with continued service. However, the extent of these changes decreases with time as increased flow resistance due to work hardening accommodates the imposed loading. Results of measured residual stresses [13] suggest this occurs within the first 100 MGT/track.

The effect of flow induced workhardening in the running surface is to increase the fatigue resistance of the material [15]. This dependence is accounted for later in the model formulation by using the fatigue behavior for work hardened material when assessing damage in that layer. Note that prestrains and periodic overstrains encountered in service situations would alter the fatigue resistance of both the work hardened layer and the softer core materials in the rail head [16,17]. Unfortunately, the effects of prestrains and overstrains are complicated and presently ill understood. For this reason they are accounted for later in the model formulation through empirical models of rail steel behavior under such conditions.

Phenomenology

To ensure that predictions of rail failures reflect field observations, it is appropriate to develop failure hypothesis which reflect the results of rail failure analysis. Results of analyses that back track transverse macrocracks to initiation sites suggest two generic classes of crack initiation [8,18,19]. One class evolves from shell like defects that lie parallel to, but below, the running surface of the rail [e.g., detail fractures (DF)]. The second class of initiators involves defects which evolve primarily on the transverse plane [e.g., transverse defects (TD)]. In the case of the DF, cracks are observed to initiate and grow on macroplanes that suggest the action of reversed shear, before they rotate onto the transverse plane. In contrast, the TD class appear to initiate at microstructural features such as inclusions with both microscopic and macroscopic growth occurring primarily on a transverse plane.

Crack Initiation Hypothesis

A number of sources suggest that shell formation may precede the detail fracture formation [8,18,19]. This is consistent with a gradient in residual stress at the interface between the work hardened running

³ In a global sense, only minor changes in residual stress occur due to periodic nonproportional flow. Thus shakedown may be said to occur globally. That is the rail head work hardens until it can accommodate the imposed load with only very confined flow. At a local scale periodic nonproportional flow essentially precludes a shakedown condition in all elements of material in the rail head, particularly in view of the statistical nature of the location and magnitude of the loading. Since fatigue analysis is done point by point through the rail head, nonproportional flow would lead to somewhat different residual stress and hardness states throughout the head. (Thus islands of various hardness would tend to develop such as have been observed by Steele [8].) While the residual deformation states in material elements may vary somewhat due to nonproportional flow, compatibility between these elements would tend to smooth perturbations suggesting that results for stabilized global residual stresses can be used for purposes of analysis.

layer and the core of the head [10]. Further, steps on shell surfaces are consistent with the alternating shear stresses that would develop at such an interface. The cyclic driving force for growth of the shear cracks would be provided by wheel passage. This driving force is coupled with large inplane tensile residual stresses (measured in this vicinity) which would tend to open the shear cracks. Periodically, the orientation of such shear/tension cracks may rotate towards the transverse plane through cracking in favorably oriented pearlite colonies. Ultimately, when the driving force for such cracks is greater on the transverse plane, the shell would rotate onto the transverse plane. In view of the presence of both shear and tension stresses in the vicinity of initiation, a multiaxial criterion is required. Analysis of Reference 10 suggests an octahedral criterion is appropriate for rails, and as such is adopted later in the model formulation.

Although shells are hereby associated with both detail fractures (DF) and occasionally with transverse defects (TD), it is not necessary to find a "shell" with every DF and TD, nor will every shell necessarily form a DF or a TD. Rather, one can expect to find shells with some DF's and a few TD's--clearly a microshear crack can rotate onto the transverse plane before a shell becomes well developed if it encounters a favorably oriented metallurgical feature early in the cracking process. That is, if the rotation onto the transverse plane occurs quickly, a true DF may be interpreted as a TD. Alternatively, defects which might otherwise initiate and grow as shells may be of sufficient size to independently initiate and continue growth as a TD. That is, the stress concentration associated with the feature may be large enough to initiate the crack on the transverse plane. It should be further noted that an appropriate failure criteria would hereby be directionally dependent, with lives to initiation and endurance limits less than that associated with initiation on a transverse plane.

Significantly, the failure hypothesis is history sensitive. This is because damage is concentrated at an interface which moves into the rail as the head work hardens. Two scenarios may develop: the penetration of the interface into the rail head can outpace the initiation process at a given interface, or this penetration can outpace the rotation of a shell onto the transverse plane. In the first instance, the damage done will not contribute to further shell formation; in the second the shell will be benign with respect to the formation of a transverse defect from the shell.

For the present formulation, all damage is assumed to concentrate at the depth and location dictated by the combination of wheel induced stresses coupled with a fixed distribution of residual and mean stresses. Such combinations are considered on an example by example basis, but in all cases the residual stress distribution is assumed to be fixed. In view of this assumption, predicted lives are conservative by the period spent stabilizing the residual stress field. As noted earlier, this is on the order of 100 MGT.

CRACK INITIATION PREDICTION MODEL

The hypothesis advanced proposes that crack initiation is controlled by shear and normal stresses on the material element in the rail head subjected to the greatest combination of thermally induced mean, flow induced residual, and wheel load induced bending

and contact stresses. The fatigue damage incurred by this material element under service histories is assessed using a modification of the linear cumulative damage theory, shown in Figure 2, in conjunction with a multiaxial damage parameter that includes mean and residual stress effects [20].⁴ The parameter, denoted D, given by

$$D = s_m \Delta \bar{\epsilon} + \Delta \bar{s} \bar{\epsilon}, \quad (1)$$

[20] is used to establish equivalence between various mean stress conditions. In this parameter s_m denotes the mean stress, $\Delta \bar{\epsilon}$ denotes the total strain range and $\Delta \bar{s}$ denotes the stress range. The bars, viz. $\Delta \bar{\epsilon}$, indicate that these parameters reflect a uniaxial equivalent for the multiaxial state. Equivalence is provided by an octahedral criterion, the choice of which is discussed in Reference 10.

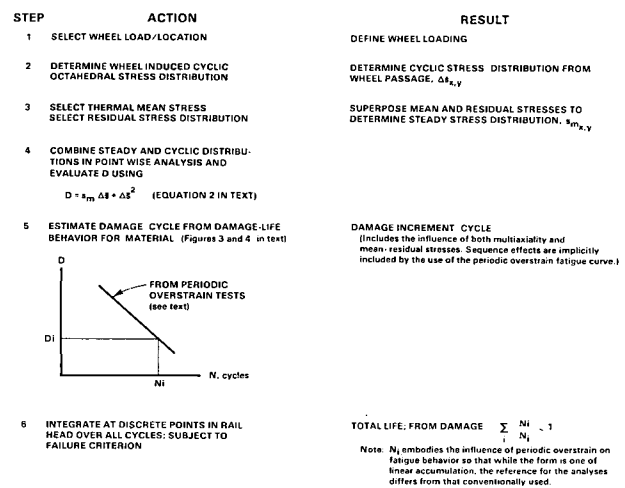


Fig. 2 Fatigue Damage Assessment Procedure

Ideally, the value of s_m in Equation (1) would be the component of the mean stress normal to the octahedral plane [21]. Unfortunately, the components of the inplane and axial mean and residual stresses on the octahedral plane cannot be directly obtained for rails. As such, lives are calculated assuming the full effect of a given directional mean or residual stress acts on the octahedral plane. This represents a lower bound on life. Corresponding calculations made assuming zero mean and residual stresses on the octahedral plane represent an upper bound on the life.

In applications such as rail where principal planes rotate, damage is directional. However, it has been shown that Equation (1) evaluated at the extremes of the cycle suitably correlates such results [20], including multiaxial mean stress effects. Also, in applications to rail steels which exhibit different fatigue resistances in different directions, life predictions for the rail are bounded by the lives predicted using fatigue properties developed for the various material orientations. The

⁴ A modified Goodman diagram could also be used in conjunction with some multiaxial criterion. However, such a diagram is not computationally convenient and thus its use would slow the analysis procedure.

orientation with the least life is assumed to indicate the location and mode of initiation. Finally, locally nonproportional plasticity, which may develop in rails under the combined out-of-phase action of lateral flange, and creep loads, and vertical loads, may be a significant consideration [22]. Fortunately, however, analysis suggests such nonproportional action contributes little to the damage process [10]. Thus, while its influence could be dealt with in terms of Equation (1), it can be ignored without much loss in accuracy.

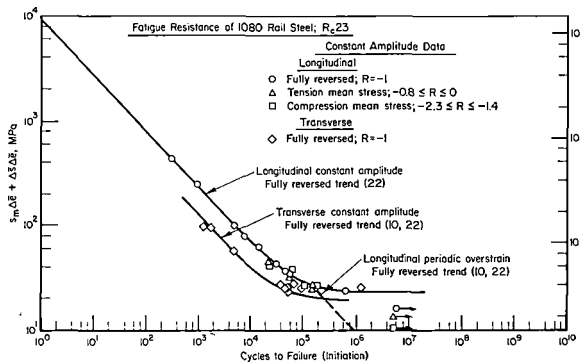
An expression relating D to the fatigue resistance of rail steels must be determined by relating values of D to the observed fatigue life of the material. Data available in the literature for rail steels are used for this purpose. Constant amplitude data from Reference [15] generates the empirical relationship between the damage parameter and life shown in Figure 3(a). Observe from Figure 3(a) that fully reversed data for the longitudinal orientation are shown as open circles while data for the transverse orientation are shown as open diamonds. Longitudinal tension mean stress data shown by open

life trend below the endurance limit in Figure 3(a), and are used in all life predictions.⁶

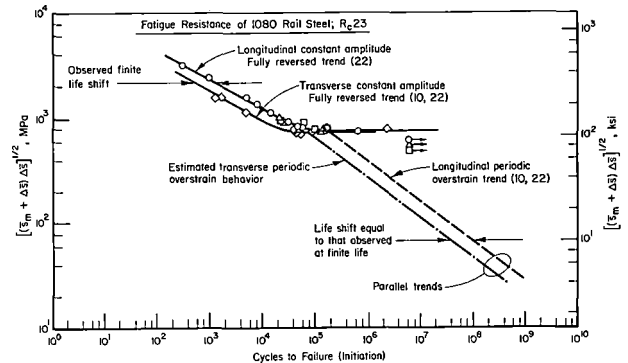
Equation (1) prescribes how cyclic, residual, and mean stresses contribute to the damage process. As written, Equation (1) involves stresses and strains and is not limited in its range of applicability. This equation can be simplified when applied to rail life prediction since stress is linearly related or nearly linearly related to total strain through the modulus of elasticity, E, for the range of lives of interest. Thus, multiplying both sides of Equation (1) and extracting the square root to retain units of stress after simplification gives

$$(DE)^{1/2} = [(s_m + \Delta s) \Delta s]^{1/2} \quad (2)$$

Since Equation (2) is used in a parametric fashion, data of Figure 3(a) may be replotted using the right hand side of Equation (2) as an ordinate, the results of which are shown in Figure 3(b). Observe that the correlation in Figure 3(a) is unchanged by this operation.



(a) General form of parameter



(b) Stress-based parameter

Fig. 3 Rail fatigue resistance characterized as a function of the damage parameter

triangles and compression mean stress data shown by open squares follow the corresponding fully reversed trend without banding for a particular condition.

Consolidation of the mean stress data indicates Equation 1 provides an appropriate basis for assessing fatigue resistance in rails, including the influence of mean stress. Note that the sign of the term $s_m \Delta e$ is controlled by the algebraic value of s_m . By definition, only positive values of D are considered to do fatigue damage⁵. Observe from the figure that the transverse data fall below the corresponding longitudinal result and thus control life in rails. These data are therefore used as a basis for all life predictions for material within the core of the rail head. Finally, since experiments show rail steels do not exhibit an endurance limit for histories similar to train loadings [16,17], periodic overstrain data have been included. They are represented by the dashed line which continues the finite

As shown by measurements at FAST [8], the growth of cracks occupies less than a few percent of the rail's life. Thus, initiation of a crack at the site of maximum damage accumulation is a good measure of rail life. Furthermore, because this crack grows so quickly, other sites with lower damage levels never develop cracks. For this reason rail life can be estimated in terms of the life to first initiation within the rail head. All calculations therefore focus on identifying the sites of maximum damage and determining the number of cycles to initiate a crack at those sites.

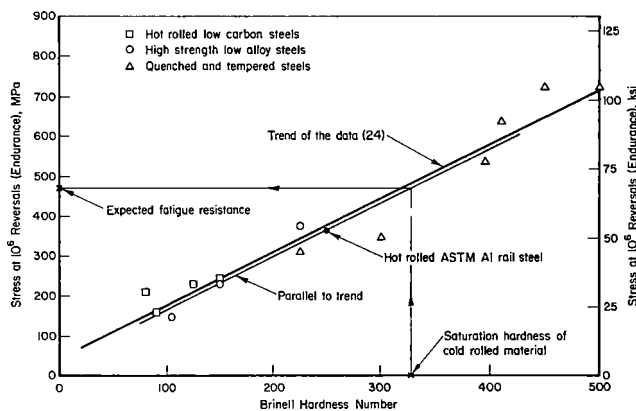
Maximum damage locations are found by evaluating the lives at various locations in the rail head for which the stresses in Equation (2) are known. Inputs

⁵ While numerically possible, negative values of D have not been observed in cases for which cracking develops. While it may be possible to generate such deformation conditions, it is difficult to envisage cracking for such cases. In any event, negative values of D are physically impossible.

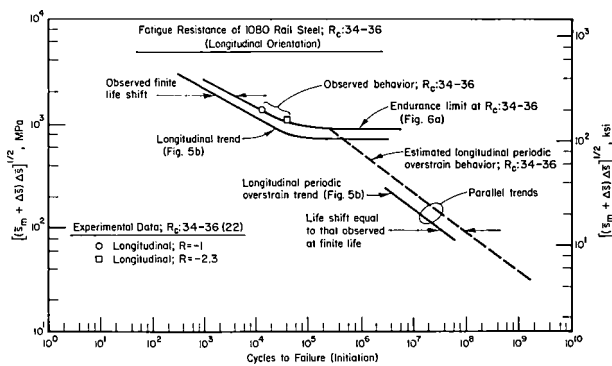
⁶ Note that the overstrain data that forms the basis for these trends reflects lives up to 10^6 cycles to initiation. These trends have been extrapolated to deal with longer lives. This has been done based on the results of more extensive experiments on a variety of materials which indicate such an extrapolation is valid [23]. However, the validity of this extrapolation has not as yet been demonstrated for rail steels. Prudence dictates verification before the present predictions are viewed in an absolute context.

to Equation (2) are based on analysis (cyclic octahedral stress due to wheel passage and thermal mean stress) and experiment (residual stress). Contours of constant damage level are estimated based on interpolation of the results of this pointwise analysis. The most refined calculations are made in regions of maximum damage or least life. Predictions of rail life are based on the least life to initiation found in this fashion, unless otherwise stated.

Contours of constant life involve material in the workhardened layer below the running surface, as well as material in the core of the head. The fatigue resistance of the core material is well characterized in terms of the data presented in Figure 3(b). However, as shown in Reference 15, the fatigue resistance of the rail steel is a strong function of the degree of work hardening. For this reason, the fatigue resistance of workhardened material makes use of the dependence of endurance limit on hardness, shown in Figure 4(a), discussed in the context of steels in general in Reference [24] and for rail steels in Reference [15]. The resultant fatigue curve is shown on coordinates of $[(s_m + \Delta s)\Delta s]^{1/2}$ and life in Figure 4(b). The endurance limit in this figure corresponds to the saturation hardness developed in rolling rectangular billets of rail steel--Rc 34 to 36 [15] as shown in Figure 4(a). The remainder of the finite life behavior follows from fairing a curve through results from fatigue experiments on samples cut from these billets, similar to that observed for materials in the core of the head.



(a) At endurance conditions



(b) Fatigue behavior for saturation hardness (Rc 34-36)

Fig. 4 Influence of hardness on the fatigue resistance of rail steel

The influence of periodic overstrain on fatigue life of hardened steels (needed to extend the constant amplitude data for analysis of variable amplitude revenue service loads) is also shown in Figure 4(b). Unfortunately, only very limited data regarding periodic overstrain effects exist for work hardened steels [24]. These data indicate that periodic overstrains reduce the fatigue behavior of work-hardened steels in a manner similar to that for hot rolled steels. As such, the overstrain trend curve for the workhardened steel has been developed by shifting as the hot rolled overstrain results in life by an amount equal to the life difference observed in the hot rolled and cold rolled material. (The result is shown as the dashed line in Figure 4(b), labelled periodic overstrain.) Note that this shift implies the workhardened material will survive about a factor of 7 longer than the corresponding hot rolled material (transverse orientation), in the range of stresses of interest. For purposes of analysis, the workhardened layer will be taken as 0.3 inch (7.6 mm) thick [8].

The final issue of significance involves scatter in fatigue data. With reference to Figure 3 and Figure 4(b), these curves represent results developed from a single piece of 60 kg/m (119 lb/yd) rail supplied by the AAR. Comparison of these trend curves with comparable published data for a variety of 1080 rail steel suggests this curve represents a lower bound behavior, with a 90 to 95 percent survival rate.⁷ The predictions of damage that develop from this curve thus relate to a lower bound response. Specifically, they only relate to hot rolled 1080 rail steels. Certainly, predictions for other rail steels are possible--however for the present purpose analyses for a single steel are adequate.

Predicted Maximum Damage Locations and Modes for Cracking

This section presents results developed for quasistatic loading of 66.6 kg/m (132 lb/yd) rail. Loading consists of repeated applications of a 134 kN (30 kip)⁸ vertical wheel load, and thus represents mean loading conditions of a unit train of 100 ton (91 x 10³ kg) cars [gross vehicle weight (GVW) = 240 tons]. The analysis seeks the largest value of D and thus the shortest life. Within limits neither heavier nor lighter loads would alter the pattern as to where damage concentrates--the life would however change.

Consider first the 30 kip (134 kN) load centrally placed on the rail head along with an assumed fixed axial residual stress pattern given by that of Figure 1, in conjunction with either zero thermal stress or 5 ksi (34 MPa) thermal stress, for tangent track. Results for this case suggest damage is concentrated below the running surface, towards the gage side of the rail, as shown in Figure 5(a) for the case of zero thermal stress. Note that the

⁷ This is true particularly for the constant amplitude data. Only limited data exist for initial and periodic overstrain conditions. The data used for those conditions represent a lower bound on the data presently available.

⁸ Stresses for this case have been developed by scaling BOEF and contact stresses developed for the case of a 19 kip (85 kN) wheel load. This is consistent with the results of FEA which indicates such a scaling is valid [25].

contours plotted represent lines of constant damage, with the numbers for each contour representing the exponent (of the base 10) for the number of applications of the 30 kip (134 KN) vertical load calculated to cause initiation. Initiation (rail failure) is indicated there to occur after 328 MGT/rail--or 656 MGT/track. Given the plane of initiation is dominated by the direction of the residual stress, initiation occurs on or near the transverse plane. That is, cracks initiate on a plane at or near perpendicular to the mean stress direction. Note that a similar initiation site is predicted to develop under the added effect of a 5 ksi (34 MPa) thermal stress, but life decreases by about 35 percent.

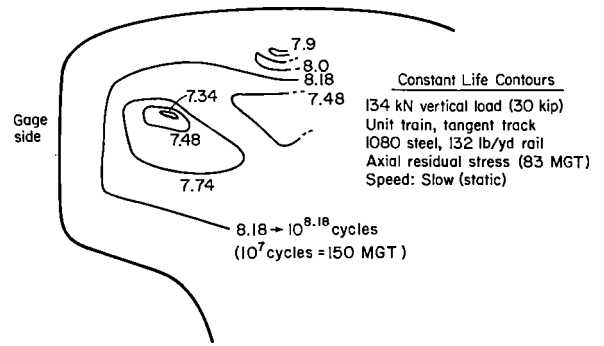
Results for the example just examined but under the action of inplane residual stresses rather than axial values, are shown in Figure 5(b). Note here that the maximum damage is concentrated further toward the gage side, about 0.4 to 0.6 inch (10-15 mm) below the running surface. In view of Figure 1, cracking for in-plane residual stresses initiates on planes associated with vertical split heads, at or near the center of the rail. Towards the gage side, the initiation behavior would be expected to be shell-like. However, in both cases the lives are close to equal to that for axial mean stresses: thus there is no indicated preference for any one mode of initiation for the case of vertical wheel loadings.

Results corresponding to parts (a) and (b) of Figure 5, except that the mean thermal and flow induced residual stresses are considered to be zero, are shown in Figure 5(c). Observe that areas of maximum damage now tend to develop in bands instead of lenses, as was suggested by parts (a) and (b). There is also some change in the value of peak damage. Cracking problems are indicated to become a problem after about 968 MGT/rail for this case.

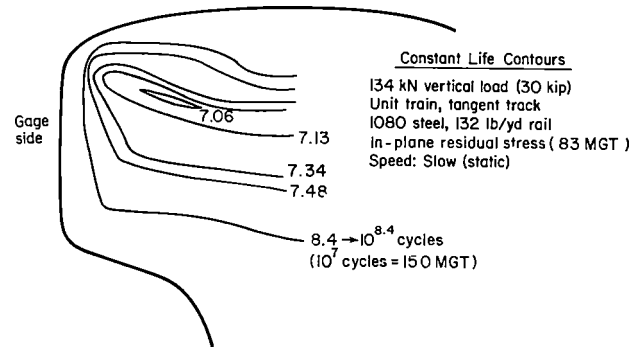
The results of these figures suggest that the concentration of initiation damage that leads to a given initiation site in service depends strongly on the character of the residual stress field. Damage calculations that account for the increases in the materials fatigue resistance due to workhardening up near the running surface indicate [as shown in Figures 5(a) and (b)] that initiation does not occur first in the contact region. Rather, these figures suggest first initiation failure occurs toward the gage side. Other residual stress measurements show patterns such as in Figure 1, except that the larger tensile stresses are concentrated on the field side [12]. These, in turn, indicate initiation is also possible toward the field side.

In summary, cracking in the transverse plane is expected to develop below the running surface with a preference toward the sides of the rail head. The results also suggest that vertical split heads and shelling are equally probable. Because the damage conditions that lead to shelling so closely match those for initiation on the transverse plane, a developing shell might easily rotate onto the transverse plane. This would be facilitated if the crack encountered some local metallurgical feature that only slightly elevated the stresses on the transverse plane. Shells, therefore, may be rationally expected to serve as precursors to detail fractures.

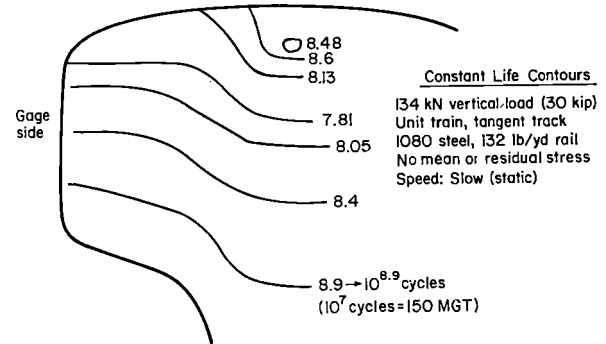
Consider next the analysis for a centrally placed wheel load of 30 kips (134 KN) coupled with a lateral flange load of 10 kips (45 KN), in the presence of a fixed residual stress field assumed to be that of Figure 1. (Lateral loading develops on the high rail on cornering as well as from lateral instabilities at lower speeds in certain classes of



(a) Axial residual stress



(b) Inplane residual stress



(c) In the absence of residual stress

Fig.5 Contours of constant damage (life) in the rail head--centered vertical load

tangent track.) Results for this case for axial residual stresses are shown in Figure 6. Observe that a lense of damage dominated by the vertical contact field is retained in the central region of the rail head just below the running surface. The presence of the lateral load shifts the patch of maximum damage toward the associated contact patch, beyond the point of maximum damage for vertical load only. By comparing Figures 5(a) and 6(a), it is evident that there is not much reduction in the life to initiation due to action of the lateral flange load. However, the magnitudes may be larger, and in the case of the creep load, its effect is confined to the contact patches. Unfortunately, detailed plots of the octahedral stress are not available for this

case. As such it is not possible to draw conclusions, except to say that the zone of maximum damage should lie closer to the running surface.

Results generated using inplane rather than axial residual stresses are shown in Figure 6(b). As with the case of vertical loading, these results suggest that vertical split heads and shelling should be expected as often as crack initiation in the transverse plane, provided that trajectories of maximum residual stresses control the plane of initiation. The patch of maximum damage lies much closer to the gage side as compared to the vertical load only case. Note too that this patch has shifted to within 0.2 to 0.3 inch (5 to 10 mm) of the running surface.

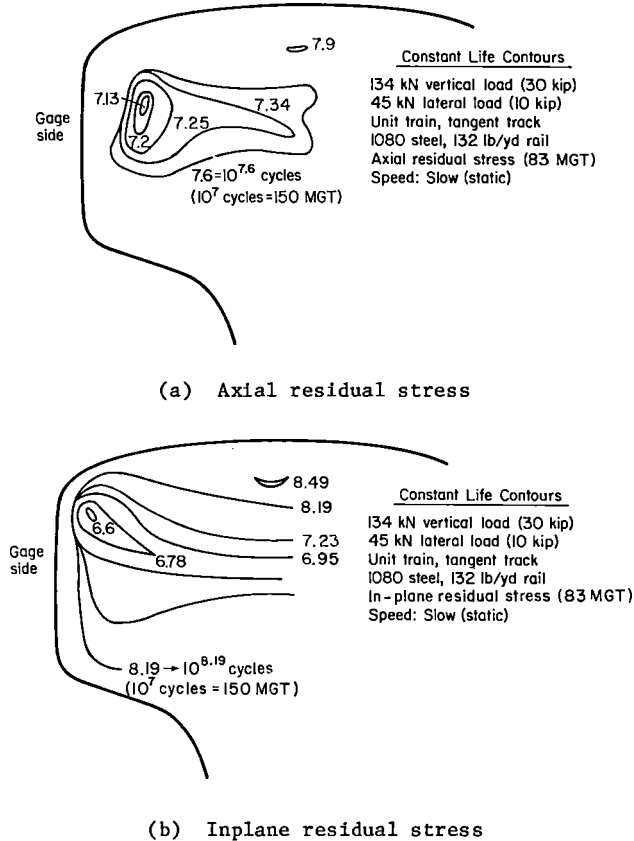


Fig.6 Contours of constant damage (life) in the rail head--centered vertical and lateral load

The residual stress pattern again tends to control the location of maximum damage. However, calculated values of maximum damage (minimum life) are not strongly dependent on the magnitude of the lateral (flange) load. This is because the term s_m tends to decrease damage due to large lateral contact stresses and increase damage elsewhere in the tension zone. In this respect consider now the just examined case of vertical and lateral loads in the context of curved track. Residual stresses for this case are assumed to be of the same character as that for a lighter weight rail, results of which are reported in Reference 13. Results for axial residual stresses are similar to the result presented in Figure 6(a) and as such are not shown. The only difference of consequence is that the patch of maximum damage lies closer to the edge of the rail head, and the life is about one half of that for tangent track. Trends

similar to Figure 6(b) also developed for inplane residual stresses. As with the axial residual stresses, the life is reduced by a factor of 2 as compared to the tangent track case.

Predicted Influence of Vertical Load Placement

Transverse offsets in wheel placement on the rail head may develop as a consequence of wheel set instabilities or curving on otherwise well maintained track. Offsets may also develop because of track whose gage has broadened. The influence of wheel offset is evaluated here for the example of an 19.1 mm (0.75 inch) offset, as compared to the case where it is centered, for vertical loading only in 66.6 kg/m (132 lb/yd) rail.

Results developed for offset loading coupled with the same assumptions made for the centrally placed load are presented in Figure 7 for the axial residual stress distribution. Comparing these results with those of Figure 5(a) suggests that the offset loading considered has only a nominal influence on fatigue resistance of rail. Predicted life for the 19.1 mm (0.75 inch) offset loading examined is about 40 percent of that for the centrally placed loading. Given the statistical nature of wheel location for tangent track, loading offset for such track is not viewed as a critical parameter. However, on curved track where offset is more deterministic, the fatigue resistance of rail could be reduced somewhat.

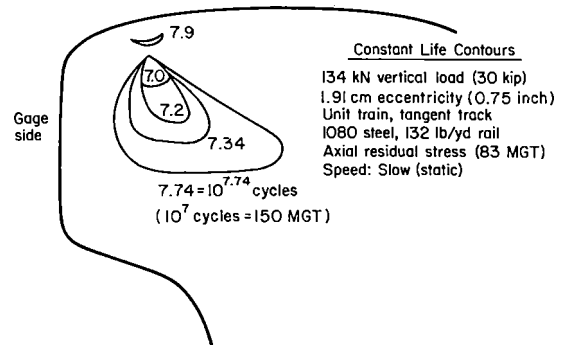


Fig.7 Contours of constant damage (life) in the rail head--offset (eccentric) vertical load

Predicted Influence of Foundation Stiffness

Maintenance of way coupled with local geological conditions can have a major effect on the foundation or roadbed stiffness for a rail. The present example considers the influence of that stiffness on predicted rail life. Specifically, results for the case of a typical vertical foundation modulus of 34.4 MPa (5 ksi) presented in Figure 5(a) will be contrasted to that for a soft modulus of 13.8 MPa (2 ksi) and a stiff modulus of 48.2 MPa (7 ksi).

Life to crack initiation is predicted to be virtually independent of foundation modulus. This is somewhat surprising in that foundation modulus is known to have a major effect on the BOEF behavior. However, the octahedral stresses on the plane which contains the load is considered herein to control rail life. This stress in turn is dominated by the contact stress field and head on web bending. Thus, the life is only weakly dependent on modulus. This prediction appears unusual in that foundation modulus is often lower in the lower classes of track, which also show a relatively high incidence of cracking. However, as discussed later in the section on speed

and class of track, this higher incidence of cracking perhaps may be ascribed to higher loads due to car dynamics (roll). For this reason, uniform differences in foundation modulus are not viewed as a critical rail life determining parameter.

Predicted Influence of Thermally Induced Mean Stress

Because track is typically laid in the summer, thermal stresses develop due to contraction of the rail during the winter. The rail undergoes one large thermally induced cycle with overall seasonal changes, and daily cycles from the heat of the day to the cool of the night. Under extreme conditions the thermal contraction may develop tensile stresses as large as 138 MPa (20 ksi). Therefore, the thermal component of the stress may significantly influence predicted life based on Equation (2).

Results for the centrally placed vertical load considered earlier are used here to assess the relative influence of thermal stress on life. For purposes of illustration, results will be presented for only the patch of damage with a life of $10^{7.34}$ cycles or 328 MGT/rail. At that site, thermal stresses of 5, 10, 15, and 20 ksi (34, 69, 103, and 138 MPa), respectively, reduce this life to 219, 142, 106, and 80 MGT/rail. These results thus suggest thermal mean stress may be a major factor controlling crack initiation in rails.

Note that the examples considered address a fixed combination of parameters. This is not to suggest that a given rail site encounters such a condition continually--rather it is done to simplify the presentation. Because the analysis approach presented is sequence independent, results for other combinations of the specific cases examined can be developed simply by linear scaling as follows. Say at a given rail location the temperature during train passage is distributed such that 50 percent of the time it is at zero residual stress and 50 percent of the time it is at 15 ksi (103 MPa). Predicted life would then be $0.5 (328 \text{ MGT/rail}) + 0.5 (106 \text{ MGT/rail}) = 227 \text{ MGT/rail}$ or 454 MGT/track. Thus, the reader can examine any set of combinations built up from any of the specific cases considered herein.

Predicted Influence of Load Level and Rail Weight

One obvious way to increase tonnage is to increase car capacity. Given that two axle trucks are retained, this results in increased wheel loads. Equation (1) indicates a strong dependence of rail life to crack initiation on applied octahedral stress range, and thus on applied cyclic wheel load. This dependence is examined here in the context of the vertical wheel loading case examined earlier. Specific cases considered include 20 and 30 kip (89 and 134 KN) loads for 119 lb/yd (60 kg/m) 19 and 30 kip (85 and 134 KN) loads for 132 lb/yd (66.6 kg/m) rail, and 30 and 50 kip (134 and 223 KN) loads for 136 lb/yd (68.6 kg/m) rail. Results of detailed FEA for these combinations indicates the following trends develop for the range of rail weights examined:

- Flange and head BOEF stress distributions are similar in a given weight of rail, and scale almost directly as a function of applied load
- The relative size of the contact stress field does not change significantly as a function of applied load
- The contact patch is highly localized, and the magnitude of the contact stresses scale almost directly as a function of applied load

- The distribution and magnitude of BOEF stresses in the head depends only weakly on the rail weight for a given applied loading

- The distribution and magnitude of the BOEF stresses depends on the rail weight in the web and flange for a given applied loading.

- Stresses in the rail head are dominated by contact stresses, head on web bending, and BOEF bending, whereas that in the flange is controlled by BOEF behavior.

Given the trends in stress as a function of load and rail weight, one would anticipate rail life to increase somewhat with rail weight for a given cyclic vertical load. However, in the absence of residual stresses, such is not observed as shown for the three weights in Table 1 by comparing the first column entries for lines B, D, and E. One would also anticipate that the life of the rail would decrease with increasing vertical load for a fixed rail weight. In contrast to trends for rail weight, such trends do develop in the absence of residual stress. This is evident in Table 1 by comparing the first column entries for lines A, C, and E with lines B, D, and F, respectively. Note that initiation here is indicated to occur on the transverse plane, and that cracking would develop in material that has been heavily workhardened. When residual stress are accounted for, failure in the workhardened material occurs at longer lives (compressive residual stresses in that area), as evident in the data from the middle column of Table 1. The results however still show the unanticipated trend of decreasing life with rail weight (observed at this same location in the absence of residual stresses) still remains. The question arises--do these results have any bearing on crack initiation in rails? Figures 5 and 6 suggest they do not. These figures consistently show that cracking is predicted to initiate below the hardened running surface.

Predictions of first initiation (i.e., rail life including residual stresses) are shown in the last column of Table 1. When residual stresses are accounted for, the anticipated trend of decreasing life with increased loads observed up in the work hardened area is retained, as evident in the table. But, in contrast to results for the hardened layer, results for first initiation show an inversion of the life trend with rail weight. That is, when residual stresses are included and first initiation is considered, the anticipated trend of increased life with increased weight is observed. With reference to the table, changes in rail weight do influence rail life, but not by large amounts [a factor of 2 develops for a change from 119 lb/yd (60 kg/m) to 132 lb/yd (66.6 kg/m)]. Residual stress again appears to be a major factor controlling rail fatigue resistance.

Rail failure (first initiation) results presented in Table 1 are reported as MGT/rail. As such, MGT/track--the usual measure of life--is equal to 2 times the lives reported. Thus predicted lives are in the range of 300 to 1000 MGT/track. As evident in the table, a large number of cycles to failure does not necessarily infer a large useful life. When life is assessed in terms of cumulative MGT--one must consider both the cycles to failure and the load carried.

Prediction of the Influence of Train Make-Up (Consist)

A given volume of goods may be moved by rail in various ways. Many trains of light GVW cars may be used. Alternatively, a few trains of heavy GVW cars

TABLE 1. Influence of Wheel Load and Rail Weight on Rail Life.

Line(d)	Rail Weight lb/yd / kg/m	Wheel Load kip/KN	Predicted Life to Initiation			
			Zero Residual(a) Cycles	MGT/rail	Typical Axial MGT/rail(b)	Residual MGT/rail(c)
A	119/60	20/89	1.17×10^8	1,170	10,500(e)	195(e)
B	119/60	30/134	3.97×10^7	595	1,650(e)	150(e)
C	132/66.6	19/85	9.1×10^7	865	17,690	525
D	132/66.6	30/134	1.99×10^7	299	1,500(f)	328(f)
E	136/68.6	30/134	4.03×10^7	605	-	-
F	136/68.6	50/223	1.11×10^7	276	-	-

- (a) Initiation in workhardened material--see Figure 5(c)--Note, rail failure is not controlled by this location.
- (b) Initiation at site corresponding to note (a)--Again, rail failure is not controlled by this location.
- (c) Results listed for axial residual stress; initiation toward gage side of head: This site controls rail failure.
- (d) Lines A, B, E, and F computed with a less refined finite element mesh than lines C and D.
- (e) Based on residual stresses estimated from data for 115 lb/yd rail
- (f) See Figure 5(a) for these results.

may be used. This poses a problem to maintenance and inspection crews in that these two different approaches to moving a fixed volume of goods may represent different increments of fatigue damage and therefore different incidences of cracking. The purpose here is to explore to what extent cracking incidence depends on train makeup.

Experimental results for rail steels show that the deformation behavior of rail steels is not strongly history sensitive--uniaxial stress and strain tend to be uniquely related regardless of the preceding deformation history [15,16]. Further, the far field stress has been shown to be uniquely related to strains at various locations throughout a notched plate made of a rail steel for differing deformation histories [26]. For this reason, the damage state characterized by Equation (1) or (2) would be essentially independent of the loading history imposed on the rail. That is the damage done by a given loading depends only on the current load--an observation substantiated by mechanics analysis [27], so long as the loading and stressing are proportional.

Given that damage is uniquely related to load, it is possible to examine the influence of train makeup in terms of the various wheel loads that are involved in a given train. The sequence of these loads, or the sequence of various trains, is not critical. However, care must be taken to use a damage life curve that reflects the influence of variable amplitude loading on the fatigue behavior of rail steels. As stated earlier, the curve denoted as periodic overstrain in Figure 4(b) is used.

The load-life to crack initiation behavior, for the case of 132 lb/yd (66.6 kg/m) rail subjected to vertical wheel loads is presented in Figure 8. For purposes of this analysis, flow induced axial residual stresses are included whereas thermal induced mean stresses are taken to be zero. The results presented relate to the area of maximum damage in the

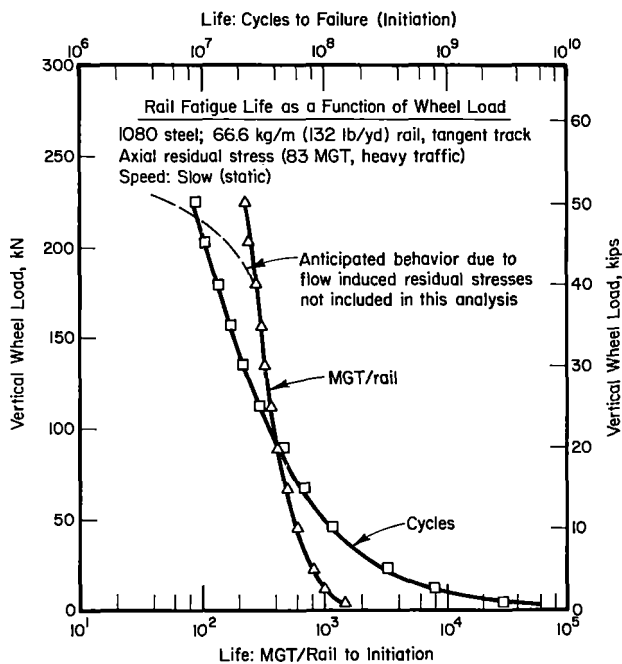


Fig.8 Rail fatigue life as a function of wheel load

rail. Recall that Figure 5 showed this area develops toward the gage or field side of the rail, about 0.4 to 0.6 inch (10 to 15 mm) below the running surface. Figure 8 shows that at higher loads the fatigue resistance is only weakly dependent on wheel load. That is, the slope of the wheel load-life line is rather steep. While the figure assumes a residual stress field associated with heavy traffic (e.g., 100 ton cars), larger residual stresses would develop if

heavier wheel loads due to increased GVW cars were encountered in service. As such, the predicted behavior for loads above the 30 kip (134 KN) level is somewhat artificial, as compared to service situations. At lower wheel load levels, the results show a marked change in the slope of the load life curves. Life assessed in terms of cycles to initiation is much more dependent on load above 7.5 kips (33.5 KN) as compared to below that load. However, in terms of MGT/rail, this break point does not occur until wheel loads approach levels below that associated with empty cars!

Recall that the results for first initiation (rail failure) presented in the last column of Table 1 suggested that wheel loading (train makeup) should be matched to weight. Differences in life, however, were not that great. Because for a given load level, contact and head-on-web stresses dominate the BOEF bending stress field in the head, the trend shown for 132 lb/yd (66.6 kg/m) rail will be similar in rail heads with similar depths. As such, the trend shown in Figure 8 reflects the behavior of a wide class of rail weights. However, this assertion must be tempered by the fact that lighter rail suffers more extensive flow, and thus develops shorter lives, as evident in Table 1.

The results of Figure 8 can be used to explore the question of inspection frequency to maximize the utility of such facilities. For example, consider inspection frequencies for track that runs fewer trains with heavier cars as compared to more trains with lighter cars. An extreme case would be that of 50 kip (223 KN) wheel loads versus 24 kip (107 KN) wheel loads, for a yearly volume of 25 MGT/track or 12.5 MGT/rail. For the lighter load failure occurs at about 380 MGT/rail, so that cracking would become a problem after about 30 years. The heavier loading would result in failure after 225 MGT/rail. Thus, at the same volume, cracking would become a problem after 18 years. Defect frequency and size increases with MGT [1,3]. Thus, the heavier used track should be inspected about twice as often based on these predicted lives.

Predicted Influence of Train Speed and Track Class

The final aspect of tonnage increases considered here is the effect of running speed and track class. Given that speed influences rail stresses as compared to the quasistatic cases examined, speed will influence life through changes in both the wheel stress and flow induced residual stresses. Data useful in characterizing the influence of speed on rail stress are reported in References 28 and 29. Pertinent observations include:

- The effect of speed is largely concentrated in the low probability regions of the distribution of wheel load versus percent wheels exceeding, as shown in Figure 9(a). A few percent of the loads significantly exceed the static (median) load, whereas a few percent fall significantly below the static load.

- The relative effect of speed on loads is more severe for lateral loads as compared to vertical loads. However, the absolute effect is greater for vertical loads.

- Worst case conditions for train makeup depends on factors such as type of car, wheel and track conditions and the magnitude of the loading. Thus, train makeup by itself is not a controlling factor.

- The influence of speeds may be much worse in the vicinity of joints.

- Impact effects from wheel flats and load magnification due to wheel eccentricities may be significant, and tend to increase with increased speed.

- The class of track has an influence on loads which is tied to speed. Lower track classes and speeds tend to generate large loads due to car roll while car bounce generates large loads at higher speeds.

- The relationship between speed and load is a combination of car, truck, wheel, track and foundation parameters. Impact and car bounce and roll tend to dominate the dependence of vertical load on speed.

The results developed in this section are typical of the influence of speed. Specifically Figure 9(a) is used in this development. Note that Figure 9(a) reflects the dynamic load magnification determined from BOEF type measurements. As such, it may not completely reflect the magnification that may be present in the region where fatigue damage accumulates the fastest. Note too that these data are developed from track laid on wood ties. Because dynamic loads depend on system damping, the effect of speed may be worse than shown if concrete ties are used in place of wooden ties. Likewise, dynamic effects would be worse in the vicinity of bridges, and transitions to and from bridges.

The dynamic load magnification factor of Figure 9(a) may be transformed into a dynamic life magnification factor using the results in Figures 4(b) and 8. Trend curves developed in this way are shown in Figure 9(b) on coordinates of percent wheels exceeding and dynamic life magnification. Note that the dynamic life magnification is represented on a logarithmic scale. The few occurrences of very large load in Figure 9(a) now correspond to reductions in life by as much as a factor of 10. This reduction is somewhat larger for the higher speeds. A similar behavior develops at the other extreme for which life is dynamically enhanced. Again this enhancement is larger for the larger speeds.

The results of Figure 9(b) show a significant fraction of the loads applied are magnified as compared to the static case. Life reductions due to these loads are as large as 0.5, for more than 10 percent of the applied loads. Conversely, an almost equal number of lower loads develop. If truly random in occurrence, reductions due to higher loads would tend to balance life increases due to lower loads. Thus the net effect of speed increases may not be too significant. This suggests that the static results may be only slightly optimistic. Significantly, the very degrading effects of bounce and roll develop at speeds below the maximum speeds employed in this country. For this reason there is no apparent benefit in running at lower speeds. Indeed higher speeds on higher classes of track may do less fatigue damage than lower speeds on lower classes of track, provided that wheel flat impact is not a serious problem.

Note that it was earlier concluded in the context of a quasistatic model that octahedral stress is not a strong function of foundation modulus. However, the loading is truly dynamic. In contrast to the quasistatic case, track modulus has an influence on the dynamic load transferred to the rail by a given wheel load. Under dynamic conditions stiffer moduli give rise to higher loads whereas softer moduli develop lower rail loads, for the same GVW [29]. Foundation modulus, therefore, does influence rail life in proportion to the increase in load due to speed-modulus-wheel load dynamic interaction. For the earlier considered limits in modulus of 13.8 MPa (2 ksi) to 48.2 MPa (7 ksi), rail for the lower

modulus would survive more than a factor of two longer than the stiffer modulus under typical dynamic conditions. Thus, modulus may be a significant factor in assessing rail fatigue resistance.

DISCUSSION

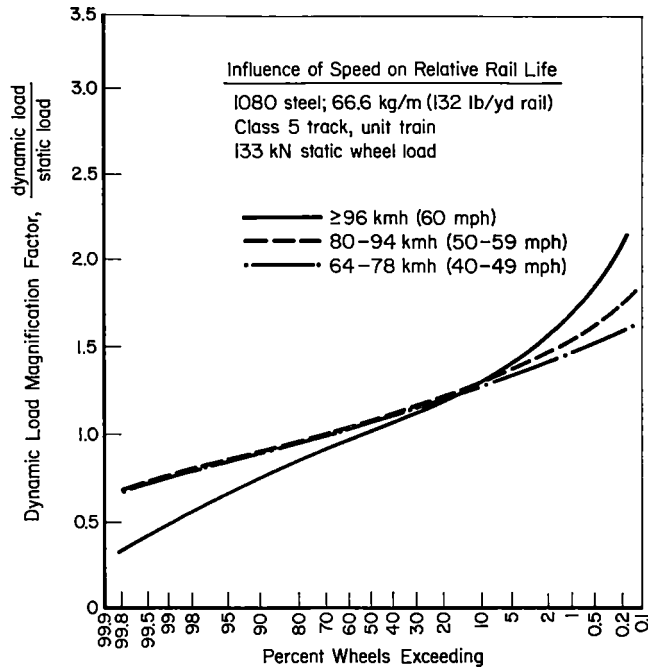
One purpose of this paper was to develop an analysis framework to predict crack initiation in the head of a rail. Since the end use of this analysis framework is the optimization of rail operational parameters to maximize both rail life and tonnage, this framework had to be sensitive to operational parameters and reasonably accurate. Based on the results presented, such a framework has been developed. However, the absolute accuracy of the model remains dependent on the as yet unverified extrapolation of periodic overstrain data following trends reported in the literature. It has been shown that flow induced residual stress, thermally induced mean stress, and the stresses due to typical vertical wheel loads are comparable under quasistatic conditions. The analyses presented suggest that longer lives will develop in heavier rail for comparable loadings. However, in contrast to the expectation that longer lives are due primarily to lower wheel induced stresses, this analysis suggests they are due to lower thermal mean and flow induced residual stresses, if fatigue controls failure.

With reference to the conference theme--increased tonnage--the desired increase can be realized for example through higher wheel loads. Table 1 indicated that wheel loads should be matched to rail weight if the maximum life of the rail is to be achieved. Further, analysis for 132 lb/yd (66.6 kg/m) rail shown in Figure 8 indicated that a rational basis exists to establish load limits as a function of rail repair/replacement schedules. Similar analysis could be made to establish whether existing rail weights can be expected to survive for economically useful lives over a range of desired tonnage increases. While useful for such life cycle analysis, studies of that nature can only be hinted at within the scope of the present paper.

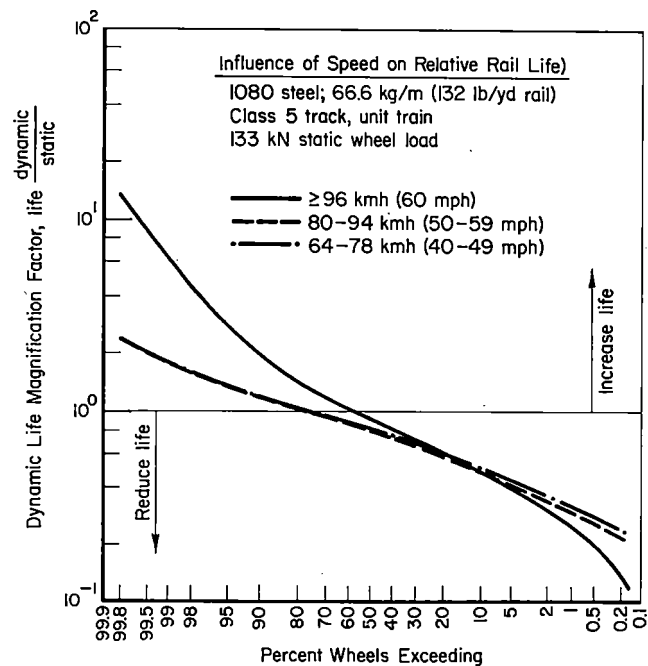
Some dynamic loadings, such as those due to increased speed and wheel flats, could certainly enhance the quasistatic initiation process considered. However, as discussed in Reference 10, the influence of these dynamic loads does not appear to be a major factor in developing fatigue resistance data. Simply put, available impact fatigue data do not indicate major life reductions would develop given the random nature of wheel flat impacts for all but chronic situations. For this reason the effects of wheel flats have not been addressed.

Figure 9(b), which explored the possible influence of increased train speed indicated it is not a major factor for higher classes of track, provided wheel flats are not a chronic problem. However, given the complex dependence of dynamic stresses on the range of system parameters involved, this observation should not be extrapolated beyond the conditions represented in Figure 9(a). Rather, the effects of speed should be considered on a case by case basis, and all systems variables known to significantly influence stresses should be explored.

There are a number of implications that derive from the analysis presented in regard to optimizing rail shape and metallurgy in order to maximize rail fatigue life. Regarding rail shape, the results of the stress analysis suggest that contact stresses and head-on-web bending stresses dominate the stress field in areas where initiation is predicted to develop, and observed to occur in service. BOEF bending stress contributes to the distribution, but does not exert a strong influence. Since life relates to cyclic stress magnitude, changes in the head to



(a) Rail loads



(b) Rail life

Fig.9 Influence of train speed on rail loads and fatigue resistance

spread the contact patch perhaps through head-on-web bending could lead to significantly longer lives. Likewise any related change in rail or wheel shape which would reduce stresses but still be compatible with existing equipment could significantly increase rail fatigue life.⁹ It is equally obvious to state that any change in metallurgy to improve materials fatigue resistance beyond that shown in Figures 3 and 4 will also enhance rail life. Clearly, hardening a portion of the rail head will achieve this goal. But, hardening will also change the residual stress distribution as compared to hot rolled rail. It may also decrease the materials fatigue resistance to higher stresses. More significant than such improvements in constant amplitude behavior would be an enhanced fatigue resistance to periodic overstrain histories. It is clearly this behavior which controls rail life. For this reason, materials for rail service should be screened for fatigue resistance using some representative service loading. Likewise, metallurgies resistant to overstrain effects should be pursued.

The form of Equation (2) suggests that rail metallurgies which retard flow induced residual stresses would lead to longer service lives. However, whether this improved flow resistance is developed via hardness or alloying additions remains a question for further laboratory experiments and analytical studies. Given that wear character will change with such metallurgical changes, care must be exercised to optimize fatigue resistance without creating related wear problems.

The failure postulate advanced has implications that carry over to decisions regarding rail replacement and repair based on field experience as portrayed for example in Weibull plots [2,3], as follows. Recall that thermally-induced mean stresses and flow-induced residual stresses are indicated to be major factors in determining rail life. Also note that what limited stress analysis exists for the influence of worn rail indicates that moderate amounts of wear do influence stresses and therefore life.¹⁰ These observations suggest that failure experience gained under one set of operational conditions may not carry over to another. Thus, in turn, they suggest that care should be exercised in developing plots of failure experience as a function of MGT.

⁹ Such a conclusion is intuitively obvious and thus has been drawn in the past. The significance of its restatement here is not to reaffirm this fact. Rather it is made because analytical tools now exist which would facilitate quantitative comparisons of such changes without resort to prototype studies. Only if specific geometries were found to develop major reductions in stress would prototype development and further study be warranted.

¹⁰ At first thought, wear is considered to increase the stresses due to decreased cross section. Associated with this is an ever changing residual stress pattern. In view of the failure postulate adopted, this changing pattern may result in damage being distributed on different layers which penetrate into the head as wear occurs. This may actually forestall initiation because damage is spread throughout the head rather than concentrated in one area. Clearly, however, there is a bound to this process, and damage accumulation will eventually lead to initiation if the rail is not removed from service due to wear.

The analysis presented clearly indicates that such plots--as for example a Weibull plot [3]--are valid and appropriate for use in situations where operational characteristics are similar. But given the complex dependence of life on operational characteristics, the results presented indicate the indiscriminate use of such plots may result in a much too early retirement, or an incidence of cracking greater than anticipated. Whether or not an unanticipated large incidence of cracking means defects could develop to larger than desired sizes or could grow to failure between inspection intervals, however, remains a subject for future studies.

The analysis suggests that vertical split heads (VSH), shelly fractures (SF), detail fractures (DF), and transverse defects (TD) should ultimately develop in relatively the same number in a given rail section. The results also suggest that shells are precursors to detail fractures. Thus, one might conclude that the results presented support the practice of pooling defect data for any or all of these defects. However, such is not the case. Recall it was postulated that the failure process which terminates in macroscopic cracking on the transverse plane may initiate on a plane other than a transverse plane. It was further suggested that microcrack growth continued on the plane of initiation until some metallurgical feature was encountered. In turn that feature facilitated rotation of the crack onto the transverse plane, where thermal mean stresses in addition to the already active flow induced residual and wheel induced octahedral stresses would grow it to a rejectable size.

The just stated failure process is clearly statistical in nature. For example, growth as a shell-like defect will occur until some micro-metallurgical feature such as a pearlite colony favors its rotation onto, and apparently rapid growth [8] in, the transverse plane. Such a situation indicates a gradually increasing incidence of shells and detail fractures as a function of MGT. Alternatively, the presence of a large inclusion would favor initiation and subsequent growth on the transverse plane. In contrast to the incidence of SF and DF failures, the incidence of the inclusion-initiated TD's would be expected to decrease with cumulative MGT under comparable conditions.¹¹ Thus, while both defect types are ultimately expected to generate a comparable incidence of failures, the sum of their respective rates which develops if such data are pooled does not yield a constant trend as a function of MGT. The pooling of such data for purposes of Weibull analyses, or for purposes of developing a service related experience base for use in the repair/replacement decision process, therefore, may be somewhat suspect.

While the failure process is clearly statistical in nature, there are equally significant deterministic operational considerations which require that care be exercised in formulating a service-experience data base. Further, because of the impact of the operational parameters on the mean life to initiation, care must be exercised in interpreting the results of such statistical analyses, and in applying the results to other service situations. Because the present deterministic framework can be easily extended to predict failure rates [30], consideration is now being given to such analysis for purposes of synthesizing the failure incidence of rails to further explore this aspect of the problem.

SUMMARY

A failure hypothesis regarding crack initiation in railroad rail was advanced and a model developed to predict rail life on that basis. Application of the model to various operational situations showed that predicted lives correspond reasonably with those encountered in service. Specifically, only a deterministic analysis using data that reflect a lower bound fatigue resistance for a 1080 rail steel was used, so that failure rates were not addressed. A number of operational parameters were examined in a sensitivity analysis to assess which of these control the fatigue damage rate process in rails. Included were: wheel eccentricity, foundation modulus, lateral loads, vertical load level, rail weight, speed, and class of track, and train make-up. The analysis performed included the effects of flow induced residual stress and thermally induced mean stresses, and limited consideration of wear effects.

The results of the study suggest that failure of railroad rails by a fatigue mechanism is largely controlled by flow induced residual stresses and by thermally induced mean stresses. The implications of these findings were discussed with respect to the optimum combination of operational parameters and rail metallurgies with a view to maximizing rail fatigue life, subject to the constraints of other failure mechanisms such as wear. Finally, the implications of this study regarding retirement for cause and the analysis of service experience using Weibull plots were discussed. It was shown that a defect type and its incidence are strongly dependent on operational characteristics, so that care must be exercised in pooling the results generated for a range of defect types and operational characteristics.

CONCLUSIONS

Major conclusions that can be drawn from the results of this study include:

- o Reasonable predictions of rail fatigue life are possible through the use of appropriate mechanics analyses and materials fatigue life data.

- o The failure postulate and failure criterion used to relate the rail head damage state to the materials fatigue life data must reflect the rail failure process if accurate predictions are to be made.

- o For the range of parameters considered, fatigue failure in a rail is controlled primarily by thermally induced mean stresses, flow induced residual stresses, and wheel induced contact stresses coupled with head-on-web bending stresses. Beam-on-elastic-foundation bending stresses contribute to wheel induced stresses, but taken alone are not a dominant factor. Lateral flange loads and wheel impact may contribute to the damage process; however, given the random nature of their occurrence they are not considered to be a factor for tangent track. However, in curves, the frequency of flange loads is large enough to make lateral loading a controlling factor. Speed in many situations is not a

11 Given the same loadings, the larger inclusions would result in early failures. Smaller and smaller inclusions require proportionally higher levels of MGT to develop failures. In the limit, the inclusion size is statistically no larger than the mean size of features associated with SF and DF formation, which is inherent in the data of Figures 3 and 4.

coupled effect of speed and poor maintenance through higher loads due to impact from wheel flats.

- o Both operational parameters and rail metallurgy could be optimized to maximize rail fatigue resistance.

- o Increased tonnage through increased wheel loads could significantly reduce rail fatigue life, particularly on lighter rails which would develop large flow induced residual stresses under such conditions.

RECOMMENDATIONS

Significantly, the stress fields which develop in rail tend to follow a number of simple characteristic patterns as functions of rail weight and wheel load. These results, selectively coupled with the results for other stress analyses that include the effect of wear, could form the basis for a simplified but still accurate model for rail stresses, for a range of loadings. This simplified stress model, coupled to a damage postprocessor that includes both fatigue and wear related failure criteria, would facilitate convenient and inexpensive simple analyses of the rail failure process. Thus, the apparent dilemma in choices to maximize rail life and increase productivity (as for example through increased tonnage) presently facing the railroads due to rail cracking, could be rationally resolved. Further, by maximizing rail life through optimum selection of rail-wheel profile, rail metallurgy, and operational parameters, replacement costs could be reduced and at the same time volume increased. That is, for example, tonnage could be increased and the consequences known in advance--adverse conditions could be predicted and avoided. In view of the results of this paper, such predictive models are clearly within reach of today's technology. Whether or not they have a place in the industry remains for industry to decide.

ACKNOWLEDGEMENTS

Much of the data base and other information used in this paper have been developed under the auspices of the Transportation Systems Center (TSC), of the Department of Transportation (DOT). The evolution of both the failure postulate and the failure criterion used in this paper was supported by the Fatigue and Fracture Technology Projects Office (FFTPO), of the Transportation and Structures Department, of Battelle's Columbus Laboratories (BCL). Likewise, all analyses presented as well as the preparation of this manuscript, were supported by the FFTPO of BCL. The support of both organizations is gratefully acknowledged.

REFERENCES

- 1 Hopper, A. T., private communication with BNL on "Analysis of Rail Flaw Statistics", done under program DOT/TSC 1708--Track Structures Metallurgy Support, January, 1982.
2. Steele, R. K., and Rieff, R. P., "Rail: Its Behavior and Relationship to Total System Wear", Proceedings 1981 FAST Engineering Conference, Denver, November, 1981, pp 115-161.
3. Besuner, P. M., et. al., "Probability Analysis of Rail Defect Data", Heavy Haul Railways Conference, Perth, Australia, 1978, paper I.4.

4. Wells, T. R., and Gudiness, T. A., "Rail Performance Model: Technical Background and Preliminary Results", AAR Report No. R-474, May 1981.
5. Perlman, A. B., Jeong, D. Y., Orringer, O., and McConnell, D. P., "Sensitivity of Rail Fatigue Life Estimates to Track Service Environment Factors, to appear in AREA bulletin.
6. Abbott, R. A., and Zaremski, A. M., "On the Prediction of the Fatigue Life of Rails", AREA--Bulletin, 1978, pp 191-203.
7. Zaremski, A. M., and Abbott, R. A., "Fatigue Analysis of Rail Subject to Traffic and Temperature Loading", Heavy Haul Railways Conference, Perth, Australia, 1978, paper I.2.
8. Steele, R. K., "A Perspective Review of Rail Behavior at the Facility for Accelerated Service Testing", FRA/TTC-81/07, June, 1981.
9. Leis, B. N., "Rationalizing Failure with the Aid of Fracture Mechanics", Decade of Progress, Vol. 2, ASME (to appear).
10. Leis, B. N., and Rice, R. C., "Selection of Failure Criteria", Interim Report on Item 4.3, Contract DOT/TSC 1663, January, 1982, from BCL to TSC; see also Sampath, S. G., et. al., "Analysis of Service Stresses in Rail", Final Report on Contract DOT/TSC 1663, from BCL to TSC, (in preparation).
11. Johns, T. G., et. al., "Engineering Analyses of Stresses in Railroad Rails", Final Report on Contract DOT/TSC 1038, March, 1981, from BCL to TSC.
12. Groom, J. J., "Residual Stress Determination", Final Report on Task 2 for Contract DOT/TSC 1426, from BCL to TSC, 1979.
13. Monthly Progress Reports on Contract DOT/TSC 1708, from BCL to TSC, January, 1981.
14. Rice, R. C., Leis, B. N., and Tuttle, M. E., "Residual Stresses and the Fatigue and Fracture Behavior of Railroad Rail", Residual Stresses, ASTM STP 776, 1982, pp 132-157.
15. Leis, B. N., and Laflen, J. H., "Cyclic Inelastic Deformation and Fatigue Resistance of a Rail Steel: Experimental Results and Mathematical Models", Topical Report to Transportation Systems Center (TSC), Department of Transportation (DOT), on DOT/TSC Program 1076, Battelle's Columbus Laboratories (BCL), June 1977.
16. Leis, B. N., "Cyclic Inelastic Deformation and Fatigue Resistance of Rail Steels", in Rail Steels--Developments, Processing and Use, ASTM STP 644, 1978, pp 449-468.
17. Broek, D., and Rice, R. C., "Fatigue Crack Initiation Properties of Rail Steels", Final Report on Contract DOT/TSC 1426, from BCL to TSC, 1980.
18. Stone, D., Association of American Railroads--Private Communication with BNL, January, 1982.
19. Steele, R. K., Transportation Test Center--private communication with BNL, January, 1982.
20. Leis, B. N., "An Energy-Based Fatigue and Creep-Fatigue Damage Parameter", Journal of Pressure Vessel Technology, Trans. ASME, Vol. 99, No. 4, November, 1977, pp 524-533.
21. Leis, B. N., and Laflen, J. H., "An Energy-Based Postulate for Damage Assessment of Cyclic Nonproportional Loadings with Fixed Principal Directions", Proceedings ASME Symposium on Ductility and Toughness in Elevated Temperature Service, San Francisco, November, 1978, MPC-8, pp 371-389.
22. Leis, B. N., and Laflen, J. H., "Problems in Fatigue and Creep-Fatigue Damage Analyses Under Nonproportional Cycling", Journal of Engineering Materials and Technology, Vol. 102, No. 1, pp 127-134, January, 1980.
23. Brose, W. R., Dowling, N. E., and Morrow, J., "Effect of Periodic Large Strain Cycles on Fatigue Behavior of Steels", SAE Paper No. 740221, 1974; see also Conle, F. A., "An Examination of Variable Amplitude Histories in Fatigue", Ph.D. Thesis, University of Waterloo, Canada, 1979.
24. Libertiny, G. Z., Topper, T. H., and Leis, B. N., "The Effect of Large Prestrains on Fatigue", Experimental Mechanics, Vol. 17, No. 2, February, 1977, pp 64-68; see also Topper, T. H., and Leis, B. N., "Fatigue Life Prediction of Stamped Structural Components--Phase II", Final Report to Ford Motor Co., from University of Waterloo, 1973.
25. Kennedy, J. C., "Stress Distributions in Railroad Rail", Interim Report on Contract DOT/TSC 1663, from BCL to TSC, (in preparation); see also Sampath, S. G., et. al., "Analysis of Service Stresses in Rail", Final Report on Contract DOT/TSC 1663, from BCL to TSC, (in preparation).
26. Leis, B. N., "Microcrack Growth Behavior of a Rail Steel", Interim Report on Item 13, Contract DOT/TSC 1663, January, 1982, from Battelle's Columbus Laboratories (BCL) to the Transportation Systems Center (TSC); see also Sampath, S. G., et. al., "Analysis of Service Stresses in Rails", Final Report on Contract DOT/TSC 1663, from BCL to TSC (in preparation).
27. Williams, D. P., Lind, N. C., Conle, F. A., Topper, T. H., and Leis, B. N., "Structural Cyclic Deformation Response Modeling", Proceedings of the ASCE Speciality Conference on Engineering Mechanics, May, 1976, in Mechanics in Engineering, University of Waterloo Press, 1977, pp 291-311.
28. Ahlbeck, D. R., et. al., "Measurement of Wheel/Rail Loads on Class 5 Track", Interim Report FRA/ORD-80/19, to Federal Railroad Administration, from BCL, 1979.
29. Dean, F. E., Harrison, H. D., Prause, R. H., and Tuten, J. M., "Investigation of the Effects of Tie Pad Stiffness on the Impact Loading of Concrete Ties in the Northeast Corridor, Final Report to Federal Railroad Administration (FRA), BCL, Program DOT-FR-9162, January 1982.
30. Leis, B. N., "An Approach for Fatigue Crack Initiation Life Prediction with Applications to Complex Components", in Fatigue Life of Structures Under Operational Loads, Proceedings of the 9th International Committee on Aeronautical Fatigue Meeting, ICAF Doc. 960, Laboratorium für Betriebsfestigkeit, May, 1977, pp 3.4/1-47.

James M. Tuten
Research Scientist

Donald R. Ahlbeck

Principal Research
Engineer
Battelle-Columbus
Laboratories
Columbus, Ohio

Determination of the Wheel/Rail Load Environment at the Facility for Accelerated Service Testing (FAST)

During the summer of 1979, a series of tests were conducted at the Transportation Test Center near Pueblo, Colorado, to determine the vertical and lateral wheel/rail loads on the Facility for Accelerated Service Testing (FAST) track. During these tests the wheel/rail loads were measured at seven wayside locations in one of the curved track sections. The loads were measured for a variety of operating conditions and consist configurations. The data were indexed and a detailed statistical data base was constructed. Using this data base, the effects of speed, train direction, vehicle weight, and vehicle component variations on the wheel/rail load environment were investigated. Statistics for the consist as a whole and also individual axle and truck statistics were generated and analyzed.

INTRODUCTION

The Facility for Accelerated Service Testing (FAST) at the Transportation Test Center (TTC) near Pueblo, Colorado was created by the joint efforts of the Federal Railroad Administration (FRA), the Association of American Railroads (AAR), the Transportation Development Agency (TDA) of Canada, and by the railroads and the Railway Progress Institute (RPI). FAST provides simulated service testing of both track and vehicle components at rates of service much higher than possible under normal revenue traffic conditions.

The facility consists of a 4.8-mile (7.7-km) loop of track divided into sections which provide many variations in track construction. Experiments include both wood and concrete ties, a variety of rail fasteners, both bolted-joint and continuous-welded rail, different rail metallurgies and ballast conditions, on both tangent and curved track.

A test train of four locomotive units and about 75 cars (primarily loaded 100-ton-capacity cars) accumulates 100 to 125 laps around the track loop each night, five nights a week at a normal operating speed of 45 mi/h (72 km/h). At this rate, the test train subjected the track to over 150 million gross tons (MGT) of loading between September 1976 and December 1977. This is about seven times faster than possible on a revenue freight track. Numerous measurements of track and vehicle characteristics have been made at planned intervals to assess component performance and to establish rates of wear and degradation.

An important aspect of the FAST experiments is a statistical definition of the wheel/rail load environment to which the track and vehicles are subjected. The load environment has been defined for typical revenue traffic in North America by several recent studies (1-3). However, the FAST train provides a unique, and in some respects, a more severe, load environment.

Instrumented wheelsets have been used to record wheel/rail loads under individual rail cars (4,5). To record loads under the complete train, wayside instrumentation was utilized in the "FAST Wheel/Rail Loads Test" conducted during the summer of 1979. After completion of these tests, a data base was generated to allow a statistical presentation of results. The wheel/rail loads data base developed during this effort is one of the most comprehensive developed to date. By combining a high degree of program flexibility with a very detailed indexing system, statistics were generated for a large number of individual test populations. This paper describes the wheel/rail load test, the development of the data base, the types of statistical formats in which the data are presented, and a brief discussion of some of the test results.

TEST DESCRIPTION

The FAST Wheel/Rail Loads Test was the first comprehensive attempt to characterize the wheel/rail load environment at FAST. At the time the test was conducted, the FAST Facility had been in operation for almost three years and had accumulated just over 400 million gross tons of traffic. By conducting a specific series of tests to determine the wheel/rail load environment, test variables which might affect the load environment could be controlled. The overall objectives of the tests were:

- Determine the lateral and vertical wheel/rail load versus speed relationship for the FAST consist on curved track;

- Determine the effects of train operating characteristics (i.e., buff, draft and drift) on wheel/rail loads at specified speeds on curve track;
- Assess the dynamic performance of a 100-ton hopper car over various sections of the FAST Track, utilizing an instrumented wheelset;
- Assess the effects of car component wear on vehicle dynamic performance;
- Determine the differences in wheel/rail loads as a function of truck type;
- Obtain load data to aid in establishing a correlation between FAST rail wear and predictive rail wear models being developed under the Track Train Dynamics Program; and
- Develop correlation between wheelset vertical and lateral load data and wayside wheel/rail load data.

Runs in 59 distinct configurations were completed during the test program. Wayside data were recorded for 12 of these test configurations for a total of 101 train passes by the instrumented wayside site. Table 1 shows the run numbers and test parameters for each of the runs for which wayside data were recorded.

TABLE 1. FAST wayside data runs

Run No.	Number of Laps	Speed (mi/h)(km/h)	Train Direction	Test Date	Operating Conditions (Sect. 07)
5	6	30 (48)	CW	6/19	Draft
6	6	34 (54)	CW	6/19	Draft
7	6	34 (54)	CW	6/19	Buff
8	6	34 (54)	CW	6/19	Drift
9	20	45 (72)	CW	6/20	Draft
10	6	30 (48)	CCW	6/21	Draft
11	6	34 (54)	CCW	6/22	Draft
12	7	34 (59)	CCW	6/22	Buff
13	6	34 (54)	CCW	6/22	Drift
14	20	45 (72)	CCW	6/20	Draft
15	6	45 (72)	CCW	6/18	Draft un-lub*
16	6	45 (72)	CW	6/18	Draft un-lub

*Curve lubricators inoperative.

Test Train Consist

The abbreviated train consist for the wheel/rail loads test was made up of cars from the FAST train. The consist was well documented and included from 54 to 56 cars pulled by three or four locomotives, depending on the particular test run. The majority of the test train consisted of loaded 100-ton hopper cars. Although the makeup of the consist was constant for each test run, it did vary slightly from test to test. The last twelve cars of the consist, however, were part of a test to determine the effect of car weight on the wheel/rail load environment, and maintained their position in the consist and in relation to each other for the duration of the test. This group was made up of 3 110-ton hopper cars, 3 100-ton hopper cars, 3 66-ton hopper cars, and 3 empty hopper cars, respectively. The different cars of the consist (excluding the weight test group) were equipped with various mechanical equipment and truck types to determine the effect such equipment would have on the wheel/ rail load environment.

Complete details of the results from this portion of the test are not presented in this paper. The data may be found in Reference 6 and will be reported in greater detail after further analysis has been completed.

Wayside Test Site Description

The wayside instrumentation was located in Section 7 of the FAST track, shown in Figure 1. This 1177-foot (359 m) CWR track section is a 5-degree (349 m radius) curve with 4-1/2 inches (11.4 cm) of superelevation and conventional wood tie construction. Seven irregularly-spaced locations were instrumented in this track section. Vertical and lateral strain gage load-measuring circuits were installed on both rails at each location by TTC personnel. The standard ORE "chevron" gage pattern on the rail web was used to measure vertical loads, while a Battelle-designed gage pattern on the rail base was used to measure lateral loads (7). The strain gage circuits were calibrated by applying known vertical and lateral loads through a special loading fixture and comparing the rail circuit response voltage with the known input loads. Values were thereby established in engineering units for step voltage changes from resistor shunt calibrations in each circuit. Four 14-channel signal-conditioning amplifier units utilizing frequency-division multiplexing were positioned at the trackside to minimize cable lengths to the strain gages. The multiplexed signals were recorded on analog tape at a central location for later processing.

Post-Test Data Reduction

Tape-recorded analog signals were converted to a digital format by a microprocessor-controlled field data reduction system. The multiplexed signals were first demodulated, then lowpass filtered at 300 Hz through 4-pole Bessel filters before analog-to-digital conversion. The microprocessor determined the peak value for each channel and each passing axle, converted the resulting voltage-related number to engineering units, and stored the peak value for printing and recording on digital cassette tape. The printer produced tables of peak values of lateral (L) and vertical (V) loads and L/V ratios for each axle passing each site.

Digital cassette tapes were then read into Battelle's CDC Cyber 74 computer system for further processing. Data were validated by comparing tabular values with oscillograph recordings to assure that signal quality was good on individual channels, that noise or tape drop-out problems were not encountered, and that axles of the train were not missed. Digital data were edited and corrected where necessary, and the validated data set was stored in an addressable file indexed by run number and multiplex number.

The next step in processing was to construct a file of indexed and sorted data values. A seven-digit index number was used to define the location (measurement site), car number, axle number, and run/lap number for each associated set of vertical and lateral load and L/V numbers. This keyed data base was then used as the basis for different statistical manipulations to produce both numerical and graphical formats.

Statistical Data Formats

In order to study the effects of various parameters, the data were organized into several statistical formats. These included numerical values of

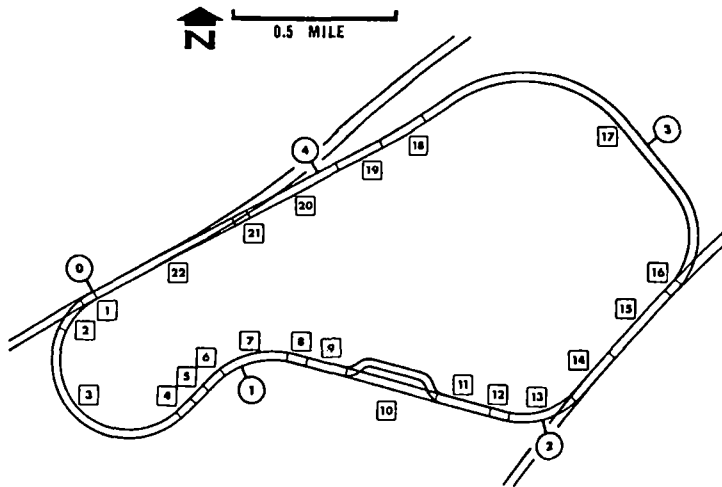


Figure 1. FAST track layout

means and standard deviations, and plots of probability densities and cumulative probability distributions. By using the keyed data base, individual populations of data points could be examined if desired, such as the lateral loads at a specific crib number produced by Axle No. 1 of Car No. 013 on the high rail. Combinations of populations were used to provide a more substantial data base, such as lumping together the lateral loads of all lead-outer wheels (Axles 1 and 3) from all 7 measurement sites for all 100-ton hopper cars.

The statistical calculations were made by dividing the total expected data range into 200 equal intervals (bins) and summing the number of peak values under a specific key number (or combination of key numbers) occurring within this interval. Using the resulting "bin count" numbers, frequency-of-occurrence histograms (probability density) and frequency-of-exceedance plots (probability distribution) were generated through computer graphics routines.

An example of the frequency-of-occurrence histogram is shown in Figure 2. This plot shows the ratio of the number of peak loads within each of 50 1.2-kip (5.3 kN) load intervals which cover the expected vertical load range of 60 kips (267 kN). By choice, the original 200 bins have been grouped by 4's. It is important to note that the quantitative results for the histogram depend on the selected load interval (bin size) and are therefore not unique. Increasing the load interval (reducing the number of bins) will increase the number of occurrences at a particular load level. This improves the averaging used for the estimate, but reduces the resolution.

Another useful format is the frequency-of-exceedance plot shown in Figure 3. This plot allows a quick determination of how many axles of the particular population will produce loads or L/V ratios greater than a given level. This format is of particular value in both fatigue and life cycle predictions. To produce this format, the number in each succeeding bin is subtracted from the total number over the range of the variable. The results are plotted on a normal probability graph so that a Gaussian distribution will appear as a straight line.

The interrelationship between lateral and vertical loads (not simply the L/V ratio) is of great interest, and is best characterized by frequency-of-exceedance of lateral load versus vertical load, as

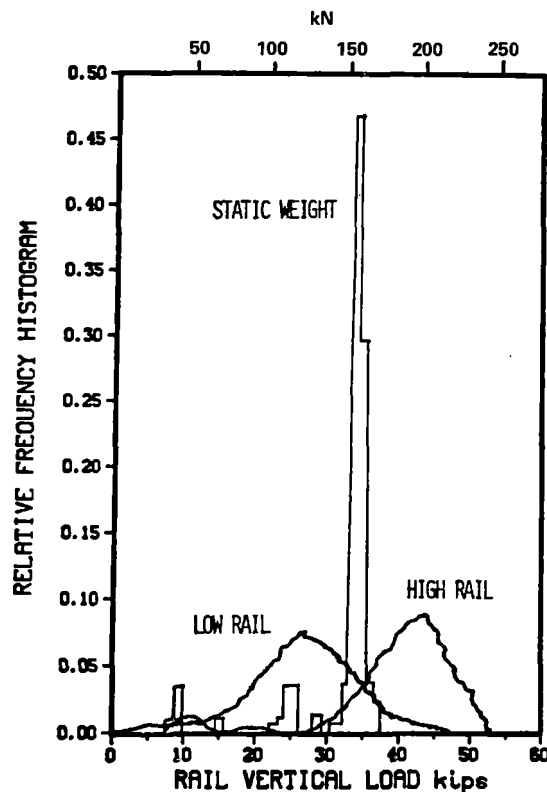


Fig. 2 Vertical load relative frequency histogram

shown in Figure 4, or by the joint probability distribution of lateral and vertical loads, as shown in Figure 5. To calculate the joint frequency-of-exceedance, the load ranges of interest were first determined. A lateral load range of -10 to +28 kips¹ (-44 to +124 kN) and a vertical load range of 0 to 60 kips (267 kN) were chosen. These ranges were then divided into 20 equal intervals (bins) to give a 20 x 20 matrix of load pairs. The total number of loads occurring in each bin of the matrix was then

¹ A positive lateral load is defined as spreading the rails.

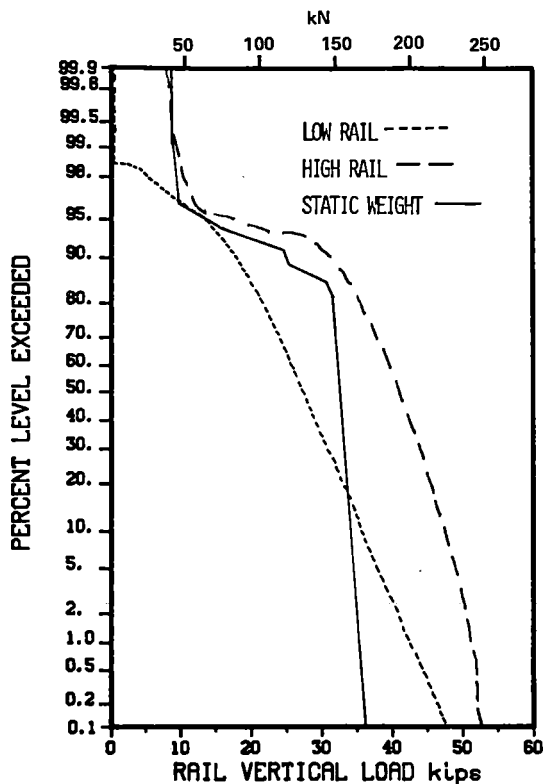


Fig. 3 Vertical wheel load exceedance distribution function

matrix, the joint probability distribution of lateral load versus vertical load and the conditional distribution (probability of L for a given V) were calculated and used to generate the different plot formats of Figures 4 and 5. Figure 5 shows that two populations of cars are apparent: first the loaded cars centered near 40 kips (178 kN), and then the three empty cars at the end of the train, centered near 10 kips (44 kN) of vertical wheel load. As a further example of this format, results from the low rail are given in Figure 6. Here, the lateral loads from two distinct populations of axles--leading and trailing--under the loaded cars are evident.

EXPERIMENTAL RESULTS

Experimental wheel/rail load data can be understood best when compared with and used in conjunction with a predictive model. Figure 7 shows the lateral loads predicted for a 100-ton hopper car in steady-state curving. Loads for each of the four wheels of a standard "three-piece bogie" were calculated using Battelle's nonlinear computer code called SSCUR2, which is based on the wheelset curving equations of Newland (8). This program accounts for the nonrigid, lozenging behavior of the freight car truck, and includes the wheel adhesion limit, flange contact, rail lateral stiffness, and suspension stops (9). Mean values of lateral load from instrumented wheelset measurements made by IITRI are shown in Figure 7 to provide verification of these predictions.

In steady-state curving, the leading wheelset of a freight car truck will assume a positive angle of attack of approximately one-half degree, resulting in

TOTAL FAST DATA HIGH RAIL

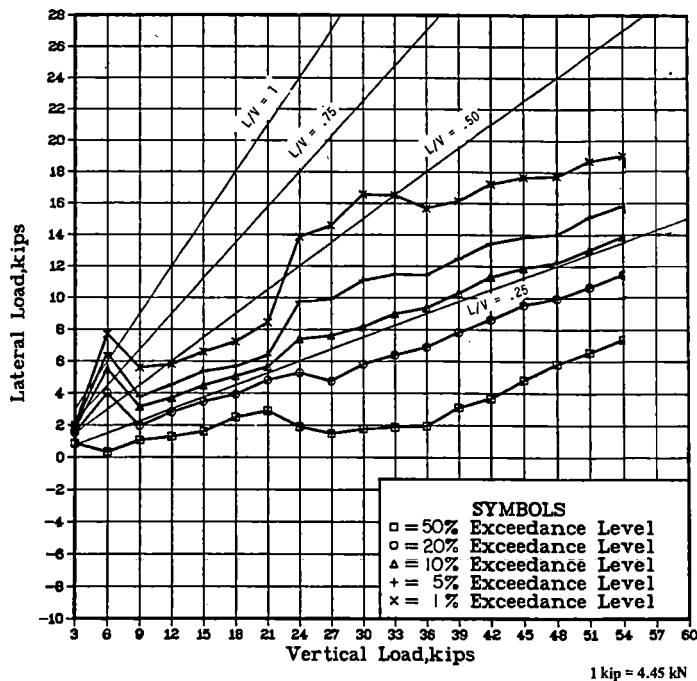


Fig. 4 Lateral load exceedance levels for high-rail FAST data

lateral creep forces on both rails directed toward the center of curvature. On a 5-degree (349 m radius) curve, the lead-outer wheel will assume flange contact with the high rail, resulting in a large oppositely-directed lateral force. This flange force may be 50 to 75 percent higher than the measured net lateral force, which is the vector sum of the flange and creep forces. As a result, the lead-outer wheel under a heavy freight car produces net lateral forces on both rails on the order of 10,000 lb (44 kN) tending to spread the rails apart.

The trailing wheelset assumes an almost neutral angle of attack, and consequently the lateral creep forces on this wheelset are substantially lower. At speeds above the "balance" speed (speed at which the centrifugal and gravity force vectors cancel), the trailing-outer (high-rail) wheel may begin to assume flange contact, but the net lateral force on the rail is low compared with the leading-outer wheel.

In using the predictive model to explore the effects of wheelset and rail parameters, the adhesion limit (the maximum horizontal force vector as a percentage of the vertical, or normal, wheel load that can be sustained without slip) has the most noticeable effect of the steady-state lateral wheel loads. An adhesion limit of 0.25 and one-half the theoretical Kalker creep coefficients (10) were used in calculating the results presented in Figure 7.

Comparing Wheelset and Wayside Loads

Wheel loads were recorded from an instrumented wheelset at the leading axle position under one of the 100-ton hopper cars at the rear of the FAST train consist (11). In addition to mean and standard deviation load values, continuous load-versus-distance plots were provided by IIT Research Institute for typical runs through the Section 7 curve. Pulses from wayside location detector targets provided identification of the instrumented wayside sites on

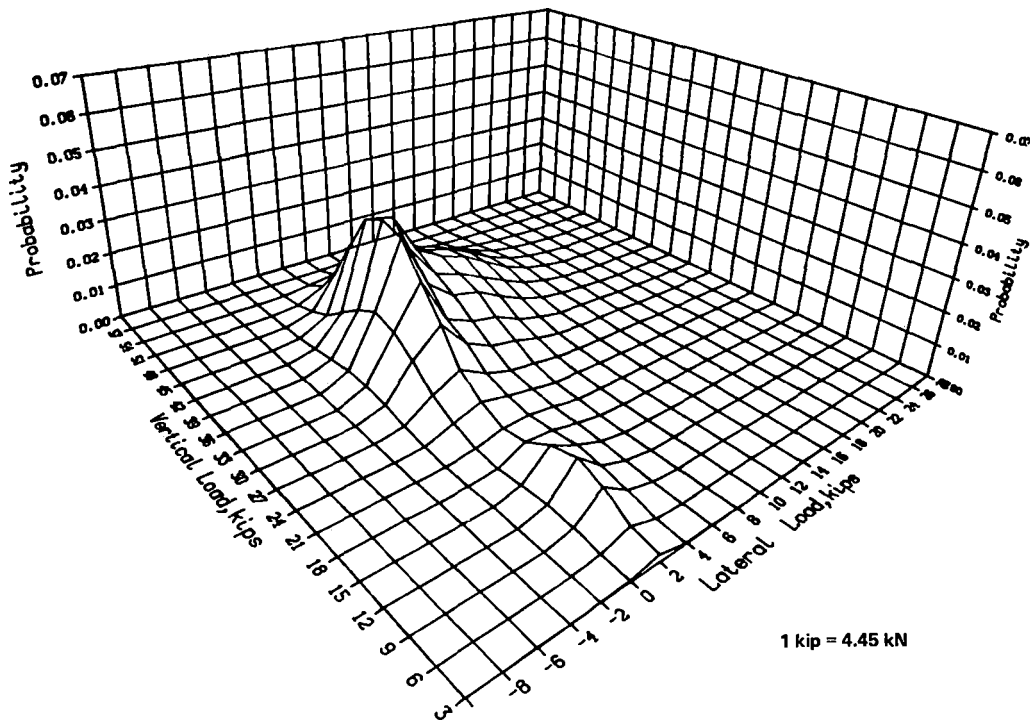


Fig. 5 Joint probability distribution of lateral and vertical load for high rail fast data

these plots and allowed a direct comparison between the two transducer systems.

Two 45-mi/h (72 km/h) runs, one in the clockwise, the other in the counter-clockwise loop directions, were chosen to compare the wheelset and way-side values in Section 7. Pronounced oscillations in

vertical loads and (particularly) high-rail lateral loads were noted in the instrumented wheelset load plots. Lateral high-rail wheel loads ranged up to 21,000 lb (93 kN) peak, and 14,000 lb (62 kN) peak-to-peak, on this leading wheelset with the primary oscillations on a 27 to 33 ft (8 to 10 m)

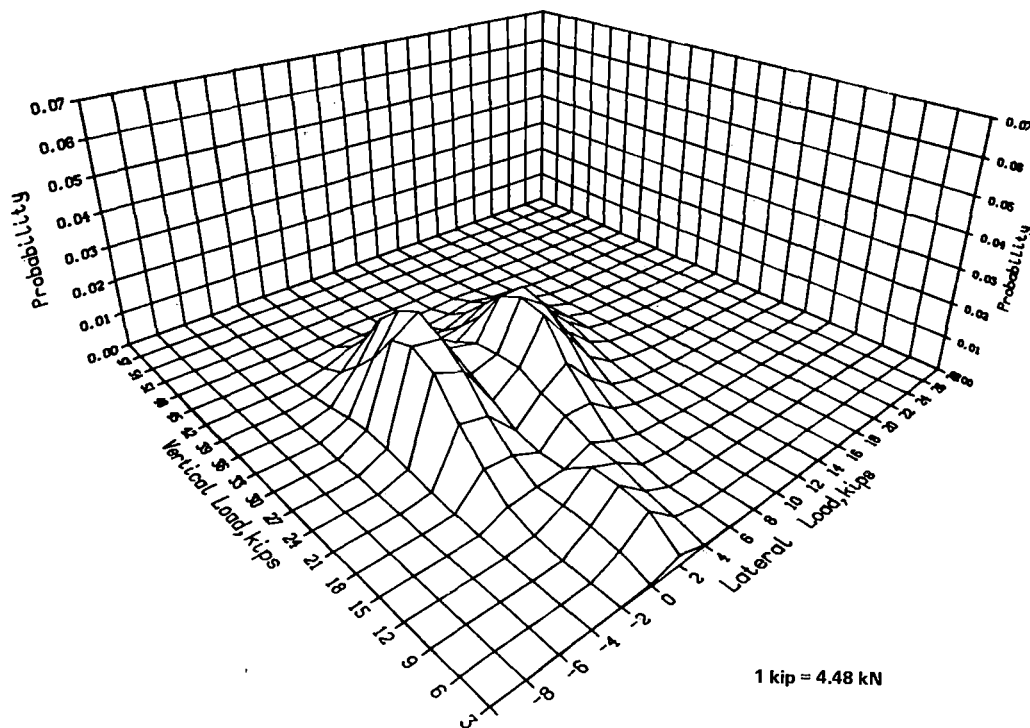


Fig 6. Joint probability distribution of lateral and vertical load for low rail FAST data

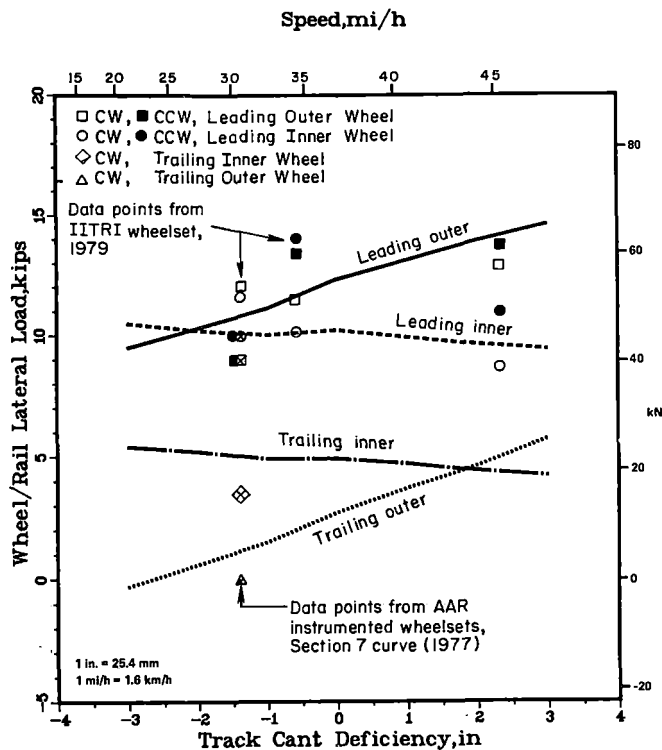


Fig. 7 Predicted net lateral wheel/rail loads under 100-ton hopper car on 5-degree curve with 4-1/2-inch superelevation

wavelength. At this speed, these wavelengths correspond to a 2.0 to 2.4-Hz frequency, a combination of roll and yaw modes of car body motion (4,5). The lateral load peaks were in-phase with the vertical load peaks on the high rail. Low-rail lateral load oscillations, on the other hand, were less than 4,000 lb (18 kN) peak-to-peak in amplitude. The high-rail load oscillations were somewhat more pronounced in the clockwise direction of running.

In comparing simultaneous track and wheelset load measurements, the high-rail lateral load circuits appeared to read an average of 2,300 lb (10 kN) lower than the wheelset (between 15 and 25 percent of the mean load), with a standard deviation of over 2,700 lb (12 kN). However, if a spatial tolerance of 2 ft (1.2 m) is allowed on the location of wayside sites relative to the wheelset load trace, a much better comparison between the rapidly-varying wheelset load signals and the short load samples from the wayside transducers is found. This tolerance accounts for location detector system response time. Lateral loads then compare within 500 lb (2.2 kN) with a standard deviation of less than 1,000 lb (4.4 kN). This is illustrated in the wheelset time history shown in Figure 8 in which the wayside data has been superimposed.

A similar comparison between wayside and wheelset vertical loads was also made as shown in Figure 8. Good correlation between low-rail track and wheelset measurements was found, with a zero mean difference and a standard deviation of 3,700 lb (16.5 kN). Again, the scatter is most probably due to the spatial uncertainty in defining the exact location of the wayside site on the wheelset load trace. High-rail vertical load measurements, however, showed the track transducers reading a consistently higher

value, on the average 9,400 lb (42 kN). The track measurements showed the nearly-equal shift in load from low rail to high rail expected at this speed (roughly 4 inches, 102 mm of cant deficiency)². While this difference is yet unresolved, it may indicate some nonlinearity or clipping in the higher range of wheelset load measurements.

A more important factor brought out by the load comparison, however, was the effect of wayside transducer spacing on the measured load spectra. Six of the seven wayside sites were located by TTC at a spacing ranging from 89 to 99 ft (27 to 30 m), the seventh being located one truck wheelbase from one of the center locations. The 27 to 33 ft (2.0 to 2.4 Hz) oscillation in high-rail lateral force at 45 mi/h therefore tends to "synchronize" with this wayside site spacing. In the clockwise direction, four of the high-rail wayside sites fell at the low portion of the wheelset load cycle, while the remaining three fell near the midpoint. In the counterclockwise direction, all but one high-rail site fell near the midpoint of the oscillation, and the remaining one fell near a load maximum. It is quite apparent that the average wayside lateral force on the high rail should be substantially lower than average wheelset lateral force in the 45 mi/h clockwise runs. This illustrates the need for randomly-chosen locations to define the wheel/rail load environment from wayside measurements with any statistical confidence (2).

Test Population Statistics

The high- and low-rail vertical load statistics for a combination of data from all test runs were shown in Figures 2 and 3, along with comparative plots of the static (weighed) wheel loads. The average wheel load measured from load scales was 30,900 lb (137 kN) with a standard deviation of 6300 lb (28 kN) for the test consist, while the mean vertical load from the wayside transducers in Section 7 was 32,200 lb (143 kN) with a slightly higher standard deviation of 7,400 lb (33 kN) as a result of curving and car dynamics.

Similar plots for the lateral loads and L/V ratios are given in Figures 9 and 10. The lateral load distributions are made up of two distinct populations, leading and trailing wheelsets in a truck, as shown by the two straight-line portions of the exceedance distribution plots which blend rather smoothly into one another. The mean lateral load was 4,700 + 4,400 lb³ (21 + 20 kN) on the high rail, and 3,000 + 4,700 lb (13 + 21 kN) on the low rail. These statistical descriptors do not reflect the basic phenomenon shown in Figure 7, that the leading wheels generate high lateral curving forces, and the trailing wheels low forces. For that reason, leading and trailing wheelsets in a curve should be handled as separate data populations. Corresponding L/V ratios were 0.12 + 0.12 on the high rail, 0.11 + 0.18 on the low rail.

The data presented represent the load environment under the modified FAST consist in Section 7,

² While the design superelevation of the Section 7 curve is 4-1/2 inches (114 mm), the intersection of the high- and low-rail mean vertical loads occurs near 30 mi/h (48 km/h), indicating an actual superelevation of approximately 3 inches (76 mm). Recent geometry measurements show a variation between 3 and 4 inches.

³ 4,700 lb mean + 1 standard deviation = 4,400 lb.

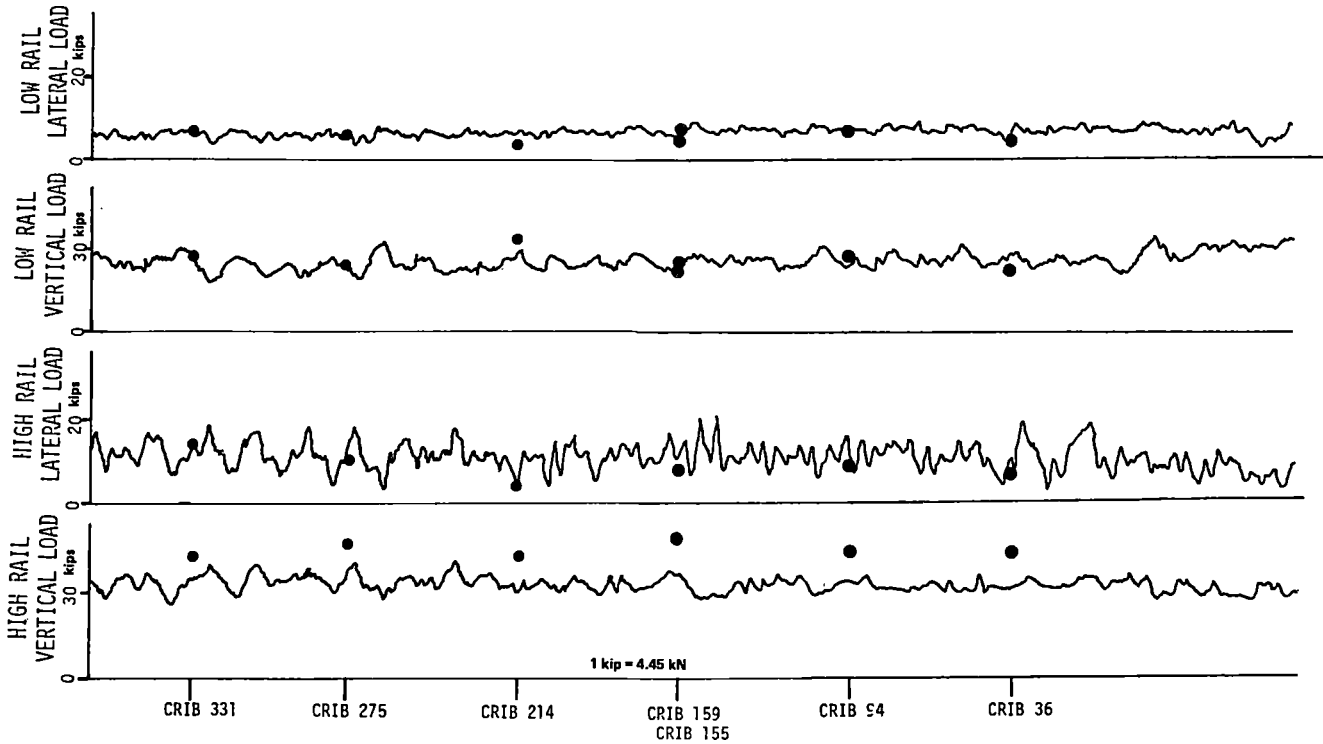


Fig. 8 Sample wheelset time history from run 9, lap 7 with corresponding wheelset data

excluding the three 110-ton cars in the consist not normally part of the FAST train for which the data were not combined in the overall statistics. Speeds of 30, 34 and 45 mi/h (48, 55 and 72 km/h) are included in the data set, where the normal operating

speed of the FAST train is 45 mi/h (72 km/h). As noted previously, data at 45 mi/h may be skewed because of speed effects with relationship to transducer spacing and the dynamic response of typical 100-ton hopper cars.

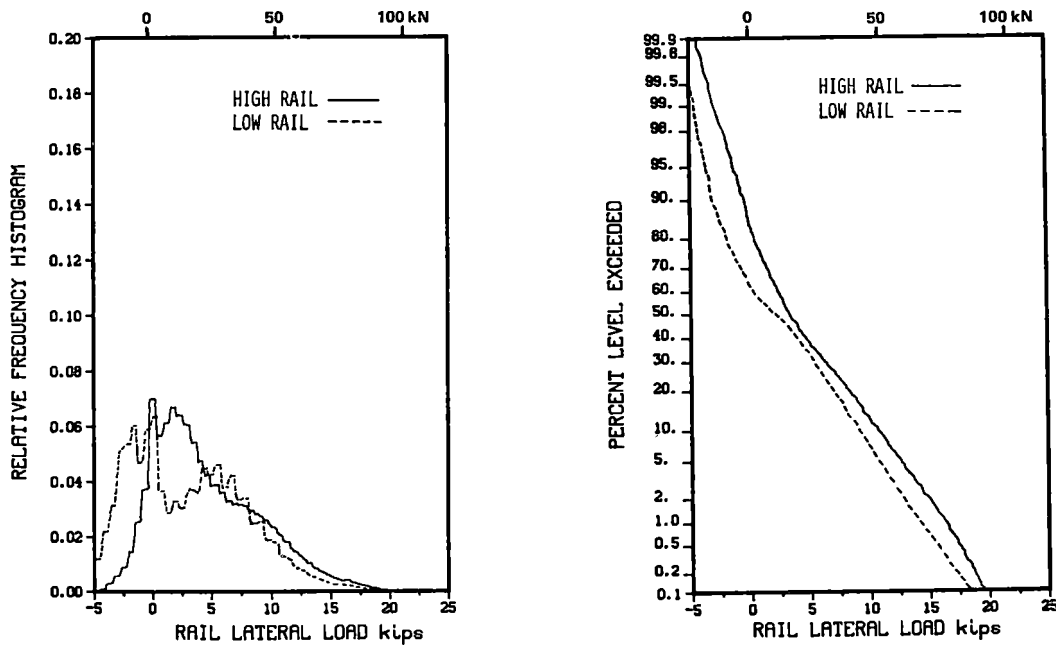


Fig. 9 Lateral load statistics for total FAST test

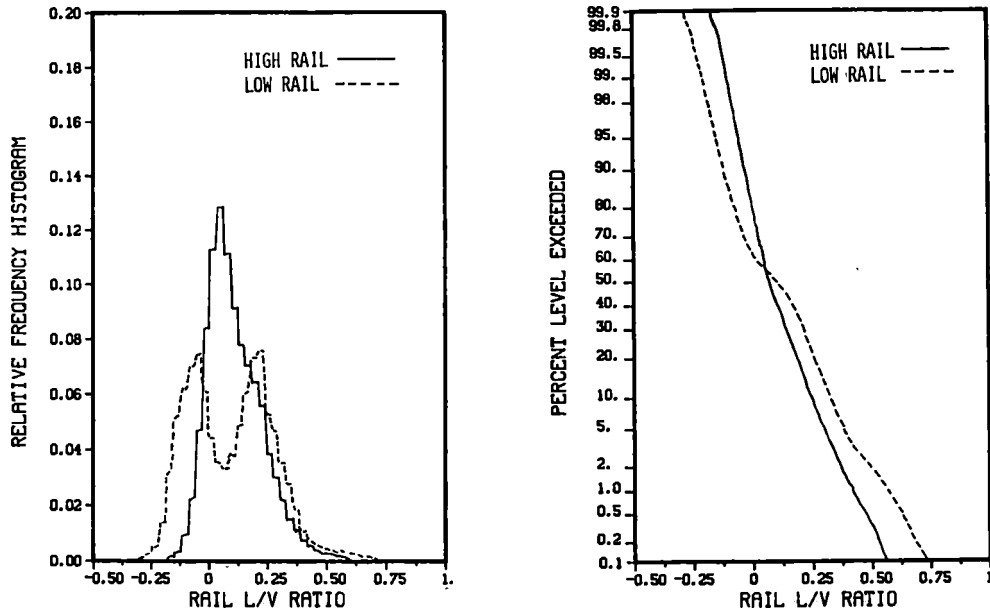


Fig. 10 L/V ratio statistics for total FAST test

Site Variations

Load measurements were made at seven different locations on the test curve. The statistics for the different sites were combined for several of the parameter variations in order to increase the population size and the statistical confidence in the results. Therefore, it was desirable to know the variation in the load statistics from site to site.

In Figure 11, the high- and low-rail vertical load exceedance functions are plotted for each measurement site from Run 9, the clockwise, 45-mi/h (72 km/h) run. The standard deviation of the mean loads from seven sites was 4 percent of the average mean load for the high rail vertical load, and 10 percent of the average mean load for the low rail vertical load.

The exceedance functions for the high-rail lateral load at each site during Run 9 are shown in Figure 12. The standard deviation of the mean loads from seven sites was 23 percent of the average mean load for the high rail. Similar results were obtained for the low rail.

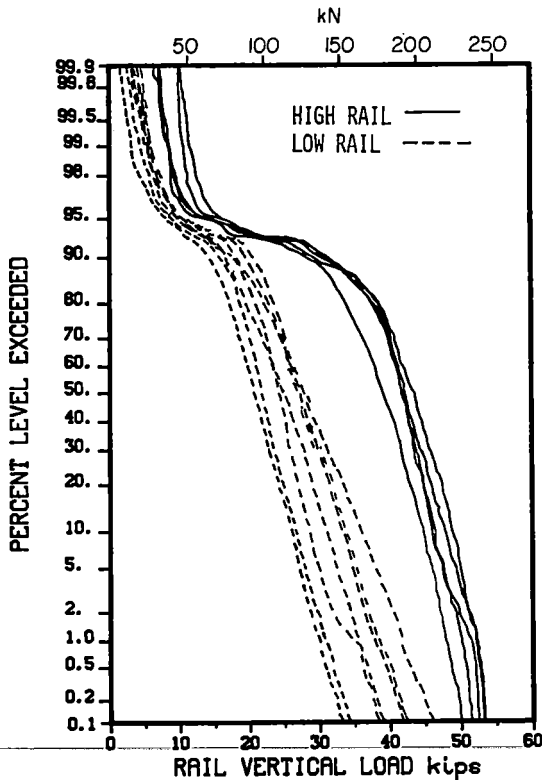


Fig. 11 Vertical load exceedance distribution functions for each site (run 9 data)

Directional Effects

One parameter investigated in this study was the effect of train direction on the wheel/rail loads. After a number of test runs around the FAST loop in the clockwise direction (in which Section 7 is a left-hand curve), the test train was wye'd to run in the same orientation of cars, but in the opposite, counterclockwise direction. The effects of direction, as "seen" from the wayside transducers, is dramatically evident in Figure 13, which shows the lateral load exceedance plots for leading axles alone. As discussed previously, the major cause of this difference was the coincidence of hopper car dynamic oscillations at 45 mi/h (72 km/h) with the average spacing of the wayside measurement sites. This effect is less critical at other speeds and with a mixture of freight car types. Wheelset load measurements (11) showed a modest difference in average leading-axle lateral loads depending on the direction, with the counterclockwise runs up to 4,000 lb (18 kN) higher, about 30 percent, than the clockwise runs. In addition, there were several cars which exhibited a definite directional bias in their curving performance. The directional bias may be due to asymmetries in wheel profile and/or truck wear. These asymmetries were substantial enough to skew the truck into a "crabbing" orientation and produce a strong directional bias for the individual trucks, as shown in Figure 14, which in turn affected the overall load statistics.

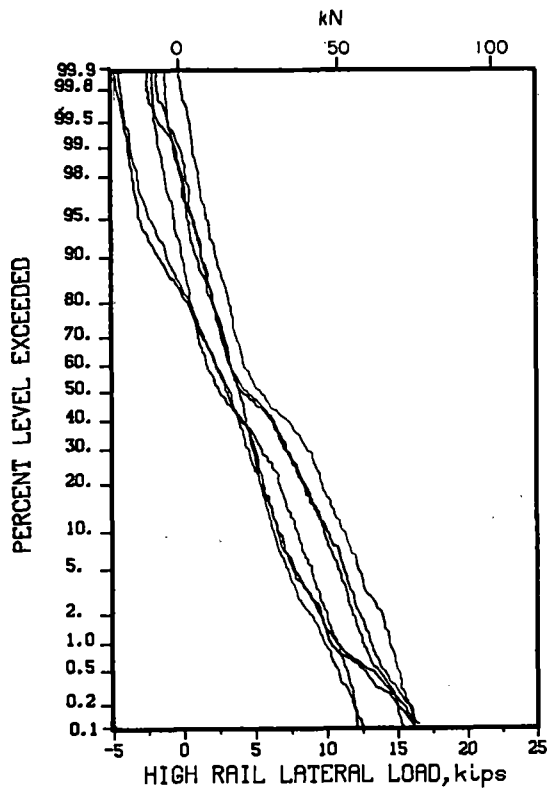


Fig. 12 Lateral load exceedance distribution functions for each site (run 9 data)

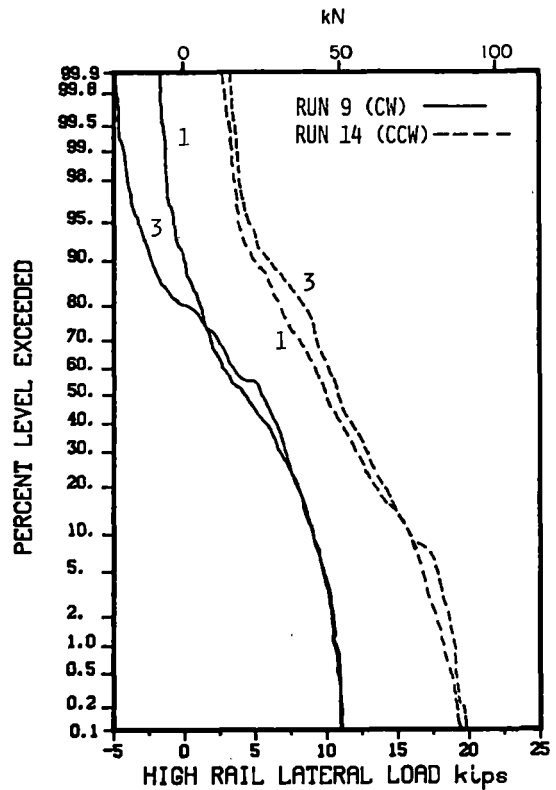


Fig. 13 High-rail lateral load exceedance distribution function for each lead axle in the CW and CCW direction

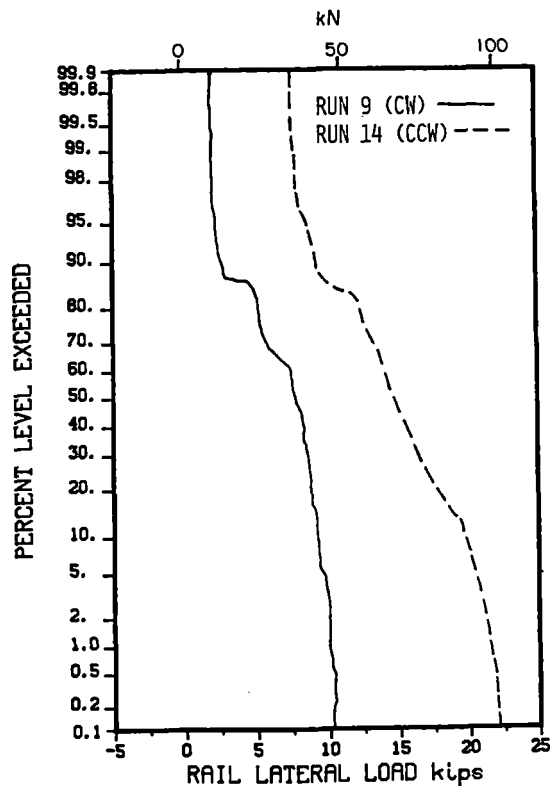


Fig. 14 High rail lateral load exceedance distribution function for the lead axle of a biased truck

No significant difference in vertical wheel load levels from runs in the two directions was noted in the wayside data.

Speed Effects

Test runs were conducted at three different speeds, 30, 34 and 45 mi/h (48, 54 and 72 km/h), in order to determine the effects of train speed on the load environment. High and low rail vertical load statistics are shown in Figure 15 for the clockwise runs, and the weight shift to the outer rail due to increased speed can be seen. (The knee in the curve at the 92 percent level merely reflects the few empty cars in the train.)

The predicted shift in lateral loads to the high rail with increased train speed is shown in Figure 7. Both wheelset and wayside measurements of mean lateral force confirm this effect. It is interesting to note, however, that an apparent dynamic resonance occurs at 34 mi/h (54 km/h). Since both high- and low-rail forces on the leading axle are higher than predicted, this phenomenon may be associated with wheelset angle of attack and truck yaw angle in the counterclockwise direction, where the Section 7 right-hand curve immediately follows a left-hand curve. (In the clockwise direction, Section 7 is preceded by a tangent section.)

The exceedance plots of Figure 16 for all cars of the consist, which includes both leading and trailing wheels on the high rail, illustrate the expected shift in lateral load to the high rail with speed, with no evidence of higher loads at 34 mi/h. This is further evidence that leading wheelset angle of attack is the primary cause of higher lateral loads at this speed.

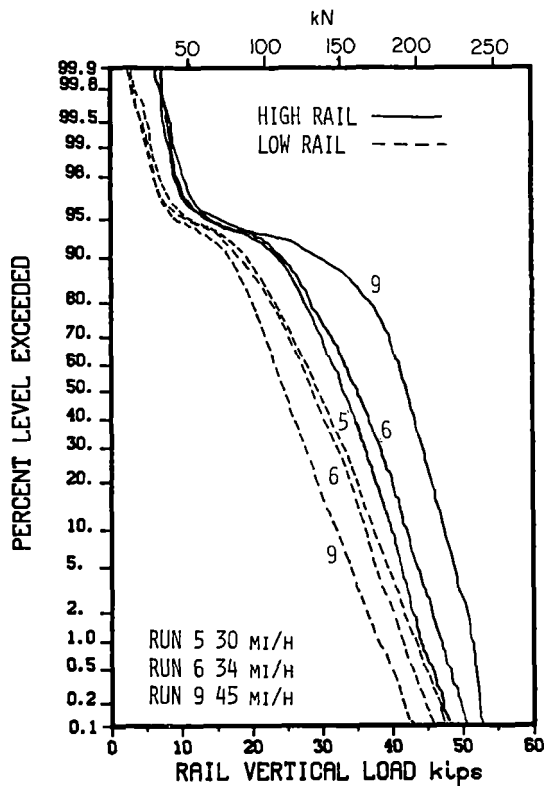


Fig. 15 High and low rail vertical load exceedance distribution functions at different speeds

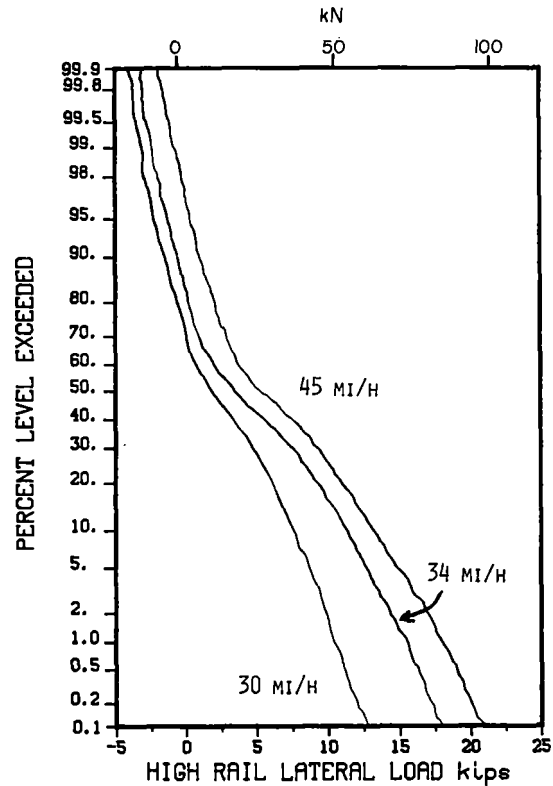


Fig. 16 High rail lateral load exceedance distribution functions at different speeds

Car Weight Effects

Vehicle weight was investigated to determine its effect on the wheel rail load environment. This was accomplished by evaluating the performance of a selected group of twelve cars in the consist. This weight test group maintained its integrity and position at the end of the test consist for all tests. The high rail vertical load exceedance distribution for each of the weight groups is shown in Figure 17. The knee in the distribution function for the 110-ton weight group is due to a lightly-loaded (comparatively) end on one of the cars in this test group. This difference in loading was noted in the static weighing of the cars. It should be noted that the full scale range on the vertical load data conversion process was 54 kips \pm zero offset. Therefore some clipping of the loads from the 110-ton cars occurred. If the load exceedance function is extrapolated (accounting for this clipping) the 110-ton cars would have generated approximately a 60 kip vertical load at the 0.1 percent exceedance level, a load which is 70 percent over the nominal wheel load. The high rail lateral load exceedance distribution function is shown in Figure 18. In this figure it is shown that the highest lateral loads were generated by the 100-ton cars. The lateral loads from the heavy 110-ton cars were actually less than the loads from the 100-ton and 66-ton cars at high exceedance percentages. The added gravitational stiffness and adhesion of the 110-ton cars due to higher weight tended to reduce the lateral load levels. The lateral loads compared favorably with the loads predicted by computer simulations for each weight class.

Other Test Variables

A number of other test variables were investigated during the FAST Wheel/Rail Loads Test. These included flange lubrication on the curve, train handling effects such as draft and buff loads, truck parameters such as centerplate diameter, and radial truck performance. Results from these different parameter variations are under evaluation and will be reported in the near future.

CONCLUSIONS

The load environment at FAST, particularly the vertical loads, was more severe than anticipated. Train speed was found to have a strong influence on loads, due partly to the shift in loads to the high rail at higher cant deficiencies, and also due to car dynamic effects. Some directional differences in lateral loads were noted in the Section 7 curve, apparently as a result of different curve entry conditions--a tangent section from one direction, a reverse curve from the other direction.

One important conclusion from these tests is that randomized locations for wayside transducers are necessary to reduce a chance synchronization with the predominant vehicle load oscillations, which may result in skewed statistical results under certain conditions. To define the statistical aspects of the load environment, random placement of at least seven transducers within a homogeneous section of track is recommended for statistical confidence in results (2,3).

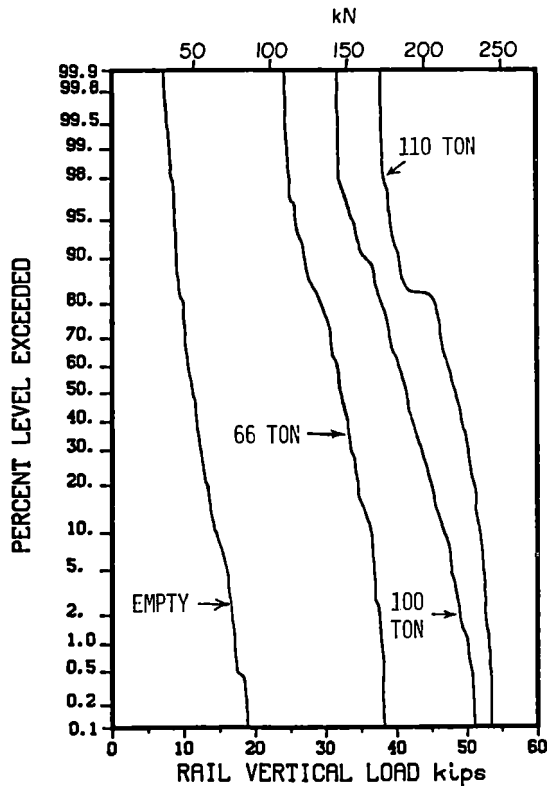


Fig. 17 High rail vertical load exceedance functions for different weight cars from run 14

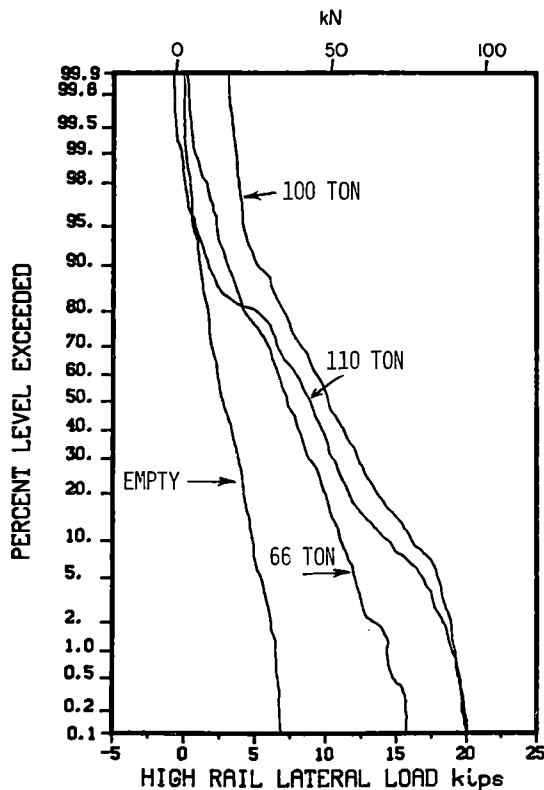


Fig 18. High rail lateral load exceedance functions for different weight cars from run 14

ACKNOWLEDGEMENTS

This paper is based on the authors' participation in the "FAST Wheel/Rail Loads Test" conducted during June-July, 1979, at the Transportation Test Center, Pueblo, Colorado. This initial work was funded by the Federal Railroad Administration under Contract DTFR53-80-C-0078 and by the Transportation Systems Center under Contract DOT-TSC-1595. During this test, the authors assisted the TTC staff during the installation and calibration of selected wayside sites on the FAST track and monitored the recording of wheel/rail load data during the tests.

Appreciation is expressed to Mr. Howard Moody of the Federal Railroad Administration and to Mr. Harold Harrison of Battelle for their assistance in completing this study, and to Dr. Milton Johnson of IITRI for providing comparative wheelset data.

REFERENCES

1. Prause, R. H., et al, "An Analytical and Experimental Evaluation of Concrete Tie and Fastener Loads", Report No. FRA/ORD-77/71, December 1977.
2. Ahlbeck, D. R., Johnson, M. R., Harrison, H. D., and Tuten, J. M., "Measurements of Wheel/Rail Loads on Class 5 Track", Report No. FRA/ORD-80/19, February 1980.
3. Ahlbeck, D. R., "Predicting the Load Environment on Railroad Track", ASME Paper No. 80-RT-7, April 1980.
4. Kenworthy, M. and Jones, C. T., "Third Dynamic Hopper Car Test", Report No. FRA/TTC-80/01, March 1980.
5. Allen, R. A. and Peters, J., "Wheel/Rail Loads Test, Hopper Car Ride Data", Report No. FRA/TTC-80/07, August 1980.
6. Tuten, J. M. and Harrison, H. D., "FAST Wheel/Rail Loads Wayside Data Reduction", Final Report, Contract DTFR53-80-C-0078 (to be published).
7. Harrison, H. D. and Ahlbeck, D. R., "Development and Evaluation of Wayside Wheel/Rail Load Measurement Techniques", International Conference on Wheel/Rail Load and Displacement Measurement Techniques, DOT/TSC, January 19-20, 1980.
8. Newland, D. E., "Steering a Flexible Railway Truck on Curved Track", Trans. ASME, Journal of Eng'ring for Ind., August, 1969, pp. 908-918.
9. Ahlbeck, D. R., Dean, F. E., and Prause, R. H., "A Methodology for Characterization of the Wheel/Rail Load Environment-A Pilot Application", Final Report, Contract DOT-TSC-1051, June 1979.
10. Kalker, J. J., "On the Rolling Contact of Two Elastic Bodies in the Presence of Dry Friction", Doctoral Dissertation, Technische Hogeschool, Delft, Netherlands, 1967.
11. Johnson, M. R., Joyce, R. P., and Mancillas, C., "Use of an Instrumented Wheelset for Measurement of Wheel/Rail Forces at the Facility for Accelerated Service Testing (FAST)", Interim Report, Contract No. TTD 79-121-1 (AAR), August 1980.

R.A. Armstrong

Scientific Officer
British Rail Research
Derby, England

T.R. Wells

Track Structure Engineer
Assoc. of American Rail-
roads, Chicago, Illinois

D.H. Stone

Director: Metallurgy
Assoc. of American Rail-
roads, Chicago, Illinois

A.M. Zarembski

Director of Research
Speno Rail Services &
Pandrol Inc., Bridgeport,
New Jersey

Impact of Car Loads on Rail Defect Occurrences

Rail defect data gathered from different sites with widely varying loading environments were analyzed with respect to defect occurrence trends. The principal loading characteristic investigated was the predominant car capacity, which determined the wheel loads and the subsequent loading of the rail. Results show that the more severe the car loading, the earlier in rail life the defects occur. A secondary loading characteristic investigated was the effects of curvature. Results were mixed, indicating that other factors also need to be considered.

INTRODUCTION

Growth in usage of high capacity unit trains and the resultant increased average car loads are accelerating rail defect formation on freight railroads. Rail defect occurrences have replaced wear as the principal criterion for rail removal on many main lines. Rail failures impose severe penalties on the railroads, since operations are disrupted, emergency repair costs incurred, and, occasionally, a derailment occurs. Research in recent years has studied both the mechanics of the actual defect formation and the statistical occurrences of defects over a line segment.

Work by Besuner, et al (1,2) on the statistical analysis of rail defect data showed that defect occurrences followed a two parameter Weibull distribution. This distribution shows that the cumulative probability of defect occurrence is a function of accumulated tonnage on the rail. Once the distribution is established, predictions of future defect rate formation can be made. This information can then be used in the planning of rail maintenance and rail replacements.

Besuner's study was limited to mixed traffic sites where the average load per car was under 70 tons (63 tonnes). Stone (3) and Zarembski (4) followed this earlier work with analyses of the impacts that 125 ton (113 tonnes), 100 ton (91 tonnes), and 70 ton (63 tonnes) cars have on rail defect occurrences. Roney (5) showed that defect occurrences differ between curves and tangent track. The overriding conclusion of all of these studies is that

defect formation starts earlier in the life of the rail, as the loadings become more severe.

Four North American sites with different average car loadings were analyzed for their defect occurrence trends in tangent track. Defect data from each of the sites were fitted to a Weibull probability distribution, from which relative comparisons were made for different average car loads. Since two of the sites also contained a significant percentage of curves, an analysis was also done on the impact of curves on rail defect occurrence probability.

STATISTICAL ANALYSIS

Fatigue life is determined by the number and magnitudes of the stress cycles experienced by the rail. In rails, larger stresses from heavier cars and curving loads shorten the fatigue life. An analysis using the Weibull distribution provides a method to compare the effects of various loading environments.

Weibull Probability Distribution

The probability of defect occurrence has been shown to be a function of the accumulated tonnage, measured in millions of gross tons (MGT; 1 MGT = 0.907 million gross tonnes [MGMT]). This function can be represented by a two parameter Weibull probability distribution. When the data are plotted on a Weibull graph, a straight line relationship results. The two parameters of the Weibull distribution are the slope of the line (α) and the characteristic of the function (β). Figure 1 summarizes the data analysis procedure which is described more fully by Besuner, et al (2).

The two parameter Weibull distribution is expressed as follows:

$$PD(MGT) = 1 - \exp\left[-\left(\frac{MGT}{\beta}\right)^\alpha\right] \quad (1)$$

for MGT, α , $\beta \geq 0$

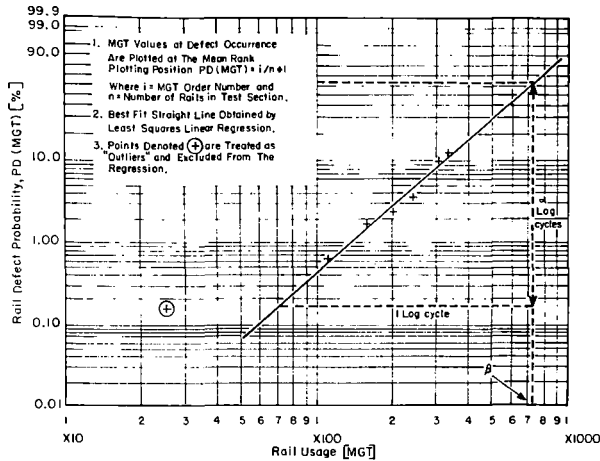


FIG. 1 SCHEMATIC DESCRIPTION OF RAIL DEFECT DATA REDUCTION AND DISPLAY.

where: PD(MGT) = Probability that a rail will have a defect before reaching a specified MGT level;

β = Characteristic (approximately the mean) usage required for a defect. β corresponds to the MGT value at which 0.632 (i.e., $1 - 1/e$) of the rails will contain a defect;

α = Slope of the Weibull line, which determines the shape of the distribution.

For most sites, several defects that are not predicted by the general Weibull distribution occur shortly after the rail installation. Consequently, the data for each site has to be examined as to whether the defect trends include early defects ("outliers") that should be ignored in determining the Weibull probability distribution. Once the "outliers" are isolated, a best-fit straight line is obtained by a least squares regression of the remaining data points. The rail defect data used in the analysis include both rail rejections during scheduled inspections and service failures.

Test Sites

The usage of heavy cars over most railroad lines has grown over a period of several years, in which time the track maintenance requirements for heavy car lines have also risen. This gradual increase has generally meant that no clear-cut adverse loading impact can be extracted from existing lines that have experienced the growth. However, test sites have been found where uniformly sized cars (unit trains) have been run exclusively over the rails, permitting an analysis of the defect trends under steady-state loading conditions.

Four North American continuously welded rail sites, each reflecting different average wheel loadings, were analyzed. Three of the sites experienced predominantly unit trains, with cars of either 70 tons (63 tonnes) net load [200,000 lb. (91 tonnes) gross weight], 100 tons (91 tonnes) net load [263,000 lb. (119 tonnes) gross weight], or 125 tons (113 tonnes)

net load [315,000 lb. (143 tonnes) gross weight]. The fourth site experienced general mixed freight traffic, and the data were taken from the studies of Besuner (1,2). Details of each site are given in Table 1. The principal analysis, comparing the effects of car loads, was confined to the tangent track sections of each site. The data available from the 100 ton (91 tonnes) and 125 ton (113 tonnes) car lines also allowed a comparison of the effects of curve versus tangent track.

Cumulative Probability Results

Rail defect data from each of the four sites that were investigated can be represented by a Weibull distribution. As illustrated in Figure 2, data from the four sites fall along straight lines on a Weibull graph. The points represent the cumulative rail failures of all types, except the mixed traffic and 125 ton (113 tonnes) car sites, where weld failures were excluded. The detrimental effects of greater car loads can be seen by comparing the probability of defect occurrence at the same accumulated MGT for the various sites. The sites with heavier car loads have a progressively higher probability of rail defects. The data from each site are shown in Figures 3 through 6, along with the results of the least squares regression for each site. The correlation coefficients (R^2 value) for each of the sites are good, with a high of 0.9934 for the 70 ton (63 tonnes) car line to a low of 0.9607 for the mixed freight line. The best-fit lines for all of the sites are shown simultaneously on a Weibull graph in Figure 7.

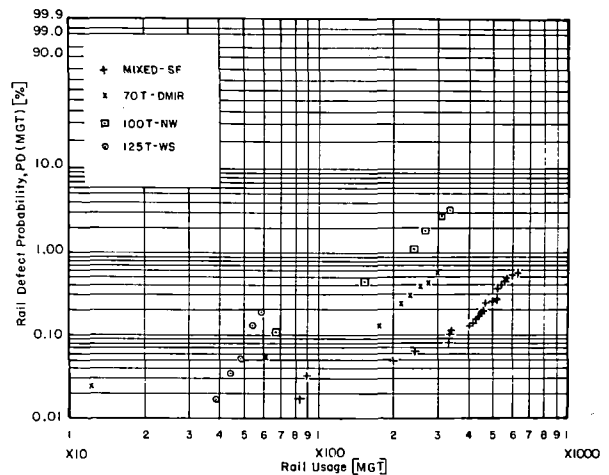


FIG. 2 CUMULATIVE PROBABILITY POINTS FOR ALL FOUR SITES.

DEFECT RATES

The representation of rail defect data by a Weibull distribution enables the long-term defect formation trends at individual sites to be predicted. From these predictions, the trends at the various sites can then be readily compared. However, maintenance of way engineers would like to predict the number of defects to be expected in a particular line segment during future maintenance planning periods.

Defect Rate Equation

The failure rate can be calculated from the Weibull parameters, α and β , using a formula derived from Equation 1. This failure rate equation is as follows:

TABLE 1. SUMMARY OF RAIL DEFECT TEST SITES

Site	Code	Length		Age (Years)	Total Tonnage		Rail Weight		Traffic Consist		Number of Defects
		Miles	km		MGT	MGMT	lb/yd	kg/m			
Santa Fe New Mexico Division	SF	22.3	35.7	16	640	580	136	68	0.4% 100 Ton 90% <70 Ton	35	
Duluth, Missabe and Iron Range	DMIR	13.0	20.8	13	304	276	132	66	95% 70 Ton	21	
Norfolk & Western Altavista Division	NW	3.1	5.0	8	338	307	132	66	80% 100 Ton	26	
Waynesburg Southern and Ten Mile Run Branch	WS	21.4	34.2	13	60	54	115	58	125 Ton	11	

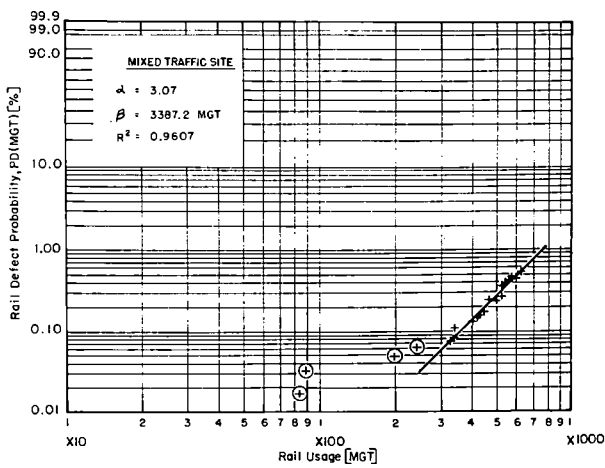


FIG. 3 CUMULATIVE PROBABILITY DISTRIBUTION FOR DEFECTS AT THE SANTA FE SITE (SF-MIXED TRAFFIC.)

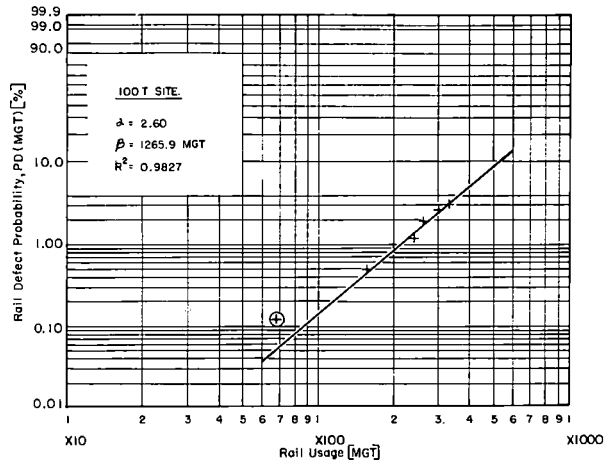


FIG. 5 CUMULATIVE PROBABILITY DISTRIBUTION FOR DEFECTS AT THE NORFOLK AND WESTERN SITE (NW-100T)

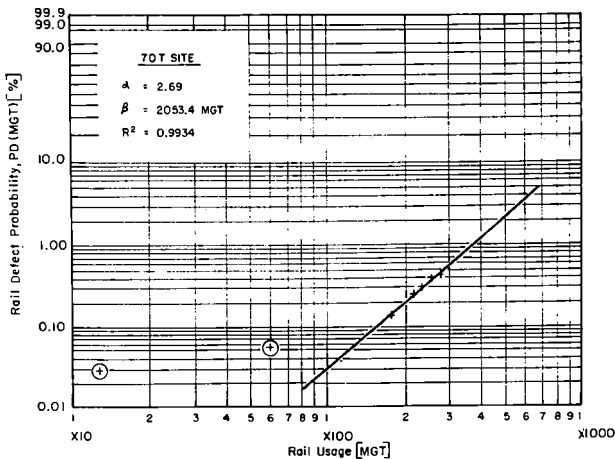


FIG. 4 CUMULATIVE PROBABILITY DISTRIBUTION FOR DEFECTS AT THE DULUTH, MISSABE AND IRON RANGE SITE (DMIR-70T)

$$\lambda (MGT) = \left[\frac{\alpha}{\beta} \right] MGT^{\alpha-1} \quad (2)$$

where: $\lambda (MGT)$ = Rate of defect occurrence, in defects/rail/MGT.

Figure 8 shows the results of plotting the calculated defect rates for each of the test sites, using the previously determined α and β parameter values.

The relative severities of the heavier traffic sites are shown graphically. All of the test sites had a Weibull slope (α) greater than 1.0, indicating that the failure rates were continuously increasing with accumulated tonnage. The accumulated tonnage on the rail at the time of a uniform defect rate is a useful indication of the severity of the heavy car loads. For example, if a defect rate of 0.1 defects/mile/MGT (0.057 defects/km/MGMT) is substituted into the rate equations for each site, the tonnage necessary to produce this rate ranges from 68 MGT (62 MGMT) for the 125 ton (113 tonnes) car line to 2199 MGT (1994

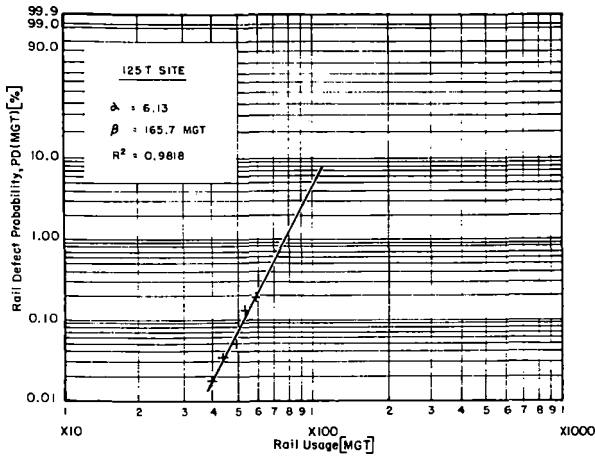


FIG. 6 CUMULATIVE PROBABILITY DISTRIBUTION FOR DEFECTS AT THE WAYNESBURG SOUTHERN SITE (WS-125T)

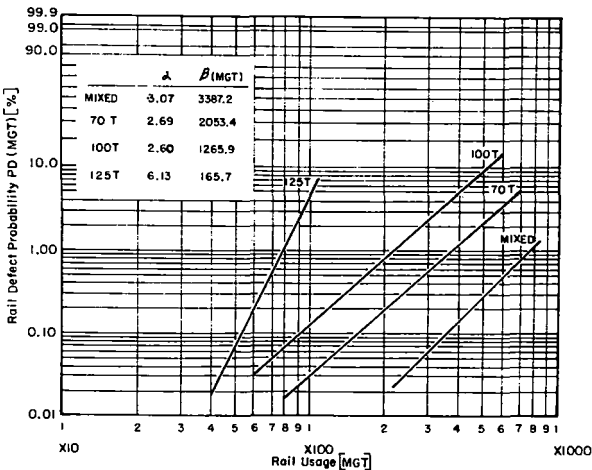


FIG. 7 BEST FIT CUMULATIVE PROBABILITY DISTRIBUTIONS FOR DEFECTS AT ALL FOUR SITES.

MGMT) for the mixed freight line. For an annual tonnage of 20 MGT (18 MGMT), the 0.1 defects/mile/MGT (0.057 defects/km/MGMT) is equivalent to 2 defects/mile/year (1.25 defects/km/year). Maintenance of way engineers often plan for rail replacements when defect rates become higher than this. Table 2 shows the tonnage levels required to produce this failure rate at all four sites. For the sites with lightly loaded cars and a high projected life, the rails may be removed before fatigue defects become a problem because of excessive head wear, or, in the case of jointed track, excessive rail end batter.

The results of this analysis show that the 125 ton (113 tonnes) car line would have 3 percent of the life of the mixed traffic site, 7 percent of the life of the 70 ton (63 tonnes) car line, and 16 percent of the life of the 100 ton (91 tonnes) car line. It must be emphasized, however, that these figures are only comparative, since all of the sites have different traffic densities. For example, the 125 ton (113 tonnes) car line has 5 MGT (4.5 MGMT) annually, whereas the mixed freight line has 40 MGT (36 MGMT) annually. Also with the exception of the 100 ton (91 tonnes) car line, these calculations are

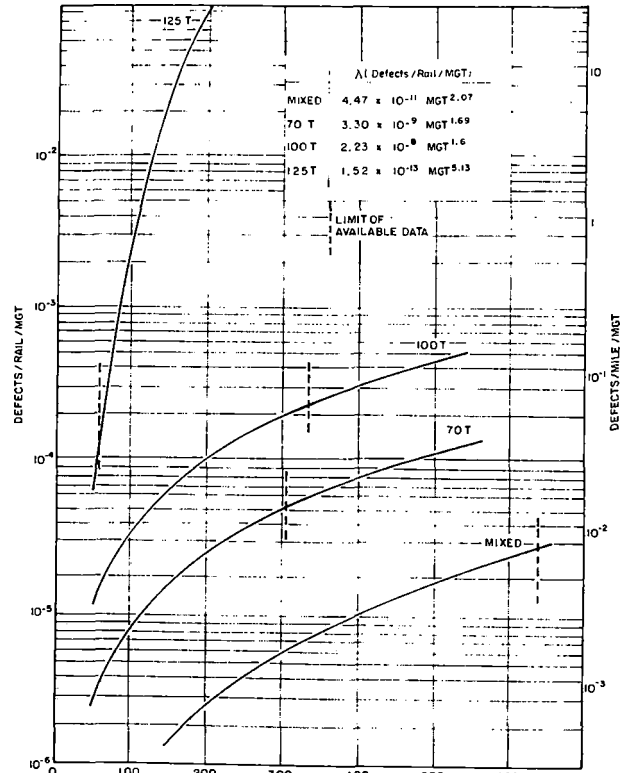


FIG. 8 RELATION BETWEEN DEFECT OCCURRENCE RATE AND RAIL USAGE.

TABLE 2. LIFE PREDICTIONS BASED ON WEIBULL PARAMETERS

Site	Life*		
	MGT	MGMT	Years
Mixed	2199	1994	110
70 T	973	883	49
100 T	433	393	22
125 T	68	62	3.4

*Life defined as a defect rate of two defects/mile/year (1.25 defects/km/year) based on a tonnage of 20 MGT/year (18 MGMT/year).

based on projections, using the trends determined from the available data.

Defect Predictions

An integration of Equation 2 produces the specific relationship needed to calculate the number of defects to be expected in specified tonnage intervals. The resultant equation is:

$$\lambda^* = \frac{1}{\beta^\alpha} \left[\frac{\text{MGT}^\alpha}{\text{MGT}_1^\alpha} \right] \frac{\text{MGT}_2}{\text{MGT}_1} \quad (3)$$

where: λ^* = Rate of defect occurrence per rail;
 MGT_1 = Accumulated tonnage (MGT) at the start of the interval;
 MGT_2 = Accumulated tonnage (MGT) at the end of the interval.

The integral is evaluated between the specified tonnages, and multiplied by the number of rails at the site to calculate the number of expected defects. This procedure was used in sample calculations for the four sites, with the results shown in Tables 3 through 6. Predictions of future defect trends are also included in the Tables for each site.

TABLE 3. DEFECT PREDICTIONS FOR MIXED TRAFFIC SITE (SF)

Tonnages MGT	λ^* Defects/Rail 1.46×10^{-11} [MGT ^{3.07}] _{MGT₁}	Number of Defects on Site	
		Predicted	Actual
0-90	1.46×10^{-5}	0.09	2
90-200	1.55×10^{-4}	0.93	1
200-247	1.54×10^{-4}	0.93	1
247-336	5.09×10^{-4}	3.1	1
336-412	7.24×10^{-4}	4.4	3
412-451	4.98×10^{-4}	3.0	3
451-477	3.86×10^{-4}	2.3	4
477-512	5.92×10^{-4}	3.6	1
512-550	7.45×10^{-4}	4.5	9
550-605	1.28×10^{-3}	7.8	7
605-640	9.54×10^{-4}	5.8	3
640-680#	1.23×10^{-3}	7.4	-
680-720#	1.39×10^{-3}	8.4	-
720-760#	1.56×10^{-3}	9.4	-

#Projected traffic and defect trends.

TABLE 4. DEFECT PREDICTIONS FOR 70 TON SITE (DMIR)

Tonnages MGT	λ^* Defects/Rail 1.23×10^{-9} [MGT ^{2.69}] _{MGT₁}	Number of Defects on Site	
		Predicted	Actual
0-13	1.22×10^{-6}	0.004	1
13-61	7.68×10^{-5}	0.27	1
61-182	1.40×10^{-3}	4.9	3
182-202	4.78×10^{-4}	1.7	2
202-222	5.65×10^{-4}	2.0	2
222-237	4.85×10^{-4}	1.7	2
237-261	8.91×10^{-4}	3.1	3
261-284	9.94×10^{-4}	3.5	2
284-304	9.82×10^{-4}	3.5	5
304-330#	1.45×10^{-3}	5.1	-
330-350#	1.26×10^{-3}	4.4	-
350-370#	1.38×10^{-3}	4.9	-

#Projected traffic and defect trends.

The accuracy of the predictions were variable. Those defects that could not be predicted were early failures, previously identified as "outliers" and excluded from the least squares analysis that determined the Weibull parameters. After these early defects were excluded from the analysis, the pre-

TABLE 5. DEFECT PREDICTIONS FOR 100 TON SITE (NW)

Tonnages MGT	λ^* Defects/Rail 8.59×10^{-9} [MGT ^{2.60}] _{MGT₁}	Number of Defects on Site	
		Predicted	Actual
0-69	5.19×10^{-4}	0.4	1
69-160	4.10×10^{-3}	3.4	3
160-246	9.52×10^{-3}	8.0	6
246-269	3.70×10^{-3}	3.1	6
269-310	7.96×10^{-3}	6.7	7
310-338	6.50×10^{-3}	5.5	3
338-380#	1.15×10^{-2}	9.7	-
380-420#	1.30×10^{-2}	11.0	-
420-460#	1.52×10^{-2}	12.8	-

#Projected traffic and defect trends.

TABLE 6. DEFECT PREDICTIONS FOR 125 TON SITE (WS)

Tonnages MGT	λ^* Defects/Rail 2.49×10^{-14} [MGT ^{6.13}] _{MGT₁}	Number of Defects on Site	
		Predicted	Actual
0-40	1.65×10^{-4}	0.95	1
40-45	1.74×10^{-4}	1.0	1
45-49.8	2.92×10^{-4}	1.7	1
49.8-55	5.29×10^{-4}	3.1	5
55-60	8.18×10^{-4}	4.7	3
60-65#	1.25×10^{-3}	7.3	-
65-70#	1.86×10^{-3}	10.8	-
70-75#	2.68×10^{-3}	15.5	-

#Projected traffic and defect trends.

diction of actual numbers of defects was generally good, over broad tonnage intervals.

The correlation coefficient calculated during the least squares analysis of the data points is an indicator of how well the defect rate equation predicted the actual defect occurrences. This is illustrated in the case of the 70 ton (63 tonnes) car line, where the correlation coefficient was the highest of all the sites, resulting in the best agreement between predicted defects and actual occurrences at this site.

EFFECT OF CURVES ON DEFECT TRENDS

Although the principal analysis was done to show the effects of changing car loads, data from the 100 ton (91 tonnes) and 125 ton (113 tonnes) car lines permitted an analysis of the effects of curves compared with tangent track. Since curved rails are more severely stressed than tangent rails, more severe defect trends could be expected on curves. The failure data from the sites with curves is shown in Figure 9. The results show that curves had a significant defect trend effect on the 100 ton (91 tonnes) car line, but, on the other hand, had little effect on the 125 ton (113 tonnes) line. Table 7 shows the calculated Weibull parameters (α, β) for both of the sites, along with the value of MGT at which the failure rate is 2 defects/mile/year (1.25 defects/km/year), calculated

in a manner similar to the defect rates shown in Table 2.

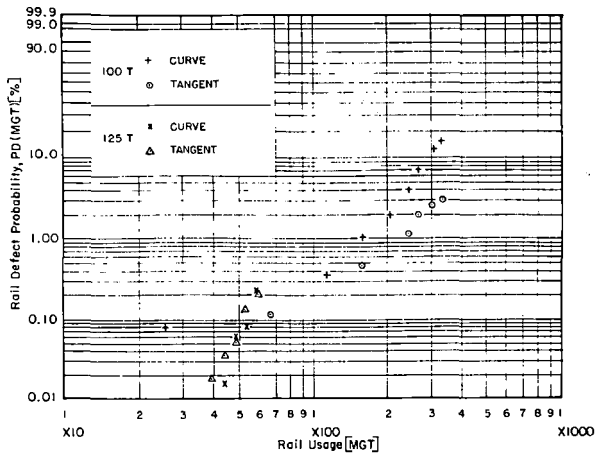


FIG. 9 EFFECT OF CURVE vs. TANGENT TRACK.

TABLE 7. EFFECT OF CURVE vs. TANGENT TRACK

Site		α	β (MGT)	Life*		
				MGT	MGMT	Years
100 T	Curve	3.5	579.3	190	172	9.5
	Tangent	2.6	1266	433	393	21.7
125 T	Curve	8.1	129.8	63	57	3.2
	Tangent	6.1	165.7	68	62	3.4

*Life defined as a defect rate of two defects/mile/year (1.25 defects/km/year) based on a tonnage of 20 MGT/year (18 MGMT/year).

Table 7 shows that there is a factor of two in the expected life of rail in tangent track, as compared with the curves, in the 100 ton (91 tonnes) car site. On the other hand, the expected rail lives for both the curves and the tangent track on the 125 ton (113 tonnes) car line are similar, with the curves exhibiting a slightly faster growth rate. Each curved site is made up of several different track curvatures. In particular, the 125 ton (113 tonnes) car site has a high percentage of curves over 6 degrees (291 meter radius), whereas the 100 ton (91 tonnes) car line had a majority of curves ranging from 3 degrees (582 meter radius) to 6 degrees (291 meter radius). The differences in the apparent curve effects between the two sites could be caused by different loading environments, as determined by operating characteristics such as speed and superelevation.

DISCUSSION

The data in this paper shows the relative impact that different car loads have on rail defect occurrences. Significant differences exist between sites handling mixed traffic, 70 ton (63 tonnes), 100 ton (91 tonnes) and 125 ton (113 tonnes) cars. The actual experience on other line segments is likely to cause variations of the calculated Weibull parameters, due to differences in the many factors that would influence the formation of defects. These include track geometry; the tie, ballast, and subgrade conditions;

operating speeds; inspection procedures; and size of rail section. Nevertheless, in this study, the major difference between each of the test sites was the car loads, which revealed significant differences in the rail defect behavior trends.

Work by Roney (5) on Australian mining railroads, that showed increasing incidences of defects on curves, has been confirmed on North American sites. The Australian sites were limited to curves that were under 2 degrees (873 meter radius), whereas the 100 ton (91 tonnes) and 125 ton (113 tonnes) sites analyzed here were both predominantly comprised of curves greater than 3 degrees (582 meter radius). Both sites that were analyzed showed that the curves had worse defect trends than the adjacent tangent track sections. However, the relative severity of curves in comparison with tangent track appeared to be site dependent. Overall, the effect of curvature was not as significant as that of increasing car loads.

The Weibull distribution is a function of accumulated tonnage on the rail, as characterized by two parameters. These parameters can be used to determine defect rates and, therefore, the numbers of defects. Once the parameters are established, calculations can be made as to future expected defects at a particular site. Predictions of the number of expected defects appear to be very sensitive to the degree to which the data fits the Weibull distribution. Defect predictions for the test sites for specific years differed from what was actually experienced, but averaged out when larger time increments were used.

Although the statistical analytical approach used in this paper was done to show the effects of increasing car loads, this defect rate prediction method can be used as an input to an overall rail planning model. The optimum rail relaying strategies could then be calculated by forecasting the defect trends, and doing an economic analysis as to the benefits of tolerating defects, as opposed to the cost of relaying the site. The Weibull distribution is currently the principal element of the planning model being developed by the Association of American Railroads (6).

CONCLUSIONS

1. The two parameter Weibull function adequately represents the probability distribution of rail defect occurrences at the four sites analyzed.
2. 0.37 percent of the rails in tangent track, equivalent to 1 rail/mile (0.625 rails/km), will have accumulated a defect after tonnages in the ratio of 1:2:4:8 for the 125 ton (113 tonnes), 100 ton (91 tonnes), 70 ton (63 tonnes) and mixed traffic sites.
3. A defect rate of 2 defects/mile/year (1.25 defects/km/year) occurs in tangent track, in the life ratio of 1:6:14:32 for the 125 ton (113 tonnes), 100 ton (91 tonnes), 70 ton (63 tonnes) and mixed traffic sites, assuming an annual tonnage of 20 MGT (18 MGMT).
4. Defect occurrences in curves are more severe than in tangent track, although the relative severities are site dependent.

REFERENCES

1. Besuner, P. M., Stone, D. H., DeHerrera, M. A., and Schoeneberg, K. W., "Statistical Analysis of Rail Defect Data," Association of American Railroads Report Number R-302, Chicago, Illinois, June, 1978.
2. Besuner, P. M., Stone, D. H., Schoeneberg, K. W., and DeHerrera, M. A., "Probability Analysis of Rail Defect Data," Heavy Haul Railway Conference, Perth, Western Australia, September, 1979.
3. Stone, D. H., "Comparison of Rail Behavior with 125-Ton and 100-Ton Cars," Association of American Railroads Report Number R-405, Chicago, Illinois, January, 1980.
4. Zarembski, A. M., "Effect of Increasing Axle Loads on Rail Fatigue Life," Association of American Railroads Report Number R-485, Chicago, Illinois, June, 1981.
5. Roney, M. D., "Meeting the 100-Ton Challenge-Report on Heavy Axle Load Lines in Australia," American Railway Engineering Association Bulletin 683, Volume 82, Washington, D.C., June-July, 1981.
6. Wells, T. R., and Gudiness, T. A., "Rail Performance Model: Technical Background and Preliminary Results," Association of American Railroads Report Number R-474, Chicago, Illinois, May, 1981.

Rails on Heavy Haul Sections on Chinese Railways

Feng Xianpei

Research Professor at
China Academy of Railway
Sciences, Chairman of
Track Committee, China
Railway Society

This paper gives a brief description of the track structure on heavy haul sections on Chinese railways and types of rails laid on those track sections. The chemical composition, physical properties and manufacturing process of the rails are also given in this paper. Five major rail defects on heavy haul sections are described and the measures to prevent the defects taken by Chinese railways and metallurgical engineers are also briefly stated. The writer concludes that although rail corrugation does not threaten traffic safety, it is still a serious problem in deteriorating parts of rolling stock, track components and track structure as a whole. Further investigation on the problem is of urgent necessity.

INTRODUCTION

The net work of Chinese railways has increased more than 30,000 km of railway track in the past three decades. At the end of 1980, the total kilometrege of Chinese railway system was about 52,000 km. It carried about 1,050 million net tons of freight and more than 900 million passengers within that year.

Within the whole network, different lines carried different amount of freight and passenger traffic. According to the statistics of recent years, on less than 20% of the main line track of the whole network carries more than 50% of the total freight traffic, especially those lines connecting production bases of raw materials and the industrial centers or export-import seaports. Most sections of the busiest main lines carried about 50 million gross tons of freight annually, and on some sections, the annual freight traffic reached 80 million gross tons. On those sections, more than 100 trains, freight and

passenger, run through everyday and became one of the busiest railway line in the world. Locomotives used for hauling passenger and freight trains are diesel and steam engines with driving axle load of 23 tons; the average loading capacity of freight cars is about 50 tons. Freight cars with loading capacity of 75 tons and average axle load of 25 tons are designed and under manufacturing, few of them has been put into operation.

Most of the heavy haul lines of railways in China are located along the east coast of the country and only a small part of those sections are in the mountainous region near the production centers of raw materials. Hence most of those heavy haul lines are on straight lines and curves with large radius, i.e. more than 600 metres (about $D = 3^{\circ}11'$ in English system). On mountainous regions, radius of curves as small as 300 metres (about $6^{\circ}22'$ in English system) is allowed. Grade of those heavy haul sections is mostly under 0.6% and 1.2% on mountainous regions with only few steeper grades.

RAILWAY TRACK ON HEAVY HAUL SECTIONS

There are two types of rails used on the track of those heavy haul sections, namely

type 50 and type 60 of Chinese Standards with actual weight of 51.5 and 60.4 kilograms per meter respectively. Sections of these rails are shown in Fig.1; The parameters of these rail sections are shown in Table 1.

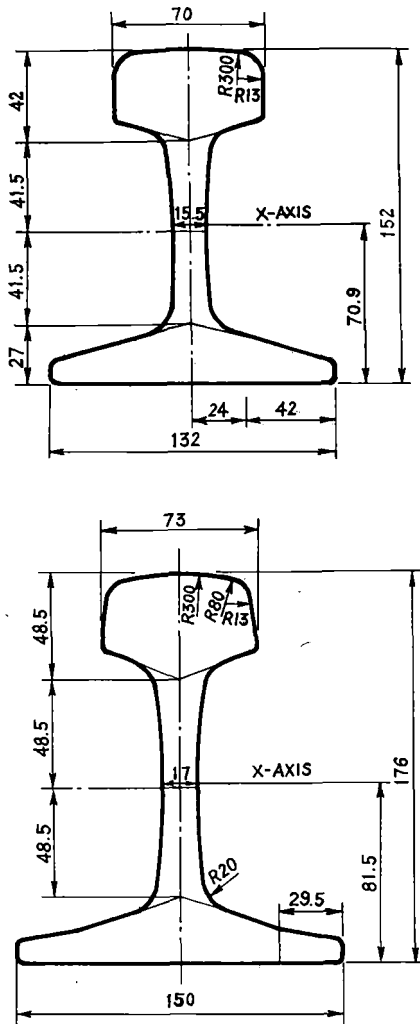


Fig.1 CROSS-SECTION OF RAILS TYPE 50 & 60

PARAMETERS OF RAILS TYPE 50 & 60 Table 1

Type of Rails	60	50
Weight kg/m	60.35	51,51
Cross-section cm ³	77.08	65.80
Moment of Inertia		
X-axis cm ⁴	3203	2037
Y-axis cm ⁴	518	377
W, Bottom Surface cm ³	393	287
W, Top Surface cm ³	339	251

1840 sleepers are laid on each kilometre of track, i.e. 54.5 cm centre to centre; and for curved track of small radius, sleepers as much as 2000 per kilometre of track, i.e. 50.0 cm centre to centre, are laid. Two kinds of sleepers are used on Chinese railways, they are treated timber sleepers and prestressed concrete sleepers, and the latter is further divided into two categories, common P.C. and broad prestressed concrete sleepers. The thickness of ballast layer under the bottom of sleeper is 30 cm on heavy haul lines and it may be thinner under broad prestressed concrete sleepers.

It is a common practice in China that railway lines should be laid with CWR except on curves with radius less than 600 m. Experiences proved that CWR of 60.4 kg/m rail laid on broad PC sleepers is very satisfactory for heavy haul lines and with good stability. Consequently, the maintenance work of track is also greatly reduced.

The damage of track caused by heavy traffic on those heavy haul sections is very serious. The impact and vibration loads caused by repeated action of heavy axles on the track destruct every component as well as the structure of the track as a whole. And due to the intervals between trains being far much smaller on those high traffic density sections than on ordinary sections, it is very difficult to carry out maintenance work normally and thence the accumulated deformation of track can hardly be removed to recover the normal conditions of the track in due time. Of all the components of the track, the steel rails which are directly under dynamic action of wheel loads are damaged more seriously.

In order to maintain rails on the heavy haul sections in good conditions, it depends upon the weight per unit length of rail laid on the track and the conditions of maintenance of track, and it also depends upon the original conditions of the rail as supplied by the manufacturer, i.e. the method of manufacturing and the original quality of the new rails.

On Chinese heavy haul railways, the rails used are lighter than those used in North

American railways, but due to cautious maintenance of track, the rails worked pretty well in the fifties. The only defect was severe rail wear on sharp curves due to less wear resisting ability of common carbon steel rails used at that time. By decreasing carbon content and increasing manganese content properly, a new type of wear resisting low alloy rail steel was produced in the early sixties after thorough investigation. This new type was the later one of the most popularly used rails in China.

All rails laid on Chinese railways are supplied by four major steel factories of the country in recent 25 years. Before 1970, all rails were rolled from open hearth steel. Steel made by LD process has also been used after 1970, but of smaller percentage.

Rails are all undergone controlled cooling after hot rolled and all the four factories have cooling pits to expell residual hydrogen content in hot rails. Twenty five years of experience proved that the result is satisfactory.

DAMAGE OF RAILS

Damage of rails on heavy haul lines is a very serious problem on traffic safety of railways. All railway personels pay great attention to avoid such damage and they have made great effort to improve quality of steel rails together with engineers of the rail factories.

The typical types of defect rails often found on the heavy haul railways are:

1. Rail wear,
2. Bolt hole breakage or star crack,
3. Transverse fissure of the rail,
4. Shelly rails, and
5. Rail corrugations.

The amount of wear of rail depends upon the radius of curve on which the rail is laid, the tonnage carried through as well as the wear resisting ability of the rail steel or the hardness of the rail top surface. The way to increase the hardness of the rail top surface is by heat treating or by using low

alloy steel.

The most commonly used kinds of steel used for rolling rail are carbon steel rails and low alloy steel rails. The chemical composition and physical properties of these rails are shown in Table 2 and Table 3 respectively.

Table 2

	Chemical Composition %					
	C	Si	Mn	Cu	P	S
U71	.64- .77	.13- .28	.60- .90		≥.040	≥.050
U74	.67- .80	.13- .28	.70- 1.00		≥.040	≥.050
U71Cu	.65- .77	.15- .30	.70- 1.00	.10- .40	≥.040	≥.050
U71Mn	.65- .77	.15- .35	1.10- 1.50		≥.040	≥.040
U70MnSi	.65- .75	.85- 1.15	.85- 1.15		≥.040	≥.040
U71MnSiCu	.65- .77	.80- 1.20	.80- 1.20	.10- .40	≥.040	≥.040

3

	Ultimate Strength kg/mm ²	Elongation %
U71	80	10
U74	80	9
U71Cu	80	9
U71Mn	90	8
U70MnSi	90	8
U71MnSiCu	90	8

Now, 'U71Mn' steel rail is widely used on Chinese railways. In comparing with 'U71' rails, the increase of maximum manganese content from 0.9% to 1.5%, the ultimate strength increased from 80 kg/mm² to 90 kg/mm². When these two kinds of rails are laid on curved track with radius of 500 m, the amount of wear of the latter is two times that of the

former after passing through same amount of traffic. For curves with radius less than 500 m, rails made of 'U70MnSi' steel give very good results in wear resisting. On curved track with radius of 350 m, the wear resisting property of rails made of 'U70Mn-Si' steel is 4 times that of rails made of 'U71' steel.

Bolt hole breakage or star crack is the most common rail damage on bolted rail tracks. It is also very prominent on Chinese railways if bolted rails are laid on heavy haul sections. Usually they are accompanied by rail end batter. CWR track has been developed in China especially on heavy haul sections. Nearly 60% of the heavy haul lines are CWR tracks, thus greatly reduces such kind of rail damage. Now, the rail manufacturers are making preparations to produce rails with the edge of bolt holes being cambered, this will be very helpful to strengthen the circumference of the bolt holes against the stress concentration around them.

Transverse fissure of rails is very dangerous to traffic safety. It is believed that the concentration of harmful gas in steel and minute particles of solid inclusions especially in the head of rail to form very small shatter cracks are the origin of the transverse fissure. Shatter crack enlarges gradually and forms egg shaped bright face inside the rail head and finally causes sudden broken of the rail transversely. Such kind of rail breakage is more dangerous on heavy haul sections due to high traffic density. In China, most of such rails are discovered by ultrasonic rail detectors before being broken. In the rail factories the adoption of controlled cooling process is very effective to the removal of residual hydrogen content inside the hot rail, however this process can not remove the metallic or non-metallic inclusions. On the heavy haul lines on Chinese railways, the rail with transverse fissure discovered on track by ultrasonic rail detectors are mostly due to non-metallic inclusions and small particles can be seen after such rails are broken manually

or by hydraulic press. Recently, rail manufacturers are installing ultrasonic detectors in their factories and each rail produced should be detected along the whole length of the rail to avoid rails with inclusions to be sent to railways. While new rails are being detected, workers should concentrate on the job. Then rail heads, webs and bases are detected one after another. Under detection rails with inclusions or other defects like pipe or segregation can be picked out automatically.

Shelly rails are another serious problem of rail damage on the gauge corner of outer rails of curved section on Chinese heavy haul railways. The result of shelly rails will be the detail fracture or compound fracture of them. In China, black spots on gauge corner of rail similar to 'Squat' in BR is often found and are thought to be the previous stage of shelly.

During the fifties and the early years of sixties, when all rails laid on Chinese railways are made of carbon steel of 'U74' or 'U71' or even of that with less carbon content, very few shelly rails had been discovered on railway tracks. But when wear resisting medium manganese rails of 'U71Mn' were widely used by Chinese railways, the amount of shelly rails increased rapidly although wear reduced at the some time. We understand that minute inclusions just beneath the surface or rail top are closely related to the formation of shelling, however, it should be noted that freight cars with loading capacity of 50 or 60 tons each had been developed and had replaced those with loading capacity of 30 tons and increased rapidly from later years of the fifties. In the meanwhile the diameter of car wheel remained unchanged, being 840 mm or 33 inches. The increase of contact force on unit area between wheel and rail must be the cause of formation of shelly other than inclusions just beneath the top surface of the rail.

Another serious problem of rails on heavy haul sections on Chinese railways is rail corrugation, although it does not threaten traf-

fic safety. Corrugation rails are very harmful to the parts of rolling stocks and it is also a problem of daily maintenance of track. When trains pass through corrugated rails, high frequency vibration deteriorates the railway structure quickly and vigorously, and it produces noise as well. In China, corrugated rails were first found in early 1960's on heavy haul railways. It was from 1958 that Chinese railways began to lay concrete sleepers on tracks of heavy haul sections; began to use diesel locomotives; axle load of freight cars as well as train speed began to increase gradually. It is believed that the cause of formation of rail corrugation is very much complicated.

From 1973 to 1974, Chinese railway engineers had made vast investigations on the conditions of rails on the heavy haul lines. They discovered that on those lines where traffic density was prominent, the service life of such rails had very close relation with the weight per unit length of the rails. It is believed that heavier rails have better resistivity to bending fatigue caused by heavy wheel loads. On few heavy haul lines in our country rails of 44.6 kg/m are still in use together with rails of 51.5 kg/m. When tonnage began to be taken in account, the service life of 44.6 kg/m rails ended after having carried 250 million gross tons of freight while for 51.5 kg/m rails, the service life increased to 500 million gross tons. On those lines where the average yearly tonnage is 25 million gross tons, the service life of the former rail will be 10 years while that of the latter, 20 years. In China, it is believed that rail service life of 20 years is most reasonable and economical. If light rails are used on heavy haul railways, service life will be short, and the work of changing rails on the track will be disadvantageous to traffic and tonnage carried. If the rails used are too heavy, certainly, rail service life can be longer than 20 years, but the initial cost is too high to bear so that it is not economical. Rails of 60.4 kg/m have been laid on heavy haul lines since 1978 with a stea-

dily increasing quantity. The parameters of that rail section is far better than those of rails of 51.5 kg/m. It is expected that such rails will carry about 800 to 1000 million gross tons of freight in the whole service life. If rails of this type are laid on lines with yearly traffic of 50 million gross tons, the estimated service life will be 16 to 20 years and it is quite reasonable in view of the current situation and development of Chinese railways. As the quality of that type of rails is further improved, rails of 60.4 kg/m will be more satisfactory. For heavy haul lines with annual tonnage up to 80 million gross tons, rails heavier than 60 kg/m should be used as suggested by Chinese railway engineers despite the case that axle load of rolling stocks and speed of running trains remain unchanged.

CONCLUSION

In China, measures have been taken by steel manufacturers and railway engineers to improve rail quality as well as working conditions, for instance, using low alloy steel rails and heat treated rails to decrease rail wear, employing controlled cooling process to eliminate possibility of transverse fissure of rail on track, and laying CWR to avoid bolt hole breakages. But there are still other rail problems remaining unsolved, such as rail corrugations. Hundreds of papers have been published all over the world discussing that kind of defect. They are very helpful to our work. Removing corrugations by grinding is only a process to improve the running surface of the corrugated rails. Further investigations should be made to prevent formation of corrugations on running surface of rails. Joint effort to investigate that kind of rail defect by specialists from different countries is in urgent need.

REFERENCE

1. "Pictorial Classification of Damaged Rails" (in Chinese), 1966, China Railway Publication Board.
2. "How To Use Rails Properly on Chinese Railways" (in Chinese) by Feng Xianpei, 1978, China Academy of Railway Sciences.
3. "Rail Damage" by C.O. Frederick, 1980, Derby Technical Center of BR.
4. "Closing the Gaps in the Track Design" by Sun Yu, 1981, Railway Gazette International, January 1981.
5. "China Railway Standards" (in Chinese).

Field Welding of Rail by the Electroslag Process

J.H. Delvetian

Associate Professor
Material Science
Oregon Graduate Center
Beaverton, Oregon

Field welding of railroad rail has up to the present time been almost exclusively limited to the thermit process. These welds, however, have been shown to be statistically more susceptible to in-service failures than any other portion of new rail or rail used in low tonnage service. A potentially cost-effective and metallurgically feasible alternative to thermit is the electroslag welding (ESW) process which is characterized by an extremely slow weld cooling rate. In this research, the feasibility of producing sound welds in a single pass by the ESW process was established despite the formidable problems of complex rail geometry, high carbon and sulfur contents of the rail and the requirement for a defect free starting capability. Process parameters were developed whereby ES welds could be deposited on 136 lb/yd rail in less than 15 minutes without the use of an expendable starting sump. The extremely slow cooling rate and the use of low carbon and sulfur filler metal allows crack-free welding of the rail. After welding, the top (runoff) riser must be cut off so that the weld can then be ground flush with the rail head.

INTRODUCTION

While in-plant rail welding systems efficiently produce high-quality welds, a limitation to the effective utilization of continuous welded rail is the need for high quality field welding process which matches the base rail properties, minimizes rail traffic disruption and minimizes the level of required operation skill. Current welding practices either do not use an additional filler metal (flash-butt welding and gas-pressure welding) or use a filler metal formulated to match rail microstructure and properties (thermit welding). In all cases, the goal is to produce a sound weld with properties equivalent to or better than those of the rail.

By far the most popular method of field joining of rail is the thermit welding process. In this process, a mixture of iron oxide and aluminum powder (reducing agent) react to produce molten iron at temperatures as high as 5000°F. Prealloyed steel shot in the mixture melts to produce a molten steel matching the rail composition. A self-tapping seal releases the molten steel at the optimum pouring temperature into a mold cavity containing the ends of the two rail sections to be joined. The primary disadvantage of this process is its inherent propensity to entrap substantial quantities of non-metallic inclusions and evolved gasses in the weld fusion zone, thus making thermit welds more susceptible to in-service failures than any other portion of the rail.

An attractive alternative to thermit welding is the electroslag welding (ESW) process which has the capability of producing defect-free weld deposits efficiently and economically. Although the application of the ESW process to rail welding is complex,

the work by Kopetman et al. (1) and Svetlopolyanskii (2) has shown that ESW can be successfully applied to the welding of crane rails. Other than this, little or no evidence is cited in the literature to suggest that the ESW process has been applied successfully to railroad rail. Under the sponsorship of the Southern Pacific Transportation Company, the purpose of this investigation was to

- a) apply the ESW process to weld 136 lb/yd carbon steel rail, and
- b) develop filler metal chemistry to produce ES weld metal with properties and microstructures equivalent to or better than those of the rail steel.

Electroslag Welding Background

Consumable guide electroslag is most commonly used for single pass vertical welding of heavy section (over 3/4 inch thick) steel plate (Fig. 1). Fusion is achieved by resistance heating an electrically conductive slag bath by continuously feeding high current carrying small diameter electrode. The slag bath and weld pool are contained by nonconsumable shoes that span the weld joint on both sides of the plate. The slag bath is maintained at a temperature and depth sufficient to melt the base metal, electrode and consumable guide tube that directs the electrode into the slag bath. The continuous deposition and solidification of metal at the bottom of the slag bath advances the weld at a rate interdependent of several variables.

The normal ES plate welding procedure requires a starting trough or run-in at least 1-1/2 inches deep to allow arc starting, transition to the slag mode, and stability to be achieved. In addition, it is necessary to establish an adequate fusion depth before reaching the critical weld members. A run-out of sufficient height to eliminate piping and slag entrapment at weld termination is also required. Both run-in and run-out are removed upon completion of the weld.

In order to utilize the electroslag process, several major modifications to the standard consumable guide process were required. These included:

1. Arc starting and run-in to promote complete fusion of the rail base and is an integral part of the completed weld.
2. Guide tube design to distribute power and filler metal commensurate with cross sectional variations in the rail as the weld progresses.
3. Cooling shoe development to provide (a) "control" heat flow distribution, (b) compatible weld contours, and (c) reusable mold components.
4. Run-off mold design that ensures sound weld metal at the head of the rail.
5. Slag depth determination to compensate for cross sectional changes as the weld progresses.

In addition to process modifications, the resulting weld metal must be properly alloyed. In the electroslag welding process, as applied to railroad rails, there are two primary means of adding alloying elements to the weld. One is to manufacture the consumable plate guide tube from material of suitable composition, which when diluted by the rail steel and the filler wire, results in a weld which matches rail properties. The other is to provide the alloying elements through the filler wire. Both methods were used in the alloy development phase of the program.

EXPERIMENTAL PROCEDURE

1. Electroslag Welding

The basic welding components, shown schematically in Fig. 2, consisted of two paralleled constant voltage DC welding power sources, each rated at 750 amps and 100% duty cycle. The dual wire drive head assembly included a digital wire feed rate monitor, while a remote panel provided contactor, wire feed speed (amperage), voltage, and oscillation control.

Two fused fluxes recommended for electroslag welding of carbon steel were used for all welds. A starting flux was used to initiate the slag bath soon after the arc was established. Once the arc was extinguished and the molten slag pool established, a neutral "running" flux was used for the remainder of the weld. Electrodes used in process adaptation were restricted to two types, both 3/32 inch diameter uncoated mild steel filler wire. One was an AWS class E70S-3 solid wire, and the other was a fabricated powder metal cored wire of AWS class E70T-G.

Starting Trough Development. A run-in design was developed that was not greater than 3/4 inch in depth and resulted in complete fusion with the base rail as possessing minimal stress concentration. Steel starting inserts (Fig. 3) of varying thicknesses and shapes were developed to meet these criteria.

Blocks of graphite, refractory, and copper were each evaluated as starting blocks to position the starting insert and to support the molten weld pool. An insulating layer between the starting insert and the backing block was finally chosen as a direction for further study. Insulating materials evaluated included graphite, zirconium sand, bonded electroslag running flux, and commercially available weld backing ceramics.

Guide Tube Development. Three basic guide tube designs were studied. The first used standard 1/2 inch guide tubes that were bent and bridged to widen electrode spacing at the rail base and narrow it as the weld puddle advances, through into the web section of the rail. The second guide tube configuration was

a plate design (Fig. 4) that allowed variations of 1/4 to 1/2 inch in guide tube thickness. The third design (Fig. 5) more nearly matched the rail shape by adding "wings" to the plate design. The guide tube shape, including electrode spacing, plate thickness, and electrode stickout distance were developed to produce satisfactory welds. Oscillation was also evaluated with the first two guide tube designs. Oscillation parameters studied included variations in distance, speed and dwell.

Cooling Shoe Design. Materials evaluated for cooling shoes included graphite, refractory, solid copper, and water-cooled copper. The final cooling shoe cavity that determines the weld shape was mainly designed to accommodate the necessary guide tube configuration. Additional cavity adjustments were made to allow vertical movement of the slag bath without causing slag entrapment and provide relief angle for shoe removal.

"Run-out" Design. The same materials were evaluated for the run-out molds as for the cooling shoes. The primary considerations in the mold design were the post weld mold removal, material compatibility with slag and weld pools, and formation of the most efficient run-out shape. The weld metal run-out had to extend well above the rail head and yet remain free of contamination from or fusion with the mold faces. Single component molds of graphite, refractory and copper were evaluated.

Slag Depth Control. Standard plate welds with uniform weld cross section require a constant slag depth of 1-1/4 to 1-3/4 inches to insure sound weld deposits. The rail joint cross section ranged from 11.7 sq in at the base to 4.5 sq in at the head. Flux additions were calculated to provide minimum effective slag depth at the rail base and near maximum at the rail head. Final adjustments were made to compensate for the slag layer that characteristically formed between the weld metal and the cooling shoes. The slag depth was monitored and adjusted by recording the weld amperage on a strip chart recorder.

Power Parameters. Both the voltage and wire feed rate (amperage) were optimized for each geometry and material. The voltage and amperage requirements were adjusted to compensate for changes in guide tube cross section, rail spacing variations, electrode types, slag depth variations, thermal conductivity differences between shoe designs and to control depth of fusion. A digital multimeter provided monitoring and control of voltage to within ± 0.5 volts.

The combination of the weld amperage trace and digital wire feed rate allowed accurate amperage control during welding and precise heat input evaluation during weld analysis.

2. Alloy Design

The 136 lb/yd standard carbon railroad rail used in this investigation had a "control-cooled" pearlitic microstructure and met the chemistry, hardness, and impact specifications given in Table I. Alloying elements were chosen on the basis of their hardenability, the ability to achieve a given hardness at the cooling rate experienced in the weld. This was done through interpreting continuous cooling transformation (CCT) diagrams and isothermal transformation (ITT) diagrams, examples of which are shown in Figs. 6 and 7, respectively. Using these diagrams, alloying elements were chosen on their ability to achieve 25 to 30 Rc hardness at the weld cooling rate of 175°F/min. (315°C/min) at

1334°F (700°C).

On this basis, carbon was added via consumable guide tube and weld filler wire additions. Both chromium-molybdenum and manganese-molybdenum alloys were chosen as filler metal wire additions. Carbon promotes a pearlitic microstructure at the cooling rates of the weld metal while the Cr-Mo and Mn-Mo alloys promote bainitic microstructures.

The amounts of alloying elements added by filler wire and by consumable guide tube materials were limited to those materials commercially available. The majority of welding filler wires are formulated to produce a certain weld metal chemistry, with very little base metal dilution, when metal transfer is through an arc as in gas metal-arc or submerged arc welding processes. Transfer characteristics of alloying elements through the electroslag slag bath are not well established, but assuming nearly 100% alloy transfer, commercially available 2-1/4Cr-1Mo, 2Mn-1/2Mo, and 0.65 carbon filler alloys were selected. Consumable guide tubes were constructed from gray cast iron and mild steel. These allowed various chemistries to be obtained in the weld.

At least two welds were made with each alloy composition. Immediately after each weld was completed, the molten slag was drawn off. Cooling shoes were removed approximately three to five minutes afterwards. The weld was then air cooled to ambient and subsequent microstructural and mechanical analysis conducted.

One weld of each chemistry was sectioned to provide all mechanical property specimens. Standard 0.505" tensile bars were machined from the rail head. Charpy V-notch, for both standard and fatigue pre-cracked impact tests, were machined from a longitudinal slab through the weld with notches located at the weld-metal centerline. The other weld provided macro sections, either transverse or longitudinal to the rail axis, and metallographic specimens. The latter were taken from the rail head in all cases. A sample was also taken for spectrographic analysis from the underside of the weld run-out or approximately at the top surface of the rail head. Carbon analysis was performed on samples from the rail head as well as elsewhere in the rail.

Tensile specimens and standard Charpy V-notch bars were tested at room temperature according to ASTM specifications. Pre-cracked Charpy V-notch specimens from each weld were also tested at room temperature for fracture toughness analysis.

Two welds were made on long rail sections for in-track testing at the FAST Track in Pueblo, Colorado, while four additional welds were made for service testing by the Southern Pacific railroad. Hence, both laboratory and full-scale field testing have been conducted or are continuing.

Macrosections of weld cross sections were surface ground, etched in a 10% nitric acid/methanal solution and examined. Specimens for optical and scanning electron microscopy were polished and etched with 2% nital.

RESULTS AND DISCUSSION

Electroslag Welding Process Modifications

Final electroslag adaptation required rail spacing of 1-1/4 inch between the rail ends (Fig. 8). The starting mold was a solid copper block grooved to support the combined steel and ceramic starting assembly.

The optimum guide tube configuration was a 1/2-inch thick winged plate type that flared the electrodes at the rail base and narrowed them at the head. The guide tube was centered above the starting insert.

Cooling shoes were copper with water cooling at the rail head. The run-out mold was a two-piece design of solid copper to produce a run-out 2-1/4 inches above and 1/4 inch wider than the rail head. The weld procedure required the starting mold and rail base to be preheated to 450°F. Flux additions were made only during the initial portion of the weld.

When the slag bath reached the top of the run-out mold, the weld was terminated and the run-out mold parted to remove the slag. While the run-out was still hot, it was readily removed with a chisel after which the rail head was finished with grinding practices common to other field welding processes. The total welding time from arc start to power off was approximately 18.5 minutes with 0.49 pounds of weld wire deposition per minute.

The finished weld (Fig. 9) had a 5/8 inch deep "run-in" beneath the rail base. A smooth transition between the weld and rail surfaces was achieved in all areas. The heat affected zone (Fig. 10) was typically 3/4 inch wide and uniform throughout. Depth of fusion was 1/4 inch into each rail resulting in a 1-3/4 inch weld zone width.

The ceramic insulation beneath the starting insert partially melted during welding and formed a smooth contour for the run-in without detrimental effects to the slag or weld pool. At the same time, it significantly reduced heat loss into the backing blocks and prevented arc impingement during weld initiation.

The winged guide tube increased contact with the slag bath and resulted in improved thermal distribution. The plate and wings carried as much as 40% of the current depending upon the material properties (3). These guide tube geometries not only improved the heat transfer uniformity into the rail base, but reduced heat concentration in the thinner rail web to control excessive depth of fusion.

The water-cooled copper shoes provided the most durable mold material. Water cooling at the rail head was important to compensate for the high heat input. Excessive depth of fusion and undercut, as well as shoe damage, resulted if water cooling was not provided in this size shoe.

The run-out mold was exposed to a high heat concentration because it contains the entire weld pool without the water cooling or a direct heat flow path into the rail. Copper was the only material evaluated that could withstand repeated exposure to the high heat concentration of the weld metal run-out.

Chemical Analysis

Table II shows the chemistries of experimental rail steels, alloyed electroslag welds and a reference thermit weld. Rail compositions were all within specifications. Carbon content varied from base to the top of the rail in the weld metal due to the change in cross sectional area of the rail changing the dilution. A distribution of dilution versus position in the rail for a 1-inch initial gap is shown in Fig. 11. A 1-1/4 inch gap was used for welds in the alloy development program in order to decrease overall dilution by about 10%. The carbon content varied from 0.38 wt.% at the starting reinforcement to 0.18 wt.% at the top of the rail head. As shown in Fig. 12, a high carbon content was not developed at the rail head even though there was a high degree of rail dilution into the weld metal. This was because the slag bath actually melts the base metal in electroslag welding. The rail steel, thus, melts 1 to 1-1/2 inches above the solidifying weld metal. This metal flows down to the molten metal pool causing the carbon content peak to be below that of base metal dilution.

Microstructure

The as-received rail steel microstructure consisted of almost 100% fine pearlite (Fig. 13). Small amounts of ferrite were observed surrounding manganese sulfide inclusions. Manganese sulfide inclusion stringers were visible extending parallel to the rail axis.

Weldments using the 2Mn-1/2Mo and the 2-1/4Cr-1Mo weld filler wires with a mild steel consumable guide tube both exhibited bainitic microstructures (Fig. 14). The 0.65 wt.% carbon weld filler wire and a mild steel consumable guide tube yielded a 90-95% fine pearlite microstructure (Fig. 15). The remaining 5-10% consisted of proeutectoid ferrite along the grain boundaries in both Widmanstätten and polygonal morphologies. Except for the small amount of proeutectoid ferrite present, this approximated the base rail steel microstructure. In comparison to the electroslag weld microstructure, Fig. 16 shows a typical microstructure at the head of an aluminothermic weld. Small amounts of proeutectoid ferrite were also present. Further adjustments in alloy content of the electroslag welds can completely eliminate the proeutectoid ferrite. Analysis of inclusions revealed that the alloyed electroslag weldments were cleaner than either the thermit welds or the rail steel itself (Fig. 17).

Mechanical Properties

The properties of the base rail steel, thermit reference welds, and alloyed electroslag welds are shown in Table III. Of the alloys investigated, only the 2-1/4Cr-1Mo and the 0.65 wt.% carbon weld filler wires, each using a mild steel consumable guide tube met hardness criteria of 24 R_C minimum. Their hardnesses at the rail head were 30 HRC and 26 HRC, respectively. Hardness traverses across the weld metal at the rail head for each of these filler wires showed fairly uniform weld metal hardnesses (Fig. 18). The standard Charpy V-notch impact toughness of the 2-1/4Cr-1Mo weld was slightly higher than that of the rail steel (3.5 ft lbs versus 2 ft lbs, respectively), at room temperature. The fracture toughness, using fatigue precracked Charpy V-notch specimens, of the 2-1/4Cr-1Mo weld was almost twice that of the rail steel (55-60 $\text{ksi}\sqrt{\text{in}}$ versus 30 $\text{ksi}\sqrt{\text{in}}$, respectively). This means that the weld metal could withstand a flaw four times the size of that of the rail steel before failure occurred. The 2-1/4Cr-1Mo wire with a mild steel consumable guide tube was used to weld a set of rails for inclusion at the FAST track for full scale testing.

CONCLUSIONS

On the basis of the matching weld/rail hardness criteria, two filler metal compositions containing (A) 2-1/4Cr-1Mo, and (B) 0.65 wt.% carbon can be used to join railroad rail with the ESW process. Both fillers attain a minimum of 24 HRC at the rail head and match or improve other mechanical properties. In the case of the weld metal deposited with 2-1/4Cr-1Mo, the fracture toughness is almost twice that of the rail steel.

The 2-1/4Cr-1Mo weldment had a bainitic microstructure while the 0.65 wt.% carbon weldment had a pearlitic microstructure which matches that of the rail steel.

This investigation demonstrated that it was possible to develop alloys for use in ESW of standard carbon railroad rail. ESW of other rail chemistries is certainly possible and weld composition, microstructure,

and hardness can be tailored to meet their requirements.

ACKNOWLEDGEMENTS

The authors wish to thank the Southern Pacific Transportation Company for sponsorship of the rail welding research program at the Oregon Graduate Center. In addition, the authors gratefully acknowledge the guidance and technical support of Mr. William E. Thomford of Southern Pacific. Helpful suggestions were also contributed by Messrs. V. E. Kahle and M. J. Karlovic.

REFERENCES

- 1 Kopetman, L. N. and Mukanaev, K. H., "Electroslag Welding of Crane Rails," Svar. Proiz., No. 5, 1967, pp. 32-34.
- 2 Svetlopolyanskii, V. I., "The Semi-Automatic Welding Electroslag Welding of Rail," Avt. Svarka, No. 3, 1966, p. 53.
- 3 Venkataraman, S., "Effects of Process Variables and Microstructure on the Properties of Electroslag Weldments," Ph.D. Thesis, Oregon Graduate Center, 1981, p. 1-14.
- 4 -----, "Specifications for Steel Rails," AREA Manual for Railway Engineering, 1979, p. 4-2-1.
- 5 -----, "Standard Specification for Carbon Steel Tee Rails," 1980 Annual Book of ASTM Standards, Part 4, p. A1-76.
- 6 -----, "Specifications for Steel Rails," AREA Manual for Railway Engineering, 1979, p. 4-2-2, 4-2-4.
- 7 Atkins, M. Atlas of Continuous Cooling Transformation Diagrams for Steel, ASM, 1980, p. 20.
- 8 -----, Atlas of Isothermal Transformation and Cooling Transformation Diagrams, ASM, 1977, p. 28.
- 9 Stone, D. H. and R. K. Steel, "The Effect of Mechanical Properties Upon the Performance of Railroad Rails," Rail Steels--Developments, Processing, and Use, ed. by D. H. Stone and G. G. Knupp, ASTM, 1978, p. 21.
- 10 Geiger, G. H., D. R. Poirer, and J. Myers, "Metallurgical Evaluation of Thermit-Type Railroad Rail Welds," University of Arizona, 1979, p. 34.

Table I.
136 lb/yd RAILROAD RAIL SPECIFICATIONS

	<u>C</u>	<u>Mn</u>	<u>Si</u>	<u>S</u>	<u>P</u>
AREA (4) (ladle analysis)	0.70/0.82	0.75/1.05	0.10/0.35	0.04 max	0.035 max
ASTM (5) (rail analysis)	0.69/0.82	0.70/1.00	0.10/0.25	0.050 max	0.040 max

Mechanical Properties (6):

Hardness--248 BHN (24 R_c) minimum

Impact--Survival from impact of a 2,000 lb. tup dropped from 22 ft.

Table II.
CHEMICAL ANALYSIS OF RAILS AND WELDS

	<u>C</u>	<u>S</u>	<u>P</u>	<u>Mn</u>	<u>Si</u>	<u>Cr</u>	<u>Ni</u>	<u>Mo</u>	<u>Cu</u>	<u>V</u>	<u>Al</u>	<u>B</u>
Rail 45400	0.73	0.043	0.033	0.93	0.225	0.09	0.09	<0.005	0.23	0.005	0.006	0.0005
Rail 20304	0.72	0.022	0.033	0.85	0.196	0.04	0.08	<0.005	0.06	0.004	0.009	0.0004
Rail 14192	0.732	0.040	0.025	0.898	0.213	0.046	0.068	<0.001	0.085	0.005	0.007	0.0003
Rail 001	0.696	0.030	0.016	0.838	0.717	0.024	0.076	<0.001	0.070	0.005	0.004	0.0003
Rail 002	0.705	0.034	0.017	0.867	0.729	0.024	0.079	<0.001	0.071	0.005	0.005	0.0004
Rail 003	0.708	0.025	0.011	0.608	0.322	0.598	0.057	0.172	0.075	0.006	0.017	0.0003
Rail 004	0.694	0.031	0.010	0.597	0.320	0.580	0.054	0.166	0.073	0.006	0.017	0.0003
Thermite Weld	0.496	0.021	0.033	1.093	0.366	0.031	0.063	0.091	0.033	0.006	0.369	0.0004
2-1/4Cr-1Mo ESRW #91	0.203	0.029	0.019	0.562	0.164	1.454	0.088	0.647	0.308	0.005	0.004	0.0004
2-1/4Cr-1Mo ESRW #53	0.142	0.028	0.016	0.587	0.175	1.827	0.086	0.755	0.322	0.005	0.006	0.0004
2Mn-1/2Mo ESRW #92	0.112	0.019	0.007	0.902	0.384	0.006	0.025	0.019	0.264	0.005	0.001	0.005
#0.65C ESRW #93	0.514	0.014	0.009	0.627	0.197	0.032	0.029	<0.001	0.248	0.004	0.007	0.0004

Table III.

MECHANICAL PROPERTIES OF RAIL STEEL AND WELD METALS

	<u>Rail Head Hardness HRC</u>	<u>Ultimate Tensile Strength ksi (MPa)</u>	<u>Yield Strength ksi (MPa)</u>	<u>Reduction in Area</u>	<u>Elongation</u>	<u>Impact Toughness (a) ft.lb. (N-M)</u>	<u>Fracture Toughness (b)</u>
Standard Carbon Rail	24 min	135(930.8)	68(468.8)	7%	12% in 2 in.(5.08 cm)	2(2.7)	26(28.3) (ref. 9)
Thermit Weld Metal	32	115(792.9) (ref. 10)	N.A.	None Detected (ref. 10)	1% in 5 in.(12.7 cm) (ref. 10)	2.5(3.4) (ref. 10)	N.A.
2Mn-1/2Mo Electroslag Weld Metal	20	85.2(587.4)	57.2(394.4)	15%	28% in 2 in.(5.08 cm)	N.A.	35(38.1)
2-1/4Cr-1Mo Electroslag Weld Metal	30	135(930.5)	90(620.5)	11%	16% in 2 in.(5.08 cm)	3.5(4.75)	57(62.1)

(a) Tested at room temperature with Charpy V-notch geometry

(b) Tested dynamically at room temperature using fatigue pre-cracked Charpy V-notch specimens

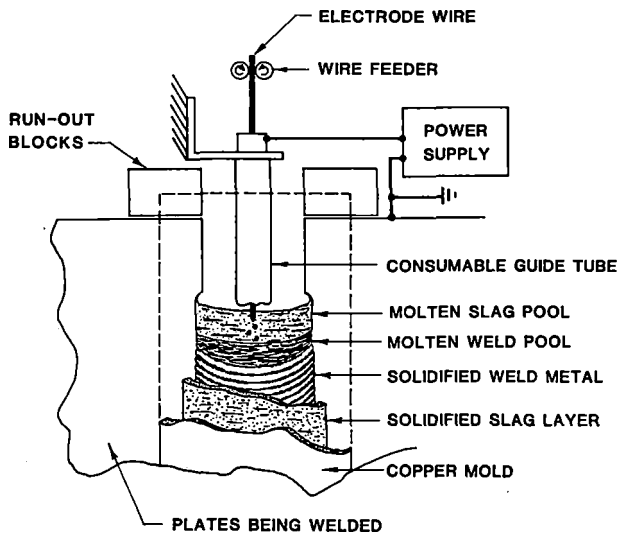
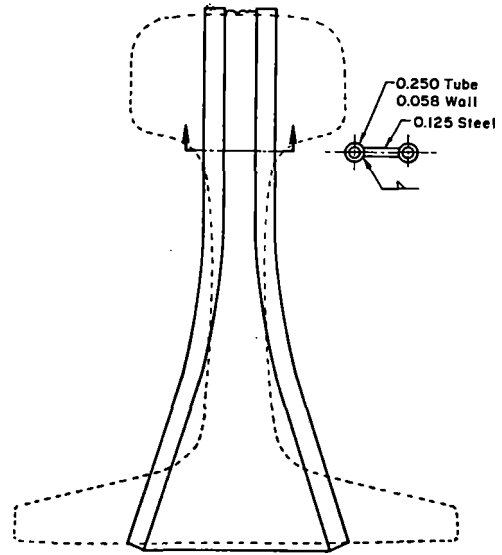


Fig.1 Diagram of Electroslag Welding Process



PRELIMINARY RAIL GUIDE TUBE

Fig.4 Plate Guide Tube

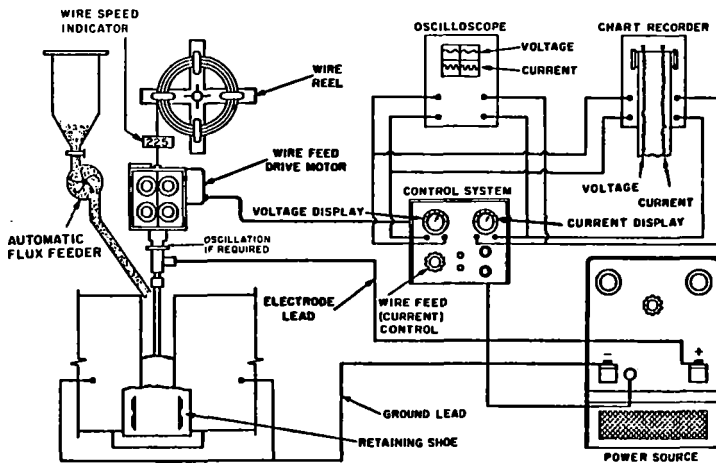


Fig.2 Schematic Diagram of Electroslag Welding Components

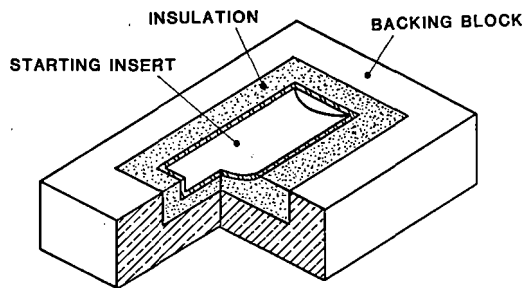


Fig.3 Starting Block Assembly

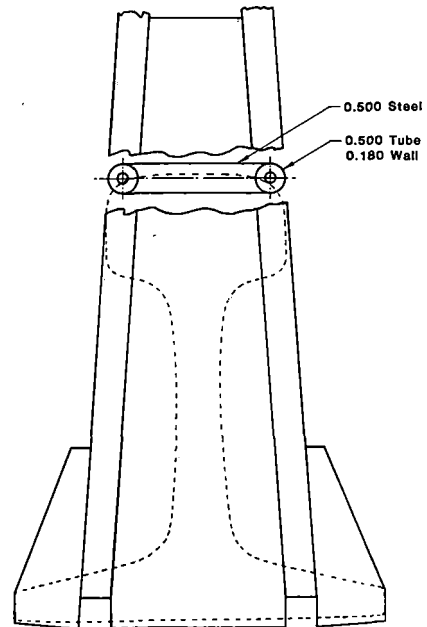


Fig.5 Wing and Plate Guide Tube

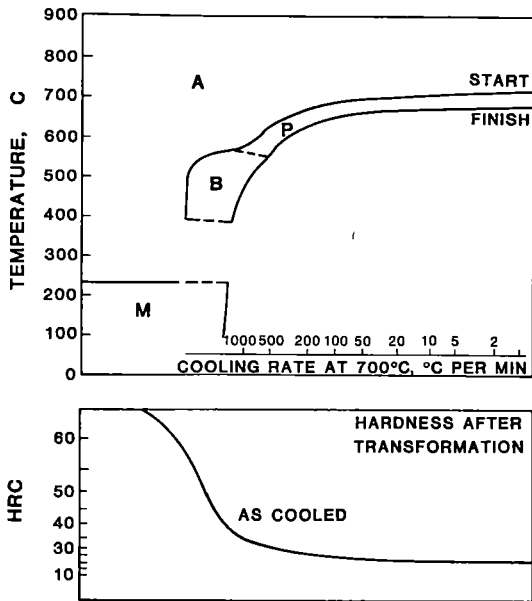


Fig.6 Continuous Cooling Transformation Diagram for a 1075 Steel (7)

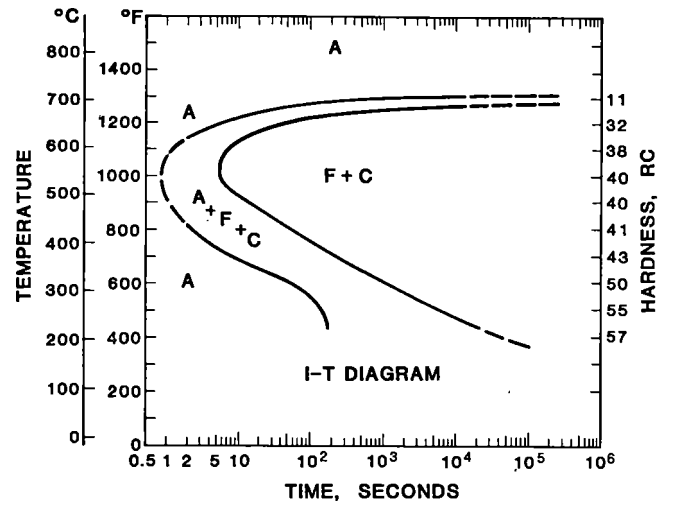


Fig.7 Isothermal Transformation Diagram for a 1080 Steel (8)

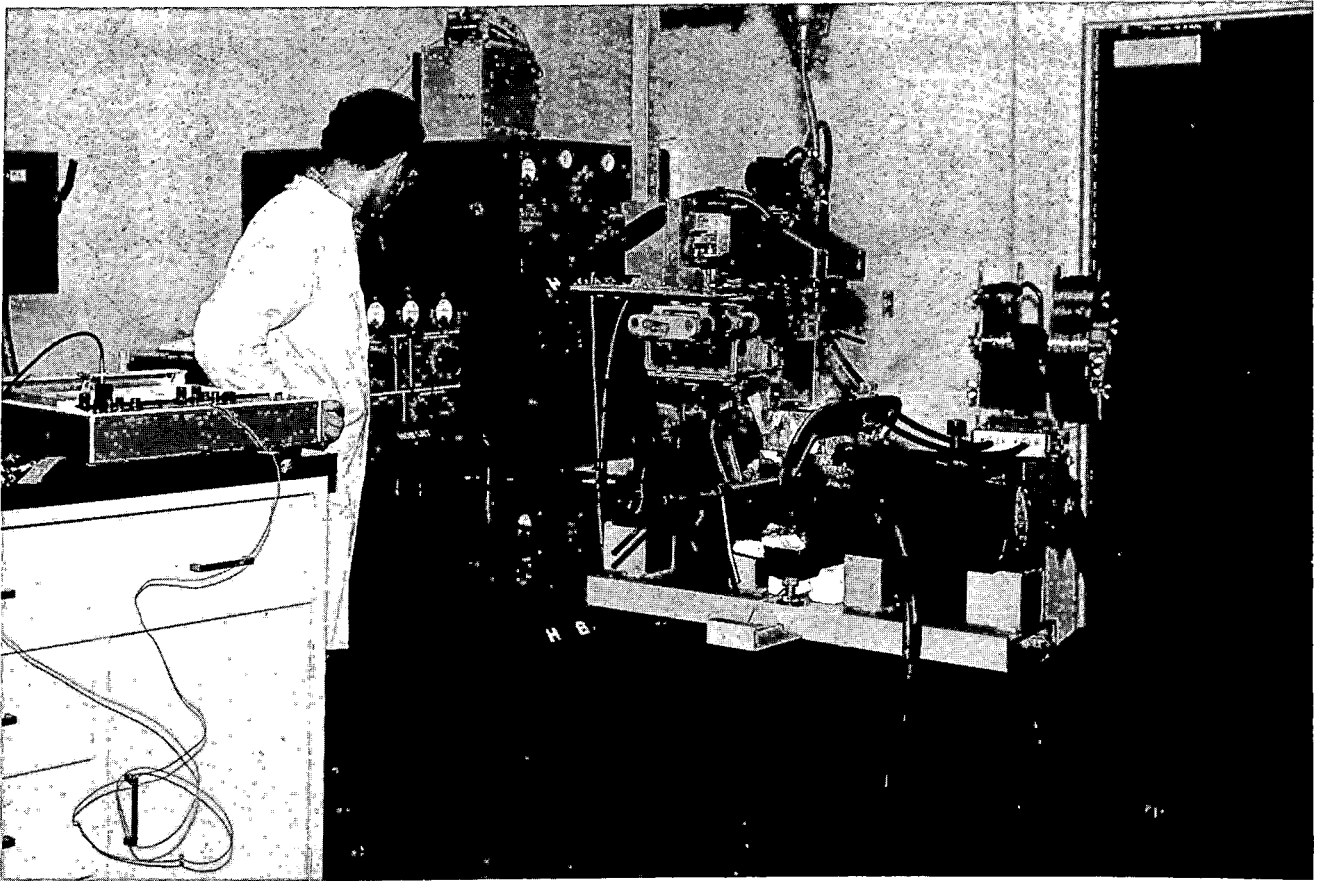


Fig.8 Electroslag Rail Weld Assembly



Fig.9 Optimized Electroslag Rail Weld

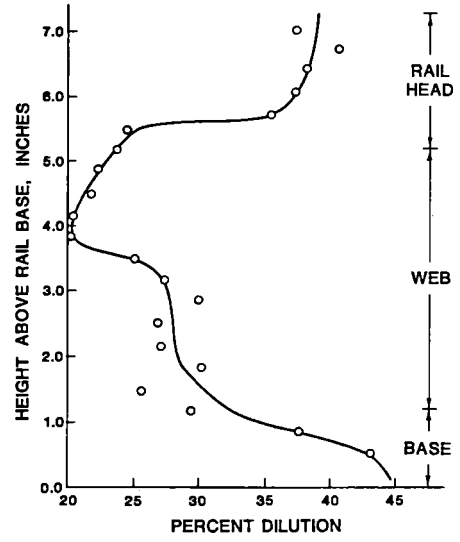


Fig.11 Dilution of Rail Steel in the Weld Metal versus Height Above the Rail Base for a 1 inch (2.54 cm) gap



Fig.10 Longitudinal Rail Section

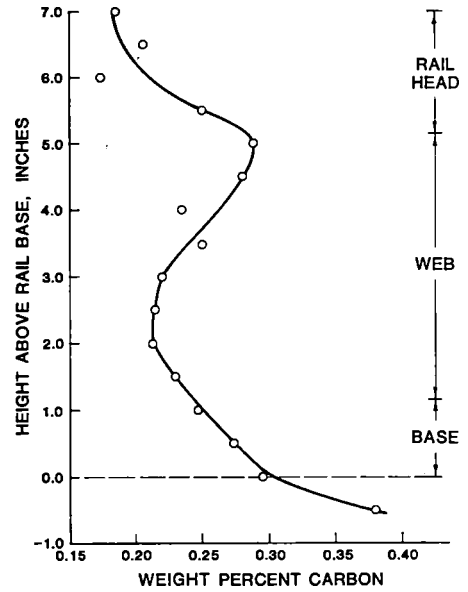
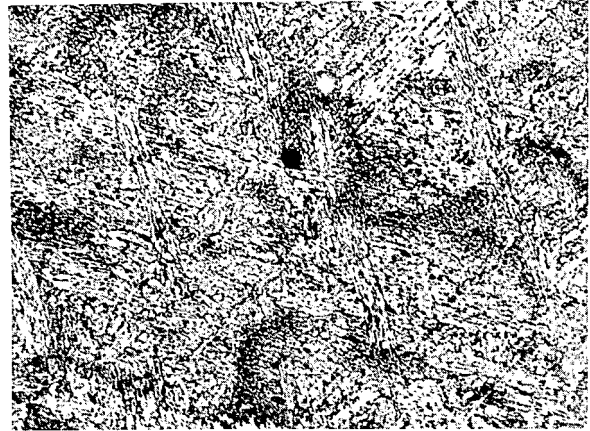


Fig.12 Variation of Carbon Content with Height Above the Rail Base for a 1-1/4 inch (3.13 cm) gap



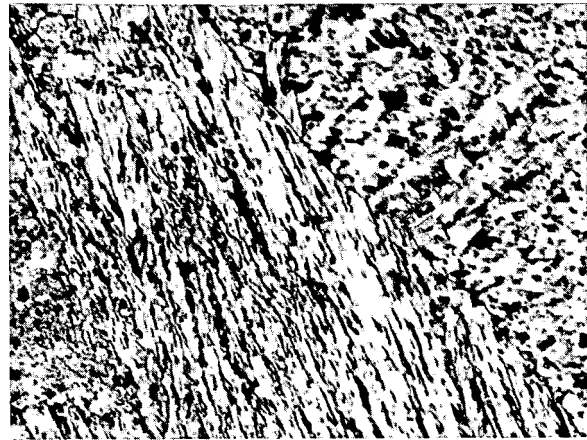
Rail Steel 250x



2-1/4Cr-1Mo Electroslag Weld Metal 250x



Rail Steel 1000x



2-1/4Cr-1Mo Electroslag Weld Metal 1000x

Fig.13 Rail Steel Microstructure (2% Nital Etch)

Fig.14a 2-1/4Cr-1Mo Weld Microstructure (2% Nital Etch)



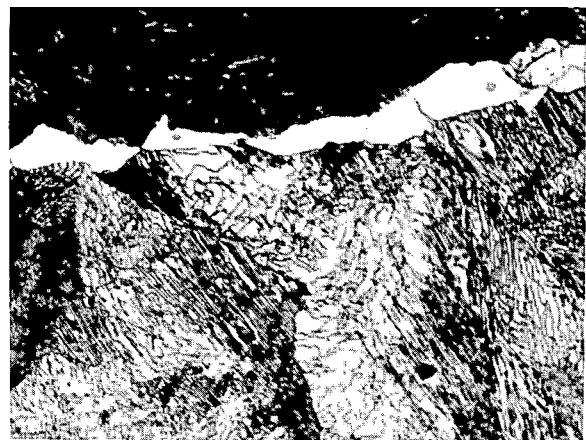
2Mn-1/2Mo Electroslag Weld Metal 250x



0.65C Electroslag Weld Metal 250x



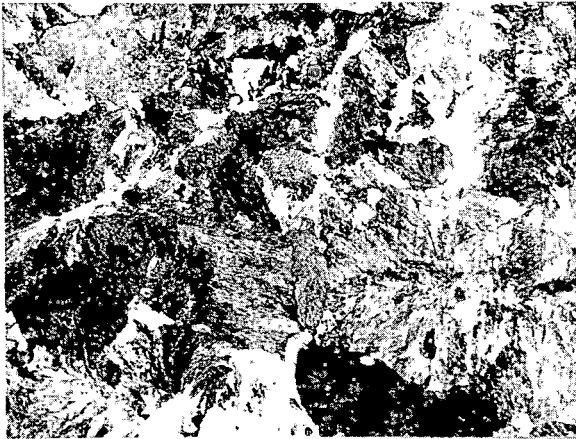
2Mn-1/2Mo Electroslag Weld Metal 1000x



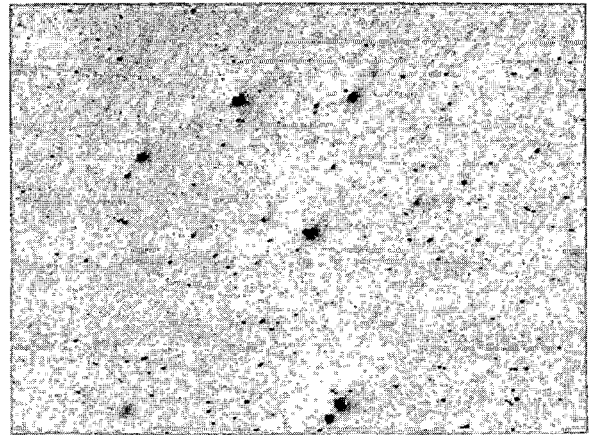
0.65C Electroslag Weld Metal 1000x

Fig.14b 2Mn-1/2Mo Weld Microstructure (2% Nital Etch)

Fig.15 0.65C Weld Microstructure (2% Nital Etch)



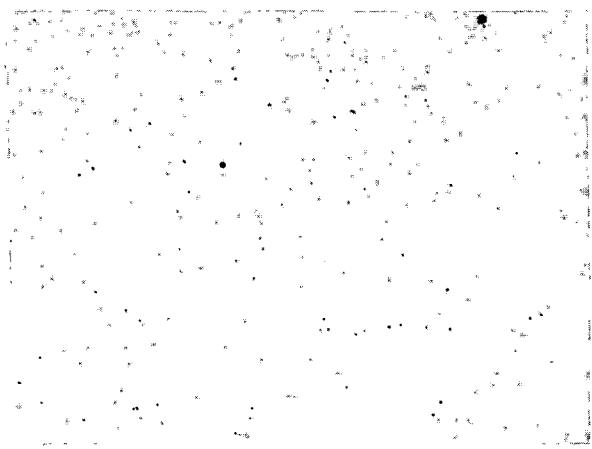
Thermit Weld Metal 250x



0.65C Weld Metal 100x



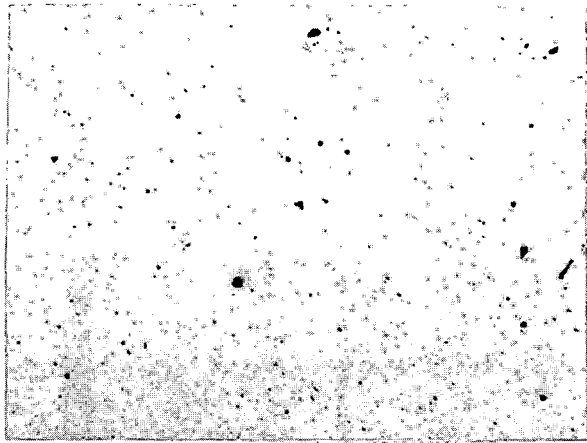
Thermit Weld Metal 1000x



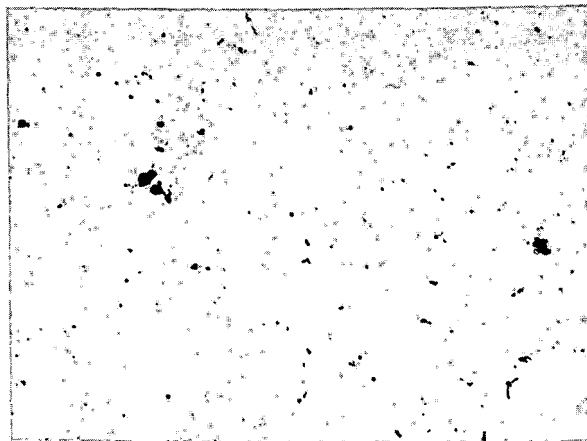
2Mn-1/2Mo Weld Metal 100x

Fig.16 Thermit Weld Microstructure (2% Nital Etch)

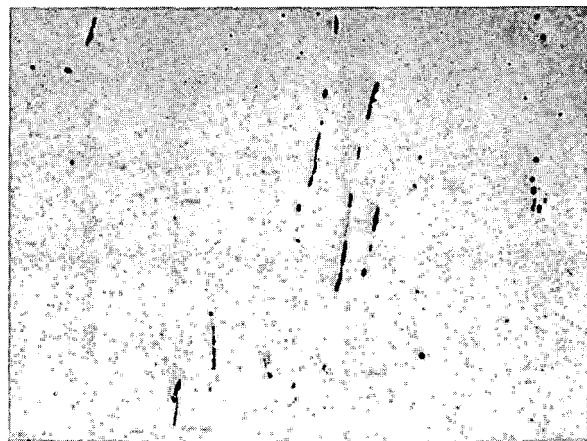
Fig.17



2-1/4Cr-1Mo Weld Metal 100x



Thermit Weld Metal 100x



Rail Steel 100x

Fig.17 Inclusion in Unetched Polished Specimens

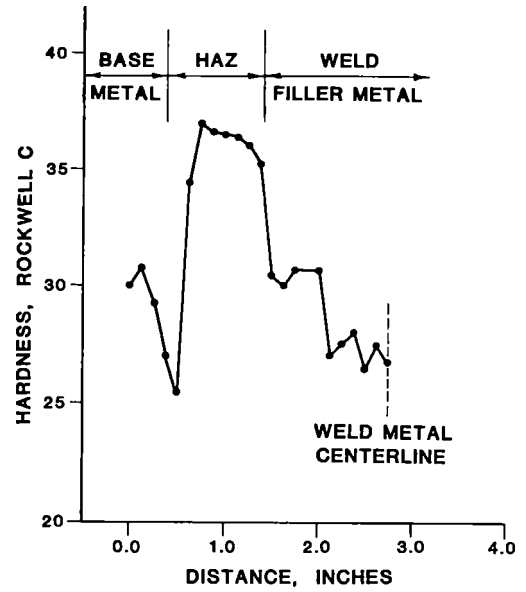


Fig.18a Hardness Traverse Through the Head Section of an Electroslag Rail Weld using a 2-1/4Cr-1Mo Filler Wire with a Mild Steel Consumable Guide Tube

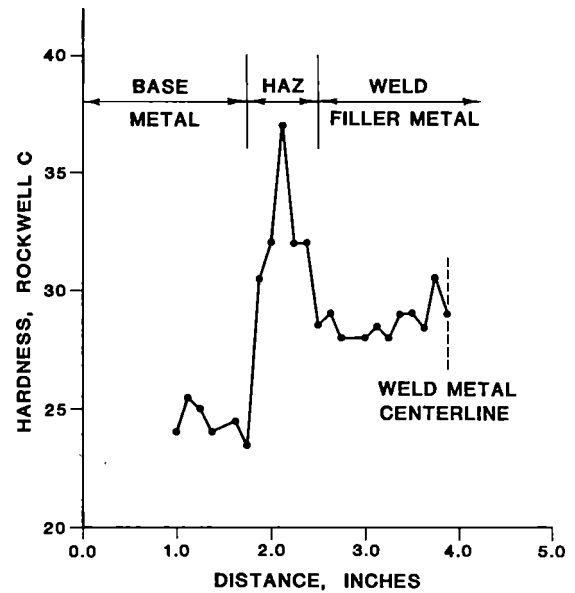


Fig.18b Hardness Traverse Through the Head Section of an Electroslag Rail Weld using 0.65 wt% Carbon Filler Wire and a Mild Steel Consumable Guide Tube

R.Y. Deroche ¹
 Y. Bourdon ¹
 A. Faessel ²
 R. Waeckerle ²
 H.P. Lieurade ³
 C. Maillard-Salin ³
 J.P. de Monicault ⁴
 J.P. le Cornu ⁴

¹ Sacilor Rail Technical
 Manager & Testing Eng.

² Sacilor-Sollac Research
 Manager & Head of Mech-
 anical Assistance Lab.

³ Head & His. Assistant
 Fatigue Testing Dept.
 French Institut de
 Recherche de la
 Siderurgie (IRSID)

⁴ Head, Static Testing
 Dept.; Assistant, The
 Fatigue Dept., French
 Laboratoire National
 D'Essais (LNE)

Stress Releasing and Straightening of Rails by Stretching

The straightness of the rails and their fatigue behaviour is a main concern for Railroads. That is why a new straightening process has been developed and patented by SACILOR. The stretch-straightening process makes the rails perfectly stress-related and fully complying with the most drastic straightness specifications. Thus, these two formerly conflicting qualities should make a profitable fatigue behaviour improvement in track to be expected. Since the yield strength is increased by stress hardening, improvements are also to be expected concerning wear and metal flow.

The straightness of the rails and their fatigue behaviour are among the most influent factors of the track maintenance cost, especially for continuous welded tracks. Increased needs of straightness made most of the rail makers cancel the old gag-press process and use the new roller-straightener facility. Then the residual stresses problem came up as the low intensity internal stresses coming from the cooling bed were turned into a high intensity stresses pattern coming from the roller-straightener and able to interfere with fatigue behaviour in an undesirable way. Furthermore, though the roller-straightener process yields an appreciable improvement to the rail-straightness quality and to the rail finishing productivity, it gives rise also to problems associated with the principle of the process : the twisting of the rail end entering the machine through the two modulus of inertia so that the use of hydraulic presses is required to get the end geometry complying with the Railroads specifications ; the wavening of the running table coming from the geometrical eccentricities of the rolls can make vibrations of the rolling stock and of the track up to a harmful level of frequency and amplitude, especially dangerous for high speed lines.

Another handicap affects the ends of the rail since a significant difference of dimensions between the ends and the body of the rail can be measured ; the run over of the rail head starts only from the second roll when the entering or leaving tip is handled by the three first rolls. The result is a widened basis and a reduced height of the rail in its central part, except 30 to 35 inches at each end keeping their rolling dimensions. It should be noticed that the variations of dimensions are increasing with growing

rail size since, with increasing bending modulus, and with a constant distance between roller axis, the vertical roll force should be increased.

Furthermore, while the bending forces are applied in the plane of symmetry through the bigger modulus straightening machine, the situation is quite different in the second straightening machine ; there, the transverse forces do not get the same reaction from the head and from the base ; as the bending of the web cannot be thwarted by the rolls, in addition very severe shearing stresses are developing in the web and base connecting area, so diagonal brittle cracks may propagate like a tunnel along the whole length of the rail without any visible traces on the outside surfaces. (Fig. 1)

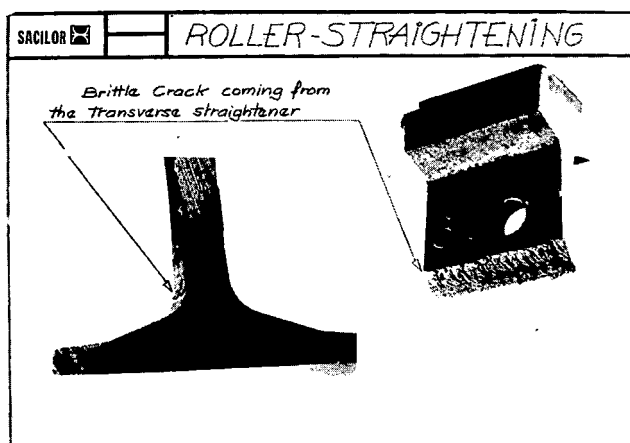


Fig. 1 Crack generated by Roller-Straightening

At least, the heterogeneous plastic strains pattern, which makes the rail straightening possible, is well known for developing high longitudinal internal stresses, the profile of which is very harmful since the higher tensile stress can be observed on the

surface of the running table and in the center line of the base, the web being in compression. The Railroads are very concerned with the tensile residual stresses of the head because they may emphasize with the service stresses but the Railroads are very concerned, also, by the tensile internal stresses located under the base which are considered as very damageable for heavy haul tracks.

That is the reason why SACILOR tried to develop a new rail straightening means - the stretch-straightening process - able to avoid the above mentioned inconveniences. Two years ago SACILOR started the first rail stretch straightening tests in the Laboratoire National d'Essais (French National Test Laboratory at COLOMBES-PARIS). This new process is now fully patented.

THE STRAIGHTNESS PROBLEM

The first stretching tests were performed by means of a 750 metric tons capacity tensile machine equipped with two fixed jaws (fig. 2-3) and able to stretch 18 meters long rail. Immediately, the need of two degrees of freedom at the jaws was discovered ; the experimental curve giving the residual general deviation of the rail versus permanent elongation shows (fig. 4), that is possible to reverse the direction of the rail general curve due to the bending moment existing in the fixed jaws ; and that makes an apparent operating point which limits the interest of the process.

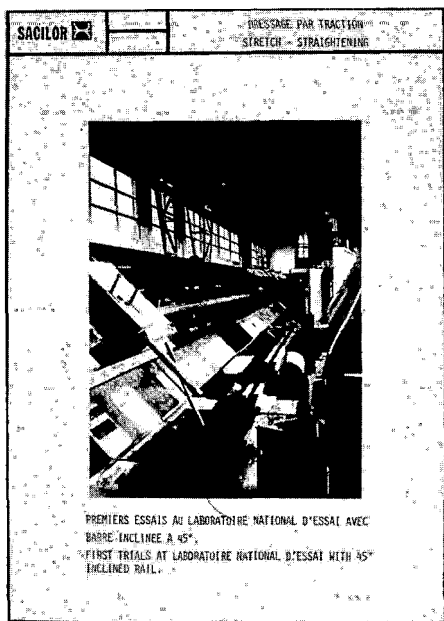


Fig. 2 Tensile Facility

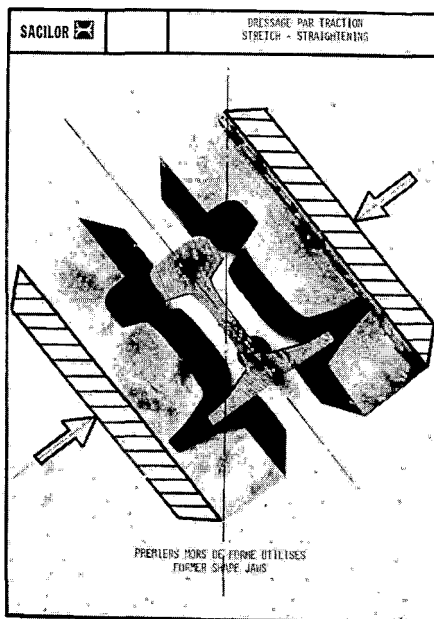


Fig. 3 Former Shape Jaws

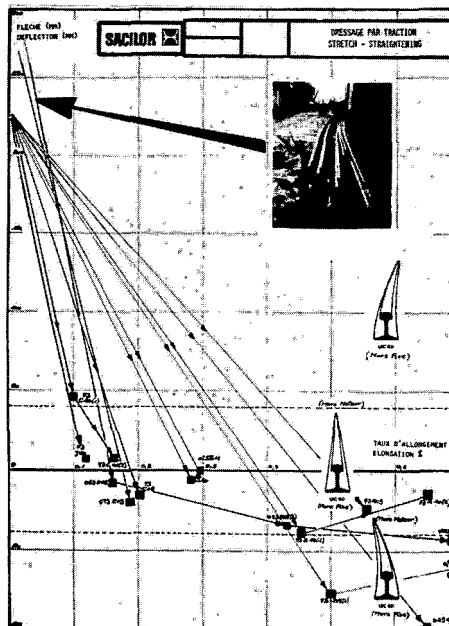


Fig. 4 Variation of the rail shape versus permanent elongation

So SACILOR developed afterwards two degrees of freedom tensile heads (fig. 5-6-7) and the stretching tests went on yielding a perfect straightness in the two directions (vertical and transverse) independently of the residual elongation as soon as this elongation keeps higher than 0.2 to 0.3 % ; the rails straightness complies with all the specifications (UTC or AREA) as well for the general curvature as well for the ends.

Now SACILOR should optimize the technology and especially the rails handling and the jaws technology.

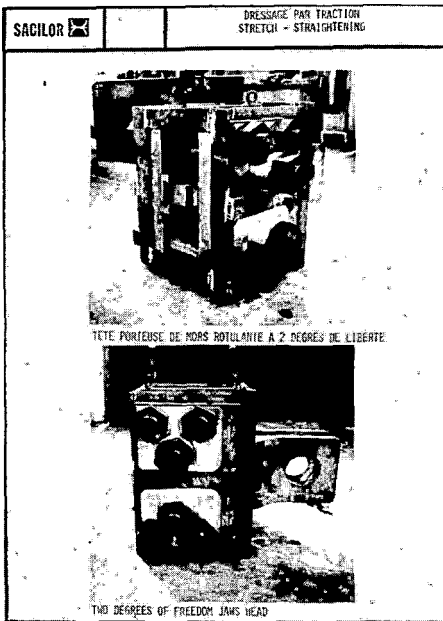


Fig. 5 Two degrees of Freedom Head

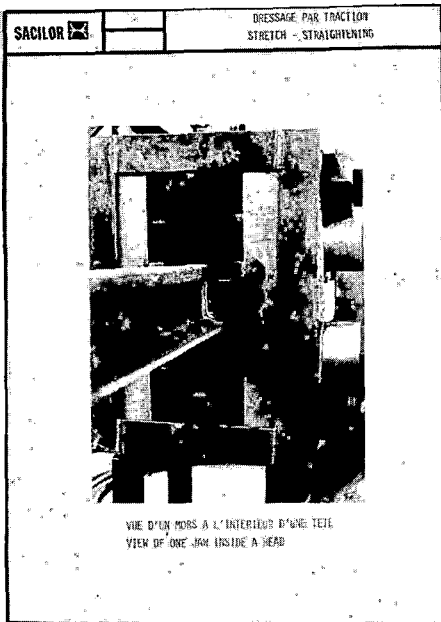


Fig. 6 View of one jaw inside a head

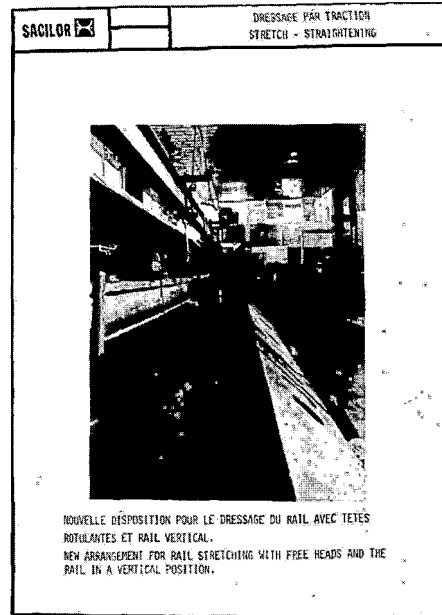


Fig. 7 Experimental arrangement

THE EFFECT ON THE RESIDUAL STRESSES

The straightening of the rail by plastic preferential strain of the shortest fibers leads to the stress-releasing of the material.

The SACILOR-RESEARCH LABORATORY has calculated the residual internal stresses evolution as a function of the permanent residual elongation (fig. 8) and this theoretical model shows that the residual stresses are efficiently reduced - in the proportion of 10 for 1 - as soon as the permanent elongation reaches 0.25 to 0.3 %.

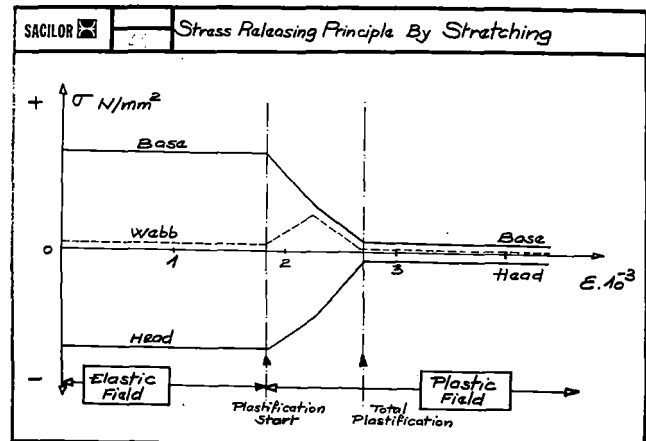


Fig. 8 Stress-Releasing by Stretching

The SACILOR MECHANICAL ASSISTANCE LABORATORY has carried out surface residual stresses measurements by means of the hole extensometric method on a UIC 60 kg/m - 950 N/mm² tensile strength usually ordered by French National Railways. (fig. 9)

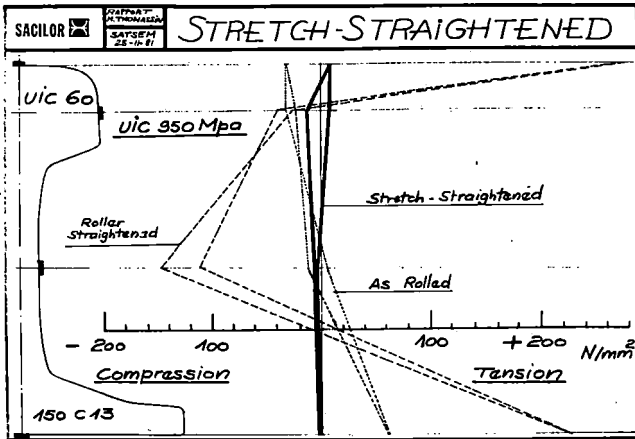


Fig. 9 Comparative results of Residual Stresses in a UIC 60 / 950 Mpa Grade (Hole Method)

The comparison between the as-rolled state, roller-straightened or stretch-straightened state can be seen in table 1.

	+ tension - compression		Longitudinal Stresses (N/mm ²)	
	As-rolled	Roller Straightened	Stretch Straightened	
Head (Running table)	+ 37	+ 282	+ 10	
Webb (center) Side A	- 15	- 113	- 17	
Webb (center) Side B	+ 10	- 143	- 21	
Base (center)	+ 61	+ 225	0	

Table 1

It should be noticed that the transverse stresses keep a very small magnitude (less than 40 N/mm²) whatever the considered state.

The French National Test Laboratory (LNE) carried out many residual stress measurements by means of the cutting method (fig. 10)

It should be mentioned that a previous experimentation on rail steel gave an acceptable agreement between the hole method, the cutting method and the trepan drilling method (this last one being developed by IRSID - French Institute for Steel Research in Saint GERMAIN - PARIS).

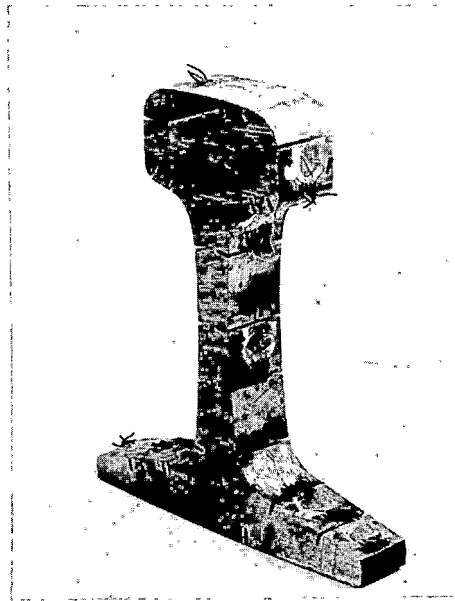


Fig. 10 Residual Stresses Measurement by Cutting Method

All the results are similar and a typical comparative residual stress profile is given in fig. 11a-b-c-d. The rail test specimen is made of UIC B wear resistant grade.

We could have closed the file of the residual stresses here. But an interesting question came up about the behaviour of the alloyed high strength rails through roller-straightening since it is well known that the residual stresses are growing like the yield strength does.

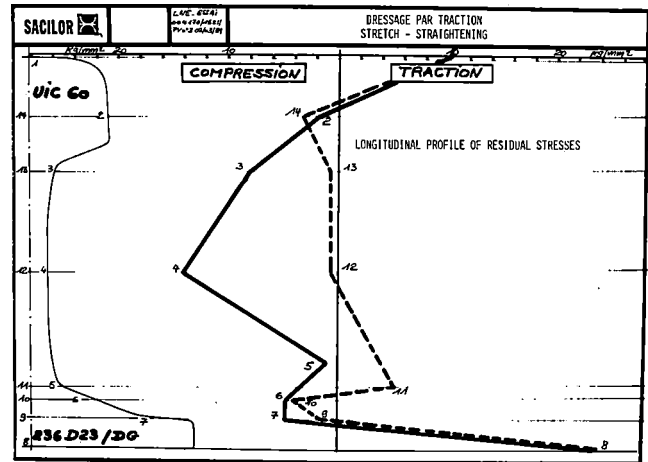


Fig. 11a

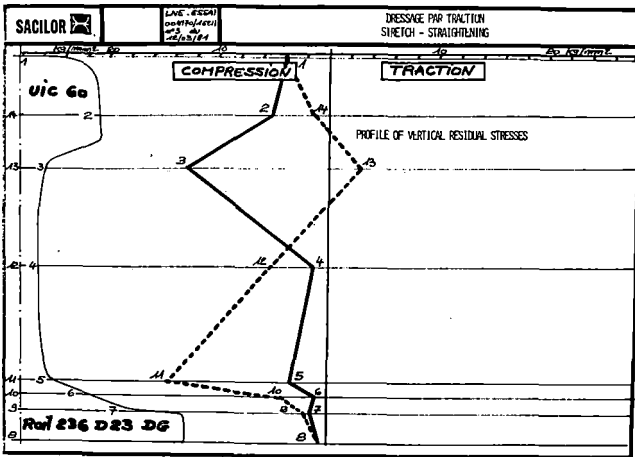


Fig. 11b

Fig. 11a and b Residual Stresses Measurements in Roller Straightened UIC 60 Rail/950 Mpa Grade (Cutting Method)

- a - Longitudinal
- b - Vertical

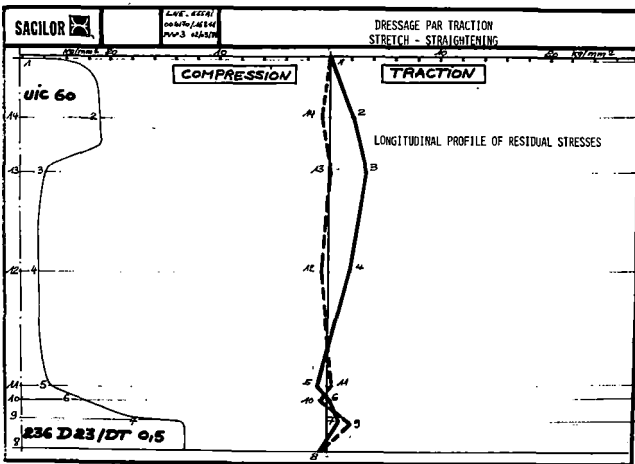


Fig. 11c

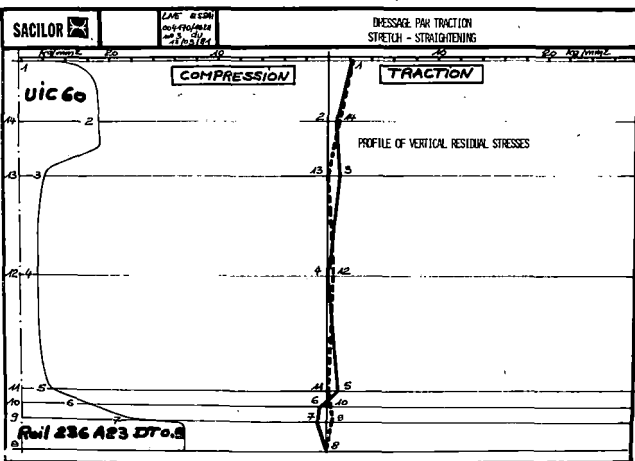


Fig. 11d

Fig. 11c and d Residual Stresses by Stretching.

- c - Longitudinal
- d - Vertical

IRSID by Trepan drilling (fig. 11 bis) method and LNE by Cutting Method, carried out a lot of measurements on a 136 RE/alloyed rails, the chemistry of which is the following :

- . Carbon : 0.720 %
- . Manganese : 0.900 %
- . Silicon : 0.750 %
- . Chromium : 0.900 %
- . Vanadium : 0.100 %

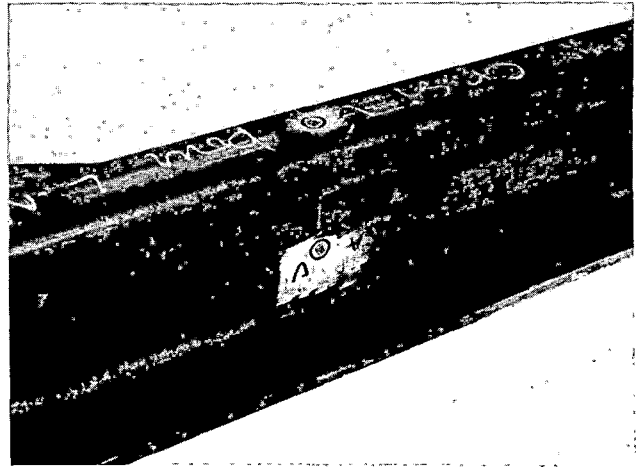


Fig. 11 bis Trepan Drilling Method

The stress values are given in the table 2 :

	Longitudinal Stresses		
	As-rolled	Roller Straightened	Stretch Straightened
Head/LNE	- 30	+ 300	+ 45
Head/IRSID	+ 38	+ 410	+ 89
Difference	68	110	44
Webb/LNE	- 120	- 100	+ 12
Webb/IRSID	- 45	- 120	+ 77
Difference	75	20	65
Base/LNE	+ 20	+ 260	+ 40
Base/IRSID	+ 87	+ 327	+ 92
Difference	67	67	52

Table 2

The lower level of residual stresses yielded by stretch straightening is truly obvious and especially in the head and in the base. (fig. 12a-b)

It can be seen that the IRSID/Trepan-Drilling method yields higher stress values, but the stress profiles are similar, only displaced of an average 70 N/mm² quantity.

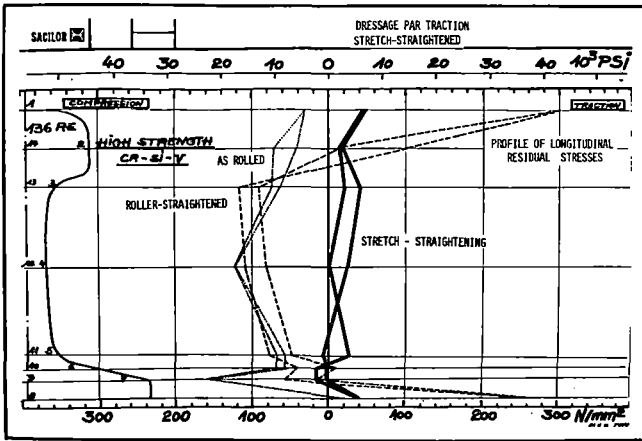


Fig. 12a Comparative Results of Longitudinal Residual Stresses in a 136 RE Alloyed Premium Rail.

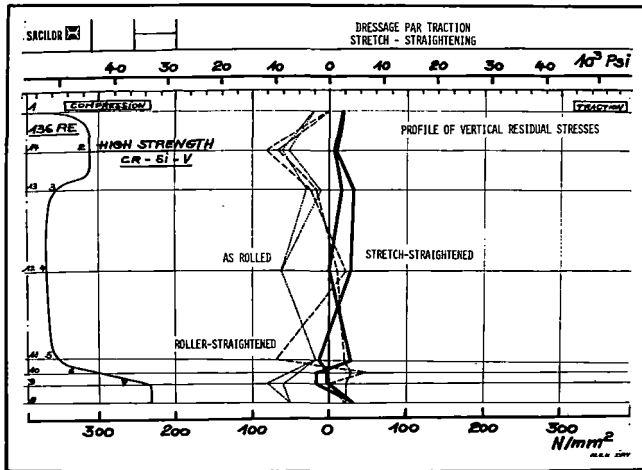


Fig. 12b Comparative Results of Vertical Residual Stresses in a 136 RE Alloyed Premium Rail.

An interesting experience consisted in stretching one 136 RE Alloyed Rail which has been previously roller-straightened (fig. 13). The strong tensile stress characterizing the roller process are efficiently reduced down to a very acceptable level.

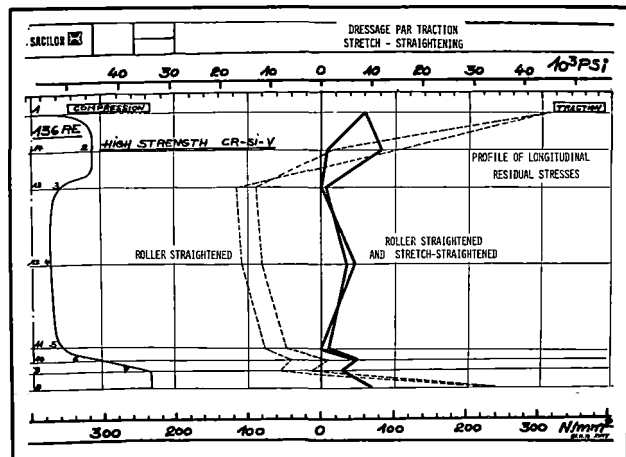


Fig. 13 Stretch Stress-Releasing of a Roller-Straightened Rail.

Finally an investigation was made in order to measure the efficiency of the stretch-straightening for 136 RE head-hardened rails (fig. 14a-b). It can be seen that the stresses regulating effect is very worthy.

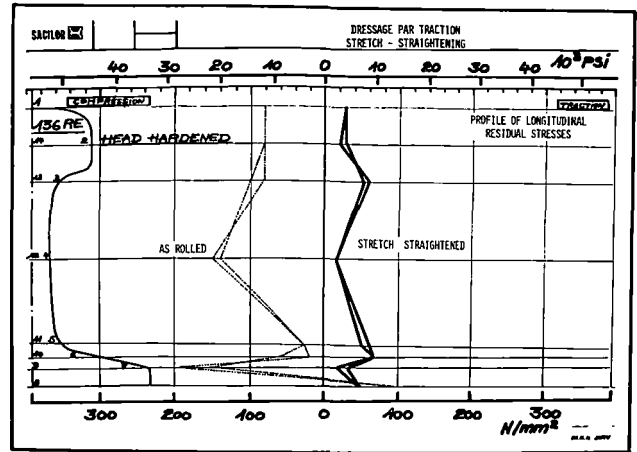


Fig. 14a Comparative Longitudinal Residual Stresses of a 136 RE Head Hardened Rail

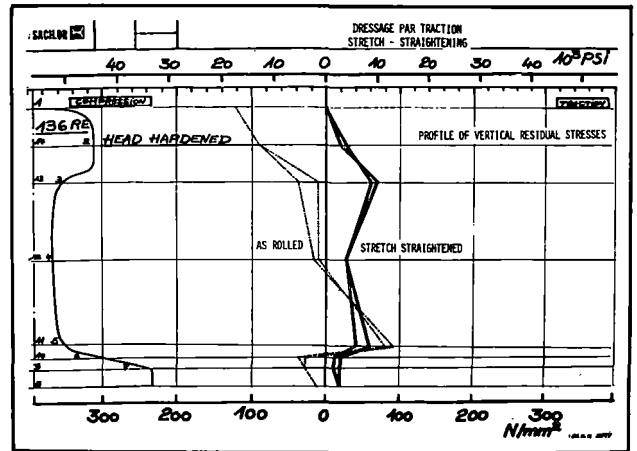


Fig. 14b Comparative Vertical Residual Stresses of a 136 RE Head Hardened Rail.

An empirical checking of the stress-releasing has been carried out by means of sawing the rail-head off the remaining profile (fig. 15) and measuring the tip upsweep during the sawing operation.

On the basis of 0.5 meter sawed length, the upsweep of a roller-straightened UIC 60 is 2 mm against 0.2 mm for a stretched rail and against 0.7 mm for an as-rolled rail.

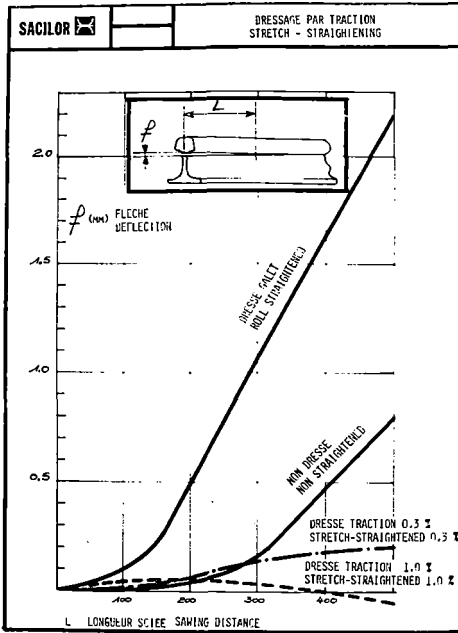


Fig. 15 Practical Residual Stresses Test

FATIGUE TESTING

Rail stretching may introduce some apprehension about damages occurring into the material and able to make eventual fatigue cracks to propagate faster. Thus SACILOR, IRSID and LNE developed together a four points fatigue bending test. (fig. 16)

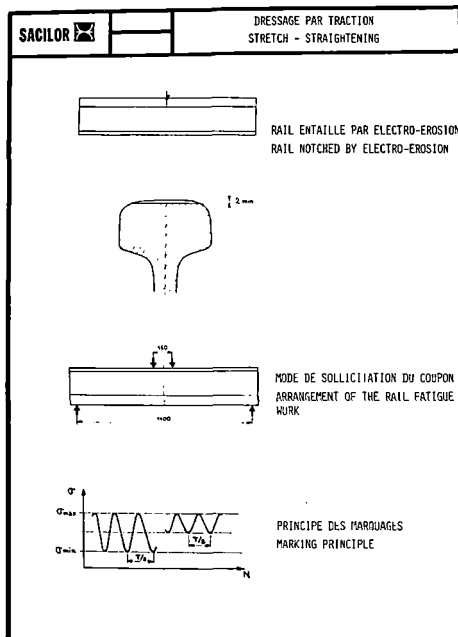


Fig. 16 Fatigue Testing Procedure

The test consists in applying on a pre-notched head rail specimen an alternative bending on a 1.40 meter base (55 inches) using a 10 Herz frequency and an approximate 90 000 Newton loading. The fatigue crack propagation is followed by means of a strain gauge extensometer and an electrical device using the electrical resistance variation during the crack propagation. Markings are made in the crack area by changing the applied stresses ratio and the curve :

$$a \text{ (Crack Depth)} = f \text{ (Number of cycles)}$$

can be plotted. This test was performed using the two UIC 60 rails mentioned in the above Residual Stresses paragraph. (fig. 17)

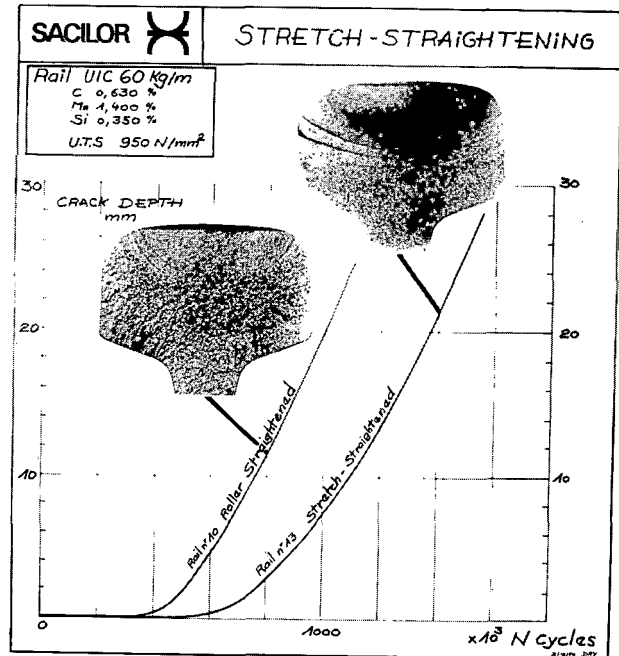


Fig. 17 Comparison of Crack Initiation and Propagation in a UIC 60 Rail/950 Mpa Grade.

The Roller-straightened rail is displaying a rather short fatigue crack area which is punctuated by brittle pops while the stretch-straightened rail displays a wider pure fatigue area coming off far from the radii of the running table.

The ratio :

$$\frac{\text{fatigue area (Stretch)}}{\text{fatigue area (Roller)}} = 1.55$$

The main parameters of the $a = f(n)$ curve can be summarised as follows, (table 3) :

	Roller Straightened	Stretch Straightened	Difference in %
Number of cycles for initiation	350,000	500,000	142
Number of cycles for propagation	750,000	1.050,000	140
Critical Length of Crack (mm)	25	28	112

Table 3

showing that, in connexion with the residual stress-releasing, the stretch-straightening improves in a very appreciable manner the fatigue behaviour, either at the initiation step, either at the propagation step. From these experimental data and from a curve of calibration giving the stress intensity factor K for a given crack depth in a full scale rail(1), IRSID calculated the Paris Law parameters m and ΔK_0 (table 4 and fig. 18) :

$$\frac{da}{dn} = 10^{-7} \left(\frac{\Delta K}{\Delta K_0} \right)^m$$

where

$\frac{da}{dn}$ is the crack propagation rate in meter/cycle

ΔK the variation of the stress intensity factor in $Mpa \sqrt{m}$

	m	ΔK_0
Roller Straightened	10.1	29.6
Stretch Straightened	6.6	31.9

Table 4

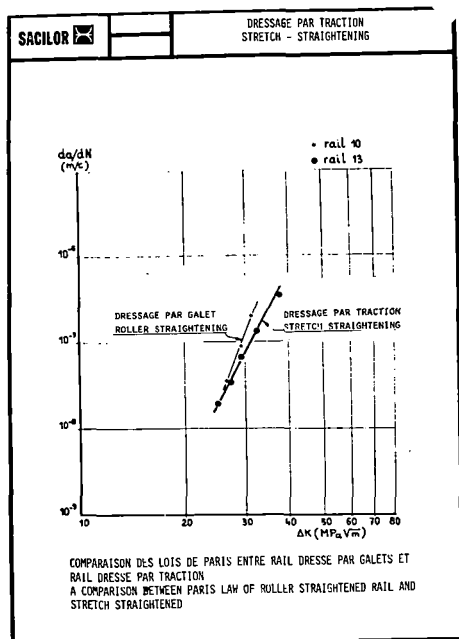


Fig. 18 Comparison of PARIS LAWS

The same fatigue tests were performed on the 136 RE alloyed rails mentioned in the Residual Stresses paragraph (fig. 19) and the main parameters for the $a = f(n)$ curve can be summarized as follows (table 5) :

D = Difference	Roller Straightened (Reference)	As rolled		Stretch Straightened		Roller + Stretch Straightened	
		D %	D %	D %	D %		
Number of Cycles for Initiation	400,000	420,000	105	850,000	212	1150,000	287
Number of Cycles for Propagation	950,000	1500,000	157	1250,000	131	1400,000	147
Critical Length of Crack (mm)	26	27	103	26	100	28	107

Table 5

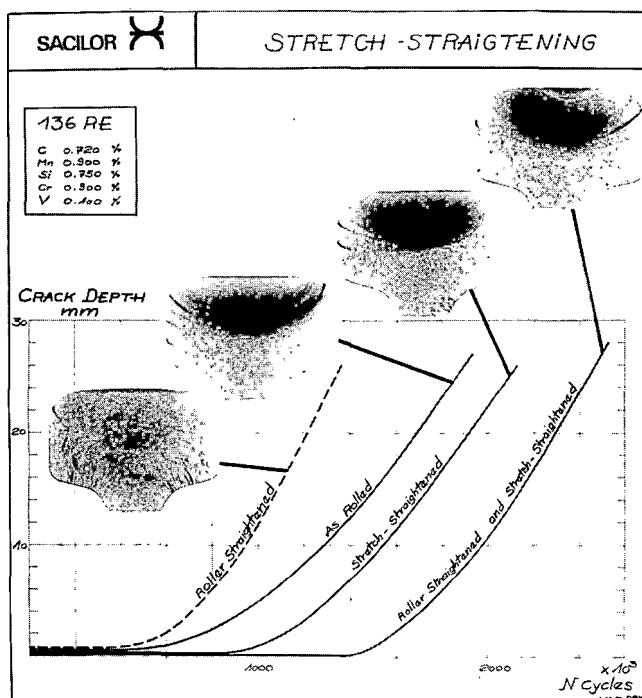


Fig. 19 Comparison of Crack Initiation and Propagation in a 136 RE Alloyed Premium Rail

The statement of the fatigue superiority of the stretching process can be done again, but it can be of interest to emphasize on some remarks :

- The as rolled fatigue characteristics seems to be very acceptable.
- The influence of a stretch-straightening subsequent to the roller-straightening operation is highly profitable because there is a clear improvement in reference to either the roller treatment either the stretch treatment. There are good reasons to believe that this fatigue behaviour improvement can be explained by a yield strength increase due to strain-hardening.
- Figure 19 shows pure fatigue areas except for the only one roller-straightened rail, the crack propagation of which was processed by subsequent brittle leaps (that is why, the curve was plotted in dotted line).

- apart from the fatigue areas, the brittle fracture of the roller-treated rail displays an irregular plane sprinkled by coarse brittle pops and rivers while the stretched-treated rail fracture plane is absolutely flat with a rather thin grain ; the stress releasing can be considered as the cause of this difference. (fig. 20)

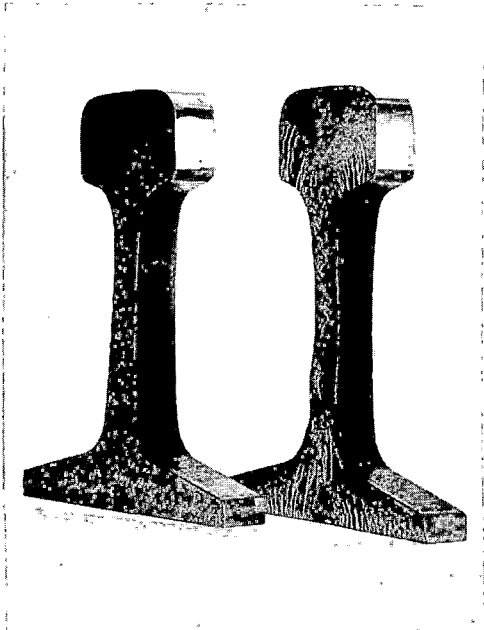


Fig. 20 Comparison of Fracture Surfaces

MECHANICAL PROPERTIES

The UIC B rail used for comparison of residual stresses and fatigue behaviour in the previous paragraphs have been tested for mechanical properties. (fig. 21)

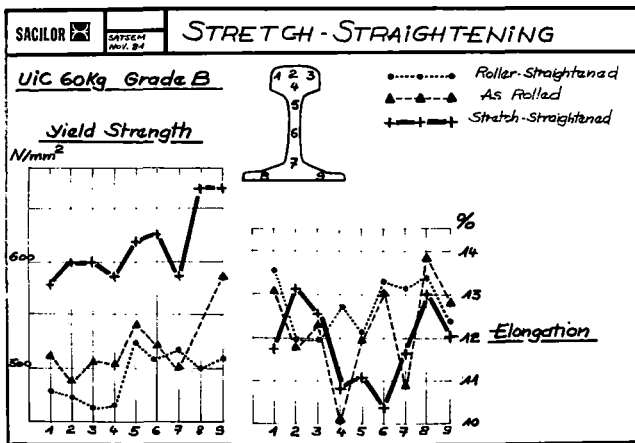


Fig. 21 Compared Mechanical Properties

While the yield strength of the roller-treated rail declines clearly (-5 %) from the as rolled state, which could be explained by a BAUSCHINGER effect, the yield strength of the stretch-treated rail is steadily raising (+ 17 %) as it can be seen in the table 6 :

YS TS	As rolled			Roller Straightened			Stretch Straightened		
	YS	TS	R=YS TS	YS	TS	R=YS TS	YS	TS	R=YS TS
Head	512	960	0.533	483	945	0.511	596	957	0.622
Webb	522	960	0.543	505	945	0.534	624	985	0.633
Base	548	992	0.552	510	980	0.520	641	994	0.644
Average	527	971	0.543	499	957	0.521	620	979	0.633

-5.3 %
+ 22.9 %
+ 17.6 %

Table 6

No sensible downgrading of the toughness (K_{1C} values) can be noticed due to the strain-hardening stretching effect, or, more exactly the stretch-straightening effect is not worse than the roller treatment to this regard :

K _{1C} in Mpa √m	As-rolled	Roller Straightened	Stretch Straightened
Head/Rolling Direction	53.2	46.5	50.5
Webb/Transverse Direction	39.0	39.1	39.0
Base/Rolling Direction	50.8	49.7	46.9
Base/Transverse Direction	41.6	41.0	40.6

Table 7

Heavy haul Railroads could be interested by this yield upgrading since a higher yield strength is generally considered as a good way for fighting against metal flow and shelling.

CONCLUSIONS

Sharper needs both for accurate geometry and for upgraded internal properties - either for High Speed Trains either for Heavy Haul Railroads - have led SACILOR to develop and patent a new straightening process.

The stretch treatment seems to be, at the present time, the only one process able to yield high quality straightness combined with very low internal stresses level, two requirements conflicting until nowadays.

SACILOR, now processing to the stretch-treatment optimization and to the industrial design, is hopeful this new process to contribute in the future to better Railroads operating conditions and, what is the main railways goal, to make the railway operation more profitable.

ACKNOWLEDGMENTS

The Authors would like to thank, namely :

- J.J. Renaud, R. Thomassin, our colleagues of SACILOR-SOLLAC Mechanical Laboratory and F. Daul of SACILOR Central Laboratory.
- D. Kaplan our colleague of Institut de Recherche de la Sidérurgie (IRSID).
- N. Courcault, B.R. Lacour, P.B. Bouquet of the Static Test Service of the Laboratoire National d'Essais (LNE).
- J. Tardy of the Fatigue Service of the Laboratoire National d'Essais (LNE).

whose active contributions have been gratefully received.

- (1) K. Morton, D.F. Cannon, P. Clayton, and E.G. Jones
THE ASSESSMENT OF RAIL STEELS
STP 644 ASTM 1978

Production of Special-Grade Naturally Hard Rails in Germany and Experience Gained in Operation

W. Heller

DR.-ING.
Krupp Stahl AG.

E. Koerfer

DR.-ING.
Klockner-Werke AG.

H. Schmedders

DR.-ING.
Thyssen AG.

When used in tight curves and on gradients under the highest axle loads, such as with iron ore railways, standard grade rail steel made according to AREA and UIC specifications no longer has a sufficiently high degree of wear resistance against material abrasion, plastic deformation and fatigue damage, for example "shelling formation". The described special-grade, naturally hard alloyed rail steel with its pearlitic basic structure has been shown to have, under extreme service stress conditions with respect to the above described kinds of wear, more than 2 to 3 times the service life in comparison with standard grade rails manufactured according to the AREA respectively UIC specifications. Special-grade, naturally hard alloyed rails are nowadays used in many parts of the world with the greatest success. Because their utilization value increases more greatly than the costs, their use is economical, especially for heavy traffic.

Special grades for railroad rails

Often, standard carbon grades manufactured to AREA¹ and UIC² standards no longer fully meet the requirements expected of them for heavily loaded tracks in particular in the case of sections having a large number of curves and those which have a marked up-grade or more accentuated down-grade. They are either subject to too great wear, or squeezing of the rail head and shelling with resulting transverse cracks occur.

In the effort to improve the service life and operating behaviour of rails used for such tracks the rail manufacturers have proceeded in two directions:

- In the USA, heat-treated rails have been developed based on the standard AREA grade which have, through subsequent heat treatment, a fine pearlitic structure in the wear zone of the rail head or over the entire rail cross-section. By this method hardness values of 320 - 380 HB are achieved.

This method has also been adopted by other countries, such as Japan and the USSR.

- In the Federal Republic of Germany a different direction has been taken. Based on the standard UIC 90 A grade with a hardness of 270 HB, the minimum tensile strength was first of all increased to 1080 N/mm², \geq 320 HB hardness (special

grade S 1100^{3;4}) by alloying with Cr or with Cr and V.

Rails of this quality prove to be perfectly adequate even when subjected to the harder conditions of mixed European goods and passenger traffic. To make possible their utilization for ore rail networks and, as experience in the USA has shown, for heavily loaded routes which are used with high axle loads, it proved necessary to improve the special grade still further in order to obtain tensile strengths of approx. 1200 N/mm² respectively hardness values of approx. 350 HB.

The present report deals essentially with the manufacture of this improved special grade as well as the experience gained so far with its utilization.

Mechanical properties and wear behaviour

The example of yield strength, tensile strength and hardness in Fig. 1 shows how these special grades differ from standard carbon grades and how they compare with heat-treated rails.

Compared with the standard AREA grade, the minimum tensile strength of 850 N/mm² has been raised to 1080 or 1150 N/mm². This corresponds to an increase of approx. 27 respectively 34 %. The yield strength for the standard AREA grade has increased from at least 430 to 590 resp. 670 N/mm². This corresponds to an increase of approx. 37 resp. 56 %. It is a known fact that the yield strength denotes the beginning of plastic deformation. With the increase in the yield strength, resistance against plastic squeezing of the rail head has therefore improved considerably.

Rails with a flattened running surface practically no longer occur where yield strengths

of over 600 N/mm^2 are involved. Compared with the standard AREA grade, the higher yield and tensile strength is accompanied by a proportional improvement in the fatigue strength so that these rails also have an essentially higher resistance against fatigue damage, such as shelling and resultant transverse cracks⁵.

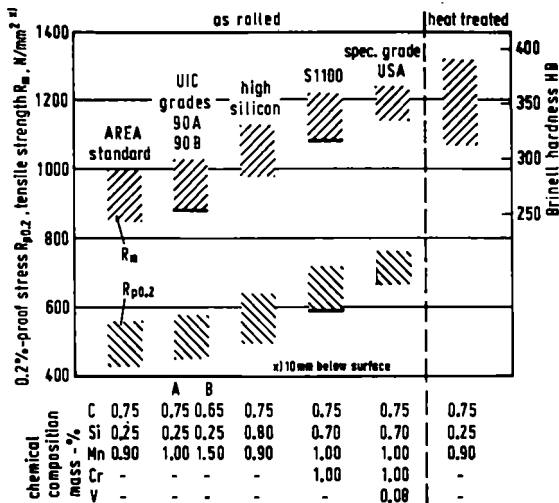


Fig. 1 Standard, alloyed and heat treated rail steels

Compared with standard grade rails, the wear resistance is doubled or nearly tripled. As can be seen in Fig. 1, the special grade naturally hard rails coincide in their average strength properties with those of heat-treated rails. In comparison with heat-treated rails they show a clearly lower variation in their strength or hardness values. This can result in heat-treated rails behaving partly more favourably and partly even somewhat more unfavourably than the special grade naturally hard rails. The average behaviour of both grades should, however, coincide.

If the variation in hardness of the rails in the rail head (Fig. 2) is studied, it can be seen that the dependency of the hardness on the distance from the running surface is less marked in the case of naturally hard grades than with heat-treated rails. This can result in heat-treated rails, whose wear behaviour is at first somewhat more favourable than that of naturally hard rails, showing wear behaviour identical to that of naturally hard rails as the operating stresses increase and even wearing to a greater extent than the naturally hard rails when subjected to high operating stresses.

Fig. 3 shows the distribution frequency of the mechanical properties (yield strength, tensile strength and elongation after fracture). It can be seen from the frequency distribution that the special-grade naturally hard rails are manufactured with a high degree of strength at close tolerances. The 95 % scatter band for the yield strength and the tensile strength thus is

100 N/mm^2 . Elongation after fracture lies above 9 %. The distributions plotted for the standard AREA grade for comparison purposes clearly show the improvements obtained in the yield strength and tensile strength.

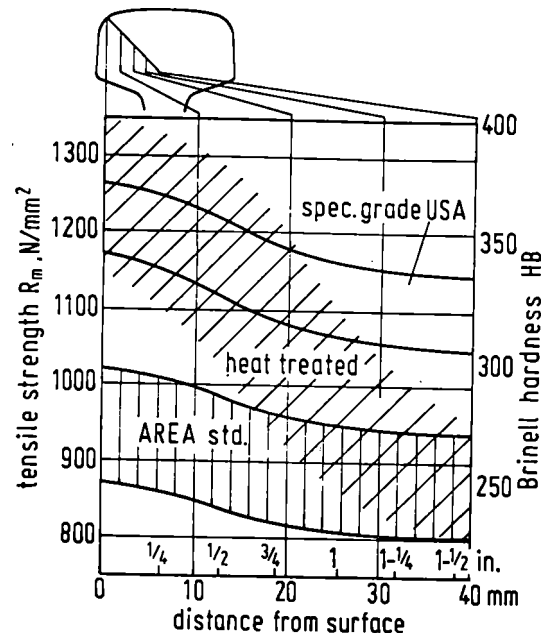


Fig. 2 Characteristic of tensile strength and hardness in rail head

Production of special-grade rails

Melting and vacuum treatment, hydrogen and oxygen content. The favourable operating and utilization properties of the special-grade rails are not only reflected in their chemical composition and mechanical properties, but also essentially depend upon the technology applied during rail production⁶.

In Germany special-grade rail steel is produced by means of both the basic oxygen and the open-hearth steelmaking process and is subjected to vacuum treatment^{7,8,9}. This is primarily to eliminate the hydrogen in the steel. Fig. 4 shows the frequency distribution of hydrogen contents in open-hearth and BOF steel, both with and without the application of vacuum treatment. For 100 % of the heats, the hydrogen distribution in non-vacuum-treated open-hearth steel shows contents which necessitate delayed cooling.

With normal BOF melting, hydrogen contents result which would necessitate delayed cooling for only around 50 % of the heats. By using vacuum treatment such low contents are obtained independent of the initial hydrogen content that, even with normal, undelayed cooling, a sufficiently large difference exists in comparison with the critical contents where flake-formation occurs. This permits cooling of the rails on the cooling bed without necessitating any special measures. Thus, the strength properties show the full effect brought

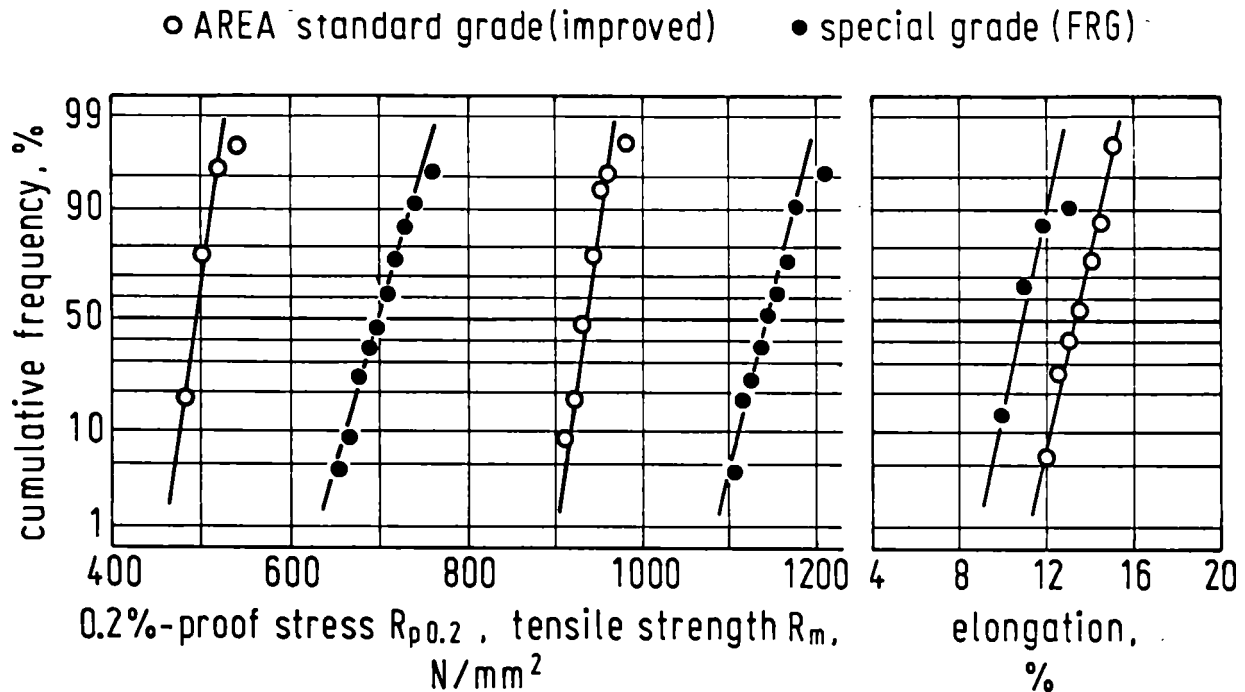


Fig. 3 Mechanical properties of rail steel for USA (sampling 17 mm below surface)

about by the chemical composition. Furthermore, undelayed cooling is a prerequisite for a rational production flow, in particular for large-length rails of up to 60 m.

In addition to the extensive elimination of the hydrogen, the oxygen in the rail steel, which can be regarded as a measure of the oxidic degree of cleanness, is simultaneously reduced to such an extent by means of improved precipitation of the deoxidizing products that only small percentages of oxidic non-metallic inclu-

sions remain in the rail steel. Fig. 5 shows the oxygen distribution in the rail head of the finished rail corresponding to the upper and center location on the ingot. In addition to the increased tensile strength and the thus increased fatigue strength, this good degree of purity has a favourable effect on the resistance of the rails against fatigue damage.

Even in the steelmaking shop itself, production of rail steel is subjected to intensive quality control. The tensile strength example in Fig. 6 shows the excellent correspondence which exists between the measured values and those values calculated on the basis of the chemical composition using a multiple regression analysis. After alloying in the ladle, the strength values which the rails will have from the respective heat can then be predicted with the greatest of certainty. If necessary, the analysis can be subsequently corrected in the vacuum installation.

Casting of the steel

Pouring of the steel into ingot moulds equipped with hot tops. In order to guarantee the favourable influence of the vacuum treatment on the quality of the finished rail, special measures are required when pouring the liquid steel to form ingots. In Germany bottom pouring of the steel into ingot moulds is practiced using hot tops, with up to 8 ingot moulds being simultaneously filled. Fig. 7 shows a schematic drawing of bottom pouring into ingot moulds using hot tops, compared with top pouring of rail steel into ingot moulds without hot tops, a method which is still practiced in some parts of the world. The low climbing rate that occurs in group casting produces a good rail surface condition.

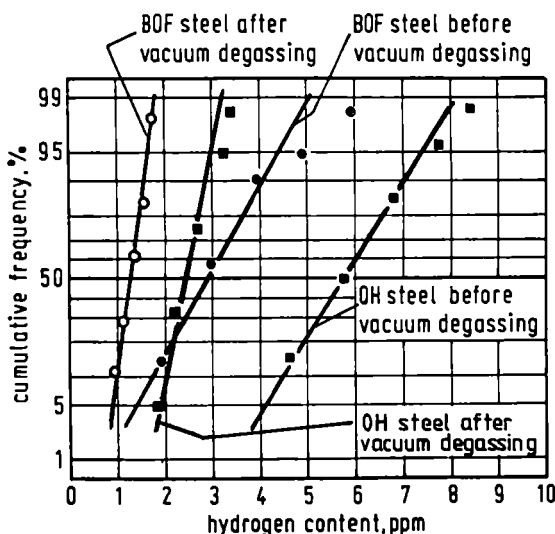


Fig. 4 Frequency curves for hydrogen contents of BOF and OH rail steels

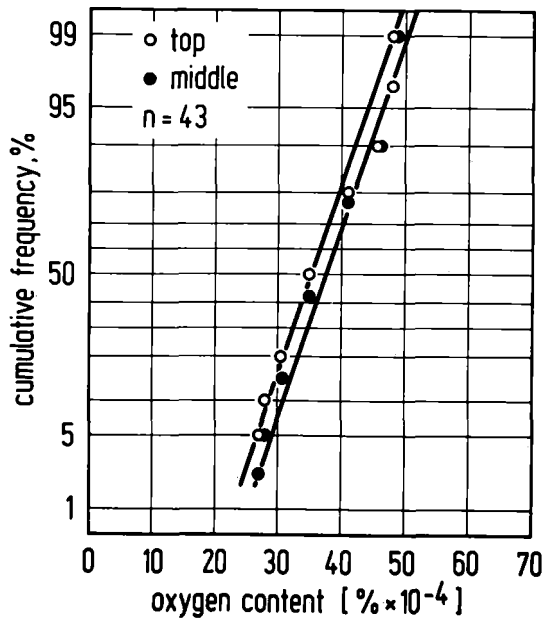


Fig. 5 Frequency curves for oxygen contents top and middle of the ingot

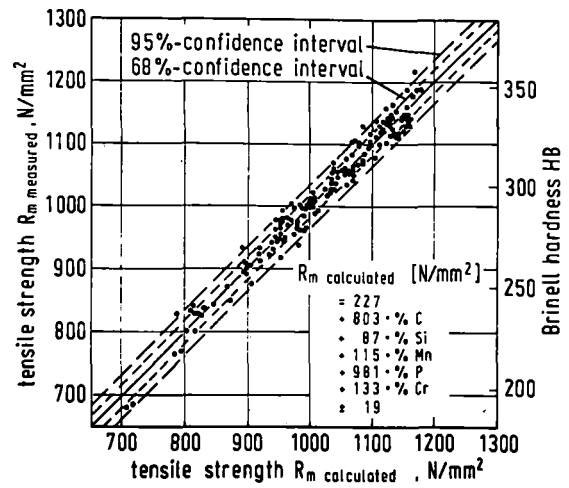


Fig. 6 Chemical composition and tensile strength of rails

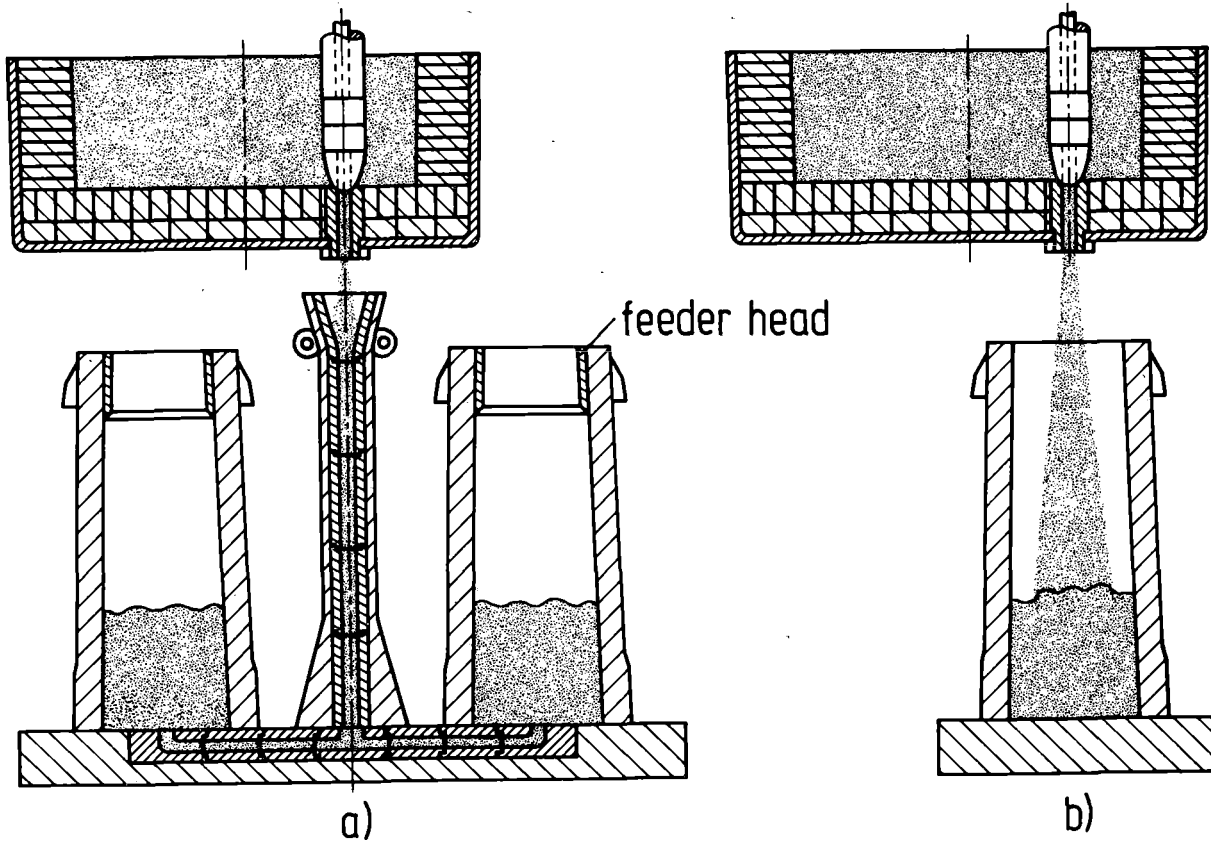


Fig. 7 Schematic representation of:
a) bottom casting of killed steel

b) top casting of semi killed steel

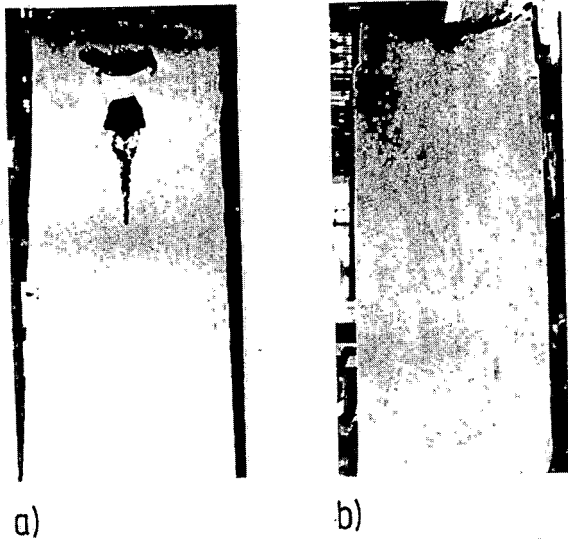


Fig. 8 Ingot: a) without
b) with hot top mould

The hot top inserted into each ingot mould keeps the steel in a liquid state in this top section for a longer period of time after pouring has been terminated so that oxides which are still present can rise from the liquid remainder of the ingot into the hot top area. Further advantages of hot top casting are the avoidance of shrinkage due to solidification and the shifting of segregation into the area where final solidification takes place, i.e. the hot top area. Fig. 8 compares, by means of Baumann sulphur prints, an ingot poured using a hot top and an ingot poured without a hot top.

Rails from ingots poured using a hot top are practically free from pipes and marked segregations because the hot top area is cropped after the ingot has been bloomed on the blooming mill. As sulphur prints of A-rails in Fig. 9 illustrate, rails originating from ingots poured using hot tops are free from segregations and pipes. The A-rail is therefore qualitatively on a par with other rails manufactured from the same ingot.

Steel casting on a continuous casting installation. For over 3 years now in Germany, strand-cast blooms made from degassed BOF-steel have been used to produce standard-grade rails and alloyed rail steels in increasing quantities and with the greatest success based on the latest steel shop casting practices¹⁰. A six-strand continuous casting installation of Concast design and with a bloom cross-section of 320 x 250 mm can be used to manufacture these blooms. The principle of continuous steel casting is illustrated schematically in Fig. 10.

Rails which are manufactured from blooms produced by this method fully satisfy all the technical specifications, as the test results obtained from extensive laboratory tests show. Their properties can at least be placed on a par with those of rails which have been produced from discontinuously cast ingots. Their service behaviour is positive.

Rolling of the rails. In addition to the metallurgical measures already discussed, the rail quality is considerably influenced with regard to its track durability by the grooving of the shape rolls. With roll pass designs used previously the crystals (dendrites) growing from the outside to the inside of the ingot during solidification stood at a perpendicular

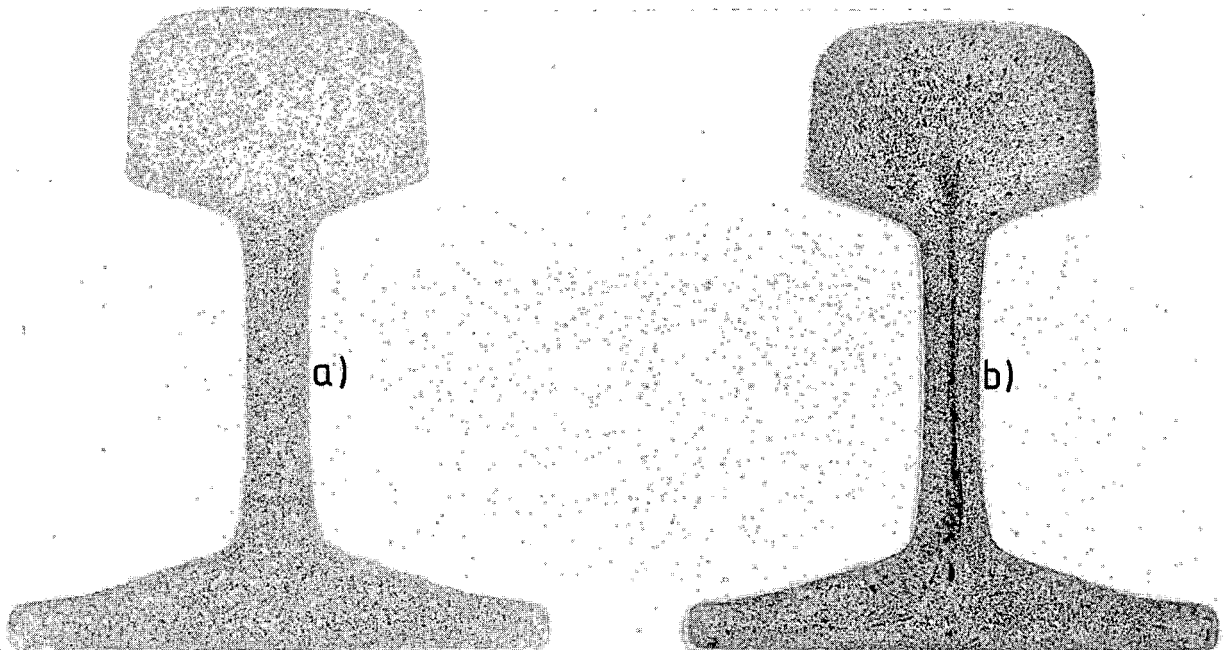


Fig. 9 Different sulphur prints:
a) bottom pouring with hot top mould
b) top pouring without hot top mould

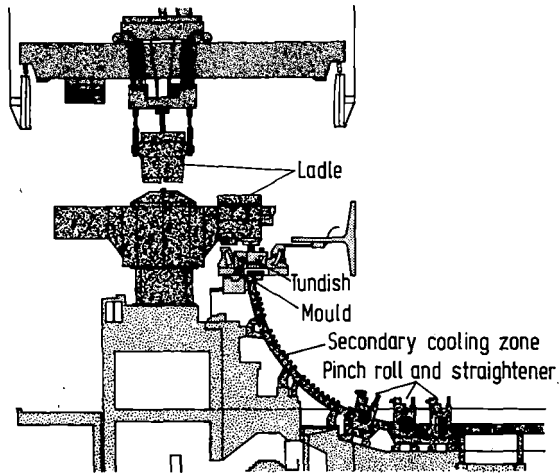
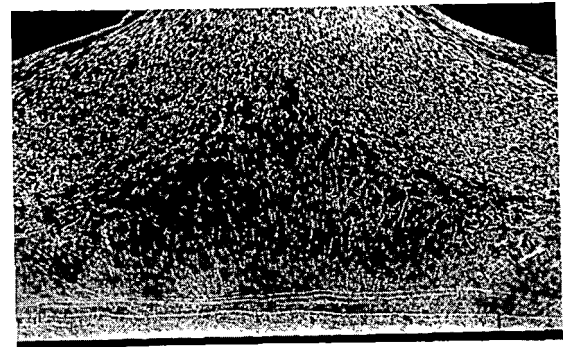


Fig. 10 Diagrammatic view of the continuous casting plant for blooms at Ruhrort works Thyssen AG

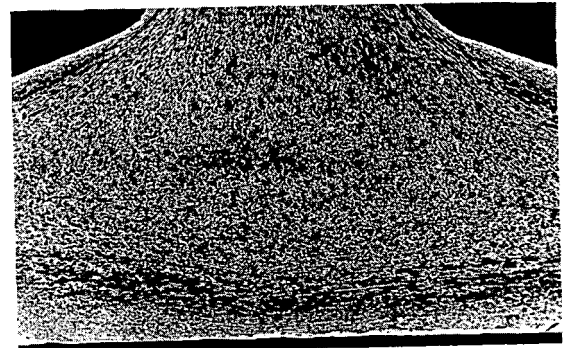
angle to the rail base. The rails would break in the base area in a longitudinal direction during the cold seasons or if subjected to certain stresses. In order to prevent this danger, the dendrites in the rail base are turned around in an almost horizontal direction by means of a special rolling procedure (Fig. 11).

This rolling process entails the initial pass bloom being split at a certain angle on the shape rolling mill corresponding to the later intended rail base and then being rolled out evenly in subsequent passes. This type of roll drafting is called drafting by splitting or Bartscherer drafting¹¹ (Fig. 12).



past roll pass design

10 mm



present roll pass design with knife passes

Fig. 11 Structure in rail base using different roll pass designs

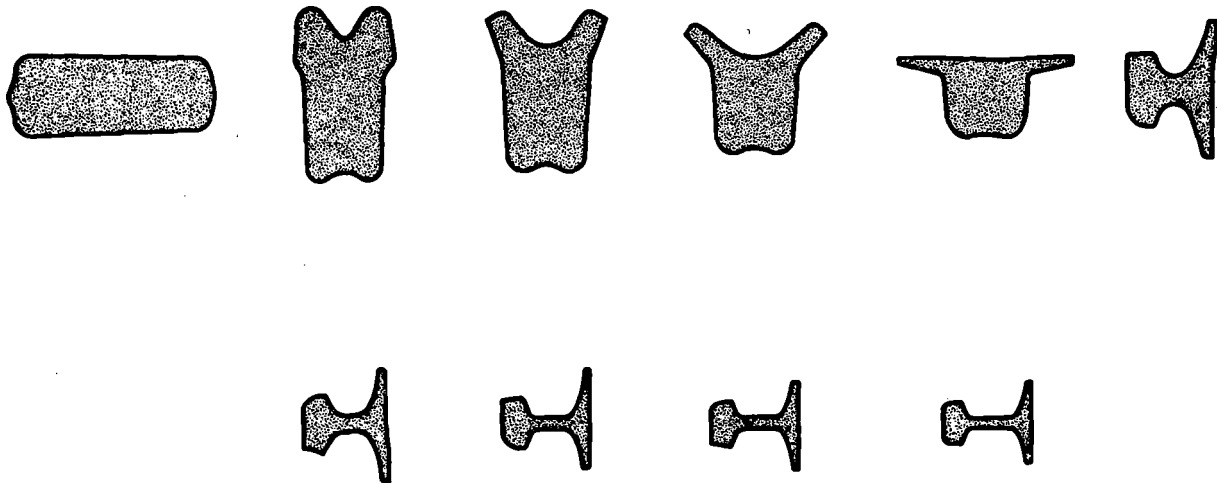


Fig. 12 Roll pass design by Thyssen or Bartscherer

Straightening of the rails. After normal, undelayed cooling of the rails on the cooling bed they are straightened on modern roller straightening machines. This method of operation guarantees rational production without any interruptions in the production flow and ensures straight rails with close tolerances, which are absolutely necessary in view of today's high-speed traffic.

Ultrasonic rail testing

Although the described metallurgical method of operation ensures an extremely high degree of rail steel homogeneity, all rails are subjected to continuous ultrasonic testing of the rail head and web after straightening to check for possible isolated non-homogeneities which are still present. The ultrasonic testing is intended both as an final check and as a control of the processes and metallurgical practices applied in the steel shop.

The vacuum treatment of liquid steel, which is applied in Germany, the bottom pouring of steel into hot top ingot moulds, and also pouring by means of the continuous casting method guarantee, together with ultrasonic testing of the rails, such a high degree of material homogeneity that the "nick and break" test specified in the AREA standard becomes unnecessary and also impact testing by the drop weight test where continuous casting is concerned.

Welding of the rails

Rails are essentially connected together as continuous track by means of flash butt and thermit welding. To remove minor local damage, e.g. where skidding has occurred, manual electrode built up welding is used.

So that welded joints and welded-on material do not impair the passage of the wheels, the mechanical and technological properties of the welds have to be equated as near as possible to those of the uninfluenced base material.

Also when welding naturally-hard, high-tensile, fine pearlitic rails, a fine pearlitic structure in the weld metal as well as in the heat-affected zone is aimed for¹². High brittle martensite hardening structure percentages have to be avoided and unavoidable soft annealing zones within the welding heat sphere of action kept to a minimum.

In Fig. 13 the TTT curve shows the transformation behaviour of the alloyed special grade. The high austenitizing temperature of 1,300 °C was selected to suit the conditions during welding.

In Fig. 13 the flash butt welding cooling curves are plotted with and without postheating. Welding together with postheating is necessary in the case of special-grade rails to guarantee transformation in the pearlite stage. For example, this is effected simply by means of a few post-heating impulses from the welding machine, as is shown in the welding diagram in Fig. 14. The cooling period from 800 to 500 °C is then prolonged to at least 5 min.

The pertinent variation in hardness is shown in Fig. 15. Such a variation in hardness guarantees favourable service behaviour of the weld.

With thermit welding the conditions of the welding technique necessitate a sufficiently long cooling-down period from the welding heat tempera-

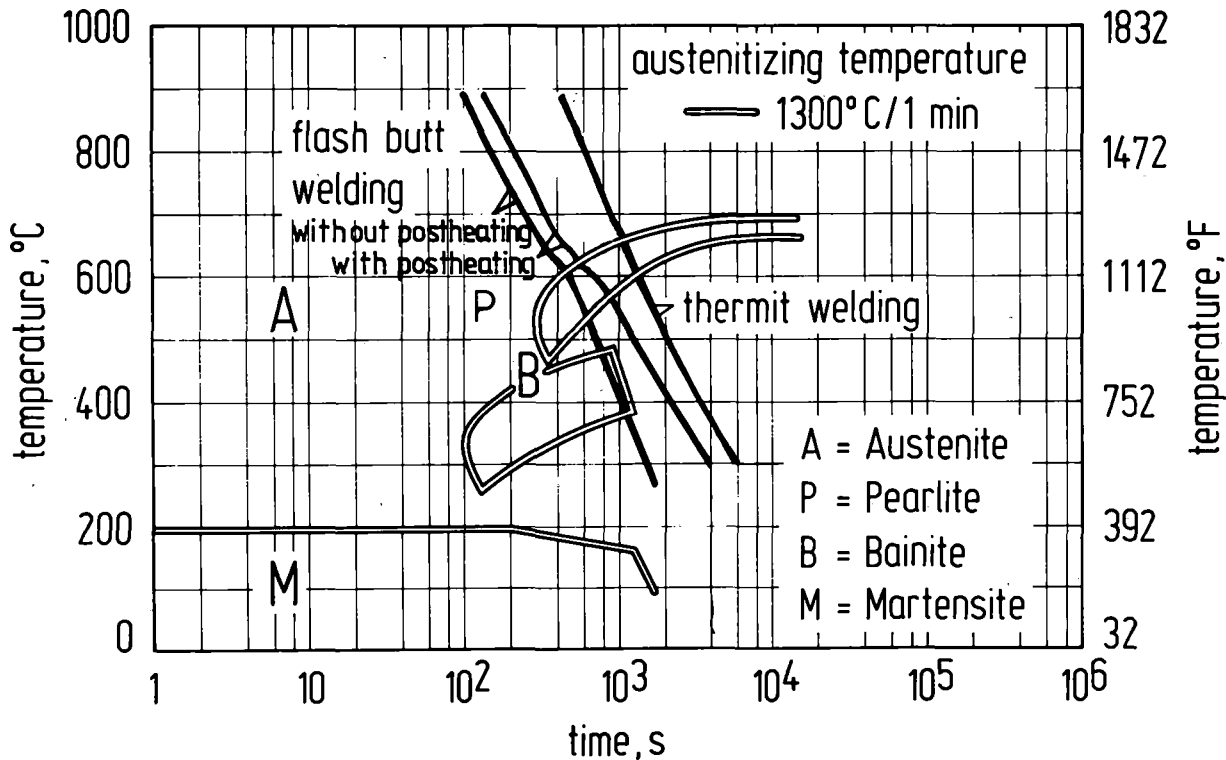


Fig. 13 TTT - diagram of wear resistant rail steel

ture to avoid hardening structures (Fig. 13).

Service behaviour of the rails

Special-grade rails of the type already described above have been in use for two decades with a great number of railway companies in Germany, Europe and Overseas, in some cases being used under the most extreme service conditions on tight curves of tracks involving gradients. Notable examples are the Gotthardt route of the Swiss Federal Railways, the rail network of the Rheinische Braunkohle AG in Germany which involves axle loads of up to 34 tons, and the Ofot line of the Norwegian State Railways, which serves primarily for the transportation of Swedish iron ores from the Kiruna mines region to the port of shipment in Narvik.

In these cases, the rails can be subjected to temperatures of as low as -30°C i.e. 0°F .

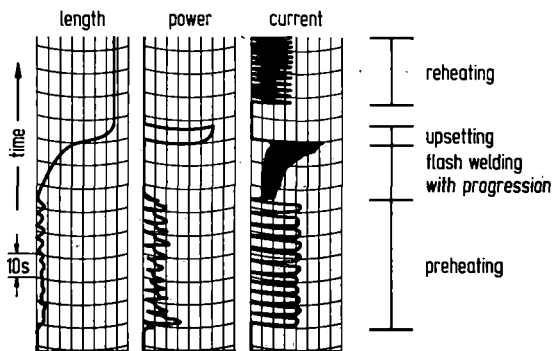


Fig. 14 Weasering tape of welding indicators

Literature

1 American Railway Engineering Association Specification for Steel Rails, 1979

2 Internationaler Eisenbahnverband, technische Lieferbedingungen für Schienen, UIC-Kodex 860, 7. Ausgabe, 1.1.79

3 Heller, W., Koerfer, E. and Schmedders, H., "Naturally Hard Special-grade Rails for Heavy-duty Transportation", Heavy Haul Railways Conference, Perth, Western Australia, September, 1978

4 Schmedders, H., "A chromium-vanadium alloyed rail steel for heavy-duty requirement" Vanadium in rail steels Proceedings of Vanitec Seminar, Chicago, Nov. 1979

5 Heller, W. and Schweitzer, R., "Untersuchungen zum Betriebsverhalten von Schienenstahl" Archiv für Eisenbahntechnik 28 (1973) pp. 81/89

6 Heller, W., Schweitzer, R. and Weber, L. Conference on "Modern Developments in Rail Steel Metallurgy and Production", Halifax, Aug. 1980

7 Hammer, R., Phlipsen, D., Schmedders, H. and Trenkler, J., "Erzeugung von verschleißfestem Schienenstahl nach dem Sauerstoffblasstahlverfah-

Special-grade, naturally hard alloyed rails used as outer rails on curves of approx. 300 m radius show approx. 2 - 3 times less wear than standard grade rails. Due to the increased yield strength there is a high degree of resistance against plastic deformation in the rail head.

Special-grade rails have proved themselves to be particularly resistant to shelling when used as outer rails on curves.

In the meantime, special-grade, naturally hard, highly wear-resistant rails have been supplied to the State Railways of Holland, Germany and Switzerland as well as to a great number of rail networks used for heavy haul transport such as in the USA, Norway, Africa, Brazil and Germany. They have stood the test with the greatest success.

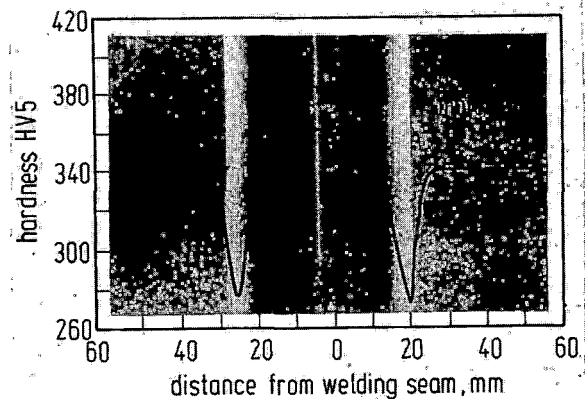


Fig. 15 Longitudinal section of flash butt welding in special grade rail

ren mit nachfolgender Vakuumbehandlung des flüssigen Stahles", Eisenbahntechn. Rdsch. 23 (1974), pp. 463/68

8 Delhey, H.-M., Fiege, L. and Vorwerk, H. Konzeption und Einsatz der DH-Vakuumanlage im LD-Stahlwerk der Fried. Krupp Hüttenwerke AG., Werk Rheinhausen

9 Heller, W., Weber, L., Hammerschmidt, P. and Schweitzer, R., "Zur Wirkung von Wasserstoff in Schienenstahl und Möglichkeiten einer wasserstoffarmen Erschmelzung", Stahl und Eisen, 92 (1972), pp. 934/45

10 Schmedders, H. and Weber, F., "Manufacture, Testing and Properties of 60-meter Rails from Strand-cast Material, Thyssen Technische Berichte, Heft 2/80

11 Lückerrath, W., "Die Verbesserung von Stahlschienen durch Umgestaltung des Primärgefüges im Schienenfuß beim Walzen". Stahl und Eisen, Vol. 57, 1937, pp. 172-79

12 Schweitzer, R. and Heller, W. "Zum Ab-brennstumpfschweißen von naturharten Schienen aus Sondergüte Chrom-Manganstahl", Eisenbahntechnische Rundschau, 23, pp. 506-16

High Strength Rails Produced by Two-Stage Flame Heating and Slack-Quenching

H. Ichinose

Assistant General Manager
Fukuyama Research Labs.
Technical Research Center
Nippon Kokan K.K.

J. Takehara

Assistant Manager
Fukuyama Research Labs.
Technical Research Center
Nippon Kokan K.K.

M. Ueda

Assistant Manager
Shape Mills
Fukuyama Works
Nippon Kokan K.K.

Three service characteristics such as wear resistance, anti-shelling and weldability have become important for rails used in tracks carrying high axle loads or fast trains. These characteristics, except weldability, become superior as strength is higher and pearlite structure is finer. A high strength rail with fine pearlite structure can be produced by alloy additions or slack-quench heat treatment. In this report, two problems are investigated in order to develop slack-quenched rails. One is heating and cooling conditions for slack-quench heat treatment. A new two-step flame heating which consists of slow heating followed by rapid heating has been developed. The other is slack-quenched rail steel with 130 kg/mm² (1274 MPa) class tensile strength and less weld softening. Simulation tests are conducted by using experimentally hot-rolled plates buried in rail heads and slack-quench facilities. Adding micro-alloy elements such as chromium, silicon, molybdenum and equating the cooling rate during slack-quenching to that after welding, the slack-quenched rails with 130 kg/mm² (1274 MPa) class tensile strength, fine pearlite and less weld softening can be developed.

1 INTRODUCTION

For tracks carrying high axleloads or fast trains, a rail steel is strongly required to have service characteristics such as wear resistance and anti-shelling. It is confirmed from our laboratory scale tests that these characteristics become superior as a strength is higher and a pearlite structure is finer.⁽¹⁾⁽²⁾ A high strength rail with fine pearlite structure can be produced by two processes. One is made with alloy additions, the other is heat treated; head hardened by slack-quench heat treatment. We produce many kinds of alloy rails with 110 kg/mm² (1078 MPa) class tensile strength and slack-quenched rails with 120 kg/mm² (1176 MPa) class tensile strength.

On alloy rails : Alloy additions can achieve further strengthening, but a weldability is harmed due to their high hardenability. A high hardenability of alloy rails and a high cooling rate after flash butt welding cause martensite formation in heat affected zone (HAZ) of flash butt welded joint. Therefore, post-weld heat treatments (PWHT) to avoid martensite formation is indispensable to higher strength alloy rails.

On slack-quenched rails : As a cooling rate after flash butt welding is slower than that during slack-quenching, the hardness of weld heat affected zone is lower than that of mother rail.

This weld softening initiates corrugations in service and decreases rail service life. The heating of rail heads in slack-quench heat treatment is generally conducted by either of high frequency induction or gas flame. We use gas flame for the heating of slack-quenched rails. A new heating process using gas

flame has been developed and adopted to manufacture slack-quenched rails.

In this report, two problems are investigated in order to develop slack-quenched rails with higher strength and finer pearlite structure. One is heating and cooling conditions for slack-quench heat treatment. The other is slack-quenched rail steels with 130 kg/mm² (1274 MPa) class tensile strength and less weld softening.

2 DEVELOPMENT OF TWO-STAGE FLAME HEATING AND SLACK-QUENCHING METHOD

2.1 Heating Condition

The CCT diagram and cooling curve for slack-quench heat treatment is shown in Fig. 1. In slack-quench heat treatment, rail heads are rapidly heated above the austenitizing temperature and then quenched by mist or compressed-air at a cooling rate which brings on pearlite transformation. The slack-quench heat treatment gives rail heads a fine pearlite structure and high hardness without tempering. In general there are two heating methods of high frequency induction and gas flame for slack-quench heat treatment. We investigate flame heating method and have developed a new heating process.

In order to establish the heating condition for slack-quench heat treatment, many experiments are conducted on rail steels. Fig. 2 shows the relation among slack-quench heat treatment conditions, microstructure and hardness. A higher cooling rate is necessary to obtain fine pearlite and high hardness when the heating temperature is below 900°C. In this region, microstructure and hardness are considerably affected by variations of heating temperature and cooling rate. On the other hand, in the region above 900°C, the heating temperature slightly influences on microstructure and hardness. A finer pearlite and higher hardness are stably obtained in accordance with increase of cooling rate.

Microstructure and hardness in the interior of

rails should be controlled as well as rail head surface. However, since the cooling of rail head is limited on the surface only, it becomes important to ensure the interior cooling rate. Fig. 3 shows the relation between a temperature gradient before mist-cooling and cooling rate obtained. The cooling rate increases as the temperature gradient increases. This tendency becomes more remarkable at the slower cooling rate. Therefore, in increasing the temperature gradient, a thermal conduction from surface to interior is promoted, resulting in the increase of interior cooling rate. It is important to control the temperature gradient in order to ensure fine pearlite and high hardness under rail head surface. Heating the rail head surface rapidly at high temperature, the steep temperature gradient brings on deeply hardened region. However, if the surface temperature is too high, the surface would be melted. Therefore, it is necessary to settle the heating conditions which control the surface temperature and interior temperature gradient properly. Fig. 4 shows the temperature distribution of the rail head cross section in case of one-step heating. The curve I and II exhibit the temperature distribution obtained by rapid heating. The temperature gradient of the curve I is too steep that the interior temperature is low and the hardened region becomes shallow. Increasing the heat input as shown by the curve II, the temperature gradient is steep and interior temperature is enough high to obtain a deeper hardened region. However the surface temperature is too high to defend melting at the surface. The curve III shows the temperature distribution heated slowly with lower heat input. In this heating condition, the interior temperature is considerably high, but the temperature gradient is so small that the interior cooling rate is not enough. As shown in Fig. 4, one-step heating is insufficient to obtain the temperature distribution required for slack-quench heat treatment. It is found that the rapid heating is useful to make the temperature gradient steep and on the other hand the slow heating is also useful to give in the deeper interior the high temperature more than 900°C.

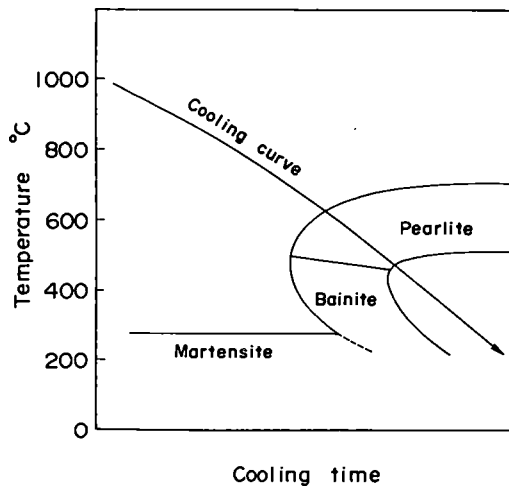


Fig. 1 CCT diagram and cooling curve for slack-quench heat treatment

On the basis of these results, a new two-step heating which consists of the first slow heating and the second rapid heating is investigated. Fig. 5 shows the influence of the preheating temperature on the temperature distribution of rail cross section in two-step heating process. Making the second step heat input constant, the first step preheating temperature is varied within the range from 350 to 650°C. The temperature gradient becomes small as the preheating temperature increases. And it is found that the preheating temperature plays an important role to decide the hardened region. Consequently, using the two-step heating process and controlling the preheating temperature appropriately, the resulting temperature distribution brings about a desired hardness distribution at the rail cross section.

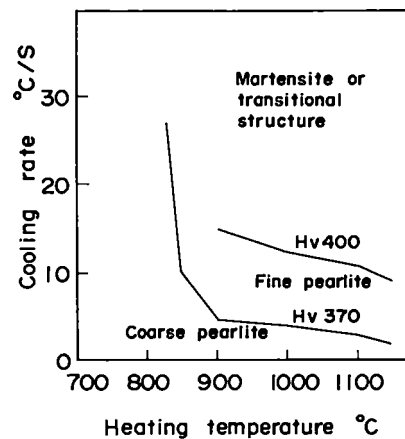


Fig. 2 Relation among slack-quench heat treatment conditions, microstructure and hardness

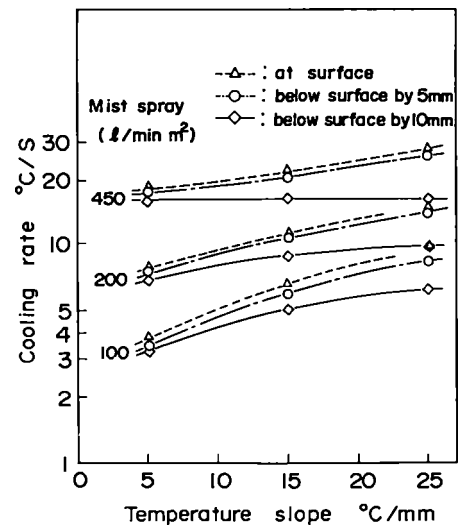


Fig. 3 Relation between a temperature gradient before mist-cooling and cooling rate obtained

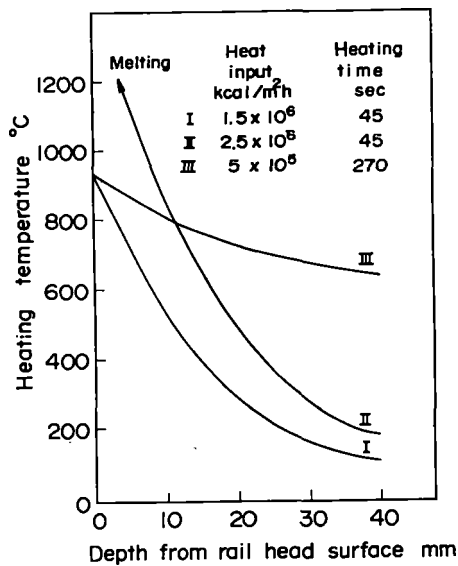


Fig. 4 Temperature distribution of the rail head cross section in case of one-step heating

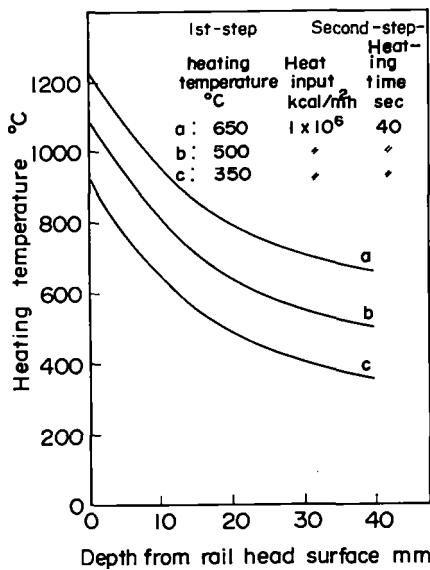


Fig. 5 Influence of the preheating temperature on the temperature distribution of rail cross section

2.2 Cooling Conditions

After heating the rail head surface and interior at the temperature above 900°C, the cooling rate ranged from 3 to 10°C/s is necessary to attain stably the hardness more than 370 Hv and fine pearlite. There are two cooling media, which are mist and compressed-air, for such a slow cooling rate. The compressed air is superior to the mist in a stability of operation, so we use a compressed-air as the cooling medium for slack-quench heat treatment.

Fig. 6 shows the general pattern of heating and cooling for slack-quench heat treatment using the new two-step flame heating method. In this case, the conditions of heat treatment include first-step preheating at the temperature 450°C, second-step rapid heating at a rate of 10⁶kcal/m²h, and compressed-air cooling under the pressure of 1.0kg/cm²G (0.098 MPaG). The region heated beyond Ar₃ transformation point is about 25mm depth from the rail head surface and a half of the depth is heated at the temperature above 900°C, where higher hardness and finer pearlite are obtained. As shown in Fig. 6, the cooling rate at the depth of 12.5mm is about 4.5°C/s, it is considered that the hardness at this depth indicates over 370Hv according to Fig. 2.

As mentioned above, a deeply hardened region with higher hardness and finer pearlite microstructure is obtained by the compressed-air cooling after two-step flame heating.

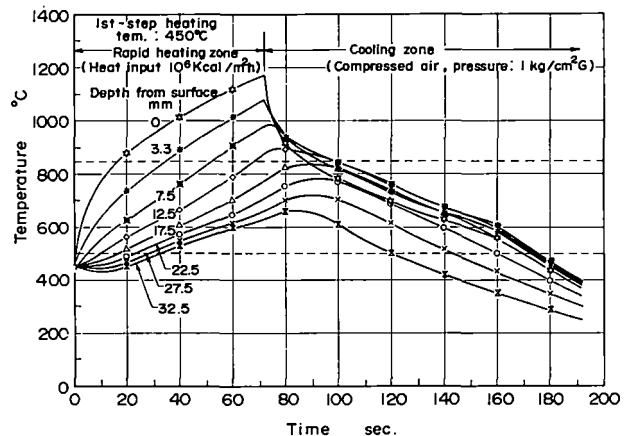


Fig. 6 General pattern of heating and cooling for slack-quench heat treatment using the new two-step flame heating method

3 DEVELOPMENT OF SLACK-QUENCHED RAIL STEELS WITH 130 kg/mm²(1274 MPa) CLASS TENSILE STRENGTH AND SUPERIOR WELD PERFORMANCE

Slack-quenched rail with 120 kg/mm²(1176 MPa) class tensile strength is produced by the new-step flame heating and compressed-air cooling. Further experiments are conducted to develop steels with tensile strength higher than 130 kg/mm²(1274 MPa) and to improve weld softening.

3.1 Test Materials and Experimental Procedure

The chemical composition of test materials is shown in Table 1. All of test materials are air-melted in 50 kg heat. The ingots are heated at 1250°C for one hour and successively hot-rolled into 40mm thick plates and cooled in atmosphere. As the heating and cooling pattern are influenced by the cross section, in which plates and rails are different, so the simulation tests as described below are conducted in the same manner as well as slack-quench heat treatment of rails. Fig. 7 shows the test specimens for slack-quench heat treatment. At first, hot-rolled plates are machined into rectangle piece and then it is buried in the rail head, where the gap between the test piece and the rail machined is filled up by welding, and finally they are joined in order

to pass the slack-quench facilities. Fig. 8 shows the test conditions of slack-quench heat treatment performed by mill facilities. The slack-quenching on test materials is conducted under constant heating conditions and varied cooling conditions. Heating conditions are composed of the first-step preheating at 500°C and the second-step rapid heating at 1000°C. Cooling rate in the temperature range of 850 to 500°C is controlled in three stage of 1.7, 3 and 5°C/s by changing the compressed-air pressure, where cooling rate is measured at 5mm below rail head surface.

Table 1 Chemical composition of test materials

	C	Si	Mn	P	S	Cr	Mo	Nb	V	So	Al	N	
1	.80	.19	1.13	.013	.012					.016	.0096		Base
2	.81	.59	1.10	.013	.011					.028	.0101		0.5% Si
3	.80	.83	1.08	.013	.011					.035	.0094		0.8% Si
4	.79	.60	1.10	.013	.011	.20				.026	.0099		0.2% Cr
5	.80	.56	1.09	.013	.011	.50				.027	.0102		0.5% Cr
6	.81	.52	1.06	.013	.010	.81				.027	.0092		0.8% Cr
7	.80	.60	1.09	.013	.012		.023			.031	.0102		0.02% Nb
8	.80	.58	1.07	.013	.011		.031			.028	.0100		0.03% Nb
9	.80	.60	1.09	.013	.010	.50	.023			.030	.0100		0.5%Cr-0.02%Nb
10	.80	.59	1.10	.013	.010			.019	.036	.0095	.002V		
11	.80	.58	1.06	.013	.012	.50	.023	.021	.030	.0102	.05Cr-0.02Nb-0.02V		
12	.80	.56	1.06	.011	.010		.06			.034	.0103		0.05% Mo
13	.80	.53	1.06	.013	.011		.10			.029	.0102		0.10% Mo
14	.78	.56	1.06	.013	.012	.49	.10			.033	.0103		0.5%Cr-0.10%Mo

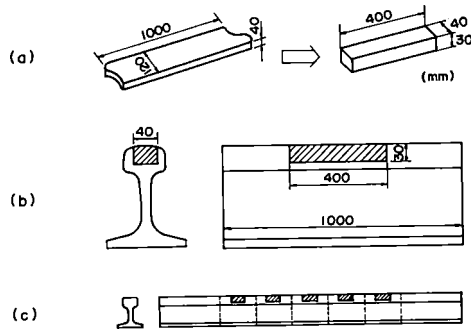


Fig. 7 Test specimens for slack-quench heat treatment

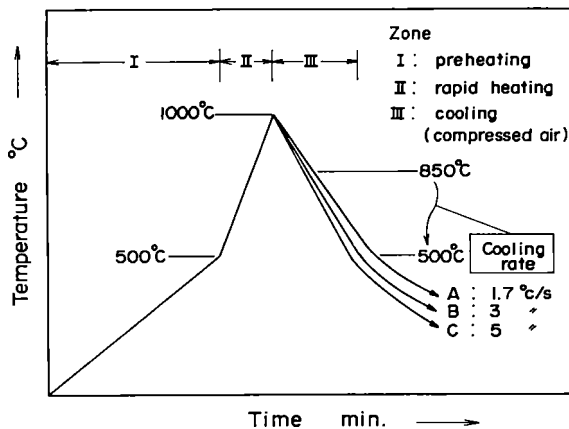


Fig. 8 Test conditions of slack-quench heat treatment

3.2 Test Results

Mechanical properties. Table 2 shows the results of tensile and hardness test performed before and after slack-quench heat treatment. Tensile specimens having a 6mm diameter are prepared from hot-rolled plates and slack-quenched rail samples at 5mm below surface. The hardness value shown in Table 2 is measured at 1mm below the surface of hot-rolled plates and slack-quenched rail samples. The depth at which hardness value indicates 340Hv is used as a parameter exhibiting a hardened region. Fig. 9, 10, 11, and 12 show the changes of 0.2%-proof stress, tensile strength, elongation and reduction area due to slack-quench heat treatment, respectively. The 0.2%-proof stress and tensile strength are increased by the range from 15 to 30 kg/mm² (from 147 to 294 MPa), from 15 to 25 kg/mm² (from 147 to 245 MPa), respectively. As shown in Fig. 9 and 10, the strength increases as the cooling rate increases. Increasing the strength level, the dependency on the cooling rate increases. As shown in Fig. 11 and 12, the elongation and reduction area are improved by 6 and 23% on the average, respectively. As for the elongation and reduction area, the dependency on the cooling rate is hardly recognized.

Table 2 Tensile and hardness test results

		Cooling condition	Tensile properties (6 th mm round bar)				Hardness	
			0.2% proof stress ₂ Kg/mm ²	Tensile strength Kg/mm ²	Elongation %	Reduction area %	Hv(0) 1mm below surface	Depth (Hv=340) mm
1	Base	R	53.4	100.8	13.3	21.5	308	
		C	77.1	121.0	16.0	31.2	348	5
2	0.5% Si	R	53.2	101.2	12.9	20.7	310	
		C	75.3	123.5	15.5	33.3	364	9
3	0.8% Si	R	55.8	104.9	13.6	22.5	313	
		C	81.4	128.0	19.1	44.4	380	13
4	0.2% Cr	R	56.3	105.1	11.8	16.5	313	
		B	74.7	123.1	19.8	46.4	354	8
5	0.5% Cr	R	64.7	111.8	10.3	15.4	334	
		B	86.4	131.9	19.8	48.2	394	11
6	0.8% Cr	R	66.6	113.6	11.7	20.8	339	
		A	82.2	129.8	19.5	44.4	390	7
7	0.02% Nb	B	91.6	136.4	19.8	48.2	415	12
		R	52.4	101.8	14.3	24.1	311	
8	0.03% Nb	C	80.9	123.6	19.8	43.0	353	4
		R	52.7	100.7	15.0	25.0	308	
9	0.5%Cr-0.02%Nb	B	73.9	117.1	20.0	45.4	342	2
		C	77.8	120.1	22.4	47.9	345	2
10	0.02% V	R	60.2	110.0	12.1	18.9	329	
		B	86.9	135.2	17.6	41.4	397	12
11	0.5% Cr	R	56.2	104.4	13.6	20.7	316	
		C	84.1	127.7	19.5	44.9	376	12
12	0.02% Nb	R	60.4	109.3	11.9	19.5	337	
		B	77.5	126.2	19.3	47.8	366	7
13	0.10% Mo	B	81.8	129.1	18.8	43.1	382	8
		R	56.1	105.1	13.1	22.2	326	
14	0.5% Cr	B	77.4	122.3	20.5	44.1	345	5
		C	85.4	129.9	18.8	43.2	383	13
14	0.10% Mo	R	57.4	105.5	14.3	23.9	327	
		A	77.3	119.5	20.5	45.6	351	5
14	0.5% Cr	B	77.6	124.3	21.7	47.0	365	11
		R	62.9	110.3	13.8	25.9	335	
14	0.10% Mo	A	93.5	134.3	20.5	50.9	409	13

Cooling condition

- R : as rolled
- A : 1.7°C/s (during slack-quenching)
- B : 3 " (")
- C : 5 " (")

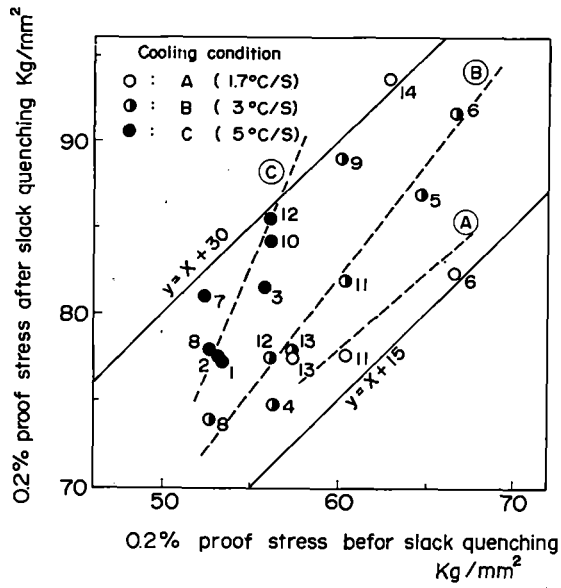


Fig. 9 Change of 0.2% proof stress due to slack-quench heat treatment

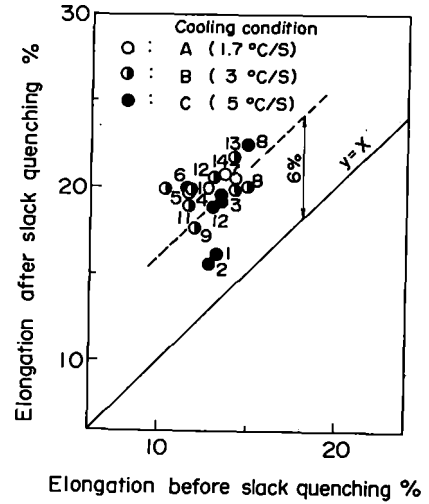


Fig. 11 Change of elongation due to slack-quench heat treatment

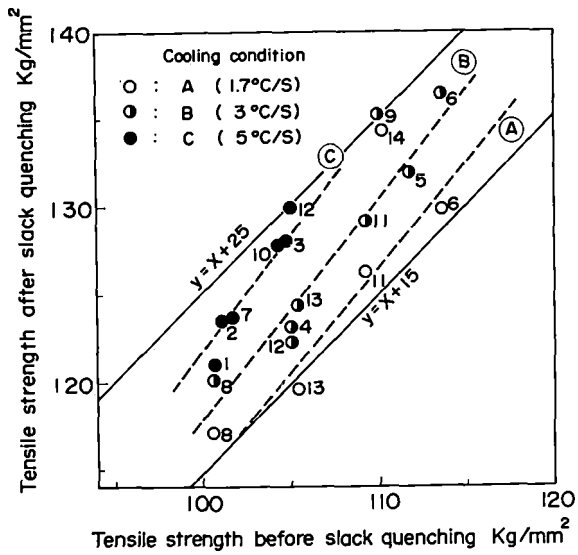


Fig. 10 Change of tensile strength due to slack-quench heat treatment

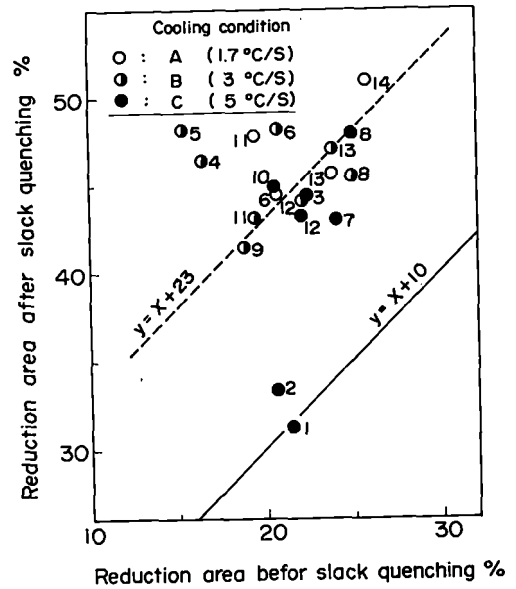


Fig. 12 Change of reduction area due to slack-quench heat treatment

Fig. 13 shows the relation between the interlamellar spacing and reduction area, where the interlamellar spacing is a minimum value and determined by observing twenty visual fields of replica. The reduction area is improved as the interlamella spacing decreases.

Fig. 14 shows the influence of micro-alloy elements on the mechanical properties in slack-quench heat treatment. Micro-alloy elements of silicon, chromium, molybdenum and vanadium contribute the strengthening of rail steels, especially chromium is most effective. Conversely, niobium addition decreases the strength and hardenability due to the restraint effect of austenite grain growth.

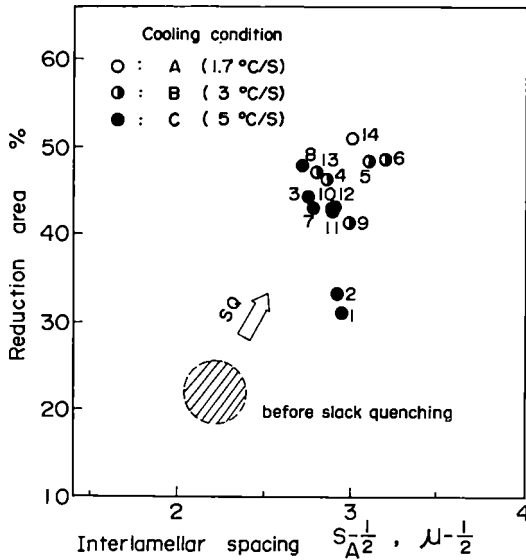


Fig. 13 Relation between interlamellar spacing and reduction area

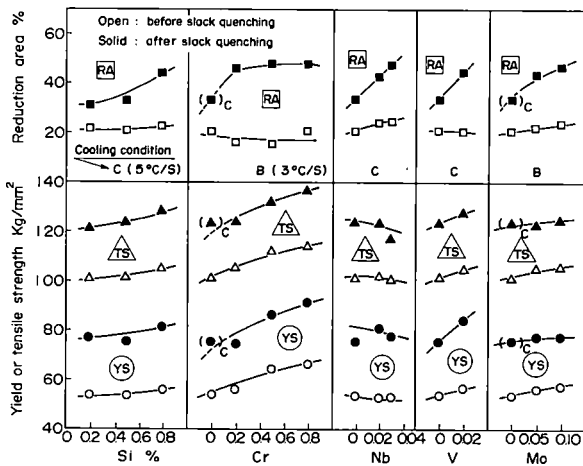


Fig. 14 Influence of micro-alloy elements on mechanical properties

Hardness distribution below surface. Increasing a wear resistance of rail steels, it is important to ensure the higher hardness of rail head surface contacted with a wheel. Moreover, hardness distributions below surface are also important in the wear resistance and anti-shelling. As a rail wear gradually increases in accordance with the increase of a passed-tonnage, it is necessary for the hardness distribution in cross section to have a sufficient hardened region in order to increase a service life of rails. As for the resistance of rolling contact fatigue like shelling, since the maximum shearing stress is usually generated at the depth less than 10mm from a contact surface, it is generally considered that a rapid hardness change at this region is not favorable.

Fig. 15 shows the relation among the surface hardness, hardened region and cooling rate, where the depth at which the hardness value indicates 340Hv is used as a parameter exhibiting a hardened region. The hardened region increases as the surface hardness or the cooling rate increases. Fig. 16, obtained from the experiment using a Formastor, shows the influence of cooling rate on the hardness and microstructure. Heating of test specimens is performed to 1000°C for five seconds and successively cooled at a rate ranged from 1 to 10°C/s. Pearlite structure is always obtained in the steel 1 regardless of the cooling rate varied. The hardenabilities of steel 1 and 10 are so low that their hardness increase due to the increases of the cooling rate are very slight. Pearlite structure is always obtained in the steel 1 regardless of the cooling rate varied. On the other hand, in case of the steel 10, bainite is elsewhere contained in pearlite at the cooling rate more than 7°C/s. The hardenability of the steel 5 is so high that the hardness increase is high even at the low cooling rate less than 3°C/s. However, though the hardness increase is remarkable at the cooling rate higher than 3°C/s, bainite and martensite generate instead of pearlite. As shown in Fig. 16, the critical cooling rate and maximum hardness at which a fine pearlite is attained are different, depending on the kind of steel.

Fig. 17 shows the schematic hardness distributions on the three types of steels with different hardenabilities. They are cooled at the cooling conditions that bring about the maximum surface hardness and fine pearlite. As the steel I has the highest hardenability in three types of steels, the lowest cooling rate is permitted. In this case, the hardened region becomes deep sufficiently and the hardness gradient near surface becomes steep slightly because of its highest hardenability. The steels of 5, 6, 9, 11, and 14 shown in Table 2 correspond to the steel I in Fig. 17. Chromium is added by 0.5% and more in this type of steel. Addition of 0.5% Chromium is indispensable to ensure the 130 kg/mm² (1274 MPa) class tensile strength with such a slow cooling rate. Since the steel III has the lowest hardenability, the hardness gradient becomes small and the hardened region becomes shallow as compared with the steel I. The steel of 1, 2, 7 and 8 shown in Table 2 correspond to the steel III in Fig. 17. The steel II has an intermediate hardenability and hardness distribution. The steel of 3, 4, 10, 12 and 13 correspond to the steel II in Fig. 17.

Consequently, the test materials of this experiment are classified into three types as shown in Fig. 17. In all of them, the steel I is most favorable in hardness distribution and weld softening described later.

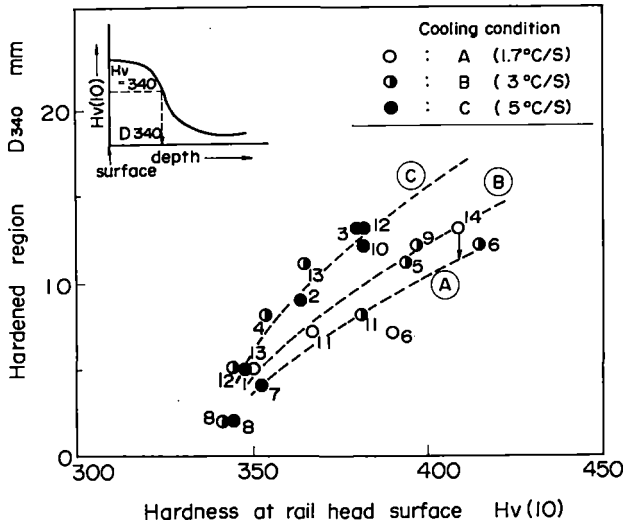


Fig. 15 Relation among surface hardness, hardened region and cooling rate

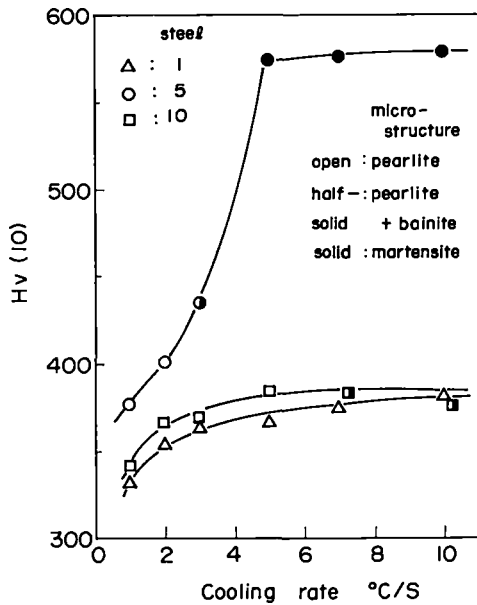


Fig. 16 Influence of cooling rate on hardness and microstructure

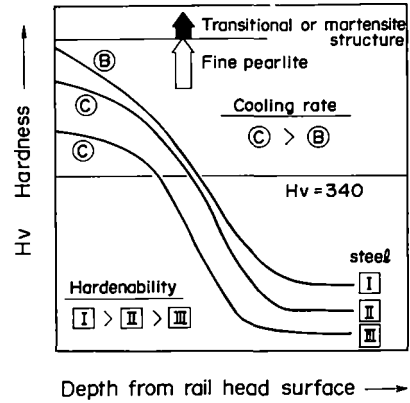
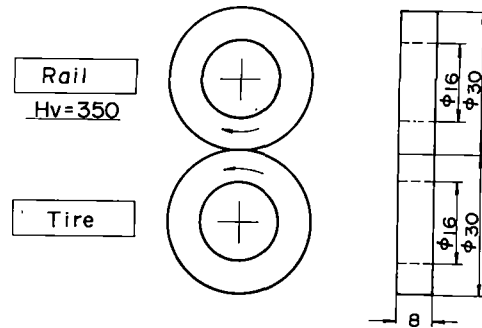


Fig. 17 Schematic hardness distribution on three types of steels with different hardenabilities

Wear resistance. Wear tests are performed on the materials after slack-quench heat treatment by using Nishihara type wear testing machine and two cylindrical specimens as shown in Fig. 18. The hardness of tire specimens is 350Hv. The weight loss of rail specimen is measured at the interval of 100,000 cycles till 500,000 cycles. Comparing to wear resistance of test material, the weight loss at 500,000 cycles is used. Fig. 19 shows the influence of hardness and microstructure on the wear resistance. Steels with different microstructures but the same hardness do not have the same wear resistance. Fine pearlite is most favorable in the wear resistance. Though the wear resistance, as well known, is improved as the hardness increases, the effect of hardness is decreased in the range over 350Hv. The effect of cooling rate is hardly recognized in Fig. 19.



Load Kg	Slip Ratio %	Cycles		Lubricant
		Rail r. p. m.	Tire r. p. m.	
50	-10.0	727	800	no

(1) Slip Ratio

$$S = (N_1 - N_2) / N_1 \times 100 \text{ (\%)}$$

N_1 : cycles of rail specimen (r. p. m.)

N_2 : cycles of tire specimen (r. p. m.)

Fig. 18 Wear test method

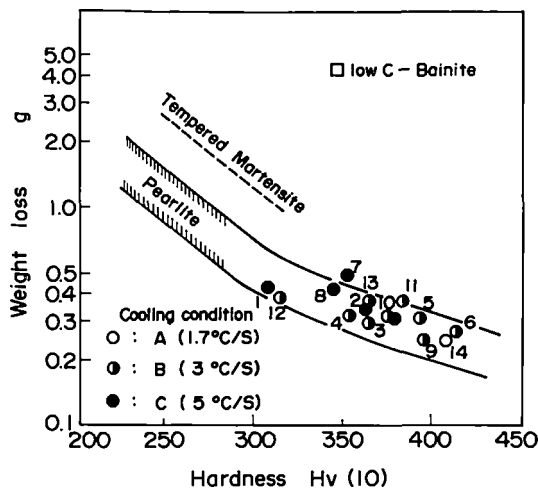


Fig. 19 Influence of hardness and microstructure on wear resistance

3.3 Discussion on the Weld Performance of Slack-Quenched Rails

In general, a site and shop welding are performed by flash butt and thermic weld methods, respectively. Fig. 20 shows schematic hardness distributions of weld joints in alloy and slack-quenched rails.

On alloy rails : The cooling rate of the heat affected zone in flash butt weld joint is approximately ranged from 1 to 2°C/s, which is higher than that after rolling of the rails. Martensite formation in the weld zone occurs due to this higher cooling rate and the high hardenability of alloy rails. Therefore, most alloy rails must be welded with a variety of post-weld heat treatments (PWHT) to avoid martensite formation. The hardness after PWHT is higher than that of mother rail. In case of thermic welding, the heat input of deposit metal is so high that the cooling rate of HAZ becomes lower than that in flash butt welding. Martensite formation in the HAZ rarely occurs, so PWHT is not performed in thermic welding.

On slack-quenched rails : Since the hardenability of slack-quenched rails is lower than that of alloy rails, martensite formation does not occur even in flash butt weld. Consequently, most slack-quenched rail can be welded without PWHT. However, slack-quenched rails, especially in carbon-manganese (C-Mn) rail steels experience a softening in HAZ both of flash butt and thermic welds. This softening is caused by the slower cooling rate after welding compared with that during slack-quenching, together with the insufficient hardenability. This weld softening increases as the difference of cooling rate between slack-quenching and welding increases and the hardenability of rail steels becomes lower.

Fig. 21 shows a philosophy to produce slack-quenched rails with high strength and fine pearlite and less weld softening. The critical cooling rate during slack-quenching to obtain fine pearlite and high hardness decreases as the carbon equivalent or hardenability of rail steel increases. The cooling rate to obtain the same hardness is different in the two types of steels, I and III on account of the high hardenability of steel I relative to steel III. The cooling rate of steel I may be slower than that of steel III. The point A means an ideal manufacturing condition, where the cooling rate during slack-quenching is equal to that after welding and neither

weld softening nor martensite formation occurs.

As shown in Fig. 20 and 21, in order to improve the weld softening of slack-quenched rails, it is effective to add micro-alloy elements such as silicon, chromium, molybdenum and equate the cooling rate during slack-quenching to that after welding. From a view of welding process, if the weld heat affected zone is cooled acceleratedly at the same cooling rate as that during slack-quenching, the weld softening of the slack-quenched carbon-manganese rails could be defended.

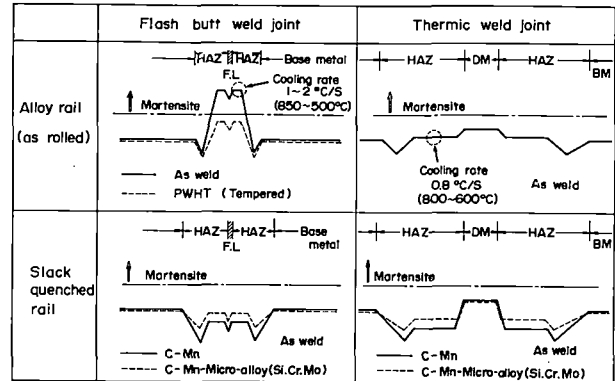


Fig. 20 Schematic hardness distributions of weld joints in alloy and slack-quenched rails

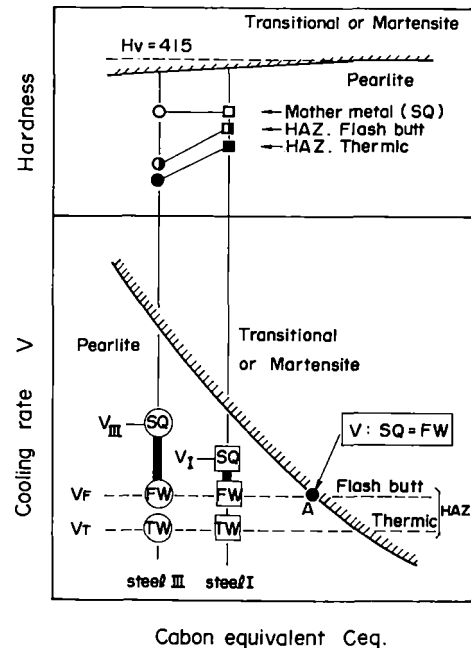


Fig. 21 A philosophy to produce slack-quenched rails with high strength and fine pearlite and less weld softening

4 CONCLUSIONS

- 1) A new two step flame heating which consists of the first slow heating and the second rapid heating has been developed. This method can attain a desired hardened region with high hardness and fine

pearlite. It is important to control the surface temperature gradient properly in order to ensure the desired hardness distributions and microstructure. The hardened region can be easily changed by controlling the first-step preheating temperature. A compressed-air is superior to a mist in a view of operation stability as a cooling medium to obtain the cooling rate ranged from 3 to 10°C/s.

- 2) Adding the micro-alloy elements such as chromium, silicon, molybdenum and equating the cooling rate during slack-quenching to that after welding, the slack-quenched rails with 130 kg/mm² (1274 MPa) class tensile strength, fine pearlite and less weld softening can be developed.

5 REFERENCES

1. Ichinose, H., Takehara, J., Iwasaki N., and Ueda, M., "An Investigation on Contact Fatigue and Wear Resistance Behaviour in Rail Steel", Proceedings of Heavy Haul Railways Conference, Perth, Western Australia, September, 1978 Session 307, Paper I. 3
2. Ueda, M., Takehara, J., Ichinose, H., "Influence of Microstructure and Strength on Wear and Contact Fatigue Properties in Rail Steels" Journal of the Iron and Steel Institute of Japan, Vol, 64. No.11 SEPT.'78. S452

Development of Weldable High-Strength Steel Rails

K. Sugino

Technical Research Office
Technical Department
Yawata Works
Nippon Steel Corp.
Japan

H. Kageyama

Technical Research Office
Technical Department
Yawata Works
Nippon Steel Corp.
Japan

H. Masumoto

Technical Research Office
Technical Department
Yawata Works
Nippon Steel Corp.
Japan

The wear resistance and failure resistance of rails can be improved by using steel of pearlite structure as the material, giving it high strength. To improve weldability, the head of a rail of steel to which alloys have been added is subjected to heat treatment. NSC has developed two types of weldable high-strength steel rails using this method.

INTRODUCTION

The requirements imposed on railways are presently very severe partly because of hard competition with other means of transportation, and a further improvement in efficiency is expected. From the user's point of view, railway transportation efficiency can be improved from two aspects : speedier transport of a large number of passengers and more efficient mass transport of cargoes. In respect of speedier passenger transport, Japan's SHINKANSEN enjoys world-wide fame. In other countries, especially in Europe, endeavors are presently being made aiming at speedier passenger transport, and the British HST and the French TGV belong to such projects (1). Typical examples of mass cargo transport are seen in countries rich in natural resources, such as the USA, Canada, Brazil and Australia, where masses of ores and other resources are transported by rail.

Such higher railway efficiency has led to increased axle load and tangential and impact forces acting on rails through wheels, thus generating a very severe environment for rails where rail failures are apt to occur due to wear and fatigue. Rail maintenance work and rail replacements have become more frequent, and rail service life has markedly been shortened. Therefore, high-quality rails capable of withstanding these severe conditions are much in demand. To meet the above-mentioned wear resistance and failure resistance, measures, such as enlargement of the rail cross section, only are insufficient and it is necessary to improve the material for rail itself. For this reason, rail manufacturers are engaged in the development of new rails. Nippon Steel Corporation developed a new high-strength head-hardened

rail (NHH rail) of fine pearlitic structure and is supplying this rail to railways.

Recently, rails have become more frequently welded upon laying. This is because, in addition to the ensuring of comfortableness, deterioration of rails and ballast due to impact upon passage of wheels is to be reduced. Therefore, besides the above-mentioned resistance to wear and failure among the necessary properties of rails, weldability is also required as an important basic characteristic. To meet these three basic characteristics, it is necessary to newly consider the metallurgical structure and composition of steel as the material for rail.

From this standpoint, NSC made an investigation to find an optimum structure and composition that meet wear resistance, failure resistance and weldability, and manufactured weldable high-strength steel rails on a trial basis based on the results of the investigation.

FACTORS GOVERNING THE WEAR RESISTANCE OF RAILS

Rail wear

The wear of rails generally takes two forms. One is the adhesive or abrasive wear in which the rail is worn by contact with wheels. The other is the plastic deformation of the rail head by axle load and this causes lateral spread of the rail which is chipped off by the wheel flange, etc. Further, there is another phenomenon which belongs to the latter category ; that is, cracks are generated in the rail surface by deformation and fatigue and flaking takes place. Rail wear in this form cannot be also disregarded.

Experiment by Nishihara type wear test equipment

It is difficult to fully simulate rail wear since rails are worn by complex internal and external conditions, as mentioned above. There, the Nishihara type wear test equipment was used to conduct comparative test for the amount of wear among several rail steels under the same test conditions. In the test, ring-shaped specimens shown in Fig. 1 were brought into contact with mating specimens rotated 5×10^5

revolutions, and the weight loss of the specimens by wear was measured and compared.

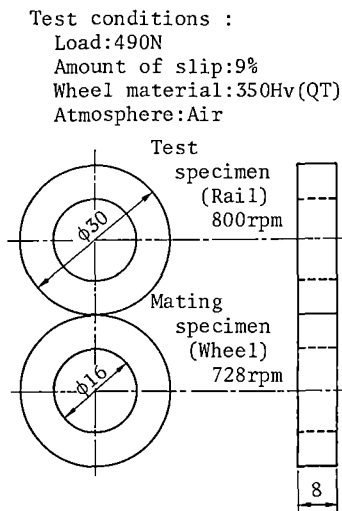


Fig.1 Nishihara type wear test specimens and test conditions

Table 1 shows the rail steels used : A to D are of pearlitic structure differing in hardness, and E is tempered martensitic structure steel made by heat treating ordinary carbon rail steel to investigate the effect of microstructure. Steel with a hardness of approximately 280 Hv obtained by increasing tempering temperature was also added. The specimen D was cut of the head of the newly developed rail (NHH), and E was chosen as the mating specimen of wheel.

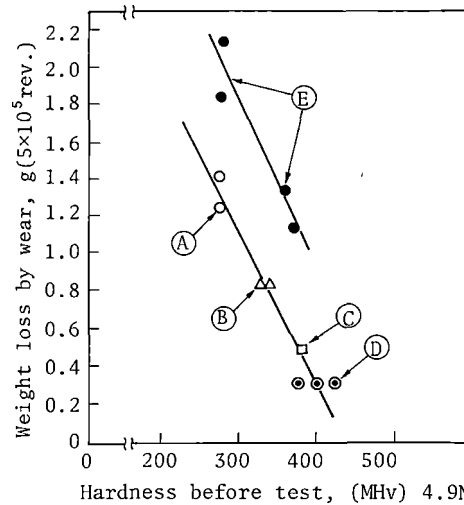


Fig.2 Relation between hardness before test and amount of wear of various rail steels

Wear resistance and material factors

The question, then, is whether the test results discussed above are in good agreement with the actual wear behavior of rails in service. Wear test was conducted on specimens cut out of rails of the same steel grades as rails of a mine railway whose wear condition was investigated for a long period of time. Fig. 3 shows a comparison between the results of this wear test and those of the investigation of wear. As far as the wear loss measured in two curved sections is concerned, both are in good correlation. Hence, the assessment based on the results of the wear test

Table 1 Chemical compositions and mechanical properties of rail steels

	C	Si	Mn	P	S	Cr	V	PS (MPa)	TS (MPa)	E1 (%)	RA (%)	Hv
A Ordinary carbon rail steel (C)	0.65	0.20	0.89	0.019	0.009	-	-	482	904	14.5	19.0	254
B High Si rail steel (HS)	0.70	0.88	1.31	0.023	0.010	-	-	593	1,030	12.0	19.0	305
C Cr-V alloy rail steel (Cr-V)	0.74	0.32	1.32	0.020	0.012	0.78	0.13	755	1,178	14.3	19.1	347
D Head hardened rail steel (fine pearlitic structure) (NHH)	0.80	0.23	0.97	0.016	0.028	-	-	852	1,265	14.3	39.7	385
E Head hardened rail steel (tempered martensitic structure) (HH)*	0.66	0.24	0.73	0.020	0.015	-	-	1,030	1,208	16.4	48.3	350

* Used also for the material of mating specimen

The results of the test are shown in Fig. 2. There is a good correlation between the amount of wear and the hardness before the test, and the higher the hardness before the test, the less the amount of wear. This agrees with a generally accepted view that the higher the hardness of steel, the greater its wear resistance. The effect of microstructure on wear proves that the tempered martensitic structure is subjected to a larger amount of wear than the pearlitic structure at the same hardness level. This means that the fine pearlitic structure is advantageous over the tempered martensitic one in production of rails, because the same level of wear resistance is kept with lower strength of rail steel with pearlitic structure.

discussed above can be valid only if it is used for the qualitative analysis of rail wear and it can be concluded that in order to improve the wear resistance of rail steels, their hardness needs to be increased with pearlitic structure. In other words, the formation of fine pearlitic structure is the guiding principle for developing new rail steels.

In this relation, as it was mentioned earlier that the toughness of the rail head against plastic deformation is an important requirement for improving the wear resistance of rails, the attempt to increase the strength of rail steel is also in the right direction to effectively satisfy this requirement.

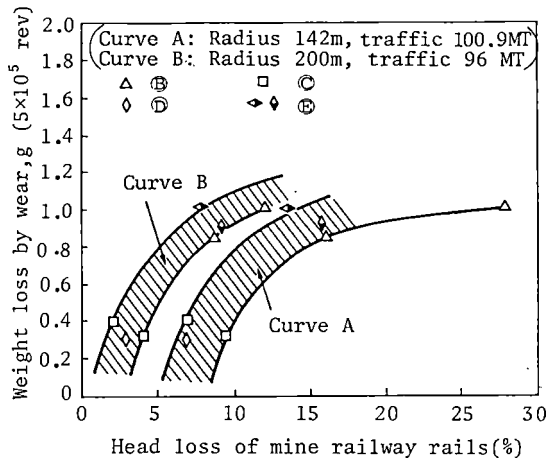


Fig. 3 Correlation between rail wear and wear test results

MATERIAL FACTORS GOVERNING THE FATIGUE FAILURE RESISTANCE OF RAILS

Fatigue failure resistance of rails

Rail wear is predicted to a large extent and measures such as rail replacement can be taken according to plan, whereas fatigue failures occur abruptly and could cause unexpected accidents such as derailment. For this reason, the failure resistance of rails can be said one of the most important properties that rails should possess. Typical failures are head check and flaking occurring at the gauge corner of a rail, shelling and corrugation observed at the gauge corner and on the running surface of a rail (2). Many of these head failures still defy clarification of their causes and energetic studies are being made. A dark spot (or shelling on the running surface of rail) belongs to this category of failure. A dark spot observed on the running surface of a rail of a high-speed railway without heavy load was investigated and the following characteristics were revealed.

The left photograph in Photo 1 shows a rail which has cracked transversely from a dark spot on the high-speed railway. Shown in the right photograph is a plan view of the same running surface of the rail. This rail, No. 2212, installed in a tangent track sustained failure after the traffic reached approximately 200 million tons. This is a typical example of case where the crack initiation point is at the central part of the running surface. The main crack originates at the place indicated by an arrow in the right photograph and runs 5 to 9 mm deep from the surface, developing a secondary crack propagating toward the base of the rail and finally leading to transverse cracking. The position at which this main crack was initiated is located on the running surface or in its neighborhood, as can be confirmed from various observations, and the propagation of this crack was, as can be partially seen in the photograph, caused by fatigue.

The appearance of such main crack from a dark spot is the same as that of flaking and pitting seen on ball-and-roller bearings, gears and rolling rolls, and therefore indicates that rolling contact fatigue causes such crack. Unfortunately because the crack initiation point on the running surface of the rail was later removed by passing wheels, further investigation became impossible (3). Then, the distribution

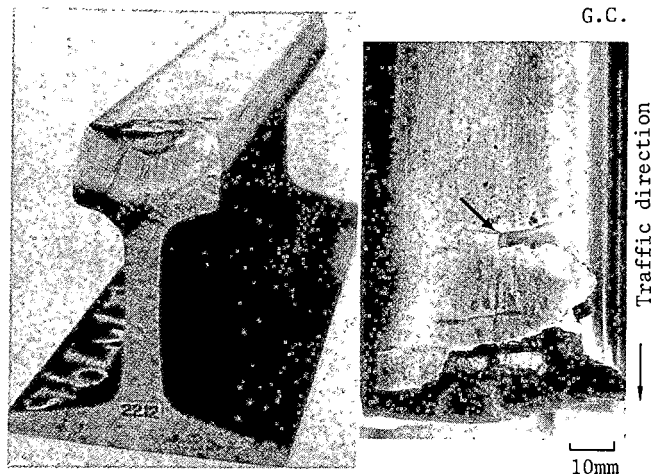


Photo 1 Rail failure from a dark spot (No. 2212 rail)

of dark spots on the running surface as shown in Photo 1 was investigated and it was found that most of them were concentrated within ± 5 mm from the centerline on the running surface of a rail, as shown in Fig. 4 (4).

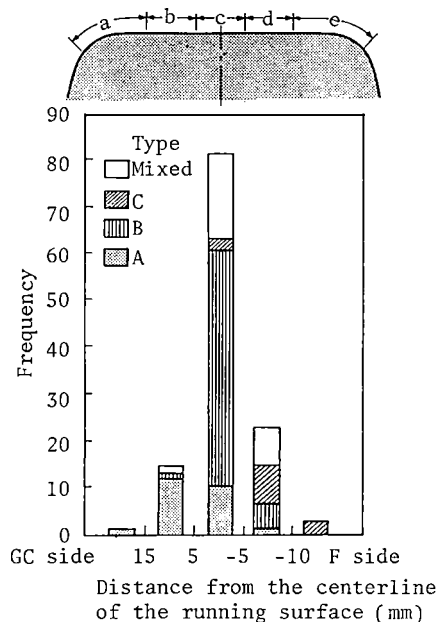


Fig. 4 Distribution of dark spots on the running surface of the rail

Photo 2 shows plastic flows observed on the running surface of No. 2212 rail. The plastic flows are very characteristic as they appear to be rotating round an axis perpendicular to the running surface. As is schematically illustrated in Fig. 5, no plastic flows heading in the traffic direction are observed near the central position of the running surface, as indicated by an arrow. However, tiny plastic flows running right angled to the traffic direction are found in this region (hereinafter called E region).

Field Side

Gauge Side

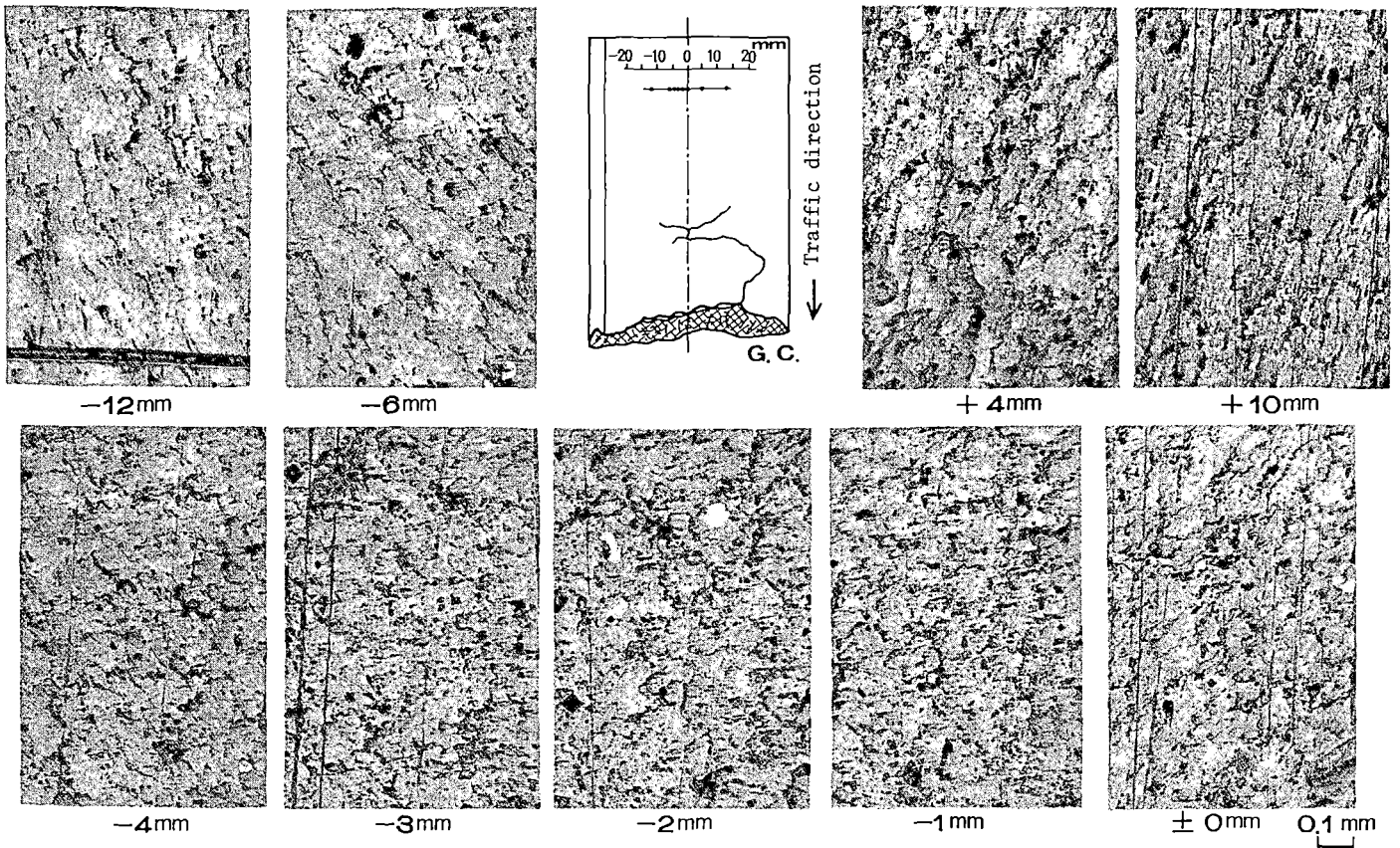


Photo 2 Plastic flow of the running surface (No.2212 rail)

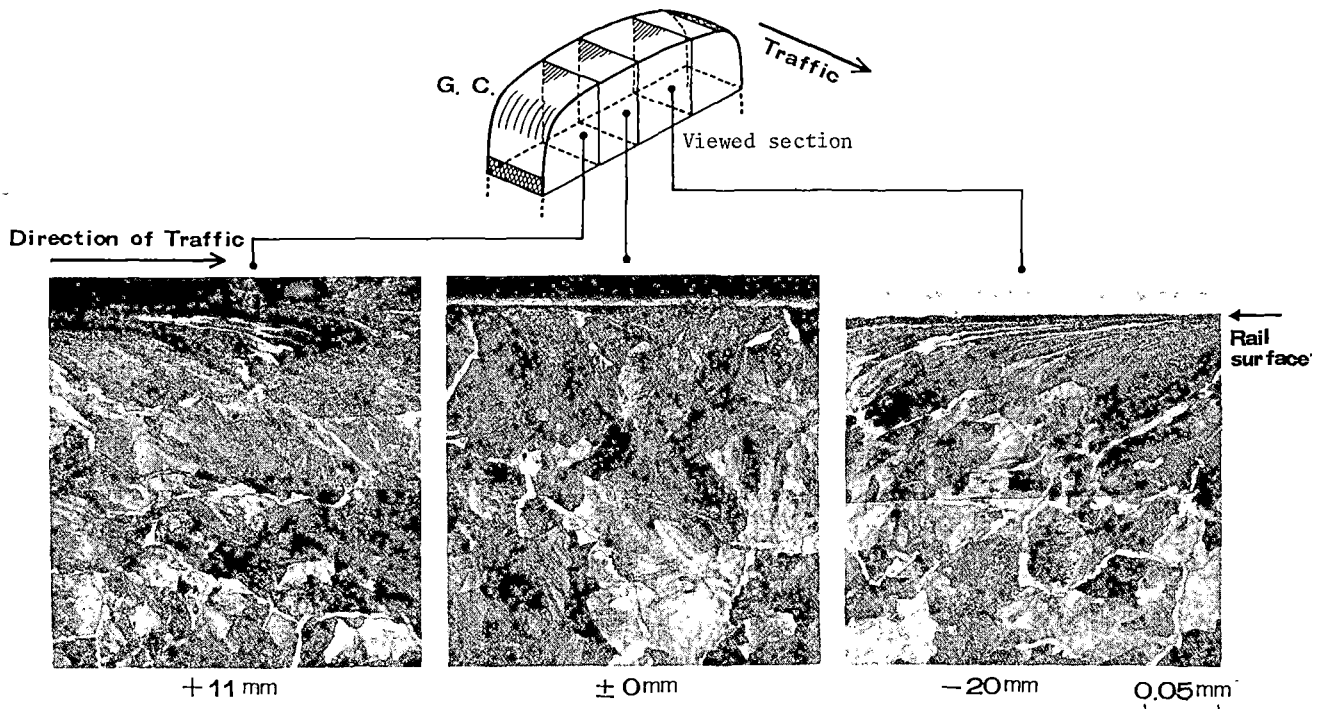


Photo 3 Optical micrographs showing plastic flow on the longitudinal-vertical section of No.2212 rail
(White layer on the rail surface is nickel plating)

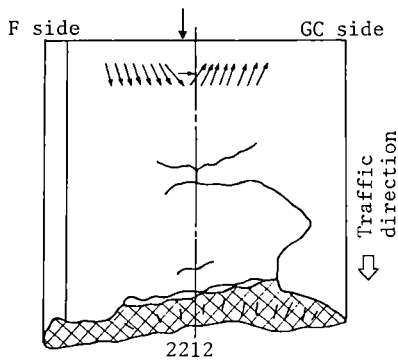


Fig.5 Schematic representation of dark spot

The E region exists at approximately -2 mm in the case of No. 2212 rail. Here, the gauge side from the centerline of the rail surface is indicated by plus (+) figure.

Photo 3 shows the longitudinal/vertical sections (L sections) of the head of No. 2212 rail at locations close to E region (± 0 mm), +11 mm to the gauge side and -20 mm to the field side. As was discussed previously, the plastic flow near the central region on the running surface can be recognized as very slight compared to those on both sides. In the zones on both sides of E region the direction of plastic flow is reversed and it corresponds to the observation that the microstructure on the running surface shows rotating plastic flow round the axis perpendicular to the surface. This can be explained well by considering that the rail surface receives from the wheels a small tangential force right angled to the traffic direction heading toward the gauge side, in addition to a positive tangential force acting in the direction opposite to the traffic direction on the gauge side and a negative tangential force acting in the same direction as the traffic direction on the filed side.

Fig. 6 represents changes in microhardness of the surface of No. 2212 rail. The hardness distribution curve is lowest in E region and increases toward both sides, well corresponding to the changes of the plastic flow discussed earlier. The measurements taken under a load condition of 4.9 N are also shown in this figure ; the hardness values in E region are almost the same as the initial hardness value of

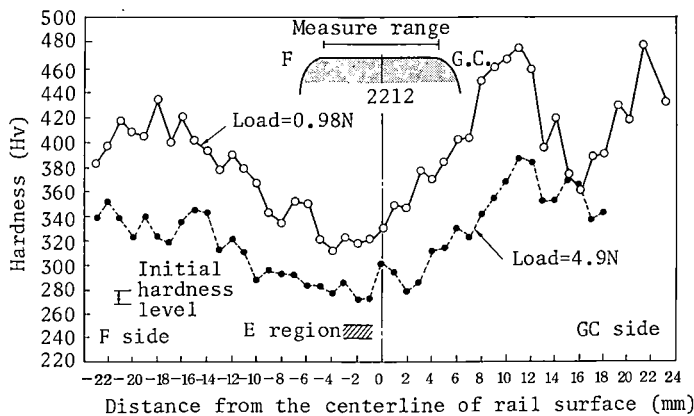


Fig.6 Hardness change on the running surface of No. 2212 rail

the base material. When the frequency of failure by position in Fig. 4, the appearance of plastic deformation and these hardness changes are correlated to each other, it is found that the failures are concentrated in E region where the change in material properties are least. This leads to a supposition that dark spots on the running surface are directly related to the initial material properties of rails, and is considered to suggest that the rolling contact fatigue of a rail by wheels has a close relation to the plastic deformation in the surface layer of a rail. In this sense, this type of failure is considered to be controlled by a different failure mechanism from that of head check occurring at the gauge corner.

Test on rolling contact fatigue of rail steels

From the results mentioned above, it was considered that the study of the rolling contact fatigue characteristics of rail steel is especially important, and the RCF test method was newly developed. This method is an application of the conventional method adopted for testing ball bearing steels, etc. (5) and uses modified Nishihara type wear test equipment. In the test by this method, a ring-shaped specimen as shown in Fig. 7 is cut out of the head of a rail and is tested with a mating specimen of a specific material (of tempered martensitic structure, Hv 350) under a constant load and slip in a lubricated condition. The life of the rail specimen is determined by the r.p.m. at which flaking takes place.

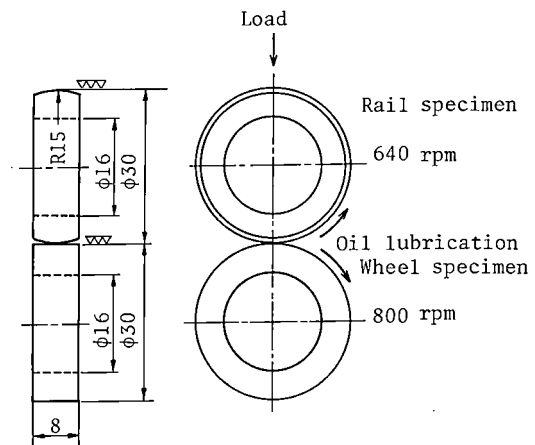


Fig.7 RCF test method

The rolling contact fatigue characteristics of several rail steels were investigated by this method. Fig. 8 shows the results of this test arranged according to Weibull's distribution probability. They are as follows :

- (1) RCF life increases with increasing the tensile strength of rail steels when ordinary carbon rail steel is taken into consideration.
- (2) An increase in life cannot be expected of rail steel of tempered martensitic structure (HH rail) in spite of its high strength.
- (3) The life of rail steel whose microstructure is changed to fine pearlite by heat treatment (NHH rail) is remarkably extended.

Thus, rail steels strengthened with fine pearlitic structure are not only improved in wear resistance, but also effective against fatigue failures.

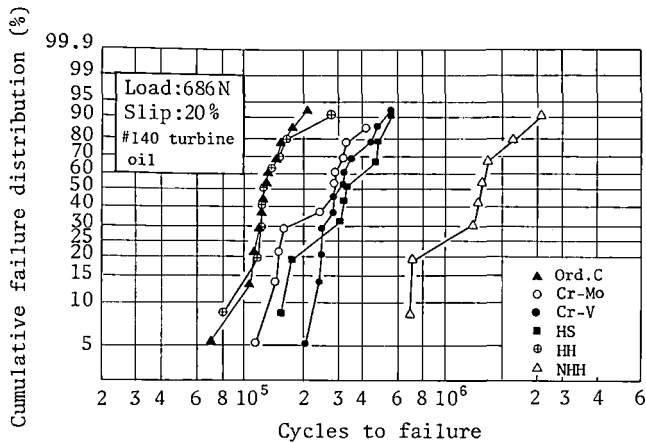


Fig.8 RCF characteristics of various rail steels

WELDABILITY OF RAILS

Necessity for weldable high-strength steel rails

As mentioned above, it was confirmed that rails of high-strength pearlitic structure have not only improved wear resistance, but also improved fatigue failure resistance and that such structure is most suitable as the structure of rail steel of heavy haul railways. This agrees with indications by other researchers (6).

For this reason, many high-strength steel rails have been developed by strengthening the pearlitic structure. These rails are broadly classified into two types. One is an as-rolled alloy steel rail, which is naturally cooled after hot rolling and whose high strength is given by addition of alloys. The other is a heat-treated high-carbon steel rail, which is subjected to rapid cooling after reheating of the whole section or the head of the rail.

Although all of these rails have good wear resistance, their weldability generally poses a problem. When alloy steel rails are welded, weld zones harden and become brittle because of high hardenability. For this reason, postweld heat treatment is sometimes carried out to soften hardened parts (7). In the case of heat-treated rails, weld zones soften from hardened parts of base-metal rails. This softening causes irregular wear and deformation of the heads of rails in service. For this reason, trials have recently been made to prevent this softening by forcibly cooling weld zones just after welding or after reheating (8). These postweld heat treatments are undesirable in that they reduce welding efficiency although they improve the behavior of weld zones. Therefore, a trial was made at NSC to develop high-strength steel rails that can be welded under the same conditions as with ordinary carbon steel rail and that do not require any postweld heat treatment.

Concept of weldable high-strength steel rails

The development of the above-mentioned rails was carried out based on the concept described below (9). To improve the performance of the weld zone of a rail, it is necessary to maintain the same pearlitic structure and strength (hardness) as those of the base metal as far as possible. For this purpose, the transformation temperature in the heat-affected zone of the

rail must be proper after welding. In this case, however, the transformation temperature cannot be changed by coercively changing the cooling rate, because the cooling rate of the heat-affected zone is predetermined by rail size and welding conditions. Therefore, it is necessary to achieve an optimum transformation temperature by improving hardenability, i.e., adding alloying elements.

In this connection, addition amounts of general alloy steel rails are large and, therefore, the structure of the heat-affected zone is more or less of martensitic structure. For this reason, the amount of alloying elements added is limited, which inevitably leads to insufficient strength of the base metal of the rail. Therefore, it is necessary to compensate for the insufficiency by increasing the cooling rate after rail rolling or reheating.

The above-mentioned concept means development of new rails by heat treatment of an alloy steel to which proper amounts of alloying elements have been added. Flash butt welding is used to weld the new rails, as a standard. Fig. 9 illustrates an example of cooling rate of the weld zone in the rail head. This figure shows also a simulated cooling rate after rail rolling.

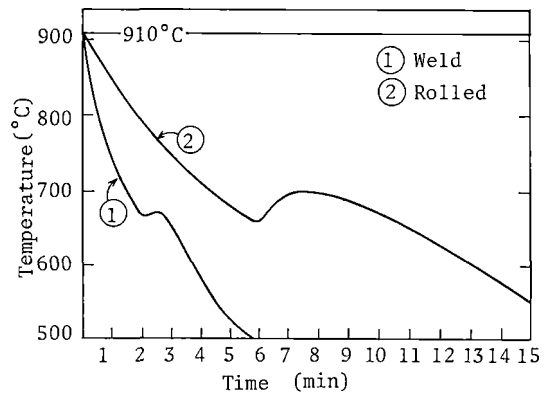


Fig.9 Typical cooling curves of 136RE rail head after weld and hot rolling

Next, it is necessary to concretely determine chemical compositions. An investigation was made into the cooling rate after flash butt welding and structure of several types of high-strength rails so far rolled. The results of this investigation were compared with a CCT diagram of each rail steel determined in the experiment, and it was found that the HAZ of flash butt welding could be roughly simulated by the structure and hardness that correspond to heating up to 1,250°C and a cooling rate of 30°C/min on the CCT diagram. These values will, of course, vary to some degree depending on rail manufacturing conditions, for example, finishing temperature upon rolling, and welding conditions.

Using the above-mentioned results, preparation of CCT diagrams and investigation of mechanical properties were carried out in the laboratory concerning a dozen or so types of heat of various kinds and amounts of alloying elements, and optimum alloying elements and their composition ranges were determined.

Strength and ductility of pearlitic steels

In general, the strength of steel showing eutectoid pearlite depends on the spacing of pearlite lamellae and the strength of the matrix that has no relation to this spacing. Therefore, the strengthening of the pearlitic structure can be achieved by making the interlamellar spacing small and strengthening the matrix, represented by solid solution hardening. The interlamellar spacing that has an important effect on the strength of steel of pearlitic structure depends on the degree of super cooling upon transformation of steel. Therefore, the interlamellar spacing can be made small by decreasing the transformation temperature. Fig. 10 shows the effect of the transformation temperature on the 0.2 % proof stress and flow stress of a 0.82C-0.26Si-0.96Mn-0.97Cr steel. This figure clearly shows that strength increases with decreasing transformation temperature. However, strength decreases abruptly when the transformation temperature decreases further below a specific point. This is because the structure becomes bainitic one.

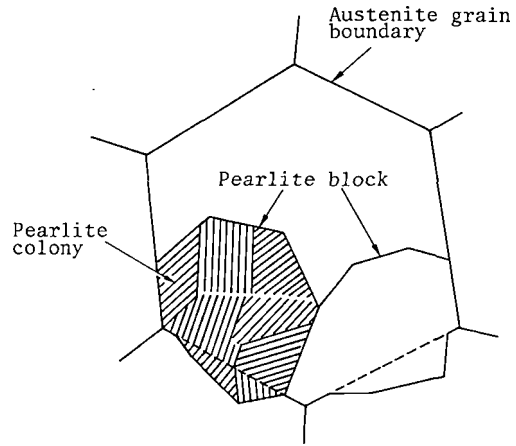


Fig.11 Schematic illustration of pearlite structure

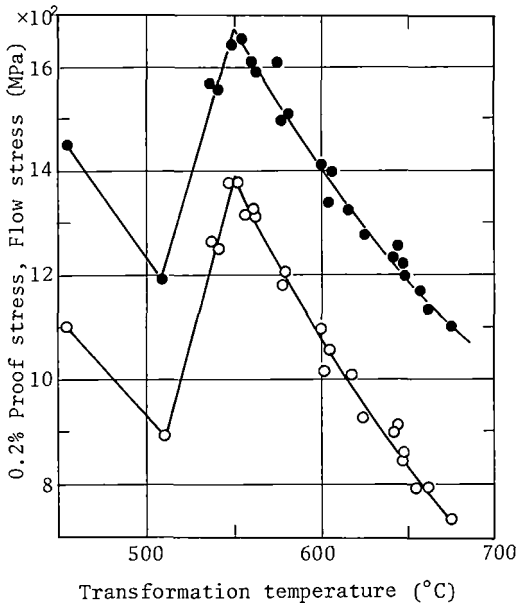


Fig.10 Effect of transformation temperature on 0.2% proof stress and flow stress (6% strain) of 0.8C-1Cr steel.

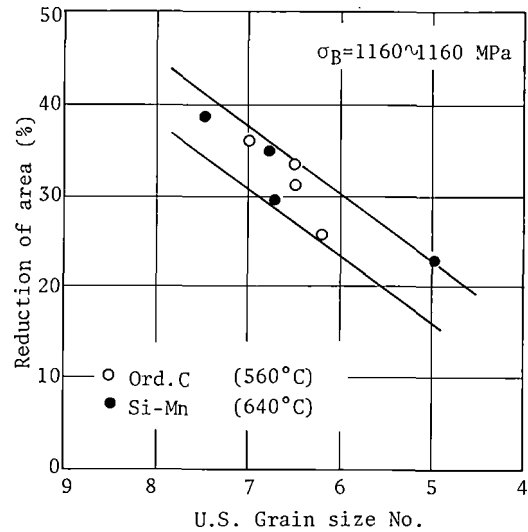


Fig.12 Relationship between reduction of area and U.S. Grain size No. of rail steels with similar tensile strength

It has become apparent that the ductility of pearlitic steels is governed by the unit of structure called "block" (10). It has been ascertained that this block is, as schematically represented in Fig. 11, the area of the ferrite in the pearlitic structure that shows the same crystal orientation. The size of this block has been found to be virtually in proportion to the austenite grain size. Therefore, ductility can be improved by making the austenite grain size small. The size of this block can be directly measured by ultrasonic waves. The reason is that different crystal orientations at the block boundary cause Rayleigh scattering, which results in the attenuation of ultrasonic waves, and that the degree of this attenuation can be related to the block size. Fig. 12 shows the relationship between the US grain size (block size) and reduction of area of an ordinary carbon rail steel and a Si-Mn rail steel of

almost the same strength ($\sigma_B = 1,160$ to $1,180$ MPa). As can be seen from the figure, the reduction of area can be well arranged by this grain size.

Fig. 13 shows changes in critical strain to failure by drawing due to the difference in tensile strength and microstructure of 0.8Si-0.6Cr eutectoid steels. It is apparent that the drawability of the pearlitic structure is by far superior to that of the tempered martensitic structure. Even with the pearlitic structure, however, the critical strain decreases remarkably when the initial strength exceeds 1.4 GPa. Therefore, a proper limit of rail steel strengthening may be set at about 1.4 GPa in view of the strength-ductility balance.

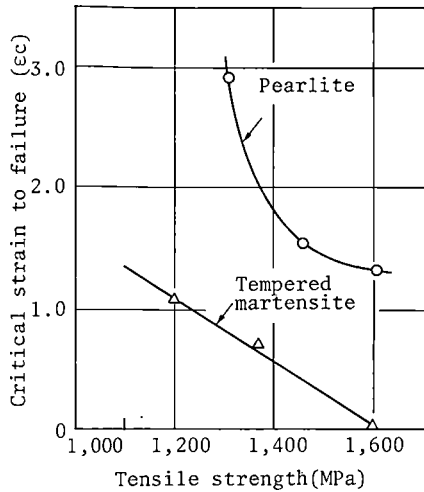


Fig.13 Effect of microstructure and tensile strength on critical strain to failure

Targets for weldable high-strength steel rails

The basic items discussed above are summarized as follows :

1. Wear resistance is improved by using steel of pearlitic structure and strengthening it. The same applies also to the improvement in fatigue failure resistance.
2. The block size is made small as far as possible from the standpoint of ductility.
3. Welding conditions must be similar to those for ordinary carbon steel rails and the hardness in the HAZ is made close to that of the hardened base metal. However, the basic structure must be pearlitic.

In consideration of these items and the results of fundamental experiments the following target values were set for the new rails to be developed : 0.2 % proof stress \geq 800 MPa, tensile strength \geq 1,250 MPa, reduction of area \geq 35 %, maximum hardness of HAZ \geq 350 Hv, and martensitic structure of HAZ \leq 5 %. Then, the two chemical compositions - Si-Mn (NS Type I) and Cr-Si (NS Type II) - given in Table 2 were selected as those which meet the above-mentioned target values. Strengthening ability, transformation characteristics, ease of segregation, improvement in

Table 2 Chemical composition of weldable high-strength rail steels

Element, %	NS-Type I	NS-Type II
Carbon	0.74 to 0.80	0.72 to 0.80
Silicon	0.85 to 0.95	0.85 to 0.95
Manganese	1.10 to 1.30	0.70 to 0.85
Phosphorus	\leq 0.025	\leq 0.025
Sulphur	\leq 0.015	\leq 0.015
Chromium	-	0.45 to 0.70
Niobium	\leq 0.02	\leq 0.02

ductility and toughness, and cost were taken into consideration in selecting these alloying elements. The CCT diagrams of Type I and Type II are shown in Fig. 14. In Type II, Cr is used to further improve the above-mentioned properties than with Type I.

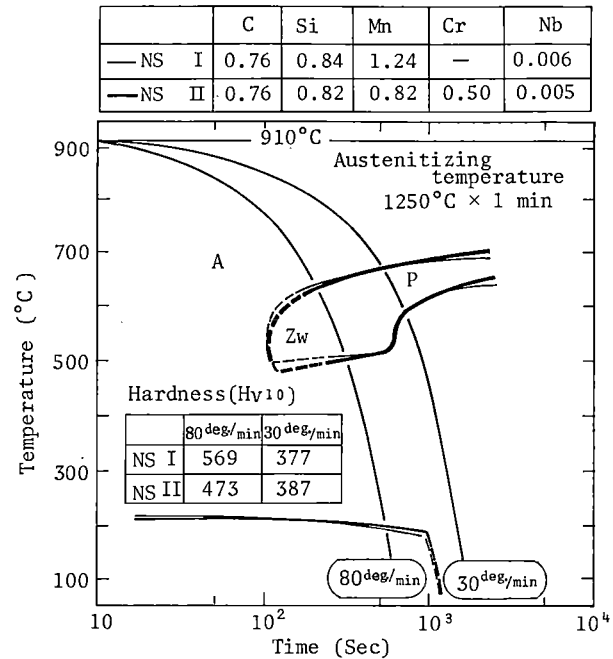


Fig.14 CCT diagrams of NS I and II rail steels

The head hardening process was selected as the heat treatment of the rail. One of the reasons is that to effectively secure the cooling rate necessary for obtaining high strength, the head of the rail is slack quenched by air from the outside by non-steady state heating of the head and also the cooling by heat conduction to the lower part of the rail is utilized at the same time. Another reason is that residual compressive stress is generated in the outer layer of the rail head when this process is employed. These residual stress can be expected to be effective in preventing the generation and propagation of cracks due to rolling contact (11).

MANUFACTURE OF WELDABLE HIGH-STRENGTH STEEL RAILS AND THEIR PROPERTIES

Manufacture

Based on the above-mentioned concept, rails Type I and Type II were manufactured to investigate the properties of actual rails. After refining in a 150 t BOF the rail steels of these new chemical compositions were subjected to the vacuum process in which adjustment of chemical compositions was conducted during degassing. After that, the steels were cast as ingots of approximately 7 t by the bottom pouring process. After soaking, these ingots were rolled to blooms 245 x 305 mm. Then, the bloom surface was dressed as required. After reheating, the blooms were rolled to rails of sections AREA 136 lbs. and JRS 60 on a universal rail mill and rails were cut by a hot saw. After cooling, these rails were straightened by a roller straightener and then cut by a cold saw. After several strict inspections, the rails were subjected to the heat treatment process.

The rail head was hardened in a continuous heat treatment line developed by NSC using heating temperatures and cooling conditions previously controlled so that the above-mentioned targets could be obtained. These rails were restraightened by a press leveler as required, and were completed through the final inspection process.

Properties

Table 3 shows the chemical compositions and average mechanical properties of these two types of rail. Type II is somewhat superior although both show almost the same properties in tests in the laboratory. Therefore, Type II will be mainly referred to in the following.

Table 3 Chemical compositions and mechanical properties of as-rolled and heat treated rail steels of NS I and NS II

	C	Si	Mn	P	S	Cr	Nb
NS I	0.76	0.84	1.24	0.023	0.009	-	0.006
NS II	0.76	0.82	0.82	0.020	0.006	0.49	0.005

Rail type	Heat treatment	0.2% proof strength	Ultimate tensile strength	Elongation	Reduction of area	Remarks
NS I	as rolled	608MPa	1098MPa	12 %	18 %	
	heat treated	873	1285	14	41	*
NS II	as rolled	608	1127	14	19	
	heat treated	902	1324	19	50	*

(*) Specimens (6 mm in diameter) were cut out of the locations 5 mm from the top surface of rail head.

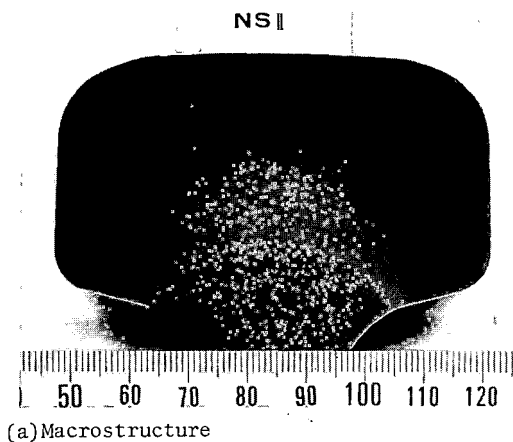
These rails show an ultimate tensile strength of approximately 1,100 MPa in the as-rolled condition. This means that even rails before heat treatment show almost the same strength level as average alloy steel rails. There is no problem in the results of various tests, such as Drop test and Nick and Break test, conducted in accordance with the AREA Specification.

Photo 4 (a) shows the macrostructure of the head of an Type II rail after heat treatment. The black part of the head indicates a fine pearlitic structure as shown in Photo 4 (b).

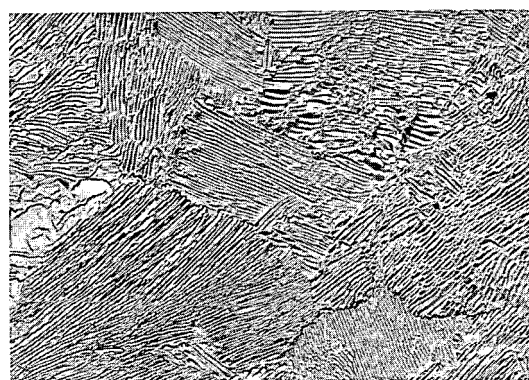
Fig. 15 shows the hardness distribution in the head section. Hardness values are from 380 to 390 Hv on the head surface and continuously decrease toward the inside. The test results of tension test specimens (6 φ) cut out of locations 5 mm from the head surface are shown in Table 3. The reduction of area is very satisfactory, with high strength kept.

Fig. 16 shows the results of US grain size measurement of an Type II rail before and after heat treatment. For comparison, the grain size of an ordinary carbon steel rail is also shown. The structure of the Type II rail shows fine grains in each of the locations and this is remarkable especially in the head after heat treatment. This is the reason why the reduction of area is good in spite of high strength. The K_{Ic} value of a specimen sampled from the head is approximately $40 \text{ MPa}\sqrt{\text{m}}$ at room

temperature and deterioration due to strengthening is not recognized.



(a) Macrostructure



(b) Microstructure (5mm from top surface) 1 μm

Photo 4 Metallurgical structure of head section of NHH rail after heat treatment

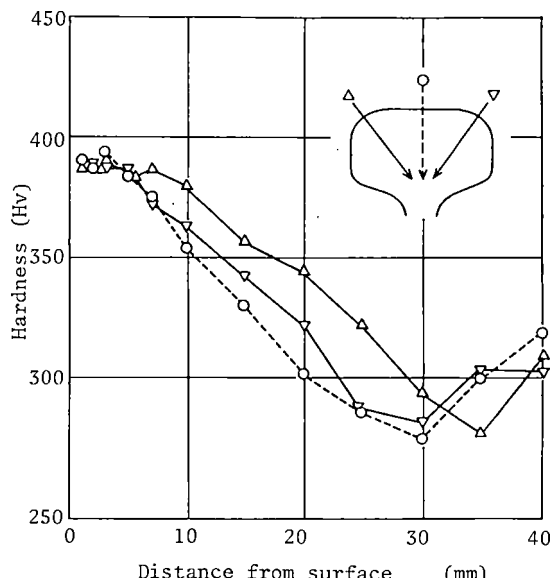


Fig.15 Hardness distribution of rail head section of NS II

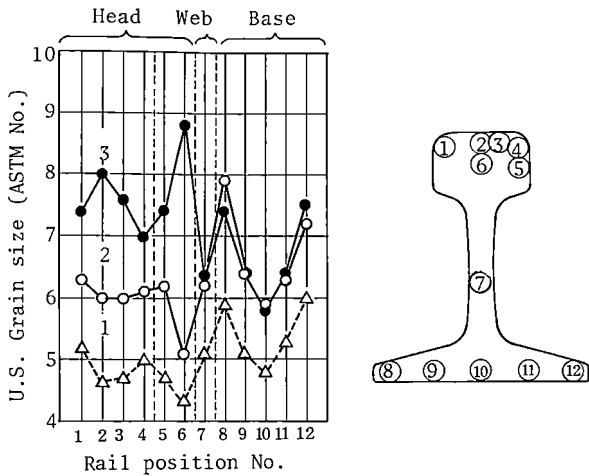


Fig.16 U.S. Grain size distribution of ordinary C and NS II rails

1. Ordinary C rail
2. NS II rail (before heat treated)
3. NS II rail (after heat treated)

Weldability

The above-mentioned rails were welded by flash butt welding and their properties were investigated. Welding was carried out under the same conditions as with ordinary carbon steel rails, shown in Table 4, and pre- and postheating were not carried out at all. Photo 5 shows the section of the center of rails welded. The formation of martensitic structure was not observed at all. Fig. 17 shows the hardness distribution in the section of the center; the hardness in the HAZ is kept above 350 Hv except with softening by a temperature rise to near the A_3 transformation temperature at which the pearlitic structure is destroyed. This is effective in making narrow the width of the softening zone formed by heating to the above-mentioned temperature range. In a three-point bending test with 1 meter span, the Type II rail showed a load of approximately 1.8 MN and a deflection of approximately 15 to 17 mm, thus demonstrating good weldability.

Table 4 Flash butt welding condition of NS II rail

Max. current density : 30,000 A/mm²
 Upset force : 45 Ton
 Upset : 13 mm

Zone	No-Load Voltage	Flashing Speed	Time
Pre-heating	7.5 V	0.22mm/sec	64sec
Flashing	6.3	"	118
Final Flashing	7.5	0.25 → 1.4	10
Upsetting	7.5	-	0.5* + 25

K355 Welding machine * Current feed

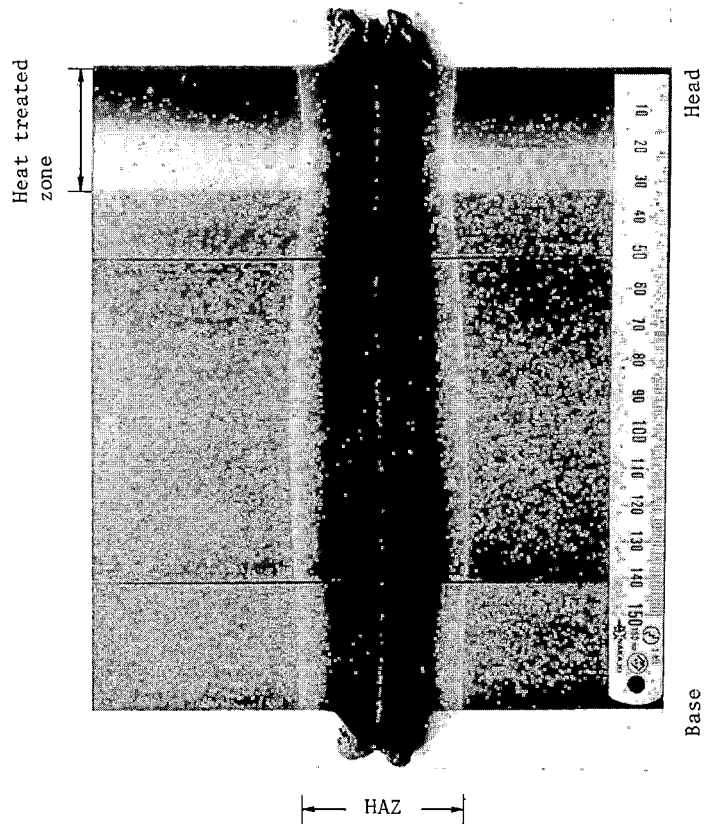


Photo 5 Macrostructure of longitudinal-vertical section of NS II rail welded by flash butt welding

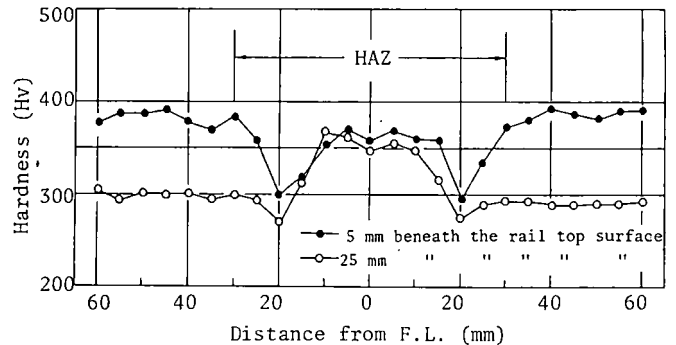


Fig.17 Hardness change on the longitudinal-vertical section of NS II rail welded by flash butt welding

SERVICE BEHAVIOR

As mentioned above, many new rails have recently been developed to improve the wear resistance and fatigue failure resistance of rails under transportation conditions of increasingly heavy load. Fig. 18 shows the average proof stress and tensile strength of so far reported high-strength rails and those developed this time. It is apparent from this figure that

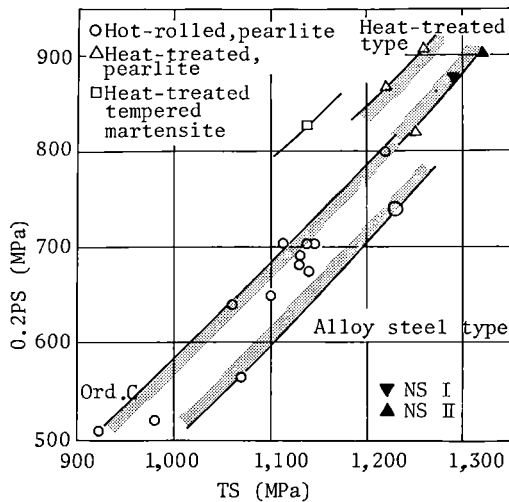


Fig.18 Strength level of rail steels

heat-treated rails provide high strength relatively easily and that the rails developed this time show the highest strength level.

These rails Type I and Type II, along with the NHH rail developed before them, were sent to the USA in April, 1979 for a laying test on the FAST. The rail Type II has been tested since December, 1979 in the third experiment. The test results are being presented in some reports. It might be said that this rail shows satisfactory results as expected, nay, more than expected, in wear resistance, failure resistance and serviceability of weld zones (12). Tests were started also with the rails NHH and Type I in December, 1980 and April, 1981, respectively. Detailed comparative examinations of the service life of these rails and their metallurgical analyses will contribute to the solution of long-pending problems relating to rails, such as wear, fatigue and corrugation and these results will lead to the development of rails of better quality.

CONCLUSION

The recent trend toward heavier load or higher speed has increased the wear and fatigue failure of rails. Therefore, rails capable of withstanding this severe situation are much in demand. Some of these concrete problems were examined and material factors were clarified to find conditions to be met for the improvement of properties of steel rails. Based on the results of such examination, new rails were developed at NSC.

- (1) The wear resistance and fatigue failure resistance of rails can be improved at the same time by making the metallurgical structure of rail steel pearlitic and giving it high strength.
- (2) As for the weldability of rails, NSC developed a manufacturing process for head-hardening of steel rails to which alloying elements have been added to obtain improved performance and the same efficiency of weld as that of ordinary carbon steel rails at the same time.
- (3) New rails NS I (Si-Mn type) and NS II (Cr-Si type) were designed as rails that meet (1) and (2) above, and rails AREA 136 lbs. and JRS 60 were manufactured on a trial basis. These rails (136 RE) are being subjected to a laying test on the FAST, USA. From the interim reports of the

test, virtually satisfactory results have been obtained with the rail NS II which was tested earlier than NS I.

ACKNOWLEDGMENT

Part of the research reported above was conducted with the support of Messrs. S. Matsuyama and R. Kurihara, senior researchers at Railway Technical Research Institute, Japanese National Railways and useful discussions were given also by the members of the research group for the wheel-rail contact problems. Further, Dr. Takahashi, Fundamental Research Laboratory, NSC, gave his cooperation concerning the basic properties of pearlitic steels. The authors wish to extend their sincere thanks to them.

REFERENCES

1. Takino, Y., "Speed up and Track in BR", Tetsudo Senro, vol. 28, 1980, pp. 124-134.
2. UIC/ORE, Docu. Leaflets Concerning the Principal Rail Flaws, Int. Rep., No. 3, 1962
3. Sugino, K., Miyamoto, K. and Nagumo, M., "Failure Process of Bearing Steel in Rolling Contact Fatigue", Trans. ISI Japan, vol. 11, 1971, pp.9-17.
4. Masumoto, H., Sugino, K., Nishida, S., Kurihara, R. and Matsuyama, S., "Some Features and Metallurgical Considerations of Surface Defects in Rail Due to Contact Fatigue", ASTM STP 644, 1978, pp. 233-255.
5. Sugino, K., Miyamoto, K. and Nagumo, M. and Aoki, K., "Structural Alterations of Bearing Steels Under Rolling Contact Fatigue", Trans. ISI Japan, vol. 10, 1970, pp. 98-111.
6. Heller, W. and Schweitzer, R., "High-Strength Pearlitic Steel Does Well in Comparative Tests of Alloy Rails", Railway Gazette International, vol. 136, No. 10, Oct. 1980, pp. 855-857.
7. Vines M.J., Townend P.H., Lancaster, G. and Marich, S., "The Flash Butt Welding of High Strength Rail", Heavy Haul Railway Conference, Session 411, paper H. 6, Sep. 1978, Perth, Australia.
8. Oketa, M., "On the Heat Treatment After Gas Pressure Welding of Head Hardened Rail", Tetsudo Senro, vol. 29, No. 1, 1981, pp. 22-25.
9. Masumoto, H., Sugino, K. and Hayashida, H., "Development of Wear Resistant and Anti-Shelling High Strength Rails in Japan", Heavy Haul Railway Conf., Session 212, paper H. 1, Sep. 1978, Perth, Australia.
10. Takahashi, T., Nagumo, M. and Asano, Y., "Microstructures Dominating the Ductility of Eutectoid Pearlitic Steels", Trans. JIM, vol. 42, 1978, pp. 708-715.
11. Nishida, S., Urashima, C., Sugino, K. and Masumoto, H., "A Study on the Fatigue Crack Propagation of Rail Steels", Proc. Int. Conf. SMA, Aschen, West Germany, 1979, pp. 1255-1260.
12. Lundgen, J.R., "FAST Results : Selected Highlights", Proc. AREA, vol. 82, 1981, pp.336-358.

Fatigue Behavior and Fracture Toughness of Standard Carbon and High Strength Rail Steels

Y.J. Park

Senior Research Associate
Climax Molybdenum Co.
1600 Huron Parkway
Ann Arbor, Michigan

F.B. Fletcher

Research Manager
Climax Molybdenum Co.
1600 Huron Parkway
Ann Arbor, Michigan

To compare the fatigue resistance of different rail steels, samples from four commercial rails were studied by strain-controlled fatigue tests. Head hardened, Cr-Mo, and Cr-V high strength rails exhibited fatigue resistance superior to that of standard carbon rail. The head hardened and the Cr-Mo rails exhibited better fatigue resistance than did the Cr-V rail. In addition, fracture toughness of standard carbon, Cr-Mo, and Cr-V rails was determined using compact tension specimens. The high strength Cr-Mo rail exhibited fracture toughness similar to that of the standard carbon rail, while the Cr-V rail exhibited inferior fracture toughness.

NOMENCLATURE

HB	Brinell hardness
$\Delta\sigma/2$	stress amplitude
$\Delta\epsilon/2$	total strain amplitude
$\Delta\epsilon_e/2$	elastic strain amplitude
$\Delta\epsilon_p/2$	plastic strain amplitude
K'	cyclic strength coefficient
n'	cyclic strain hardening exponent
σ'_f	fatigue strength coefficient
b	fatigue strength exponent
ϵ'_f	fatigue ductility coefficient
c	fatigue ductility exponent
N_f	cycles to failure
$2 N_f$	reversals to failure
E	elastic modulus
K_{Ic}	plane-strain fracture toughness
K_Q	fracture toughness based on P_Q
K_{max}	fracture toughness based on P_{max}
P_Q	load used to determine K_Q and defined in ASTM E399-81.
P_{max}	maximum load that a specimen sustains
σ_{ys}	0.2% offset yield strength in tension

INTRODUCTION

High strength premium rails have been developed as the world's railways are confronted with increasing demands for better safety, economy and load carrying capacity. Acceptance of high strength rails by the railroad industry has been based primarily upon improved wear resistance, especially in curved track, but the additional benefit of improved fatigue resistance may prove of equal or greater importance. Rails sometimes do not achieve their expected service life due to the development of fatigue defects which can be the cause of rail failures and therefore derailments (1).

A rail metallurgy experiment at the Facility for Accelerated Service Testing (FAST) has provided information on rail wear under a controlled environment (2,3). The FAST experiment has also provided useful information on rail failure behavior; appreciable lengths of rail have been replaced due to fatigue failures as well as excessive wear. In particular, a high incidence of failure has occurred during operation under well-lubricated conditions (2,4). The premature failure of rails can probably be explained by the fact that 91 metric ton (100 ton) cars are being used in the FAST track. Recent analyses (5-7) have shown that rail life is substantially reduced for wheel loadings above those of 72 metric ton (80 ton) cars because for service under such heavy haul conditions rail life is determined by its fatigue resistance rather than its wear resistance. These analytical results are in good agreement with rail defect data obtained from two mining railroads as well as from FAST (6).

Because of the importance of rail fatigue failure in heavy haul railways, this investigation centered on determining the fatigue properties of four rail steels (standard carbon, head hardened, Cr-Mo, and Cr-V) using the strain-controlled fatigue test. The strain-controlled fatigue test was employed because the strain-life approach has been recognized to be more closely related to service damage than

the stress-life (S-N) approach(8), particularly when plastic deformation is involved as is the case for rails. Even when a rail does not experience any gross plastic deformation in service, plastic strains almost always occur locally at points of high stress concentration around notches, inclusions, and other stress raisers where fatigue cracks start. In addition to the fatigue properties, the plane-strain fracture toughness (K_{Ic}) values of standard carbon, Cr-Mo, and Cr-V rail steels were determined by compact tension tests(9). The fracture toughness characterizes the resistance of a material to fracture in the presence of a sharp crack (e.g., a fatigue crack) under tensile loading and can be used to estimate the relation between failure stress and crack size for a material in service(9).

EXPERIMENTAL PROCEDURES

Materials

Four commercial rail steels were evaluated: standard carbon steel rail (hereafter referred to as carbon rail), head hardened (HH) rail, Cr-Mo rail, and Cr-V rail. The HH rail had a section size of 66.5 kg/m (133 lb/yd). All other rails had a section size of 68 kg/m (136 lb/yd). The compositions of the steels are presented in Table 1.

Table 1 - Compositions of Rail Steels

Rail Steel	Composition, Weight Percent									
	C	Mn	Si	Cr	Mo	V	Al	N	P	S
Carbon	0.74	0.93	0.38	-	-	-	0.005	0.004	0.019	0.022
HH	0.72	0.78	0.16	-	-	-	0.007	0.005	0.013	0.020
Cr-Mo	0.75	0.58	0.39	0.61	0.20	-	0.015	0.008	0.021	0.023
Cr-V	0.69	0.98	0.68	0.87	-	0.097	0.005	0.010	0.030	0.024

Hardness and Tensile Testing

A transverse section was cut from each rail, surface ground, and Brinell hardness (HB) impressions were made using a 3000 kg load. Room temperature tensile properties of each rail steel were obtained from duplicate round specimens with a gauge diameter of 12.7 mm (0.5 in.) and a gauge length of 51 mm (2 in.). The tensile specimens were longitudinally cut from the upper corners of each rail head as shown in Figure 1. In the case of the HH rail, this procedure assured obtaining tensile properties from the hardened zone. The tensile tests were performed at strain rates of $5 \times 10^{-5} \text{ sec}^{-1}$ and $8.3 \times 10^{-4} \text{ sec}^{-1}$ in the elastic and plastic portions of the stress-strain curve, respectively.

Fatigue Testing

Cylindrical fatigue specimens with a uniform gauge diameter of 6.35 mm (0.25 in.) and a gauge length of 12.7 mm (0.5 in.) were machined from the blanks cut longitudinally from the rail head (Figure 1). The gauge sections of the specimens were polished to eliminate all the circumferential tool marks. As in the case of the tensile specimens, the fatigue specimens were taken from the hardened zone of the HH rail. All fatigue tests were performed with electrohydraulic closed loop testing equipment. A Wood's metal grip was used to ensure proper axial alignment and to minimize specimen mounting stresses. Fully reversed constant strain amplitude tests were performed to determine the strain-life curve of each rail(10). At least ten

specimens were tested from each rail.

An incremental step test(11) was also conducted for each rail. A fatigue specimen was strained 1.5% in tension, unloaded, and strained 1.5% in compression. It was then restrained 1.4% in tension, 1.4% in compression, 1.3% in tension, and so on until the strain limit was 0.1%. After completion of this first incremental step "block", a second block was generated by alternately straining in tension and compression by increasing the strain limits in 0.1% increments from 0 to 1.5%. The cyclic stress-strain curve is the locus of superimposed stress-strain hysteresis loop tips. A stable cyclic stress-strain curve was obtained by applying several blocks to each specimen.

Fracture Toughness Testing

Compact tension fracture toughness test specimens were prepared from all except the HH rail. The plane of fracture was equivalent to a transverse defect in a rail, that is perpendicular to the rolling direction as shown in Figure 1.

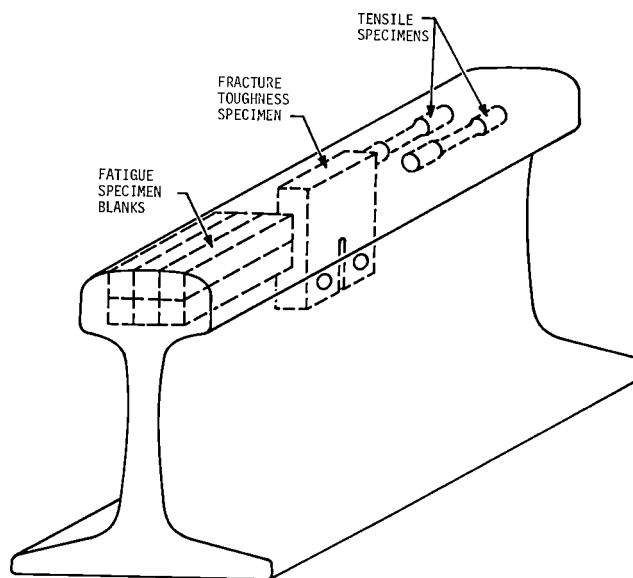


Fig. 1 Location of specimen blanks

The dimensions of the compact tension specimens are shown in Figure 2. The thickness of a particular

specimen was either 12.7 mm (0.5 in.) or 19.1 mm (0.75 in.). Fatigue precracking of each specimen was conducted at 30 Hz under load control. The specimens were pulled to failure at room temperature in a closed loop materials test system under load control and the fracture toughness was determined in accordance with ASTM Specification E 399-81(9).

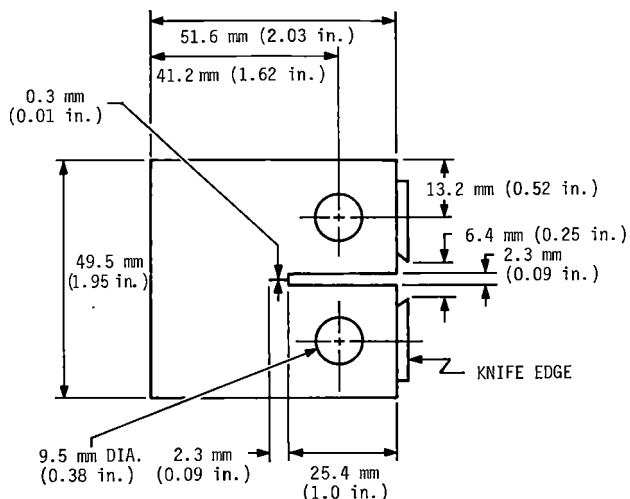


Fig. 2 Dimensions of compact tension fracture toughness test specimens. The thickness of the specimens was either 12.7 mm (0.5 in.) or 19.1 mm (0.75 in.).

Hardness and Tensile Properties

The Brinell hardness pattern in the head of each rail is presented in Figure 3. As expected, the carbon rail exhibits the lowest hardness of about 260 HB. The hardness pattern of the HH rail reveals the depth of the hardened zone. The average hardness approximately 10 mm (0.4 in.) below the rail head surface is about 330 HB, and as was mentioned earlier, the tensile and fatigue specimens were prepared from this area. The average hardnesses of the Cr-Mo and the Cr-V rails are about 330 HB and 315 HB, respectively.

Room temperature tensile properties of the rail heads are presented in Table 2. The carbon rail has the lowest strength and the Cr-V rail shows the lowest elongation and reduction of area values. The Cr-Mo rail exhibits the highest tensile strength as well as the highest reduction of area value.

Table 2 - Room Temperature Tensile Properties of Rail Steels

Rail Steel	0.2% Offset		Ultimate Tensile Strength, MPa (ksi)	Elongation in 51 mm, %	Reduction in Area, %
	Yield Strength, MPa (ksi)				
Carbon	471 (68.4)		908 (131.7)	14	19
HH	751 (109.0)		1121 (162.6)	13	24
Cr-Mo	749 (108.7)		1179 (171.0)	12	27
Cr-V	641 (93.0)		1128 (163.6)	11	18

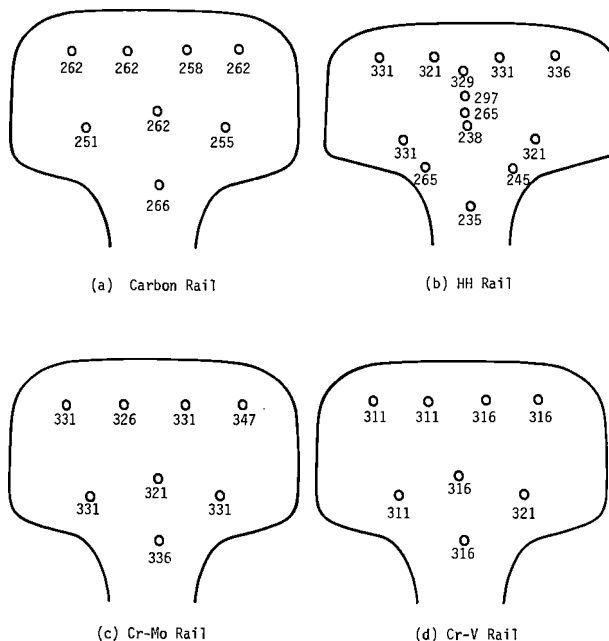


Fig. 3. Brinell hardness patterns of rails tested

Cyclic Stress-Strain Curve

The cyclic stress-strain curves obtained by the incremental step test are presented in Figure 4 along with the corresponding monotonic stress-strain curves. All four steels exhibit cyclic softening at very low strains and cyclic hardening at higher strains. The crossover from cyclic softening to cyclic hardening occurs at strains of 0.6% for carbon rail, 1.0% for Cr-V rail, 1.1% for HH rail, and 1.4% for Cr-Mo rail. Similar behavior has been observed in other pearlitic steels(12-15). The cyclic stress-strain curve of each steel can be described by the following expression:

$$\frac{\Delta\sigma}{2} = K' \left(\frac{\Delta\epsilon_p}{2} \right)^{n'} \quad (1)$$

where $\Delta\epsilon_p/2$ is plastic strain amplitude which is explained below. K' and n' are the cyclic strength coefficient and cyclic strain hardening exponent, respectively. The K' and n' values obtained from the cyclic stress-strain curves are presented in Table 3.

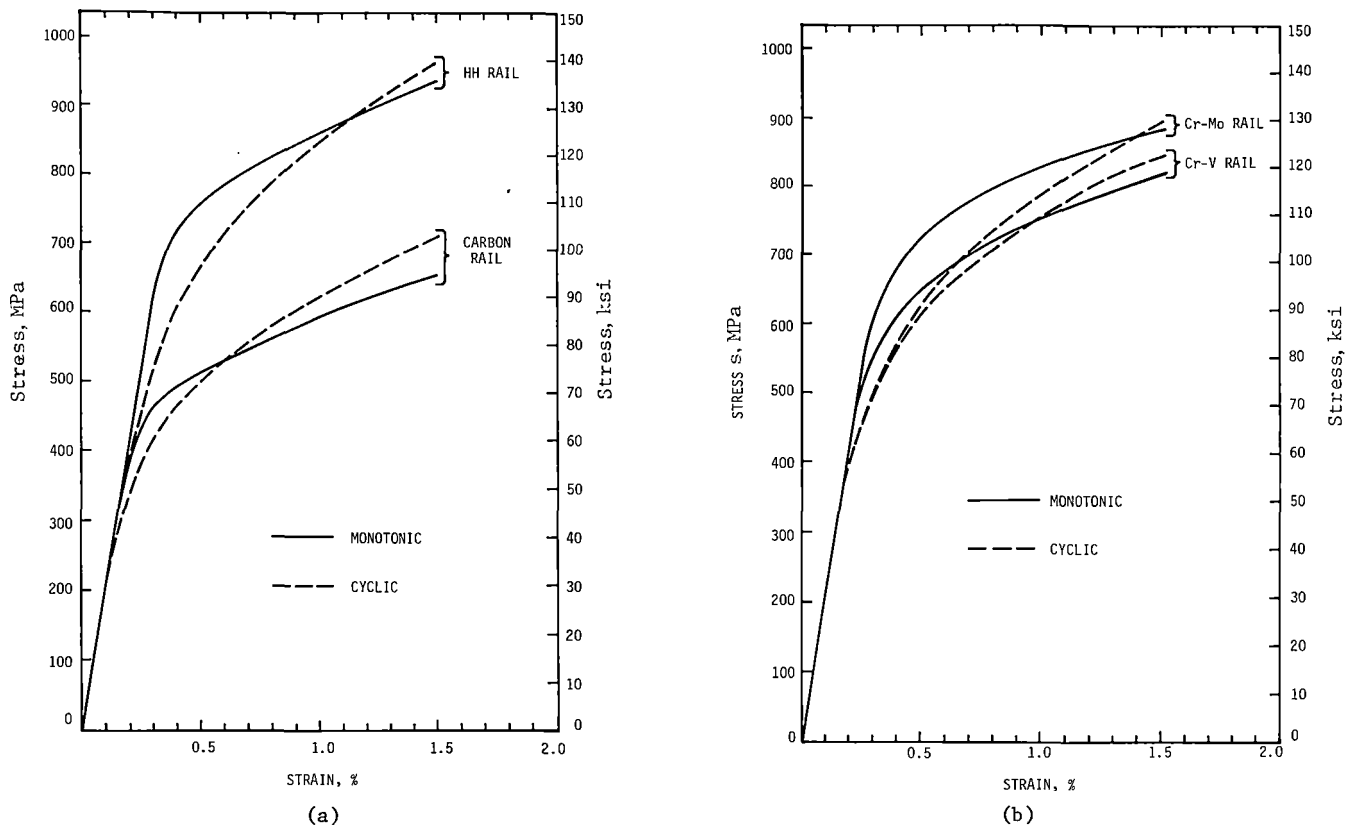


Fig. 4 Monotonic and cyclic stress-strain curves for (a) carbon and HH rails, and (b) Cr-Mo and Cr-V rails

Table 3 - Cyclic Stress-Strain Properties of Rail Steels

Rail Steel	Cyclic Strain Hardening Exponent, n'	Cyclic Strength Coefficient, K' MPa (ksi)
Carbon	0.226	1938 (281.1)
HH	0.218	2598 (376.8)
Cr-Mo	0.186	2162 (313.5)
Cr-V	0.187	1957 (283.9)

Strain-Life Curve

Fully reversed constant strain amplitude test results for the Cr-Mo rail are reported in Table 4. Similar data were obtained for other rails.

Table 4 - Fatigue Data for Cr-Mo Rail Steel

Controlled Strain Amplitude, $\Delta\epsilon/2, \%$	Reversals to Failure, $2 N_f$	Measured Stress Amplitude ($\Delta\sigma/2$) at N_f Reversals,		Calculated Strain Amplitude, %	
		MPa	(ksi)	$\Delta\epsilon_e/2$	$\Delta\epsilon_p/2$
1.50	1,140	943	(136.8)	0.465	1.035
1.50	820	894	(129.6)	0.440	1.060
1.00	2,360	843	(122.2)	0.415	0.585
1.00	2,640	839	(121.7)	0.413	0.587
0.75	5,550	765	(111.0)	0.377	0.373
0.75	5,320	762	(110.6)	0.376	0.374
0.50	13,800	687	(99.6)	0.338	0.162
0.50	16,000	629	(91.3)	0.310	0.190
0.25	242,600	469	(68.0)	0.231	0.019
0.25	327,000	478	(69.4)	0.236	0.014

The measured stress amplitude ($\Delta\sigma/2$) values at half of the reversals to failure represent steady-state values obtained for each constant strain amplitude test. The total strain amplitude, $\Delta\epsilon/2$, is the sum of the elastic strain amplitude, $\Delta\epsilon_e/2$, and the plastic strain amplitude, $\Delta\epsilon_p/2$; i.e.,

$$\Delta\epsilon/2 = \Delta\epsilon_e/2 + \Delta\epsilon_p/2 \quad (2)$$

The elastic strain amplitude can be calculated from the steady-state stress as follows:

$$\Delta\epsilon_e/2 = \frac{\Delta\sigma/2}{E} \quad (3)$$

where E is the elastic modulus of the steel. The modulus was determined separately for each steel by measuring the slope of the initial loading portion of the stress-strain curves. All values fell between 200 and 203 GPa (29,000 and 29,400 ksi).

For a number of metals including many steels, it has been shown that the plastic strain-life curve ($\Delta\epsilon_p/2$ vs. $2 N_f$) and the elastic strain-life curve ($\Delta\epsilon_e/2$ vs. $2 N_f$) are linear in a full logarithmic scale(11). The relationship between plastic strain amplitude and reversals to failure is given by:

$$\Delta\epsilon_p/2 = \epsilon_f' (2 N_f)^c \quad (4)$$

where ϵ_f' is the fatigue ductility coefficient and c is the fatigue ductility exponent. In a similar fashion the elastic strain amplitude may be expressed as:

$$\Delta\epsilon_e/2 = (\sigma_f'/E) (2 N_f)^b \quad (5)$$

where σ_f' and b are the fatigue strength coefficient and the fatigue strength exponent, respectively. Combining equations (2), (4), and (5) the total strain-life curve may be described by the following expression.

$$\Delta\epsilon/2 = (\sigma_f'/E)(2N_f)^b + \epsilon_f' (2N_f)^c \quad (6)$$

Figure 5 depicts this expression for the Cr-Mo rail. The same analysis has been carried out for each steel and the fatigue properties σ_f' , b , ϵ_f' , and c of the four rail steels are summarized in Table 5. These fatigue properties can be used to construct the strain-life curves of each rail steel similar to those shown in Figure 5.

is due to unstable fracture (pop-in) before the final fracture and has been observed in other rail steels(16-18). In several specimens, pop-in occurred twice and this behavior is referred to as Type IIa in Table 6 and Figure 6. In this case, the first pop-in load was considered as P_Q . Using P_Q and P_{max} values defined in Figure 6, K_Q and K_{max} values of each specimen were calculated. ASTM Specification E399-81 requires the use of K_Q for determining K_{Ic} , the plane-strain fracture toughness. One of the validity criteria for K_{Ic} is that the ratio $K_{max}/K_Q \leq 1.10$. However, many specimens did not meet this requirement. Consequently, both K_Q and K_{max} values are presented in Table 6 as measures of the fracture toughness, as has been done elsewhere(17,18).

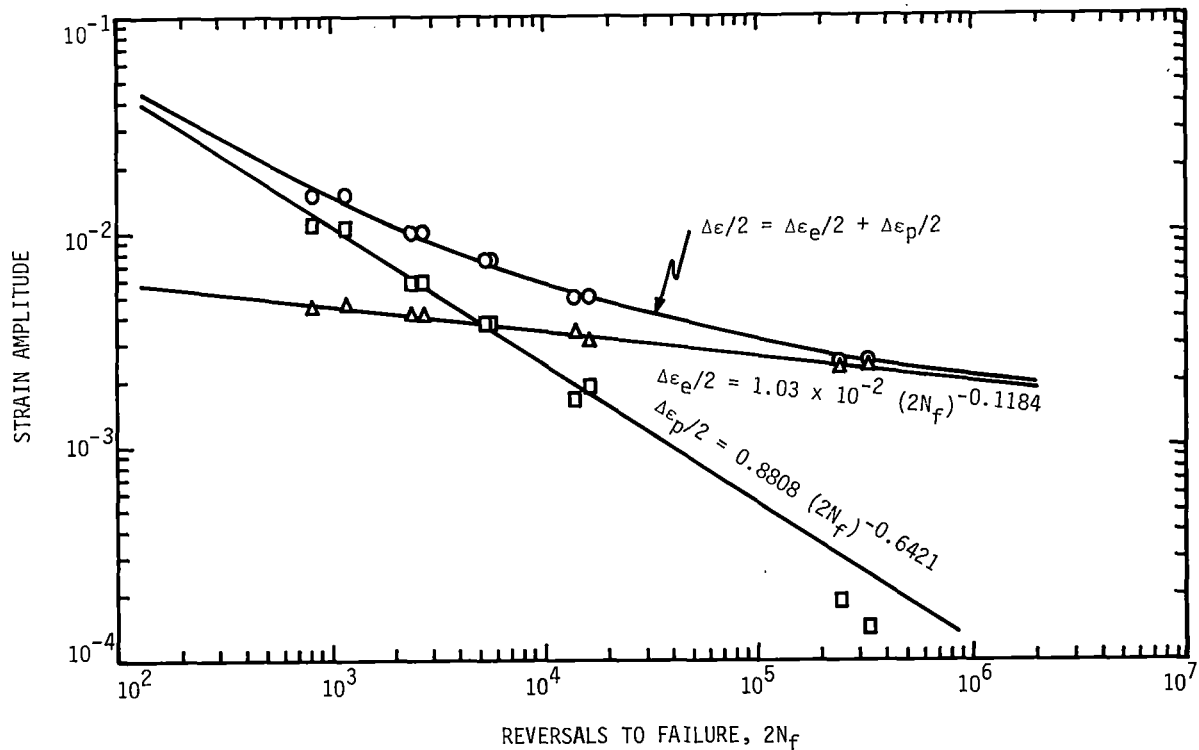


Fig. 5 Strain-life curves for Cr-Mo rail steels

Table 5 - Fatigue Properties of Rail Steels

Rail Steel	Fatigue Strength Coefficient, σ_f' MPa (ksi)	Fatigue Strength Exponent, b	Fatigue Ductility Coefficient, ϵ_f'	Fatigue Ductility Exponent, c
Carbon	1609 (233.4)	-0.1223	0.3982	-0.5313
HH	2072 (300.6)	-0.1203	0.5935	-0.5923
Cr-Mo	2089 (302.9)	-0.1184	0.8808	-0.6421
Cr-V	1762 (255.5)	-0.1098	0.5747	-0.6047

Fracture Toughness

The room temperature fracture toughness test results are presented in Table 6. Most of the Cr-Mo and Cr-V rail specimens exhibited Type II load-displacement curves(9) (Figure 6). This behavior

Another validity criterion for K_{Ic} is that $2.5 (K_Q/\sigma_{ys})^2$ is less than the thickness of the specimen ($\sigma_{ys} = 0.2\%$ offset yield strength in tension). The specimens of the carbon rail did not meet this requirement, while all the specimens of the Cr-Mo and Cr-V rails satisfied the requirement.

K_Q and K_{max} for the Cr-Mo rail and the carbon rail were virtually the same. The Cr-V rail exhibited much lower fracture toughness values than the carbon rail and the Cr-Mo rail. The average K_Q values for the carbon, Cr-Mo, and Cr-V rails were 48.0, 47.3, and 31.7 MPa \sqrt{m} (43.7, 43.1, and 28.8 ksi $\sqrt{in.}$), respectively.

DISCUSSION

Monotonic and cyclic stress-strain curves of the rail steels show that all four steels cyclically

soften at very low strains and harden at higher strains. As a consequence of the softening at low strains, the use of monotonic tensile properties, for example, in predicting the plastic flow in the rail head under cyclic wheel loading can underestimate the true plastic flow at a given load. On the other hand, the cyclic hardening behavior of the carbon rail gives a good quantitative measure of what happens to rails after they have "work-hardened" in service. It is well known that carbon rails placed in light duty service subsequent to being used in heavy haul lines exhibit improved wear resistance. Such an improvement is explained by the fact that the cyclic stress-strain curve of carbon rail exhibits higher strength than the monotonic stress-strain curve. However, all three high strength rails exhibit considerably higher strength than the carbon rail at given strains, indicating that the high strength rails would show less plastic deformation than the carbon rail under a given cyclic loading condition.

The strain-life curves of each rail can be constructed by applying the fatigue parameters in Table 5 to Equation (6). These strain-life curves are presented in Figure 7. Instead of a full logarithmic scale as in Figure 5, Figure 7 is presented in a semi-logarithmic scale to expand the strain axis. The HH and the Cr-Mo rails have superior fatigue resistance compared to the carbon rail. The Cr-V rail shows longer fatigue lives than the carbon rail at strains smaller than 0.4% but the reverse is true at strains larger than 0.4%.

The strain-life curves, however, do not give a complete picture of a rail steel's resistance to fatigue because the cyclic stress-strain response of each rail steel is not the same. As mentioned

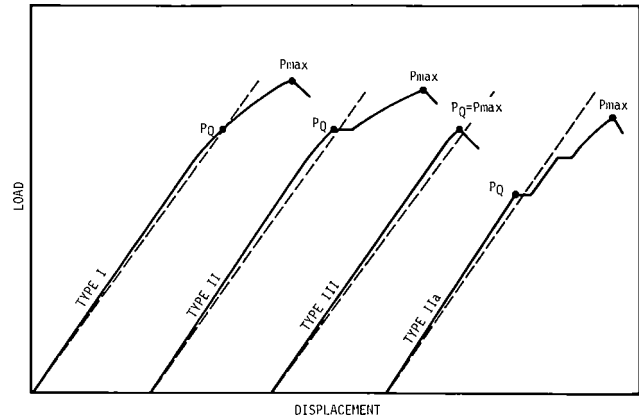


Fig. 6 Types of load-displacement curves observed in fracture toughness tests of rail steels. The dotted lines are drawn through the origins of the test records with slopes which are 95% of the slopes of the initial linear part of the records.

earlier, the carbon rail would deform more than the high strength rails under a given cyclic loading condition. To account for this difference, the strain-life curves may be converted to the stress-life (S-N) curves using the coefficients (K' and n') of the cyclic stress-strain curves. The S-N curves of the rail steels are presented in Figure 8. As expected, all three high strength rails exhibit much longer fatigue lives than the carbon rail at all stress levels. On the average, the Cr-V rail

Table 6 - Room Temperature Fracture Toughness of Rail Steels

Rail Steel	Specimen Number	Specimen Thickness mm (in.)	Curve Type	K_Q		K_{max}	
				MPa \sqrt{m}	(ksi $\sqrt{in.}$)	MPa \sqrt{m}	(ksi $\sqrt{in.}$)
Carbon	1	12.7 (0.5)	I	54.1	(49.3)	70.1	(63.8)
	2	12.7 (0.5)	I	51.7	(47.0)	52.6	(47.9)
	3	12.7 (0.5)	I	46.7	(42.5)	48.3	(44.0)
	4	19.1 (0.75)	II	43.2	(39.3)	44.8	(40.7)
	5	19.1 (0.75)	III	46.8	(42.6)	46.8	(42.6)
	6	19.1 (0.75)	I	45.4	(41.3)	61.9	(56.3)
Average:				48.0	(43.7)	54.1	(49.2)
Cr-Mo	1	12.7 (0.5)	II	53.1	(48.3)	56.8	(51.7)
	2	12.7 (0.5)	II	50.3	(45.8)	56.0	(50.9)
	3	12.7 (0.5)	II	47.0	(42.8)	48.3	(44.0)
	4	19.1 (0.75)	I	47.5	(43.2)	54.4	(49.5)
	5	19.1 (0.75)	II	41.9	(38.2)	49.9	(45.4)
	6	19.1 (0.75)	IIa	44.2	(40.2)	50.0	(45.5)
Average:				47.3	(43.1)	52.6	(47.8)
Cr-V	1	12.7 (0.5)	II	32.4	(29.5)	37.8	(34.4)
	2	12.7 (0.5)	II	31.1	(28.3)	37.2	(33.9)
	3	12.7 (0.5)	IIa	32.4	(29.5)	36.8	(33.5)
	4	12.7 (0.5)	IIa	30.7	(27.9)	37.9	(34.5)
Average:				31.7	(28.8)	37.4	(34.1)

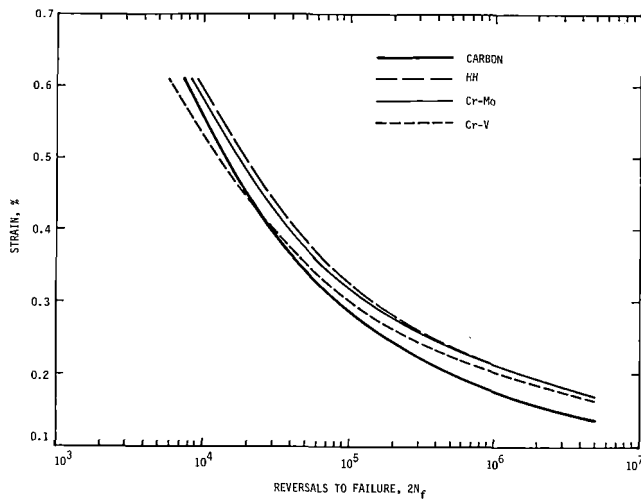


Fig. 7 Comparison of strain-life curves of the rail steels

exhibits about five times longer fatigue lives than the carbon rail, and the HH and the Cr-Mo rails show about ten times longer fatigue lives than the carbon rail.

Results from the rail metallurgy experiment at FAST support the laboratory results showing the superior fatigue resistance of the HH and the Cr-Mo rails. During the experiments at FAST, standard carbon rail exhibited the greatest number of rail head fatigue type failures. For example, in test conditions where a state of generous lubrication existed, standard carbon rail had five head-type fatigue defects, HH rail had only one head defect, and Cr-Mo rail had no head type failures in Section 03 of the FAST track(2). As mentioned earlier,

it was also observed at FAST that when rail wear rate decreased substantially because of the generous lubrication, appreciable lengths of rail section had to be replaced due to fatigue failures. It was also pointed out that recent analyses(5-7) have shown that rail life in tangent track for wheel loadings above 72 metric ton (80 ton) cars is determined by fatigue, not by wear. In these situations where fatigue is a problem, high strength rails, which are currently used by railroads mainly for good wear resistance in curved track, can also be used to improve the rail fatigue life.

Fracture toughness test results show that the Cr-Mo rail and carbon rail exhibit similar fracture toughness. This finding is in agreement with another recent investigation(18). However, some reduction of fracture toughness was observed for the Cr-V rail. The reason for this reduction may be associated with the fact that the vanadium-containing rail steels often contain vanadium carbide precipitates(19,20). The precipitates strengthen the rail steel but at the same time may deteriorate the fracture toughness of the steel. Fracture toughness of the HH rail could not be determined because of the gradation in hardness and microstructure which resulted from the head hardening process. While no conclusion could be made on the fracture toughness of the HH rail, it is expected to be comparable to the carbon and Cr-Mo rails.

Since fracture toughness is a measure of the resistance of a material to rapid (often brittle fracture) crack growth from an existing crack, it can be concluded that the carbon and the Cr-Mo rails have better resistance to rapid crack growth than the Cr-V rail. In other words, the carbon and Cr-Mo rails can tolerate either larger cracks or higher stresses before the final failure of the entire rail section than can the Cr-V rail.

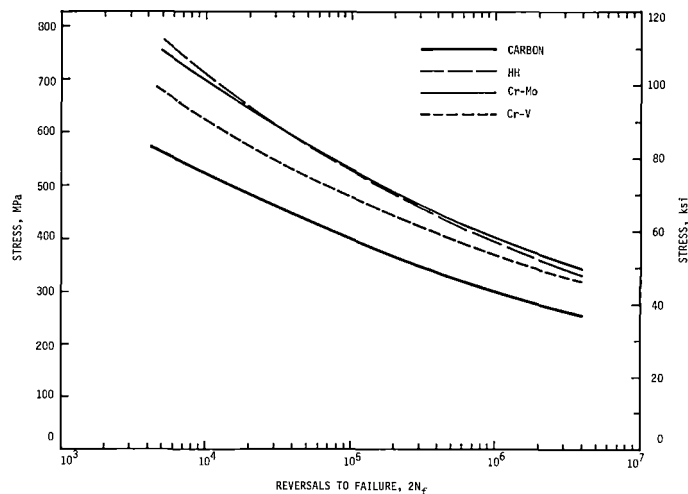


Fig. 8 Comparison of stress-life (S-N) curves of the rail steels

SUMMARY

Head hardened, Cr-Mo, and Cr-V high strength rails exhibit fatigue resistance superior to that of standard carbon rail. Therefore, the high strength rails can be used in situations where fatigue is a problem, as well as their traditional application for high wear resistance. The Cr-Mo rail and carbon rail exhibit similar fracture toughness, while the Cr-V rail is significantly less tough.

REFERENCES

- 1 Marich, S., "Development of Improved Rail and Wheel Materials," Proceedings of Seminar on Vanadium in Rail Steels, VANITEC, 1979, pp. 23-40.
- 2 "Evaluation of Rail Wear at the Facility for Accelerated Service Testing," FAST Technical Note, FAST/TTC/TN-80/04, Pueblo, CO, March 24, 1980.
- 3 Steele, R.K., "Observations of In-Service Wear of Railroad Wheels and Rails under Conditions of Widely Varying Lubrication," ASLE Preprint No. 91-LC-2B-4, American Society of Lubrication Engineers, October 5-7, 1981.
- 4 "Rail Failures, Second Metallurgy Experiment," FAST Technical Note, FAST/TTC/TN-80/07, Pueblo, CO, August 7, 1980.
- 5 Zarembski, A.M., "Effect of Rail Section and Traffic on Rail Fatigue Life," AAR Report No. R-391, Association of American Railroads, Chicago, IL, August 1979.
- 6 Zarembski, A.M., "Effect of Increasing Axle Loads on Rail Fatigue Life," AAR Report No. R-485, Association of American Railroads, Chicago, IL, June 1981; Published in AREA Bulletin 685, American Railway Engineering Association, Vol. 83, Nov.-Dec. 1981, pp. 132-143.
- 7 Final Report of the Engineering Panel for the Cost Analysis Organization Subcommittee on the Economics of the "80" vs. "100" Ton Cars, Association of American Railroads, Washington, D.C., July 1981.
- 8 Morrow, J., Wetzel, R.M., and Topper, T.H., "Laboratory Simulation of Structural Fatigue Behavior," ASTM STP 462, American Society for Testing and Materials, 1970, pp. 74-91.
- 9 "Standard Test Method for Plane-Strain Fracture Toughness of Metallic Materials," ASTM E399-81, Annual Book of ASTM Standards, Part 10, ASTM, Philadelphia, 1981, pp. 588-618.
- 10 "Standard Recommended Practice for Constant-Amplitude Low-Cycle Fatigue Testing," ASTM E606-80, Annual Book of ASTM Standards, Part 10, ASTM, Philadelphia, 1981, pp. 711-728.
- 11 Raske, D.T. and Morrow, J., "Mechanics of Materials in Low Cycle Fatigue Testing," ASTM STP 465, American Society for Testing and Materials, 1969, pp. 1-25.
- 12 Dabell, B.J., Hill, S.J., and Watson, P., "An Evaluation of the Fatigue Performance of Conventional British Rail Steels," ASTM STP 644, D.H. Stone and G.G. Knupp, Eds., American Society for Testing and Materials, 1978, pp. 430-448.
- 13 Leis, B.N., "Cyclic Inelastic Deformation and Fatigue Resistance Characteristics of a Rail Steel," ASTM STP 644, D.H. Stone and G.G. Knupp, Eds., American Society for Testing and Materials, 1978, pp. 449-468.
- 14 Park, Y.J. and Stone, D.H., "Cyclic Behavior of Class U Wheel Steel," Trans. ASME, Journal of Engineering for Industry, Vol. 103, February 1981, pp. 113-118.
- 15 Sunwoo, H., "Cyclic Stress-Strain Relations and Fatigue Crack Initiation in Pearlitic Eutectoid Rail Steels," Ph.D. Thesis, Northwestern University, Evanston, Illinois, 1981.
- 16 Fowler, G.J. and Tetelman, A.S., "The Effect of Grain Boundary Ferrite on Fatigue Crack Propagation in Pearlitic Rail Steels," ASTM STP 644, D.H. Stone and G.G. Knupp, Eds., American Society for Testing and Materials, 1978, pp. 363-386.
- 17 Fletcher, F.B. and Biss, V.A., "Microstructural Variations in Alloy Rail Webs," Climax Report No. L-311-09, Climax Molybdenum Co., Ann Arbor, MI, April 28, 1977.
- 18 Parsons, D.E., "Web Fracture-Toughness of Four Steel Rails," Lab Report MRP/PMRL 79-68 (TR), CANMET, Energy, Mines and Resources Canada, June 1980.
- 19 Marich, S. and Curcio, P., "Development of High-Strength Alloyed Rail Steels Suitable for Heavy Duty Applications," ASTM STP 644, D.H. Stone and G.G. Knupp, Eds., American Society for Testing and Materials, 1978, pp. 167-211.
- 20 Rantanen, H. and Rasanen, E., "A Study of the Microstructures of the Experimental Steels Made at Ghent University," Proceedings of Seminar on Vanadium in Rail Steels, VANITEC, 1979, pp. 16-21.

The Development of a Second Generation of Alloy Steel Rails for Heavy Haul Applications

W.H. Hodgson

BSC Track Products
Teesside Laboratories
England

R.R. Preston

BSC Teesside Research
Laboratories
England

J.K. Yates

BSC Track Products
Teesside Laboratories
England

For many years, premium quality rails having a surface hardness of HB 320/340 and a 0.2% proof stress of about 650 MPa (94 ksi) have been produced either by alloying or by separate heat treatment operation. A new technique has been developed for the enhanced cooling of the rail on the mill banks so that only the head is hardened. This has allowed BSC to produce 1% Cr steel rails with head hardnesses above HB 360 and 0.2% proof stresses above 690 MPa (100 ksi). Similarly, ARA type rails can now be provided with head hardnesses in excess of HB 300. The technique is currently being used to develop a lower alloy rail in which the hardnesses of the flash butt welds will match those of the rail head after a normal welding cycle.

1. INTRODUCTION

The demand for high strength, wear resistant rails is one which is likely to continue for many years as increasing quantities of basic raw materials are transported over considerable distances for processing or shipping. For example, in a typical iron ore development it may be necessary to transport about 50 MGT per annum, over distances of 200 to 400 km, through virgin country which imposes severe track restrictions. Good track design and the maintenance of rail head profile by grinding can reduce wear on straight lines and curves of up to 3° but local geography will often impose the need to use curves of smaller radius and these continue to give rise to severe wear problems. In such situations it is not uncommon to find that currently available rails achieve less than two years service in track.

Most wear resistant rails were developed at a time when a high proportion of the track was joined by fishplates and bolts. However, the increasing use of continuously welded track during recent years has required railmakers to ensure that their premium quality products not only possess adequate strength but also can be readily joined by flash butt or Thermit welding.

2. MICROSTRUCTURE

There is now considerable evidence^(1,2,3) to show that a steel having a fully lamellar pearlite microstructure, Figure 1 will exhibit better resistance to severe abrasion than either a bainitic or martensitic material of equal tensile strength and hardness.



FIGURE 1 Lamellar Pearlite Microstructure
X 10,000

Hyzak and Bernstein⁽⁴⁾ have further shown that the flow stress of such a steel is strongly influenced by the interlamellar spacing of the ferrite and cementite laths in the pearlite. Thus any wear resistant rail designed for use under heavy axle loads should be made from a fully pearlitic steel having the finest possible interlamellar spacing.

Work in the BSC Laboratories has shown that the abrasive wear resistance of rail steel is a function of its hardness, Figure 2,

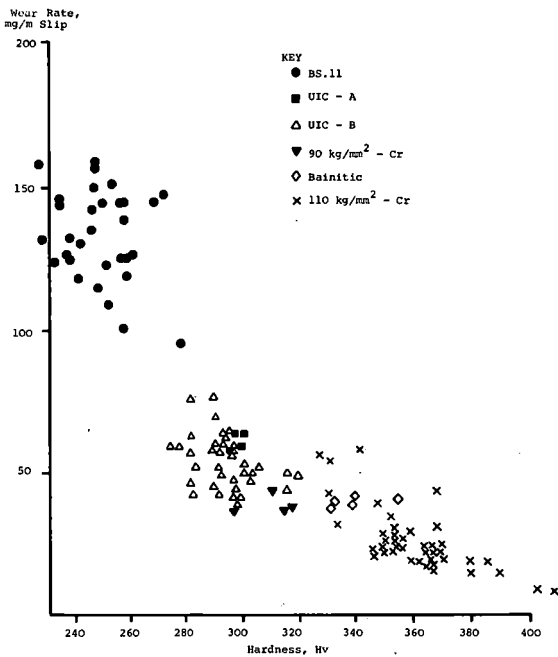


FIGURE 2 Effect of Rail Hardness on Rate of Abrasive Wear

while the hardness, in turn, increases as the interlamellar spacing of the pearlite is decreased, Figure 3.

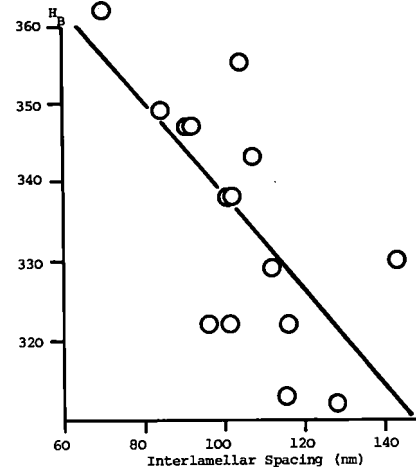


FIGURE 3 Effect of Interlamellar Spacing on Hardness of Pearlite

3. PEARLITIC RAIL STEEL

Wear resistant rails are usually made from killed steel containing 0.70 to 0.82%C and 0.6 to 1.2%Mn. The fineness of the pearlite in the microstructure is controlled by the temperature and rate at which transformation from austenite to ferrite/cementite takes place. Transformation temperature is currently controlled by either the forced cooling of plain carbon steel rails or by the natural cooling of alloy steel products, as shown schematically in Figure 4. Each method has its relative advantages and disadvantages.

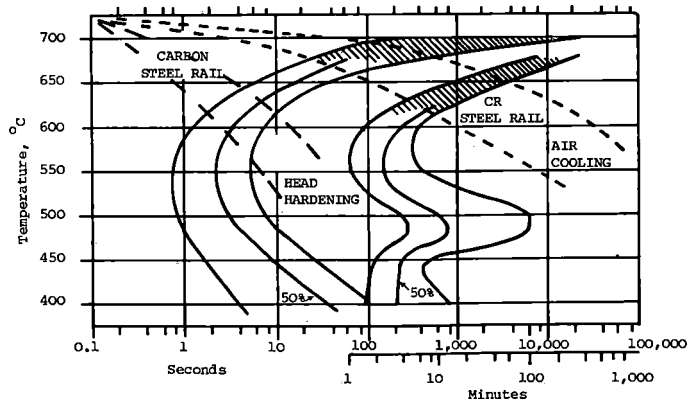


FIGURE 4 Transformation Characteristics of Plain Carbon and Alloy Rail Steels

3.1. Heat Treated Rails

- a) Plain carbon steel can normally be used so steelmaking costs are low.
- b) Substantial expenditure on capital plant is necessary.
- c) Many rails are only head-hardened in which case a softened zone of spheroidized pearlite is formed in the centre of the rail head where temperatures of only about 700°C (1290°F) are attained during the heat treatment process.
- d) Rails can be readily flash butt welded using standard procedures for normal quality sections.

3.2. Alloy Steel Rails

- a) Steelmaking costs higher due to alloy additions.
- b) No extra capital plant required.
- c) Much greater depth of hardening observed in rail head compared with head hardened products.
- d) Greater control required and possibly some post weld heating needed to avoid hard spots in flash butt welded joints.

Experience in track has generally shown that alloy rails last longer than head hardened products of similar hardness. This may in part be due to the fact that alloy rails exhibit more uniform hardening than heat treated products and there is also the possibility that the alloy additions give rise to solid solution hardening and increase the work hardening rate of the rail steel.

Thus while considerable effort has been expended, by railmakers, to refine the techniques of using either alloy additions or heat treatment to control the transformation behaviour of rail heads, very little attention has so far been paid to the rolling process as a metallurgical asset. Most rail mills merely aim to roll the product within a certain broad temperature range in order to produce a section within a defined shape and dimensional limits while avoiding the generation of excessive roll separating forces. If, however, one observes the temperature profile of such a rail, as it leaves the final mill stand to travel to the hot-saw, it can be seen to be in a metallurgically advantageous condition. The head and the upper part of the web have surface temperatures in the

range $900/850^{\circ}\text{C}$ ($1650/1560^{\circ}\text{F}$) while the thin foot tips have surface temperatures in the range $650/700^{\circ}\text{C}$ ($1200/1290^{\circ}\text{F}$), Figure 5.

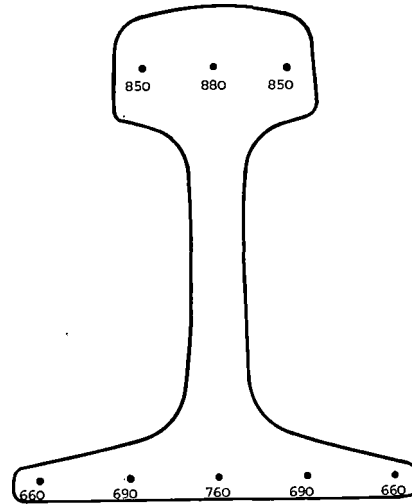


FIGURE 5 Temperature ($^{\circ}\text{C}$) Profile of Rail at Hot Saw

At this stage, it is important to avoid any acceleration in the overall cooling rate as there would be a significant risk that the toes of the rails would transform to a brittle martensitic microstructure. However, it is possible to use careful process control to exploit the temperature gradients in the rail.

4. ENHANCED RAIL COOLING

BSC (Track Products) have produced a chromium alloyed rail, of nominal tensile strength 110 kg/mm^2 (1080 MPa) for many years.⁽⁵⁾ Laboratory trials, on samples of the above rails, showed that accelerated cooling of the rail head prior to transformation could ensure the development of a fine pearlitic microstructure having hardness levels up to $H_B 400$ with 0.2% proof stress and tensile strengths up to 750 and 1200 MPa respectively.

Subsequent plant trials using powerful air fans placed underneath the cooling banks showed that similar mechanical properties could be developed in the heads of full rail lengths. A considerable amount of development work then took place to establish a production procedure in which the rolling temperature, rail spacing and air flow rates are controlled so that accelerated cooling of the rail head takes place only after the rail foot has transformed to pearlite.

Use of this procedure allows one to produce a rail in which the heavy head and thin toes have very similar mechanical properties.

The microstructure in the head of an enhanced cooled, chromium rail consists of very fine pearlite having an interlamellar spacing of about 80 nm immediately below the running surface and gradually coarsening to about 100 nm in the centre of the head. The almost exclusive use of continuously cast blooms for rail production by the BSC ensures that the product is virtually free from segregation and it is found that the centre of the head, the web and the foot all possess very similar microstructures.

A typical hardness profile is illustrated in Figure 6

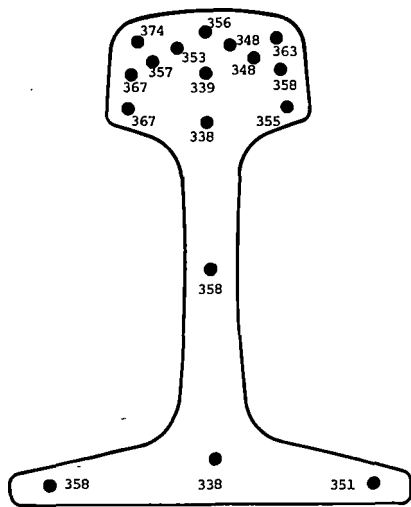


FIGURE 6 Brinell Hardness Profile of Enhanced Cooled, Chrome Steel Rail

from which it can be seen that the running surface and the sides of the head possessed hardnesses in the range H_B 355/375 decreasing to H_B 340 in the centre of the head. The web centre and foot tips possessed hardness values in the range H_B 350/360 while the heat-retaining web/foot junction resembled the centre of the head. Similar measurements carried out on a sample of head hardened rail (USS-Curvemaster) showed a hardness of H_B 339 immediately below the running surface falling to H_B 235 in the centre of the head. Hardness surveys were carried out around the "working surface" of about 450 slices of enhanced cooled, chromium rail, Figure 7 and the mean value was found to be H_B 361 with a standard deviation of 10.3

	Tensile Strength (MPa)		0.2% Proof Stress (MPa)		% Elongation	
	\bar{x}	S	\bar{x}	S	\bar{x}	S
Standard Rail	1097	25.4	655	26.1	8.0	1.1
Enhanced	1163	28	741	31	10.1	1.3

TABLE 1

Clearly a substantial increase in strength was obtained without any loss of ductility. The spread of observed proof stress and tensile strength values is plotted in Figure 8 from which the benefits derived from enhanced cooling are clearly visible.

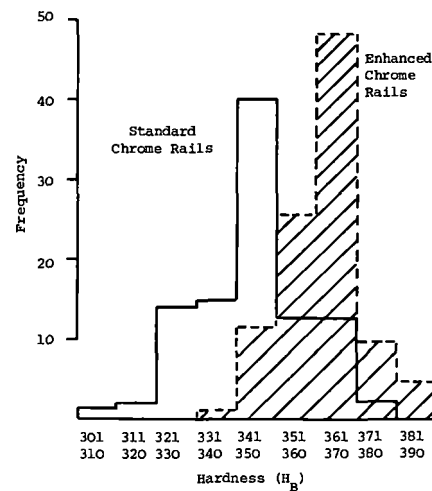


FIGURE 7 Distribution of Hardness Values Near Working Surfaces on Rail Head of Chrome Steel Rails

The results quoted above were obtained from test pieces taken from the mid-point of one half of the rail head as defined as BS 11 (1978). Measurements made on samples from positions nearer to the hardened surface provided even higher strength values:

Tensile Strength MPa		0.2% Proof Stress MPa		%Elongation	
\bar{x}	S	\bar{x}	S	\bar{x}	S
1191	31.6	790	42.4	11.4	1.2

TABLE 2

5. FURTHER DEVELOPMENTS

The proven ability to cool a rail head, on the banks, at a controlled rate has led to further promising developments.

5.1. It has been possible to reduce the upper limits on chromium and manganese content while still providing a mean surface hardness of H_B 365. This has led to a 8

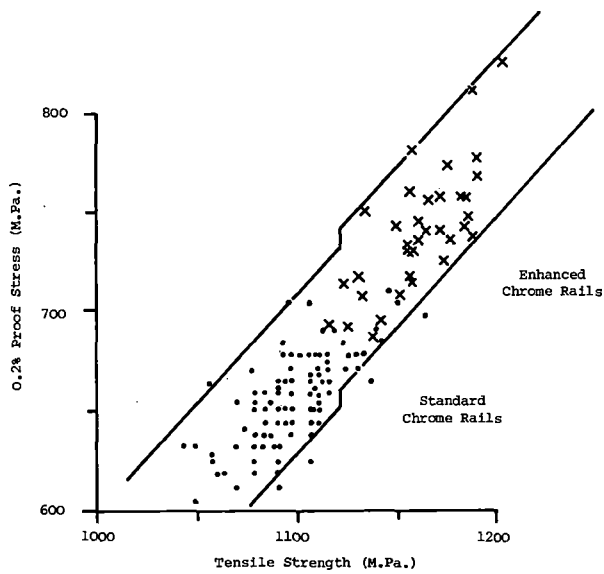


FIGURE 8 Tensile Properties of Chrome Steel Rails

useful improvement in the weldability of the rails.

5.2. Further increases in rail head cooling rate have allowed material selected from the richer end of the composition range to be processed to rails having hardness levels in excess of H_B 380. Such products can be of value in tight curves on heavy haul track.

5.3. The production route based on enhanced cooling has also been applied to rails based on the standard AREA composition. Useful improvements in mechanical properties are achieved as shown in the table below:

TABLE 3

	Tensile Strength MPa		0.2% Proof Stress MPa		% Elongation		H_B	
	\bar{x}	S	\bar{x}	S	\bar{x}	S	\bar{x}	S
Standard	928	26.4	485	15.2	11.4	0.6	261	10.2
Enhanced	946	12.89	549	16.5	12.2	1.1	282	8.5

The value of enhanced cooling of AREA type rails is illustrated in Figure 9.

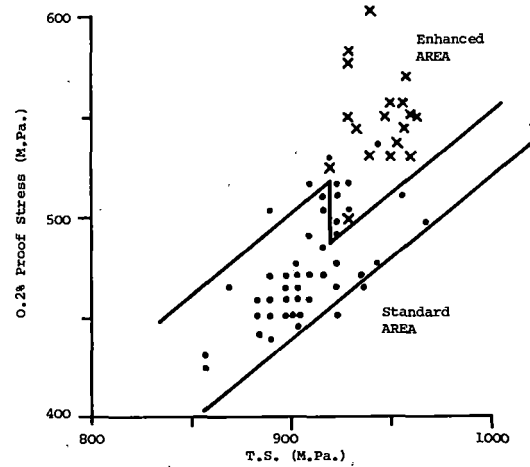


FIGURE 9 Tensile Properties of AREA Rails

5.4. Further increases in surface hardness of AREA type rails can be achieved either by the use of even higher rail cooling rates or by using "high residual" steels at current fan cooling rates. Both routes are under development for the production of a new grade of rail having a minimum surface hardness of H_B 300. Such rails should be of great value in tangent track and shallow curves on heavy haul railroads.

5.5. The most exciting development involves the use of steel composition and controlled cooling combinations to provide wear resistant rails which can be readily joined by normal flash butt welding procedures and where the hardness of the weld will match that of the rail head.

The majority of joints between such rails are made by flash-butt welding. In this process the rail ends to be jointed are held in copper grips which act as both clamps and electrodes. Preheating is achieved by applying a number of high current (60-90 kA) impulses across the interface between the two rails. They are then parted sufficiently to establish a low voltage arc or flashing action which cleans the rail ends and ensures uniform heating. The rails are then forced together under a hydraulic force of 40 to 60 tonnes so that molten and soft steel is forced out of the joint. This extruded material is then quickly removed by shearing and grinding. The remaining steel in the region of the joint is in the hot forged condition and Vines and Lancaster⁽⁶⁾ have reported it to possess an austenite grain size of about 70 μm (ASTM 4/5).

This weld material then proceeds to cool down passing through the transformation range 720 to 500°C (1328 to 928°F) at a rate reported by Marich and Curico⁽⁷⁾ for 65.5 kg/m (132 lb/yd) rails to be 1.1 °C/s (2.0 F°/s). Fletcher⁽⁸⁾ reported a rate of 1.0°C/s (1.8 F°/s) for similar sized rails while Pell⁽⁹⁾ has reported a cooling rate of 0.7°C/s (1.3 F°/s) between 800 and 400°C (1472 and 752°F) for 56.4 kg/m (113 lb/yd) rails. For a plain carbon steel, of the AREA type, this results in a fully pearlitic structure having a hardness of approximately H_B 296 (33Rc). Such rails supplied in the hot-rolled condition would probably have a head hardness of H_B 260 (29Rc); hence that region of the weld close to the joint will be harder than the parent rail. If, on the other hand, a rail of the same composition was supplied in the heat treated condition it would probably have a surface hardness of H_B 340 (37 Rc) and, in this case, the weld would be softer than the parent rail.

During the forging operation there is a narrow zone, in each rail, in which the microstructure is still pearlitic, but the temperature is in the range 600 to 700°C (1112 to 1292°F). Robbins et al⁽¹⁰⁾ have shown that when pearlite is deformed in this temperature range the cementite lamellae rapidly spheroidize and the hardness of the steel falls. Thus a narrow softened zone is usually observed on each side of the main

weld zone. This is illustrated in Figure 10.

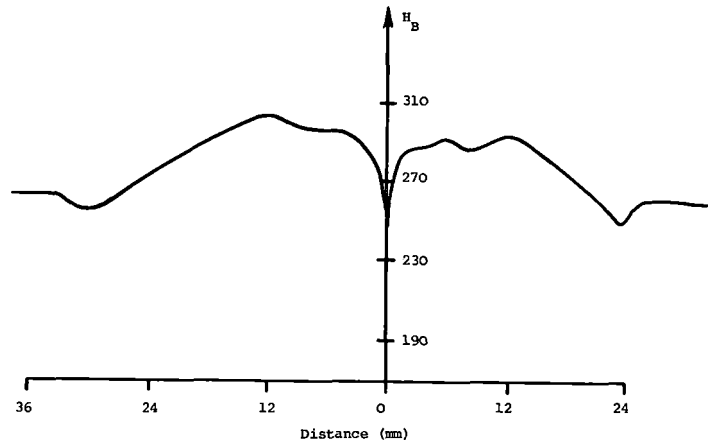


FIGURE 10 Hardness Profile Across Flash Butt Weld Between Two AREA Rails

which shows a hardness traverse across the head of a typical flash-butt weld between two AREA rails.

When alloy steel rails of the 1% Cr type are flash-butt welded in the simple manner described above, the region near the joint will always be harder than the parent rail because the head cooling rate on the rolling mill banks is typically 0.2°C/s (0.36 F°/s) over the range 720 to 500°C (1328 to 928°F) whereas the weld zone will normally cool at least four times faster. In order to avoid the formation of very hard weld zones between such rails it is normal to supply heat to the joint after the forging stroke in order to reduce the cooling rate in this region. This, of course, tends to increase the time and cost involved in the flash-butt welding of alloy steel rails.

Clearly the ideal situation would be to supply rails of a composition and processing route such that after normal flash-butt welding the weld zone would possess a hardness equal to that of the parent rails. The magnitude of this hardness would have to be sufficiently high to resist rail head wear under the relevant operating conditions. In the case of heavy haul railroads the accepted value seems to be about H_B 340 (37 Rc). Thus the composition of the steel should be chosen so that after a standard flash-butt welding operation, the austenite, in the joint having a grain size of about 70 μm , could cool through the temperature range 720 to 500°C (1328 to 928°F) at the rate of 1.1 °C/s (2.0 F°/s) and transform into lamellar pearlite with a hardness of H_B 340 (37 Rc). In order to develop this level of hardness the mean interlamellar

spacing of the pearlite will need to be approximately 97 nm, Figure 3.

In addition, the cooling rate of the rail heads on the mill banks must be controlled so that an identical microstructure is developed in the rolled product. This cooling rate may not necessarily be the same as that observed in the flash-butt weld because the austenite grain size of the hot rolled rail head may differ from that of the hot-forged weld. In the case of the BSC rail mill, at Workington, the austenite grain size of the rail heads just prior to transformation is in the range 60-90 μm (ASTM 4-5) and therefore the relevant cooling rate would be expected to be very close to 1.1 $^{\circ}\text{C}/\text{s}$ (2.0 $^{\circ}\text{F}/\text{s}$).

At the beginning of this work the two main problems were therefore to:

- a) identify a suitable steel composition,
- b) provide a reliable form of enhanced cooling on the mill banks at Workington.

Experimental ingots of steel containing 0.70% C, 0.30% Si and 1.10% Mn with varying chromium contents were rolled, in a laboratory mill, using a schedule designed to simulate the rolling and cooling of a rail head at Workington Works. It was then possible to plot a graph of hardness versus chromium content for normally processed rails, Figure 11.

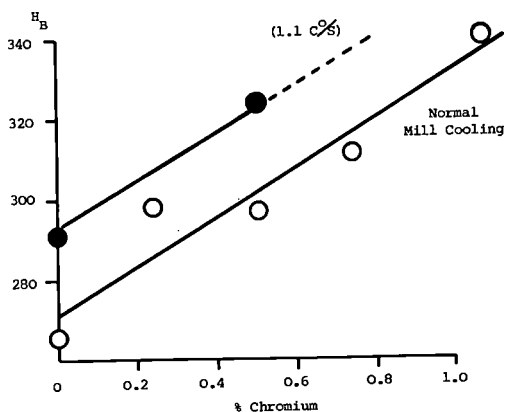


FIGURE 11 Effect of Chromium Content on Hardness of 0.7 %C, 1.1% Mn Rail Steel

In subsequent experiments similar ingots were rolled to the same schedule but the surface cooling rate after rolling was increased to 1.1 $^{\circ}\text{C}/\text{s}$ (2.0 $^{\circ}\text{F}/\text{s}$). The hardness values for these samples are also shown in Figure 11 from which it can be seen that, at the higher cooling rate, the chromium content could be reduced to approximately 0.8% and the rails would still possess a surface hardness of about H_B 340. Similar experiments were carried out for steel samples with varying manganese contents and it was shown that over the range 0.5 to 1.0% the effect of manganese on surface hardness was very similar to that of chromium. Current experiments therefore involve the use of the accelerated cooling facility on the mill banks at Workington to process a number of rail steel heats having suitably reduced chromium or manganese contents. The rails will then be flash-butt welded together and hardness traverses carried out across the joints.

6. CONCLUSIONS

6.1. A controlled cooling facility has been constructed on the BSC rail mill at Workington which allows one to increase the cooling of rail heads, prior to transformation to pearlite, without prejudice to the properties of the webs and feet.

6.2. This facility was used initially to increase the rail head hardness of products made from existing steel specifications. Subsequently it was used to provide wear resistant rails from slightly leaner steels having a restricted range of alloy contents.

6.3. Enhanced cooling has also been used to develop a "super AREA" type rail with a minimum surface hardness of H_B 300.

6.4. Current developments are aimed at the provision of a low alloy steel rail, with a surface hardness of about H_B 340, which on being flash-butt welded using a standard procedure will produce a weld zone of hardness identical with that of the rail head.

7. ACKNOWLEDGEMENTS

We would like to acknowledge the efforts of our colleagues in both BSC Track Products and the Teesside Research Laboratories who have provided the data used in this paper. Thanks are also required for the General Manager, BSC Cumbria and the Director Technical BSC for permission to publish the work.

REFERENCES

1. W Heller and R Schweitzer
Railway Gazette International, October
1980, pp 855-857.
2. S Bhattacharyya
Wear, 60, (1980) pp 133-141.
3. H Ichinose, J Takebara, N Iwasaki and
M Ueda
First Heavy Haul Conference. Session
307.
4. J M Hyzak and I M Bernstein
Met. Trans, 7A (1976). pp 1217-1224.
5. J D Young
First Heavy Haul Conference, Perth,
Australia September, 1978. Session 217.
6. M J Vines and G Lancaster
Metals Forum, 2 (1) (1979) pp 29-33.
7. S Marich and P Curcio
BHP Melbourne Research Laboratory
Report No. MRL/083/75/008, August, 1975.
8. F B Fletcher
Climax Report No J-4162-01 June, 1976.
9. G M Pell
British Rail, Technical Note TN-MET 22,
March, 1980.
10. J L Robbins, O C Shepard and O D Sherby
J.I.S.I., 202 (1964) pp 804-807.

P.J. Lugg

M. Welding. I.
 Assistant (Welding)
 Civil Engineering Dept.
 British Railways Board HQ
 Marylebone, London

B.R. Experience With Rail Welding

The welding of rails in the course of construction, maintenance and repair of the permanent way has been practiced on railways in Britain for over 50 years. Originally, gas welding was the predominant process used both for maintenance and joining of rails, but the programme of modernisation embarked upon in the 1950's introduced alternatives. Changes in the previous standard of track construction led to changes in welding procedures and processes. Continuous development and improvements in welding techniques have led to the current situation where the welding of rails is a normally accepted resource employed in good management of the permanent way. With improved quality control and staff training, the standard of welding has risen to a high level of reliability with, where applicable, new processes being embraced as they become available.

INTRODUCTION

The welding of rails in Britain is not a recent innovation. As long ago as 1820 John Birkenshaw proposed to weld together his 6m long wrought iron rails in an attempt to eliminate the problem associated with the great number of joints in "railways" then being constructed. It was however, not until the early 1920's that the use of the then available welding processes was seriously considered as a method of eliminating joints between rails and, also, to assist in the maintenance of crossings to a satisfactory standard.

The processes adopted at that time were gas welding (using oxygen and acetylene) and manual metal-arc (M.M.A.) with either bare wire or asbestos wrapped electrodes. The rail generally in use at that time was to British Standard Specification No. 9 (B.S.9), bullhead section, with (except in a few experimental sites where steel or concrete sleepers existed) timber sleepers to which cast iron chairs were fastened. With the exception of a few prestige express passenger trains, speeds were generally of the order of 110 - 130 k.p.h., with freight trains (consisting mainly of four-wheeled vehicles) having a maximum speed of 96 k.p.h. Steam locomotives were almost the only form of traction and the heaviest axle load (and this on a locomotive) was 22½ tons. Thus, the construction of the permanent way, the use to which it was subjected, and the requirements of any welding of rails undertaken were largely compatible, and a fair margin of tolerance was present in their relationships.

During the years immediately preceding the war, oxy-acetylene welding to build-up crossings, etc., was beginning to displace M.M.A. as the preferred process. Although gas welding was not without its problems (generally shelling-out of the deposited weld metal), several failures of the parent rail were occurring where M.M.A. welding maintenance had been carried out. (These failures were, much later, attributed to incorrect welding procedure.) With the difficulty of obtaining fuel for the mobile welding sets and the problems associated with their maintenance, the period 1939 - 45 saw the gas welding maintenance procedure established as the accepted standard, with M.M.A. used only in a few areas. This was the situation extensively obtaining at the time of Nationalisation (1.1.48) and, in respect of maintenance welding of rails, was little changed when the British Railways Modernisation Plan was announced in January, 1955.

The Modernisation Plan initiated major changes in the previous character of the railway; changes that were in due course to considerably affect the role of rail welding in both construction and maintenance of the permanent way. On main lines, initially, continuous welded rail (C.W.R.) of flat bottom section was to be installed on either concrete or hardwood sleepers. The steam locomotive was to be phased out and replaced by diesel, diesel-electric or electric traction, and a general trend towards higher speeds was encouraged. The need for long welded rails (L.W.R.) stimulated the establishment of production lines where rails, 18m long, could be flash welded into the longest practicable lengths, later to be welded into C.W.R., on site.

At this period, particular attention was focussed on these two welding functions, whilst the maintenance aspect of welding was often allowed to decline, although a large amount of this work was still carried out on all Regions to varying standards. It was only after many years of service

experience with the modernised railway system that the importance of maintenance and repair welding was fully appreciated and attention given to improving standards in its application. The experience obtained in adopting, employing and developing these rail welding applications on B.R. is outlined in the following pages.

FLASH WELDING

Prior to 1939, attempts to eliminate rail joints and to produce L.W.R. had been made by making joints using oxy-acetylene, electric-arc or alumino-thermic processes. However, the London Passenger Transport Board (L.P.T.B.) had undertaken a considerable programme of flash welded rail installation and, as a result largely of their experience, in 1954 a production line to manufacture L.W.R. by flash welding was commissioned at Redbridge (near Southampton) on the Southern Region. This plant enabled B.R. to produce rails of 183m length in the flat bottom rail section then being introduced, as well as the then extensively used bullhead section running rails and conductor rails.

The production line route and equipment installed at Redbridge set a broad pattern for the other L.W.R. production depots and lines subsequently operated by B.R. The production route favoured was generally as shown in FIGURE 1, with each of the operation stations positioned at 18m intervals. This arrangement allowed for the functions to be carried out concurrently, thus improving the rate of production. It was assumed, then, that the rate of production would be governed by the capacity of the

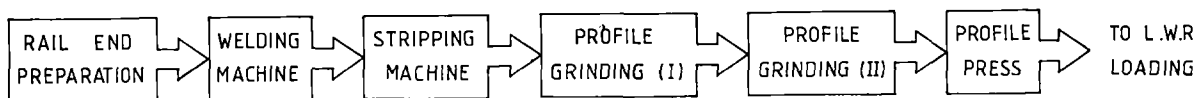
flash welding machine, and a rate of 8 welds per hour was considered acceptable. To meet the necessary criteria, the welding machine selected for that installation was designed and manufactured by Messrs. A.I. Welders Ltd., of Inverness, Scotland, and this choice was influenced by the experience gained with a similarly manufactured machine (although of older concept) which had given satisfactory service for many years producing the L.W.R. for the L.P.T.B. lines.

During the next eight years, rail welding depots (R.W.D.) were commissioned at five other locations (one on each of the then existing Regions) as follows:-

- 1956 CHESTERTON (Near CAMBRIDGE)
- 1958 CASTLETON (Near MANCHESTER)
- 1960 HOOKAGATE (Near SHREWSBURY)
- 1961 DINSDALE (Near DARLINGTON)
- 1962 MOTHERWELL (Near GLASGOW)

In this way, the whole of the B.R. network was reasonably conveniently served with a supply of L.W.R. in lengths of between 91.5m and 365.75m, dependent upon the geographical constraints of the supplying depot. The location of these depots is shown in FIGURE 2, and all of these are still in production and supplying the current needs of L.W.R. for B.R. Approximately 700 track km of new rail and 200 track km of serviceable (i.e. recovered, worn rail, subsequently re-used in lower category lines) are produced each year.

TYPICAL CURRENT ARRANGEMENT



PROPOSED FUTURE ARRANGEMENT

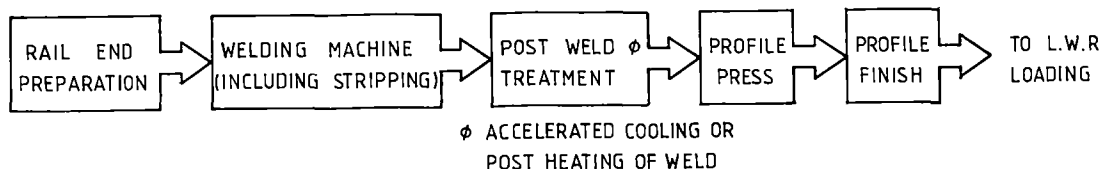


Fig.1 Long welded rail production routes



Fig.2 Location of rail welding depots

- | | |
|----------------|----------------|
| (1) Redbridge | (4) Hookagate |
| (2) Chesterton | (5) Dinsdale |
| (3) Castleton | (6) Motherwell |

The equipment in the depots is generally that originally installed, with only subsequent minor modifications, except in the cases of Redbridge and Motherwell Depots where the originally installed flash welding machines were replaced in 1963 and 1974 respectively. With the exception of Motherwell, where an APHF40/80 type machine is now installed, all the welding machines currently in use are of the APHF30/60 type, manufactured by A.I. Welders Ltd., and were designed to allow the welding of F.B.98 section rail (cross sectional area 6200mm²) in normal quality steel. It is testimony to their design that they are now satisfactorily welding rails of F.B.113A section (cross sectional area 7185mm²) generally of normal quality steel and, when required, of wear resisting qualities 'A' and 'B', 110kg chromium, and, more recently, low-carbon A.M.S. These machines are electro-pneumatic/hydraulic in operation and the welding parameters are set by manipulation and adjustment of hydraulic/pneumatic valves, electrical relays and timers, and mechanical stops. Some 1.6 million flash welds made by these machines are now

installed on B.R. and the quality of weld obtained from these machines is demonstrated by a level of breakage (in service) in 1980, of less than 4 per 100,000 installed in track. (See FIGURE 3)

Regular quality control checks are made to ensure that the standard of weld quality produced at each of the depots does not fall below the minimum acceptable standard. The test applied is either the falling weight (tup) test or slow bend test. The prescribed minimum standards for each test for welds made between new rails of F.B.113A section in normal quality rail steel are:-

Drop Weight Test

The weld must survive without breaking, and with a deflection of not less than 45.5mm, three "drops" (one each from 2135, 2745 & 3355mm) of a 1194kg weight. The weld being tested must be centrally positioned between supports 1220mm apart and when tested the rail (weld) foot must be in tension.

Slow Bend Test

The weld must sustain without breaking, a load of at least 121927kg, with a minimum deflection of 31.75mm. When tested the rail (weld) foot must be in tension.

The application of these standards appears to be ensuring that welds of a satisfactory quality are consistently produced; welds that break in service usually have their fracture originating from flat-spot (lens) type defects on the weld centre line or from "arc-burns" associated with the electrode contact arrangements. The great increase in the incidence of cracked flash welds reported from 1979 onwards (see FIGURE 3) is attributable to a single, well defined source. For many years, at some R.W.D.'s, the welding upset was removed by manual operation of pneumatic hammer and chisels. This inevitably led to notches being introduced into the remaining upset and, by a process of fatigue, these may grow into longitudinal horizontal cracks if the rail is allowed to remain in service for extended periods: such a defect is shown in FIGURE 4. The introduction of automatic weld upset trimming machines into all depots eliminated this problem, but a considerable number of hand trimmed welds remain in track and are being given special attention to ensure that any cracks are detected, and the weld removed if necessary.

B.R. has now embarked upon a programme of rationalisation of the existing depots, the aim being to reduce their number and improve the performance of those that remain. This will entail the renewal of all the major items in each of the remaining production lines and, where necessary, a re-arrangement of the sequence of the processing events. This latter requirement will allow the final profile finishing of the weld to be carried out with the weld at ambient temperature, rather than (as at present) whilst still hot from the welding operation. The proposed production route will be broadly as shown in FIGURE 1, and the first line to be established on this basis will be at Redbridge.

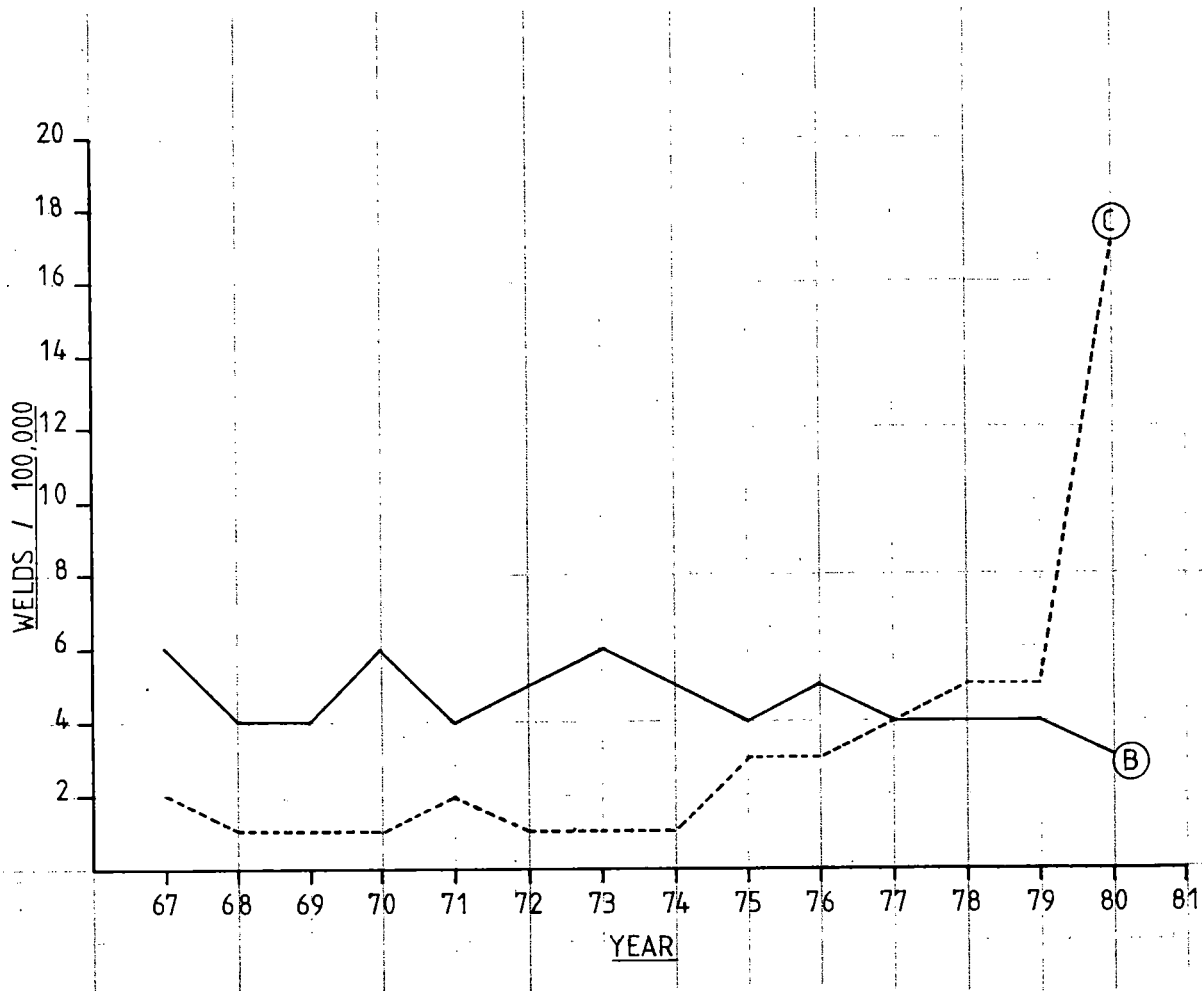


Fig.3 Broken and cracked flash welds for 100,000 population

(B) Broken
(C) Cracked

The welding machine selected for installation at Redbridge is, again, manufactured by A.I. Welders Ltd. and is due to be installed in mid-1982. It will have the capability of welding normal quality rail of a maximum cross sectional area of 10,000mm² at a continuous rate of 20 welds per hour. Having a forging load of 60964kg it will be possible to weld rails of wear resisting qualities 'A' and 'B' (the use of which is increasing on B.R.) 110kg chromium, and low-carbon A.M.S. rail without difficulty. A solid state control system with P.C.B.'s will be incorporated and this will be flexible enough to allow both coarse and fine control of all the necessary parameters. Consistency of quality will be enhanced by a closed-loop feed back control system, and verification of the quality of each weld produced will be obtained in the first instance by a monitoring system providing considerably more information than that which is obtained at the moment. For the first time (on B.R.), the decision has been taken to instal a flash welding machine (for rails) which also incorporates a weld upset trimming arrangement. (Previously, the weld upset has been removed by a separate machine placed downstream of

the welding machine, see FIGURE 1). Whilst it is appreciated that this proposed arrangement will reduce the overall production rate which can be achieved by using separate machines for welding and trimming, considerations of space and the advent of 36.5m rails for welding (and for which the new layout is designed) support the adoption of this change in philosophy.

In addition to the concern to produce welds of the highest possible standard, special attention is also being given to achieving the best possible obtainable alignment of the rail ends being welded and the profile of the finished weld and weld area. These most important aspects (particularly on high speed lines) have been the subject of considerable research, and the new welding machine will incorporate an automatic alignment system (to locate the rail ends within a tolerance of + 0.3mm in both vertical and horizontal planes) without any intervention by the machine operator. It is also anticipated that an indication of the achieved alignment will be displayed, either in digital or linear form, outside the welding machine. A further development being investigated will use this information to give an indication of

what correction will be required (either by pressing or machining) to the finished weld at the final profiling point.

production rate called for in the modified welding lines. Work is also proceeding (in conjunction with London Transport) on the finishing of flat-bottomed section rail by hot-rolling to profile. There is some promise shown in this method which has been successful (experimentally) when used on welded bullhead section rails.

With the introduction of new welding machines giving welds of superior quality and alignment, making welds between longer "short" rails, together with much superior running surface profile finishing of the weld and immediate surrounding areas, it will be possible to deliver to site rails of 182.5m length to an improved standard. Trains to convey 32 each rails of these lengths at speeds to a maximum of 96 k.p.h. are now being built, thus allowing adequate distribution from fewer production points, which latter facet will allow more consistent quality control.

THERMIT WELDING

The application of the aluminio-thermic process for joining together rails came into widespread use on B.R. in the early 1950's, when the requirement to instal C.W.R. called for a method of site welding together L.W.R. produced in depots, by flash welding. Additionally, until sufficient flash welding depots had been established to meet the demand for long rails, considerable quantities of L.W.R. were produced (at temporarily established "depots") by Thermit welding together 18m long rails into 91.5m lengths.

The first Thermit welds had been installed on the Southern Railway in 1929 (by contractors), therefore, some experience of its effectiveness was available and this was compared with the alternative method of site welding (the Phillips Electric Arc) being used in some areas of the London Midland Region. Drawing, also, on the experience being gained in Germany in the application of the Thermit process to the re-construction of the Deutsche Bundesbahn (D.B.) tracks, the decision was taken to employ the then available Thermit process as a standard for site welding on B.R. Many thousands of welds were made using that welding system, employing as it did a long pre-heat (approximately 25 minutes) and necessitating the manufacture of refractory moulds on site. The shortcomings of this method of Thermit welding gradually made themselves apparent and by the mid-1950's a change had been made to the Thermit SmW process (the Thermit "Quick" Weld). With this process came the use of factory made refractory moulds, an improvement in the method of pre-heating and a great reduction in the time required to make a weld. (See FIGURE 5)

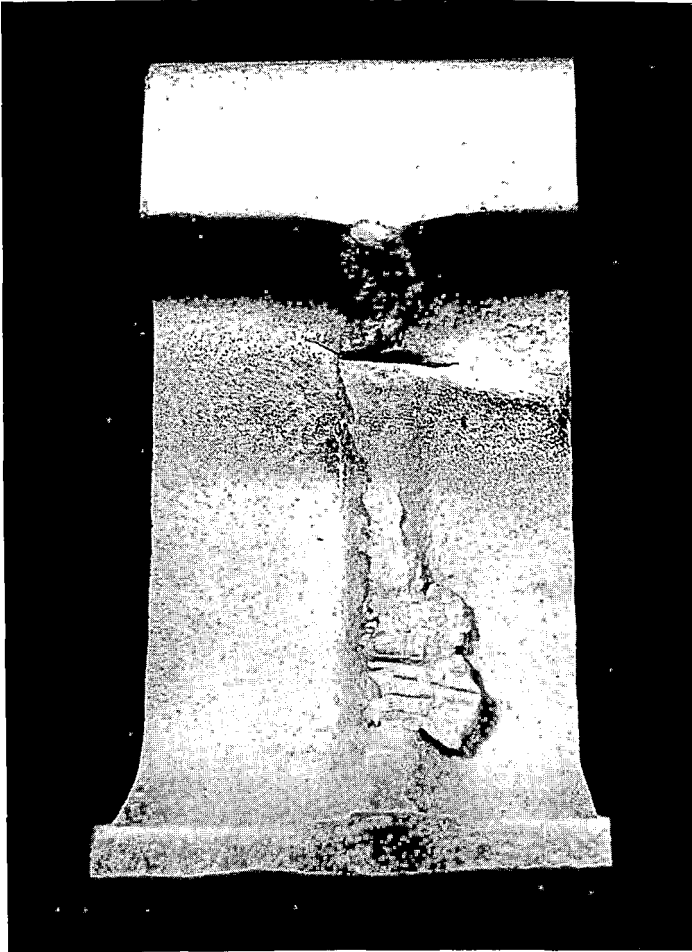


Fig.4 A crack in the upper fillet radius which has initiated at a chisel mark

In order to speed the rate of production, yet allow the rail to be finish profiled at ambient temperature, accelerated cooling - initially by air blast and followed by water spray - will be employed in the refurbished welding lines when welding normal quality steel rails. When called for (e.g. when welding chromium steel rails) provision will be made, in the production line, to carry out post-heating treatment to the weld, this being the procedure preferred by B.R.

Investigation into the manner of producing a final finished profile to the running surface at the weld has included evaluation of several different methods. Various milling procedures, electro-chemical machining (E.C.M.) and many alternative methods of grinding have been considered. Of these methods, the most effective, so far, appears to be grinding; although a major change in the application of the existing procedure will be necessary to give the required consistent standard of finish at the

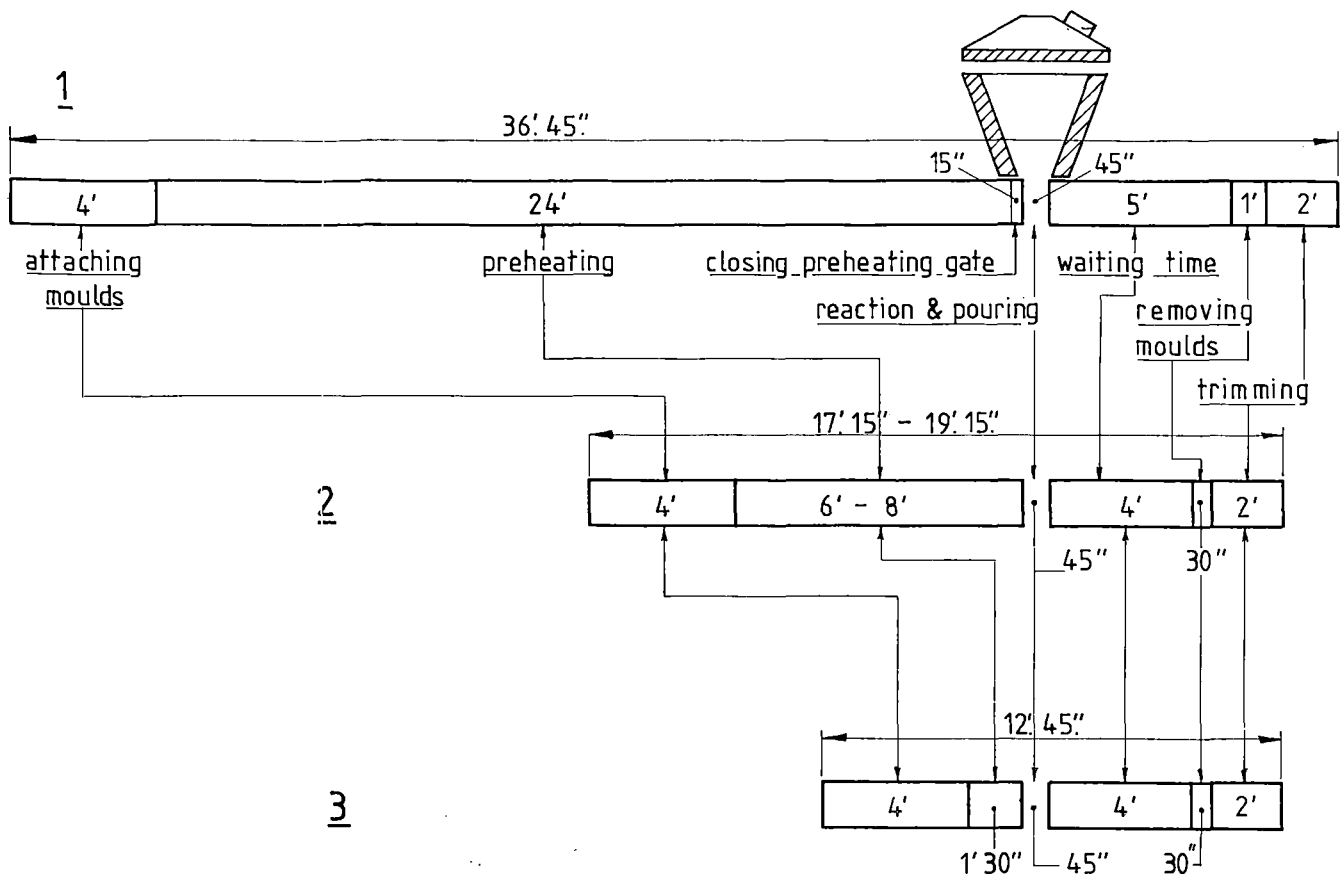


Fig.5 Time to make thermit welds
(excluding alignment of rail ends)

- (1) Original Thermit (full fusion) weld
- (2) Thermit SmW ("Quick") Weld
- (3) Thermit SkV (short pre-heat) weld

As a result of the apparent ease with which welds could then be made on site, not enough attention was given to the necessity for adequate training and supervision of welders carrying out the task. One or two weeks tuition was considered adequate in many cases and supervision by staff with little knowledge of welding - and, in particular the necessary requirements for Thermit welding - was not unknown. Some 8 - 10 years were to elapse before the results of this attitude manifested themselves in the form of an increase in the rate of Thermit weld failures. This was accentuated by a change in the mean stress free temperature range (from 65°F - 75°F to 21°C - 27°C) when fastening down C.W.R. lengths. An examination of the failed welds showed that in the vast majority of cases the failures emanated from lack of fusion defects as a result of incorrect pre-heating. With this information to hand, the necessity to have a formalised training arrangement was appreciated and led, initially, to the preparation of the first handbook of instructions, the observance of which would enable a satisfactory weld to be made on every occasion. Subsequently, the preparation of

a specification for aluminothermic powders for rail welding was set in hand, and in January, 1973, this document was published as B.R. Specification No. 552. This contained details of the required analysis within which Thermit portions must be contained, together with the strength of weld, determined by slow bend testing, which must be produced from such portions. The requirements of this test which are now the standard test criteria for welder examination, also, are as follows:-

Minimum load at failure 920KN
Minimum deflection at failure 7mm

(For new F.B.113A section rail of normal quality.)

The availability of these documents and the application of their requirements improved the standard of Thermit welding, but failures continued to occur as a result of lack of fusion defects and it appeared that these were attributable to a large degree to the subjective observation, by the operator, of the necessary pre-heat condition. In

the mid-1960's, development had taken place in Germany of an advanced Thermit welding technique requiring only a very short pre-heating period, and following a visit to the D.B. (who were adopting this system as a standard) it was decided to carry out full scale field trials on B.R. Thus in November, 1970, the first Thermit SkV (Thermit "Short Pre-heat") welds were installed.

Requiring only 1½ minutes pre-heating (timed by a stop-watch) and employing a larger portion than hitherto, the Thermit SkV weld has now become the standard site weld on B.R., and the process is used to weld not only normal quality steel rails but, also, wear resisting grades 'A' and 'B' and 110kg chromium. The basic weld as originally introduced has since been modified and the form now used is designated SkV-F. This has a weld collar (rib) of flatter section which allows for the weld to be easily cut out (if it is required to replace one of the adjoining components), and another weld to be made in exactly the same place. The advantage of this facility is particularly useful where switch and crossing components which have been welded in situ have to be replaced due to wear.

An increase in the number of Thermit welds breaking in service was seen in 1979 (see FIGURE 6) and on February 15, 1980, a passenger train travelling at 154 k.p.h. was derailed when passing over an undetected broken Thermit SkV-F weld. Fortunately no fatalities resulted and the number injured was relatively low. At the subsequent public inquiry it was determined that the initiating cause of failure of the Thermit joint was a gross lack of fusion defect resulting, most probably, from the operators (who made the joint) not adhering fully to the correct procedures as defined in the appropriate instructions. In consequence, the Inspecting Officer (of the Department of Transport) made recommendations regarding the level of training to be given to those actually carrying out welding operations and to those called upon to employ welders in the course of carrying out various works such as relaying, re-railing, etc. Recommendations were also made concerning the advisability of N.D.T. examination of Thermit welds, and a procedure has been formulated and is being instituted.

It is proposed to use specialised ultrasonic techniques to examine the whole cross section of the weld and, in particular, to look for the presence of lack of fusion defects in the foot of the rail. The procedure adopted recognises that not all "defects" in an alumino-thermic weld are potential sources of failure, but that in some areas (e.g. the foot tip) the presence of a defect (particularly if associated with lack of fusion) is potentially more hazardous than a similar size of defect elsewhere (e.g. in the rail head section). It is, therefore, proposed to give a numerical value to the presence of defects, the value being "loaded" dependent upon location within the weld section. In this way an assessment of weld quality may be made and, if any weld exceeds a pre-determined "points value", its removal can be arranged before possible failure. It is not intended to examine all welds made in track in this way, but each welder will have at least one weld examined (at random) each six months. As a result, some 3500 of the 55000 welds made each year will be examined and any undesirable trend should be

detected before it becomes a source of trouble. This sampling technique may, therefore, be considered a quality control procedure and its employment may not necessarily lead to the detection of all welds containing defects likely to cause failure of the joint.

All these, and other quality control procedures (many of which were already in operation prior to the incident at Bushey on 15.2.80) are already showing the attainment of an improved standard: of some 28000 welds produced already in 1981, only 20 have subsequently broken.

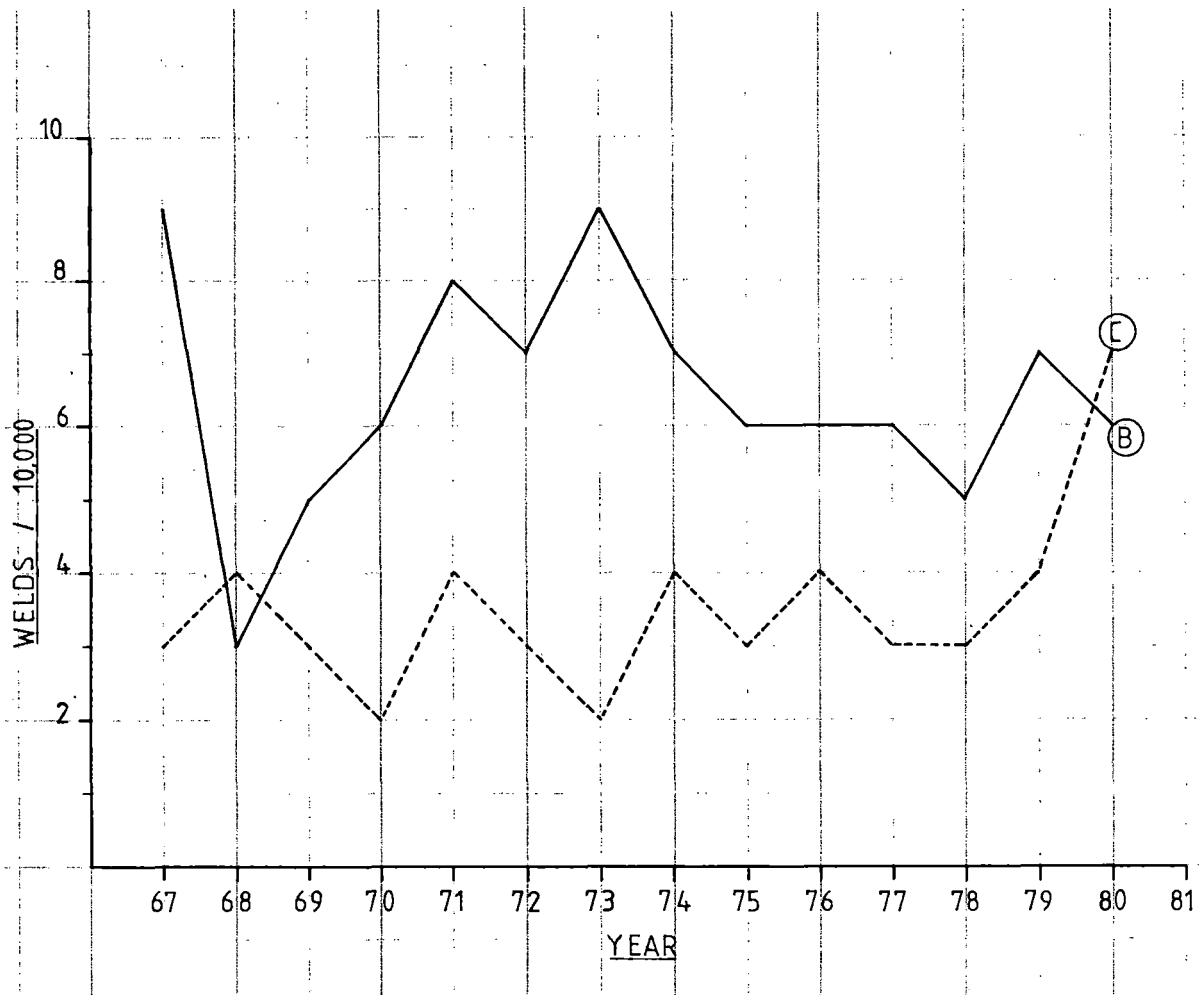


Fig.6 Broken and cracked Thermit welds for 10,000 population

(B) Broken
(C) Cracked

Whilst considerable effort has been expended in improving the quality of normal welding operations, development of the Thermit processes and their application has not been allowed to stagnate. In the development of improved rail steels and, particularly, wear resistant steels, Thermit processes have been developed, modified or adapted to allow the greatest use to be made of rails having special characteristics. Thermit welds are now in running lines laid with 110kg. chromium steel rails and, of particular benefit, a large number of Thermit welds have been made in low-carbon A.M.S. rails laid in heavily trafficked suburban tunnel lines. Many of these latter employ a slab track construction and a welding procedure suitable for use in this type of track has been developed. In addition to using the Thermit welding process (generally of the SkV type) as a constructional feature in crossing vees manufactured in unconventional formats and non-standard materials, it has also been used to fabricate the rail components of a right-angle crossing - the first application (in this way) ever made.

The displacement of the alumino-thermic process, for site welding, by other systems is not foreseen in the near future on B.R. It remains a reasonably versatile operation requiring a limited amount of equipment, few staff, and little or no occupation of running lines, other than that required to make the joints. Development will continue, as at present, to make the process less operator dependent and suitable for use in far more circumstances. It is possible that in some cases, (e.g. the repair of surface damage of rails), localised repair may be more speedily and effectively made by employing an alumino-thermic welding process than by the generally accepted current procedures employing either M.M.A. or semi-automatic electric arc welding.

ELECTRIC ARC WELDING

The restoration of the worn and damaged surfaces of crossings has for long been carried out on B.R. by electric arc welding. For many years this process was used alongside gas welding, and the final commitment to change was largely stimulated by:-

- (i) Increases in speeds and axle loads and the

associated higher rates of wear which led to increased costs in the renewal of track (rail) components. This in turn led to

- (ii) The greater use of wear resisting materials that could not be welded by other than the electric arc processes.

Initially, M.M.A. was only used to re-surface crossings manufactured from normal quality rail steel. Little regard was paid to the importance of pre-heating (although the need for such was well known) and electrodes of very many different types and manufacture were used. The choice of electrode was often based on ease of deposition rather than metallurgical and mechanical suitability of the resulting weld metal, and the welding procedure was modelled on that which for so many years had been adopted for gas welding. The portable welding sets purchased for track welding operations were standard, commercially produced sets, with either petrol (2-stroke or 4-stroke) or diesel engines as the prime mover; equipment more suitable for the less demanding quality of mild steel welding, rather than the high standard demanded for satisfactory rail welding.

In the mid-1950's, a survey of the welding maintenance work being carried on throughout B.R. was undertaken and, as a result, a more uniform policy was initiated. The choice of electrode was limited with approval only being given to those that met pre-determined requirements. Recommendations were made in respect of the type of welding machines to be used and the necessity for, and minimum level of pre-heat to be employed, were defined. With these guidelines applied, the employment of M.M.A. welding maintenance of crossings was adopted on a more widespread scale and, in particular, on the more heavily used lines. The results obtained were found to be more consistent and reasonably satisfactory and with the experience gained it became apparent that improvements in both quality and consistency could (and should) be attained.

By the early 1969's, the rate of introduction of cast high manganese steel ("Hadfield Steel") crossings had gained momentum, and with service experience it was soon found that their life could be much prolonged by judicious maintenance welding. Due to the nature of the material, greater care and attention had to be given to the execution of the work, but the rewards - both financial and in the reduction of disruption to train running due to changing worn out units - were found to be substantial.

It was not long before the necessity to formally standardise all crossing maintenance welding procedures became paramount, and in August, 1977, was published the first edition of the Civil Engineering Handbook No. 32 "General Instructions for Track Working". This comprehensive document (which also contained instructions relating to the thermit welding of rail joints) is the standard reference for all B.R. and defines all the important parameters and factors to be observed to ensure an adequate standard of welding. Procedures for welding of both normal quality and high manganese steel crossings are included, but as yet the welding of switches is not permitted on B.R. although it is anticipated that a suitable procedure will in due

course be formulated.

The availability of Handbook No. 32 gave staff greater confidence to attempt the welding of components which may, previously, have been discarded either as "beyond reclamation" or "not worth the effort", and this was particularly so in the case of cast A.M.S. steel crossings. It had been agreed that this type of crossing should be the standard unit wherever possible on heavily used lines of A1 - A4, B2 - B4, C3, C4, D4 and D3 Categories (see FIGURE 7), and in these environments, blemishes inherent in the casting of these units were quickly revealed, and in many cases, equally quickly rectified by welding.

In some cases, however, what had seemed on initial examination to be a relatively minor maintenance welding procedure became, once preparation for welding had been undertaken, a major repair. This new factor of the welders' job first led to dismay that "unknown" problems could be encountered when carrying out welding on these crossings. This widely held attitude was soon dispelled (by advice and training) and there evolved a class of welder having the ability and confidence to tackle the more major repair with complete success. There became, as a result, two classes of welder, one who could undertake both repair and maintenance of all types of crossings, and another group having skills allowing only for maintenance welding. This structure is recognised by B.R. and welders are graded, and paid, taking into account their particular abilities.

It should be noted that all welders must be proficient in at least three thermit welding jointing procedures, rail bonding, powder-spray welding, and at least two M.M.A. welding procedures before undergoing training for repair welding. The division between "maintenance" and "repair" welding is defined in the following way:-

Maintenance Welding

Where the need to excavate damaged or defective material and make good by welding is confined to a depth of less than 15mm below the normal running surface of the rail.

Repair Welding

Where there is a need to excavate damaged or defective material and make good by welding to a depth in excess of 15mm below the normal running surface of the rail.

Although the more highly skilled welders initially showed their ability when called upon to repair cast crossings, they were also required, in some locations, to repair rails damaged by wheel burn. A satisfactory procedure was devised for this particular task and a great many successful repairs were made in both jointed and C.W.R. track; with the financial benefits being particularly marked in the latter case. It was fortuitous, perhaps, that experience of the repair of wheel burn damage was gained in many areas for, in about 1972, a "new" - or previously unrecognised - defect was identified as a rolling contact fatigue defect, now known throughout B.R. as a "squat".

		SPEED - MILES / HOUR			
		OVER 100	75 to 99	50 to 74	49 or less
ANNUAL GROSS TONNAGE TONS (MILLIONS)	OVER 12	A 4	B 4	C 4	D 4
	5 to 12	A 3	B 3	C 3	D 3
	2 to 5	A 2	B 2	C 2	D 2
	2 or Less	A 1	B 1	C 1	D 1

Fig.7 Track categories

The squat defect was found to be distributed throughout the whole system, but particularly on A and B category lines (see FIGURE 8), i.e. those having high speeds and high gross tonnages of traffic. The defect is first seen as a small circular indentation about 5mm in diameter and up to 2mm in depth, but when well developed, has the characteristic appearance shown in FIGURE 9. Cracks initiate, radially, at an angle of about 10° - 15° to the horizontal which, subsequently, branch downwards into the rail head to form transverse cracks at about 55° to the vertical; whilst the original (near horizontal) crack continues to propagate. Many of these features also are to be found in wheel burn damage and a slight modification to the procedure employed to repair wheel burns has allowed the successful repair of many thousands of squats. Providing the repair of squats is carried out before they have grown too large (a maximum length of 50mm is allowed) a wholly satisfactory weld repair may be made - generally without any interruption to normal traffic - and a subsequent failure rate of less than one in two thousand is being experienced.

The most highly trained and graded track welder on B.R. is required to be proficient in at least 17 different welding skills, of which 11 are mandatory and the remaining 6 are optional and selected (in co-operation with local management, to suit the particular area's needs) from a further 14 skills. Welders are formally examined (at Regional Welding Schools) every 2 years; with an on-the-job examination at six-monthly intervals. The levels of quality referred to in this paper are specific to particular applications, but are very representative

of the standards applied and achieved in all the welding operations undertaken.

In order to enhance this situation, which has resulted from over 50 years of experience and application, a continuing research and development programme is being pursued. Taking into account the many advances being made in the science of welding, particular attention is being paid to the reduction of the influence of the operator and an increase in output from equipment. Mention has already been made of developments of this type in the rail welding depots producing L.W.R. by the flash welding process. On site, automation of the electric welding processes, improvement in the thermit processes and the use of friction welding to make attachments to rails are some of the activities already in well advanced stages.

The use of improved equipment and consumables in accordance with procedures that have been tested and verified in the field, following extensive laboratory and workshop evaluation, will continue to be the policy pursued by B.R. This will ensure that, as in the past, future operations will include welding maintenance and repair of rails as a major and very important resource in the attainment of the necessary standard of permanent way for high speeds and heavy axle loads.

The writer wishes to acknowledge, with thanks, the permission of the Director of Civil Engineering, B.R.B. Headquarters, to publish this paper.

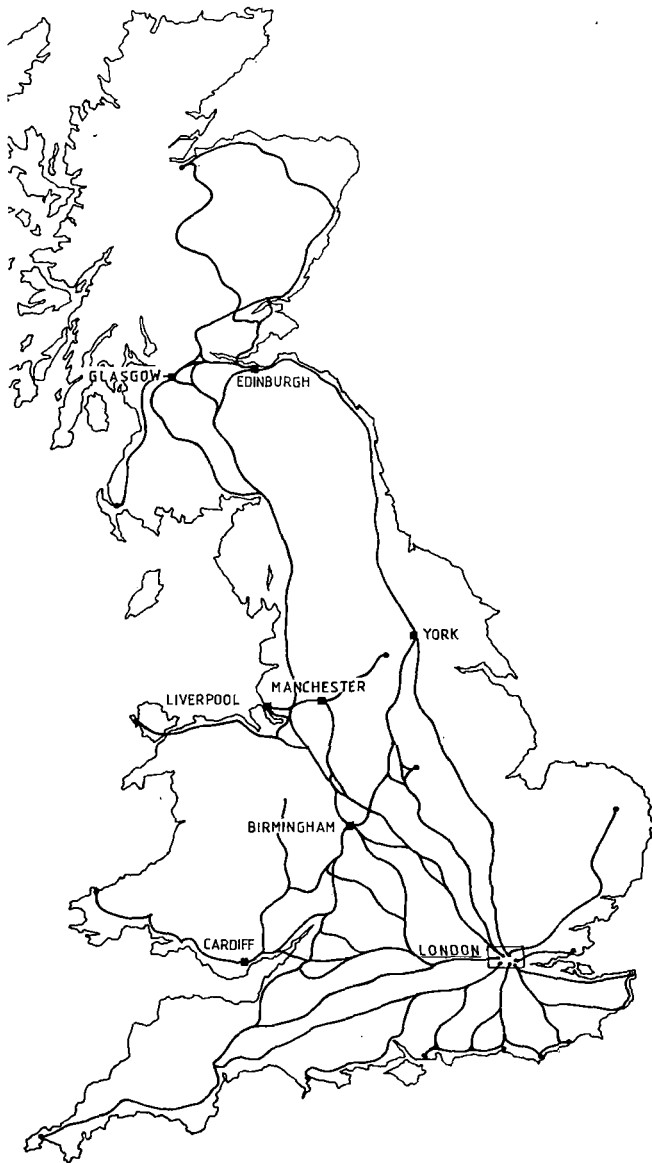


Fig.8 Routes of principal A and B category lines

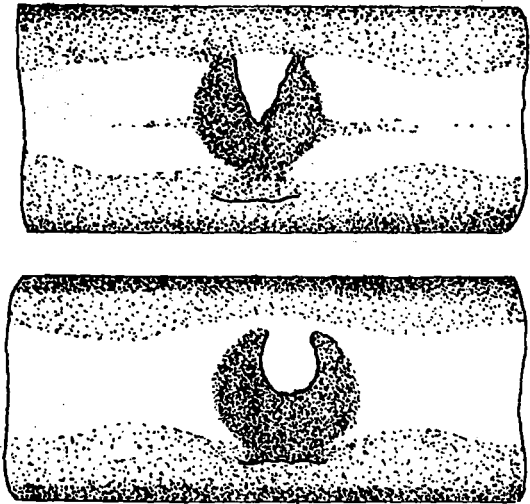


Fig.9 Typical appearance of squats

Rail: Its Behavior and Relationship to Total System Wear

Roger K. Steele

Ph.D., Experiment Manager
Rail Metallurgy
Federal Railroad
Administration

Richard P. Reiff

Experiment Monitor
Rail Metallurgy
Boeing Services
International, Inc.

The main intent of this paper is to provide a clear and accurate summary of what has been learned about rail in the FAST experiment. However, this information might be of limited or uncertain utility to the reader were it not related to observations made in the real world of railroad operation. In addition, the subsequential improvement in understanding the FAST results that can be derived from laboratory examination will be emphasized. The information available for both wheels and rails will be utilized in a unified fashion to provide some insights about total systems (wheel and rail) wear. Illustrations will be given to show how some of the information can be utilized.

This paper is divided into three main topic areas:

- o WEAR and METAL FLOW
- o WELDED RAIL END BATTER
- o FATIGUE and FRACTURE

Because the discussion of each topic will sometimes utilize information which is presented elsewhere in this conference proceedings, the reader is urged to refer to these other sections as he proceeds.

INTRODUCTION

At present, the third rail metallurgy experiment (RME III) is in progress. Over the period of time since the beginning in September 1976, the objectives of the experiment have evolved gradually from determining wear and metal flow behavior alone to include the study of welded rail end batter and defect formation and growth in rails and welds as well.

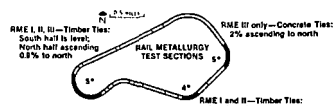
The features of the FAST train are summarized in Table I. The train reverses direction each day. The average train speed is about 41 mph and typically 120 laps of the 4.8 mile loop are made each day imposing approximately 1 MGT of traffic per day on the track. Thus 1 MGT on the track equals approximately 500 miles of vehicle travel.

As shown in Figure 1, the rail metallurgy test sections have been located in Section 3 for all three experiments and in Section 13 for experiments I and II, and Section 17 (5° Curve) for the current (III) experiment. Section 3 is a 5° curve essentially level on its southerly half and ascending to the north with a 0.9% grade on its northern half. Section 13 is a 4° curve on level grade. The 5° curve at Section 17 ascends to the north at a 2% grade.

TABLE I. THE FAST TRAIN.

Motive Power:	Four 4-axle, 2000hp locomotives.
Car Equipment:	Ninety-nine cars in FAST pool; Ninety-two 100-ton open-top hopper; Six 100-ton tank; One 70-ton TTX.
Lading:	Hoppers—expanded shale (simulated coal lading); Tanks—water; 100-ton design cars—loaded to gross weight on rail of 263,000 lbs ± 2,000 lbs.
Nominal Consist:	Four units plus 70 cars; 9200 trailing tons; 0.87 hp per trailing ton.

In all three experiments the rail in Section 3 has been 132, 136 or 140 lb/yd. The rail in Section 13 has been 115 lb/yd while that currently in Section 17 (5° curve) is all 136 lb/yd. The physical arrangement of the rails in Section 3 in each experiment is also shown in Figure 1. The essential feature of each design is that it provides replication of different metallurgies in different places in the curve to assess the contribution of position-in-curve effect. The designs used previously in Section 13 in the first and second experiments were



FIRST EXPERIMENT													
Segment	A	B	C	D	HH	HSi	FHT	CrMo	Std	F	G	H	J
Tie Plate Cant	1:40	1:30	1:14	1:14			1:30		1:40	1:40	1:18	1:30	1:14

SECOND EXPERIMENT															
Metallurgy	Std	HH	CrMo	FHT	HSi	Std	HH	CrMo	FHT	HSi	Std	HH	CrMo	FHT	HSi
Tie Plate Cant	1:40		1:30		1:14		1:40		1:30		1:14		1:40		1:40

THIRD EXPERIMENT																
Std	HH	CrMo(A)	SiCr	1%Cr	CrMo(C)	HH	Std	FHT	HH	Std	CrMo(A)	SiCr	1%Cr	CrMo(C)	Std	HH
	SiMn				NNH		SiMn		NNH		SiMn		NNH			NNH
	2/81				12/80		2/81		12/80		2/81		12/80			12/80

NOTE: Cant by 1:40 throughout / CrMo(A)=Bafoid / CrMo(C)=Weldable

FIGURE 1. RAIL METALLURGY TEST SECTIONS.

similar to those used in Section 3 except that only four metallurgies (Std, HSi, FHT, and HH) were present instead of the five present in Section 3. In the current experiment standard carbon and head hardened rail are the control (reference) rails and each have been replicated four times in Section 3. The other metallurgies are replicated only twice except for fully heat treated rail which is positioned only at the center of the curve. The originally installed CrMo(A) has been replaced by SiMn (HH) rail; one half of the control head hardened rail has been replaced with new head hardened rail. In Section 17, head hardened rail is the control rail and SiCr(HH), 1 Cr, and CrV are each replicated twice in the curve.

Three tie plate cants, 1:14, 1:30, and 1:40 were utilized in the first and second experiments; however, only the 1:40 cant is utilized in the current experiment.

The essential features of each experiment are summarized in Table II. An important variable in each experiment has been lubrication. Even though two track lubricators had been installed initially, the first 40-45 MGT of the first experiment were char-

TABLE II. EXPERIMENT FEATURES.

Experiment	Dates	Tonnage	Tie Plate Cants	Lubrication Pattern
RME I	8/76 - 8/77	135 MGT	1:14, 1:30, 1:40	Poorly lubricated—first 45 MGT; Well lubricated—remaining 90 MGT
RME II	12/77 - 6/79	290 MGT	1:14, 1:30, 1:40	Well lubricated for entire period except for brief (35 MGT) lubrication experiment
RME III	12/79 - present	190 MGT to date	1:40 only	Alternating well lubricated (~35 MGT) and dry (~15 MGT)

NOTE: In the well lubricated periods, the lubricators were shut down every 2 to 3 MGT for half-MGT intervals to facilitate rail flaw inspection

acterized by ineffective lubrication. Over a period of time, two more lubricators were added and the level of lubrication approached what would be termed most charitably as "generous" after 45 MGT. The lubricators were utilized in the second experiment throughout the 290 MGT period of that experiment, with the exception of a brief period of 22 MGT where only one lubricator was used as part of a lubrication experiment. The level of lubrication throughout the second experiment was sufficiently generous that comparisons between the different metallurgies have not yet been made reliably. In the current experi-

ment, an alternating pattern of lubricated and dry running has been employed (with much improved measurement instrumentation to provide wear information in both lubrication regimes and also as part of an effort to minimize fatigue damage to the rail. Two properly functioning track lubricators have been found more than adequate to generously lubricate the entire loop. An important note to remember is that the lubricated period has not ever represented continuous lubrication; the lubricators are shut down every 2-3 MGT for about 1/2 MGT to "clean" the rail for inspection.

The average ladle analyses of the test rail in the 1st and 3rd experiments are given in Table III. Several significant details should be pointed out. The FHT rail installed in Section 3 RME I had relatively low carbon and manganese levels compared to those of the other metallurgies; however, the FHT rail in Section 13 had comparable carbon levels to those of the premium rails although its manganese content was lower. In the current experiment, the FHT rail is high in both carbon and manganese relative to the other non-alloy rails.

TABLE III. AVERAGE LADLE ANALYSIS OF RAIL IN THE FAST METALLURGY EXPERIMENTS: RME I & III

Section	Rail Type	WEIGHT PERCENT (w/o)							
		C	Mn	P	S	Si	Cr	Mo	V
RME I Section 03 (132 lb/yd)	Std	0.78	0.86	0.027	0.025	0.15	—	—	—
	HSi	0.76	0.86	0.028	0.027	0.63	—	—	—
	FHT	0.69	0.81	0.018	0.032	0.18	—	—	—
	CrMo	0.80	0.82	0.026	0.025	0.25	0.78	0.20	—
	HH	0.79	0.84	0.009	0.018	0.16	—	—	—
Section 13 (115 lb/yd)	Std	0.73	0.86	0.024	0.020	0.17	—	—	—
	HSi	0.77	0.88	0.029	0.024	0.68	—	—	—
	FHT	0.77	0.81	0.020	0.041	0.15	—	—	—
	HH	0.77	0.88	0.015	0.025	0.18	—	—	—
RME III Sections 3 and 17 (5°) (132, 136, & 140 lb/yd)	Std	0.76	0.86	0.022	0.024	0.18	—	—	—
	FHT	0.81	0.93	0.018	0.041	0.20	—	—	—
	HH	0.77	0.83	0.021	0.030	0.17	—	—	—
	NNH	0.76	0.93	0.020	0.020	0.22	—	—	—
	SiCr (HH)	0.76	0.82	0.020	0.006	0.82	0.50	—	—
	SiMn (HH)	0.76	1.24	0.023	0.009	0.84	—	—	—
	1 CR (A)	0.71	0.73	0.014	0.021	0.27	1.16	—	—
	1 CR (B)	0.73	1.30	0.023	0.026	0.30	1.25	—	—
	1 CR (C)	0.75	0.88	0.030	0.027	0.23	0.95	—	—
	CrV (A)	0.67	1.15	0.009	0.013	0.34	1.11	—	0.11
CrV (B)	0.72	1.27	0.014	0.030	0.22	1.04	—	0.087	
CrMo (A)	0.72	0.79	0.009	0.023	0.25	0.78	0.21	—	
CrMo (C)	0.79	0.60	0.026	0.016	0.26	0.61	0.17	—	

In the first and second experiment each different metallurgy was provided in its entirety by a single manufacturer. However, in the current experiment the 1% chromium rail has been provided by three manufacturers and the CrV and CrMo rail by two manufacturers. The two CrMo rails tested in the current experiment have significantly different manganese, chromium, and molybdenum levels. The lower alloy levels in CrMo(C) permit it to be welded without postheat although an additional preheat cycle is recommended. CrMo(A) is much more similar in composition to the CrMo rail tested in the first experiment.

In the case of the 1% Chromium rail the variation in manganese level (0.73 to 1.30 w/o) and chromium level (0.95 to 1.25 w/o) is very significant. The variation in chromium, manganese, and vanadium levels in the CrV rails is less significant. A few words are appropriate for the SiCr(HH) and SiMn(HH) rails. Both of these are alloy rails which are head hardened; their alloy compositions have been adjusted to provide the benefits of increased hard-

enability at the heat affected zones of flash butt welds without the need to resort to postheating.

The average ladle analyses of the AREA standard carbon rail tested in the first and third experiments is very similar. However, significant variations have occurred among ladle analyses for individual standard rail heats. Much more will be said about this in the discussion of equivalent carbon effects.

WEAR AND METAL FLOW

The measures of wear and metal flow are shown in Figure 2. In the first (and second) experiment all the measures were obtained from rail profiles having a long term variability of $\pm 0.020'' - 0.030''$ on any dimension. When wear rates were reduced by lubrication (by as much as a factor of 10 in some cases) as in RME II, the total wear which occurred in a period of observation was comparable with the "noise" characteristic of the profilometer; This is the reason that RME II has not provided a reliable assessment of the effects of different metallurgies and tie plate cants.

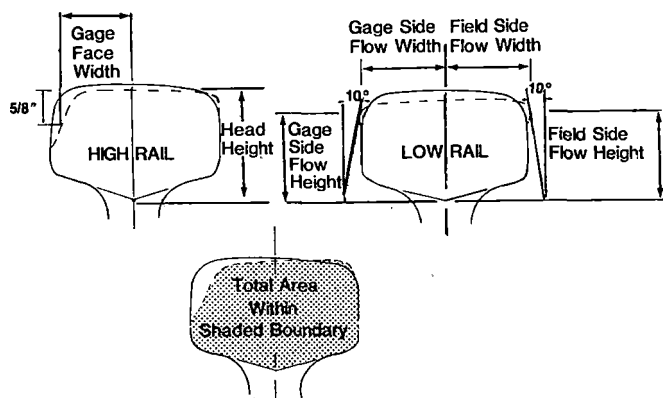


FIGURE 2. DIMENSIONS AND AREA DETERMINATION.

To correct this problem, a series of "snap" gage type instruments has been developed for use in RME III. These instruments accomplish dimensional measurement through the use of dial gauges and have a long term variability of $\pm 0.002'' - 0.003''$. They are used to generate gage face, head height loss, and lateral metal flow information. Cross sectional head area loss still needs to be determined from profilometer traces.

In addition to wear rate information which will be presented in the following paragraphs, reference will be made to the term "figure of merit". The figure of merit (FM) provides a relative assessment of how much better a premium rail is than standard rail. Most simply it is calculated by dividing the average wear rate of standard rail by that of the comparison rail. Because statistically there is some variability in the wear rates of both standard and premium metallurgies, dividing one average wear rate by another is not rigorously correct. Properly, the technique used commonly to calculate the probability distribution function of lateral to vertical wheel loads ratio should be used. The expression for making this calculation is given below.

$$\text{PDF}(Z) = \frac{\sigma_x \sigma_y}{\pi (\sigma_y^2 - Z^2 \sigma_x^2)} \exp \left\{ -\frac{1}{2} \left[\left(\frac{\mu_x}{\sigma_x} \right)^2 + \left(\frac{\mu_y}{\sigma_y} \right)^2 \right] \right\} + \left[\frac{\mu_x \sigma_y^2 + Z \mu_y \sigma_x^2}{\sqrt{2\pi} (\sigma_y^2 - Z^2 \sigma_x^2)^{3/2}} \right] \exp \left\{ -\frac{1}{2} \frac{(\mu_y - Z \mu_x)^2}{(\sigma_y^2 - Z^2 \sigma_x^2)} \right\} \text{erf} \left[\frac{\mu_x \sigma_y^2 + Z \mu_y \sigma_x^2}{\sigma_x \sigma_y \sqrt{(2 \sigma_y^2 + Z^2 \sigma_x^2)}} \right]$$

where:

$$Z = \text{Figure of Merit} = \frac{\text{wear rate of Std rail}}{\text{wear rate of comparison rail}}$$

$\mu_{x, y}$ = Wear rate means of comparison and standard rails, respectively

$\sigma_{x, y}$ = Variances of wear rates for comparison and standard rails, respectively

The inputs needed are the average wear rates and the variances for each metallurgy. The difference between the simple method and the rigorously correct method will be shown in a subsequent paragraph.

Table IV presents the average gage face wear rates of the different metallurgies tested in Section 3 in RME I. The wear rates given are the averages for all positions-in-curve and all tie plate cants as determined by two independent analyses, one performed by

TABLE IV. AVERAGE GAGE FACE LOSS.

SECTION 3: RME I	Below Lubrication Transition		Above Lubrication Transition	
	Rate, ln/MGT	FM	Rate, ln/MGT	FM
Std	0.0086	1	0.0012	1
HiSi	0.0061	1.4	0.0012	1
FHT	0.0059	1.5	0.0011	1.1
CrMo	0.0041	2.1	0.0011	1.1
HH	0.0032	2.7	0.0007	1.5

$$\text{FM} = \text{Figure of Merit} = \frac{\text{Average Wear Rate of Std Rail}}{\text{Average Wear Rate of Comparison Rail}}$$

the AAR and the other by the Transportation Systems Center. The lubrication transition occurred at 40 - 45 MGT. In the dry (below transition) regime, the CrMo and HH exhibited the least gage face wear with both HiSi and FHT having intermediate wear resistance. The improvement in lubrication that occurred near 40 - 45 MGT greatly reduced gage face wear rates but not uniformly for each metallurgy. While the wear rate of standard rail diminished by a factor of seven, that of each premium rail was reduced by a significantly smaller factor such that improved lubrication reduced the wear rate of HH rail by a factor of only four and one half. This occurrence is termed a metallurgy:lubrication interaction.

This interaction is reflected also in the reduction in the magnitude of the figures of merit of the premium rails upon improvement in lubrication. Thus, premium rails do not offer as great advantage relative to standard rail in the lubricated regime as they do in the dry regime.

The greater uncertainty in establishing the relative benefit of premium rails in the lubricated regime can be seen by comparing the figure of merit probability distribution functions shown in Figure 3. The distributions are relatively narrow in the dry

regime and the FM peak value positions agree well with those calculated from the ratio of average wear rates. However, in the lubricated regime, the distributions are broader and the FM peak values do not agree as well with the ratio of average wear rates. Nevertheless, clearly the distributions tend to superimpose in the lubricated regime whereas they are distinctly separate in the dry regime. This behavior suggests that the metallurgy-lubrication is indeed real.

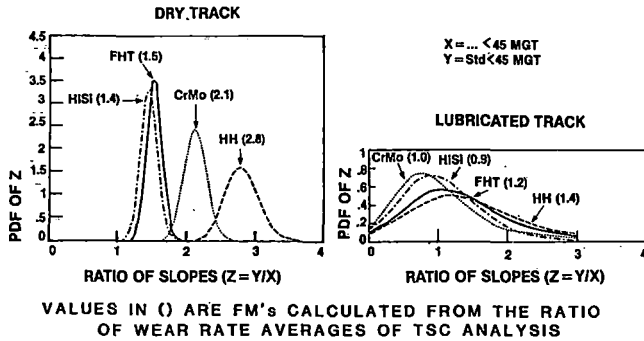


FIGURE 3. PDF OF SLOPE RATIOS.

In spite of this greater uncertainty in the FM values in the lubricated regime, in the following sections, the simple ratio of average wear rates will be used as a measure of the figure of merit.

One of the potential difficulties with a field type of test is that there may be variations in behavior at different positions in a test curve—a so called position-in-curve effect. If allowances are not made for this possibility in the design of the experiment, there exists the risk that no meaningful information may be derived from the experiment. Indeed, Section 3 does appear to exhibit a position-in-curve effect which is a function of the level of lubrication. As shown in Table V in the dry regime, the south end of Section 3 yielded wear rates about 20% higher, on the average, than those observed in the center and north end of the curve. However, in the lubricated regime, the center of the curve exhibited the highest wear rate, and the relative variation in wear from the south end of the curve to the center was greater than that attributable to different metallurgies, on the average.

TABLE V. POSITION-IN-CURVE EFFECT.

SECTION 3 (In/MGT): RME I

	Below Lubrication Transition	Above Lubrication Transition
Section 02 End	0.0052	0.0012
Middle	0.0054	0.0017
Section 04 End	0.0064	0.0006

NOTE: Average of all metallurgies and tie plate cants

The three different tie plate cants used under the high rail of Section 3 also had an effect that appeared to depend upon the level of lubrication; this is shown in Table VI. In the dry regime the 1:14 cant plate caused about 20% higher wear rates than did either 1:30 or 1:40 cant plates on the average. However, there is an important caveat: the wear of standard AREA carbon rail was so rapid on the 1:14 cant plates that the rail shape very quickly conformed to the shape of the average wheel contour and the wear rate of standard rail then became the same as that on the other tie plates. When wear rates dropped due to the presence of "generous" lubrication, the tendency of steeper cant to increase wear rate became more noticeable across all three cants. Because the wear rate of standard carbon rail was much lower, the effect of higher cant persisted longer. The reader must remember, however, that the intent of using high cant is to "unload" the gage corner and thereby delay shell/TD formation—not to reduce wear. In the lubricated regime, where fatigue of rail will become more important, the slightly higher wear rate on 1:14 cant plates might be more than compensated for by greater resistance to shelling and TD formation.

TABLE VI. TIE PLATE CANT EFFECT.

SECTION 3 (In/MGT): RME I

	Below Lubrication Transition	Above Lubrication Transition
1:40	0.0053	0.0008
1:30	0.0053	0.0011
1:14	0.0062	0.0013

NOTE: Average of all metallurgies and positions in curve

The gage face wear rates in Section 13 (115 lb/yd rail, 4° curvature) are summarized in Table VII. In the dry regime, the wear rates for all metallurgies were only slightly higher at the center of the curve than at the ends. However, this trend was much more pronounced for standard carbon rail. In the lubricated regime, the center of the curve exhibits noticeably less wear than the ends for all metallurgies. This pattern was opposite to that observed

TABLE VII. GAGE FACE WEAR RESULTS FROM SECTION 13.

(In/MGT)	Position-in-Curve				Average	Average Figure of Merit
	Metallurgy	A	B	C		
Below Transition						
HH	0.0021	0.0017	0.0025	0.0021	0.0022	3.5
HISI	0.0052	0.0049	0.0045	0.0043	0.0047	1.6
FHT	0.0038	0.0038	0.0034	0.0037	0.0037	2.1
Std	0.0063	0.0092	0.0094	0.0060	0.0077	1.0
Average	0.0044	0.0049	0.0050	0.0046		
Above Transition						
HH	0.0014	0.0012	0.0003	0.0010	0.0010	1.3
HISI	0.0025	0.0001	0.0006	0.0014	0.0012	1.1
FHT	0.0020	0.0001	0.0010	0.0012	0.0010	1.3
Std	0.0016	0.0010	0.0010	0.0016	0.0013	1.0
Average	0.0019	0.0006	0.0007	0.0013		

A = Section 02 End

B, C = Middle

D = Section 04 End

in Section 3. The figures of merit for those metallurgies common to both Section 3 and 13 are very similar to those in Section 3, i.e., HH exhibited the best gage face wear resistance while HiSi and FHT fell into an intermediate group. Also the metallurgy: lubrication interaction has been observed again.

To assess the effect of curvature (assuming that the rail section itself does not affect the wear rate), the ratio of wear rates in Section 13 and Section 3 (1:40 cant only) have been calculated and tabulated in Table VIII. On the average, the ratio was 0.8 suggesting a linear relationship between wear rate and degrees of curvature. However, the ratio can vary considerably for each metallurgy and from the dry to the lubricated regime. If the ratios for gage face wear (in the dry regime) are multiplied against head area loss rates from Section 3, a linear relationship of wear rate with curvature is indeed suggested in Figure 4, at least for standard, HiSi, and HH rails. Ratioing the head area loss on the basis of gage face loss is valid for the FAST data because, as will be shown in the next paragraph, the head height loss rate was relatively small compared to gage face wear rates.

TABLE VIII. RELATIVE GAGE FACE WEAR IN SECTION 03: RME I:

RATIO: WEAR RATE SECTION 13
WEAR RATE SECTION 03

Metallurgy	Below Transition	Above Transition
Std	0.804	0.906
HiSi	0.746	0.671
FHT	0.617	0.809
HH	0.846	0.993
Average	0.753	0.845

OVERALL AVERAGE = 0.799

NOTE: Average of all positions in curves; 1:40 tie plate cant only

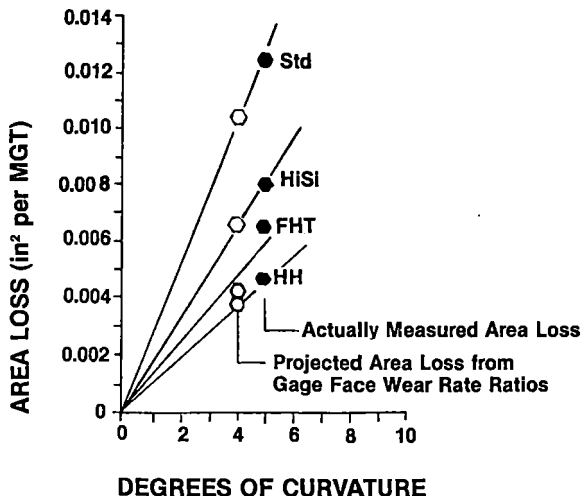


FIGURE 4. EFFECT OF TRACK CURVATURE.

The high rail head height loss rates in Section 3 for each of the metallurgies on each of the three tie plate cants are summarized in Table IX. Overall, the head height loss rates were about one-third the gage face wear rates. There is an important difference, though, in the ranking of the metallurgies, i.e., CrMo and FHT had the highest resistance while HiSi and HH fell into an intermediate category. Also, the 1:30 and 1:14 cant plates tended to produce lower head height loss rates than did the 1:40 cant; the effect became more pronounced for the better performing rails. There was virtually no head height loss in the lubricated regime on any of the premium rails.

TABLE IX. HEAD HEIGHT LOSS RATES.

SECTION 3 (Below Lubrication Transition at 45 MGT): RME I

Cant	1:40		1:30		1:14		Average	
	Rate /MGT	FM	Rate /MGT	FM	Rate /MGT	FM	Rate /MGT	FM
Std	0.0026	1.0	0.0022	1.0	0.0023	1.0	0.0024	1.0
HiSi	0.0014	1.9	0.0012	1.8	0.0013	1.8	0.0012	2.0
FHT	0.0010	2.6	0.0008	2.8	0.0006	3.8	0.0008	3.0
CrMo	0.0007	3.7	0.0005	4.4	0.0005	4.6	0.0006	4.0
HH	0.0013	2.0	0.0011	2.0	0.0009	2.6	0.0011	2.2

The relationship of gage face wear rate and head height loss rate seems to be a function of both the metallurgy itself along with the cant ratios. This is illustrated in Figure 5 for the ratio of gage face wear rate to head height loss rate. The FHT rail exhibited the greatest sensitivity to cant while standard and HH exhibited the least. It is not clear why different metallurgies should behave so differently but this behavior does suggest that a proper assessment of the wear resistance of a given metallurgy requires both gage face and head height loss measurements.

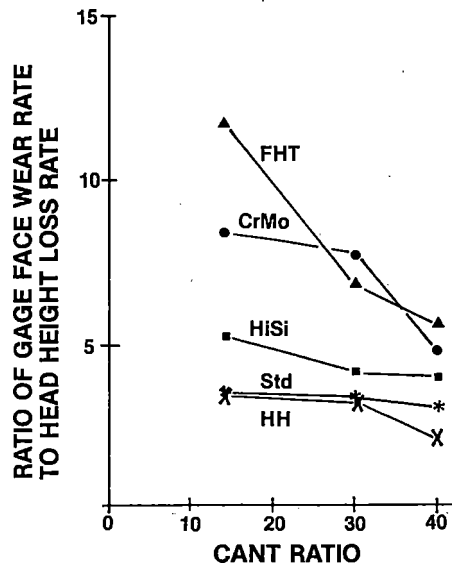


FIGURE 5. RATIO OF GAGE FACE WEAR RATE TO HEAD HEIGHT LOSS RATE.

By having both gage face and head height loss rates, a reliable estimate of relative area loss can be made by creating a composite FM from the dimensional loss rates. The composite FM is

$$\sqrt{\text{FM (gage face)} \times \text{FM (head height)}}$$

The good agreement between the composite FM's and the observed area loss FM's is shown in Figure 6.

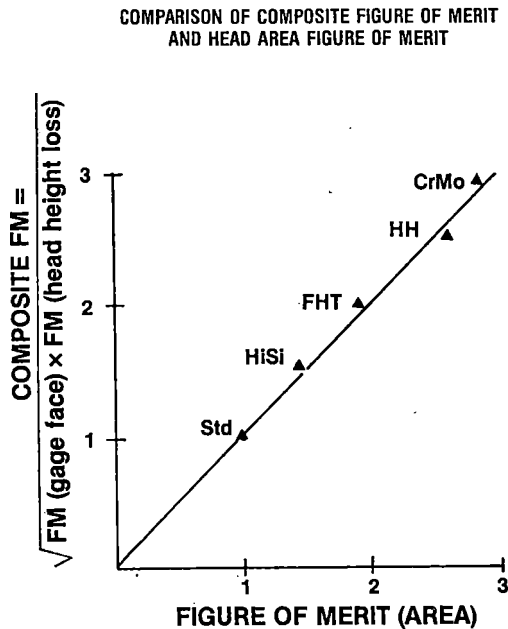


FIGURE 6. FIGURE OF MERIT (AREA).

Turning now to the low rail, the head height loss rates in each of the ten track segments of Section 3 in each lubrication regime are plotted in Figure 7. Virtually no position-in-curve effect was detected in the dry regime but in the lubricated regime the center portion of the curve had substantially higher wear rates than the ends for all metallurgies. The head height loss rates of the different metallurgies were generally less in the lubricated regime. This fact and the occurrence of a position-in-curve effect in the lubricated regime are of some interest because the running surface of the low rail of the curve was not lubricated. Thus, it appears that the head height loss behavior of the low rail was governed by the lubrication level on the high rail.

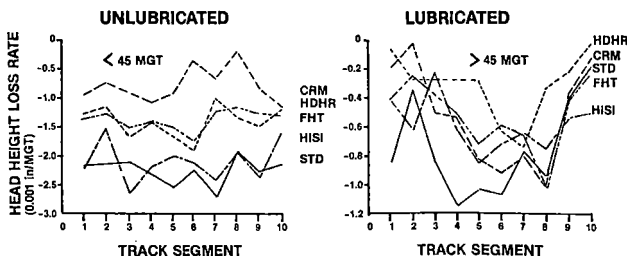


FIGURE 7. HEAD HEIGHT LOSS OF LOW RAIL: RME I.

The metal flow behavior of the low rail is more difficult to describe simply. To do this, both the heights and widths to the point at which a 10° (from the vertical) tangent touches the gage or field side flow lips have been measured. The typical behavior of standard carbon rail in Section 3 is illustrated in Figure 8. The most significant dimensional change was the increase in height to the flow lip on both field and gage sides. This occurred at a rapid rate for the first 35 to 55 MGT as metal crowded into the gage and field corner of the rail. After this period, there is a leveling off of height on the gage side and a gradual reduction in height thereafter on the field side. It is not clear whether the maximum points on the head height curves were associated with the change in lubrication on the outside rails. The width dimensions behaved somewhat differently on gage and field sides. On the gage side, the tangent to the flow lip actually receded for 80 to 90 MGT whereafter it moved more rapidly outward. However, on the field side, there was a gradual increase in width for approximately 100 MGT followed by a leveling off thereafter. The leveling off may be the result of sustained lubrication on the high rail.

LOW RAIL: RME I

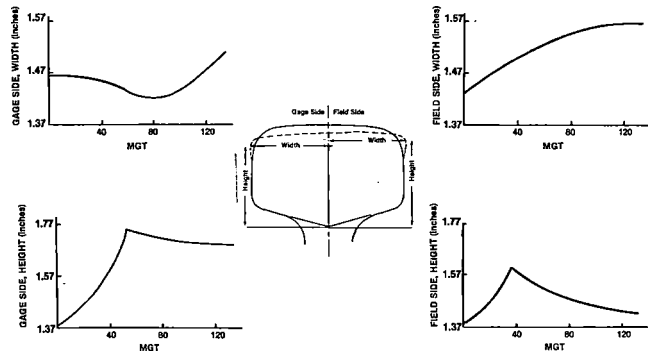


FIGURE 8. METAL FLOW BEHAVIOR OF STANDARD RAIL.

HiSi rail behaved in a fashion similar to standard carbon rail except that field side lateral flow (i.e., width increase) was observed only in the north and south end segments of Section 3 suggesting a very pronounced position-in-curve effect. No statistically significant widening on the gage side was observed at all. None of the other premium metallurgies exhibited any measurable metal flow.

The wear behavior of rail can be related with various degrees of success to its mechanical properties. The most commonly used of these properties is hardness. Figure 9 presents the head area loss figures of merit plotted against gage face hardness ratio which was determined with a 3000 kg indenting force tester at the very end of the RME I experiment (after 45 MGT dry and 90 MGT lubricated). Because the hardness measurements were made only after the active test of the rail had been completed, the behavior observed must not be expected necessarily to be appropriate for a single lubrication regime, dry or lubricated. Nevertheless, the results do suggest that increased hardness achieved in different ways does not necessarily lead to the same improvement in wear resistance. It appeared that increased hardness achieved through heat treatment

alone did not provide as much improved overall wear resistance (gauge face and head height) as did alloying. Also, the alloy rail appeared to be more affected by the level of lubrication than did the heat treated rail.

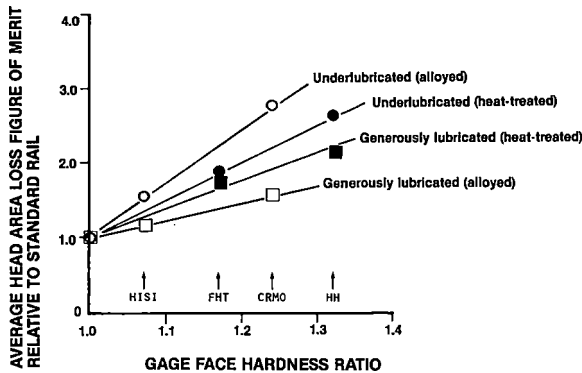


FIGURE 9. EFFECT OF RELATIVE GAGE FACE HARDNESS UPON AREA LOSS FIGURE OF MERIT: RME I SECTION 03.

There appears to be some interest in the industry toward utilizing a mechanical property parameter such as yield strength as a measure of wear resistance. Some recent work by the University of Connecticut¹ suggests that this may be appropriate for resistance to head height loss but may not provide good correlation with gauge face wear resistance. Figure 10 plots the figures of merit for head height loss and for gauge face wear against the cyclic and static 0.2% offset yield strengths. Perhaps because head height loss may be predominantly a metal flow process, the agreement between head height loss figure of merit and yield strength (both cyclic and static) is good. But the relationship between either yield strength and the gauge face figure of merit is much poorer primarily because of the behavior of the FHT rail. As will be discussed later, the mechanism of wear on the gauge face may be associated more with shear band cracking than ease of plastic flow, and, therefore, a fundamental correlation of gauge face wear with yield strength might not be expected.

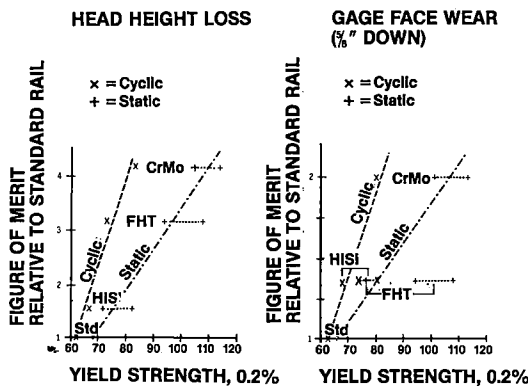


FIGURE 10. RELATIONSHIP OF WEAR BEHAVIOR TO YIELD STRENGTH.

The fact that about ten different heats of standard and HiSi rail each were incorporated into the high rail of Section 3 (RMEI) has permitted an evaluation of the effect of chemistry upon wear resistance. Although there will be differences from one heat to another due to small variations in mill processing, the fact that all rails came from the same mill has made determination of chemistry effects less complicated. The method that has been adopted to illustrate the effect of chemistry has been to convert carbon, manganese, and silicon contents to equivalent carbon in the manner described by Clayton² such that:

$$C_{eq} = w/o C + w/o Mn/4.75 + w/o Si/10$$

Figure 11 is a plot of gauge face wear rate in the dry regime versus equivalent carbon calculated from ladle analyses after corrections have been applied for position-in-curve effects. Within the range of chemistry of the standard carbon rails tested, there was an approximate 50% variation in gauge face wear rate. Within the range of equivalent carbon calculated from the extremes of C, Mn, and Si, content allowed by the AREA specifications* on rail, there could be as much as a 3:1 variation in wear rate. This behavior suggests that there may be some merit in segregating rails at the high end of the equivalent carbon range for more severe usage (in the fashion of "blue" rails some years ago). Also perhaps a very low cost premium rail could be developed near or just above the upper end of the current allowable AREA range.

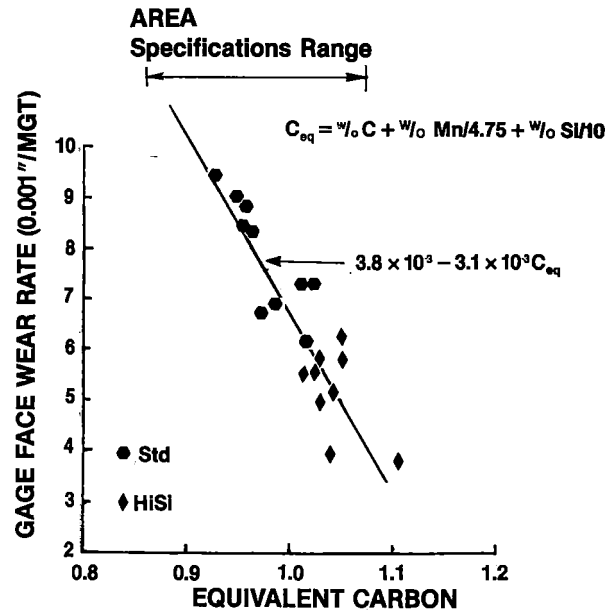


FIGURE 11. EFFECT OF EQUIVALENT CARBON LEVEL ON GAGE FACE WEAR RATE: RME I.

In order to compare the FAST rail wear behavior with that of other types of operations Figures 12a and 12b show the FAST wear data at 5° curvature along with families of curves from other sources. By comparison with the data of Hay, et. al.,³ (Northern Pacific and Burlington Northern), the FAST wear environment is roughly twice as severe. Interestingly, the Hay data show the 132 lb/yd FHT wearing at about the same rate as standard rail. How-

*A lubrication block is one lubricated interval of 30-40 MGT and a dry period of 10-15 MGT.

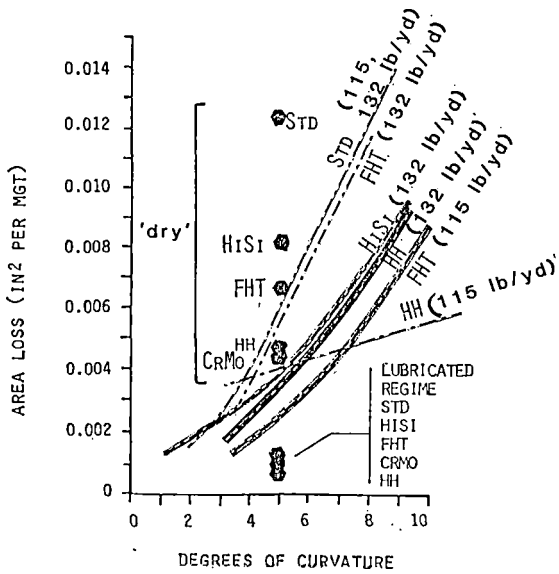


FIGURE 12a. FIELD COMPARED TO FAST DATA (COMPARING HAY et. al).

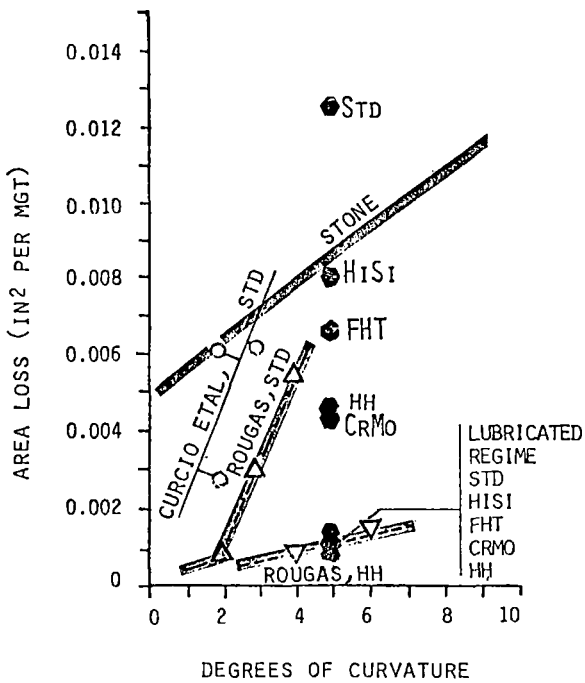


FIGURE 12b. FIELD COMPARED TO FAST DATA (COMPARING STONE, CURCIO, ROUGAS).

ever, the 115 lb/yd FHT performed substantially better. In a similar manner the FAST 115 lb/yd FHT rail performed substantially better on a 4° curve than one would have predicted from linearly interpolating the 132 lb/yd FHT wear rate at 5° back to 4° curvature. Data from Rougas⁴ for 100 ton cars operating on the Bessemer and Lake Erie (Figure 13b) suggest that the FAST environment is roughly twice as severe for standard carbon rail and perhaps four times as severe for HH rail. The FAST wear rate of standard rail seems to be about 50% greater than that reported by Stone⁵ for the Waynesburg Southern

operating at low speeds with 125 ton cars. However the Australian experience with 100 ton cars (albeit reported with lubrication) at low curvatures does extrapolate linearly to wear rates close to those observed at FAST.

Another set of comparisons can be made by taking the linearly interpolated FAST wear rates for standard AREA carbon rail (refer to Figure 4) to calculate lives using 25% head area loss the condemning limit and plotting them upon the data for other railroads as shown in Figure 13. At 5° curvature, the FAST calculated rail life would fall toward the low end of the distribution observed for other railroads. However, as curvature decreases the FAST wear lives calculated from linearly interpolated wear rates fall toward the high side of the distribution more so as the curvature decreases.

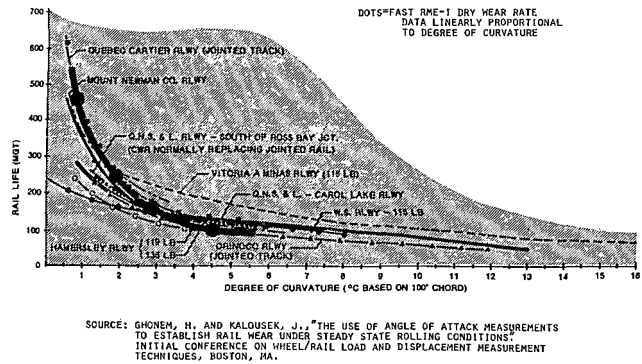


FIGURE 13. COMPARISON OF WEAR RATE DATA DIFFERENT SOURCES WITH THAT FROM RME I.

The distinction of RME III by comparison with RME I is that a greater variety of metallurgies were tested with vastly improved measurement techniques under conditions of planned variation in lubrication level. Attempts were made to provide reasonably close control on the wheel mix of the train. In spite of these controls, there were significant variations in the wear rates of the rails from one lubrication block* to the next. This sort of variation in the dry regime is shown in Table X for the four different standard rail heats tested. The wheel mix and character of the train are given at the top of each column along with the type of mechanical experiment run in that period. The wear rates in the Block II dry regime typically were about 25% higher than those of block I; yet there was virtually no change in the wheel mix or train consist. Then, in Block III, the wear rates dropped, typically by about 40%; the only significant change in the consist was the introduction of some cars of the wheels IV experiment. If B and C wheels were grouped together as 'hard' wheels, the hard wheel content of the train varied from 45% in Block I to 40% in Block II, and then to 53% in Block III; clearly the introduction of hard wheels was not associated with any detectable increase in rail wear rate.

The changes in dry rail wear rate from one lubrication block to another were also associated with a

change in the character of the position-in-curve effect for standard rail. Figures 14a thru 14c illustrate the position-in-curve effect in each lubrication block. From Block I to II, the effect became more pronounced with rail at the south end of the curve exhibiting 25 to 30% greater wear rate than the same heat of rail in the north end. However, in Block III the position-in-curve effect had virtually disappeared.

TABLE X. GAGE FACE WEAR RATES OF STANDARD RAIL: RME III.

(NO LUB REGIME)

Heat #	Segment	BLOCK I		BLOCK II		BLOCK III		
		55% U 42% C 3% B	Valt +RT	60% U 38% C 2% B	Valt +RT +WWI	47% U 43% C 10% B	RT+ WHIV	
21178	III	0.00578	24	0.00717	-40	0.00430		
$C_{eq}=0.94$		0.00561	37	0.00769				
21180	I	0.00502	21	0.00609	-26	0.00448		
$C_{eq}=0.995$		III	0.00654	21	0.00789	-39	0.00483	
		IV	0.00626	35	0.00847	-39	0.00514	
21181	I	0.00557	21	0.00576	-27	0.00506		
$C_{eq}=0.94$		II	0.00668	21	0.00812	-39	0.00492	
		IV	0.00765	33	0.01021	-42	0.00590	
21187	II	0.00507	14	0.00576	-49	0.00292		
$C_{eq}=0.97$								

VALT - Variable Axle Load Test
 RT - Radial Truck Test
 WWI - Wheel Wear Index
 WH IV - Wheels IV Experiment

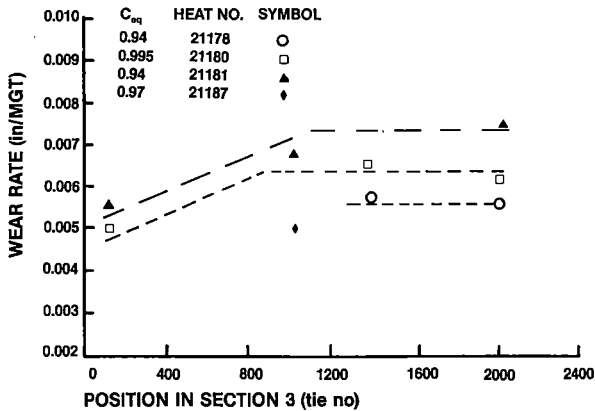


FIGURE 14a. BLOCK I: RME III.

Some variation in superelevation had occurred throughout this period at tie ranges shown in Figure 15. By the dry period of Block I, the superelevation had diminished somewhat from its initial construction level. However, just before the beginning of the dry period in Block II, the superelevation was restored to its initial construction level and it has stayed at that level to the end of operation prior to the summer 1981 installation of concrete ties into Section 3. Thus, the change in superelevation seems unlikely to be associated with the changes in wear rates and in position-in-curve effect.

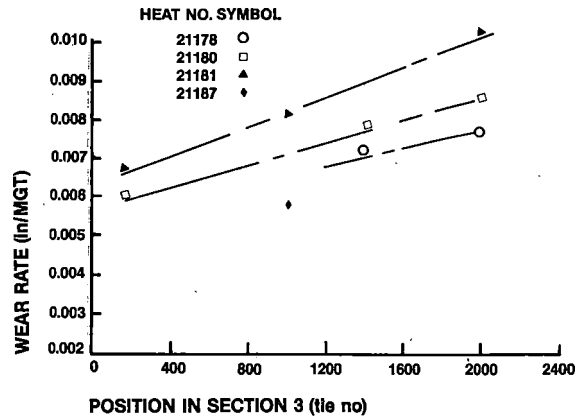


FIGURE 14b. BLOCK II: RME III.

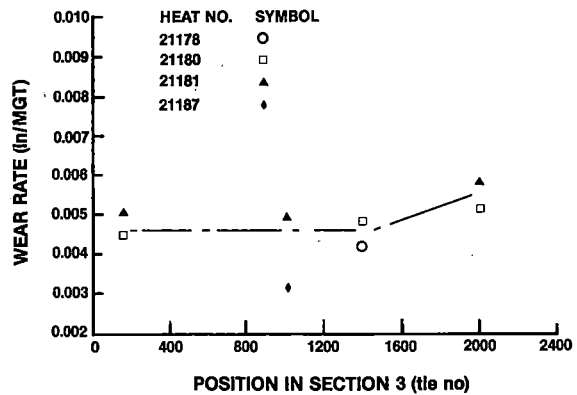


FIGURE 14c. BLOCK III: RME III.

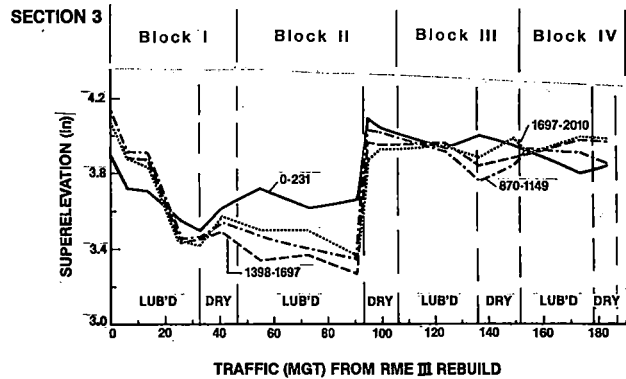


FIGURE 15. VARIATION IN SUPERELEVATION WITH TRAFFIC: RME III.

An overall view of how the wear rates of all test rails in Sections 3 and 17 changed from one lubrication block to the next is given in Figures 16a thru 16d. In the dry periods (Figures 16a and 16b), the premium rails exhibited far less variation in wear rate than did standard rail. Indeed SiCr (HH) exhibited only a mild decrease in wear rate across all four lubrication blocks. FHT rail exhibited a more marked and consistent decrease in wear rate through that period perhaps is indicative of a difference in the gage face resistance of the surface

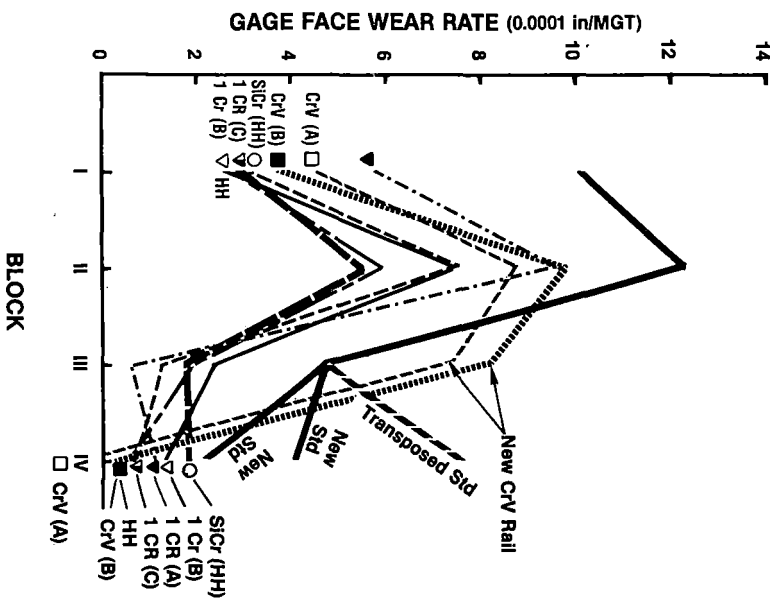
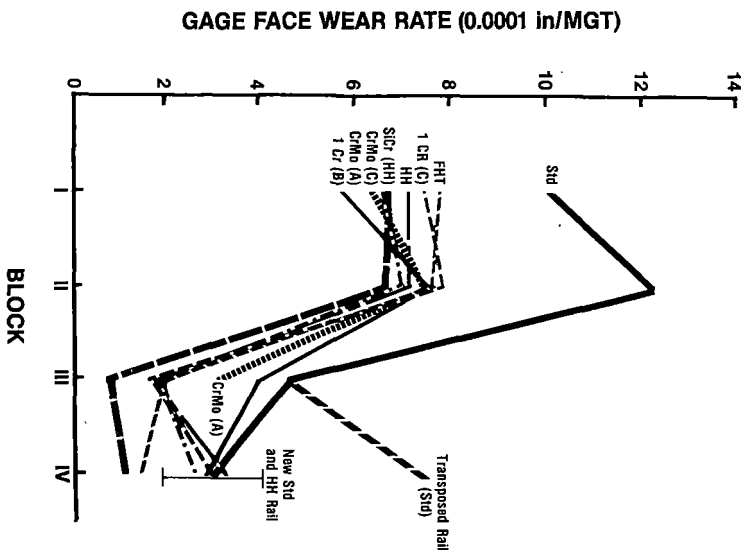


FIGURE 16d. GAGE FACE WEAR RATES; SECTION 17; LUBE.

GAGE FACE WEAR RATE (0.001 in/MGT)

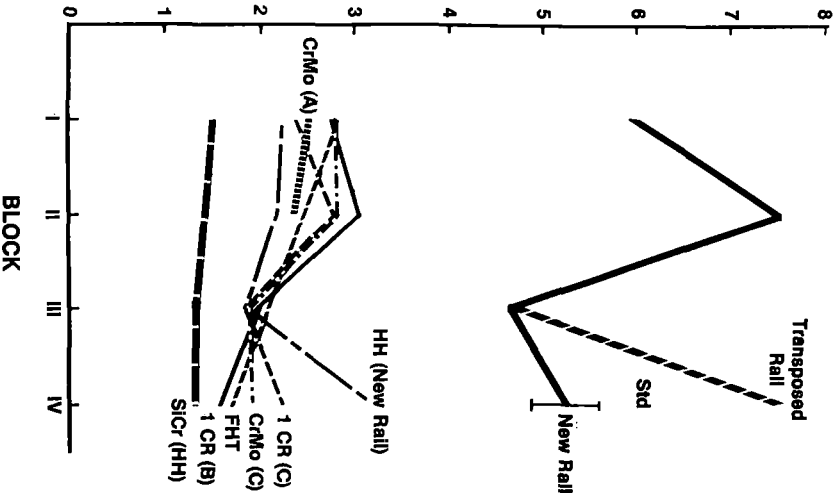


FIGURE 16a. GAGE FACE WEAR RATES; SECTION 03; DRY.

GAGE FACE WEAR RATE (0.001 in/MGT)

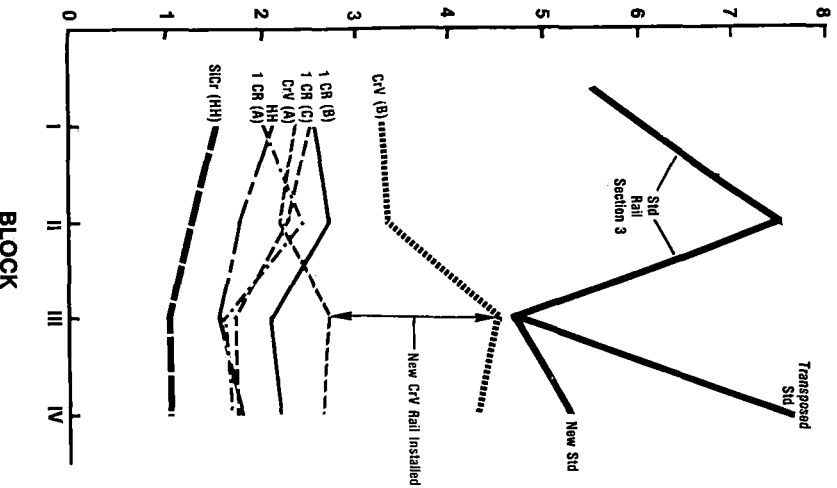


FIGURE 16b. GAGE FACE WEAR RATES; SECTION 17; DRY.

material as opposed to the material further within the rail head. Clearly, though, in the dry periods, SiCr(HH) rail stood by itself as the most resistant rail to gage face wear. All the other metallurgies except for CrV(B) were clustered together, intermediate in performance. The CrV, from two different manufacturers, which was tested only in the 5 curve of Section 17, exhibited differences in performance. While that rail from supplier 'A' behaved about the same as that of the other intermediate group rails, that from supplier 'B' exhibited notably poorer gage face wear resistance.

A similar situation existed for CrMo(A) rail. Within one stretch of rail very large differences in wear rate could occur. The magnitude of this variation is shown in Table XI; at the low wear rate end, the rail performed better than any of the other intermediate group rails, but at the high wear rate end, it performed only slightly better than did standard carbon rail. Notably, it did not exhibit the large change in wear rate observed for standard carbon rail in Blocks I and II.

TABLE XI. CrMo(A) AS A SPECIAL CASE; GAGE POINT WEAR RATES FOR DRY REGIME: RME III.

Segment	Group	Block I	Block II
I	Hi Wear Rate	0.0048"/MGT	0.0048"/MGT
	Lo Wear Rate	0.0018"/MGT	0.0019"/MGT
II	Hi Wear Rate	0.0046"/MGT	0.0049"/MGT
	Lo Wear Rate	0.0032"/MGT	0.0029"/MGT

Invariably when new rail, from the same heats as tested before, was installed in the course of the operation at the beginning of the lub'd period, the wear rate in the subsequent dry period would be greater than that of the same rail just removed from test. This was true for new standard and HH rail (Block IV), and new CrV rail (Block III). In the case of new standard rail introduced in Block IV, the average wear rates were not quite so high as those of the rail originally installed upon construction. Standard carbon rail transposed from the low rail has exhibited an exceptionally high gage face wear rate compared to the same heats of rail installed initially in the high rail.

The behavior of the test rail in the lubricated periods generally has been the same from one block to the next as has the behavior of the rail in the dry periods (Figures 16c and 16d). However, in lubricated periods of Block III, the same factor which led to the general decrease in wear rates observed in the dry periods, lowered wear rates of the premium rails far more relative to that of standard rail than would have been expected.

Only in Block III do the figures of merit of the premium rails in the lubricated periods approach those values observed in the dry period. This can be seen in Table XII. The discrepancy appeared only in the lubricated portion of Block III; in the dry period, the figures of merit of all rail except CrV were generally the same as those observed in the other dry periods. A suitable explanation for the anomalous behavior of the rail in the lubrication portion of Block III is not at hand.

TABLE XII. FIGURES OF MERIT FOR GAGE FACE WEAR: RME III.

Metallurgy	BLOCK I		BLOCK II		BLOCK III		BLOCK IV	
	Sec. 3	Sec. 17*	Sec. 3	Sec. 17*	Sec. 3	Sec. 17*	Sec. 3	Sec. 17*
	L	NL	L	NL	L	NL	L	NL
Std.....	1.0	1.0	/	/	1.0	1.0	/	/
HH.....	1.6	2.7	/	/	1.7	3.5	/	/
FHT.....	1.4	2.1	-	-	1.7	3.0	-	-
SiCr(HH).....	1.7	4.0	1.5	3.7	1.9	5.2	1.7	3.8
A.....	-	-	0.8	2.8	-	-	1.1	2.6
B.....	1.9	2.2	1.6	2.3	1.6	2.5	1.4	2.3
C.....	1.5	2.5	1.5	2.3	1.6	2.7	1.4	2.7
1 CR.....	-	-	-	-	-	-	-	-
A.....	1.8	2.4	-	-	1.6	3.2	-	-
B.....	1.9	2.2	-	-	1.7	2.7	-	-
C.....	1.6	2.2	-	-	1.7	2.7	-	-
CrMo.....	-	-	-	-	-	-	-	-
A.....	-	-	1.0	2.5	-	-	1.2	2.8
B.....	-	-	1.2	1.8	-	-	1.0	1.9

* Adjusted against Section 3 by assuming HH in both sections is equivalent

In addition to gage face wear rates some information is available from transverse profile measurements* about head height loss rates of the outside rail. Because of the relatively short lube and no lube periods in each lubrication Block, the results from Blocks I and II have been averaged for presentation in Table XIII. Perhaps because a greater effort was made to keep the running surface free of lubricant, the variation in head height loss rate from lubricated to dry regimes is far less obvious (and less consistent) than it was in the first experiment.

TABLE XIII. HEAD HEIGHT LOSS RATES FOR HIGH RAIL ONLY.

Metallurgy	Section 3		Section 17	
	Lub'd.	Dry	Lub'd.	Dry
Std.....	0.0007	0.0021	---	---
HH.....	0.0004	0.0002	0.0005	0.0004
FHT.....	0.0004	0.0007	---	---
SiCr(HH).....	0.0010	0.0013	0.0003	0.0007
1 CR.....	0.0003	0.0009	---	---
CrMo(A).....	0.0007	0.0005	---	---
(C).....	0.0005	0.0003	---	---
CrV.....	---	---	0.0006	0.0016

Interestingly, the SiCr(HH) rail which exhibited outstanding resistance to gage face wear in the dry periods is grouped with CrV rail in an intermediate category in this regime. All other premium rails exhibited height loss rates less than 0.001"/MGT. In view of the wide scatter inherent in transverse profilometry measurement values, all those metallurgies showing rates less than 0.001"/MGT must be considered to be performing the same.

Metal flow measurements made on the standard carbon low rail with the snap gage type instrument are shown in Figures 17a and 17b. As with the standard carbon (low) rail in the first experiment, the major metal flow was to the field side. However unlike the behavior observed in the first experiment, the lateral flow seemed to have increased rapidly with each succeeding dry period. Because measurements were made only at the end of dry periods, it cannot be established whether most flow occurred in the lubricated or in the dry regimes. But, the fact that flow increased after each dry period in contrast to the levelling off (on the field side)

* Regrettably, the head height loss snap gage did not become available until the beginning of the third lubrication block.

observed in the lubricated period of the first experiment, does suggest that lubrication of the high rail has a beneficial effect on metal flow on the low rail. There was not sufficient metal flow of any of the premium rails to make a judgement about their relative performance.

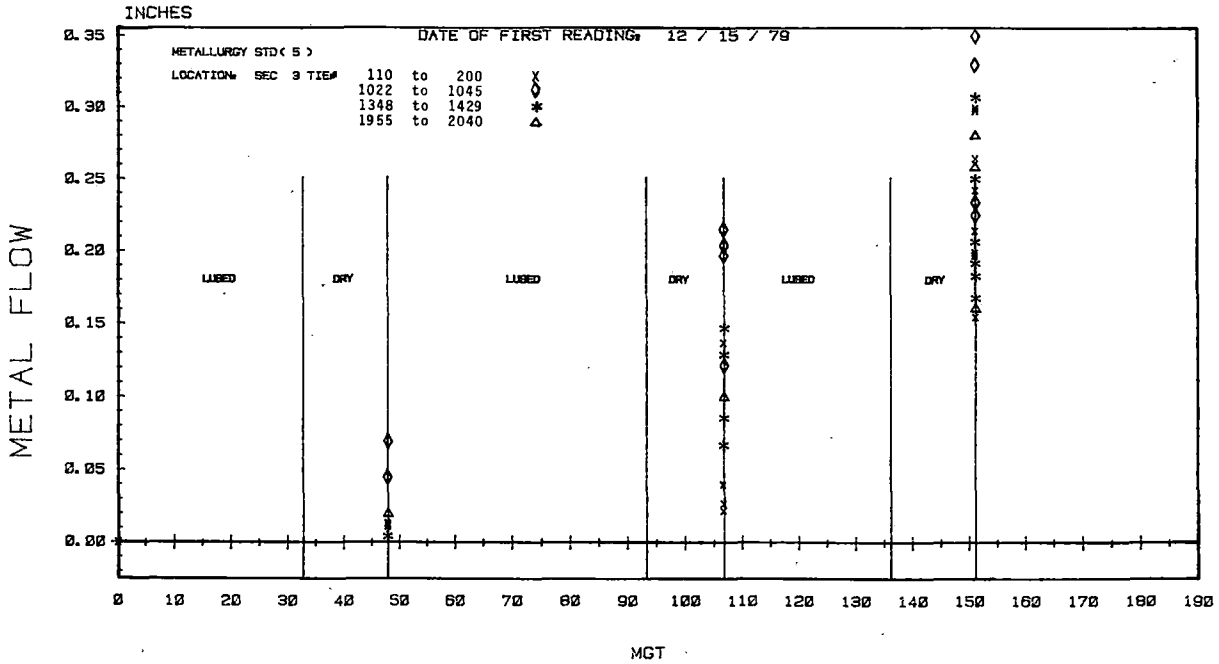


FIGURE 17a. METAL FLOW LOW RAIL FIELD MEASUREMENT
SNAP GAGE: RME III.

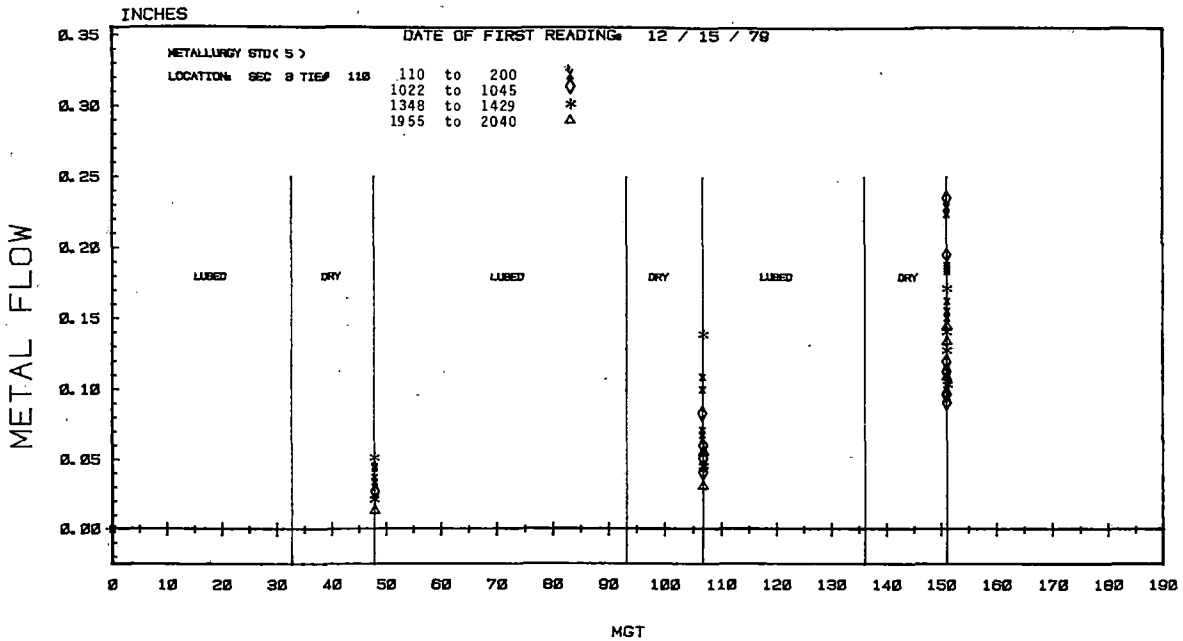


FIGURE 17b. METAL FLOW LOW RAIL GAGE MEASUREMENT
SNAP GAGE: RME III.

Considerably more attention has been paid to hardness of rails in the current experiment than was paid in the first experiment. Both light load (~1 kg Eseyaw) and high load (3000 kg Brinell) indentation tests have been made at intervals throughout the period of the experiment. Figure 18 presents both types of hardness data for the running surface together at various times during the experiment. As can be seen not all the different metallurgies behaved the same. For instance, SiCr(HH) seems to have exhibited a consistent increase in hardness with exposure to service as determined by both measures of hardness. CrMo(A), on the other hand, seems to have exhibited a continued increase in light load hardness with service but a slight reduction in high load hardness after a maximum was reached following a period of service. 1 Cr exhibited a peak in high load Brinell hardness followed by a slight drop although light load hardnesses appear to have continued to increase with service exposure. Most interestingly standard carbon rail exhibited a peak followed by a decrease in both measures of hardness. The light load is not particularly suitable for making comparisons over long periods of time, but it does provide a reasonable basis for comparison when readings are taken in the same time period. Thus, the indicated continued increase in hardness for SiCr(HH) and the peaking followed by a decrease for standard rail are probably true.

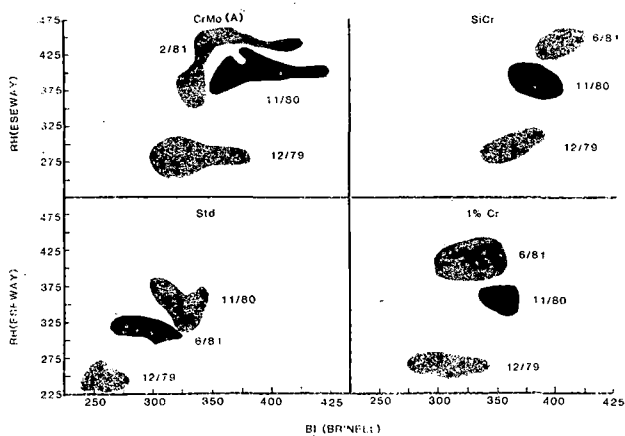


FIGURE 18. HARDNESS POPULATION DISTRIBUTION.

Using the as-worn gage face hardnesses after the second lubrication block along with the average wear rates of each metallurgy, the relationship between wear rate and hardness may be plotted as shown in Figures 19a and 19b for the different lubrication regimes. A semi-logarithmic format has been chosen because a straight line plot of dry regime wear rate against hardness would imply zero rate at 430 BHN - not a very believable situation. The slope of the line in the dry regime is considerably steeper than that in the lubricated regime - a consequence of the behavior observed in the first experiment, the lateral flow seemed to have increased rapidly with each succeeding dry period. Because measurements were made only at the end of dry periods, it cannot be established whether most flow occurred in the lubricated or in the dry regimes. But, the fact that flow increased after each dry period in contrast to the levelling off (on the field side)

metallurgy:lubrication interaction. Most data falls closely along the straight lines; however, both FHT and CrMo(A) are not with that group of data. The CrMo(A) is believed to be at least partially bainitic and therefore may be quite hard but will possess poor wear resistance. The poorer gage face wear performance of FHT rail than would be expected from its hardness is less easy to explain. However, the gradual diminution of its gage face wear rate as metal is removed from the gage face, suggests that there may be a microstructural gradient from the rail surface to the interior. An interesting (but unexplained) observation shown in Figure 19b is that in the first lubricated period the wear rate of rails in Section 17 (5°) was notably less than the same metallurgies (same heats) in Section 3. However, as comparison of Figures 16c and 16d reveals, in the second lubricated period, the wear rates in Section 17 (5°) increased to about same average level as those in Section 3 although the spread of values was substantially greater.

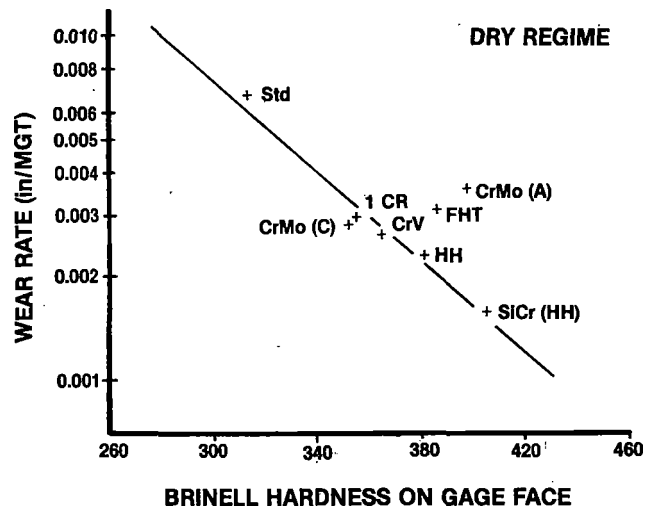


FIGURE 19a. WEAR RATES AS A FUNCTION OF HARDNESS: RME III.

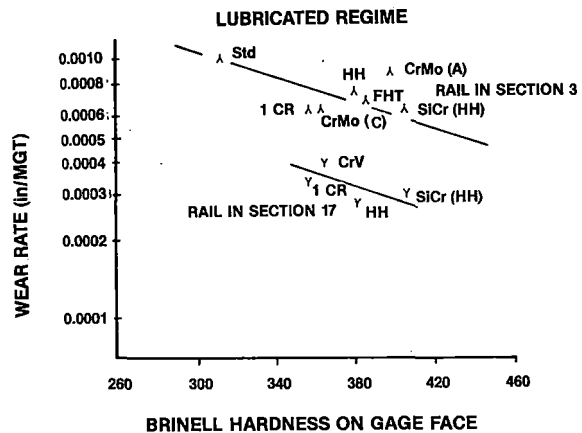


FIGURE 19b. WEAR RATES AS A FUNCTION OF HARDNESS.

One further use may be made of the gage face wear data from the current experiment and that is to extend the formulation for the contribution of equivalent carbon to alloying elements. There has not been enough data available to accomplish this in a rigorously correct statistical fashion, but if the assumption is made that the alloying elements do not interact with each other, (i.e., the effect of X w/o Cr in a Cr alloy would be the same as X w/o Cr in a CrMo or CrV alloy) and that mill processing variables from one manufacturer to another do not dominate over the alloy effects, then one can extend the formulation by first considering the 1 Cr alloy to assess the contribution of Cr and then CrMo and CrV alloys to assess the Mo and V. The basic tenet of this approach is that the slope of the wear rate vs C_{eq} plot is the same, regardless of how the alloy elements contribute equivalent carbon terms. In doing this the 1 Cr(B) and CrV(B) have been excluded from the development of the formulation because they do indeed seem to behave differently from the other alloys of the same nominal composition from different manufacturers. Figure 20 shows that the wear data of the alloy rails (excluding those of manufacturer B) cluster around the dashed line (extrapolated from the standard rail data of the current experiment) parallel to the line observed for Std and HiSi of the first experiment when equivalent carbon is calculated according to the equation:

$$C_{eq} = w/o C + w/o Mn/4.75 + w/o Si/10 + w/o Cr/6.4 + w/o Mo/3.8 - w/o V/4.4$$

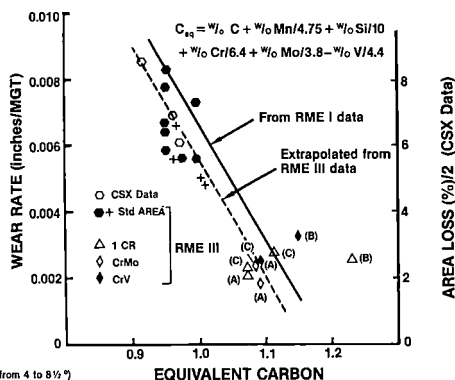


FIGURE 20. EFFECT OF EQUIVALENT CARBON EXPANDED TO INCLUDE ALLOY ADDITIONS: RME III.

s formulation implies that Cr does not have quite as strong an effect on wear as does Mn and that Mo has a slightly stronger influence than does Mn. Vanadium appears to have a negative effect, i.e., its presence may strengthen the alloy but does not improve its wear resistance. Caution is urged in applying this formulation too widely because mill processing variables (as in the case of manufacturer B) clearly can dominate over the alloying contribution. Nevertheless, the results from FAST do raise a serious question of whether vanadium provides the improvement in wear resistance that it is thought to provide.

To summarize now for the topic of wear and metal flow:

- o Typical maximum gage face figures of merit
 - Alloy rail = 3
 - Heat treated std carbon rail = 3
 - heat treated alloy rail = 4
- o The relative benefit of lubrication depends upon the type of rail.
- o Within the full allowable AREA chemistry range a 3:1 variation in gage face wear rate would be expected.
- o Hardness and yield strength are not necessarily good indicators of gage face wear resistance.
- o Metal flow on the low rail does seem to be influenced by lubrication on the high rail.
- o Significant metal flow (low rail) was observed only in standard and HiSi rail.
- o Uncontrolled variations in rail wear and metal flow behavior from one lubrication block to the next substantially weaken comparisons made among blocks; strongest comparisons are made within individual blocks.

WELDED RAIL END BATTER

The introduction of continuous welded rail (cwr) has vastly improved the geometric stability of the track structure. Nevertheless, the localized change in the metallurgical character of the rail that can occur in the vicinity of welds can ultimately lead to a loss of running smoothness which, like corrugations, can promote the development of localized track geometry irregularities, such as the kink shown in Figure 21. Loss of surface, pulverizing and movement of the ballast, release of anchoring action with ensuing movement of ties, and enhanced running of rail are some other annoying problems that seem associated with batter and corrugations.



FIGURE 21. A KINK ASSOCIATED WITH WELDED RAIL END BATTER.

The different metallurgies, types of track, and lubrication levels existing at FAST permit a fairly comprehensive experiment for both flash butt and

thermite welds. At least one plant weld of each metallurgy on the high rail and low rail has been monitored in Section 3 and Section 17 except for FHT where only one site was monitored initially. The primary type of measurement is longitudinal profilometry accomplished with the instrument shown in Figure 22. The instrument produces a paper trace whereon the vertical displacement along the rail is magnified 17 times and the longitudinal dimension is reduced by nearly 4:1. A built-in calibration step permits direct calibration of the instrument on each trace.

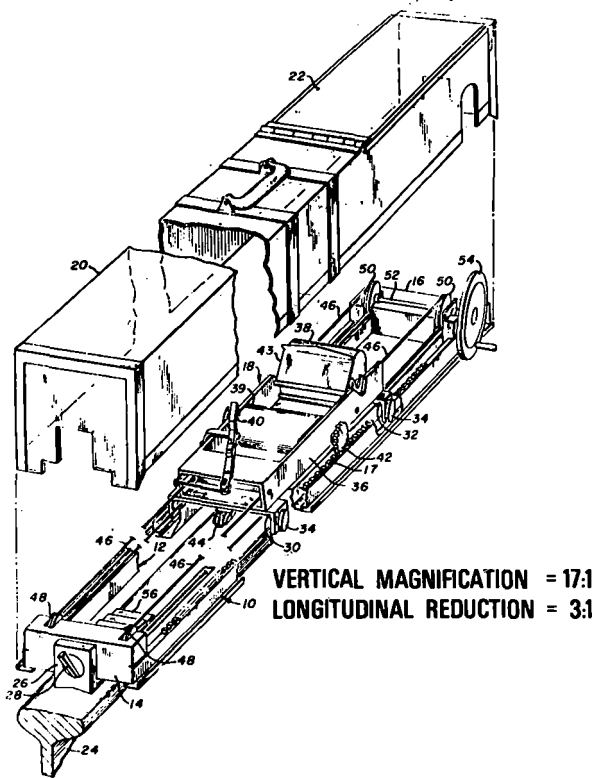


FIGURE 22. LONGITUDINAL RAIL PROFILOMETER.

The weld behavior observed has fallen into the three general categories: single dippers, double dippers, and peaked as shown in Figure 23. The distinction between the double dipper and the peaked configuration is in the position of the valleys and the height of the peak. The valleys of the double dipper occur in the heat affected zones (HAZ) next to the welds whereas in the case of the peaked configuration, the valleys develop outside the HAZ in the base rail. Also, the peak tends to rise above the smooth running surface of the rail.

The heat treated rails exhibited a single dipper behavior, the alloy rail welds were double dippers, and standard carbon rail exhibited the peaked behavior. Some examples of the type of batter found are shown in Figure 24. An unusually bad weld developed 0.05" of batter in 50 MGT whereas a good weld developed only 0.02" of batter in 175 MGT.

Welds of two metallurgies, CrMo(A) and CrV, were tempered at 1000°F for 20 minutes after welding because no post heat that could be applied following

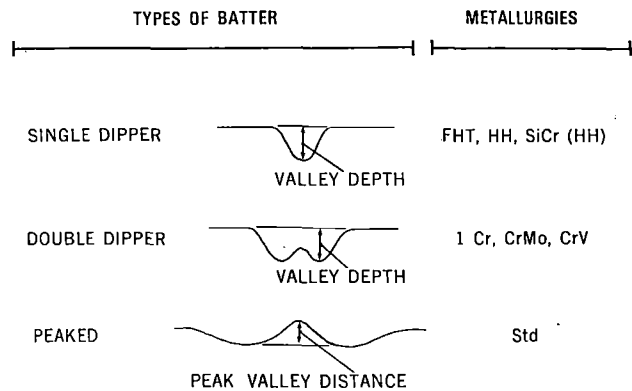


FIGURE 23. CATEGORIES OF WELD BEHAVIOR.

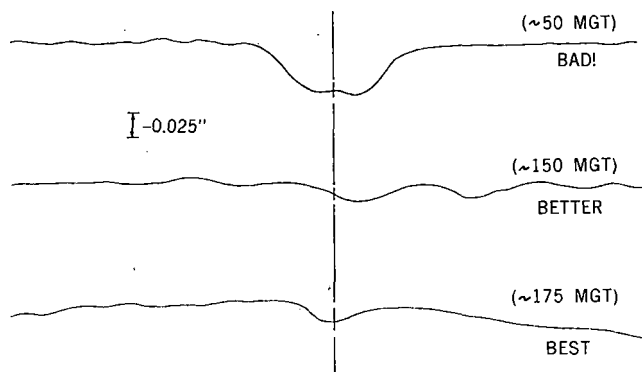


FIGURE 24. EXAMPLES OF WELDED RAIL END BATTER.

weld upset was found to be able to prevent the occurrence of substantial quantities (>30%) of untempered martensite in either the front or back of the base.* Some of these tempered welds performed extremely poor. The behavior of a typical tempered CrMo weldment is compared with the behavior of a weld of weldable grade CrMo that requires no post heat in Figure 25. Although the weldable grade developed about 0.035" batter by the end of the second dry period (106 MGT), the tempered weldment had developed nearly 0.09" of batter at 90 MGT; had not the weld been ground, batter might well have reached 0.150" by 150 MGT. A similar behavior was observed with the CrV rail as shown in Figure 26. For comparison, a 'properly'** postheated weld is shown to exhibit very little batter. It was with these tempered weldments that the aggravating effect of dry running was first noticed.

*The problem appeared to be associated with the development of an uneven heating pattern across the rail base which was especially severe upon post heating.

**The word 'properly' should be interpreted to mean avoidance of untempered martensite; however the postheating practice required seventeen 3 second pulses separated by 27 second intervals.

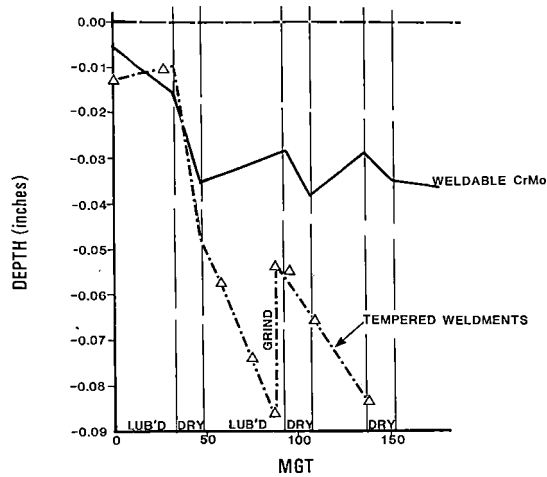


FIGURE 25. CrMo RAIL/VALLEY DEPTH INSIDE/RAIL SECTION 03.

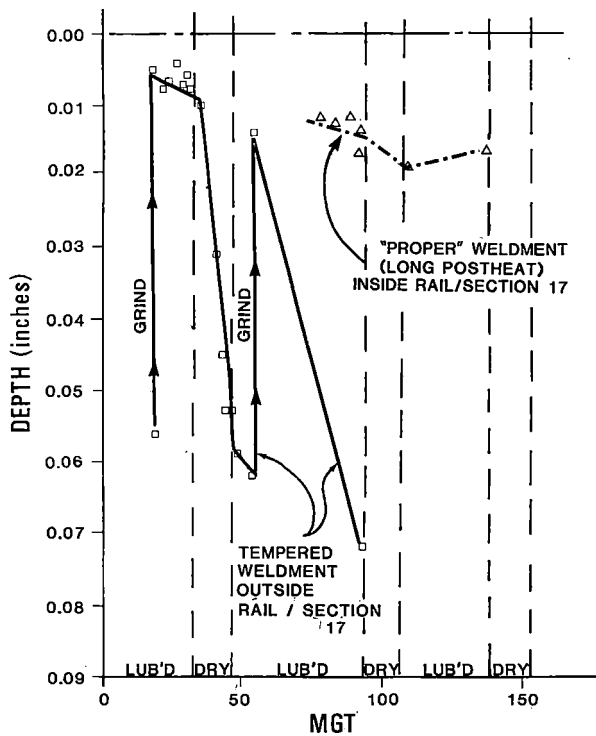


FIGURE 26. CrV RAIL/VALLEY DEPTH.

The behavior of a standard carbon flash butt and a thermite weld in tangent track is shown in Figure 27. Although the initial surface irregularity of the thermite weld was much greater than that of the flash butt weld, the batter development of both types of welds was remarkably similar. After the initial lubricated period, the thermite weld had exhibited some smoothing out of the initial irregularity, even though the width of the HAZ of the thermite weld was much greater than that of the flash butt weld.

By way of comparison, a flash butt weld of standard carbon rail in the 5° curve (Section 3) developed a

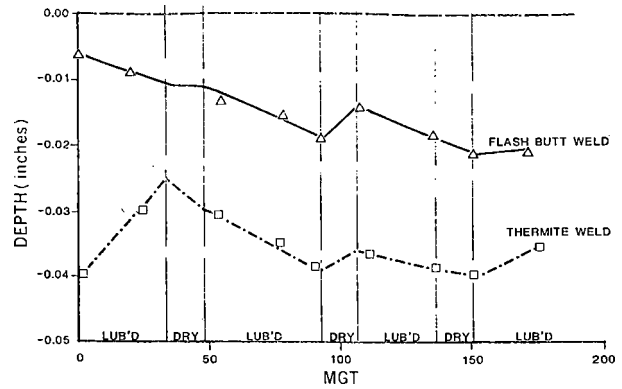


FIGURE 27. AREA STANDARD CARBON RAIL/VALLEY DEPTH FLASH BUTT AND THERMITE/TANGENT WELD.

somewhat different growth pattern (Figure 28). While the valley depth change beneath a smooth surface was not unlike that of a weld in tangent track (except perhaps in the third dry period), a peak had developed above the smooth running surface, probably as a consequence of the smooth running surface receding below the initial running surface while the metal at the weld bond line did not recede. The peak to valley height showed a strong tendency to grow much more rapidly in the dry periods than it did in the lubricated period with the exception of the first lubricated interval. This behavior was somewhat similar to that of the tempered CrMo(A) and CrV and of the CrMo(C) as well.

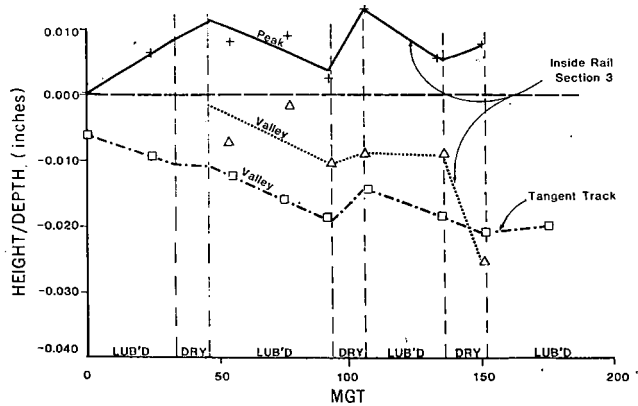


FIGURE 28. AREA STANDARD CARBON RAIL/VALLEY DEPTH AND PEAK HEIGHT.

Figure 29 illustrates the behavior at CrMo(C) on the inside and outside rail. The same general pattern has been observed on both rails, although the effects of dry and lubricated operation seem somewhat more pronounced on the inside rail where batter depth increased by about 0.03" in about 175 MGT. It is important to note again that only the outside rail was lubricated effectively and that the running surface of the inside rail was almost always dry.

However, on weldments which exhibited good resistance to batter, the effect of dry running to accelerate batter was not so certain. As shown in Figures 30 and 31 for 1 Cr and SiCr(HH) respectively,

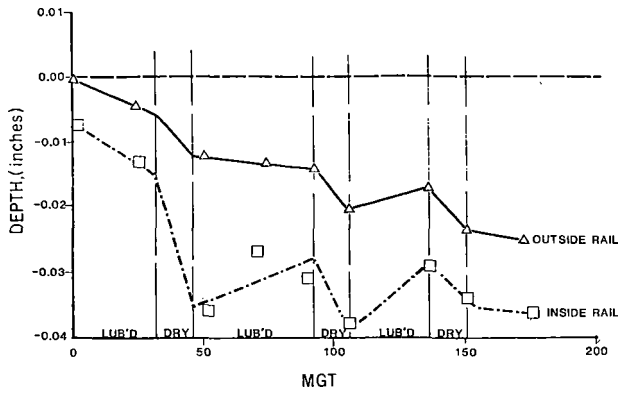


FIGURE 29. CrMo(C)/VALLEY DEPTH.

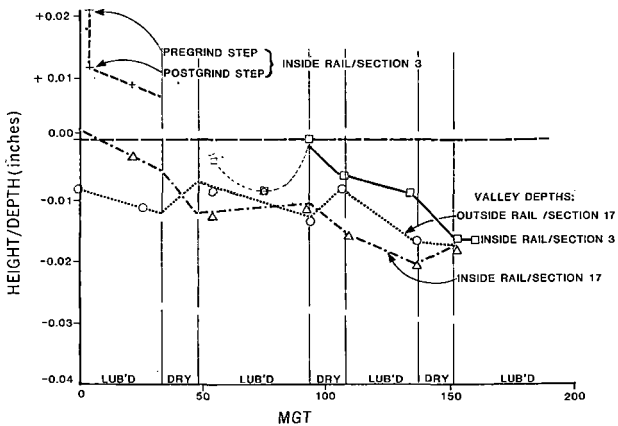


FIGURE 30. 1 Cr/VALLEY DEPTH AND STEP HEIGHT.

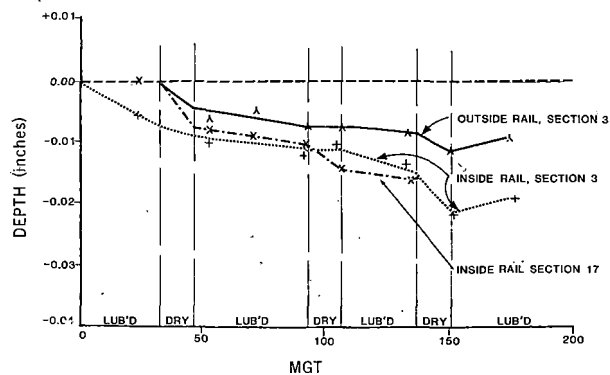


FIGURE 31. SiCr(HH)/VALLEY DEPTH.

there appeared to be some variability in behavior. However, perhaps this lower sensitivity to lubrication is related to the fact that the SiCr alloy has been designed so as to harden upon cooling after welding at the rates (slack quenching) characteristic of the weld and HAZ without post heat. In a similar sense, the 1 Cr welds have been given a very unusual post heat to prevent the formation of untempered martensite which tests had shown would otherwise have occurred on the welder used. For these superior weldments, batter depth would have reached only 0.02" at 150 MGT.

There were some differences in the behavior of heat treated standard carbon rails. Figure 32 shows that an FHT weldment in the outer rail was battering at a rather low rate after the first lubricated period with little or no effect of dry operation. An outside rail HH weldment also was exhibiting minimal batter. However, the inside rail HH weldment which was monitored in the same region, exhibited a rather exceptional batter propensity. The damaging effect of dry operation was particularly noticeable. Grinding at 80 MGT did nothing to slow the deterioration (in a fashion similar to the behavior of the tempered CrMo and CrV). Subsequent checks of other FHT and HH weldments in test Sections 3 (FHT + HH) and 17 (HH only) revealed that other FHT weldments in both inside and outside rail exhibited total batter similar to that of the monitored weldment. However, the HH was behaving in two different fashions--one group of about one-half the weldments had exhibited very little batter while the other half had exhibited total batter similar to that of the inside rail weldment shown in Figure 32. At this time we have no clear explanation for the behavior; with the exception of the SiCr(HH) rail, all rails for which information is presented here were welded on the same (60 kA) welder in the same time frame.

A comparison of inside rail weldments is given in Figure 33. The figure shows that SiCr(HH) and 'properly' post heated 1 Cr and CrV were all about

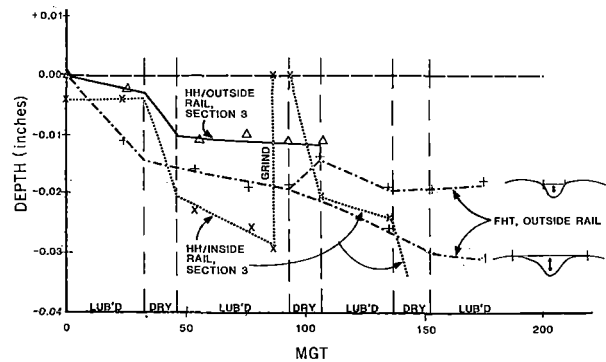


FIGURE 32. HEAT TREATED AREA STANDARD CARBON RAIL/ VALLEY DEPTH.

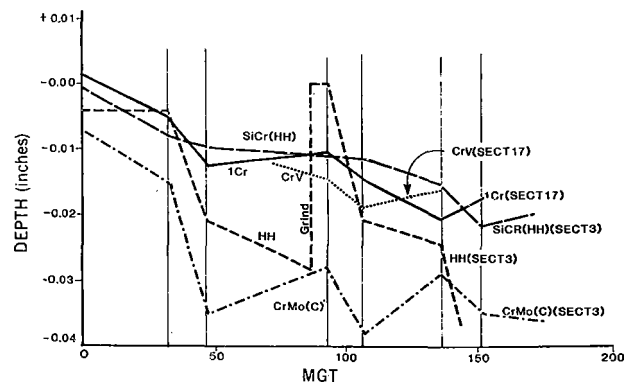


FIGURE 33. COMPARISON OF MAXIMUM VALLEY DEPTHS OF PREMIUM RAIL/INSIDE RAIL.

the same in performance but that weldable grade CrMo(C) had developed somewhat greater batter (mostly in the dry periods). The batter depth increase of the HH weldments in the lubricated periods was not unlike that of SiCr(HH), 1 Cr, and CrV weldment but it appeared to be particularly susceptible to dry operation.

In the alloy rails, the valleys of the 'double dip' occurred in the HAZ on either side of the weld bond line, and, therefore, one might expect a relationship between the depth of batter and the surface hardness. Figures 34a thru 34d plot the hardness profile and the surface profile together and show the correlation, such as it is, between surface hardness and batter. Although the valleys did indeed tend to occur at the places where the hardness, at least initially, was lowest, substantial valley depth occurred without the presence of low surface hardness. Likewise, large dips in hardness occurred without the presence of deep batter at these points. Thus, running surface hardness, at least as measured in the field, would not seem a good indicator of batter resistance.

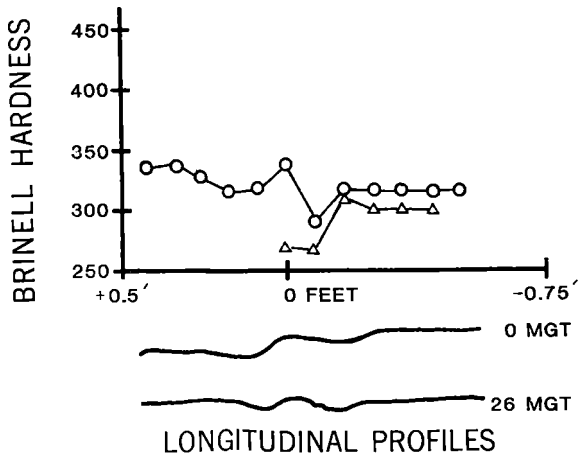


FIGURE 34a. 1 Cr RAIL 1ST LUBRICATION PERIOD.

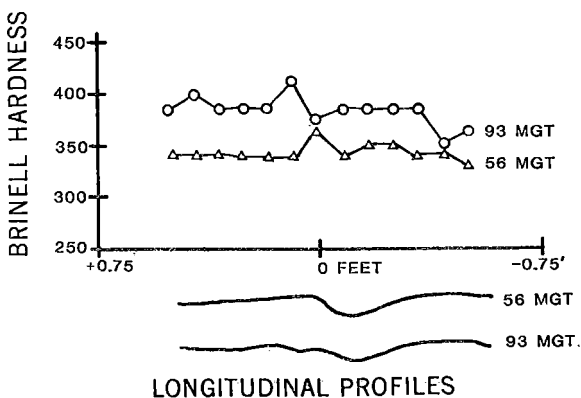


FIGURE 34b. 1 Cr RAIL 2ND LUBRICATION PERIOD.

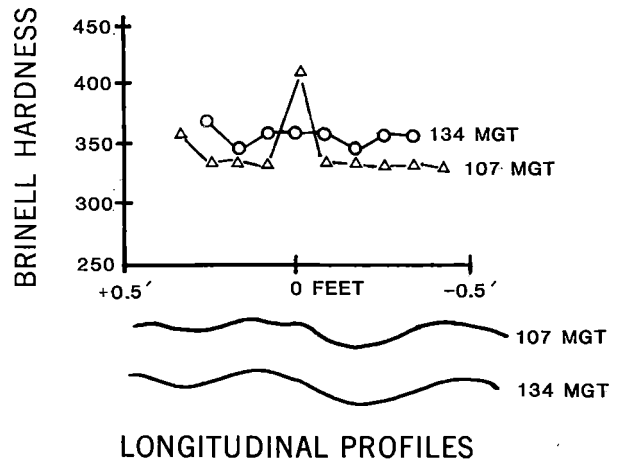


FIGURE 34c. 1 Cr RAIL 3RD LUBRICATION PERIOD.

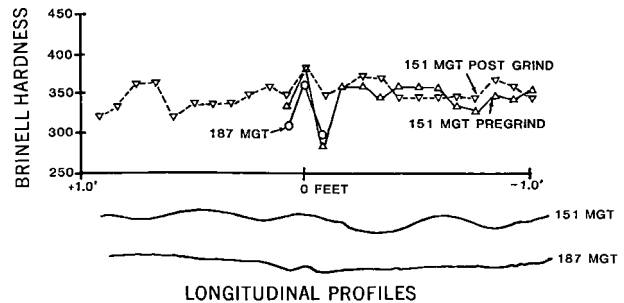


FIGURE 34d. 1 Cr RAIL 4TH LUBRICATION PERIOD.

If the value of hardness in the HAZ does not control batter development, the width of the HAZ may. The superior performance of the 'properly' post heated 1 Cr and CrV weldments as opposed to the performance of the CrMo(C), which does have a wide HAZ, suggests that attention should be paid to the influence of different combinations and types of preheat and post heat for alloy rail.

The width of the HAZ appeared to be a function of the temperature at which the pearlite transformation started in the upset (forged) region of the weld. Post heats fall into two major categories-- the short delay and the long delay. The short delay practice involves holding the weld in the welder for 20-40 seconds after completion of upset and then applying numerous heating pulses (typically of 2-6 second duration) separated by intervals comparable in length to the heating pulses. Thus heat is added to the weldment when it is still hot so that stripping may follow post heating. The long delay practice involves waiting 60 seconds or longer following completion of upset before the post heat cycles are applied. In this delay period, the weld is stripped while it is still hot and, if an external stripper is used, returned to the welder following stripping. After the rail is locked up again in the welder, one or two relatively long pulses (6-10 seconds) are applied to the weldment with a rather long interval (20-30 seconds) between pulses.

In the case of the 'properly' post heated 1 Cr and CrV weldments seventeen 3-second pulses separated by

27-second intervals were applied. The cooling paths each type of practice would follow are shown conceptually on the continuous cooling transformation diagram (Figure 35). The important difference between the two practices is that the long delay practice introduces the additional heat needed to prolong the cooling process at a substantially lower temperature. The interlamellar spacing of the pearlite (S_p) is inversely proportional to the temperature difference below the eutectoid temperature (1333°F) at which the pearlite transformation takes place. Thus, the lower temperature, at which the pearlite reaction occurs for the long delay practice, will result in a more refined microstructure in the weldment.

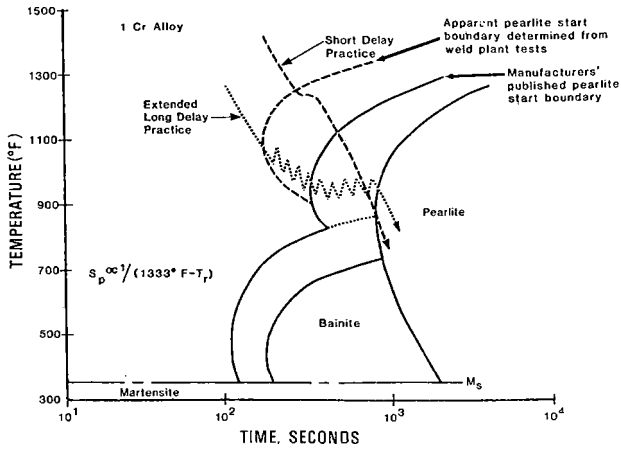


FIGURE 35. COOLING PATHS ON THE CONTINUOUS COOLING TRANSFORMATION DIAGRAM.

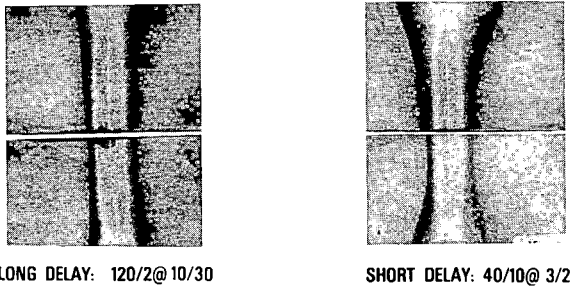


FIGURE 36a. PHOTOGRAPHS OF MACROETCHED PIECES FROM CrMo RAILS.

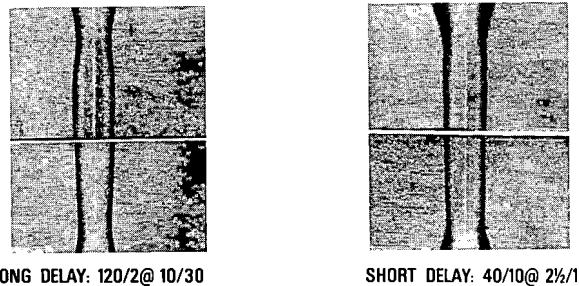


FIGURE 36b. PHOTOGRAPHS OF MACROETCHED PIECES FROM 1 Cr RAILS.

Figure 36a and 36b illustrate the fact that the short delay practice can cause the distance between the HAZ boundaries at the running surface to be about twice as large as that produced by the long delay practice--at least for CrMo(A) weldments on the 60 kA welder. The hardness profile in each of these welds just below the running surface is shown in Figures 37a and 37b.

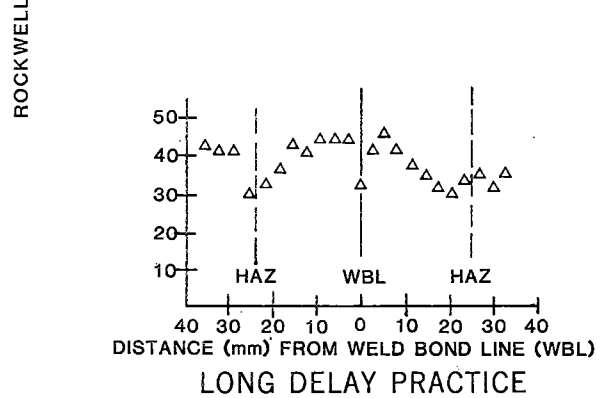
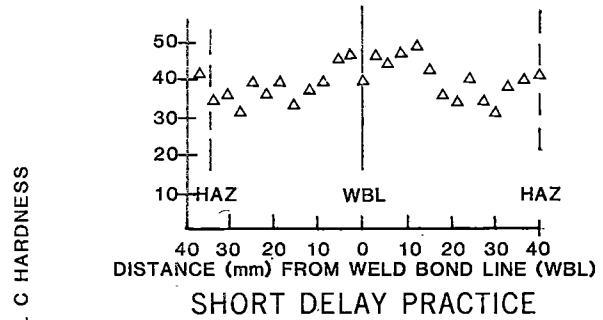


FIGURE 37a. HARDNESS AS A FUNCTION OF DISTANCE FROM WELD BOND LINE CrMo RAIL.

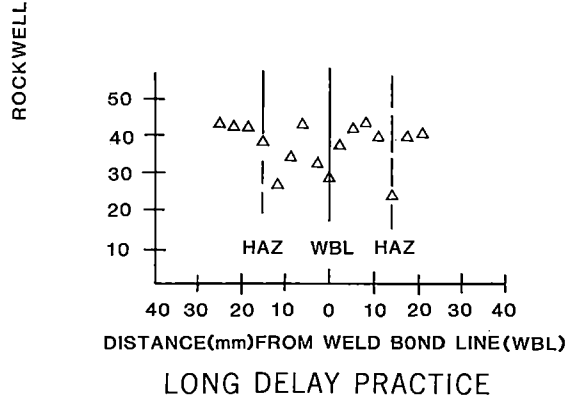
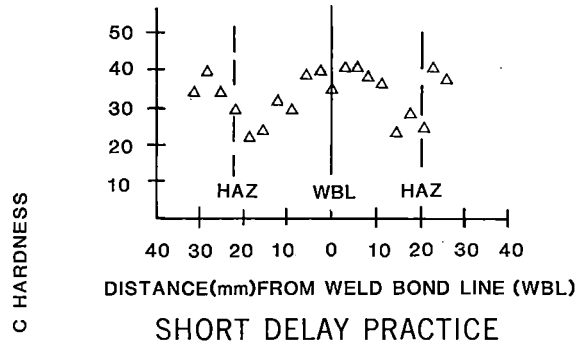
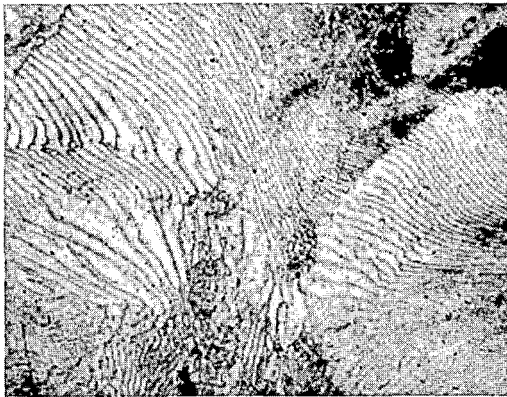


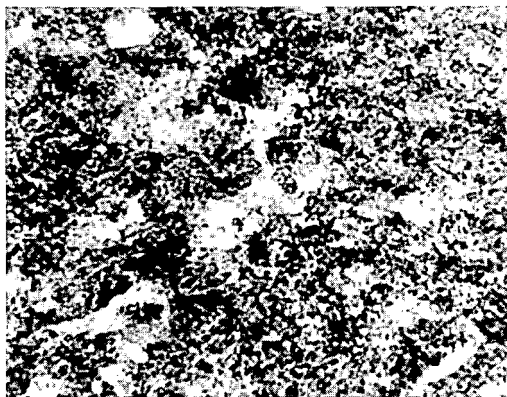
FIGURE 37b. HARDNESS AS A FUNCTION OF DISTANCE FROM WELD BOND LINE 1 Cr RAIL.

The minimum hardness was about the same for either practice, but the extent of the softer region was much greater with the short delay practice for each metallurgy.

The very poor behavior of the tempered CrMo and CrV weldments can be understood in terms of the change in microstructure which the tempering operation induced. Figure 38 illustrates the decomposition of the pearlite structure which had occurred. The decomposition would not have been expected if the temperature of tempering truly were 1000°F; the structure is characteristic of heating to 1250°F or higher.



1600X
A. PROPER PEARLITIC MICROSTRUCTURE



1600X

FIGURE 38. DECOMPOSED PEARLITIC MICROSTRUCTURE IN BATTERED CrV WELD.

Up to this point in the discussion, only depth of batter has been considered. Another important characteristic parameter is the wavelength. One way of treating both amplitude and wavelength (really wave shape) of any continuous curve is the Fourier series. The mathematical representation of this is given as

$$\text{HEIGHT} = A_0 + \sum [A_j \cos(jx) + B_j \sin(jx)]$$

A_0 , A_j , and B_j are empirically determined constants for increasing values of j (as many as needed to provide a suitable description of the curve), and x is the distance along the rail from the weld centerline.

This technique has been used to describe the running surface of a flash butt weldment of standard carbon rail located in Section 3. To simplify the process slightly the wave shape has been made symmetrical about the weld centerline. Separate sets of coefficients for dry and lubricated running have been obtained as a function of MGT by assuming that the change in batter that developed in any one dry or lubricated interval was unaffected by what happened in the immediately-previous period so that the changes in all dry periods and in all the lubricated periods can be summed separately.

For each lubrication regime, seven coefficients and A_0 have been found to provide an adequate description of the batter process in the weld considered. Figure 39 illustrates how these coefficients and constant A_0 changed with tonnage. Clearly the dry periods led to rapid, apparently non-linear, increases in the coefficients after about 30 MGT (dry) of traffic. Lubrication on the other hand tended to lead to a fairly steady value for each of the coefficients. It is also worth noting that coefficients seem to behave in a grouped fashion. For instance, in the dry regime, A_0 and A_1 seemed virtually identical, A_2 was nearly constant near zero, A_3 and A_7 were identical, and A_4 , A_5 , and A_6 were all virtually identical. Thus, in reality the variation of four coefficients and one constant adequately described the batter development.

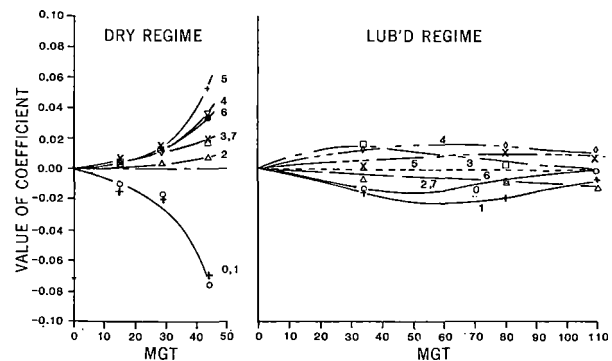


FIGURE 39. VARIATION OF FOURIER SERIES COEFFICIENTS.

The variations in the constant and coefficients have been used to reconstruct the batter profile for a condition of 40 MGT of pure dry operation and for 100 MGT of pure lubricated operation. These curves are shown in Figure 40. In the dry regime, the development of pronounced secondary batter can be seen after 30 MGT. Indeed, small undulations that are close to the weld up to 30 MGT seem to spread rapidly along the rail after 30 MGT has been exceeded. The actual experimentally observed profile after three 15 MGT dry periods plus three lubricated periods totalling 110 MGT is shown as a dashed line on the right hand side of the weld centerline. Clearly secondary batter had developed but the amplitude was far less than would be predicted for purely dry operation, perhaps because of the bene-

ficial effect of lubrication in diminishing the amplitude of batter that had developed in the previous dry cycle.

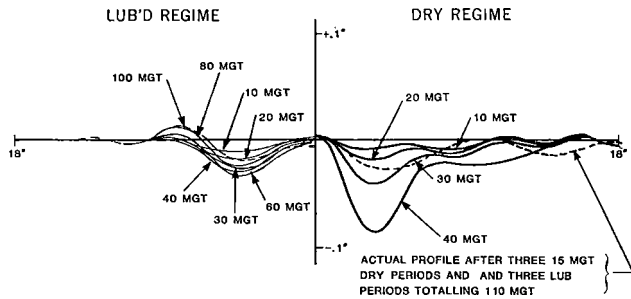


FIGURE 40. BATTER PROFILES FROM CENTERLINE OF FLASH BUTT WELD.

To summarize the welded rail end batter topic:

- o In some cases but not all, dry operation clearly accelerated batter development.
- o The batter rate of standard carbon rail on tangent track was about the same as that on a 5° curve.
- o The batter rate of inside and outside rail weldments on a 5° curve was generally about the same.
- o Standard carbon rail thermite welds battered at about the same rate as did flash-butt welds.
- o There is the hint that long delay post heat practices for alloy rail reduce batter development.
- o The batter rate may be highly dependent on the characteristics of the flash butt welder.
- o A Fourier Series representation of batter appears to provide a suitable description of both amplitude and wavelength (wave shape).

RAIL FATIGUE AND FAILURE BEHAVIOR

The rail metallurgy experiment at FAST has been designed primarily to study wear and metal flow. Yet when the wear rate was reduced massively by lubrication as in the case of the second experiment, rail fatigue became a major concern. The consequences of that fatigue were not inconsiderable as shown in Figure 41. This derailment resulted from three detail fractures that failed one after the other in a very short periods of time under the train. In 177 MGT, the heat of rail from which the failed rail had come had developed seven detail fractures - an extraordinary number.

The rail and weld failure history for the first and second experiment are given in Table XIV. The weld failure problem in the first experiment was magnified by (1) inexperience in making thermite welds to the extent that twice as many field welds failed as were installed initially in Section 3 and (2) the

plant welding of many dissimilar metallurgies together.*



FIGURE 41. PHOTO OF FAST TRAIN DERAILMENT.

TABLE XIV. RAIL AND WELD FAILURE HISTORY.

	Plant Welds	Field Welds	Head Defects
First Experiment (135 MGT)			
Section 03	44 (180)	44 (22)	2
Section 13	17 (64)	17 (10)	7
Second Experiment (250 MGT)			
Section 03	10 (120)	12 (0)	15 (27/mile)
Section 13	4 (48)	8 (0)	7 (10/mile) (30/mile)

*Defect rate adjusted to eliminate failures and rail length associated with "dirty" standard rail. The number in parentheses () is the number of welds installed upon initial construction.

The distressingly large number of weld failures in the first experiment in addition to rapid wear in the dry period necessitated the redesign and reconstruction of the metallurgy test sections at 135 MGT. The second experiment fared substantially better in terms of both plant and field weld failures. However, the prolonged period of operation achieved by improved lubrication allowed a far greater number of transverse fatigue failures to develop in Section 3.

The locations of all plant weld and head type failures in the high rail of Section 3 are shown in Figure 42 by metallurgy and tie plate cant. Without counting those transverse failures of questionable attribution (due to close proximity to a mechanical joint), standard carbon rail developed five failures (44/mile of high rail). HiSi rail developed only two failures (18/mile of high rail). HH rail developed only one valid fatigue failure. FHT had only one head failure, but it was at a segment end. CrMo rail had no head type fatigue failures.

*with care, there is no reason that dissimilar metallurgies cannot be welded together; there may, however, then be a batter problem.

(HIGH RAIL ONLY)

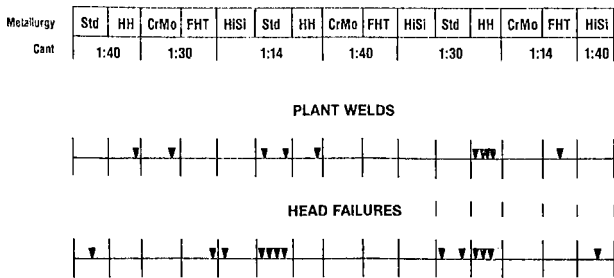


FIGURE 42. FAILURE BY METALLURGY.

HH exhibited the most plant weld failures⁶ in Section 3; in addition, there were others elsewhere in the track. More will be said about the nature of these failures later. Standard carbon rail had two plant weld failures while CrMo and FHT rail had only one plant weld failure each within the metallurgy test section. In Section 13, standard carbon rail had two plant weld failures, while FHT and HiSi had one failure each. It is important to know that except for CrMo, all rail was welded at the same plant in the same time frame.

The 1:14 cant was associated with a total of nine failures, the 1:30 cant with ten failures, and the 1:40 cant with three failures. However, some of these did occur near segment ends (as can be determined from Figure 42) and these must be viewed as suspect. A further consideration is the fact that the experiment design itself placed the Std, HiSi, and HH rails on the 1:14 and 1:30 cants in the mid-region of the curve while these same rails on the 1:40 cant were positioned at the ends of the curve. Thus, what appears as a tie plate cant effect may actually be a position-in-curve effect. The lateral wheel loads as determined from instrumented wheel set measurements at approximately 279 MGT into the second experiment are shown in Figure 43; no exceptional variations at any particular place in the curve were observed on these runs. However, the central one third of Section 3 was observed to have suffered more loss of track alignment than either of the end thirds (Figure 44).

SECTION 3, 45 mph (nominal)
LUBRICATED

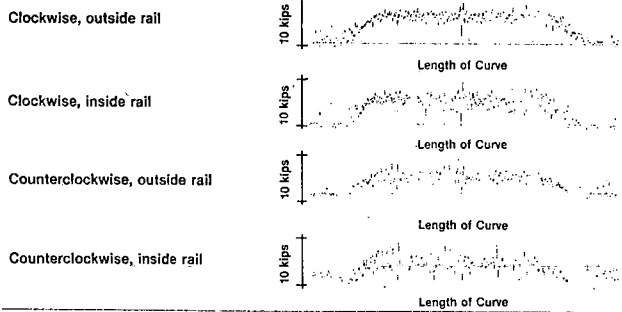


FIGURE 43. LATERAL WHEEL LOADS IN 5° CURVE.

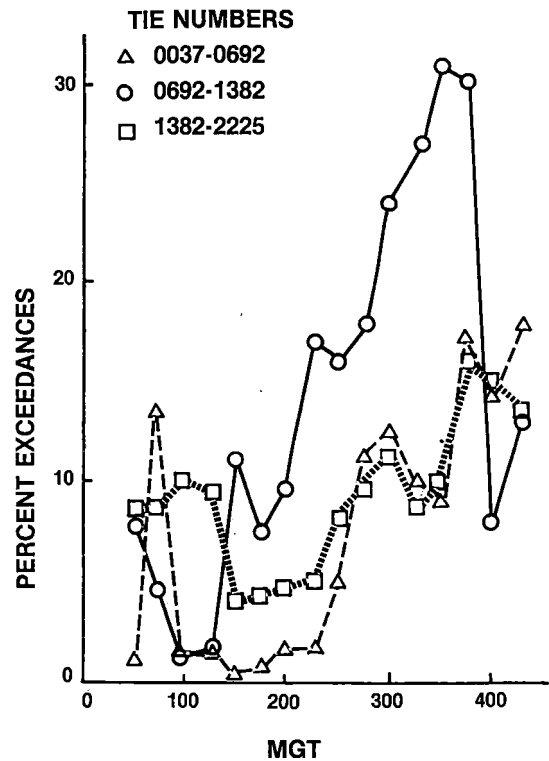


FIGURE 44. LOSS OF ALIGNMENTS BY TIE POSITION.

The relationship between rail failure at FAST and tonnage is shown in the Weibull plot of Figure 45 for standard carbon rail in both the 5° curve (Section 3) and in tangent track. The 'failures' in tangent track were not listed as detail fractures but rather as horizontal separations; they occurred in cwr track remote from welds. The line for the two HiSi failures also is shown. For comparison with rail defect behavior from actual U.S. railroad service, the upper and lower bounds within which the AAR/AREA/AISI survey⁷ data fall are plotted along with the defect occurrence line for the Waynesburg Southern Railroad⁵ upon which 125 ton cars are operated, albeit at lower speeds than those at FAST. The FAST rail failure experience is substantially more severe than that of more conventional U.S. railroad operations where car weights average closer to 75 tons. However, the Waynesburg Southern experience is very similar to that of FAST.

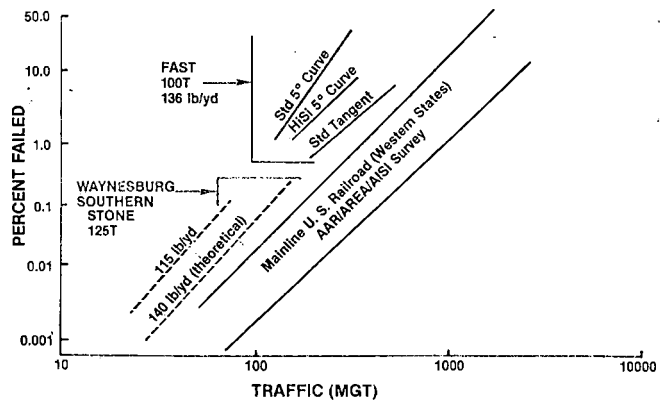


FIGURE 45. AFFECTS OF TOTAL TRAFFIC ON RAIL FAILURES.

The effect of wheel load can be seen by using the FAST rail failure data in conjunction with the defect data of the Waynesburg Southern and two sites (SF1, SF2) of the AAR/AREA/AISI survey where wheel loads are known. The one percentile tonnages have been taken from the Weibull plot (Figure 45) and plotted on a log-log basis (Figure 46). Typically, the slope of the plots was near -1.5. A theoretical prediction by Perlman et. al.,⁷ (estimated at the five percentile life) using an amplified and attenuated Union Pacific load spectra is shown to have a just slightly lower wheel load dependency than that observed for service information. Laboratory tests for contact fatigue performed by British Rail⁹ and Nippon Steel¹⁰ exhibited slopes of -1.5 and -0.7 respectively.

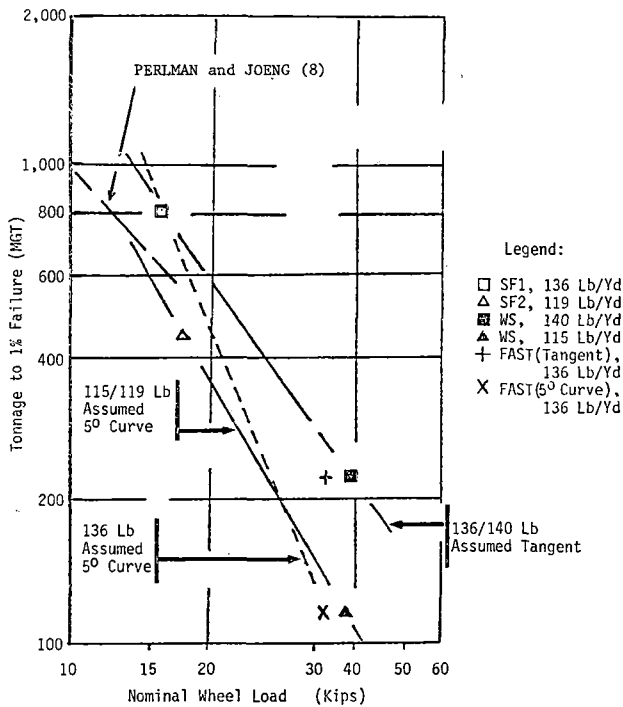


FIGURE 46. WHEEL LOADS VS RAIL FAILURES.

A derailment, such as that shown in Figure 41 resulting from rail failures at multiple undetected rail flaws serves as a substantial stimulus to determine what are the deficiencies of the inspection system used and to correct them. One indication of how well the inspection system is performing is the size distribution of defects found. Figure 47 shows the transverse defect size distributions before and after the derailment along with an estimated distribution for the nation as a whole based upon data from the Sperry Rail Service.* Prior to the derailment, the greatest number of transverse defects found at FAST fell into the range of 10 to 30%--a situation somewhat less conservative than

*The Sperry information has been given in the size categories: small, medium, and large. This author considered 'small' as 5 to 15%, 'medium' as 16 to 30%, and 'large' as >30% of the cross sectional head area.

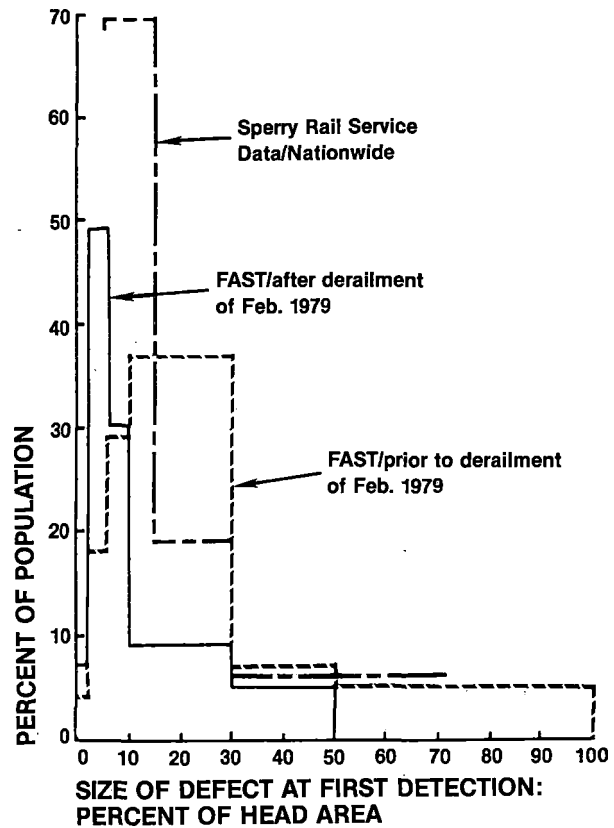


FIGURE 47. TRANSVERSE DEFECT SIZE DISTRIBUTION.

that for the nation as a whole where the estimated peak occurrence was 5-15%. After the derailment, corrections in the inspection procedure and in the system itself caused the peak occurrence to shift to the range of 2 to 5%.

An examination of some of the rail failures that have occurred at FAST will prove informative.

A sideview of a typical HH rail plant weld failure is shown in Figure 48. At first glance, the crack appears to have been a horizontal failure near the mid-web region which turned to run vertically as the crack grew away from the weld. However, upon closer examination, one can see that the horizontal crack actually initiated from a vertical transverse crack which had originated in the head-web fillet region. The appearance of the transverse crack is shown in Figure 49. Each growth ring represents one day of operation (1 MGT) so that the vertical crack would appear to have been growing for well over 20 MGT. The origin of the vertical crack occurred at the edge of the upset region at a location where shear drag was particularly severe as shown in Figure 50. Decarburization also was observed in the vicinity of the origin. As indicated previously, the greatest number of these types of failures occurred in HH weldments even though all other metallurgies except CrMo were welded in the same weld plant in the same time frame.

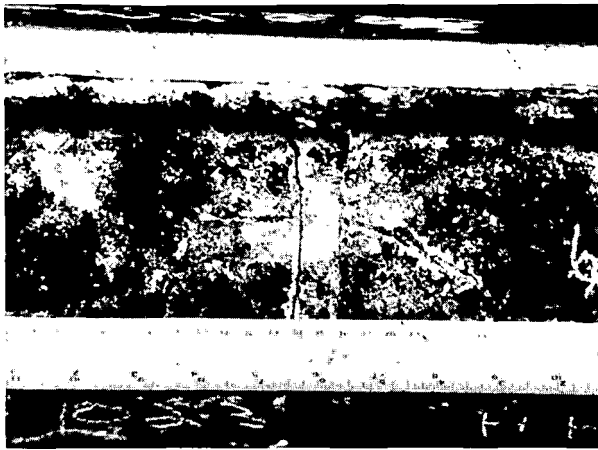


FIGURE 48. TYPICAL RAIL PLANT WELD FAILURE.



FIGURE 49. PLANT WELD FAILURE TRANSVERSE VIEW.

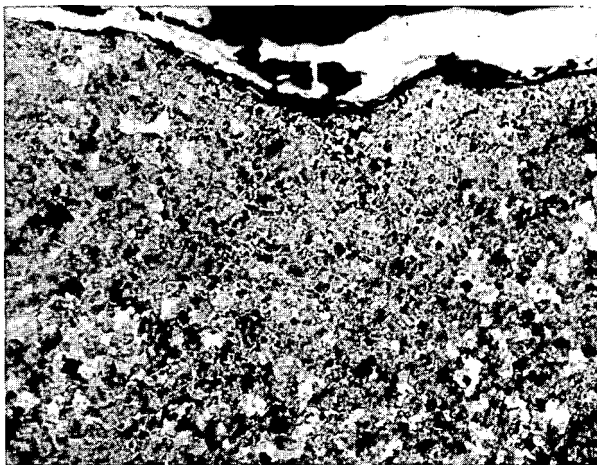


FIGURE 50. ORIGIN OF VERTICAL CRACK.

Figure 51 shows a typical 'long' life failure of a thermite weld. The failure was somewhat unique because a clear cut indication of a fatigue crack can be seen at the edge of the cast region. In addition, a shiny battered region on the opposite side of the weld suggests that the crack traversed this region slowly enough to allow the surfaces to come together and develop the battered pattern. The circular shape of the battered region suggests that the possibility that it may also have been an origin. Many thermite weld failures fall into the 'infant mortality' category. Such a failure is shown in Figure 52. Although the weld was made in accordance with 'proper' procedure, shrinkage cracks developed in the head-web fillet region. Subsequent examination of the cracks revealed finger-like dendrites protruding from what was the liquid-solid interface (Figure 53). The solidification process had been starved of liquid metal. The likely cause was insufficient preheat or insufficient superheat of the liquid metal prior to pouring. Though the procedure may have been 'proper', it clearly was not adequate for the cold, windy day on which the weld was made.



FIGURE 51. THERMITE WELD FAILURE.

Failures of rails or plant welds have been rare in the metallurgy test sections in the approximately 190 MGT accumulated thus far in the third experiment. There have been a few failures though. Figure 54 illustrates the appearance of a transverse failure of a 1 Cr rail. The failure had developed from a longitudinal vertical fatigue crack in the rail base which in turn had initiated from a base

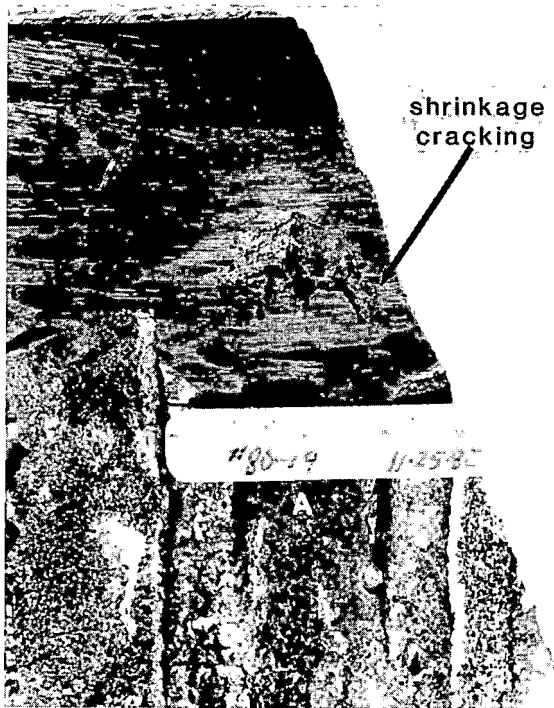


FIGURE 52. WELD FAILURE DUE TO COOLING SHRINKAGE.

SEM OF DENDRITES
IN WELD METAL 300X

HIGHER MAGNIFICATION
OF DENDRITES 1000X

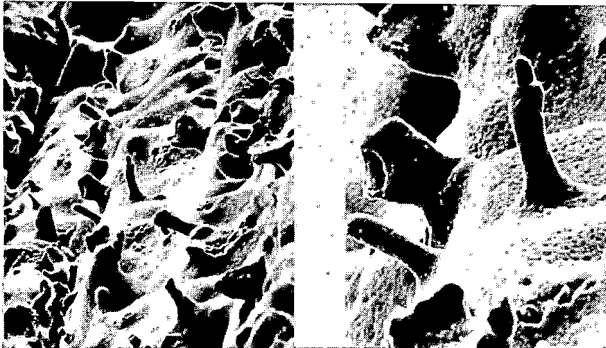


FIGURE 53. DENDRITE FORMATION IN SHRINKAGE CRACKS.

TRANSVERSE FAILURE IN RAIL,
SHOWING POINT OF INITIATION AT
PRE-EXISTING FLANGE CRACK

CRACK IN RAIL FLANGE

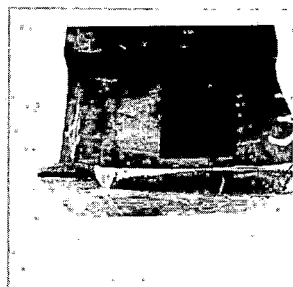
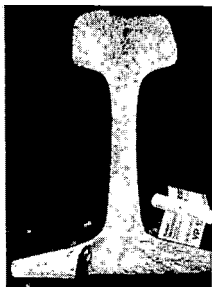


FIGURE 54. TRANSVERSE FAILURE OF ALLOY RAIL.

seam adjacent to a plant weld. The seam itself was approximately 30-40 mm long and 0.7 mm deep (Figure 55). The fact that the rolling practice of this manufacturer at this time left the base slightly concave downward combined with the clamping action of the electrodes at the welding plant is believed to have contributed to initiating a small base crack that subsequently grew under service. Action has been taken by the manufacturer to reduce the number of seams and to prevent concave base occurrence.



FIGURE 55. MICROGRAPH OF TRANSVERSE SECTION THRU THE LONGITUDINAL CRACK SHOWING THE DEPTH OF THE BASE SEAM.

A base crack and a plant weld failure have occurred in the SiCr(HH) rail. The base crack, shown in Figure 56, originated at the lower edge of the base surface. Metallographic examination revealed that the origin region had been subjected to mechanical action that had produced a 'white' etching layer; in addition, decarburization had occurred in this region; this was not common elsewhere along the rail. These features are shown in Figure 57. Clearly, damage had been done to the rail but gouges or dents from anchors or from an accidental blow of a spike maul were not observed. The weld failure is shown in Figure 58. Unlike other weld failures in HH rail, the crack had no vertical component at the upset region. The origin of this crack was a scratch through a brand mark that was located just on the edge of the upset region. The scratch was probably created upon stripping of the weld. In addition an island of decarburization was found about 0.04" below the surface at the crack origin (Figure 59). It is not clear why the decarburized region occurred below the surface of the rail.

Perhaps the most spectacular rail defect that develops at FAST is the detail fracture-from-shell. The one shown in Figure 60 is one of many that have occurred in the second metallurgy experiment. Each growth ring represents the period in which the train runs in one direction (~1 MGT usually). When the train reverses direction, the crack plane changes orientation slightly. Thus as the crack grows, its plane of growth alternates back and forth, the average growth being roughly perpendicular to the

BASE FAILURE, SiCr (HH) RAIL



CLOSE UP VIEW OF FATIGUE CRACK
SURFACE AT THE END OF BASE

FIGURE 56. OVERALL AND CLOSE-UP VIEWS OF FATIGUE CRACK
SURFACE AT THE END OF BASE.

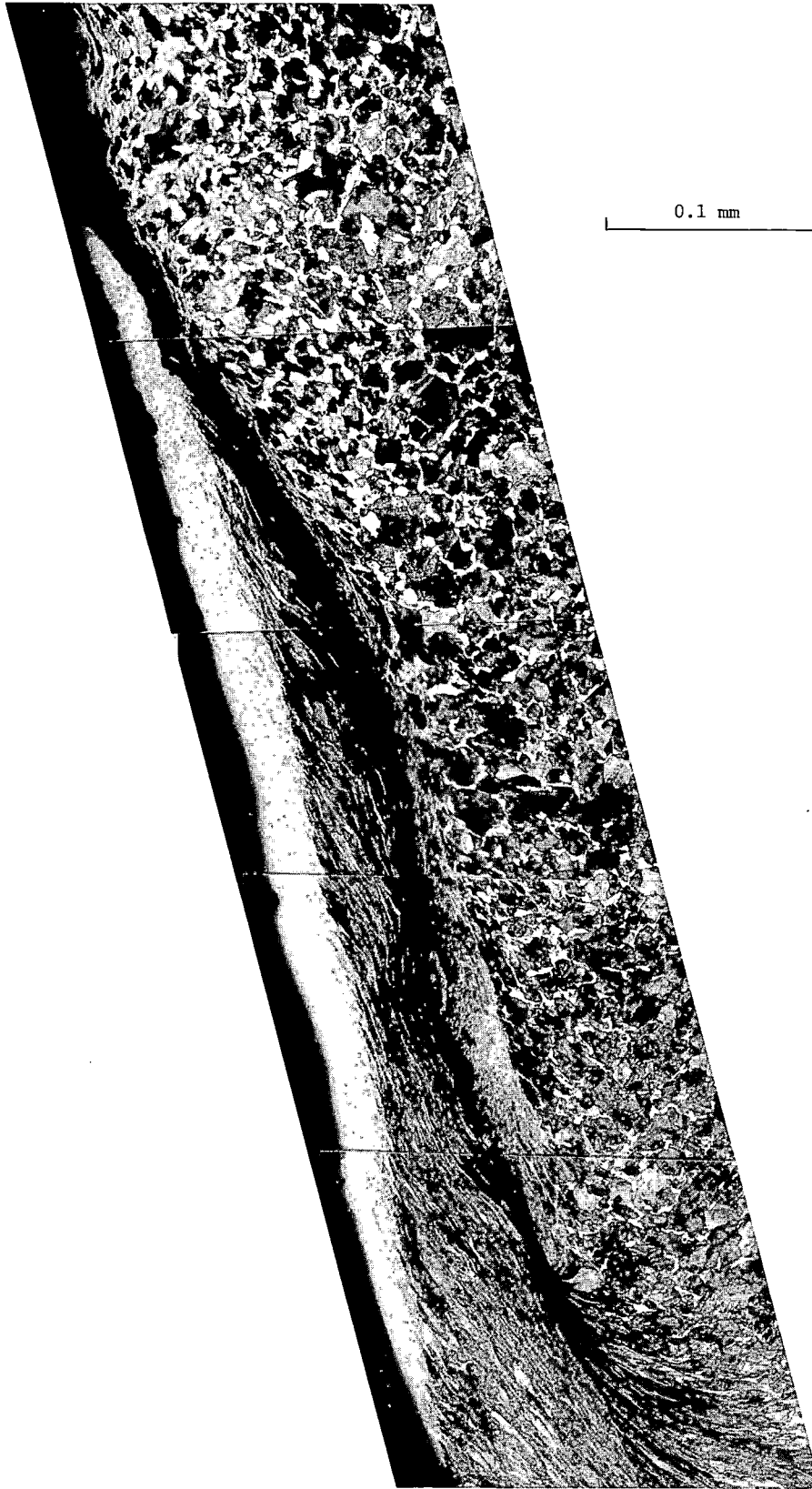
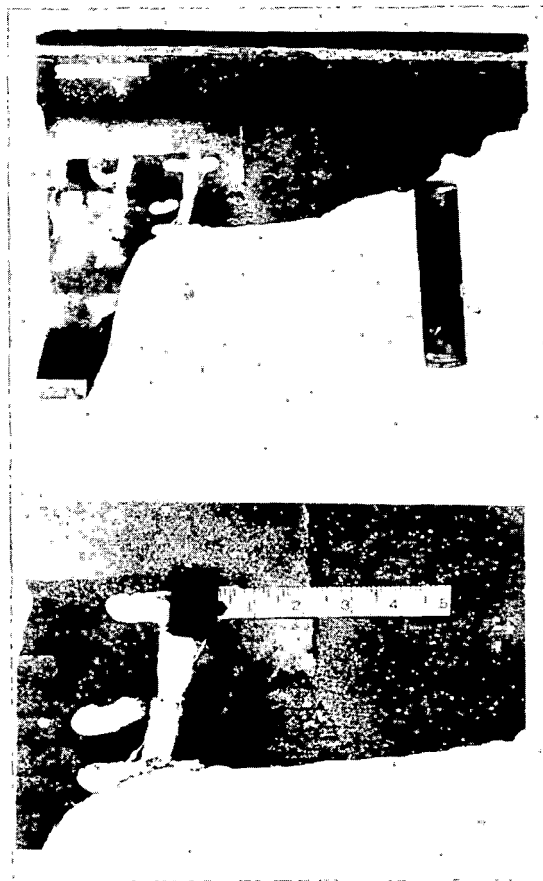


FIGURE 57. MICROGRAPH OF TRANSVERSE SECTION SHOWING
WHITE ETCHING LAYER AND DECARBURIZATION
AT EDGE OF RAIL BASE.

FAILURE AT A PLANT WELD
SiCr (HH) RAIL



CLOSE UP VIEW OF WEB SURFACE
(1 mm/Div)

FIGURE 58. FAILURE AT A PLANT WELD SiCr (HH) RAIL.

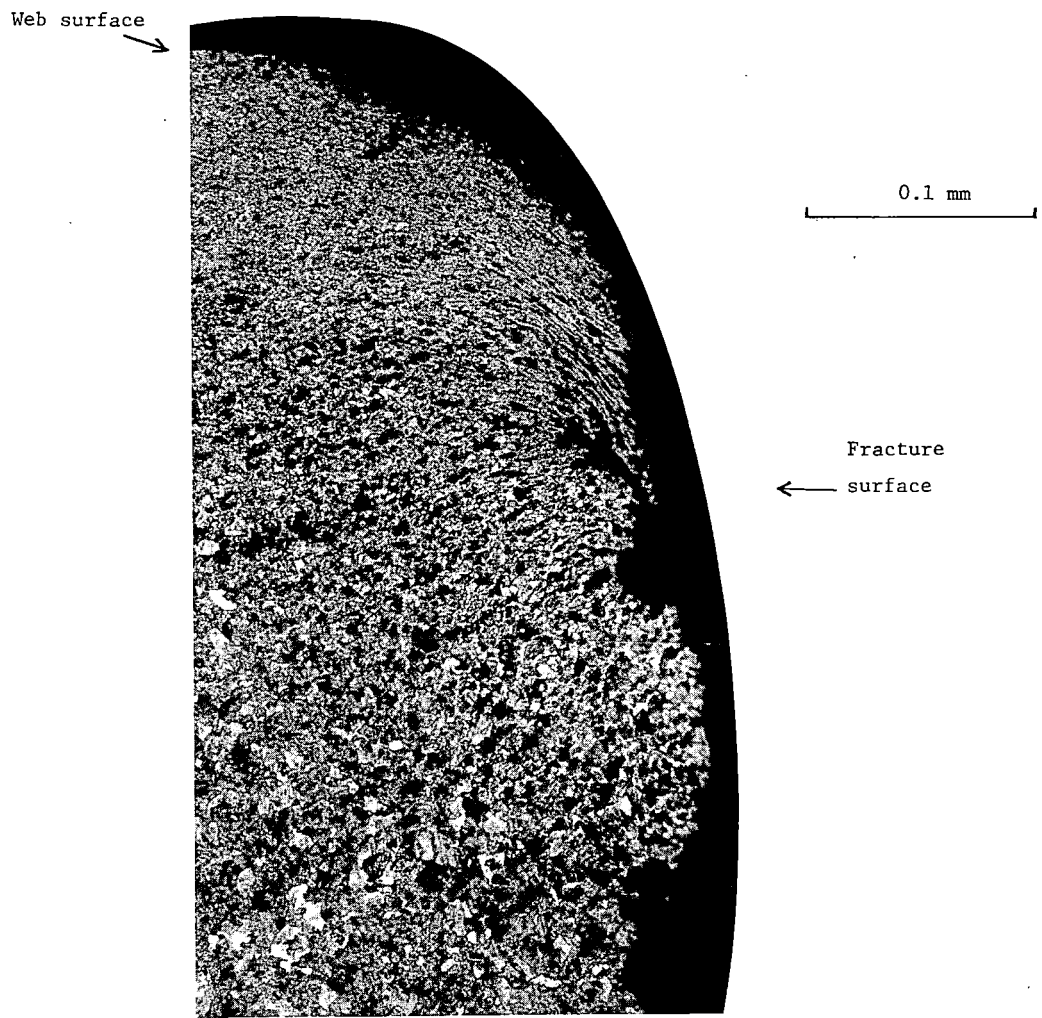
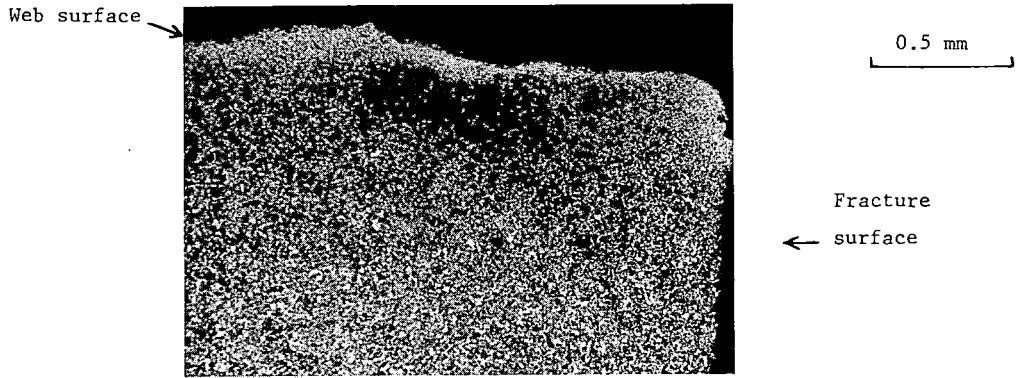


FIGURE 59. MICROGRAPH OF LONGITUDINAL TRANSVERSE SECTION THRU THE HORIZONTAL FRACTURE SHOWING A POCKET OF DECARBURIZATION NEAR THE WEB SURFACE.

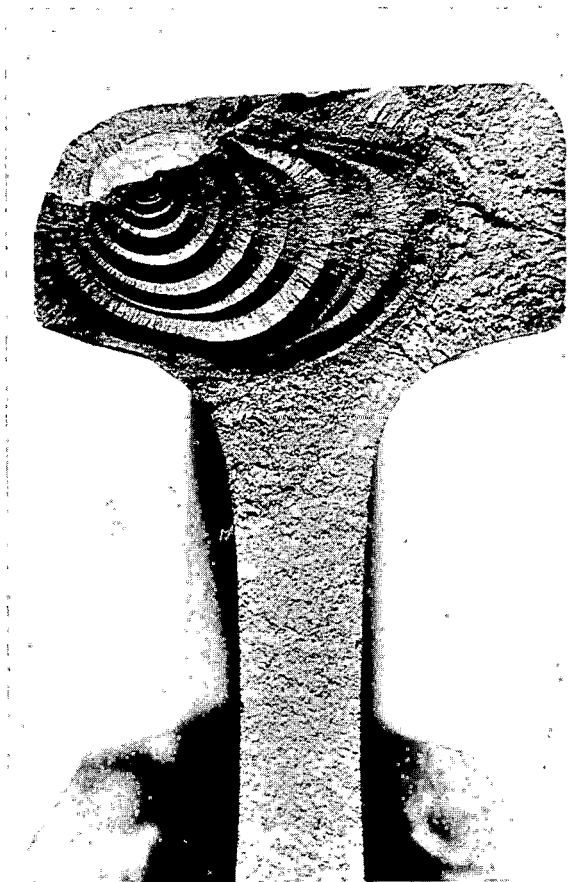


FIGURE 60. DETAIL FRACTURE FROM SHELL.

rail axis. This reversible zig-zag pattern has been very useful for tracking crack growth as will be shown shortly. The pattern also develops on the shell portion of the crack as shown in Figure 61. Here the shell surface has been exposed by sectioning. The origin of the shell is internal beneath the gage corner of the rail. Probably 10 or more MGT had passed before the shell even approached the gage face of the rail. The shell surface gave no indication of grease being present in the crack. Thus, the presence of a fluid (grease) in the shell appears not to be necessary for growth of the crack. After the shell had grown approximately 3/4" from its origin, the detail fracture developed. A vertical longitudinal section taken through the origin of the shell and the origin of the detail fracture is shown in Figure 62. The detail fracture can be seen to be only one of many incipient 'detail fractures' which developed at the valleys of the zig-zag shell surface. There appears to be a critical distance, 1/2" to 1" at FAST (on a curve) for shell growth before bifurcation leads to the dominant detail fracture. The shell proceeded on its zig-zag path

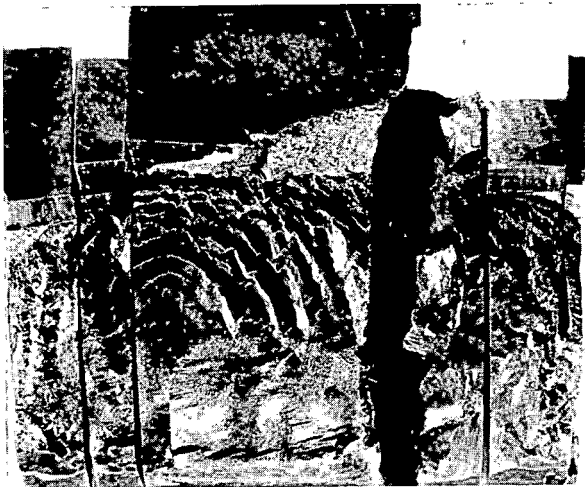


FIGURE 61. VIEW OF SHELL SURFACE.

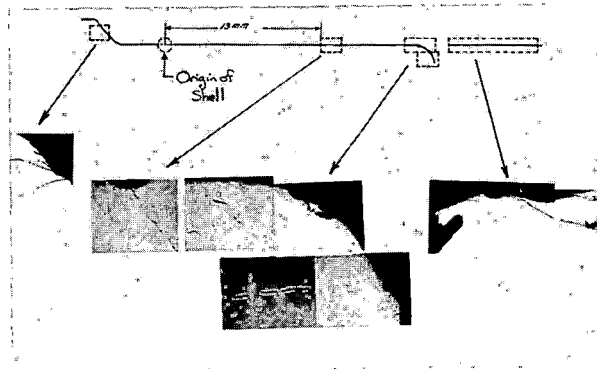


FIGURE 62. RELATIONSHIP OF SHELL ORIGIN TO POSITION OF TD AND DEVELOPMENT OF SECONDARY CRACKS.

even after the detail fracture had started to turn into a vertical plane. No special features such as inclusions seem to be necessary for the detail to develop. However, one would expect inclusions to play a part in the initiation of the shell. Alas, although no inclusions were identified as being associated with shell origin, perhaps they were lost upon sectioning. Microhardness traverses were run across a transverse vertical plane through the rail near the shell (but not actually containing the shell) and a hardness contour map was drawn from the traverses. This is shown in Figure 63. The region in which the shell developed seems to be characterized as an intrusion or lense of somewhat softer metal than much of that around it. This suggests that the shell may form in a region of cyclically softened metal 1/4" to 1/2" below the running surface.

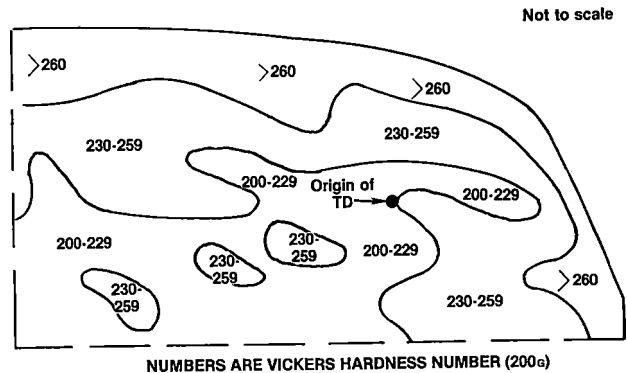


FIGURE 63. HARDNESS MAP OF TD-CONTAINING RAIL.

The zig-zag path of the crack suggests that shear stresses also play a part in the growth of the crack perhaps by causing the residual principle stresses to rotate alternately one way and then the other as the train reverses direction.

The growth rings that are so clearly delineated on the surface of the detail fracture permit some simple calculations to be made which will help define the environment in which the crack grows. There are two dominant stress systems which must govern the growth of the transverse crack--the flexural stress system induced by the passage of the wheel and the steady stress system which is generated by the combined effect of thermal stresses and residual stresses resulting from the cyclic work hardening of the upper part of the head. The rolling action of the wheels may be expected to induce residual compression in the near-surface region but as is the case with shot peening, the region beneath that in residual compression must provide a balance of forces by being in residual tension.

Ignoring the shear stress contribution (since it appears the shear stresses will act only when the crack is under compression and not growing), a rather simple linear elastic fracture mechanics approach can be used to estimate the combinations of flexural and residual stresses which would have caused the observed crack growth. The flexural stresses can be related approximately to an equivalent wheel load (made up of both vertical and lateral components) by beam-on-elastic-foundation methods. Crack growth can be calculated from the integrated form of the Forman expression given below. The general method is described in the reference.¹⁰

$$\Delta K \approx 1.13 \Delta \sigma \sqrt{a}$$

$$da/dN = B \cdot \Delta K^n / [(1-R) K_c - \Delta K]$$

$$[1.13^n/2] [B] [\Delta \sigma^n] [\Delta N] =$$

$$[(1-R) K_c / (n-2)] [1/\Delta K_c^{n-2}] \Delta K_c - [1/(n-3)] [1/\Delta K_c^{n-3}] \Delta K_c$$

$$\Delta K_{\text{threshold}} = \Delta K_{\text{threshold}}^{R=0} (1-R)^{1/n}$$

The observed growth is shown in Figure 64. The values of B, n, and K_c needed in the Forman expression were derived from specimen crack growth information generated from the failed rail as well as the other sources shown in Figure 65. Because the observed specimen crack growth data of the failed rail was very near the upper bound of the Broek and Feddersen¹² data set, and also near to the behavior observed by Barson and Imhof,¹³ the following parameter values were selected:

$$B = 3 \times 10^{-9} \text{ in/cycle}$$

$$n = 3.32$$

$$K_c = 50 \text{ ksi} \sqrt{\text{in}}$$

The calculated rail crack growth curves are compared with the observed crack growth of the transverse defect in Figure 66, with the nearest calculated residual stress/wheel load set bracketing the observed curve. For a crack size of 0.4" radius, the combination of wheel load and residual stress needed to make the crack grow in the observed fashion is plotted in Figure 67.

Subsequent to completion of Forman crack growth analysis, Battelle, Columbus Laboratories¹⁴ completed a determination of residual stresses in the failed rail by destructive sectioning methods. The results are given in Figure 68. The residual stress in the region where the crack would have been about 0.4" in radius is near 20 to 30 ksi. Thus, from Figure 67 the equivalent wheel load would be expected to fall between 35 and 45 kips. The actual average vertical wheel load is about 33 kips, suggesting that the effective lateral force augment of the vertical load is between 2 and 12 kips. Typical observed lateral forces in Section 13 (where failure occurred) are near 10 kips. Though the technique does not have great precision in defining the growth environment, it does provide realistic approximate estimates and the success in its use encourages extension to provide some insight into the effects of material and service parameters on rail performance and that, in turn, upon the needs for rail defect inspection.

The key points concerning the FAST rail failure experience to be remembered are:

- o A possible penalty of improved wear life achieved by lubrication is a shift to fatigue as the failure mode.

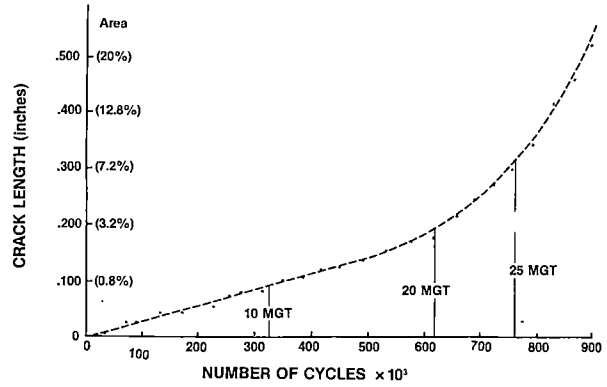


FIGURE 64. OBSERVED CRACK GROWTH.

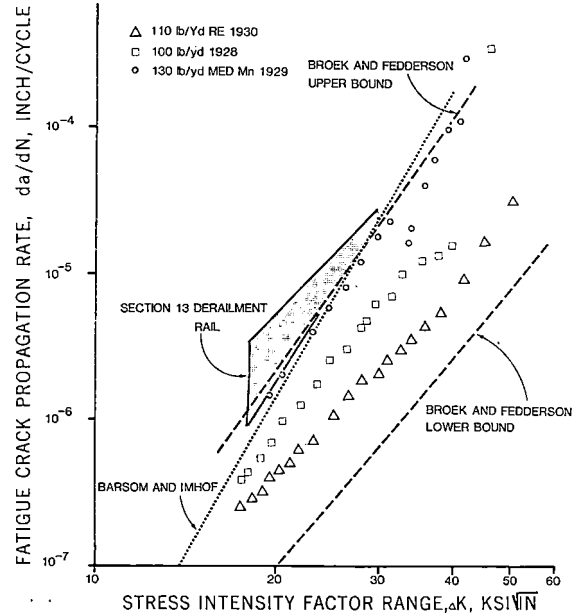


FIGURE 65. VARIABILITY OF FATIGUE CRACK PROPAGATION RATE BEHAVIOR.

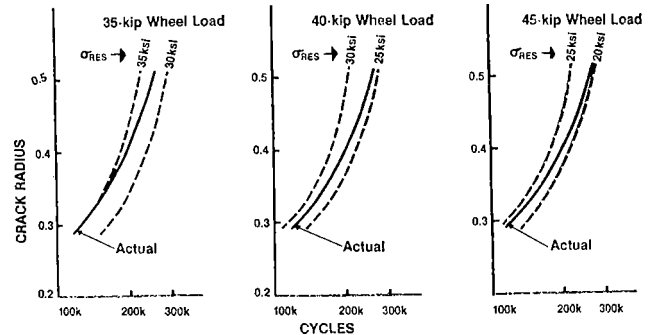


FIGURE 66. COMPARISON OF ACTUAL CRACK GROWTH WITH FAMILIES OF CALCULATED GROWTH CURVES.

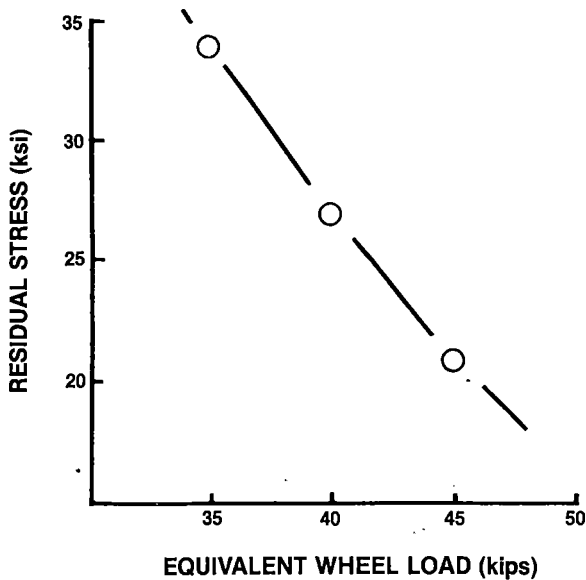


FIGURE 67. WHEEL LOAD/RESIDUAL STRESS COMBINATIONS FOR OBSERVED CRACK GROWTH.

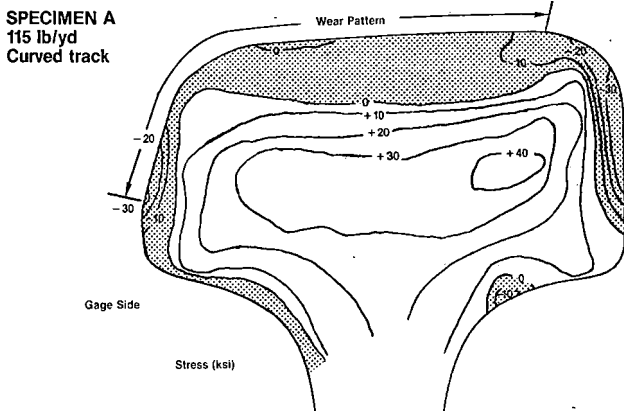


FIGURE 68. AXIAL RESIDUAL STRESS AT 177.7 MGt.

- o From FAST data and from other sources, it would appear that doubling the nominal wheel load reduces the rail life (at a specified percentile) by a factor of two to four.
- o At FAST, the detail fracture is a non-unique bifurcation of the shell crack.
- o Simple linear elastic fracture mechanics predictions of crack growth behavior match observed rail transverse crack behavior reasonably well.

DISCUSSIONS

Much of the information presented in the preceding sections qualifies as "interesting, but...." In the following paragraphs some illustrations will be given to show how this information may be used and how laboratory examinations can help improve our understanding of the processes which are operative.

The metallurgy:lubrication interaction can be understood in terms of variation in surface shear stress with lubrication when adjustments are made for

material characteristics. The importance of surface stress level on the wear progress has been shown by Bolton¹⁵ who observed that in laboratory tests, the logarithm of the wear rate (in the 'mild' wear regime) was a linear function of contact stress. Battelle-Columbus Laboratory studies of Hertzian contact have shown that the amplitude and the location of the maximum octahedral shear stresses change as a function of the friction coefficient at the wheel/rail interface. This variation is illustrated in Figure 69. When the friction coefficient at the surface is zero, the maximum octahedral shear stress is located about 0.1" beneath the surface with an amplitude of 53 ksi for a 19 kip vertical wheel load. However, when the friction coefficient reaches 0.5, the maximum shear stress comes to the surface and increases in magnitude to nearly 80 ksi. In this same range of friction coefficient, the surface shear stresses change from about 25 ksi to nearly 80 ksi. An approximate relationship between the logarithm of shear stress (in ksi), wheel load (kips), and friction coefficient is given in the equation shown below.

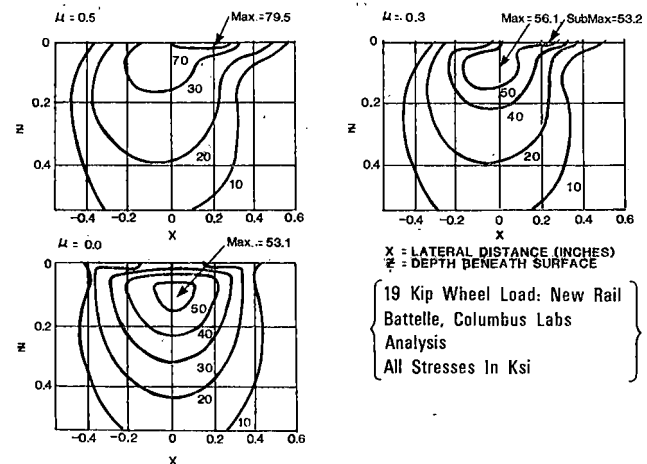


FIGURE 69. SHEAR STRESSES AS A FUNCTION OF FRICTION COEFFICIENTS.

$$\text{Log } \tau_{\text{OCT}} = \text{Log} \left[10.55 \left[\text{WL} \right]^{0.301} \right] + 0.9976 \left[\mu \right]$$

SURFACE OCTAHEDRAL SHEAR STRESS WHEEL LOAD FRICTION COEFFICIENT

However, the fact that the metallurgies respond in different degrees to the lubrication level requires that a material sensitive parameter be included in any expression which seeks to relate wear rate to surface stress state. A second equation has been obtained empirically to fit the FAST data when the shear stress is based upon 19 kip wheel load for illustration.

$$\text{Log } W = -3.4437 + 27.41 \left[\frac{\tau_{\text{OCT}}}{H} \right]^{2.5}$$

WEAR RATE HARDNESS (A SURROGATE PARAMETER) COMPOSITE NUMBER FOR A WIDE RANGE OF μ

Brinell hardness has been used as the material sensitive parameter. In reality hardness is a surrogate parameter which we must use because it's the only material parameter which is generally available. However, hardness, as such, is unlikely to have any effect upon the wear process itself. As is shown later, in the dry regime, wear may be more related to a ductility parameter such as the true fracture strain either cyclic or static. In the lubricated regime where little or no asperity contact is likely to occur, the mechanism may be more related to the high cycle endurance strength.¹⁷ In an empirical sense, the difference in the slope of the wear rate vs hardness plots given in Figures 19a and 19b reflects the variation in hardness sensitivity. Thus the exponent 2.5 used is in effect, a weighted composite value for the entire range of friction coefficient from dry to lubricated.

In spite of these approximations, the approach does provide a good prediction of wear rate across a range of lubrication if the dry regime at FAST is assumed to be characterized by a friction coefficient of 0.5 while that of the lubricated regime is taken as 0.1. Figure 70 illustrates that the agreement between the observed and predicted gage face wear rates of the different metallurgies tested in the current experiment was within 0.001"/MGT in the unlubricated regime and 0.0002"/MGT in the lubricated regime. The poorer-than-expected performance of CrMo(A) may be related to its metallurgical structure; it is believed to be at least partially bainitic. Bainitic rail steels have been shown to exhibit much poorer wear resistance than do pearlite rail steels.¹⁸ The behavior of the FHT rail is more difficult to understand. The rail has consistently exhibited poorer gage face wear resistance than its hardness would suggest that it should (even though higher carbon FHT rails were selected intentionally in the current experiment). However, its rapid decrease in wear rate from one lubrication block to the next and the fact that it is processed in the mill by oil quenching followed by tempering admits to the possibility that its surface layers at least may not be entirely pearlitic.

The transition in modes is shown conceptually in Figure 71 as the friction coefficient changes. A variant on the model is a transition to severe wear

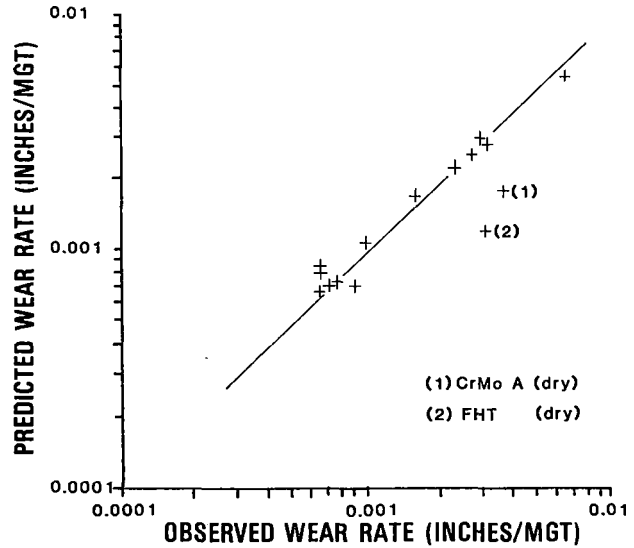


FIGURE 70. PREDICTED VS. OBSERVED GAGE FACE WEAR RATES.

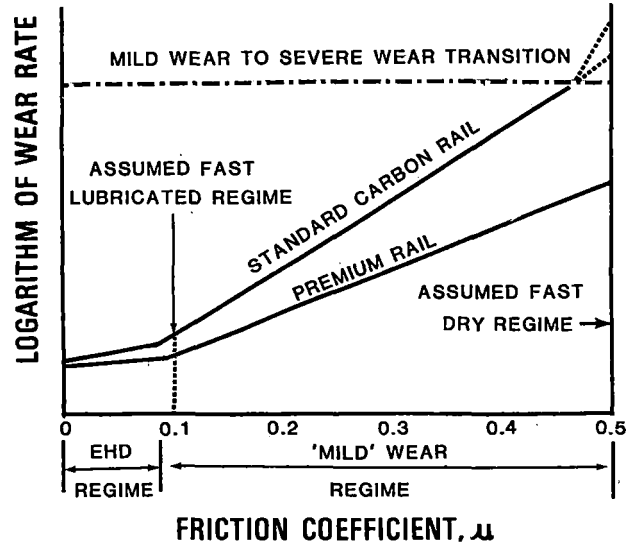


FIGURE 71. CONCEPTUAL VIEW OF CHANGE IN WEAR MECHANISM WITH INCREASING FRICTION COEFFICIENT.

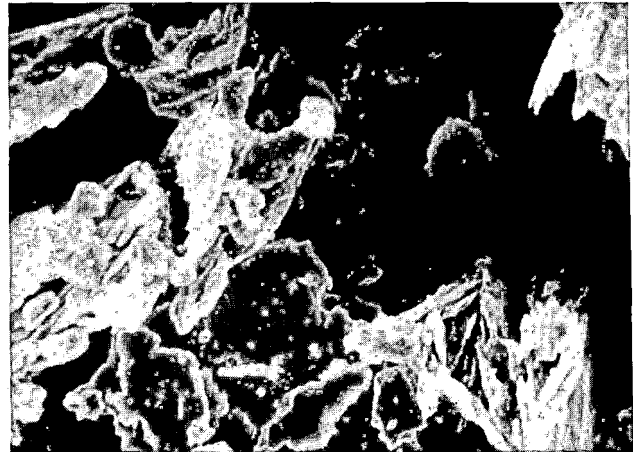
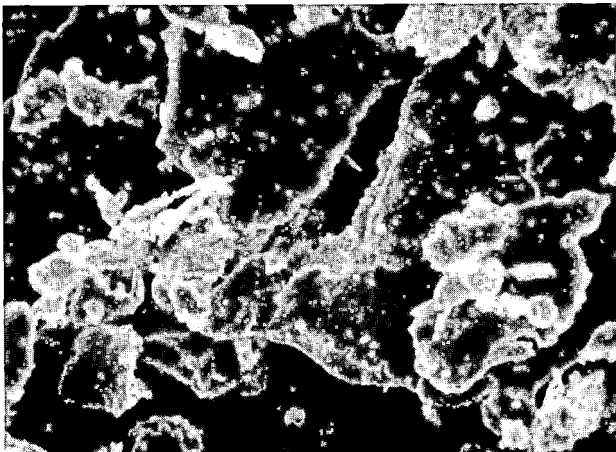


FIGURE 72. WEAR DEBRIS.

for standard rail above a critical wear rate. Wear debris collected at FAST in the previous experiment during a brief dry period was observed¹⁹ to be primarily flakes about 80µm and 140µm long for standard and head hardened rail respectively as shown in Figure 72. Bolton et al, have observed flakes of this size in a mild wear regime suggesting that a wear model based on a mild wear mode may be appropriate to the dry regime of FAST operations.

By combining both wheel and rail wear rate data from FAST in a manner proposed by Rabinowicz²⁰ some predictions can be made about the total rail/wheel system wear. The framework in which this can be done is shown in Figure 73 wherein the logarithm of wear rate is plotted against the logarithm of the ratio of rail to wheel hardness. The underlying presumption is that if the hardness of one component (the wheel) is fixed, the wear rates can be related to the hardness ratios of the two components. In proposing that the diagram shown in Figure 73 can be used to treat total system wear, Rabinowicz noted that there are several assumptions that are appropriate for adhesive wear processes:

- (a) The wear rate of the softer component depends only on the inverse of its hardness (wear rate $\propto 1/\text{Hardness}$).
- (b) The wear rate of the harder component is related to the square of the ratio of lower hardness to greater hardness of the two components of the couple.
- (c) The specific wear rates of the two components of a couple will be equal when hardnesses are equal.

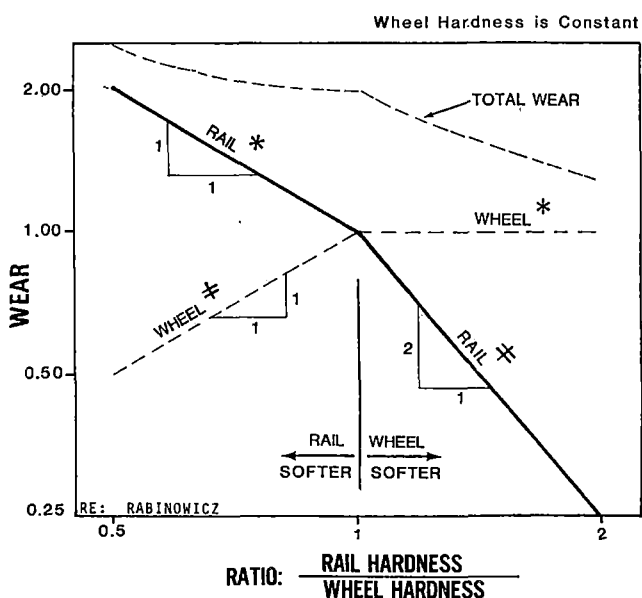


FIGURE 73. COMBINED PRESENTATION OF RAIL/WHEEL WEAR INFORMATION.

Thus, at rail:wheel hardness ratios greater than unity the wheel will be the softer component, and because its hardness is fixed, its wear rate will not change as the rail becomes harder. As the rail

becomes harder, its wear rate will be related to that of the wheel as the inverse of the rail:wheel hardness ratio squared, i.e., $1 \times [2]^{-2} = 1/4$ at a hardness ratio of 2. When the rail:wheel hardness ratio is less than unity, the rail will be the softer component, and because its hardness is changing (decreasing to the left), its wear rate will increase in proportion to the hardness ratio to the -1 power. The wheel which is fixed in hardness will be the harder component to the left of unity hardness ratio, and its wear rate will be governed by assumption (b) such that at a rail:wheel hardness ratio of 0.5 (where the rail wear rate is 2) that of the wheel will be $2 \times [0.5]^2 = 0.5$.

The total system wear is the sum of the wheel and rail wear rates. At a rail:wheel hardness ratio of 0.5, the total wear rate will be 2.5 diminishing nonlinearly to 2.0 at a rail:wheel hardness ratio of unity. At a rail:wheel hardness ratio of 2, the total system wear rate has diminished to only 1.25. Thus, a 4:1 change in hardness of rail relative to that of wheels which, in theory, would reduce the rail wear by a factor of 8, would reduce the total system wear by a factor of only 2.

In order to utilize the FAST rail and wheel wear rate data in the fashion proposed by Rabinowicz, the wear rates of each component must be cast into the same units, and adjustments must be made for the different wear exposures of rails and wheels. To start this process for gage face wear of rail and flange wear of wheels, all of the curves at FAST are converted to equivalent 5° curvature by assuming that:

- (a) rail wear is a linear function of curvature as suggested by Figure 4, and
- (b) that those factors which influence rail gage face wear rate will influence flange wear rate proportionally in the same fashion.

Table XV shows that the total of 9346' at 3°, 4°, and 5° curvature converts to 8246' of equivalent 5° curvature.

TABLE XV. AMOUNT OF EQUIVALENT 5° CURVE.

SECTION	OVERALL LENGTH	EQUIVALENT 5° CURVE
3(5°)	3670'	3670'
7(5°)	1000'	1000'
13(4°)	1250'	1000'
17(5°)	1300'	1300'
17(3°)	2126'	1276'
TOTAL	9346'	8246'

Using the amount of equivalent 5° curvature, the exposure ratio between wheels and rails can be calculated. The approach to do this is summarized as:

- o WHEEL FLANGE EXPOSURE =
 $8250/9.425 = 875$ EXPOSURES/LAP
 CIRCUMFERENCE OF 36" DIA. WHEEL
- o BUT EACH WHEEL IS OUTSIDE LEAD WHEEL ONLY
 ONCE EVERY FOUR DAYS $\rightarrow 218.8$ EXPOSURES/LAP
 ON AVERAGE
- o RAIL EXPOSURE = 320 WHEELS/2 = 160
 EXPOSURES/LAP
- o EXPOSURE FACTOR = $219/160 = 1.4$

A point on the circumference of a 36" diameter wheel flange will strike the gage face of the rail 875 times in traversing the approximately 8250 feet of equivalent 5° curvature. But each wheel is the outside lead wheel only once every fourth day so that on an average, a point on the flange strikes the gage face of the rail only about 219 times per lap of the loop. On the other hand, a point on the gage face of the rail in the curve will be struck by the outside lead wheel 160 times, (one half of the approximately 320 wheels on one side of the train). Thus while a point on the wheel flange will see an average of 219 wear events per lap, a point on the gage face of the rail will see 160 wear events per lap. Therefore, the wheel to rail exposure ratio is about 1.4, i.e., the wheel flange receives about 40% more exposure than does the rail gage face so that 1 MGT is approximately 350 miles of vehicle travel.

Although hardnesses are available for the gage face of each of the different rail metallurgies (see Figure 19a), flange face hardnesses of wheels are not readily obtained with the instrumentation available at FAST. Therefore, to estimate flange face hardness, the microhardness data taken from near the flange surface to a depth of about 5½ mm as shown in Figure 74²⁷ for a FAST U wheel, have been used to determine that the flange metal near the surface is about 20 BHN harder than the base metal. Thus, the estimated flange hardness is taken as the measured rim Brinell hardness plus 20 BHN.

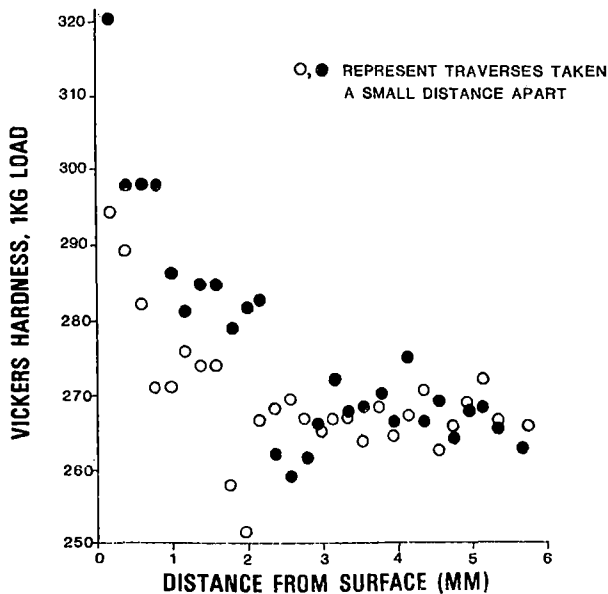


FIGURE 74. HARDNESS PROFILE IN A WHEEL FLANGE.

The dry regime wear rates of rails from both the first and third (current) experiments and wheels (corrected for exposure ratio) from both the Wheels III (VALT) and Wheels IV experiments²² are plotted in Figure 75. The wear rate of rail in the current experiment (1st dry block) appears to be consistently less than that observed in the first experiment although the wear rate dependence on hardness is about the same.

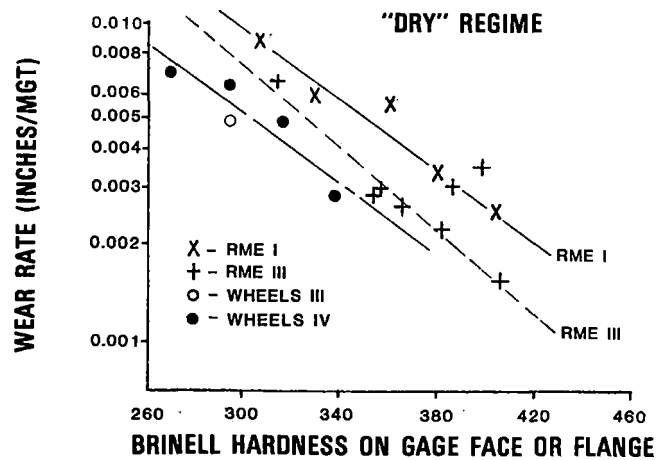


FIGURE 75. WEAR RATES AS A FUNCTION OF HARDNESS.

The rail and wheel (corrected) wear rates are plotted against hardness ratio in Figure 76. The hardness ratios have been calculated as follows for the wheel mix given in Table XVI:

- o Rails: average hardness of a given metallurgy divided by average overall wheel flange hardness
- o Wheels: average overall hardness of the rail curves divided by average hardness of individual wheel types.

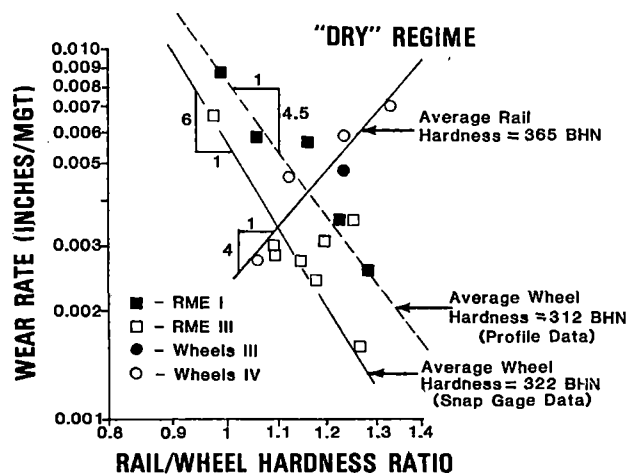


FIGURE 76. WEAR RATES VS. HARDNESS.

The wear rates and hardnesses of rails and wheels are summarized in Tables XVII, XVIII, XIX, and XX. The significant finding is that the slopes of the

TABLE XVI. WHEEL MIX OF TRAIN (RME III/BLOCK I).

DRY REGIME

WHEEL TYPE		
C	B	U
43%	2%	55%

TABLE XVII. RAIL GAGE FACE WEAR RATES.

Metallurgy	Dry	Lub'd	
		Sect 3	Sect 17
Standard (Std)	0.0066	0.0010	--
Fully Heat Treated (FHT)	0.0031	0.0007	--
Heat Hardened (HH)	0.0023	0.00075	0.00028
Silicon Chrome (CrSi(HH))	0.0016	0.00065	0.00030
Chrome Molybdenum (CrMo)	(C)	0.0029	0.00065
	(A)	0.0036	0.00090
Chrome Vanadium (CrV)	0.0027	--	0.00040
1% Chrome (1Cr)	0.0030	0.00065	0.00034

TABLE XVIII. WHEEL FLANGE WEAR RATES (CAST WHEELS/ DRY REGIME ONLY).

Experiment Identification	Flange Wear Rate, Inches/1000 Miles (15.8mm/1000 km)	Normalized Wear Rate, Inches/MGT (28mm/100kg)	
Wheels III			
U (untreated)	0.014	14000 miles of running (22540 km)	
C (treated)	0.0063*		0.0049
Wheels IV			
Sub U	0.221	7000 miles of running (11270 km)	
U	0.174		0.0070
B	0.135		0.0063
C	0.090		0.0049

*estimated for a C vs U wheel figure of merit of 2.2 based upon a straight line drawn through the Wheels IV data plotted in Figure 4a.

TABLE XIX. RAIL HARDNESS.

Metallurgy	Mean Hardness, BHN	
	Running Surface	Gage Face
Standard (Std)	324	314
Fully Heat Treated (FHT)	366	386
Head Hardened (HH)	355	381
Silicon Chrome (SiCr(HH))	391	405
Chrome Molybdenum, C (CrMoC)	344	353
Chrome Molybdenum, A (CrMoA)	383	398
Chrome Vanadium (CrV)	372	365
1% Chrome (1Cr)	348	353

TABLE XX. WHEEL HARDNESS, SIDE OF RIM (WHEELS IV EXPERIMENT/CAST ONLY).

Class of Wheel	Average Brinell Hardness
Sub U	249
U	273
B	295
C	317

rail lines are near -6 (RME III) and -4.5 (RME I), much steeper than might have been expected for a purely adhesive wear process in the cases where rail is harder than the average wheel hardness. The steep slope of the wheel plot cannot be compared with the horizontal line of Figure 73 because there the wheel hardness was assumed to be constant. Thus, for rails (and wheels also) the steeper slope than that expected for purely adhesive wear suggests that there is some other mechanism of wear that dominates over that of the adhesive component.

By using a somewhat different format, i.e., wear rate ratio* vs hardness ratio, the FAST wheel and rail wear rate data can be compared with that of other investigators. The FAST data for wheels and rails is shown in Figure 77 to be very close to that of Clayton²³ for field observations and Jamison²⁴ for laboratory tests, all three of which have disposition inclined more steeply than that for adhesive wear. Only the information of Marich & Curcio²⁴ approaches a slope of -2. However, before leaving this topic the data of Jamison should be examined more closely. Some specific data has been plotted in Figure 78. It appears that when the relative humidity is low, the slope of the wear rate ratio vs hardness ratio plot becomes quite steep. However, when the relative humidity is high, the disposition of the data is far less steeply inclined. This leads one to wonder if the FAST data would appear differently disposed if it were determined in a more humid area (although the Clayton field data was determined in the UK -- certainly a more humid environment than that of Pueblo, Colorado).

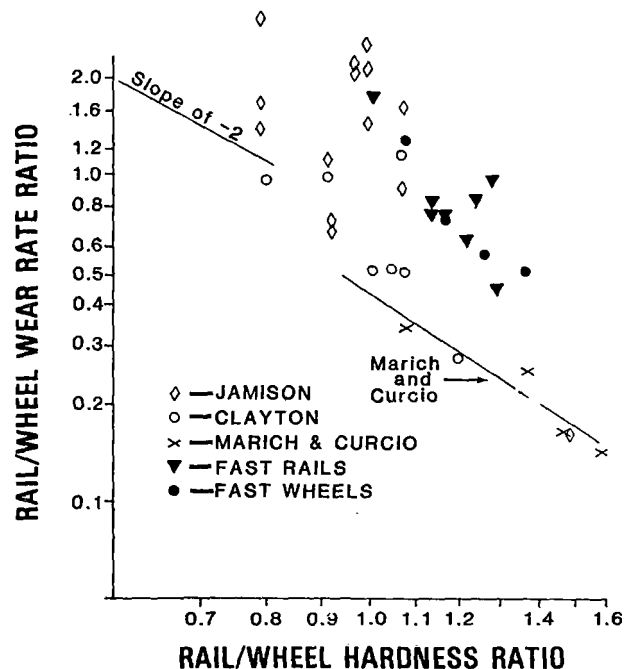


FIGURE 77. RAIL/WHEEL WEAR RATE RATIO AS A FUNCTION OF RAIL/WHEEL HARDNESS RATIO.

*the rail/wheel wear rate ratios have been calculated in the same fashion as the rail/wheel hardness ratios.

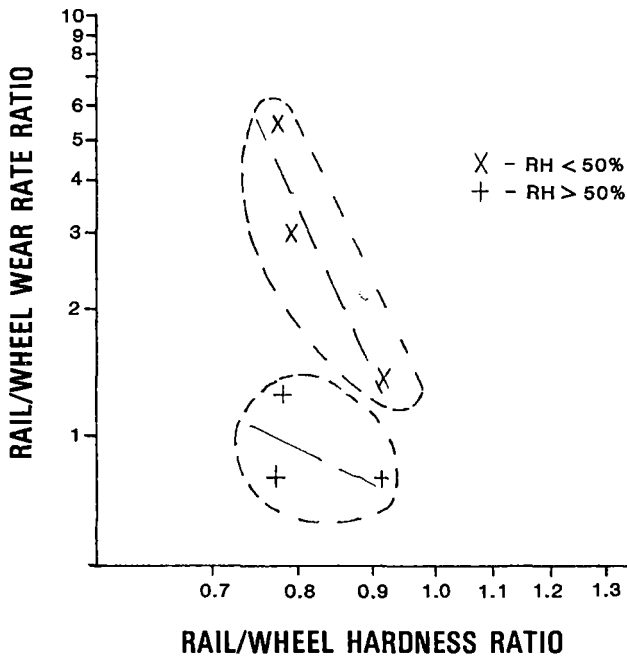


FIGURE 78. JAMISON DATA.

Some additional insight can be gained by plotting the individual wheel and rail specimen wear rates of Marich and Curcio²⁵ and Marich and Mutton²⁶ in the fashion proposed by Rabinowicz. This is done in Figure 79. The wheel data tended to show two different behavior patterns; in one case (upper right) the wheel wear rate decreased as the rail hardness increased while in the other case (lower left) the wheel wear rate increased very slightly as the rail hardness increased over a limited range. Strangely, when 360 BHN rail was substituted for 270 BHN rail the wheel wear rate diminished for a given rail to wheel hardness ratio. The rail behavior in each case (each investigation) behaved somewhat similarly

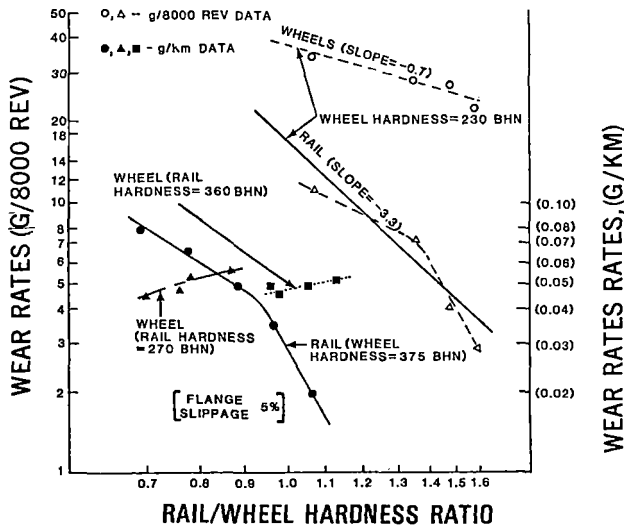


FIGURE 79. LABORATORY RAIL: WHEEL DATA OF 'MARICH AND CURCIO' AND 'MARICH AND MUTTON'.

although the data sets were displaced from each other. In each case there appeared to be a 'knee' in the plot such that at rail to wheel hardness ratios below the 'knee' the slope was much less than it was above the knee--a behavior not unlike that suggested by Rabinowicz.

In Figure 80, the FAST rail data has been plotted to show the effect of varying rail hardness against U wheels of fixed hardness assuming that the assumptions specified previously are appropriate.

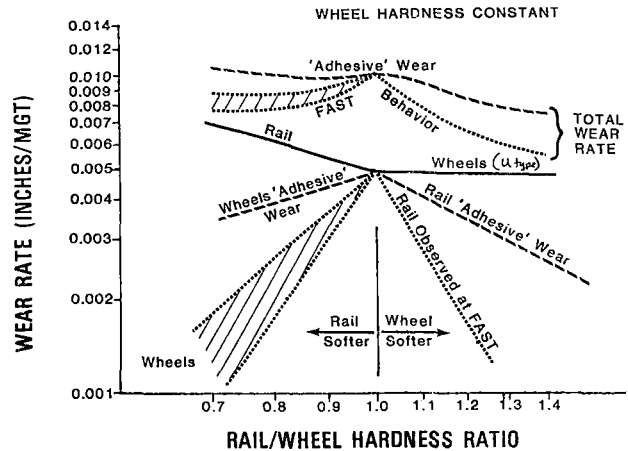


FIGURE 80. CONCEPTUAL ARRANGEMENT OF WEAR RATE FOR ADHESIVE AND FOR FAST DATA.

At fixed wheel hardness and at rail:wheel hardness ratios less than unity the relationship between rail and wheel wear rates would be represented by a rail line sloped upward to the left and a wheel line sloped downward to the left. For 'adhesive' wear the rail slope would be -1 and that for wheels would be +1. However, if the observed (at FAST) slopes for rails and wheels (-6 and +4 respectively) were used, the wheel slope would be between +3 and +5. This presumes that the wear rate of the softer component (the rail) would still be inversely related to the first power of hardness.

The total system wear rate is the sum of the wheel and rail wear rates at each hardness ratio. The wheel and rail lines for adhesive wear are also shown in Figure 80. For essentially adhesive wear, a 2:1 increase in hardness ratio (from 0.7 to 1.4) would be expected to yield only a 27% reduction in total system wear rate. For the actually observed FAST behavior, the maximum system wear rate would be expected to occur at unity hardness ratio with a reduction in system wear rate (~44%) occurring at hardness ratios approaching 1.4.

A somewhat different approach can be used to estimate the effect on rail wear rate of changing the type of wheel. This is shown in Figure 81. The presumption is made that the slope of the rail wear rate vs hardness ratio plot is not influenced by the wheel hardness, and for that matter, that the hardnesses themselves are not functions of the character of the mating materials. For purposes of illustration, the effect on wear rate of head hardened rail of changing from all U wheels to all C wheels is considered for both the 'adhesive' (rail slope of -2) wear and the observed FAST wear (rail slope of -6). If C wheels which wear at about one half the

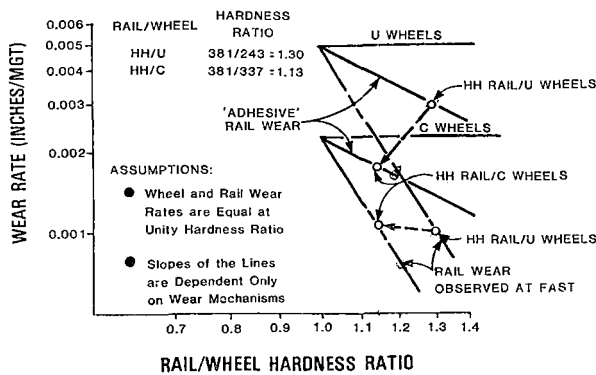


FIGURE 81. ILLUSTRATION OF CHANGES IN WEAR RATES RESULTING FROM CHANGE IN WHEEL TYPE FROM U TO C.

rate of U wheels replaced U wheels in an adhesive wear process, the wear rate of head hardened rail would diminish from about 0.003"/MGT to just under 0.002"/MGT. However, if the process involved were not purely adhesive but were that observed at FAST, the wear rate of head hardened rail would increase very slightly from just below 0.001"/MGT to just over 0.001"/MGT.

Thus, analysis suggests that either improvement or deterioration of wear performance of one component is possible by increasing the hardness of the mating component. Which will occur depends upon the slope of the rail line, (i.e., presumably the slope is a function of the mechanism of wear), the magnitude of the change in hardness and the relative difference in the wear rates of the component (wheels in this illustration) which is changed. The change in hardness and the relative difference wear rate of the component changed are really related to each other. With some simple mathematical manipulation one can show that the point at which a change from one wheel type to another will produce no change in rail wear rate is given by the relationship shown below.

$$\left(\frac{HR_U}{HR_C} \right)^n = FM$$

Rail: Wheel Hardness Ratio

Slope Of Wear Rate vs. HR Plot

Figure Of Merit Of C vs. U Wheels

An appropriate question at this point is "What wear mechanism might be associated with the steep rail wear rate vs hardness ratio plots observed at FAST?". Metallographic examination of cross sections taken through the gage faces of high wear rate (low equivalent carbon) and low wear rate (high equivalent carbon) rails (see Figure 82) suggests that the mechanism of wear involves cracking in the shear bands which develop beneath the gage face due to extensive plastic deformation resulting from many wheel passages. The cracks in the shear bands are shown in Figure 83. The depth of the shear band cracking is much greater (0.001" to 0.002") in the case of the high wear rate rail. Subsequent re-

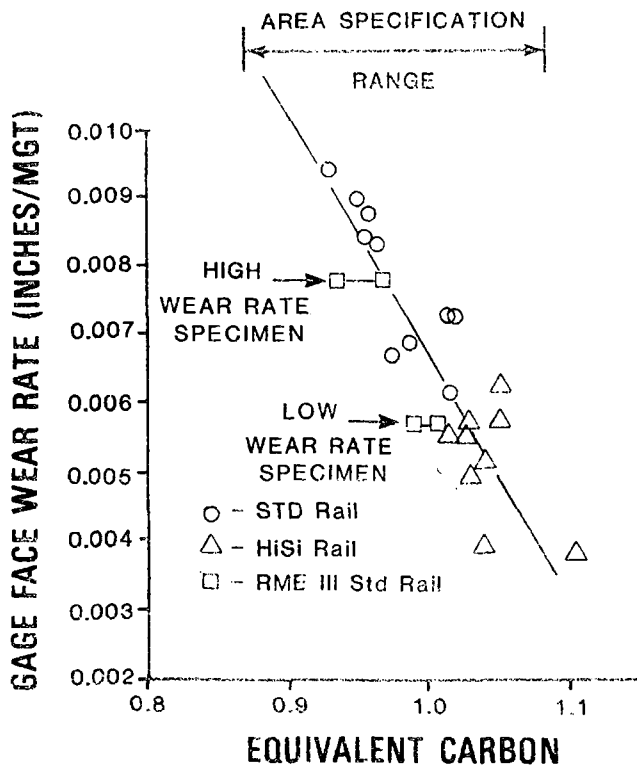
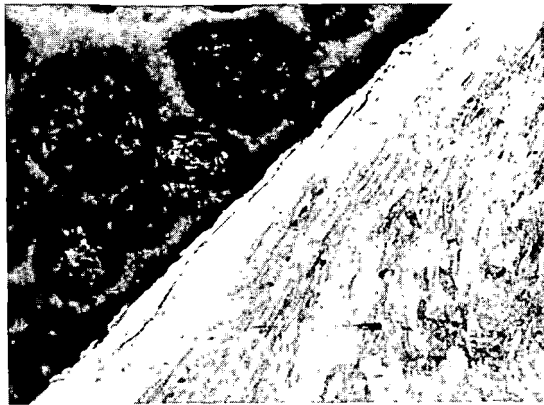


FIGURE 82. EFFECT OF EQUIVALENT CARBON LEVEL ON GAGE FACE WEAR RATE.

peated polishing and etching examinations have suggested that the cracks initiate beneath the surface and that nonmetallic inclusions may be associated with crack occurrence. Similar behavior has been observed in wheels as shown in Figures 84a, 84b, and 84c. These observations imply that the cleanliness of the steel may influence its wear resistance--a rather unexpected possibility.

Some further insights can be gained by observing the hardness variations beneath the gage face and the flow of metal down the gage face. Figures 85a and 85b illustrate the variations in hardness beneath the gage face surface for both the high wear rate and low wear rate rails. Traverse I (from the running surface just over the gage corner) reveals virtually no difference between rails. However, traverse II (from the gage face just below the gage corner) reveals that the high wear rate was substantially softer at a depth near 1mm, although both rails had about the same near surface hardness. In Figure 86, the hardness variation across the region of metal flow at the lower edge of the gage face is shown. Again the high wear rate rail exhibited greater softening beneath the surface. The hardness behavior beneath the surface suggests that metal flow down the gage face may account in part at least for 'loss' of metal from the gage face. The fact that even heavily worked regions may be as soft or softer than the base metal implies that cyclic softening may influence the 'wear' process--at least that part related to metal flow.

Up to this point in the discussion, attention has focused on the use and interpretation of wear information from FAST. Similar exercises may be undertaken with the rail failure information presented previously.



LOW WEAR RATE (200x)

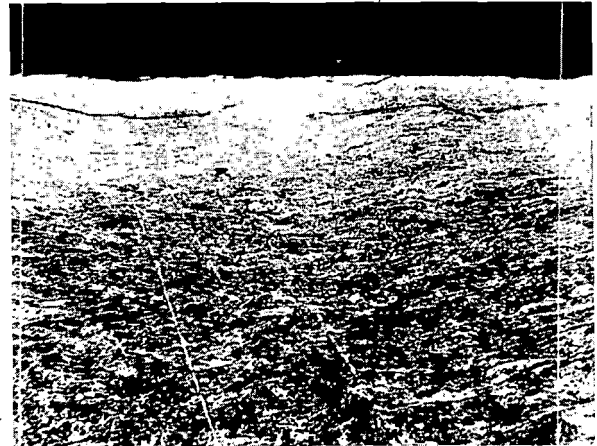


HIGH WEAR RATE (200x)

FIGURE 83. PHOTOMICROGRAPHS OF TRANSVERSE SECTIONS THROUGH GAGE FACE OF HIGH AND LOW WEAR RATE STANDARD CARBON RAILS.



CLASS "U" 600 X
a.



CLASS "C" 400 X
b.



CLASS "C" 400 X
c.

FIGURE 84a, b, & c. PHOTOMICROGRAPHS OF TRANSVERSE SECTIONS THROUGH FLANGE OF U AND C WHEELS.

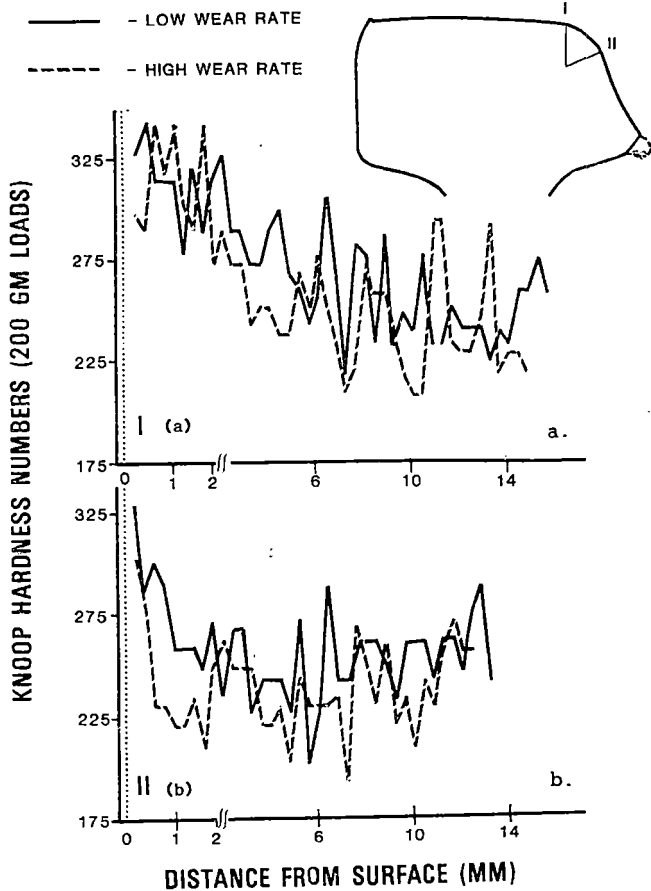


FIGURE 85a & b. HARDNESS VARIATION WITH DEPTH.

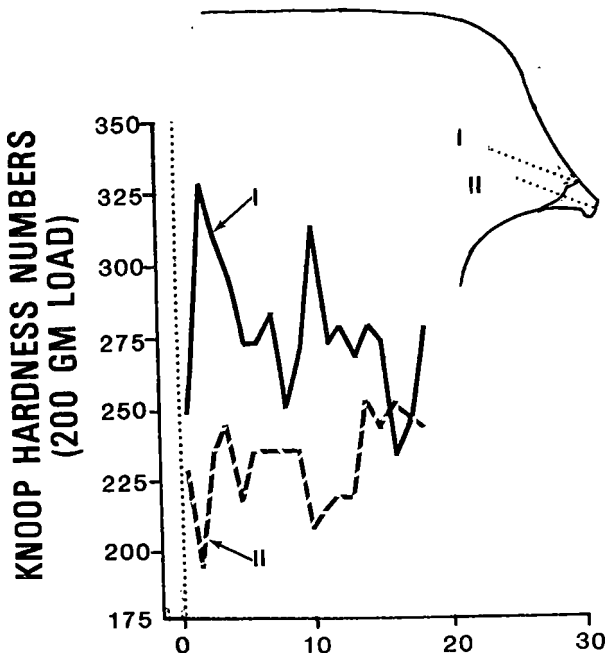


FIGURE 86. HARDNESS VARIATION WITH DEPTH.

The fact that the observed crack growth behavior at FAST seems reasonably in agreement with a prediction made from a rather simple crack growth model indicates that the approach could be applied usefully to more conventional railroad operating conditions to see the influence of a variety of factors upon transverse crack growth and especially upon the capabilities required of rail inspection to assure safety.

Table XXI summarizes a set of base line conditions which would be appropriate for a line in good physical shape carrying a large number of heavy cars (but not entirely loaded unit trains) on a conventional standard carbon rail of recent manufacture having seen enough service to have developed a reasonably high residual tensile stress state within the rail head. Also given in the table is a summary of the formulation and other relationships needed for making the calculations; the method is described in the reference.¹⁰

TABLE XXI. CONDITIONS FOR CALCULATION OF TRANSVERSE CRACK RADII FOR FAILURE IN PERIOD SPECIFIED.

(CENTRAL TRANSVERSE FISSURE/CENTER 0.4" DOWN)

Base Line Conditions :	RMS Wheel Load = 23.2 kips	$K_D = 30 \text{ ksi } \sqrt{\text{in}}$
	$\sigma_{RES} = 30 \text{ ksi}$	$K_F = 50 \text{ ksi } \sqrt{\text{in}}$
	Track Modulus = 1500 psi	$B = 3 \times 10^{-6} \text{ in/cycle}$
	Threshold = $\Delta K_{TH}^{R=0} (1-R)$	$n = 3.32$
	$\Delta K_{TH}^{R=0} = 7 \text{ ksi } \sqrt{\text{in}}$	
Crack Growth Formulation :	$\Delta K \approx 1.13 \Delta \sigma \sqrt{a}$	$\Delta \sigma =$ stress range calculated from beam-on-elastic foundation theory
	$da/dN = B \cdot \Delta K^n / [(1-R) K_c - \Delta K]$	$a =$ crack radius
		$K_c = K_F$ in fatigue situations
		$= K_D$ in impact situations
	$\Delta K_{threshold} = \Delta K_{threshold}^{R=0} (1-R)^{\gamma}$	$\gamma = 1$ for rail steel
		$R = \sigma_{min} / \sigma_{max}$

The results of baseline calculations are given in Table XXII. The defect sizes shown represent the upper limit of inspection sensitivity which would be required to avoid the occurrence of service failures under the baseline conditions at the tonnage rates and in the inspection periods specified. For instance, if a line having the characteristics and traffic specified carried only 1 MGT/yr and inspections were to be made at 2 year intervals, the inspection system would need to be able to find defects no smaller than 21% with 100% reliability to assure freedom from service failures. However, if the line were to carry 50 MGT/yr and inspections were still to be made once every two years. The inspection system would need to be able to find a 0.3% defect with 100% reliability.

Table XXII TONNAGE RATE

Period	1 MGT/yr	10 MGT/yr	20 MGT/yr	50 MGT/yr
1 month	0.68" (29%)	0.63" (25%)	0.59" (22%)	0.50" (16%)
3 months	0.67" (28%)	0.55" (19%)	0.47" (14%)	0.33" (7%)
6 months	0.65" (27%)	0.47" (14%)	0.36" (8%)	0.22" (3%)
1 year	0.62" (24%)	0.36" (8%)	0.25" (4%)	0.13" (1%)
2 years	0.58" (21%)	0.25" (4%)	0.15" (1%)	0.07" (.3%)

10% defect size boundary
10% defect size boundary

Typically, for most inspection systems, the reliability in finding defects drops significantly for defects less than 10% in size. Thus the dotted boundary in the table represents a sort of an upper boundary on inspection interval. For instance, with a 10% sensitivity system and the rail, track, and operation conditions specified, inspections ought to be made, monthly at maximum for 50 MGT/yr, quarterly for 20 MGT/yr line, and twice yearly for a 10 MGT/yr line.

The situation described in the previous paragraph applies to a rail with a relatively high internal residual stress state such as might be achieved after many hundred MGT of service. If for some reason, such as lighter wheel loads, wear, or grinding, a lesser internal residual stress state were achieved, a longer inspection interval would be tolerable. For instance, as shown in Figure 87, at 50 MGT/yr and 20 ksi residual tensile stress, inspections once each 6 months would be adequate; at 15 ksi residual tensile stress, inspections once each year would be adequate. The effect at 1 MGT/yr also is shown in the figure. Although the effect of residual stress on limiting defect size is greatest at 1 MGT, because almost any currently available inspections system would find 10% defects reliably and almost certainly inspections would be made at least once every 2 years, residual stress variations up to and even slightly exceeding 30 ksi would in a practical sense have no effect upon the inspection process.

TRACK STIFFNESS = 1500psi / RAIL TOUGHNESS = 30ksi $\sqrt{\text{in}}$

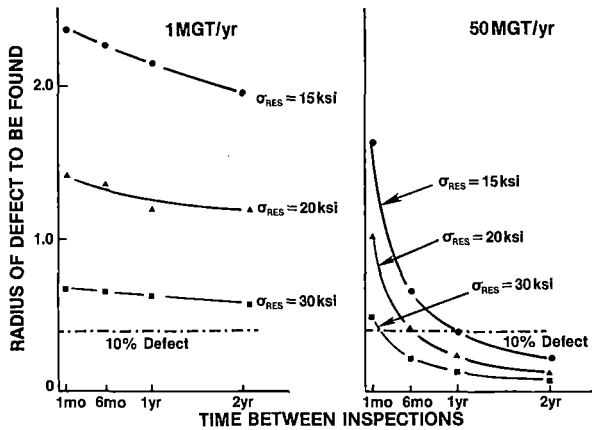


FIGURE 87. EFFECT OF RESIDUAL STRESS LEVEL.

The effects of variations in rail toughness and

track stiffness are shown in Figures 88 and 89. Given that any inspection system generally used would find 10% defects reliably and that inspections would be made at least once every two years, improving the fracture toughness (K_{Ic}) from 30 ksi $\sqrt{\text{in}}$ to 40 ksi $\sqrt{\text{in}}$ would have no real benefit at 1 MGT/yr (unless service conditions changed). However, at 50 MGT/yr improving toughness from 30 ksi $\sqrt{\text{in}}$ to 40 ksi $\sqrt{\text{in}}$ would permit the inspection interval to be lengthened from about 2 months to 3 months. Of course improved toughness is always an advantage because it provides added reserve against rupture particularly under conditions of high impact loading such as flat wheel passages. But the degree to which it provides benefit will depend upon inspection frequency and tonnage rate. The effect of reduced toughness is a bit clearer. For both 1 MGT/yr and 50 MGT/yr, with the 10% defect inspection system, a rail having a toughness of 20 ksi $\sqrt{\text{in}}$ could not be considered safe-by-inspection at any of the periods for which the calculations were made.

RESIDUAL STRESS = 30ksi / TRACK STIFFNESS = 1500psi

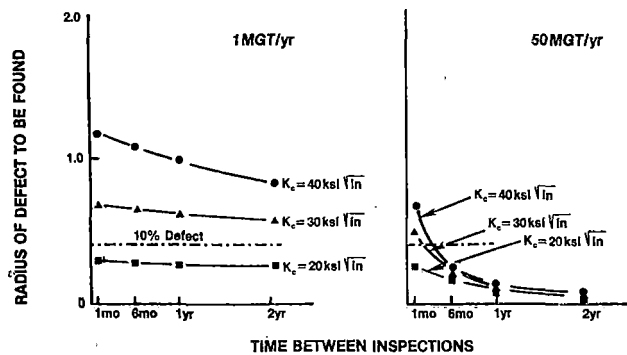


FIGURE 88. EFFECT OF RAIL TOUGHNESS, K_{Ic} .

RESIDUAL STRESS = 30ksi / RAIL TOUGHNESS = 30ksi $\sqrt{\text{in}}$

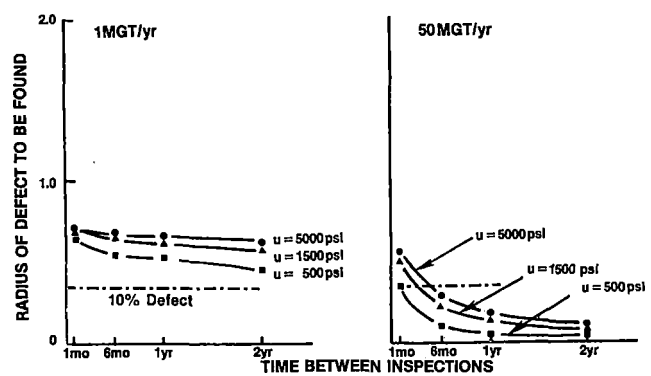


FIGURE 89. EFFECT OF TRACK STIFFNESS, ν .

Increase in track stiffness from 500 psi to 5000 psi would seem to have little real benefit on a 1 MGT/yr line (Figure 89). But at 50 MGT/yr, an increase in track stiffness from 1500 psi to 5000 psi would permit some extension of the inspection interval from approximately 3½ months to 5 months while loss of track stiffness to 500 psi would require shortening of the inspection interval to about one month.

Of course, the numbers discussed here cannot be applied rigorously to actual operation situations

because nobody really knows what the residual stress level is in a given rail at a given time. Nor does one know what the track stiffness or the toughness of the rail really are. The value of this exercise is to alert the reader to the idea that adverse changes that he sees occurring in the track may necessitate increased inspection, the degree of increase depending upon the tonnage carried.

The defect and rail failure information shown in Figure 45 can be utilized in a similar fashion to plan rail inspection on a more rational basis. The FAST data is useful in this respect to help assess the impact of wheel load on defect occurrence. However, to illustrate the utility of this type of data (number of defects as a function of traffic), the mean defect behavior of that found in the AAR/AREA/AISI survey will be employed to study the effects of different types of inspection policy. A central concept of the analysis which follows is that the more rail defects found at a given inspection (at fixed inspection sensitivity and reliability) the greater will be the likelihood that a few of these could have been service failures. This is illustrated conceptually in Figure 90. The rationale for this view is the fact that at FAST many transverse service failures occurred prior to the derailment of February 1979 when the peak defect population occurred in the 10-30% size range, but relatively few transverse type service failures have occurred now that the peak defect population is in the 2-5% size range.

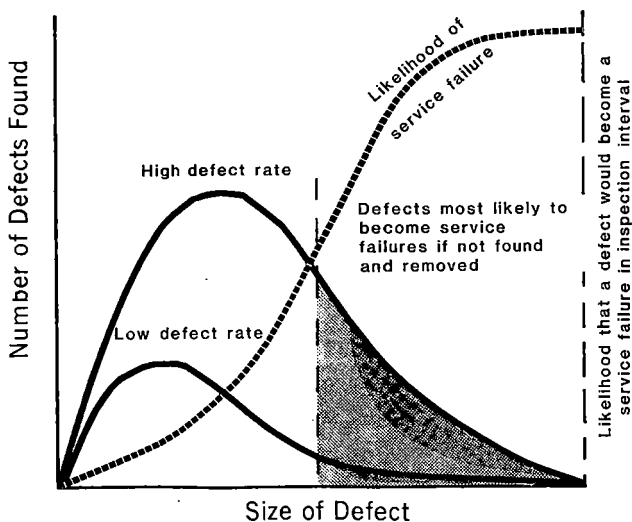


FIGURE 90. SIZE OF DEFECT.

The exercise may be accomplished mathematically starting from the Weibull expression for portion defective, $F(x)$, as a function of tonnage:

$$F(x) = 1 - \exp\{-\frac{(x-\gamma)^\beta}{\alpha}\}$$

where β , γ , and α are constants which describe the life distribution and x is measured in units of 100 MGT. For the mean survey behavior (and presuming only one defect per rail length), $\gamma = 0$, $\beta = 3.21$ and $\alpha = 16318$. The defect rate, $Z(x)$, the instantaneous slope of the defect vs MGT plot, is given as:

$$Z(x) = \beta(x-\gamma) \frac{\beta-1}{\alpha}$$

For the mean survey behavior, the defect rate curve is shown in Figure 91. There are two obvious main categories of inspection rationale that can be considered:

- (1) Constant inspection rate i.e., fixed intervals of time or tonnage between inspections (basically, the philosophy is that of the current FRA track standards), and
- (2) Variable inspection rate wherein the interval between inspections or the number of inspections per unit of exposure (time or tonnage) is varied in some systematic fashion.

Without becoming burdened with the mathematics of how to do this we may nevertheless benefit from a comparison of the constant rate inspection philosophy with two variable rate inspection philosophies, one adjusting the inspection rate (interval) in proportion to the defect rate and the other adjusting the number of inspections in proportion to the defect rate. To make each approach truly comparable, the variable rate methods have been scoped to find the same total number of defects as does the constant rate approach in 500 MGT of service.

The resulting intervals between inspections for each approach at a tonnage rate of 20 MGT/yr are shown in Figure 92. Note that as the rail sees more service and its defect rate increases (Figure 91), the interval between inspections becomes smaller and smaller while that for the current FRA approach (constant rate inspection) remains fixed. Figures 93 and 94 show that for both of the variable rate philosophies, the number of defects found per unit of track distance per inspection increases and then tends to level off or even drop slightly. The current FRA approach yields a continuing increase in defects found in each inspection as the rail grows older. At fixed inspection sensitivity and reliability, the longer the interval between inspections as the rail accumulates more tonnage, the greater the number of defects present in the inspection interval and the greater the likelihood that some of the population present will either have been service failures before the next inspection or, if not discovered by the next inspection, will be service failures before the following inspection.

A relevant question at this time is whether a variable (increasing) rate inspection philosophy is reasonable in view of the practicalities of rail inspection. Figures 95a through 95d illustrate different approaches currently required (FRA) or proposed (modified FRA and AREA) along with a 'linearized' version of the variable rate approach. When all are superimposed together on one plot (Figure 96) it becomes clear that the variable rate approach (linearized version) is extremely consistent with a combination of both the proposed FRA modification and the AREA recommendation. Common sense has triumphed again.

This type of analysis can be carried one stage further if assumptions are made about the distribution of defects actually generated in the rail and also about the shape of the inspection reliability curve. Figure 97a illustrates what the size distribution of detected defects should look like given

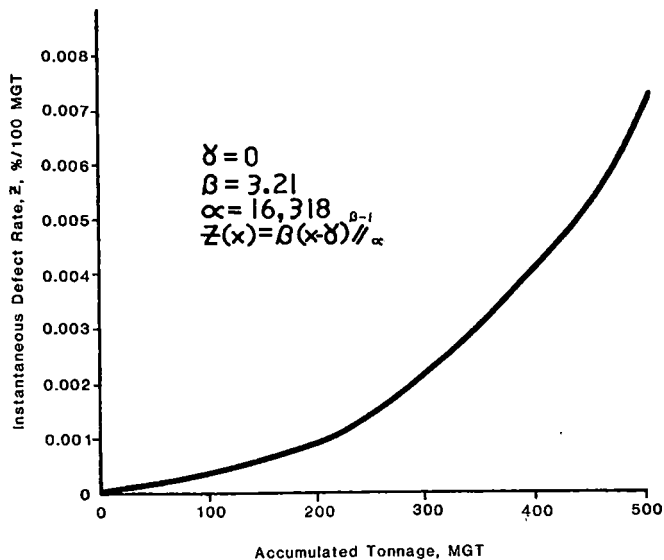


FIGURE 91. INSTANTANEOUS DEFECT RATE AS A FUNCTION OF SERVICE EXPOSURE.

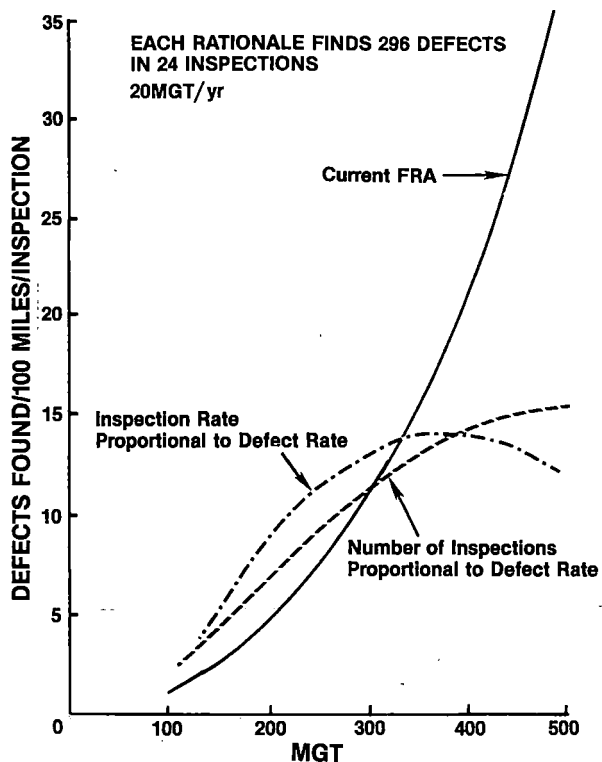


FIGURE 94. DEFECTS FOUND AS A FUNCTION OF TONNAGE.

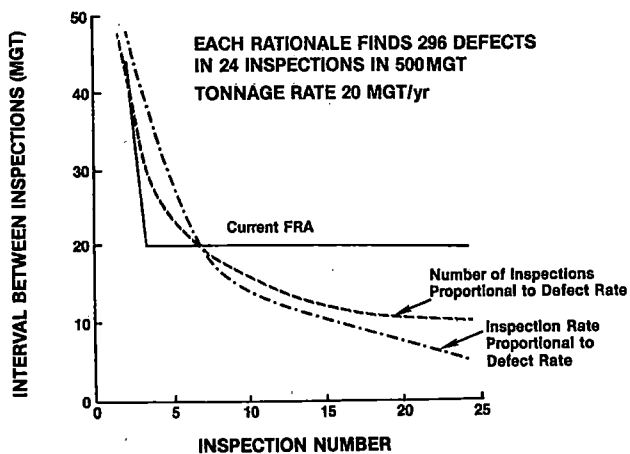


FIGURE 92. VARIATION OF INTERVAL BETWEEN INSPECTIONS.

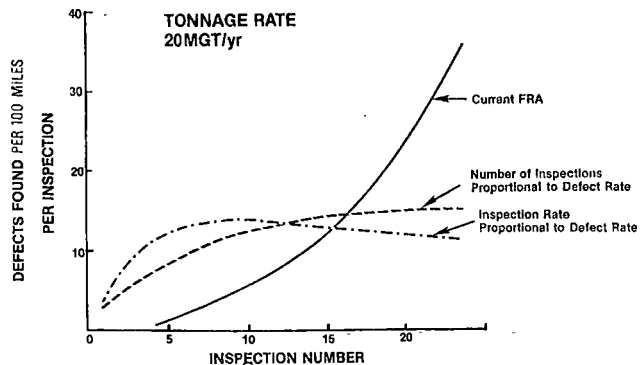


FIGURE 93. DEFECT FOUND AT EACH INSPECTION.

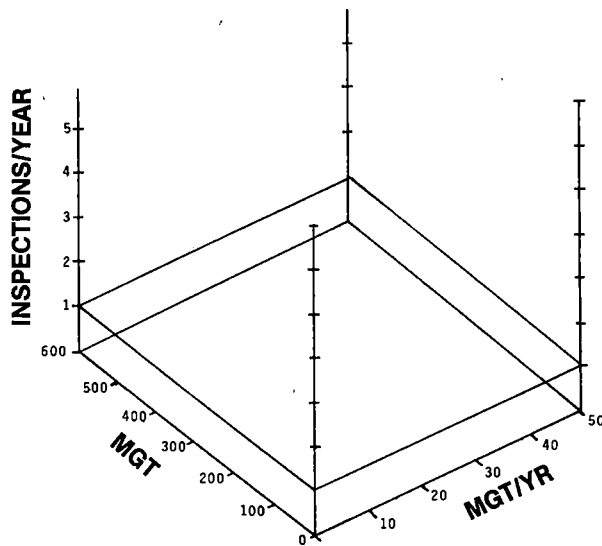


FIGURE 95a. CURRENT FRA INSPECTION REQUIREMENTS.

the assumed total defect size distribution and the assumed inspection reliability function. The detected defect distribution is not unlike those shown in Figure 47. Because no inspection process is absolutely 100% effective there will a high likelihood that some defects will remain undetected as shown in Figure 97b.

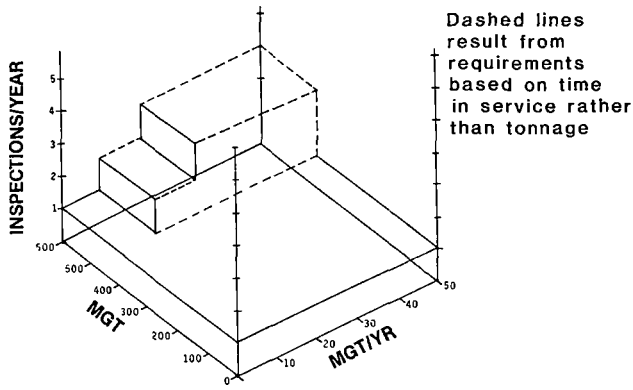


FIGURE 95b. PROPOSED FRA INSPECTION REQUIREMENTS.

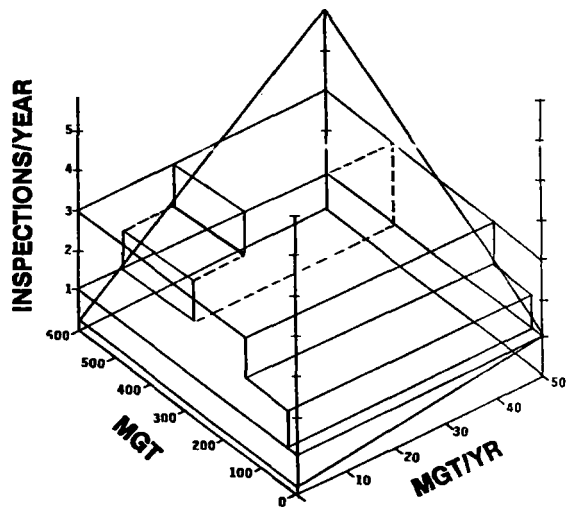


FIGURE 96. COMBINED RECOMMENDATIONS.

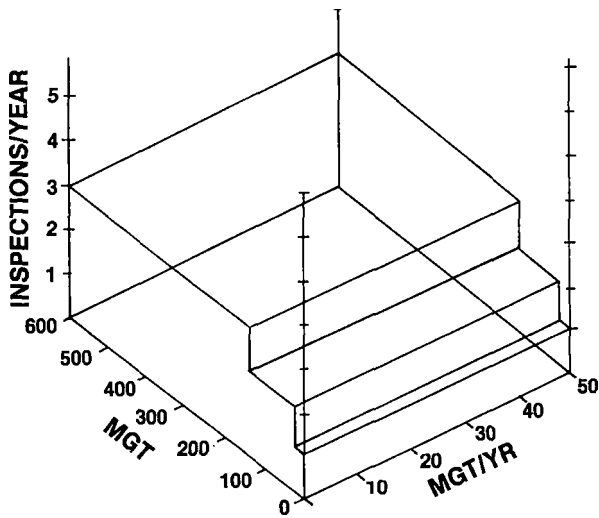


FIGURE 95c. PROPOSED INSPECTION REQUIREMENT BY AREA COMMITTEE 4, SUBCOMMITTEE 9.

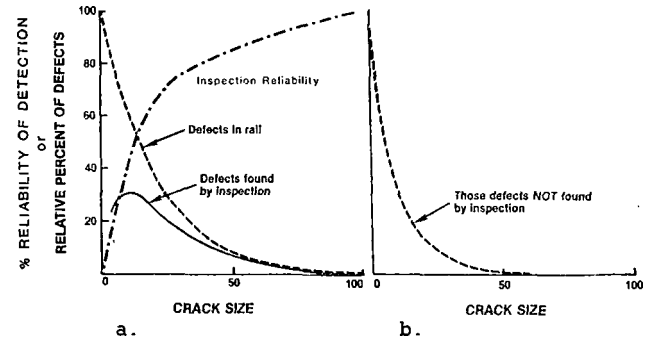


FIGURE 97a & b. ASSUMED DEFECT SIZE DISTRIBUTION.

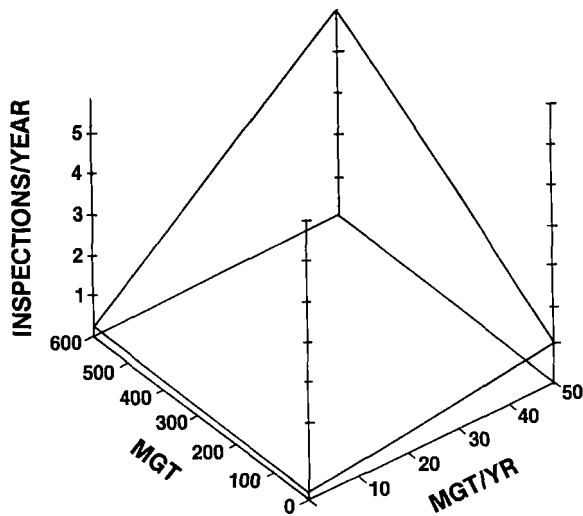


FIGURE 95d. INSPECTIONS PROPORTIONAL TO DEFECT RATE (LINEARIZED VERSION).

Typically transverse defects (detail fracture type) in the size range from 20 to 40% growth can become rapid.²⁷ Thus, some idea of the likelihood of service failure occurrence can be gained by estimating the number of defects likely to reach 30% size or more in less than the inspection interval. This has been done for the current FRA (constant interval) approach (Figure 98a) and a variable rate approach (Figure 98b) wherein both approaches find the same number of defects in 400 MGT and seven inspections. Note that for the variable interval approach the peak occurrence shifts to smaller defect sizes with each subsequent inspection and that the total number of defects found as well as the number greater than 30% in size tends to level off with tonnage. However, the constant interval approach maintains the peak occurrence at about the same size and the total number of defects found as well as the number greater than 30% in size increases non linearly with tonnage.

CONCLUDING REMARKS

The important findings of FAST tests for each topic (wear and metal flow, welded rail end batter, and rail failure) have been summarized at the end of each section and will not be repeated here. What

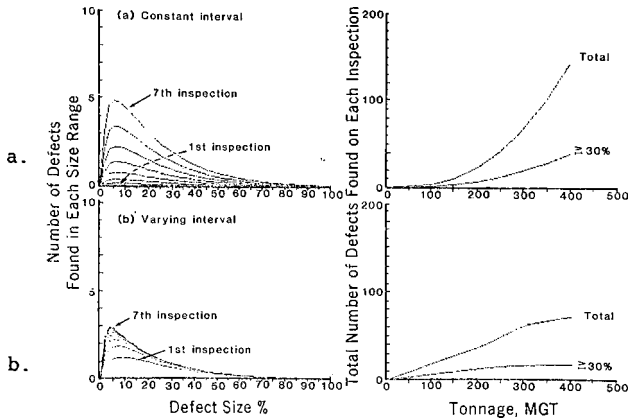


FIGURE 98a & b. DEFECT SIZE DISTRIBUTION AND TOTAL NUMBER OF DEFECTS FOUND.

the 'Discussion' section has sought to show is that there is a great deal that can be done with the information generated at FAST, both in terms of wear and metal flow and also fatigue and failure of rail, and that FAST provides a very suitable test bed upon which to study mechanisms (of wear, for instance) while at the same time generating more practical comparative information which can provide shorter term benefits to the railroad industry. Greater benefit will be derived from the information generated at FAST only if it is related more clearly to real world environments where good measurements and records of service environments are obtained only with much greater difficulty.

Acknowledgements: The information presented here in this chapter on Rail has become available thru the sustained and sometimes painful efforts of a large number of people over the course of several years. We must express our gratitude to the following individuals

Mike Hargrove } Kate Shade }	Association of American Railroads
Tim Suazo } Ebby Moin } Glenn Brave } Les Ott } Lahnona Krumanocker }	Boeing Services International

and Jesus Prieto, Ferrocarriles Nacionales de Mexico

PHOTO COURTESY OF G. KRAUSS, COLORADO SCHOOL OF MINES.
FIGURES 48, 49, & 50.

PHOTO COURTESY OF MANUFACTURER.
FIGURES 54, 55, 56, 57, 58, 59, & 84a, b, & c.

REFERENCES

- 1 McEvily, A. J. and Minakawa, K. - "Metallurgical Evaluation of FAST Rail Steels," Final Report, August 1981, U.S. DOT Contract DOT-TSC-1551, University of Connecticut.
- 2 Clayton, P. - "The Relationships Between Wear Behavior and Basic Material Properties for Pearlitic Steels," *Wear of Materials 1979*, American Society of Mechanical Engineers, New York, N.Y., pp 35-44.
- 3 Hay, W. W., Reinschmidt, A. J., Bakas, P. T., and Schuch, P. M. - *Economic Evaluation of Special Metallurgy Rails*, Report No. ENG-76-2002, University of Illinois at Urbana-Champaign, Urbana, IL, January 1976, NITIS #PB 525 024.

- 4 Rougas, M. - 1975 Technical Proceedings of the 12th Annual Railroad Engineering Conference, Report No. FRA-OR&D-76-243, October 1975, pp 41-44.
- 5 Stone, D. H. - *Comparison of Rail Behavior with 125-Ton and 100-Ton Cars*, Report No. R-405, Association of American Railroads, Chicago, IL, January 1980.
- 6 Curcio, P., Marich, S., and Nisich, G. - "Performance of High Strength Rails in Track," Paper I.10, *Heavy Haul Railways Conference*, Perth, Western Australia, September 1978.
- 7 Stone, D. H. - *Track Train Dynamics Contributions to Rail Metallurgy*, AREA Bulletin 673, Vol. 80, pp 528-543, June-July 1979.
- 8 Perlman, A. B. and Jeong, D. Y. - "The Effect of Track Load and Structure Characteristics on the Fatigue of Rail," Department of Mechanical Engineering, Tufts University, December 1980.
- 9 Frederick, C. O. and Jones, E. G. - "A Review of Rail Research on British Rail," TRB Meeting, January 1980, Washington, D.C.
- 10 Ichinose, H., Takehara, J., Iwasaki, N., and Ueda, M. - "An Investigation on Contact Fatigue and Wear Resistance Behavior in Rail Steels," Paper I.3, *Heavy Haul Railways Conference*, Perth, Western Australia, September 1978.
- 11 Steele, R. K. - "Fatigue Crack Growth and Fracture Mechanics Considerations for Flaw Inspection of Railroad Rail," *Materials Evaluation*, October 1980, Vol 38, No. 10, pp 33-38.
- 12 Feddersen, C. E. and Broek, D. - "Fatigue Crack Propagation in Rail Steels," *Rail Steels - Developments, Processing, and Use*, STP 644, American Society for Testing and Materials, Philadelphia, PA, 1978, pp 414-429.
- 13 Barsom, J. M. and Imhof, E. J. - "Fatigue and Fracture Behavior of Carbon-Steel Rails," STP 644, American Society for Testing and Materials, Philadelphia, PA, 1978, pp 387-413.
- 14 Groom, J. J. - *Residual Stress Determination*, DOT-TSC-1426, Battelle-Columbus Laboratories, November 26, 1979 (Draft Report).
- 15 Bolton, P. J., Clayton, P., and McEwen, I. J. - "Wear of Rail and Tire Steels Under Rolling/Sliding Condition," ASLE Preprint 80-LC-5B-3.
- 16 Johns, T. G., Davies, K. B., McGuire, P. M., Sampath, S. G., and Rybecki, E. F. - "Engineering Analysis of Stresses in Railroad Rail: Phase I," Battelle-Columbus Lab Report G6266-0101, June 1977, Columbus, Ohio.
- 17 Stone, D. H. and Steele, R. K. - "The Effect of Mechanical Properties Upon the Performance of Railroad Rails," ASTM STP644, 1976, pp 21-48.
- 18 Marich, S. - "Research on Rail Metallurgy," AREA Bulletin, June/July 1977, #633, Vol. 73, page 597.
- 19 "Rail Lubrication Studies at the Facility for Accelerated Service Testing," FAST/TTC/TM-80/08, TTC, US DOT, Pueblo, Colorado.
- 20 Rabinowicz, E. - "Wear Coefficients-Metals," pp 501-502 in *Wear Control Handbook*, ASME 1980.
- 21 Allen, R. - "The Mechanical Aspects of Wheel/Rail Wear," Report No. FRA/TTC-82/01, page 217.
- 22 Marich, S. and Stone, D. H. - "Metallographic Examination of Cracked Wheel Flanges from FAST," paper 5-2, Proceeding of the 6th International Wheelset Congress, Colorado Springs, Colorado, October 1978.
- 23 Clayton, P. - "Lateral Wear of Rails on Curves," *Tribology*, pp 83-90, Illustrated Mechanical Engineer, London, 1978.
- 24 Jamison, W. E. - *Wear of Steel in Combined Rolling and Sliding*, ASLE Report No. 80-LC-5B-1.
- 25 Marich, S. and Curcio, P. - "Development of High-Strength Alloyed Rail Steels Suitable for Heavy Duty Applications," ASTM STP 644, page 188.

²⁶ Marich, S. and Mutton, P. J. - "An Investigation of Severe Wear Under Rolling/Sliding Contact Conditions Existing in Heavy Haul Railways," Seventh International Wheelset Congress, Vienna, October 1981.

²⁷ Rail Defect Manual, Sperry Rail Service, 4th Printing 4/68, page 39.

QUESTIONS AND ANSWERS

Question 1

If hardness and yield strength are not good indicators of gage face wear, what do we strive for to obtain better performance?

Answer

In most cases as-worn surface hardness, and by inference, initial hardness as well, will provide a good correlation with wear resistance. However, some notable exceptions have been pointed out. Likewise, both static and cyclic yield strength seem well related to head height loss rate, but not to gage face wear rate in all cases. Because gage face wear rate (under FAST conditions) appears to involve a shear band cracking process, cyclic ductility (cyclic true fracture strain) may prove to be a better predictor of gage face wear resistance. Work by Paul Clayton at British Rail does suggest that there is a good correlation between wear rate and the total plastic strain at a fixed stress level. Really, though, at this time we don't know enough about the nature of the wear process itself to suggest that any mechanical test parameter will be a truly reliable predictor of wear resistance. However, were I responsible for attempting to find, and control the quality of, a better rail, I'd watch hardness, equivalent carbon level, and microstructure.

Question 2

What, if any, is the effect of lubrication on failures?

Answer

Effective lubrication clearly prolongs the life of rail long enough to allow fatigue to become an important concern. We have not seen any indication that lubricant acts as a hydraulic 'wedge' to propagate a crack. However, the reduction of the friction coefficient at the wheel/rail interface that is achieved by effective lubrication would be expected to move the point at which the maximum shear stresses occur to greater depths beneath the running surface and to reduce the amplitude of these stresses. These changes could well alter the rate and location at which fatigue cracks develop. The FAST results suggest that modest wear may actually serve to prolong rail life by deferring fatigue as a competitive mode of failure.

Question 3

Where are lubricators located?

1. On curve where flange first contacts high rail, or
2. Tangent, if tangent is gage tightened? If so how much?

Answer

In the past, lubricators have been located in tangent track just prior to the entry to the spirals. Most recently lubricators have been located in tangent track, in some cases thousands of feet from the curves which they must lubricate. Track gage has not been tightened in such cases. Perhaps, because FAST is a closed loop and our lubricators in these tangent track installation 'geyser' so much even on the lowest output setting, we are able to get effective lubrication of a high rail (inside loop rail in Section 7) up to two or more miles from the lubricator (in Section 20). FAST does not represent a challenge to achieve a lubricated state but rather to prevent it from overwhelming us.

Question 4

Is there any relationship between change in wear rates vs. work softening and/or work hardening of the rail with traffic?

Is there any evidence of work hardening or work softening behavior at FAST?

Answer

Probably yes. We see that a high wear rate standard carbon rail (low equivalent carbon) does exhibit a layer of what appears to be softened material beneath the surface deformed region and that metal pushed down the gage face is far softer than we'd expect to observe for metal so heavily deformed. Likewise, the region in which a shell has developed in one of our failed rails appears to be softer than much of the metal around it. We suspect that the work softened material may be more prone to fatigue damage. However, the region (0.001-0.002" beneath the gage face) in which wear debris is generated does not seem softer than nearby regions. Thus, at this time we are unable to estimate the effect of work softening on wear itself.

Question 5

Have you (or anyone) looked at these rail samples under transmission electron microscopy? Does this shed any light on the origins of wear in the different rail samples as well as the influence of lubrication?

Answer

No, we have not yet used the transmission electron microscope to examine the character of the metal in the vicinity of the wear inter-

face. To do so would be an extremely useful exercise in that such examination would help define the nature of the deformation processes occurring in the region of debris generation. Thus we could anticipate more accurately what characteristics should be sought for an improved rail--even an improved standard carbon rail. Use of preferred orientation determination techniques (X-ray diffraction) also would provide valuable insights into the processes which occur at the rail/wheel interface.

Question 6

Is the rate of metal flow on rail uniform through age? If not, how does it vary?

Answer

Apparently not! Although data from the first rail metallurgy experiment does show a steady rise and then a levelling off of low rail lateral flow to the field side (in the lubricated regime), information from the third experiment (not available at the time of the Conference presentation) suggests that lateral flow on both field and gage side of the low rail occurs at an increasing rate after each lubrication interval.

Question 7

Have you analyzed the economic cost of different rails based on your data (not including transportation)?

What is the difference between type B, C, & U wheels you showed on graph in Phase III?

Answer

No, but Mike Hargrove at AAR in Washington has been using the FAST rail wear data to calibrate a rail life model prepared by the Canadian Institute of Guided Ground Transport. This model would then be exercised to provide economic cost analysis. Although we've not performed an economic analysis, an improved standard carbon which might have 50% better wear resistance at less than 10% additional cost would appear to be highly attractive and, based upon the FAST rail wear results, would appear to be easily within reach.

With regard to wheel designations, U and C class wheels have the same carbon content, but the C wheel is rim hardened (somewhat akin to head hardened rail). A B class wheel is rim hardened but has a lower carbon content than the C wheel.

Question 8

You infer that there is a substantial improvement in wear due to lubrication, but you did not mention any specific comparison in quantitative terms. What would be the FM (figure of merit) comparing dry standard rail vs lubricated standard rail, dry CrMo, lubed CrMo, dry HH and lubed HH, etc?

Answer

The generous lubrication which we've encountered at FAST improves the wear resistance of standard rail by about a factor of 8 to 10. However, the wear resistance of the better premium rails will improve by a factor of 4 to 5 only. Thus, the figure of merit of premium rails relative to standard rail diminishes significantly as the level of lubrication improves as with SiCr(HH) where the figure of merit exceeds 4 when dry, but is less than 2 when well lubricated. Similar changes occur for the other premium metallurgies.

Question 9

Is gage face wear, head loss, and total wear rate measurement compared to initial no service conditions of each rail metallurgy or compared to a nominal rail section? If the latter comparison, how are the wear rates of different rail sections reconciled?

Answer

The FAST wear measurements have been made by comparing the profiles after service exposure at each measurement site to the initial actual profiles at that site.

Question 10

Is there any information available why a bainitic structure does not fit into the hardness wear characteristic? Why is a bainitic microstructure wearing different than a pearlitic one of approximately the same hardness--test heats with 4.3% Cr, ~400 HBN, structure fully bainitic, done in Germany about six years ago, showed higher wear rate than 1% Cr pearlitic rail steel with ~320 HBN?

Answer

We don't know enough about the mechanism of wear and the relationship of wear to mechanical behavior to explain why bainite and martensite exhibit poorer wear resistance than pearlite of the same hardness. However, it is interesting to note that both bainite and martensite are the products of shear transformations while the pearlite transformation is a two phase nucleation and growth process. As a consequence of the shear transformation, the morphology of the iron carbides in bainite and martensite (tempered) is very different from that of pearlite. Although we can say these differences exist, alas it is not clear why they should imbue bainite and martensite with inferior wear characteristics.

Question 11

You mentioned in your talk that two (or more) types of head hardened rail has been tested and that the second type tested seems to wear somewhat more rapidly than the first.

Do you think this is due to something the manufacturer is doing in the heat treating process, or is it due to chemistry? Is it statistically significant? Are you allowed to name names if it is? Does it have anything to do with rail cleanliness?

This question is asked because we are buying two different types of HH rail at the moment (Nippon and NKK). About 15 years ago we bought some Curvemaster and it failed, mainly with the shell.

Answer

Both conventional standard carbon head hardened and silicon chrome head hardened rail have been tested thoroughly. The silicon chrome rail is an alloy specially designed to benefit from slack quenching (as in the flash butt welding operation). The gage face wear resistance of the silicon chrome head hardened rail is about one-third better than that of conventional head hardened rail when running dry. However, its head height loss resistance (running dry) may not be so good as that of conventional head hardened rail. Both rails are approximately comparable when running in the lubricated state. The difference in chemistry probably is chiefly responsible for the difference in gage face wear resistance.

We try to avoid naming manufacturers. But we do see differences in behavior for rails of nominally the same chemistry which are likely due to differences in processing from one manufacturer to another.

With regard to cleanliness, yes, much to our surprise we think there may be a relationship between gage face wear (not just fatigue failure, i.e., shelling) and the inclusion content of the steel. But this is not yet well established.

Question 12

Does rail design, specifically the slope of gage face side, affect gage face wear? (Slopes of 140 RE and 136 RE rails are different.)

Also, has corrective head grinding affected gage face wear?

Answer

Wear at FAST is rapid enough in the dry regime so that all rails will quickly adopt the same profile after a short period of service. Thus, the original slope of the side of the rail is quickly lost and is replaced by a slope characteristic of the average wheel tread/throat/flange configuration. However, the rate at which this new contour progresses down the side of the rail head may indeed be a function of the head design (as well as of metallurgy). We really don't know. However, once the new contour has extended to the 5/8" gage point, the wear measurements now are all taken at the same representative geometry and the wear rate is governed by the inherent wear resistance of the metallurgy.

We have been able to detect experimentally any effect of corrective head grinding upon gage face wear but this lack of relationship may be attributed to the fact that the experiment has not been designed to study the effect of grinding on gage face wear.

Question 13

You will be interested in the grain refinement being found in hot rolled (not controlled rolled) steel if V&N are present. This observation needs more investigation to be sure. Do you have nitrogen contents of the V rails?

Answer

No, unfortunately, we don't know the nitrogen content of the vanadium containing rails. It would be appropriate for us to find out. We're not sure what structural features other than pearlite interlamellar spacing need be controlled to assure good wear resistance. The relationship between vanadium and nitrogen levels and microstructural refinement is intriguing and this relationship may offer some aid in understanding why chrome vanadium compositions have not done better than we have observed.

Question 14

Has the mechanism of rail wear been investigated from the standpoint of nucleus of origin, i.e., what effects have metallurgical grain size and steel cleanliness been upon wear initiation and progression? If not, is there any plan to investigate these factors?

Answer

We believe the gage face wear process itself is a shear band failure process which may well depend on steel cleanliness. Of course the formation of shells (and TD's) by a fatigue process has long been felt to be related to steel cleanliness. The question at hand is "how much cleanliness is worth paying for?". We have just started to attempt to develop the correlations which might answer that question.

Question 15

Were climatic changes or differences correlated with wear rates, i.e., seasons of high or low humidity which varied from block to block or snow quantities or temperatures?

Answer

We have not been able to detect any relationship between wear rate and the season of the year and the temperature or humidity. Admittedly, we've not gone at this in a rigorous fashion. Though we've not seen a clear correlation (would that we could use this explanation to rationalize our block to block variations), we have an open mind on the subject.

Question 16

Would the introduction of anomalies in the wheel bearing area cause greater metal flow or a more rapid loss of head height?

If so, would there be a difference in rate between dry and lube?

Answer

I interpret this question to mean "will features such as welded rail end batter, engine burns, and corrugations act to accelerate the wear process?". In theory, the higher dynamic forces occurring under such conditions might be expected to accelerate wear. Our measurement techniques have not been sensitive enough yet to shed light on this question.

Question 17

How can my railroad measure the amount of (or effectiveness of) lubricant film on gage face at a specific distance from a lubricator?

Answer

There appears to be no simple, reliable method of measuring the amount of lubricant film in the field. The best approach is to determine the wear rate (preferably with an instrument having a 0.001" measuring sensitivity) in both the dry and lubricated states at the same place in track. If the lubricated wear rate is one-fifth to one-tenth that of the dry state, you are obtaining effective lubrication.

Question 18

Why didn't you use equivalent carbon content of wheels and rail vs. wear rate instead of wheel and rail hardness vs. wear rate as a predictor of overall wear?

Answer

If wear rate were only a function of equivalent carbon, conceivably this would be possible. But heat treatment also influences wear rate at a given equivalent carbon level. Therefore, some parameter such as hardness is used which is responsive both to chemistry and heat treatment. From a practical point of view, hardness is a good parameter because it can be measured so easily.

Question 19

In the derailment of the FAST train traced to detail fracture, why was it not possible to detect the initiation of the fracture or the fracture itself during growth with the detector cars which, it is assumed, are used to greater extent at FAST?

Answer

There were three TD's within one 20' piece of rail. On one inspection, the detection system

picked up two of the three defects but the operator noted neither of the two which appeared on the strip chart record. A few days later on the next inspection, the vehicle had reversed direction and only one of the defects was detected. The defect was detected again on the next inspection (vehicle travelling in the same direction as on the day that the strip chart record indicated two defects); the second defect was not observed. The one which was observed was indicated as a 8% TD--smaller than the size requiring joint bar installation.

This unfortunate series of events resulted from two major causes which have been corrected subsequently. The first of these was that the strip chart record was not examined at the end of the day's run to determine whether defects were found but not entered on the log. The second was the fact that the twelve 70° transducers (six in each rail wheel) were not all functioning at equal sensitivity and that no periodic test of sensitivity of each transducer was required. The fact that three 70° transducers within a group are wired in parallel means that the loss of sensitivity of one or two of these cannot be detected without using a procedure designed to check each transducer individually. Rail inspection at FAST is made every 2-3 MGT which is an appropriate interval. But, inspection at any interval will be ineffective if all parts of the inspection system are not known to be functioning properly.

Question 20

Has there been any consideration of steel metallurgy (for rails) as related to failure rate and impact properties?

Might not the variable hardness zones found in (some) rail fractures be associated with steel solidification dendritic patterns (i.e., higher % C segregation at dendritics)?

Answer

Fracture toughness (both static and dynamic) which can be a function of the type of metallurgy can, as shown in the text, have a large effect on the performance of the rail and upon the inspection sensitivity and intervals required. However, FAST has not been able to provide an effective assessment of how different metallurgies behave because so few premium rails have failed due to fatigue of the rail (as opposed to the weld) itself. Although FAST wheel loads are high, there are virtually no flat wheels which could provide the impact loading needed to increase the rail failure rate. Basically, FAST has not been designed as a fatigue test.

With regard to the second question, the 'softened' zone is only about 3/8" below the running/gage surface and is not found on the field side of the rail. It's hard to imagine that the effects of dendritic segregation would occur only at this depth on the gage side of the rail head while they have been destroyed (by prior hot rolling) on the field side of the head.

Question 21

Has any study been made on flat wheel effect on rail failure or growth of defect?

Answer

FAST has not assessed the effects of flat wheels because philosophically it has focused primarily on wear. From time-to-time proposals have been made to include an assessment of flat wheels not only on rail behavior (primarily rail and weld failure) but also on concrete tie structural behavior and upon track geometry deterioration. Many years ago an AAR study provided some information on the magnitude of loads that flat wheels could induce. More recently British Rail studies have sought to simulate the effects of flat wheels by grinding 'dips' in rail itself. There seems to be no work that actually ties the impact forces generated by flat wheels to flaw growth.

Question 22

Based on population of detail fractures and failed shop welds in certain premium rails, would you change your FM figures given yesterday based on wear?

Answer

The figure of merit, as we have used it, does not consider rail or weld failure behavior. As such, the figure of merit is just one of several factors which must be considered in making a judgement about which rail metallurgy to select for a particular service application. Some factors such as inherent wear resistance, corrugation tendency, and fatigue susceptibility of the rail itself cannot be altered readily once a metallurgy is selected. However, welded rail end batter and susceptibility to weld failure, in many cases, can be modified by changing the welding practice.

Question 23

It would seem, at least superficially, that the mechanism providing rail end batter is somewhat similar to that providing rail corrugation. Would the author care to comment on this? Does it perhaps indicate common dynamic mode(s) of similar frequency(s)?

Answer

Perhaps corrugation and welded rail end batter behaviors are the railroad engineering counterparts of the old question "which came first--the chicken or the egg?". The configuration of the batter may indeed depend on the nature of the dynamic forces acting upon the weldment just as the dynamic forces are themselves likely to be a function of the batter configuration. Part of the experiment, which has not yet been implemented, is a determination of the loads which result from vehicles passing over welds with different degrees of batter.

Question 24

Isn't rail end batter influenced by speed? If so, isn't FAST very limited in batter analysis as it applies to the real world? (Real world defined as Western railroads and their high speed, high efficiency operation.)

Answer

Speed will very likely influence the forces which will develop as a wheel traverses a weld. The rate at which batter develops probably is dependent upon the magnitude of these forces. In this respect, FAST is indeed very limited in scope. However, it seems unlikely that differences in speed, or in other operating parameters for that matter, will cause single dippers to become double dippers and vice versa. Nor does it seem likely that a CrMo weldment performing poorly relative to a CrSi (HH) weldment at FAST would be found to be the better weld if the train speed were very different. Perhaps similarly the strong effect of lubrication seen at FAST would occur in the real world as well. Indeed the FAST experiment is severely limited, not so much because a wide range of speeds are not utilized, but because a wider variety of welding machines and practices have not been encompassed. Insofar as is known to the writer, the welded rail end batter study at FAST, for all its limitation, is the only source of quantitative information available anywhere.

T.S. Eyre

Brunel University
Dept. of Metallurgy
Uxbridge
England

Wear of Pearlitic Steel

Laboratory wear tests have been carried out to produce the two forms of wear, white layer (scuffing) and delamination which have been observed to occur in service on rail steel. The steel used in this study is somewhat lower in carbon (0.35 compared to 0.65) and although most of the experiments have been carried out on the pearlitic form, some quenched and tempered conditions have been included. A pin on disc machine has been used for the white layer study and a conical diamond on flat reciprocating machine was used for the delamination study. The metallurgical similarities between service observation and the damage produced on the laboratory machines, suggest that these results form a sound basis for further examination of the wear mechanisms and the precise conditions under which they form.

INTRODUCTION

This investigation carried out in two separate but interrelated parts using the same experimental material, a pearlitic steel of 0.35 percent carbon. In both cases attempts were made to control the wear conditions to examine two types of wear which have been reported to occur in the use of rail steel. These are firstly scuffing or adhesive wear leading to the formation of white layer and secondly deformation and fracture leading to wear by delamination. The former occurs on the rail head and would appear to be associated with the problem of rail corrugations which occur on tangent rail. The latter is associated with side face wear which is a problem on curves due to the sideways thrust of the wheel flange.

WHITE LAYER

A pin on disc machine was used in which the main variable was the pin sliding against a standard disc (Table 1) at a sliding speed of 1 m/sec^{-1} at 20°C and a relative humidity of 55-70% RH. Frictional resistance and wear were measured continuously during the experiments. The pin is 6.25 mm diameter, 5 cms long with flat ends which rub against a 12.5 cm diameter, 1.5 cm thick steel disc.

Wear rate of the pin is plotted against the applied normal load in Fig. 1 and it will be seen that up to 10 kgs the wear rate is directly proportional to load, it then falls to a lower

TABLE 1

Pin and disc details

Disc	BS970, pt 2, 1970, Grade 533A99 $750 H_V \pm 10$
Pin	BS970, pt 1, 1970, Grade 080M42 $210 H_V \pm 10$

value before rising steeply again. Observations during the course of these experiments indicated that oxidative wear occurred up to 10 kgs, mixed metallic/oxidative wear coincided with the wear rate reduction and finally metallic wear produced a very high wear rate. During oxidative wear the debris which is red/brown at low loads changes to a black debris at intermediate loads and at higher loads a very much larger metallic debris was produced. Fig. 2 shows the fine scale granular debris produced at low loads and the plate like debris at very high loads. X-ray diffraction was used to verify that $\alpha\text{Fe}_2\text{O}_3$ occurred at low loads, Fe_3O_4 and FeO at intermediate loads and αFe predominates at high loads. The reason for the reduction in wear rate at intermediate loads in the oxidative wear region was further investigated by preparing transverse taper sections through all of the worn pins and the more important features are shown in Fig. 3. At low loads surface deformation is evident and the oxide layer is easily observable (Fig. 3a). At intermediate loads as well as thicker patchy oxide there is a white layer surface constituent in between the oxide (Fig. 3b). At higher loads there is surface deformation and oxide,

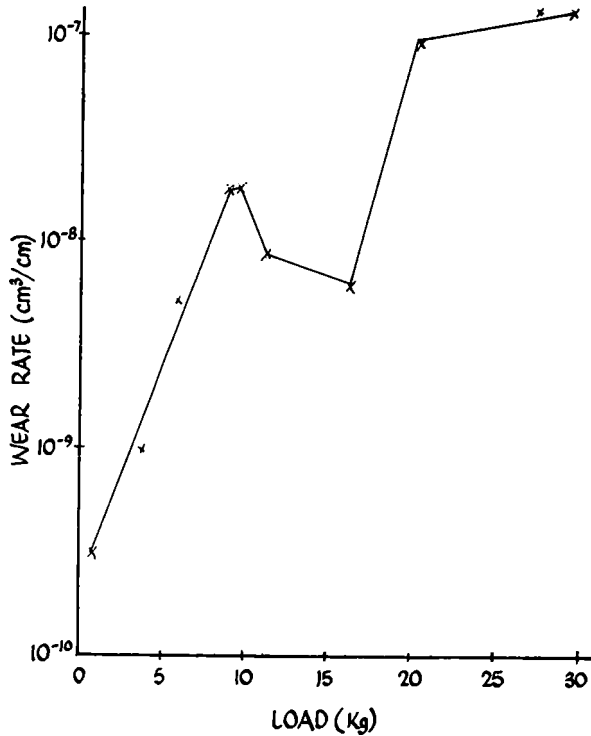


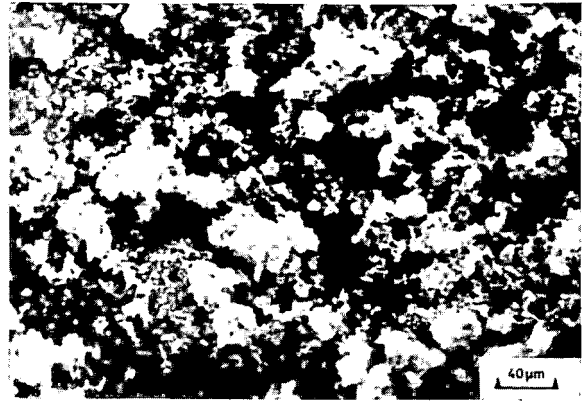
Fig. 1. Wear rate transition for a pearlitic (0.35%) steel.

both in the surface valleys and entrapped in the worked surface layers and there is no obviously discernable white layer surface constituent present (Fig. 3c). In spite of considerable difficulties involved with surface micro-hardness measurement it was possible to obtain good impressions in the white layer surface constituent giving values in the range of 800-1000 H_v and these were the highest hardness values obtained on all the wear surfaces tested.

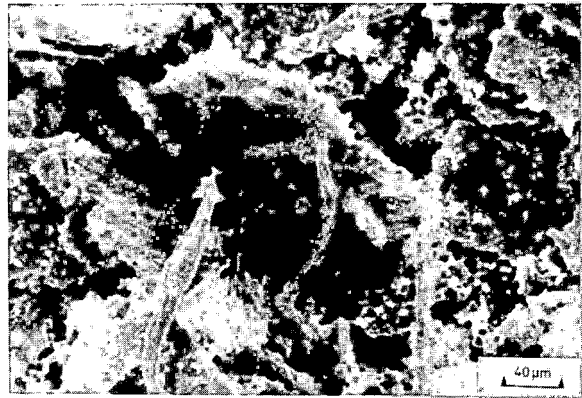
The same overall results were obtained with this same steel in other microstructural conditions produced by heat treatment, namely where a reduction in wear rate occurred at intermediate loads, white layer surface constituent was always present on the wear surface of the pin. A low carbon steel (0.1%C) was also tested which did not exhibit an intermediate reduction in wear and no evidence of white layer was detected on the wear pin surface.

Of the various heat treated conditions evaluated the martensitic condition was inferior to the normalised and various tempered conditions, in spite of its considerably higher hardness. Once more therefore it is demonstrated that there is no simple relationship between wear behaviour and hardness under sliding conditions.

The frictional resistance was measured during all of these experiments and in general there was an overall reduction in coefficient of friction as the load increased, it was as high as 0.6 - 0.8 at around 4 kgs in the oxidative wear region and around 0.2 at loads above 20 kgs in the metallic wear region. The results for the normalised 0.35 percent carbon steel were fairly consistently below



Granular debris from low load tests



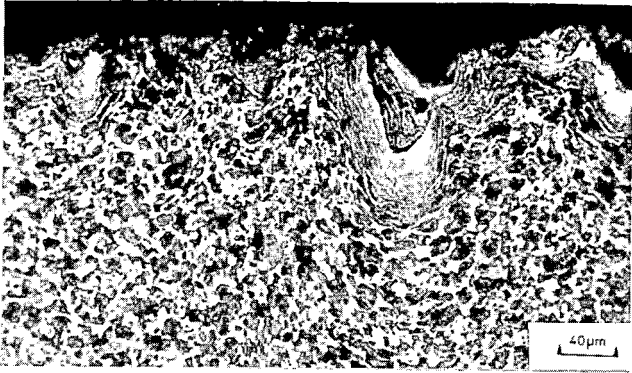
Platelike debris from high load tests

Fig. 2. Wear debris produced under sliding conditions.

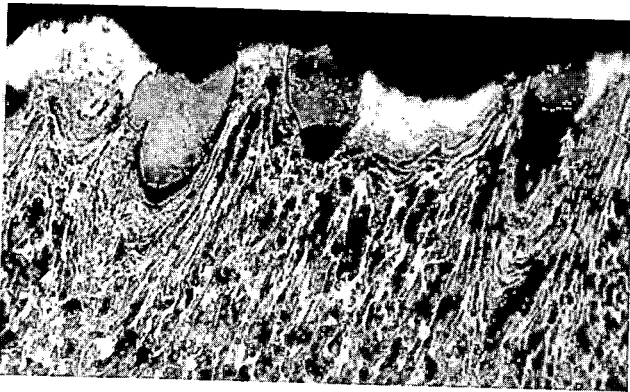
0.4. The scatter in results however were considerably greater than the scatter in the wear results and it would be misleading therefore to try to read too much into these.

DELAMINATION WEAR

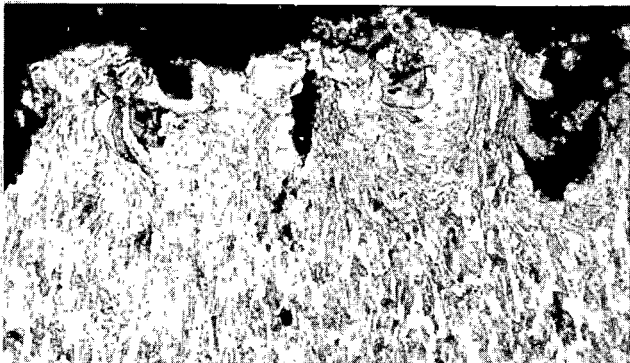
These experiments on a plain carbon steel in both the pearlitic and heat treated conditions were carried out with a conical ended diamond from a hardness machine. This was rubbed along a flat plate of the steel in a reciprocating mode over the same track at a speed of 2 cms long, at various loads and number of passes. The tests were carried out at 20°C and 55 - 70% RH. Friction was not measured during these experiments. Volume wear was calculated from measurements of the width of the wear track and related to the load for both single and multi passes. It will be observed that wear volume is directly proportional to the applied load and inversely related to the hardness (Fig. 4). The single and multi pass experiments show that wear is not directly related to the number of passes. These differences no doubt relate to the work hardening occurring in the material below the wear track during the test, shown in Fig. 5a. A direct SEM view in Fig. 5b shows the plate like delamination wear of the surface and in Fig. 5c these features



Load 10 kg, oxide and beginning of white layer formation



Load 12 kg, oxide and considerable white layer



Load 30 kg, deformation and oxide but no white layer

Fig. 3. Microsections taken transverse to the wear direction on the pin.

are also observed in the wear debris collected. There is evidence from Fig. 5a and 5b and also more detailed examination of the track (Fig. 5d) that wear occurs by crack formation below the surface which then propagates to the surface with the eventual release of plate like wear debris from the surface. The experimental evidence therefore agrees with the delamination theory of wear⁽¹⁾.

One of the difficulties in measuring wear is illustrated in Fig. 6 in which it is observed that wear is composed of both material being displaced and also removed. As more displacement occurs, particularly for ductile metals the inaccuracy involved in measuring the track width increases. In spite of this however it is not considered that this

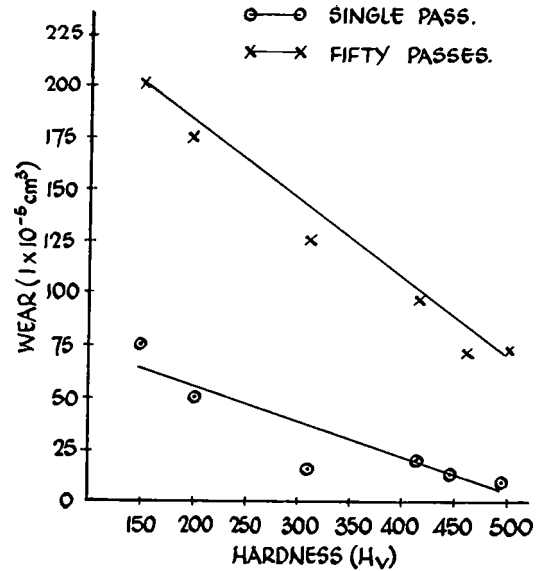


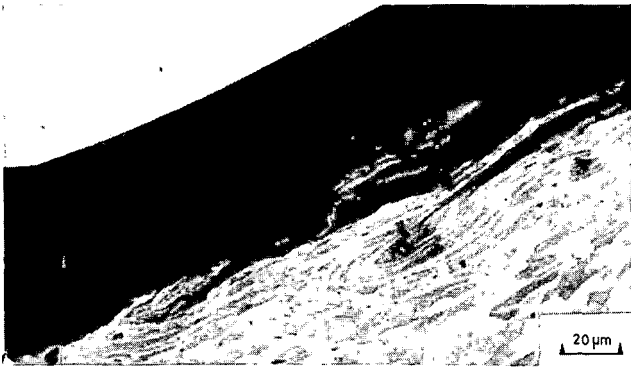
Fig. 4. Wear volume related to both the hardness of the steel and the number of passes.

invalidates the overall results obtained in this investigation.

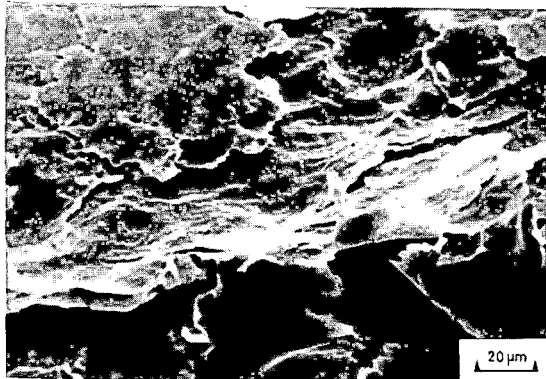
Microhardness readings taken through these worn surfaces give increases of about $100 H_V$, these were more reproducible at the higher loads, for example at 15 kgs, values of around $400 H_V$ were obtained, and at a depth of 0.10 mm this was down to $270 H_V$. These results indicate that work hardening is involved in this wear process and this is confined to a very shallow layer following the contours of the surface in contact with the diamond cone. When maximum work hardening has occurred maximum wear resistance is obtained. Debris is produced when further deformation cannot be accommodated and fracture occurs.

DISCUSSION

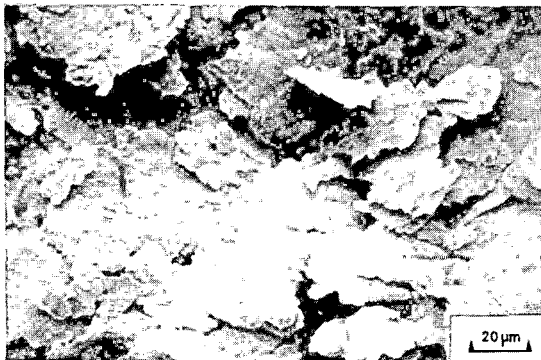
In the adhesive wear experiments the transitional wear behaviour of steel has been demonstrated and it has been observed that there are two basic wear mechanisms. These are initially oxidative wear at low loads and metallic wear at high loads and it is the high wear rate regime which conforms to our normal understanding of adhesive wear, which occurs by metal shear, transfer from one surface to the other and then debris formation. The debris collected has features which are characteristic of these two types of wear which therefore could have been identified by examination of the debris only. At intermediate loads white layer forms at the wear surface and this is extremely hard. The reduction in wear rate could be due either to the energy consumed in the process of white layer formation leaving insufficient to maintain metal removal, or the presence of this hard layer itself could strengthen the surface oxide and thus increase



Deformation and fracture of the wear track



Delamination of the wear track surface



Platelike wear debris



Initiation of delamination

Fig. 5. Metallurgical damage of the wear track both below and on the surface and the wear debris produced.

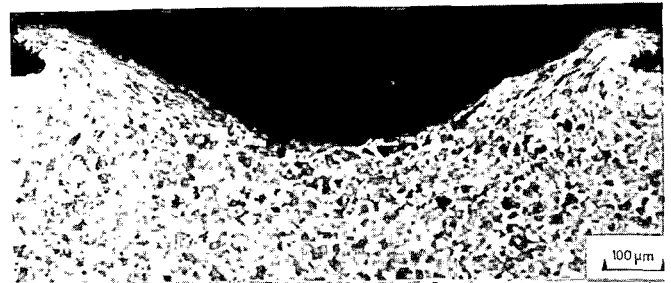


Fig. 6. Cross section of the wear track showing both removal and deformation along the edges of the wear track.

its resistance to wear. Protection, by whatever mechanism only operates over a relatively narrow load range. White layer has been observed on the head of rail in service and would appear to be related to the problem of rail corrugations. Under conditions of normal rolling contact between a rail and wheel it should not be possible to produce white layer which only forms under conditions of slip between the surfaces. This may indicate that there is greater slip in the rail/wheel situation than has previously been supposed. White layer observed on rail head and produced in this investigation have many similarities. A pin on disc machine therefore appears to be ideal to examine the conditions under which white layer forms as well as providing a method for the preparation of white layer for subsequent metallurgical investigation. There has been considerable conjecture about the precise mechanism of formation of white layer which may be accounted for by either (2):-

1. Shear transformation at low temperature.
2. High temperature phase transformation.

However the various arguments for these ideas will not be further explored here because more information about their structural and chemical characteristics are required before any reasonable theory can be put forward.

In this investigation delamination wear occurs under ploughing conditions, in which both adhesion and cutting have been minimised by the selection of a conical diamond indenter. Wear occurs by deformation, work hardening and fracture. Fracture is observed after only a few passes and therefore a fatigue process is not considered to be the controlling mechanism. Fracture occurs in the work hardened layer immediately below the wear surface and then connects to the surface with the production of a plate like metallic wear debris. Wear is highest in the early stages and wear resistance increases as work hardening occurs. Wear is greatest for the steel in the softest condition and decreases with increase in the heat treated hardness. Wear occurring on the side rail in curves has many similarities to delamination observed in this investigation. The wear technique used here would therefore appear to be appropriate to the study of wear of rail steel in curves⁽³⁾.

CONCLUSIONS

1. White layer can be produced on pearlitic steel on a pin on disc wear machine under conditions of slip and under dry rubbing conditions. White layer only occurs under narrow specific conditions of load.
2. Delamination wear can be produced on pearlitic steel on a conical diamond on flat reciprocating wear machine under dry rubbing conditions. Wear occurs by deformation, work hardening and fracture from below the surface to produce a plate like metallic wear debris.
3. Wear debris is characteristic of the type of wear which is responsible for producing it and its characterisation provides a suitable diagnostic technique. This of course must be based upon prior information of the type illustrated in this investigation which can be used to produce a "Wear Atlas" for the combination of materials investigated.
4. There is a marked similarity between the types of wear produced in this investigation and those observed in the wear of rail steel.

ACKNOWLEDGEMENTS

The results presented in this report were obtained during the course of research carried out by U.D. Laad, M. Phil., and K. Krishnan, M.Tech. of the Tribology Group at Brunel University.

REFERENCES

1. N.P. Suh., The Delamination Theory of Wear., Wear, 25, 111-124, (1973).
2. T.S. Eyre., A. Baxter., The Formation of White Layer at Rubbing Surfaces. Metals & Mats., 6, 435-439, (1972).
3. P.J. Bolton., P. Clayton., I.J. McEwen., Wear of Rail and Tyre Steels under Rolling/Sliding Conditions. ASME/ASLE, Lub. Conf. San Francisco. ASLE Report No. 80-LC-58-3. (1980).

Hardness, Microstructure and Wear Behavior of Steel Rails

Wilhelm Heller

Director: Engineering
Krupp Stahl AG
West Germany

Reinhard Schweitzer

One of the most important service properties of rails is high resistance to wear. Wear depends on the multifarious conditions of a wear system and in the case of the wheel-rail system on the combination of wheel and rail materials such as moisture and grease, the prevailing frictional conditions and the stresses induced. In laboratory tests these conditions can only be partly reproduced. Nevertheless, laboratory tests were made as these permitted a large number of different rail steels to be examined on a uniform basis. Selected steels were then rolled into rails and tested under severe service conditions up to high gross loadings. Laboratory tests and track tests showed the microstructure and tensile strength or hardness to be the main influencing factors:

- bainitic rail steels wear faster than pearlitic steels of the same hardness,
- within a microstructure group the resistance to wear increases with increasing hardness,
- with pearlitic steels hardness depends on the interlamellar spacing; for this reason the resistance to wear on as-rolled alloyed rails is the same as that on heat-treated rails with pearlitic structure and equal hardness.

These results represent the general trend of rail steel wear with a relatively large scatter due to the above mentioned variety of operational conditions. Nevertheless, the question whether there is an additional influence exercised by the rail steel itself is being examined with some expectation.

INTRODUCTION

The rail undergoes dynamic loading in service as a result of axle loads capable of bringing about fatigue damage. Different types of fatigue cracking in rails, including horizontal cracking at the web-flange joint, have been reported (1).

Recent investigations (2) have shown that rail buckling occurs when a vertical load (axle weight) and a horizontal load (cornering force) are applied on the rail head. This phenomenon results in repeated bending of the web, particularly in the web-head transition area. This loading, on which is superimposed the general bending of the rail, can lead to fatigue cracking on the rail ends (Figure 1). This cracking can occur in more heavily loaded rails (frequently the case of switch rails).

While stress level measurements have been carried out (2), no fatigue data are presently available which take into account the surface condition actually encountered.

This surface condition can correspond either to an as-rolled condition or a machined condition (case of switch rails).

In the case of as-rolled rails, two extreme cases may be considered: condition of a well maintained rail (sufficient lubrication) and the condition of a corroded rail (in particular in the case of insulated joints).

This study endeavors to provide data, using specimens in accordance with Figure 2, on fatigue crack initiation by bending in a rail web as a function of the surface condition of the rail.

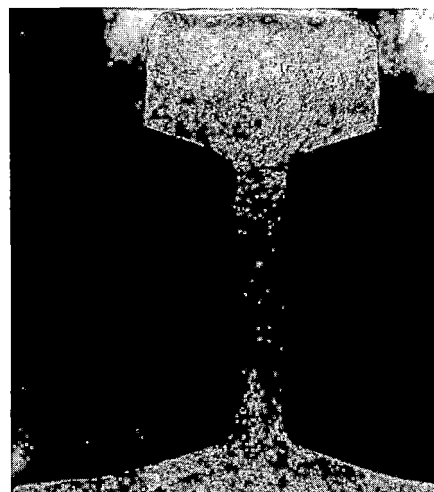


Fig.1 End of a cracked rail

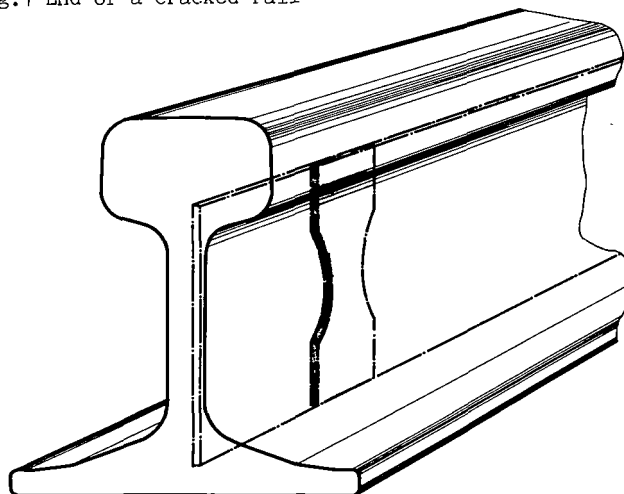


Fig.2 Specimen location

STEEL PROPERTIES STUDIED

Test Grades

This study concerns three rail coupons of naturally hard grade. Two of these coupons, reference 1207 A and B, come from the same bar and were adjacent.

Chemical Analysis

The chemical compositions of the steel used, according to the plant acceptance report, are given in Table 1.

Coupon reference	C	Mn	P	S	Si
1207 A and B	0.625	1.360	0.023	0.020	0.160
1449	0.615	1.560	0.042	0.020	0.235

Table 1 - Chemical composition (%) of the steel used

Mechanical Properties

The mechanical properties obtained on cylindrical specimens (5 mm diameter) are given in Table 2.

Coupon reference	YS (MPa)	UTS (MPa)	Elong. (%)	Red. of Area (%)
1207 A and B	510	935	12.8	25
1449	445	875	12.4	23

Table 2 - Mechanical properties of the steels used

The specimens are sampled in the rail web perpendicular to the rolling direction and as close as possible to the rail surface.

SURFACE CONDITIONS INVESTIGATED

The surface condition of the specimens studied can be characterized by several parameters:

- . Macrogeometry
- . Roughness level
- . Surface work hardening
- . Metallurgical structure
- . Residual stresses.

Macroscopic Observations

The different surface condition studied correspond to the following:

- A very corroded surface of a rail withdrawn after in-service cracking; the photo in Figure 3-1 shows the surface in question.

Two cross-sections of the useful part of the specimen (Figure 3-2) has made it possible to measure the depth of some craters with the shadowgraph.

- An as-rolled surface.

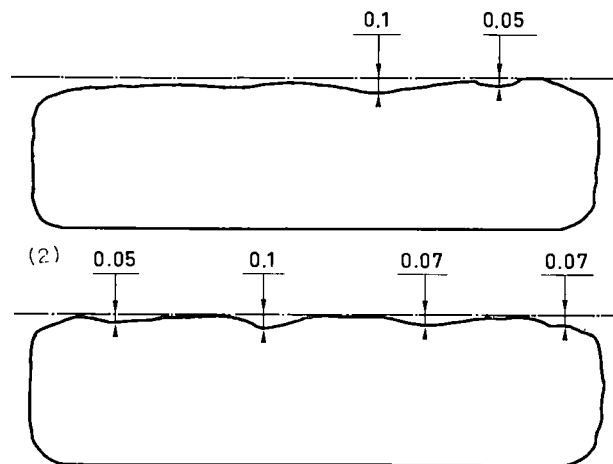
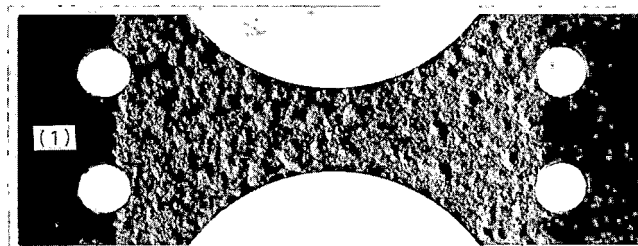
- Two machined surfaces from a rail profiled either with a half-worn or completely worn tool. Profiling consists in milling the rail end, this profile modification allowing the connection to switches and crossings. The machining is carried out with a carbide tool. Carbide inserts are fitted on a tool-holder whose surface contour corresponds to the shape to be obtained: profile milling. The surfaces obtained exhibit finely striated areas (due to the microgeometry of the carbide inserts) separated into

steps (due to offset which can exist between two series of adjacent inserts according to the contour of the tool) (Figure 4-1). The minimum section of the specimen is located at the center of a striated area (at an equal distance from two successive steps).

To characterize these surface conditions, we measured the thickness variations by the displacement of a dial gauge. The results of these measurements are given in Figure 4-2.

There is not significant difference between the heights of the steps found for each surface condition. On the specimens machined with a worn tool, we observed a small additional offset located about 1 mm from a step and corresponding to a geometrical defect in an insert (clinging chip, for example).

- Ground surfaces used as references. The grinding was carried out in the longitudinal direction along an axis parallel to the fatigue stress, with a lubricated 32 A 46 HVPE grinding wheel.



— theoretical profile
all dimensions in millimetres

Fig.3 Specimen taken from a corroded rail

- (1) Surface of a specimen
- (2) Cross-sections of a specimen

Roughness

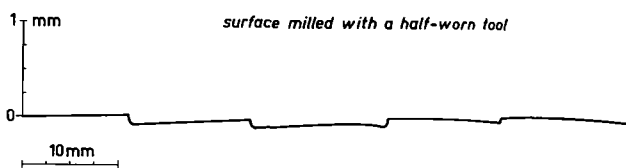
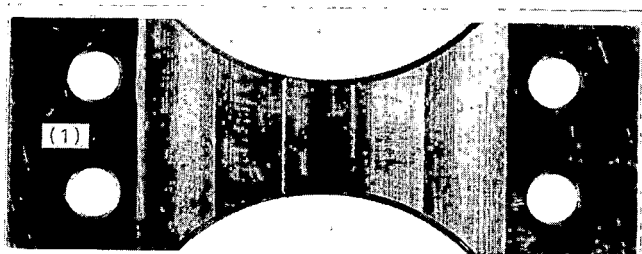
Roughness measurements were carried out on the central area of ground, as-rolled and machined specimens.

The roughness characteristics are given in Table 3. They are not directly comparable but provide a basis for the qualitative evaluation of the different surface conditions.

The values corresponding to the as-rolled condition contain errors. It was not possible for us to completely remove the scale without attacking the surface. It is thus possible that some scale areas were not removed, thereby increasing the roughness levels measured.

Surface condition	R _t	R _p	R _a	Tracing direction
Ground	4.3	1.5	0.6	Transverse
As-rolled	32.3	11.2	4.4	Longitudinal
Milled with half-worn tool	10	3.9	1.4	Longitudinal
Milled with worn tool	6	1.8	0.7	Longitudinal

Table 3 - Roughness characteristics (in μm)



(2)

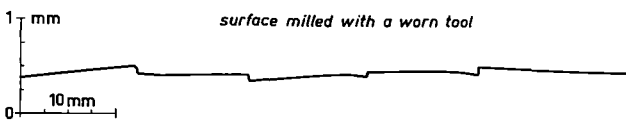


Fig.4 Specimens taken from profiled rails

- (1) Specimen surface
- (2) Longitudinal profiles of specimens

Work Hardening

To determine the level of work hardening produced by machining, we measured the Vickers hardness under a load of 10 daN. This load corresponds to a compromise between the size of the indentation (if the length of the diagonal measured is large, relative reading error is small) and the depth of the indentation (this depth should be smaller than the work-hardened thickness). In our case, the depth of the indentation is less than 0.1 mm.

Hardness measurements were carried out on:

- the machined surfaces (ground or milled);
- the non-work-hardened base metal, after fine mechanical polishing; the measured values constitute a real reference;

- the as-rolled surface; the measured values then constitute a reference on the product.

As the results exhibit a scatter band, we carried out several measurements. The histograms of the results obtained are given in Figure 5.

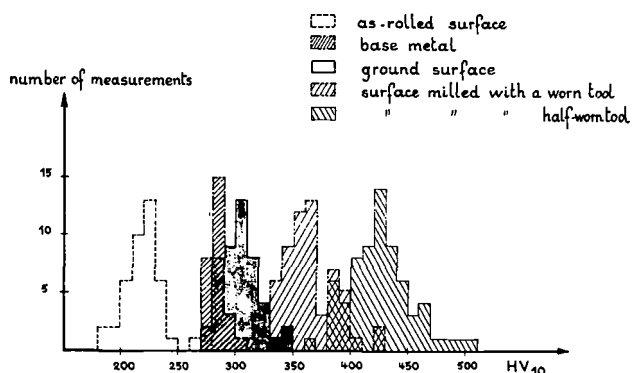


Fig.5 Hardness histograms

In each case, a distribution of data is obtained which can be estimated by a normal law. These distributions are significantly different. The averages and the standard deviations of the hardness measurements are given in Table 4.

Surface condition	Average	Standard deviation
As-rolled	219	15
Mechanically polished	285	6
Ground	304	17
Milled with worn tool	365	26
Milled with half-worn tool	425	28

Table 4 - Averages and standard deviations of HV₁₀ hardness values

Hardness measurement is a simple means of characterizing work-hardening. Two points should however be noted:

- Hardness values can take into account a modification in the metallurgical structure of the material. It may however be considered that a surface structural modification due to the heating caused by machining (change to a hardened structure) corresponds, like work-hardening, to an increase in the number of dislocations.

- Hardness values are probably influenced by the presence of residual stresses (3). Given the size of the indentations, this influence is limited and falls within the scatter band.

Metallurgical Structure

Observations were carried out on a polished section after Nital etching (Figure 6).

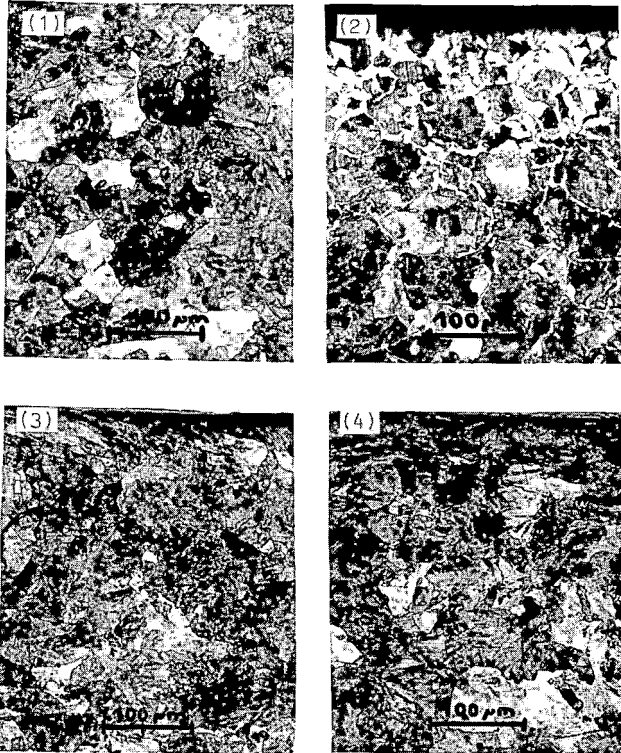


Fig.6 Microstructure

- (1) Internal rail structure
- (2) Surface structure of as-rolled rail
- (3) Surface structure of rail machined with half-worn tool
- (4) Surface structure of rail machined with worn tool

- The rail structure (Figure 6-1) is very fine pearlite.

- Hot rolling produces slight surface decarburation to a depth of 0.1 mm (Figure 6-2).

- Corrosion destroys the decarburized layer.

- Grinding destroys the decarburized layer and produces slight work-hardening of the pearlitic structure.

- Rail-end milling causes extensive work-hardening (Figure 6-3 and 4). In addition, one can observe on the cross-section of the specimens the existence of a surface layer not etched by the Nital. Owing to the small thickness (in the order of 4 μm for rails machined with a half-worn tool, and 8 μm for those machined with a worn tool), it is not easy to characterize this layer. However, as machining conditions are very severe, it is possible that the surface temperature of the rail exceeds 720°C during machining, the surface structure could then be a quenched structure.

Residual stresses

Surface residual stresses were measured by the X-ray diffraction technique.

The different measurements carried out on machined specimens yielded a wide scatter band.

This scattering, much greater than the uncertainty of the measurement method, reveals the very rapid variation of the residual stresses with local machining conditions.

- For the ground surface condition which corresponds to laboratory machining, the residual stresses measured in the longitudinal direction are small (the measured stresses vary from -30 MPa to +140 MPa).

- For the milled surface conditions, the measurements show considerable tensile stresses (varying from +400 MPa to +900 MPa).

EXPERIMENTAL CONDITIONS

Specimen

The specimen had a thickness of 4 mm. The edges of the specimen were machined by means of a form tool (r = 1 mm) so as to avoid initiation points of fracture.

The section of the specimens in the useful zone is 80 mm² (20 x 4 mm²) for profiled surfaces (reference FA 1-2) and 60 mm² (15 x 4 mm²) for the other cases (reference FA 1-3).

Sampling Method

The specimens are sampled in the web of the rail perpendicular to the rolling section.

The rail surface is kept on one side of the specimen; the other side is ground (Figure 2).

Experimental Setup

The tests were carried out under repeated bending on a plane bending machine with a maximum bending moment of 60 m·N.

The specimen is mounted so that the surface to be tested is under tension. Different stress rates between 300 and 700 MPa are applied. The maximum life of a specimen was set at 5.10⁶ cycles. Beyond this limit, the specimen is considered to be unfractured.

Analysis of Results

The test data are processed by means of a program using the mathematical representation of the Wöhler curve proposed by Bastenaire (4):

$$N = A \frac{e^{-[(S-E)/B]^C}}{S - E}$$

where : A, B, C are curve parameters,
E is the endurance limit.

The curves obtained correspond to respective fracture equiprobabilities of 10, 50 and 90%.

TEST RESULTS

Presentation of Results

The different Wöhler curves plotted by computer, as well as the scatter band of the test results, are shown in Figures 7-1 to 7-4.

The analysis of the tests conducted on the specimens sampled from the rail machined with a worn tool (Figure 7-3) was performed manually, computer analysis not being possible owing to the small number of specimens.

The results obtained on ground specimens coming from rail coupons from two different bars are given in Figure 7-1. The test results relative to different surface conditions can be regarded as directly comparable since the two rail coupons exhibit similar fatigue properties in the ground condition.

The conventional endurance limits (values at 5.10^6 cycles) and the corresponding standard deviations (s) are given in Table 5. This table gives the ratio σ_D/σ_{DR} , in which σ_D is the endurance limit for a given surface condition and σ_{DR} the endurance limit obtained on specimens in the corresponding ground condition.

Coupon reference	Surface condition	σ_D	σ_D/σ_{DR}	s
1207 A	Ground	549	1	20
1207 A	As-rolled	425	0.77	22
1207 B	Machined with half-worn tool	586	1.07	27
1207 B	Machined with worn tool	380	0.69	-
1449	Ground	529	1	25
1449	Corroded	261	0.49	14

$$U_{Gaus} = 1.28$$

Table 5 - Endurance limit under repeated bending and standard deviations calculated for each surface condition (in MPa)

Fracture Surface Appearance

The fracture surfaces obtained on a ground specimen and on a corroded specimen are shown in Figure 8.

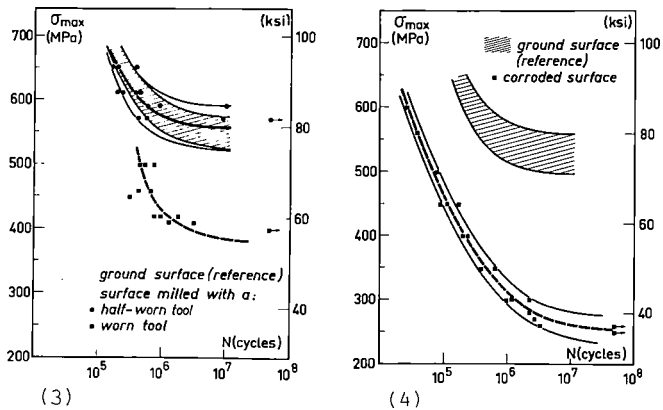
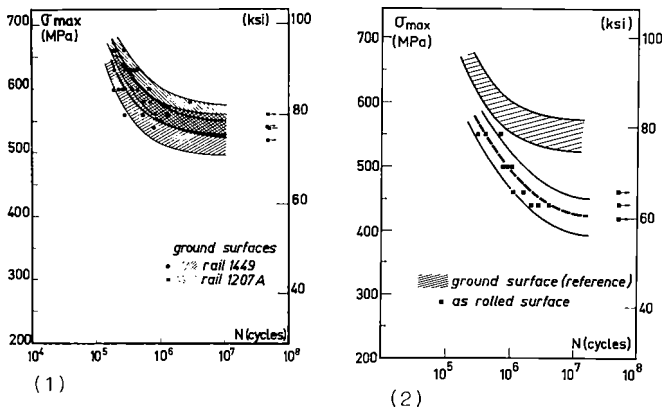


Fig.7 Wöhler curves

- (1) Ground specimens coming from two different rails
- (2) As-rolled condition
- (3) Profiled conditions
- (4) Corroded condition

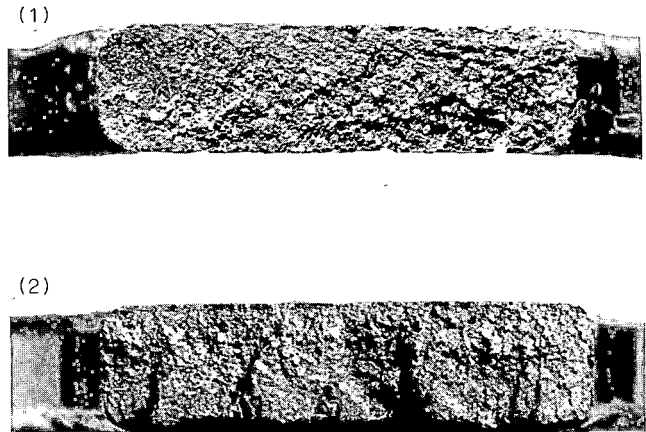


Fig.8 Fracture facies

- (1) - Ground specimen
- (2) - Corroded specimen

In the case of the corroded specimens, the cracks initiate from corrosion pitting which can be in very different transverse planes.

For the other cases, the fracture surface is generally plane.

For specimens conserving the skin of the machined rail:

- . With a half-worn tool:
 - 3 fractures (21%) occurred at the level of a step separating two successive tool passes.
 - the other fractures occurred in the central part of the specimen.
- . With a worn tool:
 - 4 fractures (33%) occurred at the level of a step.
 - 3 fractures (25%) occurred about 1 mm from a step (zone corresponding to a visible offset on the longitudinal section of the specimen).
 - the other fractures occurred in the central part of the specimen.

The large steps and offsets on the surface of the specimen induce stress concentrations in the corresponding location. And, this location is in a larger section than that of the useful zone. The theoretical nominal stress (without stress concentration) is thus small in this section. We do not know the value of the stress concentration fracture K_T relative to this case. However, by approximation on the basis of known cases (5), we find $K_T = 1.2$. The value of the product $K_T \cdot \sigma_{f \text{ step}}$ is then near the bending stress in the minimum section. Since the stresses are of the same order, the fractures can occur in the minimum section just as well as at a step. If a step coincided with the minimum section of the specimen, the endurance limits would doubtless be smaller.

DISCUSSION OF RESULTS

Effect of Parameters Characterizing the Surface Condition on Fatigue Behavior

As-rolled surface This surface condition leads to a lowering of the endurance limit by slightly more than 20% compared with the corresponding ground condition. This reduction can be attributed to the greater roughness and to the surface decarburization in the as-rolled condition, as well as to the surface work-hardening caused by machining in the ground condition. It is however rather small compared to that (30 to 40%) generally observed with high yield strength steels (6 and 7). This can be explained by the fact that the steel decarburized on the surface and not work-hardened is not highly sensitive to the notch effect and hence to surface roughness.

The plastic volume defined by Kuegel (8) is moreover located entirely in the decarburized layer. This volume, for which the stress is higher than 95% of the maximum stress, has a thickness equal to:

$$\frac{e}{2} (1 - 0.95) = 0.1 \text{ mm} = \text{decarburized depth.}$$

Machined surfaces In the case of the half-worn tool, the endurance limit is near that obtained for the ground condition ($\sigma_D/\sigma_{DR} = 1.07$).

On the other hand, in the case of the worn tool, the endurance limit drops by about 30% compared to the ground condition. To explain these differences, the effect of different parameters may be considered:

Roughness: If one considers the two types of machining on profiled rails, the fatigue lives are not in relation with the measured roughnesses. In fact, the highest endurance limit (milling with half-worn tool) is obtained for the highest level of R_t . However, if one considers the fact that the results of roughness measurements entail a certain scattering, it may be assumed that the values of R_t are of the same order of magnitude (6 and 10). In addition, in the case where the surface is machined with a half-worn tool, the striations are larger and also more numerous, and there is a stress concentration distribution.

Work-hardening: Work-hardening considerably increases the mechanical properties of the surface and hence its fatigue strength. In the case of the half-worn tool, there is a significant improvement (HV10 average = 425) to compensate for the harmful effect of roughness. On the other hand, in the case of the worn tool, the substantially smaller improvement in the surface properties (HV10 average = 365) does not allow a total compensation.

Metallurgical structure: If the existence of quenched surface layer is assumed, its mechanical properties are very high. The improvement in fatigue strength resulting therefrom is however negligible owing to the small thickness of this quenched layer in relation to the plastic volume (8).

Residual stresses: Although very extensive, the measured residual stresses involve only a layer with a thickness smaller than 10 μm . The influence of these stresses on fatigue strength consequently appears to be limited.

Corroded surface The presence of corrosion pitting facilitates fatigue crack initiation at stress levels substantially smaller than for the other surface conditions studied. This mechanism results in a very substantial reduction in the endurance limit. One in fact observes a halving of the endurance limit when the ground condition is used as a reference, and a drop of 40% compared to the as-rolled condition.

Furthermore, in the case of in-service stresses, the possible presence of a corrosive environment further accelerates crack initiation leading to shorter service lives.

Influence of Surface Condition on the Scattering of Results

The ratio of the standard deviation (s) on the endurance limit (σ_D) provides an idea of the relative scatter band of fatigue test data as a function of surface condition.

This ratio varies between 3.6 and 5.4. The lowest value is obtained for a ground condition; the highest value corresponds to the corroded condition.

For a rail receiving normal maintenance, it is possible to use as a guide the value $s/\sigma_D = 5\%$.

Influence of Surface Condition in the Limited Endurance Range

The results obtained for each surface condition were compared with the results on ground specimens coming from the same rail coupon (Figures 7-1 to 7-4).

Whereas the differences in the applied stress rates are very pronounced for long fatigue lives (endurance limit range), they are attenuated in the range of short lives ($N < 10^5$ cycles).

CONCLUSION

The study of the influence of surface condition on the endurance limit under repeated bending in specimens taken from the web of naturally hard rail grades has made possible to elucidate the following points:

The as-rolled condition leads to an endurance limit (425 MPa) 20% lower than the reference condition obtained by grinding (550 MPa).

In the case of a milled condition, the endurance limit level depends on the work-hardening level produced by the machining operation (tool wear, depth of pass, etc...). In the case of a half-worn tool, the endurance limit can be of the same order of magnitude (585 MPa) as for the ground condition, whereas the use of a worn tool leads to a drop in the endurance limit (380 MPa) of about 30% compared to the reference condition.

The presence of corrosion pitting in the case of a poorly maintained rail produces a halving of the endurance limit (260 MPa). This stress level is to be related to the multiple initiations observed in this case on the fracture surface of the specimens.

The relative scattering of the results obtained in surface conditions encountered on rails in service can be estimated by $s/\sigma_D = 5\%$ (where σ_D is the endurance limit and s the standard deviation of the test results).

ACKNOWLEDGEMENTS

The rails used were furnished by the SNCF. The residual stress measurements were carried out by ENSAM, Paris. We extend our thanks to the SNCF and ENSAM for their contribution to this work, with special thanks to J.L. Lebrun who carried out the residual stress measurements.

REFERENCES

1 "Avaries et Rupture des Rails", Catalogue de Défauts des Rails, UIC Document, 1959, n° 1321.

2 Gence, P., Deroche, R.Y., Lieurade, H-P., "Problèmes d'Ordre Mécanique et Métallurgique posés par la Tenue des Joints Eclissés - Application au Cas des Aiguilles Courbes", Revue Générale des Chemins de Fer, to be published.

3 Frelat, J., "Principe d'une Méthode Non Destructive pour Caractériser l'Etat de Contraintes Internes d'une Pièce", Proceeding of the Seminary on Residual Stresses, Centre de Recherche de Voreppe, 1978.

4 Bastenaire, F., La Fatigue dans les Matériaux Editions Ediscience, 1973, pp. 107-144.

5 Peterson, R.E., Stress concentration factors, Wiley interscience publication, 1974, p. 98.

6 Pomey, G., Rabbe, P., "Influence de l'Etat de Surface et d'une Entaille ou d'un Trou sur le Comportement en Fatigue de Divers Aciers de Construction Soudables", Revue de Métallurgie, mars 1970, pp. 205-215.

7 Cazaud, R., La Fatigue des Métaux, Editions Dunod, 1969, pp. 375-393.

8 Kuegel, R., A Relation Between Theoretical Stress Concentration Factor and Fatigue Notch Factor Deduced from Concept of Highly Stressed Volume, Proceeding ASTM, n° 61, 1961, pp. 732-748.

H.P. Lieurade

IRSID

C. Maillard-Salin

IRSID

R.Y. Deroche

SACILOR

L. Beaujard

IRSID

Influence of Surface Conditions on Repeated Bending Behavior of Naturally Hard Rails

The web of a rail is subjected to repeated bending loads in service. On particularly loaded rail ends, the cyclic stress rate can be such that it generates surface crack initiation and then fatigue cracking at the web-flange joint. In this case, the fatigue behavior of the rail depends on:

- the applied stress amplitude;
- the crack initiation resistance of the rail surface;
- the fatigue-crack-growth resistance of the rail steel.

The purpose of this study is to quantify the influence of the applied stress rate and surface conditions on the initiation life of a fatigue crack. The endurance limits and the Q_{max} -N curves (number of cycles to fracture) were determined on specimens sampled in rails having the following surface conditions:

- as-rolled
- machined
- corroded.

The ratios of the different endurance limits obtained to the endurance limit determined on ground specimens vary between 0.5 and 1. The results were analyzed as a function of roughness, work hardening, surface structure and residual stress conditions.

Rail wear is of major economic significance for railways. In the wheel-rail system, wear is a function not just of the rail material but of all the factors involved.

In tight curves, in particular, rails are subject to higher wear. To counteract this, all the factors in the wear system, i.e. materials and operating conditions, have to be analyzed and then optimized on the basis of the findings.

As rail manufacturers we have repeatedly been faced with the task of increasing the wear resistance of rail steels without impairing other important service properties such as weldability and resistance to failure.

We have been testing special grades of alloyed rails since 1961.

Since 1972 chemical composition and microstructure have been systematically examined on a broad basis in comprehensive research projects, initially in laboratory melts and then in shop melts. The rails thus produced are being tested up to high gross loads in in-service test tracks.

The chemical composition, microstructure and mechanical properties have already been reported on (1, 2). In the following, the results relating to wear behaviour are summarized.

RAIL MATERIALS

Fig. 1 outlines again the main lines of development for rail steels. Two of the lines followed in as-rolled steels were:

Pearlitic Rails

Particular importance was attached to the development of as-rolled rails starting from the UIC grade 90 A with about 0.75 % C and 1.0 % Mn and a minimum tensile strength of 880 N/mm² (250 HB). By adding silicon and, most importantly, 1 % chromium, the tensile strength is increased to a minimum of 1,080 N/mm² (315 HB). As the micrographs show, this effect is attributable to the reduction of the interlamellar spacing in the pearlite. Adding 0.1 % V then further increases the tensile strength to a minimum of 1,180 N/mm² (345 HB), mainly through additional vanadium carbonitride precipitates.

By way of comparison we also followed the line of development in which rails are heat-treated to finely spaced lamellar pearlite. Rails of AREA standard composition are re-austenitized and subjected to accelerated cooling. In addition, we subjected rails to accelerated cooling directly after rolling by means of special measures (2). In both cases, as with the as-rolled, alloyed rails, a pearlitic microstructure with small interlamellar spacing and a high degree of hardness is obtained.

Examinations have shown that the strength of both the heat-treated and the alloyed rail steel derives from the geometrical characteristics of the pearlite (3).

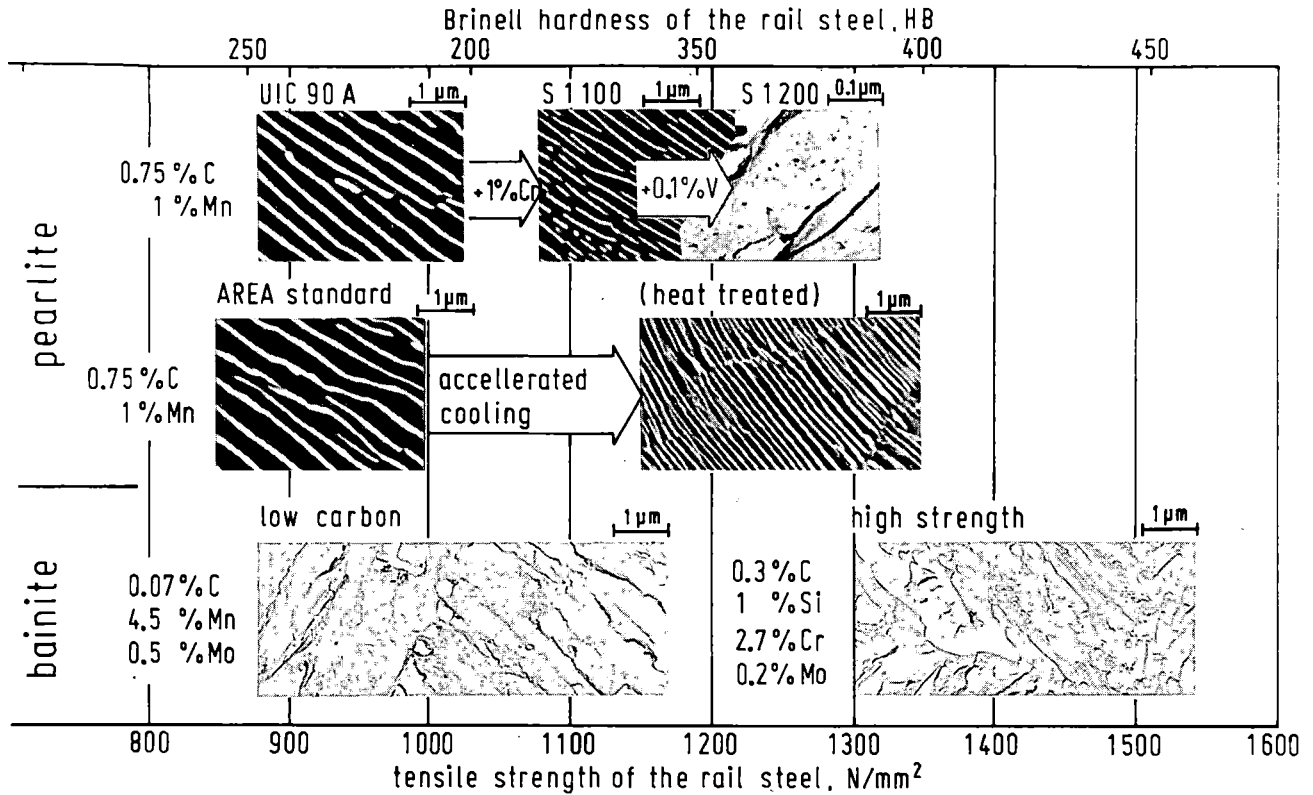


Figure 1 Lines of development for high strength rail steels

Bainitic Rails

As-rolled rails with a bainitic microstructure are an innovation. We have produced them in two variants:

a low-carbon grade with approx. 0.07 % C, 4.5 % Mn and 0.5 % Mo and a tensile strength between 900 and 1,150 N/mm² (270 to 345 HB)

and

a high-strength grade with 0.3 % C, 2.7 % Cr and 0.2 % Mo and a tensile strength of between 1,300 and 1,500 N/mm² (390 to 460 HB).

The microstructure of the low-carbon rails is a coarsely acicular bainite and that of the high-strength rails a finely acicular bainite with finely dispersed precipitates.

TESTING AND MEASUREMENT OF WEAR

The influence of rail steels on wear was first determined in laboratory tests and subsequently in-track. Fig. 2 shows the testing and measuring procedure.

The rolling-sliding wear test is designed to simulate track conditions as far as at all possible. A roll made of wheel material runs over a roll made of track material with 0.7 % slip. The amount of wear

is determined by weighing the rolls after set sliding distances and the specific abrasion i.e. the abrasion in relation to the sliding distance is given as the result.

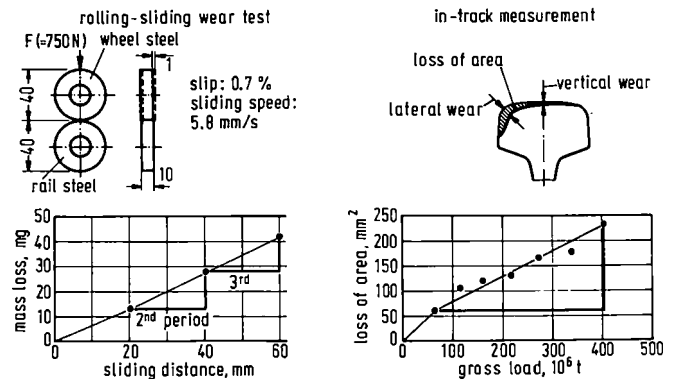


Figure 2 Testing and measurement of rail steel wear

In the track, the rail section is recorded by a scanning device at intervals of approximately one year. Measurements are then obtained of the loss of area, of vertical and lateral wear as compared with the original section. The rails were tested up to high gross loads, often in excess of 300 · 10⁶ t. A specific amount of wear, e.g. the loss of area in relation to 100 · 10⁶ t, is given as the result.

RESULTS OF LABORATORY TESTS

Fig. 3 shows the results of the rolling-sliding wear test for pearlitic rail steels in a tensile strength range from 700 to 1,250 N/mm² (200 to 370 HB). The specific amount of wear is plotted logarithmically against the hardness of the rail steel examined. UIC R2 wheel steel with a tensile strength of 780 N/mm² (220 HB) served as the wheel material. It can be seen that the hardness and tensile strength of the rail steel have a marked influence. If the tensile strength is increased by 200 N/mm² or the hardness by 65 HB, wear is almost halved. The results - shown here for comparison - of a purely sliding test carried out as part of recent British research work on pearlitic steels from laboratory melts would indicate that hardness exerts an even greater influence (4). The different gradient is evidently attributable to the differences between the two wear systems.

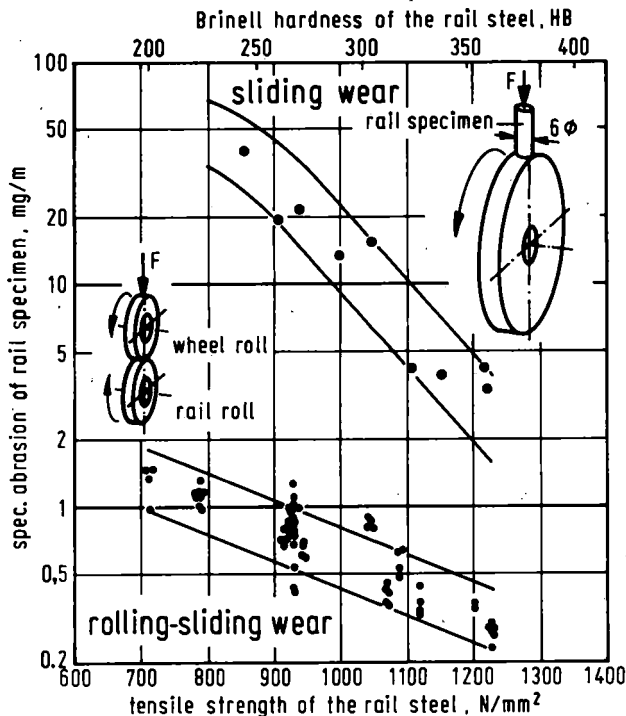


Figure 3 Results of laboratory wear test on pearlitic rail steels

For the bainitic steels no such clear-cut results were obtained in laboratory testing. However, since operational wear systems can never be perfectly simulated, laboratory testing can furnish only preliminary information on the in-track behaviour of rails; operational trials remain the only decisive test.

RESULTS OF IN-TRACK MEASUREMENTS

The measurement results of pearlitic rails in the in-service test tracks of

the German Federal Railway (DB)
the Swiss Federal Railways (SBB) and
the Rheinische Braunkohlenwerke AG,
(lignite industry), (RBW)

are outlined in Fig. 4. The rails are laid as high rails of curves with radii between 250 and 620 m (7° and 2.5°). As Fig. 4 shows, the tracks also differ in terms of axle load and speed. The axle load at RBW's industrial siding is 340 kN, 50 % higher than on the other two lines. The speed of 45 km/h (28 mph) is, however, only half as high.

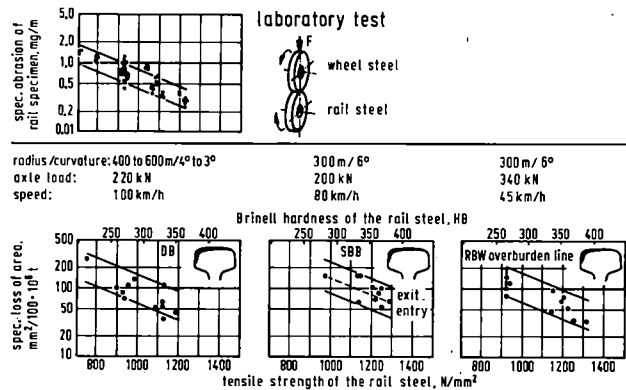


Figure 4 In-track measurements of wear in curves at high rails of pearlitic steels

Despite the different operating conditions, the logarithmic plotting of the specific amount of wear against the hardness of the rail steel shows a uniform relationship in all three tracks. The inclination of the scatter in the laboratory tests in Fig. 4, top left, can be transferred to the results from the three test tracks, i.e. here, too, wear is almost halved by increasing the tensile strength of the rail steel by 200 N/mm² and, thus, hardness by 65 HB.

The width of scatter is determined by local operating conditions. A rail of lower tensile strength at a certain part of the track behaves exactly like a part of higher tensile strength at another. In the SBB test track the scatter can be narrowed, for example, by regarding as separate the rails leading into the curve (entry) and those leading out of the curve (exit): in those leading out of the curve the wear is considerably higher.

Further results regarding the influence of the rail steel are discussed in reference to the track at RBW. On the left in Fig. 5 the scatter of the wear behaviour of pearlitic rails in the high rail of tight curves in the overburden line is presented again. It can be seen that the wear of the heat-treated pearlitic rails follows the same law as the as-rolled pearlitic rails. Under the same

operating conditions wear is exclusively a function of hardness. This is easily explained by the homogeneity of the microstructure: the resistance to wear as well as hardness and tensile strength are evidently determined by the interlamellar spacing of the pearlite.

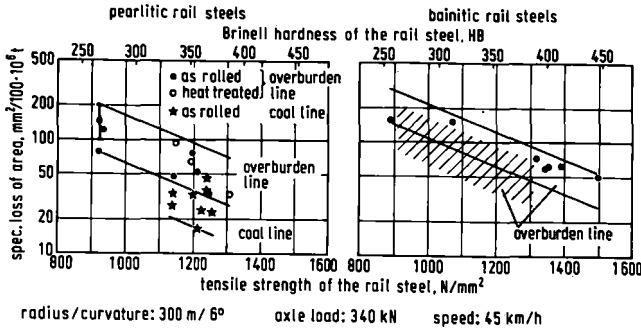


Figure 5 Wear in curves at RBW (high rails)

By contrast, as the diagram on the right in Fig. 5 shows, bainitic rails of the same hardness wear more. The scatter of the specific wear of bainitic steel rails lies higher, but has the same inclination. This result agrees with that obtained at the SBB test track. Hardness is thus a clear factor in resistance to wear only within one microstructure group. Wear of the bainitic rail steels is, however, so much higher, that in terms of resistance to wear it is not worth using such more highly alloyed steels. The wear is, however, not as much as found previously in laboratory tests (5).

The results of the wear measurements on the test track at RBW also give an indication of the influence of the operating conditions. From the diagram on the left in Fig. 5 it can be seen that the high-tensile pearlitic rails in the high rail of the coal line exhibit appreciably less wear than those with the same radius, and subject to the same axle load and same speeds in the overburden line. This may have to do with the material being transported which, should it fall from the waggons, is likely to reduce wear, in the case of coal, or increase wear, in the case of overburden. The reason may also lie in the different design of the waggons.

If we disregard the favourable results from the coal line and collate those from the pearlitic rails in all the other tracks, we obtain the representation on the left in Fig. 6 for "generous lubrication". Here too, there is a uniform, if somewhat wider scatter which reflects the specific wear of the high rails in curves subject to high loads. This may be surprising, but it is an indication that rail wear has indeed been reduced. As a loss of area of 100 mm², which represents about 2 mm lateral wear, does not obtain until after 100 · 10⁶ t in high-tensile rails, these rails can also be used in tight curves subjected to gross loads of at least 500 · 10⁶ t.

	radius/curvature	axle load kN	speed km/h	mph		radius/curvature	axle load kN	speed km/h	mph
• OB	400 to 500 m / 4° to 3°	220	100	62	• FAST	350 m / 5°	300	65	40
○ SBB	300 m / 6°	200	80	50					
• RBW	300 m / 6°	340	45	28					
○ ore line	300 m / 6°	250	50	31					

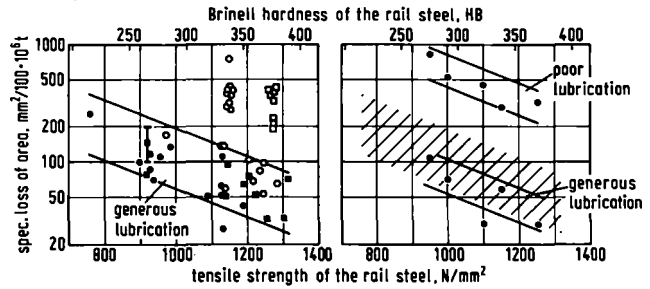


Figure 6 Wear in various curves (high rails, pearlitic)

This good result is not just attributable to the improvements made in the rail steels, but also to lubrication of the rails and wheel flange lubrication. The graph on the right in Fig. 6 again clearly shows the influence of lubrication, using the results from the FAST-track in Pueblo as thus evaluated by us (6). With generous lubrication the amounts of wear are low and fall within the scatter of the in-service test tracks that we studied. With poor lubrication wear increases by roughly a factor of 7. High amounts of wear in the high-tensile pearlitic outer rails of curves in one special case at SBB and an ore line are thus probably attributable to peculiarities in the operating conditions e.g. inadequate lubrication (Fig. 6, left). Our research into as-rolled high-tensile pearlitic rails indicates, however, that even in the case of such special operating conditions it is still possible to optimize the rail steel's resistance to wear.

In general, it should be possible, by suitably improving the operating conditions and selecting the suitable rail steel to completely overcome problems of rail wear. Lubrication alone, however, would lead to fatigue damage, if the high cyclic stress, which is continuously active in the same region underneath the gauge corner when wear is low, is not counteracted by the high fatigue strength of the high-tensile rail steel.

CONCLUSIONS

1. Within a given microstructure group (pearlite, bainite) resistance to wear is determined by the hardness of the rail steel.
2. As-rolled pearlitic rails and heat-treated pearlitic rails of equal hardness exhibit the same resistance to wear because of their homogeneous microstructure.
3. Bainitic rails wear more quickly than pearlitic rails of the same hardness.

4. Given appropriate improvement of the operating conditions, e.g. lubrication and the selection of a suitable rail steel, a high service life of over $500 \cdot 10^6$ t can be expected even for tight curves.

REFERENCES

1 Heller, W., and Schweitzer, R., "Untersuchung und betriebliche Erprobung neuartiger naturharter Schienenstähle", Techn. Mitt. Krupp - Werksberichte, Vol. 37, 1979, pp. 79/87.

2 Heller, W., and Schweitzer, R., "Untersuchungen und Betriebserprobungen von Schienenstählen im Rahmen des Rad/Schiene-Forschungsvorhabens", Berichtsband Internationale Schientagung 1979, Heidelberg, VDEh, pp. 177/217.

3 Flügge, J., Heller, W., Stolte, E., and Dahl, W., "Einflußgrößen für die mechanischen Eigenschaften perlitischer Stähle", Arch. Eisenhüttenwes., Vol. 47, 1976, pp. 635/640.

4 Clayton, P., "The Relations between Wear Behaviour and Basic Material Properties for Pearlitic Steels", Wear, Vol. 60, 1980, pp. 75/93.

5 Masumoto, H., Sugino, K., and Hayashida, H., "Development of Wear Resistant and Anti-Shelling High Strength Rails in Japan", Conf. Papers of Heavy Haul Railways Conference, Perth, Western Australia, Sept. 1978

6 Steele, R.K., "A perspectival Review of rail behaviour at the Facility for Accelerated Service Testing", Conf. Papers 19th Annual Conference of Metallurgists, Halifax, Nova Scotia, August 1980.

Rail Corrugation Growth Performance

L.E. Daniels

P.E.
Rail Corrugations
Experiment Monitor
Boring Services Inter-
national, Pueblo,
Colorado

N. Blume

Staff Engineer
Rail Corrugations
Boring Services Inter-
national, Pueblo,
Colorado

The purpose of this paper is to supply rail corrugation growth data, to determine the effect of various track parameters on corrugation growth, to estimate the additional track maintenance cost caused by corrugations and to determine optimum rail corrugation grinding depths. The problem termed Rail Corrugations has stimulated the interest and speculations of railroad personnel for about 80 years. However, the basic mechanism of corrugations is still not understood. In 1979, FAST technical personnel were directed to establish a test with the objective of providing operating railroads with better methods to treat corrugations. An experiment was designed which would first provide an understanding of corrugation growth and then based on that data establish an investigation of corrugating mechanisms. This report contains the results of the first step. In summary, it first presents the layout, measurement and conduct of the FAST Rail Corrugation Experiment. Corrugation growth rates are presented. Factors affecting corrugation growth are then evaluated and discussed. The effects of corrugations on track maintenance are presented. Rail grinding is then discussed. Current theories on corrugating mechanisms are reviewed. Finally, the paper's conclusions are summarized with recommendations for revenue service application and recommendations for additional research.

DESCRIPTION OF THE TEST LAYOUT, MEASUREMENT AND CONDUCT TECHNIQUES

FAST provides a variety of rail metallurgies, track grades and tie configurations, allowing evaluations of these factors relative to corrugation development under a controlled full service environment. Figure 1 shows the FAST loop, the corrugation test zones, and rail lubricator locations.

Figure 2 illustrates the track geometry for the FAST loop. Rail Corrugation test zones are shown as solid blocks. Note the large difference in ruling grade between the 5° curve in Section 17 (2% Grade) and the much flatter contour in Section 3 (0.9% and 0.1%).

Figure 3 shows a detailed layout of the metallurgies tested in FAST Test Sections 3 and 17 (5° curve only). These sections are used for corrugation growth characterizations.

Section 13 (4° curve) is used to observe corrugation growth from an artificial corrugation the shape of a battered weld.

THE FAST TRACK

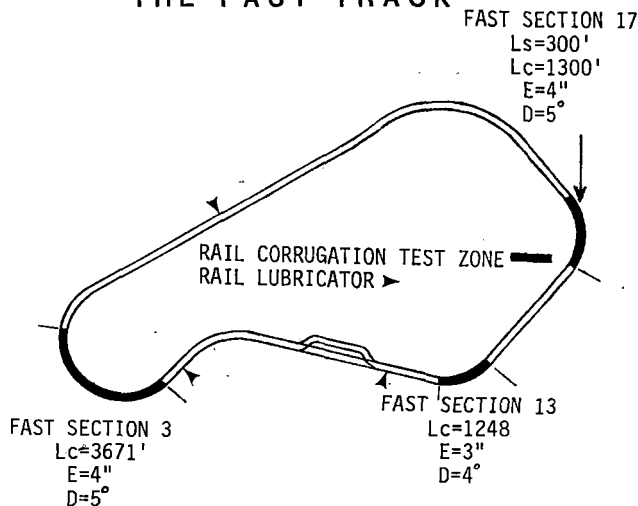


FIGURE 1. RAIL CORRUGATION TEST ZONES.

FAST TRACK CHART

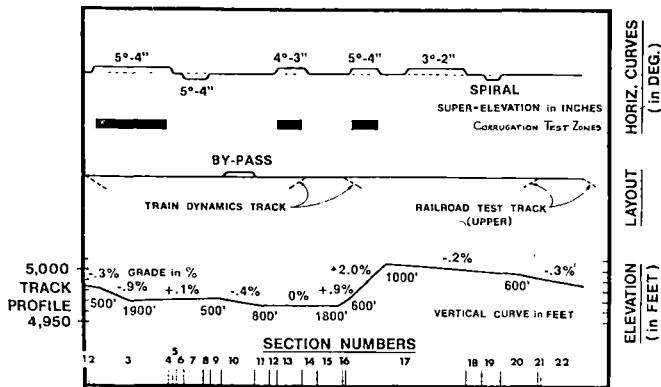


FIGURE 2. FAST TRACK GEOMETRY.

TABLE A. RAIL METALLURGY LADLE ANALYSIS AND AVERAGE HARDNESS.¹

METALLURGY	WEIGHT PERCENT (W/O)								WORK HARDENED BRINELL (AVG) TOP OF HEAD
	C	Mn	P	S	Si	Cr	Mo	V	
Std. Carbon	0.76	0.86	0.022	0.024	0.18	----	----	----	324
Fully Heat Treated	0.81	0.93	0.018	0.041	0.20	----	----	----	366
Head Hardened	0.77	0.83	0.021	0.300	0.17	----	----	----	355
Silicon Chrome	0.76	0.82	0.020	0.006	0.82	0.50	----	----	391
1% Chrome	0.73	0.97	0.022	0.025	0.27	1.12	----	----	348
Chrome Vanadium	0.69	1.21	0.012	0.022	0.28	1.07	----	----	372
Chrome - Moly (A)	0.72	0.79	0.009	0.023	0.25	0.78	0.21	----	383
Chrome - Moly (C)	0.79	0.60	0.026	0.016	0.26	0.61	0.17	----	344

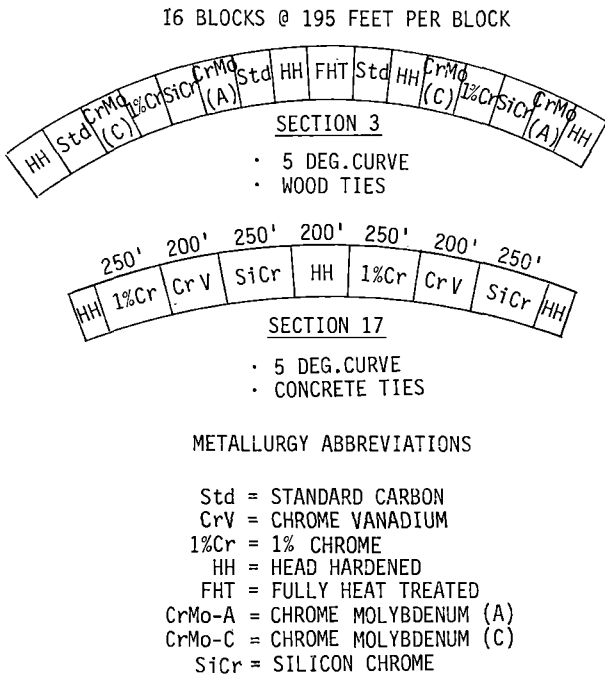


FIGURE 3. RAIL METALLURGY LAYOUT.

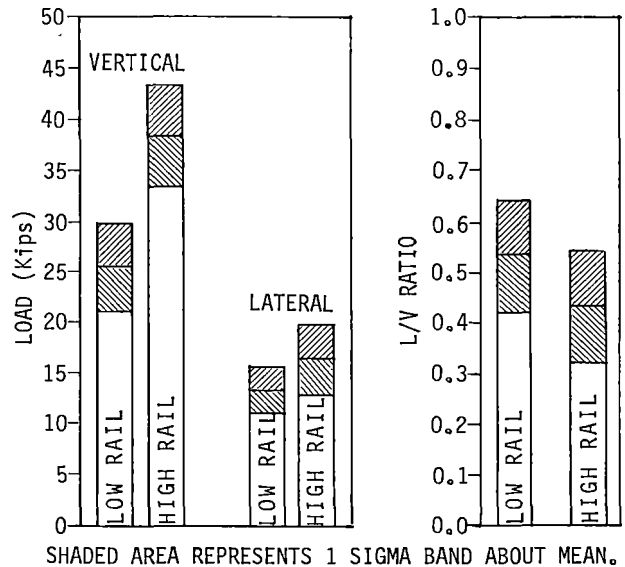


FIGURE 4. PEAK WHEEL LOADS AND L/V RATIO PLOT FOR A 5° CURVE.

Table A lists the chemical content and average brinell hardness for the test metallurgies.

The load spectrum is controlled to insure uniformity throughout the test. Typical loads are shown in Figure 4.

Revenue service vertical loadings in mixed freight are much lower than at FAST. Lateral loading at FAST is nearly the same as that in revenue service.

The test period was from December 1979 through August 1981. During this period 187 million gross tons (MGT) were accumulated on test metallurgy.

The rail lubrication alternated between full lubrication and no lubrication. The periods of each lubrication are shown in Table B.

TABLE B. LUBRICATION PERIODS.

MGT	LUBRICATION CONDITION
0	Lubricated
32.945	Non-Lubricated
47.879	Lubricated
93.559	Non-Lubricated
106.711	Lubricated
136.122	Non-Lubricated
151.196	Lubricated
178.919	Non-Lubricated
187.026	Lubricated

Field measurements to document corrugation growth and characterize parameter changes with MGT are taken at the lubrication cycle beginning and end, and before and after pertinent maintenance activity.

Field measurements are:

- o Continuous Longitudinal Rail Profile - rail head surface of the entire FAST loop is recorded on tape, then reduced to corrugation wavelength and amplitude distributions by metallurgy.
- o M-S Longitudinal Profile - 36" long rail head surface tracing of selected locations of developed corrugations.
- o Transverse (X-Section) Rail Profile - taken on corrugation peaks & valleys in conjunction with the M-S Longitudinal Profile.
- o Rail Hardness - Brinell hardness at selected peak & valley and at non-corrugated locations.
- o Track Stiffness - Average vertical stiffness.

Train operations (speed, braking, throttle setting) are monitored continuously during all train movements.

Track Maintenance is monitored by technical personnel. Maintenance activity is dictated by general FAST operating policy which sets FRA Class 4 as a minimum operating standard.

Postmortem metallurgical evaluations were performed on a set of corrugated chrome-molybdenum-C samples at 187 MGT. Evaluations include:

- Micro Hardness
- Scanning Electron Microscope

RAIL CORRUGATION GROWTH RATES

Rail Corrugation growth rates are based on the profiles of the entire running length of each test metallurgy subsection. Since rail corrugations occur predominately on the low rail at FAST, only low rail data will be presented here.

CONTINUOUS LONGITUDINAL PROFILE

Rail running surface profiles are measured with an eddy current proximity sensor mounted midpoint in a 6-foot ski riding on the rail (Figure 5).

In this experiment the ski carriage is towed at 4 mph. The measurement accuracy at this speed is $\pm .005$ " vertical (amplitude) and ± 0.5 " longitudinal (wavelength).

DATA APPEARANCE, REDUCTION AND CHARACTERIZATION

The output of the continuous longitudinal profile is a continuous record of rail running surface variations.

Figure 6A shows the raw data from this measurement on new rail and Figure 6B shows the wavelength

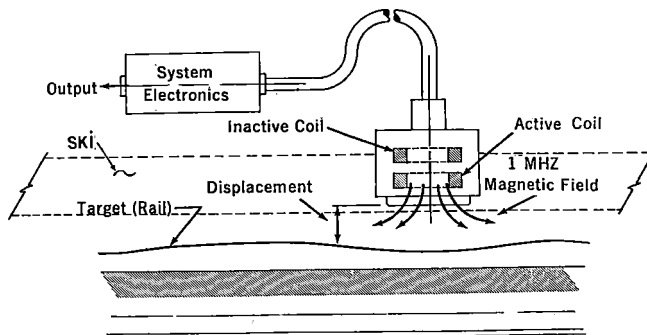


FIGURE 5a. SCHEMATIC OF EDDY CURRENT SENSING DEVICE.



FIGURE 5b. PHOTOGRAPH OF SKI AND RAIL MOUNTED CARRIAGE.

distribution of each profile.

To contrast a new rail surface with a corrugated surface, profiles are shown in Figures 7A at the beginning of the test and Figures 7B after 151 MGT of test for standard carbon rail.

The profiles for each metallurgy subsection are reduced into the more manageable joint probability distribution of wavelength and amplitude shown in Figure 8. These distributions form the data base for corrugation characterizations.

The corrugation amplitude parameter is termed "severity" and is the amplitude at the deepest wave (95% exceedence) between 5" and 10" long. The parameter representing the amount of rail that is corrugated is termed "extent" and is the percent of the metallurgy subsection which contains wavelengths between 5" and 10" long.

A typical plot of rail corrugation severity and extent is shown as a function of MGT in Figure 9.

In Figure 9, it is observed that corrugation growth is different between lubricated and dry test periods.

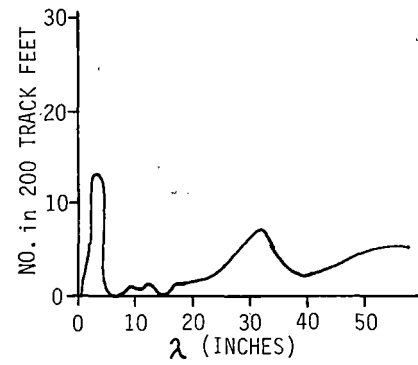
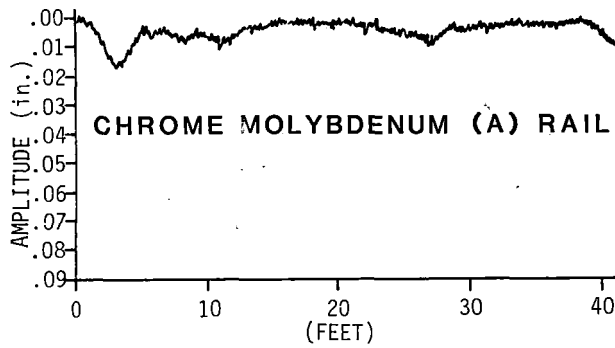
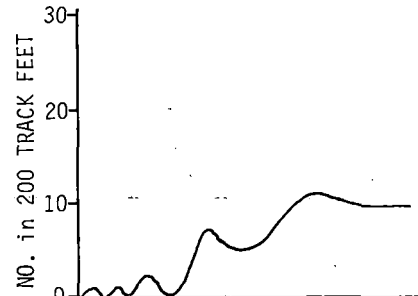
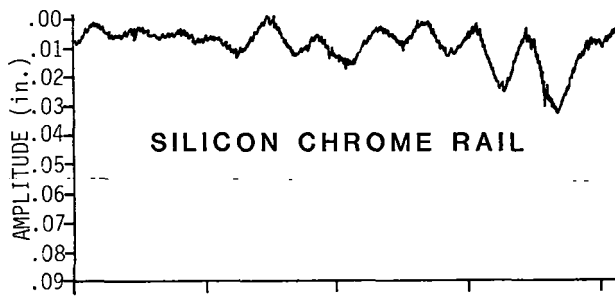
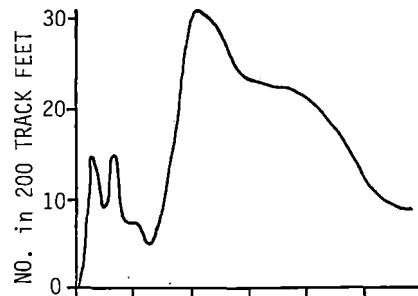
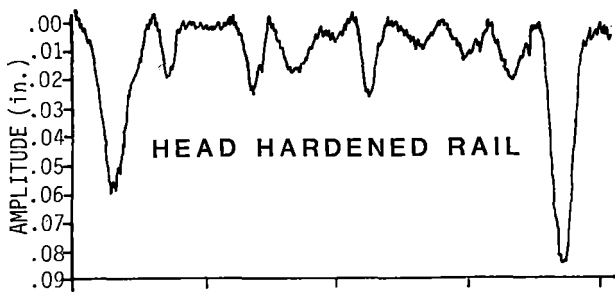


FIGURE 6a. TYPICAL INITIAL RAIL PROFILES.

FIGURE 6b. WAVELENGTH DISTRIBUTION (200').

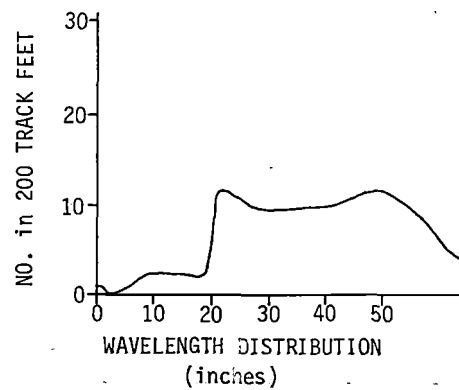
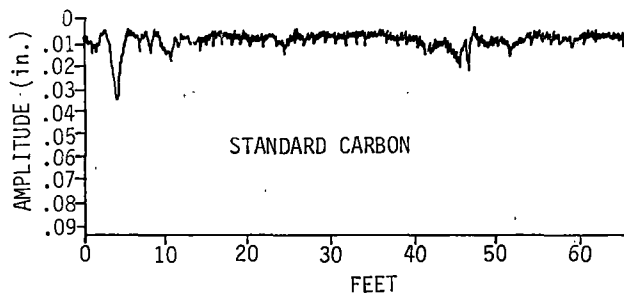


FIGURE 7a. NEW RAIL SURFACE PROFILE.

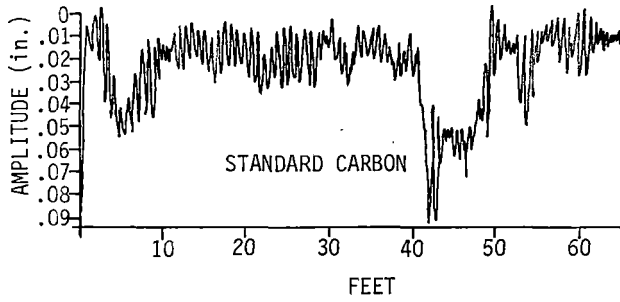
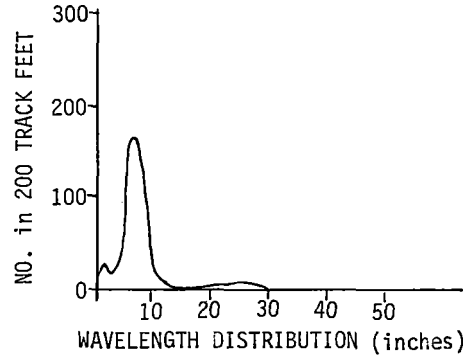


FIGURE 7b. CORRUGATED PROFILE AFTER 151 MGT.



SECTION NUMBER: 03	
TIE NUMBER: 1337 I	
TAPE NUMBER: 43-2	
R-O-T NUMBER: 151-196	
MEASUREMENT DATE: 8/10/16	
METALLURGY: STANDARD CARBON	
MAINTENANCE: BEGIN LUBE	
HYSTERESIS: 12	
A-TO-D SPAN: 128	
SUMS:	9 14 65 276 127 13 5 3 5 6 6 1 0 1 0 0 = 532
5.0-6.25	0 2 3 2 1 0 1 0 0 0 0 0 0 0 0 0 = 10
6.25-7.5	6 7 27 58 19 6 2 1 1 2 1 0 0 0 0 = 130
7.5-8.75	2 3 16 60 37 4 0 0 1 1 2 0 0 0 0 = 126
8.75-10.0	1 1 9 43 23 2 1 1 1 2 1 0 0 0 0 = 86
10.0-11.25	0 1 6 52 17 1 1 1 0 1 1 0 0 0 0 = 81
11.25-12.5	0 0 3 28 13 0 0 0 1 0 0 0 0 0 0 = 45
12.5-13.75	0 0 2 15 10 0 0 0 0 0 0 0 0 0 0 = 27
13.75-15.0	0 0 0 12 4 0 0 0 0 0 0 0 0 0 0 = 16
15.0-16.25	0 0 0 5 2 0 0 0 0 0 0 0 0 0 0 = 7
16.25-17.5	0 0 0 0 0 0 0 0 0 0 0 0 0 0 0 = 3
17.5-18.75	0 0 0 0 0 0 0 0 0 0 0 0 0 0 0 = 0
18.75-20.0	0 0 0 0 0 0 0 0 0 1 0 0 0 0 0 = 1
20.0-21.25	0 0 0 0 0 0 0 0 0 0 0 0 0 0 0 = 0
21.25-22.5	0 0 0 0 0 0 0 0 0 0 0 0 0 0 0 = 0
22.5-23.75	0 0 0 0 0 0 0 0 0 0 0 0 0 0 0 = 0
23.75-25.0	0 0 0 0 0 0 0 0 0 0 0 0 0 0 0 = 0
SUM OF DISTANCE COUNTS = 4596	

FIGURE 8. AMPLITUDE/WAVELENGTH MATRIX.

Figure 10 is the replot of the data in Figure 9 such that lubricated periods are connected to lubricated periods and non-lubricated periods are connected to non-lubricated periods. Figure 10 shows that lubrication has a marked effect on the extent parameter and, to a lesser degree, on the severity parameter.

Further, we observe that the growth rate of the corrugations can be approximated by a linear relationship for each lubrication condition.

Using this format, the raw severity and extent data is presented for each metallurgy in Figures 11 and 12.

It is important to note in Figures 11 and 12 that the range of performance within each metallurgy is not uniform. That is, corrugation growth rates vary between test subsections of the same metallurgy. Referring to Figure 3, this variance in performance takes place within as little as 400 track feet on the same curve. This inconsistency is often repeated in revenue service where corrugations behave erratically from curve to curve which are otherwise equal in terms of construction, design and incident service.

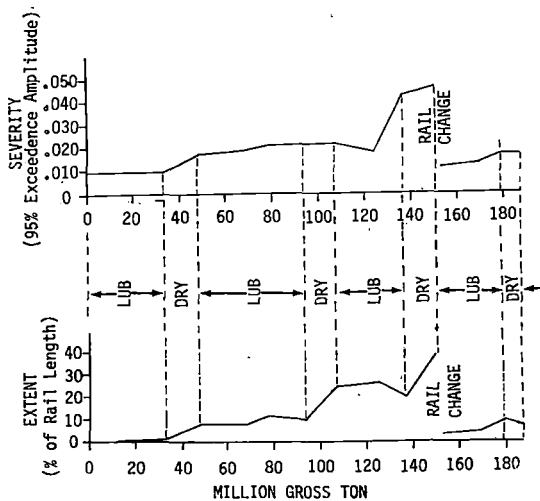


FIGURE 9. RAIL CORRUGATION GROWTH; STANDARD CARBON RAIL 5° CURVE, HARDWOOD TIES.

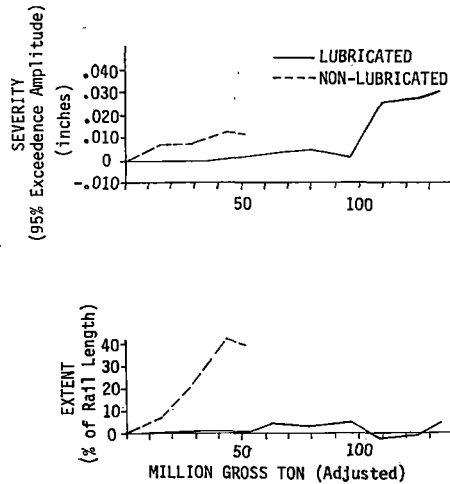
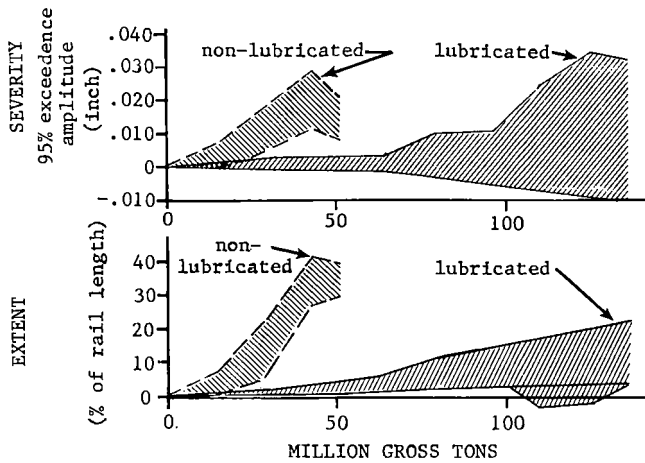
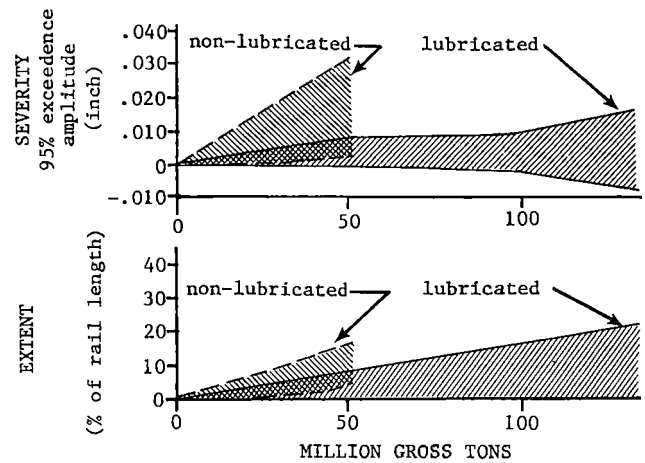


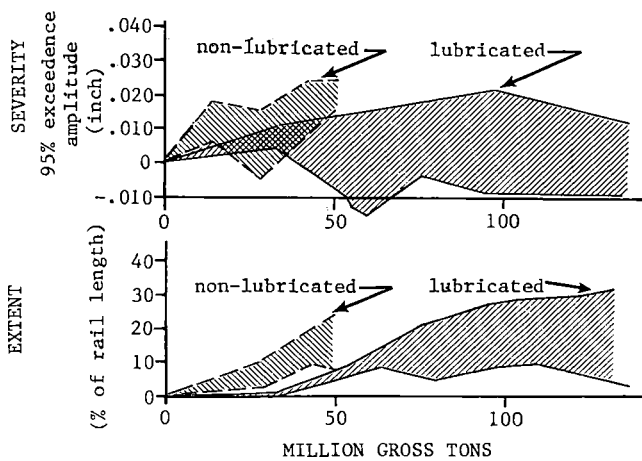
FIGURE 10. RAIL CORRUGATION GROWTH BY LUBRICATION CONDITION; STANDARD CARBON RAIL, 5° CURVE, HARDWOOD TIES.



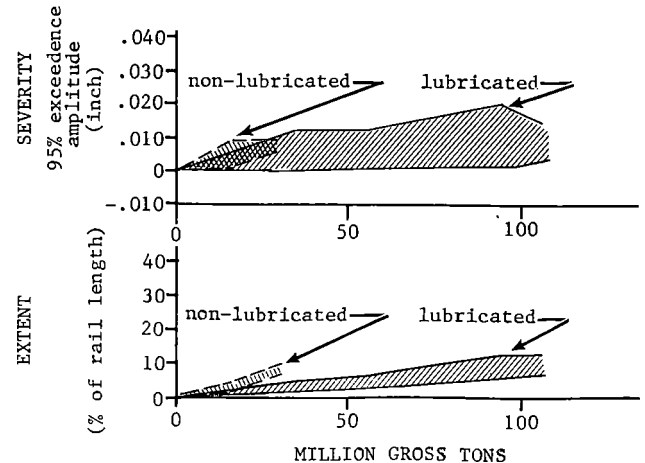
(a.) STANDARD CARBON.



(b.) HEAD HARDENED.



(c.) CHROME-MOLYBDENUM (C).



(d.) CHROME-MOLYBDENUM (A).

FIGURES 11a. - 11d. RAIL CORRUGATION SEVERITY AND EXTENT RAW DATA.

In passing, we cannot validate nor contradict assertions² that the amplitude of corrugations stabilizes after a sufficient number of passes (of vehicle axles), based on the data in Figures 11 and 12.

CORRUGATION GROWTH DATA

In Tables C, D, E, and F. growth rates are stated for each metallurgy separately for FAST test section 3 and section 17. Different growth rates are calculated for lubricated and nonlubricated test conditions.

The growth rates are linear (i.e., of the form: $y = mx + b$) based on the general appearance of the data in Figures 11 and 12, and based on statistical tests of other relationship forms.*

*The linear form, power and log functions were tested. The linear form produced the highest correlation coefficient.

The statistical significance of each growth rate is shown under the column "Growth \neq 0?"

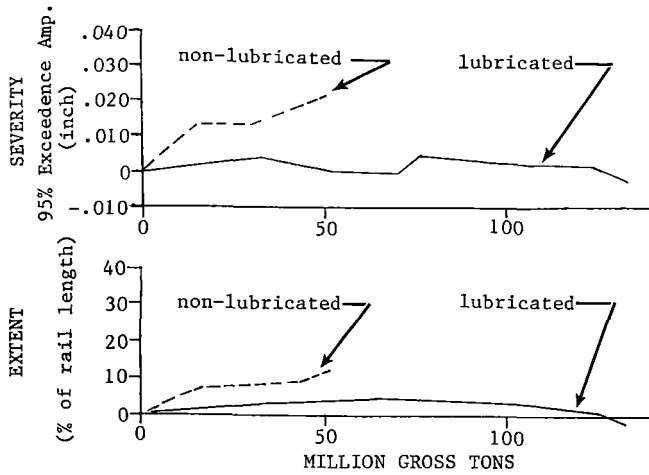
FACTORS AFFECTING CORRUGATION GROWTH

In this section the effects of individual parameters on corrugations will be examined. It must be understood that the observed correlation between any parameter and corrugations is not exclusive of other interactions in the track/train system.

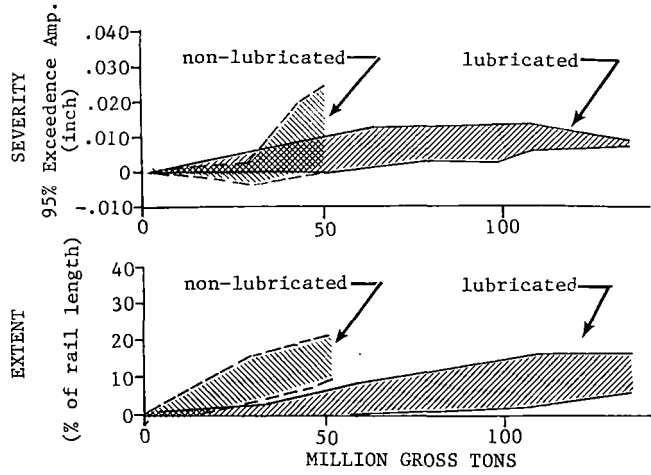
Previously observed influences of lubrication and metallurgy will be examined more objectively. Also, other influences such as track geometry, surface roughness, track modulus, train operations (speed) track construction (tie type), will be investigated.

EFFECTS OF RAIL LUBRICATION

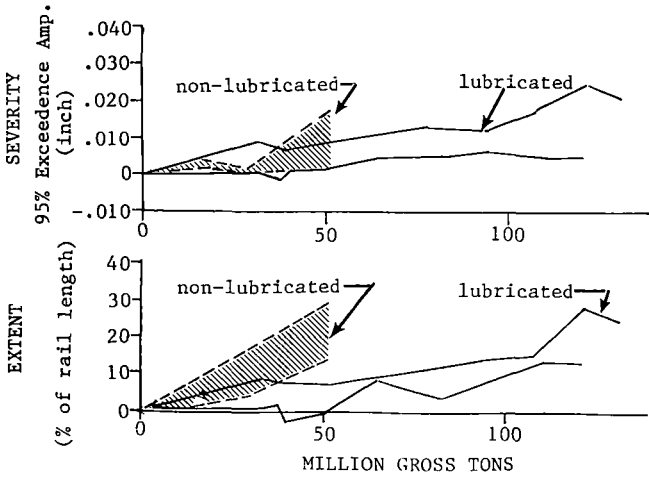
Lubrication at FAST is applied only to the gage face of the high rail during lubricated periods. While some lubricant occasionally reaches the low rail,



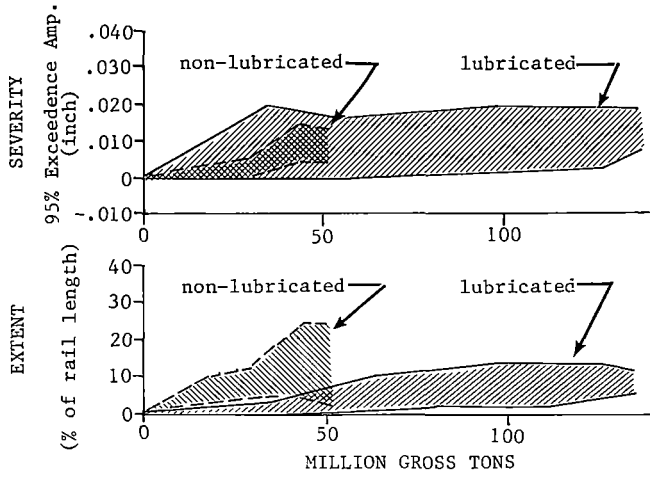
(a.) FULLY HEAT TREATED.



(b.) 1% CHROME.



(c.) CHROME VANADIUM.



(d.) SILICON CHROME.

FIGURES 12a. - 12d. RAIL CORRUGATION SEVERITY AND EXTENT RAW DATA.

TABLE C. CORRUGATION GROWTH RATES.
SEVERITY - SECTION 3¹
By Metallurgy

Metallurgy	Lube Condition	Growth Rate 10 ⁻³ in/ MGT	Growth Rate Error 10 ⁻³ in/MGT	Constant 10 ⁻³ in	Constant Error 10 ⁻³ in	% Variation Explained	F*	Degrees of Freedom Reg/Resid	F Table (.95)	Growth ² ≠ 0 ?
Std	Lub'd	.1534	.0480	-4.6630	10.4211	29.0	10.2	1/25	4.2	yes
	Dry	.3482	.0947	-1.8395	6.8136	51.0	13.5	1/13	4.7	yes
CrMo - C	Lub'd	.0320	.0682	-.1403	12.0600	1.3	.2	1/17	4.4	no
	Dry	.3095	.1526	2.8724	8.9600	33.9	4.1	1/8	5.3	no
HH	Lub'd	.0672	.0180	-.6565	3.6444	33.3	14.0	1/28	4.2	yes
	Dry	.2998	.0672	-.7557	6.8016	40.7	19.9	1/29	4.2	yes
CrMo - A	Lub'd	.0800	.3408	.3445	7.5207	11.6	1.8	1/14	4.6	no
	Dry	.2589	.1156	.0672	3.2491	55.6	5.0	1/4	7.7	no
FHT	Lub'd	-.0104	.0197	1.8400	2.4378	3.4	.3	1/8	5.3	no
	Dry	.4015	.0672	2.3847	2.7890	92.2	35.7	1/3	10.1	yes
SiCr	Lub'd	.0489	.0423	6.9300	7.5488	7.4	1.3	1/16	4.5	no
	Dry	.1987	.0431	-.2613	2.5770	58.3	11.2	1/8	5.3	yes
1% Cr	Lub'd	.0817	.0163	1.0023	3.9540	43.3	25.2	1/33	4.1	yes
	Dry	.2309	.0815	-2.6385	6.7670	30.9	8.0	1/18	4.4	yes

¹Section 3 has Wood Ties, .9% to 0% Grade, Constant Speeds, Grade 4 Ballast(various sources), 5° Curves

Severity of Corrugations = [Growth Rate ± Growth Rate Error (10⁻³ in/MGT)] x MGT + [Constant ± Constant Error (10⁻³ in)]

²Growth ≠ 0; "yes" means significant growth; "no" means no significant corrugation growth.

TABLE D. CORRUGATION GROWTH RATES.
SEVERITY - SECTION 17¹
By Metallurgy

Metallurgy	Lube Condition	Growth Rate 10 ⁻³ in/ MGT	Growth Rate Error 10 ⁻³ in/MGT	Constant 10 ⁻³ in	Constant Error 10 ⁻³ in	% Variation Explained	F*	Degrees of Freedom Reg/Resid	F Table (.95)	Growth ² ≠ 0 ?
HH	Lub'd	-.0037	.0286	3.8925	6.1790	0.1	0.0	1/24	4.3	no
	Dry	.2998	.0672	-.7557	6.8016	40.7	19.9	1/29	4.2	yes
SiCr	Lub'd	.0489	.0219	2.1543	3.8717	24.3	5.1	1/16	4.5	yes
	Dry	.1987	.0577	-2.1218	3.8683	70.2	18.9	1/8	5.3	yes
CrV	Lub'd	.1284	.0301	-.9644	5.2498	50.3	18.2	1/18	4.4	yes
	Dry	.1808	.0819	-.7311	4.8118	37.8	4.9	1/87	5.3	no
1% Cr	Lub'd	.0817	.0163	1.0023	3.9540	43.3	25.2	1/33	4.1	yes
	Dry	.2309	.0815	-2.6385	5.7671	30.9	8.0	1/18	4.4	yes

¹Section 17 has Concrete Ties, 2% Grade (some in vertical curve) varying speed (35-50 mph), Grade 4 Ballast (various sources) 5° Curve

Severity of Corrugations = [Growth Rate ± Growth Rate Error (10⁻³ in/MGT)] × MGT + [Constant ± Constant Error (10⁻³ in)]

²Growth ≠ 0; "yes" means significant growth; "no" means no significant corrugation growth.

TABLE E. CORRUGATION GROWTH RATES.
EXTENT - SECTION 3¹
By Metallurgy

Metallurgy	Lube Condition	Growth Rate %/MGT	Growth Rate Error %/MGT	Constant %	Constant Error %	% Variation Explained	F*	Degrees of Freedom Reg/Resid	F Table (.95)	Growth ² ≠ 0 ?
Std	Lub'd	.0812	.0223	-.6041	4.8322	34.8	13.3	1/25	4.2	yes
	Dry	.7492	.0836	-3.6803	6.0102	86.1	80.4	1/13	4.7	yes
CrMo - C	Lub'd	.1501	.0502	-.3126	8.8910	34.4	8.9	1/17	4.5	yes
	Dry	.3253	.0902	-.2301	5.2960	61.9	13.0	1/8	5.3	yes
HH	Lub'd	.0929	.0255	-1.0319	5.1651	39.0	17.9	1/28	4.2	yes
	Dry	.2079	.0327	-.3513	3.3141	58.2	40.3	1/29	4.2	yes
CrMo - A	Lub'd	.0947	.0155	.0763	1.9812	72.6	37.1	1/14	4.6	yes
	Dry	.2626	.0752	-.5491	2.1140	75.3	12.2	1/4	7.7	yes
FHT	Lub'd	.1272	.0168	-1.6628	2.0814	87.8	57.3	1/8	5.3	yes
	Dry	.2153	.0415	1.4007	1.7226	90.0	26.9	1/3	10.1	yes
SiCr	Lub'd	.0970	.0139	1.8677	2.4805	75.3	48.7	1/16	4.5	yes
	Dry	.0950	.0254	-.7897	1.4918	63.5	14.0	1/8	5.3	yes
1% Cr	Lub'd	.0987	.0142	-.0664	3.4489	59.4	48.3	1/33	4.1	yes
	Dry	.3079	.0544	-.0453	4.5184	64.0	32.0	1/18	4.4	yes

¹Section 3 has Wood Ties, .9% to 0% Grade, Constant Speeds (≈ 40 mph), Grade 4 Ballast (various sources) 5° Curve.

Extent of Corrugations = [Growth Rate ± Growth Rate Error (%/MGT)] × MGT + [Constant ± Constant Error (%)]

²Growth ≠ 0; "yes" means significant growth; "no" means no significant corrugation growth.

TABLE F. CORRUGATION GROWTH RATES.
EXTENT - SECTION 17¹
By Metallurgy

Metallurgy	Lube Condition	Growth Rate %/MGT	Growth Rate Error %/MGT	Constant %	Constant Error %	% Variation Explained	F*	Degrees of Freedom Reg/Resid	F Table (.95)	Growth ² ≠ 0 ?
HH	Lub'd	.0929	.0243	-1.4337	5.2506	30.0	10.3	1/24	4.3	yes
	Dry	.2079	.0325	-.3513	3.3141	58.2	40.3	1/29	4.2	yes
SiCr	Lub'd	.0358	.0132	1.2322	2.3253	31.6	7.4	1/16	4.5	yes
	Dry	.2644	.0764	.6621	4.4854	75.3	24.4	1/8	5.3	yes
CrV	Lub'd	.1825	.0284	-2.6582	4.9548	69.6	41.3	1/18	4.4	yes
	Dry	.4486	.1041	-1.0707	6.1118	69.9	18.6	1/8	5.3	yes
1% Cr	Lub'd	.0987	.0142	-.0664	3.4489	59.4	48.3	1/33	4.1	yes
	Dry	.3079	.0544	-.0453	4.5184	64.0	32.0	1/18	4.4	yes

¹Section 17 is Concrete Ties, 2% Grade (some in vertical curve), varying speed (35-50 mph), Grade 4 Ballast (various sources), 5° Curve

Extent of Corrugations = [Growth Rate ± Growth Rate Error (%/MGT)] × MGT + [Constant ± Constant Error (%)]

²Growth ≠ 0; "yes" means significant growth; "no" means no significant corrugation growth.

the low rail lubrication condition is either completely "starved" or boundary lubricated; generally the former, even during lubricated test periods.

Table G presents the results of the statistical comparison between lubricated and non-lubricated growth rates.

Comparisons in Table G are provided for each metallurgy in each of general test zones to minimize the effects of differences of tie type, grade and train operations.

The statistical results in Table G show that significantly higher growth rates occur in either the severity or extent parameter for every metallurgy except the chrome-molybdenum-C rail, which showed no difference.

The "Ratio Dry/Lub" is a mean quotient of the two growth rate population distributions,⁶ rather than a simple ratio of the average growth rates.

Ratios shown with a "(?)" are not accurate because the lubricated growth rate is shown to be equal to zero (Refer to Tables C through F), and a ratio with zero in the denominator is, as always, undefined.

High rail lubrication is a significant factor in reducing corrugation growth.

Rail lubrication is thought by some^{3,4,5} to have an adverse effect on corrugation growth (increases corrugation) through hydrodynamic pressure within rail surface fatigue cracks.

Since the low rail at FAST is not lubricated, this theory cannot be evaluated.

Corrugations are also thought to result from wheel/rail stick-slip. The beneficial effect of lubrication on reducing corrugations could be the result of reducing the opportunity for wheel/rail stick-slip.

EFFECTS OF RAIL METALLURGY

Numerous authors^{8,9,10,11,12} suggest that "improved" metallurgy is at least a partial, if not the whole, solution to corrugation occurrence and development. Difference in rail corrugation growth rates between metallurgies are shown in Table H.

From Table H, significant differences between metallurgies occurred only during non-lubricated conditions and only for the extent parameter (% of rail

TABLE H. DIFFERENCE BETWEEN METALLURGIES.

WOOD TIES: .1% - .9% Grade (Section 3)											
SEVERITY						EXTENT					
Lubricated			Dry			Lubricated			Dry		
Growth		Rank	Growth		Rank	Growth		Rank	Growth		Rank
Metallurgy	Rate	Rank	Metallurgy	Rate	Rank	Metallurgy	Rate	Rank	Metallurgy	Rate	Rank
FHT	~0		CrMo - C	~0		Std	.0812		SiCr	.0950	1
CrMo - C	~0		CrMo - A	~0		HH	.0929		HH	.2079	2
SiCr	~0		SiCr	.1987		CrMo - A	.0947		FHT	.2153	2
CrMo - A	~0		1% Cr	.2309		SiCr	.0970		CrMo - A	.2626	2
HH	.0672	No Difference	HH	.2998	No Difference	1% Cr	.0987		1% Cr	.3079	2
1% Cr	.0817		Std	.3482		FHT	.1272	No Difference	CrMo - C	.3253	2
Std	.1534		FHT	.4015		CrMo - C	.1501		Std	.7492	3

CONCRETE TIES: .65% - 2% Grade (Section 17)											
SEVERITY						EXTENT					
Lubricated			Dry			Lubricated			Dry		
Growth		Rank	Growth		Rank	Growth		Rank	Growth		Rank
Metallurgy	Rate	Rank	Metallurgy	Rate	Rank	Metallurgy	Rate	Rank	Metallurgy	Rate	Rank
HH	~0	1	CrV	~0		SiCr	.0358	1	HH	.2079	1
SiCr	.0489	1	SiCr	.1987		HH	.0929	1	SiCr	.2644	1
1% Cr	.0817	2	1% Cr	.2309		1% Cr	.0987	1	1% Cr	.3079	1
CrV	.1284	3	HH	.2998		CrV	.1825	2	CrV	.4486	2

1. Significant difference between all metallurgies taken at 95% confidence level.
2. Severity Growth rates is 10⁻³ in/MGT; Extent Growth rate is % of rail length/MGT.
3. Ranking is based on a 2 Standard Deviation spread between average growth rates.

TABLE G. EFFECT OF LUBRICATION ON RAIL CORRUGATION GROWTH.

SECTION 3 (Wood Ties, Constant Train Speed ≈ 42 mph, 0-.9% Grade, Grade 4 Ballast)								
METALLURGY	SEVERITY				EXTENT			
	Ave Growth Rate (10 ⁻³ in/MGT) Lubricated	Dry	Significant Difference ?	Ratio Dry/Lub'd	Ave Growth Rate (%/MGT) Lubricated	Dry	Significant Difference ?	Ratio Dry/Lub'd
FHT	-.0104 ^{NS}	.4015	yes	17.08(?)	.1272	.2153	no	1
HH	.0672	.2998	yes	3.94	.0929	.2079	yes	1.75
SiCr	.0489 ^{NS}	.1987	yes	1.63(?)	.0970	.0950	no	1
1% Cr	.0817	.2309	yes	2.62	.0987	.3079	yes	3.00
CrMo - C	.0320 ^{NS}	.3095 ^{NS}	no	1	.1501	.3253	no	1
CrMo - A	.0800 ^{NS}	.2589 ^{NS}	no	1	.0947	.2626	yes	2.63
Std	.1534	.3482	no	1	.0812	.7492	yes	8.13

SECTION 17 (Concrete Ties, Variable Speed - 35 to 50 mph, 2% Grade, Grade 4 Ballast)								
METALLURGY	SEVERITY				EXTENT			
	Ave Growth Rate (10 ⁻³ in/MGT) Lubricated	Dry	Significant Difference ?	Ratio Dry/Lub'd	Ave Growth Rate (%/MGT) Lubricated	Dry	Significant Difference ?	Ratio Dry/Lub'd
HH	-.0037 ^{NS}	.2998	yes	8.25(?)	.0929	.2079	no	1
SiCr	.0489	.1987	yes	3.86	.0358	.2644	yes	8.60
1% Cr	.0817	.2309	yes	2.62	.0987	.3079	yes	3.00
CrV	.1284	.1808 ^{NS}	no	1	.1825	.4486	yes	2.35

NS: Growth rate not significantly different from zero, i.e., Growth rate = 0.

statistical test for parallel slopes at 95% confidence interval

length which corrugated) in Section 3. Under non-lubricated high rail conditions in Section 3 (wood ties, .1% - .9% grade, constant train speed \cong 40 mph), silicon chrome metallurgy resisted corrugations best of those tested, and standard carbon rail performed worst.

In Section 17 (concrete ties, 2% grade, variable train speed between 35 and 50 mph), head hardened, silicon chrome and 1% chrome metallurgies have significantly lower corrugation rates than the chrome vanadium rail, except for the severity parameter under non-lubricated conditions, where no difference is observed.

The results for Section 3 in Table H provides an indication, although not conclusive evidence, that high rail lubrication can minimize the rail corrugation non-lubricated performance differences between premium metallurgies and standard carbon rail.

Further, it is noted that the best corrugation performance is achieved by an alloyed heat treated rail (silicon chrome) followed in performance by the heat treated standard carbon metallurgies (head hardened and fully heat treated), then alloyed non-heat treated metallurgies (chrome-moly A & C, and 1% chrome), then, last, by standard carbon rail.

The differences in performance shown through statistical analysis can only be understood in terms of mechanical properties of the metallurgies. The metallurgical property generally associated with corrugations is yield strength in shear.^{5 12} Other properties of interest are yield strength in tension and cyclic yield strength and rail hardness.

Tensile and cyclic yield strengths are available from an earlier FAST test, but not from the current test. Rail hardness and yield strength are shown in Table I.

Table I shows an inverse relationship between

TABLE I. RAIL HARDNESS AND CYCLIC YIELD STRENGTH.

Rail Metallurgy	a Ave. Dry Extent Growth Rate (%/MGR)	Ranking	c Initial Brinell Hardness	c Work Hardened Brinell Hardness	d Yield Stress	
					Uniaxial (ksi)	Cyclic (ksi)
Section 3						
SiCr	.0950	1	365	391		
NH	.2079	2	316	355	98	90
FHT	.2153	2	362	366	95	74
CrMo - A	.2626	2	355	383		
1% Cr	.3079	2	315	348		
CrMo - C	.3253	2	314	344	113	82
Std	.7492	3	276	324	66	61
Section 17						
NH	.2079	1	316	355	98	90
1% Cr	.3079	1	315	348		
SiCr	.2644	1	365	391		
CrV	.4486	2	344	372		

NOTES:
a Growth Rates and ranking are those shown in Table H, non-lubricated
b Brinell Hardness before traffic: 3000 kg, 10 mm ball
c Brinell Hardness averaged over test duration excluding initial measurements: 3000 kg, 10 mm ball
d Yield stress from samples in earlier FAST test

Brinell hardness and corrugation growth, i.e., higher hardness results in lower corrugation growth rate.

The following relationships show good correlation between hardness and corrugation growth (Section 3 data only):

$$\text{Ext}_{NL} = -.005 \times \text{I.H.} + 1.98;$$

correlation coefficient = .85

where Ext_{NL} = Non-lubricated extent growth rate

I.H. = Initial hardness of rail

$$\text{Ext}_{NL} = -.007 \times \text{W.H.} + 2.95$$

correlation coefficient = .82

where W.H. = Work hardened rail hardness

[Note: perfect correlation = 1.00; No correlation = 0.]

This general trend is followed in the Section 17 data except for chrome vanadium. Insufficient data eliminates the opportunity to establish correlation between Section 17 hardness and corrugation growth rates.

Yield stress data in Table I is insufficient to establish any reliable relationships. The values for uniaxial yield stress in Table I can be compared to work by Mair and Groenhout¹² who estimate that "a material 0.2 percent proof stress of 670 M Pa [97 ksi]... is adequate to avoid corrugation formation." This appears to be a reasonable estimate for heavy haul operations based on the FAST data in Table I. This yield stress is approximately equivalent to a Brinell hardness of 354 BHN.

It is of interest to compare the corrugation growth rate to the rail hardness at the time each measurement is taken.

Figure 13 is a plot of individual hardness values and corrugation growth by lubrication periods ("x" is data collected during lubricated periods; "o" is data collected during non-lubricated).

While substantial data scatter is observed in Figure 13, the relationship between extent growth rate and Brinell hardness during non-lubricated periods is:

$$\text{Ext}_{NL} = -.004 (\text{BHN}) + 1.772$$

Ext_{NL} = Non-lubricated extent growth rate

BHN = Brinell Hardness

This relationship is very close to the regression relationship obtained using initial rail hardness values from Table I.

There is no relationship between hardness and corrugation growth during lubricated periods. This proves conclusively that lubrication on the high rail eliminates any effects that metallurgy (i.e., differences between standard and premium metallurgies) has on corrugation growth. This further substantiates the conclusion that lubrication is an effective means for controlling corrugation development.

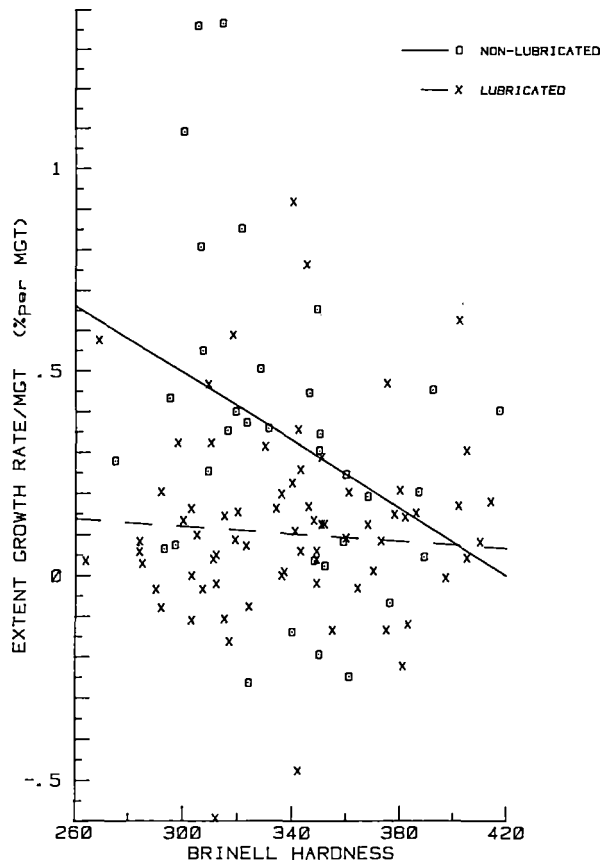


FIGURE 13. CORRUGATION EXTENT GROWTH RATE VS BRINELL HARDNESS.

From Figure 13, we also observed that no corrugation growth was observed when rail hardness was 422 BHN or greater (zero intercept on abscissa) even during non-lubricated operations.

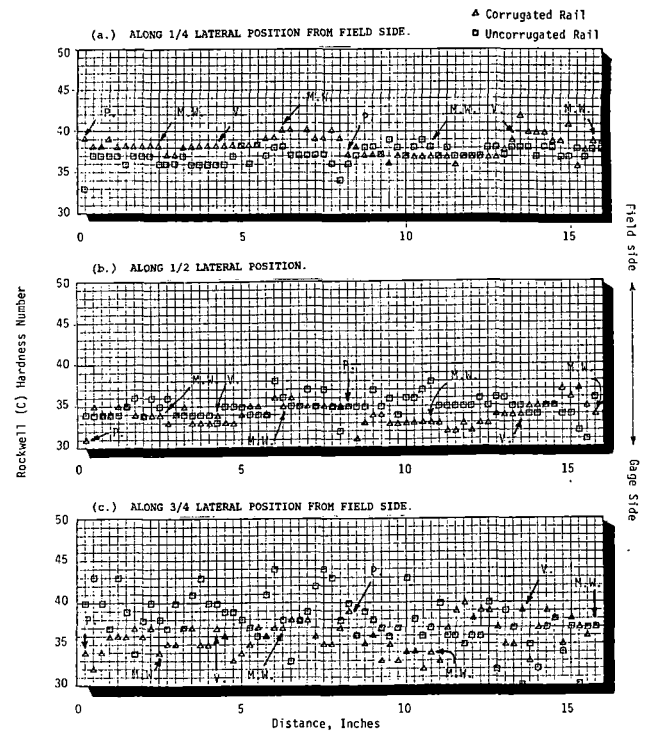
A second topic concerning hardness and corrugations is the assertion that the peak and valley hardnesses vary.

Figure 14 shows a hardness trace of a heavily corrugated rail and, overlaid, a trace of non-corrugated rail. Hardness measurements were taken in the laboratory using a Rockwell (C) tester. The rail sample had accumulated 187 MGT at the time of measurement. No hardness differential consistent with corrugation peak and valleys was apparent.

Figure 15 shows the progressions of corrugations during the field test for the sample shown in Figure 14. Again there is no clear indication that peak and valley hardnesses vary.

METALLURGICAL TRANSFORMATIONS

Rail surface transformations resulting from wheel slippage or normal work hardening have been associated with corrugations. Clayton and Allery¹¹ suggest that a "white phase" material described as a very hard, slow etching, transformation product about 0.17 mm thick on the rail surface was worn from valleys but not from peaks. [Clayton and Allery's work was done on "short wave" corrugations].



FIGURES 14a. - 14c. ROCKWELL (C) HARDNESS NUMBER VARIATIONS ALONG 16 INCHES OF CORRUGATED AND UNCORRUGATED RAIL.¹³

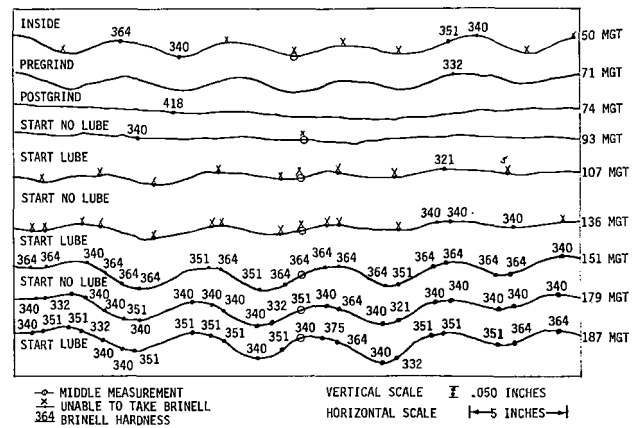


FIGURE 15. PEAK AND VALLEY BRINELL HARDNESS.

Optical micrographs were taken on the corrugated rail samples used in Figures 14 and 15. A neighboring non-corrugated rail was similarly examined. The white etching phase can be seen in very small traces on the rail surface at the mid-wave and peak locations. This phase is seen more in the valley than in other corrugated portions. A relatively thick layer, 1.2 mm, of white etching phase (untempered Martensite) frequently was found on the surface of the uncorrugated section.¹³ (Figure 16)

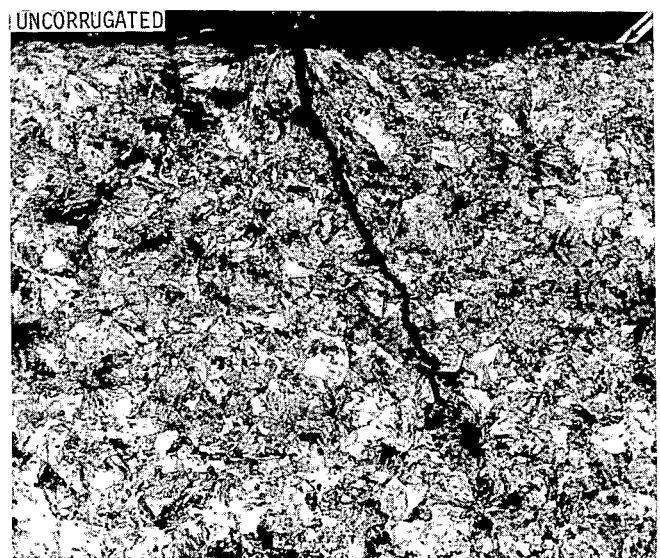
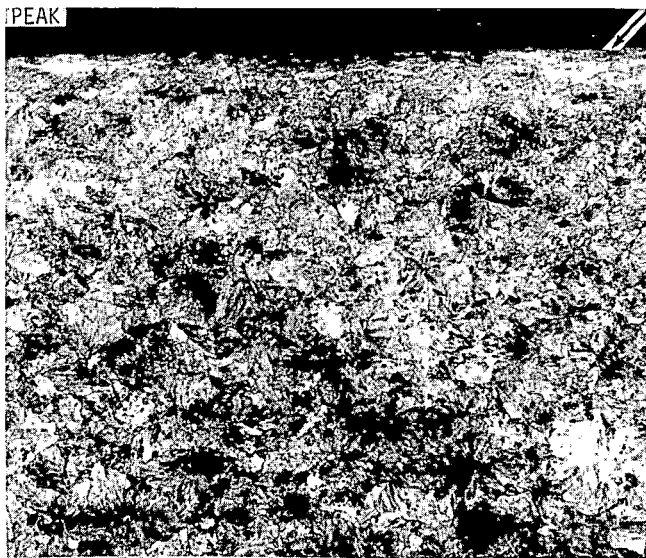
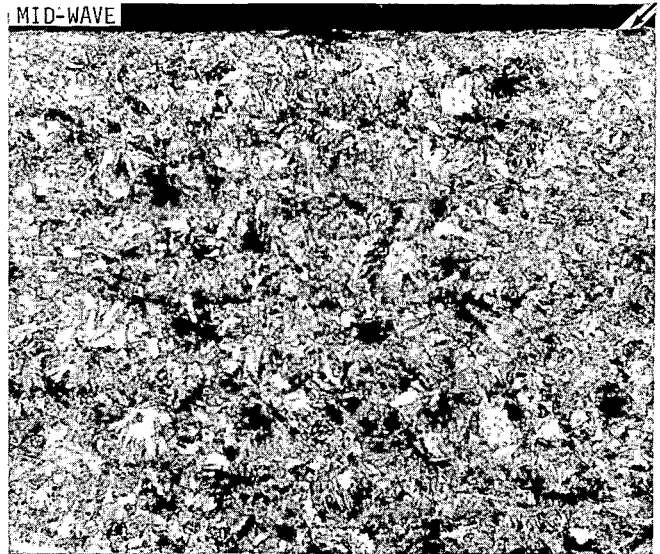
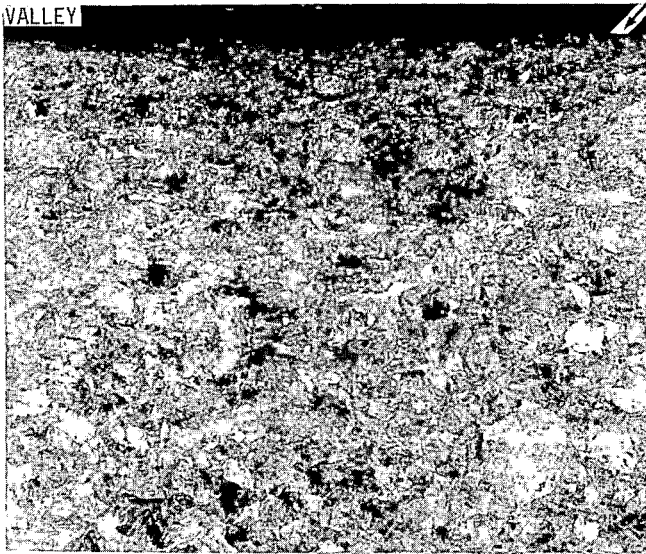


FIGURE 16. MICROSTRUCTURE OF RAIL SECTION AT THE 1/2 LATERAL POSITION OF THE RAIL HEAD (a.) VALLEY, (b.) MID-WAVE, (c.) PEAK CORRUGATED PORTION OF THE RAIL, (d.) UNCORRUGATED SECTION (VERTICAL-LONGITUDINAL PLANE). ARROWS SHOW RAIL SURFACE. ALL PHOTOMICROGRAPHS @ 100X, ETCHED WITH 2% NITAL.

The British researchers hypothesized that the brittle transformed layer formed wear flakes in the valleys and corrugations formed as a result of the wear. This hypothesis conflicts with observations of FAST corrugation samples.

Photos of a FAST corrugated rail surface, Figure 17, show that the rail surface is relatively free of gouge marks which could be expected from gross wheel slip. This appearance is interpreted as the result of a "mild" wear and deformation process.¹⁴

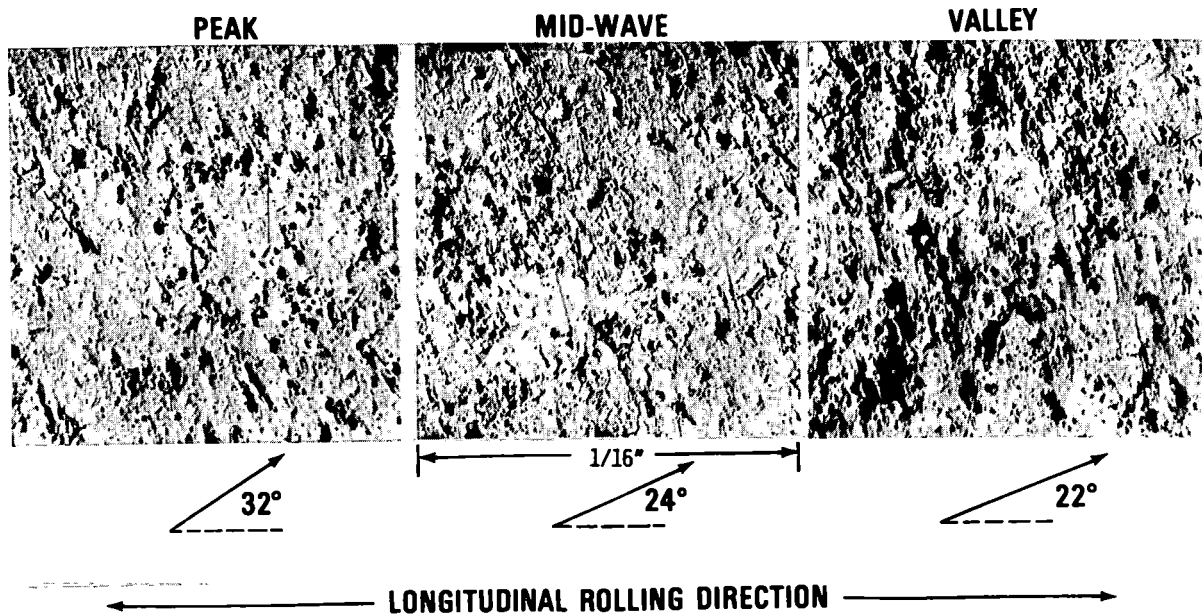


FIGURE 17. RUNNING SURFACE SEM PHOTOMICROGRAPHS
1 INCH FROM FIELD, CORRUGATION DEPTH
= 0.032".

To summarize the results of the effects of metallurgy on corrugation growth:

- o Metallurgy is a significant factor in corrugation growth.
- o Silicon chrome had the lowest corrugation growth rate and standard carbon rail had the highest growth rate in Section 03 (wood ties, uniform speed \cong 40 mph, .1% to .9% grade).
- o Silicon chrome, 1% chrome and head hardened metallurgies had lower growth rates than the chrome vanadium rail in Section 17.
- o Hardness measurements generally show an inverse relationship with corrugations under non-lubricated rail conditions.
- o Results approximately agree with Mair and Groenhout estimates that rail with a minimum yield stress of 670 M Pa (97,175 psi) is necessary to resist corrugation growth.
- o For 100 ton car loading, such as at FAST, no corrugation development is expected for metallurgies work hardened greater than 422 Brinell, which converts to a yield stress of 790 M Pa (114,547 psi).
- o Hardness does not vary consistently with corrugation peak and valley.
- o Metallurgical transformations at the rail surface, such as white etching layer, have no direct causal influence on corrugation development.

THE EFFECTS OF SURFACE ROUGHNESS

For the purpose of this report, we categorize surface roughness into micro-roughness and macro-roughness.

Micro-roughness of the rail surface is the small "asperities" within the contact patch. This level of roughness has not been measured at FAST.

The larger roughness shapes, macro-roughness, are features of the running surface affecting the smooth rolling line of the wheel. Fredrick¹⁵, Johnson¹⁶, have addressed the problem and shown that perturbations in the rail surface such as a battered weld or a dipped joint produce dynamic wheel/rail loads up to 3 times the static loading. The oscillation established by the perturbation loading depends on the shape of the rail surface dip and the system damping.

A number of artificial rail surface perturbations were placed in Section 13 (4° curve, 0% grade, wood ties - refer to Figure 1). The shape of the perturbations approximated the maximum allowable low shop weld in AREA rail welding specifications. The artificial weld shapes were ground at mid-point in the rail lengths to avoid influence of the heat affected zones at actual welds. [Note: rail was service work hardened @ beginning of test.] Prior to installing the artificial weld shapes, the entire curve was ground, new ties installed and track geometry was placed to new construction tolerances.

Figure 18 shows a typical progression of the artificial perturbation profile. We observe that no corrugation or secondary batter occurred at the artificial perturbation. Instead the waveform

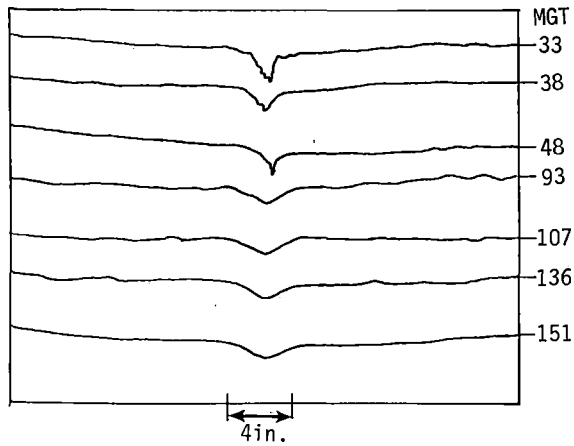


FIGURE 18. ARTIFICIAL CORRUGATION SURFACE PROFILE.

diminished in depth as the surrounding surface wore. This leads us to the conclusion that surface roughness the shape of a battered weld is not a sufficient condition for the initiation of corrugations if other track parameters such as track surface, line and gage are tightly controlled.

The general rail running surface roughness of the test metallurgies were shown at the beginning of this paper (Figure 6) to have unique distributions for each metallurgy.

Figures 19 through 25 show typical spectral distributions from the initial continuous profile of each metallurgy rail surface.

The wavelength distributions in Figure 19 through 25 illustrate that the initial roughness is largely concentrated in the 17.5 inch to 35.0 inch wavelengths. Further the head hardened rail is initially much rougher than the other metallurgies.

Using the area under these curves a relative measure of surface roughness, the roughness of each metallurgy relative to carbon rail is shown in Table J.

Table J shows that there is no relationship between initial roughness and future corrugation growth.

EFFECTS OF TRACK GEOMETRY

This report will review corrugation performance relative to designed track geometry (curvature, grade and superelevation) and relative to deviations from design track geometry (track gage).

Design Track Geometry - Curvature:

Corrugation growth rates increase with track curvature for two different metallurgies, Figure 26. Extrapolations to curves greater than 5° is not justified because data is limited by the FAST track layout (no curves over 5°).

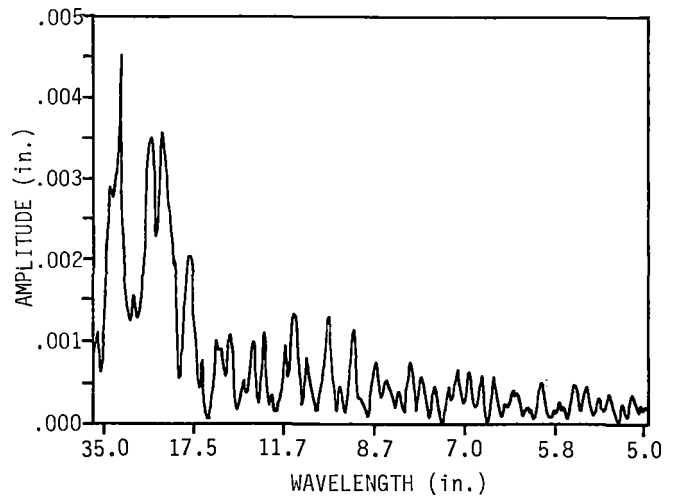


FIGURE 19. HEAD HARDENED INITIAL SURFACE ROUGHNESS.

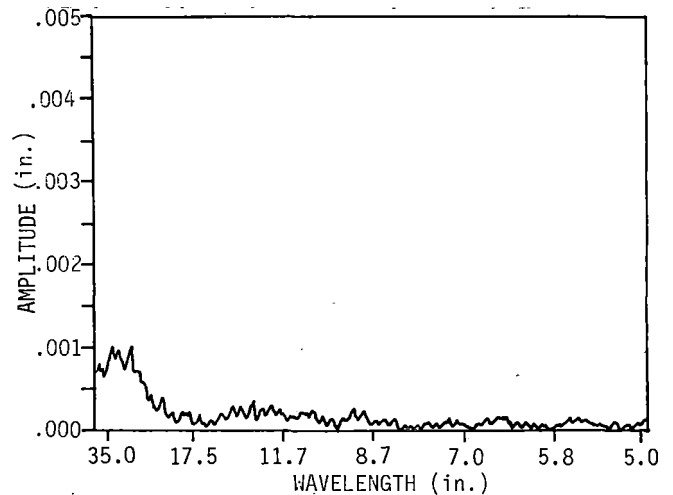


FIGURE 20. STANDARD CARBON INITIAL SURFACE ROUGHNESS.

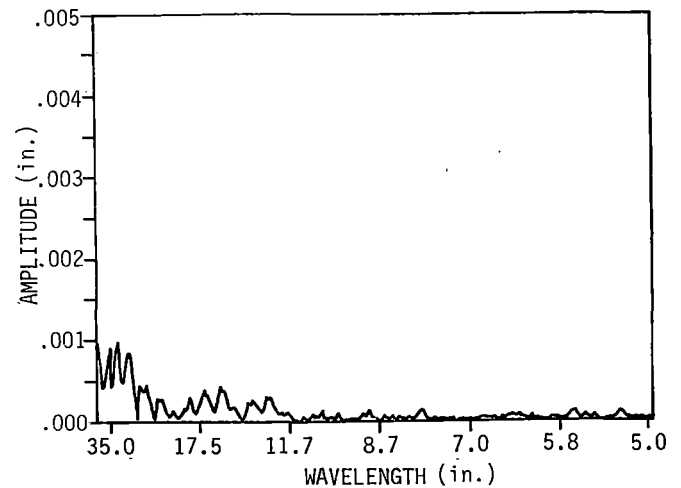


FIGURE 21. CHROME-MOLYBDENUM (A) INITIAL SURFACE ROUGHNESS.

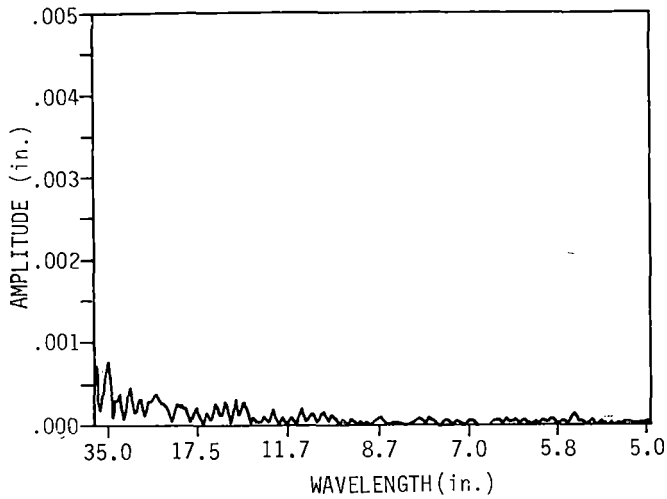


FIGURE 22. SILICONE CHROME INITIAL SURFACE ROUGHNESS.

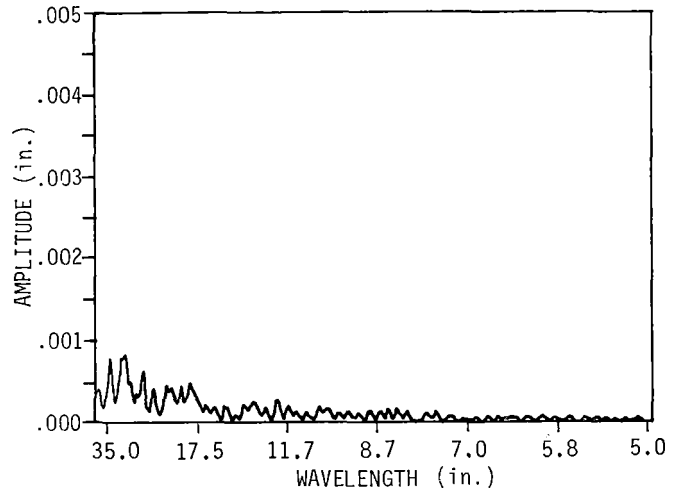


FIGURE 25. FULLY HEAT-TREATED INITIAL SURFACE ROUGHNESS.

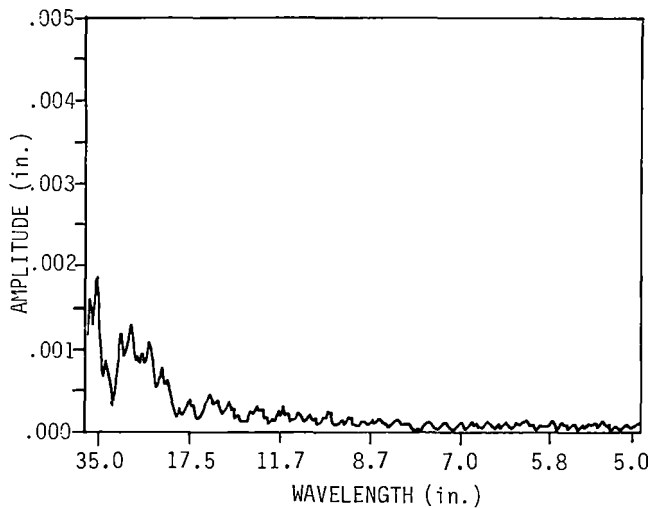


FIGURE 23. 1% CHROME INITIAL SURFACE ROUGHNESS.

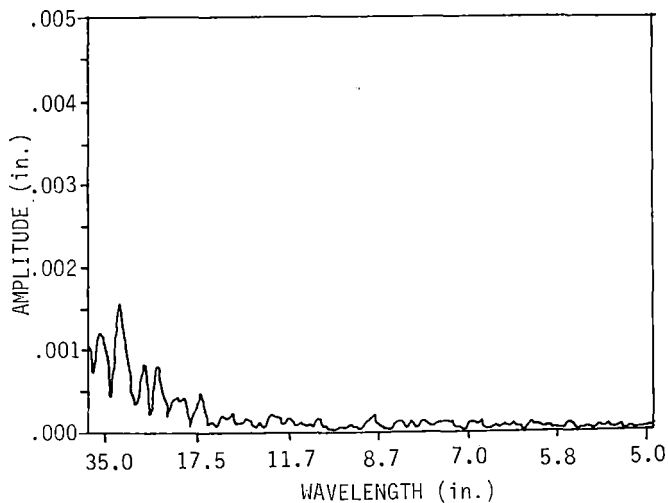


FIGURE 24. CHROME-MOLYBDENUM (C) INITIAL SURFACE ROUGHNESS.

TABLE J. RELATIVE INITIAL SURFACE ROUGHNESS.
(Section 03)

Metallurgy	Initial Surface Roughness Relative to Carbon Rail	Extent Growth Rate (Non-Lube) (%/MGT)
Head Hardened	3	.208
Std. Carbon	1	.749
Silicon Chrome	0.4	.095
1% Chrome	0.4	.308
Chrome Moly-C	0.3	.325
Chrome Moly-A	0.2	.263
Fully Heat Treated	0.2	.215

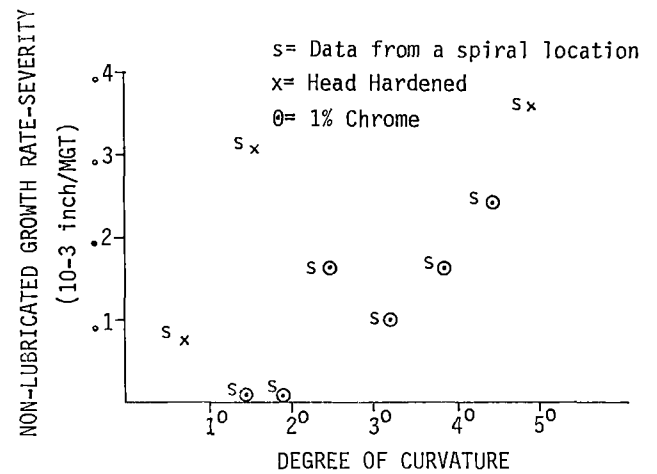


FIGURE 26. EFFECT OF CURVATURE HEAD HARDENED RAIL SECTION 17 - CONCRETE TIES.

Design Track Geometry - Grade:

Corrugation growth relative to track grade is difficult to evaluate in this test. The basic difficulty is that there is no directly comparable test sections where the only variable is grade.

However, we may compare the performance of the same metallurgy located on the 2% grade (Section 17) and the gentler .9% and .1% grades (Section 3) if it is kept in mind that tie type is different in Section 17 (concrete ties) and Section 3 (wood ties).

Table K is a comparison by metallurgy of Sections 17 and 3. Table K shows the average corrugation growth for each metallurgy separately in Section 3 and Section 17. For each measurement (severity and extent) and each lubrication condition.

Generally, no statistical difference exists between growth rates in the two sections for the same metallurgy. Where differences in performances are seen (head hardened - severity, lubricated; silicon chrome - extent), numerical differences are small. The only substantive difference in the growth rates occurred for the silicon chrome rail in non-lubricated condition (extent).

Where no significant growth rate difference exists between Section 3 and Section 17 the values may be

TABLE K. DIFFERENCE BETWEEN SECTION 3 (WOOD TIES, .1 - .9% GRADE) AND SECTION 17 (CONCRETE TIES, 2% GRADE).

Metallurgy	Section 03 Growth Rate Slope	Section 17 Growth Rate Slope	F*	Degrees of Freedom Reg/Resid	F Table	Significant Difference in Growth Rates Between 3 & 17 yes/no
Lubricated Rail, Severity Growth (Inches x 10 ⁻³ /MGT)						
Head Hardened	.0672	-.0037	4.4	1/52	4.0	yes
Silicon Chrome	.0478	.0497	0.0	1/32	4.2	no
1% Chrome	.0672	.0928	0.7	1/31	4.2	no
Non-Lubricated Rail, Severity Growth (Inches x 10 ⁻³ /MGT)						
Head Hardened	.3919	.2429	1.3	1/27	4.2	no
Silicon Chrome	.1468	.2506	2.0	1/16	4.5	no
1% Chrome	.2622	.1996	0.1	1/16	4.5	no
Lubricated Rail, Extent Growth (Percent/MGT)						
Head Hardened	.1078	.0780	0.7	1/52	4.0	no
Silicon Chrome	.0970	.0358	10.2	1/32	4.2	yes
1% Chrome	.1110	.0785	2.2	1/31	4.2	no
Non-Lubricated Rail, Extent Growth (Percent/MGT)						
Head Hardened	.2470	.1817	1.0	1/27	4.2	no
Silicon Chrome	.0950	.2644	17.2	1/16	4.5	yes
1% Chrome	.3129	.3031	0.0	1/16	4.5	no

averaged together to give a corrugation growth rate representative of the given metallurgy (Tables C, D, E, F).

Conventional wisdom that steeper grades are a more severe environment (higher traction/braking) leads us to the expectation that corrugation growth should be worse on the 2% grade in Section 17. Further, some industry personnel observe that concrete ties contribute to accelerated corrugation rates which would aggravate the already "severe" environment in Section 17.

However, we do not observe any consistent difference in corrugation growth between the steeper grades in Section 17 and relatively flat grades in Section 3, even with the difference in tie type, which should contribute to even greater differences.

Therefore, track grade has no influence on corrugation growth rates.

Gage and Superelevation:

Track parameters and metallurgy properties have been evaluated independently up to this point in the report. However, the assessment of gage and superelevation demands that the interdependence of all parameters be recognized.

This evaluation will establish relationships between track geometry and rail contact stress.

The basic concept employs work by Mair (Ref. 12) in which a steel 0.2 percent yield stress is sought to resist maximum applied contact stresses.

We wish to reformulate that thought slightly to determine whether a given yield stress is exceeded by applied contact stresses. That is:

$$\text{Condition for yielding: } \frac{\sigma_{\text{app}}}{\sigma_{\text{allow}}} \geq 1$$

where σ_{app} = applied maximum normal stress (psi)
 σ_{allow} = maximum allowable normal stress for a given steel.

Our hypothesis is that a severe condition for corrugations exists if the ratio $\sigma_{\text{app}}/\sigma_{\text{allow}}$ is equal to or greater than 1.

Mair provides the following relations

$$\sigma_{\text{app}} = \left(\frac{.16 E P}{(1 - \nu)rw} \right)^{1/2}; \quad \sigma_{\text{allow}} = 2.31 (1 - \mu)Y$$

where E = Young's Modulus $\cong 30 \times 10^6$ psi
P = Applied wheel load

ν = Poisson's ratio $\cong .3$
r = roll radius $\cong 18$ inch
w = width of contact patch $\cong .5$ inch
 μ = coefficient of friction $\cong .20$, non-lubricated
Y = rail yield stress (psi)

σ_{app} is based on the Hertz formula, σ_{allow} is based on von Mises yield criterion, the effect of tangential slip on the limit of elastic behavior and on the shakedown limit (loading limits for yield).

The unknowns are the rail yield stress, Y, and the applied load, P.

The rail yield stress is estimated from Brinell hardness data

$$y.s. \text{ tension} = \frac{BHN}{6} \text{ (1422 psi/kg mm}^2\text{)}$$

from Tabor (Ref. 17)

The applied load, P, is for our purposes, the vertical wheel/ rail load at the low rail. Appendix A illustrates the relationships and nomenclature for estimating the applied low rail load. The resulting relation for low rail load is a function of gage, superelevation, degree of curvature, and vehicle velocity. Measurements for each parameter are taken by an EM-80 Track Geometry Car at the same time as other corrugation data. The loads predicted by this approach are within 2% of mean low rail loads measured at FAST.

Figure 27 plots the stress ratio ($\sigma_{app}/\sigma_{allow}$) for the various metallurgies against corrugation growth rates.

Figure 27 demonstrates that track geometry parameters contribute in a complimentary fashion to increase the probability of corrugations by increasing the applied stress on the low rail.

The original hypothesis that a high incidence of corrugation will occur if the stress ratio $\sigma_{app}/\sigma_{allow}$ exceeds a value of 1 is confirmed.

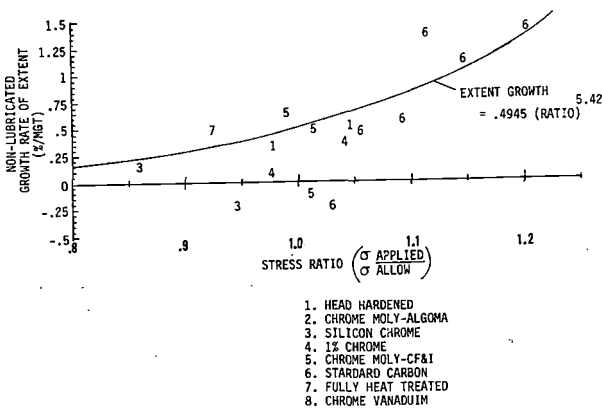


FIGURE 27. CORRUGATION GROWTH WITH RAIL STRESS RATIO

The relative effect of each of the parameters can be assessed using the relationships established in this analysis.

The principal influences are summarized:

- o The rail yield stress is the single most important parameter controlling the stress ratio
- o Increasing gage will increase the load on the low rail, but the effect is very weak (a gage increase of .5 inch will increase the low rail load less than 1%)

- o Increasing the speed relative to the superelevation (or reducing the superelevation relative to the speed) will reduce the low rail load. The effect of changing the superelevation/speed relationship is stronger than that for gage because the velocity term is squared. A change in the parameters is only recommended when the existing condition is marginally within the corrugation risk condition (i.e., stress ratio is .85 - .90, using .2% yield stress). The various situations involving traffic requiring different curving speeds (station entry, passenger vs freight) are known corrugation prone locations which is caused by the lower speed traffic based on this analysis. As additional proof of this point, the speed profile in Section 17 is distinctly different, shown in Figure 28, for the clockwise and counterclockwise direction (due to the steep grade). The data from the lower speed range describes the stress ratio in Figure 27 better than either of the high speed range or an average of the high and low speeds.

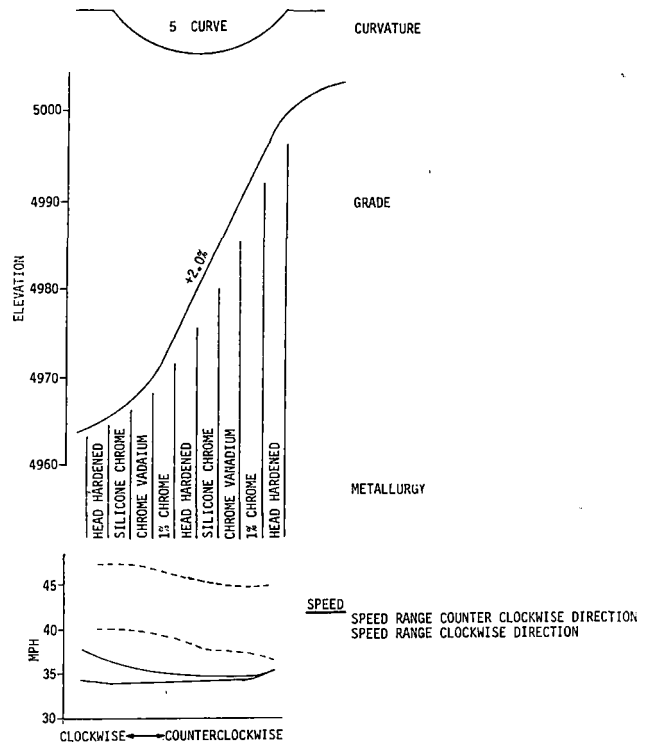


FIGURE 28. SECTION 17 TRAIN SPEED PROFILE.

False flange contact on the rail head as a result of wide gage is frequently cited as a cause of corrugations. The FAST consist contains few wheels with false flanges, yet corrugations have formed in abundance. Figure 29 shows a heavily worn profile for FAST. We conclude that the presence of a false flange is not a necessary condition for corrugation formation.

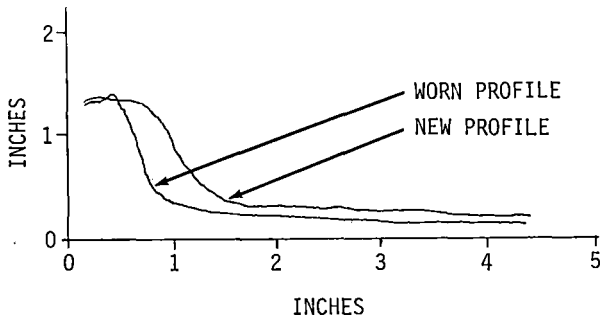


FIGURE 29. FAST WHEEL PROFILES, NEW AND WORN.

EFFECTS OF TRACK MODULUS

Track modulus is related to the dynamic response of the track.

Figure 30 is a plot of the track modulus with corrugation growth divided into lubricated and non-lubricated data groups.

It is evident from this plot that the data scatter is too great to draw any correlation between track modulus and corrugation growth.

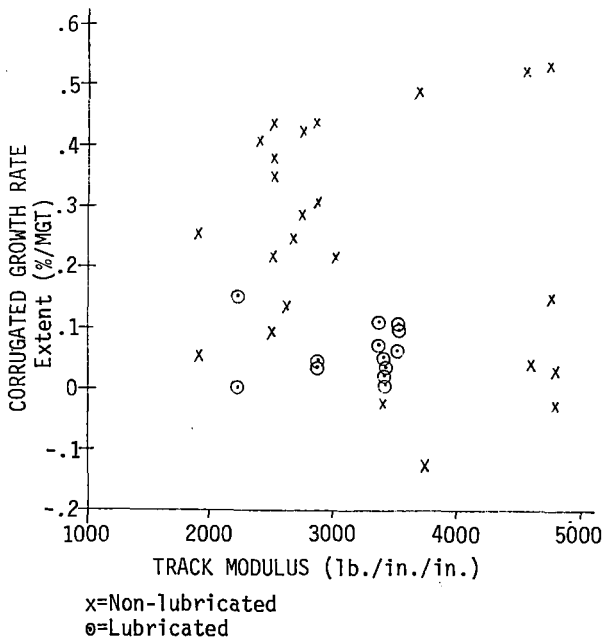


FIGURE 30. TRACK MODULES AND CORRUGATION GROWTH.

EFFECTS OF TIE TYPE

Earlier statistical results on the comparison of track grades was also a simultaneous comparison of concrete vs wood tie.

Informal observations by industry personnel suggest that corrugation growth is greater on concrete ties than on wood ties. The FAST experience contradicts those observations, based on the comparison referred to above. However, there could be aspects of the wood tie vs concrete tie comparison which would be evident in revenue service and not at FAST.

The concrete tie adds substantial mass to the track, directly effecting the track dynamics. Also, the concrete tie has different resonating frequencies than the wood tie. We will review briefly the latter.

The resonating frequency of interest is that which produces the corrugation wavelength. This frequency can be found by multiplying the observed wavelength of corrugations on the rail by the train speed. This exercise produces estimated corrugating frequencies of 108 Hz in the wood tie section and either 110 Hz or 89 Hz on concrete ties (remember there are two different operating speeds on the concrete ties caused by the grade and train direction on the grade).

The natural, or resonant, frequency of the wood and concrete ties installed at FAST are given in Table L.

TABLE L. TIE RESONANT FREQUENCIES.

Tie Type	Natural Frequencies (Calculated)
Wood	87 Hz
Concrete (Mfr. A)	92 - 163 Hz
Concrete (Mfr. B)	103 - 112 Hz

It appears from Table L that if concrete ties had a significantly greater contribution to corrugations than wood ties it would be because the concrete tie natural frequency occurs at the same natural frequency as the corrugating mechanism (whatever it may be) whereas the wood tie does not, at least not so precisely.

TRACK MAINTENANCE AND CORRUGATIONS

This section will discuss corrugation effects on track maintenance.

The cost of corrugations is unknown. Nearly every introduction to the rail corrugation problem associates rail removals, rail grinding and undocumented losses such as freight damage, track instability and loss of track geometry with rail corrugations. The perception of damage is real, but accurate cost related assessments of corrugations' effects are non-existent.

This evaluation intends only to estimate increases in track maintenance caused by rail corrugations.

Raw FAST maintenance manhours are not directly relatable to specific industry use. Every operating railroad establishes different operating policies and practices. FAST cannot, and does not, intend to replicate every deviation in application. However, since the practices used are uniform to FAST, relative comparison between test sections is valid. (Maintenance for experimental purposes has been removed from the data.)

Track maintenance at FAST is dictated by FRA Class 4 as a minimum operating condition; the rail corrugation experiment imposed no restrictions regarding the method or timing of maintenance.

In order to assess whether any relationship exists between corrugations growth and track maintenance, corrugation growth (severity, extent) is overplotted with total accumulated track maintenance against MGT in Figure 31.

Figure 31 shows that the increment in total maintenance manhours closely parallels corrugation extent measures and, to a lesser degree, severity measures.

Also in Figure 31 are the accumulated manhours for various types of maintenance: joints, tamping and lining, and rail. The sum of these three curves at any point equals the total maintenance curve

The consistency of this plot provides an indication that corrugations do effect maintenance and the effect is immediate. That is, there is no time delay between the corrugating effects and the need for maintenance.

More importantly, it is not the level of corrugations that generates maintenance, rather it is the rate of growth of corrugations that appears to stimulate maintenance. Based on this observation we can evaluate the parallel growth rate of corrugations and the rate of accumulation of maintenance.

Figures 32 and 33 show maintenance manhours per MGT (for 200' of track) as a function of corrugation extent growth rate in the same period. The data has been segregated into lubricated and non-lubricated periods. Data is taken from the wood tie test sections only. The severity growth rate, as shown in Figure 31, is not a good predictor of maintenance.

Figures 32 and 33 show that high corrugation rates generate significant maintenance during non-lubricated periods and that the maintenance increases at least as a cube power of the corrugation extent growth rate.

Before discussing the maintenance demand further, Table M compares the extent growth rates from Table I with the maintenance rates from Figures 32 and 33.

In Table M, several data points considered to be outliers are not included in the relationships shown for maintenance with corrugations (outliers are noted in Figures 32 and 33). Further, the data population is small, therefore extensions to revenue service are somewhat risky.

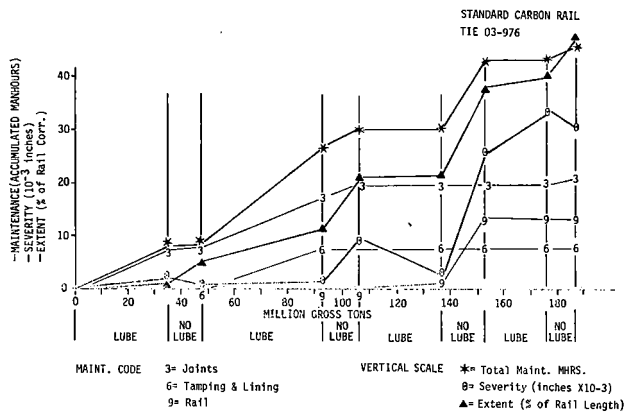


FIGURE 31. TRACK MAINTENANCE AND CORRUGATION GROWTH.

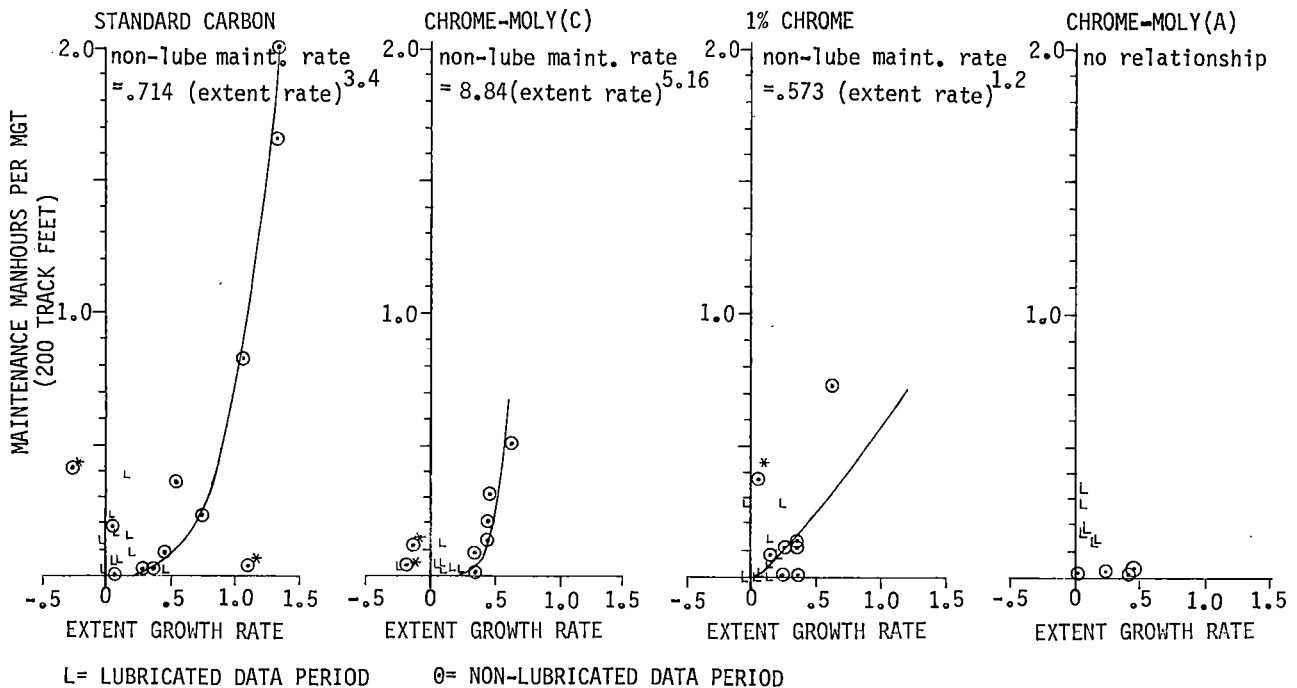
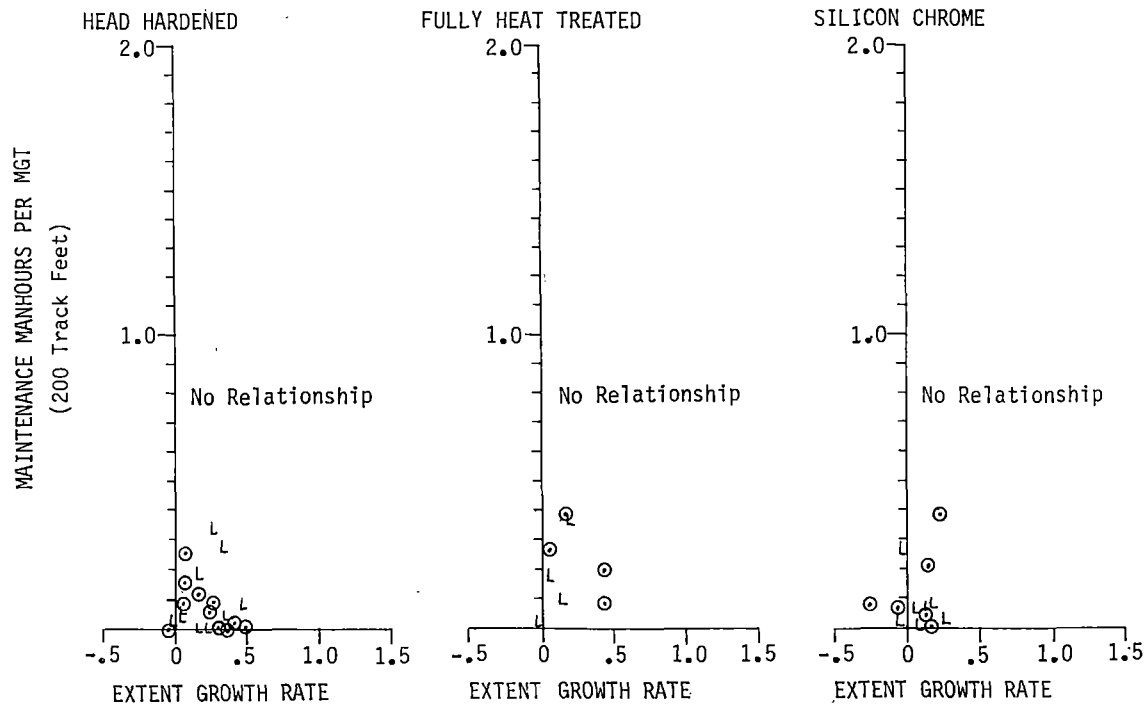


FIGURE 32. EFFECT OF CORRUGATION GROWTH ON MAINTENANCE SECTION 03: WOOD TIES, 0.1% - 0.9% GRADE. *DATA POINTS CONSIDERED AS OUTLIERS.



L= Lubricated Data Period O= Non-Lubricated Data Period

FIGURE 33. EFFECT OF CORRUGATION GROWTH ON MAINTENANCE
SECTION 03: WOOD TIES, 0.1% - 0.9% GRADE.

TABLE M. COMPARISON OF RAIL CORRUGATION GROWTH (EXTENT)
WITH MAINTENANCE ACCUMULATION
(NON-LUBRICATED)

Metallurgy	Extent Growth (%/MGT)	Statistical Rank (From Table I)	Non-Lubricated Maintenance Relationship
Silicon Chrome	.095	1	No Relationship
Head Hardened	.208	2	No Relationship
Fully Heat Treated	.215	2	No Relationship
Chrome Moly-A	.263	2	No Relationship
1% Chrome	.308	2	MHR/MGT = .573 (Extent Growth) ^{1,2}
Chrome Moly-C	.325	2	MHR/MGT = 8.84 (Extent Growth) ^{5,16}
Standard Carbon	.749	3	MHR/MGT = .714 (Extent, Growth) ^{3,4}

The conclusions are:

- o Corrugations effect total track maintenance, but only under non-lubricated high rail conditions.
- o The level of corrugations is not a factor in increasing maintenance demand. Rather, the rate of corrugation growth is the principal cause of increased maintenance.
- o Total track maintenance increases at least as a cube power of the corrugation.
- o Remedial maintenance for corrugations should be implemented if the extent growth rate exceeds 0.5% per MGT to avoid highly accelerated maintenance demand.
- o All of the heat treated metallurgies had corrugation growth rates low enough that no significant increase in maintenance is observed.

However, the consistency of maintenance rates with corrugation growth rate rankings, shown in Table M, substantiate that higher corrugation rates increase the maintenance rates.

The corrugation growth rate above which maintenance begins to accelerate is about 0.5% of the rail length per MGT. That is, if new corrugations are generated at a rate of more than 0.5% of the curve length (or other measure of total track length which is prone to corrugation) per MGT, then immediate maintenance measures are desirable.

From Figures 32 and 33, high rail lubrication minimizes, if not completely nullifies, the effect of rail corrugations on track maintenance.

Also, the growth rates of all heat treated metallurgies were at a slow enough rate that corrugations caused no noticeable increase in maintenance.

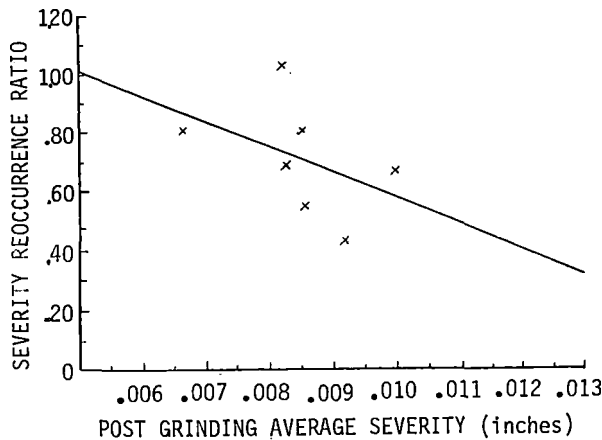
RAIL GRINDING

The preceding discussion provided a criteria for "when to grind?" (when corrugation extent growth exceeds 0.5%/MGT of a given curve.)

"How to grind?" is a frequent question.

The FAST experiment included grinding trials using grinding depth as the test variable. Figure 34

shows the reoccurrence rate of corrugations as a function of grinding depth.



$$\text{Severity Reoccurrence Ratio} = \frac{\text{Growth Rate Before Grinding}}{\text{Growth Rate After Grinding}}$$

FIGURE 34. GRINDING DEPTH VS REOCCURRENCE RATE.

Figure 34 shows that the average remaining batter, corrugation or other rail non-uniformity after grinding must be 0.005" deep (or less) to reduce subsequent corrugating rates to that observed prior to grinding. Otherwise corrugations will return at a higher rate.

Because data points are limited and somewhat scattered, an obvious recommendation is to grind corrugations and weld batter such that no surface deformity remains after grinding. There is no evidence to suggest that overgrinding (grinding deeper than the maximum deformity) has any benefit.

Grinding techniques generally applied in North American Railroads attempt to reprofile the rail cross sectional shape to that of the original profile. This practice was followed at FAST (except that the maximum angle from vertical that the FAST equipment can attain is 30° which leaves a square at the field and gage corners).

An alternate grinding approach is used by the Australians which is proven to reduce wear, rail failures and curving resistance of the train. No claim is made regarding the technique's benefit to reducing corrugation development, so no further discussion is warranted. For those interested, References 24 and 25 describe the theory and practice of this technique.

REVIEW OF CORRUGATING THEORIES

Formulating a comprehensive corrugation mechanism theory is beyond the scope of this paper. However, our understanding of corrugations can be enhanced by reviewing some of the outstanding technical work in this area.

In this review, we choose to cite work which either forms the most well-developed theory or is frequently referenced in the literature. The background sources chosen are those providing the most comprehensive technical explanation of the subject matter.

Corrugation formation theories have a common interest in identifying the variables describing the wheel rail contact environment. The "patch" formed by the contact of the wheel and rail is a complex modification of Hertzian theory. Kalker¹⁸ presents a complete review of contact theory. These contact forces at the mating surfaces are dependent on the complex mechanics of vehicle curving, described by Elkins¹⁹ and by Cooperrider and Law.²⁰

The theories of corrugating mechanisms fall into two broad categories: (1) wear mechanisms and (2) system vibrations (wheel/rail instabilities).

In the category of wear mechanisms, two theories are noted: first, wear from hydrodynamic pressure in fatigue cracks and second, wheel/rail stick-slip.

Corrugations caused from wear flakes created under hydrodynamic pressure of lubrication infiltrating fatigue cracks on the rail surface has been introduced in the section "Differences Between Lubricated and Non-Lubricated Corrugation Growth." Since FAST does not accumulate an appreciable amount of lubricant on the low rail, the theory cannot be objectively evaluated. Corrugations did form in the absence of lubrication on the low rail. Further, corrugation formation where lubricant is present has not been sufficiently documented in revenue service to substantiate this theory.

While lubricant on the head of the low rail may accelerate corrugation growth, the presence of lubricant on the head of the low rail is not a sufficient condition for corrugation formation.

"Stick-slip" is the second wear theory associated with corrugations. The hypothesis generally states that uniform rolling of both wheels on the same axle is inhibited by non-uniform resistance between wheels. Depending on the theory, either flange contact, unequal rolling radii or contact force imbalance, an additional resistance is created on one wheel which is not present at the other wheel and since the wheels are connected by a solid axle, one wheel must slide to catch up to the other.

The first of the stick-slip theoreticians, King and Kalousek,⁴ state that a "stick-slip" effect results from the fact that the wheel set acts as one piece and the wheel on the high rail must travel further than the one on the low rail during curve negotiation. Assuming that the effective radius is the same for both wheels, the wheel on the high rail would be forced to rotate more than the wheel on the low rail. This differential in wheel revolutions places the axle in torque until the adhesion forces at the wheel/rail interface become insufficient on either high or low rail resulting in a "slip effect".

A more scientific approach is taken to the same theme by Rajkumar.²¹ Using a field validated vehicle curving model, it is shown that the effective rolling radii difference is not equal and that either wheel may be the "lagging" wheel depending on

friction on each rail. Where both rails are dry, the low rail wheel will slip. Where the high rail is lubricated the high rail wheel will slip. This set of mechanics is purported to support a "mild" slip corrugation mechanism coupled with a plastic deformation corrugating process observed by T. J. Devine, et. al.¹⁴ and by Harrison and Johnson.¹⁶

The period of predicted stick-slip is very close to the wavelengths of corrugations at FAST, using FAST track, vehicle and train operations as input to the model.

However, this model implies corrugations should occur on every railroad curve. This, obviously, is not true.

Maintaining the thread of thought that corrugations are an oscillatory mechanism of the wheel relative to the rail, we search for a set of ideas that explain the uniqueness of a section of corrugating track which segregates it from its neighboring track that has the same nominal characteristics, in all respects, yet does not corrugate. This set of circumstances, found too frequently in revenue service, may be rooted in the more complex world of dynamic response of the system.

Dynamic systems are the collection of connected components which respond to inputs to the system. A system of independent elements performing in unison are "stable". When components move out of unison the system is "unstable".

Two approaches are presented here that appear to have significant merit in explaining corrugations. The first, by Clark, Newton, and Elkins²² includes all elements of the track and vehicle from the unsprung mass of the wheel down through the ballast to affect a solution which in essence finds that the maximum contact force amplitude is associated with rail vibrations over the tie. That is the tie affects rail vibrations and in turn increments the wheel/rail contact force. This work alerts us to the importance of the tie, rail, wheel as a system, and the theoretical work is substantiated by field measurement. The theory suggests that corrugation initiation, or at least heaviest corrugations would occur, over a tie.

Unfortunately, corrugations do not initiate exclusively over ties at FAST. Also, the amplitude of corrugations did not increase with a pattern consistent with tie locations.

The last theory combines the dynamic relations of the structural elements of the track and the unsprung mass with the surface geometry (roughness) of the rail to formulate an exquisitely clever statistical approach to wheel/rail contact. The author of this theory, Nayak,²³ implies that contact forces can be generated under the yield stress at corrugating frequencies because the frequency of occurrence is high as a result of oscillations in the contact, the material may then fatigue producing the observed metal flow. The author documents the short-comings of the results, not the least of which is the fact that the model only considers vertical plane vibrations.

It is extremely important that the work referenced

in the preceding paragraphs should be considered as valuable source material for research on corrugations. The negative comments concerning each theory are intended as a balance to show that the complete mechanism of corrugations has not yet been discovered.

SUMMARY

The conclusions of this report are:

- o Corrugation growth is linear within each lubrication condition.
- o High rail lubrication significantly reduces corrugation growth on all metallurgies except Chrome Molybdenum-C.
- o Rail metallurgy is a significant factor in non-lubricated corrugation growth.

In Section 03 (45 mph, .1%-.9% grade, wood ties), silicon chrome had the lowest corrugation growth rate; standard carbon rail had the highest growth rate.

In Section 17 (35 to 50 mph, 2% grade, concrete ties), silicon chrome, 1% chrome, and head hardened metallurgies had lower growth rates than the chrome vanadium rail.

- o Rail head hardness measurements show a consistent inverse relationship with corrugation growth.
- o High rail lubrication essentially eliminates the non-lubricated differences between carbon rail and premium metallurgies.
- o No rail corrugation development was observed for metallurgies work hardened to greater than 422 Brinell, which converts to a yield stress of 790 MPa (114,547 psi) for 100 ton car loading such as at FAST.
- o Little or no corrugation development is expected for metallurgies with yield stress of 670 MPa (97,175 psi), confirming Australian estimates by Mair and Groenhout.
- o Rail head hardness does not vary consistently with corrugation peaks and valleys.
- o Metallurgical transformations at the rail surface, such as the white etching layer, have no causal influence on corrugations.
- o A rail surface anomaly the shape of a low weld is not a sufficient condition for the initiation of corrugations if other track parameters of surface, line and gage are tightly controlled.
- o There is no relationship between initial rail surface roughness and future corrugation growth.
- o Corrugations growth rates appear to increase with increasing track curvature.

- o Corrugation growth is no different on 2% grade than that on a .9% or .1% grade. No difference is observed between concrete and wood ties.
- o Low rail stress ratio ($\frac{\sigma_{app}}{\sigma_{allow}}$) greater than .85 (using .2% offset yield) are highly conducive to corrugation formation and the corrugation growth rate increases non-linearly with stress ratio.
- o The rail yield stress is the single most important parameter controlling stress ratio.
- o Increasing the gage will increase the low rail load, but the effect is small.
- o Increasing the speed relative to the superelevation (or reducing the superelevation relative to the speed) will reduce the low rail load.
- o False flange contact on the top of the rail head is not a necessary condition for corrugation formation.
- o No correlation could be found between track modulus and corrugation growth.
- o Track maintenance increases non-linearly as a function of corrugation extent growth rate above .5% MGT. Track maintenance appears to be independent of any corrugation absolute level.
- o Rail lubrication completely negates the above correlation of corrugations with maintenance.
- o Rail should be ground, such that the remaining maximum amplitude of any surface deformation is .005" or less. Remaining corrugation depths greater than .005" increases the rate of corrugation reoccurrence over the growth rate observed prior to grinding.
- o Major theories of corrugation mechanics are reviewed and each theory, while aiding our understanding of the problem, is not universally consistent with observed corrugation development.

The above conclusions are a tremendous step forward in the understanding of corrugation growth. While the corrugating mechanism is still not fully understood, these results provide railroads with corrugation treatment techniques which greatly increase the productivity of money spent on corrugations.

Recommended treatment techniques to reduce corrugation growth are:

1. Lubricate the high rail of curves.
2. If corrugation elimination is sought using premium metallurgy, specify a metallurgy with a minimum yield stress of 97,000 psi.
3. When the extent growth rate (% of the length of curve) is above 0.5% per MGT, immediate remedial track maintenance is recommended.
4. When grinding, remove corrugations to the point when the maximum remaining surface anomaly is less than .005" deep.

5. Maintain the track and control the operating speeds such that a low rail stress ratio of .85 is not exceeded.

Results imply that maintenance of the track to the highest possible standard reduces the probability of corrugation occurrence. This generates a trivial recommendation since we safely assume that railroads maintain their track to the highest level permissible by available economics.

These results provide new insight into corrugation development and into management of corrugations. However, the results suggest further research.

Recommended future research includes:

1. Description of wheel/rail contact forces through modeling of the vehicle/track system.
2. Better understanding of metal wear and fatigue mechanisms.
3. Accurate characterization of component material properties and of component design properties (stiffness, mass, elasticity).

ACKNOWLEDGEMENTS:

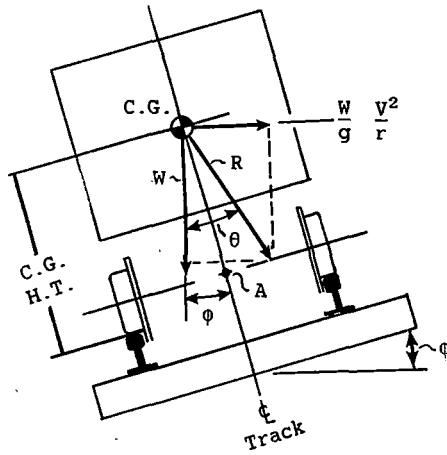
The authors express their deepest appreciation to Mr. T.J. Devine, Griffin Wheel Co., FAST Rail Corrugation Experiment Manager, for his intelligent development of this experiment. The authors also wish to acknowledge significant contributions of B.R. Rajkumar, R. Margasahayam, and J.A. Gardner. Finally, the individuals at FAST who manage and collect data are expressly thanked for their patience, dedication and skill.

REFERENCES

1. R. K. Steele and R. P. Reiff, "Rail: Its Behavior and Relationship to Total System Wear", FAST Engineering Conference Proceedings, pp. 116, 151.
2. K. L. Johnson and C. G. Gray, "Development of Corrugations on Surfaces in Rolling Contact", Proceedings of the Institution of Mechanical Engineers, Vol. 189, 13/1975.
3. J. Kalousek and R. Klein, "Investigation into Causes of Rail Corrugations", AREA Bulletin 656, p. 429.
4. F. E. King and J. Kalousek, "Rail Wear and Corrugation Studies", AREA Bulletin 658, p. 619.
5. J. Kalousek, Track/Train Dynamics Report #4, Rail Corrugations, CP Dept. of Research Report No. 5488-75, Feb. 1975, p. 61.
6. L. E. Daniels, "Probability Density For Ratios of Variables With Different Population Distributions", Boeing Services International, Inc., Transportation Test Center, _____
7. J. Eisenmann, "Formation of Short Pitch Corrugations in Rails," Heavy Haul Conference, Paper I.6, Melbourne, Australia, 1978.
8. R. I. Mair and R. A. Jupp, "Rail Track for Heavy Unit Train Operation," Annual Engineering Conference, The Institution of Engineers, Townsville, Australia, May, 1976.

9. R. I. Mair, R. A. Jupp, and R. Groenhout, "The Characteristics and Control of Long Pitch Rail Corrugation at Heavy Axle Loads", Heavy Haul Conference Paper No. I.8, Melbourne, Australia, 1978.
10. "The Mechanism of Long Pitch Corrugation Development and Its Implications - A Qualitative Summary", Rail Dynamics Committee, Technical Note 1, 9/1975, Broken Hill Proprietary - Mount Newman Mining Report 75/010, p. 13.
11. P. Clayton and M. B. Pallery, "Metallurgical Aspects of Surface Damage Problems", British Rail, Darby, England, 1980.
12. R. I. Mair and R. Groenhout, "Prediction of Rail Steel Strength Requirements - A Reliability Approach," Rail Steel - Developments, Processing, and Use, ASTM STP 644, D. H. Stone and G. G. Knupp, Eds., American Society For Testing and Materials, 1978, pp. 342-360.
13. E. Moin, "Metallurgical Examination of Corrugated Rail Section," Dr-154 Transportation Test Center Nov. 1981, Pueblo, Colorado.
14. T. J. Devine, L. E. Daniels, N. Blume, "Rail Corrugations at FAST: December 1979 through August 1981," FAST Engineering Conference Proceedings November 1981, Transportation Test Center, Pueblo, Colorado.
15. C. O. Fredick, "The Effect of Wheel and Rail Irregularities on the Track," Heavy Haul Railways Conference, paper G.2, Perth, Australia, 9/1978.
16. D. Harrison, K. L. Johnson, "Final Report of Investigations into Rail Corrugations," Department of Engineering, University of Cambridge, CUED/C -Mech TR15, 1978.
17. D. Tabor, "The Hardness of Metals," Oxford Press, 1951, Page 16. Tabor states that the ratio of ultimate tensile strength to Brinell Hardness $\cong .33$. We have made the further assumption in this paper that the yield strength is $\cong .5$ the ultimate tensile strength.
18. J. J. Kalker, "Survey of Wheel - Rail Rolling Contact Theory," Vehicle System Dynamics 5 (1979), Pages 317-358.
19. Two References
 - A) J. A. Elkins, B. M. Eickhoff, "Advances in Non-Linear Wheel/Rail Force Prediction Methods and Their Validation," British Railways Board, November 1979, ASME Winter Conference, N.Y., 7 December 1979.
 - B) J. A. Elkins, R. J. Gostling, "A General Quasi-Static Curving Theory for Railway Vehicles," Proceedings 5th Vehicle Systems Dynamics - 2nd IUTAM Symposium, held at Technical University, Vienna, September 19-23, 1977.
20. N. K. Cooperrider, E. H. Law, "Rail Vehicle Dynamics - Class & Text, January, 7-11, 1980.
21. B. R. Rajkumar, "Wheelset Torsional Stick-Slip and Rail Corrugations," Transportation Test Center, to be published.
22. R. A. Clark, S. C. Newton, J. A. Elkins, "A Investigation into the Dynamic Effect of Railway Vehicles Running on Corrugated Rails," British Rail Research, Darby, England, unpublished.
23. P. R. Nayak, "Contact Vibration of a Wheel on a Rail," Journal of Sound and Vibration, (1973) 28 (2), 277-293.
24. M. D. Roney, "Meeting the 100-ton Challenge; Report on Heavy Axle Loads in Australia," AREA Proceedings, Bulletin 683, Vol. 82 (1981), June-July.
25. P. H. Townsend, C. J. Epp, P. J. Clark, "Bogie Curving Trials, Rail Profiling and Theoretical Modelling to Reduce Rail Deterioration and Wheel Wear on Curves." Heavy Haul Railways Conference, Perth, Western Australia, 9/1978, National Library of Australia ISBN 090942112.

APPENDIX A.



$$R = \sqrt{W^2 + \left(\frac{W}{g} \frac{v^2}{r}\right)^2}$$

$$\theta = \text{Tan}^{-1} \left(\frac{\frac{W}{g} \frac{v^2}{r}}{W} \right) = \text{Tan}^{-1} \left(\frac{v^2}{gr} \right)$$

where $W = \text{Weight @ one axle}$
 $\approx 66000 \text{ lb}$

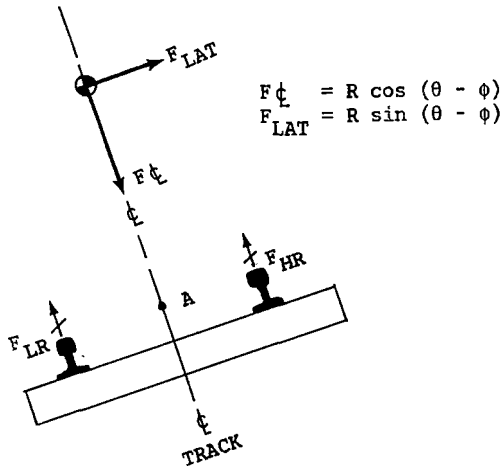
$v = \text{Vehicle velocity (fps)}$

$g = 32.2 \text{ ft/sec}^2$

$r = \frac{50 \text{ ft}}{\text{Sin } (\frac{1}{2} \text{ Deg Cu})}$

$$\phi = \text{Tan}^{-1} \left(\frac{\text{Superelevation (inch)}}{\text{Gage} + \text{Rail Hd. Width}} \right)$$

Resolve R into components thru \perp Track, F_{\perp} ,
 and perpendicular to \perp Track, F_{LAT}



$$F_{\perp} = R \cos (\theta - \phi)$$

$$F_{\text{LAT}} = R \sin (\theta - \phi)$$

Sum Forces perpendicular to tie and Sum Moments about A,
 Solve for Low Rail Reaction, F_{LR} :

$$F_{\text{LR}} = \frac{F_{\perp}}{2} - F_{\text{LAT}} \left(\frac{\text{C.G.Ht.}}{G} \right) = P$$

where $G = \text{Track Gage} + \text{Tread Width}$

Tan Licheng

Associate Research
Professor in China
Academy of Railway
Sciences, M.Sc. in
Moscow Institute of
Transport Engineering,
USSR, 1955

The Investigation on Wheel/Rail Interaction and Rail Corrugations

This paper presents a theory which describes the main causes of short wave and long wave corrugations. The key problem is to eliminate relaxation vibration of wheelset on track, to reduce or avoid rail corrugations. Finally, suggestions and problems for further research are put forward.

NOMENCLATURE

B	braking force, kg
F	inertia force, kg
K	braking shoe pressure, kg/cm ²
M	braking torque, kg·cm
r	radius of wheel, cm
u	creepage, %
v	velocity of train, km/hr
W	wheel load, T
	angle of wheel rotation, rad/s

SUBSCRIPTS

1. right or inner wheel
2. left or outer wheel

INTRODUCTION

Rail corrugations have been a very complicated issue concerned in railroad all over the world. As early as in the year 1895 the research work was started. Lots of papers and materials were published and many of the writers approached the subject from different angles. All of these have made a significant contribution to working out the problem eventually. Nevertheless, there exist quite a many different schools of thought throughout the world and so far none of the theories on the causes of either short wavelength or long wavelength corrugations has been widely accepted or proved to be efficient. It is, therefore, still the question that railroad engineers and research workers are working hard for. Evidently, while a train runs over a section of corrugated track, the result is serious ---- not only noise and vibration but also locomotive and rolling stock destruction can be caused, and even safe driving can be disturbed, thus leading to the increase of transport expenditure. The method of renovation nowadays is either grinding or replacing the old rails with new ones. It is beyond doubt that the question discussed is of great economical significance.

Corrugations are divided into two types, short wavelength corrugations and long wave-

length corrugations. The former has a pitch about 30-80 mm and the latter 200-600 mm. It is sometimes of a definite periodicity, but mostly of random process. The research work in various nations, therefore, has been concentrating on explaining the reasons which bring about corrugations of long wavelength and short wavelength and studying them respectively [1]. The directions of research are described in many papers. They are roughly known as follows:

studying the original non-smooth-going caused by rail straightener itself;

considering the material and composition of rail and the technology of heat treatment; under the viewpoint of residual stress of rail; and

studying the contact vibration of wheel and rail.

Many writers do the work with a viewpoint of studying the vibration of wheel/rail system, probing into the torsional vibration of wheel set, the vibration of wheel disc and the natural frequency of track vibration. Besides, some of the writers also study the influence caused by ultrasonic vibration of rail.

Many writers suggest that because of the different distances covered by outer wheel and inner wheel while passing through a curve, stick-slip happens and thus bringing about corrugation.

In addition to those stated above, there are still other considerations such as the influence due to sleeper interval and track elasticity, etc.

On the First International Heavy Haul Railway Conference, three articles deliberating rail corrugation were raised [2, 3, 4].

In our country, the problem of rail corrugations had been discovered after sixties, and recently, serious rail corrugations have been found on the outer rail on long and steep down grade section with small radius of curvature ($R = 300m$), especially in mountain regions. This is very disadvantageous to safe-driving and results in the deep concern of the question. [5, 6]

STUDYING OF CORRUGATION MECHANISM ON THE STANDPOINT OF WHEEL/RAIL INTERACTION.

We consider that the occurrence and development of corrugations (including plastic fluidity of metal) have much to do with the interaction and variation of interaction between wheel and rail.

It is known there exist vertical, longitudinal and lateral interaction forces between wheel and rail. Lateral force produces during hunting and curve negotiation while longitudinal force during tractive force of various kinds of locomotives is brought into action.

Studying rail corrugations, the action on rail by wheels of various kinds of locomotives and rolling stocks together with the reaction on wheels by rail, i.e. the situation of wheel tread, should be fully considered simultaneously.

In short, the first thing to do is to study wheel/rail action, and then locomotives rolling stocks, track and materials, technology as well.

SITE INVESTIGATION

Based on the above standpoints, while carrying out site investigation we not only directly measured rail corrugations, but also went to steam-, diesel- and electrical-locomotive depots as well as passenger and freight car depots to inquire about the states of locomotive braking and traction, and tread of various kinds of wheels.

(1) Investigation On Rail Corrugations.

Owing to the fact that most corrugations occur on long and steep down grade with small curve in mountain regions, we did several investigations in such districts and made practical measurements of corrugations there. The following tables 1 and 2 present the measured data on two pieces of corrugated rail as examples.

Table 1

Trough/Pitch of Rail Corrugation

Slope %	Radius of Curvature R(m)	Superelevation h(mm)	Speed of Train v(km/hr)	Rail
15.4	300	90	Passenger, Freight Car 70 Car 55	Outer Rail
Trough (mm) Pitch (mm)	0.98/255, 0.70/245, 0.66/300, 0.06/315, 0.74/295, 1.36/340, 0.38/205, 0.67/245, 0.51/325, 0.24/425, 0.20/240, 0.14/245, 0.36/320, 0.43/235, 0/110, 0.38/195, 0.40/360, 0/120, 0.36/225, 0.33/255, 0.35/240, 0.14/265, 0/270, 0.30/165,	1.12/455, 0.68/370, 1.32/480, 0.91/290, 0.97/385, 1.06/390, 0.35/255, 0.58/370, <u>0.34-0.17*</u> 490 0.17/365, 0.51/290, 0.32/225, 0/175, 0.20/110, 0/320, 0.25/170, 0.50/190, 0/145, 0.17/145, 0.35/225, 0/130, 0.26/170, 0.46/202, 0/315,	0.88/340, 0.66/300, 0.20/190, 0.68/275, 0.45/300, 0/350, 0.57/320, 0.57/265, 0.73/265, 0.61/370, 0.28/190, 0.32/345, 0.26/235, 0.48/255, 0.24/220, 0/305, 0.07/185, 0/410, 0.31/215, <u>0.67-0.12*</u> 370 0/110, 0.41/170, 0.12/405, 0.29/255,	

* Within the range of the full corrugation wave 490 mm and that of the full corrugation wave 370 mm pitch two troughs were observed in each case.

Corrugation Interval of Rail

Table 2*

Slope %	Radius of Curvature R(m)	Superelevation h(mm)	Speed of Train v(km/hr)	Rail
18.1	300	90		Outer Rail
Corrugation Interval (mm)	45, 45, 45, 40, 40, 65, 40, 45, 40, 30, 30, 45, 60, 45, 45, 20, 20, 30, 45, 40, 35, 35, 45, 30, 35, 55, 45, 45, 45, 35, 40, 40, 30, 30, 40, 35, 40, 45, 30, 35, 35, 35, 40, 35, 50, 35, 50, 45, 30, 40, 45, 45, 30, 35, 45, 35, 25, 35, 25, 35, 20, 35, 30, 45, 55, 30, 25, 35, 25, 25, 40, 40, 35, 40, 30, 25, 30, 30, 30, 40, 40, 40, 45, 35, 32, 31, 25, 27, 25, 25, 30, 35, 53, 35, 32, 37, 25, 40, 35, 35, 40.			

* The rail measured is a long quenched one. On the top surface of rail exist local small shellings at intervals shown in the table with depth about 0.07 mm.

(2) Preliminary Analysis on Rail Corrugations.

For the moment we are not inclined to make statistical analysis for the data measured. From table 2 it is clear that pitches are of random property, the maximum pitch being 480 mm (there are practically two troughs lying within the range of the full corrugation wave having a pitch of 490 mm) and the minimum 110. In general, pitches round 200 mm are rather shallow, while those round 300 mm are deeper. It is necessary to point out that these data are the results of definite development stage of rail but not the initial state of it. Within the ranges of the two pitches with asterisk there are two troughs of different depth. This implies that they are resulted from the development of two corrugation waves of smaller pitches. Thus it can be seen that pitches over 200 mm and 300 mm are mostly likely to be the results of the development of smaller ones.

It can also be seen from table 2 that the pitches of short corrugations are within 20-65 mm. From the same table it is found that on the curve of small radius both long pitch and short pitch rail corrugations are possible. Be sure, it is an important fact.

(3) Investigation on the Condition of Wheel Tread.

Through careful observation on wheel treads of tender, steam-, diesel- and electrical locomotives, freight car and passenger car, we found a very important phenomenon that the wheel treads were not smooth enough but with bright spots alternating with dark ones. The bright spots are crests and the dark ones are troughs. Table 3 is an instance for the pitches between bright and dark spots.

Corrugation Interval of Wheel Table 3

Freight Car	35, 35, 45, 35, 37, 42, 50, 58, 50, 50, 50, 50, 45, 40, 45, 45, 53, 55, 37, 70, 52, 58, 45, 45, 47, 44, 50, 40, 40, 32, 56, 50,
-------------	---

	36, 50, 40, 70, 65, 80, 55, 60, 80, 65, 75, 51, 45, 46, 35, 38, 38, 30, 48, 31, 36, 20, 27, 38, 42, 32, 26, 24, 64, 58, 51, 42, 54, 64, 49, 50, 67, 54, 75, 35, 65, 110, 80, 110, 105, 35, 80, 67, 60, 120, 160, 55, 135, 140.
Passenger Car*	45, 37, 45, 45, 50, 48, 50, 60, 26, 45, 45, 40. * On the tread circle of one of the wheels there are bright spots alternating with dark ones, the corrugation interval being round 48 mm.
Steam Locomotive	70, 70, 70, 70, 62, 76....
Tender	30, 40, 30, 25....
Trailing Wheel	No difference between bright and spots
Diesel Locomotive	Round 50 mm and 100 mm.
Electrical Locomotive	The same as above.

(4) Preliminary Analysis on Wheel Corrugations.

According to the data investigated, on the tread of trailing wheel of steam locomotive, there isn't the difference between bright and dark spots. Besides this exception difference between bright and dark spots exists on treads of all kinds of locomotives and cars, i.e. all the wheels having action of tractive force or braking force produced visible differences between bright and dark spots, the pitch being round 50 mm or 100 mm.

(5) Relation Between Rail Corrugations and Wheel Corrugations.

It is seen from the analysis of the above data that wheel as well as rail yields corrugations, and the pitches are approximately coincident. Corrugations occur either on high rail or on low rail. It does not occur simul-

taneously on both rails, but occurs early or late on either rail. The pair of wheels of wheelset yields corrugations. And corrugations of long wavelength are developed from short ones. Hence a unified theory on the formation of short pitch and long pitch rail corrugations can be thus established.

CHARACTERISTICS OF WHEEL/RAIL UNDER EXERTING FORCES AT BRAKING ON LONG AND STEEP GRADE OF SMALL RADIUS OF CURVATURE.

The purpose of this paper stress on the study of rail corrugations on long and steep grade of small curvature, hence the characteristics of wheel/rail under exerting force should be mastered. And what the characteristics then? They are:

The adhesion force between wheel and rail decreases due to lateral slip, and

Superelevation and curve widening of rail gauge exist in curved section.

On railroad for both passenger and freight trains it is difficult to have an adequate superelevation that can meet the different requirements of both passenger train and freight train. If superelevation is not sufficient, the vertical load on outer rail will be higher than that on inner rail while a train running through at a high speed. In other words, when the adhesion weight of outer rail is higher, the possible tractive or braking force will be larger. In this case corrugations are the frequent outcome. On the contrary, corrugations will frequently occur on inner rail. Despite the analysis stated above, it is still in urgent need to inquire into the mechanism producing rail corrugations.

PHENOMENA OF DRY FRICTION BETWEEN WHEEL/RAIL AND WHEEL/BRAKE SHOE.

The friction between wheel and rail is dry friction. When longitudinal force exists between them, wheel yields, relative to rail, elastic and plastic slip. This is sometimes called 'creep' and was discovered as early as in 1926[7]. From then on, many researchers have devoted great effort to this problem,

among them Kalter[8] has gone deep into the subject since 1973. Logston and Itaml have made painstaking experiments and studied on friction-creep of locomotives[9]. And Figure 1 is quoted from their thesis. It is shown in this figure that the relation curve of friction(adhesion) coefficient versus creep rises initially and falls after passing a maximum, i.e., a two-valued relation lies

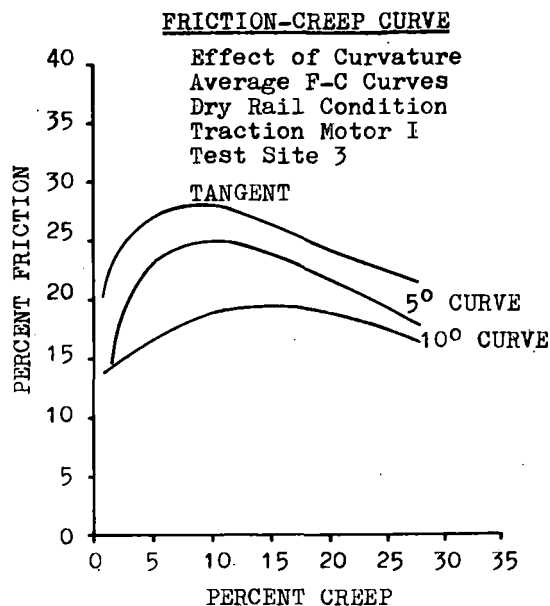


Fig.1 Effect of Curvature (Dry Rail)

between them. The max. point represents the max. value of adhesion coefficient. Passing the max. adhesion coefficient falls to such an extent that skid of wheels may happen. On the basis of the non-linear vibration theory [10,11,12], relaxation vibration might take place under certain condition.

When braking is applied, wheel will similarly produce elastic and plastic slip(creep) relative to rail. Its regular pattern must be the same as that appearing while pulling (but may be different in quantity). Wheel friction against brake shoe also decreases at a rate corresponding to the increase of wheel speed relative to brake shoe, and therefore relaxation vibration might occur under certain situation at braking.

At present there is still lack of both theoretical and experimental investigation on the relation between braking adhesion coeffi-

cient versus creepage.[13]

FORMATION OF RELAXATION VIBRATION AND WHEEL/RAIL CORRUGATION AT BRAKING.

(1) Relation between Braking Force and Rotating Angle of Wheel.

The relation between friction and creepage (or relative speed) at braking can be transferred into the form of relation between braking force and rotating angle of wheel. Braking force is equal to the product of braking friction coefficient by wheel load. And creepage, too, can be changed into rotating angle[14]. Fig.2 is a sketch map of it.

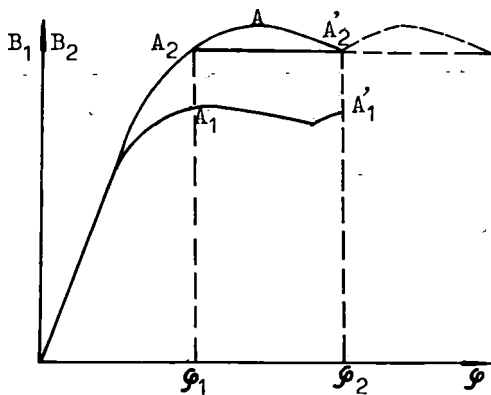


Fig.2 Sketch Map of Relation between Braking Force and Rotating Angle of Wheel

(2) Relaxation and Formation of Corrugation

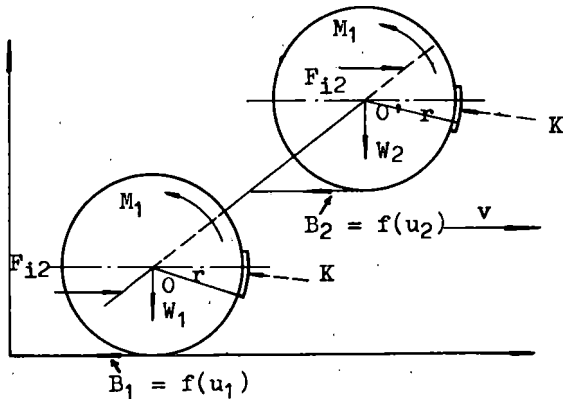


Fig.3 Wheel Under Force At Braking

A train is braked as it is running on a curved section. Under normal conditions, the pressures of brake shoes are equivalent, and hence the braking torques of both wheels are equal, i.e., $M_1 = M_2$ (Fig.3). If superelevation of outer rail is not sufficient, $W_2 > W_1$, otherwise, $W_2 < W_1$. Fig.3 shows the situation in the former case. The braking force on outer wheel is larger than that on inner wheel, i.e., $B_2 > B_1$. At the beginning of braking, the two wheels turn a same angle respectively (ϕ_1) in the direction opposite to movement of train (See A_1 and A_2 in Fig. 2. At this moment car axle of wheelset does not transmit torque), and in the meanwhile the adhesion of inner wheel reaches the critical value. Because there still exists excess of the braking torque of inner wheel, its value being $M_1 - B_1$, this excessive torque will be transferred through axle under torsion to outer wheel whose braking adhesion force is approaching maximum value, and thus the braking torque of outer wheel is increased. Under such conditions, the adhesion force of outer wheel exceeds the maximum. From Fig.2, we see, after the max. the curve falls, adhesion force decreases and the rotation of outer wheel is accelerated, causing inverse spin. The torsional angle of axle automatically relaxes and adhesion is restored (at A'_2 and A'_1). Relaxation vibration continuous in this way and corrugations, therefore, appear on outer wheel and rail. This is the mechanism of producing corrugations.

Corrugation pitch is decided by the circumference length corresponding to difference of torsional angles ($\phi_2 - \phi_1$) or difference of creepages. If the average creepage within the range from A_2 to A'_2 is 15%, the pitch produced by passenger car wheel of diameter 915mm will be

$$\pi D u = 43 \text{ mm,}$$

and that by freight car wheel of diameter 850 mm will be

$$\pi D u = 40 \text{ mm.}$$

Here, we have set forth the mechanism of the formation of corrugations through physical model, as to the mathematical model about

relaxation vibration and the evaluation process of non-linear differential equations, we are going to carry them out on the basis of the experimental curve $B = f(u)$ and elaborate in next paper.

(3) Characteristics of Pitch Distribution and Evidence on Property of Random Process.

Pitches are of different Properties of random process. The reason is that there is certain property of random process in friction coefficient and creepage. It has something to do with the functions causing variations of wheel load, contact area between wheel and rail [15], the magnitude of lateral force, and especially with rail surface conditions which are under the influence of weather. Therefore, pitches inevitably possess the property of random process. Logston and ItamI wrote in their paper, "The value of percent friction and percent creep for an outwardly similar rail condition have a wide spread, and that the friction-creep relationship between steel wheel and rail is hard to predict. Even on tangent track, large variations are possible in friction-creep curves whose peaks will vary from 10 to 50% friction and 2 to 20% creep depending upon rail conditions."

Short wavelength corrugations recorded in relevant papers are 43 mm, 50 mm [16] and 60mm in Germany, England and Japan respectively. The differences between them are owing to different railroad facilities in those nations such as locomotives, rolling stocks, rails together with structural materials and running speed, especially running speed. And this can be explained by the theory presented in the paper.

CONCLUSION.

(1) The theory put forward in this paper can be used to illustrate the mechanism of the formation of rail corrugations. Corrugations exist not only in rail but also in wheel.

(2) It is necessary to study the process of formation of long wavelength corrugations

from short wavelength ones through interaction between rolling stock and track.

(3) It is an urgent task to study the relation between braking adhesion coefficient and creep on curves of small radius.

(4) Corrugations can be reduced and even eliminated through further comprehensive investigation on locomotives, rolling stocks, track, and material and its technology.

SUGGESTIONS.

(1) Minimize variations of wheel load and unbalance of left and right wheel loads by means of comprehensive consideration of locomotive, rolling stock and track as a system.

(2) Make equivalent as far as possible the braking forces or tractive forces of both wheels of a wheelset.

(3) Establish rational superelevation of outer rail in curves of small radius.

(4) Minimize diameter difference between wheels of a wheelset.

(5) Select adequate material and corresponding technology for wheel and rail.

(6) Operate train in a rational way.

REFERENCES.

1. Hou Yunqing, "Rail Corrugations", Institute of Information, Ministry of Railway, China, Specialized Information 81-4, (1981).
2. J.B.C. Taylor, A.M. Crawley, "Some Aspects of the Problem of Rail Corrugations", Proc. of 1st International Heavy Haul Railway Conference (1978).
3. R.I. Maix; M.A. Jupp; R. Groenhout, "The Characteristics and Control of Long Pitch Rail Corrugation at heavy Axle Loads", Proc. of 1st IHRC (1978).
4. J. Eisenmann, "Formation of Short Pitch Corrugations in Rails", Proc. of 1st IHRC (1978).
5. Lei Teng, Tan Licheng, Cheng Guangzu, Fang Fubao, "Some Problems on Relationship between Wheel and Rail in China" (1980).
6. Cui Zhenzhi, "Investigation on Rail Corrugations in Shi-Tai Railline" (1980).
7. F.W. Carter, "On the Action of a Locomotive Driving Wheel", Proc. Roy. Soc., A112,

151-157 (1926).

8. J.J. Kalker, "On the Rolling Contact of Two Elastic Bodies in the Presence of Dry Friction", Delft University of Technology, The Netherlands, Reprint of Doctor Thesis (1973).

9. C.F. Logston, Jr. G.S. Itaml, "Locomotive Friction-Creep Studies", Trans. of the ASME August 1980, Vol. 102/275.

10. E.E. Babakov, "Theory of Vibration", (1958).

11. J.J. Stoker, "Nonlinear Vibrations in Mechanical and Electrical Systems", (1950).

12. A.A. Harkewich, "Self-exciting Vibrations", (1954).

13. V.M. Kazarenov, B.L. Karbaiky, "Calculation and Investigation of Autobrake", (1961)

14. Tan Licheng, "Investigation on Distribution of Tractive Force on Power Wheels of Steam Locomotive", (1955).

15. J.R. Mitchell, "The Curving of Railway Vehicles", Paper to the 2nd Symposium on the Relation between Wheel and Track Organized by China Academy of Railway Sciences of the Ministry of Railways, Beijing, October 1980.

16. C.O. Frederick, "Rail Damage", Paper to the 2nd Symposium on the Relation between Wheel and Track Organized by the CARS of the Ministry of Railways, Beijing, October 1980.

P. Mutton

Senior Experimental
Officer
BHP Melbourne Research
Laboratories
Melbourne, Australia

C. Epp

Senior Research Officer
BHP Melbourne Research
Laboratories
Melbourne, Australia

S. Marich

Senior Principal Research
Officer
BHP Melbourne Research
Laboratories
Melbourne, Australia

Rail Assessment

The economic need by railway systems to operate at higher axle loads has led to a demand for improved materials, including rail steels. The final choice of material for such conditions depends on both technical and economic factors. To quantify these, it is essential that the material be subjected to a detailed and often long term in-track assessment programme. A programme of this nature has been conducted at the Mt. Newman Mining Company Pty. Ltd. and Hamersley Iron Pty. Ltd. for the case of rail steels. The results obtained in the study are used to discuss the relevant experimental and technical factors which can influence the analysis; such factors include rail lubrication, original rail profiles, wheel wear, material properties, rail fatigue, operating conditions and experimental techniques.

INTRODUCTION

Rails are the most costly single item used in track by heavy haul railway operators. Under such operating conditions, typified by the iron ore railways in Western Australia, in particular the Mount Newman Mining Company Pty. Ltd. (MNM) and Hamersley Iron Pty. Ltd. (HI), it has been shown that the life of standard carbon AREA rails in curved track is only two to four years or 100 to 200 million gross tonnes of traffic¹. Consequently, any delay in rail replacement results in considerable benefits in terms of deferment in expenditure and reduced interference to traffic. This aspect, together with the economic necessity by railway systems to operate at maximum capacity², including higher axle loads, has led to numerous recent developments in rail steel technology.

The deterioration processes which determine the life of rails in track are wear, fatigue and plastic deformation; these factors have been discussed in previous publications³⁻⁶. Using a knowledge of these deterioration processes, the initial assessment of rail materials can rely on data obtained in laboratory tests. Some of the more important material characteristics which give an indication of performance are:

- Tensile strength and ductility
- Hardness
- Cyclic strength and resistance to deformation
- Work hardening behaviour
- Wear resistance
- Fatigue crack initiation and growth
- Static and dynamic fracture toughness
- Weldability
- Cleanliness level

The final choice of material, however, depends on both technical and economic aspects. To quantify these, to allow for any effects which cannot be simulated in the laboratory, and to provide information which can be used to validate laboratory data, it is essential that the materials under consideration be subjected to a detailed and often long term in-track assessment programme. Such a programme was initiated at MNM and HI in 1973 and is still in operation, although its nature has changed considerably over the years.

This paper reports on the methods adopted in establishing and carrying out the rail in-track studies, the results obtained and in particular the many factors which can influence these results.

IN-TRACK TEST PROGRAMME

Details of the rail materials and track characteristics covered in the study have been given in a previous publication¹ and are summarised as follows:

Rails

Type: AREA standard carbon, alloy and heat treated (both head and through hardened).
Section: AREA 66 kg/m and 68 kg/m.
Properties: 0.2% proof strength ranging from 490 MPa to 870 MPa, tensile strength ranging from 950 MPa to 1260 MPa.
Country of Manufacture: Australia, Japan, U.S.A., Germany and Russia.
Steelmaking: Semi killed and fully killed ingots.
Microstructure: Predominantly fully pearlitic.

Track

Geometry: High and low legs of curves ranging in radius from 395 metres (4.4°) to 1160 metres (1.5°) and length from 400 metres to 1300 metres.
Welding Practice: Continuously flash butt welded track with thermit field welds.
Sleepers: Timber or concrete.
Superelevation: 12 mm to 58 mm.

Grade: -0.46% to +1.50%.
 Lubrication: Molybdenum disulphide based grease using track mounted lubricators placed at mine end of each curve, activated by all wheels in loaded trains.
 Axle Load: 30 tonnes mean.
 Vehicle Speed: 15 km/hr to 60 km/hr.
 Annual Traffic: Approximately 50 million gross tonnes.

The initial evaluation of some of the high strength alloy rails under actual operating conditions was conducted at MNM in a curve of radius 870 metres (2°). The primary objective of this trial was to assess the resistance of the higher strength rails to corrugation formation. Consequently a total of 90 rails were laid in the high leg of the curve in groups of three according to the 0.2% proof strength characteristics as measured by the manufacturer on air cooled samples from the A rails of each ingot. Standard carbon rails were laid adjacent to the other rail types in several parts of the curve as a basis for comparison. This procedure enabled a correlation to be established between resistance to corrugation formation and the strength of the material. It also allowed the following practical guidelines to be established for the other in-track trials, particularly in terms of obtaining valid rail wear data over the life of the rail:

(a) The placement of standard carbon rails among the higher strength rails can result in considerable track maintenance problems, due to their higher maintenance requirements particularly surface grinding for corrugation control, and their relatively short replacement time. Consequently, subsequent in-track trials restricted the inclusion of standard rails to both ends of the experimental curves, until sufficient performance data were obtained on both high strength and standard rails. Thereafter, the experimental curves contained only high strength rails, laid in both high and low legs according to rail type in groups consisting of at least five rail lengths.

(b) As mentioned previously, wear and plastic deformation of the material are important factors in determining rail life. In the current study rail head profiles were recorded with a Seiki profile gauge as shown in Figure 1. The gauge reproduces a 1:1 profile, with a repeatability between successive measurements within 10 mm² of the rail head area, provided regular (daily) calibration checks are carried out. The rail head area is then measured using a planimeter, with all material outside the

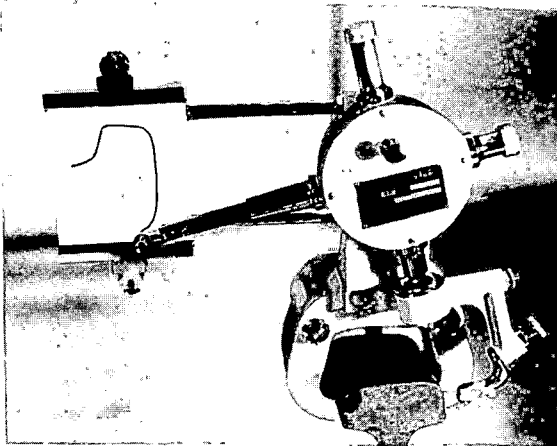


FIG. 1: SEIKI GAUGE

original profile being regarded as "lost". The resulting head area loss, expressed as a percentage of the original area, therefore represents metal loss due to the combined influence of both wear and plastic flow. The performance of any rail material relative to standard rail for a particular set of operating conditions can then be determined from the ratio of the respective head area losses¹. The accuracy of the technique has been determined by comparing field measurements with rail head areas measured directly on rail sections removed from track. The results obtained are summarised in Table I. Using statistical analysis (t-test) it can be shown that there is no significant difference in the mean of the two sets of data at a confidence limit of 90% or higher. At this confidence limit, the direct (D) and in-track (T) percent rail head loss measurements are related by the expression:

$$- 1.9 < T - D < + 2.7$$

Therefore, for an in-track measurement of 10% head loss, the direct head loss could be in the range 7.3% to 11.9%. In determining the relative performance of different rail types, it is therefore essential that the rails exhibit considerable losses in head area, unless a significant (more than 30) number of data points are measured.

(c) In comparing the performance of different rail types, it is also necessary to account for different section sizes. For example; in the current study, rails with 66 kg/m and 68 kg/m sections were tested. Obviously the same amount of head loss would represent a smaller percentage on the larger rails and would give them an apparent superiority. This aspect can be taken into account by either expressing material loss as an area or modifying the values of percent head loss by an appropriate amount to compensate for the difference in section size.

TABLE I: COMPARISON OF TRACK AND DIRECT MEASUREMENTS

PERCENT RAIL HEAD LOSS	
TRACK MEASUREMENT	DIRECT MEASUREMENT
9.2	9.2
9.4	8.3
9.8	8.6
10.9	10.9
11.4	12.1
13.0	14.1
13.7	14.2
13.9	12.5
14.0	14.6
14.2	12.8
14.2	15.3
14.5	13.4
15.0	14.3
15.6	16.6
16.7	15.5
17.0	17.0
18.7	16.5
18.8	18.6
19.6	19.2
19.6	19.2
26.1	25.5

(d) A major source of error in determining percentage head loss and rail performance is associated with the value given to the original rail head area. The study has shown that it is incorrect to regard this parameter as a constant, because of the variation in original rail head size which can occur due to rolling tolerances. This is of particular importance for the case of experimental high strength steels produced for the first time on a limited quantity basis by a manufacturer. An example of the influence which the original rail head area can have on the prediction of rail performance is shown in Table II for the case of a 873 metre radius curve (2°), in which rail measurements were taken after approximately 100 million gross tonnes of traffic. For the standard rails, it can be seen that even though differences existed between actual and nominal original areas, the average of the actual percent head loss values (13.5%) is within measurement error of the nominal value (13.4%). The experimental rails, on the other hand, exhibited considerable differences in original areas. In this case, valid predictions of rail performance could be made only by recording the profiles of the rails prior to any traffic and using these values in calculating percentage head losses.

TABLE II: INFLUENCE OF ORIGINAL RAIL HEAD AREA ON RAIL PERFORMANCE

STANDARD CARBON RAIL - 66 kg/m					
ORIGINAL HEAD AREA (mm ²)		HEAD AREA AT 100 MGT (mm ²)	% HEAD LOSS		
ACTUAL	NOMINAL		ACTUAL	NOMINAL	
2840	2852	2470	13.0	13.4	
2850	2852	2470	13.4	13.4	
2860	2852	2470	13.6	13.4	
2870	2852	2470	13.9	13.4	
HIGH STRENGTH RAIL - 66 kg/m					
RAIL TYPE	ORIGINAL HEAD AREA (mm ²)		HEAD AREA AT 100 MGT (mm ²)	PERFORMANCE RATING	
	ACTUAL	NOMINAL		ACTUAL	NOMINAL
STD. CARBON	2860	2852	2470	1.0	1.0
Cr-Nb-V	2940	2852	2615	1.2	1.6
Cr-Nb-V	2800	2852	2475	1.2	1.0
Cr-Mo	2930	2852	2715	1.8	2.8
Cr-Mo	2810	2852	2595	1.8	1.5

(e) In the initial stages of the study, rail head measurements were taken at the 1/3, 1/2 and 2/3 locations along the length of several rail types in the experimental curves to determine the variability within rail lengths. The results are shown in Table III and Figure 2. It is apparent that the variation measured within any one rail length is within the

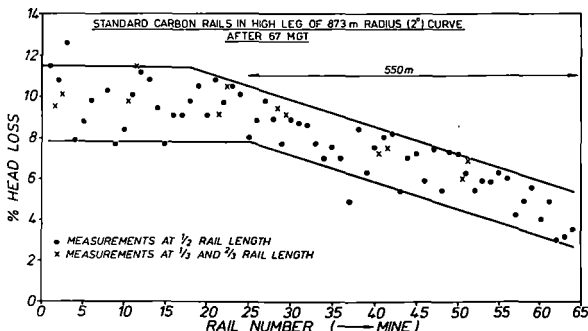


FIG. 2. VARIATION OF RAIL WEAR WITH MEASURING POSITION.

TABLE III: INFLUENCE OF MEASURING POSITION ON WORN RAIL HEAD AREA

PERCENT HEAD LOSS		
1/3 LENGTH	MID RAIL	2/3 LENGTH
9.4	10.8	10.1
9.1	9.7	10.5
9.8	10.1	11.5
9.1	7.7	9.4
7.2	8.0	7.5
8.4	8.7	9.1
8.2	8.0	7.4
6.9	6.3	6.0
10.1	9.1	8.4
7.5	6.5	7.9
8.0	7.3	6.6

scatter observed throughout the curve. The consistency of the data is most likely due to a combination of relatively low operational vehicle speeds and very good track geometry, both of which would tend to reduce dynamic vehicle/track interaction. Thereafter, rail head measurements have been taken at mid rail length position in rails 13.5 metres in length and at 1/3 and 2/3 rail length positions in rails 25 metres in length. It should also be noted that throughout the rail life the measurements are always taken at the same location.

(f) A further aspect which must be taken into account when assessing different rail types is the tonnage to which the rails have been subjected. It is evident from Figure 3 that rails do not follow a linear relationship with tonnage until later in their life. This is particularly so for the lower strength materials. Consequently the predicted relative lives of the various rail types can change considerably depending on the tonnage at which the assessment is made; this could influence the final economic decision. Table IV summarises the relative performance of the rail types calculated at the different traffic levels. For this case, it is obvious that any predictions made after 42 MGT and 66 MGT of traffic would result in incorrect recommendations. In any in-track assessment programme it is therefore essential that the rails be measured at regular

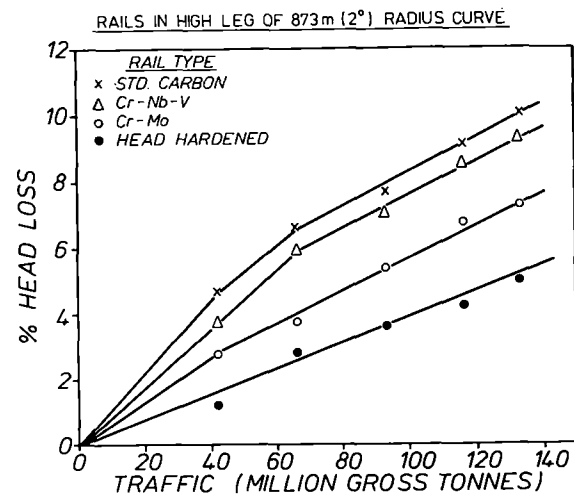


FIG. 3. RAIL WEAR AS A FUNCTION OF TRAFFIC.

intervals until their wear behaviour can be confidently defined. The reason for the observed behaviour is most likely due to different work hardening characteristics of the rail materials under both monotonic and cyclic compression^{4,7}. However, as discussed in a later section, the head profile of the original rails may also have an influence on the initial rail wear performance.

TABLE IV: RELATIVE RAIL PERFORMANCE AT DIFFERENT TRAFFIC LEVELS

RAIL TYPE	PREDICTED RAIL LIFE				
	42 MGT	66 MGT	93 MGT	116 MGT	133 MGT
STD. CARBON	1.00	1.00	1.00	1.00	1.00
Cr-Nb-V	1.26	1.12	1.08	1.08	1.08
Cr-Mo	1.69	1.76	1.43	1.36	1.38
HEAD HARDENED	3.88	2.36	2.13	2.19	2.00

(g) As mentioned previously¹, the in-track assessment of rails can be influenced by track maintenance practice and in particular rail rectification by grinding. Obviously the amount of metal removed during a grinding operation will depend on the mechanical properties of the material. It has also been shown, however, that grinding may influence the subsequent wear rate by removing different proportions of work hardened material¹. If grinding is conducted, it is therefore necessary to take rail profiles immediately before and after the operation to quantify such effects.

(h) The measured performance of rails in track is also influenced by their location in a curve. As illustrated in Figure 4, for high strength rails and relatively short curves (less than approximately

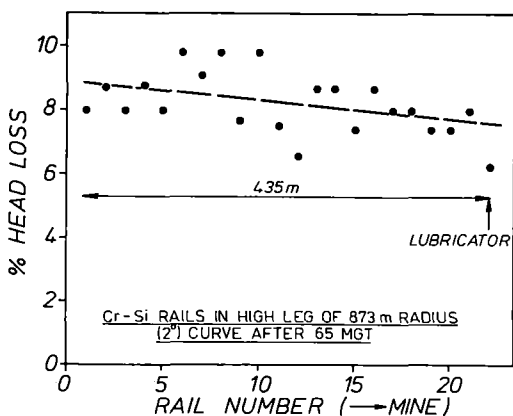
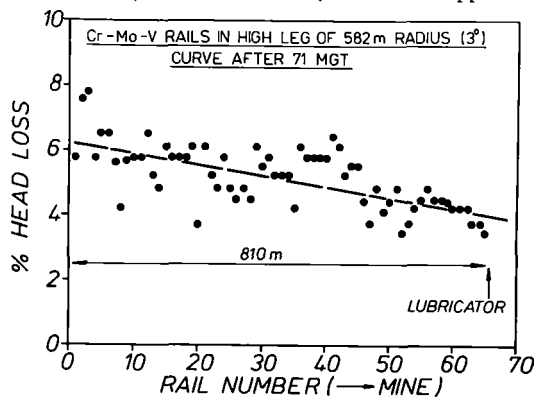


FIG. 4. VARIATION OF RAIL WEAR WITH CURVE LOCATION.

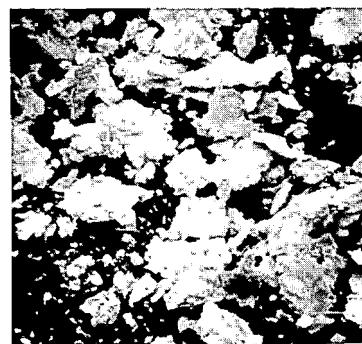
500 metres) it is generally observed that the rail wear varies linearly along the curve. If this condition holds, the method described previously¹, which compensates for such a variation, can be used. As shown in Figure 2, however, lower strength rails in longer curves can exhibit a linear change in wear over, in this case, 40 rail lengths (550 metres) and thereafter the wear remains relatively constant. The rails invariably exhibit lower head losses at the mine end of curves, i.e. where the curve lubricators are located. For this reason, as discussed in a later section, it has been proposed that lubrication can have a major influence on rail assessment and determination of relative performance.

An examination of wear debris collected at various locations within curves has indicated differences in wear behaviour with varying lubrication conditions. As shown in Figure 5, the debris from standard carbon rails in the 873 metre radius curve discussed above (Figure 2) consisted predominantly of metallic flakes. However, it is evident that the flake size from the generously lubricated end of the curve is very much smaller than that from the poorly lubricated end. If such differences in flake size are considered to result from changes in subsurface stress levels as a function of gauge face friction, then the smaller flake size at the lubricated end of the curve is consistent with the lower wear rate. In any in-track rail assessment programme, it is therefore essential to characterise the wear behaviour of rails over the full range of lubrication conditions.

(i) Rail wear in curves can vary considerably with track location. In this study no attempt was made to determine all possible causes of such



(a) x 30



(b) x 30

FIG. 5: STANDARD CARBON WEAR DEBRIS

- (a) GENEROUSLY LUBRICATED
- (b) POORLY LUBRICATED

variability. However, the study has shown that, within the range of operating variables examined, the relative performance of different rail types remains reasonably constant. For example the relative performance of several rail types determined after 80-90 MGT of traffic in curves of varying radius (580-875m) and vehicle speed (20-60 km/hr) summarised in Table V shows that the predicted lives of the rail types in the different curves does not vary by more than 10%.

TABLE V: RELATIVE RAIL PERFORMANCE IN DIFFERENT CURVES

RAIL TYPE	PREDICTED RAIL LIFE (CURVE RADIUS - TRAIN SPEED)			
	873m-20km/hr	873m-45km/hr	873m-60km/hr	582m-16km/hr
STD. CARBON	1.00	1.00	1.00	1.00
Cr-Nb-V (1)	1.15	1.08	1.12	1.10
Cr-Nb-V (2)	0.91	0.96	0.93	
Cr-Nb-V (3)	1.05	1.01	1.10	1.08
Cr-Mo	1.44	1.43	1.33	1.40

It must be stressed that the accuracy and validity of any in-track rail assessment programme rely on the testing of the materials over the full range of operating conditions existing in the railroad system.

TECHNICAL FACTORS INFLUENCING RAIL PERFORMANCE

In the previous section several factors were recognised and quantified as having an influence on the practical aspects of establishing a valid, long term in-track rail assessment programme. The major emphasis of this section will be on those technical factors which have been found to directly influence the wear behaviour of rails in-track and consequently their assessment.

Material Properties

The rails tested in the first of the experimental curves were examined in detail in terms of mechanical properties and chemical analysis, following their removal from track. The results have been plotted against the rate of material loss, determined over the life of the rails, in Figures 6 and 7. The carbon equivalent (CE) was calculated using the formula:

$$CE = C + \frac{Mn + Si}{4} + \frac{Cr}{2} + \frac{Mo + V}{5} + \frac{Nb}{3}$$

It can be seen that the rate of material loss is inversely proportional to strength, but there is considerable scatter in the data; higher levels of correlation were obtained with carbon equivalent and material hardness. This is to be expected since under high axle load conditions rail material is lost

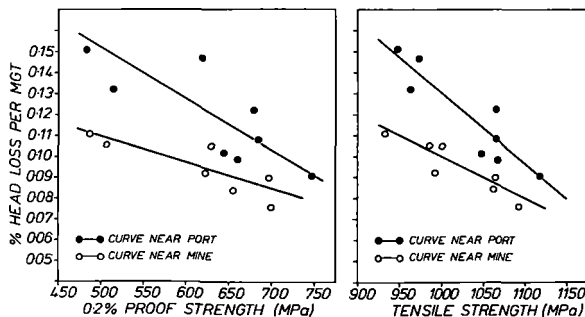


FIG. 6. WEAR RATE AS A FUNCTION OF RAIL STRENGTH.

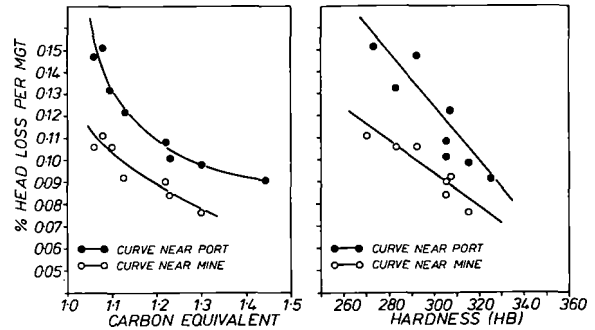


FIG. 7. WEAR RATE AS A FUNCTION OF CARBON EQUIVALENT AND HARDNESS

primarily through wear processes and, as discussed in a later section, wear rates are strongly dependent on material hardness.

Data obtained at the FAST experimental track in U.S.A. have also shown a strong influence of carbon equivalent on wear rate⁸. Thus, for underlubricated conditions, a 0.1 reduction in carbon equivalent yielded a 50% increase in wear rate. For a similar carbon equivalent range and variation the current results show increases in rail wear rates of 30% for the rails near the port end of curves (moderately lubricated) and 21% for the rails near the mine end (well lubricated). Indeed it can be seen from Figures 6 and 7 that the rails operating under well lubricated conditions are influenced less by material characteristics. This aspect will also be discussed in more detail in a later section.

Rail Transposition

It has been generally recognised that rails which have been subjected to an amount of traffic will exhibit an improved performance under higher loading conditions than new rails. To the authors' knowledge, however, this aspect has not been quantified. In the current study, high strength rails of various types were laid in both high and low legs of a 873 m radius curve. The performance of the rails in both legs was monitored at regular intervals (see Figure 3) until 132 MGT of traffic. Thereafter the rails were transposed, their original profile restored by grinding and the assessment continued. Table VI shows the results obtained in the high leg of the curve on the original new rails and the transposed rails (originally in the low leg) after an equivalent tonnage. It is evident that the transposed rails exhibit much lower wear rates, particularly those of lower strength levels (standard carbon and the first four alloy types in Table VI). This behaviour is most likely due to work hardening of the rails while in the low leg of the curve prior to transposition.

TABLE VI: COMPARISON OF WEAR IN NEW AND TRANSPOSED RAILS

RAIL TYPE	% HEAD LOSS		RELATIVE PERFORMANCE TRANSP./NEW
	NEW RAILS 66 MGT	TRANSP. RAILS 62 MGT	
STANDARD CARBON	6.6	4.2	1.5
Cr-Nb-V (1)	5.9	3.5	1.6
Cr-Nb-V (2)	6.5	3.9	1.6
Cr-Nb-V (3)	6.3	3.7	1.6
Cr-Nb-V (4)	5.6	2.6	2.0
Cr-Nb-V (5)	4.8	4.1	1.1
Cr-Mo-V	3.2	2.5	1.2
HEAD HARDENED	2.8	2.0	1.3

In considering the use of such a technique, the costs associated with transposition and rail rectification have to be considered. The results, however, show sufficient potential benefits to warrant a continued investigation.

Rail Profiles

Figure 8 shows wear data obtained in a curve containing three types of head hardened (HH) rail. In setting up the trial the rail types were laid in strings of alternate types to account for wear variations along the length of the curve. For this case, the HH rail of type 1 is used as a basis of comparison.

It can be seen that rail types 2 and 3 exhibit a slightly better performance (10-15%). However, as shown in Table VII at earlier tonnages (in the range 77-108 MGT) the field data indicated the type 2 rail to exhibit a much higher predicted life. The observed variation in wear behaviour could not be explained in terms of either chemistry or mechanical properties and in particular hardness distribution. A more detailed examination of the original profiles of the rail types 1 and 2 on the other hand, revealed that even though both products were within dimensional tolerance specifications, considerable differences existed in their respective crown profiles. Thus, whilst the type 2 rail showed reasonable symmetry with a crown radius of approximately 300 mm, the type 1 rail was asymmetric with a crown radius of 500 mm on one side and a flat region on the other half.

In an effort to verify the impact of these profile differences on wear performance, the bogie curving simulation model developed at the BHP Melbourne Research Laboratories⁹ was used with the actual rail profiles and operating conditions as inputs. The simulation results indicated that the very subtle differences in profile could give rise to an improvement in the initial wear rate of up to 50% for the type 2 rail by the influence of rail profiles on vehicle/track interaction characteristics.

In this case, the influence of rail profiles was observed even at relatively large tonnages because of the high resistance to deformation of these material types. A similar effect would soon disappear in materials with lower strength. However, the findings again emphasise the need to assess rails over a considerable tonnage before reaching any final decision on rail performance. They also highlight the importance of examining any railway problem using a multi-disciplinary approach which can appropriately define the vehicle/track interaction.

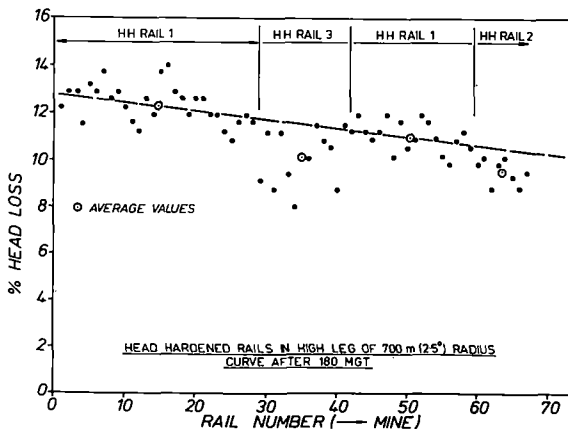


FIG.8. HEAD HARDENED RAIL WEAR.

TABLE VII: RELATIVE PERFORMANCE OF HEAD HARDENED RAILS

RAIL TYPE	PREDICTED RAIL LIFE				
	77 MGT	94 MGT	108 MGT	131 MGT	180 MGT
HH 1	1.00	1.00	1.00	1.00	1.00
HH 2	2.00	1.71	1.54	1.13	1.11
HH 3	1.20	1.30	1.29	1.20	1.15

Rail Fatigue

So far in this text the assessment of the various rail types has been discussed in terms of rail life predictions based on material loss. However, as mentioned in the Introduction, material fatigue also plays an important role in determining rail life, particularly in curves of larger radii and in tangent track. Indeed, some fatigue defects such as shells, transverse defects and horizontal split heads necessitate immediate replacement of the defective rails and therefore can have a major influence on maintenance planning, traffic movements, safety and costs. Consequently, any in-track rail assessment programme has to be conducted for a sufficiently long time to ensure consideration of all possible life controlling mechanisms.

In the current study, several of the high strength rail types examined, including two of the head hardened types, developed shell defects after only 60 to 100 MGT of traffic, as illustrated in Figure 9. Obviously, the development of such defects curtailed the advantages of these rails related to their better wear and deformation behaviour.

Detailed examination of the defective rails revealed that the occurrence of the shells was associated with manufacturing procedures rather than material characteristics. In most rails, the defects were nucleated by large oxide inclusions which have been shown to have a detrimental effect on the fatigue performance of rails^{10,11}. In one of the head hardened rail types, nucleation of the defects occurred at a martensitic band which had formed 3-5 mm below the rail surface due to an incorrect manufacturing process.

The detailed analysis of rail fatigue should be considered during a rail assessment programme since the solution to a problem can often be easily achieved, particularly if the problem is not associated with the basic material properties.



FIG. 9: TYPICAL SHELL DEFECT

Rail Lubrication

As pointed out previously, the use of rail lubrication, applied at the mine (entry) end of curves, results in an increasing wear rate through the curve length. This is particularly evident over the first 500 metres (Figure 2). The wear rates of all rail materials are reduced by the use of rail lubrication, but the extent of the reduction depends on the rail type. Therefore, the performance rating given to the various high strength rail materials is dependent on the effectiveness of lubrication.

Figure 10 shows the mean wear rates of standard carbon and several high strength rail materials as a function of distance from the lubricator position. The wear rates, expressed as percentage head loss per million gross tonnes per degree of curvature, are mean values from several curves of 600-800 m radius (2-3°), normalised to an original area of 3150 mm² (equivalent to 68 kg/m rails). The benefit of lubrication is greatest for standard carbon rail and decreases for the high strength rail materials.

The mean wear rates for well lubricated and moderately lubricated positions (50 m and 500 m respectively from the lubricator) are shown as a function of rail hardness in Figure 11. It can be seen that the effect of lubrication is to reduce the slope of the wear rate/hardness relationship. Included in Figure 11 are the results from a 5° curve in the FAST experimental track⁸, the change from unlubricated to lubricated conditions in this case being a reflection of improved lubrication practice rather than increasing distance from the lubricator. The FAST results consequently show a greater reduction in wear rate for the lubricated condition.

Table VIII summarises the influence of lubrication on predicted life for five high strength rail types relative to standard carbon rail, which has been given the base figure of 1.0 for both lubricated and unlubricated conditions to emphasise the larger difference in performance observed under unlubricated conditions. The mean values in the table are higher than the typical values reported in previous sections, reflecting the use of mean wear rates rather than actual head loss data to compare performance.

TABLE VIII: INFLUENCE OF RAIL LUBRICATION ON RELATIVE PREDICTED RAIL LIFE*

RAIL TYPE	PREDICTED RAIL LIFE		
	UNLUBRICATED	LUBRICATED	MEAN
Std. Carbon	1.00	1.00	1.00
Cr-Nb-V	1.74	1.58	1.66
Cr-Mo	2.10	1.77	1.94
Cr-Mo-V	2.86	2.35	2.61
Head Hard. (1)	2.73	2.03	2.38
Head Hard. (3)	3.55	2.23	2.89

* Using mean wear rates over rail life.

The influence of flange lubrication on relative wear performance has also been investigated using the bogie curving model mentioned above. The simulation involved varying the coefficient of friction at the wheel flange/rail gauge face contact from a value of 0.1 (generously lubricated) to 0.56 (unlubricated); the results indicated a potential variation in wear performance of 2.5:1 between the respective lubrication conditions. Under typical track conditions in the MNM and HI railroads, the friction coefficient would be expected to vary from 0.15 (well lubricated) to 0.35 (poorly lubricated); in this case the variation in wear performance would be 1.6:1.

The results of the bogie curving simulation further emphasise the influence of lubrication practice on rail wear rates and relative performance.

Wheel Wear

A major factor which requires consideration in the economic assessment of rail steels is the effect of different rail types on wheel wear. This aspect is most difficult to determine in service because of the many other factors which can influence wheel life. Consequently, use must be made of either full scale or laboratory test facilities.

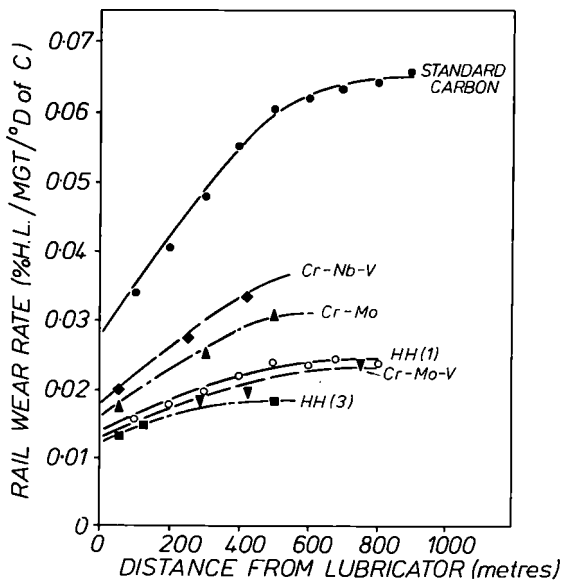


FIG. 10: WEAR RATE AS A FUNCTION OF DISTANCE FROM LUBRICATOR

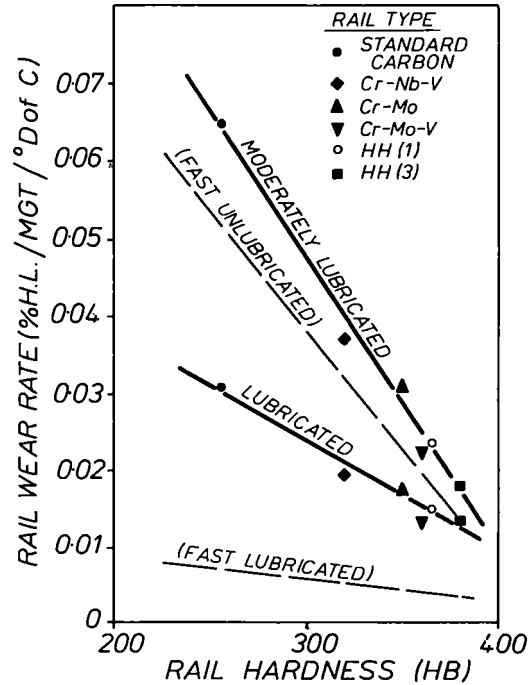


FIG. 11: WEAR RATE AS A FUNCTION OF HARDNESS AND LUBRICATION

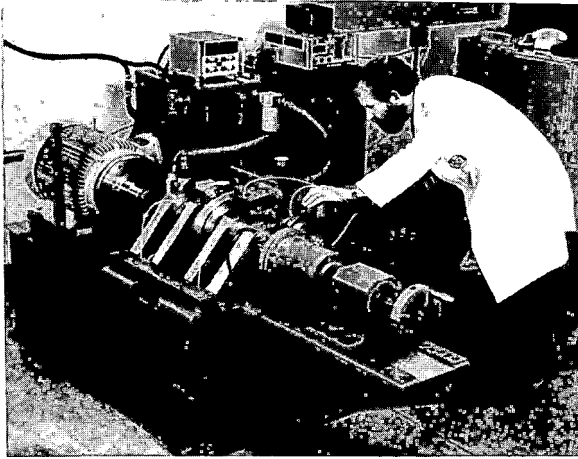


FIG. 12: LABORATORY WEAR RIG

Figure 12 shows the laboratory test rig constructed at the BHP Melbourne Research Laboratories for investigating wheel/rail wear behaviour under varying loading conditions. The initial tests conducted in this rig under accelerated conditions (20% maximum slip at the wheel flange/rail gauge face interface) indicated that high strength rails, in particular head hardened types, do not increase the wear rate of AAR Class C wheels¹². As illustrated in Figure 13, more recent tests conducted under slip conditions similar to those occurring in track (2.5% slip) have similarly shown no effect of head hardened rails on wheel wear rates at an axle load of 30 tonnes and a range of lateral force levels. These results have been supported by observations made at the FAST track in the United States of America⁸.

The data in Figure 13 also shows that the relative performance of standard carbon and head hardened rails in the laboratory test is equivalent to that determined under actual in-track conditions. It must be emphasised, however, that the present results are relevant only to the materials and operating conditions examined.

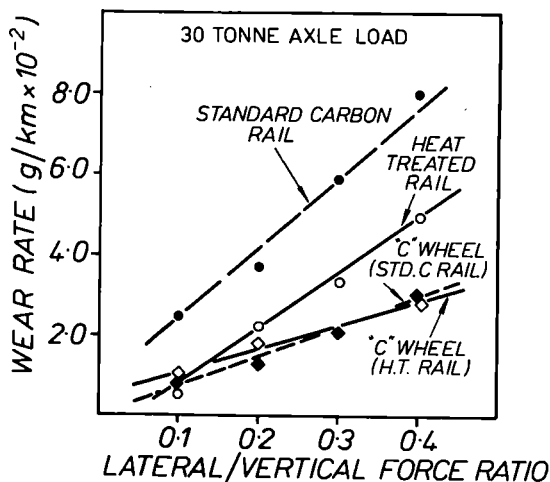


FIG. 13. VARIATION OF RAIL/WHEEL WEAR WITH RAIL TYPE AND LATERAL LOAD.

CONCLUSIONS

The in-track testing of rails is an essential part of any rail assessment programme since the final decision will have a major influence on the long term planning and economics of railway operations. Such a study has been conducted on the high axle load, iron ore railroads at Mt. Newman Mining and Hamersley Iron in Western Australia.

Because of its extended nature, a programme of this kind has to be sufficiently flexible to cope with the many changes which can be introduced by routine and new track maintenance procedures. It must also be structured and managed to ensure the full involvement of track maintenance personnel.

The current study has shown that valid quantitative data can be obtained from field measurements. However, there are many practical and technical aspects which can influence the results and hence require consideration in the analyses.

The following practical factors are regarded as being of major importance:

- 1 The accurate measurement of rail profiles.
- 2 The laying of experimental rails in curves such that a valid comparison may be made between the different rail types.
- 3 The measurement of original profiles of rails in experimental track sections.
- 4 The extension of the study to sufficiently large traffic tonnages so that the performance predictions made at the lower tonnages may be validated.
- 5 The allowance for any track maintenance practice and in particular rail head rectification.
- 6 The allowance for differences in rail wear with curve location, particularly when single track lubricators are used in combination with lower strength rails.
- 7 The testing of rails over the full range of operating conditions existing in the system.

The following technical factors have a direct influence on the in-track life and assessment of rails:

- 1 Material hardness and carbon equivalent are parameters closely related to rail wear.
- 2 Work hardening characteristics can influence the performance of transposed rails.
- 3 Variation in original rail profiles can lead to considerable differences in the initial performance of rails, through their influence on vehicle tracking characteristics.
- 4 Rail fatigue is usually associated with manufacturing procedures and can result in a severe curtailment of other material advantages.
- 5 Rail lubrication is probably the most important and complex technical parameter influencing wear behaviour. Appropriate lubrication practice can give marked reductions in the wear rates of materials, together with reducing the variation in performance of different material types.
- 6 At 30 tonne axle loads, wheel wear rates are not influenced by high strength rails of the head hardened type.

Although the above factors make rail evaluation on a cost/performance basis more complex, their inclusion in an assessment programme is necessary to establish the most cost effective rail replacement and maintenance strategies.

ACKNOWLEDGEMENTS

The reported work has used information from several studies which are part of a joint railroad research programme between the Mt. Newman Mining Co. Pty. Limited, Hamersley Iron Pty. Limited and The Broken Hill Proprietary Co. Limited. The authors are grateful to all three companies for their continued support and permission to publish this work.

REFERENCES

- 1 Curcio, P., Marich, S. and Nisich, G., "Performance of High Strength Rails in Track", Proceedings of the Heavy Haul Railways Conf., I.E. Aust., 1978, Session 313.
- 2 Purcell, M.S., "Economics of a Heavy Haul Railway", Proceedings of the Heavy Haul Railways Conference, The Institution of Engineers, Australia, 1978, Session 104.
- 3 Marich, S., "Research on Rail Metallurgy", AREA Bulletin, Vol. 78, No. 663, June/July 1977, pp. 594-610.
- 4 Marich, S. and Curcio, P., "Development of High Strength Alloyed Rail Steels Suitable for Heavy Duty Applications", ASTM STP 644, May 1978, pp. 167-198.
- 5 Marich, S., "Development of Improved Rail and Wheel Materials", Proceedings of the Symposium on Vanadium in Rail Steels, VANITEC, 1979, pp. 23-40.
- 6 Marich, S. and Mutton, P., "Rail Requirements for Heavy Haul Rail Systems", Proceedings of the 34th Australasian Institute of Metals Annual Conference, 1981, pp. 5-10.
- 7 Stone, D.H., Marich, S. and Rinnac, C.M. "Deformation Behaviour of Rail Steels", Presented at the U.S. Transportation Research Board Annual Meeting, Washington, January 1980.
- 8 Hargrove, M.B., Mitchell, F.S., Steel, R.K. and Young, R.E., "The Wear Behaviour of High Rails Tested in the First Metallurgy Experiment - 0 to 135 MGT", U.S. Department of Transportation Report No. FRA/TTC-81/04, September 1981.
- 9 Marich, S. and Lamson, S., "A Strategy and Procedure for the Development and Application of a Bogie Curving Model", Proceedings of the Railway Engineering Conference, The Institution of Engineers, Australia, 1981, pp. 62-67.
- 10 Marich, S., Cottam, J.W. and Curcio, P., "Laboratory Investigation of Transverse Defects in Rails", Proceedings of the Heavy Haul Railways Conference, The Institution of Engineers, Australia, 1978, Session 303.
- 11 Chipperfield, C.G., Skinner, D.H. and Marich, S., "Influence of Inclusions on the Fatigue of Rail Steels", Presented at the International Iron and Steel Institute Annual Conference, Sydney, March 1981.
- 12 Marich, S. and Mutton, P., "An Investigation of Severe Wear Under Rolling/Sliding Contact Conditions Existing in Heavy Haul Railways", Proceedings of the 7th International Wheelset Congress, 1981, Paper 10.

E.E. Laufer

Technical University
of Nova Scotia
Halifax, Canada

H. Ghonem

Assoc. Professor
Dept. Mechanical Engr.
Univ. of Rhode Island
Kingston, Rhode Island

J. Kalousek

Assoc. Research Officer
National Research Council
of Canada
Vancouver
British Columbia

D.H. Stone

Director: Metallurgy
Assoc. of American
Railroads
Chicago, Illinois

Aspects of Plastic Deformation and Fatigue Damage in Pearlitic Rail Steel

Increased plastic flow of rail material brought about by the introduction of 100 ton and 125 ton capacity cars in the fleets of many North American railroads has become a matter of concern to a large number of railway engineers. This problem is particularly troublesome in curves where the shakedown limit of rail material is reduced due to the presence of curving traction forces in the rail/wheel contact zone. The occurrence of shelly spots, shells and flaking, caused by the fatigue failure of rail material, is always accompanied by plastic flow. In order to establish the manner in which plastic flow affects or is affected by the cracks, two rails, removed from main line curves, were sectioned and examined under Scanning and Transmission Electron Microscopes. Electron Microscope observations of dislocations are correlated to some existing theoretical models of microcrack formation and the directionality of broken pearlite colonies is examined in view of current contact stress and residual stress theories. The field observations were confirmed by laboratory experiments with the accurately known loading histories.

INTRODUCTION

As the world trend shifts toward higher speed, longer and heavily loaded trains, plastic deformation and associated damage, in particular longitudinal and transverse cracks, as shown in Fig. 1, have been viewed as serious problems effecting the rail head operational life.

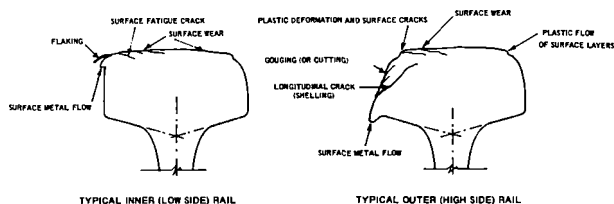


Fig. 1 Plastic deformation and associated damage in the rail head.

Considerable attention has been devoted to studying the degree of rail head deformation during service and its effect on the formation of contact fatigue cracks, changes in mechanical properties and the contact stress field (1-5). Surface topography and local changes in microstructure due to rail head deformation and the effect of metallurgical parameters in promoting subsurface cracks were studied (6-10). Other studies included the description of rail monotonic and cyclic deformation characteristics and their effect on the rail's fatigue resistance (11,12). However, beyond a preliminary study made by Stone and Marich (13), little has been contributed to the re-

lationship between rail plastic deformation and the damage process and the contact stress field or the rail steel microstructure characteristics. This paper is a preliminary attempt to characterize such a relationship and to describe the initiation and propagation of longitudinal cracks based on the rail microstructural response to the externally induced parameters during the deformation process.

PLASTIC DEFORMATION

Introduction

While the microstructure of alloyed rail steel, in the as-rolled conditions, consists of pearlite and ferrite grains, rail steel with a tensile strength of 700-900 N/mm² are composed predominantly of pearlite grains with about 25 percent ferrite. Rails with tensile above 900 N/mm², which represents the majority of heavy section rails, have a pure pearlitic grain structure. The important variable in the microstructure of pearlite is the distance between its adjacent lamellae. The increase in yield strength and, consequently, resistance to plastic deformation, varies inversely with the interlamellar spacing of the pearlite. The early stages of plastic deformation in the pearlitic rail steel matrix, as in any polycrystalline structure subjected to external stresses, take place within individual grains or, specifically, within lamellae in highly stressed regions. As a result, a dislocation pile up occurs at the ferrite-cementite boundaries. When the density of such a pile-up is accelerated due to the increase in the level of internal stress or the increase in the loading cycles, Frank-Read sources are activated in the lamella interface, emitting dislocation loops which on the one hand neutralize the stress concentration of the original pile-up and, on the other hand, enable the slip to continue across the lamella interface or to the neighbor grain. Such a slipping process will continue with each loading cycle on the rail head causing a microscopic "monotonic" increment in deformation. When such an increment is integrated with respect to time, it results in gross plastic deformation. Another mode

of the deformation may occur when the slipping process alternate in direction causing "alternating" plasticity. Each of these deformation modes depends on the nature of the stress state that activates the dislocation multiplication process in the rail head. Such stresses while depending on the mechanical properties of the rail microstructure are a product of the stress field in the rail/wheel contact zone. Therefore, the knowledge of this stress field would enable us to characterize the mode of plastic deformation in the rail head. This will be briefly discussed in the next section.

Contact Stresses and Associated Deformation

In the rolling/sliding motion between wheel and rail, two forms of forces are transmitted to the contact zone, i.e., the normal force, N , and tangential force F . The latter may result from geometrical constraint, yaw or lateral motion of the wheelset or due to an application of external lateral forces (14). These combined forces acting on the contact zone, the geometry of which could be calculated on the basis of conformal (15,16) or counterformal constraints, produce a stress field whose three dimensional stress tensor component could be computed by using different analytical and numerical techniques (17,18). The important factor in such calculations is to recognize that the octahedral shear, and not the maximum shear component, is what controls the amount of maximum repeated plastic deformation of the stresses matrix, see Lundberg and Palmgren (19) and Greenert (20).

Under free rolling contact conditions, the subsurface octahedral shear reaches equal and opposite peak values on either side of the axis of symmetry of the contact zone. This occurs at point $x_1 = +0.866a$ and $x_3 = -0.5a$ measured from the origin of that zone, where a is its major axis. When tangential force is added to the contact interface, it is found (21) to increase one of the peak values of the octahedral shear and to decrease the other. As the tangential force increases in the contact zone, the maximum subsurface octahedral shear increases in value and its location slowly decreases in depth. At the same time an additional peak of shear stress equal to $T = \mu P^*$, where μ is the coefficient of friction and P is the maximum normal pressure, is introduced on the surface at the center of the contact zone. As is known, the shake down state exists when the amount of energy dissipated in plastic flow never exceeds a finite limit so that purely elastic behavior will occur after a fixed number of load cycles. The work of K. Johnson (22) shows that, when the tangential force exceeds $0.367P$, the surface shear exceeds the subsurface octahedral shear so that the shake down is controlled by the surface stress. The coefficient of friction in wheel/rail interaction ranges between 0.2 - 0.25 in a lubricating-dry condition; thus, T does not reach the $0.367P$ value estimated by K. Johnson. Analytical techniques exist to determine if shake down state is satisfied in structure such as rail head, see for example Ref. (23). Experimental observations indicate however that such state cannot be reached during the service life of the rail head of which the plastic deformation is an accumulative process with time. The question then concerns the depth of the plastically deformed zone and the mode of its deformation. The

*The surface shear traction does not greatly influence the subsurface distribution of strain. The subsurface plastic deformation caused by partial slip is not likely to differ significantly, therefore, from the one of complete slip, see Ref. (22).

work of Ravitskaya (24) shows that in carbon rail the depth ranges from 8-15 mm, while in alloyed rail steel it ranges from 3-6 mm. Such depth depends on the wheel load, the microstructure of the rail head matrix and surface and the subsurface strain hardening characteristics of such structure.

As previously explained the mode of deformation in a polycrystalline structure depends on the form of the applied stress. In the deformed zone of the rail head, aside from the compressive stress resulting from the normal force, the stress applied on the surface is basically of a different character than the one acting on the interior. While the surface stress maintains a single direction following the traction force direction, the subsurface octahedral shear is an alternating stress.

In addition, the plastic flow of the subsurface layers being highly constrained in relation to that of the surface layer, these layers also possess different microstructures. The surface layer consists of a fine grain structure with a high degree of preferred orientation while the subsurface layer is a coarse structure with randomly oriented grains. Such differences manifest themselves in the degree of the severity of deformation pattern exhibited, Fig. 2(a). The subsurface, under the effect of alternating shear, deforms in an "alternating" or "zigzag" pattern, shown in Fig. 2(b), while maintaining the integrity of its lamella structure. The surface layer, measured with an $100 \mu\text{m}$ depth in Fig. 2(a), is a fragmented layer

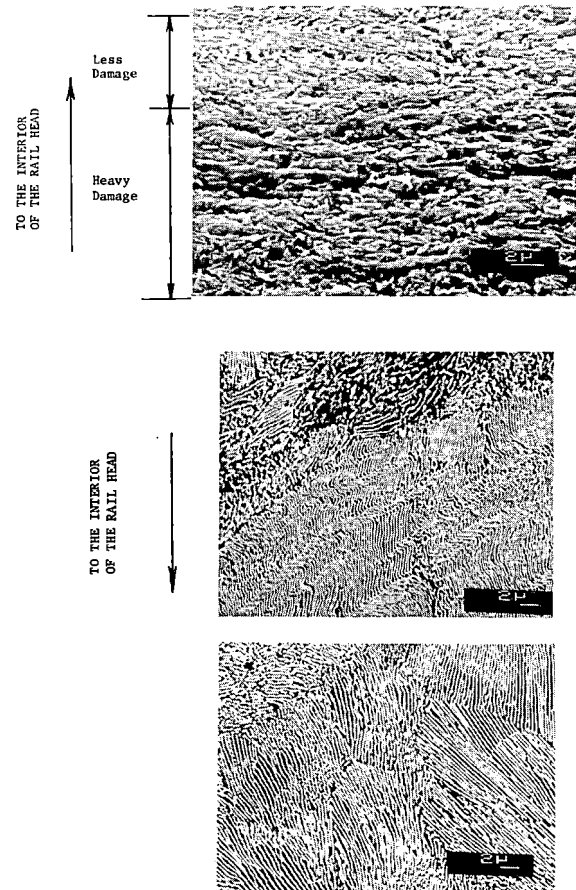
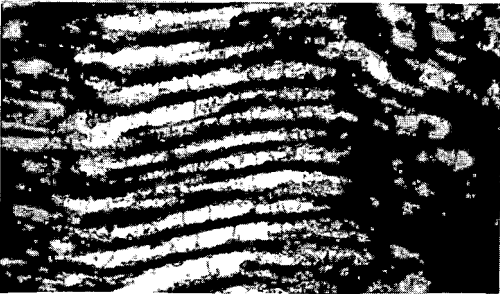


Fig. 2(a) Deformation pattern of the heavily damaged surface layers, (b) Zigzag pattern of deformed lamellae, and (c) Lamellae arrangement in undeformed grains.

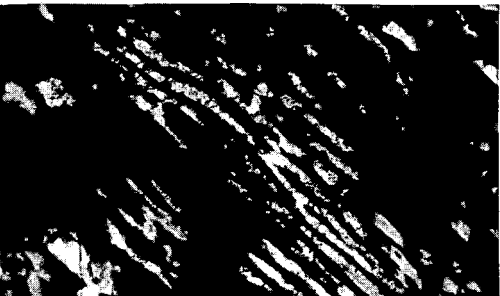
consisting of heavily deformed broken "short" lamella. Such a structure has been shown by Rigney (25) to consist of a cellular structure which develops during an initial break-in* period of the rail surface. Indeed, when viewing the dislocation pattern in the two layers discussed, using the Transmission Electron Microscope, one can observe that at a depth of 5 mm from the surface, Fig. 3, the dislocations pile up at the ferrite-cementite boundary with no tangled dislocations in the ferrite region. The density of the tangled dislocations and consequently the cell structure increases while approaching the surface at depths of 1 mm and 500 μm shown in Fig. 3(b) and (c).



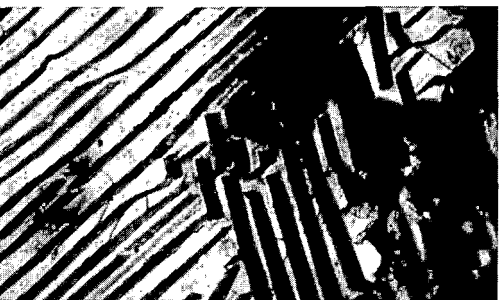
(a)



(b)



(c)



(d)

Fig. 3 Dislocation pattern in used rail at depth (a) 5 mm (b) 1 mm (c) 500 μm compared with this of new rail at depth (d) 1 mm.

*Break-in period is where the original microstructure of the surface is gradually changing to a cell structure of accommodating large strains in the sliding direction.

With this argument in mind, it should be recognized that the deformed zone in the rail head consists of two distinctive layers; i.e.:

- (i) a heavily deformed surface having a thickness* of 100 μm - 1 mm followed by,
- (ii) a plastically deformed subsurface layer with a thickness of 3-5 mm (depending on the rail type).

Behavior analysis of these layers or their mathematical modelling must consequently be treated independently.

While the ability to quantitatively characterize the stress and strain fields in both these two layers is equally important, the work in the following section will concentrate on developing a simple model for estimating the total strain in the surface due to the effect of the surface traction force.

Simplified Model

As described before, the critical factor in quantitatively describing the plastic flow in the outersurface layer of the rail is the surface traction force resulting from wheel/rail sliding. Such force is characterized by parameters such as the magnitude and direction of sliding in the contact zone and the position of this zone on the rail surface. Interdependence of these parameters should initially be discussed as follows:

Contact Zone Position. In order to establish the position of the contact zone, one should consider an overall spatial orientation between a wheelset and track rather than limit such analysis to a single wheel and rail. In the case of a tangent track a wheelset is kept at the center of the track by gravitational forces. It contacts the rails at two points which are approximately symmetrical with respect to the center of the track or the wheelset. In curves, however, the situation is more complex. A wheelset may contact the rail at either two or three points, depending on its angular alignment and lateral displacement. These two variables, yaw misalignment (also referred to as skew angle or angle of attack) and lateral displacement, are interrelated. However, angle of attack is considered an independent variable.

The angle of attack may vary randomly in any given population of wheelsets in ranges from -20° to about $+60^\circ$ depending on the degree of curvature, location of the wheelset in a freight car and other variables affected by track irregularities. Field measurements (28) have shown that angle of attack is highest on the leading axle of a leading truck (LL) and in the vicinity of zero to slightly negative for a trailing axle on a trailing truck (TT). For example, the mean values measured in five degree curves were as follows: $\alpha_{LL} = 28^\circ$; $\alpha_{TL} = 10^\circ$; $\alpha_{LT} = 24^\circ$; and $\alpha_{TT} = 5^\circ$ (L:Leading, T:Trailing). Although lateral displacements were not measured during these tests, it has been analytically well established that with an increase in the angle of attack the wheelset displaces laterally until flange contact is established at the

*In the work of Rigney and Hirth (26) it is shown that the thickness, t , of the highly deformed layer would vary with load by some power less than unity. Tsuya (27) has estimated that the thickness for such layer (for copper) equals L^n where $n \approx \frac{1}{2}$.

range of $\alpha = 8' - 14'$. A value of $8'$ is typical of a dry rail and an upper limit value of $14'$ is typical of a fully lubricated rail.

Since this paper is concerned with plastic flow being experienced by the outer or high rail in curves, let us analyze more closely the possible situation which may occur at this location. The left side of Fig. 4 shows three examples of contact between worn wheels and worn high rails. Case I shows a contact ellipse typical of interaction between trailing

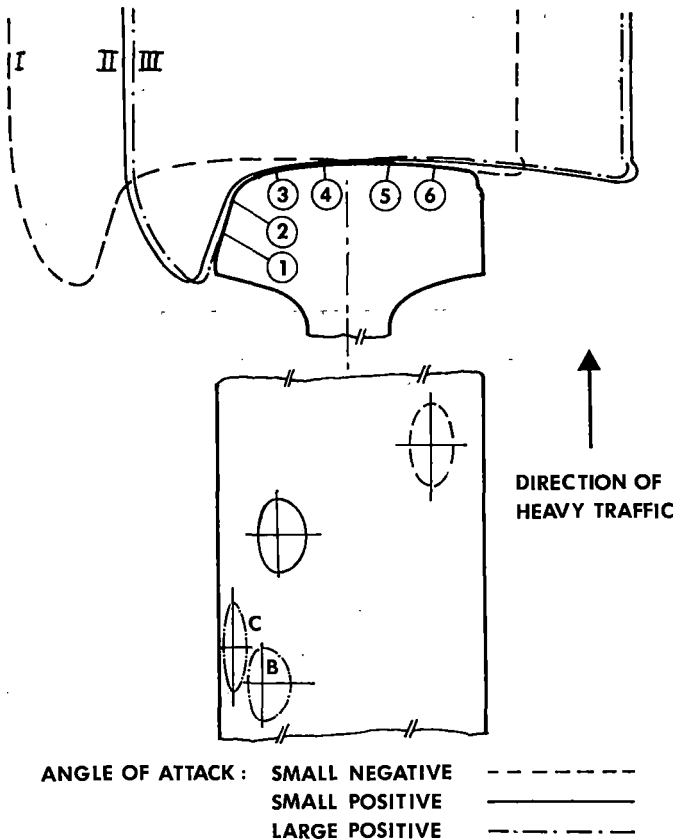
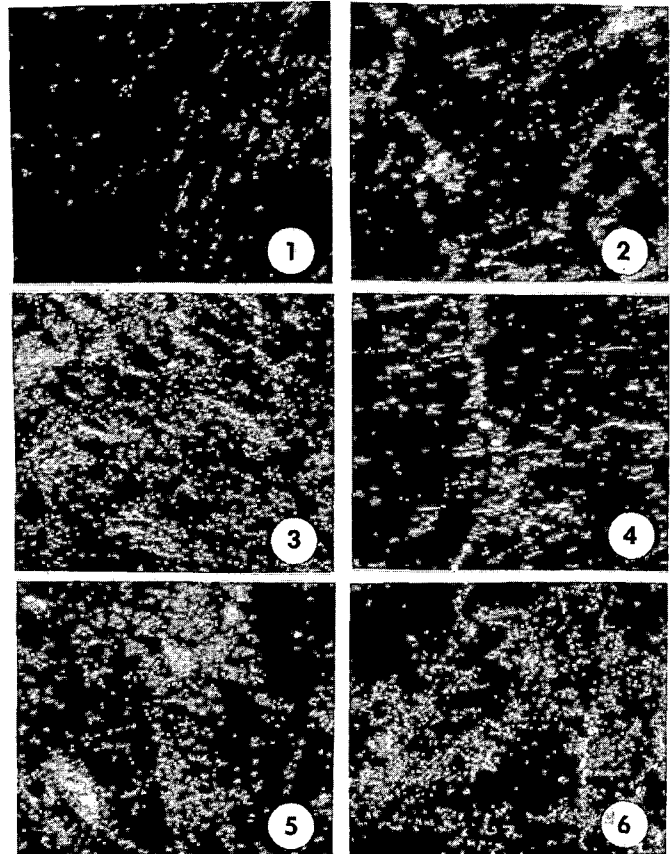


Fig. 4 Surface characteristics of contact position on the rail head.

wheelsets of trailing trucks and high rails. Both, angle of attack and lateral displacement, are slightly negative, bringing a flange of low wheels very close to the gauge corner of the low rail. Case II is typical of wheelsets with a small positive angle of attack in which hard flanging is absent and both vertical and lateral load components are supported by one contact ellipse having high conicity with respect to track center line. Case III is typical of large angles of attack where a third point of contact between a pair of rails and wheelsets is firmly established. This situation is referred to as hard flanging. As a rule, a flange contact C is located forward of tread contact B. Thus, knowledge of angle of attack, lateral displacement and tread profiles of wheels and rails has helped us establish the locality and shape of contact ellipses. These same misalignments, however, are responsible for the presence of sliding within the zone of contact during the wheelset's negotiation of curves.

Surface Traction. The length and direction of sliding within the zone of contact could be observed

experimentally on rail or wheel surfaces. The right side of Fig. 4 shows the micrographs at six locations of the rail surface taken from an eight degree curve. Locations 1 and 2 are from the flange contact while the other four are from the tread contact. The largest amount of sliding appears at the flange contact and a trajectory of wheel asperity rubbing rail takes on a shape of extended cycloid. Therefore, if the wheel flange contacts the upper half of the gauge side of the rail, the rubbing trajectory will exhibit a large downward component. However, if the contact zone is



located at the lower half of the gauge side of the rail, the rubbing marks will have a large longitudinal component. Wheelsets contacting the tread of the high rail with a positive angle of attack will produce surface tractions with appreciable lateral components. In fact, these tractions are almost perpendicular to the direction of travel of wheels in the case of large angles of attack.

These tractions produce significant shear stresses in the surface layer(s) of rail material causing plastic deformation and flow towards the gauge side the high rail. The fact that at Location 6 the rail material is pushed towards the field side of the rail can be attributed to a negative angle of attack which not only brings the wheelsets into contact at this location but also produces tractions with appreciable lateral components pointing in the opposite direction from tractions at Locations 3 to 5. Since these tractions have lateral and longitudinal, as well as spin components, the underlying plastic flow also appears to be in the direction of the resultant of these components, as shown in Fig. 5. This figure

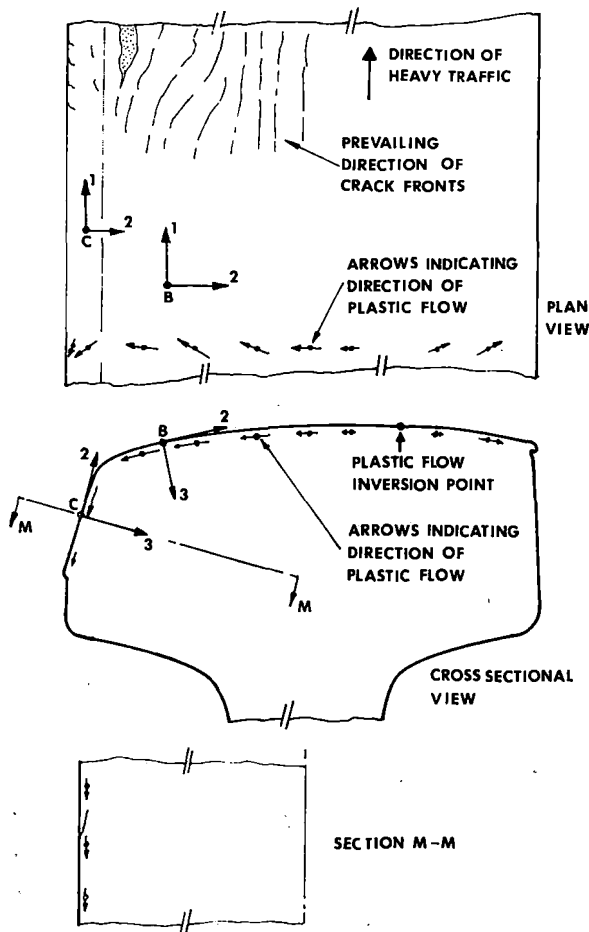


Fig. 5 Configuration of surface tractions on the rail head.

also depicts the prevailing direction of surface microcracks which are, not surprisingly, perpendicular to the direction of surface tractions.

While the surface tractions and direction of plastic flow have been discussed on the basis of experimental observations, the direction and magnitude of these tractions and, therefore, the amount of slippage in the contact zone, could analytically be calculated by using, for example, a theory of Kalker's (29). A detailed analysis of such calculations is presented in Ref. (30).

Now, having characterized the surface traction, the rail surface would be assumed to have the following features during the deformation process:

1. The average surface roughness and asperities would stabilize after the passage of the first few cycles and thus the magnitude of the coefficient of friction is a constant.
2. The extent of wheel material transfer to the rail surface would be extremely limited due to the hardening and the cold working effect of the surface. Furthermore, the work function of this surface would be in a level that produces a minimal reaction to the external environment; therefore no chemistry or phase change would occur during the deformation process. When invoking these conditions, a steady state of plastic deformation is assumed to occur in the rail surface and the magnitude of strain in this surface is the same for each cycle or wheel

passage.

As mentioned before, the integral amount of slippage within the area of contact can mathematically be calculated. If this amount is δa , the frictional work done in the zone of contact can then be estimated as:

$$W = F\delta a$$

$$= \mu N\delta a$$

Furthermore, the plastic work per unit volume in the area of contact could be calculated as the product of the flow stress, τ_f , in the sliding direction and the average net strain, ϵ_t , per cycle in the severely deformed layer. It is shown by Rigney and Hirth (26) that both τ_f and ϵ_t depend on the depth, d , of this layer.

The plastic work could then be written as:

$$W_p = \tau_f \epsilon_t d \delta b \delta a$$

where δb is the width of the plastically deformed zone. It should be noted here that both δa and δb are independent of the geometry of the contact area but depend on the normal pressure distribution in such an area. Under steady state conditions which are assumed to exist, the plastic work is equal to frictional work, therefore:

$$\tau_f \epsilon_t d \delta b \delta a = \mu N \delta a$$

which could be written as:

$$\epsilon_t = \frac{\mu N}{d\delta b} \tau_f^{-1}$$

The flow stress τ_f for a constant value of ϵ_t in pearlitic structure could be approximated by:

$$\tau_f = \tau_0 + K \ell^{-0.5}$$

where τ_0 is the average frictional stress and K is the Hall-Petch slope. For pearlitic structure, these two constants are estimated as:

$$\tau_0 = 76.4 \text{ MPa};$$

$$\text{and } K = 0.5 - 0.68 \text{ MN/m}^{3/2}$$

Furthermore, in the previous equation ℓ is generally considered the interlamella spacing or the average grain size. In the present analysis, however, the grain boundary and most of the bulk features are totally obliterated in the surface layer. ℓ is then taken here as an average of the cell size in the deformed surface layer.

Equation can be written, therefore, as:

$$\epsilon_t = \frac{\mu N}{d\delta b} (\tau_0 + (K/\sqrt{\ell}))^{-1} / \text{cycle}$$

This equation expresses the average net strain/cycle as a function of parameters that represent the load criterion on the rail surface and parameters that represent the microstructure properties of the rail material. This expression, however, suffers a major problem: in order to determine its validity, surface strain for each loading cycle in the direction of the metal flow should experimentally be measured. An X-ray diffraction method or a chemical marker technique could be used, together with Auger analysis, to measure

the variation of gross strain with depth in the near-surface region. Such experimental verification of the previous equation is part of the author's current research activities.

RAIL HEAD DAMAGE

Rail head damage is a term that covers a wide scope of defects which results from the severe conditions of wheel/rail loading and lead either to the fracture of the head section or to the early removal of the rail from service. Of the defects that have been identified and classified in several articles (31,32), the combination of subsurface longitudinal and transverse crack has been the focus of studies in the past decade (33-35). The important characteristic of such cracks is that they initiate and propagate to their critical length without surface exposure. It is estimated that they are responsible for a high percentage (90% in some cases (35)) of failure in heavy haul lines. A general view of their appearance in the head cross section is shown in Fig. 6.

In this section of the paper a model is developed to explain the initiation and propagation processes of the longitudinal crack.

The Longitudinal Crack

As described in the excellent work of Marich (33), the longitudinal crack is the crack which runs horizontally along under the inside gage corner of the high rail head at curved regions of a track. Its path as shown in Fig. 7 is inclined at an angle between 30°-60° to the vertical plane with a depth range of 3-12 mm measured from the running surface depending on the rail steel type. As this crack propagates longitudinally and laterally inside the rail, it culminates in the removal of a thick portion of the surface metal at the gage corner as illustrated in Fig. 8. This phenomenon, commonly referred to as heavy or light shelling, depending on the severity of the damage, could occur as an isolated incident on the rail curve or at several locations on the same rail length, see Fig. 9.

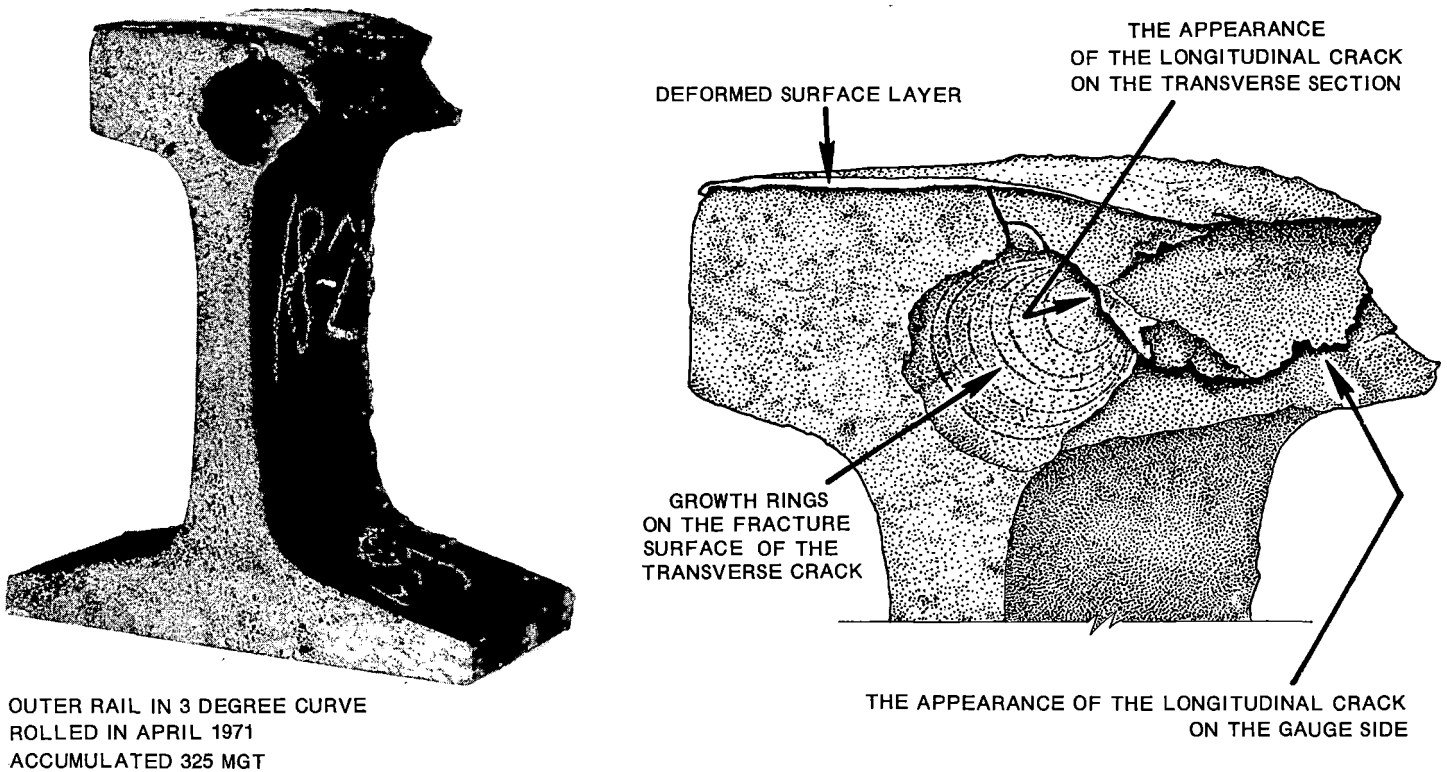


Fig. 6 General view of longitudinal transverse cracks.

It has been established that in this crack combination the longitudinal crack is formed initially and that a transverse crack is subsequently created at a location on the interface of the longitudinal crack (24).

In this concept, assuming that the general rules of the fatigue damage process apply, the fracture surface of the longitudinal crack acts as a free surface on which the transverse defect is initiated. The initiation mechanism of the longitudinal crack, however, is the least understood since it is assumed to take place in the deep layer of the rail matrix.

Models describing the initiation mechanism of this crack (33) have been proposed on the assumption that locations of random inclusions or phase transformed regions in the rail head can act as initiation sites. Keeping in mind that specimens examined in some of these studies were manufactured a decade ago, the increase of rail steel matrix cleanliness as a result of development in steel making and rolling processes did not reduce the appearance of such cracks or alter their geometrical appearance in the rail head. Microscopic examinations, in fact, showed that longitudinal cracks can exist in regions of the rail head that are free of traces of inclusions or severe

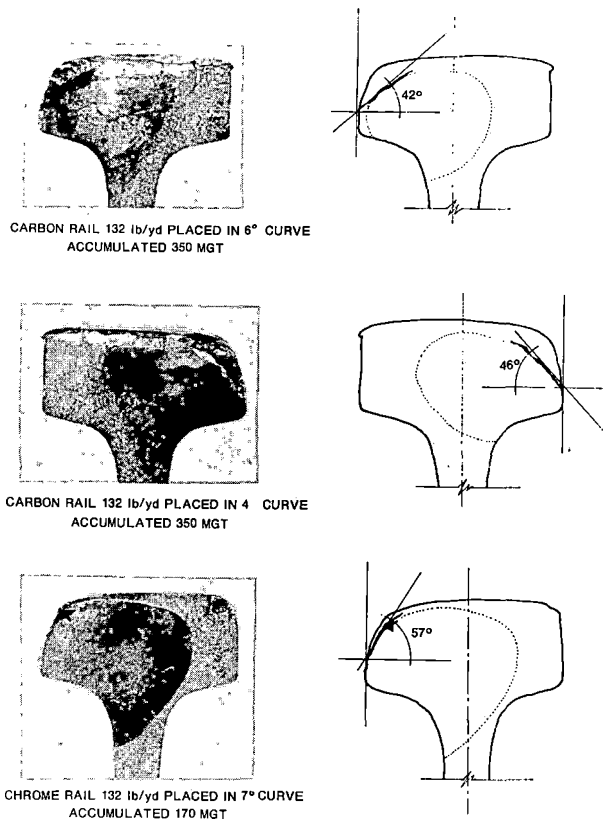
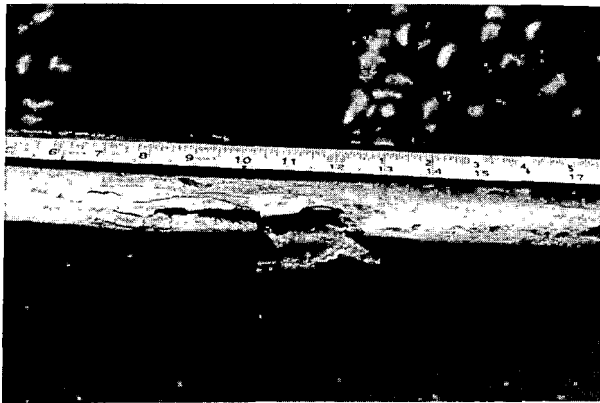


Fig. 7 Geometry of the longitudinal crack in the rail head.



(a)



(b)

Fig. 8 Appearance of shelling; (a) surface, (b) transverse.



Fig. 9 Multiple "light" shelling on a rail length.

impurities. Such observations are consistent with the general laws of fatigue processes, one of which states that the internal fatigue cracks occur under favorable conditions in the presence of a free surface (the inclusion/matrix interface could be viewed as a free surface). It becomes reasonable then to assume that in addition to the hypothesis of inclusion, other mechanisms that include the effect of stress field and rail microstructure parameters should exist for the initiation of longitudinal cracks. In this section, a model for such mechanisms is introduced.

Initiation Mechanism

In the first part of this paper, it was shown that the outer surface layer of the rail head will experience an incremental unidirectional plastic flow that continues during the operational life of the rail. As the metal flow advances along the gage corner of the rail, it terminates in a form of displaced layers accumulating along the corner. The edge of each of these displaced layers will either interact with a previous layer, having a different magnitude of deformation or with an elastic matrix that did not suffer deformation. Such interaction was observed to generate a number of surface intrusions as shown in Fig. 10.

As the rail head gage corner conforms to the wheel profile contour, the wheel/rail contact zone, in hard flanging positions, could include regions of the gage side as low as position 1 in Fig. 8. The tangential surface stresses acting in this zone create a large tensile stress in the area of its rear boundary (36). If any of the surface intrusions previously described fall into this area, it is highly probable that the cyclic repetition of this tensile stress results in such an intrusion opening into the rail matrix, see Fig. 11. Simulated work using a laboratory wheel/rail wear rig confirmed that such surface crack initiation mechanism exists.

The number of wheel cycles, N_i , necessary for this initiation process to be completed, i.e., for the surface intrusion to reach the threshold length a_{th} ,

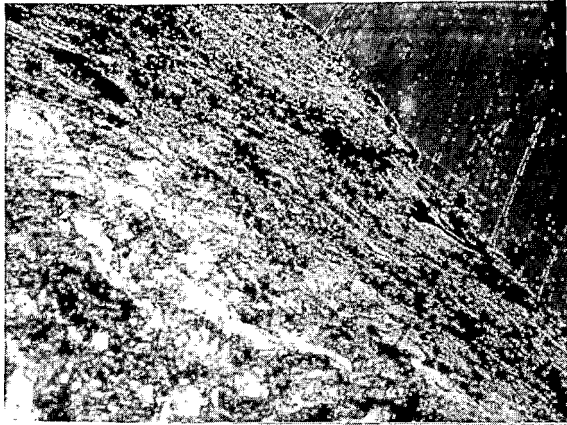


Fig. 10 Surface intrusion on the gauge side of a rail.

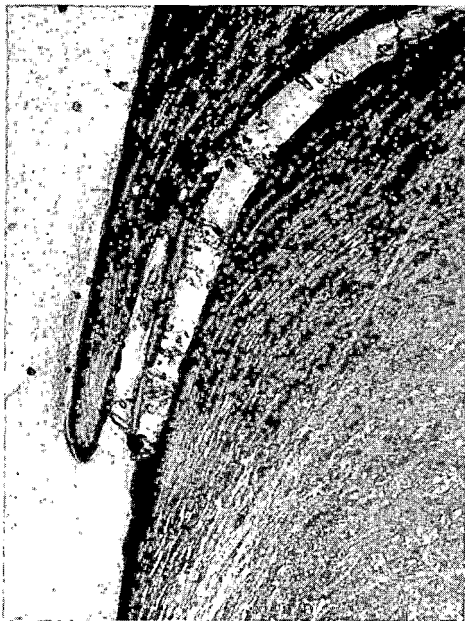


Fig. 11 Development of a surface into a surface crack.

can be calculated from the knowledge of the magnitude of tensile stress in the rear boundary of the contact zone, the hardening characteristics of the rail surface, a_{th} which can be evaluated by calculating the threshold stress intensity factor, K_{th} , for pearlitic rail steel. Analytical models for calculating N_1 exist; they will not be detailed in this paper, see Refs. (37,38).

As the crack develops inside the rail head, it enters a plastically deformed region. The orientation of the crack propagation plane or plateau within this zone is governed, in addition to the active shear stress component, by the magnitude and orientation of residual stresses and hardening characteristics of the matrix in this zone.

Residual stresses and hardness values were measured in the corner gauge of an unfailed portion of a rail that had developed a longitudinal crack. Fig. 12 shows hardness contours connecting points of equal hardness in the deformed gauge corner. Each of the

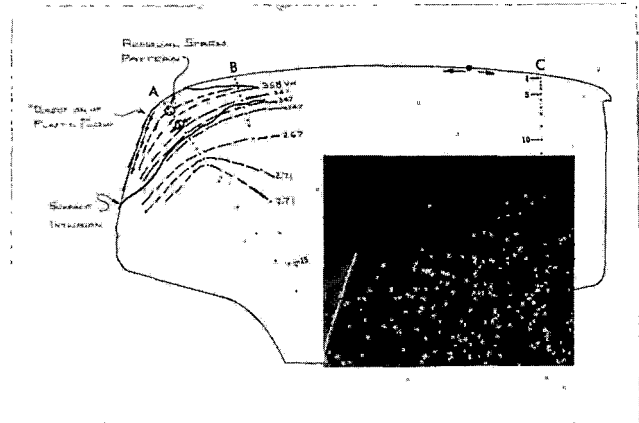


Fig. 12 Hardness contours in the gauge corner.

contours separates a layer (or layers) of different deformation or hardening level and Figs. 13 and 14* indicate the pattern of radial and transverse stresses in this region. While radial stresses, below 3 mm of the running surface of the rail, are in a form of tensile stress,** thus aiding a crack to propagate in a direction parallel to the surface of the rail head corner, all other stresses, Fig. 14, are in compression, preventing any crack from propagating in a perpendicular direction to the rail surface or from linking with the heavily deformed layer of this surface.

The optimum path for a crack's propagation is, therefore, a plane of uniform hardening (parallel to the gauge corner) subjected to tensile residual stresses and passing through the transitional region between a plastically deformed structure and elastic material. This region has been shown by Marich et al. (13) to be, in fact, work softened. The geometry of this path is similar to what observed in the large portion of failing rail cross sections.

In the model described above the propagation process is achieved through combined propagation modes; Mode I governed by the influence of the tensile radial residual stresses and Mode II (in-plane shear) due to the shear stress component of the externally applied wheel/rail contact stresses. In this latter mode of propagation, the fracture surface is subjected to a fretting fatigue process that leads to the appearance of spherical particles as shown in Fig. 16.

The effective stress intensity factor, therefore, as reported by Shah (39) and utilized by Marich (33), is the sum of the stress intensity factor associated with each mode, i.e.,

$$K_{ef} = K_I + K_{II}$$

$$= 2\sigma \sqrt{a_{th}}/\pi + 0.8 \tau \sqrt{a_{th}}/\pi$$

*Mitchell, C.M. and Laufer, E.E., AIME Meeting, Las Vegas, 1980.

**Radial residual stresses of an average of 200 MPa, shown in Fig. 13 could actually be capable of opening grain boundaries inside the microstructure. These openings could act as crack initiation sites. Such phenomenon is observed to occur in the rail head, see Fig. 15.

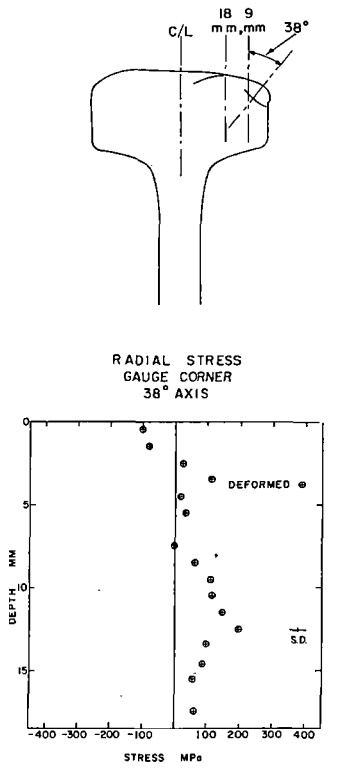


Fig. 13 Radial residual stress pattern in the gauge corner.

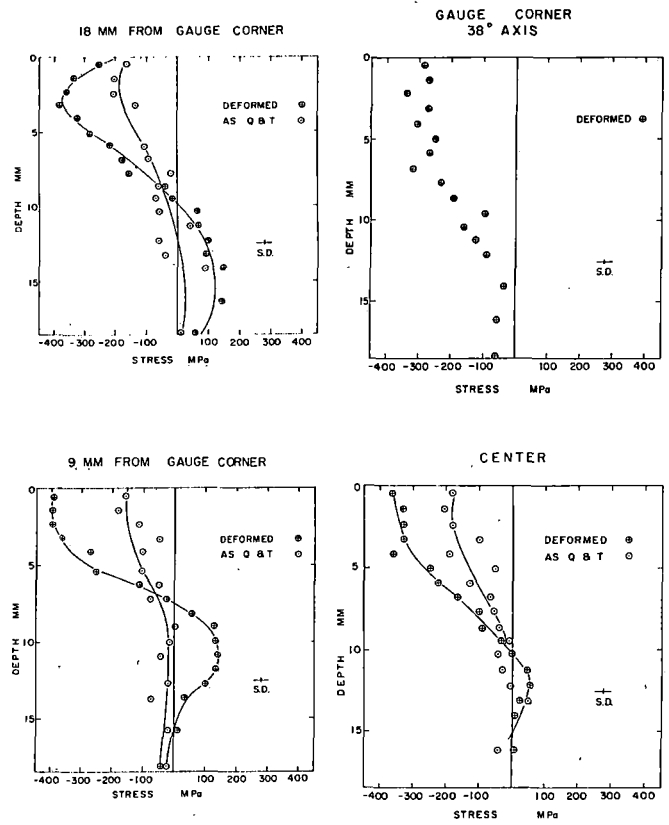


Fig. 14 Transverse residual stress pattern.



Fig. 15 Grain boundary openings on the fracture surface 11,000x.

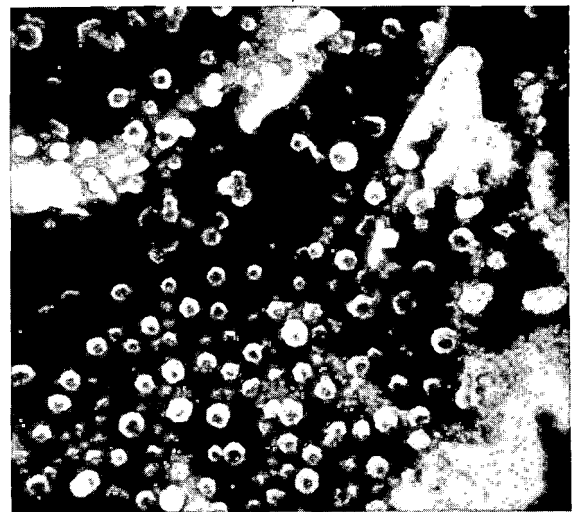


Fig. 16 Spherical particles on the fracture surface of the longitudinal crack 1,000x.

where K_{ef} is taken to be the maximum threshold stress intensity factor determined by Broek and Rice (40) and utilized by Marich. It equals $14.8 \text{ MPa}\sqrt{\text{m}}$ for fully eutectoid steel. a_{th} is the threshold crack length, i.e., the minimum length of a crack which will lead to

fatigue crack propagation.

τ is the shear stress component along the fracture surface = 530 MPa (33).

σ is the tensile residual stresses (the effect of thermal contraction of the rail and vertical and bending are negligible) σ is taken as 200 MPa, see Fig. 13.

From the above equation a_{th} is shown to be 300 μm . This value is much larger than the diameter of a typical inclusion or inclusion/matrix diameter of any cluster of inclusion which are normally observed in the rail head microstructure. It has to be acknowledged, however, that inclusions larger than 300 μm - although not typical - exist in the rail head and could lead to the appearance of internal cracks.

CONCLUSIONS

1. The deformed zone in the rail head consist of two distinct layers, I, a heavily deformed surface having a thickness of 100 μm - 1 mm followed by, II, a plastically deformed subsurface layer with a thickness of 3-5 mm depending on the rail type.

2. A new model is proposed to explain the phenomenon of initiation of a longitudinal crack in the rail head. In this model service intrusions on the gage face of the high rail are considered the initiation sites of these cracks.

REFERENCES

1. Tamazaki, T. and Sugiyama, T., "Experiments on Horizontal Crack Propagation in Rail Head," Quarterly Report, Railway Tech. Res. Inst., Vol. 22, 1981.
2. Akaoka, J. and Hirasawa, K., "Fatigue Phenomenon under Rolling Contact Accompanied with Sliding," Bulletin of JSME, Vol. 2, 1959.
3. Allmen, N.J., "The Effect of the Ratio of Wheel Diameter to Wheel Load on Extent of Rail Damage," Proc. 45th Conv. AREA, Vol. 47, 1946.
4. Toth, L. "Fatigue-Wear Testing of Rails Under Rolling Load," Acta Tech. Acad. Sci. Hung., 70: 445, 1971.
5. Marich, S., "Research on Rail Metallurgy," AREA Bulletin 78, 1977.
6. Fastenrath, F., ed. "Railroad Track, Theory and Practice," Frederick Ungar Pub. Co., N.T., 1977.
7. Park, Y.J. and Bernstein, I.M., "Effective Grain Size for Cleavage Fracture in Pearlitic Eutectoid Steel," Int. Fracture, Waterloo, Canada, 1974.
8. Parsons, D.E., "Chemical Composition and Impact Transition Temperature of Carbon and Alloy Rail Steels (1951-1977)," CANMET, Report MRP/PMRL 77-4(R), 1977.
9. Marich, S., "Development of Improved Rail and Wheel Materials," Proc. of Seminar on Vanadium in Rail Steels, Chicago, Nov., 1979.
10. Leis, B.N. and Laflen, J.H., "Cyclic Inelastic Deformation and Fatigue Resistance of Rail Steels-Experimental Results and Mathematical Models," DOT-TSC-1076, 1977.
11. Leis, B.N., "Cyclic Inelastic Deformation and Fatigue Resistance Characteristics of a Rail Steel," ASTM, STP 644, 1976.
12. Stone, D.H. and Steele, R.K., "The Effect of Mechanical Properties Upon the Performance of Railroad Rails," ASTM, STP 644, 1976.
13. Stone, D.H. and Marich, S., "Deformation Behavior of Rail Steels," Transportation Research Record 744.
14. Brickle, B.V., "The Steady State Forces and Moments on a Railway Wheelset Including Flange Contact Conditions," Ph.D thesis, The Loughborough University, 1973.
15. Paul, B. and Hashemi, J., "An Improved Numerical Method for Counterformal Contact Stress Problem," Department of Transportation, Report No. FRA-ORD-78-26, 1977.
16. Hashemi, J. and Paul, B., "Contact Stresses on Bodies with Arbitrary Geometry, Application to Wheels and Rails," Department of Transportation, Report No. FRA-ORD-79-23, 1979.
17. Johnson, K.L. and Jefferis, J.A., "Plastic Flow and Residual Stresses in Rolling and Sliding Contact," Proc. Symp. Fatigue in Rolling Contact, London, 1963.
18. Martin, G.C. and Hay, W.W., "The Influence of Wheel-Rail Contact Forces on the Formation of Rail Shell," University of Illinois, 1970.
19. Lundberg, G. and Palmgren, A., "The Dynamic Capacity of Roller Bearings," Acta Polytech., Stockholm, No. 7, 1947.
20. Greenert, W.J., "The Toroid Contact Roller Test as Applied to the Study of Bearing Materials," J. Basic Engng., Trans. Amer. Soc. Mech. Engrs., 84, 1962.
21. Smith, J.O. and Liu, C.K., "Stresses Due to Tangential and Normal Loads on An Elastic Solid with Application to Some Contact Stress Problems," ASME, J. of Applied Mechanics, Trans. ASME, 75, 1953.
22. Merwin, J.E. and Johnson, K.L., "An Analysis of Plastic Deformation in Rolling Contact," Proc. Inst. Mech. Engrs., 177, No. 25, 1963.
23. Hodge, Jr., P.G., "Plastic Analysis of Structure," McGraw-Hill, N.T., 1959.
24. Ravitskaya, T.M., "Features of the Initiation and Development of Internal Fatigue Cracks Considered on the Examples of Rail Failure," Problemy Prochnosti, No. 11, 1974.
25. Rigney, D.A., and Glasser, W.A., "The Significance of Near Surface Microstructure in the Wear Process," Wear, 46, 1978.
26. Rigney, D.A. and Hirth, J.P., "Plastic Deformation and Sliding Friction of Metals," Wear, 53, 1979.

27. Tsuya, T., "Microstructures of Wear, Friction and Solid Lubrication," Tech. Rep. No. 81, Mech. Eng. Lab., Igusa Suginami-Ku, Tokyo, 1976.
28. Ghonem, H., Gonsalves, R. and Bartley, G., "Comparative Performance of Type II and Premium Trucks," Trans. of ASME, 80-RT-8, 1980.
29. Kalker, J.J., "Rolling with Slip and Spin in the Presence of Dry Friction," Wear, 1966.
30. Kalousek, J., Rosval, G. and Ghonem, H., "Lateral Creepage and Its Effect on Wear in Rail/Wheel Interfaces," Proc. of Int. Symp. on Contact Mechanics and Wear of Rail Wheel Systems, University of Waterloo, Canada, 1982.
31. Schoeneberg, K.W., "Rail and Research - Problem Definition," Association of American Railroads, Tech. Report No. R-120, 1973.
32. Monaghan, B.M., "Rail Life Study and Recommendations," Quebec North Shore and Labrador Railway, Quebec, 1961.
33. Marich, S., Cottam, J.W. and Curcio, P., "Laboratory Investigation of Transverse Defects in Rails," Heavy Haul Railway Conference, Perth, Australia, 1978.
34. Ito, A. and Kurihara, R., "Shelling of Rails Experienced in Japanese Railways," Bulletin of Permanent Way Soc. of Japan, Vol. 13, 1965.
35. Skinner, D.H. and Judd, P.A., "A Metallurgical Study of Fatigue Defects in Rails," Aust. Inst. Mining, 34th Annual Conference, Queensland, 1981.
36. Masumoto, H., et al., "Some Features and Metallurgical Considerations of Surface Defects in Rail Due to Contact Fatigue," STP 644, 1978.
37. Ghonem, H. and Provan, J.W., "Micro-mechanics Theory of Fatigue Crack Initiation and Propagation," Int. J. of Fracture Mechanics, Vol. 13, No. 4, 1981.
38. Ghonem, H., "Longitudinal and Transverse Cracks in the Rail Head," Proc. of CANSAM, Vol. 1, 1981.
39. Shah, R.G., "Fracture under Combined Modes in 4340 Steel," ASTM STP 560, 1974.
40. Broek, D. and Rice, R.G., "Fatigue Crack Growth Properties of Rail Steels," Battelle, Report No. DOT-TSC-1076, 1977.

The Influence of Wheel/Rail Interaction on System Performance

C. Epp

Senior Research Officer
BHP Melbourne Research
Laboratories
Melbourne, Australia

R. Okey

Research Officer
BHP Melbourne Research
Laboratories
Melbourne, Australia

Wheel and rail wear represent major costs in heavy axle load unit train operations. The desire to improve operating efficiency has led to an examination of standards and practices in use on these systems. An important aspect of research activities has been the development of simulation models to provide better understanding of system parameter interactive effects. Models have been set up to study wheel/rail profile interaction and its influence on three-piece truck curving and tangent track performance. These have been used for designing and evaluating wheel and rail profile modifications. Field trials have shown improvements in performance associated with profile grinding of rails and the use of wear adapted wheel profiles. The study has shown that track quality, wheel and rail profiles and truck component tolerances have a direct influence on system performance.

INTRODUCTION

Under heavy axle load unit train conditions, wheel and rail wear significantly influence system performance and operating costs. A joint research programme, between Mt. Newman Mining Co. Pty. Ltd., Hamersley Iron Pty. Ltd. and The Broken Hill Proprietary Co. Ltd., has examined means by which iron ore railroad operations in Western Australia could be improved. This has involved extensive field trials and the collection of data to evaluate system changes¹⁻³.

A prime requirement for achieving a better understanding of railroad operations has been the development of system models. These include a steady state curving model and a dynamic tangent track lateral response model for three piece trucks^{4,5}. Considerable emphasis was placed on the modelling of wheel and rail profile combinations. These models were used for assessing system parameter interactive effects, the design and evaluation of modified wheel and rail profiles.

CURVE RAIL PROFILING

Under the action of heavy axle loads, severe rail profile wear takes place. Plastic flow, particularly in association with standard rail materials, constitutes a significant part of these profile changes. A consequence of this is the reduction in wheelset rolling radius differential. This leads to higher flange guidance forces in curves thereby accentuating both wheel flange and rail side wear.

Rail maintenance machinery, such as the Speno grinding unit, is commonly used to restore the pro-

file and to rectify surface irregularities. This, in association with gauge widening resulting from rail side wear, can help to improve the curving performance. For coned wheels, increased gauge or more specifically greater wheel/rail lateral clearance directly increases the maximum rolling radius differential. Its influence on tread and flange energy consumption, derived from the curving model, is shown in Fig. 1. The specific flange energy is based on the product of flange force times relative slip, whilst the tread energy term is defined by the sum of creep forces times creepage.

The results indicate that a preferred gauge or wheel/rail lateral clearance exists for minimum tread energy. In contrast, flange energy is seen to decrease progressively with increasing clearance. This factor dominates and points towards wider gauge for improved performance under conditions of new wheels and rails. However, gauge widening is limited by practical constraints and leads to adverse conditions in the case of worn wheels when reversed tread conicity sections contact the rail.

A more effective means for increasing rolling radius differential is to modify the profiles. This should be confined largely to the rail profiles in curves as high rolling radius differences or conicities are not desired for tangent running. Maximum effect is achieved by asymmetric profile grinding of rails. This is within the scope of rail grinders and is a practice adopted by the major iron ore railroads in Western Australia.

Initial field trials, previously reported⁶, showed the favourable effect of rail profiling to reduce curve wear. Subsequently, analytical techniques were developed further to allow changes in wheel and rail profiles to be evaluated. As a result of this work, initial ground rail profiles were refined to reduce material removal whilst achieving a suitable wheelset rolling radius differential.

Figure 2 illustrates the relative change in rolling radius differential for coned wheels on standard and asymmetric profile ground rail sections. For the ground rail a base value is generated with

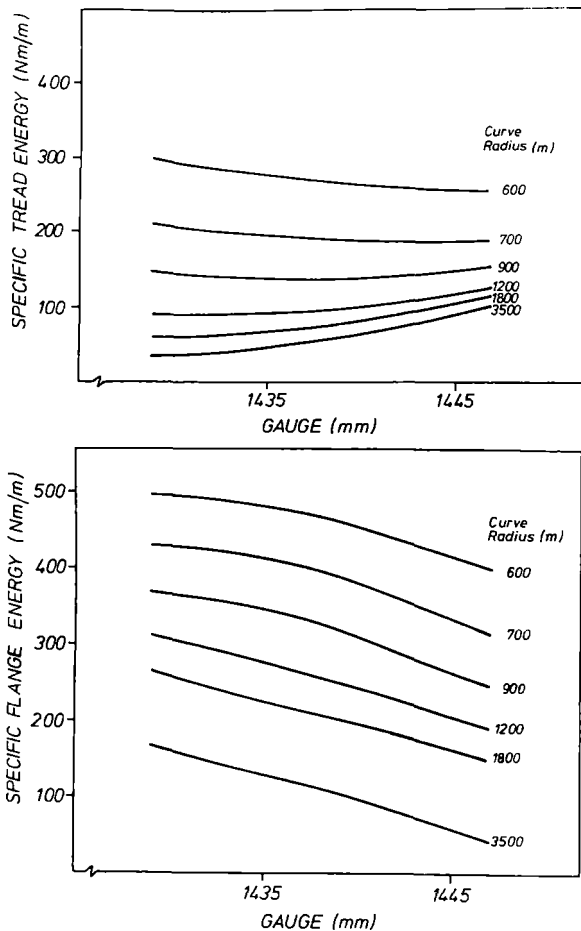


FIG.1 VARIATION OF TREAD AND FLANGE ENERGY WITH GAUGE FOR A 'LOADED' TRUCK (NEW WHEEL AND RAIL PROFILES)

the wheelset centralized. This allows a larger rolling radius differential to be achieved at the point of high rail flange contact than is the case for standard rail profiles.

Similar changes occur with worn wheel profiles and assist in the curve negotiation by reducing flange forces and wear. Asymmetric profiling avoids the need for high conicity wheels which conflict with the requirements for tangent track operation. Nevertheless, some increase in the effective conicity of new wheels is desirable to reduce their sensitivity to diameter mismatch and differential wear across axles.

CURVING PERFORMANCE

Curving simulations were conducted to establish representative base data for wheel/rail energy consumption. The variables examined included evenly wearing AAR wheels at various stages of their service life, profile ground rail, a range of curve classes and levels of flange lubrication.

The results are shown in Fig. 3 and also include the combination of new coned wheels with standard rail sections. The comparison of new wheels on standard and profile ground rail illustrates the improvements associated with asymmetric profiling. In the sharper curves, up to 2000 m radius, a 40-50% reduction in flange energy is indicated. For shallower curves larger reductions result whilst steady state

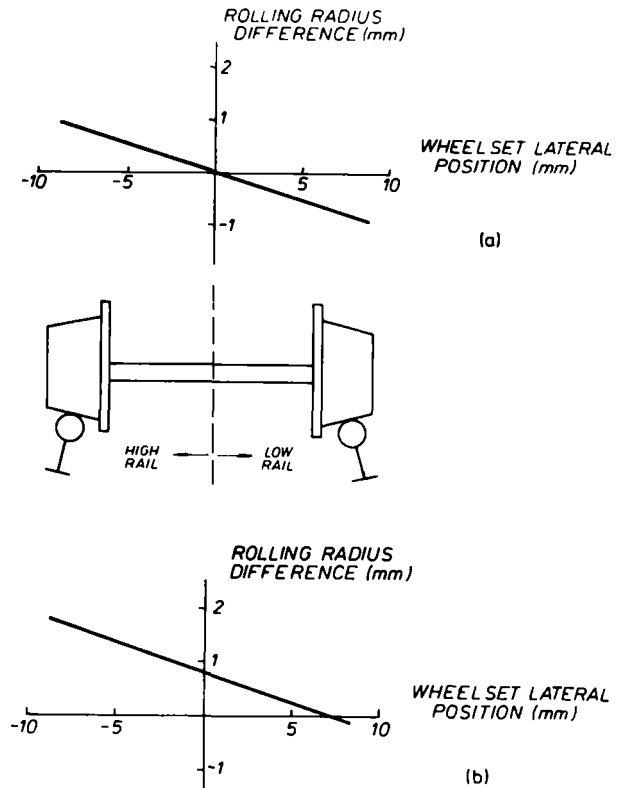


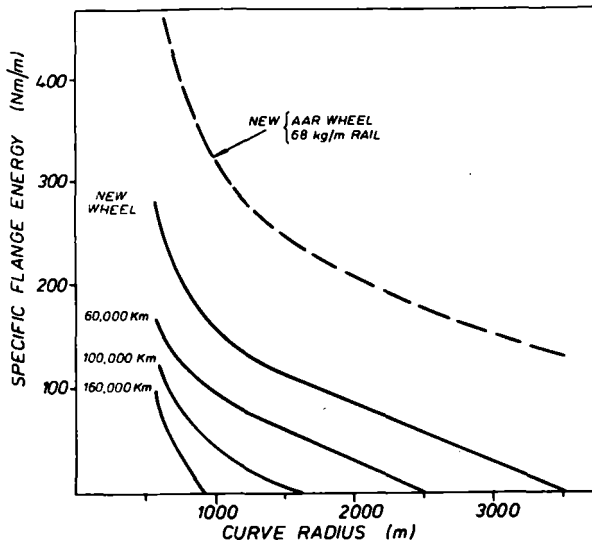
FIG.2 ROLLING RADIUS DIFFERENCE FOR CONED WHEELS ON (a) STANDARD RAILS AND (b) ASYMMETRIC PROFILE GROUND RAILS

flanging in curves above 3500 m is absent. Proportionately greater improvements can be expected for worn-in wheels as steady state flanging is suppressed further.

New wheels were found to consume the highest level of flange energy. Their flange wear performance improves progressively as they wear in, this being most noticeable in the flange throat area. In general, a stable profile condition was reached after 70,000 km of service for evenly wearing wheelsets. However, a more rapid bedding in was apparent for unevenly wearing wheelsets.

Further improvements in performance, beyond the initial bedding in period, as shown in Fig. 3, are associated with moderate tread profile changes and subsequent flange wear. These factors combine in providing increased rolling radius differential. This benefits the curving behaviour unless tread hollowing and reversed tread conicity counter their effect. In general, three stages of wear, the initially high, the moderate and accelerated wear rates are noted. For unevenly wearing wheelsets, the accelerated mode occurs at an earlier stage of the service period and may suppress the moderate wear stage.

The combined flange energy for loaded plus empty vehicle trucks in a 900 m radius curve is shown in Fig. 4. This shows the influence of flange lubrication in reducing wear. The typical variation of total tread energy for several curves is shown in Fig. 5. Flange friction was found to have little influence on the tread energy. Although tare was close to 20% of the loaded condition, the empty vehicle truck in general represented about 30% of the loaded energy levels.



FLANGE FRICTION 0.25
 AXLE LOAD 30 TONNE
 GAUGE 1435 mm

FIG. 3 FLANGE ENERGY PER LOADED TRUCK ON ASYMMETRIC PROFILE GROUND RAILS

The reported higher tread energy on the low rail wheels⁷ were found to apply for wheels in their early wear stages. This differential is pronounced under poorly lubricated flange conditions. In the latter wear stages, the tread energy at the high and low rails is largely equalized. At higher flange friction values, the total energy consumption per truck was relatively constant with service period. This results from the increase in tread energy whilst flange energy reduces.

Evenly wearing wheelsets seem to offer a satisfactory wheel life. The major problem from an operations point of view is to control the extent and degree of uneven wheel wear which significantly lowers the fleet average wheel life.

The base data on curving performance were used for evaluating an energy based wear model and the relative performance of modified wheel and rail profile designs.

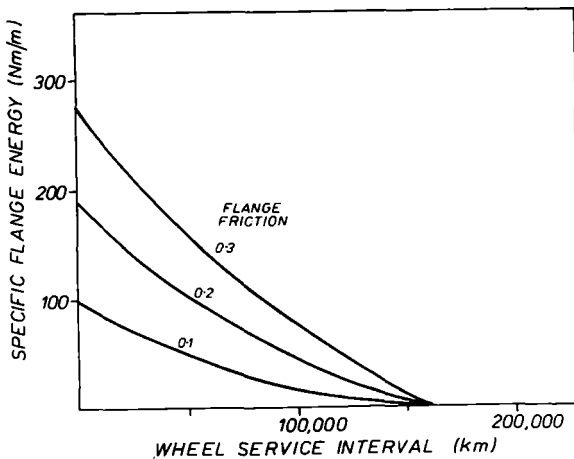


FIG. 4 FLANGE ENERGY FOR LOADED PLUS EMPTY TRUCK IN 900m RADIUS CURVE WITH PROFILE GROUND RAILS

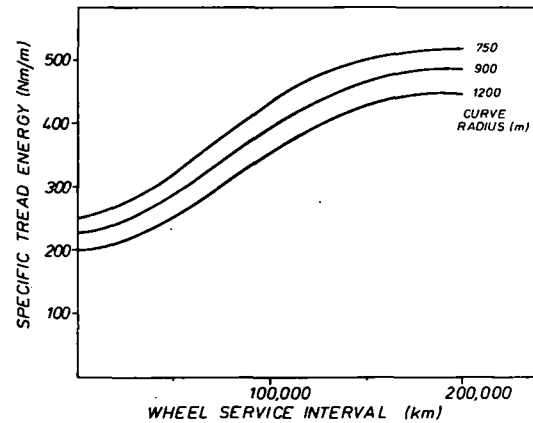


FIG. 5 TREAD ENERGY FOR LOADED PLUS EMPTY TRUCK IN CURVES WITH PROFILE GROUND RAILS

RAIL WEAR

The revised ground rail profile designs for curves were evaluated in the field. Rail instrumentation was placed at several points within test curves to allow mean wheel/rail lateral forces to be estimated. Measurements were taken prior to and following profile grinding. These indicated a general reduction in lateral forces for flanging axles.

In a 1200 m radius curve a close to 90% reduction in mean lateral force was noted, whilst a 50% reduction was observed in a 750 m radius curve. Typically a 30% reduction in dynamic force variation was also found after rail profiling.

A 50% reduction in lateral force is representative of the relative improvements between new and profiled rails indicated in Fig. 3. The much larger reduction in the 1200 m radius curve is associated with the higher lateral forces for the worn rail prior to rail grinding. This was some 35% greater than that expected for new wheels on new rail sections.

Detailed rail profile measurements at 4.5 million gross tonne (MGT) intervals showed significant wear reductions. Projected wear rates, including allowances for periodic profile restoration, indicated a 75% increase in rail life in shallower curves and a 50% improvement in sharper curves.

Wear rates for standard wheel and rail materials were also derived from laboratory tests under simulated heavy axle load conditions⁸. Applied loads and measured slip conditions in combination with a friction-creep relationship were used to compute specific energy inputs to the test specimens. A close to linear relationship between energy input and material wear was found to apply for a range of contact conditions approaching the yield of wheel and rail materials. Rail side wear was nominally three times greater than either rail head, wheel tread or flange wear. Specific energy estimates at the wheel/rail interface should therefore provide a good indication of wear in the form of debris.

Specific energy levels, derived from the simulation work, were used to predict the ground rail wear rates in the field. A vehicle fleet with evenly wearing wheelsets was assumed and the corresponding energy terms were scaled for a 4.5 MGT interval. These were converted into rail material loss using the laboratory measured specific wear rates.

Comparison of predicted and measured wear showed a consistent underestimation. Typically rail top wear was underpredicted by about 75% whilst side wear was around 25% below the measured values. Plastic flow, not accounted for by the laboratory wear rates, was thought to account for part of the discrepancies, particularly at the rail head. As well, the assumption of ideal or evenly wearing wheelsets for the total fleet was expected to give an underestimation of actual wear.

Uneven wheel wear of varying degree is often observed on three piece trucks. This is commonly attributed to initial wheel diameter mismatch and side frame length differences or truck component tolerances in general⁷. Sensitivity analyses conducted have shown this to be the case⁹. In particular, asymmetric truck performance and wheel wear is highly sensitive to inter axle alignment. This is shown in Fig. 6 where the misalignment acts in a manner so as to increase the severity of flanging. For larger inter axle angles, the relative change in tread energy was found to be more than twice that at the flange.

On the basis of these trends, an upper estimate of 25% side wear and 50% of rail top wear could be attributable to vehicles with asymmetric tracking characteristics. However, the number of vehicles accounting for the bulk of this wear need not be large due to the substantial energy increases with axle misalignment. Further work is being conducted in the area of component tolerances and their influence on vehicle performance.

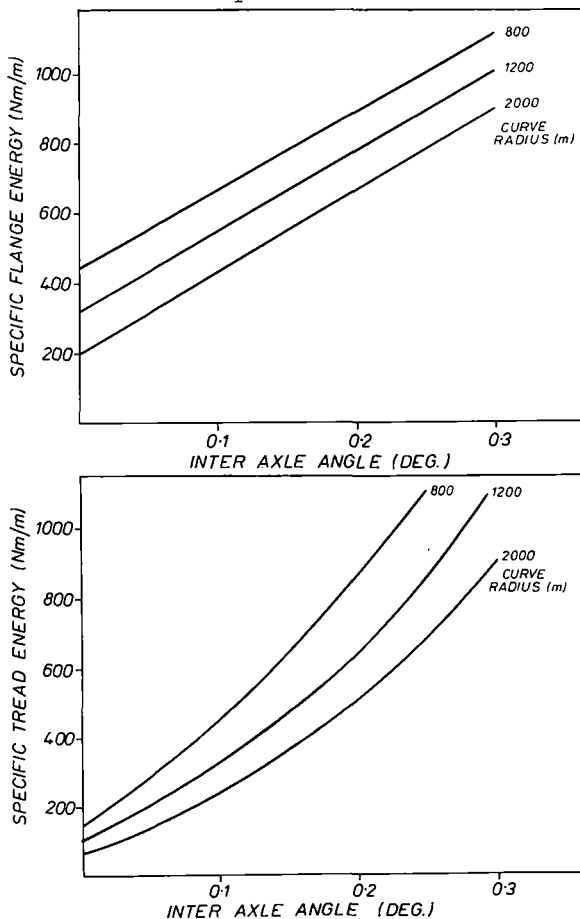


FIG. 6. INFLUENCE OF INTER AXLE ALIGNMENT ON ENERGY CONSUMPTION PER LOADED TRUCK IN CURVES (SERVICE WORN WHEELS AND RAILS)

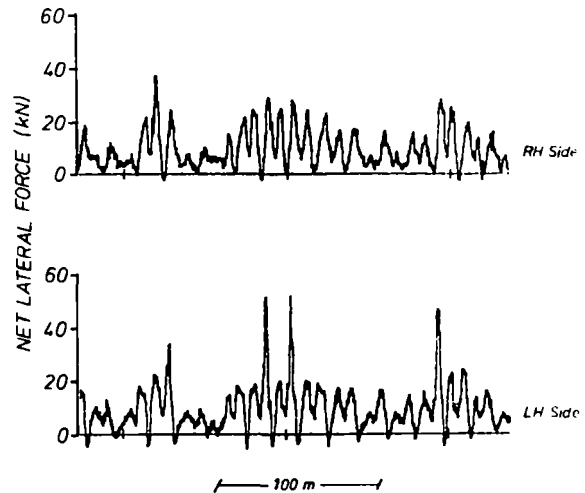


FIG. 7. SIMULATED LEAD AXLE NET LATERAL FORCES FOR TRUCK WITH WORN-IN WHEELS

TANGENT TRACK PERFORMANCE

A three piece truck lateral response model was developed to examine the influence of wheel/rail profile interaction and track quality condition on system performance. The model incorporates non linear creep coefficients and limiting tread and flange friction levels. The track is described by the average alignment, gauge and twist derived from track geometry recordings.

Flange forces associated with two point, tread and flange contact are calculated. Tread creep and flange friction forces and the corresponding slip values are used to derive the levels of energy dissipation. Fig. 7 shows typical outputs of leading axle net lateral forces. These are representative of measured wheel/rail forces, with the larger triangular force pulses corresponding to a flanging condition.

Simulations were conducted with wheel profiles sampled from trucks exhibiting even wheel wear. Three track qualities were also included, representing the average and extreme conditions on the iron ore rail-road systems. Typical wheel tread and flange energy levels for 30 tonne axle load conditions are shown in Figs. 8 and 9.

For increasing wheel service period, trends similar to those from the curving simulations were found to apply. The upper levels of tread energy in the latter wear stages represented about 50% of those for 1200 m radius curves. The initially high flange energy levels also moderated with time in service.

The relative low values around 50,000 km service were attributed to a small false flange resulting from the action of brake blocks. This was not evident for wheels at greater mileages.

Earlier re-machining of wheel profiles can lead to a reduction in total energy consumption. However, this is not warranted because of the increased frequency of machining and associated costs. In addition, new wheels suffer a higher degree of flange wear which requires proportionately greater amounts of tread metal removal to restore the profile. The period for which worn wheel profiles should remain in service is being given further consideration. This will involve the selection of tread and flange wear limits to optimize the overall wheel maintenance costs.

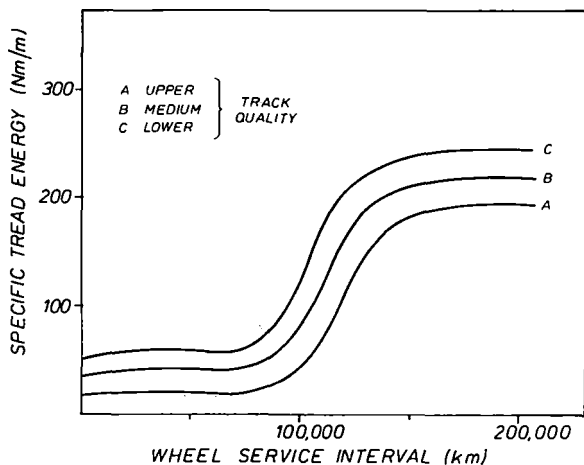


FIG. 8. VARIATION OF TREAD ENERGY PER LOADED TRUCK WITH WHEEL SERVICE INTERVAL AND TRACK QUALITY.

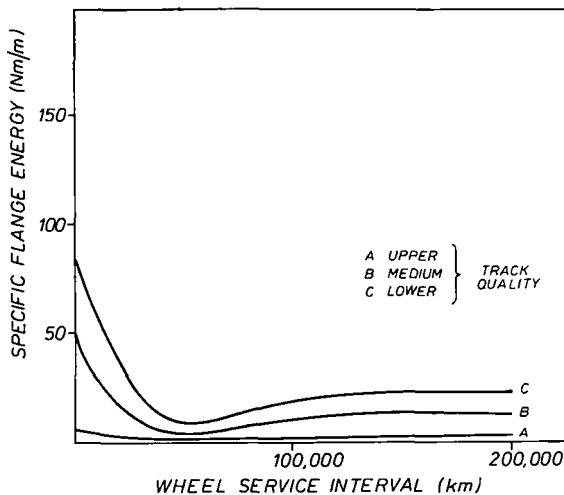


FIG. 9. VARIATION OF FLANGE ENERGY PER LOADED TRUCK WITH WHEEL SERVICE INTERVAL AND TRACK QUALITY.

Track quality was seen to have a direct influence on system performance. For the cases examined a 75% differential in the average wheel/rail energy was noted between extreme track qualities. The potential savings associated with improved track quality will depend on the track standards on a given system, the practical limitations and hence costs for improving standards.

Effectiveness of maintenance machinery and rates of track degradation are being monitored on the iron ore railway systems. This information in combination with wheel and rail operating costs will lead to better utilization of maintenance machinery.

TANGENT RAIL PROFILING

Rail profiling in tangent, similar to that in curves, has been introduced on the iron ore railroads.

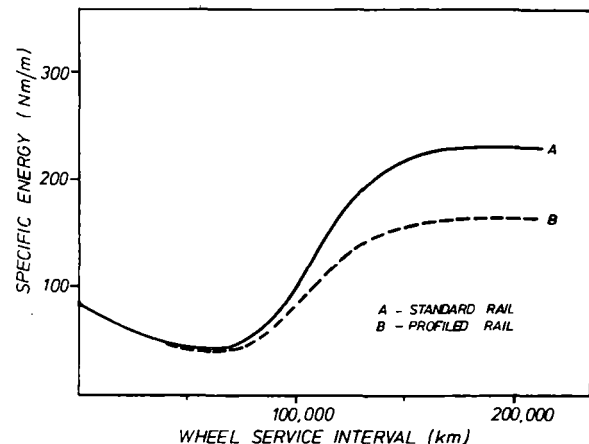


FIG. 10. VARIATION OF TOTAL ENERGY PER LOADED TRUCK WITH WHEEL SERVICE INTERVAL ON STANDARD AND PROFILE GROUND RAIL

Field trials, have shown this to have a favourable effect on vehicle response and rail wear. To some extent this is due to a moderation of the rail head running band deviations, which act as inputs to vehicle lateral behaviour. However, these changes are not readily quantified by conventional track geometry measurements. A more direct influence of rail profiling, which can be assessed, is the interactive effect between wheel profiles and the ground rail profile.

Supporting computer simulations, as shown in Fig. 10, have shown that average energy consumption on profile ground rail is some 25% less than that on standard rail profiles. This was primarily due to a reduction in tread energy of worn-in wheels, these having seen close to equal service on standard and profile ground tangent rail. Whilst benefits of rail profiling are apparent, the question remains as to the extent which can be realized once the system has fully adjusted. Wheel and rail profile changes will be monitored to allow grinding procedures to be refined.

WHEEL WEAR

The relative wear rates of materials established under laboratory conditions are indicative of the relative wear performance in track on a given system¹. The difficulty arises in predicting absolute wear rates due to the uncertainty and variability of system parameters. In this regard, wheel and rail wear performance between systems can vary considerably.

In the rail wear predictions it was apparent that the state of vehicles in the fleet can have a major influence on the in-track wear rates. In general, the state of the track system can be defined more readily than that of vehicles. Wheel wear performance should therefore be more readily predicted, and give a better indication of the applicability of the energy based wear model to field operation.

Wheel tread and flange energy estimates were obtained from the simulation results. Curve rails were profile ground whilst standard and profile ground tangent rail data were averaged to account for the introduction of profile grinding on tangent. The average flange friction factor on tangent rail was taken as 0.3 and that on curves as 0.25. Worn wheel profiles, track curvature and length were also taken into account in deriving an average

specific energy over a 220,000 km service interval.

For curves and tangent track of medium quality, the average specific flange energy for a loaded plus empty truck was 36 Nm/m. The estimate for tread energy was nominally 210 Nm/m. In both cases the empty vehicle condition represented about 30% of the loaded case. Using laboratory measured wear rates, these energy levels translated into wheel cross sectional area losses of some 30 mm² at the flange and around 125 mm² for the tread.

Comparison of these profile changes with evenly wearing wheelsets showed very good agreement. Total cross sectional area change was 160 mm² when referenced to a new wheel profile. Of this 28 mm² was considered as flange wear defined by an arbitrary 45 degree normal in the flange throat.

A somewhat greater discrepancy in wear prediction is possible due to the uncertainty of the actual distance travelled and tonnage carried by individual vehicles, as well as slight variations in the initial flange thickness of reprofiled wheels.

The calculation procedure adopted here does not allow the precise wear profile to be predicted as has been attempted in other studies¹⁰. However, given representative field data, the approach used permits typical energy and wear levels to be satisfactorily estimated.

Improvements in system performance can be achieved through better track quality and the use of rail profiling. The highly sensitive nature of wheelset alignment on performance as noted in the curving studies was also found to apply for tangent running, as shown in Fig. 11.

These trends are consistent with the high variability of wheel wear found in service. Although inter axle alignment error is not the only contributing factor, its importance was highlighted during instrumented vehicle tests.

A strain gauged wheelset was fitted as the lead axle of a truck with a one button side frame length difference. This provided increased scope for axle misalignment and resulted in a distinct tracking bias. The greater tendency to flange on the shorter sideframe side was evident from the associated higher force peaks as shown in Fig. 12.

The tracking bias was also apparent in curves. Invariably higher lateral forces were recorded when the shorter side frame was on the high rail side. The converse was the case when the inter axle alignment assisted in steering. This resulted in the absence of steady state flanging in a shallower 1200 m radius curve. In this instance distinct

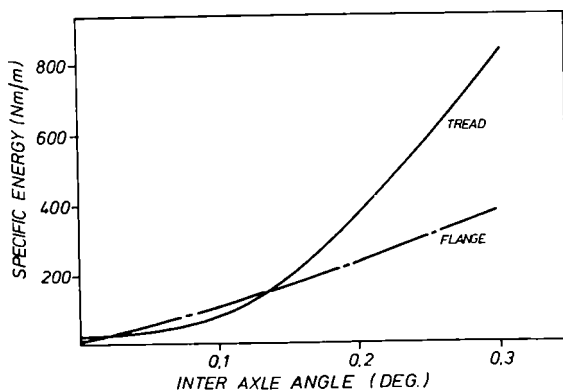


FIG. 11. INFLUENCE OF INTER AXLE ALIGNMENT ON ENERGY CONSUMPTION PER LOADED TRUCK ON TANGENT (NEW WHEELS AND RAILS)

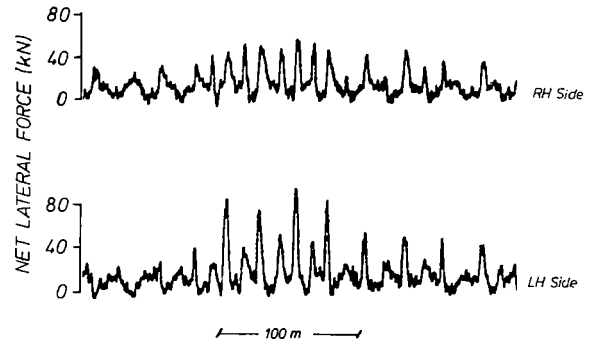


FIG. 12. MEASURED LEAD AXLE NET LATERAL FORCES FOR TRUCK WITH UNEQUAL SIDEFAMES (30 TONNE AXLE LOAD)

kinematic truck oscillations were noted, whilst the net lateral outer rail forces were small and directed in the opposite sense to flanging forces.

Asymmetric tracking accentuates differential wear, particularly for wheels in a new condition. This often results in three times greater flange wear in relation to evenly wearing wheelsets. Consequently greater emphasis has to be placed on the control of component tolerances to improve the useful life of wheelsets and to reduce maintenance costs.

MODIFIED WHEEL PROFILES

Standard conical wheel profiles are generally unsuited to heavy axle load applications. Tread contact stresses are high and so accentuate surface fatigue of both wheel and rail materials. The simulation studies also showed that new wheels consumed three times the fleet average flange energy. Poor flange detail and high flange energy levels combine to cause the initially high wear rates seen in service.

Numerous "worn" wheel profiles have been designed and evaluated on railroad systems. An important aspect is that profiles be based on service worn profiles and to modify these to overcome specific operating problems. For heavy axle load applications, the initially high flange wear, subsequent tread hollowing and fatigue influence the useful wheel life.

Modified wheel profiles designed for the iron ore operations in Australia incorporate a progressively contoured tread and flange throat detail¹¹. This has permitted average contact stress levels to be reduced to the range 600-700 MPa. These are regarded as stabilized values established under simulated 30 tonne axle load conditions^{8,12}.

The combination of the modified wheel and profile ground rail resulted in a higher mid range effective conicity. A controlled increase in rolling radius differential was also achieved when approaching flange contact as shown in Fig. 13. These characteristics are beneficial to the curving performance. They also reduce the wheel diameter mismatch sensitivity causing differential wheel wear.

Curving simulations for this wheel profile showed a flange wear performance similar to that of fully worn-in AAR wheels. The tread energy, although 25% less than that of worn-in wheels, was close to the system average. These trends were also apparent in the tangent track simulations. Flange wear projections on the assumption that the modified wheel

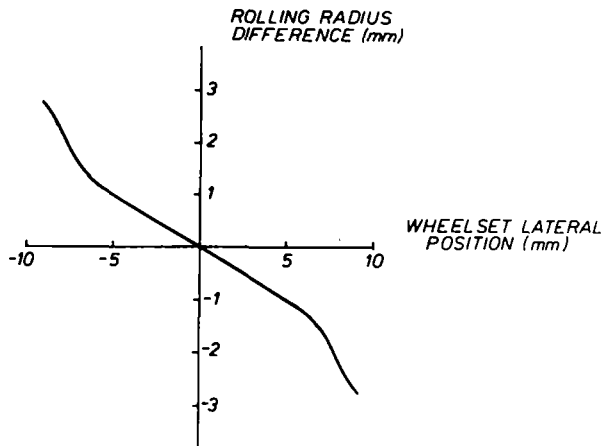


FIG.13. ROLLING RADIUS DIFFERENCE FOR MODIFIED WHEELS ON PROFILE GROUND TANGENT RAILS

was close to a fully stabilized wear profile suggested a 30-40% improvement over standard wheel profiles.

The major benefit of wear adapted wheel profiles is seen in terms of reduced flange and rail side wear. This allows wheel service periods to be extended. However, remachining prior to existing flange wear limits may be preferred to improve wheel utilization and operating efficiency.

Modified profile wheels have been placed in service and their wear rates are being monitored in relation to standard AAR profile wheels. To date, although at small mileages, the wear adapted profiles are performing favourably. Flange wear on modified profile wheels is on average 30% less than that on standard profile wheels.

This estimate is based on AAR flange thickness readings. These do not reflect the full extent of profile changes away from the measuring point. In terms of cross sectional area, the flange metal loss of modified wheels was considerably smaller than that for standard wheel profiles. The relative profile changes shown in Fig. 14 also indicate a lesser degree of tread profile change for the modified wheel. This reflects the benefits of reduced tread contact stresses to control plastic flow.

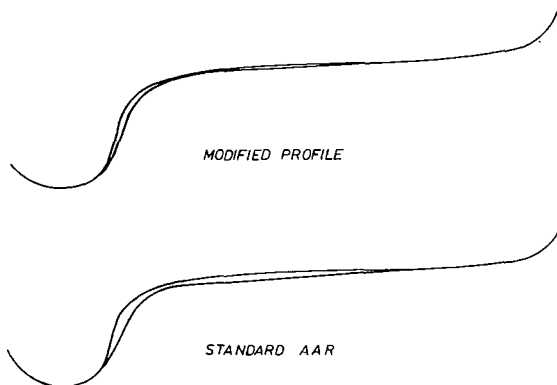


FIG.14. RELATIVE PROFILE CHANGES FOR MODIFIED AND STANDARD AAR WHEELS

Further measurements are required to give a clearer indication of the improvements. As well, truck component tolerances require closer examination to estimate their influence on asymmetric wheel wear, which was evident on the test vehicles. This will provide a better assessment of theoretical predictions and the potential improvements associated with wear adapted wheel profiles.

CONCLUSIONS

Rail side wear and wheel flange wear in curves can be significantly reduced through the use of asymmetric rail profile grinding. This overcomes the need for high conicity wheel profiles to improve the curving performance which place limits on stable tangent track running.

Simulation studies indicated that standard conical wheels consumed a high level of flange energy. This reduced considerably as wheels wore in to a stable profile. However, tread energy was found to increase with service, levelling off in the latter wear stages. Under poorly lubricated flange conditions, the total energy consumption in curves was relatively constant. Flange lubrication reduced the flange energy particularly for wheels in their early service period.

Truck response sensitivity analyses have shown component tolerances to influence asymmetric wheel wear. Of these, axle misalignment in trucks was found to have the greatest effect. The associated asymmetric tracking of vehicles was thought to be a major cause of increased rail wear in the field.

An energy based wear model can be used to satisfactorily predict wheel wear in service. Modified wheel profiles have been designed and evaluated using this model. Initial field trials have indicated improved flange wear performance in relation to standard AAR profiles.

The studies have highlighted the importance of controlling truck component tolerances, track quality, wheel and rail profiles to achieve improvements in system performance.

ACKNOWLEDGEMENTS

The reported work has been based on information derived from several studies which are part of a joint railroad research programme between the Mt. Newman Mining Co. Pty. Ltd., Hamersley Iron Pty. Ltd. and The Broken Hill Proprietary Co. Ltd. The authors wish to thank these companies for their continued support and permission to publish this work.

REFERENCES

- 1 Mutton, P., Epp, C., and Marich, S., "Rail Assessment", submitted to the 1982 Heavy Haul Conf.
- 2 Lamson, S.T., "An Evaluation of Rail Profile Grinding", BHP Melb. Res. Labs. Report MRL/CB28/81/008, January 1981.
- 3 Gutierrez, J.P., "Study of Experimental Bogies", BHP Melb. Res. Labs. Report MRL/CA23/80/020, December 1980.
- 4 Lamson, S.T., "Bogie Curving Model - A Refined Calibration", BHP Melb. Res. Labs. Report, MRL/CB28/80/003, September 1980.
- 5 Okey, R.C., "The Tangent Track Three-Piece Bogie Model Conversion to Digital Computer Format and Validation", BHP Melb. Res. Labs. Report MRL/CB28/81/018, November 1981.

Determining the Economical Timing for the Grinding and Renewal of Rail

M.D. Roney

Senior Research Officer
BHP Melbourne Research
Laboratories
Melbourne, Australia

S.T. Lamson

Research Officer
BHP Melbourne Research
Laboratories
Melbourne, Australia

M.B. Baggott

Superintendent
Permanent Way
Mt. Newman Mining Co., Pty.
Port Hedland, Australia

The Mt. Newman Mining Company operates 421 kms (253 mi) of mainline track supporting traffic volumes of about 50 million gross tonnes (55 MMGT) per annum with axle loads nominally of 30 tonnes (33 tons). The relatively rapid consumption of rail that this traffic entails, in combination with only a minimal prospect for second position use of rail, places a premium on the timely maintenance and replacement of rail. In cooperation with the BHP Melbourne Research labs and Hamersley Iron Pty., Mt. Newman has arrived at policies for grinding of rails and for rail renewal that are founded upon specific prediction of wear and defect occurrences rates. These predictions are processed through cost models to arrive at a minimum cost policy. The results of the background research studies are discussed within the framework of Mt. Newman's current rail management plan.

INTRODUCTION

Decisions on the appropriate timing for maintenance and renewal of rail have traditionally been based upon the subjective judgement of an experienced trackman. In the absence of specific information on the effect of his aging rail on system cost, he must typically rely upon visual indications of rail distress and rules of thumb. Inevitably, this leads to some conservatism, as the penalty attending overutilization of rail is far more apparent than the wastefulness of overmaintaining or of underutilizing its tonnage capacity. Just as in the case of an aging piece of equipment, the continued utilization of a rail in a given location must be periodically re-examined to determine the least cost strategy among the options of doing nothing, maintaining (eg. grinding), or replacing the rail.

The prospects for objective rail management have been the subject of research activity at BHP Melbourne Research Laboratories (MRL) for three years, under the joint sponsorship of Hamersley Iron Pty.Ltd. and the Mt. Newman Mining Co. Through this effort, it has been found possible to interpret the available physical indicators of welded rail conditions, rail wear and defect counts in economic terms. The basic cost models that have arisen from this research

have now been implemented at Mt. Newman (MNM) as an innovative procedure for the planning of annual maintenance and replacement programs.

Mt. Newman Mining is an ideal test bed for a scientific approach to rail management. The railway is a heavy axle load (nominally 30 tonnes (33 tons)), high density (50 million gross tonnes per annum (55 MMGT)) ore hauling railroad which, by April 1982, had carried approximately 570 million gross tonnes (630 MMGT). Being a trunk line operation in an isolated environment, very little prospect exists for reuse of the continuously welded 66 kg/m (132 lb/yd) rail in second position. Therefore, premature renewal carries a particularly high penalty. Thankfully, the acute need for maximum first position rail utilization is matched by an engineering information system that is capable of supporting the data requirements of advanced analyses. The Mt. Newman track history system can retrieve such important parameters as exact timing and location of service and detected rail failures, rerails, transpositions, Speno grinding (including the number of passes), and rail wear.

Using the techniques described in Mt. Newman projects an average life for tangent standard carbon rail of about 700 MMGT, with much of this being projected to last beyond 1,000 MMGT.

FRAMEWORK FOR RAIL MANAGEMENT DECISIONS

The key to the objective evaluation of the appropriate action to be taken at a

given site is the quantification of the cost impact of the aging rail. Continuously welded rail can be seen to be affected by tonnage accumulation in the following ways:

1. As the rail head cross sectional area is reduced through wear, flexural stresses increase and contribute to the rate of occurrence of internal defects and flexural fatigue.
2. As rail wears, the rail profile becomes distorted and a less favourable wheel/rail contact condition results. This accelerates the wear of both rail and wheels.
3. As the rail gauge face wears, gauge is widened, increasing the probability of corrugation development on the low rail due to false flange contacts, and marginally increasing derailment risk.
4. As the rail accumulates tonnage, the top surface and gauge corner of the rail develop surface spalls, shells and corrugations, thus increasing dynamic loadings and accelerating deterioration of wheel, rail and rolling stock.
5. As the rail accumulates tonnage, the rate of occurrence of internal defects accelerates, incurring increased inspection costs, emergency rail plug replacements, interference to traffic and increasing derailment cost expectations.

Both Mt. Newman and Hamersley Iron are unique in their capacity to perform preventative rail grinding using an asymmetric rail profiling technique that improves vehicle tracking. Mt. Newman employs two - 28 stone grinders year round to control rail surface distortion in 421 km (253 mi) of mainline track. As a result, plastic flow distortion, contact fatigue, and the earlier problem of sinusoidal wear⁽¹⁾ are controlled to a high degree and are rarely the cause of rail renewal.

The cost effects of wearing rail are illustrated conceptually as Figures 1, 2 and 3. Figure 1 shows the escalation of system cost with tonnage accumulation that is due to occurrence of fatigue-induced internal rail defects, i.e. those rail defects that develop through the initiation and growth of cracks in high stress areas within the rail. The defects that both show this strong sensitivity to tonnage accumulation are transverse defects (TD's), analogous to detail fractures from shell, horizontal split heads (HSH's) and vertical split heads (VSH's). The occurrence of one of these defects incurs a direct cost that is comprised of:

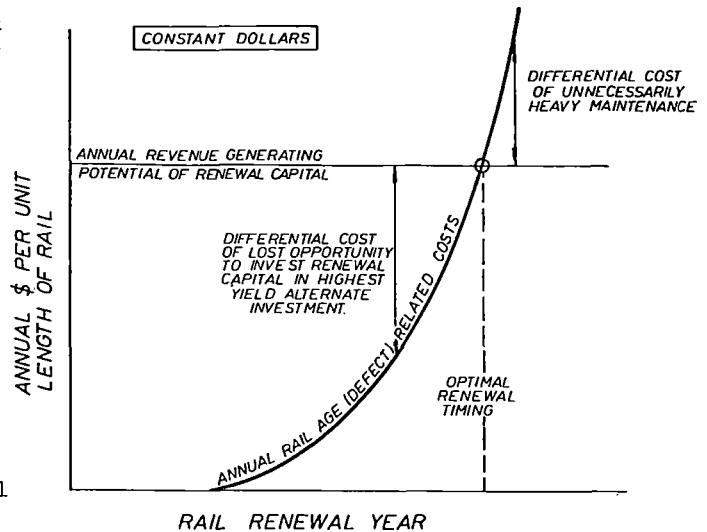


Fig. 1: Response of Internal Defect-Related Costs to Tonnage Showing Economic Fatigue Life

- the unit cost of clamping the defect immediately upon detection
- the unit cost of a rail plug
- the cost of two thermite welds
- the unit cost of weld inspection

In addition to this, there is an indirect cost that must be considered. This includes the:

- unit variable cost of ultrasonic inspection
- the expected unit cost of emergency repairs to that portion of defects that fall in service
- the expected unit cost of interference to traffic during emergency rail plug replacement
- the expected unit cost of the extremely low probability that a derailment will result from an undetected defect
- the expected unit cost of slow ordering traffic between detection and repair of large detected defects
- the expected unit cost of replacing that portion of the welds added with the rail plug that will fail at a later date
- the expected cost in foreshortened life of ballast, equipment and adjacent rail resulting from a potential irregularity in rail surface introduced with the installation of the rail plug.

Therefore, as defect occurrence rates increase, this is reflected in an increasing cost function of the form shown in Figure 1. A tradeoff is ultimately reached where the annual maintenance cost exceeds the value of deferring renewal of the rail for a further year. The latter is defined by $P(k - \Delta Cr)$, where P is the current after-tax cost of renewing a unit length of rail, k is the acceptable rate of return on investment and ΔCr is the cost escalation rate for rail renewal. The crossover point represents the economic renewal timing for rail that is governed by internal fatigue. In fact, this cost function alone defines a high percentage of tangent rail renewals, where lateral wear, the chief cause of head losses, is minimal.

The second important tonnage related cost is that due to the accumulation of rail head wear. This cost function is not immediately apparent without a consideration of the interaction of profile grinding and wear.

The application of profile grinding in curves in Mt. Newman Mining trackage has three main objectives:

- (i) To reduce the rate of side wear on high rails. This is achieved by maintaining an asymmetrical profile for both high and low rails. This profile has been designed to improve the steering ability of the three piece bogies used in the fleet. The result is lower flange force and less side wear, with a slight penalty in increased vertical head loss.
- (ii) To minimize the irregularities on the running surface of the rail head. Experience has shown that this treatment is effective for the prevention or control of the corrugation problem. Measurements of the depth of deformation at the corrugated track sections (usually short and following an irregularity such as a bad weld) have shown that this depth grows almost exponentially with tonnage unless regrinding is carried out.
- (iii) To reduce the head checking problem on the gauge corner of high rails. This is achieved by grinding the top of the gauge corner where most of the head checks are present. This treatment also reduces the direct wheel loading on the rail gauge corner where most sub-surface fatigue defects initiate. At present it is too early to quantify the effect of this treatment on the defects due to their slow growth rate. However, theoretical analyses predict that the defect rate would be reduced.

Accordingly, the physical consequences of decisions on rail grinding cycles are illustrated in Figures 2 and 3. Figure 2 compares the conceptualized progression of head loss in an unground rail with two levels of grinding. The nonlinearity in the wear curve is due to the self-accelerating feedback of a worn running surface profile to the generation of unfavourable tracking conditions. The effect of grinding is to restore the initial tracking attitude. Field tests have shown that the heavy axle train traffic can cause the ground asymmetrical rail profile to lose its shape within a few months and wear again begins to accelerate. Therefore, the accumulated wear curve for ground rail is composed of a repeated pattern of nonlinear wear joined by stepwise loss of material in the grinding operation. Experience has shown that the averaged head loss of ground rail is less than the head loss for unground rails, indicating that the treatment is effective.

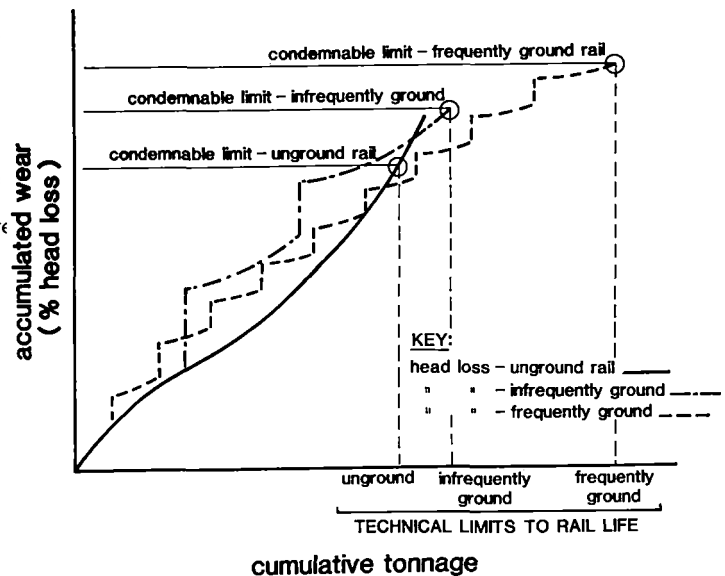


Fig. 2: Progression of Accumulated Head Wear vs Tonnage and Maintenance Policy

The decision of whether or not to grind is an aspect of rail management that has been positively decided in favour of a policy of rigorous grinding. The question of current interest to Mt. Newman Mining is which grinding cycle length to adopt. As indicated in Figure 2, both wear and the number of grinding passes required to restore the desired rail profile increases with the length of the grinding cycle.

The expiration of rail life on a strict wear criterion is currently based upon a technical limit, the condemnable limit of head loss. It is recognized that this is

in fact an economic threshold, however the collection of the necessary data on the cost of sustaining high head losses is a risky business as it requires interpolation from observations with severely worn rail. Limitations on rail head loss stem from flexural fatigue in the head/web fillet area, wide gauge and a shorter wheel climb derailment path. A test site of the standard 66 kg/m (132 lb/yd) rail that has had 20 mm (0.8 in.) of vertical head height removed by machining has been in service now for almost five years without indication of distress. Parallel experience at Hamersley Iron with large head losses has led to the conclusion that, with profile grinding and driven by a low salvage value, condemnable wear limits can be increased. Consequently, Figure 2 assumes the use of the previous standard of 25% head loss when profile grinding is not applied. The profile ground options assume this to be extended to match current thinking that this limit should be in the 35% range. Most of this difference is attributable to the lower relative component of gauge face wear in a profile ground rail with similar head loss.

Figure 3 illustrates the tonnage relationship of corrugations and gauge corner shelling and spalling. Without grinding, surface distress develops at an accelerating rate. Grinding is able to control surface fatigue such that condemnable thresholds are never reached. The condemnable threshold is defined as a corrugation or shell depth that is too deep to repair economically by grinding. Even with grinding, there is a slight increase in the rate of reoccurrence of surface distress due to the inability to completely remove all memory. Again, experience has shown that this can be tolerated within a pre-established grinding cycle. Although a technical or economic limit of rail contact fatigue is rarely seen under current Mt. Newman practice, there is a cost tradeoff between sustaining the consequences of higher levels of rail distress versus paying more for frequent grinding.

Translation of the system cost implications of Figures 2 and 3 is not straight forward. The annual direct cost of rail wear, including contact fatigue, has little impact on the track maintenance budget, except where this wear produces irregularities that increase tie and ballast loadings. The associated deterioration of tracking performance does, however, have an impact upon concomitant wheel wear, which represents a cost that is actually incurred on an annual basis due to the existence of widely varying states of wear within the wheel population. Fuel consumption and bogie maintenance costs (where wear is manifested as corrugations) are similarly incurred more or less continuously. The major impact of rail wear on track costs is the cyclic expense of curved rail replace-

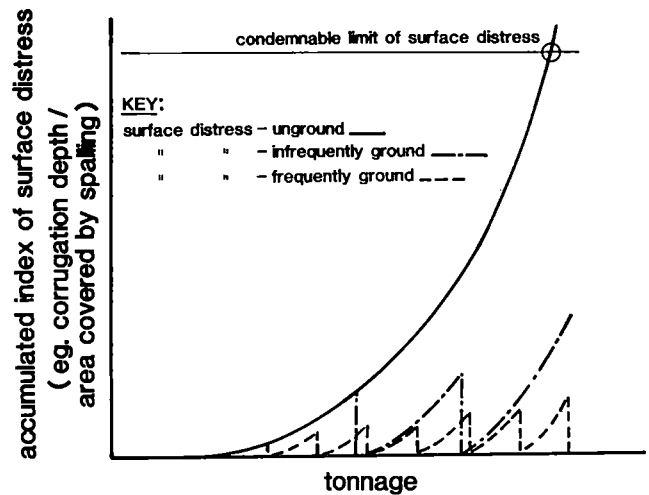


Fig. 3: Accumulated Contact Fatigue Damage vs Tonnage and Maintenance Practice

ment due to the relatively rapid progression to condemnable wear limits, which ideally reflect opportunity costs.

Grinding is capable of checking this acceleration of wear and a relatively constant annual cost level is established which includes a fixed grinding cost once a scheduling policy has been set. The cost of periodic grinding, including leasing fees, fuel consumed and the cost of track time, varies with the grinding cycle. There are also decided economies of scale on grinding activity due to the non-productive time associated with moving the grinder to the work locations. Therefore, a longer grinding cycle with greater grinding effort at each work location would reduce the unit cost per grinding pass. Counteracting this is the penalty associated with sustaining a higher level of concomitant wheel wear and the fact that the number of grinding passes required to remove irregularities (eg. corrugations) increases at faster than a linear rate.

It is clear from this framework that the most important rail management decisions facing Mt. Newman Mining are:

1. At what defect rate threshold is it economical to renew rail and how can this threshold be anticipated?
2. How can annual costs be minimized through intelligent scheduling of grinding?

In fact there is a third aspect which deals with the condemnable limit for head wear. Investigation of this policy will continue as more data become available.

It has been recognized by both Mt. New-

man Mining and Hamersley Iron that objective economic evaluation of these rail management options based upon sound scientific principles could generate important payoffs and MRL was commissioned to try to quantify the cost behaviour implied by Figures 1-3. The investigations that addressed these areas are discussed in the following two sections.

ESTIMATION OF AN ECONOMIC RAIL FATIGUE LIFE

As previously mentioned, the key to understanding cost tradeoffs related to defect occurrences is the discernment of defect (TD, HSH and VSH) production rates from field data, in combination with the estimation of a total unit cost of a defect.

Statistical Basis for Predicting Defect Occurrences

The pattern of escalating TD, HSH and VSH defect rates with time (Figure 4) can be explained if defect occurrences are thought of as earlier failures from a larger distribution encompassing the fatigue lives of the entire population of rails. The hypothesis that the fatigue lives of a population of engineering components (specimens) will distribute themselves according to a quantifiable statistical distribution has been verified for a diversity of applications. The art of identifying this distribution from early failures so that future fatigue occurrences can be projected has been given a strong scientific basis in the Weibull technique. (2)

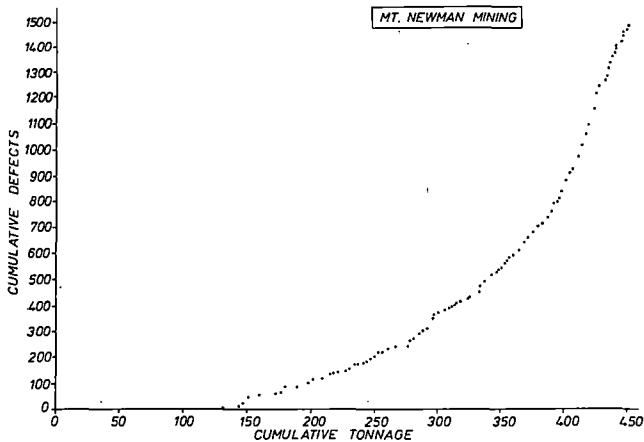


FIG. 4. DETECTED DEFECTS vs. TONNAGE IN MT. NEWMAN MAINLINE TRACK.

Fig. 4: Detected Defects vs Tonnage in Mt. Newman Mainline Track

This fatigue life distribution has the general shape shown in Figure 5. The exercise that is followed is to identify the form of the Weibull distribution that fits the historical pattern of failures. The well tried assumption is made that the rate of defect occurrence will continue to

follow this same statistical behaviour. Therefore, it is possible, once the particular distribution has been specified, to predict the rate of occurrence of defects in future years.

A detailed analysis of Mt. Newman Mining Co. service and detected TD's, VSH's and HSH's up to 435 MGT (Figure 4) quickly demonstrated a pitfall of previous Weibull analyses of rail: over-aggregation of data. The study began by segregating the rail plant into groupings that were meaningful from a defect causality point of view. It was found that variation in track geometry, metallurgy, and whether or not the rail had been transposed, resulted in significantly different defect production behaviour. Conceptually, the failure distribution of all rails can be viewed as shown in Figure 6. It is therefore not possible to produce reliable estimates of defect rates unless the rail groupings contain a certain minimum level of homogeneity. This objective was met by segregating the rail sample according to variation in the above parameters.

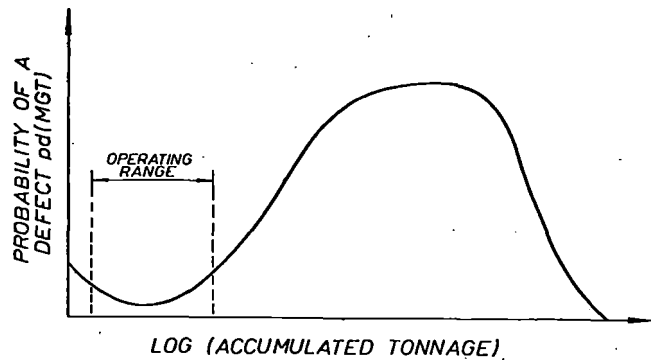


Fig. 5: Idealised Rail Subsurface Fatigue Life Distribution

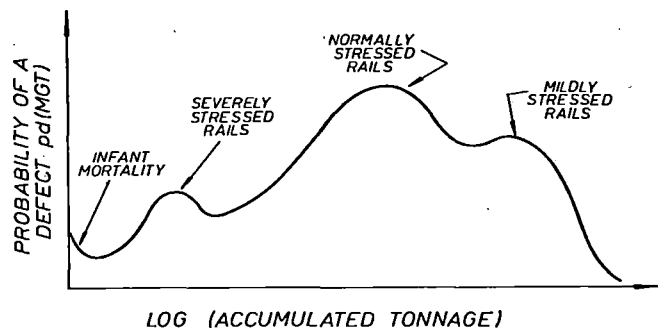


Fig. 6: Typical Multimodal Subsurface Fatigue Life Distribution

Ordering the Data

Within each of these groupings, defect occurrences must first be assigned order numbers. These order numbers account for variations in the number of rail specimens that have reached progressively higher service tonnages as transposition or renewal of rail changes the age mix. The specific formula used to order rail defects was:

$$N_i = N_{i-1} + \frac{(S+1) - N_{i-1}}{1+R} \quad (1)$$

where N_i = Order number of the i^{th} defect

N_{i-1} = Order number for $(i-1)^{\text{th}}$ defect

S = Total number of specimens in the sample including original length of rail and all subsequent re-rails. A specimen was defined as the typical 3.43 m length of rail removed with a defect detection. The use of such a structural unit provides a basis for normalizing defect data and of relating it to failure probabilities.

R = Number of specimens still in sample at service tonnages exceeding that at which the i^{th} defect was detected.

Choice of Plotting Positions

Once the recorded defect occurrences have been ordered in such a manner, each progressive occurrence represents an "observation" of the cumulative probability of rail failure associated with the timing of its detection. This observed cumulative probability of failure, termed a "rank", is assigned to each failure in a group according to a statistically-based formula. It is not possible to say that, for example, 10% of a population of ten rails would have failed at the precise tonnage of the first recorded failure. Each ordered failure is itself an observation from a distribution of possible timings for the appearance of a defect in that position in the order. The solution is to use a plotting position (rank) that, in the long run, will lead the positive and negative errors of the location of points on the plot to cancel themselves out. This can be either a mean rank or a median rank.

It has been found that the danger of underestimating the slope of the cumulative distribution plot is minimized through the use of the median plotting position, which ensures that a point is just as likely to fall to the right as the left of the maximum likelihood line. The median rank convention also results in a slightly steeper (more conservative) slope than the mean rank and was subsequently adopted for the current study. The median rank of the i^{th} defect is given by:

$$F(\text{MMGT}) = \frac{N_i - (1 - \ln 2) - (2 \ln 2 - 1) \frac{(N_i - 1)}{S - 1}}{S} \quad (2)$$

where $F(\text{MMGT})$ = the estimated cumulative probability of finding a defect in a given rail specimen by tonnage MMGT.

The choice of the unit of rail usage, in this case MMGT, has an effect upon the results. The unit must be an homogeneous measure of cumulative service. For the case of an ore line, where the axle load composition of traffic has historically remained unchanged, the use of million gross tonnes would not introduce a bias into the results. On the other hand, a traffic mix that is characterized by a changing axle load mix or speed profile must be represented by some form of weighted gross tonne measure. (2)

Estimating the Underlying Statistical Failure Distribution

The Weibull distribution function can, through the simple expedient of adjusting the values of the parameters describing the function, represent a wide range of different fatigue life distributions, which are characteristically highly dispersed and skewed. The form of the cumulative distribution function can also be easily linearized and therefore lends itself to parameter estimation using linear least squares regression.

The general form for the cumulative probability distribution for the (two-parameter) Weibull distribution, using MMGT as the unit of usage, is:

$$F(\text{MMGT}) = 1 - \text{EXP} \left[- \left(\frac{\text{MMGT}}{\theta} \right)^\alpha \right] \quad (3)$$

where α = the Weibull slope parameter

θ = the characteristic life or scale parameter. This is also the expected timing before the occurrence of a defect in any given rail specimen.

This probability distribution function must be fit to the "observed" ranking of cumulative failure probabilities based upon the transformed defect data in order to define the underlying statistical distribution. This is facilitated by transforming the data to produce a linear representation. Eq. (3) can be plotted in linear form on a graph where the X-axis is $\ln(\text{MMGT})$ and the Y-axis is $\ln(1 - F(\text{MMGT}))$. A straight line best fit to the transformed experimental data represents the estimated Weibull distribution that explains the timing between the occurrence of fatigue defects within the rail grouping. Extrapolation of this straight line fills in the remainder of the distribution, enabling future year failures to be predicted.

Figure 7 shows a sample curve fit to

four groups of untransposed tangent rail. Note that the Weibull distribution is fully described by the slope and intercept of this line on the Weibull-transformed axes. Note also that the close fit to the data confirms that defect production in railroad rails is a result of a Weibull distribution of fatigue lives.

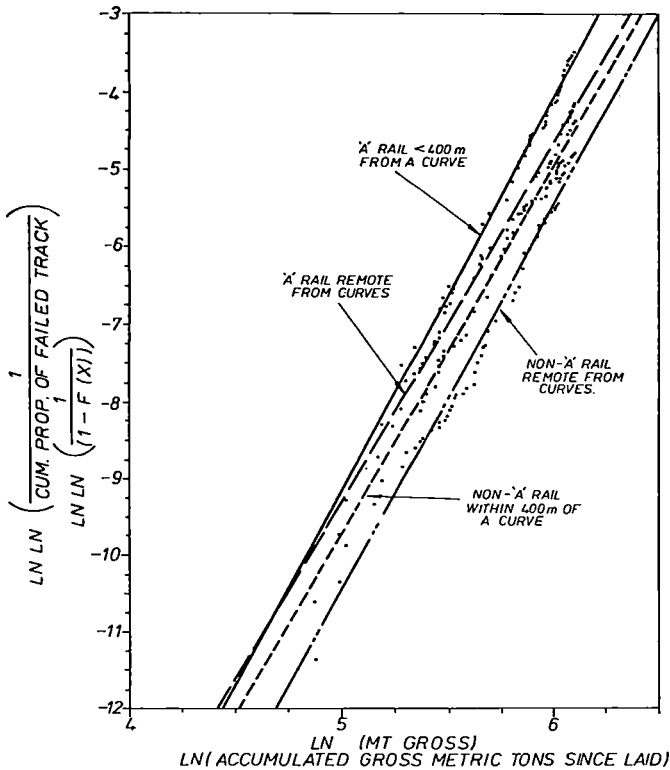


Fig. 7: Weibull Transformed Cumulative Defect Probabilities vs LN of Tonnage for Original Position Rail

Selection of Rail Groupings

As previously mentioned, the existence of characteristics that vary from location to location and which consistently influence defect production behaviour represents the largest source of inaccuracy in the estimation procedure. The analogy is the use of a system averaged unit cost for track maintenance over the railway. This cost may be an accurate representation of the average cost over the system, but has little applicability to any given track section.

This fact is disturbing in light of the extreme variability noted between locations in the Mt. Newman track. This is illustrated in Figure 8, which plots densities of recorded defects in alternate tangent and curved track.

This comparison shows curvature-induced influences, high defect areas of some 20-30 km, low defect areas of some 50-60 km and high variability within a given class and within tangent sections. Examination of clustering of defects found a large tendency for defect reoccurrences within the same 13.7 m (39 ft) rail length and within a distance of up to 200 m (650 ft) from the initial defect.

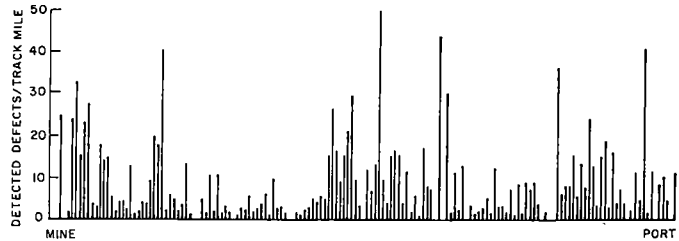


Fig. 8: Density of Detected Defects in Alternate Tangent and Curved Line Segments

Test of Defect-Producing Factors

A test was made of various explanatory variables for this behaviour. The test procedure involved segregating the sample of rails in present and past service into groupings based upon significant variation in the test variable. Defect cumulative probabilities vs tonnage were calculated for each grouping based upon computerized defect statistics and transposition and renewal records. These were then transformed for linear least squares fitting to a Weibull cumulative probability distribution function. The best-fit Weibull parameters were then compared for the different groups. Significant differences indicated that the test parameter was in fact exerting an influence on defect production behaviour. Lack of significant differences inferred that the influence was unsupported by the data.

The statistical analysis showed that track curvature was responsible for consistently greater rates of defect occurrence, in spite of a maximum curvature class of only 3 degrees. This is logical in view of the additional lateral loading and tangential forces. Figure 9 is an illustration of the estimated defect rate functions for different curvature classes reconstructed from the best fit statistical distribution. The defect rate function can be derived from the Weibull best fit parameters and defined as:

$$\text{DEFECT OCCURRENCE RATE PER RAIL KM/MMGT} = \frac{1000}{L_p} \times \frac{\alpha (\sum \text{MMGT})^{\alpha-1}}{\theta^\alpha} \quad (3)$$

where L_p = average rail plug length (m)
 $\sum \text{MMGT}$ = accumulated gross tonnage since rail was laid or transposed
 α = the Weibull slope parameter
 θ = the Weibull characteristic life

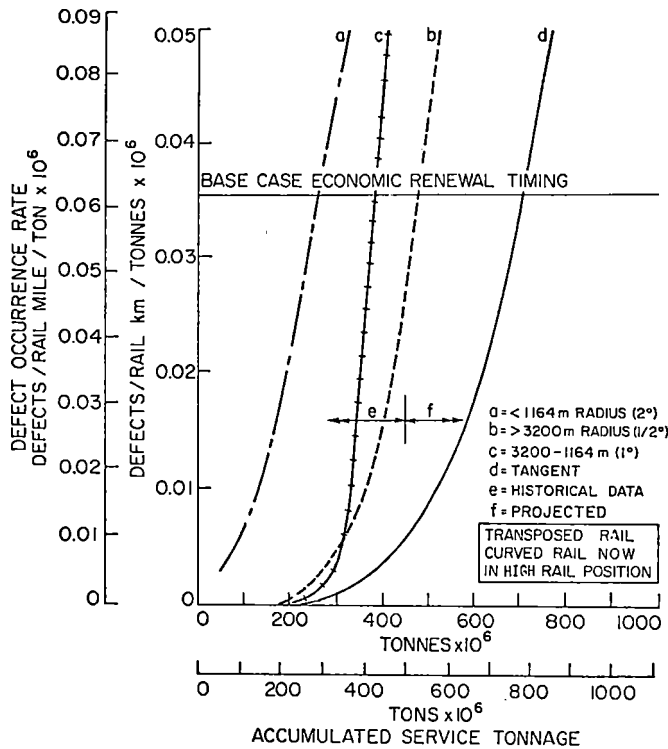


Fig. 9: Comparison of Defect Rate Function for Different Curvatures

It was similarly shown that defects were produced at a higher rate in tangent rails adjacent to curves.

Transposed rails performed better than rails that had not been transposed (Figure 10), consistent with the concept that the fatigue damage potential is higher in the gauge corner than in the field side of both curved and tangent rails.¹ These results also led to the realization that it was possible to provide guidelines on the economic transposition timing.

Finally, the cleanliness of the rail metallurgy was shown to have a significant effect on defects. Using as proxies for rail cleanliness: A-ingot position rails in semi-killed steel (dirty), all other ingot positions in semi-killed steel (average), and fully-killed rail steel (clean), a consistent and dramatic ranking resulted (Figure 11). This reinforces the conclusions of previous MRL studies (3), which have shown that these types of defects invariably initiate from a cluster of non-metallic rail

¹ Transposition of tangent track in addition to curves was adopted as a policy initially to control sinusoidal wear patterns due to lateral oscillation of the short wheelbase ore cars. The benefit in increased fatigue life has been a fortunate side benefit.

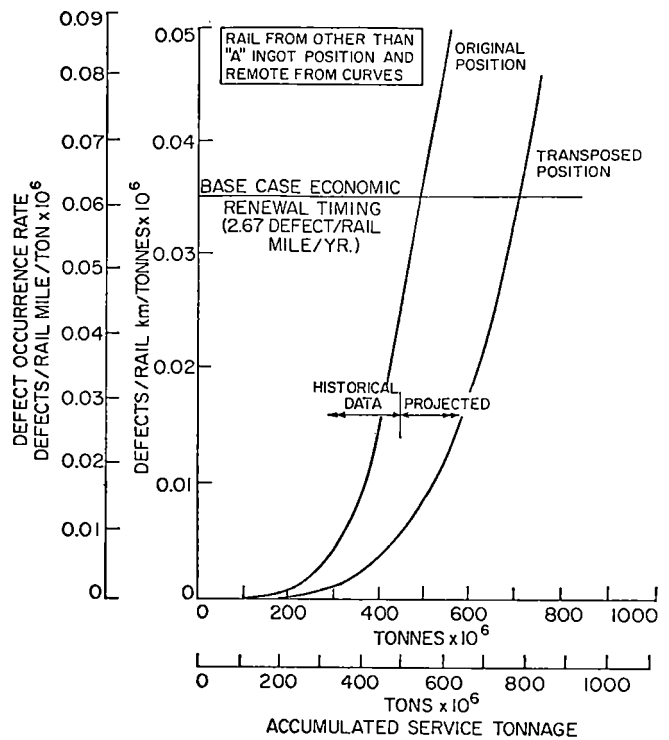


Fig. 10: Comparison of Defect Functions for Transposed vs Untransposed Tangent Rail

inclusions introduced in the steel-making practice.

Economic Fatigue Life of Rail

The defect rate functions presented in Figures 9-11 meet the requirements necessary to provide quantification of the defect cost function conceptualized in Figure 1. If this representation were to be followed strictly, the assignment of an all-inclusive unit cost of a defect would yield the cost function which would be compared with an economic threshold. In fact, it is possible to cancel out the units of dollars and to directly establish the approximate defect rate at which renewal would be optimal.² Using Mt. Newman cost data to quantify all direct and indirect costs of incurring a rail defect, a threshold defect rate of 1.6 defects/rail km/year (2.7/rail mi) was established. This is shown in Figures 9-11, which illustrate the intersection of the defect rate functions and the defect rate threshold representing the effective expiration of the rail's fatigue life. This inter-

² This must account for differences in the tax treatment of expense vs capital, differential cost escalation between rail renewal and those annual costs affected by defects and the traffic density projected at the time of renewal.

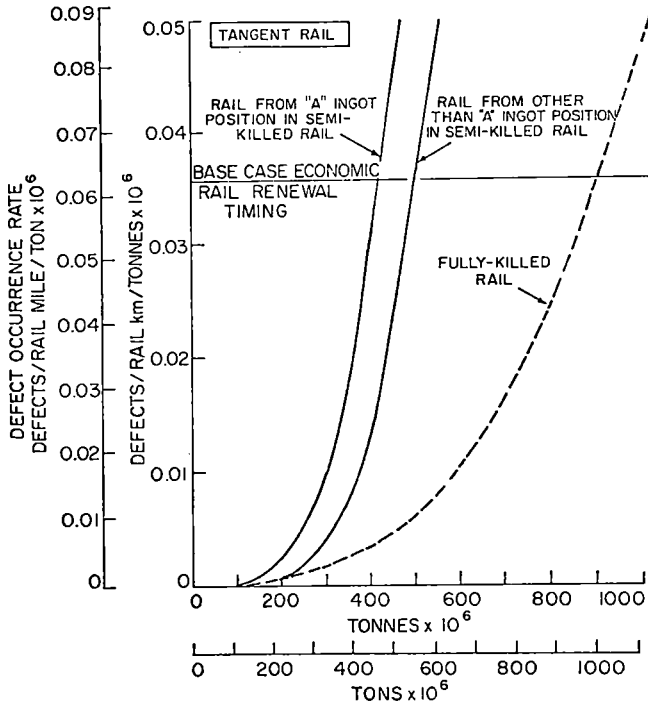


Fig. 11: Comparison of Defect Functions for Rail Samples with Characteristic Differences in Cleanliness Levels

section point would represent the economic renewal timing for rail that will not reach its wear allowance first. Typically, this means tangent rail. Lateral rail wear in Mt. Newman curves, is, in spite of profile grinding, quite rapid. This is probably related to the hot, dry environment, a characteristic shared with the U.S. FAST experiments.

Weibull statistics and class-level economic renewal timings for samples of those classes of rail found to be significantly different are included as Table 1. Note that specific renewal timings will vary with financial assumptions. Under any reasonable scenario, these economic renewal timings are considerably longer than originally anticipated by the operators.

The class lives calculated in this study are useful for long term planning but give little guidance to the selection of specific candidates for renewal. Clearly, one of the results of the study was the realization that large benefits could be gained by planning annual rail programs to consider the natural distribution of rails with different economic fatigue lives. As a result, Mt. Newman and MRL jointly developed the capability to automatically perform similar analyses of very specific rail groupings.

Table 1: Base Case Economic Fatigue Lives for Selected Rail Classes

(numbers in brackets give lives in millions of gross tons (Imp.))

Class Description	Weibull Slope	Characteristic Life (MMgt)	Economic Fatigue Life (MMgt)
Untransposed tangent rails, non-'A' ingot, > 400m from curves (1300 ft)	4.99	1207 (1330)	500 (550)
Transposed tangent rails, non-'A' ingot > 400m from curves (1300 ft)	4.92	1620 (1780)	715 (787)
Untransposed tangent rails from 'A' ingot position, 400m from curves	4.64	1108 (1220)	420 (460)
Untransposed tangent rail, fully killed	3.94	2242 (2470)	900 (990)
Transposed rail in curves of 1164-3200m radius (1°)	8.81	704 (775)	390 (430)
Transposed rail in curves of >3200 radius (2°)	2.61	1410 (1550)	261 (290)

* Assuming a rate return of 15% rail renewal cost escalation rate of 7% and a net rail salvage value of \$100/tonne (\$91/ton).

INTERPRETATION OF DEFECT STATISTICS IN THE PLANNING OF ANNUAL RAIL PROGRAMS

The concept of monitoring rail defects and deducing which areas of track should be railed had been evolving over a number of rerailling years at Mt. Newman Mining. At various stages in this evolution it was thought that choosing sections to be railed would be based on total number of defects, the number of defects in the last 12 months or convenient rerailling lengths combined with subjective evaluation of "overall rail quality". With the completion of the rail defect study, it was decided that what had been considered the longer term strategy of objective economic evaluation of economic fatigue lives could be immediately adopted.

A computer program was therefore developed jointly with MRL (Figure 12) which performs the same statistical evaluations of historical defect behaviour as outlined above for any selected rail location. A second program was added to convert this to an economic renewal timing based upon the occurrence of fatigue type defects. As the defect study had indicated a large residual clustering in defect behaviour, even after normalization for tonnage accumulation, curvature, transposition and metallurgy, it was decided to break down the rail grouping contained in each of these classes into smaller modules.³

³ This is consistent with a general philosophy, pioneered at Mt. Newman, that the rail plant should be considered as a collection of distinct modules. The idea was to maintain each module uniformly. Such an approach has an obvious advantage from a planning viewpoint.

Therefore, mainline track was segregated into individual curves of 400 m lengths of tangent rail. The 400 m length was chosen as the most economical rerailling module. For Mz. Newman Mining, a total of 920 different rerailling modules were developed in this way.

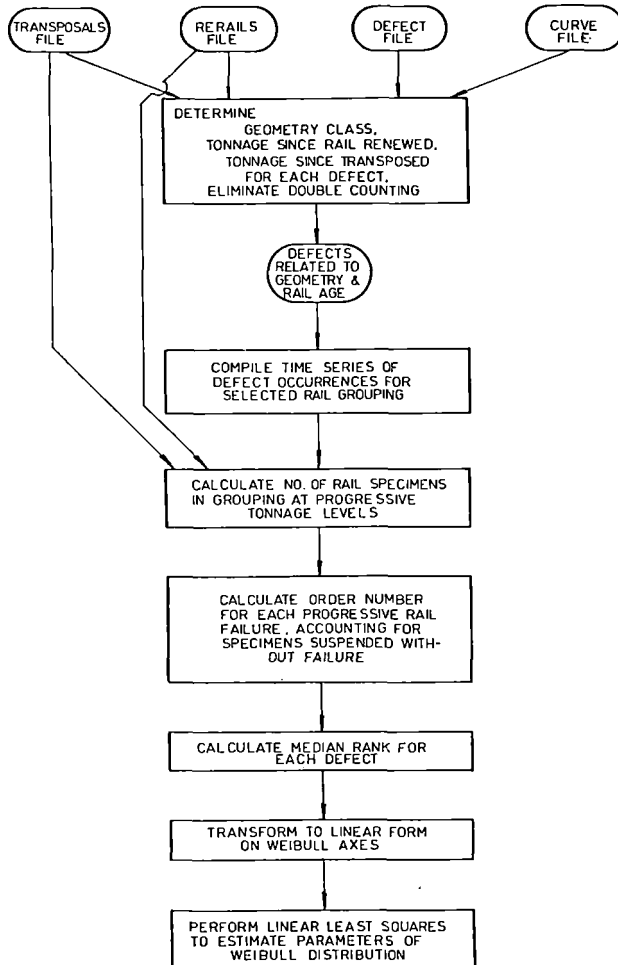


Fig. 12; Flowchart of Computations Performed for Statistical Analysis of Defects

Each of these modules has been analyzed independently by the economic fatigue life model. The theory has been that it is more economical to accept the error due to the projection of defects from small samples than to lose specificity by trying to develop a detailed projection using a larger group. A factor that contributes to this philosophy is the fact that the sections with a higher priority for renewal will also be the ones that are most accurately estimated. There are two distinct reasons for undergoing the complicated Weibull analysis. The first is to identify those modules which should be considered for the next rerailling program. The second is to predict for the other

modules when it will be economical to reraill them. The rules followed in performing these analyses are as follows.

The first step in the evaluation is to make a total defect count for each module. If the total number of defects in a module is greater than 3 then that module is considered a candidate for renewal in its own right.⁴ Within each of these modules, defects are classified into whether they occurred in original position rail or transposed rail. Therefore, where transposition has occurred, separate Weibull curves are computed based upon the defect behaviour of the rail in its original position. The Weibull curves are fitted to the historical data using the least squares method regression. The curves are then extrapolated in order to simulate the defects expected in future.

The methodology used to choose when rerailling should occur in the future is to compute total equivalent annual costs (EAC) assuming rerailling in each of the next 15 years. The option producing the lowest EAC is the year rerailling should be carried out, and corresponds to the year when the projected defect rate reaches the economic threshold.

This section of the computations can also display the EAC for each component of the total cost such as the defect cost, rerailling etc. It can also give expected future defect occurrences for that module. This has proven to be a handy tool in gang programming in a large scale sense.

Analysis Reliabilities and Results

As with any predictive tool, this system relies on the accuracy of the defect data input. There have been unexplained data trends but generally the high coefficient of determination computed during regression indicates that the Weibull process can be

⁴ As a rough guide any module with more than 7 defects will require rerailling provided the time series for the defect is of the Weibull type and generally exponential in shape. (i.e. rate increasing with time). But every module is different and extreme care should be exercised when generalising such as this.

⁵ All the data are now known for past costs and for predicting future costs. Those data are:

- rerailling costs
- transposing costs
- defect rates (present and future)
- opportunity cost (for investing the money for rerailling into some other venture)
- escalation rates
- tonnage rates (past, present and future)
- derailment cost

ORE YEAR

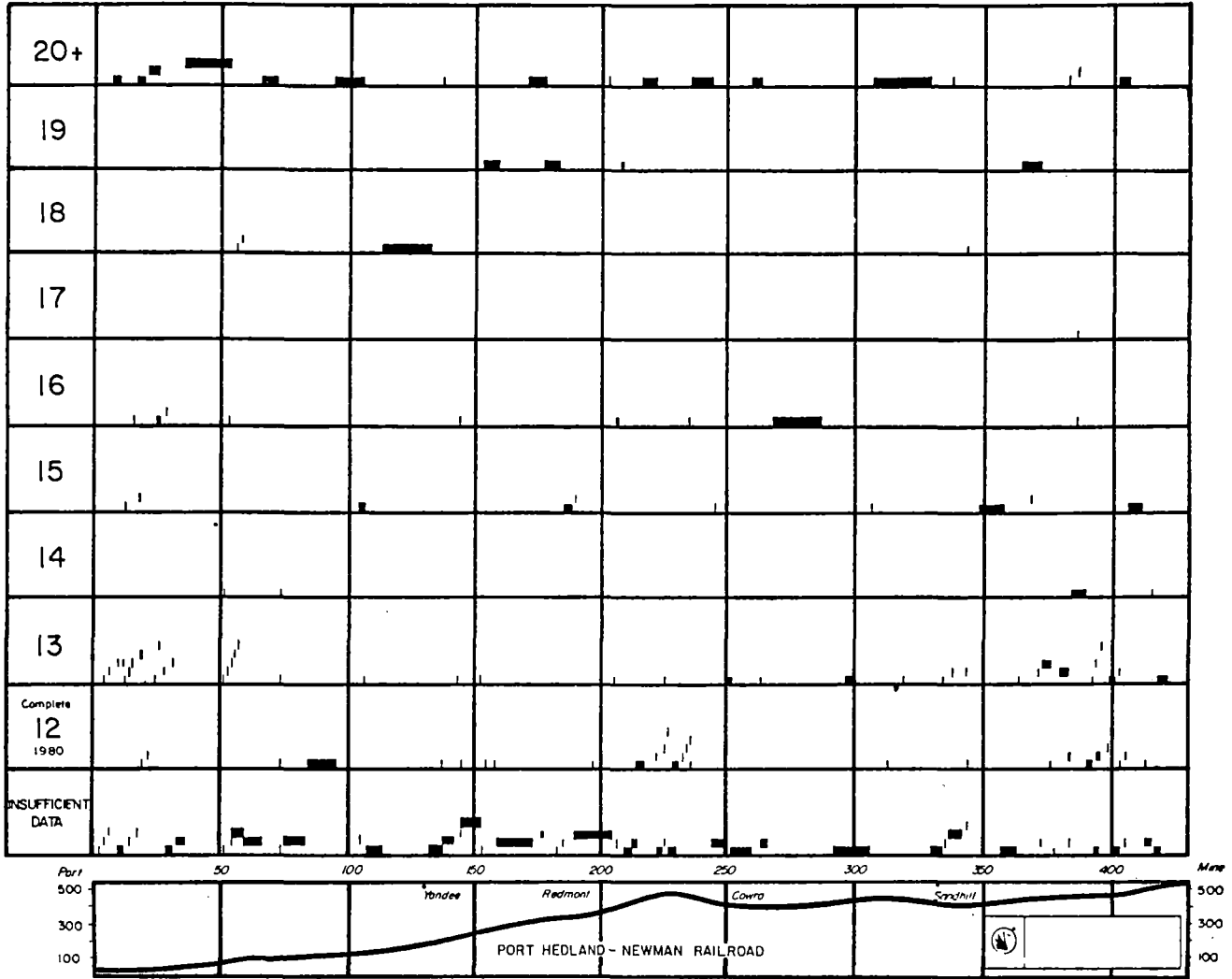


Fig. 13: Mt. Newman Rail Renewal Program Based Upon Projected Rail Fatigue Lives

applied and there is confidence in the data.

Mention has been made of selecting for Weibull analysis those modules with more than three defects. The process is also applied to those modules that have not been selected by aggregating those exhibiting similar characteristics and projecting defect behaviour, therefore coming to some conclusion about that group as a whole.

This is invaluable for planning material deliveries and rerailling contracts well into the future and is really used as a long term planning tool. These combined sections with their low numbers of defects will show long life. In some instances no analysis is possible because of lack of data.

A rerailling plan based upon projected fatigue lives has been developed using this model, and is shown in Figure 13. As more data are collected and as one moves closer to those distant years further analysis is required and the rerailling predictions will

change. Already, however, the system has saved Mt. Newman Mining about \$1 M deferments of planned rerailling, the penalty associated with the conservatism that governed rerailling decisions in the past.

JOINT OPTIMIZATION OF RAIL GRINDING CYCLE AND RAIL RENEWAL TIMING

The final step in the implementation of Phase I of the rail management system was to bring together the economics of rail wear and rail defects. The influence of rail wear in tangents and rail fatigue in higher degree curves is small and condemnation by either factor will override the other. Curves of $\frac{1}{2}^\circ$ or 1° , however, will experience contributions from both wear and fatigue so the economics are more interesting.

The above model must therefore be combined with the cost contributions of wear, based upon the behaviour shown in Figure 2,

before it can provide accurate estimates of curved rail life. In particular, the grinding practice must be considered as it influences both annual system costs and the cyclic cost of curved rail renewals.

Just as in the case of rail renewal, intelligent scheduling of grinding can have a substantial effect on system costs. This was recognized by Mt. Newman Mining and Hamersley Iron, who commissioned MRL to extend the rail management concept to the optimization of the grinding cycle within the framework of a total rail cost model.

MRL responded with the development of a model that finds the grinding cycle that minimizes the discounted incremental contribution to system costs. The foundation for this effort was a quantification of the following relationships, essential to the optimization of rail grinding cycles:

- (i) The rate of rail head wear as a function of the tonnage level for various types of rail steel and in various curve geometries (i.e. degree of track curvature).
- (ii) The associated rate of wheel tread wear and cost of wheel tread reconditioning (by remachining or replacement).
- (iii) The rate of rail side wear (on the gauge side) as a function of the tonnage level for various types of rail steel and in various curve geometries (i.e. degree of track curvature).
- (iv) The associated rate of wheel flange wear and cost of wheel flange reconditioning (by remachining or replacement).

Preliminary rail wear vs tonnage relationships were developed from a monitoring of wear in three test curves, (Figure 14). These base relationships were then expanded to incorporate the effect of curvature and rail metallurgy by overlaying the parametric wear sensitivities determined in MRL bogie curving simulations and laboratory wheel/rail wear experiments respectively. The flowchart for this development is included as Figure 15.

The relationship between the wheel and rail wear rates determined in the laboratory experiments was also used to derive the wheel wear characteristics from the rail wear characteristics. The cost of wheel tread and flange wear caused by rail head and side wear respectively was calculated from the wheel maintenance cost data. The procedure is summarized in Figure 16. It uses the data from the annual survey of wheel problems and wheel maintenance cost in conjunction with the established rail wear characteristics to establish the wheel maintenance cost that can be associated with each percent rail wear in a given km.

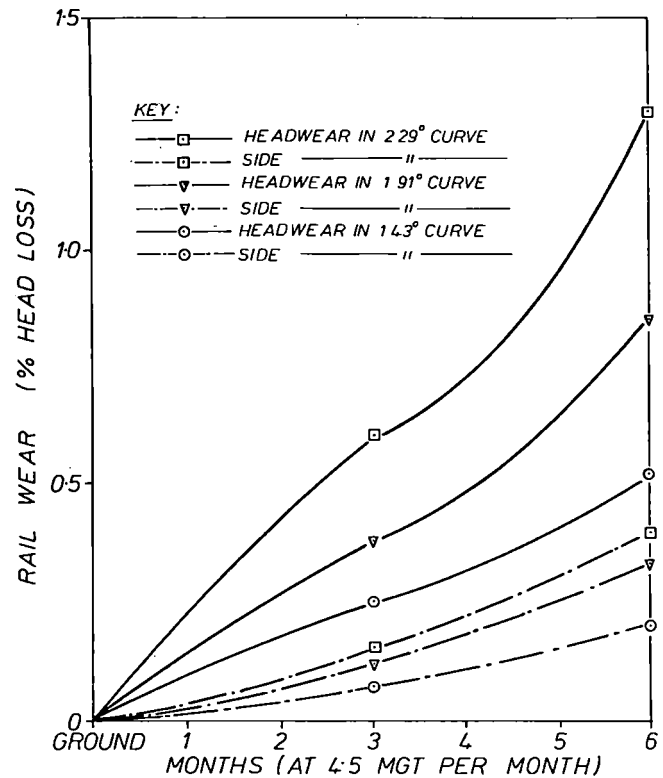


Fig. 14: Rail Wear in the Grinding Test Curves (High Rails, Std. Carbon)

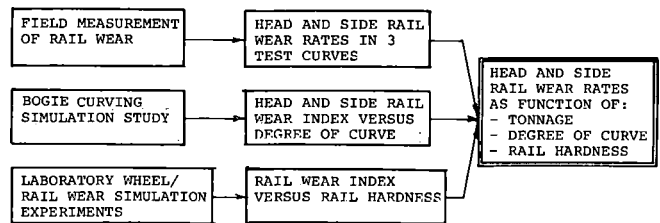


Fig. 15: Flowchart for the Determination of Rail Wear Functions

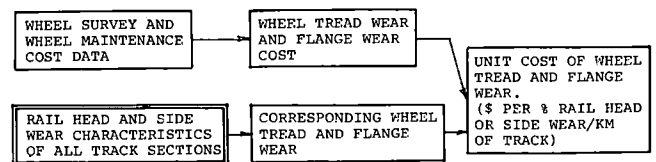


Fig. 16: Flowchart for the Determination of Wheel Wear Cost

The next phase of the development involved assessing the relationship between the grinding effort required and the grinding frequency. The number of grinding passes needed to restore the rail to an optimal condition is dependent on three main rail deterioration rates:

- (i) The rate of the wear of the running surface in the rail head. This problem causes the loss of the profile asymmetry. The result is the development of

a crown slope that is counter to that required to steer the bogie through the curve. When this becomes prominent, profile restoration grinding is required.

- (ii) The rate of rail surface (contact) fatigue. This problem requires the rail surface restoration grinding treatment.
- (iii) The rate of rail corrugation development. This problem does not always develop, particularly if high strength rails are used. For the track sections which are subject to corrugations, the corrugation prevention grinding treatment is required.

The rate of development of these respective problems is monitored in the test curves. Preliminary results were combined with the theoretical investigation in the laboratory to establish the grinding requirement function. Figure 17 shows a sample application of this function. It gives the number of grinding passes required to completely restore the condition of rails in the 2 degrees curve class for a range of candidate grinding cycles.

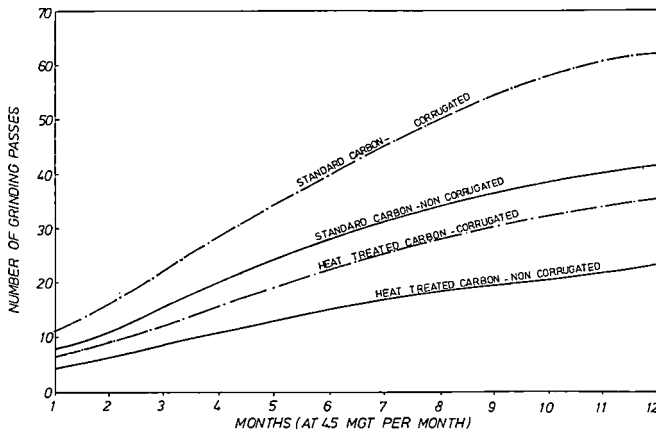


Fig. 17: Grinding Requirement for Standard and Heat Treated Carbon Rails in 2 Degrees Curve Class

Preliminary Model Application

A preliminary application of the model has been made in the joint optimization of grinding cycle and replacement timing for rails in the 2 degree curve class. The optimization is appropriate for 1981 system characteristics, i.e. 30 tonnes (33 ton) axle load and 50 million gross tonnes (55 MMGT) of traffic per year. Two rail types are considered: the standard carbon which has been used in the past and the heat treated carbon rail which has been adopted for future rail replacement. With regard to input from track conditions, the optimization considers two cases: the typical case where rails are subjected to surface deterioration such as head checking, but do not

corrugate, and the problem where rails are subject to a recurring corrugation problem.

The planning horizon extends 30 years into the future. This time span is estimated to be the economic life of the whole railway. All costs are discounted to present value and are appropriate for 1 km of rail in track.

Results of the preliminary model application are summarized in Table 2. It shows the optimal grinding cycle is 4 and 8 months for standard and heat treated carbon rails respectively. At these cycles, grinding contributes some 25% of head loss and rail wear 10%.

Table 2: Optimal Rail Management Policies for Rails in 2 Degrees Curve Class

DESCRIPTION	UNIT	STANDARD CARBON		HEAT TREATED CARBON	
		TYPICAL	CORRUGATED	TYPICAL	CORRUGATED
Economic Rail Life	Year	5	5	11.5	11.5
NPV of Rail Management Cost over 30 Years	\$	223 089	253 000	148 741	167 438
Cost of Defect	%	13.1	11.2	11.0	9.4
Cost of Rail Wear	%	41.9	35.9	57.8	49.7
Cost of Grinding	%	54.0	53	31.2	40.9
Estimated Total No of Defect		7	7	10	10
Total Rail Head Wear	%	7.5	7.5	7.0	7.0
Total Rail Side Wear	%	3.2	3.2	2.8	2.8
Total Grinding Loss	%	16.5	23.1	12.4	19.3
Number of Grinding Passes on Running Surface		2	10	2	12
Total No. of Grinding Passes at Each Cycle		20	28	18	28
Physical Rail Life	Year	6.5	5.5	18	13.75
Grinding Cycle	Month	4	4	8	8

The effect of corrugations is increased demand for grinding, causing higher overall cost. The number of grinding passes on the running surface represents the extra grinding requirement to control corrugations.

In general, heat treated carbon rails require less grinding, last longer and are cheaper to use in the long run, given current and projected tonnage levels. Rail wear and grinding are the two major cost items; defect-related cost, though significant is not the controlling factor for curve rails.

In practice, it is not always possible to follow the optimal plan, particularly when the grinding program, which incorporates many different curves with different

optimal grinding cycles has to be planned to maximize the grinder usage. An examination of the effect of suboptimal grinding cycles on the overall cost associated with standard carbon in the typical (i.e. non-corrugated) 2° curved track condition has been carried out. Figure 18 summarizes the results. It shows that if a sub-optimal cycle must be used, it is cheaper to experience a small delay than to grind prematurely.

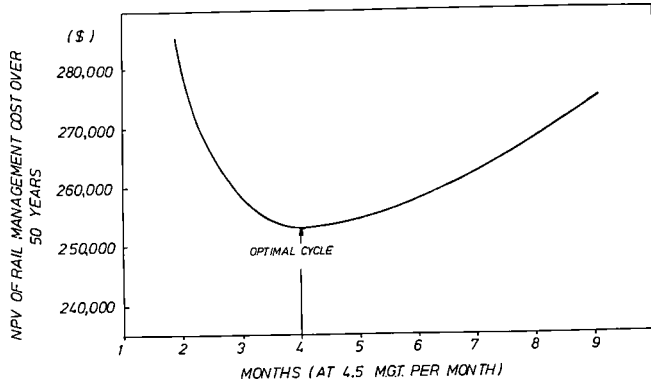


Fig. 18: Net Present Value System Cost for Standard Carbon Rails in 2 Degree Curve Class vs Grinding Cycle

CONCLUSION

With the joint sponsorship of research of MRL aimed at understanding the costs of rail wear and defect production, combined with a concerted effort to see the results of these efforts implemented, Mt. Newman has moved into an era of objective rail management. The aim is to gain an ability to predict the cost behaviour of the wheel/rail system such that it is always possible to estimate the least cost strategy. The most effective way of understanding this behaviour is through the use of a rail management model such as the one outlined herein. Such a framework enables complex interactions to be estimated and will generate an updated prediction of the least cost strategy for any change in technical or financial parameters. It is also particularly amenable to future refinements and addition of modules. This factor is particularly important as management of a track plant can best be described as "trying to hit a moving target". The rail management model framework ensures that, with the addition of future modules, Mt. Newman's permanent way management will be able to centre on what the railway will be doing tomorrow rather than reacting to problems after they have already occurred.

BIBLIOGRAPHY

- 1 Nisich, G.L. and Oliver, B.D., "Transposing as a Measure to Combat Hunting", Proceedings of the First International Heavy Haul Railways Conference, Perth, W.A., September, 1978.
- 2 Besuner, P.M. et al., "Probability Analysis of Rail Defect Data", Proceedings of the First International Heavy Haul Railways Conference, Perth, W.A., September, 1978.
- 3 Marich, S. et al., "Laboratory Investigation of Transverse Defects in Rails", Proceedings of the First International Heavy Haul Railways Conference, Perth, W.A., September, 1978.

Development of Rail Profile Grinding at Hamersley Iron

B.H. Longson

BASc, (Civil) MIE Aust.
Senior Engineer
Railways Technical
Hamersley Iron Pty.Ltd.
Australia

S.T. Lamson

B. Eng. (Mech) MIE Aust.
Research Officer
BHP Melbourne Research
Laboratories
Australia

The development and testing of a special ground rail profile to improve the curving characteristics of the three piece bogie is described. Field trials indicated a substantial reduction in wheel flanging force and a large increase in rail life. The application of the technique of rail profile grinding is discussed with respect to methods used, efficiency and optimisation of cycles. The impact of Hamersley Iron's railway maintenance costs is shown to be significant.

1. INTRODUCTION

Hamersley Iron operates a 400km, standard gauge, mostly single track railway for the haulage of iron ore from its two mines to the port. Its unit trains normally consist of 180 cars each weighing 120 tonnes fully loaded and exerting an axle load of 30 tonnes on the track. The level of traffic is approximately 60 million gross tonnes (MGT) per year and train speeds range up to 80km/h.

Bogies are the standard three piece design which tend to exhibit a lack of steering control in curves and a tendency to hunt in the empty condition on straights. The traditional problems of severe wear on the gauge face of high rails in curves (30% of mainline track) and on the flanges of wheels were of concern as was the snaking rail wear pattern on tangent track. To counter rail corrugations on curves and reduce the effect of the sinusoidal side wear, a new rail grinder was obtained in 1978.

The use of a rail grinder to attempt to control head profile had been on trial at Mt Newman Mining Railroad for several years (1). A joint research programme involving Hamersley Iron, Mt Newman Mining Co and Broken Hill Proprietary Limited had been aiming at rectifying the problems of rail and wheel wear by various techniques. Of these the rail profile development study proved to be the most successful. The study used a bogie curving computer model to develop a novel rail profile which aimed to reduce wheel/rail wear by improving the bogie tracking characteristics. Field tests of this profile were conducted to verify its predicted performance.

Based on promising results from the early trials

a practical method of carrying out in-track rail re-profiling was developed. With further experience and minor modifications to improve efficiency the technique has led to significant rail and wheel maintenance savings.

2. RAIL PROFILE DESIGN

2.1 Concept

The development of the special rail profile is based on a simulation study of the three piece bogie curving characteristics using the Bogie Curving Model. This model was set up in 1978(2) and accurately calibrated to the lateral wheel/rail interaction characteristics at Hamersley Iron(3). It provided a reliable prediction of the bogie curving performance under the various track/vehicle parameter modifications.

The three piece bogies used in the Hamersley Iron fleet have the leading and trailing axles nominally constrained to remain parallel to each other. This configuration prevents the simultaneous achievement of radial alignment of both axles hence causing poor curving characteristics. The axles can slide relative to each other forming a bogie frame distortion called lozenging. This enables the wheelsets to fit within the curve but does not improve their radial alignment.

The conicity of the wheel tread generates a rolling radius differential when the wheelset is displaced from the track centre line. In curves, part of this rolling radius differential is required to compensate for the difference in radius of curvature between high and low rails. The remaining difference in rolling radius produces a partial wheel slip in the longitudinal direction called longitudinal creepage. This longitudinal creep force tends to steer the bogie into the radial position where misalignment is equally distributed between the leading and trailing wheelsets. This configuration would be sufficient to reduce the heavy flanging in

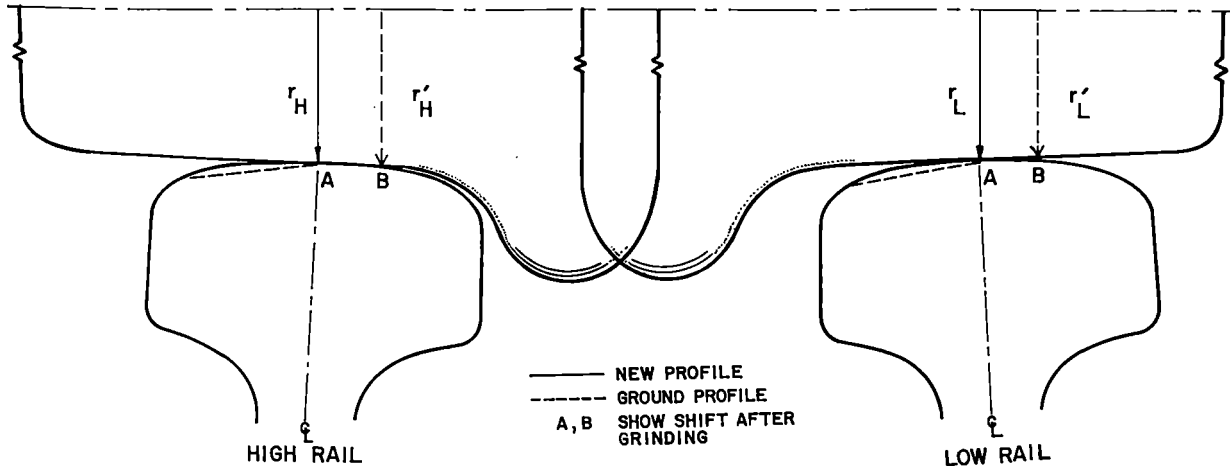


FIGURE 1. Effect of grinding on wheel/rail contact positions

most of the Hamersley Iron curves since they are relatively flat.

Specifically, the bogie curving model predicts that if the rail profile can be modified to increase the rolling radius differential to 3mm, the non-flanging curving mode can be achieved for curves up to 3 degrees (greater than 600 metres). Knowing the present range of wheel profile conditions in the fleet (i.e. from new wheels to worn wheels), it can be shown that the required rolling radius differential can be achieved by modifying the existing railhead profile to an asymmetrical shape (Figure 1).

There are a number of constraints which restrict a larger increase of rolling radius differential. The two most prominent are:

- (i) Transverse fatigue defect prevention. This requires the avoidance of wheel loading within 15mm of the gauge corner of high rails (field corner of low rails).
- (ii) Excessive contact stress prevention. This requires the wheel/rail contact band to be at least 25mm wide.

2.2 Design Features

The designed profile for the high rail (Figure 2) has five segments, the characteristics of which are:

Segment (1) on the gauge corner is designed to avoid contact with the flange root of most wheels.

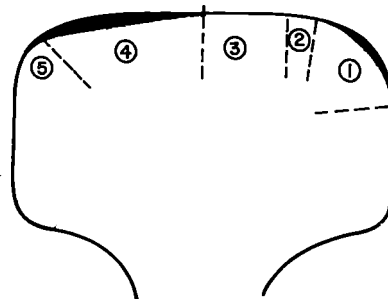
Segment (2) is designed to take the loading near the flange root. Its radius of curvature is comparable to that of the tread near the flange root of worn-in wheels.

Segment (3) is designed to take the tread load. Its radius of curvature is slightly less than that of most wheel treads. Together with Segment (2) the specified contact band width is provided.

Segment (4) is designed to avoid wheel contact. This segment requires the most grinding. The slope is critical for the grinding interval.

Segment (5) is merely a trim of the corner and removal of material for possible transposition.

The profile for the low rail is a transposed image of the above, i.e. Segment (5) becomes the gauge corner.



SHADED AREAS INDICATE DIFFERENCE FROM A.R.E.A. 68 KG/M (136 LB) PROFILE.

FIGURE 2. Designed ground rail profile

3. RAIL GRINDING TESTS

3.1 Objectives

Initially, the tests aimed to assess the performance of the new rail profile in terms of the wheel/rail interaction forces. In the longer term they aimed to determine the rail wear characteristics of the profile.

The tests had a further objective of providing detailed knowledge of the grinding method and how the current grinding practice could be modified to achieve the desired rail profiles.

3.2 Test Curves

Three test curves representing a typical range of degrees of curvature at Hamersley Iron were selected.

TABLE 1
TEST CURVE DATA

Curve	Length	Radius	Rail Type	Rail Wear
25km	1200 m	1220 m (1°30')	Carbon Low Carbon High	New New
27km	400m	915 m (2°)	Carbon Low CrV High	15% (trans- New posed)
34km	500m	764 m (2°20')	Carbon Low Carbon High	New New

3.3 Instrumentation

3.3.1 Strain Gauges. The primary aim of the strain gauge technique was to record the lateral rail bending stress due to the lateral wheel/rail interaction forces, with the minimum interference from vertical wheel loads. Linear gauges were used, mounted longitudinally, at the lower corner on both sides of the rail head. This arrangement enabled the measurement of rail bending stress on both sides of the rail without strain gauge damage when flange contact occurred. The strain gauges were calibrated using a track spreading instrument fitted with a hydraulic jack.

The gauge wiring was designed to record only the stress differential between the left and right hand sides of the rail head. As a result, the symmetrical bending stress due to vertical load was eliminated while the change in lateral bending stress was amplified.

It had been known from previous measurements using an instrumented wheel set that the lateral wheel/rail interaction forces in Hamersley Iron track vary at a predominant wave length of 25m. To measure the average forces under this condition, strain gauges were placed at three locations with a spacing of 12m (1/2 wave length) and 6m (1/4 wave length) between them. The average signal obtained from these locations would be close to two thirds of the true average of the wheel/rail interaction forces. This accuracy was satisfactory for the ground rail assessment which was based on the change in force level before and after grinding.

3.3.2 High Resolution Wear Gauge. In order to accurately measure the rate of wear of the profile over a reasonably short time span, a special wear gauge was developed. It consisted of a reference frame and a depth micrometer. The frame was designed to permit repetitive set up of an accurate reference from which rail profiles could be measured using the micrometer. The maximum error on rail profile measurement was 0.05mm. In practice this was reduced by employing multiple readings, using two independent operators and using reference points for calibration.

3.4 Test Procedures

- (i) The three curves with new rail were instrumented with strain gauges and lateral wheel/rail interaction forces were measured under the passage of three loaded trains.
- (ii) Both high and low rails were ground using the designed profile. Further lateral wheel/rail force measurements were recorded.

(iii) The rail head and side wear rates were measured separately every month for six months using the high resolution rail wear measuring gauge. No further grinding took place during this period.

(iv) The changes in rail profile were monitored every three months using a Seiki rail gauge.

This procedure ensured that both short term performance and long term wear characteristics of the rail profile could be assessed. The first result was necessary for the fine adjustment of the rail profile during the grinding test. The second result was essential for the evaluation of the longer term benefits and the incorporation of the method into a rail grinding maintenance programme.

3.5 Grinding Details

The grinding was carried out using an RR28E machine manufactured by Speno International. This machine has 12 x 15 HP reprofiling motors mounted on two trolleys on the outside of the two vehicle axles. These are able to be altered over a wide range of angular positions. It also has 16 x 15 HP rectification motors fitted between the axles on two mobile chassis. These units allow only a maximum 15° movement relative to the vertical axis of the rail and are primarily directed at the running surface.

The grinding stones were set to remove sufficient material from the new profile to create a profile similar to that shown in Figure 2. Their angles and relative positions produced grinding across the full rail head during each pass. This required a higher concentration of stones on the sloping side (8 stones) to produce a sufficiently high grinding rate. Results were checked with templates and some minor adjustment of stone angles was required to ensure an accurate test profile. Including run in and adjustments, approximately 40 passes were used to achieve the profiles on standard carbon with the machine travelling at a speed of about 6km/h.

A spring loaded punch was used to indent the rail and by measuring the depth the rate of metal removal was determined. On the field side of the high leg about 0.02mm was removed per pass and on the gauge corner about 0.05mm was removed. The average head loss per pass was about 0.05%. The harder alloy rail required about 25% more grinding effort.

4. GROUND RAIL TEST PERFORMANCE

4.1 Lateral Wheel Force Results

The short term assessment aimed at evaluating the effectiveness of the ground profile in improving the curving characteristics of the bogies.

Analyses of the strain gauge data recorded in the test curves before and after grinding showed large reductions of the lateral wheel/rail interaction forces at the leading wheelset. The forces at the trailing wheelset showed some variations but the magnitude of these variations as well as their mean force levels were relatively small and would not significantly influence wheel/rail life.

Table 2 summarises the lateral wheel/rail interaction forces associated with the leading wheelsets of the three piece bogies in the fleet. The results showed substantial reductions of the lateral forces acting on the high rails. Of most significance was the reduction in the flange forces. This indicated that the side wear of high rails and flange wear of wheels would be drastically reduced. The results generally showed that the ground rail would be most effective

in curves less than 2 degrees (i.e. about 900m radius). For sharper curves (> 2 degrees) the reduction of flange force is very significant but is insufficient to indicate a non-flanging curving mode. This result generally correlates with the simulation study since the rolling radius differential achievable with the ground rail was $\approx 2.5\text{mm}$, slightly short of the 3mm target required to achieve a non-flanging curving mode in Hamersley Iron curves right up to 3 degrees (600m radius).

Table 2 also shows significant reductions in the standard deviations of the lateral wheel/rail interaction forces associated with the leading wheelsets. The average reduction is about 30%. Since there is no curve-degree-dependent trend associated with these reductions, it can be concluded that they were achieved mainly from the improved uniformity of the ground rail profiles. As these standard deviations represent the dynamic components of the lateral wheel/rail interaction forces, their reductions indicated that the derailment risk (associated with high L/V wheel climb) will be lower, and the rate of deterioration of track and vehicle components will be reduced.

TABLE 2
REDUCTIONS IN LATERAL WHEEL/RAIL INTERACTION FORCES

TEST CURVES	RAIL PROFILE	MEAN FORCE LEVEL (kN)			STD DEVIATION (kN)	
		HIGH RAIL	LOW RAIL	FLANGE	HIGH RAIL	LOW RAIL
25km 1220mR (1°30')	Pre Grinding	35.03	31.59	51.62	20.90	19.92
	Post Grinding	3.60	18.16	6.76	16.93	11.27
	% Force Reduction	90	43	87	19	43
27km 915mR (2°)	Pre Grinding	35.17	27.60	47.77	19.10	12.16
	Post Grinding	7.59	12.73	5.33	13.56	8.57
	% Force Reduction	78	54	89	29	30
34km 764mR (2°20')	Pre Grinding	38.95	38.61	62.56	18.66	13.13
	Post Grinding	17.48	29.35	31.84	12.65	10.77
	% Force Reduction	55	24	51	32	18

4.2 Wheel/Rail Wear Results

The long term effect of rail profile grinding was predicted to be a reduction in wheel and rail wear. It was impractical to measure the change in wheel wear in the relatively short period of the grinding trial (6 months). The measurement of rail wear in the test curves was carried out monthly using the high resolution wear gauge which allowed the separate recording of head wear and side wear. The performance of the ground rail was judged mainly on the rate of side wear of the high rails, since this was the most severe wear problem to be overcome.

4.3 Analysis of Results

Figure 3 shows the head and side wear characteristics of high rails in the test curves during the initial period of six months following the profile grinding. The wear rate of the CrV alloy rail in the 27km curve high leg has been converted to the equivalent standard carbon wear rate using a wear ratio of 0.6 determined in laboratory wear tests. The wear levels are generally low, particularly the side wear. There was no evidence of a plastic flow problem on low rails and the wear rates were comparable with the head wear rates of high rails.

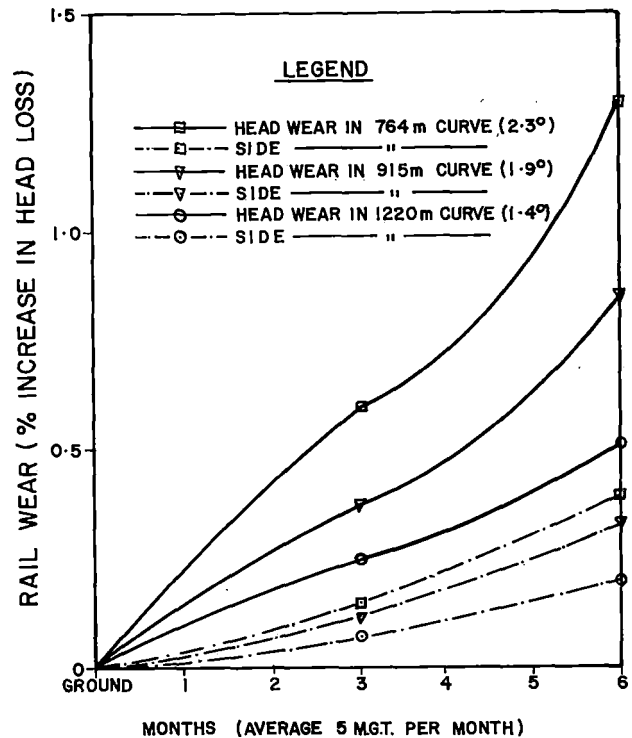


FIGURE 3. High rail wear in test curves

There was limited data on the wear characteristics of these rails before the grinding test to enable a direct comparison with the ground rail wear rates. However, by assuming that the rail profile grinding practice continued regularly, say at a uniform 6 monthly interval, a projection of the ground rail life could be made and the projected lives compared to the average rail lives recorded in the past for these curves.

Table 3 shows this comparison. The projection was based on the rail wear rate, an approximate 1.5% rail head loss during reprofiling, and a maximum allowable rail head loss of 35%. The theoretical improvements on rail lives were shown to be very substantial. The results showed that profile grinding would be more effective in flat curves than in sharp curves. It was also noted that because of its low side wear rate, the profile ground rail would reach the condemnation age without requiring transposition as was the practice in the past.

TABLE 3
INCREASE IN RAIL LIFE BY PROFILE GRINDING

CURVE RADIUS	RAIL LIFE (#) (MGT)		THEORETICAL % INCREASE	% INCREASE TO DATE
	NO GRINDING	WITH GRINDING		
1220m (1°30')	255	465	82	50
915m (2°)	225	390	73	38
764m (2°20')	195	330	69	31

(#) Based on a maximum head loss allowable for 35%

5. RAIL GRINDING PRACTICE

In-track grinding has been widely adopted by railroad operators as a standard rail maintenance tool, but perhaps due to the expense, its use has been restricted. Discussions have been published in the literature on guidelines for effective grinding practice. The concerns, hence the directions of the discussions, centred around corrugation and plastic flow (4,5). Extension of rail grinding technique to the control of rail wear by reprofiling is relatively new(6).

Historically Hamersley Iron had used rail grinding primarily as a tool for rectifying rail corrugations. This entailed using a large number of passes with all of the stones directed on the top of the railhead. At the worst locations some 40 - 50 passes were used each cycle to remove corrugations. This was carried out on a fairly frequent basis and the grinder was pressed to cope with the demand. Some attempts were also made to control tangent snaking rail patterns but machine capacity became a limiting factor.

With the indication of positive results from the rail grinding trials a decision was made to adopt rail reprofiling as a maintenance policy. The grinding test had provided the knowledge to formulate guidelines for a cost effective application of in-track reprofiling. In particular the test showed that grinding efficiency and an optimal grinding cycle were the two most critical factors.

5.1 Grinding Efficiency

The rail grinding test confirmed the simulation study results that bogie performance (hence wheel/rail wear) is highly sensitive to the rail profile. Accurate profile grinding must therefore be maintained to ensure that improvements are achieved in lieu of further damage to the vehicle/track system. The first measure to achieve accuracy in grinding is to set the correct reference for the grinding stone angles. This requires the setting of the stones to be carried out on an accurately aligned tangent track location with a stable foundation. The second measure is to develop appropriate quality control monitoring to ensure that the ground rails are produced correctly, not only in terms of their profile specifications but also their orientation with respect to the track plane. One simple method which can be

used is to spray paint the rail head for about 1 metre upon completion of grinding. After passage of a suitable number of trains the rail is inspected to see where the wheels have worn off the paint. This indicates the contact band location and width which is very important in determining whether the profile is working properly to control the bogies.

The correct profile must be produced with the minimum volume of rail metal removal since the loss of railhead, in whatever form, has a detrimental effect on rail life. With proper grinding, a very substantial reduction in overall rail wear can be achieved. However, experience has shown that an unskilled grinding operator can easily do the reverse. Proper supervision and inspection are required to achieve results.

It would be beneficial to monitor changes in the profiles of the wheels in the fleet and adjust the ground rail profile accordingly. A significant decline in the previous high rate of flange wear has been experienced at Hamersley. The trend is now toward wear on the wheel tread but at a lower overall rate. This is a positive result which nevertheless should be watched so that the best match up of wheel and rail is achieved.

5.2 Optimum Grinding Cycles

In rail grinding management, it is important to aim for a simultaneous achievement of rail profile restoration, surface defect removal and corrugation prevention. Following the introduction of profile grinding a certain period was required to introduce the profile on all curves on Hamersley's track. The initial grinding required an average 20 - 25 passes per curve. It took some 14 months to get on top of both curves and tangents. In terms of corrugations this meant getting to the point where, with an improved contact situation, a system based on prevention rather than cure was achieved.

It was recognised that the planning for the operation of the grinder would benefit from a computerised data processing system. An appropriate subsystem was created as part of Hamersley's Track Information System which comprises a series of data bases. The historical information on each particular location is stored and used to schedule grinding cycles and plan the efficient use of the machine. When the crucial data on the rate of rail deformation via corrugation or profile loss is determined as a function of tonnage, then the most effective grinding cycle can be developed. This will ensure the minimum removal of rail metal and the least overall grinding effort.

The scheduling of the grinding cycle has a direct effect on rail lives. Hamersley started out with cycles related to time and the history of corrugation at each location. Since then a policy of grinding fewer passes (about 10 each location) per cycle has been adopted. These act as a profile touch-up and retard any development of corrugation. Cycles are now being determined for a range of radii based on tonnage rather than time.

There appears to be a trend to fewer total passes now being required for a given level of haulage; but with tonnages fluctuating this has yet to be confirmed. As further experience is gained the process is being fine tuned toward the development of optimum grinding cycles. In general, the optimisation of the rail grinding cycle must be based on a broader consideration of the effect of rail grinding on the various components of the overall rail maintenance cost (Figure 4). This will ensure that the overall maintenance cost is minimised - not just the rail replacement cost.

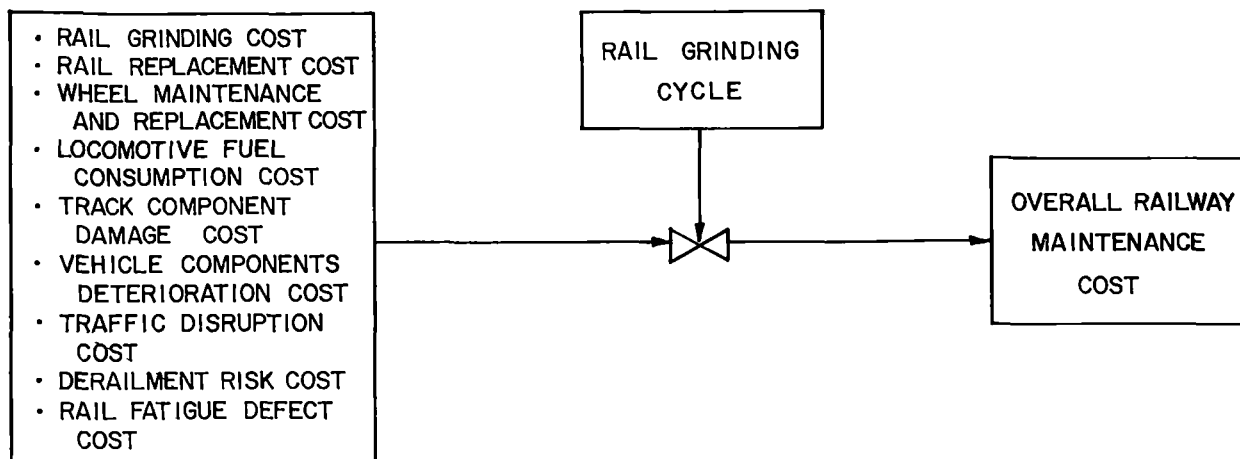


FIGURE 4. Effect of grinding cycle on overall railway maintenance cost

5.3 Grinding Capacity

To be able to grind efficiently and optimize cycles, one must have adequate grinding capacity. This aspect should not be neglected with track occupancy time on most railways being short and becoming shorter all the time.

When Hamersley was in the midst of its problems with corrugations and tangent hunting wear, it was considered that an additional grinder would be necessary. The other option was to face massive re-railing programmes. With the development of re-profiling the need for the additional capacity was eliminated.

Currently at Hamersley productive grinding time is about 1,700 hours per year based on a 24 hour shift, 5 days per week, with one third of the time allocated to cold shut maintenance (as opposed to running maintenance) and two thirds available for grinding. With traffic of 18 loaded/empty trains per day about 63 per cent of the machine's available time is actually spent grinding. Allowances must be made for breakdowns, major overhauls and travelling. It is felt that, should the need arise, there remains a reasonable reserve capacity available. In 1980 whilst hauling 60 MGT, some 16 000 pass kms were ground, split roughly equally between curves and tangents. A trend toward a decreasing grinding requirement for a given level of haulage is expected once the initial profile has been established.

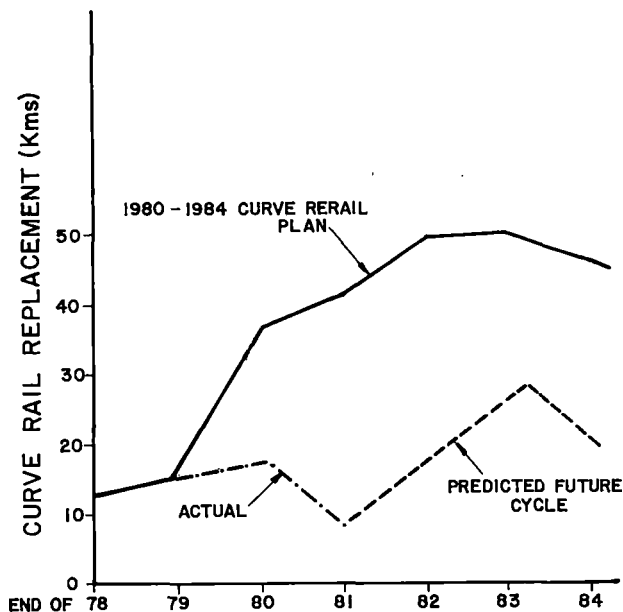


FIGURE 5. Actual versus predicted curve rerail

6. BENEFITS

The benefits from the use of profile grinding at Hamersley Iron have been and continue to be substantial.

In Table 3 is an indication of the actual increases in rail lives achieved to date. It is unlikely that the theoretical levels predicted will be achieved due to minor errors in the profile, surface condition requirements etc. However, by concentrating on the areas of grinding efficiency and optimisation of cycles, it is felt that further improvements in rail life can be made. The impact of reprofiling in terms of actual annual rerail requirements is well illustrated in Figure 5.

On most curves minimal side wear occurs, with the tendency being toward a gradual, uniform reduction in the rail head thickness. The development of severely worn gauge faces has halted and there is a decreased risk of wheel climb derailments associated with this shape change. This stabilised rail head wear, as shown in Figure 6, has also generated confidence in increasing the allowable rail wear replacement limit to 35% or greater. The need for transposition with the associated labour and equipment costs will be eliminated in future.

There are a host of other benefits being gained such as fewer fatigue defects, more accurate ultrasonic rail testing and better control of weld profiles. Finally, there is a corresponding but as yet unquantified

fied benefit being experienced in reduced wheel wear and remachining costs.

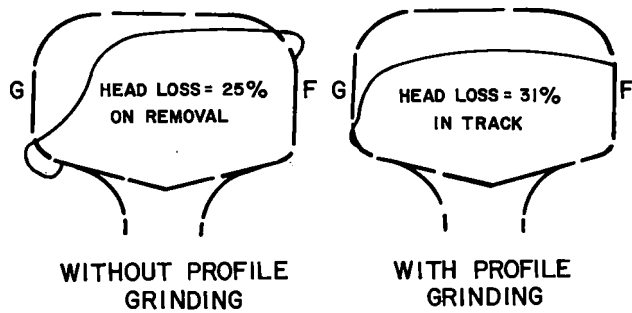


FIGURE 6. Typical worn rail shapes

A conservative estimate indicates savings in re-rail costs alone due to curve reprofiling at about \$1.0m per year. This more than justifies the annual curve grinding cost of \$0.6m, especially when one considers that the equivalent of this amount was being spent in 1976 on corrugation removal.

7. FUTURE

Despite the great steps made in the development of reprofiling, there remains much that can be done to improve the technique. Although production requirements are currently being met, there are arguments for a much faster or efficient grinding rate which potentially could be achieved by such means as improved grinding materials, a faster operating speed or perhaps the use of planing or milling heads. In this respect, Hamersley Iron is looking at improvements to the existing machine, as well as investigating the possibilities for future advancements in technology.

There was an early recognition of limitations in determining the correct number of passes and the level of deterioration of the profile for a given location. This, coupled with a desire to accurately measure rail wear for predicting replacement requirements, led Hamersley to investigate an automatic, non-contact, profile measuring system. A prototype based on the electronic scanning of a sectioned light sheet projected on the rail head is now under test.

One further point worth making is that the success of the asymmetric rail profile has led to a serious consideration to having this profile rolled for new rail. It would appear to be economic to avoid the initial grinding requirements and higher wear rate associated with standard profiles, despite the potential logistic and operational concerns caused by specifying an asymmetric profile. The standard AREA profiles may not be the best suited for maximum rail life. This does not seem such a revelation when one considers how wheel profiles are tending to depart from the AAR standard to the so-called worn wheel profile.

8. TANGENT PROFILE

For simplification, details of tangent rail grinding have been excluded. However, it is necessary to make some mention of the situation since tangents require nearly half the annual

grinding effort at Hamersley Iron.

In the early stages, extensive grinding (up to 60 passes) was directed to attempts at breaking up the side wear pattern. However, by using a version of the curved rail profile on an interim basis, far fewer passes are being required. This method has been successful in controlling the hunting problem which threatened to cause premature rail replacement. A similar exercise to produce a profile specifically designed for tangent track using a computer model, is in the process of being completed. Besides concentrating on reducing snaking wear and surface deterioration, it will aim to reduce stress levels in order to extend the fatigue life of tangent rail.

9. CONCLUSIONS

Simulation studies of the three piece bogie curving characteristics using a computer model produced a rail profile which could be used in curves to reduce the wheel/rail interaction forces and wear.

Field testing of this profile by in-track grinding, followed by the measurement of the lateral wheel/rail interaction forces, verified that significant reductions in these forces can be expected.

Monitoring of test curves over a significant time duration confirmed that rail wear, especially side wear of high rails, decreased dramatically.

The technique of rail profile grinding has been developed and refined into the most important track maintenance tool which Hamersley currently use.

Extensive use of rail profile grinding has substantially reduced Hamersley's maintenance cost, but, to maximise the benefit, the rail grinding method must be efficient and the cycle must be optimised.

REFERENCES

- 1 Downs, L.H., and Oliver, B.D., (1979). "Some Developments in Track Maintenance on Mt Newman Mining's Track". Proc. Third International Rail Sleeper Conference, 1979, 24-28 September. The Rail Track and Sleeper Association, Australia. Session 4, Paper 5.
- 2 Townend, P.H., Epp, C.J., and Clark, P.J. (1978). "Bogie Curving Trials, Rail Profiling and Theoretical Modelling to Reduce Rail Deterioration and Wheel Wear in Curves". Proc. Heavy Haul Railways Conference, Perth, Session 203.
- 3 Marich, S, and Lamson, S, (1981). "A Strategy and Procedure for the Development and Application of a Bogie Curving Model". Railway Engineering Conference, 1981, Sydney, 7-10 September. (The Institution of Engineers, Australia. National Conference Publication No. 81/9)
- 4 Marich, S and Mutton, P.J. (1981). "Rail Requirements for Heavy Haul Rail Systems". Proc. 34th Annual Conference of the Australian Institute of Metals, 10-14 May 1981. Surfers Paradise, Queensland, Australia.
- 5 Bramwell, S. (1979). "Rail Maintenance - Grinding". Proc. Third International Sleeper Conference, 1979, 24-28 September. The Rail Track and Sleeper Association, Australia. Session 8, Paper 6.
- 6 Bruno, A.T., (1981). "Rail Grinding: a closer look". Railway Track and Structures February 1981

The Use of Rails on British Railways

M.C. Purbrick

B.Sc. (Eng), F.Eng.,
F.I.C.E.
Director of Civil
Engineer
British Railways

British Rail's policy for the use of rail in its intensity used, multipurpose, track network was defined 15 years ago and is unusual in its insistence on the relatively low rail weight of 113lb/yard. Although freight vehicles of 100 ton laden weight (25 ton axle load) regularly run at 60 mph on this network, the policy is nevertheless successful and cost-effective. This paper outlines the reasoning behind B.R.'s original decision, and its experience to date with this rail with particular reference to factors seen as shortening the life of the rail, are described. Finally, B.R.'s plans to get even longer life out of this light-weight rail in the future are foreshadowed.

INTRODUCTION

The British Railways system contains some 22,000 miles of track or 11,000 miles of route. The majority of track carries both passenger and freight traffic. Passenger services which are operated by the High Speed Train run at 125 mph (200 km per hour) with 17 ton axle weights and some 10 million miles a year are run by this fleet of trains; the highest in the world at that speed on track not specially built for high speed operation. On the same tracks trains of 25 ton (25.4 tonne or 28 US tons) axle weight operate at speeds up to 60 mph, with gross train loads up to 3000 tons. B.R. runs an average of 275 "Merry-go-Round" trains (these carry coal, oil, iron ore etc. in 100 ton wagons) each day, with an average gross tonnage of 1500 per train. A further 125 Company trains and 100 Freightliner trains operate daily, each with a gross trailing tonnage of 1000 or over. The biggest single point to point flow is about 26 million tons per year, and a number of the fastest passenger routes carry tonnages of the order of 21 million.

B.R. is the only European Railway system to use 25 ton axles, most other systems only allowing 20 tons.

The use of rails in this intensively used mixed system where they are subjected to high dynamic loading from high speed trains and reasonably high loading from the freight operation is discussed. Causes of limited life are reviewed and methods of obtaining longer life outlined.

RAIL POLICY ON B.R

Rail Specification And Manufacture

The bulk of the rail steel used by B.R. is to British Standard 11:1978 Normal Grade. Limited quantities of A Grade and B Grade wear resistant steel together with Austenitic 12/15% Manganese (AM) Steel are also used. A small number of rails made from 110 kg/mm² Chromium Grade and Austenitic 12/16% (weldable) Manganese steel have been installed. The British Standard is very similar to UIC specification. All of the rails are purchases from British Steel Corporation. Other than the A.M. steel they are rolled from continuously cast basic oxygen steel; A.M. steel being rolled from ingots teemed from an electric arc furnace. Until recently the finished rail length has been 60 ft but now B.S.C. are supplying 120 ft length rails.

Installation

Most of the rail bought by B.R. is depot-welded by the Flash-butt Welding Process into lengths up to 1000 ft. After conveyance to site by train it is welded again, by the Thermit Skv-F process, to form Continuously Welded Rail Track (CWR). About 10,000 miles of this track now exist on B.R. (i.e. nearly 50% of all track).

Rail Section

B.R.'s decision about the rail section to adopt as standard for its CWR track was made in the late 1960s following a programme of analytical and experimental work undertaken by B.R.'s R.&D. Division in co-operation with the British Steel Corporation. (1, 2). For C.W.R., it was found that for 25 ton axle weights the fatigue life of B.R.'s 110A rail section (which was identical with UIC 54) was such that for B.R. traffics and operating conditions there was no case for increasing rail weight on purely rail strength grounds. To cure problems encountered with bolt hole fatigue in rail webs at fishplated joints however the web section was thickened up to form the BS113A

section which has since 1969 been B.R.'s standard rail.

This decision has borne the test of time. The critical part of the rail was identified as the upper fillet and to date there have been virtually no failures that could be traced to excessive fatigue stress in this part of the rail and this is made clear in the part of the paper which deals with the causes of defects leading to the removal of rail from the track.

Nevertheless, B.R. has kept its policy under continuous review, particularly in view of the expectation of many European Railway engineers that a heavy rail section would reduce the pressure between the sleeper and the ballast and thus reduce the rate of deterioration of track geometry. We have taken part in the work of ORE Committee D 117 (3, 4) which showed that little difference was found in the geometric performance which could be attributed to the differing rail sections. Following the conclusions of the D 117 Committee therefore, we have so far retained the BS113A rail as standard and have achieved reduced sleeper/ballast pressure by reduced sleeper spacing. Thus although we carry heavier axles than the rest of Europe we do not intend to follow their trend towards UIC 60 rail.

FACTORS LIMITING RAIL LIFE - 1 - RAIL DEFECTS

Any defect in a rail which is likely to lead to a fracture requires in most cases the removal of a length of the rail from service.

Whenever a rail is removed from service due to either a break or the detection of a crack or defect the cause of removal is analysed and coded using the UIC standard catalogue of Rail Defects, and the coded information fed into a complete programme for analysis.

Type Analysis Of Rail Defects

Rail failures are first analysed by type, viz. whether the failure is due to:

- (a) Corrosion
- (b) Inadequate maintenance
- (c) Inherent defect of rail
- (d) Inadequate Specification
- (e) Effects of traffic
- (f) Welding Defects

In a normal year the significant classifications are (b), (c), (e) and (f).

Failures due to inadequate maintenance are predominantly those associated with rail joints and will not be further discussed.

Failures due to inherent defect of rail may be divided into gross defects, such as major inclusions, piping, vertical splitting etc., and Taches Ovales. Failures due to the effect of traffic include "Squats" and wheelburns. Welding defects are predominantly from Thermit Welds. Notes on some of these follow.

Gross Manufacturing Defects. These cracks, flaws etc. arising from the making and rolling of the rail, predominantly occur in older rails. Two recent developments have virtually eliminated these defects from new rail - viz. the introduction of continuous casting and the provision of routine ultrasonic rail examination at the steelworks.

Taches Ovales. This well known and very dangerous form of internal defect is usually on B.R. initiated by an exceedingly minute hydrogen crack. Because the quantities of H₂ present are so small (mean value 1.36 ppm in finished rail) it takes several years for the H₂ present to migrate far enough for a few atoms to coalesce into a nucleus. Hence the defect is typical of the older rail (where H₂ levels at the time of manufacture were higher). This type of defect accounts for 12-15% of all failures on B.R., and over 80% of "failures" are found by ultrasonic means and removed from the track before they break.

Squats. The type of rail running surface defect known on B.R. as a squat consists of a rolling contact fatigue initiated surface defect propagating at a shallow angle of and then turning down to form a transverse fracture see Fig.1

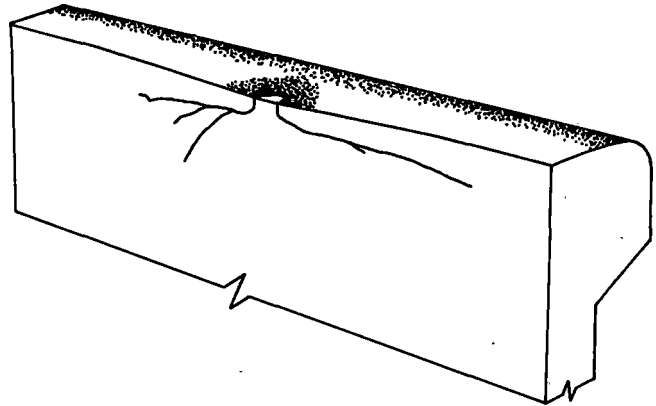


Fig. 1. A Developing Squat Defect

This type of defect has only appeared in the last 10 years. It is a particularly serious form of defect as the cracks running parallel to the head of the rail prevent the ultrasonic detection of any developing transverse fracture. The cause is not fully understood but is believed to be due to high stresses from the wheel and rail contact forces which are dependent on wheel and rail profiles. It is thought that there may be a relationship between these defects and corrugations. The stress situation in the rail head which is of fundamental importance continues to receive attention by our Research Department (5, 6). It is possible to carry out a repair of a squat by welding provided it is carried out before the defect has grown too large. Consideration is currently being given to the use of higher strength steel on heavily worked lines which may assist in reducing these defects.

Wheelburns. As will be well known this common defect takes the form of depressions in the running surface of the rail caused by wheel spin which lead to high dynamic stresses and subsequent fatigue cracking or continuous transformation of the running surface causing hardened micro structures with subsequent fatigue or brittle fracture. These defects are commonly on B.R. repaired by grinding out to unflawed material and replacing with sound metal by Manual Metal Arc Welding.

		SPEED - MILES / HOUR			
		OVER 100	75 to 99	50 to 74	49 or less
ANNUAL GROSS TONNAGE TONS (MILLIONS)	OVER 12	A 4	B 4	C 4	D 4
	5 to 12	A 3	B 3	C 3	D 3
	2 to 5	A 2	B 2	C 2	D 2
	2 or Less	A 1	B 1	C 1	D 1

Fig. 2 B.R. Track Categorisation

Welds. The Flashbutt and Thermit welded joint connecting the 60 ft lengths of rail have to withstand a very hostile environment due to thermal tension and the bending and impact loads imposed by the trains moving over them. Both types of weld can be liable to fatigue and brittle fracture if the weld is defective as a result of the manufacturing process. Flashbutt weld failures are relatively few (1 in 25,000 of the total installed population per annum) and do not present a serious problem. The Thermit Weld is however particularly sensitive to the skill and craftsmanship of the welder. As a result the proportion of failures is much greater than with FB Welds, particularly early in the life of the weld. In 1980, which was a bad year 0.18% of welds were failed within a year of manufacture. The problem is being tackled by increased training of the welders together with improvements in quality control. This subject is dealt with in detail in Mr. Lugg's paper to this Conference (7).

Analysis Of Rail Failures By Age, Tonnage & Speed

In addition to the type analysis described above, rail failures are analysed according to age and track classification.

Track Classification. For all aspects of track maintenance and renewal B.R. use a 4 x 4 matrix of speed and weight of traffic for the classification of track. The matrix is shown in Fig.2 above.

Statistical Trends in Rail Failures. Using these classifications the cumulative rate of rail failures can be plotted against age of rail. This is shown if Fig.3 overleaf.

Track Categories A4 and A3 show a very pronounced deterioration trend after being in the track 12 years. In B4 the trend is less marked and C4 even less so. All other categories approximate to a linear deterioration with age. It is interesting to note that the worst situation occurs on the high speed routes A4 and A3 where high quality track is maintained.

On the heavy weight slow speed routes D4 a very low rate of failure exists. Our statistics at the moment, do not permit the division of traffic on the A4 and A3 routes between high speed and heavy axle but a new recorder is being developed which will give this information so that further analysis can be carried out.

Whilst the development of defects can be contained by ultrasonic inspection there is always a possibility of failures occurring between examinations.

The costs incurred as a consequence of unexpected rail failure are considerable, even without taking account of the consequences of a passenger train derailment. Equally, if a rail is found to be defective as a result of ultrasonic examination, the process of obtaining emergency possession, cutting in and restressing CWR is a most uneconomic one compared with programmed rerailing. These considerations are leading B.R. towards a decision to renew all rail in A4, A3 and B4 routes after 12 years service. It would be the intention to re-use the recovered rails in lower category lines (a so-called Cascading Policy). The possibilities and implications of this policy will be further discussed below.

FACTORS LIMITING RAIL LIFE - 2 - EFFECTS OF TRAFFIC

The considerations outlined in the above paragraphs apply to the removal of rail to prevent the catastrophic development of internal flaws. However rail life has other important determining factors arising directly as a result of the wear caused by trains. Four of these factors will now be discussed, viz. Corrugations, Sidewear, Footwear and Headwear.

Corrugations

Although corrugations have existed in a limited number of places on B.R. for many years, in the last 15 years the incidence has increased greatly and continues to grow. Despite considerable research the phenomenon is still not understood. The problem is

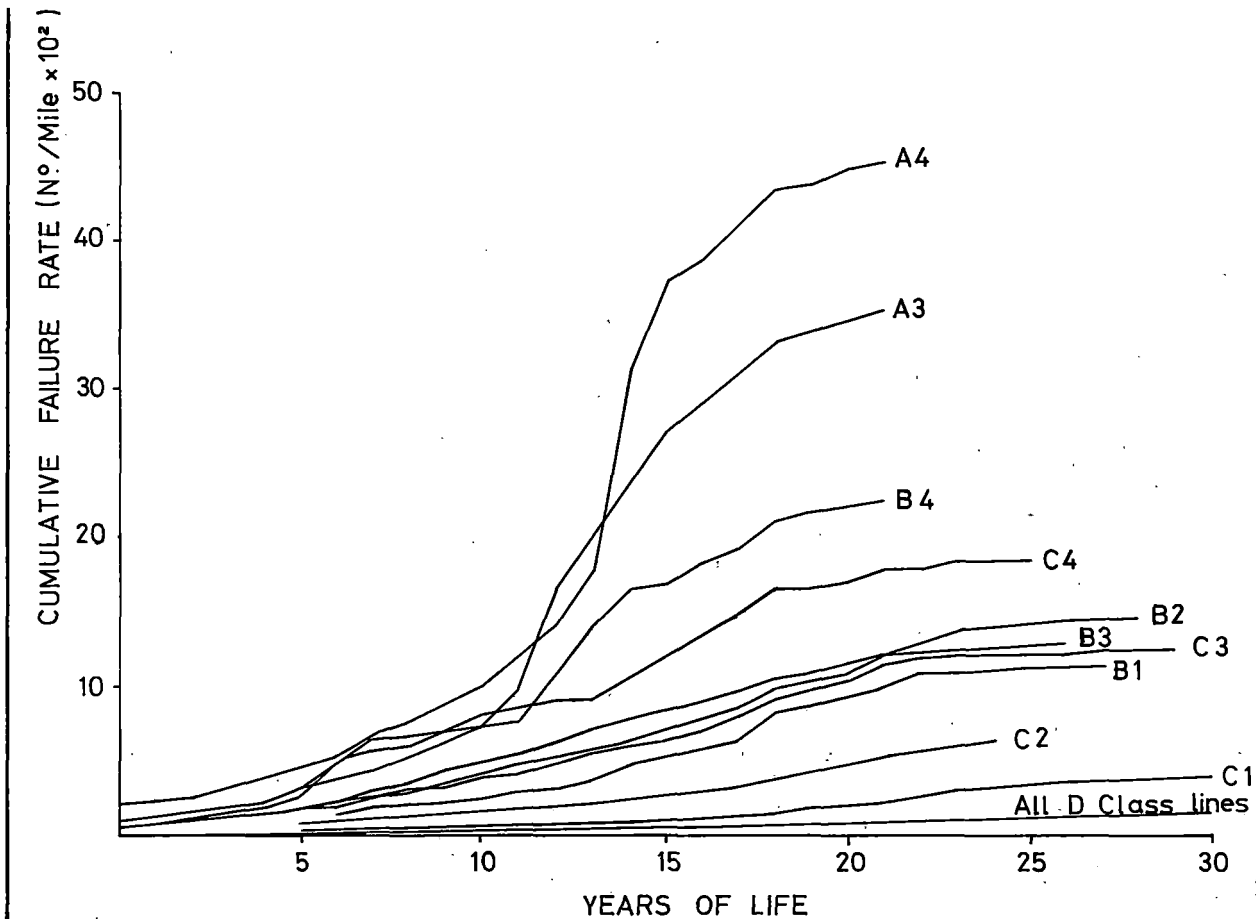


Fig.3 Cumulative Rate of Rail Failures Plotted Against Age for Track in Various Categories

being met by grinding but this is only a palliative and after a time the corrugations return. Experiments have shown however that new rail if ground immediately it is installed develops corrugations much more slowly. Further work is now being undertaken to investigate the cause of corrugations that have been shown to exist on new rail and the benefits of removing these before installation.

Sidewear

The combination of track curvature and vehicle characteristics - angle of attack of wheel flanges and bogie rotational stiffness - make this a very variable problem. Lubrication from rail lubricators produces significant reduction of wear rate but on B.R. there is still scope for further extension of this method. Wear resistant steels are used in sharp curves particularly B Grade. The use of B Grade rail has been limited in the past to jointed track due to welding difficulties, but these problems have in principle been solved and this rail was used as CWR on the Mersey Loop and Link Scheme. Rolled AMS rail has been used in limited quantities but is extremely difficult to weld and when welded can only be used in tunnels due to its high coefficient of thermal expansion. It was so used when the Eastern Region suburban lines were electrified and extended in tunnel from Kings Cross to Moorgate.

Trial lengths of Grade A rail and of 1% C (110 kg/mm² UTS) rail have been laid and these rail steels are likely to be used much more extensively in the near future.

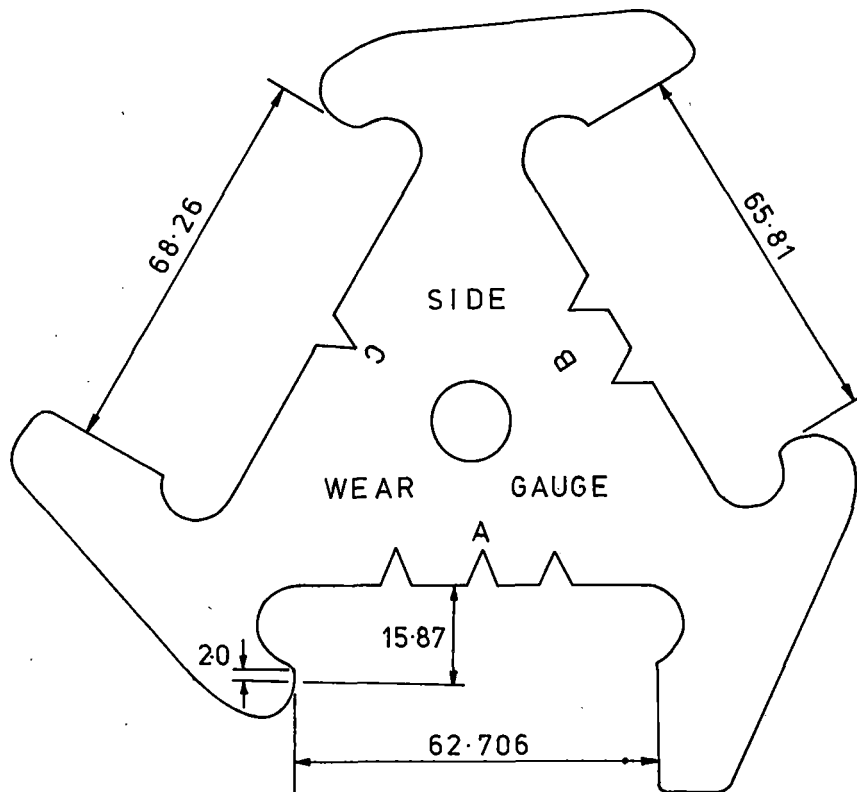
Considerable data has been obtained on wear on a selected number of sites and the information is contained in a B.R. Research Division Report (8). A number of years ago it was seen to be necessary to define more precisely the criteria for the limits of permissible side wear in order to ensure rail was not being removed prematurely. This was done by means of an easily used gauge as shown in Fig. 4 overleaf and Appendix A. By this means the life of rail subject to sidewear has been significantly increased.

Footwear

Some wear has been experienced at the edge of the foot in early baseplate types of fastenings where it was in contact for gauge retention purposes, with the shoulder of either a cast iron or rolled steel baseplate. This does not occur with the current standard fastening used on B.R. with concrete sleepers and Pandrol clips with replaceable insulators which retain the gauge.

Headwear

Some hardware is inevitable. However on B.R. in straight track in normal circumstances the loss of head depth due to abrasion by passage of traffic is quite small - only say 1 mm for 50 million tons of traffic. The work referred to in reference 1 and 2 showed that for the 25 ton axle loads no stress



Dimensions in millimetres.

Fig. 4. B.R. Standard Side—Wear Gauge

problem arises for less than 12 - 15 mm of head wear and B.R.'s practice is to permit up to 9 mm of headwear on "A"; 12 mm on "B"; 15 mm on "C" and 18 mm on "D" class tracks respectively. This latter wear level, coupled with permitted side wear, is the most that can be allowed without risk of contact between wheel flange and fishplate.

Loss of depth occurs more rapidly on Curved Track due to the creepage or slip of wheels on both high and low rail, and due to crushing when substantial weight transfer occurs. This is mainly a problem on the low rail on heavy cants where it is necessary to cater for both fast passenger trains and slow moving freight.

METHODS OF EXTENDING RAIL LIFE

As outlined in the previous paragraphs there is usually plenty of metal to go at in a rail head, and except on a very small proportion of tracks carrying combinations of very fast and very heavy traffic there is no real problem caused by the generation of internal or surface fatigue cracking.

B.R. has therefore become very concerned with the problems involved in effectively making as much as possible of the rail head available for use. This has meant finding ways of removing corrugation, and of making sidworn or headworn rail suitable for reuse. The Speno Rail Grinding train is used to combat corrugation. For many years B.R. simply turned or transposed its sidworn rail. However, this created problems with high frequency bogie oscillations on fast passenger trains and it has been

realised that it is of fundamental importance when re-using rails to restore an acceptable head profile. A good head profile also helps to minimise wheel maintenance. Hence we have been collaborating with Messrs. Plasser and Theurer on the development of a rail profiling machine. Thirdly, to assist in making ourselves as cost-effective as possible in the process of transposing or cascading rails, we have been developing various machines to assist in these activities. These various devices are reviewed below.

Speno Rail Grinding

The Speno Rail Grinding Train is well known and needs no description here. B.R. now has two of these trains on hire. They are used more or less exclusively on the removal of corrugations and a mileage of 1000 per annum is being achieved. During the grinding process the rail head profile is restored to an acceptable profile and this substantially improves the ride of passenger vehicles. When the Speno Train was first taken into regular use it was hoped to be able to use it for reprofiling the whole upper surface of rail selected for transposing. However this was found to take too long.

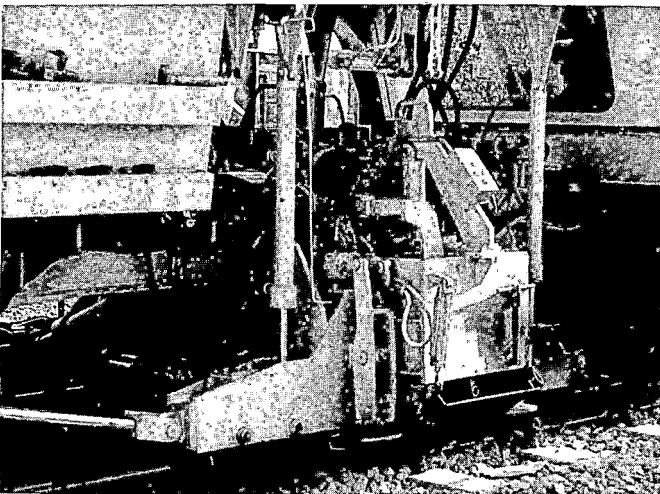
Plasser Rail Reprofilng Machine

Reprofiling of heads of worn rails has been carried out in Europe using multiple planing machines or milling machines in conventional workshops for many years. The method is costly; rails must be removed from the track, transported to the workshop, installed in the machine and then despatched for re-use.

Continuously welded rails must be cut into standard lengths and re-welded. British Railways have not adopted this process and until six years ago the practice of transposing to obtain further life from worn rail was common. Because of the need to improve the wheel rail contact as mentioned above studies were initiated into the design of a profiling carriage and tool holder capable of machining ends of rails in situ on the track. On examining the power required for such an operation it very soon became evident that in excess of 200 hp was necessary and this meant a major machine (Fig.5).



Plasser and Theurer undertook to manufacture the profiling carriage and tool holder (Fig.6)



and install it on a track machine based on one of the Standard O7 tamper/liners; the planing head taking place of the tamper banks and associated equipment. In order to develop sufficient adhesion to carry out the planing operations it was necessary for all four axles on the machine to be driven. After trials and evaluation and development work of the system of use, the machine was purchased and is now in normal

use as part of the Civil Engineering Department's plant fleet.

The technique that has been developed to reprofile one running edge on the head of the rail is illustrated in Fig.7 overleaf. To form the radius on the running edge, three cuts are made, first as in 2. at 45° and then a second with two cutting edges, one at $67\frac{1}{2}^\circ$ and the other at $22\frac{1}{2}^\circ$, to start forming the radius and a third cut as in 6 using a radiused tool which produced the finished profile. The datum point for the whole planing operation is the centre of the railhead and it is for this reason that the final cut is made at the centre of this datum. If it is required to reprofile the other running edge this can be done by repeating cuts 2, 3 and 6. The cutting speed is most important, and experience to date shows that the best results achieved with a planing speed of 0.9 metres per second. All operations are normally done on both rails at the same time. Tool positions are set up manually before operations are commenced and the procedure monitored by the operator who sits inside the machine using a split screen video system. The tools utilised are tungsten carbide disposable cutters which are entirely satisfactory in dealing with all steels up to grade B.

The planing produces considerable quantities of swarf and chip breaker tools are needed to ensure that this is broken up into an easily handleable size. The swarf is picked up from the track via a magnet suspended on short crane arms positioned on a vehicle trailed behind the main machine.

Before the start of reprofiling work it is essential that the track is tamped and lined to ensure that the rails are free from dips or misalignments. Best results have been achieved on continuous welded rail but good quality jointed track can also be dealt with satisfactorily. In good conditions it is possible to reprofile completely both rails on 1,200 metres of track within a normal eight hour possession.

In the first six months of use the machine has very satisfactorily reprofiled over 20 miles of track. This has enabled B.R. to avoid purchasing the equivalent length of new rail and the machine has therefore covered its capital cost twice over in that time.

Attempts have been made to remove severe corrugation by the use of this machine but so far because it is found necessary to take a minimum depth of cut of 0.5 mm to give a successful cut the use of the machine this way does not appear too promising. However work is still being undertaken in this area.

Rail Changing and Positioning Machines

It is easy to change, turn or transpose rails of 60 ft (18 in) length either by hand or with a crane. Means have been developed for offloading rails up to 1000 ft long from trains, and for handling such rails on the ground, but the methods are time consuming and costly. Much time and effort has however been spent on efforts to devise track-mounted machines that would unload and change rails in one operation, or that would automatically transpose CWR without having to cut the rails. With this end in view a Plasser Rail Changing Machine was purchased in 1979. This machine is intended to move long welded rail from sleeper ends into rail seats and vice versa, or to transpose rail. It is still in course of development.

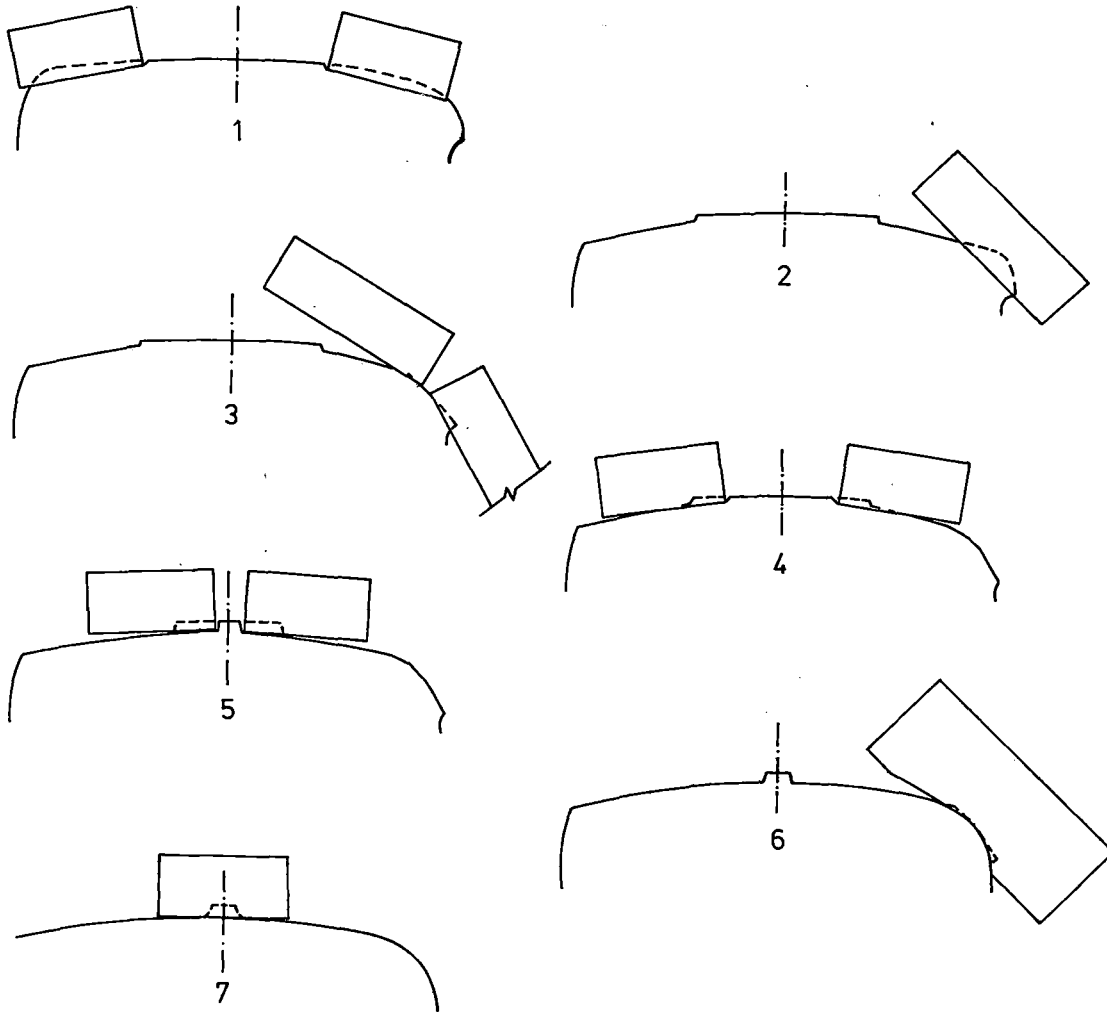


Fig. 7 Rail Profiling Sequence of Operation

Future Policy

Our current thoughts on our forward planning for the re-use of rail, based on the maximisation of in-situ life by the use of the Speno Train for combating corrugation, and the maximisation of reuse by reprofiling with the Plasser Rail Reprofiling machine are that in the ultimate rather more than 40% of the rail arising from renewal/rerailing in any one year should go back into running lines. The use of new rail would be limited to A, B₄ and C₄ category routes. Rail from Categories A and B₄ would be cascaded into an appropriate lower category after 12 years. Rail in other categories would be cascaded similarly when it had reached the appropriate limiting depths. Jointed rail removed in this way would be cropped and thermit welded and all serviceable long welded rail whether recovered welded or recovered as jointed and then welded, would be reprofiled as part of the process of returning it to use.

CONCLUSION

By these various means which have been very briefly outlined B.R. is proposing to increase its average rail "life" from 35 years to at least 50 years and hopefully beyond that. The cost reduction that accrues each year will make a real contribution to more economic and viable operation of our system. In doing so the fundamental importance of safety on a mixed system which includes high speed passenger operations has had to be carefully taken into account.

REFERENCES

- 1 Experimental Stress Analysis of Rails
A.S.Babb Proc 1 Mech E 1965 Vol.180
Pr.1 No.41
- 2 The implications of Running Heavy Axle Loads on
B.S. 110 A Rail
J.C.Loach and D.Lindsay
B.R. & R.&D.D. Report E 579. Dec.1965
Unpublished
- 3 RP2 ORE Committee D117
Study of the changes in the track level as a
function of the traffic and of the track
component.
- 4 RP7 ORE Committee D117
Study of the change in track geometry as a
function of traffic. Additional results.
- 5 B.R. R.&D.Division Technical Note TN GTM15
Cheeswright P.R. A critical review of
Residual Mass Measurement in rails.
- 6 B.R. R.&D.Division Report MR MET 1
Frederick C.O.& Jones E.G. A review of Rail Research
in British Rail.
- 7 B.R. Experience with Rail Welding
P.J.Lugg 2nd Heavy Haul Conference Papers
1982.
- 8 B.R. R.&D.Division Report TM WR 13
Harvey R.F. A summary of Rail Wear Measurements
made by the Research & Development Division
between 1977 and 1981.

APPENDIX A

TRIANGULAR SIDEWEAR GAUGE

Method of Use

The gauge is used by placing it on the rail head with one of the long, notched, straight faces of the gauge parallel with the running table of the rail. The straight portion of one corner extension is placed against the outer face of the rail and the rounded nose of the extension at the adjacent angle of the triangle on the worn running face. The side of the triangle with one notch is defined as "C", with two notches it is "B" and with three notches it is "A".

If the "C" face of the triangle (i.e. 1 notch) does not rest on the rail head then the sidewear is classified as "slight".

If the "C" face rests loosely on the rail, but the "B" face does not then the sidewear is classified as "medium".

If the "B" face just rests on the rail with both the straight extension and the rounded nose also in contact with the rail the sidewear is classified as "heavy".

If the "B" face rests loosely on the rail but the "A" face does not, then the sidewear is classified as "severe".

If the "S" face rests on the rail the sidewear is classified as "beyond tolerance."

Application to Lines where the Permanent Speed Restrictions is 60 mile/h or more

Where trains travel at 60 mile/h or more rails should be turned, transposed or replaced at the degree of wear classified above as "heavy". This means that the Permanent Way Supervisor should initiate programmed arrangements for attention at appropriate times to accord with his experience of the rate at which the rail wears when the rail is at the "medium" sidewear condition.

Application to Lines where the P.S.R. is less than 60 mile/h

All rails must be turned, transposed or replaced before they become sideworn to the "beyond tolerance" condition. If any rails are found to be in this condition, immediate action must be taken to turn, transpose or replace.

Because of the wide variations in the rate at which sidewear takes place on sharp curves it is not possible to lay down hard and fast rules as to the stage at which programmed action has to be initiated, but as a guide the following are suggested:

When rerailling is required arrangements for rerailling should be initiated at the "heavy" sidewear condition.

When turning or transposing is required arrangements should be initiated at the "severe" or "heavy" stage depending upon the rate of wear and difficulty of arranging possession.

M.J. Abbott
Chief Civil Engineer

R.A. Dean

D.G. Pearce

R.J. Chamberlain

Rebuilding the Kwinana to Koolyanobbing Railway in Western Australia as "A New Generation Track"

Despite being opened for traffic in the late 1960's Westrail's 490km standard gauge mainline between Kwinana and Koolyanobbing required rebuilding by 1983 to maintain a safe and efficient service. The line carries around 10 million gross tonnes of traffic per annum of which over 50% is iron ore and wheat hauled in unit bulk haul trains. Axle load and speed for these trains were initially 24 tonnes and 70km per hour respectively but these have been subsequently reduced to 22.5 tonnes and 50km per hour on account of the inadequacies of the track structure. The technical and economic case for rebuilding the track structure was presented at the "Heavy Haul Railways Conference" held in Perth in 1978. This work showed that a heavier (new generation) track structure was required: the most cost effective being 60kg per metre rail on concrete sleepers with modern resilient fastenings. Rebuilding of the railway is currently proceeding to schedule and should be substantially completed in 1982. This paper follows on from the earlier paper and details the rebuilding planning; physical processes including logistics, tender evaluation and finally the operation of the task. It will outline decisions which led to the use of modern sophisticated equipment such as the P811 rerailling/re-sleeping machine and the SRS switch exchange equipment. The problems associated with:

- the change of sleeper type from timber to concrete,
- the handling and fixing of the FIST BTR and PANDROL fastenings,
- the handling of 60kg per metre rail in long lengths, and
- rebuilding the track structure under time constraints due to traffic density,

will be discussed together with how these problems were effectively and economically solved.

Summary

Deterioration of the track structure of the 1435mm gauge railway between Kwinana and Koolyanobbing in Western Australia resulted in investigation during the years 1975-78 to determine the best form of renewal. Technical research and evaluation studies indicated that replacement of the existing 47kg/m rail, 230mm x 115mm hardwood timber sleepers 19mm square dogspike fastenings and rail anchors, with continuously welded 60kg/m rail, prestressed concrete sleepers and resilient fastenings was the most cost effective combination for traffic consisting of predominantly unit bulk trains operating with axle loads of 24 tonnes.

Rehabilitation and upgrading of some 500km of this railway without serious dislocation to revenue earning rail traffic represented a major task. This paper traces the planning and evaluation of upgraded track standards, establishment of a concrete sleeper factory, rail welding depot and new rerailling and resleeping techniques.

1 INTRODUCTION

The Kwinana to Koolyanobbing railway is part of the standard gauge (1435mm) railway which links Perth with the Eastern States of Australia (see Figure 1.).

The Kwinana to Koolyanobbing section of railway completed in 1967 comprised 47kg/m rails of 13.7m mill lengths flashbutt welded into 109.7m lengths and converted into continuously welded rail in the track by Thermit welding. Timber sleepers were 2440mm in length with a section of 230mm x 115mm at 610mm intervals together with double shouldered steel sleeperplates, dogspikes, and deep bowed type rail anchors.

Track geometry was of a high standard such that gradient and alignment were favourable, waterway structures sound, the track formation built of good quality materials well compacted and crushed rock ballast of good quality to a depth of 230mm below sleeper.

Train speeds commenced at 110 and 130 km/hr for locomotive hauled passenger stock and rail car operation respectively. General freight was permitted to operate at 90km/hr and unit trains of ore and grain at 70km/hr where the axle load reached the maximum permissible 24 tonnes.

It soon became apparent that with the combination of the rapidly escalating annual tonneages and track deterioration, these speeds could not be sustained. As a consequence of a number of derailments in 1973 due to track failure, the maximum speeds of all trains were reduced between 10 and 15 per cent and axle loading of unit trains reduced from 24 tonnes to a maximum of 21 tonnes except for grain and iron ore which were permitted to be loaded to 22 and 22.5 tonnes respectively. However, the track structure continued to deteriorate with degradation of rail and sleepers being particularly marked.

Detailed examination revealed that sleepers would become service expired between the years 1979 and 1982 and the remaining safe rail life reached progressively between 1981 and 1986.

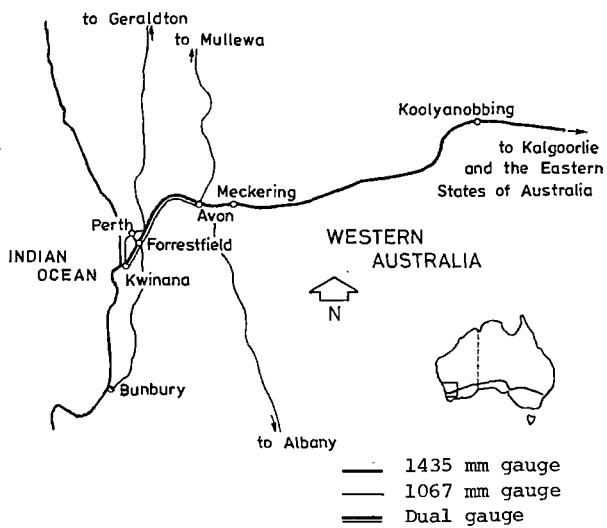


Fig.1 Location of Railway

Traffic expectations of 10 million gross tonnes by 1985 have been exceeded, this figure being achieved in 1976. Conservative estimates predict that traffic will continue to grow by at least 3 per cent a year.

2 SELECTION OF TRACK STRUCTURE

The technical justifications for the selection of 60kg/m rail on concrete sleepers using resilient fastenings was presented at the previous Heavy Haul Railways Conferences in Perth.¹

2.1 Sleepers

In order to assess the economic merit of timber and concrete sleepers, tenders were called internationally for the following three types:-

- (i) preserved hardwood sleepers of 230mm x 150mm section to be fitted with Pandrol baseplates, clips and lockspikes.
- (ii) concrete sleepers for Pandrol fastenings supplied with cast-in shoulders suitable for Pandrol clips, insulators and rail seat pads and
- (iii) concrete sleepers for Fist-BTR fastenings: supplied with cast-in tubes suitable for Fist-BTR clips, pins and ribbed type (R) rail seat pads.

Tenders were received from eight firms with the design expertise for concrete sleepers coming from Australia, England, France, Germany, South Africa, Sweden and the United States of America.

The tender showed that the concrete sleeper with Fist-BTR fastenings was the total least cost followed by the concrete sleeper with Pandrol fastenings, with the treated timber sleeper with Pandrol fastenings the most expensive. These were approximately in the proportion of 1:1.08:1.38.

After lengthy negotiations, a contract was signed with John Holland (Constructions) Pty Ltd in association with Grinaker (Precast) Pty Ltd from South Africa, for the production of:-

- (i) 540 000 standard gauge sleepers for Fist-BTR fastenings.
- (ii) 250 000 dual gauge sleepers for Fist-BTR fastenings.
- (iii) 170 000 dual gauge sleepers for Pandrol fastenings.

The production of the concrete sleepers commenced in June 1978 with the original contract recently reaching completion (July 1982). The factory produced 1120 sleepers daily from 7 lines.

It is thought that the dual gauge concrete sleepers for 1435mm and 1067mm gauge railway tracks are the first of this type designed and produced in the world.

Dynamic testing of the sleepers to verify the fatigue capacity of the sleepers was considered essential to prove the design of the concrete sleepers.

A one kilometre dual gauge Pandrol test section,

with 400 metre radius curves, was installed in February 1979. This was intended for observation under traffic conditions, prior to the balance of the dual gauge sleepers being produced, in case it was found necessary to vary the design. The traffic loading of 8.5MGT was not sufficient to cause faults to develop before production commenced however in August 1980 cracks began to develop on sleepers adjacent to rail welds. By August 1981, 55 sleepers or 4% of the trial section sleepers, had visible cracks, mainly around the narrow gauge rail seat as indicated in Figure 2 below.²

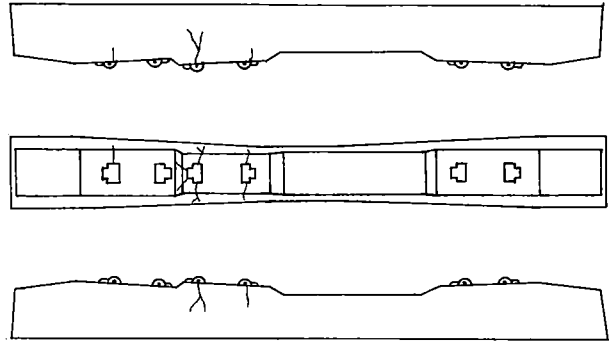


Fig.2 Concrete sleeper crack patterns (August 1981)

Strain gauges were installed on sleepers still without cracks adjacent to thermit and flashbutt welded joints and also between the welds. Figure 3 below indicates the analysis of results as recorded in August 1981. The shaded area shows that the tensile stress in the sleepers monitored is close to the ultimate tensile strength of 5.65MPa and explains the development of cracks in other sleepers.

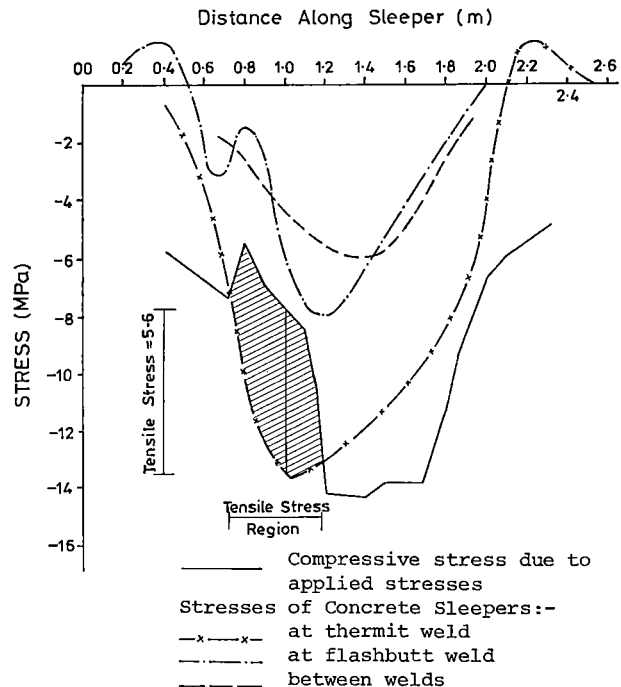


Fig.3 Compressive and tensile stress profile

It is clear from both visual observations and strain measurements that support conditions contrary to design assumptions are responsible for the development of cracks in the dual gauge sleepers.

A further trial section has been established to examine the influence of tamping patterns and ballast condition on dual gauge track.

At the time of preparation of this paper, the dual gauge sleepers that were installed in the test section and developed cracks around the Pandrol shoulders, referred to above, are the only sleepers that have shown any signs of not performing up to expectation. The production run dual gauge sleepers installed by the p811 machine have not developed any faults.

2.2 Rail

Manufacture of rail in Australia is only available through Broken Hill Pty Ltd. The 60kg/m rail used was to a new Australian Standard, being the first rail rolled to metric dimensions in Australia, and with improved tensile rail strength to a minimum of 900MPa.

Delivery is by rail from Whyalla South Australia, in 27.4m lengths, to the new flashbutt welding depot at Midland.

The rail is transported in coupled pairs of rail wagons fitted with bulkheads at each end of the consist and slotted side stanchions which secure greased timber gluts to obviate the need for chains thereby increasing the speed of loading and unloading.

Unloading at Midland is performed by an electromagnetic travelling gantry, lifting six rails at a time.

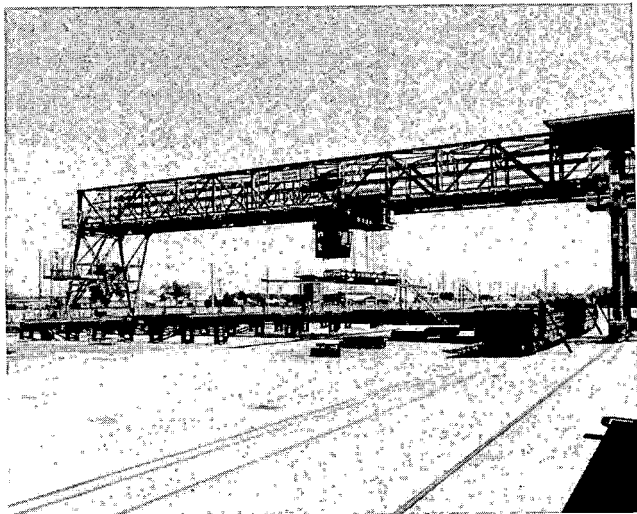


Fig.4 Electromagnetic travelling gantry

Unloading a wagon with 51 rails 27.4m in length, and stacking takes approximately 1 hour.

The lifting magnets used are:

4 x Mecal R.L. 300 x 1500 - S
Power 3.1Kw: 220V DC

Overall lifting spread of magnets 10017mm (35'-10 3/8").

Two magnets at each end spaced 552mm (1'-9 3/4").

There was a problem at the beginning of the project, with rails dropping off the magnets. This was overcome by eliminating the upward deflection of the rails at the centre by inserting a wooden block to maintain straightness of the rail at the same level as the magnets.

2.3 Fastenings

To match the requirements of the concrete sleeper contract, an order was placed for the following fastenings:-

1 761 000 sets of Fist-BTR	83%
495 000 sets of Pandrol	17%

2.3.1 Fist-BTR. A new organisation, Rail Track Fasteners Pty Ltd, was formed to produce these fastenings in Western Australia. A set of fastenings consists of:-

- (i) one clip - toe load 2500kg.
- (ii) one pin with nylon coated insulation.
- (iii) one High Density Poly Ethylene (HDPE) rail seat pad 12mm thick, and ribbed (R-type).

This fastening system requires a 3 man team for installation. Early efforts by the track laying contractor to develop a machine for application was abandoned as were earlier attempts in South Africa.

The Fist-BTR fastening system is quite bulky and the storage and handling presents more of a problem than some other fastening systems.

Performance in the track to date, under axle loads up to 25 tonnes, has been excellent.

2.3.2 Pandrol. Pandrol Australia tendered to produce the required fastenings in Western Australia. The set of fastenings as finally ordered consists of:-

- (i) two E2003 series clips - toe load, 1000 kg.
- (ii) two fibre glass reinforced gauge plate insulators.
- (iii) a 5mm flat HDPE rail seat pad.

These fastenings were ordered for the up dual gauge main between Avon and Forrestfield yards. This 110km section carries 8.5 MGT per annum with only 36% of the length tangent track and 19% of the length with curves below 600 metre radius (2.9°).

It was considered advantageous to use the "top of the sleeper" type fastening in this section to facilitate transposition of the rails when it is required, due to rail wear on the curves.

Pandrol clips type 401A have been used throughout all of the new turnouts.

3 RAIL WELDING AND HANDLING

The decision to use 60kg/m rail supplied in mill lengths of 27.4m required the construction of a new flashbutt welding depot.

Fortunately, a narrow gauge railway marshalling

yard that was made redundant through previous reconstruction work, was available near the former rail welding depot at Midland.

The experience of overseas railway welding depots was drawn upon to design the new depot, which for its' size is considered to be one of the most efficient in the world.

3.1 Flashbutt Welding

Installation of a new A.P.H.F. 60R welding machine and Mark VI Stripper manufactured by A.I. Welders Ltd of Inverness, Scotland was carried out by the Company in 1979. These machines have performed satisfactorily, producing up to 72 welds per 8 hour day of a high quality weld trimmed to close tolerances in particular, on the underside of rail foot to avoid the necessity to respace sleepers at flashbutt welds.

The rail is flashbutt welded into 274m (900ft) strings and moved forward by powered rollers to where it is stored awaiting dispatch.

3.2 Loading

Side loading of the 274m rail strings was adopted in preference to end loading systems popular elsewhere, as it was found that optimisation of the system enabled three men to undertake loading together with other duties. This system using a series of fixed load-out gantries has the advantage of minimising the number of specially equipped rail wagons required to transport long welded rail strings to the work face, enables rapid and efficient stock-piling of long welded rail strings at the welding depot, provides a rail transshipping facility and also represents a back-up system to the electromagnetic travelling gantry.

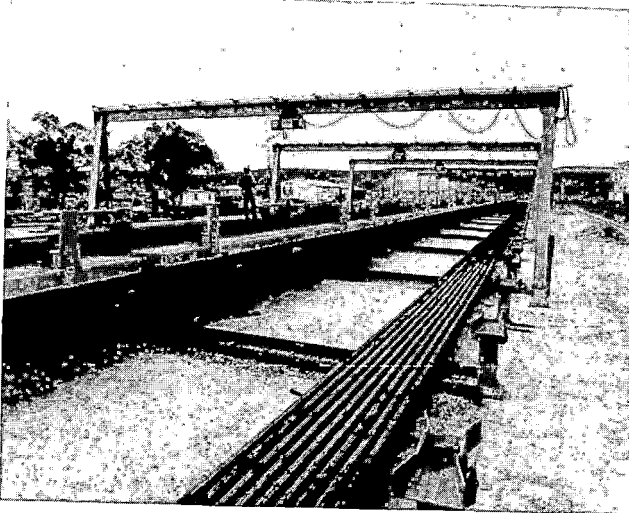


Fig.5 Load-out gantries

The loading of 30/274m rail strings on 3 layers on the rail wagons can be completed by the 3 men in 3 hours.

4 RESLEEPERING AND RERAILING

Tenders for the replacement of rail and sleepers

in the track were called throughout the world. The specification was flexible in the manner of achievement of the required result, so that contractors would have the greatest freedom in determination of method and machinery. Track occupancy was only guaranteed for one five hourly period daily. The lowest and successful tenderer was Roberts Construction (Pacific) Pty Ltd, who commenced work in May 79.

Roberts Construction had previous railway experience in South Africa and Australia and they nominated the main item of plant, the P811 track renewal machine developed by Valditerra of Italy and marketed throughout the world by Canon Pty Ltd. Roberts purchased this original machine, modifying and strengthening it for the Western Australian project.

4.1 P811 Track-renewal machine

On commencement of the work on site, it was immediately clear that the P811 track renewal machine as supplied, had major difficulties in meeting the specification for the project.

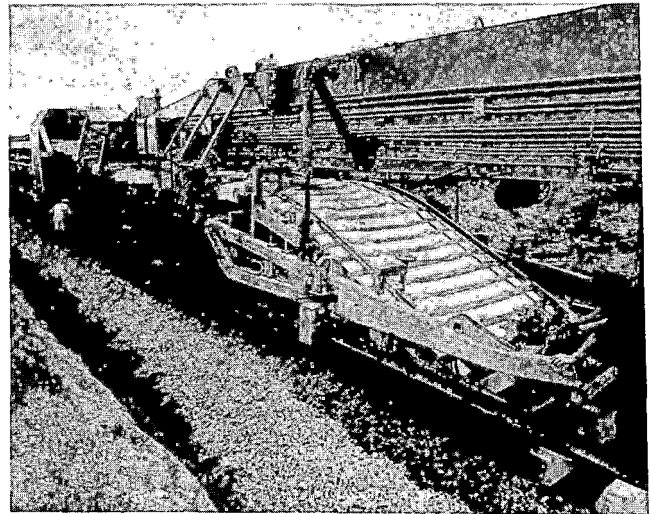


Fig.6 P811 Track Renewal Machine

Fundamental problems related to:-

- (i) the depth and quantity of ballast to be ploughed out under the machine to achieve the specification and
- (ii) the aligning of Fist type concrete sleepers to allow the new rail to be threaded in without damaging the sleeper shoulder or rail seat pads.

The P811 machine as used in Italy had been required only to level out the ballast bed prior to placing Pandrol type concrete sleepers with cast in steel shoulders. Level adjustment was achieved by use of a ballast cleaner following the resleepering and rerailing. Ballast cleaning was not required on the Western Australian Project.

Roberts Construction decided to close down operations to allow further modification to the

machine.

In order to prevent the main ballast plough becoming choked with ballast and severely hampering the timber sleeper recovery wheel, additional shoulder ballast ploughs were mounted under the leading section of the P811 machine. These ploughs are retractable and hydraulically operated. Their function is to plough ballast from the end of the sleeper. This reduces the demand on the main plough and provides a channel into which ballast can be pushed thus preventing "bogging down".

An automatic sleeper spacing and lining frame was designed and mounted behind the operator on the concrete sleeper chute. The frame individually spaces each sleeper and ensures that the outside shoulders of the Fist pad recesses on one side are all aligned. Damage still occurs on occasions, but is greatly reduced dependant upon operator proficiency.

Work recommenced in July 1979.

It was found that the P811 machine had considerable difficulty in pushing the load of concrete sleepers and ploughing ballast depth required. The tractive effort was not sufficient and wheel slippage occurred frequently.

It was apparent that the machine would not plough 50mm below the underside of the timber sleepers. It was considered that 25mm was achievable without unduly overloading the machine. This has now been adopted.

Problems with traction still occur when pushing nine loaded concrete sleeper wagons on steeper grades (0.67%).

A learning course of some weeks then followed while supervisors, operators and labourers alike became familiar with the operation of the machine and achieved the current level of efficiency.

The resleepering and rerailling of 548m and sometimes 812m within the five hour track occupancy is readily achieved using the P811.

The P811 track renewal machine performs its task exceptionally well. The machine does not operate continuously as it is required to stop, start, - stop, start for a variety of reasons. It has been found that where something commences to go wrong, it is better to stop the machine and fix it immediately. The greatest delay to the operation is caused by broken timber sleepers, which have to be removed manually. Actual time occupied in resleepering and rerailling activities would be less than one half of the total time. Progress of the machine is about 300m per hour.

Following the P811 machine, a manual gang applies the fastenings keeping a strict control of the rail temperature between 35°C and 45°C. The 274m rails are then thermit welded using the S.M.W.(F) process.

On completion of the days work, there is approximately 600m of new track without crib or shoulder ballast under a 25km/hr speed restriction, thence 1200m of track with new crib and shoulder ballast under a speed restriction of 40km/hr, thence

6000m of initial tamped, aligned and levelled track under a speed restriction of 80km/hr to allow consolidation under normal rail traffic prior to final levelling, lining and tamping after which the restriction is removed.

The P811 was preferred to the gantry type operations for the following reasons:-

- (i) Gantry operation would require the opening out of the daily section i.e. 548m to permit the preparation of the ballast bed to receive the concrete sleepers.
- (ii) A major break down would leave a large gap to be relaid by other means, which would not be completed in the time scheduled.
- (iii) Recovery of materials would be more time consuming and tend to be left if inconvenient to a later date.
- (iv) Overall completion of the track in the 5 hour track occupancy would be more doubtful, therefore the risk of delay to trains, with a penalty up to \$2 000 per hour, could be expensive.
- (v) The gantry could not work through the sections without being obstructed by bridges, culverts and the low level landings and also work through level crossings would not be as convenient.
- (vi) The P811 recovers the timber sleepers as part of the resleepering process, with the sleepers all stacked on the wagons for return to a depot for unloading.

4.1.1 Use of P811 on new construction. Upgrading works required that sections of the mainline between Forrestfield and Kwinana be duplicated. The contractor was required to construct approximately 17km of new track on new formation and opted to use the P811 machine to perform the work.

Subgrade was generally sand topped with 230mm of crushed limestone which formed an ideal base for constructing temporary track.

Rail (60kg) was distributed from the adjacent main line onto the new formation and slewed into position on temporary tie bars using a rubber tyred Pettibone crane.

Tie bars consisted of strips of mild steel plate onto which had been welded pandrol type steel shoulders for securing the rail and holding gauge. Tie bars were spiked to the formation on the correct alignment at 3 metre centres. Once the rail was placed and secured, spikes were removed.

Pandrol clips were applied on the outside only on every second tie bar on tangent track and both sides of every second tie bar on curved track.

In order to prevent possible damage to the concrete sleepers from centrebinding effects when placed directly onto the formation, a carefully controlled centre dump of ballast was made from hoppers onto the temporary track. The angle of the main ballast plough on the P811 was then adjusted to

give a slightly hollowed ballast bed to receive concrete sleepers. This procedure also reduced the number of lifts required by the tamper to achieve the final ballast depth. Approximately 60mm of ballast was placed under the sleepers during tracklaying by this method.

The remaining clips were knocked off and tie bars pulled out ahead of the main ballast plough as the P811 progressed.

Specially made timber sleepers were used to ramp down from the concrete sleepered track to the temporary track.

Once in full production track was laid at the rate of 822 metres every second day. Alternate days being spent on preparation ahead and destressing behind the rail head.

5 WORK PERFORMED BY WESTRAIL DAY LABOUR STAFF

Completely new designs have been drawn up by Westrail's engineering staff for all turnouts required in the upgraded railway. The essential features of the new turnouts are that all crossings are rail-bound cast manganese, switches are jointless, all fastenings are resilient (Pandrol) and preserved timbers 250mm x 150mm support all assemblies.

Westrail day labour staff replace all turnouts ahead of the contract rerailling and resleepering activity. These turnouts which are up to forty metres in length and twenty four tonnes in weight presented a major task where located in confined space, difficult terrain and with limited track occupancies, if they were to be installed using conventional equipment available.

Westrail investigations led to Sweden where newly developed on-track turnout exchanging equipment manufactured by Swedish Rail System in that country was witnessed under operating conditions. The system was selected as the most suitable for Westrail's needs and has made replacement of turnouts into a relatively simple operation.

The system, new to Australia, enables existing turnouts to be removed from the track in one piece, transported to a convenient location in station yards for dismantling whilst simultaneously new turnouts are transported from assembly point in station yards and placed in the vacated position in track.

A typical operation involves transport of the old and new turnouts approximately 800m in either direction, removal and installation being completed in two to three hours, the first trains proceeding through the new turnouts at 15 km/hr.

As soon afterwards as possible the turnouts are tamped, switch operating mechanisms commissioned representing a further two hours when speed of trains is increased to 25 km/hr increasing to 50 km/hr within a few days.

To test efficiency and flexibility, Westrail staff platelaid 3km of trial dual gauge track, using Pandrol concrete sleepers and timber sleepers with Pandrol plates and clips. This trial section was located in an area with limited access. Panels 54.8m long were made up and transported by the S.R.S.

trolleys over a distance of about 8km through a number of reverse curves of radius 600m (2.9°).



Fig.7 S.R.S. Turnout Exchanger

Westrail day labour staff also undertake re-railing and resleepering through major highway and public roadway level crossings in conjunction with highway and local road authorities ahead of the contract rerailling, resleepering activity being done.

Radio control is being established over the total length of the upgraded railway, not only to assist the upgrading activity but also for improved railway operating purposes later.

6 PROGRESS OF THE PROJECT

Despite a considerable delay whilst satisfactory modifications were developed and effected to the P811 by the contractor, increased production since restarting has enabled lost time to be made up.

At the time conference papers went to print in October 1981, 340 track kilometres of the railway were completed and it is anticipated that a total of 460 kilometres will have been completed by September 1982.

7 CONCLUSION

Greatly increased tonneages of rail traffic, in excess of those forecast when the railway was completed in 1967, together with deficiencies of the original 47kg/m rail, 230mm x 115mm section timber sleepers with dogspike fastenings made it necessary to upgrade the Kwinana-Koolyanobbing railway during the years 1979-1983 to preclude unacceptable restrictions to the traffic flow on this section of railway which constitutes a major portion of the main East-West trunk route.

Technical research and evaluation studies indicated that prestressed concrete sleepers with resilient fastenings and 60kg/m continuously welded rail was the most cost effective combination for

traffic which has predominantly unit bulk haul trains operating with axle loads of 24 tonnes. When completed it will constitute a heavy duty track capable of meeting transport needs through to the 21st Century with high technical reliability and operating efficiency at reasonable cost.

The virtual reconstruction of some 500km of this railway without serious dislocation of revenue earning rail traffic commenced mid 1979 and is proceeding to programme with the assistance of the latest overseas equipment not previously seen in Australia, demonstrating a practical and economic means of achievement.

8 ACKNOWLEDGEMENTS

The author thanks the Commission of Westrail, Mr W I McCullough for permission to publish this paper.

9 REFERENCES

1. J F Hoare and A F Payne. Track Structure for the Kwinana to Koolyanobbing Railway. The Institution of Engineers, Australia and the Australian Institute of Mining and Metallurgy - Heavy Haul Railways Conference, Perth, Western Australia, September 1978.

2. Avon Valley - Trial section - Concrete sleeper crack patterns Data Report No. 2 Westrail PS-81/11.

3. A B Holm, Westrail Develops New Standards for Kwinana - Koolyanobbing Upgrading, Railway Gazette International, Developing Railways 1980.

The Effects of Track and Traffic Parameters on the Development of Track Vertical Roughness

G.S. Lane

Research & Development
Division
British Rail
Derby
United Kingdom

This paper deals with the theoretical prediction of the deterioration of vertical track profile. A computer model is described which uses theoretical methods of predicting static and dynamic tie-ballast forces, together with experimentally determined ballast settlement properties, to calculate the deterioration. A wide range of track irregularities can cause track deterioration and calculations are presented which show how the roughness developed depends on track and vehicle parameters. These calculations help to show the relative importance of each type of irregularity and also of specific vehicle parameters. They can also be used to assess the effects of railroad system changes on the track maintenance requirements (and hence costs); and to help in defining the maximum permissible magnitude of track irregularities.

NOMENCLATURE

a	settlement after first cycle of unit load, m
b	constant in settlement law
c	constant in settlement law, m
C	track damping per rail, Ns/m
d	constant in settlement law
F	tie-ballast force, N
k	track stiffness per rail end, N/m
m	track mass per unit length per rail, kg/m
M	unsprung mass per wheel, kg
N	number of load applications
T	traffic, tonnes gross
v	speed, m/s
x	ballast settlement, m
α	irregularity ramp angle, radians
σ	standard deviation of vertical track profile, m

SUBSCRIPTS

o	present value
1	degree of freedom
2	degree of freedom
a	particular deterioration mechanism
i	mechanism number
m	maintenance period
r	other deterioration mechanisms
T	total

SUPERSCRIPTS

max maximum value

INTRODUCTION

In order to increase the capacity of a freight railroad changes must be made which may affect capital, operating and maintenance costs. If total costs are to be minimised a means is required of assessing, in advance, the effects of such changes. This paper is concerned with the prediction of the track maintenance part of the full cost equation. Attention is concentrated on the deterioration in the vertical geometry of the track, i.e. the development of track roughness, under the influence of repeated traffic loading. This factor is of prime importance in the assessment of track geometrical quality and is therefore directly related to track maintenance requirements and costs.

A full experimental approach to this problem is not possible. It is impractical to perform tests on more than a small number of the wide variety of possible system variations and so it is necessary to evolve a reliable theoretical approach. With a firm theoretical basis, the experimental work can be limited to verification of the theory for specific cases. Previous BR theoretical work, however, has

been restricted to the calculation of vehicle-track forces (1). This has allowed limits on vehicle parameters to be established such that individual track loads are kept to within prescribed limits, but has not allowed inclusion of cumulative damage criteria.

In the present work, the effects of vertical track settlement under repeated static and dynamic loadings are taken into account. The model under development takes the form of computer programs which allow prediction of the deterioration in vertical track geometry as a function of track, vehicle and traffic mix parameters. The predictions can be used in the evaluation of maintenance requirements and costs. The model can also be used to define, on the basis of maintenance requirement criteria, the limiting values for vehicle parameters and the maximum permissible magnitudes of geometric track faults.

It must be emphasised that the work addresses the problem of geometrical deterioration of the track resulting from the variability of the track structure and the existence of various types of track irregularities. The deterioration and service life of individual track components is not considered, although the loading predicted as function of traffic will be relevant to this problem.

DESCRIPTION OF THE BR TRACK DETERIORATION MODELS

General

Geometrical track deterioration can result from many types of irregularity or non-uniformity in track or vehicles. Deterioration due to a particular factor may depend on other vehicle and track properties in its own distinct way, so decisions based on models of individual mechanisms can be unreliable. (As an example of this, it is shown later that consideration of a dipped rail joint alone suggests that increasing axle load will reduce track deterioration). A consideration of all major modes of deterioration is, therefore, required.

Computer models are now in an advanced stage of development for various types of vertical track irregularity. These fall essentially into two categories:

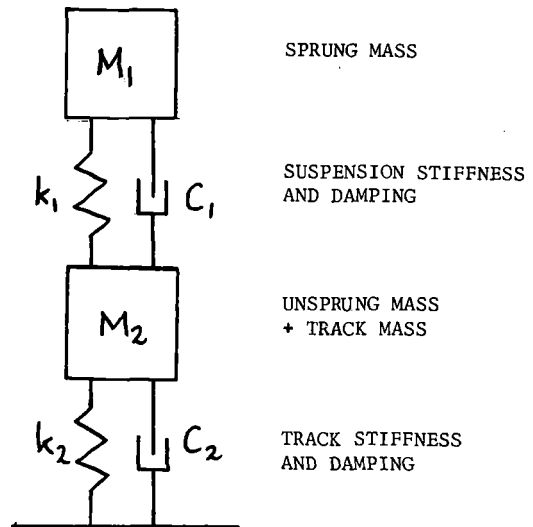
1. Models for localised, "discrete" irregularities such as those at bolted rail joints, rail welds, hard or soft spots in the formation.
2. Models for "extended" spatially distributed irregularities. In this general category we include the effects of variability in ballast and sub-grade stiffness and settlement properties; the effects of rails which are not naturally straight; the effects of variable tie spacings, etc.

When these models have been fully validated it will be possible to combine them to produce an overall description of the deterioration of vertical track geometry under traffic loading.

At the present time, lateral (alignment) deterioration has not been considered.

The Discrete Irregularity Model

Versions of this model are available for the variety of discrete irregularities mentioned above (2). The difference appears in the calculation of the dynamic increment to wheel-rail force in the vicinity of the irregularity. The first version of this model was for ramp type irregularities at bolted joints and used a simple formula for dynamic force based on a one degree of freedom system. The later versions for other irregularities use a more detailed two degree of freedom model (Fig 1).



TWO DEGREE OF FREEDOM MODEL

NOTE: For higher frequency effects the parameters are redefined to include Hertzian contact.

Fig 1 Model for calculation of dynamic forces

The programs operate in a deterministic manner. The length of track modelled is typically 20 - 30 ties with the irregularity at the centre. Starting from a fully defined track, traffic mix and sets of vehicle parameters, the histories of loaded and unloaded track profiles are built up using a step by step procedure. The starting point for the calculation is generally taken to be the track immediately after maintenance. In order to form a complete model of the maintenance - deterioration - maintenance cycle, it is necessary to describe the transfer function of the maintenance operation. This forms an important element in the model.

At any stage in the calculation each axle type is 'run across' the model and the peak tie-ballast forces are calculated, including the effects of static and dynamic wheel-rail forces and any voids which may have developed. The array of peak ballast forces is then used to calculate the settlement, x , at

each tie position using experimentally determined settlement laws. The peak forces applied to the ballast are different for the different tie positions and so differential settlement occurs. This leads directly to non-uniform track profile and hence to increased track roughness. The basic form of settlement law used at present is:-

$$x = F^b \{ a + c (\log N)^d \}$$

where a = settlement at first cycle for unit load
 F = tie ballast force
 N = number of applications of force F
 b, c, d are constants

In order that constant load data, as represented by the above equation can be used in a changing load environment, a 'strain hardening' assumption is adopted. When a settlement x_0 has been reached under a variety of loads, it is required to calculate the next increment of settlement, Δx_0 , for N cycles of the present load. This is based on the number of cycles, N_0 , which would have given the settlement x_0 if the previous loads had been constant and equal to the present load, F_0 . The value of N_0 can then be found:-

$$\log N_0 = \left\{ \frac{1}{c} \left(\frac{x_0}{F_0^b} - a \right) \right\}^{1/d}$$

and hence the value of Δx_0 :-

$$\Delta x_0 = c F_0^b \left\{ [\log (N_0 + \Delta N)]^d - [\log N_0]^d \right\}$$

Note that although a strain hardening assumption is used, it would be straightforward to include any description of the settlement under varying loads. This is an advantage of the step by step procedure over a purely analytical approach where a specific assumption must be made (3).

At any step in the calculation the individual settlements for each axle type are calculated from the above relationships and summed to give the total for the particular step. This is then used; (a) to estimate the loaded and unloaded profiles and corresponding track roughness, and (b) to re-define the state of the track for the next stage of the calculation.

The full capabilities of the program can be gauged by considering the input data (track, vehicle, traffic mix). These are given in the Appendix. Sensitivity analysis can be performed on variation of any of these input data. The output of the program includes histories of loaded and unloaded levels and the corresponding standard deviations which describe track roughness. Assuming that a maximum track roughness can be specified, the output can be used to determine track maintenance periods and therefore the maintenance cost associated with the specific irregularity concerned.

The Extended Irregularity Models

These models are again deterministic and operate in the same way as the discrete irregularity model; the essential difference is that the extended model considers a track length of many more ties, typically 100 but up to 500 or 1000 have been used for special purposes. Because of this larger number of ties different methods are used for the calculation of dynamic forces and in the estimation of peak tie force, the objective of the changes being to reduce computing time to an acceptable level. Inputs and outputs are equivalent to the discrete model.

The main types of irregularities for which the extended model is used concern the inherent variability of track properties over a long length of track. This leads to non-uniform tie ballast forces which, when applied to non-uniform settlement properties, lead to increased differential track settlements and therefore to increased track roughness. The dynamic wheel-rail forces will also increase and lead to a further contribution to track roughness.

Combination of Models for Different Mechanisms

A full description of the deterioration in geometry of any length of track requires modelling of many mechanisms. There is no reason in principle why the extended model should not be generalised to include discrete effects. However most interactions, e.g. between the effects of dipped welds and the variability of ballast stiffness, are unlikely to be important and the combined approach carries a severe penalty in terms of computing time. The BR approach to date has been to assume independence between the various mechanisms and to use separate programs to study each. In this way the dependence of different deterioration mechanisms on track and vehicle parameters can be seen clearly. If the mechanisms are assumed to be independent the track roughness resulting from a combination can be simply estimated. The roughness for mechanism i is calculated by the program as the variation in standard deviation of level with traffic (time), $\sigma_i(t)$. The total track roughness $\sigma_T(t)$, for n mechanisms is then given by:-

$$\sigma_T(t) = \sqrt{\sum_{i=1}^n \sigma_i(t)^2}$$

THE PARAMETRIC DEPENDENCE OF TRACK DETERIORATION FOR DISCRETE IRREGULARITIES

General

In this section, various types of discrete irregularity are considered and it is shown that the resulting deterioration can depend on vehicle and track parameters in distinct ways. The relevance of this to the problem of increasing freight railroad capacity is that it helps to quantify the trade-off between installation standard and maintenance cost and indicates where attention should be concentrated in track maintenance procedures.

Deterioration Due to the Effects of Ramp and Joints or Welds

Ramp-type irregularities lead to dynamic wheel-rail forces which can be calculated from a one degree of freedom model (4).

$$\text{dynamic force} = \alpha v \sqrt{kM} \text{ per wheel}$$

where α = total ramp angle
 v = vehicle speed
 k = track stiffness per rail
 M = Unsprung mass per wheel

The discrete irregularity program uses a more general form of equation which includes correction terms for track damping and track mass:

$$\text{dynamic force} = \alpha v \sqrt{\frac{M}{m+M}} \left\{ 1 - \frac{C}{4\sqrt{k(m+M)}} \right\} \sqrt{kM}$$

where m = track mass per unit length per rail
 C = track damping per rail

Ramp irregularities can have several distinct origins. The rails supplied to BR have usually been roller straightened, a process which cannot be fully effective at the rail ends. If rails with partly straightened ends are bolted or welded together with

the bulk of the rails rectilinear an irregularity occurs in the vicinity of the join. If the ends are dipped downwards an irregularity shown in fig 2 as type A results. Surprisingly, for rail ends turned upwards an irregularity similar to type A can occur when the rails are welded together with continuity of slope at the weld. This is because the self weight of the track flattens the rail on the ballast except in the vicinity of the weld where an effective dip occurs. A second type of irregularity, type B in fig 2, occurs if straight rails are welded at an angle. Again, the rail will flatten under the self weight leaving a visible dip at the weld, but in this case the effective span of the irregularity is much larger. A range of irregularities intermediate in character between types A and B is of course possible,

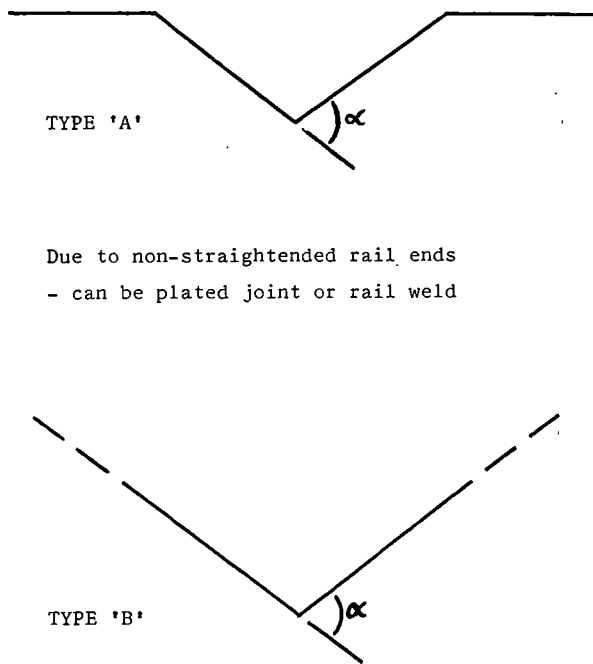


Fig 2 Ramp irregularity types

Although in track the different types are difficult to distinguish, they respond in different ways to the axle loads and unsprung masses of the traffic. This is particularly relevant to the case of freight traffic and the costs associated with using heavier cars. In order to demonstrate the differences which can occur for different types of irregularity, calculations of the deterioration in vertical level have been performed for types A and B, for the carriage of 4M tonnes of freight goods. BR freight cars of various axle loads, unsprung masses and speeds have been assumed. For the study of the effect of axle load the vehicle parameters for a BR 100 tonne car were used and the car was assumed to be loaded to give

specific axle loads. In all cases the traffic has been restricted to 4M tonnes in order to minimise computing time. Conclusions can be based on this relatively low tonnage since deterioration tends to increase logarithmically and by 4M tonnes the trend has been set.

Variation with Severity of Irregularity, and with Traffic Speed. In all cases the roughness developed after a certain tonnage is approximately linear with the severity of irregularity defined by ramp-angle, α , figure 3. The deterioration under freight traffic is less severe for type A irregularities than for type B although in each case the dynamic increment to wheel-rail force is initially the same. Turning to the effects of speed, see fig 4, there is a strong dependence for type A but very little for type B.

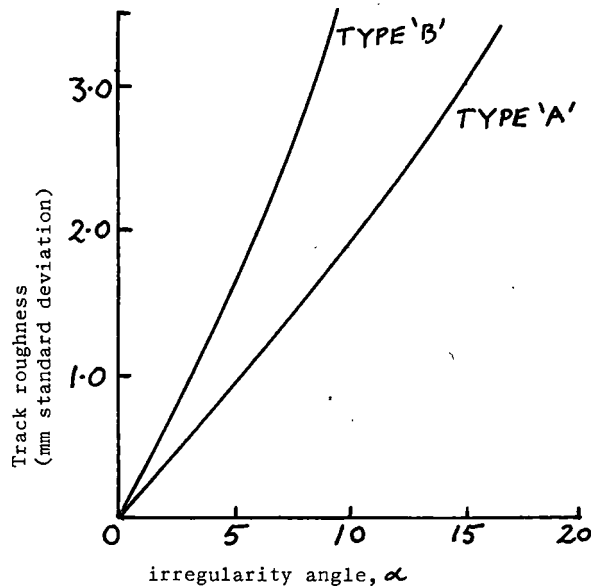


Fig 3 Ramp irregularities - dependence on α .

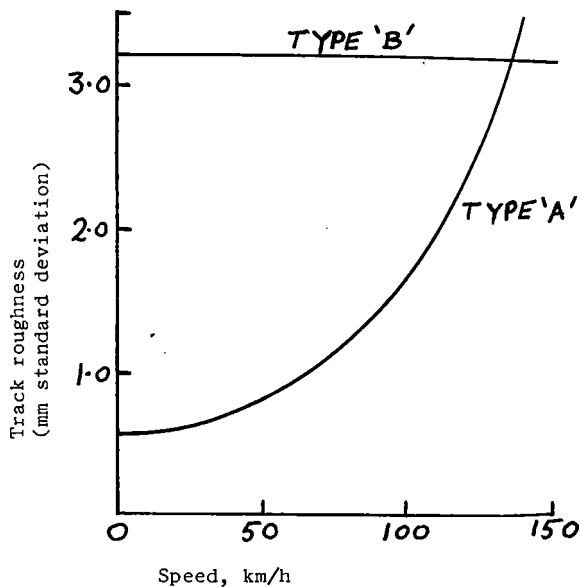


Fig 4 Ramp irregularities - dependence on speed

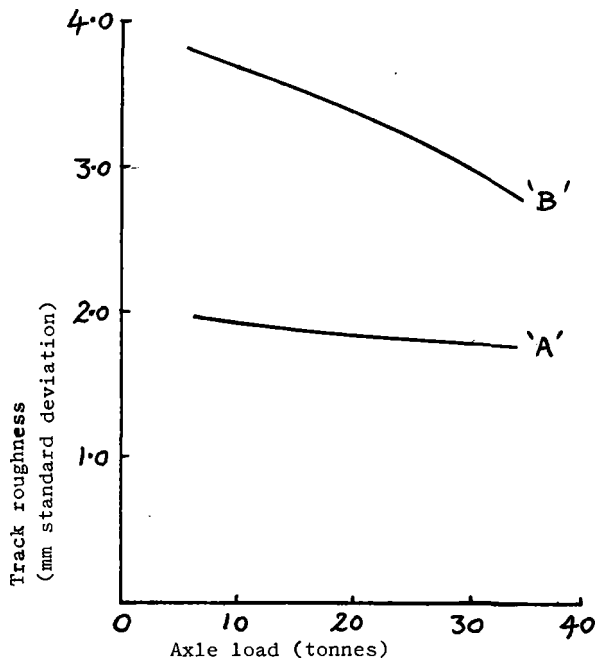
The explanation of these effects arises from the fact that there are two mechanisms contributing to the deterioration in level:

1. Differential settlement resulting from the dynamic increment to wheel-rail force in the vicinity of the irregularity. This effect is directly proportional to speed and to the square root of the unsprung mass for a given ramp angle. For high speed (200 km/hour) passenger traffic on BR it predominates.

2. The tendency for the natural shape of the irregularity to become imprinted on the ballast under the action of traffic. This effect is largely independent of dynamic forces and is therefore independent of speed and unsprung mass of the vehicle. It would therefore tend to predominate at low speeds.

The final deterioration is thus a combination of contributions from these two effects. Both effects are proportional to ramp angle and so the linear dependence on this parameter would be expected. However, the irregularity types A and B are fundamentally different as regards the imprint mechanism. For type A the imprint mechanism predominates up to about 50 km/hour and above this the dynamic force effects become important. For type B the imprint mechanism is more severe and predominates at all speeds. The deterioration is, therefore, largely independent of speed.

Variation with Axle Load.



Ramp angle - 10 m radians

Traffic - 4 M tonnes gross

Fig 5 Ramp irregularities - dependence on axle load

The variation of track roughness with axle load for both types of irregularity, Fig 5, is at first sight anomalous - the calculations predict that for the higher speeds increasing axle load reduces track roughness from the initial value. This surprising result is, in fact, a necessary consequence of studying in isolation one individual deterioration mechanism. At the higher speeds the deterioration is controlled by the effects of dynamic forces; to be more precise by the differential settlement caused by the dynamic forces in the vicinity of the irregularity. The magnitude of this differential settlement depends on the ratio:-

$$\frac{\text{Static force + dynamic increment}}{\text{Static force}}$$

Now the dynamic increment is a function of speed and unsprung mass, not of static wheel load, and so the ratio decreases for increasing axleload which explains the apparently anomalous dependence for higher speeds.

Variation with Unsprung Mass. It is generally not possible to vary this factor independently of the other vehicle parameters but its importance in determining the magnitude of dynamic forces has been recognised for a long time. As regards deterioration of track profile, its significance depends on the mechanism concerned. To show this for types A and B ramp irregularities, it has been assumed that the unsprung mass of BR 100 tonne freight vehicles can in fact be changed. Fig 6 shows the predicted dependence of track roughness on unsprung mass. For type A irregularities, where the dynamic force mechanism is significant, the roughness increases with unsprung mass. The dependence is not strong, since at lower speeds the imprint mechanism contributes and at higher speeds the dynamic forces are proportional to the square root of unsprung mass. For type B irregularities the imprint mechanism predominates and the roughness is largely independent of unsprung mass.

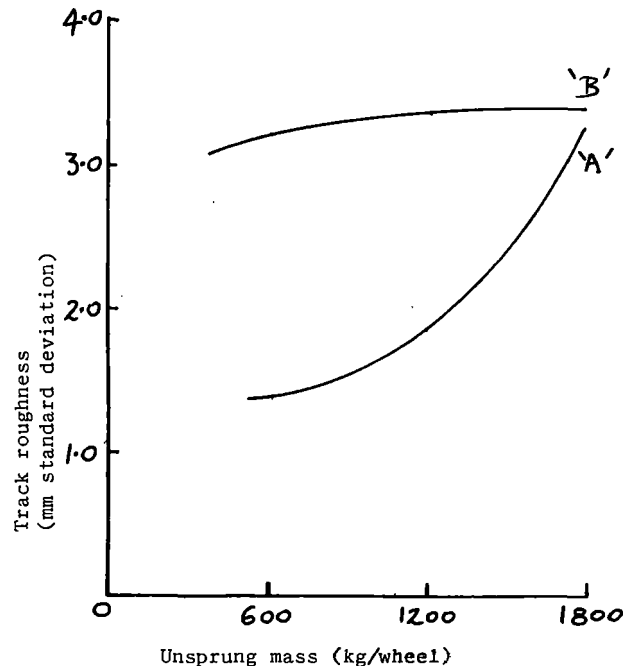


Fig 6 Ramp irregularities - dependence on unsprung mass

The calculations show, therefore, that from the point of view of geometrical deterioration and for relatively low speed freight vehicles, unsprung mass has only a small effect on deterioration at ramp irregularities. A similar conclusion has been reached by Frederick (3) for the case of ramp irregularities. It must be emphasised that this conclusion may not be true for higher speeds and for effects such as rail or wheel damage which depend strongly on dynamic forces and hence on unsprung mass.

Implications for the Freight Railroad. As far as the freight railroad is concerned the message is clear, the type B irregularity - welding of rails at an angle - must be avoided. Type A irregularities - due to non-straightened rail ends - are of less importance to a relatively low speed freight railroad but if there is any chance of high speed passenger traffic using the line, these irregularities must also be considered. If it is thought that Depot or site welding practice may lead to rails welded at an angle, improvements here or weld straightening will lead to a reduction in subsequent track maintenance cost.

Use of Discrete Irregularity Calculations to Define Permissible Limits to the Size of Track Faults

On BR, it is hoped to use calculations of the type described above to provide a basis on which the limiting magnitude of specific types of track fault can be judged. This approach is at an early stage and involves some assumptions but is providing a framework on which the cost of various options can be assessed. The approach and assumptions can be described as follows:-

- a. Consider type of track, traffic etc, and decide on maximum acceptable track roughness. Such values of roughness expressed in terms of standard deviation of level for different traffic and speeds, have been defined for BR.
- b. Estimate the proportion of roughness contributed by the irregularity type in question. For example if mechanism 'a' is estimated to produce 50% of roughness then $\sigma_a = \sigma_r$ where σ_a = roughness contributed by mechanism 'a'.

σ_r = roughness contributed by all other mechanisms.

Now the total roughness is given by:-

$$\sigma_T = \sqrt{\sigma_a^2 + \sigma_r^2}$$

For passenger traffic, the maximum value of σ_T may be about 2 mm and so the maximum value of σ_a is 1.4 mm.

- c. Decide on an acceptable maintenance period, represented by traffic, T_m .
- d. Use the track deterioration program to predict the variation of roughness with severity of irregularity, α , for traffic T_m .
- e. The value of α corresponding to the roughness contribution σ_a then represents the maximum permissible severity of the irreg-

ularity (See Fig 7).

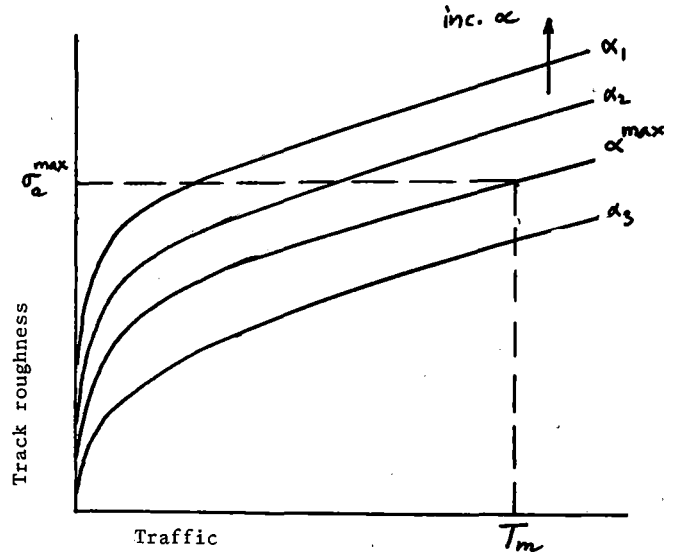


Fig 7 The relationship between the maintenance period and the maximum values of track roughness and ramp angle.

The above procedure has several areas of uncertainty in particular the choice of limiting values of standard deviation and the proportion contributed by each mechanism. Values for the former are being evolved on BR from experience; and for major mechanisms of deterioration the latter does not have a large effect on the final result. Of great significance, however, is the choice of track standard for the traffic concerned and it is here that the commercial judgement enters - the balance between installation cost, track standard and maintenance cost.

THE PARAMETRIC DEPENDENCE OF TRACK DETERIORATION FOR EXTENDED IRREGULARITIES

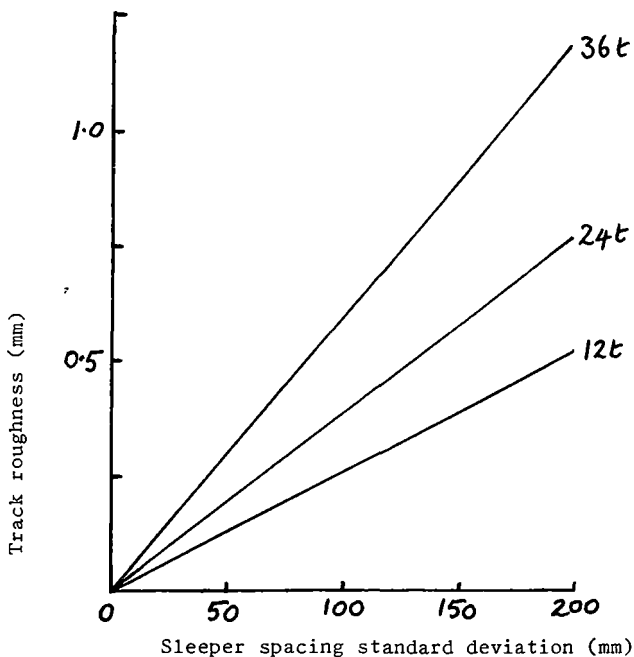
General

In this section extended irregularities are considered. The computer programs which deal with these are not in such an advanced stage of development as those for discrete irregularities. For instance, the calculation of dynamic effects has been included in the program, but at the present stage this facility has not yet been fully tested. In the calculations described below, therefore, effects due to dynamic forces have been omitted. However, it is shown that 'static' effects caused by the variability in ballast and sub-grade properties and in track parameters make a significant contribution to the development of track roughness. For this work a version of the extended program was written which allows any or all track parameters and ballast properties to be chosen at random from a Gaussian distribution, the means and standard deviations of which are taken from typical track measurements. Many possible effects could be considered but attention will be concentrated on the variability in tie spacing and ballast support stiffness, and the way in which these interact with axle-

load. In addition the effect of the natural shape of the rail will be demonstrated.

The Effect of Variability in Tie Spacing at Different Axle Loads

In the absence of dynamic effects differences in tie spacing will have no effect on deterioration rate provided it is constant. A scatter in tie spacing will lead to a variation in the force applied to the ballast even when all other factors are constant. This effect would be expected to increase for heavier axleloads. Fig 8 shows the predicted effect as a function of tonnage for a mean tie spacing of 700 mm with standard deviations up to 200 mm and for axle loads up to 36 tonnes. For normal scatter in tie spacing the effects are small but for heavier axles it is worth taking care, when installing track, to ensure accuracy of tie placing.



NOTE: - track roughness is given in terms of standard deviation of loaded vertical profile

Traffic 3 M tonnes gross

Fig 8 Extended irregularities - the effect of variability in tie spacing on track roughness

The Effect of Variability in Ballast Stiffness at different Axle Loads

Ballast stiffness, in this context, is taken to mean the ratio of the tie-ballast force at an individual tie to the deflection of that tie. As far as the ballast is concerned this is a more fundamental quantity than the track modulus defined as the ratio of wheel load to rail deflection since the latter includes the effect of the rail and this tends to

mask the variability in the ballast itself. Measurements on BR show a wide variety of ballast stiffness values but on a typical freight track measurements indicate that stiffness follows a normal distribution and the standard deviation can be 20 MN/m for a stiffness of 50 MN/m.

Using the above mean and various standard deviations calculations have been made of the track deterioration for 3 million tonnes of freight traffic carried by 12, 24 and 36 tonne axles, see Fig 9

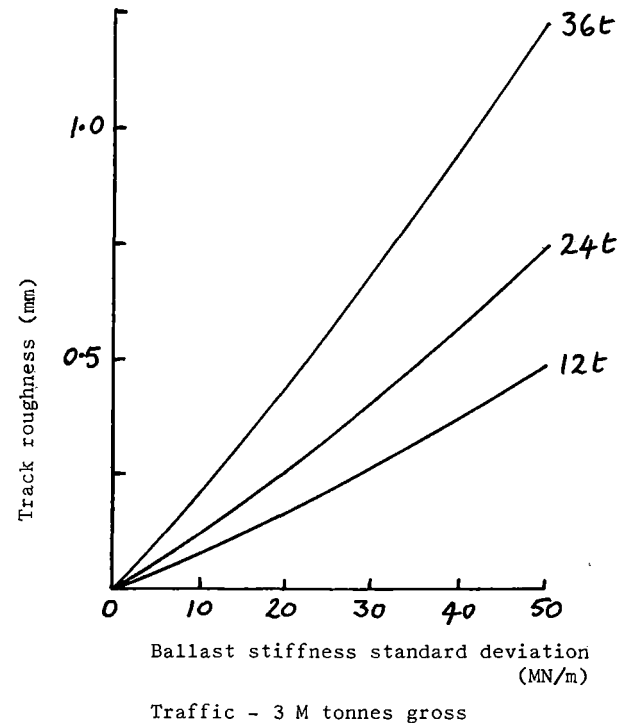


Fig 9 Extended irregularities - the effect of variability of ballast stiffness on track roughness

It is clear that if larger freight cars are to be used to reduce unit costs, considerable benefit will be realised if the ballast specification can be tightened so that the variability is reduced. A similar conclusion may well apply to the sub-grade, but at the present stage of development of the track deterioration programs this cannot be modelled explicitly.

The Effect of Natural Rail Shape

The concept of natural rail shape is relatively new. It can be defined as the longitudinal shape the rail would assume in a gravity free environment. When rails are produced the cooling process leaves them far from straight. A roller straightening process is required to give rails of acceptable standard. However there are two problems which arise:-

- a. It is very difficult to gauge the effectiveness of the straightening process, particularly at longer wavelengths (5 m and upwards).
- b. By the nature of the process the rails cannot be fully straightened in the vicinity of the rail ends.

Although the track maintenance process will mask the natural rail shape, it is believed that under the influence of traffic it will become imprinted into the ballast and contribute to track roughness. The extended track deterioration programs can accept natural rail shape data and be used to predict the effect of this for any combination of other parameters. Techniques for the measurements of natural rail shape have been developed on BR (5).

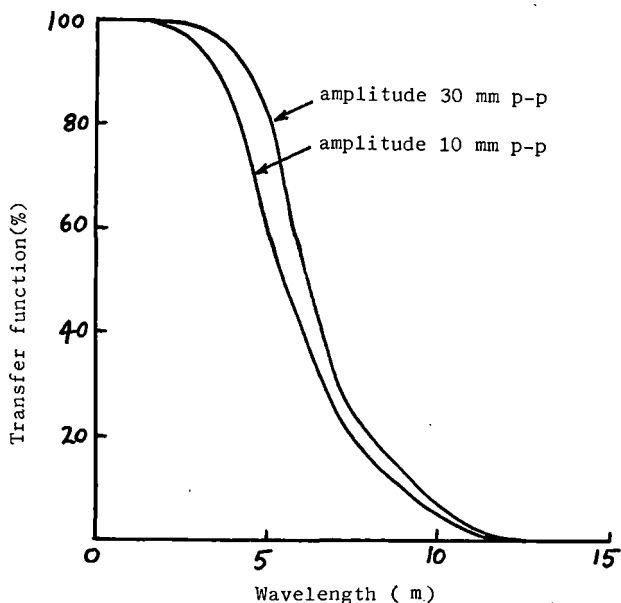


Fig 10 The effect of sinusoidal rail shape on track roughness

The importance of natural rail shape would be expected to be strongly dependent on the wavelength. In order to examine this theoretically calculations have been made for hypothetical sinusoidal rail shapes with wavelengths up to 15 metres. In Fig 10 the predicted roughness developed is shown as a function of wavelength in terms of a transfer function. This is defined as the ratio of the amplitude of the (sinusoidal) loaded top to the amplitude of the natural rail shape. Wavelengths up to 10 m are clearly important.

DISCUSSION

It has been stated that the prediction of track deterioration and maintenance requirements is desirable for existing, uprated or new railroads and that a purely experimental approach to the problem is not possible. The work described in the paper is providing the necessary theoretical background to the problem. The techniques which are being evolved are an advance on previous methods of calculation which give forces only; cumulative damage phenomena, in partic-

ular the deterioration of vertical track profile, can be predicted. Many mechanisms leading to this form of track deterioration have been identified and it has been shown that dependence on track and vehicle parameters can vary widely.

In the context of the freight railroad it has been shown that mechanisms depending on the imprint of the irregularity, or rail, shape on the ballast bed must be reduced to a minimum if heavy cars are to be used. Mechanisms depending on the dynamic force effects which occur at discrete irregularities are of less importance. However, dynamic force effects must be considered in the broader context.

The calculations made using the extended program which are presented above, exclude the effects of dynamic forces. The discrete irregularity calculations suggest that this may be acceptable for short wavelength effects (motion of the unsprung mass on the track spring). However, in the case of the extended program, where long wavelength irregularities may develop, lower frequency sprung mass effects will occur (motion of the sprung mass on the suspension spring). Although consideration of this problem is at an early stage, first indications are that these effects can be significant especially for heavily loaded freight cars. Significant dynamic increments to wheel load can occur which will lead to increases in track roughness.

Summarising, the prediction of track deterioration is a complex topic which should form an essential part of the overall decision making process when considering ways of increasing freight railroad capacity. The implications for track maintenance requirements of any proposed method of operating a railroad system can be considered by using track deterioration program predictions to:-

- a. Decide which mechanisms are important.
- b. Set limits to the maximum permissible magnitude of irregularities.
- c. Exhibit the implications and show the value of improving installation or renewal track standards.
- d. Predict maintenance requirements and hence costs.

The program can be used to test the value of any changes in track parameters or standard, in vehicle parameters and in operating procedures.

CONCLUSIONS

1. The problem of predicting track maintenance requirements is complex. It must be tackled in order to minimise the costs of running given railroad, whether capacity is to be increased or not.
2. A full experimental approach to the problem is not possible. A reliable theoretical description is thus required for interpretation of experiments and extrapolation to other conditions.
3. Previous theories have provided calculations of forces due to specific track irregularities. In the present work these have been extended to include the effects of repeated loading. Theoretical models of the deterioration of vertical track geometry for

various mechanisms have been developed.

4. This type of track deterioration can occur as a result of many mechanisms. For different mechanisms the deterioration rate depends on track, vehicle and traffic mix parameters in different distinct ways. The importance of each mechanism thus depends on the characteristics of the railroad system.

5. Increased freight railroad capacity generally is taken to mean larger, heavier cars. If this is the case attention must be paid to installation maintenance and renewal track standards. Stringent specifications and uniformity of standards along the length of the track are essential.

6. For increased speeds track uniformity is also required but in this case individual irregularities must be controlled. Where possible reductions in vehicle unsprung mass would be beneficial.

7. The theoretical models developed offer the possibility of including calculation of the deterioration in vertical track geometry, and hence estimation of maintenance cost, in the decision making process when considering changes to a railroad system with a view to minimising costs and/or increasing capacity.

ACKNOWLEDGEMENTS

The author wishes to thank Mr C O Frederick, Mr J C Lucas and Dr M J Shenton for their detailed comments on the manuscript. He would also like to thank British Railways Board for permission to publish this paper.

REFERENCES

1. Frederick, C.O. "The Effect of Wheel and Rail Irregularities on the Track", Proceedings of the Conference on Heavy Haul Railways, Institute of Engrs of Australia, Perth, September 1978.
2. Lane G.S. "Track Deterioration at Discrete Vertical Irregularities - description of a Computer Model", Technical Note TN TS 33, British Rail Research and Development Division, November 1978
3. Frederick, C.O. "The Effect of Rail Straightness on Track Maintenance", presented at the Symposium on Advanced Techniques in Permanent Way Design and Maintenance, Madrid 1981, to be published.
4. Nield B.J., Goodwin W.H., "Dynamic Loading at a Rail Joint", Railway Gazette, 15 August 1969, p616.
5. Round D.J. "The Influence of Rail Shape on Track Deterioration", British Rail and American Association of Railroads joint Seminar on Rail Technology, Nottingham, UK, 1981, to be published.

APPENDIX TRACK DETERIORATION PROGRAM INPUT DATA

1. Track parameters

Rail section (weight and 'EI')
Sleeper weight
Sleeper spacings*
Sleeper voids (if any)*
Formation support stiffnesses*
Formation settlement coefficients*
Track damping ratio

2. Vehicle parameters

Number of axles/vehicle
Axle loads
Unsprung masses
Suspension stiffnesses
Sprung masses
Wheel radii
Suspension damping

3. Traffic mix parameters

Number of axle types
Proportion of each axle in total traffic
Vehicle speeds
Total traffic to be considered

* These factors can vary along length of the Track model

- belt conveyance
- rail-bound conveyance

non-rail-bound conveyance is not at all employed in the opencast mines of the Rhenish Lignite Area. When opencast mining was started on an industrial scale, rail-bound conveyance was the transport system primarily used, and since the mid 50s preference has gradually been given to belt conveyance.

COMPARISON BETWEEN RAIL-BOUND AND BELT CONVEYANCE

The quantities of up to 200 000 m³/d to be handled in opencast mines can be transported with either of the two means of conveyance. Compared with belt conveyance, rail-bound conveyance can more easily be adapted to varying quantities by changing the train length or frequency; on the other hand, belt conveyance proves advantageous because the belt is easy to install and more suitable for steep gradients.

Though the adaptation to different materials to be transported is easier with rail-bound conveyance, it is still possible with belt conveyors, too, by means of appropriate distribution points.

Compared with rail transport, malfunctions occur less frequently belt conveyor systems; nevertheless they are on the whole more susceptible to failures because a malfunction interrupts the whole transport system while in most cases of malfunctions in a rail transport system still part of the masses can be transported.

The costs of installing the belts amount to many times those of rail installation whereas rail-bound transport is more expensive as far as the labour costs are concerned.

The above advantages and disadvantages resulted in the decision to general use belt conveyors in the immediate opencast mining field and, on the other hand, to give preference to rail-bound conveyance in the wider opencast mining area, i.e. for transports to lignite consumers and outer dumps.

CONCEPTION AS TO HEAVY-LOAD RAILROAD TRANSPORT

General

After the second world war, the Rhenish Lignite Area was faced with a special task. A major part of the opencast mines operated under favourable conditions in the south of the Rhenish Area approached exhaustion.

For two reasons, the necessary development of further opencast mines called for a more efficient transport system:

- The extraction from greater depths entailed larger overburden quantities. These could be handled economically only by using newly developed mining equipment with an increased capacity of 100 000 m³/d - bucket-wheel excavators.

For handling the increased mass flow, new lignite and overburden freight cars as well as locomotives had to be developed for railroad transport; this necessarily resulted in higher axle loads, in turn requiring a heavier superstructure.

- The new opencast mines in the northern part of the Rhenish Lignite Area were more than 30 km away from the preparation plants in the south. The lignite had to be transported via new track systems from the mining fields to the consumer.

Rolling stock

The freight cars developed in the 50s were laid

out for being loaded from mining equipment with a capacity of 100 000 m³/d. This corresponds to a mass flow of 1.4 m³/s and 2.7 t/s respectively.

The loading capacity of a freight car had to be adjusted to this mass flow; in addition, the empty weight and the net load were to be in a favourable ratio to each other. Since these trains run on mine-owned tracks only and are not used on public railroads, there was no reason to stick to the clearance measurements for the public railroad system when planning high-capacity freight cars.

One restrictive condition, however, was the use of a standard-gauge track in order to allow a transfer of the trains running on public railroads. The basic conception of the freight cars at the time developed has remained the same until today.

THE HIGH-CAPACITY OVERBURDEN FREIGHT CAR (FIGURE 2)

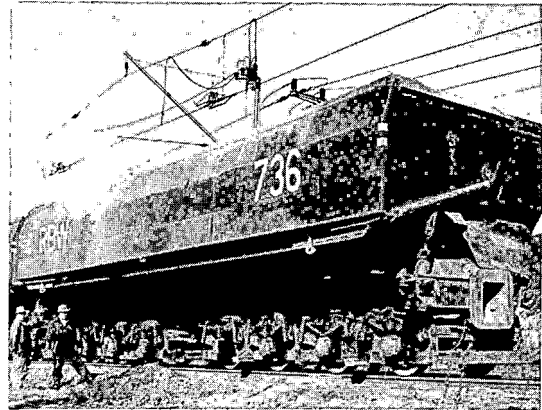


Figure 2 shows a high-capacity overburden freight car has a loading capacity of 96 m³ and is laid out as a side-dumping freight car. The empty weight is 62 t. With an average overburden weight of 1.8 t/m³ the freight car has a gross weight of 240 t. The load of the car box is transmitted to the wheels via one bridge girder and four two-axle bogies with a wheel base of 1 500 m. The wheels which are relatively small for reaching a favourable dumping angle have a running tread diameter of 850 mm.

THE HIGH-CAPACITY LIGNITE FREIGHT CAR (FIGURE 3)

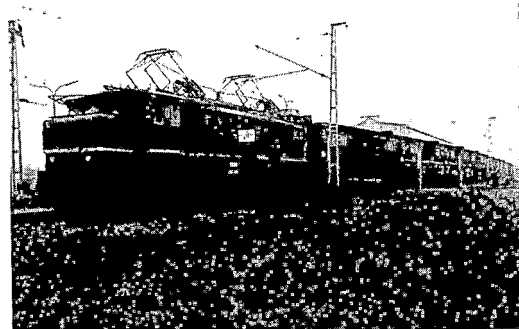


Figure 3 shows a high-capacity lignite freight car has a loading capacity of 114 m³ and is laid out as a saddle-bottomed car. Since the bulk weight of the run-of-mine lignite is lower than that of the over-

burden, the freight car is much lighter and therefore equipped with two two-axle bogies only. With an empty weight of 29 metric tons, the gross weight is approx. 125 metric tons and the axle loads amount to approx. 30 metric tons.

THE ELECTRIC LOCOMOTIVES (FIGURE 4)



Figure 4 shows a 6 kV electric locomotive

The trains available in the Rhenish Lignite Area until the end of the second world war were operated with direct-current locomotives. Their overhead line voltage was 1,2 kV. This mains system did not suffice for handling the quantities to be conveyed due to the new opencast mining technology. The new electric locomotives were to draw train tonnages of 2 000 t over 10 to 14 % gradients. The train speed was to vary between minimum loading movements and maximum speeds of 60 km/h. Besides, the locomotive was subjected to wireless remote-control during the loading operation.

To meet these requirements, a new mains system with singlephase alternating current with a frequency of 50 Hz and an overhead line voltage of 6 kV was introduced.

The traction motors of the electric locomotives are direct-current motors as used in former times, which have proved successful due to both their favourable behaviour when moving slowly during the loading operation and their robust construction.

The alternating current taken from the overhead line had thus to be converted into direct current on the locomotive, by applying various systems in the course of time.

The first locomotive type was the motor-generator set consisting of a singlephase synchronous motor, a direct-current generator, and an exciting generator for the synchronous motor.

Then, mercury vapour current converter locomotives followed. The latest development is the phase-angle-controlled thyristor converter locomotive.

Power feeding is optional, either via main power trolleys in the field of fixed tracks, or via side power trolleys in the field of shiftable tracks.

CLEARANCE (FIGURE 5)

Owing to the dimensions of the high-capacity vehicles running on mine and mine-connecting railroads, a larger clearance was selected for these lines. Here, the distance between the tracks is

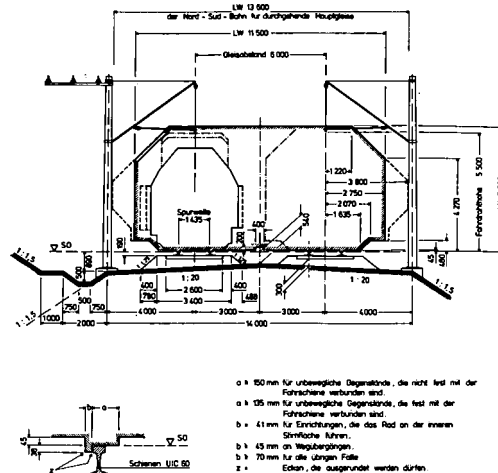
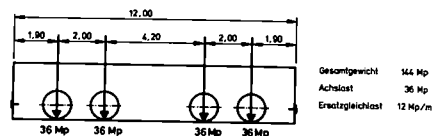


Figure 5 shows clearance

6.00 m on the clear track compared with 4.00 m with standard-gauge public tracks. The distance of 6.00 m is enough for a train on the neighbouring track to pass an overburden car inclined towards the roadbed axle.

LOADING DIAGRAM (FIGURE 6)

Lastenzug des normalspurigen Kohlewagens



Lastenzug des normalspurigen Abraumwagens

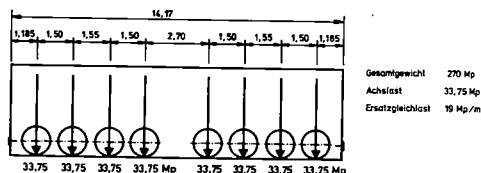


Figure 6 shows a loading diagram

According to the axle loads and the distances resulting from the high-capacity freight train, a new loading diagram was established which is the basis for determining the dimensions and load-carrying capacities of all bridges. The loads contained in this diagram are far higher than with the heaviest load train "S" of the Deutsche Bundesbahn (public railroad system of the Federal Republic of Germany).

Superstructure

The heavy rail loads and axle loads required the superstructure to be strengthened. It became obvious that the S 49 rail so far usual to standard-gauge railroads did not meet the requirements of the heavy-load transport in the Rhenish Lignite Area. For this reason, a new S 64 rail was developed with a weight of 64 kp per meter. The high resistance and

inertia moments of this rail stiffen the overall superstructure and distribute the axle loads via several ties on ballast and superstructure. In addition, the longer cross-section of the rail head with increasing wear permits a longer service. Recently, the S 64 rail has been replaced by the UIC 60 rail, the largest rail profile of the European railroads.

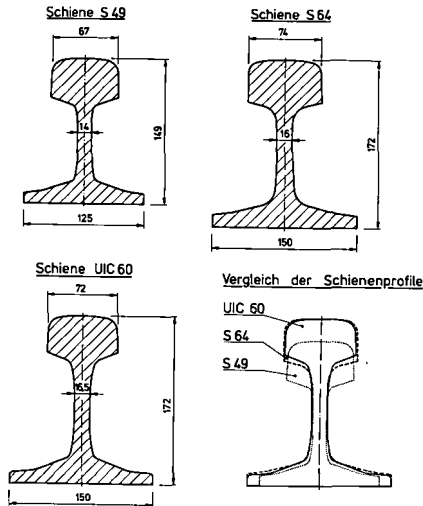


Figure 7 shows the various rail profiles

The strength of the rail steels lies between 900 N/mm^2 and $1\,200 \text{ N/mm}^2$, with the higher strengths used in the curves subjected to particularly high requirements.

In the Rhenish Lignite Area, the following kinds of tie are laid:

- wood ties
- prestressed concrete ties
- steel ties.

While the Deutsche Bundesbahn increasingly lays prestressed concrete ties, the railroad system in the Rhenish Lignite Area continues to be equipped above all with wood ties.

A major reason for this is that derailments caused by malfunctions as to the rolling stock (axle breaking, hot axle) must constantly be reckoned with in the lignite railroad system. In this context, the prestressed concrete tie proved to react more sensitively to derailments than the wood tie. Subsequent to derailments, repairs to the superstructure are more expensive both in terms of money and time with prestressed concrete ties than with wood ties. The hollow steel tie is used for shiftable tracks.

Rail fastening

There are three modes of fastening the rail to the wood tie:

- K-support fastening
- clamp-clip fastening (Spannbügel-Befestigung) Deenik system)
- SKI 3 clamp-clip fastening

These fastening methods have proved successful for the forces exerted when passing over the rails.

Switches

The standard switch type used in the Rhenish Lignite Area is the EW 300 - 1 : 9 single turnout. The originally guideless transition in the crossing-frog section caused problems to lignite heavy-load transport.

On the one hand, when passing over the guideless section, the wheels of the overburden and lignite cars due to their low diameter lead to a high wear of the crossing frogs and wing rails because the tires are differently worn. On the other hand, however, the impact arising from passing through the crossing section causes material to fall constantly off the freight cars and dirty considerably the ballast.

To eliminate these disadvantages switches with mobile crossings are nowadays installed similar to those used for express train lines of the Deutsche Bundesbahn (Figure 8).

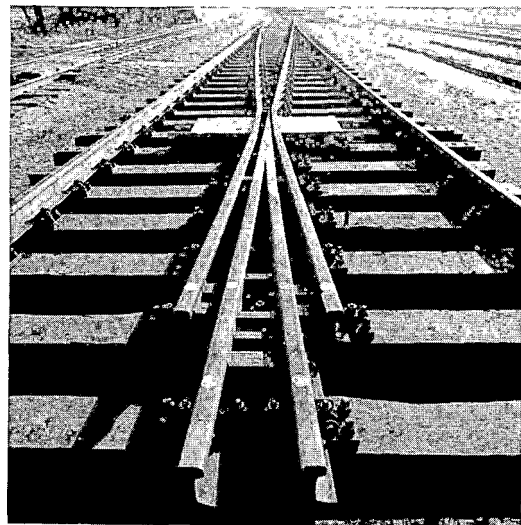


Figure 8 shows a mobile crossing of a switch

THE RAILROAD SYSTEM IN THE RHENISH LIGNITE AREA

North-South Railroad

Centerpiece of the present railroad system (Figure 9)

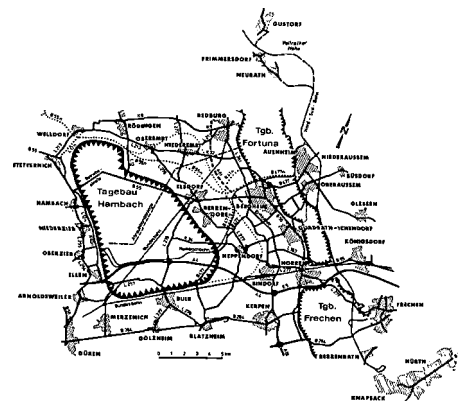


Figure 9 shows a map of the North-South Railroad and of the Hambach Railroad

is the so-called North-South Railroad having a length of 31 km. It was built in the 50s to connect the new lignite fields in the north to the consumers in the south. This railroad has track connections to all the mines and lignite consumers in its area. It is the heavy-load rail collector in the Rhenish Lignite Area and permits a balance between changing qualities mined and quantities received.

It was clear from the very beginning of the planning that the quantities to be transported have a volume justifying a generous location with gentle gradients and large radii. The maximum gradient aimed at was not steeper than the braking gradient at which the speed is to slow down when the fixed speed limit is exceeded. If possible, braking was to be avoided to keep the wear as low as possible.

A comparison between the annual costs of gradients between 6 and 8 ‰ led to a most favourable maximum gradient of 6 ‰.

When selecting the radii, it was likewise of prime importance to keep the wear as low as possible. With 3 exceptions, a minimum radius of 1 000 m was fixed for the clear track of the North-South Railroad. As far as there are track curves having radii below 1 500 m in the maximum gradient, the resistance to curvature was taken into account, and the gradient lowered to achieve a constant resistance to tension. With the determination of the maximum gradient and the minimum radius, the location elements were given.

Since the North-South Railroad was to be connected to the various mines, power stations, and briquetting plants, and any blocking of the run-of-mine lignite had to be avoided, its middle section had to be laid on the east side of the mines. In the south, this railroad line passes through a worked-out area. In the north, it makes a wide curve and bypasses the ridge situated east of Neurath.

In its course, the North-South Railroad crosses three lines of the Deutsche Bundesbahn (Horrem - Rommerskirchen, Cologne - Aachen, Mödrath - Benzlath), two mine railroad lines, the Cologne - Aachen superhighway, two highways, six main roads, and several other routes. The gradient is a function above all of the position of these railroads and roads. It is shown in Figure 10.

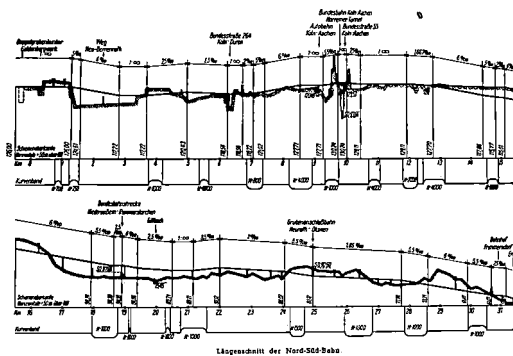


Figure 10 shows the gradient of the North-South Railroad

The deepest point of the North-South Railroad is the Frimmersdorf transfer point in the north. Up to the vertex, a height difference of 69 m is to be overcome in the main load direction. Location difficulties arose with the ascent from the Erfttal

(valley of the Erft river) near Frimmersdorf, and with the transition zone from the Gillbachtal (Gillbach valley) to the Ville hills near Oberaußem. For reasons of overall planning (largescale power plant, mine exits, main workshop), Frimmersdorf station is situated crosswise to the Erfttal.

The hills in the vicinity of this valley were overcome solely by a cut up to 16 m deep. As to Oberaußem, the situation is similar. Here, a dam height of 14 m and a cut depth of 12 m had to be accepted to balance the immediate gradient of 30 ‰. In the exhausted area in the south, the North-South Railroad is to be found on overburden dumps in part piled-up only immediately before the track system was installed.

Stations are only in Frimmersdorf and Knapsack, i. e. the final points of the North-South Railroad. The individual facilities are by 8 branching-off points connected to the North-South Railroad.

Hambach Railroad

The Hambach Railroad is a new railroad connection between the slewing center of the Hambach opencast mine where the development was started in 1978, and the North-South Railroad in the area of the Niederaußem township (Figure 9). It is planned to transport the lignite from the Hambach opencast mine where mining will start in 1983 to the consumers along the North-South Railroad - power stations and briquetting plants. In 1983, the quantity to be transported per year will be no more than 5 million t and until 1995 rise to 50 million t - i. e. the total output of the Hambach opencast mine.

Besides lignite transports, only workshop transports are directed on this line; it will not serve overburden transport.

The Hambach Railroad since 1980 under construction and scheduled to start operating in 1983 will be 21,5 km long. It is a double-track, fully electrified line having a loop in the bunker section in the Hambach opencast mine. Here, the loading facilities are installed in which the material is loaded from the belt conveyors in the opencast mine on the lignite freight cars. From this point, the railroad runs along available or planned roads to the North-South Railroad with townships being bypasses. The location elements selected are the same as those of the North-South Railroad, namely a minimum radius of 1 000 m and a maximum gradient of 6 ‰. It is only in the bunker loop that the empty-car track has a curvature radius of 200 m. The clearance, too, with its clear height of 5,80 m and clear width of 5,50 m corresponds to the North-South Railroad. With a distance of 6,00 m between the tracks, the double-track railroad has a total width of 14,00 m.

For operational reasons, the railroad is to be laid out as a grade-separation structure. Therefore and because of the improved immission protection, it runs in a cut nearly all over its length. Only for crossing the Wiebach, Giesendorfer Fließ, and Erfttrivers, the line is installed on a dam (Figure 11). About 30 bridges had to be built for crossing communication lines and water courses. On account of the high population density in the Rhineland, much attention was paid to immission protection. Thus, protective measures are taken along the new railroad near townships, namely noise protection walls are built lateral to the line running on the dam to cross the Erfttal (Figure 12). These protective walls have a height of 4,00 to 5,00 m above the rail top. The railroad crosses a large wood area and two nature reserves. That is why considerable greening and

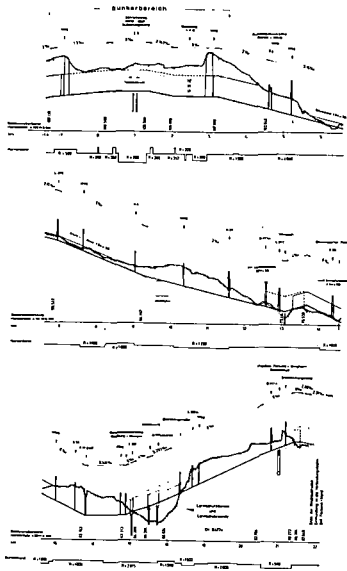


Figure 11 shows the gradient of the Hambach Railroad

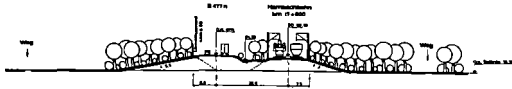


Figure 12 shows a gross section of the Hambach Railroad in the Erfttal

planting measures are taken on cut slopes and dams as well as on surfaces beside.

For the superstructure, UIC 60 rails with a strength of 900 to 1 100 N/mm² will be used. They will be fastened by means of UNI 60 bearing plates, Ss 8 tie screws, SKL tensioning clamps, intermediate plastic layers, and Lupolen plastic bases. The switches to be installed will be wood switches as mostly used by Rheinbraun. Superstructuring work will be started in spring 1982. As signal control, the Hambach Railroad will be given three track-diagram signal boxes, SpDr 60 type from Messrs. Siemens, via remote control connected to the Auenheim central signal station; from here they are distant-controlled. In the case of a malfunction, however, they can locally be controlled, too. The trains are operated with alternating current, 6 kV, 50 Hz. The locomotive is supplied directly via the overhead line to which a feeding line of 25 kV,

50 Hz is connected. Power feeding takes place in two transformer substations consisting of one 25 kV and one 6 kV switchgear as well as auxiliary and control facilities.

RAILROAD TRAFFIC REGULATION

The Rheinbraun railroad system serves the transport of overburden and lignite as well as related workshop and maintenance transports. The overburden and lignite cars can be loaded either directly from the excavator or via inserted load-transferring facilities or belt conveyors.

For direct loading,

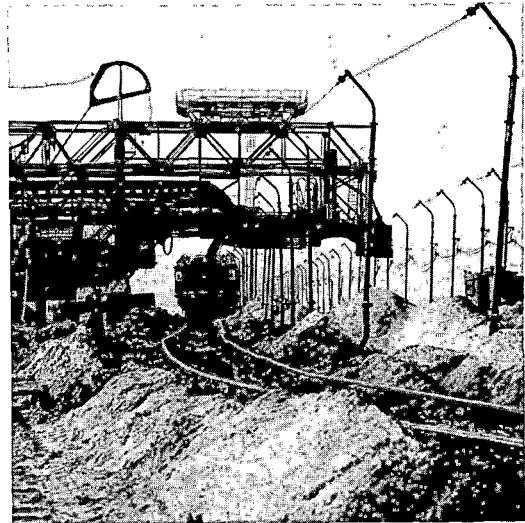


Figure 13 shows train loading directly from the excavator

the train runs on shiftable tracks under the excavator where it is loaded with overburden and lignite while moving slowly according to VHF radio instructions. The shiftable tracks are laid without ballast immediately on the soil subgrade. For this purpose, hollow steel ties with 110 x 350 x 3,000 mm measurements are used. Movable pin connections serve to fasten the rails to the ties. The position of the shiftable tracks is not exact, thus leading to high maintenance and wear. Today, direct loading from the excavator is only practised in the Frimmersdorf opencast mine where it will likewise be totally dispensed with in the course of the change-over to the Garzweiler opencast mine.

If load-transferring facilities are inserted, the train runs under a stationary loading installation where it is filled with overburden or lignite - likewise with VHF-controlled slow motion. In this case, the tracks are stationary, too, and have the usual design. Evitable overloading during the loading operation causes a severe dirt problem.

The overburden trains are unloaded into dump trenches (Figure 14), the lignite trains into bunkers (Figure 15). The overburden dump trench consists of a trough besides the track, the dumping operation is released by compressed air. To prevent the overburden freight cars from turning over while the material is dumped, a supporting structure is installed beside the track on which the running gear of the freight car rests with a bracket. The track itself requires a solid foundation to meet the dynamic impact during the dumping operation. The lignite cars are unloaded into

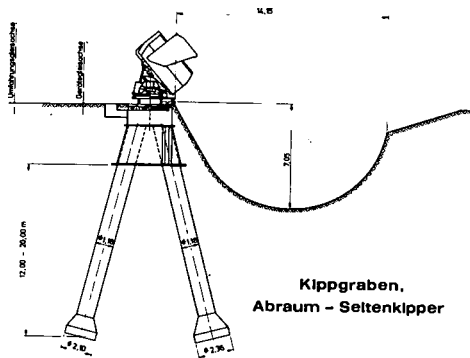


Figure 14 shows a cross section of a dump trench

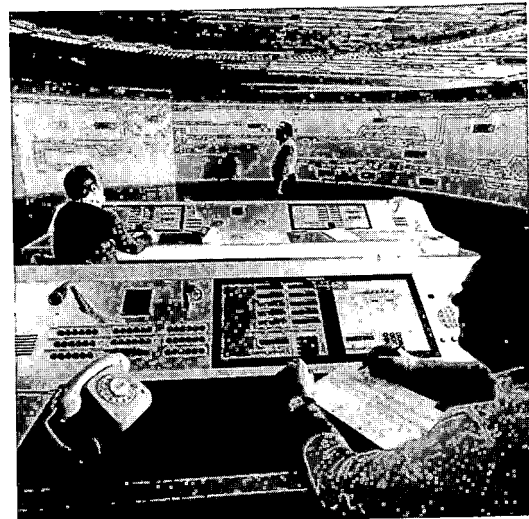


Figure 16 shows the Auenheim central signal station

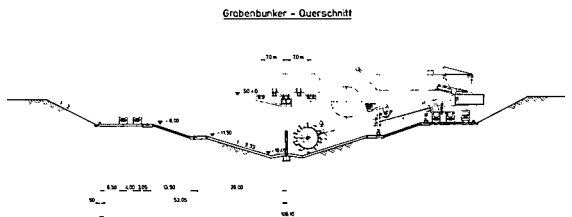


Figure 15 shows a cross section of a bunker

the bunkers of the power stations and briquetting plants. The bunkers consist of a bridge structure as long, or half as long as the train, built above a storage bunker. Depending on the shape of the storage bunker, trench and slot bunkers are distinguished. The material is dumped by opening the side gates of the lignite cars employing compressed air. The dumping operation can be started from the locomotive or by hand at every single freight car.

Depending on the available bunker length, the trains must be divided to be unloaded.

Today, a train consisting of 10 freight cars and 1 locomotive is usual for overburden transport. It is only in track sections of a steep gradient - more than 6 ‰ in the mine railroads - that trains consisting of 8 freight cars are used. In future times, the lignite trains will have 14 freight cars (in former times 10 freight cars) and one locomotive. Rheinbraun does not operate its trains according to a timetable, but in accordance with the operational requirements. All the locomotives are equipped with radio sets and have constant radio contact with the Auenheim central signal station from where the instructions are given (Figure 16).

On account of the high efficiency, the tracks are equipped with modern signalling systems. These include track-diagram signal boxes, an automatic electric block system, an electric train number announcing, and train describers at specific checkpoints. Wrong running - running on the wrong track - is likewise signal-controlled. The overrunning of a stop signal is excluded by a magnetic train control, installed 200 m in front of the signal and causing an automatic train stop if the train driver does not react correctly. For the operation of trains with a banking locomotive, signal imitators are installed at train length in front of the signal.

MAINTENANCE WORK

Rolling stock

The overburden and lignite cars as well as the locomotives are maintained in the Grefrath main workshop the equipment of which is suitable for any kind of maintenance work. This work primarily includes the vehicle tests prescribed under the BOA (regulations as to connecting railroads - BOA = Betriebsordnung für Anschlußbahnen) and the resulting repairs. Axle breaking is a severe problem, frequently causing derailments and subsequent damage. By ultrasound testing it is attempted to recognize defects and damage which may cause axles to break, and to stop operating the vehicles in time. In addition to maintenance work, the main workshop has recently rebuilt and improved vehicles in many cases, thus serving immission protection. In this connection, sound-absorbed wheels, special plastics for running gears and brakes as well as noise-reducing measures taken at the compressors of the locomotives are to be mentioned. In the Frimmersdorf opencast mine far away from the main workshop, there is a branch workshop for minor repair work.

Superstructure

Track maintenance is carried out by Rheinbraun's own staff and equipment. Here, the main problem is the

substantial dirt caused by trickling material - overburden and lignite - which penetrates through untight freight car gates or falls down over the side walls in case the freight cars are overloaded. This trickling material causes the ballast to bond or cake which then does no longer drain properly. This results in damage to the track system and in the necessity of cleaning and maintaining the ballast. For carrying out this work, most advanced equipment and machinery are available; the most important among those are track-tamping machines, switch-tamping machines, flank-cleaning devices, and equipment to clear the space between 2 ties.

Tracklayer gangs primarily working in switch sections cannot yet be dispensed with because the degree of mechanization for maintaining the switches is not yet satisfactory. Besides mere track maintenance, minor reconstruction work is done out of Rheinbraun's own resources. The machinery and track construction cranes required for this purpose are available, too. Special vehicles are used for checking and maintaining the electric facilities - overhead lines and signals. In this connection, the 1979/80 severe winter is worth mentioning when operational difficulties arose from freezing switches. To exclude repetitions, all the switches required for ensuring the main transport are now equipped with electric switch heatings.

TRACK SYSTEM AND QUANTITIES TO BE TRANSPORTED

The Rheinbraun railroad transport system

BIBLIOGRAPHY

- (1) Gärtner Die Einführung eines schweren Schienenprofils und die technische Entwicklung der Oberbaugestaltung im Braunkohlentagebaubetrieb (Braunkohle 1953, Hefte 1 - 4)

(The introduction of a heavy rail profile and the technical development of the superstructures in lignite opencast mines)
- (2) Gärtner Entwicklungstendenzen in der Geräte- und Fördertechnik (Braunkohle 1955)

(Developments in equipment and mining technologies)
- (3) Freisburger/ Braunkohlenbergbau und Eisenbahn Wöckel (Die Bundesbahn 1955)

(Lignite mining and rail transport)
- (4) Fries/Meyer Der Bahnbetrieb Fortuna und seine technische Entwicklung (Braunkohle 9/1977)

(The Fortuna railroad system and its technical development)
- (5) Goergen Der Kastenwagen - ein möglicher Wagentyp für den Abraumtransport (Braunkohle 12/1964)

(The box-type freight car - a car type to be used for overburden transport)

had reached its climax in the 50s and 60s. At that time, most transports both of overburden and lignite took place on tracks. Later on, the quantities transported by rail were on the decline, and the track lengths were reduced, too. This downward tendency will change with the start-up of the Hambach Railroad. Quantities and transport capacities of the railroad system will again rise considerably from 1983.

WEAR

The Rheinbraun heavy-load transport revealed numerous wear problems. In this connection, the rail wear is most important to be mentioned which was intolerably high with the first S 64 rails having a strength of 700 N/mm². In many years' tests, numerous rails were tested in rail sections most heavily loaded (Rath loop in the Fortuna opencast mine). The test rails were Krupp, Klöckner, US-Steel, and Bethlehem-Steel rails. The tests resulted in a strength increase up to 900 N/mm², or 1 000 N/mm² with an extremely heavy rail load. Recent strength tests of more than 1 100 N/mm² show that the structure and alloying play quite an important role. It is likewise of importance whether the railroads in question are overburden or lignite lines. The tests are being continued. Besides the wear of the rail itself, the wear of the welded rail joint must be considered because here the rails can easily break. In addition, wear problems occurred at the fastening material, intermediate layers and bases, ties, and switch slide plates. The present state is satisfactory.

- (6) Goergen Massentransport im Tagebaubetrieb (Fördern u. Heben 14/1967)

(Mass transport in opencast mines)
- (7) Heitkemper Projektierung der Hambachbahn (Braunkohle 4/1980)

(Projection of the Hambach Railroad)
- (8) Heitkemper Rheinbraun-Tagebau Hambach: Hambachbahn (Energiewirtschaftliche Tagesfragen 5/1981)

(The Rheinbraun Hambach opencast mine: Hambach Railroad)
- (9) Leuschner Die Fördertechnik im Rheinischen Braunkohlenbergbau (Erzmetall 10/1969)

(Mining technology in the Rhenish Lignite Area)
- (10) Rauch Das Rheinische Braunkohlenrevier und seine Nord-Süd-Bahn (Eisenbahntechnische Rundschau 10/1955)

(The Rhenish Lignite Area and its North-South Railroad)
- (11) Rauch Die Nord-Süd-Bahn im Rheinischen Braunkohlenrevier (Braunkohle 1953, Heft 9/10)

- The North-South Railroad in the Rhenish Lignite Area)
- (12) Schmidtalbers Der Entwicklungsstand des Oberbaues bei normalspurigen Gleisanlagen bei der "Rheinische Braunkohlenwerke AG" Köln (Braunkohle 5/1968)
- (State of development regarding the superstructure with standard-gauge tracks used by the "Rheinische Braunkohlenwerke AG", Cologne)
- (13) Schmidtalbers Erfahrungen mit dem Auftrags-schweißen bei S 64-Herzstücken (Braunkohle 1/1969)
- (Experience gained with deposition welding of S 64 crossings)
- (14) Schmidtalbers/ Die heutigen Großraumwagen mit Langhammer mehr als 90 m³ Inhalt im rheinischen Braunkohlenrevier (Braunkohle 1970, Heft 1, 5, 10; 1971 Heft 1)
- (Today's large freight cars with a capacity of more than 90 m³ used in the Rhenish Lignite Area)
- (15) Schmidtalbers Entwicklungsstand des normalspurigen Zugbetriebes im rheinischen Braunkohlenrevier (Teil 1 u. 2) (Bergbau-WISS 18/1971)
- (State of development regarding normal-gauge rail conveyance in the Rhenish Lignite Area)
- (16) Schmidtalbers Der Eisenbahnbetrieb bei der "Rheinische Braunkohlenwerke AG" Köln (unveröff. Manuskript 1974)
- (Rail transport at the "Rheinische Braunkohlenwerke AG", Cologne)
- (17) Schultze Fernsteuerung des Kippvorganges an 95 m³-Abraumwagen - eine Maßnahme zur weiteren Rationalisierung des Abraumzugbetriebes - (Braunkohle 6/1970)
- (Remote control of the dumping operation of 95 m³ overburden freight cars - a measure for further rationalizing overburden railroad transport)
- (18) Schultze Erfahrungen mit hochfesten Schienen bei der "Rheinische Braunkohlenwerke AG" (Braunkohle 7/1972)
- (Experience gained with highly stable rails used by the "Rheinische Braunkohlenwerke AG")
- (19) Schulze Einführung beweglicher Herzstückspitzen in Weichen und Kreuzungen bei der "Rheinische Braunkohlenwerke AG" (Braunkohle 6/1969)
- (Mounting of mobile crossing frogs to switches and crossings at the "Rheinische Braunkohlenwerke AG")
- (20) Würz Gleisverschmutzung und maschinelle Gleisreinigung in Tagebauen (Braunkohle 4/1961)
- (Track soilage and mechanical track cleaning in opencast mines)

Zeng Shugu

Research Engineer
China Academy of Railway
Sciences
Beijing, China

Failure of Heavy Haul Track & Its Design

A limit state method of track design is proposed with safe fatigue life of rail and accumulative deformation of ballast as performance criteria, which stem from the deterioration behaviour of heavy duty track. It is aimed to yield such a track structure as will satisfy a preset period between general overhauls and a suitable quota of track maintenance. For use as the design load in its broadest sense, spectra of track load, amplitude of vibrational acceleration, frequency and power are obtained from field measurements. Through laboratory tests are acquired the resistance properties of rail and ballast under the action of repeated loading. Safety criterion is determined appropriately in accordance with past operating experiences. Then calculations are performed for safe fatigue life of rail and accumulated deformation of ballast following respectively the modified Miner's rule of linear cumulative damage and the empirical rule of ballast cumulative deformation.

NOMENCLATURE

a vertical vibrational acceleration (g) of top of ballast prism
D spring constant (kg/cm) for rail support
EI flexural stiffness ($kg \cdot cm^2$) of rail section
J_p mean square deviation (T) of wheel load
J_{2a} mean square deviation (kg/cm^2) of total stress amplitude
K stress scatter coefficient
k rate of stiffness factor (cm^{-1}) for rail relative to support
l sleeper spacing (cm)
m mass of sleeper, ballast and subgrade taking part in vibration ($kg \cdot sec^2 \cdot cm^{-1}$)
n_i number of stress (σ_i) occurrence
N_i number of times of load passed corresponding to stress
N_a accumulated gross number of times of load passed
P wheel load (T)
P_{min} minimum alternating load (T)
P_{max} maximum alternating load (T)

P_s test load (T) for ballast cumulative deformation
p compressive stress (kg/cm^2) at top of ballast
Q load (T) transferred from rail to sleeper
R radius (mm) of wheel tread or rail head
T annual traffic volume (in 100 million tons)
U coefficient of resilience (kg/cm^2) for rail support
U₁ spring constant (kg/cm) for rail pad
V train speed (km/h)
W coefficient of track state
Y accumulated deformation (mm) of ballast
 α safety criterion
 β rate of ballast settlement (10^{-5} mm/occurrence)
r_p load ratio
 γ_{σ} stress ratio
 σ_a half amplitude of stress (kg/cm^2)
 σ_{2a} total amplitude of stress (kg/cm^2)
 σ_m mean stress value (kg/cm^2)
 σ_t tensile stress (kg/cm^2)
 λ vehicle coefficient

PERFORMANCE CRITERIA FOR HEAVY DUTY TRACK AND LIMIT STATE DESIGN

The principal problems now confronting China's heavily trafficked main trunk lines are unduly short overhaul cycles and unduly large maintenance volumes. The necessary repair work simply could not be accomplished during regular train intervals, while it is practically impossible to provide

enough track work "slots" in the train diagram without cutting down scheduled traffic targets. In consequence, technically, good working condition of the track could hardly be maintained. Economically, the result is undesirably high consumption of materials as well as man-power.

The overhaul cycle is controlled by the service life of track components. The amount of track work depends on the deterioration of track geometry due to cumulative track deformation. Hence the performance criteria for heavy duty track are stated as follows:

1 The track components are to have adequate service life so that durability of the track could be ensured;

2 The rate of track cumulative deformation is not to go beyond a certain limit specified in accordance with particular operating conditions and competence in track maintenance, so that the track might be kept in a good working state.

A specific state of the integrated track structure or any of the track components is named the limit state of performance if the performance criterion could not be satisfied on the specific state being overrun.

Strong randomness is inherent with the external forces acting on the track (including external loads, thermal deformation or constraint deformation), the geometry and material properties of track components, and various other factors affecting track performance. Therefore, the limit state, which is controlled by the above mentioned factors, and beyond which the track will not work properly, can only be described by some method of statistical analysis based on a probability approach. The method of reliability design for engineering structures is especially useful to heavy duty track in that it is itself a limit state design founded on the probability theory.

LIMIT STATE TRACK DESIGN BASED ON RAIL SAFE FATIGUE LIFE AS PERFORMANCE CRITERION

Safe fatigue life of rail denotes the gross passing traffic tonnage the rail is capable of carrying during its entire service period from the day it is laid to the day it is removed from the track. This tonnage is the main index used at present in this country in determining the general overhaul cycle of the track.

A group of rails is deemed to have attained its limit of safety life when the number of damaged or broken rails (from this group due to different causes) which are removed from the track has come up to a specified quantity so that their continued service would no longer guarantee safety of operation. Statistical figures from the track maintenance department have shown that, for a certain type of rail, each classification of rail defect has a definite proportion in the total number of damaged rails. Table 1 gives statistical data for 50 kg/m rails prepared by a maintenance division in regard to the damages incurred during a particular length of time.

With respect to the description of the limit state of safe fatigue life, the same effect is obtained either by control over the accumulated total number of damaged rail or by control over the accumulated number of damaged rail due to a specific classification of defect. For instance, using the data given in Table 1, we may take either

Table 1 Statistics of defects (50 kg/m rail)

Classification of defect	Oval flaw	Propagated crack in rail head due to engine burn, spalling, etc.	Crack around bolt hole	Total number of damaged rail
Number of damaged rail	202	108	140	450
Percentage	45	24	31	100

the total number of damaged rail, 450 pcs (100%), or the number of damaged rail due to oval flaw, 202 pcs (45%), and we will arrive at the same service life or accumulated gross passing tonnage.

In this paper, we shall base our description of the limit state of rail and calculations for rail safe fatigue life on oval flaw, the principal classification of defect of the 50 kg/m rails which are used most extensively on our trunk railway lines.

Study on the fatigue life of rail began in 1973 in this country (1) - (5). The American Railway Engineering Association has carried out a series of studies on this subject (6) - (8). The same was conducted in West Germany, Japan and some other countries (9) (10).

Calculated Point and Nominal Stress

The maximum tensile stress is taken as the nominal stress in the calculations, because the fatigue origin of flexural members in general usually appears in the region where the tensile stress is highest. In the case of rails under traffic, however, the fatigue origin mostly appear in the head (Fig 1) inspite that there is high tensile stress in the base. This has something to do with the wheel/rail contact stress in the head. We have made field measurements of the stressing conditions at different parts of the rail (Fig 2). The figure shows the factual existence of two types of basic deformations -- flexural deformation and contact-rolling deformation -- at the head and at the web; and that there is only flexural deformation at the edge of the base.

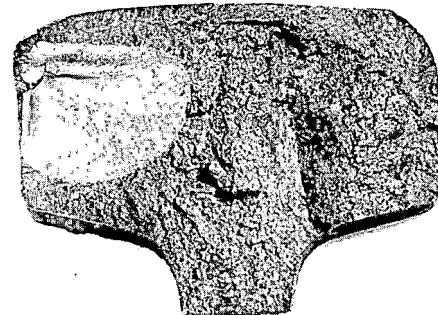


Fig 1 Photo of track rail with oval flaw

It is indicated by our fatigue tests with real rail sections (Fig 3, 4) (11) that fatigue origins which lead to fatigue failure always occur in the base when the stress ratio γ_p (of load P) = $P_{min}/P_{max} > 0$. The same tests also indicate that marks of injury or fine cracks that

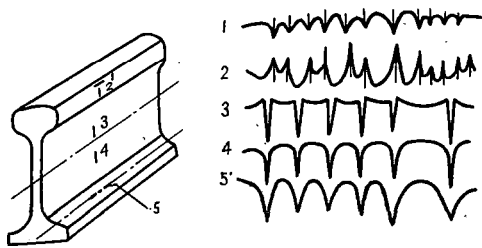


Fig 2 Stress waveform for different parts of rail

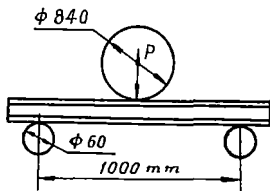


Fig 3 Three-point test for flexural fatigue

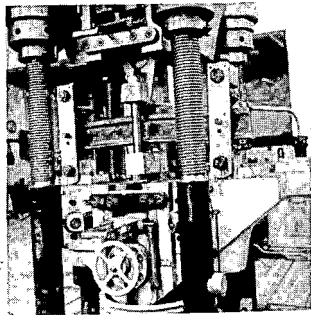


Fig 4 Photo showing test apparatus

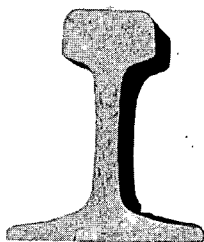


Fig 5 Photo showing fatigue origin in rail base

are found in the rail head before testing will not extend during testing. But when $\psi_p < -0.1$, the fatigue origins are all found in the head (Fig 6) and injuries and cracks found before testing

will develop quickly. Contact stress only will

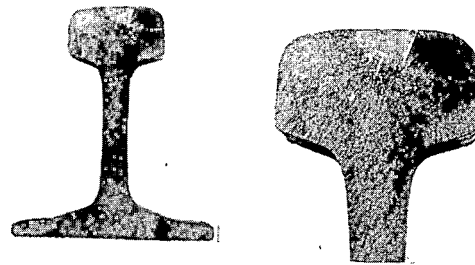


Fig 6 Photo showing fatigue origin in rail head

not lead to rail break without the presence of bending stress.

The previously mentioned field tests have proved that two basic types of deformation, the flexural deformation and the contact-rolling deformation, factually occur in the railhead. And the laboratory tests have proved that contact deformation plays an important role in the formation of fatigue origin and that the existence of flexural deformation and its changing of signs are necessary conditions for the propagation of fatigue cracks.

In calculating the life of rail with oval flaw when fatigue origin appears in the head, we take a point on the centre line of the rail head 5 mm below its top as the calculated point. The reason is that fatigue origin most probably will appear nearby this point. The longitudinal stress at this point which is dependent on both the flexural deformation of the rail and the wheel/rail contact-rolling deformation is taken as the nominal stress. The contact stress is calculated according to the Herz's equations (12).

In Fig 7 is shown the waveform of nominal stress. We can see that the tensile stress in the rail head assumes a small value with trivial fluctuation. This stress is supposed to be constant

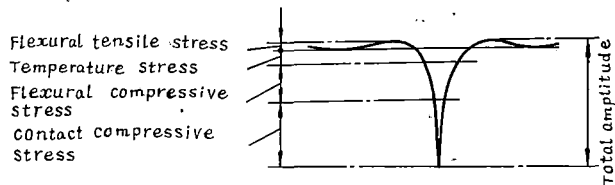


Fig 7 Waveform of nominal stress

so as to simplify calculation. Its value is calculated from track measurements to be $\sigma_1 = 270 \text{ kg/cm}^2$ for 50 kg/m rail and $\sigma_1 = 212 \text{ kg/cm}^2$ for 60 kg/m rail, on the safe side. The temperature stress is also assumed to be constant in the calculation, because: (1) as the temperature stress has a much longer fluctuation cycle than the wheel load stress, it is nearly a constant within the fluctuation cycle of wheel load stress; (2) experience has indicated that only very slight damage

is inflicted upon the rail by fluctuation of temperature stress. What influence temperature stress has on rail fatigue is mirrored in the variation of the mean nominal stress.

With the foregoing process of simplification, the nominal stress turns out to be a pulsating reversal stress orientated toward the negative direction (taking tensile stress as positive, compressive stress as negative) and referenced to the maximum stress (temperature stress plus flexural tensile stress) as a datum. This stress is represented by the radial line QP in the fatigue limit graph (Fig 8) (13).

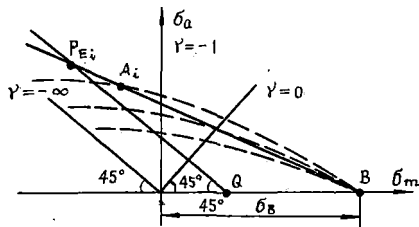


Fig 8 Fatigue limit graph and pulsating reversal stress line QP

Fatigue Test on Rail Section and Modified Fatigue Curve

Laboratory fatigue test on rail section is modelled on the traditional three-point mechanical test (Fig 3, 4). The value of u is calculated after the equation $k = 1/4 = (u/4EI)^{1/4}$ (14). This test model is comparable to our timber-sleepered track on weak subgrade. The value of l should be made sufficiently small to adapt itself to concrete-sleepered track.

The test results are plotted to give a fatigue curve, with the nominal stresses at the calculated point as ordinate. Since the working stress ratio γ_σ of rail is varying, the fatigue curve obtained by the traditional method for a constant value of γ_σ cannot be used for evaluation of rail fatigue life.

Data from laboratory fatigue test on rail section is used to plot the modified fatigue curve (Fig 9), for which the stress ratio consistently agrees with the working stress ratio of the rail (shown in Fig 8 as pulsating reversal stress represented by the radial line QP). The following procedure is followed.

1 From the test load, calculate the nominal stress which correspond to the maximum and the minimum values of the test load for the i -th test section. Plot point A_i on the fatigue limit diagram (Fig 8) against the mean stress value σ_{mi} and the half amplitude value σ_{ai} . Connect point A_i with point B, which lies on the abscissa and represents rupture strength σ_B , to obtain the constant life curve expressed in terms of the fatigue life N_i of the test section.

2¹ Point E_i , the intersecting point of line QP and the constant life curve BA_i , represents a stress value that is the fatigue strength of rail with a stress ratio exactly equal to the factual working stress ratio of the rail. We indicate this fatigue strength by the total stress amplitude

σ_{2a} .

3 A point M_i can be obtained and plotted on the S-N curve from the σ_{2ai} and N_i values of the i -th test section.

4 Following the preceeding procedure, a group of M points are found corresponding to a set of test sections. From the group of M points a straight line is obtained by least square reduction. This straight line is the modified fatigue curve S-N.

Spectra of Train Load and Rail Working Stress

The wheel load spectrum as shown in Fig 10 is obtained through statistical calculations on the basis of ample field measurements of rail stresses under our currently operating wheel loads. Subject to normal distribution, this spectrum has a mean value of 8.25 tons, which comes close to the mean static wheel load. Its mean square deviation may be expressed by the following experimental formula:

$$J_p = 1.937 + 0.0123V \quad (30 \text{ km/h} < V < 90 \text{ km/h}) \quad (1)$$

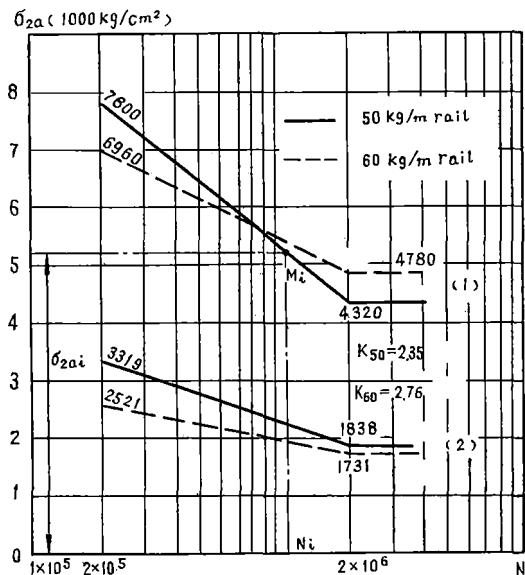


Fig 9 S-N curve
(1) Modified fatigue curve
(2) Safe fatigue life curve

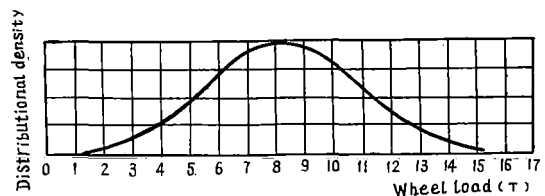


Fig 10 Probability distribution of train wheel load

From a certain wheel load, a corresponding value of nominal stress may be acquired with this and taking further account of flexural tensile stress and temperature tensile stress, a spectrum of nominal working stress (Fig 11) also may be acquired in terms of σ_{2a} , the total stress amplitude. The mean value and the mean square deviation of this spectrum are given in Table 2.

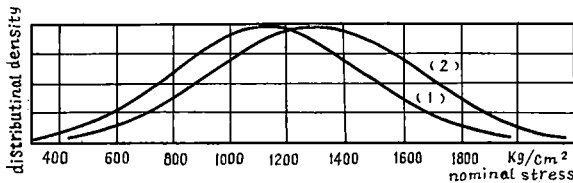


Fig 11 Spectrum of nominal working stress
(1) 60 kg/m rail
(2) 50 kg/m rail

Table 2 Statistical Eigenvalues of nominal working stress spectrum

Type of rail (kg/m)	Mean value (Total stress amplitude) (kg/cm ²)	Mean square deviation (Total stress amplitude) (kg/cm ²)
60	1130	232.6 + 1.629 V
50	1293	261.2 + 1.617 V

Safety Criterion and Safe Fatigue Life Curve

Safety criterion is an eigenvalue indicating the reliability level (or failure probability) of a structure. To determine this criterion, account should be taken not only of technical and economical factors, but also of possible social effects.

For 12.5 m rails, we judge that limit state of normal service of the rail is reached, when the accumulated number of damaged rails comes to 2 pcs per kilometer of track. (referring to Table 1, the corresponding number of oval flaw rails per kilometer is 0.9.) Matching this, the safety criterion α is 2.24 and the reliability index is 0.9875.

When the service rail reaches its limit state, the gross passing tonnage carried during its entire service period is approximately 480 million tons for 50 kg/m rail and 270 million tons for 43 kg/m rail, according to statistical data taken from the track liad with concrete sleepers under train speed of 60 km/h. Those figures then are considered as the respective allowable gross passing tonnages. Analysis of statistical data for haul tonnage and train composition over the investigated line sections enables us to derive from the allowable gross passing tonnage the allowable total number of passing axles N_a (Table 3).

A corresponding spectrum of allowable service stress (L-N curve) may be derived from N_a and the curve of stress spectrum as shown in Fig 11. If we consider the track rail as a test piece, then the unstationary repeated train load will be the test load. Here the rail fatigue strength curve

Table 3 Allowable gross passing tonnage and allowable total number of passing axles for several types of rails

Type of rail (kg/m)	Allowable gross passing tonnage (100 million tons)	Allowable total number of passing axles N_a (10^6 times)
43	2.7	13.9
50	4.8	24.8
60*	8.4	43.4

* The tabulated figure of gross tonnage for 60 kg/m rail is obtained by deduction according to the method suggested in this paper, on condition that the same safety criterion as for 43 kg/m and 50 kg/m rails is adhered to.

corresponding to the allowable service stress spectrum may be obtained by the Lokat method making reference to the shape of the modified fatigue curve of the same rail (15). We call the curve thus obtained the allowable service fatigue curve or the safe fatigue life curve. The implied meaning is that the working stress will not exceed the allowable fatigue strength of the rail so long as the practical working stress remains within the range of the allowable service stress spectrum. In other words, the rail herefrom may be safely used against a safety criterion of 2.24.

There is a proportional relationship between the modified fatigue curve and the safe fatigue life curve and is denoted as the coefficient K, which we call the scatter coefficient. It is a synthetic parameter indicating the scattering state of the mechanical strength of track rail, the scattering state of non-conformity between the practical working stress spectrum and the spectrum we have obtained through a limited number of tests, the proximity of Miner's hypothesis of linear cumulative damage as used in the Lokat method, the field conditions which could hardly be simulated in laboratory experiments, and so on. The calculated results are given in Table 4.

Table 4 Scatter coefficient of rail

Type of rail	Scatter coefficient K
50 kg/m	2.35
60 kg/m	2.76

Calculation of Rail Cumulative Damage

The cumulative damage is calculated by applying the modified Miner's rule of linear cumulative damage. The modification comprises extending the inclined portion of the fatigue curve downward beyond the fatigue limit and calculating the damage for all low stress values (Fig 12).

$$q = \sum \frac{n_i}{N_i} \quad (2)$$

According to Miner's rule, low fatigue stresses are assumed to be producing little damage. This holds under the assumption of constant load amplitude. However, under unstationary repeated load, low fatigue stress will produce damage in that they promote the fatigue origin formed under excess

stresses. This is why the Miner's rule must be modified.

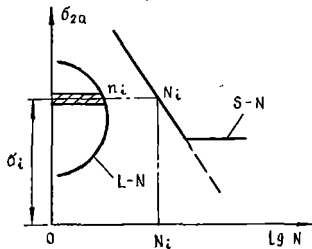


Fig 12 Modified Miner's rule of linear cumulative damage

The modified Miner's rule proves to be quite suitable for calculation of fatigue life by the method of comparison.

Evaluation of Rail Safe Fatigue Life.

From statistical information from some typical line sections, the allowable gross passing tonnage values (Table 3) of certain types of rails have been estimated against a prescribed safety criterion for particular operation and track conditions. Evaluation of the rail safe fatigue life makes use of those data, either to derive the life of the same type of rail under other operation and track conditions by comparison of their cumulative damage, or to predict, following the principle of equivalent safety criterion, using available rail data, the life of a certain new type of rail. Following are the working procedures:

- 1 Draw the modified fatigue curve from fatigue test results of rail sections. The safe fatigue life curve (Fig 9) is obtained by introducing the scatter coefficient (Table 4).
- 2 Derive the working stress spectrum from axle loads, track conditions and train speeds, in line with the following propositions: the working stress spectrum obeys normal distribution, the mean spectral stress value equals the mean static stress value, the mean square deviation conforms to the results by the empirical equation as shown in Table 2.
3. Calculate the cumulative damage separately by employing the modified Miner's rule for equal times of load application, for the previously mentioned typical line sections, over which the statistical data have been collected and for sections the life of which is to be predicted.
- 4 The safe fatigue life of the rail on the line sections for which the life evaluation is made will be inversely proportional to the cumulative damage obtained in the foregoing manner, under the given condition of allowable gross tonnage operating on the typical section (Table 3).

The above method enables us to plot control diagrams for calculation of the safe fatigue life of home-made 50 kg/m and 60 kg/m rails (Fig 13). The safe fatigue life of rail under any operation conditions and track conditions can be obtained

directly from these diagrams. They also may help in the choice of a desirable track structure for specific operation conditions and specific cycle of track overhaul (safety life).

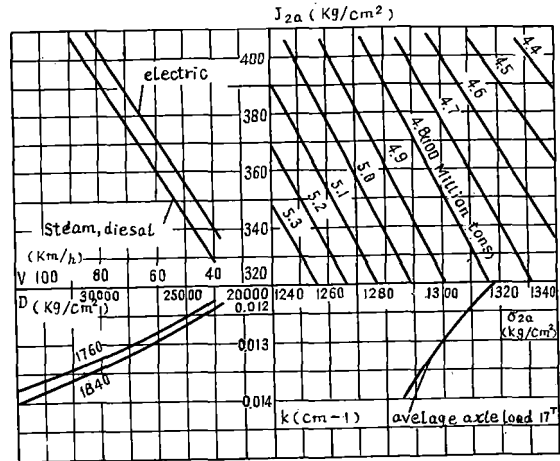


Fig 13(a) Control diagram for calculation of fatigue life of 50 kg/m rail

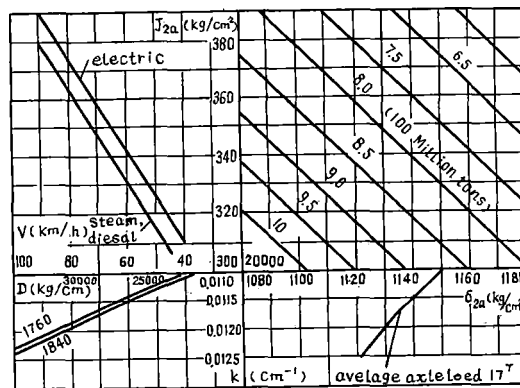


Fig 13(b) Control diagram for calculation of fatigue life of 60 kg/m rail

In addition to these, we have made calculations over the safe fatigue life of 60 kg/m rail (Table 5) for an average axle load of 25 tons, concave wheel tread radius of 450 mm and 381 mm (16) and rail head radius of 600 mm.

LIMIT STATE TRACK DESIGN WITH CONTROLLED CUMULATIVE DEFORMATION OF BALLAST AS PERFORMANCE CRITERION

The amount of track maintenance work is related

Table 5 Safety fatigue life of 60 kg/m rail for various conditions

Axle load (T)	17			25		
Rail head radius (mm)	300			300	60	
Tread radius (mm)	∞	450	381	∞	450	∞
Safety fatigue life (100 millions)	8.4	21.6	23.4	1.8	6	2.8
Ratio	1	2.6	2.8	0.21	0.71	0.33

to the extent of deterioration of track geometry due to uneven settlement. As indicated by measurements taken in Japan, there is a rough proportion between the mean value and the mean square deviation of the residual settlements at different points of the track (17). The mean square deviation is what mirrors the unevenness of settlement and the extent of deterioration of track geometry. Therefore, the rate of increase in residual settlement offers a measuring index of the track maintenance volume.

On our existing trunk lines where the trackbed is in good condition, track settlement results chiefly from consolidation, attrition and sliding of ballast. Under the condition that the working state of the trackbed would not be noticeably altered due to any change of operation conditions, the relative stability of the present trackbed will be maintained, and track settlement will remain dependent on ballast cumulative deformation.

Behaviour of Ballast Cumulative Deformation under Repeated loading

Tests have been carried out in a number of countries in order to have knowledge of the behaviour of ballast cumulative deformation under repeated loading (18) - (20). The process of ballast settlement has been found through the tests to break down into two phases. The first phase is one in which the ballast consolidates gradually as a result of the movement, interspersion and relocation of ballast particles. As a consequence of the reduction of voids in the ballast, it becomes compacted and settles. This phase does not take long. What people are concerned about and has become the focus of study is the second phase, a regular working phase follows after the ballast has reached a state of relative stability. In this phase, the main causes producing settlement are the fragmentation, attrition and lateral movement of ballast along with the sliding of the ballast shoulder.

The apparatus used in our tests on ballast cumulative deformation are shown in Figs 14 and 15. The test track is 2 m long laid after the fashion of the Class I trunk line track, with 50 kg/m rail, concrete sleeper (3 pieces), ω-type rail fastenings, 7 mm rubber pad under rail base, crushed stone ballast of 30 cm depth under the bottom of sleepers. A cushion of sand 80 cm in thickness is placed under the ballast to simulate such resilience as provided by the subgrade for the track. Below the sand layer is a rigid concrete base. Load from a hydraulic fatigue test machine is applied to the rail by way of a load beam, the load frequencies being 4.17 and 8.34 Hz. The tested parameters are the settlement of the tops of the rail, the sleeper and the ballast (or the bottom of the sleeper), the pressure exerted onto the sleepers by the rail, and the compressive stresses at the tops of the ballast

(or the bottom of the sleeper) and the sand cushion, for static and dynamic load conditions separately. Also tested are the vibrational acceleration under dynamic loading along three directions at the tops of the ballast and the sand layer.

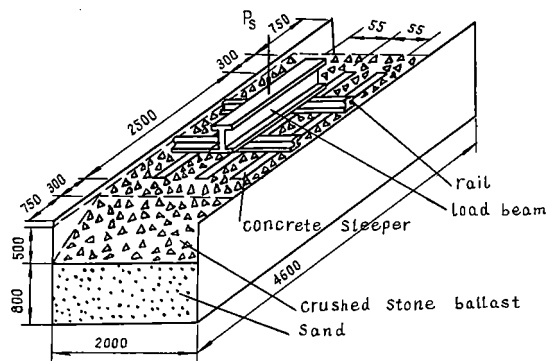


Fig 14 Test apparatus for ballast cumulative deformation (dimensions in mm)

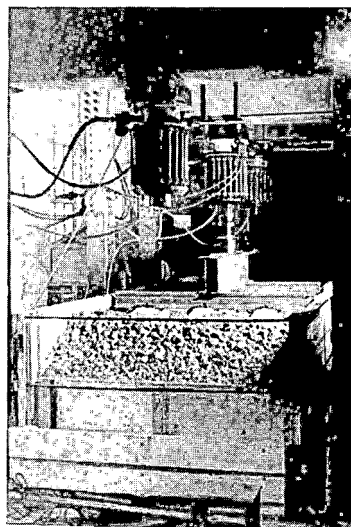


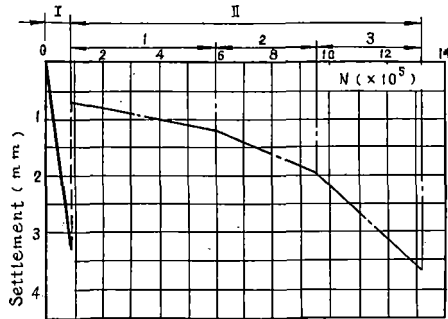
Fig 15 Apparatus used for ballast test

The ballast cumulative deformation curve as shown in Fig 16 is plotted using the test results. A preliminary conclusion is drawn that there is a rough proportion between the rate of settlement β and the product of stress multiplied by the square of the acceleration, i.e., (Fig 17)

$$\beta \propto p \cdot a^2 \quad (3)$$

Influence on Ballast Cumulative Deformation by Stress and Vibrational Acceleration of Ballast

As demonstrated by our test results, for ordinary train loads, the ballast stress may be calculated using the theory of distribution angle, and a rough proportion is found between the stress and the total settlement of the ballast. In the total



Working Phase	load Ps	β	p	a	a_*	pa^2	pa_*^2	
		$\frac{mm}{10^5}$	kg/cm^2	g		$10^{-3} kg \cdot g^2 \cdot cm^{-2}$		
Consolidation phase I	2-15	3.67	0.971	0.1	0.153	9.71	22.7	
relatively Stable Phase II	1	2-15	0.075	0.971	0.1	0.153	9.71	22.7
	2	2-17.5	0.228	1.133	0.1158	0.316	15.2	113
	3	2-20	0.472	1.295	0.138	0.526	24.6	358

Fig 16 Cumulative deformation curve of ballast

a — frequency range 0 ~ 250 Hz
 a_* — frequency range 2 ~ 10000 Hz

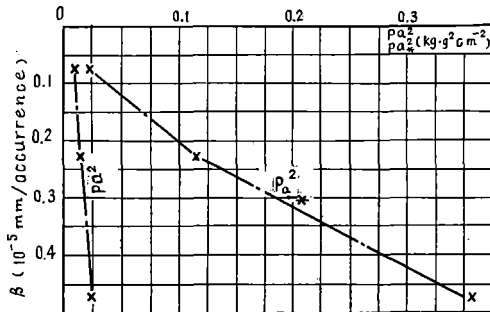


Fig 17 β / pa^2 relationship

settlement, both the elastic settlement in general and the residual settlement take a definite proportion. Hence it may be approximated that a rough proportional relationship is existing between the stress and the residual deformation.

The stability of the ballast prism is maintained by interlocking and friction forces between ballast particles. These forces diminish considerably under vibration (21). In studying the influence of ballast vibration upon cumulative deformation, we have measured the vibrational acceleration of different components on the track. The amplitude characteristics (Table 6), the frequency spectrum (Fig 18) and the power spectrum parameters (Table 7) are analyzed. Statistical analysis of the relationship between the parameter values of ballast acceleration and the volume of track maintenance

is made (22) (23). The preliminary conclusion is that the work volume is roughly in proportion to the mean power of vibrational acceleration of ballast (Table 7). The power spectrum of acceleration describes the intensity of vibrational acceleration, while the mean power represented by

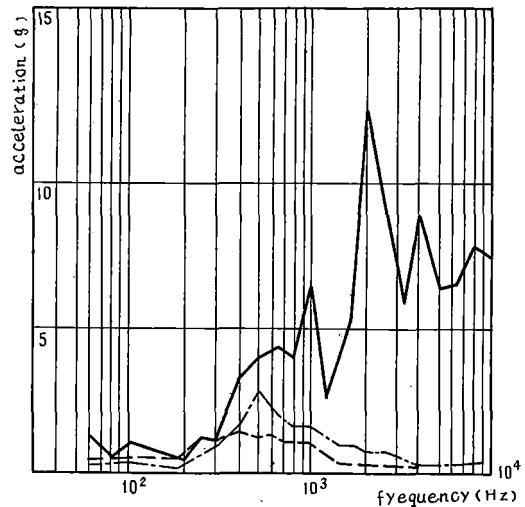


Fig 18 Frequency spectra of rail, sleeper and ballast acceleration for quarter points of rail
 — rail
 - - - sleeper
 . . . ballast

Table 6 Vibrational acceleration of ballast (taking a maximum value from each passing train for statistical calculation)

Measurement		Rail joint (Gap 7.5 - 10 mm, 1.5 mm mid ordinate deflection for 1 m chord)	Quarter point of rail length
Ballast acceleration (g)	Average	14.4	3.6
	Max.	23.6	4.4

the area contained by the power spectrum curve and the absciss describes the mean energy of vibrational acceleration. Hence it may be reckoned that the cumulative deformation and the volume of track maintenance are proportional to the energy potential of vibrational acceleration. This conclusion is

Table 7 Comparison of mean power of ballast vibration acceleration

Frequency range	0 -- 936 Hz		0 -- 468 Hz	
	measurement index	ratio	measurement index	ratio
Measurement taken at joint	2.4805	34.9	1.3906	27.42
Measurement taken at quarter point	0.0688		0.058	

in agreement with the laboratorial test result that cumulative deformation of ballast is proportional to the square of its vibrational acceleration.

Influence of Track Parameters upon Ballast Vibrational acceleration

The working state of ballast may be described by ballast stress and ballast vibrational acceleration. On certain eigenvalues of these two parameters depends also the rate of accumulation of ballast deformation. According to the data published in Japan, the ballast vibrational acceleration and the track parameters bear the following relationship:

$$a = \sqrt{U_1} \cdot \frac{1}{\sqrt{m}} \cdot \frac{1}{\sqrt{EIU}} \quad (4)$$

Calculation of Ballast Cumulative Deformation

By equations (3) and (4), and assuming that there is an approximately proportional relationship between the amount of settlement and the annual traffic volume T, train speed V, vehicle parameter, and track condition W (17), then the equation for ballast cumulative deformation can be expressed as:

$$Y \propto p \cdot a^2 \cdot T \cdot V \cdot W = p \cdot T \cdot V \cdot W \cdot \frac{U_1}{EIUm} \quad (6)$$

By the limit state track design with ballast cumulative deformation as its performance criterion means to carry out the track design on the basis of a certain limit value of its ballast cumulative deformation Y.

If a specific track state which the present maintenance technique can keep under given operating conditions is defined as the limit state, conforming to a certain safety criterion, the annual limit value of settlement can be calculated from equation (6). By method of comparison, the track conditions required for other operation conditions can be determined.

Let us take, as a typical case, our ordinary goods line carrying 30 million tons per annum with an average train speed of 60 km/h on a track structure that is extensively seen in this country (50 kg/m rail, 1840 pcs of concrete sleeper to one kilometer, crushed stone ballast 30 cm thick under sleeper, rail pad having a stiffness factor of 120 T/cm), assuming for the time being the coefficient of track state W = 1, and introducing, our vehicle parameter. Supposing the volume of maintenance work needed for such a track equal to 100, the volumes calculated for other cases are

given in Table 8.

Table 8 Comparison of the volume of maintenance work needed under different track conditions

Rail (kg/m)	Stiffness factor of rail pad (T/cm)	Sleeper	Average axle load (T)	Volume of maintenance work
50	120	Concrete	17	100
60	120	"	17	60
50	60	"	17	58
50	120	Broad concrete	17	13
50	120	Concrete	25	184

CONCLUSIONS

1 In consideration of the randomness of the failure state of track structure, load, strength of materials and the working state of the track, it is considered appropriate to employ the limit state design based on probability theory.

2 The basic performance requirements of heavy duty track may be stated as: (1) durability which depends upon the track components having sufficient service life; (2) proper amount of maintenance work and constant good working order of track which depend upon the integrated track structure having reasonable rate of cumulative deformation.

3. To raise the average axle load of goods wagons to 25 tons has considerable effect on the safe fatigue life of rail and the amount of maintenance work. Wagons of 25 ton axle load ought to be tried out on some branch lines to gather experiences before they are to be used in quantity.

4 Concave-shaped wheel tread and increased rail head radius help reduce wheel/rail contact stress and extend rail life. Research work in this field is necessary in the future.

5 Track maintenance work may be cut down by way of enlarging rail section, laying broad concrete sleepers, enhancing the resilience of rail pad, and improving the spring system of wagons;

Additions to the above conclusions is expected in the course of further accumulation of test results, since theoretic work and experiments on the design of heavy duty track are still under way.

ACKNOWLEDGEMENT

This work is accomplished by the concerted efforts of all those participants under the research program "Study on the Theory of Design of Heavy Duty Tracks".

REFERENCES

1. 铁研院 铁建所, 铁路钢轨的疲劳设计 1976
2. 铁研院 铁建所, 按不稳定重复荷载, 有限期使用寿命的钢轨承载能力计算方法 1977
3. 曾树谷、马焯, 铁路钢轨的疲劳损伤和寿命估算 《铁道部科学研究院论文集》第4期 1979
4. 铁道部第一设计院, 钢轨疲劳承载能力的计算 《铁路工程技术设计手册第三篇》1979

5. 上海铁道学院主编. 按疲劳强度条件计算钢轨的承载能力 《铁路轨道及路基》高校试用教材 1979
- 6 R.A. Abbott. "On the Prediction of the Fatigue Life of Rails" A.R.E.A., 1978 1/2
- 7 R.A. Abbott. "Fatigue Analysis of Rail Subject to Traffic and Temperature" Heavy Haul Railway Conference. 1978
- 8 A.M. Zarembski "Effect of Rail Section and Traffic on Rail Fatigue Life" A.R.E.A. 1979 6/7
- 9 W. Kraft. "Grenzbelastung der Schiene S49 in Gleisen und Weichen" Der Eisenbahn ingenieur. 1974 No3
- 10 渡边 偕年: 60 kg V-ルの诞生
《铁道线路》1967 № 8
11. 铁研院, 铁建所. 国产 60 kg/m 钢轨的疲劳试验
1979
- 12 F.B. Seely. "Advanced Mechanics of Materials" (2nd Ed.) 1955
- 13 日本材料学会 金属材料疲劳设计便览 1978
- 14 J. Eisenmann. Theoretische Betrachtungen über die Beanspruchung des Schienenkopfes am lastangriffspunkt" E.T.R. 1965 1/2
- 15 L. Sors. "Fatigue Design of Machine Components" 1971
- 16 F.E. King. "Rail Wear and Corrugation Studies" A.R.E.A. 1976 6/7
- 17 佐藤. 裕: 轨道力学 1978
- 18 M.J. Shenton. Deformation of Railway Ballast under Repeated Loading Condition" 1975
- 19 В.Г. Альбрехт. Современные конструкции верхнего строения железнодорожного пути 1975
- 20 佐藤. 裕: 繰返荷重による道床沉下の実験
《铁道技术研究報告》61. № 8
- 21 Г.Г. Желнин. Устойчивость рельсо-ципальной решетки сдвигу при высоких скоростях движения.
《ЦНИИ. м.п.с》 вып 592
- 22 铁研院, 铁建所. 混凝土轨枕上的弹性垫层试验报告
1969
- 23 铁研院, 铁建所. 轨道结构振动特性的测试
1979

Correlation Analysis of Concrete Cross Tie Track Performance

Harold Harrison

Senior Research Engineer
Applied Dynamics
& Acoustics Section
Battelle's Columbus Labs.

Howard Moody

Program Manager
Office of Research
& Development
Federal Railroad
Administration

A comparison was made of track performance at FAST and four revenue service test sites. Dynamic measurements under traffic, combined with physical measurements of track stiffness, settlement and visual inspections provided the basis for comparing the usefulness of results at FAST with other results acquired in revenue service. The lack of rail seat flexural cracks at FAST was determined to be related to well maintained wheels whereas, at some revenue sites, wheel flats were shown to cause significant tie cracking on up to 100% of the test ties. The relative performance of wood and concrete tie track settlement was shown to be similar when ballast support and maintenance procedures are the same. Gage holding is superior for concrete ties.

INTRODUCTION

The Facility for Accelerated Service Testing (FAST) was created to make comparative evaluations of track systems and components, as well as mechanical systems and components over their life cycle (within the FAST environment). These evaluations can be made by measuring and determining the rate of degradation and/or the failure mode of the components and hence the systems. The results can be used to establish track and mechanical component performance standards or specifications, system performance indices, and long term track and mechanical system maintenance requirements. Some of these results may be influenced by the specific environment in which they occur, such as climate, while others may be influenced by the accelerated testing process. A true accelerated service test is produced by increasing the loading or the rate of loading. The accelerated test is not appropriate if, in the process of increasing the load or changing the rate, something is left out, such as impact loading, or if the increase in loads creates other failure modes not seen in revenue service. The purpose of the correlation study was to determine whether FAST is truly representative, in an accelerated manner, of revenue service conditions.

The area of study chosen was concrete tie track, because there was not a great deal of empirical information available about concrete tie performance for North American conditions. After evaluating over sixty potential locations, four distinctly different, revenue service sites available met a variety of requirements established for this program.

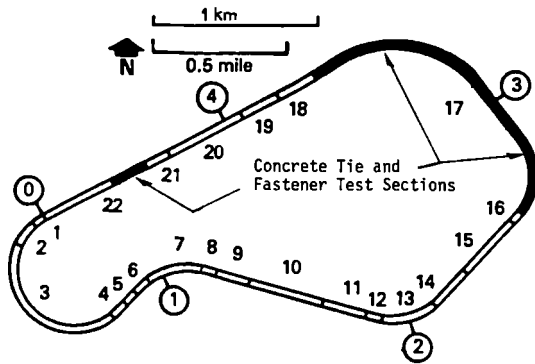
The study was begun in September, 1979, by Battelle's Columbus Laboratories under contract to the Federal Railroad Administration. The four test sites chosen are outlined in Table 1. In general, the components were very similar to those in FAST.

Table 1. Test Site Statistics

Location	Date Installed	Track Configur.	Traffic	Tonnage	Rail	Ties	Fasteners	Ballast
ATSF Leeds, IL MP 102	1974	Tangent	Mixed freight to 70mph; AMTRAK to 79mph	20MG/yr; 140MG/yr to date	135# RE CWR	8"6" and 9" prestressed concrete at 24"	3 types of elastic clips; 2 types of pads	Area #4 granite
AMTRAK NEC ... Aberdeen, MD MP 58.7	1978	Tangent	Mixed freight to 70mph; AMTRAK to 110mph	20MG/yr; 70MG/yr to date	140# RE CWR	8"6" prestressed concrete at 24"	1 type of elastic clip; 1 type of pad	Area #24 trap rock
C&O Luraine, VA MP 11.6	1974	3° curve	Mixed freight unit coal trains 43mph	30MG/yr; 220MG/yr to date	122# CWR	8"6" and 9" prestressed concrete at 25"	2 types of elastic clips; 2 types of pads	Area #4 granite (embank)
NSW Kunda, VA MP 261	1974	Tangent	Unit coal trains 45mph	50-60 MG/yr; 260MG/yr to date	132# RE CWR	8"6" and 9" prestressed concrete at 24" and 26"	1 type of elastic clips; 2 types of pads	Area #3 granite

The analysis compared performance at the revenue service sites to the performance of concrete and wood tie track in Section 22 and concrete tie track in Section 17 at FAST. The FAST locations are shown in Figure 1 along with the track configuration. The speed at FAST is generally in the range of 40-45 mph (18-20 m/s), with 2 in. (50 mm) underbalanced conditions in the curves. The exception to this is a 5 degree curve in Section 17 where in the counterclockwise direction the consist speed at times drops to 25 mph (11 m/s).

In general, the test sites contained prestressed monoblock concrete ties of equivalent length and strength to those being tested at FAST. Bending strength in the rail seat region of the ties exceeded 300 kip-in. (34 kNm) in most cases, which conforms to the American Railway Engineering Association requirements for ties at 30 in. (760 mm) spacings even



The Fast Track

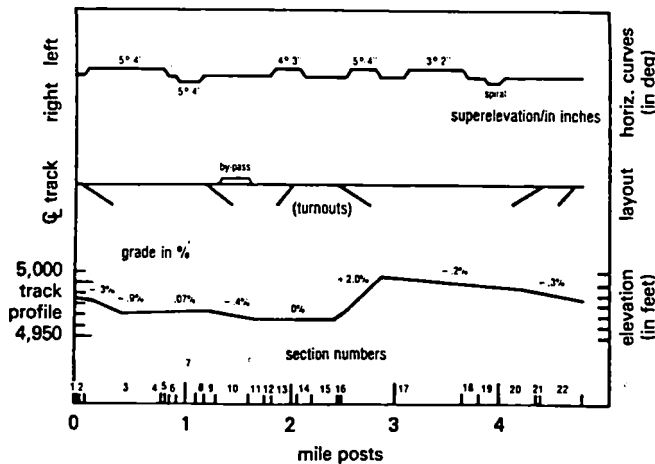


Fig.1 Diagram of the FAST track

though the ties were at 24 in. (610 mm) to 26 in. (660 mm) spacings. The fastener clips and pads were generally similar to those at FAST. The ballast and subgrade types and conditions were different at each site as were the traffic density and mix, and the track construction. This tended, through careful analyses of the data, to improve the correlation analysis by providing a broader spectrum of service conditions to compare with FAST results.

At Leeds (near Streator, IL.) on the Atchison, Topeka and Santa Fe Railway Company an additional wood tie test zone was evaluated and compared to the concrete tie test zone. The primary comparison of wood and concrete tie track was through ballast and subgrade evaluation, and settlement. Both test sections were on one track assuring the same traffic.

TEST DESCRIPTION

To understand the relationships between FAST and revenue service, extensive data were collected and analyzed. These data on track performance were broken down into three basic groups as follows:

1. Primary performance measures of geometry and component degradation
2. Governing structural characteristics: vertical and lateral track stiffness, transfer function of the pads, subgrade moisture content, subgrade elastic and plastic limits, ballast degradation and general ballast condition
3. Loading and load response: wheel/rail loads, tie strains, and ballast strains.

The specific data requirements are summarized in Table 2. The test was structured to compare these data and similar data from FAST and to determine the applicability of FAST tests to revenue service.

This paper emphasizes two aspects of the results of the analyses: (1) the load and loading response, and (2) the track settlement, which are the most important indices in comparing FAST with revenue service.

Table 2. Summary of performance and data requirements

Primary Performance Measures

- A. Tie, Fastener/Pad/Insulator Inspections, (e.g., tie crack summaries)
- B. Survey-to-Benchmark, lateral, vertical settlement
- C. Maintenance Record from the Railroad
- D. Tonnage Accumulation

Governing Structural Characteristics

- A. Vertical Track Modulus
- B. Lateral Track Stiffness
- C. Ballast Density and Gradation
- D. Ballast and Subgrade Material Properties
- E. Ballast Bearing Strength/Stiffness
- F. Subgrade Penetration Resistance
- G. Material Stress-Strain Properties
- H. Moisture Content

Loading and Load Response

- A. Vertical and Lateral Loads and Consist Definitions
- B. Tie Strains
- C. Rail/Tie Accelerations
- D. Ballast Strains

DISCUSSION

Tie Cracking

Visual inspection for cracks has been a standard procedure for determining the condition of concrete ties. Flexural cracks in the rail seat region as well as in the tie center are generally an indication of tie loading greater than design loads. Other types of cracks may be related to factors such as manufacturing defects or dragging equipment impacts. Of particular interest in this discussion are the transverse rail seat cracks which generally range from 1 to 6 in. (25 to 150 mm) long extending from the bottom surface of the tie as shown in Figure 2. In more advanced cases, ties can have cracks extending up to the top surface after branching out toward the fastener shoulders on either side of the rail seat.

In June, 1980 while data were being acquired at the Aberdeen test site, an improved technique was used to aid in visually inspecting for cracks in the concrete ties. Using this technique, cracks were made visible which would not previously have been detected. The results of the visual inspection

CONCRETE TIE

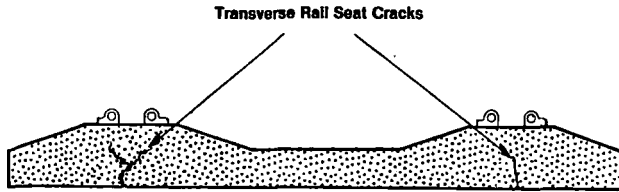


Fig. 2 Concrete tie transverse rail seat cracks

showed that over 70 percent of the rail seats were cracked after only 35 million gross tons (MGT) of total traffic. Using this technique at the other sites allowed for a consistent set of statistics which revealed considerably more cracked ties than was previously anticipated considering that the results from FAST had shown no rail seat cracks after 450 MGT. A summary of the most recent inspections at each site is shown in Table 3. Note that at Aberdeen, the percentage of cracked rail seats increased to over 90 percent after an additional year of traffic (about 25 MGT).

Table 3. Summary of tie inspections

Location	Number Inspected	Number Cracked	Percent Cracked	MGT	Traffic Loads
FAST	600	0	0	425	Heavy; no flats
Streator	80	11	14	125	Medium; moderate flats
Richmond ...	80	44	55	220	Heavy; moderate to severe flats
Aberdeen	60	56	93	60	Light, medium; high speed flats
Roanoke	48	48	100	260	Heavy; severe flats

While no crack on any tie inspected had progressed to the point where the tie was no longer functional, the history of concrete tie performance in this country indicates that these types of cracks will considerably shorten the 50-year life expectancy of the tie. As can be seen by the brief description of the traffic loads in Table 3, severe flats on freights and wheel irregularities on high-speed passenger trains correlate well with the occurrence of cracked ties. At FAST, where wheels are maintained in very good conditions no cracks were observed in any of 600 ties inspected even though the nominal wheel loads are higher at FAST than at any other location.

Track Loading

Figure 3 is a summary plot of dynamic wheel loads measured at each of the four revenue sites and at FAST. Of particular importance are two regions of the curve. The middle range of the percent level exceeded (50 being the median value) shows that the

nominal traffic loads at each site are uniquely different. This can be explained by direct observation of the types of vehicles at each of these test sites. For example, Santa Fe predominantly carries trailers and containers on flat cars, both loaded and empty, and some mixed freight, with only an occasional car loaded to the maximum 100-ton capacity. This produces the lowest wheel load spectrum of any of the sites. The Chessie System runs loaded, unit trains in one direction and empty, unit trains returning in the opposite direction thus producing two separate populations, with a small population of mixed freights filling in the middle of the two load ranges. At the other extreme, FAST traffic is nearly all loaded, 100-ton cars, and the Norfolk and Western Railway Company (N&W) operates unit coal trains loaded to 70, 85, and 100-ton capacities.

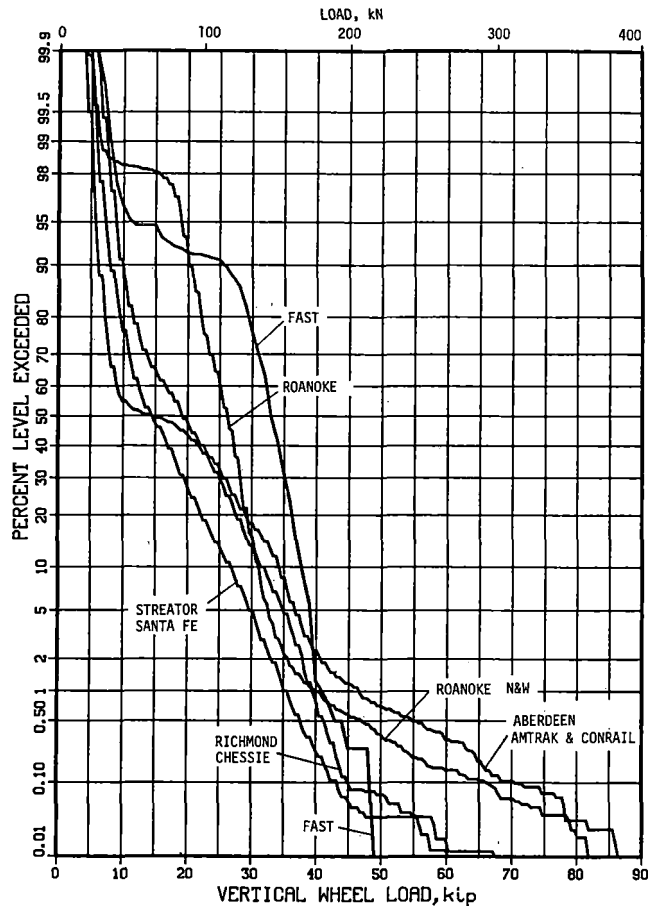


Fig. 3 Summary plot of dynamic wheel loads at all sites

As shown in Figure 4, detailed evaluation of train consists acquired for the same period that dynamic data were taken reveal a very close match between the gross loads tabulated by the railroads and the corresponding dynamic loads measured at the test site; at least over some 90 to 95 percent of the entire population of vehicles. However, the lower portion of Figures 3 and 4 show in each fleet a small but important population of wheels having irregularities including spalled and eccentric profiles, and slid flats. At most sites these irregular wheels

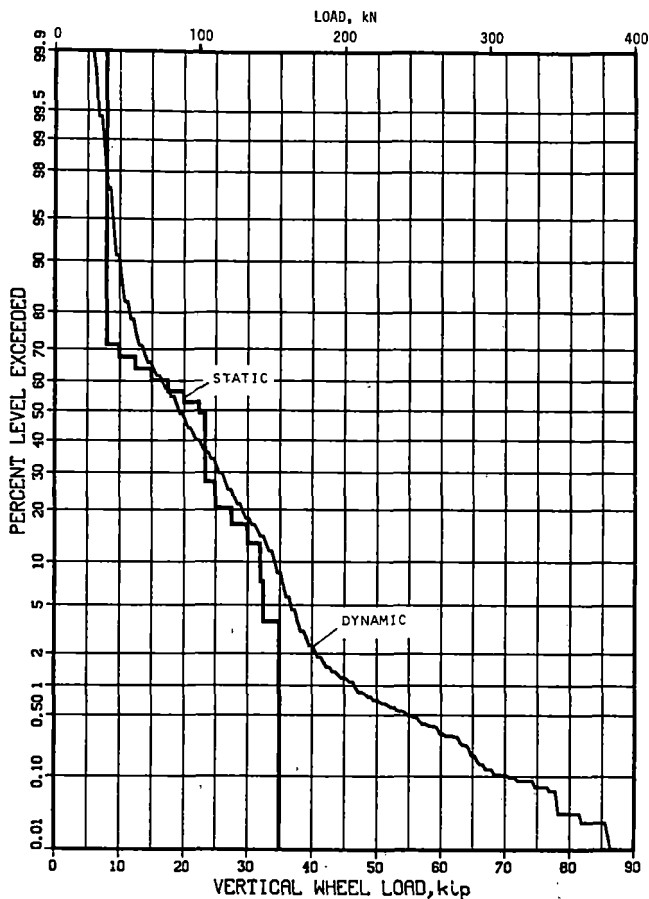


Fig. 4 Combined passenger and freight static and dynamic wheel loads at Aberdeen (Amtrak and Conrail)

constitute 0.1 to 5 percent of the entire axle population rolling over a single narrow zone on the track. Because wheel circumferences are on the order of 10 ft (3 m) and wheel loads were measured only over a 10- or 12-in. (250-300 mm) zone, the actual population of wheel irregularities can be assumed to be about 10 times greater. Well-maintained wheels such as those at FAST can generate loads up to 1.5 times their static weight on smooth, tangent track, while poorer wheel conditions can produce loads between 3 and 5 times their static weight! [Although well beyond the linear range of the data system, single events have been estimated at greater than 125 kips (550 kN).]

Tie Loading Response

Tie responses to wheel/rail loads were measured with full-bridge strain coupons developed for this program. Each of seven instrumented ties randomly selected at each test site, were gaged at one rail seat and at the tie center. Although it was originally assumed that a 300 Hz data bandwidth was sufficient to characterize the bending moments, a detailed examination of the dynamic response of the ties at Aberdeen, at the maximum recorded bandwidth (2000 Hz) showed that data must be analyzed to bandwidths near 1200 Hz to achieve 95 percent of the "true" strain amplitudes experienced in the ties.

The resulting rail seat bending strains are shown in Figure 5 and it can be seen that they are strongly dependent on the corresponding load spectrum

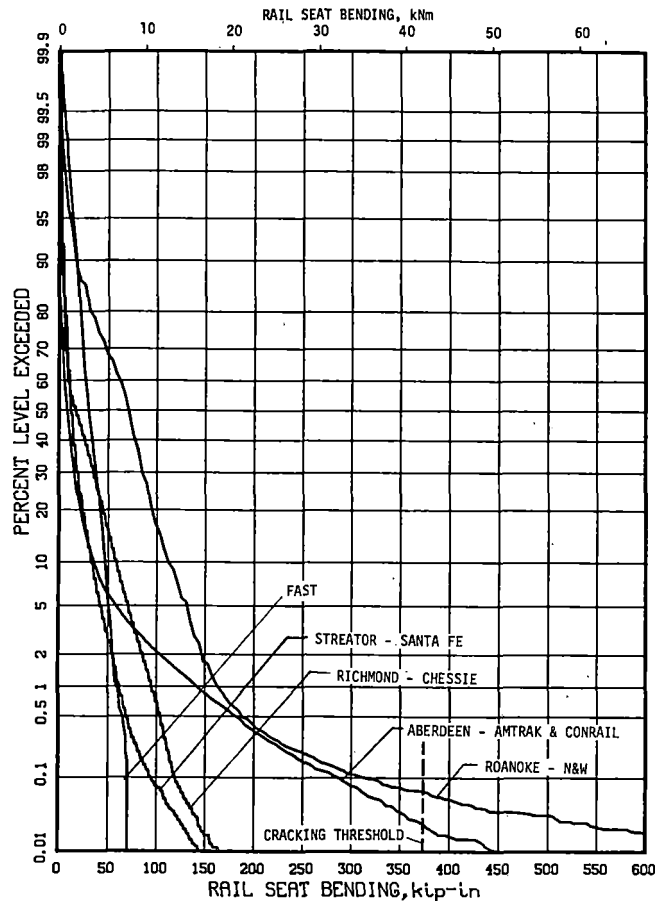


Fig. 5 Summary of tie bending at all sites

shown in Figure 3, particularly at the higher bending load levels. At the bottom of the plot, the 0.01-percent levels of rail seat bending moment are almost directly related to the percentage of ties cracked as shown in Table 3. In general, the higher the percentage of cracked ties, the longer the cracks. The most severe cracks were found on the ties at the Roanoke test site, probably due in part to having about four times as much traffic accumulated as at Aberdeen.

The nominal cracking strength of most ties in the rail seat region is about 375 kip-in. (42 kNm) which is well above the 300 kip-in. (34 kNm) static requirement for ties designed to the AREA specification. This cracking strength is exceeded at Aberdeen once every 1 or 2 days at any one tie location and at Roanoke about five times per day. If Figure 5 were expanded to the lower probability, higher bending loads, it would be obvious that even at the other revenue sites that the cracking limit would be exceeded eventually at each tie location. Wheel inspection techniques and the maintenance programs on each railroad will determine at what point on this otherwise ever-expanding scale that the curve becomes truncated. At FAST where every wheel is frequently inspected and maintained to a high degree, the curve can be seen to truncate at or about the 0.1-percent level (this is larger than the whole population at FAST). Although similar, heavy-haul traffic exists on Chessie and N&W, the data indicate a difference in wheel conditions on these two railroads.

Data analyzed at Aberdeen were separated into freight and passenger categories as well as by speed bands. That highest loads and bending moments were caused by passenger coach equipment at speeds above 80 mph (36 m/s), indicate a speed effect above the 70-80 mph (32-36 m/s) region. Compared to this, no significant speed effects were observed within the nominal speed ranges for freight traffic at any of the test sites.

Track Stiffness

A series of physical measurements were taken at each of the test sites as well as at FAST (FAST data were acquired through FAST operations). Vertical track stiffness measurements were made during the initial site visits, and where possible, both before and after surfacing.

Vertical track stiffness was measured by loading both rails at one tie with a hydraulic jack system suspended beneath a loaded hopper car. Resulting deflections were measured with a surveyor's theodolite, sighted on a machinist's scale attached to the rail directly beneath the applied load. Figure 6 is a summary of the mean track vertical deflection to the point load application as determined by averaging the responses of 7 to 10 locations at each revenue test site, and by periodic measurements at one location at each test zone in FAST Section 22. Note that the consolidated stiffness of

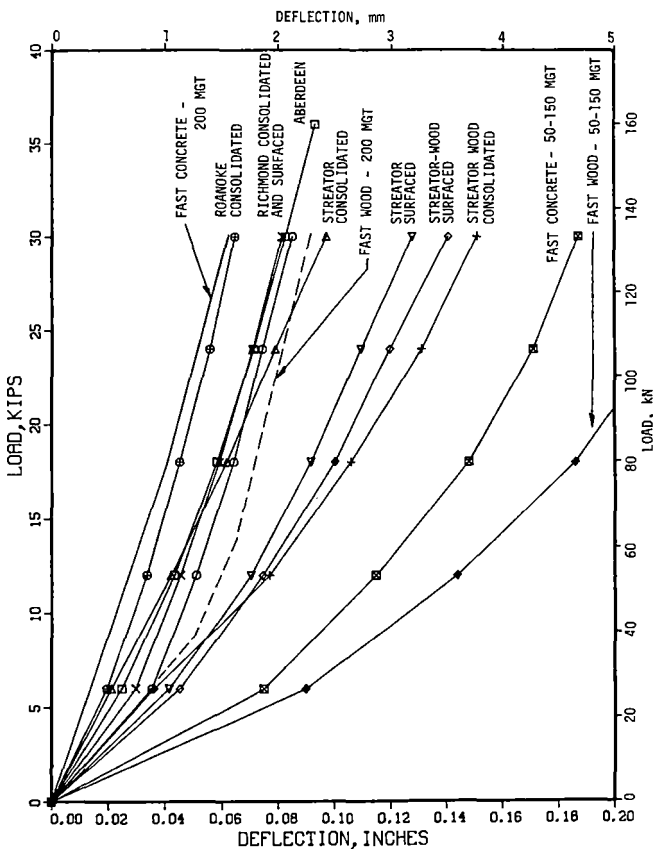


Fig. 6 Summary of track stiffness at all sites

the four revenue concrete tie test sections all fall in a small range of values to the left of the plot. The stiffness of the freshly-surfaced concrete tie track at Streator as well as the wood tie section at Streator both show more "slack action" at lower load levels resulting in overall lower secant stiffnesses;

about one-half of that of the consolidated concrete tie sections. The average of the 50,100, and 150 MGT concrete- and wood-tie values from FAST do not appear to fit the same patterns of secant stiffness that were acquired at 200 MGT or at the revenue sites. The large variation in the two sets of data from FAST would indicate that the technique of selecting single ties for stiffness measurements will not guarantee average results.

Two observations can be made from evaluating the results of the revenue sites.

(1) The tangent stiffness at maximum nominal wheel loads for a given track would not be substantially altered by surfacing, which indicates that this stiffness is controlled by the portion of the track structure remaining consolidated. However, the secant stiffness, which is influenced strongly by the amount of free play directly beneath the tie, will be adversely affected by the loss of consolidation generated by surfacing, and

(2) as shown in Figure 7, the variability of track stiffness is strongly influenced by surfacing. That is, thoroughly consolidated track will generally show a very low variation of stiffness from one location to another. Whereas freshly surfaced track will show a large variation in support from one tie to the next. This variability of support will contribute to an immediate deterioration in the initial surface established by the tamping operation as the track begins to settle.

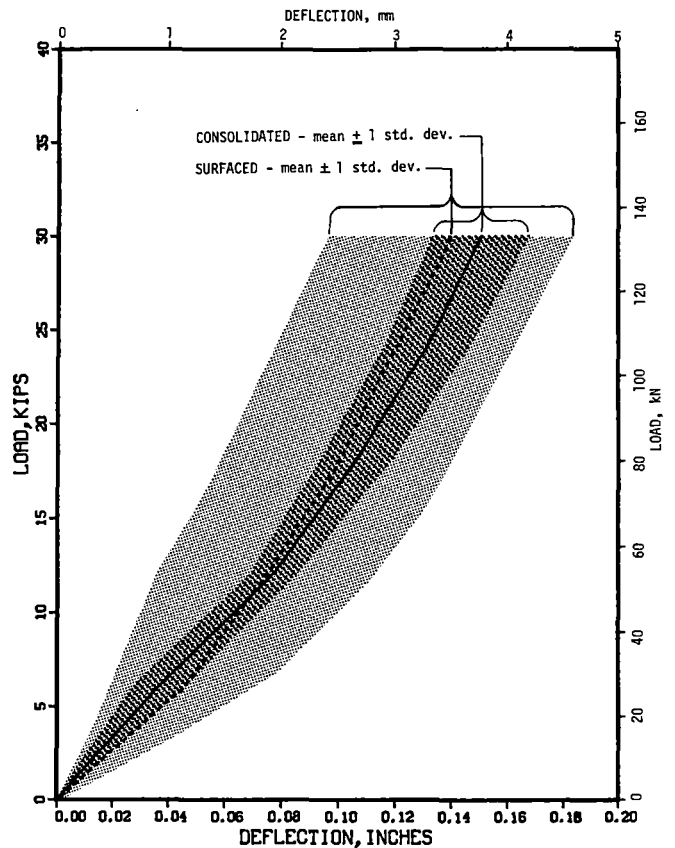


Fig. 7 Track vertical response to point load application at Streator-Wood

Track Settlement

Survey-to-benchmark measurements were taken at each site then continued at 6-month intervals for two

years. These measurements were made at 10 ft (3 m) intervals over spans of track between 450 and 600 ft (137-183 m) long. The surface of each rail, the corresponding cross level, and the alignment of one rail were all measured at each site. The absolute space curves were then processed to eliminate overall curvature and grade effects so that the nominal roughness and settlement could be seen more easily in graphical plots. Ten-foot (3 m) intervals were considered sufficient to develop characteristic roughness, considering that these sites did not have any anomalies in running surface caused by bolted joints or special track work. Comparing the data at different visits allowed both qualitative and quantitative evaluations of settlement performance. Of particular interest was the absolute settlement and whether or not there was a underlying relationship between increased roughness as a function of absolute settlement or tonnage accumulated over the site.

As an example of the survey-to-benchmark data, Figure 8 shows the absolute surface of one rail in the concrete tie test zone in Section 22 at FAST (corrected for average grade). The uppermost curve is the baseline after surfacing (at 93.2 MGT). Subsequent surveys were made at the intervals since surfacing noted on the right. The lower family of curves represent the net settlement relative to the baseline for each measurement. Visually, there is a subtle increase in roughness particularly at discrete locations such as the "hard spot" at station +100. Statistically, these rough spots do not correlate strongly with absolute settlement even when examined at the 5-percent exceedance level; the limit of practicality for the small population of values acquired at each site. It must be emphasized, however, that these data were collected over deliberately-chosen, homogeneous sections of track containing no obvious anomalies such as joints, engine burns, grade crossings, or culverts.

roughness is primarily driven by discrete anomalies within the track structure, either in terms of local imperfections in the running surface or abrupt changes in stiffness or strength within the track structure. None of these anomalies were observed within the chosen test sites, except at the ends of the concrete sections where the track stiffness changes caused some transients in the running surface to develop.

Figure 9 is a summary plot of mean settlement at each test site beginning with a survey made as close as practical to the moment that the site was freshly surfaced. Instances when it was not possible to get an initial space curve immediately upon completion of surfacing, required estimating the initial settlement occurring under the first trains passing over the test site. However, of more importance are the resulting characteristic settlement rates of each of the sites once the initial consolidation of the upper ballast layer has occurred. As Figure 9 shows, all sites tended to follow one of two general ranges of settlement rates: a very low settlement rate on the order of 500 MGT/in. (20 MGT/mm) at the one extreme and as high as 38 to 40 MGT/in. (1.5-1.6 MGT/mm) at the other. At three of the sections surveyed: Streator-concrete, Streator-wood, and Aberdeen, some form of seasonal effect seemed to be causing accelerated settlements during the winter and early spring. Moisture levels measured at the base of the ballast section as well as rainfall statistics do not seem to correlate with this seasonal effect. This effect may be associated with either freeze/thaw cycles or perhaps to an increased track modulus when the ballast is frozen causing higher pressures in the ballast and subgrade. There was no indication of a similar effect at Richmond which does not have heavy frost or FAST where moisture levels are low.

Two wood tie test sections at FAST and at Streator were surveyed along with the concrete tie

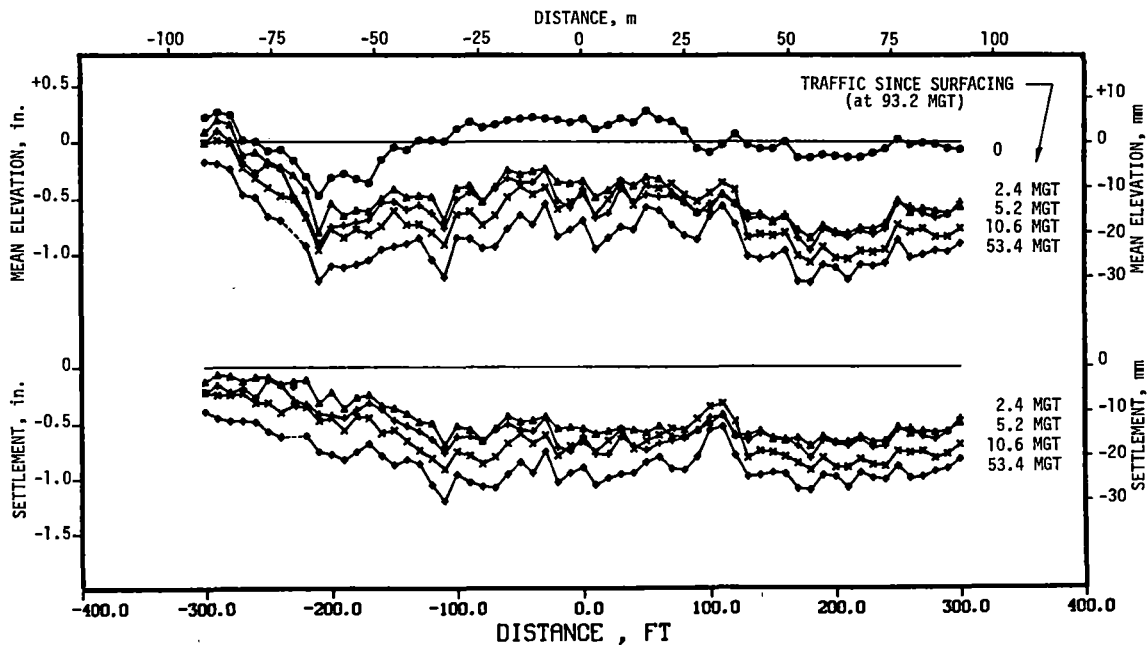


Fig. 8 Settlement of concrete tie test zone in Section 22, FAST.

Overall, track geometry was also sufficiently smooth to minimize any vehicle dynamics which otherwise might cause fluctuating loads. These results tend to confirm the observations that relative track

sections to compare the relative performance of wood and concrete ties. At FAST, in Section 22, wood and concrete ties were built upon identical roadbeds and identical ballast beds, built and maintained at the

same times and with common procedures. By contrast, the Streator test sites consisted of newly-built (1974) concrete tie track including about 12 inches (30 mm) of fresh Georgia granite below the bottom of the tie and a wood tie control section with an old, 8-in. (200 mm) ballast bed of small, thoroughly

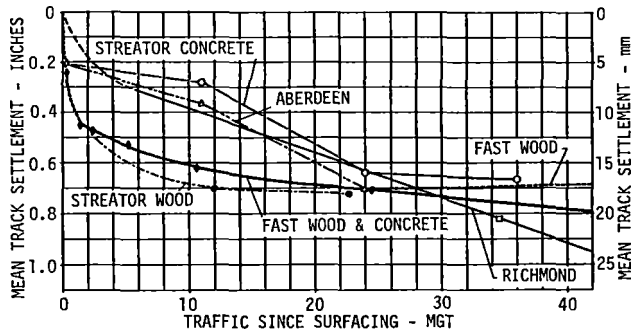


Fig. 9 Summary of mean track settlement

fouled material representing mature, mainline track with the expected mix of new and old ties with random lengths and support conditions. The results of these two site comparisons show that when constructed under identical conditions that wood ties at the traditional 19-1/2 in. (495 mm) spacing and concrete ties at the currently excepted 24-in. (610 mm) spacing produce almost identical settlement rates and comparable degrees of track roughness. By contrast, there was a slight advantage in quality of surface and line of the concrete test section over the adjacent control wood tie section at Streator. This may be attributed primarily to differences in the ballast sections and possibly, tie condition. One clear advantage that the concrete ties have over the wood ties is their ability to maintain a very accurate and consistent gage as seen in Figure 10.

CONCLUSIONS

FAST Versus Revenue Service

- The FAST track has larger mean loads than the revenue sites with significantly lower maximum loads than most sites.
- Concrete tie performance evaluation is not accelerated because the maximum loads are lower.
- The results from FAST show that the removal of flat wheels from revenue service traffic would significantly increase the performance of concrete ties.
- The relatively new track construction at FAST is not representative of track conditions normally found in revenue service except where major reconstruction accompanies the installation of concrete ties.

Wood Versus Concrete

- No significant difference in settlement or roughness was observed at FAST.
- Slightly poorer performance of the wood tie track at Streator may be attributed to ballast condition and wood ties of varying condition.
- Concrete tie flexural cracking is caused primarily by poor wheel conditions (speed and tie pad flexibility have been shown to alter the severity).
- With rigid pads, concrete ties designed for 300 kip-in. (34 kNm) bending moments and used on 24-in. (610 mm) centers cannot endure all revenue wheel conditions without cracking (in all probability, these poor wheel conditions also cause considerable damage to rolling stock and may contribute to plate cutting on wood ties).

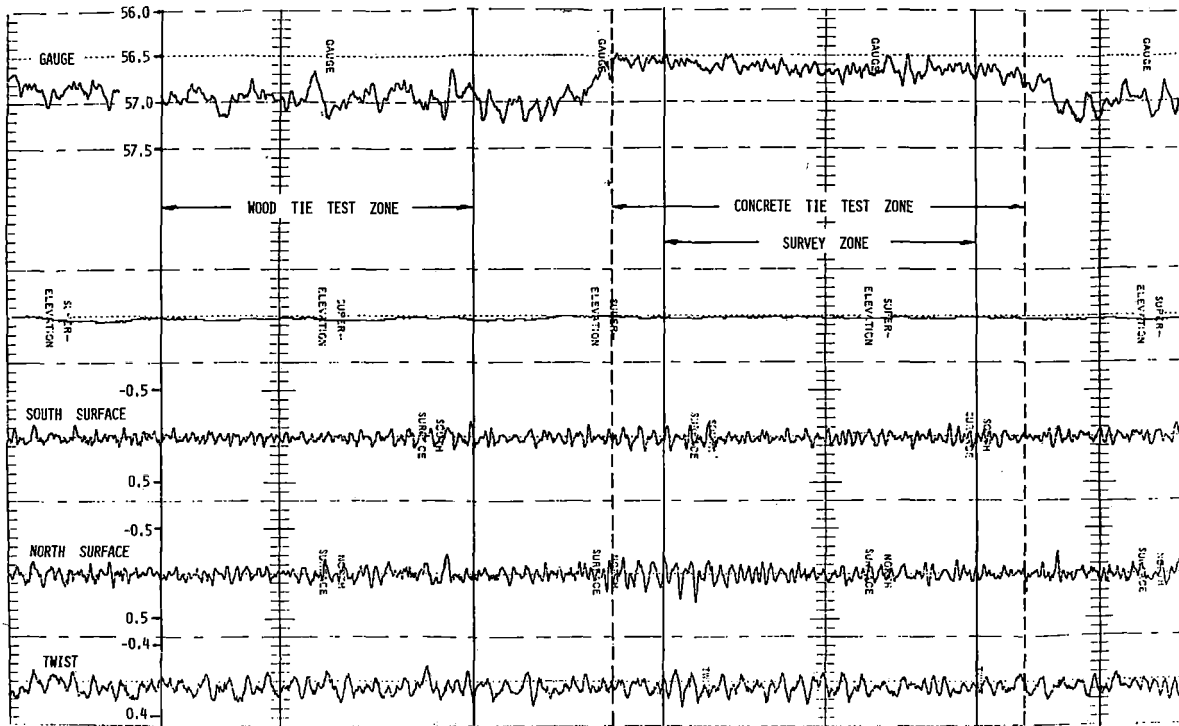


Fig. 10 Track geometry at Streator (Leeds) wood and concrete tie test sites.

Fastener Performance in Concrete and Wood Tie Track

Howard G. Moody

Program Manager
Federal Railroad
Administration

L.E. Daniels

Principal Engineer
Boeing Services
International, Inc.

Premature failure of wood ties and increasing problems in maintaining track gage, have in recent years led railroads and railroad researchers to investigate replacing the cut spike with alternative fastening systems. Included in these fastening systems are concrete tie systems, as well as alternative wood tie fastener systems. Several of these systems have been tested on wood and concrete tie track at the Facility for Accelerated Service Testing (FAST). Data will be presented to show the reasons for using the alternative fasteners and to compare them with the wood tie spike system. Concrete tie fastener performance will also be discussed. Comparing these tests with laboratory tests will show the need for a laboratory test specification that replicates field conditions. Studies used to develop this paper show that alternative fastening systems need better design to handle the traffic conditions on North American Railroads.

DESCRIPTION

FAST is a test track at the Transportation Test Center in Pueblo, Colorado. The FAST objective is to accelerate the life cycle of track and mechanical components so that in a period of time one fifth to one tenth of revenue service applications component evaluations can be made. To accomplish this a 76 car train is operated over a 4.8 mile loop, as shown in Figure 1, for 16 hours a day, five days a week. This consist is primarily composed of loaded 100 ton hopper cars. In one night's operation, over one Million Gross Tons (MGT) of traffic are accumulated on the track (1). Since the beginning of the test in September 1976, there have been 630 MGT of traffic.

The concrete tie fastener tests are in Section 17 and the wood tie fastener tests are in Section 7. As shown in Figure 1, Section 17 consists of several track configurations, including a tangent, a 3° curve, and spirals into and out of the curves. The area of primary interest is the 5° curve which is on a 2% grade. Section 7 is a 5° curve but it is only .07% grade. The average train speed in both sections is 40-45 mph with 2" over balanced conditions, except when the consist is operating in the counter-clockwise direction in Section 17. In that mode the train speed can be as low as 25 mph.

In the 5° curve of Section 17, there have been only two major tests, one from zero to 425 MGT and the other from 425 MGT to the present (about 630 MGT) (2). In a few instances entire lots of fasteners have been changed out because of track maintenance problems or unsatisfactory fastener performance.

In Section 7, there have been three major component

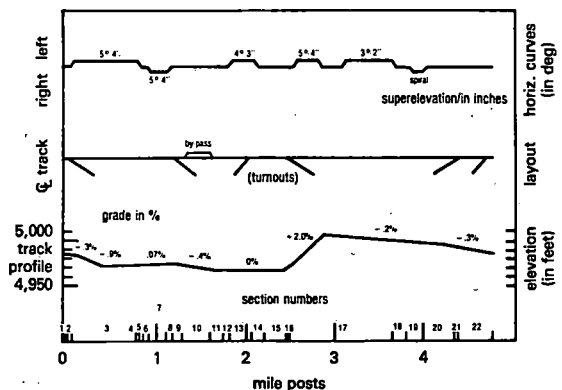
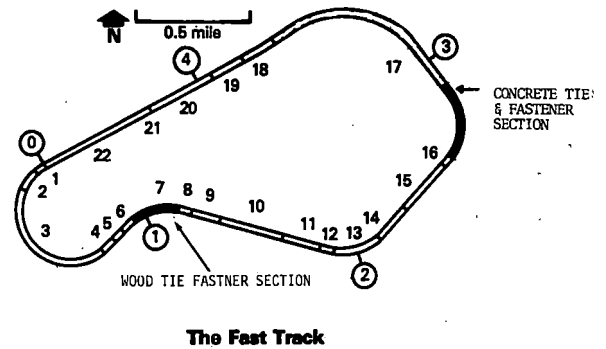


FIGURE 1. DIAGRAM OF THE FAST TRACK.

tests to date (2). As was the case in Section 17, two early tests were terminated because of track maintenance problems and fastener performance problems. The third test on this series has proven to be a much more significant test of fastener performance. The results of this test are still incomplete, but an interim evaluation has provided valuable information on the use of alternative wood tie fasteners.

TEST ENVIRONMENT

The test environment consists of the track configuration, the track geometry (generally held to FRA Class 5), and the wheel/rail loads. The wheel/rail loads in vertical and lateral planes are the primary determinant of component performance and characterize the test at FAST when comparing performance against other tests in revenue service and in the laboratory.

The wheel/rail loads at FAST are different for each curve. In Section 17, 5° curve the largest vertical loads and the highest mean vertical load are on the high rail. The highest lateral loads, however, are in the low rail. The vertical and lateral loads probability distributions are shown in Figures 2a and 2b. The occurrence of high lateral loads on the low rail is due largely to the position of the vertical load on the rail head. There is no flanging on the low rail. With increasing tonnage the low rail head begins to flatten which accentuates the lateral load. The maximum lateral load is about 24 kips which is enough with most of the fasteners used in the 5° curve to cause substantial fastener fallouts and fractures. About 80% of all clip fallouts and fractures were on the low rail gage side.

In Section 7, however, the more severe environment was on the high rail. In Figure 3, data for both the vertical and lateral loads are shown for Section 7, and several revenue service sites. These include data taken on low speed branch line track on the Chessie and main line track on the Western Pacific, Union Pacific and Canadian National Railroads. It is abundantly evident that although the vertical loadings at FAST are considerably higher than those in revenue service, the lateral loadings are not. As can be seen in Figure 4, a plot of L/V ratios, the result of the higher vertical loads at FAST is a lower L/V ratio. The L/V ratio is usually an indicator of the severity of loading and is the essential variable for evaluating fastener load environment.

As previously mentioned, when compared to other revenue service sites, FAST does have higher mean vertical loads but the highest peak vertical loads at the 1% level and above are less (3). These data are shown in Figure 5, a cumulative probability distribution of vertical loads at FAST and four revenue service sites. These four sites are all on concrete ties and all but one on tangent track. The reason for the higher peak vertical loads is wheel irregularities on revenue service.

These high peak vertical loads cause concrete tie cracks. One possible means of attenuating some of these large loads is to use a resilient tie pad with concrete ties. Early concrete ties in North America almost exclusively used rigid tie pads which do not

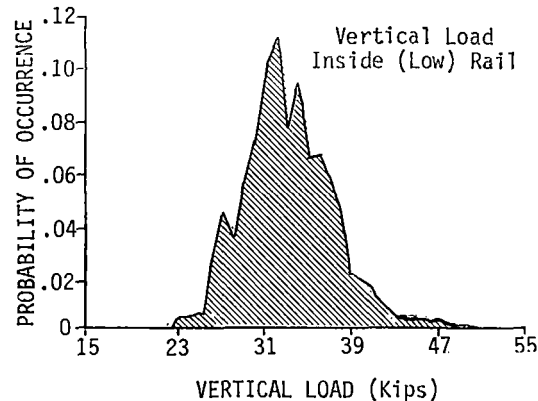
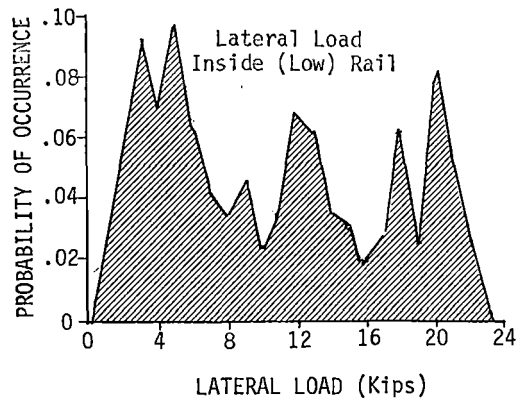


FIGURE 2a. LOAD ENVIRONMENT SECTION 17 LOW RAIL.

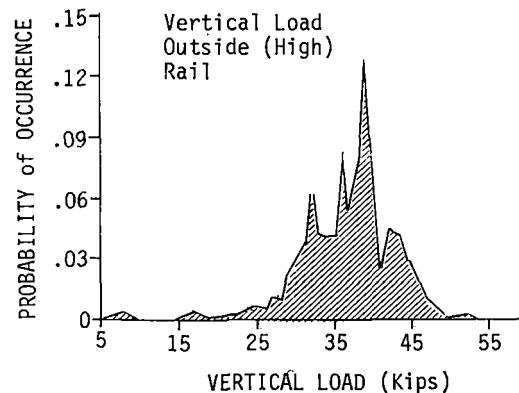
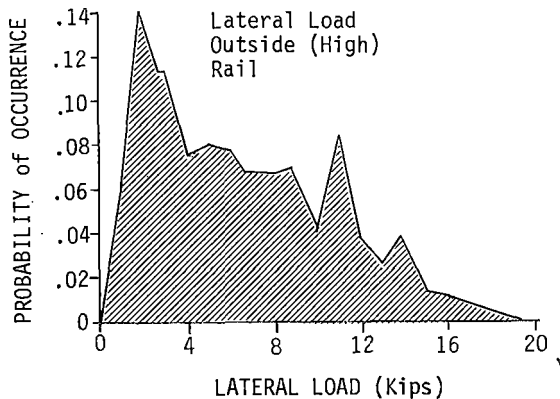


FIGURE 2b. LOAD ENVIRONMENT SECTION 17 HIGH RAIL.

attenuate these large loads well. However, the rigid pads were used in the belief that this reduced fastener clip deflection. This makes the choice of the pad important in concrete tie fastener design. This, as shown later in this paper, was in fact not true. The rigid pad resulted in more clip deflection than the resilient pad.

COMPONENT PERFORMANCE

Previous work by Ahlbeck (4) has shown large force/deflection differences in wood tie track. Typical results are shown in Figure 6, which analytically represent different track fastener types and conditions based on tests on SNCF, British Rail, Transportation Test Center track, and on the branch line track on the Chessie Sytem. Rigid track (very stiff track) is represented by a high lateral stiffness. This results in minimal rail head deflection for very large lateral loads. Representative of this type of track would be concrete ties and fasteners and the alternative systems on wood tie track.

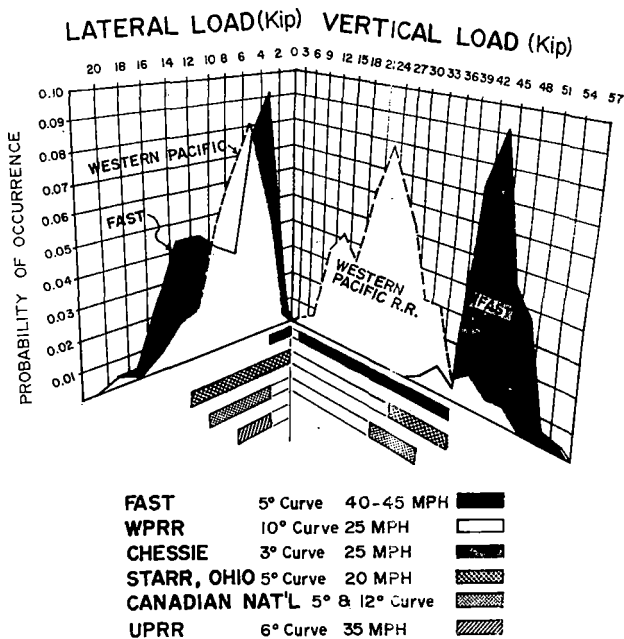


FIGURE 3. LOAD ENVIRONMENT SECTION 7 AND REVENUE SERVICE.

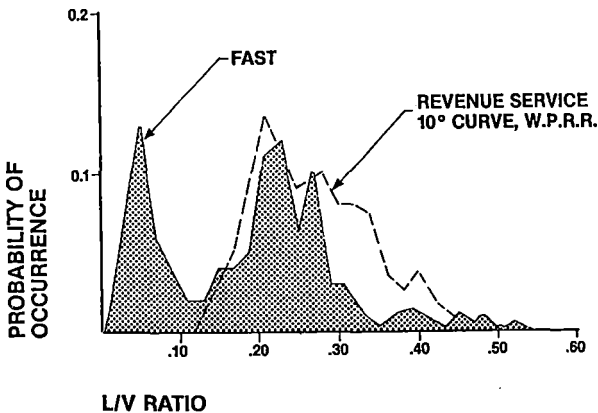


FIGURE 4. L/V RATIO COMPARISON.

Intermediate stiffness is shown as wood tie/cut spike track (new construction). This is very similar to the conditions of the wood tie cut spike segment in Section 7, which is used as a control segment for the alternative fasteners,

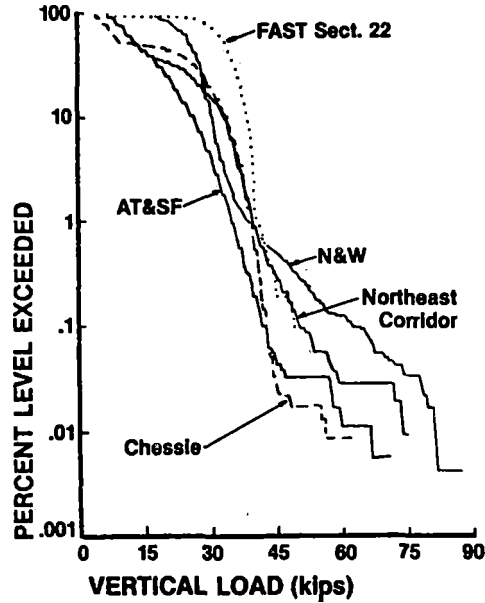


FIGURE 5. FREIGHT TRAFFIC VERTICAL LOAD DISTRIBUTIONS.

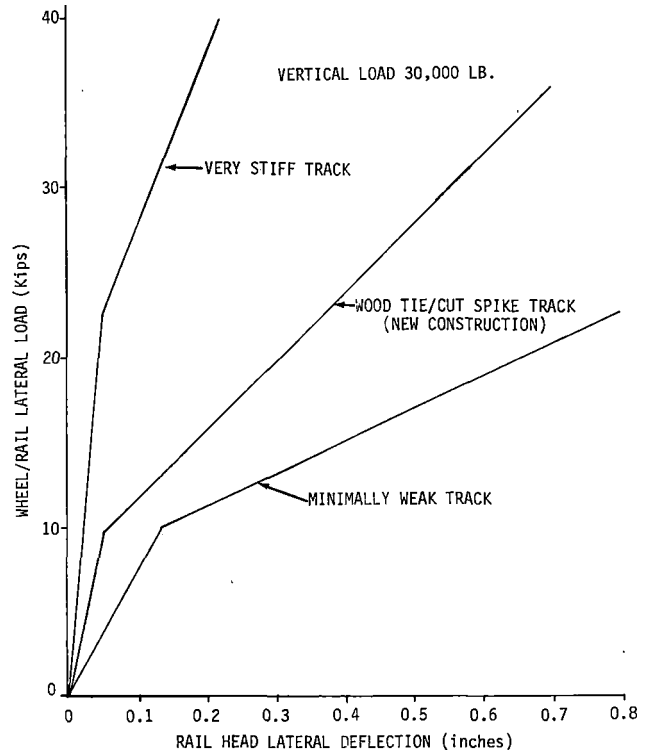


FIGURE 6. LATERAL FORCE/DEFLECTION RESPONSE FOR DIFFERENT LATERAL STIFFNESS.

The third condition, which is represented by minimally weak track, is the type of track which could lead to a wide gage condition. It is this condition which has led railroad engineers to look at alternative fastening systems.

At FAST the wood tie cut spike segment has begun to show some deterioration, but as can be seen in Figure 7, a plot of lateral fastener stiffness, the values at 257 MGT, are no where near those of minimally weak track. Other data from alternative fastening systems show greater lateral restraint as shown in Figure 8. This is expected since the inherent design assumption is high lateral stiffness.

There is one important relationship between the FAST data and the revenue service data. In both cases, the inflection point where the piece wise linear plot changes slope is at a point where the L/V ratio equals .33. This point can be interpreted as the value of the coefficient of friction of the steel tie plate on wood. Consequently, before the lateral spring, which in this case is the cut spike, is engaged, a sizable amount of frictional resistance must be overcome.

In Figure 9, the L/V relationships are shown for FAST and the revenue service site on the Western Pacific Railroad. These data were shown previously in the test environment discussion. FAST does not produce large occurrences of L/V's above .33, as does revenue service for this case.

Ahlbeck (4) in his paper represented the stiffness laterally as both rail head and base stiffness. The FAST data were separated into two categories, rail base deflection as shown in Figures 7 and 8, and rail head minus rail base in Figure 10. The rail head minus rail base or rail rotation adds a linear component to the overall deflection. This deflection should be considered when measuring track dynamic gage.

Because the alternative fasteners, as has been shown are much more rigid than the cut spike system, they allow less dynamic rail excursion. However, as a result, more load is being transmitted into the clip than into the cut spike.

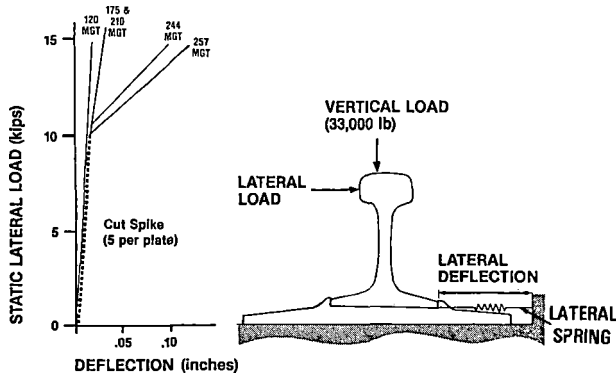


FIGURE 7. LATERAL RAIL BASE FASTENER STIFFNESS OF CUT SPIKES.

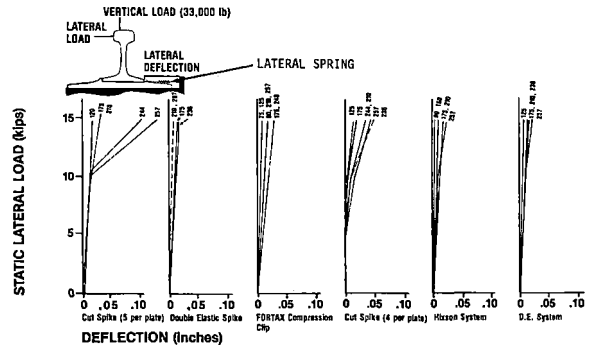


FIGURE 8. LATERAL RAIL BASE FASTENER STIFFNESS OF VARIOUS FASTENERS.

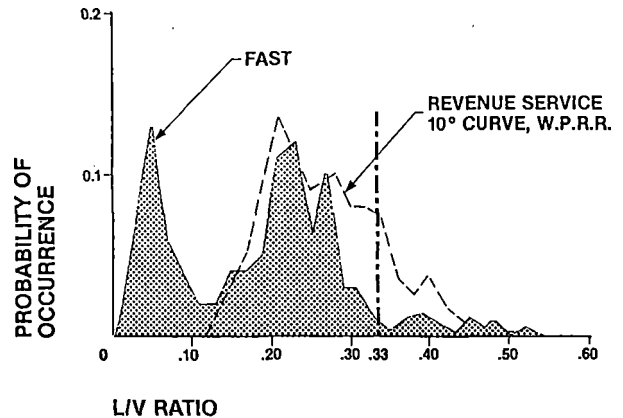


FIGURE 9. L/V RATIO COMPARISON.

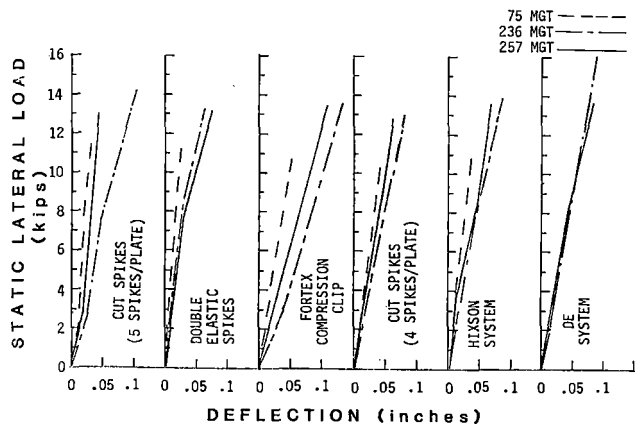


FIGURE 10. RAIL HEAD DEFLECTION, RAIL HEAD MINUS RAIL BASE.

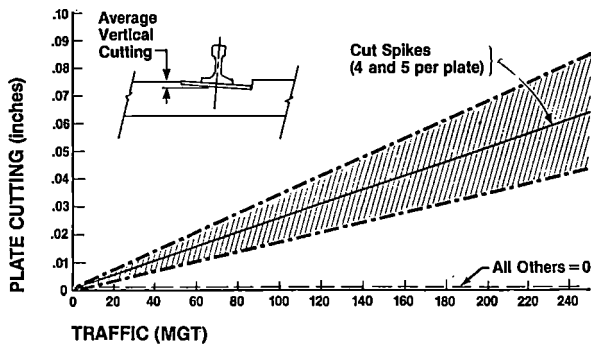
In both concrete and wood tie track component performance of some alternative fastening systems has not been satisfactory. In the wood tie section, there have been considerable difficulties with fastener component damage. Early tests resulted in tie plate failures, clip fallouts, and hold down fastener fractures and fallouts. Performance has been somewhat better in the third test, although component failures as shown in Table 1 have been higher on most of the alternative fasteners than on the cut spike system.

TABLE 1. TOTAL FASTENER FAILURES.
(280 MGT of Service 8.5 Million Load Cycles)

FASTENER SYSTEM	FAILURES*	% SURVIVING
INTMA Double Elastic Spike	None	100%
Cut Spike (4 spikes per plate)	None	100%
Cut Spike (5 spikes per plate)	1 Plate	99+%
D.E. Clip and Plate	3 Clips	Clips99% Plates100%
FORTAX Compression Clip	15 Clips	94%
Hixson Clip and Plate	16 Clips 3 Plates	Clips93% Plates98%

*COMPONENT FAILURE: Complete loss of component function, either from breakage or from slipping free from its mounting.

One other measure of wood tie fastener performance is plate cutting. Plate cutting potentially occurs because of abrasive damage, tie crushing, or decay. Decay, although an issue in revenue service, is not an issue at FAST because of the limited test time and dry environment. Tie crushing also is not an issue because the stress produced by the highest wheel loads does not even approach the compression strength of the wood ties used in this test. It is abrasion, therefore, that is the prime cause of tie plate cutting at FAST. This correlates well with the results as shown in Figure 11 for vertical tie plate cutting. The cut spike fasteners showed some minimal tie plate cutting, whereas, the other fasteners did not. With the increased lateral movement, as shown previously, there is abrasive wear accumulating on the cut spike ties.



NOTE: Hixson Plate and Clip configuration does not permit measurement comparable to other systems.

FIGURE 11. VERTICAL TIE PLATE CUTTING.

In concrete tie track in the 5° curve, fastener performance has been marred by clip fallouts and fractures, as well as pad failures. Prior to these fasteners being introduced into FAST, they were tested, along with the concrete ties using the recommended specification of the American Railway Engineering Association (AREA), "Manual for Railway Engineering," Chapter 10. These tests showed no component failures or performance problems. There appeared to be enough differences between the laboratory (specification) performance and the field performance to warrant an investigation into this relationship.

Rail to tie deflections in all planes on concrete

and wood tie track at FAST were taken to characterize the deflection environment for laboratory tests (5). Measuring the deflections was chosen because it provided a direct one to one relationship from the field to the laboratory. Load information, a possible alternative, would require precise knowledge of the track stiffness which would complicate the process. On wood tie track, the results could be used to initiate a specification rather than modify an existing one as with concrete ties.

Two test sites were selected for Section 17 and Section 7. These sites were selected to be representative of a full range of fastener types. In the concrete tie track, the major difference was in tie pad stiffness and in wood tie track, the difference was in the design of the elastic clip. In one case, the clip attached directly to the tie plate and the other, the clip was driven into the tie. These design variations on concrete ties resulted in differences in fastener response which affected the laboratory tests.

The measurements were taken, as shown schematically in Figure 12, in all three planes of rail to tie movement. The locations of deflection transducers were:

- Vertical deflection at the "field side left" position,
- Vertical deflection at the "field side right" position,
- Vertical deflection at the "gage side left" position,
- Lateral deflection at the rail head,
- Lateral deflection at the rail base, and
- Longitudinal deflection at the field side base.

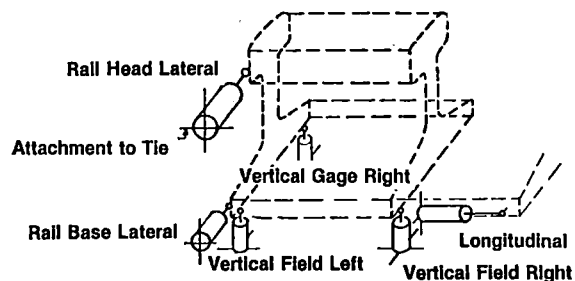


FIGURE 12. POSITIONS OF DISPLACEMENT TRANSDUCERS.

The three vertical deflections combined to determine clip deflection, rail/tie rollover, and rail/tie rocking. The difference on rail head lateral and rail base lateral can also define rollover. Rail base lateral defines lateral excursion. In addition, in one segment in each section, the clips were strain gaged to provide a correlation with the deflection measurements.

Measurements were taken with a consist composed of 20-100 ton loaded cars, and two GP 38 locomotives. Data were taken on both the high and low rail, and

in most cases, in the clockwise and counterclockwise directions. The counterclockwise runs were deleted in the wood tie segments due to time constraints. A minimum of one run was taken at 40-45 mph at each location.

Data from each of the test runs in three locations in each segment were recorded on strip charts. These data provided the following results.

1. The highest clip strain and deflection in Section 17 was produced in the gage side clip on the low rail. This location is also the principal location for clip fallout and fracturing.
2. The highest clip deflections and strains occurred in the counterclockwise train operation on the low rail on Section 17. This can be attributed to train action which results in the gage and field side deflections being in phase during clockwise operation and out of phase in the counterclockwise operation. Consequently, in one case the deflections cancel each other and in the other they are additive.
3. Clip deflections and strain were about 30% greater on the rigid pad which had a spring rate of 5-8 Mlb/in than on the resilient pad which had a spring rate of 1.4 Mlb/in. The location of one of the measurement sites near a weld on the rigid pad may have skewed the results slightly. The two deflection ranges could conservatively be considered to be about equal. This is in contrast to the expected result which would have the greatest deflections occurring on the resilient pad.
4. Clip strain was lower by 50% on the wood tie track compared to concrete tie track even though rail head deflections were similar. This is probably due to the plate bending on the wood ties. The shoulder on the concrete ties is a rigid cast iron insert which would not be expected to deflect when loading.
5. There was less tie rocking with resilient tie pads than with rigid tie pads in the concrete tie section. The deflections from the two vertical field side transducers are about equal with the resilient pad, and substantially different with the rigid pad (this results in tie rocking).
6. In both the concrete wood tie track, there was a distinct difference in the response of the rail on the high and low rails. By looking at the relative amount of motion of the rail and head lateral transducer and the rail base lateral transducer, it can be discerned that flanging occurs on the high rail which produces lateral head and base excursions of nearly the same magnitude, and that rail rocking occurs on the low rail due to the change in the point of contact of the vertical load.
7. In the wood tie segments, there was evidence of considerable plate bending in the

spring clip segment when compared to the elastic clip segment. This is because the spring clip reacts against the tie plate and the elastic clip reacts against the wood tie. Correspondingly, there is more tie rocking in the elastic clips segment where the tie is more rigid.

There are two current concrete tie and fastener specifications in use in the United States. One of these was developed for Amtrak, and the other for the American Railway Engineering Association (6). There is no comparable wood tie fastener specification. The two specifications have several tests which define fastener performance. These tests, as listed below, are not mutually exclusive to one specification or the other.

1. Strength of fastener insert in the tie - Fastener insert test, pullout test and torque test.
2. Pad separation load - Fastening uplift test.
3. Insulation capability of tie and fastener - Electrical impedance test.
4. Fastening resistance to fatigue - Fastening repeated load test and fastening push pull test.
5. Rail longitudinal restraint capability - Fastening longitudinal restraint test.
6. Gage widening resistance - Lateral load restraint test.
7. Pad resistance to permanent set - Tie pad load/deflection test.
8. Fastener set and yield test - Rail clip load - deflection test and toe load test.

Three were selected to be reviewed: fastening repeated load, fastening longitudinal restraint, and lateral load restraint test. These tests were selected because they are direct tests of fastener life cycle performance (7). The other tests are more indirect indicators.

The lateral load restraint test was used to develop appropriate clip strain and rail to tie deflections in the laboratory that would represent the actual field data.

The maximum deflections of the rail head relative to the tie were about .100" from both wood and concrete tie track. Rail tie vertical deflections of the rail clips in the concrete tie sections and the rail clips and tie plates on the wood tie sections were nearly .040" peak to peak in compression and uplift.

The concrete tie lateral restraint test was conducted at several L/V angles from 20 to 30 degrees to the vertical with several pad types. Figure 13 is a schematic of the fixture used in this test. Clip deflections were measured directly from the clip to correct for inconsistencies in interpreting the vertical deflections from the field test. Also, the rail head lateral deflections were measured. Figure 14 shows the results of load application at 20° and 30° angles for a rigid polyethylene pad

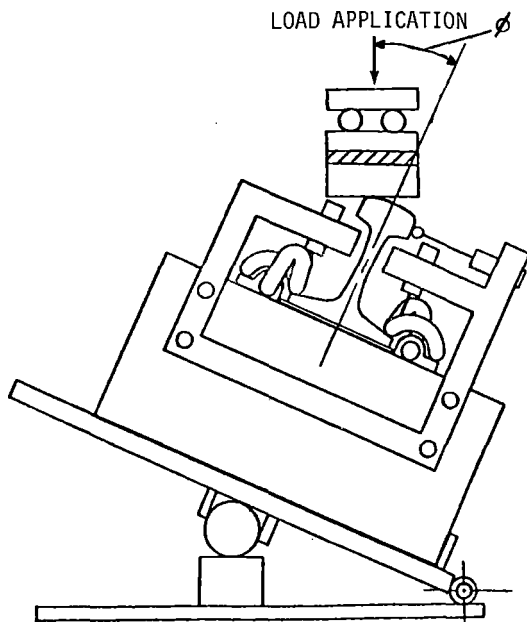


FIGURE 13. LATERAL RESTRAINT LOADING AND MEASUREMENT SCHEMATIC.

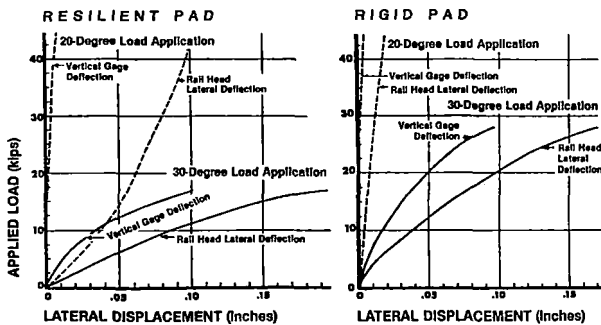


FIGURE 14. RESULTS OF LATERAL RESTRAINT TESTS.

(5.0M-8.0M lb/in spring rate) and a resilient (flexible) neoprene pad (1.4 Mlb/in spring rate) which approximate the spring rate of the two pads in the FAST test segments. Results show that lateral displacement and the corresponding clip displacement are both highly dependent upon the angle of application and the pad spring rate. The AREA specification lateral restraint test is conducted at a 20° angle with a 41,000 lb load applied at the gage corner, and the rail rollover test is conducted at a 30° angle with a 20,500 lb load. The lateral displacement test is designed to determine the shift in the rail base with load. In this case, there was little rail base displacement. Consequently, there was little difference in performance due to pad stiffness. However, there was a substantive difference in the rollover test due to pad stiffness. This bias, in all probability, is not a realistic representation of the actual field test since the effects of load spreading onto adjacent ties is not considered. A more appropriate test might be to calculate the rollover in the fastening

repeated load test.

One of the most significant outputs of this static lateral restraint test showed differences between load applications at a 20° angle and a 30° angle. At a 20° angle, there is only .015 inches of lateral deflection produced by a 30,000 lb load. This is representative of the range of deflection experienced in the field test. At a 30° angle, the deflections were well over .100 inches at the rail head which is more representative of the field test results. The most important laboratory test is the fastener repeated load test. The repeated load test would define fastener component performance and would be applicable for both wood and concrete tie fastening systems.

Even though most concrete tie fastening systems passed the AREA and Amtrak repeated load tests, in severe service conditions such as FAST, component fractures and clip fallouts occurred and often in large numbers. In the AREA specification, a compression and an uplift load are applied at a 20° angle. In the Amtrak test, the load is applied at an 18° angle. As was noted previously, these angles of application did not produce the desired rail deflection as reflected in the field test.

A range of L/V angles from 20 to 27 degrees were tried to produce approximate deflections with a final angle of 24 degrees being selected. To meet the specified deflection goals of .100" rail head deflection and clip uplift deflection range of 0.40" for the gage corner clip by 10 percent, a range of loads was required for each pad type on concrete ties. The rigid pad required 20,000 lbs compression and 2,400 lbs uplift load. The resilient pad required 13,000-16,000 lbs compression and 1,600-2,000 lbs uplift load. The range of loads was required to adjust for seating of components and to maintain the required deflections. Figure 15 shows the loading schematic for the fastener fatigue test for concrete tie fasteners.

At 653,000 cycles of the repeated load test conducted at 2 Hz, the gage corner clip was noticed to be cracked in two locations. These locations as shown in Figure 16 are the same locations where clip fractures had occurred at FAST. However, because the test was being conducted using the maximum deflection values, the failure occurred earlier in the laboratory than at FAST. There were no fatigue failures at FAST with newly installed clips until 1.2 million cycles (40 MGT) in the first experiment.

It was interesting to note that during the 653,000 cycles, the clips begin to work out and had moved about 1/2" prior to the fractures being noticed. This, to some extent, indicates a relationship evident in the field between deflection magnitude and clip fallout.

The wood tie fastener repeated load test, as shown in Figure 17, was conducted using the same fixturing and the wood tie fastener components from Section 7, Segment 6. At 1,090,000 cycles, the tie plate failed in a fashion similar to those at FAST. This time the ratio of simulated cycles in the laboratory to the field was 1/3. There were two interesting physical problems that needed to be overcome in order to properly conduct the test. The tie plate area needed to be adzed slightly so that the deflections produced in the laboratory would closely match

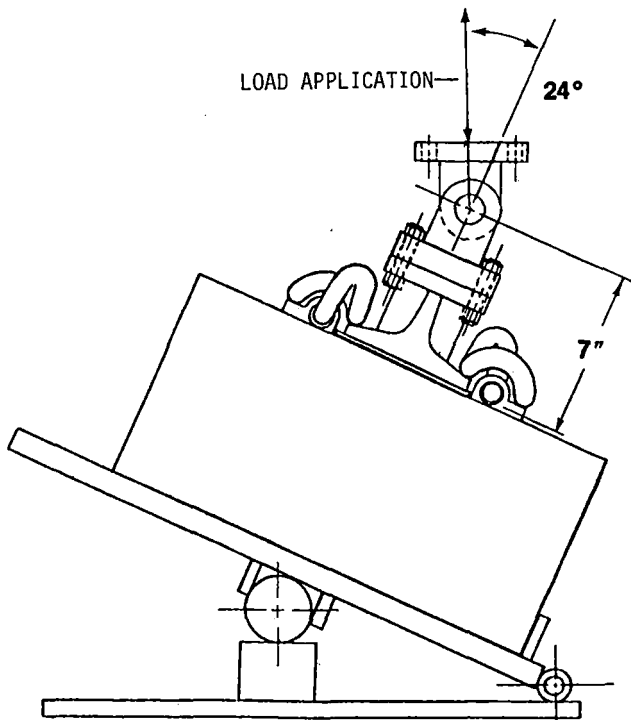


FIGURE 15. LOADING SCHEMATIC FOR CONCRETE TIE FASTENER FATIGUE TEST.

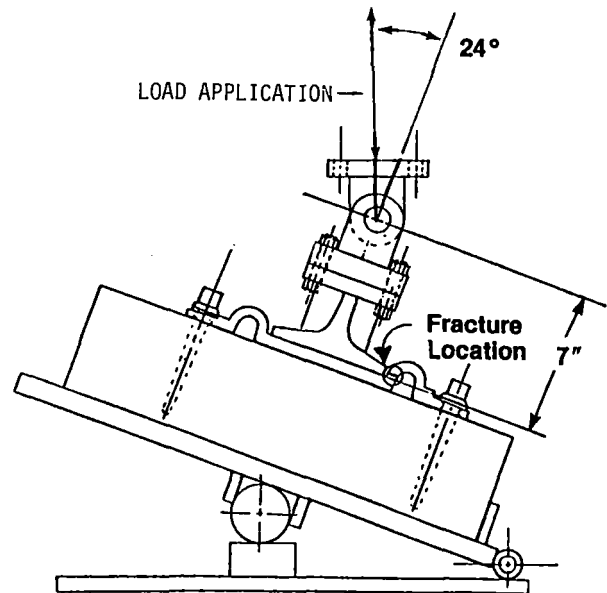


FIGURE 17. WOOD TIE FASTENER FATIGUE TEST SCHEMATIC AND FAILURE.

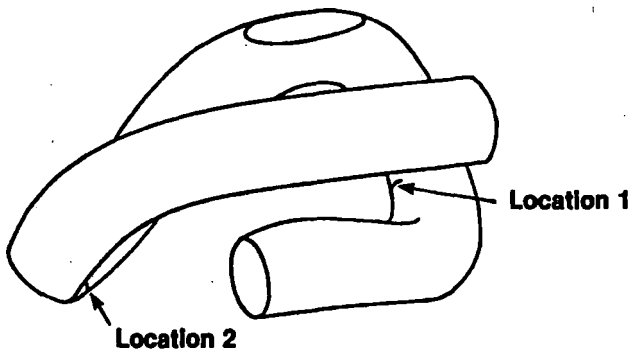


FIGURE 16. CONCRETE TIE FASTENER FATIGUE TEST CLIP CRACKS.

those measured on track. This was a "seating" of the tie plate which occurs in track as a small amount of tie plate cutting. In addition, when conducting the test, it was necessary to constantly tighten the screw spikes to prevent them from working out of the tie. The working out of the screw spike was a frequent occurrence in the FAST track.

Longitudinal restraint tests were also conducted as a part of the laboratory work. There were considerable difficulties encountered during the initial setup which is shown in Figure 18. The fastener clips did not provide consistent toe loads as a results of installation variances. These variations in toe load resulted in a difference of 15% in longitudinal restraint values.

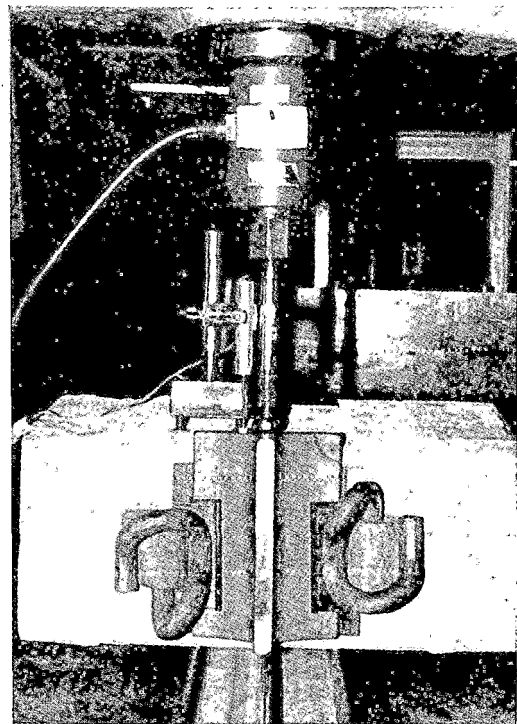


FIGURE 18. LONGITUDINAL RESTRAINT TEST CONCRETE TIE FASTENER.

Consequently, a consistent toe-load was provided by applying a known vertical load through the fixture shown in Figure 19. Even with this fixture, it was necessary to constantly change out the pad and insulators to get repeatable results on concrete tie

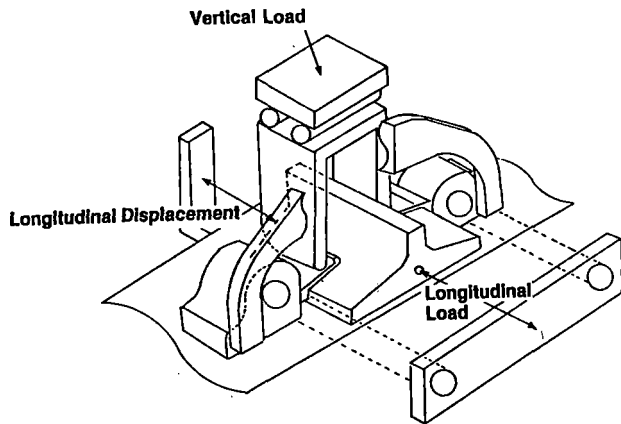


FIGURE 19. MEASUREMENT OF LONGITUDINAL RESTRAINT UNDER CONTROLLED VERTICAL LOAD.

fasteners. These results are shown in Figure 20 which show a large difference in longitudinal restraint, the point at which continuous slip is obtained with different pad types and with and without insulators. In general, resilient pads have higher coefficient of friction (μ) than rigid pads. For wood tie fasteners where there are no pads, slip occurs at a slightly lower load than with the resilient pads because of the lower friction between the rail steel and the steel tie plate. These results are shown in Figure 21.

CONCLUSIONS

The fastening system, whether it is the traditional cut spike and tie plate or the more recent alternative fastening systems that restrain the rail more rigidly, seem to be one of the most critical elements in the railroad track system. Large vertical and lateral loads are transmitted from the rail through the fastener system into the tie. The traditional cut spike has become a marginal fastener on some areas, particularly in curves of over 4° .

Alternative fastening systems have been designed and tested at FAST and in revenue service. There have been many critical problems to overcome, particularly component performance problems. These alternative fasteners on wood ties have resulted in less tie plate cutting and greater lateral strength. However, component failures in these fastening systems have resulted in premature termination of some tests and have cast a shadow over the applicability of these fasteners in revenue service. This is a critical problem since it has been shown that FAST is probably not as severe as one, and possibly many more, revenue service locations. An appropriate laboratory test for these fasteners would help the designer and the railroad engineer in improving upon and selecting fasteners for use in revenue service.

Concrete tie fasteners also need to be improved. One relatively inexpensive and productive means to do so would be to exclusively use a resilient tie pad with concrete ties. In another paper presented at this conference, the need for a resilient pad to help prevent excessive tie cracking has been established. Rail/tie deflections at FAST have shown

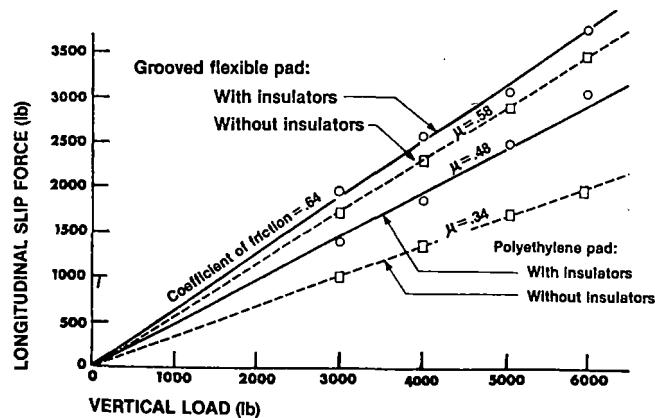


FIGURE 20. RESULTS OF LONGITUDINAL RESTRAINT TESTS CONCRETE TIE FASTENERS.

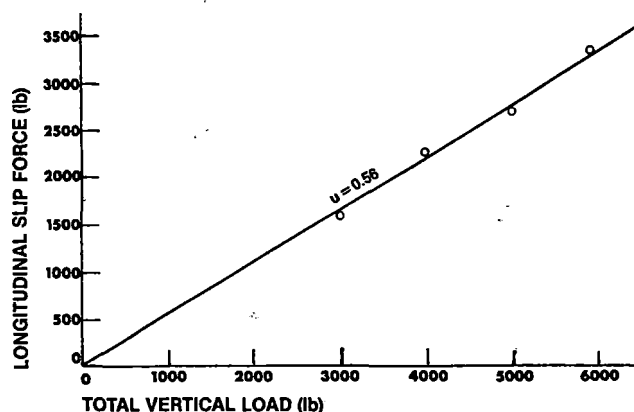


FIGURE 21. RESULTS OF LONGITUDINAL RESTRAINT WOOD TIE FASTENER.

conservatively that clip deflections are less using resilient tie pads rather than rigid pads. Additional data taken on the Northeast Corridor last November on a 1° curve in high speed track show that in revenue service this trend is also apparent. These data shown in Figure 22 indicate that the maximum deflections are one half as great on resilient pads than on rigid pads. There is also evidence that longitudinal restraint is improved with a resilient tie pad.

As with wood tie fasteners, an appropriate specification for concrete tie fasteners needs to be developed. The current specification, while perhaps suitable for large radius curves and tangent track, is not applicable for small radius curves. For each application judgement must be used in selecting the loads and deflections for the laboratory repeated load and longitudinal restraint tests. Since the majority of these systems are being designed for use on curves, the angle of application of the repeated load test needs to be increased from the current $18-20^\circ$ to $24-27^\circ$. Longitudinal restraint tests need to be repeated several times to obtain consistent results. Consideration should be given to applying a vertical load in uplift and compressing while conducting longitudinal restraint tests. This would be more representative of field conditions.

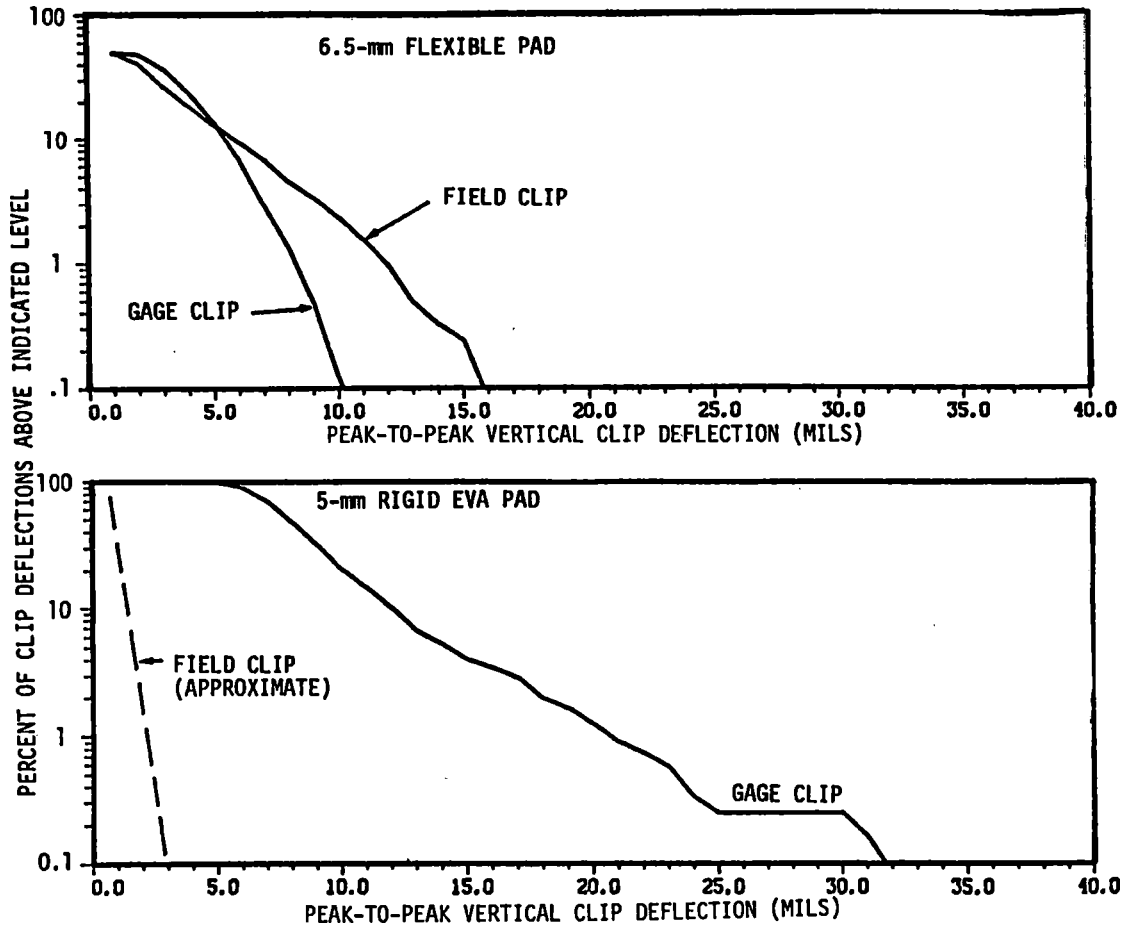


FIGURE 22. FASTENER DEFLECTIONS ON A 1° CURVE ON NORTHEAST CORRIDOR TRACK.

Current fastener tests at FAST may prove to the railroad community that there are economic alternatives to the cut spike fastener. To improve the reliability of results a more appropriate specification needs to be used and better definition of revenue service conditions. Until then there is too much guesswork in selecting fasteners.

ACKNOWLEDGEMENTS

Revenue service data collection and analysis for this report was performed under the direction of F. E. Dean and H. Harrison, Battelle Columbus Laboratories. Data collection at FAST was performed by FAST Instrumentation under the direction of R. L. Jackson, during the FAST Concrete Tie Experiment monitored by J. E. Heiss. The authors thank these individuals, as well as, the personnel at FAST who supported the data collection, data processing and operation management, for their professionalism and dedication.

References

1. Description of FAST Track and Mechanical Experiments, TN 79-02, February 1979.
2. H. G. Moody, et al, "Tie and Fastener Performance", FAST Conference Proceedings, Report No. FRA/TTC-82/01, February 1982.
3. F. E. Dean, "The Effect of Tie Plate Stiffness on the Attenuation of Impact Strain in Concrete Ties," Report No. FRA ORDB2/18, March 1982.
4. D. R. Ahlbeck, "The Effects of Track Modulus on Vehicle-Track Dynamic Interaction", ASME/IEEE Joint Railroad Conference, April 1982.
5. F. E. Dean, "Measurements of Rail/Tie Deflections and Fastener Clip Strains at FAST", IR8/03, May 1982.
6. American Railway Engineering Association, Manual for Railway Engineering Chapter 10, 1981.
7. F. E. Dean "Investigations of Rail Fastener Performance Requirements", Report No. FRA ORDB2/10, March 1982.

Effect of Tie Pad Stiffness on the Impact Loading of Concrete Ties

F.E. Dean
D.R. Ahlbeck
H.D. Harrison
J.M. Tuten

Research Engineers
Applied Dynamics and
Acoustics Section
Battelle's Columbus
Laboratories
Columbus, Ohio

The effect of tie pad stiffness on high-impact wheel/rail loads and concrete tie strains were investigated by field and laboratory measurements and analytical simulation. The simulations and track measurements demonstrated that wheel irregularities on high-speed passenger traffic in the Northeast Corridor frequently produce wheel/rail loads over four times the static wheel load. Concrete tie strains above the level known to cause tie cracking were measured at frequencies of occurrence averaging one event in less than two days at an average tie location. Measurements on heavy haul freight lines have shown similar results. The laboratory tests successfully reproduced the impact phenomena measured in track and the level of tie strain which causes tie cracking in static bending tests. It was demonstrated that major reductions in tie stiffness can reduce the levels of impact strain caused by wheel flats, but that elimination of cracking will require both a more flexible tie pad and a program to remove the worst wheel conditions.

* MGT = million gross English tons
Mmt = million metric tonnes

INTRODUCTION

The reconstruction of the Amtrak Northeast Corridor track includes 400 track-miles of prestressed concrete ties. Many of the ties, with service histories ranging from a few months to about two years, have developed "hairline" cracks under the rail seats. While there is no evidence of structural failure, there is concern over the crack development because:

a. The ties were designed under the latest strength specifications of the American Railway Engineering Association and Amtrak [1,2], and should have sustained all anticipated loads without cracking.

b. The cracks are of the same type which have eventually led to failure (loss of bending strength) in earlier designs of lower-strength ties.

This investigation was conducted to identify the cause of the crack development and to recommend corrective action which would minimize component replacement. The investigation was carried out in several phases:

a. Existing data on vertical loads and tie bending moments from the Northeast Corridor track were evaluated to determine whether processing over a wider frequency bandwidth would reveal high response levels. This study [3] identified impact loads from a small percentage of high-speed passenger train wheels as the probable cause of the cracks. Similar data from the Norfolk and Western (N&W) concrete tie test site near Roanoke, Virginia show that comparable loads are caused by a small percentage of loaded coal cars and that this has resulted in 100 percent tie cracking through the test section after 250 MGT (227 Mmt)*

b. Impact loading tests were conducted with a one-tie laboratory test arrangement to determine the effects of tie pad stiffness on the attenuation of bending strain [4]. The tests revealed that major reductions in tie pad stiffness, using pads of up to 9-mm thickness, could reduce the bending strains below the level which causes cracks.

c. To verify the results of the laboratory tests, new field measurements were conducted on the NEC track at Aberdeen, Maryland using pads of different stiffness. Pads were substituted in a test zone to obtain loads and strain data over a 5-day period for each pad. The field tests provided proof that flexible pads which are adaptable to the current fastener system can significantly reduce the occurrence of strains which can cause cracks [5].

d. Analytical simulations of impact loading on wood and concrete tie track verified that wheel flats of the type found on passenger trains in the Northeast Corridor could produce impact loads with the range of amplitude and frequency content which has been measured. Some effects of train speed are also presented.

ANALYSIS OF DYNAMIC LOADS AND TIE BENDING MOMENTS FROM THE NEC AND N&W TESTS

Dynamic wheel/rail loads and tie bending moments were first measured on the Northeast Corridor track at Aberdeen, Md. during June, 1980. Strain gage circuits illustrated in Figure 1 measured the vertical and lateral loads at single location. The methods by which these circuits are calibrated and the data processed are described in Reference [5]. Strain gage coupons were attached to one rail seat and to the center of each of seven ties, as illustrated in Figure 2. Using the loading fixture shown in Figure 2, the outputs of these coupons were directly calibrated in terms of the bending moments sustained by the ties. Wheel/rail load and tie bending moment data were collected for both freight and passenger traffic over a 5-day period. Only the vertical load and rail seat bending moment circuits produced load magnitudes of interest to the impact loads investigation.

To process the data, a 300-Hz filter bandwidth was initially chosen because previous experience had shown that this bandwidth was adequate for measurements under normal freight service. However, the NEC track carries a unique combination of freight and high-speed passenger traffic. Much of the passenger traffic travels above 70 mph (113 km/h). A closer examination of the original data, particularly for the high-speed passenger traffic, showed that the tie response was highly oscillatory under most wheels. In addition, no rail seat bending moments were found above the "cracking threshold" of 375 kip-inch (42.4 kN-m). This threshold was established as the mean of bending moments which produced first cracking in static bending tests of similar ties [6].

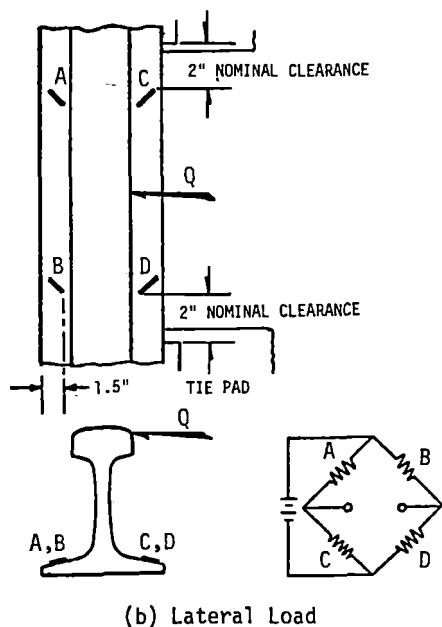
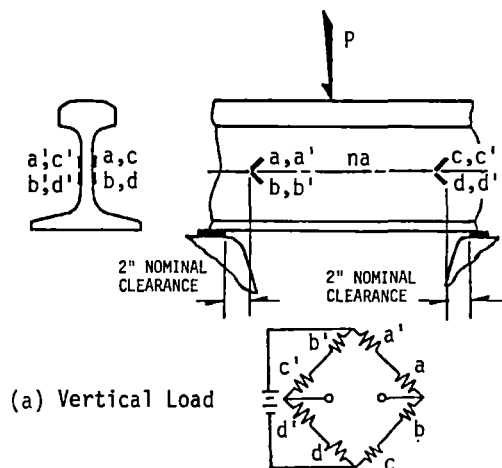


Fig. 1 Strain Gage Circuits to Measure Lateral and Vertical Wheel/Rail Loads

The need for processing the data over a wider frequency bandwidth was clearly indicated. This involved a tradeoff: as the filter bandwidth was increased, the system noise and uncertainty associated with a given signal also increased. After evaluating processing at bandwidths of 800, 1200 and 2000 Hz, the 1200-Hz bandwidth was selected. This bandwidth provided about 93 percent of the signal amplitude obtained at 2000 Hz while reducing the system noise to about half the 40 kip-inch (4.5 kN-m) level encountered at 2000 Hz.

Plots of peak rail seat bending moment vs. frequency of occurrence were compiled from data processed with 300- and 1200-Hz bandwidths. In Figure 3, the results are shown separately for three types of traffic: passenger traffic above 70 mph (113 km/h) passenger traffic below 70 mph, and freight traffic, most of which passed the test site at speeds between 40 and 60 mph (65 and 97 km/h). At frequencies of occurrence below 1 percent, the data for each type of traffic show substantial increases in strain level due to the expansion of frequency bandwidth. A vertical line indicates the previously discussed cracking threshold.

The right side of Figure 3 shows that less than 0.1 percent (1/1000) of the measured bending moment peaks for high-speed passenger traffic exceeded the cracking threshold. Because the measurement sites were scattered, inputs could not be captured from all wheel flats. For the low-speed passenger and freight traffic, the cracking threshold is reached at even lower frequencies of occurrence. However, since an average of 540 passenger axles per day passed the measurement site above 70 mph (113 km/h) the frequency with which an average tie location encountered a potential cracking event was once in 1.8 days.

Major effects of wheel impacts can be seen in the vertical wheel/rail loads data of Figure 4. The full-scale range of the analog-to-digital data conversion system was 82 kips (365 kN). Between 0.1 and 0.2 percent of the peak loads from high-speed passenger traffic exceeded this level, which is approximately 4 times the average static passenger wheel load of 20 kips (89 kN).

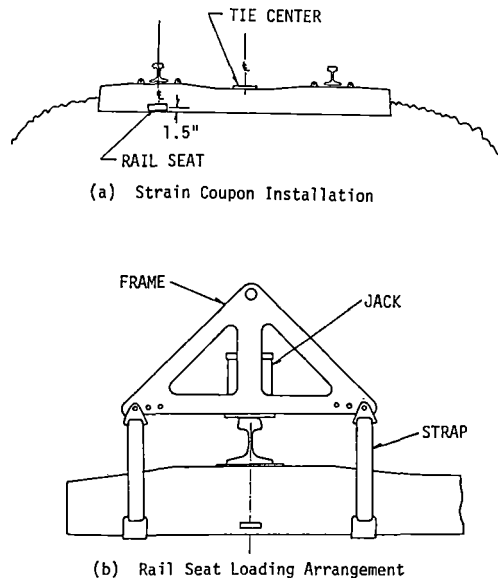


Fig. 2 Installation and Calibration of Strain Gage Coupon to Measure Tie Bending Moment

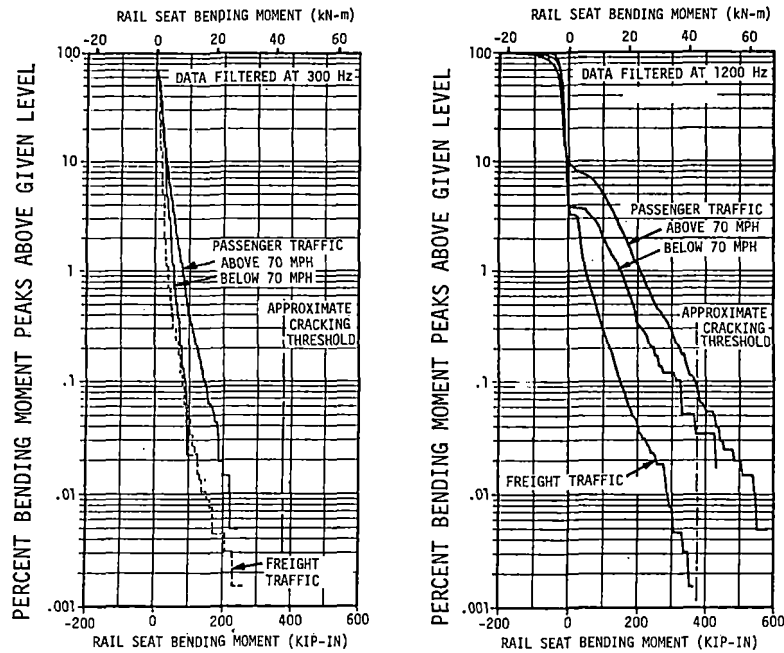


Fig. 3 Rail Seat Bending Moment vs. Frequency of Occurrence for Data Filtered at 300 and 1200 Hz

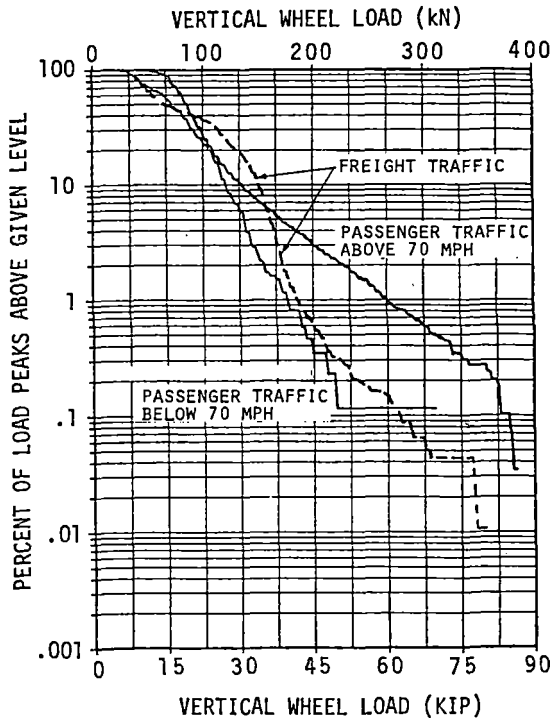


Fig. 4 Exceedance Levels of Vertical Wheel/Rail Load for June 1980 Tests at Aberdeen

It should be emphasized that these data were collected on well-maintained track without rail surface irregularities or visible geometry errors. The occurrence of severely cracked ties at rail joints and battered welds indicates that cracking-level tie strains can be produced at track anomalies by the passage of normal or near-normal wheels.

Dynamic loads and tie bending strain data were also collected on a Norfolk and Western (N&W) concrete tie test segment near Roanoke, Virginia. Although the N&W track carries only freight traffic at 35-45 mph (56-72 km/h) there are similarities in track construction, loading environment and tie performance on the two tracks. All ties in the N&W site contained rail seat bending cracks and most contained center bending cracks. The instrumented ties were designed to the same rail seat bending strength specifications and were placed at the same 24-inch (61cm) spacing as the NEC ties. Tie bending moments and vertical loads for the two sites, including both freight and passenger traffic for the NEC, are compared in Figure 5. The loading environments are very similar despite the fact that the extreme loads for the NEC track were produced almost exclusively by high-speed passenger traffic, while all loads on the N&W were the result of relatively low-speed freight traffic. In both cases, the extreme loads are caused by wheel irregularities.

LABORATORY STUDY OF THE EFFECTS OF TIE PAD STIFFNESS ON IMPACT LOADS

One possible solution to the cracking problem consists of replacing the current tie pad with a more flexible pad which could better attenuate impact loads. This offers the potential of reducing the impact loading from rail anomalies (engine burns, battered welds, joints) as well as from the irregularities of train wheels. To assess the potential effects of pad substitutions, a loading fixture was constructed and tests were conducted with the "single-tie" arrangement shown in Figure 6. Tie bending moments were measured

by the same methods used in the field measurements. By variations of the shim inserted between the impact hammer and the hammer head, it was possible to closely match the time history of tie bending moment which had been measured in the field. Typical time histories produced by the passage of a flat wheel over a field measurement site and by a single blow of the drop hammer are illustrated in Figure 7. An assortment of the pads is shown in Figure 8.

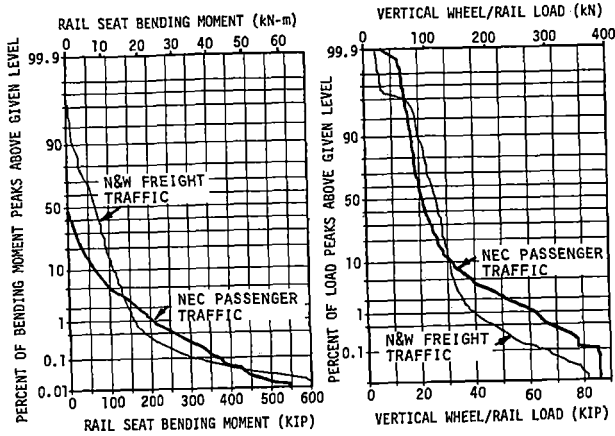


Figure 5. Comparison of Loading Environments for Northeast Corridor and Norfolk & Western Test Sites

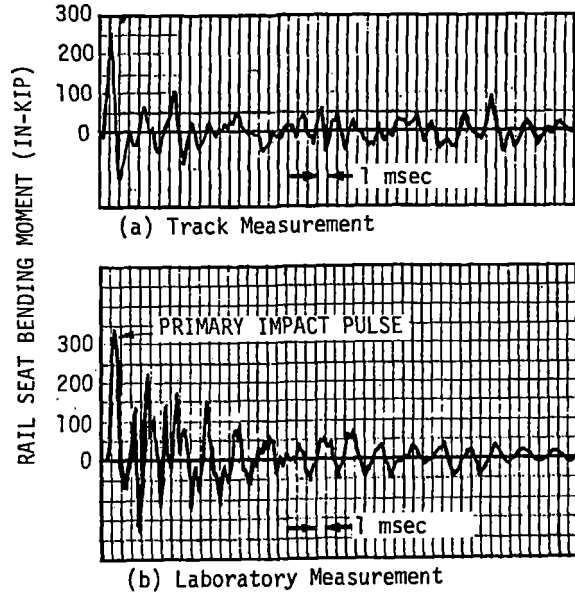


Fig. 7 Typical Time Histories of Tie Bending Moment from Track and Laboratory Measurements

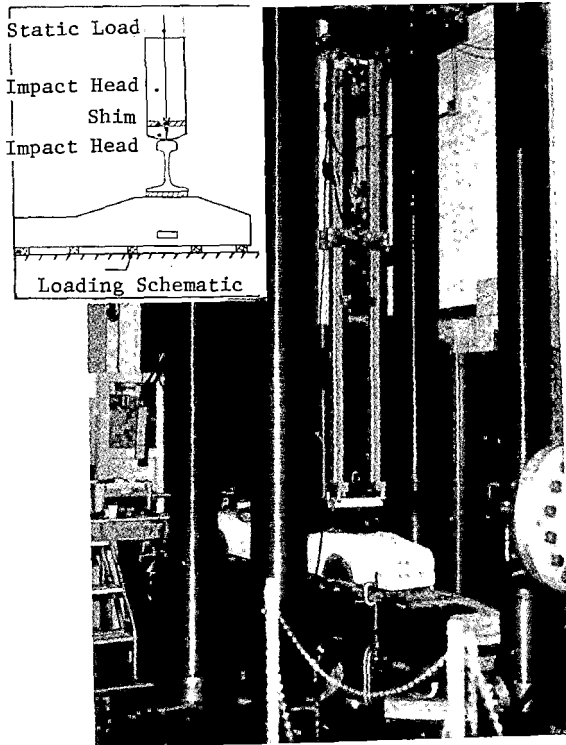


Figure 6. Impact Loading Fixture

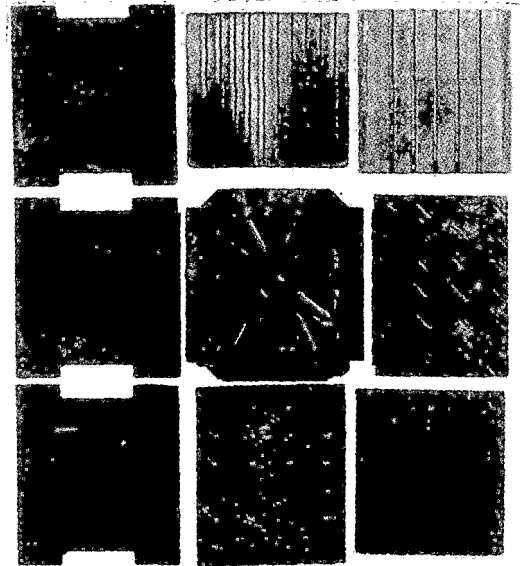


Fig. 8 Concrete Tie Test Pads of Different Materials, Thicknesses and Grooving

Nondestructive Pad Tests

For the rigid plastic pad originally installed on the NEC track and for eight potential alternatives of 5-mm nominal thickness, the peak bending moments from low-level (non-crack) drops are shown in Figure 9. The right side of the figure shows similar comparative results for two grooved pads of increased thickness. Most of the flexible pads were grooved to increase flexibility.

The vertical force-deflection characteristics of each pad were measured statically and at loading/unloading rates of 9 cycles per second. (This loading rate has since been increased to 10 cycles per second). For each pad, a value of "dynamic stiffness" was determined as the slope of the line connecting 4 and 20 kips (17.8 and 89.0 kN) during the pad compression portion of the dynamic loading cycle. Figure 10 shows the load-deflection results for the three pads which were later selected for field testing.

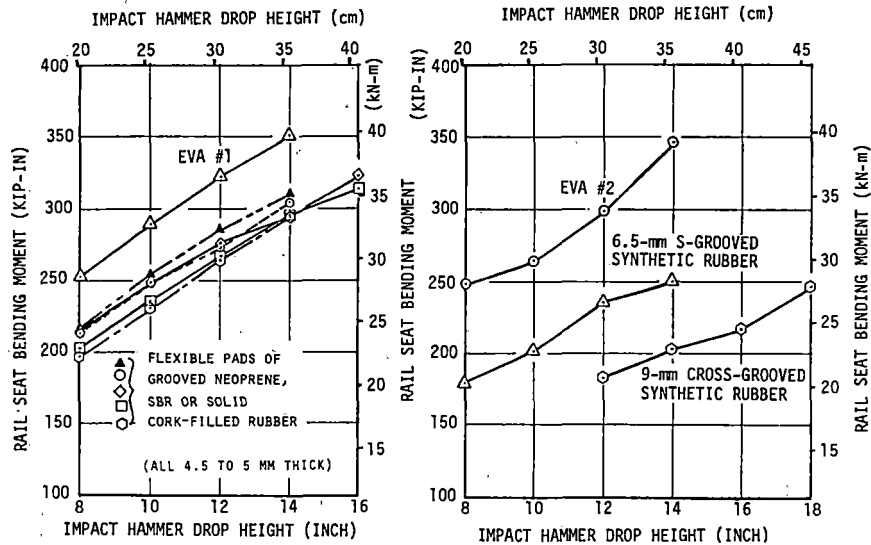


Fig. 9 Effect of Tie Pad Substitutions on Impact Bending Moment at the Rail Seat

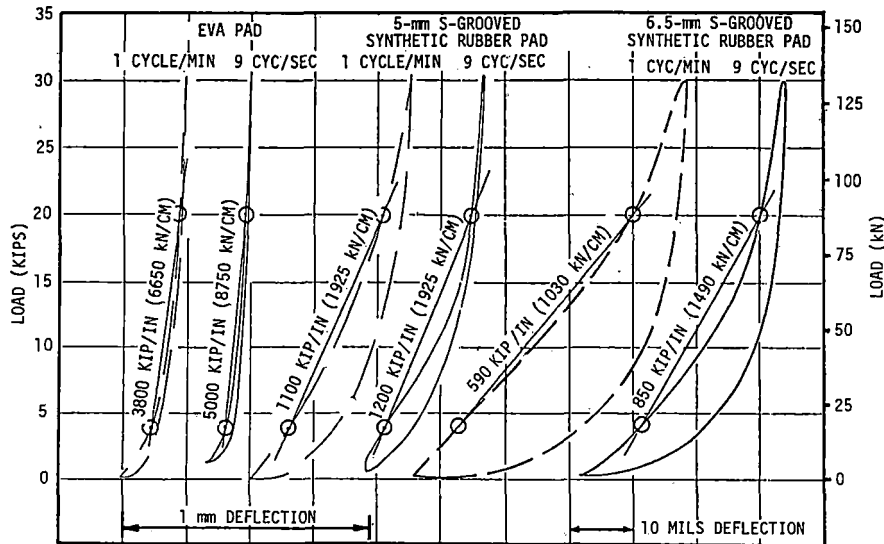


Fig. 10 Typical Load-Deflection Plots from Tie Pad Stiffness Tests

From comparable peak bending moments at each of the drop heights in Figure 9, a mean percentage bending moment reduction was calculated for each alternative pad. The static and dynamic values of pad stiffness were obtained from data of the type illustrated in Figure 10. The results are compiled in Table 1 along with the stiffness values for a number of pads which were not selected for impact testing.

The results show that with two exceptions, bending moment attenuation increases as pad stiffness decreases. However, the rate of attenuation does not reach 20 percent until the dynamic values of pad stiffness fall below 1 million lb/in. (1.75 MN/cm), which is one-fifth of that of the current rigid plastic (EVA) pad. Further reductions in impact bending strain were only obtained with pads of increased thickness.

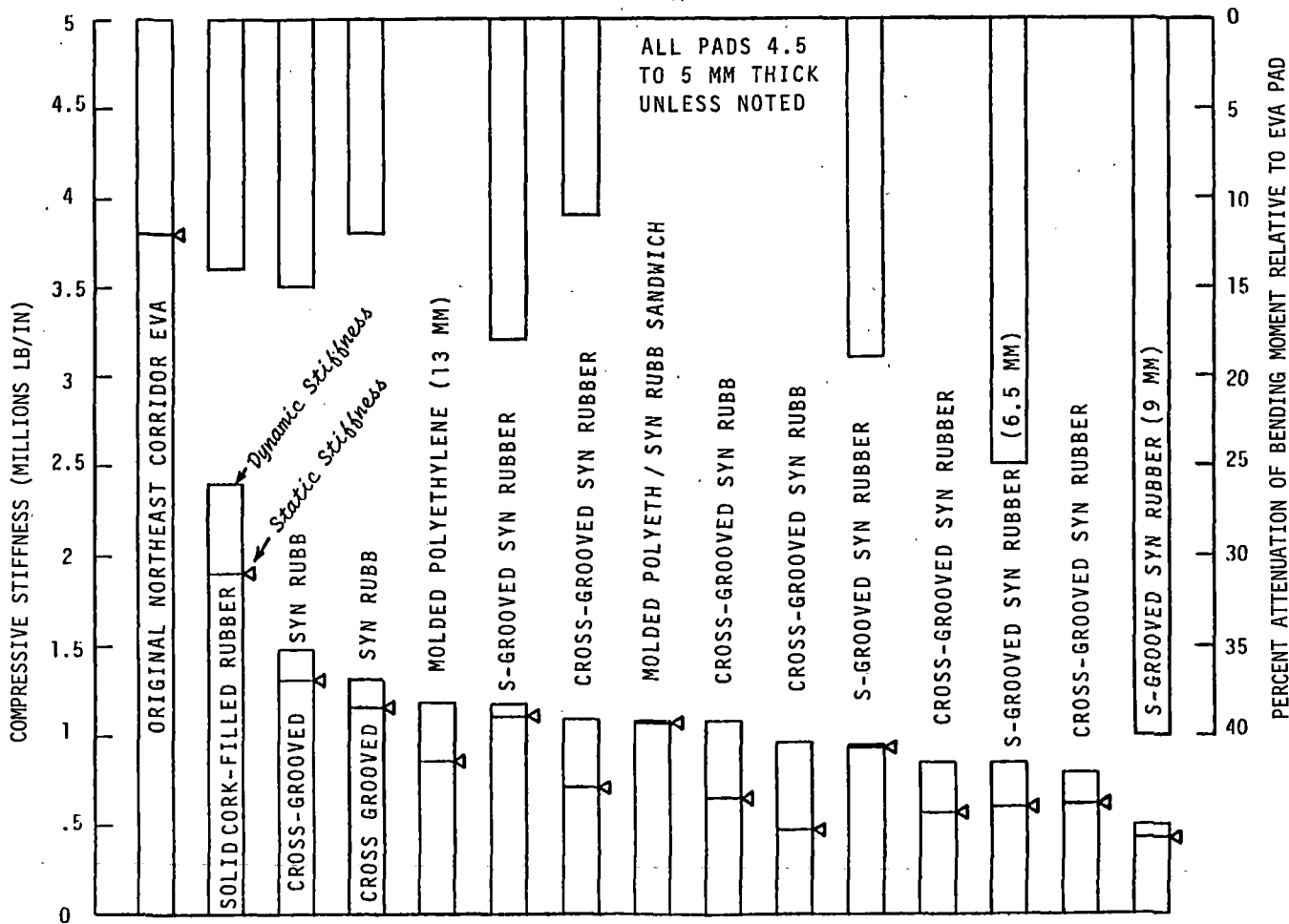
Destructive Tie Tests

Noninstrumented, destructive impact tests were conducted on two ties to determine the range of drop heights required to produce advanced cracks of the type found in track. The rail seat areas of each tie were stresscoated. One end of each tie was impacted at heights varying from 14 to 36 in. (35.6 to 91.4 cm) in 2-inch (5.1-cm) increments from 14 to 20 inches (35.6 to 50.8 cm) and 4-inch (10.2 cm) increments thereafter.

Crack progression under the rail seats is shown for two rail seats in Figure 11. Also shown in the figure is the typical crack "y" shape which developed both in service and in the lab tests. Cracks were first detected at the drop height of 16 inches on each tie.

After completion of the first test (Tie 0432), it was discovered that cracks had developed at the nonimpacted rail seat as well as the impacted rail seat. Subsequent tests produced the same result. In each case, total crack height on the nonimpacted end was 70 to 80 percent of the total crack height on the impacted end. Maximum crack heights for the two ends of each tie are compared in the box of Figure 11. This result demonstrates that a stress wave propagates across the tie with little attenuation of the initial amplitude.

Table 1 Tie Pad Stiffness and Impact Attenuation Rates from Basic Tests



It should be noted that without the Stresscoat applied to the ties faces, few if any of the laboratory cracks would have been detected. In contrast, cracks on tie in track were visible either with an alcohol spray or with no surface treatment. It can be concluded that service-produced cracks are well-developed before they become visible, and that repeated working under normal service loads causes the cracks to widen.

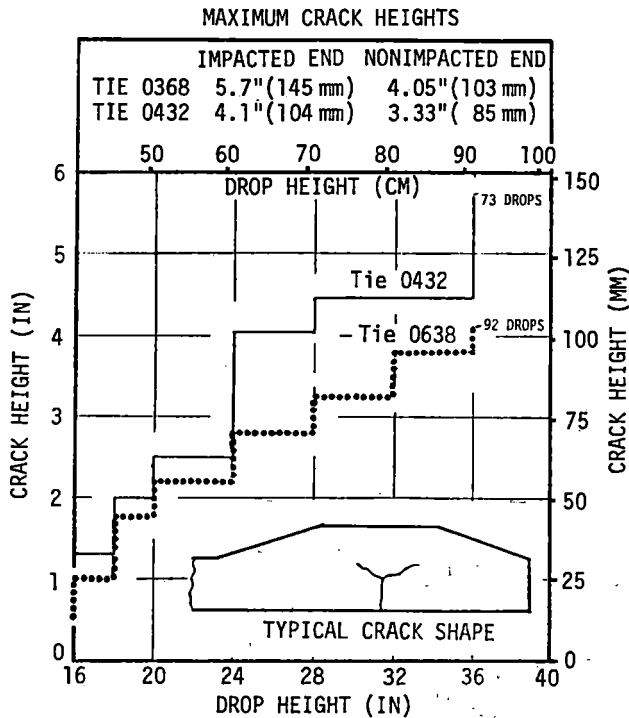


Fig. 11 Crack Development vs. Impact Hammer Drop Height

TRACK MEASUREMENTS TO VERIFY THE EFFECTS OF PAD STIFFNESS ON IMPACT LOADS

The laboratory tests demonstrated that major reductions in pad stiffness could significantly attenuate tie impact loading. To verify that the results of the one-tie laboratory test could be reproduced in track, a field test program was again conducted on the NEC track at Aberdeen, Md. The instrumented zone shown in Figure 12 was established within a segment of 50 ties where pad substitutions were made. Measurements included vertical wheel/rail load and tie bending moments at the rail seats. Additional measurements of rail/tie deflection were made on a nearby high-speed one-degree curve.

The three pads selected for testing are those whose stiffness properties are illustrated in Figure 10. The currently used rigid plastic pad was included to provide a direct comparison with the effectiveness of the flexible pads. The 5-mm synthetic rubber pad provided the best attenuation of impact loads among the laboratory test pads of "standard" thickness (4.5-5mm). The 6.5-mm synthetic rubber pad provided the most effective attenuation among pads which might be used with the current Pandrol fastener clip.

Each of the three pads was installed in the 50-tie test section for a period of 5 days. To minimize the possibility of crack development during the tests, the tests began with the softest pad and ended with the hardest. For each installation, data were collected for approximately 5000 axles, of which approximately 50 percent were passenger train axles. Most of the passenger traffic passed the site at speeds between 70 and 110 mph (113 and 177 km/h). While most freight traffic fell within the range of 40 to 60 mph (64 to 97 km/h).

Tie bending strain coupons were installed under the west rail on 5 consecutive ties and under the east rail on the center tie. This provided a zone length slightly greater than a wheel circumference; thus for one rail, all wheel impact conditions would be identified at some point in the zone.

From the 5 days of data collected with each of the three test pad installations, statistical summaries of peak tie bending moments and vertical wheel/rail loads were compiled for an average tie location and an average load measurement site (crib). The data show the influence of tie pad stiffness on impact loads for several classifications of traffic and ranges of speed.

Passenger Traffic. The attenuation of bending moments by pad substitutions can be seen in Figure 13(a). Bending moments above the "cracking" threshold of 375 inch-kips occurred with the following frequencies:

Pad Type	Exceedance Frequency	Avg. No. Days Between Exceedance
Rigid Plastic	1/1300	2.6
5-mm Flexible	1/2200	4.4
6.5-mm Flexible	1/14,000	28

While the most flexible pad did not eliminate the occurrence of bending moments above the cracking threshold, these events were reduced significantly. This reduction could minimize both the requirements for improvements in wheel conditions and the damage from normal wheels passing over track defects.

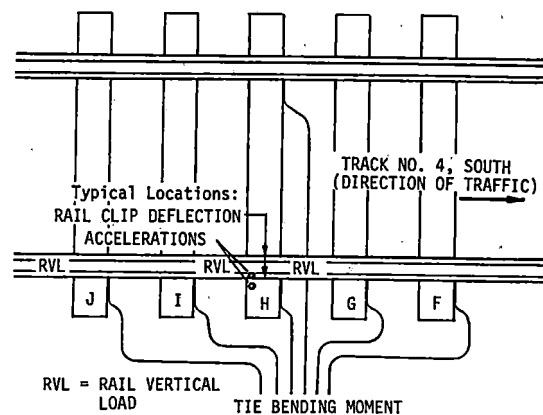


Figure 12. Layout of Instrumented Zone

Figure 13(b) shows the exceedance levels of vertical wheel/rail loads produced by passenger traffic. While the results for the rigid plastic and 5-mm flexible pads are nearly identical, those for the 6.5-mm pad show a significant reduction in the frequency of occurrence of potentially crack-producing loads. By matching exceedance percentages from the cracking threshold of bending moment (375 inch-kips), the cracking threshold of vertical wheel/rail load can be placed at about 80 kips with the EVA pad.

It should be noted in Figure 13 that for each type of pad, a few events produced such high strain levels that they saturated the data system. It is unlikely that any pad within the practical range of thickness could attenuate such events sufficiently to prevent cracking. These very low-probability events point to the need for improvements in wheel tread conditions along with the use of a more flexible pad.

Wheel Tread Conditions. A number of wheel impact conditions were traced and the wheels photographed. Typical spalled conditions are indicated in Figure 14(a) and occurred on both Amfleet and conventional passenger cars. However, the worst impacts were produced by longer wavelength (12-18 inch) irregularities of the type illustrated in Figure 14(b) which are characteristic of the conventional passenger equipment (with disc brakes). This particular wheel

produced a measured vertical load of 85.8 kips. The irregularity consisted of a flattening or chording of the wheel circumference over a length 12 inches. The area contained very little spalling of the type which is usually associated with "flat" wheels. The wheel was placed on a truing machine which permitted the measurement of the radial distance from a fixed reference, across the wheel tread, at several selected stations across the chorded area. The radially measured tread depth varied by about 0.09 inches from the edges to the center of the chorded area along a path adjacent to the tape line. These longer-wavelength irregularities are more difficult to identify than are wheel spalls. This emphasizes the necessity for a regular program of wheel inspection and truing.

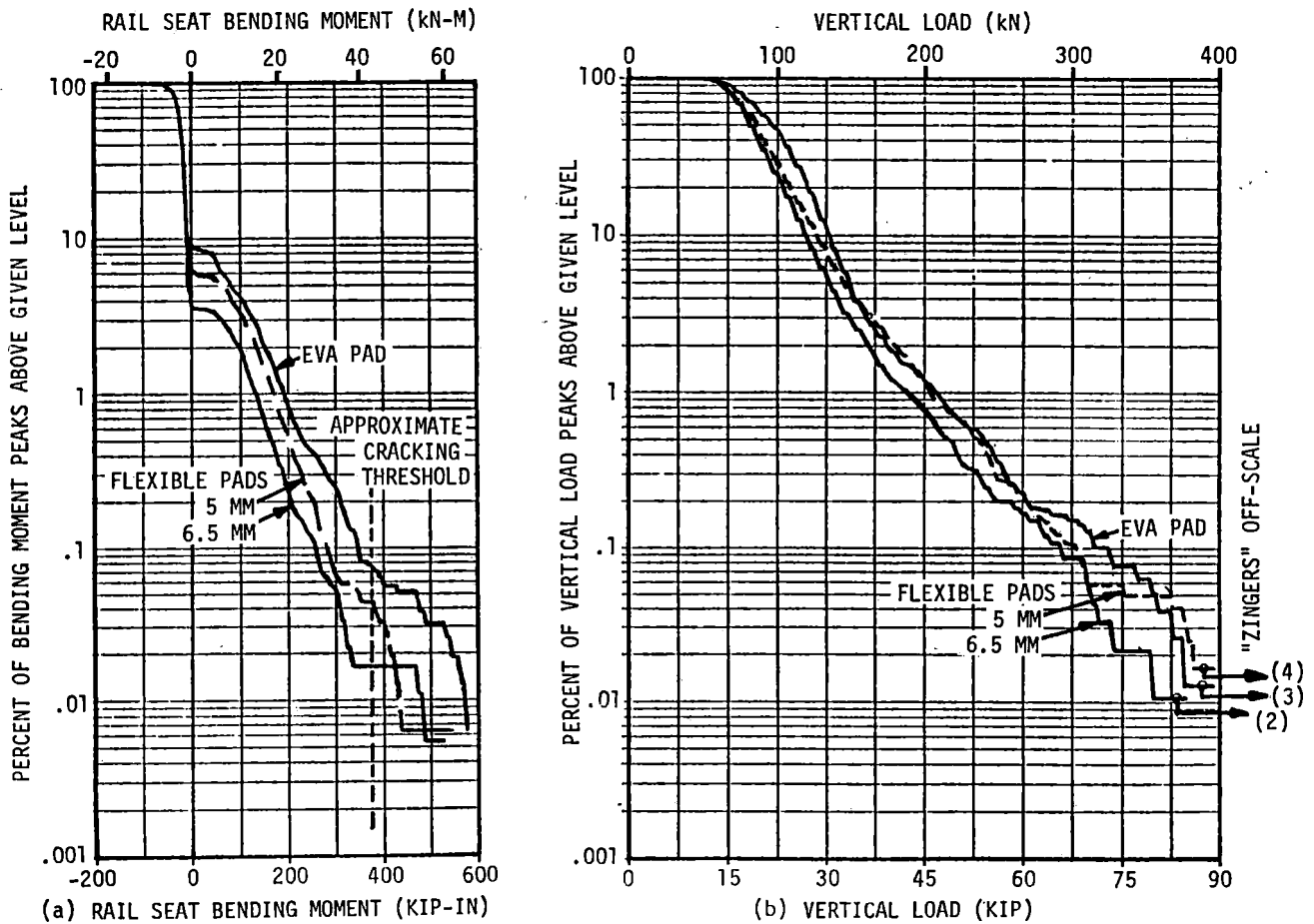
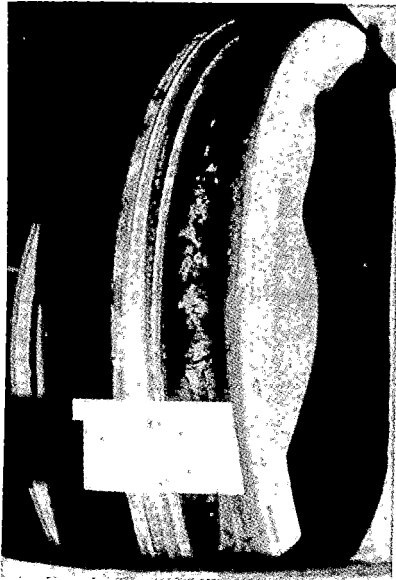
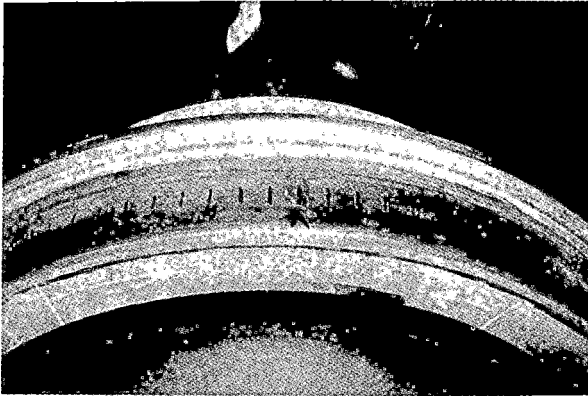


Fig. 13 Exceedance Levels of Rail Seat Bending Moment and Vertical Load for Northeast Corridor Passenger Traffic over 70 mph, Three Types of Pads



(a) Spalled Wheel



(b) Long-Wavelength Wheel Flat

Figure 14. Typical Wheel Tread Conditions

Vertical Deflection of the Fastener Clip. Among the issues involved in a pad conversion is the possibility that a more flexible pad will produce greater rail clip deflections and cause the clips to fail in fatigue. Because the highest deflections occur on curves, deflections were measured on a one-degree curve in Aberdeen where most passenger train speeds were 80-100 mph and most freight train speeds were 40-50 mph. The greatest deflections were invariably caused by freight trains.

Fastener clip vertical deflections were measured on the field and gage sides of the high rail only. Most of the rail movement had been observed on this rail rather than on the low rail. Pad substitutions were made to permit measurement of deflections on both the current rigid plastic pad and on the 6.5-mm flexible synthetic rubber pad. The measurements were made on the field and gage sides of the high rail with noncontacting deflection sensors as shown in Figure 15. These sensors have a very high frequency response (50 KHz), which contrasts with the very low frequency response (50 Hz) of most conventional deflection measurement devices.

Frequency-of-occurrence plots in Figure 16 compare levels of peak-to-peak vertical clip deflections (rail/tie deflections at the clip toe) for measurements on the rigid and flexible pads. The measurements verify a trend which had been indicated in earlier measurements at FAST [7]: peak-to-peak deflections were higher for the rigid pad than for the flexible pad. Much of this difference was due to greater uplift deflections which occurred at the gage side of the high rail on the rigid pad. In addition, the rail tended to rotate about the field side corner of the rail base with the rigid pad, while a more balanced rotation occurred with the flexible pad. These results indicate that there may be no detriment to clip fatigue life when the flexible pad is substituted.

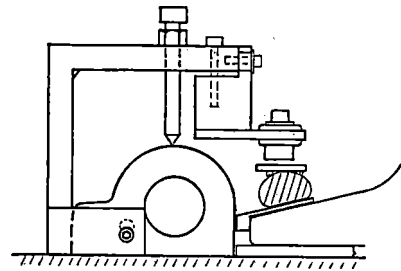


Figure 15 Measurement of Vertical Rail Clip Deflection

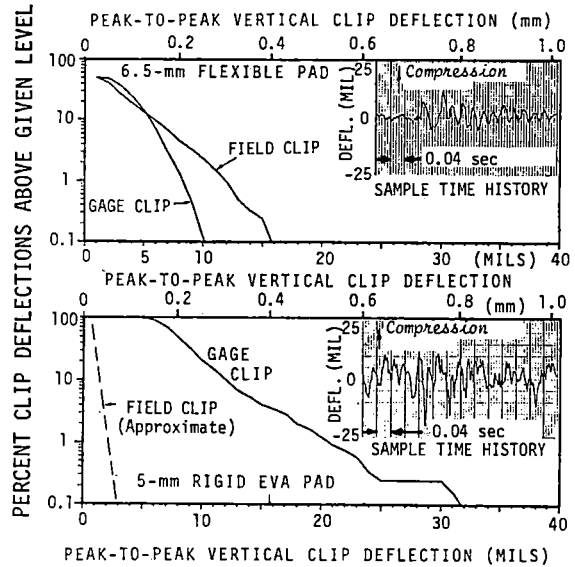


Fig. 16 "Peak-to-Peak" Vertical Clip Deflections on a High-Speed, One-Degree Curve of the Northeast Corridor Track

ANALYTICAL SIMULATION OF IMPACT LOADS

A simplified discrete-mass representation of the wheelset, rail and track structure, similar to that described by Bjork [8] was used initially to investigate wheel/rail impact loads. Developed as part of a methodology for predicting the wheel/rail load environment [9], Program IMPACT was validated by comparing its predicted results with measured wheel/rail loads under both loaded and empty 100-ton hopper cars on wood tie track. An example of vertical load under a flat wheel on an empty car, measured within the short influence zone of a wayside strain-gage bridge circuit, is shown in Figure 17 compared with the "continuous" load output from the computer model. (Note that the measured load falls to zero as the wheel passes out of the wayside measurement zone.)

Computer simulation runs were made using a British Rail "rounded flat" shape [10] to simulate both empty and loaded 100-ton cars on CWR woodtie track, and the peak loads plotted in Figures 18 and 19 were compared with measured impact loads [11,12]. Wheel flat lengths were implied from the measured data from the load pulse time duration, knowing the train speed. Several parameters were used to verify the computer simulation: these included peak vertical load, the natural frequency of load oscillations, the speed at which the wheel became "airborne" for a particular flat length, and the peak vertical accelerations of the rail. All these factors correlated well between predicted and measured values.

In this model, the tie and ballast masses were lumped together, and track parameters were based on measured dynamic modulus, [11,13] and beam-on-elastic-foundation formulae. The model was then used in this configuration to explore impact loads on concrete ties. Preliminary results using NEC track structure parameters and Amcoach vehicle parameters showed unrealistically high loads to occur at speeds near 30 mph (48 km/h) a phenomenon not observed in wayside measurements on the NEC track near Aberdeen, Md. or near Bradford, RI. The model was therefore expanded to include both the tie and ballast effective masses as separate degrees of freedom. The model then predicted somewhat lower wheel/rail peak loads in the 30 to 40 mph (48 to 65 km/h) speed range, and peak rail/tie reaction forces in the 65 to 85 mph (105 to 137 km/h) speed range.

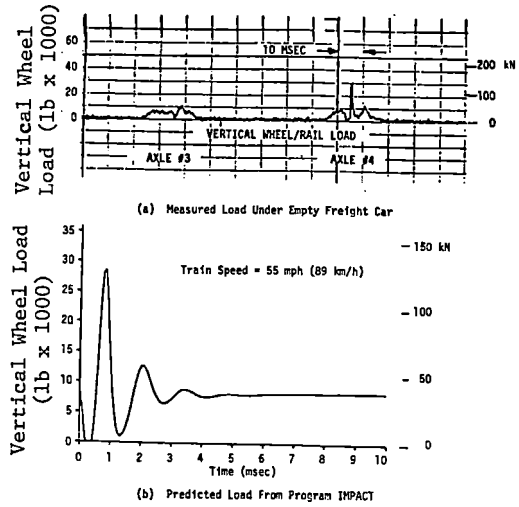


Figure 17 Comparison of Measured and Predicted Vertical Wheel Load Under Empty Freight Car. CWR Wood-Tie Track

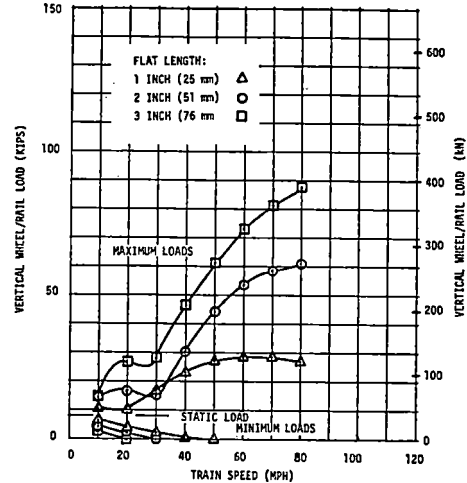


Figure 18 Vertical Wheel/Rail Impact Loads Under Simulated Empty (100-T) Freight Car, Wood-Tie Track Structure--Program IMPACT, BR "Rounded" Flat Shape

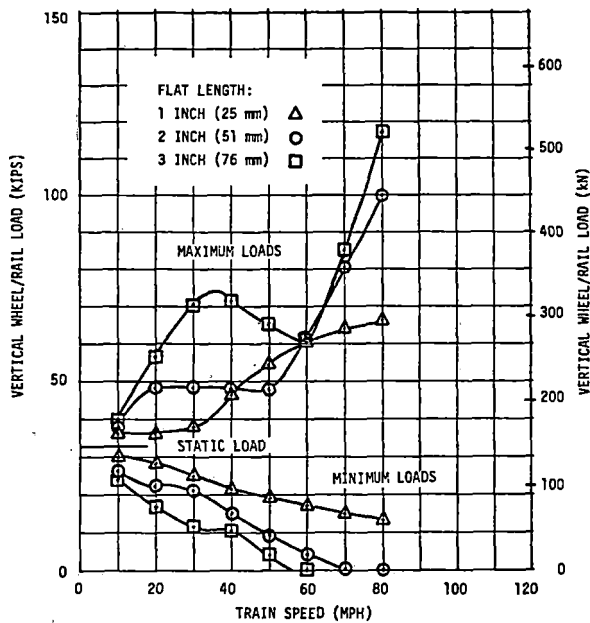


Figure 19 Vertical Wheel/Rail Impact Loads Under Simulated 100-Ton Freight Car, Wood-Tie Track Structure--Program IMPACT, BR "Rounded" Flat Shape

Initial predictions from the model of the effects of a softer rail seat pad are shown in Figure 20 for a simulated Amcoach with a 2-inch (51mm) rounded wheel flat. The model predicts that the peak load at the wheel/rail interface will actually be higher at speeds above 70 mph (113 km/h) with the softer pad than with the stiff pad. This high wheel/rail force peak in the simulation consists of a very short-duration impact (less than 0.5 millisecond) followed by rebound of the rail with loss of contact, and then the longer-duration force peak that is reacted at the rail/tie interface. This short-duration force peak has not been observed in the wheel/rail force measurements, and in strain gage patterns may be isolated by part of the rail effective mass from this impact force. On the other hand, the rail head and wheel rim may have sufficient resilience and distributed mass that this wheel/rail impact load is attenuated in the real case, and artificial in the simulation.

The model predicts a substantial reduction in the rail/tie reaction load with softer pads, which is verified both by the laboratory tests and field measurements. The rail/tie loads plotted in Figure 20, are of course, shared by several ties. From the beam-on-elastic-foundation relationships, the percent of wheel load supported by a tie directly under the load is 39.4 percent with the stiff pad, 37.0 percent with the softer pad. The dynamic effects under a short-duration impact load would probably result in a much higher percentage of the rail/tie reaction load being transferred to the nearest tie.

As discussed earlier, several high impact loads were correlated with actual wheel profiles during the field measurement phase of the study. The wheel previously shown in Figure 14(b) produced the wheel profile shown in Figure 21, and resembles a dipped rail joint more than the traditional wheel flat shape. The idealized sine curve of Figure 21 was programmed for simulation, and series of runs with Program IMPACT were made, varying pad stiffness over the range tested on the NEC track. A plot of the impact load at the rail/tie interface is shown in Figure 22 for the softer pad and an 80-mph (129 km/h) train speed. Results for this range of pad stiffness values are plotted in Figure 23. The peak load predicted for the softer pad is roughly 15 percent lower than the measured load, indicating that there is some dynamic stiffening of the pads under impact loading. From the model, the peak loading was found to occur 7 inches (178 mm) beyond the profile "cusp", which corresponds with the secondary "batter" profile error evident in Figure 21.

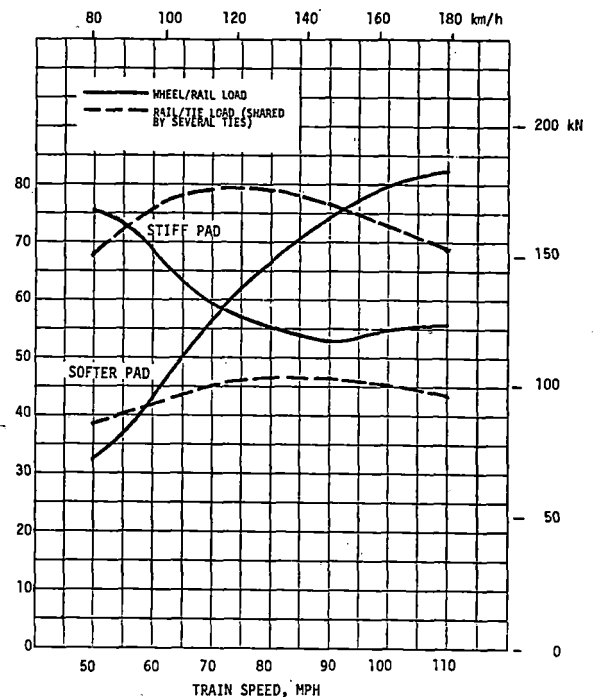


Figure 20 Predicted Effects of Rail Seat Pad Stiffness on Wheel/Rail and Rail/Tie Loads--Simulated Amcoach with 2-inch (51 mm) Wheel Flat

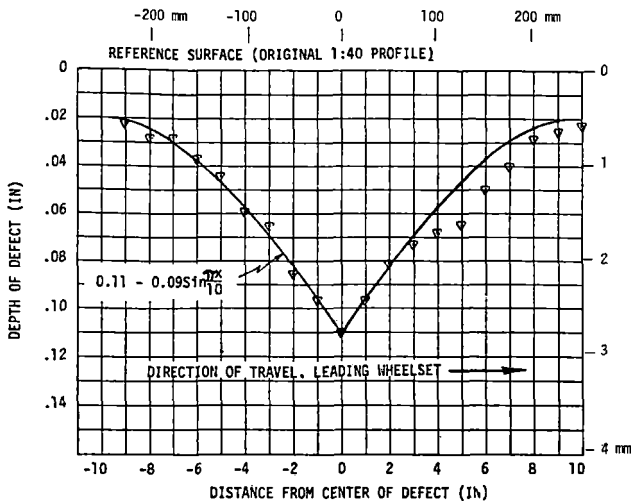


Figure 21 Plot of Maximum Defect (at 2.1 in from Field Face), Profile Measurements on Wheel #7, Car #4710, 36-in Diameter Wheel with about 200,000 MI of Wear

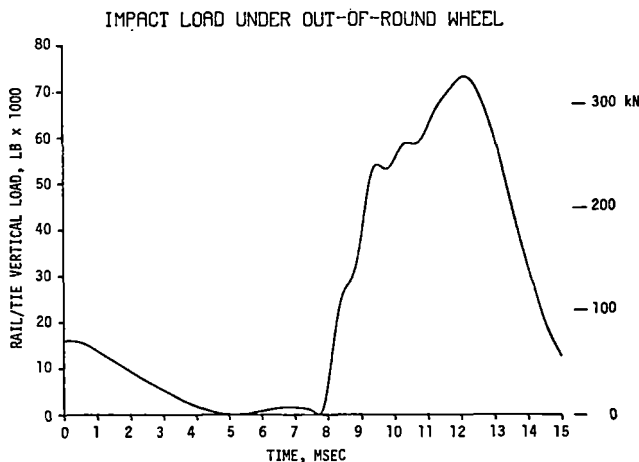


Figure 22 Simulation of Impact Load at Rail/Tie Interface Due to Wheel Profile of Figure 20--Passenger Car at 80 MPH (129 KM/H), Softer (6.5 MM) Pads

Measurements of wheel/rail loads with other pad stiffness showed several impact loads greater than 90,000 lb (400 kN) under passenger cars on the stiff (EVA) pads. One exceptional impact load (not the same wheel shown in Figure 17) was measured exceeding 135,000 lb (600 kN), well into the nonlinear range of the signal conditioning amplifier, on the intermediate-stiffness (5 mm) pads.

Both the rail and the tie are, in reality, complex distributed structures and can be modeled only crudely as lumped masses. Particularly, the beam response of the tie due to an asymmetric impact (one rail seat) seems to have a strong effect on pulse shape measured in the field and laboratory. A dynamic finite-element model can be used to model the

track structure in greater detail. British Rail currently employs an analytical model of the wheel/rail impact load and the track structure response, with the dynamic system represented as a Timoshenko beam on discrete elastic supports, with the rail normal modes of vibration handled as a Fourier series [14]. The use of the one-dimensional model described above for the investigation of a three-dimensional problem has, however, provided helpful insights into the wheel load impact phenomenon.

CONCLUSIONS AND RECOMMENDATIONS

a. Cracks at the rail seats of concrete ties on the Northeast Corridor are caused by the impacts resulting from wheel irregularities on a very small percentage of passenger car wheels. Similar cracks under rail seats of concrete ties at the N&W test site are caused by a small percentage of loaded hopper cars with flat wheels.

b. The substitution of a more flexible pad can definitely reduce the rate of occurrence of impacts with the potential to cause tie cracks. The pad should have an approximately linear load-deflection characteristic of about 1 million pounds per inch or lower. Other required properties include tensile strength and resistance to compressive set, age hardening and abrasion.

c. The long-term durability of flexible pads should be evaluated through track and laboratory tests appropriate for the specific service environment. Service histories of pads to date indicate a life expectancy of 10 years with an increase in spring rate over that time period.

d. Although flexible pads will improve the life expectancy of concrete ties, long term durability cannot be assured without a comprehensive program of detecting and retrueing the small percentage of wheels which cause the more severe impacts.

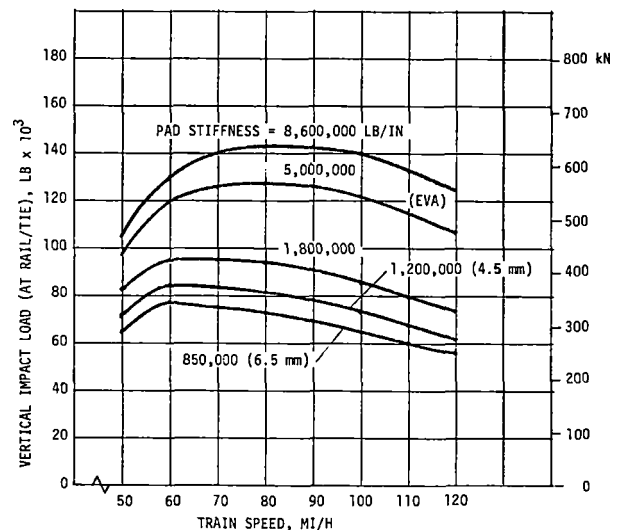


Figure 23 Effects on Rail/Tie Reaction Load of Rail Seat Pad Stiffness--Impact Due to Wheel Profile of Figure 6, NEC Concrete Tie Track

ACKNOWLEDGEMENTS

This program was sponsored by the Federal Railroad Administration (FRA) with the assistance of the National Railroad Passenger Corporation (Amtrak). The successful completion of the program resulted from the work of many people. As the sponsor's technical representative, Mr. Howard G. Moody of the FRA Improved Track Structures Research Division participated actively in all planning phases and coordinated activities among Battelle, the FRA, Amtrak and several pad manufacturers. Other key participants included Mr. Ted R. Ferragut of the FRA Office of Intercity Programs, Mr. Daniel L. Jerman of Amtrak, Mr. Dennis C. Wilcox of Amtrak and Mr. Gregory E. Mester of Deleuw, Cather/Parsons. Battelle researchers and technicians who conducted the field and laboratory tests and data evaluations included Dale Dawley, Edward Hiltner, Dale Punkett, Kenneth Schueller, Tony So, Paul Southerland and Matthew Zelinski. The contributions of all of these people are greatly appreciated by the authors.

REFERENCES

- [1] "Manual for Railway Engineering", American Railway Engineering Association, Chicago, Illinois, Chapter 10(Revised 1981).
- [2] "Concrete Tie Technical Provisions, Part 3 - Execution", National Railroad Passenger Corporation, Revised November 8, 1977.
- [3] Tuten, J.M., "Analysis of Dynamic Loads and Concrete Tie Strain From the Northeast Corridor Track", Technical Memo by Battelle's Columbus Laboratories to the Federal Railroad Administration, Improved Track Structures Research Division, Contract DOT-FR-9162, May 1981.
- [4] Dean, F. E. and Harrison, H. H., "Laboratory Study to Determine the Effects of Tie Pad Stiffness on the Attenuation of Impact Strain in Concrete Ties", report by Battelle's Columbus Laboratories to the Federal Railroad Administration, Improved Track Structures Research Division, Contract DOT-FR-9162, January 1982.
- [5] Dean, F. E. and Harrison, H. D., et al., "Investigation of the Effects of Tie Pad Stiffness on the Impact Loading of Concrete Ties in the Northeast Corridor", report by Battelle's Columbus Laboratories to the Federal Railroad Administration, Improved Track Structures Research Division, Contract DOT-FR-9162, January 1982.
- [6] Dean, F. E., "Tests to Determine the Effects of Service Loading on the Bending Strength of Concrete Ties", Transportation Test Center FAST Report No. 81/11, December 1981.
- [7] Dean, F. E., "Measurements of Rail/Tie Deflections and Fastener Clip Strains at the Facility for Accelerated Service Testing", Transportation Test Center FAST Report No. 81/03, December 1981.
- [8] Bjork, J., "Dynamic Loading at Rail Joints--Effect of Resilient Wheels", Railway Gazette, June 5, 1970, pp. 430-434.
- [9] Ahlbeck, D. R., Dean, F. E., and Prause, R. H., "A Methodology for Characterization of the Wheel/Rail Load Environment", draft final report, Contract No. DOT-TSC 1051, June 1979.
- [10] Lyon, D., "The Calculation of Track Forces Due to Clipped Rail Joints, Wheel Flats and Rail Welds", British Rail Research Dept., Tech. Note TS.2, February 1972.
- [11] Ahlbeck, D. R. et al., "Measurements of Wheel/Rail Loads on Class 5 Track", Report No. FRA/ORD-80/19, February 1980.
- [12] Ahlbeck, D. R. and Tuten, J. M., "LRC Trainset Cant Deficiency Tests--Vehicle/Track Dynamic Response From Wayside Measurements", Summary Report Under Contract No. DOT-FR-64113, Task 475, January 9, 1981.
- [13] Nessler, G. L., Prause, R. H. and Kaiser W. D., "An Experimental Evaluation of Techniques for Measuring the Dynamic Compliance of Railroad Track", Report No. FRA/ORD-78/25, July 1978.
- [14] Newton, S. G. and Clark, R. A., "An Investigation Into the Dynamic Effects on the Track of Wheel-flats on Railway Vehicles", Journal Mechanical Engineering Science, IMechE 1979, Vol. 21, No. 4 1979.

Theoretical Tendon Stresses Induced during Fatigue Testing of Prestressed Concrete Sleepers for a Heavy Haul Railway Line

J.S. Maree

Principal Engineer
B.Sc. Eng. (Civil)
Assistant Track Engineer
Track Development
Chief Civil Engineer's
Office
South African Transport
Services
Johannesburg
South Africa

The South African Railways Track Laboratory regularly carries out production control and special tests on semi-rigid monolithic prestressed concrete sleepers, in order to assess the structural adequacy of sleepers supplied under tender and sleepers manufactured for development purposes. As part of the standard test, the sleeper section under test is pre-cracked by subjecting it to a bending moment 15% higher than the theoretical cracking moment. A fatigue test is then carried out on the cracked section (i.e. on the prestressing tendons) for two million cycles or until failure occurs. This paper describes a theoretical model which allows calculations of the tendon stresses induced during the fatigue test, as well as the ultimate moment of resistance of the sleeper section. This model was used to adjudicate tenders for two million heavy haul prestressed concrete sleepers with savings of R1 million on the R50 million (R1 = approximately \$1 US) contract for the coal line and now (October 1981) again for 4 to 5 million concrete sleepers (R110 million). In Appendix 2 the effect of the first year of 20t axle load (56 MGT) on the coal line is compared with the last year (37 MGT) of 18.5t axle loads.

NOMENCLATURE

A_c	area of concrete
A_t	area of tendons
A_i	area of ith tendon
c.g	centre point of gravity
E_c	Young's modulus for concrete. (between 30 and 50 GPa).
E_s	Young's modulus for prestressing steel (210 GPa)
e	eccentricity
F_c	compressive force in concrete
F_s	tensile force in steel tendons
f_{pbi}	tendon stress in ith tendon
f_{cu}	characteristic concrete cube strength
f_y	characteristic strength of steel tendons
I	second moment of area.
M	bending moment
M_u	ultimate moment of resistance.
P_e	effective total prestress
β_1, β_2	bond factors
γ_m	partial safety factor for strength.
ϵ_c	maximum compressive strain in concrete
ϵ_{cu}	maximum compressive strain in concrete at failure

ϵ_{pa}	additional strain produced by applied loading
ϵ_{pb}	tensile strain in tendon
ϵ_{pbi}	tensile strain in ith tendon.
ϵ_{pe}	strain in tendon due to effective prestress
σ_c	concrete prestress.

INTRODUCTION

In the South African Railways Track Laboratory, the standard method of assessing the structural adequacy of prestressed concrete sleepers includes the following test of the fatigue capabilities of the steel tendons (wires, strands or bars) :

(1) The sleeper section (rail seat or sleeper centre) is subjected to pure bending (i.e. no shear) until the concrete in tension (bottom surface at rail seat or top surface at sleeper centre) is cracked to the outer layer of prestressing tendons. Prior to this stage, the externally applied bending moment is resisted by both the concrete and tendons in tension and the concrete in the compression zone. Once the concrete in tension has cracked, the tensile force resisting the external bending moment must be provided solely by the prestressing tendons. The bending moment which initiates cracking of the concrete is known as the actual cracking moment, as opposed to the theoretical bending moment which, by definition, is that bending moment which induces a tensile stress of 6,20 MPa in the concrete.

(2) The sleeper section is then subjected to a repeated loading with each cycle varying uniformly from about 20 kN (or any small value) to a force which induces a bending moment of 1,15 times the theoretical cracking moment. The frequency of load application is normally 500 cycles per minute, and the load is applied for 2 million cycles or until failure occurs.

(3) If, after the application of 2 million cycles, the sleeper can support with no further crack growth the force corresponding to 1,15 times the theoretical cracking moment, the requirements of this test will have been met. Also, the cracks shall preferably not be wider than 0,05 mm with the load completely removed.

Failure of the sleeper in the above test before 2 million cycles have been completed may occur in one or more of the following modes :-

- (1) Breaking of the tendons when their fatigue strength is exceeded.
- (2) Gross slippage between the tendons and the concrete (bond failure).
- (3) Failure of the anchorage zone, where one is used.
- (4) Shear failure of the sleeper in the shear span. Fig. 1 illustrates the concept of shear span for the rail seat test and the sleeper centre test.

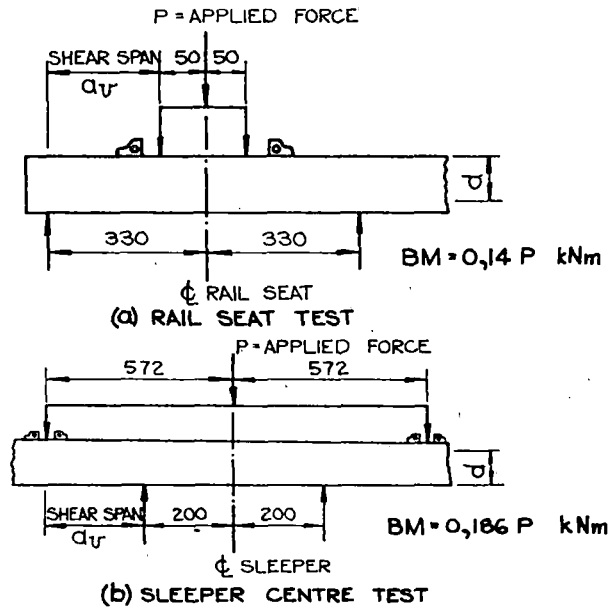


Fig. 1 Support conditions and loading for rail seat and sleeper centre

Prestressed concrete sleepers are normally not reinforced for shear. It may be expected that the shear failure mode is strongly dependent on the shear - span/depth ratio a_v/d . For the conditions shown in Fig. 1 the value of the ratio will be about 1,6 for the rail seat test and 2,0 for the sleeper centre test (assuming heavy haul S.A.R. PY or FY sleepers). If the failure mode is one of shear, it will therefore take on one of the following forms : web-shear crack, flexure-shear crack followed by diagonal-tension failure, shear-tension failure or shear-compression failure.

The need arose in the past for a reliable prediction of the stresses induced in the prestressing tendons during the fatigue testing as described above, for the following reasons :

- (1) for judge, before testing, whether or not the tendons would complete the full 2 million cycles,
- (2) to plot a theoretical S-N (stress vs cycles to failure) fatigue curve for the prestressing tendons, on completion of testing.

This paper describes a theoretical model which allows calculation of the tendon stresses induced during fatigue testing of prestressed concrete sleepers in the S.A.R. Track Laboratory, as well as determination of the ultimate moment of resistance based on the CP110 stress block and strain approach.

MATHEMATICAL MODEL

A General Flexural Theory

The following assumptions are made :

- (a) The compressive stress in the concrete due to the applied bending moment during fatigue testing is directly proportional to the distance from the neutral axis, at which the stress is zero. This in turn assumes that the maximum concrete stress induced does not exceed the limit - of - proportionality ("elastic limit") for the concrete.
- (b) The ultimate limit state of collapse is reached when the concrete strain at the extreme compression fibre reaches a specified value ϵ_{cu} .
- (c) At failure, the distribution of concrete compressive stresses is defined by an idealized stress/strain curve.
- (d) The tensile strength of the concrete is ignored. This in turn assumes that the section up to the neutral axis is fully cracked.

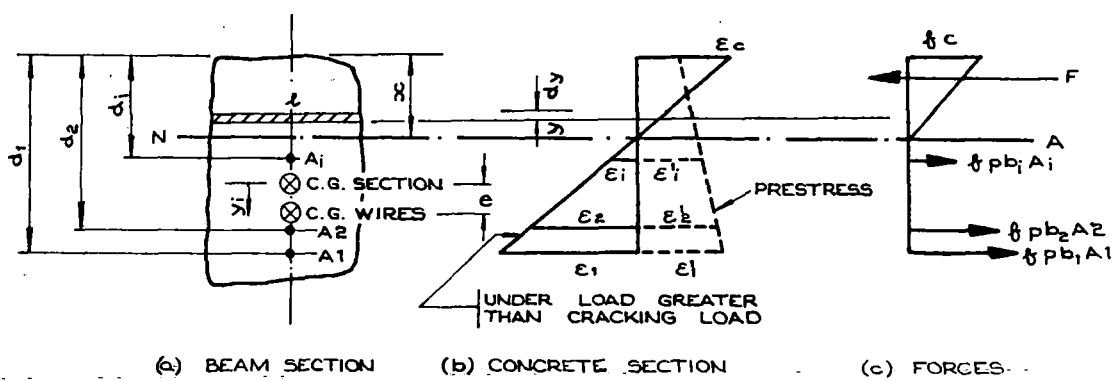


Fig. 2 Elastic analysis for cracked section

(e) The stresses in the reinforcement are derived from the appropriate stress/strain curve. Consider the beam section shown in Fig. 2(a).

Concrete strains under load greater than cracking load. The neutral axis is at a distance x from the top of the compression zone. The maximum compressive strain in the concrete is ϵ_c . The concrete strain at any distance d_i from the top of the compression zone is :

$$\epsilon_i = \left(\frac{d_i - x}{x} \right) \cdot \epsilon_c \quad (1)$$

Concrete strains due to the effective prestress only. The concrete strain at any distance y_i from the centre of gravity of the section is :

$$\epsilon_i' = \left(\frac{1}{E_c} \right) \sigma_c' \quad (2)$$

where σ_c' is the concrete prestress and given by :

$$\sigma_c' = \frac{P_e}{A_c} + \frac{P_e \cdot e}{I} \cdot y_i \quad (3)$$

Strain in tendon due to the effective prestress only.

$$\epsilon_{pe} = \frac{P_e}{A_t E_s} \quad (4)$$

Strain in tendon when a load greater than the cracking load is applied to the sleeper section. The strain in the tendon at distance d_i from the top of the compression zone may be considered to be made up of two parts :

- (a) the strain ϵ_{pe} due to the effective tendon prestress after losses and,
- (b) the additional strain ϵ_{pa} produced by the applied loading. Thus

$$\epsilon_{pb} = \epsilon_{pe} + \epsilon_{pa} \quad (5)$$

The additional strain ϵ_{pa} can be evaluated by considering the change in concrete strain at the level of the tendon. In Fig. 2(b), the broken line represents the strain distribution in the concrete produced by the effective prestressing force. Thus ϵ_i' is $(1/E_c)$ times the concrete prestress at the tendon level (Eqn. 2). The strain ϵ_i is the average concrete strain at that level under the applied bending moment during fatigue testing (Eqn. 1). Where effective bond exists, the additional strain in the tendon is $\epsilon_{pa} = \epsilon_i' + \epsilon_i$. In an unbonded post-tensioned beam ϵ_{pa} will be less than $\epsilon_i' + \epsilon_i$. In general, we can write :

$$\epsilon_{pa} = \beta_1 \epsilon_i' + \beta_2 \epsilon_i \quad (6)$$

where the bond factors β_1 and β_2 may be taken as unity for pre-tensioned beams or bonded post-tensioned beams, for unbonded post-tensioned beams, β_1 is often taken as 0,5 and β_2 as between 0,1 and 0,25.

Combining Eqns (1), (2), (3), (4), (5) and (6) gives :

$$\epsilon_{pbi} = \frac{P_e}{A_t E_s} + \beta_1 \frac{1}{E_c} \left(\frac{P_e}{A_c} + \frac{P_e \cdot e}{I} y_i \right) + \beta_2 \epsilon_c \left(\frac{d_i - x}{x} \right) \quad (7)$$

for the i th tendon.

Equilibrium equations for applied moment M.

Internal force equilibrium. The total tensile force resisted by the steel tendons, F_s , must be equal to the total compressive force on the concrete, F_c .

Referring to Fig. 2(a), the compressive force on a fibre of height dy and width l is

$$dF_c = \frac{y}{x} \cdot \sigma_c \cdot l \cdot dy$$

The total concrete force is thus :

$$F_c = \int_0^x \frac{l y \sigma_c}{x} dy$$

or

$$\frac{F_c}{\sigma_c} = \int_0^x \frac{l y}{x} dy \quad (8)$$

where l is a function of y for any section other than rectangular.

The total steel force is :

$$F_s = E_s \sum_{i=1}^n \left(A_i \epsilon_{pbi} \right) \quad (9)$$

where n is the total number of tendons. Defining $E_s/E_c = a_e$ and equating F_c to F_s :

$$E_c \epsilon_c \int_0^x \frac{l y}{x} dy = E_s \sum_{i=1}^n A_i \epsilon_{pbi} \quad (10)$$

$$\epsilon_c \int_0^x \frac{l y}{x} dy = a_e \sum_{i=1}^n A_i \epsilon_{pbi}$$

Moment equilibrium. Taking moments about neutral axis,

$$M = \sigma_c \int_0^x \frac{y^2}{x} l dy + E_s \sum_{i=1}^n A_i \epsilon_{pbi} (d_i - x) \quad (11)$$

Equations (7), (10) and (11) can now be solved for the unknowns in the problem, viz :-

- x , the depth of the neutral axis;
- ϵ_c , the maximum compressive strain in the concrete;
- ϵ_{pb} , the total tensile strain in any tendon.

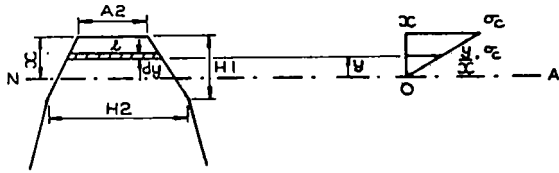
Limits of validity of theory. The above equations are valid only if both the concrete stress - depth distribution and steel stress-strain distribution are linear. For concrete, the stress-strain curve may be approximated by a straight line only up to about 50 % of the maximum stress. If the cube strength is 60 MPa, the cylinder strength is $0,8 \times 60 = 48$ MPa i.e. 50 % of this is 24 MPa. Now, if E_c equals 30 GPa,

this gives a limiting strain of $24 \times 10^{-3} / 30 = 0,0008$ which is only 22,9 % of the value at which concrete is assumed to exhibit visible crushing viz. 0,0035.

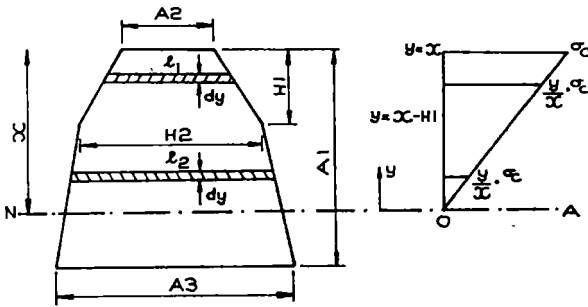
Prestressing steel does not have a definite yield point, but it is assumed in CP110 that the limit-of-proportionality is about 0,7 time the 0,2 % proof stress. Now, if the proof stress is 1 500 MPa, this gives $0,7 \times 1\ 500 = 1\ 050$ MPa. If E_s equals 200 GPa the limiting strain is 0,0053.

THEORY APPLIED TO PRESTRESSED CONCRETE SLEEPERS

The integrals in Eqns. (10) and (11) can be evaluated for sleeper sections (rail seat and centre). This is done in Appendix 1. The results are given below.



(a) $x < H1$



(b) $x > H1$

Fig. 3 Calculation of total concrete force F_c and moment M_c

(i) $x < H1$

$$\frac{F_c}{\sigma_c} = \frac{x}{2} \left[A2 + \left(\frac{H2 - A2}{H1} \right) \frac{x}{3} \right] \tag{12}$$

$$\frac{M_c}{\sigma_c} = \frac{x^2}{3} \left[A2 + \left(\frac{H2 - A2}{H1} \right) \frac{x}{4} \right] \tag{13}$$

(ii) $x > H1$

$$\begin{aligned} \frac{F_c}{\sigma_c} &= \left[H2 - A2 + x \left\{ \left(\frac{A3 - H2}{A1 - H1} \right) - \left(\frac{H2 - A2}{H1} \right) \right\} - H1 \left(\frac{A3 - H2}{A1 - H1} \right) \right] \\ &+ \frac{(x - H1)^3}{3x} \left[- \left(\frac{A3 - H2}{A1 - H1} \right) + \left(\frac{H2 - A2}{H1} \right) \right] \\ &+ A2 \cdot \frac{x}{2} + \frac{x^2}{6} \left(\frac{H2 - A2}{H1} \right) \end{aligned} \tag{14}$$

$$\begin{aligned} \frac{M_c}{\sigma_c} &= \frac{(x - H1)^3}{3x} \left[H2 + \left\{ \left(\frac{A3 - H2}{A1 - H1} \right) - \left(\frac{H2 - A2}{H1} \right) \right\} x \right] \\ &+ \frac{(x - H1)^3}{3x} \left[- H1 \cdot \left(\frac{A3 - H2}{A1 - H1} \right) - A2 \right] \\ &+ \frac{(x - H1)^4}{4x} \left[- \left(\frac{A3 - H2}{A1 - H1} \right) + \left(\frac{H2 - A2}{H1} \right) \right] \\ &+ A2 \cdot \frac{x^2}{3} + \frac{x^3}{12} \cdot \frac{(H2 - A2)}{H1} \end{aligned} \tag{15}$$

SOLUTION PROCEDURE FOR ELASTIC ANALYSIS

The unknowns : x , ϵ_c and ϵ_{pbi} can be solved for using the following procedure^{Pb}:

- (1) Choose x .
- (2) Substitute x into Eqn (7) giving ϵ_{pbi} in terms of ϵ_c (for $i = 1, 2, \dots, n$).
- (3) Substitute x into Eqn (13) or (15) depending on the value of x
- (4) Substitute ϵ_{pbi} and Eqn (13) or (15) into Eqn (11)
- (5) M is known, therefore calculate ϵ_c
- (6) Substitute ϵ_c and x into Eqn (12) or (14) depending on value of x , and see if Eqn (10) is satisfied.
- (7) If not, choose new value of x and repeat steps (1) to (6) until Eqn (10) is satisfied.
- (8) This yields x , ϵ_c and hence ϵ_{pbi} and f_{pbi} , the tendon stresses.

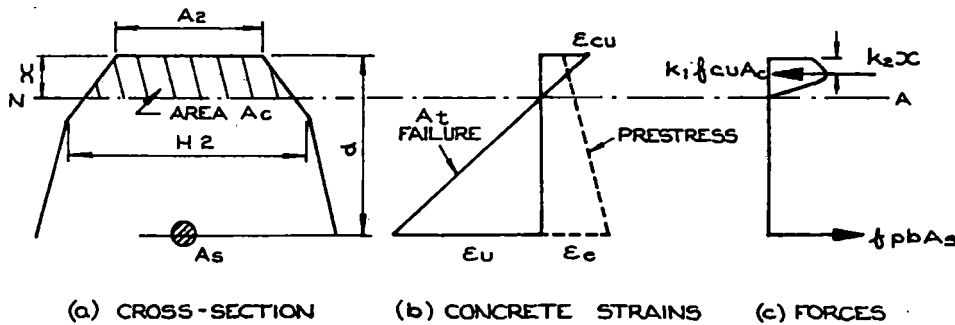


Fig. 4 Ultimate flexural conditions

**CALCULATION OF ULTIMATE MOMENT OF RESISTANCE
USING CP110 STRESS BLOCK AND STRAIN APPROACH**

Consider the sleeper section shown in Fig. 4(a).

From assumption (b), the maximum concrete compressive strain has a specified value ϵ_{cu} at the instant of collapse. Therefore, the concrete strain at a distance d from the top of the section can be obtained immediately from the geometry of Fig. 4(b). The tendon strain ϵ_{pb} at the ultimate condition is made up of two parts :

- (a) the strain ϵ_{pe} due to the effective tendon prestress after losses and,
- (b) the additional strain ϵ_{pa} produced by the applied ultimate moment M_u . Thus

$$\epsilon_{pb} = \epsilon_{pe} + \epsilon_{pa}$$

The prestress strain ϵ_{pe} is f_{pe}/E_s if the stress is within the elastic limit, but may in any case be determined from f_{pe} and the stress/strain curve. The additional strain ϵ_{pa} is given by :

$$\epsilon_{pa} = \beta_1 \epsilon_e + \beta_2 \epsilon_u$$

ϵ_u may be obtained from the geometry of Fig. 4(b), so that

$$\epsilon_{pa} = \beta_1 \epsilon_e + \beta_2 \cdot \frac{d-x}{x} \cdot \epsilon_{cu}$$

Now,
$$\epsilon_{pb} = \epsilon_{pe} + \epsilon_{pa}$$

$$= \epsilon_{pe} + \beta_1 \epsilon_e + \beta_2 \epsilon_{cu} \cdot \frac{d-x}{x} \quad (16)$$

The tendon stress f_{pb} corresponding to ϵ_{pb} can be obtained from the CP110 design stress/strain curve for ultimate limit state (Fig. 5).

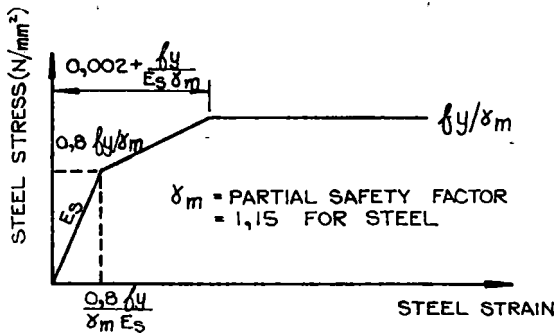


Fig. 5 Design stress/strain curve for ultimate limit state - CP110

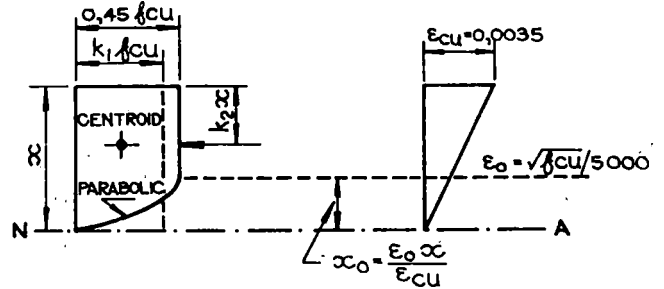
Applying the equilibrium condition to Fig. 4(c):

$$f_{pb} A_t = k_1 f_{cu} A_c \quad (17)$$

where k_1 is the ratio of the average compressive stress to the characteristic concrete strength f_{cu} .

Fig. 6(a) shows the idealized stress block adopted in CP110 for ultimate strength calculations in design. CP110 further assumes that the ultimate concrete strain is constant at $\epsilon_{cu} = 0,0035$, and that the parabolic part of the stress block ends at a strain

$$\epsilon_o = \sqrt{f_{cu}}/5000$$



(a) STRESS BLOCK (b) STRAIN DISTRIBUTION

Fig. 6 Design stress block for ultimate limit state - CP110

From Fig. 6,

$$k_1 = 0,45 \left[1 - \sqrt{f_{cu}}/52,5 \right] \quad (18)$$

$$k_2 = \frac{\left[2 - \frac{f_{cu}}{17,5} \right]^2 + 2}{4 \left[3 - \frac{\sqrt{f_{cu}}}{17,5} \right]} \quad (19)$$

The ultimate moment of resistance is :

$$M_u = f_{pb} A_t (d - k_2 x) \quad (20)$$

f_{pb} is obtained from solving Eqn (17) by trial-and-error of the unknown value x .

SOLUTION PROCEDURE FOR ULTIMATE ANALYSIS

- (1) Choose x .
- (2) Calculate ϵ_{pb} from Eqn (16) with $\epsilon_{cu} = 0,0035$
- (3) Obtain f_{pb} from Fig. 5
- (4) Calculate total steel force $\sum f_{pb} A_t$.
- (5) Calculate total concrete force $k_1 f_{cu} A_c$.
- (6) Check that steel force equals concrete force.
- (7) If not, choose new value of x and repeat steps (1) to (6) until steel force equals concrete force.
- (8) Calculate M_u from Eqn. (20).

Comment on Ultimate Moment Calculation

The procedure for calculating the ultimate moment of resistance of a sleeper cross section is on the CP110 stress and strain approach. This calculation method underestimates the actual moment of resistance as observed in the laboratory

(by between 30 % and 50 % of the actual value). The underestimation is probably as a result of assuming the concrete has failed when the outer fibre strain is 0,0035 (whereas in fact it may be more in practice), and of using the design stress/strain for steel shown in Fig. 5, which contains inherent partial safety factors as laid down by CP110.

Further work is done to improve the ultimate moment calculation procedure by using a more basic and less conservative approach than that in CP110. The results should be available at the time of the Conference.

COMPUTER PROGRAM

The elastic and ultimate flexural analysis described above requires in iterative solution of Eqns. (7) to (15) (elastic analysis) and Eqns (16) to (17) (ultimate analysis). A computer program CRACK was written in BASIC language to automate the solution of these equations.

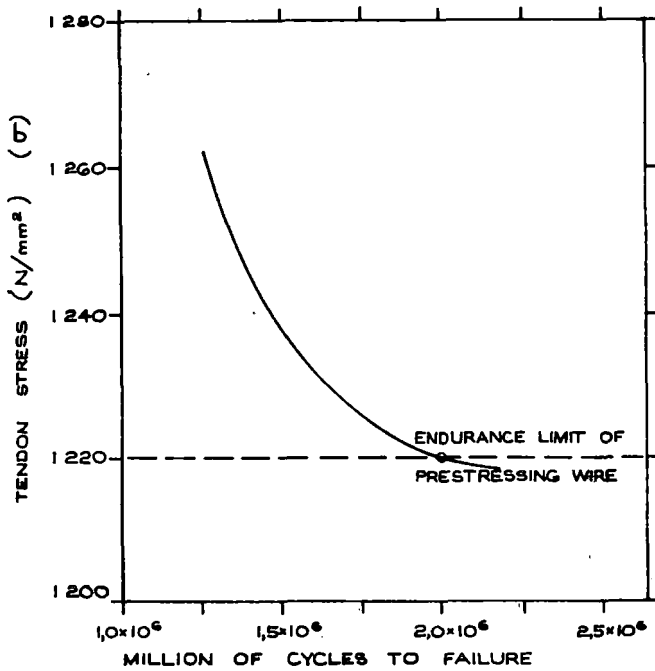


Fig. 7 Tendon stresses versus number of cycles to failure

Fatigue tests done in the past in the S.A.R. Track Laboratory on concrete sleepers supply almost sufficient data to plot master S-N curves (i.e. the stresses induced in the bottom tendons were calculated using the program CRACK and the results plotted versus the number of cycles to failure) as shown in Fig. 7 for each of the different tendons used by the suppliers of concrete sleepers.

Further tests are planned and master S-N curves should be available in due course.

ACKNOWLEDGEMENTS

The General Manager of the South African Transport Services is thanked for permission to publish this paper.

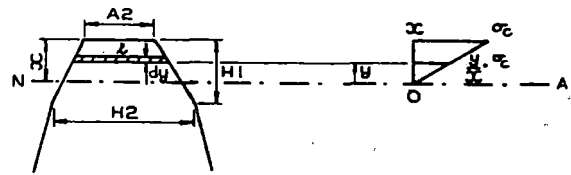
REFERENCES

1. Speers C.R. "Theoretical Tendon Stresses Induced during Fatigue Testing of Prestressed Concrete Sleepers", S.A.R. Report 24.594/10/79.
2. Maree J.S. "Die Effek van die Eerste 20 t Asbelastingjaar op die Steenkoollyn se Spoorstawe", S.A.R. Report 24.616/01/81.
3. Besuner P.M., Stone D.H., Schoeneberg K.W. and De Herrera M.A. "Probability Analysis of Rail Defect Data", Proceedings of the Heavy Haul Railways Conference, The Institution of Engineers, Australia, September 1978, Session 308, Paper I.4.

APPENDIX 1

CALCULATION OF CONCRETE FORCE AND MOMENT FOR ELASTIC ANALYSIS OF PRESTRESSED CONCRETE SLEEPERS.

Force F_c .
(1) $x < H_1$



(a) $x < H_1$

$$l = A_2 + \frac{(H_2 - A_2)(x - y)}{H_1}$$

$$dA = l \cdot dy$$

$$F_c = \int_0^x \frac{y}{x} \cdot \sigma_c \cdot dA = \sigma_c \int_0^x \frac{y}{x} \cdot l \cdot dy$$

$$\frac{F_c}{\sigma_c} = \int_0^x \left[A_2 + \frac{(H_2 - A_2)(x - y)}{H_1} \right] \frac{y}{x} dy$$

$$= \int_0^x A_2 \frac{y}{x} dy + \int_0^x \frac{(H_2 - A_2)(x - y)}{H_1} \frac{y}{x} dy$$

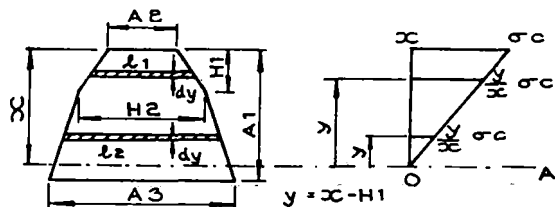
$$= A_2 \left[\frac{y^2}{2x} \right]_0^x + \frac{(H_2 - A_2)}{H_1} \left[\frac{y^2}{2} - \frac{y^3}{3x} \right]_0^x$$

$$= A_2 \frac{x}{2} + \frac{(H_2 - A_2)}{H_1} \frac{x^2}{6}$$

$$= \frac{x}{2} \left[A_2 + \frac{(H_2 - A_2)}{H_1} \frac{x}{3} \right]$$

$$= \frac{x}{2} (A_2 + C_9 \frac{x}{3}) \tag{21}$$

(ii) $x > H_1$



$$\begin{aligned}
l_1 &= A2 + \frac{(H2 - A2)}{H1} \cdot (x - y) \\
l_2 &= H2 + \frac{(A3 - H2)}{A1 - H1} \cdot (x - H1 - y) \\
\frac{F_c}{\sigma_c} &= \int_0^x \left[H2 + \frac{(A3 - H2) \cdot (x - H1 - y)}{(A1 - H1)} \right] \frac{y}{x} \cdot dy \\
&+ \int_{x-H1}^x \left[A2 + \frac{(H2 - A2) \cdot (x - y)}{H1} \right] \frac{y}{x} \cdot dy \\
&= \int_0^x H2 \cdot \frac{y}{x} \cdot dy + \int_0^x \frac{(A3 - H2)}{(A1 - H1)} \left(y - \frac{y^2}{x} - H1 \cdot \frac{y}{x} \right) dy \\
&+ \int_{x-H1}^x A2 \cdot \frac{y}{x} \cdot dy + \int_{x-H1}^x \frac{(H2 - A2)}{H1} \cdot \left(y - \frac{y^2}{x} \right) \cdot dy \\
&= H2 \left[\frac{y^2}{2x} \right]_0^x + \frac{(A3 - H2)}{A1 - H1} \left[\frac{y^2}{2} - \frac{y^3}{3x} - \frac{H1 \cdot y^2}{2x} \right]_0^x \\
&+ A2 \left[\frac{y^2}{2x} \right]_{x-H1}^x + \frac{(H2 - A2)}{H1} \left[\frac{y^2}{2} - \frac{y^3}{3x} \right]_{x-H1}^x \\
&= H2 \cdot \frac{(x - H1)^2}{2x} + \frac{(A3 - H2)}{A1 - H1} \left[\frac{(x - H1)^2}{2} \right] \\
&+ \frac{A3 - H2}{A1 - H1} \left[-\frac{(x - H1)^3}{3x} - \frac{H1 \cdot (x - H1)^2}{2x} \right] \\
&+ A2 \left[\frac{x}{2} - \frac{(x - H1)^2}{2x} \right] + \frac{(H2 - A2)}{H1} \left[\frac{x^2}{2} - \frac{x^3}{3} - \frac{(x - H1)^2}{2} \right] \\
&+ \frac{(H2 - A2) \cdot (x - H1)^3}{H1 \cdot 3x} \\
&= \frac{(x - H1)^2}{2x} \left[H2 - A2 + \frac{(A3 - H2)x}{A1 - H1} - H1 \cdot \frac{(A3 - H2)}{A1 - H1} \right] \\
&+ \frac{(x - H1)^2}{2x} \left[-\frac{(H2 - A2)}{H1} x \right] \\
&+ \frac{(x - H1)^3}{3x} \left[-\frac{(A3 - H2)}{A1 - H1} + \frac{(H2 - A2)}{H1} \right] \\
&+ A2 \cdot \frac{x}{2} + \frac{x^2}{6} \cdot \frac{(H2 - A2)}{H1} \\
&= \frac{(x - H1)^2}{2x} \left[H2 - A2 + x \frac{(A3 - H2)}{A1 - H1} - H1 \cdot \frac{(A3 - H2)}{A1 - H1} \right] \\
&+ \frac{(x - H1)^2}{2x} \left[-\frac{(H2 - A2)}{H1} x \right] \\
&+ \frac{(x - H1)^3}{3x} \left[-\frac{(A3 - H2)}{A1 - H1} + \frac{(H2 - A2)}{H1} \right] \\
&+ A2 \cdot \frac{x}{2} + \frac{x^2}{6} \cdot \frac{(H2 - A2)}{H1} \\
&= \frac{(x - H1)^2}{2x} \cdot (X4 + x \cdot X5 - H1 \cdot H3) \\
&+ \frac{(x - H1)^3}{3x} \cdot (-X5) + A2 \cdot \frac{x}{2} + \frac{x^2}{6} \cdot C9. \quad (22)
\end{aligned}$$

Moment M_c (Taking moments about N.A.)

(i) $x < H1$.

$$\begin{aligned}
\frac{M_c}{\sigma_c} &= \int_0^x l \cdot \frac{y}{x} \cdot y \cdot dy \\
&= A2 \left[\frac{y^3}{3x} \right]_0^x + \frac{(H2 - A2)}{H1} \left[\frac{y^3}{3} - \frac{y^4}{4x} \right]_0^x \\
&= A2 \cdot \frac{x^2}{3} + \frac{(H2 - A2)}{H1} \left(\frac{x^3}{3} - \frac{x^4}{4} \right) \\
&= A2 \cdot \frac{x^2}{3} + \frac{(H2 - A2)}{H1} \cdot \frac{x^3}{12} \\
&= \frac{x^2}{3} \cdot (A2 + C9 \cdot \frac{x}{4}) \quad (23)
\end{aligned}$$

(ii) $x > H1$

$$\begin{aligned}
\frac{M_c}{\sigma_c} &= H2 \left[\frac{y^3}{3x} \right]_0^{x-H1} + \left[\frac{(A3 - H2)}{A1 - H1} \frac{y^3}{3} - \frac{y^4}{4x} - \frac{H1 \cdot y^3}{3x} \right]_0^{x-H1} \\
&+ A2 \left[\frac{y^3}{3x} \right]_x^{x-H1} + \frac{(H2 - A2)}{H1} \left[\frac{y^3}{3} - \frac{y^4}{4x} \right]_{x-H1}^x \\
&= \frac{(x - H1)^3}{3x} \left[H2 + \frac{(A3 - H2)}{A1 - H1} x - A2 - \frac{(H2 - A2)x}{H1} \right] \\
&+ \frac{(x - H1)^3}{3x} \left[-H1 \cdot \frac{(A3 - H2)}{A1 - H1} \right] \\
&+ \frac{(x - H1)^4}{4x} \left[-\frac{(A3 - H2)}{A1 - H1} + \frac{(H2 - A2)}{H1} \right] \\
&+ A2 \cdot \frac{x^2}{3} + \frac{x^3}{12} \cdot \frac{(H2 - A2)}{H1} \\
&= \frac{(x - H1)^3}{3x} \left[H2 + \left\{ \frac{(A3 - H2)}{A1 - H1} - \frac{(H2 - A2)}{H1} \right\} x \right] \\
&+ \frac{(x - H1)^3}{3x} \left[-H1 \cdot \frac{(A3 - H2)}{A1 - H1} - A2 \right] \\
&+ \frac{(x - H1)^4}{4x} \left[-\frac{(A3 - H2)}{A1 - H1} + \frac{(H2 - A2)}{H1} \right] \\
&+ A2 \cdot \frac{x^2}{3} + \frac{x^3}{12} \cdot \frac{(H2 - A2)}{H1} \\
&= \frac{(x - H1)^3}{3x} \cdot (X4 + x \cdot X5 - H1 \cdot H3) \\
&+ \frac{(x - H1)^4}{4x} \cdot (-X5) + A2 \cdot \frac{x^2}{3} + \frac{x^3}{12} \cdot C9 \quad (24)
\end{aligned}$$

APPENDIX 2

EFFECT OF THE FIRST 20 t/AXLE YEAR ON THE RAILS OF THE COAL LINE

INTRODUCTION

At the end of 1976 the first trainload of coal was off-loaded at Richards Bay harbour. By the end of June 1979 110 million gross tons (MGT) was carried on the coal line from Broodsnyersplaas to Richards Bay. (500 km). Trains were made up by 18,5 t/axle coal trucks with electric locomotives of 22 t/axle. Most of the trucks were equipped with high stability Scheffel bogies. Since July 1979 the axle loads were increased to 20 t.

During the last 18,5 t/axle year 37 MGT was carried and 56 MGT during the first 20 t/axle year. This line carried the highest traffic on the South African Railways during 1979/80.

From Broodsnyersplaas to Richards Bay (See map in Appendix 3) the minimum track structure is 200 mm of ballast below the 215 kg prestressed concrete sleepers placed at 700 mm spacing. The minimum ballast shoulder width is 250 mm. From Broodsnyersplaas to Vryheid (300 km) 57 kg/m HCOB rails were used. On the section from Vryheid to Richards Bay 128 km of 48 kg/m HCOB rails were used originally. At the end of June 1980 only 99 km of these were left in the track. The main reason for replacement was wear on curves. Of the 65 km of 57 kg/m HCOB rails 57 km was still in the track at the end of June 1980. No rails were replaced north of Vryheid.

The following data can be analysed to evaluate the effect of the 20 t axle loads :

- (a) Maintenance costs;
- (b) Maintenance effort e.g. what was required to retain the track within a certain standard;
- (c) Component life e.g. points and crossings, block joints, rail wear, rail breaks, etc.

DISCUSSION OF AVAILABLE DATA

Maintenance Costs

The previous method of book-keeping for maintenance costs was unsatisfactory, but a revised method now introduced will yield important data on cost of maintenance.

Maintenance Effort

Due to problems with the two track geometry cars information on the rate of deterioration of track geometry is not sufficient.

Component Life

Sufficient information on the life of specific components is not available.

The only data available is the record of reported rail defects stored on computer with other track data. The Vryheid - Richards Bay section (200 km) is the line on the S.A.R. with the worst history of broken rails in the thermit weld area. Breaks occur at a rate of more than 40 per year for every 1000 thermit welds. On the Broodsnyersplaas - Vryheid section (300 km) breaks occur at 6 per year for every 1000 thermit welds which tie in with the average for the S.A.R.

RAIL BREAKS

In fig. 8 all reported cumulative broken rails for Vryheid - Richards Bay (200 km) and Ermelo - Vryheid (200 km) are shown against time. A big increase of breaks with the introduction of the 20 t axle loads was observed.

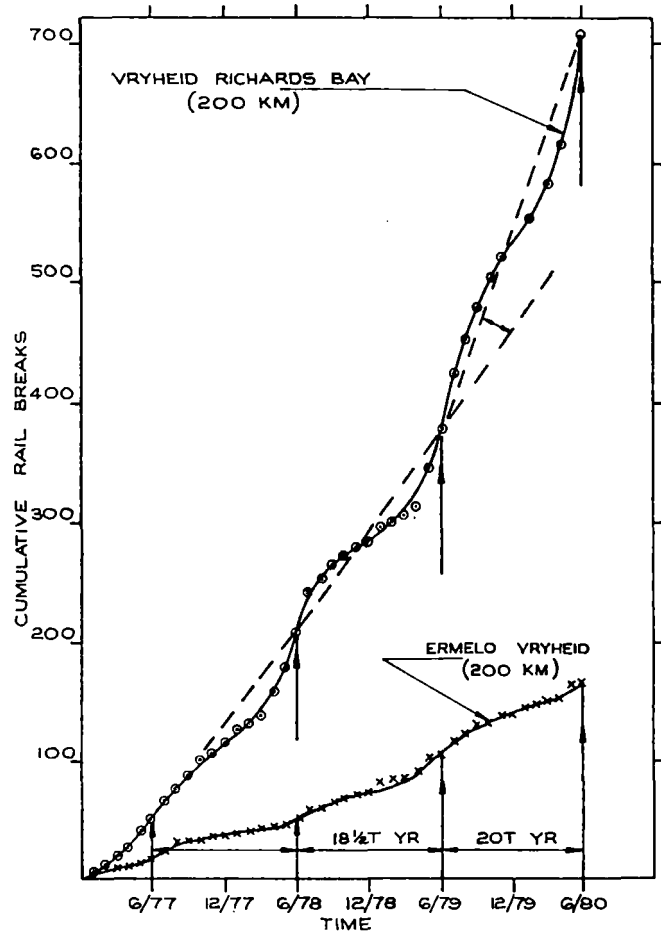


Fig. 8 All reported broken rails against time.

In fig. 9 the same breaks are plotted against MGT. It is now clear that the increase in rail breaks on the Vryheid - Richards Bay section can not only be ascribed to the increase in axle loads (mostly 48 kg/m rails). The Ermelo - Vryheid section shows a decrease of broken rails after the introduction of the 20 t axle loads.

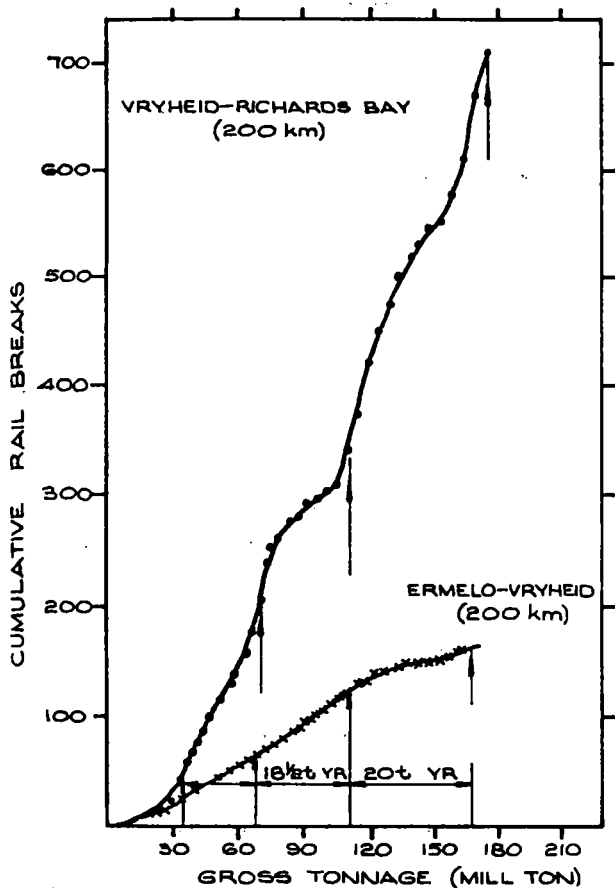


Fig. 9 All reported broken rails against traffic (MGT)

As discussed under the Weibull-analysis the comparison between the 57 kg/m south of Vryheid and the same length (57 km) directly north of Vryheid can be seen in fig. 10

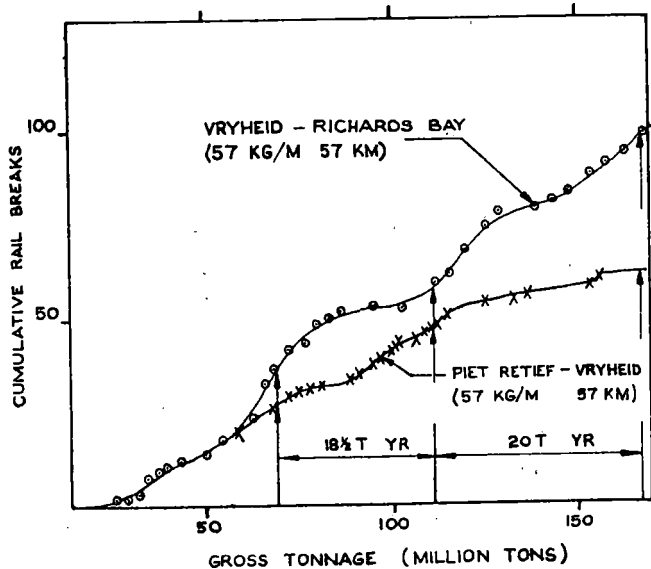


Fig. 10 Comparison of broken rails Vryheid-Richards Bay and Piet Retief-Vryheid.

PROBABILITY ANALYSIS OF BROKEN RAILS

The two - parameter Weibull distribution (3) is represented by the equation.

$$PD(MGT) = \begin{cases} 1 - \exp \left[- (MGT/\alpha)^\beta \right] \\ MGT, \alpha, \beta \geq 0 \end{cases} \quad (25)$$

where PD (MGT) = Probability a rail will have a defect before a certain tonnage.

α = Characteristic usage required for a defect. Corresponds to the MGT value at which 0,632 (i.e. $1 - e^{-1}$) of the rails will contain a defect.

β = Weibull shape, slope or scatter parameter.

The defect occurrence or "failure" rate is given by :

$$\lambda(MGT) = \beta / \alpha^\beta \left[MGT \right]^{\beta-1} \quad (26)$$

Let N_n = $\lambda \cdot k$ = rate of defect occurrence per km at a given tonnage.

k = Number of rails in one track km.

Let N = $\sum N_n$ = accumulated defects/km at given tonnage.

$$= \int_0^{MGT} \lambda d(MGT) \\ = k (MGT/\alpha)^\beta \quad (27)$$

With the information stored on computer of rails in track, gross tonnage, rail break history and ultrasonic test results a program was developed to predict the accumulated defects/km for any section. The program calculates the MGT over a rail until it breaks, performs a statistical regression analysis to determine the relation between $\log_e \log_e MGT$ and $\log_e \log_e$ probability. The correlation coefficient (R) and the values of the parameters α and β are printed. The results are plotted on a "computerized" Weibull probability paper. With α and β known predictions of the expected defects (N) can be made at any tonnage by using equation (27). From a Weibull analysis with the reported broken rails at the end of June 1979 (end of the last 18,5 t year) the expected broken rails at the end of June 1980 (end of the first 20 t year) is calculated. The predictions are done assuming the axle loading has remained at 18,5 t.

Experience has shown that predictions from 100 MGT are not always realistic. Predictions after 150 MGT compared well with real conditions. As a check α and β were determined again using data at the end of June 1980. With these α and β values the theoretical breaks/km are compared with the reported breaks/km.

Vryheid - Richards Bay (48 kg/m)

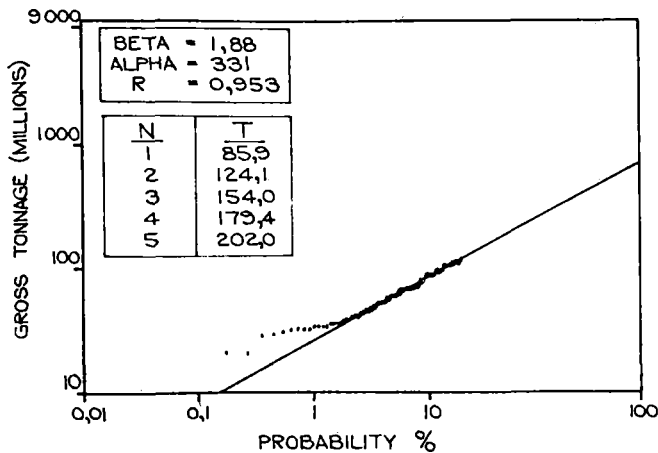


Fig. 11 Weibull-analysis 48 kg/m broken rails Vryheid-Richards Bay end June 1979

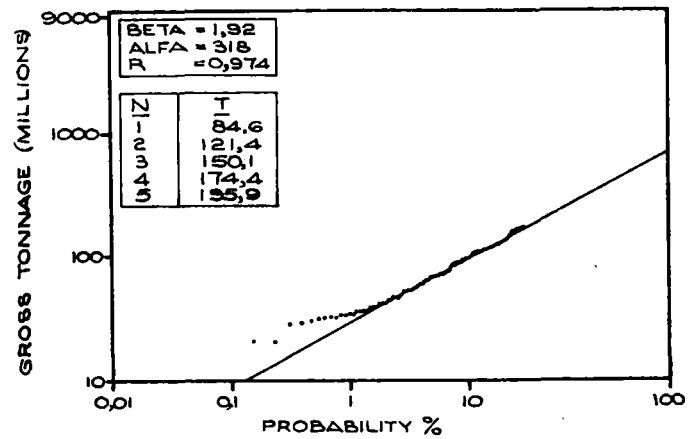


Fig. 12 Weibull-analysis 48 kg/m broken rails Vryheid-Richards Bay end June 1980.

TABLE NO. 1

SUMMARY OF CUMULATIVE BREAKS/KM ACCORDING TO WEIBULL ANALYSIS.

SECTION	BREAKS/KM REPORTED		BREAKS/KM PREDICTED		BREAKS/KM THEORETICAL AS AT END JUNE 1980		
	N ₇₉	N ₈₀	N ₈₀	R	N ₇₉	N ₈₀	R
ERMELO - PIET RETIEF 57 KG/M - 100 KM	0,3	0,5	0,5	0,96	0,3	0,5	0,98
PIET RETIEF - VRYHEID 57 KG/M - 100 KM	0,6	0,7	1,1	0,98	0,6	1,0	0,98
VRYHEID - RICHARDS BAY 57 KG/M - 57 KM	0,9	1,5	3,0	0,97	0,9	1,8	0,97
VRYHEID - RICHARDS BAY 48 KG/M - 99 KM	1,7	3,1	3,5	0,95	1,6	3,6	0,97

N₇₉ = Cumulative breaks end June 1979
 N₈₀ = Cumulative breaks end June 1980
 R = Correlation coefficient.

The plots are shown in fig. 11 (June 1979, 110 Mt) and fig. 12 (June 1980, 166 MGT). Correlation coefficients of 0,95 and 0,97 were obtained. With α and β from fig. 11 the expected breaks/km (N_{expected}) at 166 MGT are calculated.

$$\alpha = 331 \text{ MGT}$$

$$\beta = 1,88$$

$$N_{\text{expected}} = 3,5 \text{ breaks/km.}$$

After 166 MGT 305 breaks were reported for the 99 km of 48 kg/m rails still in the track.

$$N_{\text{reported}} = 305/99$$

$$= 3,1 \text{ breaks/km}$$

Less breaks actually occurred than expected.

The plots for the other sections are not included but the results are given in table No. 1. The section from Broodsniersplaas to Ermelo was not analysed due to too little breaks.

Discussion of Weibull Analysis

Neither the 48 nor the 57 kg/m rails showed more breaks than predicted. More breaks occurred on the 48 kg/m rails than on the 57 kg/m rails. The increase in rail breaks for the 57 kg/m sections is very interesting.

The 57 kg/m rails in the Vryheid - Richards Bay section only carried 5 MGT more than the section north of Vryheid.

The 57 kg/m rails in the Vryheid - Richards Bay section are situated in the heart of Zululand far from developed areas, with big changes in temperature and sharper grades.

The weathered tillite formation could also contribute to the increase in rail breaks.

CONCLUSIONS

Graphs of cumulative breaks against gross tonnage on natural scale and Weibull analysis show an increase in rail breaks in 48 and 57 kg/m rails can not be attributed to the increase in axle loads from 18,5 t to 20 t. The growth in traffic is the decisive factor.

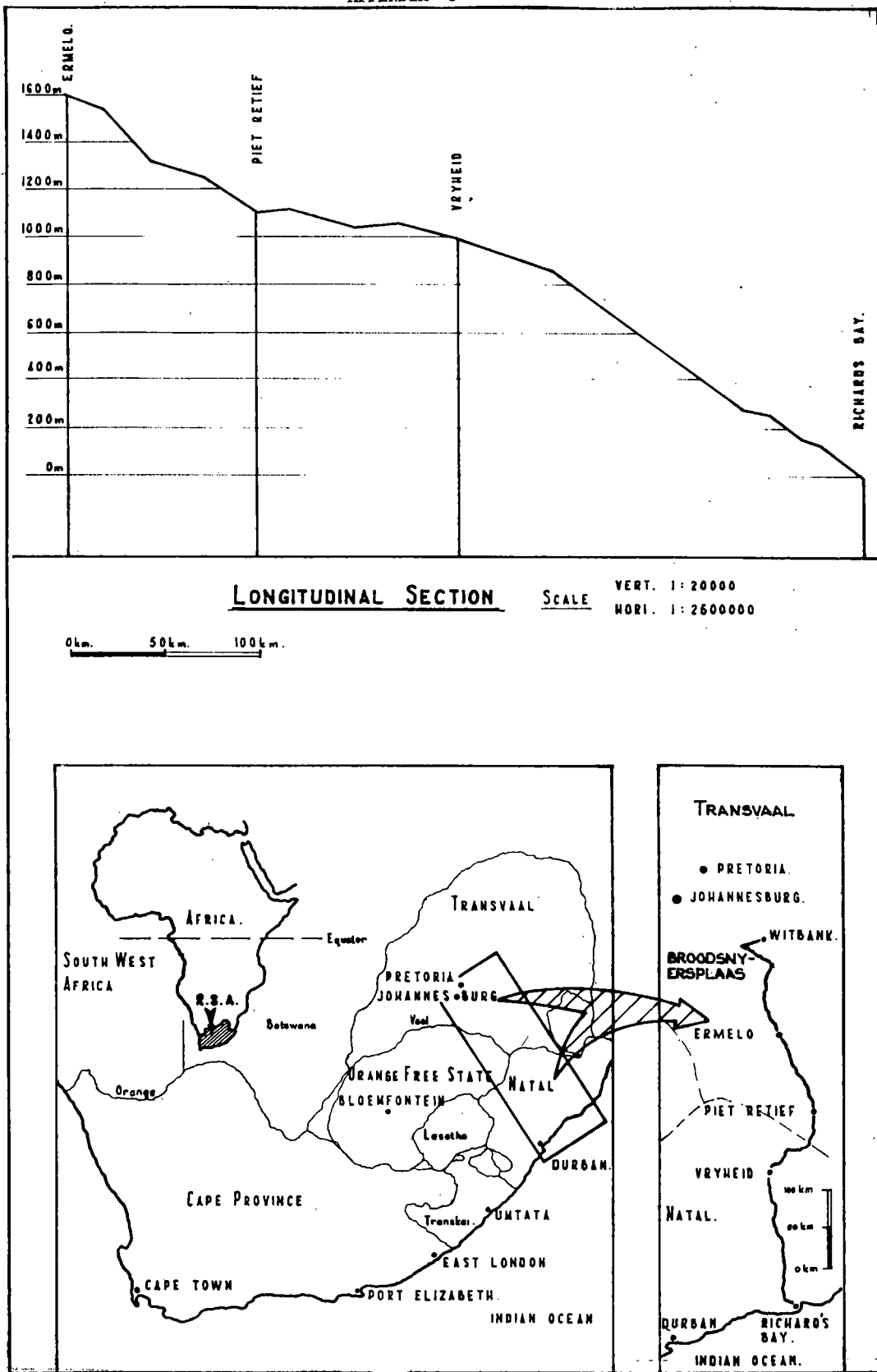
Requests to increase axle loads from 18,5 t to 20 t on 215 kg concrete sleepers at 700 mm spacing can be granted without fear of a drastic increase in rail breaks. The condition of the track is of utmost importance and can only be evaluated by track maintenance personnel.

The change to Scheffel bogies for 20 t/axle trucks should be a priority. A transition period of (say) three years can be considered.

Rail defects should however be analysed before a decision to increase the axle load is taken, because defects increase with fatigue life.

This analysis stressed the importance of sound thermit welds. The SKV (minimum pre-heat) thermit welds introduced last year could reduce the problem.

An economical method to test thermit welds must be developed. Strategic thermit welds (e.g. in tunnels, on high bridges, etc.) on the coal line are now examined radiographically. This method is however too expensive and specialised.



Map showing the Coal Line

D. Leshchinsky

Research Engineer-Track
Research & Test Department
Assoc. of American
Railroads

J. Choros

Senior Research Engineer
Research & Test Department
Assoc. of American
Railroads

A.J. Reinschmidt

Manager
Track Research Division
Research & Test Department
Assoc. of American
Railroads

A Simplified Methodology to Evaluate the Effect of Heavier Axle Loads on Track Substructure Performance

A simplified methodology to evaluate the effect of heavier axle loads on track substructure performance is presented. The track geometry deterioration mechanism, as related to the substructure is postulated. Based on that, damage factors which account for heavier axle loads are defined as inequalities. The quantities needed to calculate the damage factors are determined through the beam on elastic foundation and through the integrated Boussinesq equations, all presented in a convenient ready to use chart format. The experimental input data needed is the track modulus characterizing the track where the heavier axle load effect is to be evaluated. The non-linear system response is evaluated through the value of the track modulus corresponding to the proper axle load. The methodology presented in this paper offers also a convenient technique to check the effect of changes in the track structure.

Throughout the history of the railroad industry the need for greater productivity has been, in part, achieved by the continued growth of car size and capacity. Unfortunately, the increased transportation productivity provided by larger and heavier cars may, in some cases, be partially offset by increases in other costs.

One major element of railroad costs is the maintenance of the track structure and its associated foundation. The railroad industry is unique in being the only major mode of transportation which is required to maintain its own right-of-way. However, this maintenance requirement gives the railroad the unique opportunity to optimize the total transportation system, in light of the interaction of vehicle and track maintenance costs.

The costs of track maintenance can be related to several distinct degradation mechanisms, each of which is governed by a particular set of laws and considerations. A degradation mechanism which requires constant attention is the loss of line and surface. The deterioration of surface is the result of the accumulation of permanent settlement in the ballast and subgrade layers of the track structure. Traditional methods of assessing the loads which exist at various levels in the track structure have been linear with respect to the applied load. Thus, any evaluation of the effect of increased car size would show a linear increase in the loads throughout the track structure. However, nature is infrequently a linear system. In most cases, the load-displacement functions of natural materials exhibit significant non-linear properties.

Previous efforts to assess the effects of varying load levels on ballast and subgrade, considering non-linear effects, have required extensive analysis resources. The difficulty associated with applying these techniques has limited their use. This paper presents a simplified methodology for evaluating the effect of varying loads on the subgrade, considering the non-linear properties of the substructure. The simplified nature of this technique should overcome the major limitation of earlier attempts to evaluate the effect of heavier axle loads.

TRACK SUBSTRUCTURE CONTRIBUTION TO THE SURFACE GEOMETRICAL DETERIORATION

In order to develop a methodology which will enable the evaluation of heavier axle load effects on track performance, the track geometry deterioration mechanism, as related to the substructure, should be postulated.

As discussed in [1], the track surface geometrical deterioration is based upon differential permanent settlements. The magnitudes of the differential permanent settlements are related to the magnitudes of the permanent settlements; i.e., the greater the permanent settlement the greater the potential for larger differential settlement, and hence, the faster the track surface deteriorates.

Figure 1 is a qualitative illustration of a typical track settlement response, resulting from one loading cycle applied at the rail head. In this figure, the subscript, p , on the displacement axis represents the permanent settlement which is retained at rail level after the completion of the loading cycle. The permanent settlement is generated by the materials that have inelastic properties, mainly the ballast and subgrade. Due to the non-linear nature of the load-displacement relationship of inelastic support materials, an increase in axle load from W to $W+\Delta W$ will result in permanent settlements which are

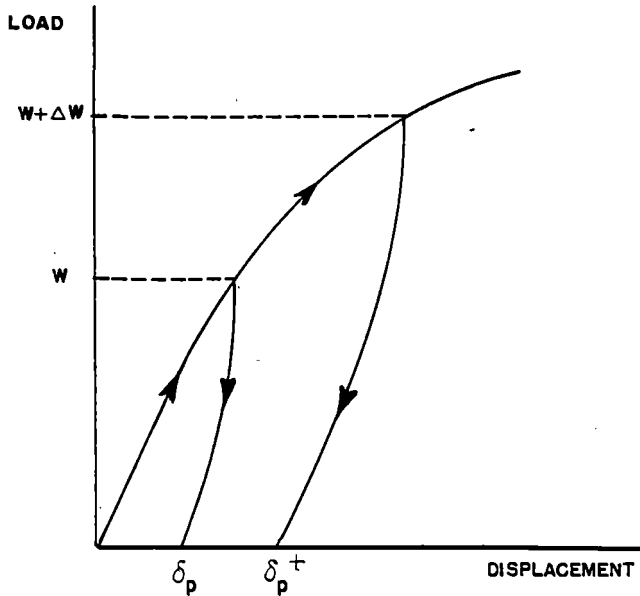


Figure 1. Typical Track Displacement Response to One Loading Cycle

greater than (or equal to) the relative increase in the axle load (see Figure 1). Based on the above, a damage factor may be defined as follows:

$$DF = \delta_p^+ / \delta_p \geq (W + \Delta W) / W \quad (1)$$

where: DF = damage factor,

δ_p^+ = permanent settlement under heavier axle load ($W + \Delta W$), and

δ_p = permanent settlement under existing axle load (W).

Practically, the permanent settlement after one loading cycle is very small, and hence, very difficult to measure. Therefore, the damage factor must be defined as an inequality and its lower limit value may be estimated. Equation (1) may be defined as follows:

$$DF \geq 1 + \Delta W / W \quad (2)$$

Similarly, a damage factor may be separately defined for each one of the components that contribute to the geometrical surface deterioration; namely, subgrade and ballast. The damage factors for these materials will take the following forms:

$$(DF)_b \geq R / R_0 \quad (3.a)$$

$$(DF)_s \geq q / q_0 \quad (3.b)$$

where: R_0 , R = maximum tie reaction under existing axle load, W , and heavier axle load, $W + \Delta W$, respectively

$(DF)_b$ = damage factor for ballast,

q_0 , q = vertical stress as induced at the subgrade-ballast interface by existing axle load, W , and heavier axle load, $W + \Delta W$, respectively, and

$(DF)_s$ = damage factor for subgrade

As can be seen from equations (3), the damage factors (or the track geometry deterioration indicators) are related to the forces exerted at the top of the ballast layer or to the vertical stresses induced at the top of the subgrade. The advantage of using these factors is that one may evaluate the track structure changes which are required (such as adding ballast or decreasing the tie spacings) in order to obtain value 1 for the factors. A value of 1 for the damage factor indicates that the design modifications will permit the increased axle load to be applied without increasing the permanent deformation accumulated under these loads. The following parts of this paper present a simplified methodology to evaluate the damage factors as defined by Equations (3).

PROPOSED METHODOLOGY FOR DETERMINING DAMAGE FACTORS

Utilization of the subgrade and ballast damage factors as defined by Equations (3) requires knowledge of the tie reaction and the vertical stress distribution. Currently, several different methods to evaluate the necessary data are available [2]. Some of the methods to evaluate the stress distribution are based on empirically derived equations through curve fitting of experimental test results [3]. Application of such a method is limited to locations where load and track structure characteristics are similar to the location where the equations were derived. Other empirical methods (such as the pyramid stress distribution) requires a considerable amount of judgement in determining the input data (e.g., the angle of vertical stress distribution and the tie effective bearing area). The more sophisticated methods, such as the finite element, require the characterization of each track structure component. In order to do this, an extensive laboratory investigation is required in order to characterize the subgrade and ballast. This renders such methods impractical in most cases. Thus, most of the existing methods that might be used to evaluate the effect of heavier axle load are either over simplified or over complicated.

The proposed methodology is based on a two-step technique. These steps are:

1. Determination of the tie reaction using the beam on elastic foundation method [4].
2. Evaluation of the stress distribution using the Boussinesq method [5].

Figure 2 illustrates the geometrical and physical significance of the mathematical symbols and notations used hereafter. Note that the applied load, denoted as P , may represent the existing axle load, W , or the heavier axle $W + \Delta W$. Using the beam on elastic-foundation theory in a discrete fashion, it can be shown that the tie reaction immediately below the applied load is as follows:

$$R_{d_0} / P = 1 - e^{-\lambda a / 2} \cos(\lambda a / 2) \quad (4)$$

where: $\lambda = (U / 4EI)^{1/4}$

U = track modulus,

EI = rail stiffness,

a = tie spacing, and

R_{d_0} = tie reaction immediately below the applied load P .

In order to determine the reaction of a tie away from the applied load, so as to enable the usage of the superposition method for several axles, the following equation may be developed (based on the beam on elastic foundation model):

$$\frac{R_d}{P} = \frac{e^{-\lambda d}}{2} [\cos \lambda d (1 - e^{-\lambda a} \cos \lambda a) + e^{-\lambda a} \sin \lambda a \cdot \sin \lambda d] \quad (5)$$

where: d = distance from applied load, P , to nearest mid-space adjacent to the tie under evaluation, and

R_d = the reaction of the tie located $d + a/2$ away from the applied load P (see Figure 2).

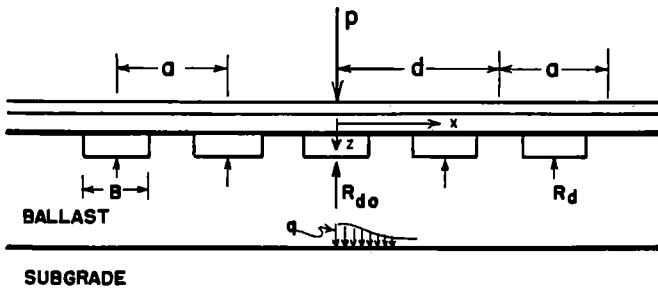


Figure 2. Symbols and Notations used in the Methodology

Equations (4) and (5) are represented in a non-dimensional format in Figures 3 and 4, respectively.

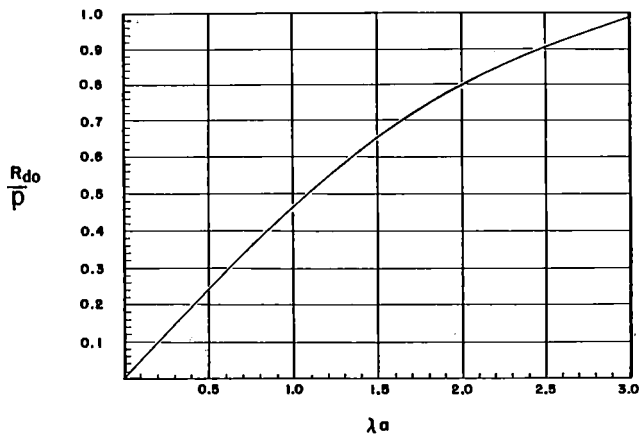


Figure 3. Non-Dimensional Presentation of Tie Reaction, R_{d0} Immediately Below the Applied Load, P , vs the Track Structure Properties

For a given track, the track modulus can easily be evaluated for the typical existing axle load ($P=W$) and for the heavier axle load ($P=W+\Delta W$). Then, for the existing rail the tie spacing (EI and a), the maximum tie reactions, R_0 and R , as obtained under W and $W+\Delta W$, can be determined through Figure 3, (single axle) or Figures 3 and 4 (using the superposition method for multiple axles). Once R and R_0 were determined, the ballast damage factor (Equation 3.a) can be calculated. If the purpose of this exercise is to obtain a design which results in a

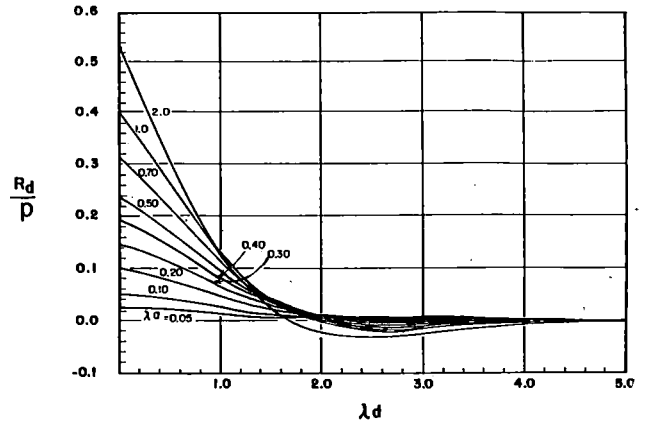


Figure 4. Non-Dimensional Presentation of Tie Reaction, R_d at a Distance of $d + a/2$ from the Applied Load, P , as a Function of Different Track Structures

damage factor of 1 for the load $W+\Delta W$, the proper tie space or rail cross section may be selected so as to obtain $R = R_0$. It should be noted that knowledge of the track modulus is essential and the technique to find it is described in [6].

In order to evaluate the effect of a heavier axle load on subgrade performance (or to determine the subgrade damage factor), the stress distribution should be known. For this purpose the Boussinesq method was used. This method was found to be in quite good agreement with measured stresses in different soil conditions [5]. From [7] it can be seen that in a practical depth range, there is reasonable agreement between the Talbot [3] and Boussinesq stress distributions. In order to generate easy to use charts, the Boussinesq equation (for concentrated force) was integrated using the computer program suggested in [5]. Figure 5

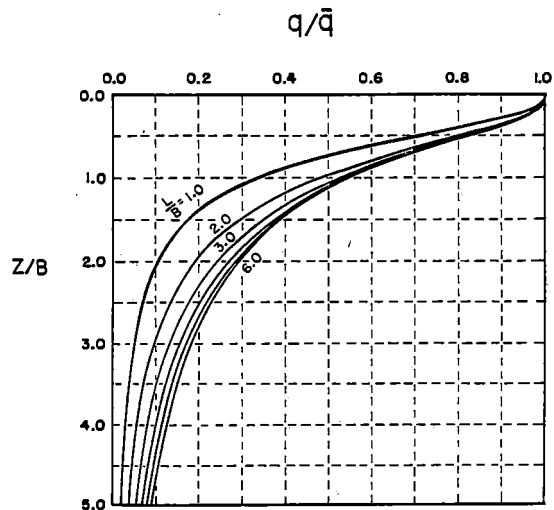


Figure 5. Non-Dimensional Presentation of the Vertical Stress Distribution, q , at Various Depths, z ($x=0$), as a Function of Effective Tie Bearing Dimensions, L/B

shows the vertical stress distribution (q) with depth (z) calculated at a point at the tie center line under the rail seat. Note that the stress and depth axes are non-dimensional. The term, B , represents the tie width and the term, \bar{q} , represents the assumed average (uniform) stress at the tie bottom ($z=0$). The term, L , represents the effective load bearing length of the tie bottom, and hence, $B*L$ is the effective tie bearing area. Therefore, \bar{q} is the tie reaction, R , divided by the effective bearing area. Also, note that each curve shown on Figure 5 is plotted for a constant ratio of L/B . As can be seen, the stress distribution is affected very little by this ratio. Since it has been shown that the effective bearing length of a tie is greater than $3B$, a unique curve of stress distribution calculated for $L/B = 4.5$ is presented in Figure 6 for practical use.

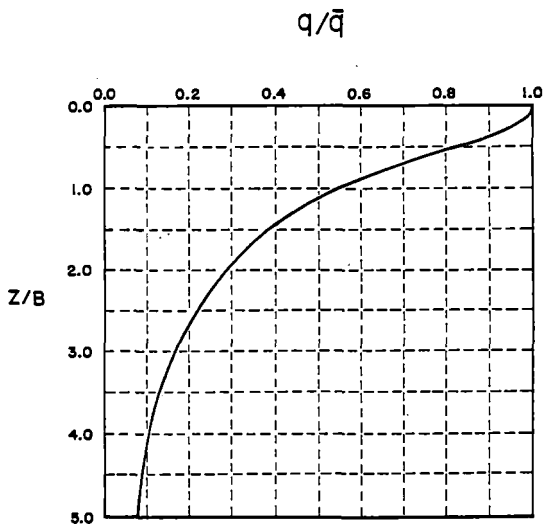


Figure 6. Non-Dimensional Presentation of the Vertical Stress Distribution, q , at Various Depths, z ($x=0$), as a Function of Average Effective Tie Bearing Dimensions ($L/B=4.5$)

Figure 7 is a representation of the vertical stress

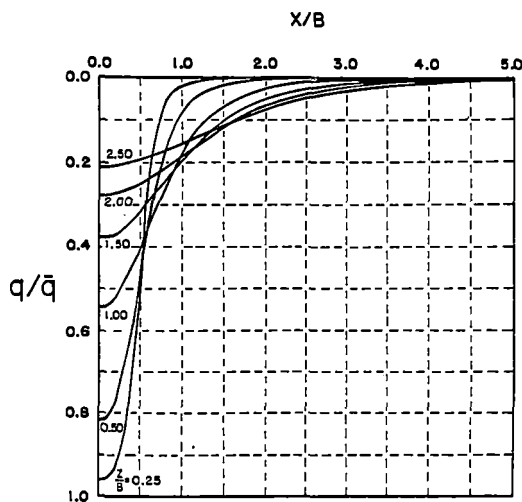


Figure 7. Non-Dimensional Presentation of the Vertical Stress Distribution, q , at Various Depths, z , along the Track, x

distribution along a horizontal distance from the loading center line at various depth levels. This figure may be used for superposition purposes.

EXAMPLE OF THE APPLICATION OF THE PROPOSED METHODOLOGY

Consider as an example the following track structure: Rail weight 132 lb/yd ($EI=2.5 \times 10^9$ lb-in⁴), tie spacing $a = 19.5$ inch, tie width $B = 9$ inch, and ballast thickness $Z = 12$ inch. The existing typical axle load is $P_0 = 25$ ton. The measured track modulus under this load is $U = 1000$ lb/in/in. Since a single axle is given, one may use Figure 3 to obtain:

$$R_o = R_{d_o} = 0.17 P_o$$

However, to determine the vertical stress level at the ballast-subgrade interfaces ($Z = 12$ inch or $Z/B = 12/9$), the reaction of the adjacent ties should be evaluated. Through figures 4, 6 and 7, the following ratio can be obtained:

$$\frac{q_o}{\bar{q}} \cong 0.45$$

where: $\bar{q} = R_o/A$, and

$$A = B*L = \text{effective tie bearing area}$$

hence: $q_o \cong 0.45 R_o/A$

Now, the effect of the increase in axle load may be evaluated. Assume that the typical axle load is increased to $P = 33$ ton and the corresponding track modulus (measured) is $U = 1500$ lb/in/in. The change of the track modulus with load is attributed to the non-linear response of the track support system (e.g., see [6], p. 22, Figure 9). This is why it is important to measure the track modulus under the proper load. Following the procedure described above, it can be shown that:

$$R = 0.19 P$$

$$q \cong 0.45 R/A$$

Therefore, if the track structure is left unchanged, the following damage factors will be obtained (Equation 3):

$$(DF)_b \geq R/R_o = (0.19 \times 33)/(0.17 \times 25) = 1.48$$

$$(DF)_s \geq q/q_o = 0.45 R/0.45 R_o = 1.48$$

The fact that both damage factors are equal is only due to the particular data chosen here. It should be noted that the ratio of axle loads, P/P_o is only 1.32, which is less than the damage factor values. In order to achieve a ballast damage factor equal to 1, the ordinate on Figure 3 should be equal to $0.17 P/P = 0.13$. The corresponding values on the abscissa, $\lambda a = 0.26$, will produce the same maximum tie reaction under the increased axle load as it was under the existing axle load and track structure.

If the same rail is used, the tie spacing must be decreased to 13.3 inch to obtain a λa value of 0.26. From a practical standpoint, this is almost impossible: the space left between the ties for the tamper blades (4.3") is not enough. If 140 lb/yd rail ($EI=2.81 \times 10^9$ lb/in²) is used, the tie space required is increased to 13.6 inches. Therefore, the goal of a ballast damage factor of 1 may practically be unachievable. However, a significant portion of the track geometrical deterioration is contributed by the subgrade. It can be shown that if the same track

structure is maintained, and for the same track modulus, increasing the ballast thickness from 12 inches to approximately 17 inches ($L/B = 1.9$) will produce a subgrade damage factor of 1 (the ballast damage factor will remain 1.48).

It should be noted that an important input data requirement is the relevant track modulus. Since the determination of the track modulus is relatively simple [6], it is suggested that this modulus be evaluated for any modified track structure and vehicle weight used in the analysis. It is an iterative approach which converges very fast.

This procedure provides a simplified methodology to determine the effect of varying wheel loads on track deterioration while still considering the nonlinearities of the track structure. However, this methodology should be verified by further in-track measurements.

ACKNOWLEDGMENTS

The authors express their appreciation to Dr. A. M. Zarembski, Director-Research and Development, Pandrol, Inc., formerly Manager-Track Research Division, Association of American Railroads, for his contribution to the development of this methodology.

REFERENCES

- 1 Leshchinsky, D., "Development of a Track Quality Index," Association of American Railroads - Technical Center, Chicago, Ill., Report No. WP-100, Feb. 1982.
- 2 So, W., Martin, G. C., Singh, B., Chang, I. C., and Chang, E. H., "Mathematical Models for Track Structures," Association of American Railroads - Technical Center, Chicago, Ill., Report No. R-262, Apr. 1977.
- 3 Talbot, A. N., Second Progress Report, Special Committee on Stresses in Railroad Track, 1919, p. 808
- 4 Hetenyi, M., Beams on Elastic Foundation, University of Michigan Press, Ann Arbor, Mich., 1958
- 5 Bowles, J. E., Foundation Analysis and Design, 2nd Edition, McGraw-Hill Book Co., 1977.
- 6 Choros, J., Zarembski, A. M., and Gitlin, I., "Vertical Track Modulus: Test Results and Comparison of Analysis Techniques," U. S. Department of Transportation, Federal Railroad Administration, Washington, D. C., Report No. FRA/ORD-79/34, Nov. 1979.
- 7 Ireland, H. O., Railroad Subgrade Stresses, Bulletin 641, AREA, pp 382-386.

Ernest T. Selig

Professor
Dept. Civil Engineering
Univ. of Massachusetts
Amherst, Massachusetts

Jorge E. Alva-Hurtado

Geotechnical Engineer
Lima, Peru

Predicting Effects of Repeated Wheel Loading on Track Settlement

Over a period of time, railroad track will settle as a result of permanent deformation in the ballast and underlying soil layers produced by traffic loading. This paper presents a methodology to calculate this settlement as a basis for maintenance life prediction. A three-dimensional computer model is used to estimate the stress state in the roadbed materials caused by train loading. Stresses representative of these computed values are applied to samples of ballast in repeated-load triaxial tests to obtain permanent strain behavior of the material. These strains are integrated to estimate settlement. This method can take into account the main factors influencing the deformation behavior, including axle load and number of cycles, rail and tie characteristics, and properties and thickness of the ballast and underlying layers. The paper also provides a review of related previous research.

NOMENCLATURE

A_0, A_1, A_2, A_3	coefficients in resilient Poisson's ratio equation
c	Mohr-Coulomb cohesion
E_i	initial tangent modulus
E_r	resilient Young's modulus
h_i	thickness of i^{th} sublayer
K	horizontal/vertical soil stress ratio
K_1 to K_6	parameters in equations for resilient modulus
N	number of load cycles
n	soil porosity
p	$(\sigma_1 + \sigma_3)/2$
q	$(\sigma_1 - \sigma_3)/2$
q_f	failure shear stress = $(\sigma_1 - \sigma_3)/f$
R	ratio of applied cyclic stress to static deviator stress at failure
R_f	failure ratio
s	number of sublayers
Δq	cyclic shear stress
δ^P	total permanent deformation
ϵ_1	permanent strain after first cycle
ϵ_N	permanent vertical strain after N cycles

ϵ_i^P	permanent vertical strain in i^{th} sublayer
θ	bulk stress = $\sigma_1 + \sigma_2 + \sigma_3$
ν_r	resilient Poisson's ratio
σ_1	major principal stress
σ_2	intermediate principal stress
σ_3	minor principal stress or confining pressure
σ_{oct}	octahedral normal stress
τ_{oct}	octahedral shear stress
ϕ	Mohr-Coulomb friction angle

SUBSCRIPTS

f	field
t	triaxial

SUPERSCRIPTS

$-$	effective stress
-----	------------------

INTRODUCTION

Railroad track deforms elastically under each application of wheel loading, but settles as a result of the inelastic deformation in the ballast and underlying soil layers produced by the accumulation of many cycles of traffic loading. The elastic deformations determine the track stiffness and the fatigue life of the track components. The inelastic behavior produces the track settlement that deteriorates the track geometry, hence requiring maintenance to resurface and line the track. The purpose of this paper is to present a method to predict the elastic and inelastic behavior of railroad track structures under traffic loading, which is applicable to estimating maintenance life for new or existing railroad track as it is influenced by ballast properties.

The methodology involves: 1) use of a three-dimensional computer model to predict the elastic state of stress imposed on the roadbed materials by the train loading, 2) determination of equivalent stresses to which the samples will be subjected in laboratory tests, 3) testing of the ballast material to obtain the properties, and 4) integrating the test results to estimate track settlement. The approach for accomplishing each of these tasks will be described following a review of related previous research.

BEHAVIOR OF GRANULAR MATERIALS

In general, types of loading can be broadly categorized as either monotonic or cyclic. Monotonic loading has been extensively investigated for many years, and therefore is better understood. However, the type of loading influencing the behavior of the track system is cyclic. Unfortunately, there is no general constitutive law available to account for the effect of cyclic loading in ballast and roadbed materials.

Two distinct behavior patterns have been noted for granular materials under cyclic loading (Fig. 1).

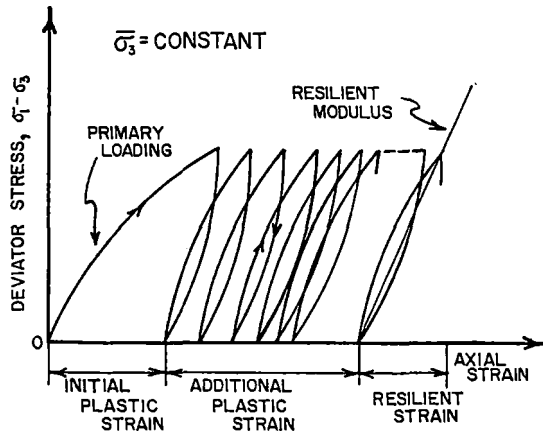


Fig. 1. Representation of Stress-Strain Curve from a Triaxial Sample Under Repeated Load

The first is the recoverable or resilient behavior; the second is the permanent deformation behavior. The typical behavior of a granular material, under moderate levels of repeated stress, is that after the first few cycles, the material becomes "elastic" because the irrecoverable strain is small compared to the recoverable strain. However, significant permanent strain can still accumulate after a large number of cycles.

Resilient Behavior

Most of the investigations of resilient behavior (for example, Refs. 1 to 9) have been accomplished by triaxial repeated load testing using constant confining pressures. However, Allen (Ref. 6) and Brown and Hyde (Ref. 12) used cyclic confining pressure as well as cyclic deviator stress. Allen and Thompson (Ref. 14) concluded that, although the constant confining pressure tests overestimated the resilient modulus, the use of the constant confining pressure triaxial test was justified as a means of characterizing the resilient response of granular materials because the

error was not great and the testing equipment was simpler.

The resilient response is usually characterized by a resilient modulus (E_r) and resilient Poisson's ratio (ν_r). The resilient modulus is defined as the repeated deviatoric stress at constant confining pressure divided by the recoverable portion of the axial strain. The resilient Poisson's ratio is equal to the negative ratio of the recoverable portion of the radial or lateral strain divided by the recoverable portion of the axial strain at constant confining pressure.

The resilient modulus has been found to be a function mainly of the state of stress. Two predictive equations have been developed for granular materials to relate the modulus to the stress state. These are

$$E_r = K_1 \theta^2 \quad (1)$$

and

$$E_r = K_3 \sigma_3^{K_4} \quad (2)$$

where K_1 , K_2 , K_3 and K_4 = constants determined from regression analysis of the laboratory data,

θ = bulk stress or the sum of the three principal stresses = $\sigma_1 + \sigma_2 + \sigma_3$, and

σ_3 = the minimum principal stress or confining pressure.

Thus the resilient stiffness of a roadbed material is not constant for any layer, because the stress state varies with location in the system.

Some values of resilient modulus for the FAST track materials were determined by Thompson (Ref. 11). As an example, results for the granite ballast, gravel subballast, and sand subgrade are shown in Fig. 2. The ballast data came from repeated loading tests,

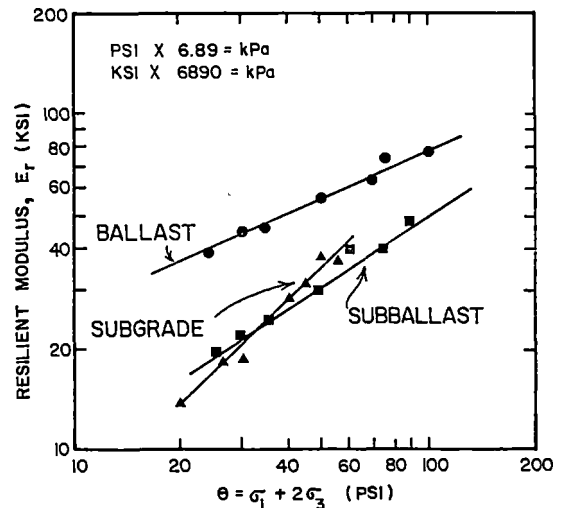


Fig. 2. Resilient Modulus Relationship to Bulk Stress for FAST Wyoming Granite Ballast, Subballast and Subgrade (Ref. 11)

where the specimens were initially conditioned at a confining pressure of $\sigma_3 = 15$ psi (103 kPa), with 5000 repetitions of a deviatoric stress of $\sigma_1 - \sigma_3 = 45$ psi (310 kPa). The same specimen was used on the seven resilient moduli determinations by stage

testing involving 5000 repetitions at each stress condition.

From repeated load testing with constant confining pressure, Hicks (Ref. 5) represented the resilient Poisson's ratio as a function of the principal stress ratio (σ_1/σ_3) as follows:

$$v_r = A_0 + A_1 \left(\frac{\sigma_1}{\sigma_3}\right) + A_2 \left(\frac{\sigma_1}{\sigma_3}\right)^2 + A_3 \left(\frac{\sigma_1}{\sigma_3}\right)^3$$

Allen (Ref. 6) performed repeated load testing with constant and variable confining pressure. He found that the results varied with the stress path. However, Brown and Hyde (Ref. 12) indicated that if both types of tests are interpreted in terms of the ratio of volumetric strain to shear strain, the results from both tests are compatible.

Hicks (Ref. 5) and Allen (Ref. 6) indicated that the resilient response after thousands of cycles can be obtained after approximately 100 load cycles. They also indicated that one specimen can be used to measure the resilient response for a range of stress levels and that the sequence of stress application had no significant effect on the results, as long as stress states were well below failure. Kalcheff and Hicks (Ref. 15) also reported that the number of stress repetitions and stress sequence had little effect on the resilient properties of granular materials. They recommended that the resilient response of granular materials be determined after 150 to 200 load repetitions.

Morgan (Ref. 7) and Brown (Ref. 9) indicated that the resilient modulus increased with the number of cycles, but reached equilibrium values after approximately 10,000 cycles of deviator stress. Boyce, Brown and Pell (Ref. 16) indicated that the resilient modulus is sensitive to stress history, but this can be reduced by using only a few cycles of each stress state and avoiding high ratios of deviator to confining stress.

For granular materials, the rate of load application and load duration does not significantly affect resilient properties (Refs. 1, 6, 15, 16 and 17).

From tests conducted on well-graded crushed gravel and crushed rock, Hicks and Monismith (Ref. 17) concluded that resilient modulus at a given stress level increased with increasing particle angularity or surface roughness. Haynes and Yoder (Ref. 4) observed higher resilient modulus values for gravel specimens than for crushed stone when both were compacted to the same relative density. Allen (Ref. 6) found that the effects of material type on the resilient parameters are slight compared with the effects of changes in the state of stress. Allen conducted repeated load testing on crushed stone, gravel and a blend of the two. In general, the crushed stone yielded slightly higher values of E_r than the gravel. The modulus of the blend material was normally between those of the other materials. Tests by Robnett, et al. (Ref. 10) showed that material type is not a major factor affecting the resilient response of granular materials.

Hicks (Ref. 5) observed decreases in the resilient moduli of well-graded materials as the fines content (percent passing number 200 sieve) increased. Barksdale (Ref. 3) tested various soil-aggregate blends and concluded that a 20% soil/80% aggregate blend exhibited higher values of resilient modulus at low stresses than a 40% soil/60% aggregate blend specimen. At higher stress levels, the situation was reversed. Haynes and Yoder (Ref. 4) observed little change in resilient modulus values of well-graded aggregates for

changes in the percent of fines ranging from 6.2 to 11.5 percent.

Hicks (Ref. 5) concluded that for a given stress condition, the resilient modulus increased with an increase in density. Poisson's ratio, however, was only slightly influenced by density. Allen (Ref. 6) investigated the variation of resilient parameters with density for crushed stone, gravel and a blend of both. Generally, the resilient modulus increased as density increased. However, the Poisson's ratio showed no consistent variation with density changes.

Hicks (Ref. 5) indicated that for sands and gravels at different degrees of saturation, the resilient modulus decreased as the degree of saturation increased, so long as comparisons were made on the basis of total confining pressures. Comparisons on the basis of effective stresses indicated that the resilient moduli for 100 percent saturated samples differed only slightly from those for dry samples.

Permanent Deformation Behavior

The permanent deformation behavior of granular materials, and in particular ballast, under the application of repeated loading had been studied both in the laboratory (Refs. 2, 3, 13, 18, 19 and 20) and in the field (Refs. 21 and 22). Both types of studies indicated that the response under each load is essentially elastic, but with number of load applications and traffic, there is an accumulation of permanent strain.

The effect of stress level on the permanent deformation of ballast limestone is illustrated in Fig. 3. Knutson (Ref. 13) concluded that an increase in

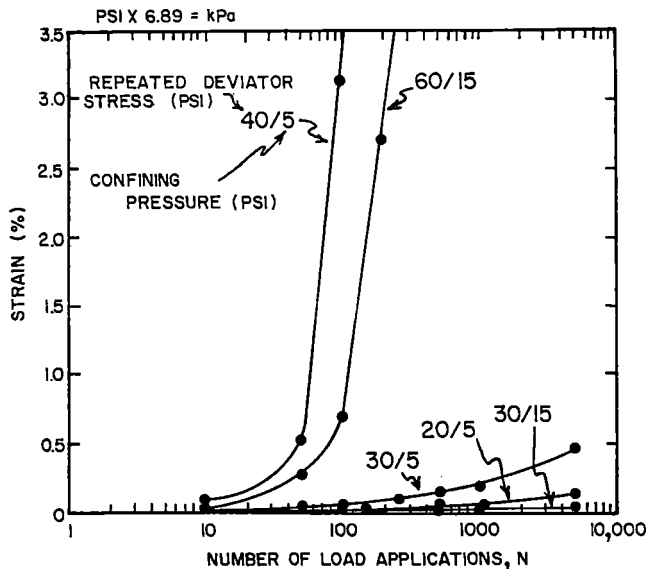


Fig. 3. Effect of Stress Level on Permanent Deformation Response of Low Density Limestone (Ref. 13)

stress ratio (repeated deviator divided by confining pressure) resulted in additional permanent deformation for ballast samples. However, stress ratio by itself cannot be used to predict adequately the permanent deformation behavior of ballast materials. For a given stress ratio, for instance four, the development of permanent deformation with number of cycles will be different for two different confining pressures in the triaxial test. The lower confining

pressure, for instance $\sigma_3 = 5$ psi (34 kPa), produces much lower permanent deformation than the higher confining pressure, for instance 15 psi (103 kPa), as shown in Fig. 3. Knutson indicated that the stress level effects were difficult to discern because both the deviator stress and the confining pressure, and not merely the ratio of the two, must be considered.

Barksdale (Ref. 3) concluded that the permanent deformation decreased significantly as the confining pressure increased for a given deviator stress. The rate of accumulation of permanent deformation at low repeated deviator stress is proportional to the number of load applications, but at deviator stresses above a critical value, the rate of permanent deformation accumulation increased with increasing number of load applications (Fig. 4).

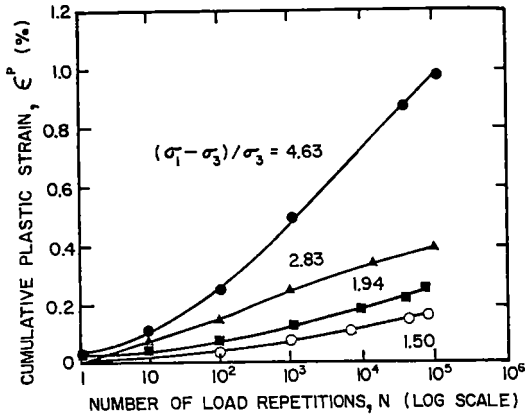


Fig. 4. Influence of Number of Load Applications and Magnitude of Deviator Stress on Permanent Deformation (Ref. 3)

Brown and Hyde (Ref. 12) and Knutson (Ref. 13) have shown that, unlike the resilient behavior, the permanent deformation behavior is dependent on the load application sequence or stress history. The total permanent deformation was less when a specimen was subjected to gradually increasing stress levels than when the highest stress level was applied first.

Field evidence of the importance of the primary loading on the permanent deformation of ballast has been presented by ORE (Ref. 19). This research concluded that smaller loads cause negligible settlement, and that a small number of large dynamic loads determines the deterioration of the track level, rather than the general level of the axle loads.

Allen (Ref. 6) found that an increase in density resulted in a decrease of permanent deformation and that crushed material experienced less permanent deformation than gravel. ORE (Ref. 19) indicated that permanent deformation is proportional to the initial porosity and is thus inversely proportional to initial density. Knutson (Ref. 13) concluded that no specimen parameter has more influence on the permanent deformation behavior than the degree of compaction (Fig. 5).

Knutson (Ref. 13) found no significant differences in the permanent deformation behavior of crushed limestone, crushed basalt and gravel. The effects of material properties such as particle index and flakiness index were not consistent and therefore no conclusions were drawn with respect to those properties. Knutson also reported the effect of gradation on permanent deformation behavior. In general, the AREA number 4 gradation tended to resist permanent deformation less than did the AREA number 5 gradation or the "well-graded" materials.

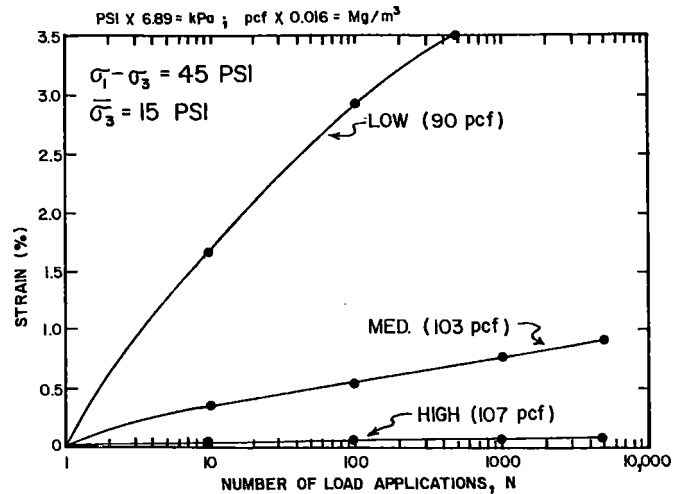


Fig. 5. Effect of Density on Permanent Deformation Response of Limestone Ballast (Ref. 13)

Raymond and Williams (Ref. 23), based on Olowokere's work (Ref. 18), studied stress-strain-volume change relationships as a function of number of cycles for triaxial compression repeated load testing of Coteau dolomite ballast. A large axial strain was observed at the end of the first cycle, the magnitude being a function of confining pressure and deviator stress. The amount of strain occurring in each successive cycle tended to decrease. The hysteresis was also greatest in the first cycle and decreased with subsequent cycles until the loading curves eventually coincided with the corresponding unloading curves. Permanent axial and volumetric strains increased approximately linearly with the logarithm of the number of load cycles (Fig. 6). Olowokere also observed

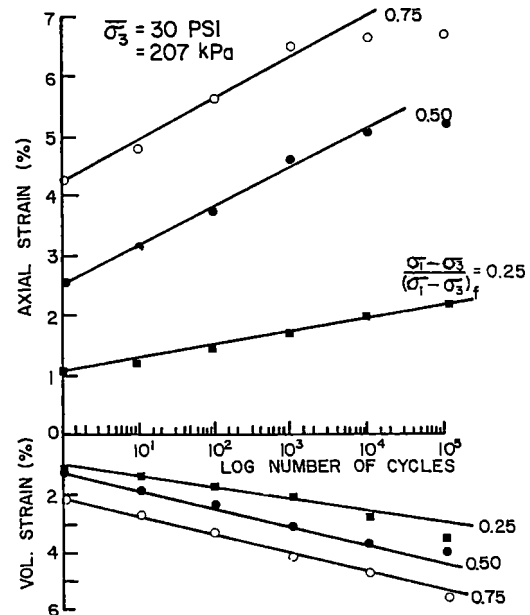


Fig. 6. Strain Response of Coteau Dolomite Ballast as a Function of Number of Repeated Load Cycles (Ref. 18)

that: 1) for a given material and a given density, increasing the ratio of repeated deviatoric stress to the deviatoric stress at failure will result in increased permanent deformation, and 2) for a given ratio of repeated deviatoric stress to deviatoric stress at failure and for the same material and initial density, the permanent deformation increases with increasing confining pressure. The work of Olowokere was extended by Raymond and Williams (Ref. 23) to include extension tests. However, only one density was used in both types of tests.

The Office of Research and Experiments (ORE) of the International Union of Railways (Ref. 19) undertook studies, both in the laboratory and in the field, to determine the behavior of the ballast layer in track under the action of repetitive loads. Laboratory repeated load tests were made on Derbyshire limestone and Meldon stone ballasts. Different densities were tested. The results indicated that under controlled stress conditions the ballast permanent strain can be predicted by the equation:

$$\epsilon_N = 0.082(100n-38.2)(\sigma_1-\sigma_3)^2(1+0.2 \log N), \quad (3)$$

where ϵ_N = permanent strain after N loading cycles,

n = initial porosity of the sample,

$\sigma_1-\sigma_3$ = deviator stress, and

N = number of repeated loading cycles.

The main points that arose from the predictive equation were that:

1. The development of the permanent deformation of the ballast (deformation/load cycle) was greatest for the first cycle and reduced considerably as the number of cycles increased.

2. The deformations produced by subsequent loading can be related to that produced at the first loading by:

$$\epsilon_N = \epsilon_1(1 + 0.2 \log N) \quad (4)$$

This relationship was independent of initial porosity, stress levels, or material type.

3. The permanent deformation was very dependent on the initial compaction of the ballast.

4. The permanent deformation was proportional to the square of the applied deviatoric stress.

Shenton (Ref. 20) continued the laboratory testing undertaken by ORE mainly to determine and qualify the effects of changes in the applied loading pattern. He made the following conclusions:

1. The first load cycle produced a large permanent strain followed by a period where the permanent strain is proportional to the log of the number of cycles. This is the same as ORE (Ref. 19).

2. There is a large variation in ballast strains from test to test, even when the ballast samples are identically prepared and subjected to the same stresses.

3. The permanent strain is proportional to the axial stress raised to a power ranging from 1 to 3.

4. The permanent strain is determined mainly by the largest load when two load levels are applied.

5. The permanent strain accumulation is reduced if full load removal is not allowed between load cycles.

6. The ORE relationship for permanent deformation at cycle N as a function of permanent deformation at cycle 1 was also obtained for Ballidon limestone tested at three different densities.

Hargis (Ref. 2) studied the permanent

deformation behavior of a limestone gravel subjected to repetitive loading. He developed a regression model to predict permanent deformations with the repeated application of loads. The independent variables were the number of cycles of loading, N, and the ratio of cyclic deviator stress to maximum static deviator stress, R. The regression model was of the form:

$$\log \epsilon_N = -1.8688 + 0.1666 \log N + 2.4048R, \quad (5)$$

where ϵ_N is the predicted vertical permanent strain in percent.

Brown (Ref. 9) conducted a series of laboratory repeated load triaxial tests on a crushed granite with a 0.2-in. (5.1-mm) maximum particle size. He found that, under drained conditions, the permanent strain reached equilibrium values after approximately 10,000 cycles of deviator stress. The permanent strain at equilibrium was related to the applied stresses by:

$$\epsilon_N = 0.01 (q/\sigma_3) \quad (6)$$

where q was the repeated deviator stress and σ_3 was the confining pressure.

In a recent extension of Brown's work, Hyde (Ref. 24) investigated the influences of loading sequence and using cyclic confining pressure. The limited study of loading sequence showed that while the resilient modulus was unaffected, the permanent deformation behavior was significantly affected. The permanent strain which developed after about 100,000 cycles of gradually increasing level of successive applications was less than half of the value resulting when the highest stress level was applied constantly.

PAVEMENT APPROACH TO DEFORMATION PREDICTION

Much more research has been carried out on the prediction of inelastic deformation (rutting) of pavements than on inelastic settlement of track structures under repeated traffic loads. Because of the similarity of many aspects of the two problems, the approaches developed for pavement deformation prediction have formed the basis for track settlement prediction.

Monismith and Finn (Ref. 25) indicate two design approaches related to rutting from repeated traffic loading. One involves limiting the vertical compressive strain at the subgrade surface to some tolerable amount associated with a specific number of load repetitions, e.g., the Shell Co. criteria (Ref. 26). By controlling the characteristics of the materials in the pavement section through materials design and proper construction procedures, and by insuring that materials of adequate stiffness and sufficient thickness are used so that this strain level is not exceeded, permanent deformation equal to or less than some prescribed amount is thus expected.

The other approach involves prediction of the actual amount of deformation which might occur in the pavement system using material characterization data developed in the laboratory together with an analysis procedure used to represent the pavement structure. The analysis procedure represents the pavement structure as a linear or nonlinear elastic layered system with material properties from repeated load triaxial compression tests. Relationships between permanent strain and applied stress must also be available for each of the pavement components.

This method, as presented by Barksdale (Ref. 27), is a simplified engineering approach that consists of subdividing each layer of the pavement structure into sublayers. Then linear or nonlinear elastic layer theory is used to determine the major principal stress (σ_1) and average confining pressure (σ_3) at the center of each sublayer beneath the wheel load, as shown in Fig. 7. Because the principal planes are

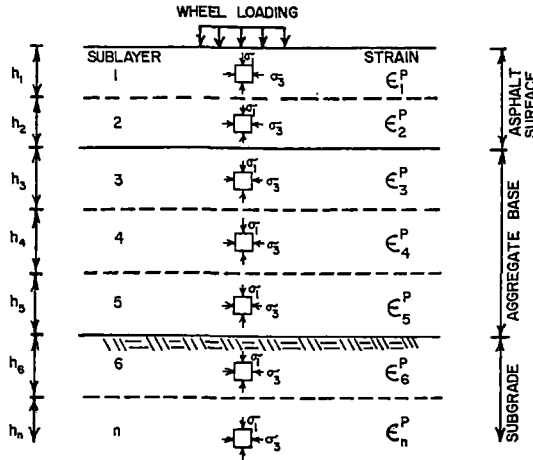


Fig. 7. Idealization of Layered Pavement Structure for Calculating Permanent Deformation (Ref. 27)

vertical and horizontal at these locations, this stress state can be simulated in the laboratory by the triaxial test.

The permanent strains can be calculated at the center of each sublayer by using the relationship between permanent strain and applied stress from laboratory results for the desired number of load applications. The total permanent deformation is then obtained by summing up all of the products of the average permanent strain occurring at the center of each layer and the corresponding sublayer thickness. This step can be mathematically expressed as

$$\delta^P_{\text{total}} = \sum_{i=1}^s (\epsilon_i^P h_i) \quad (7)$$

where δ^P_{total} = total permanent deformation beneath the wheel load,

ϵ_i^P = average permanent strain in the i^{th} sublayer,

h_i = thickness of the i^{th} sublayer, and

s = total number of sublayers.

The values of permanent strain ϵ_i^P are obtained from laboratory tests for a given i^{th} state of stress at various number of load repetitions.

Barksdale (Ref. 27) proposed a method to relate the permanent axial strain caused by repeated loading to the state of stress in the triaxial test based on a modification of the hyperbolic model of Duncan and Chang (Ref. 28). The strain after 100,000 cycles of well-graded materials can be predicted by

$$\epsilon_N = \frac{(\sigma_1 - \sigma_3)/E_i}{1 - \left(\frac{(\sigma_1 - \sigma_3)(1 - \sin\phi)R_f}{2(c \cos\phi + \sigma_3 \sin\phi)} \right)} \quad (8)$$

where ϵ_N = permanent axial strain,

$\sigma_1 - \sigma_3$ = deviator stress,

σ_3 = confining pressure,

E_i = hyperbolic initial tangent modulus,

c, ϕ = Mohr-Coulomb parameters for cohesion and friction angle, and

R_f = a ratio of the stress difference at failure to the stress difference where the stress-strain curve approaches infinite strain, i.e., $(\sigma_1 - \sigma_3)_f / (\sigma_1 - \sigma_3)_{\text{ult}}$.

The above approach to predict permanent deformation has been used by a number of investigators (Refs. 29 to 34). Brown and Bell (Ref. 35) extended the approach to predict permanent deformation in off-axis locations by using stress invariants. They stated that a firm conclusion about the validity of the approach was not considered possible on the evidence presented, and therefore the need for future work was indicated.

STRESS ANALYSIS OF TRACK STRUCTURE

The approach taken for track permanent settlement prediction is similar to that represented by Eq. 7 for flexible pavements. The first step is the determination of the stresses in the layers of ballast, subballast and subgrade resulting from train loading. For this purpose, a three-dimensional model, GEOTRACK, was developed that represents the track structure by a pair of rails resting on ties, supported by five nonlinear-elastic layers that characterize the ballast and underlying materials (Ref. 36). The complete state of stress can be calculated at any depth beneath the ties for specified wheel loads placed on the rails. These stresses are then converted to equivalent stress for the laboratory property tests.

The computed stress states and their use in prediction of track performance will be illustrated using as a case study the track section 18B at the Facility for Accelerated Service Testing (FAST) track at Pueblo, Colorado. Details of the track section and the methods of analysis may be found in Refs. 22, 37, 38 and 39.

Field Stress States

The track section 18B consisted of 136-lb (61.7-kg) jointed rail on 7-in.-high by 9-in.-wide by 8.5-ft-long ties (178-mm by 229-mm by 2.6-m) at 19.5-in. (495-mm) center-to-center spacing. The ties were resting on 15 in. (381 mm) of granite ballast, under which was a 6-in. (152-mm) layer of compacted well-graded gravelly sand subballast. The subgrade under the subballast was silty fine to medium sand. The properties for the ballast, subballast and subgrade required by GEOTRACK are given in Table 1. The unit weights are based on field data. The unit weights, together with the assumed ratios of horizontal to vertical stress, K , are used to estimate the geostatic stresses. The resilient Poisson's ratio values are assumed from data on similar materials, since measurements were not available. The initial resilient moduli were the values used for the first iteration with the GEOTRACK program. However, the program subsequently determined the moduli from the stress-dependent formulation of Eq. 1 using the parameter values for K_1 and K_2 obtained from laboratory tests reported in Ref. 11. For comparison, the final resilient moduli, after convergence of the computer

Table 1. Soil Layer Properties for FAST Section 18B

Material	Unit Weight (lb/cu ft)	Resilient Poisson's Ratio, ν_r	Resilient Modulus, E_r (psi)			
			Initial	Final	K_1	K_2
Granite Ballast	106	0.37	30,000	41,000	7735	0.509
Subballast	144	0.37	20,000	12,300	2182	0.687
Upper Subgrade	112	0.33	10,000	7,400	523	1.083
Lower Subgrade	112	0.33	5,000	12,600	523	1.083

NOTE: The ratio of horizontal to vertical geostatic stress, K, is assumed to be 1 for the ballast and 0.5 for the other layers; lb/cu ft x 0.016 = Mg/m³; psi x 6.89 = kPa.

solution by 3 successive iterations to obtain consistency between E_r and the stress states, are also given in Table 1. These final values of E_r were found to be independent of the assumed initial values.

The calculated distributions of principal stresses with depth beneath the wheel load in section 18B are shown in Fig. 8. These stresses decrease rapidly

increasing geostatic stress, since the stresses from the train load continue to decrease with depth in the subgrade.

Octahedral stresses were used to represent the three-dimensional system of stresses by those relating to volume change and those relating to shear distortion. The total field octahedral normal stress (σ_{oct_f}) and total field octahedral shear stress (τ_{oct_f}) are determined from the total principal stresses by the expression

$$\sigma_{oct_f} = \frac{\sigma_{1f} + \sigma_{2f} + \sigma_{3f}}{3}, \quad (9)$$

and

$$\tau_{oct_f} = 1/3 \sqrt{(\sigma_{1f} - \sigma_{2f})^2 + (\sigma_{2f} - \sigma_{3f})^2 + (\sigma_{3f} - \sigma_{1f})^2}, \quad (10)$$

where σ_{1f} , σ_{2f} and σ_{3f} are the three total principal stresses from the field. These total stresses consist of the stresses from train loading predicted from GEOTRACK plus the geostatic stresses from the material unit weights.

The distribution of octahedral stresses with depth is shown in Fig. 9. The normal stress decreases rapidly with depth in the ballast layer, becoming slightly negative at the bottom of this layer. In the subballast, the normal stress is positive and approximately constant. In the subgrade, the normal stress increases gradually with depth. The shear stress is relatively constant in the ballast layer, except near the bottom where it is highest. After decreasing rapidly across the ballast-subballast interface, the shear stress remains relatively constant with depth.

Stresses for Laboratory Tests

The stress paths produced in the field by the imposition of wheel loads were simulated in the laboratory with cyclic (repeated load) triaxial compression tests. The test facility used permitted varying only the axial load (deviatoric stress), while maintaining the cell pressure (lateral stress) constant. The equivalent stress states for the laboratory tests were determined by equating the predicted field octahedral stresses (Fig. 9) to the octahedral stresses in the laboratory triaxial test.

The octahedral stresses in the axisymmetric triaxial test are defined by

$$\sigma_{oct_t} = 1/3(\sigma_1 + 2\sigma_3), \quad (11)$$

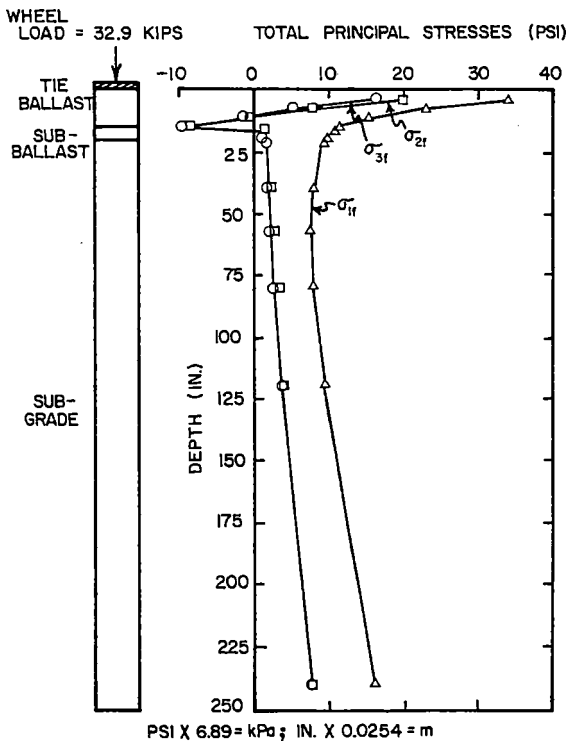


Fig. 8. Variation of Total Principal Stresses with Depth below Wheel Load from GEOTRACK for FAST Section 18B

with depth in the ballast, where the geostatic stress is small. The horizontal stresses theoretically are tensile at the bottom of the ballast layer because the subballast has a lower modulus than the ballast. However, in the actual track these stresses can never be tensile because the ballast would be in a failure state. The total stresses generally increase with depth in the subgrade. This is a result of the

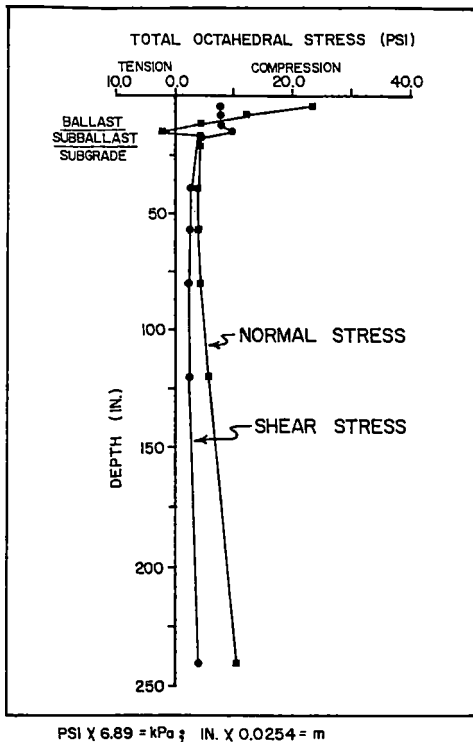


Fig. 9. Distribution with Depth Below Wheel Load of Total Octahedral Stresses for FAST Section 18B

and

$$\tau_{oct_t} = \frac{\sqrt{2}}{3} (\sigma_1 - \sigma_3) \quad (12)$$

Values for σ_1 and σ_3 are obtained by equating σ_{oct_t} (Eq. 11) to σ_{oct_f} (Eq. 9) and τ_{oct_t} (Eq. 12) to τ_{oct_f} (Eq. 10).

The calculated equivalent triaxial stresses for section 18B are shown in Fig. 10. The distributions of σ_1 and σ_3 with depth are generally similar to those for the corresponding principal stresses in the field (Fig. 8). This is expected for the locations directly beneath the point of wheel load application in the track because at these locations, the principal planes are approximately horizontal and vertical, and the horizontal principal stresses σ_{2f} and σ_{3f} are approximately equal.

The stress path for the equivalent triaxial stress states in the middle of the ballast layer is shown as line AB in Fig. 11. Point A is the unloaded state representing only the geostatic stresses. Point B is the loaded state which combines the geostatic stresses with the stresses from the train load. Since σ_3 is not constant for stress path AB, a further modification must be made to provide an equivalent stress path having σ_3 constant. Two alternatives were considered (Fig. 11). One is path CB, which matches the maximum or loaded stress state of AB. The other is path DE, which matches the mean stress state of AB. The results with both CB and DE will be presented to demonstrate the best approach.

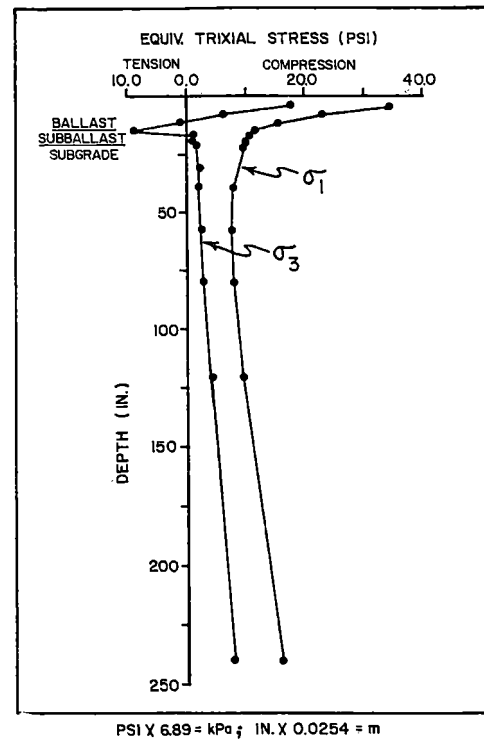


Fig. 10. Distribution with Depth Below Wheel Load of Equivalent Triaxial Stresses for FAST Section 18B

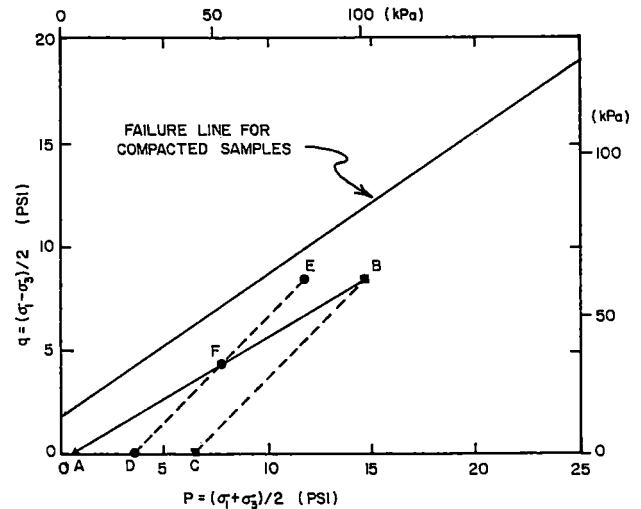


Fig. 11. Stress Paths for Middle of Ballast Layer in FAST Section 18B

BALLAST PROPERTY DETERMINATION

The GEOTRACK model is used to determine the stress paths for the property tests for a particular track structure. However, resilient properties are required before the GEOTRACK model can be run to determine the stress paths. In some cases these resilient properties can be assumed based on prior experience. On the other hand, the resilient parameters can be experimentally determined by conducting constant confining pressure cyclic triaxial tests based on a representative range of confining pressures and deviator stresses. For ballast, the effective confining pressures should be in the range of 3 to 12 psi

(21 to 83 kPa). The deviator stress at any confining pressure should be selected so that the maximum shear stress is in the range of 20 to 60% of the failure shear stress and the minimum shear stress is zero, i.e., no shear stress reversal.

Triaxial test procedures used for the FAST predictions are described in Ref. 39. A minimum of 1000 cycles should be applied before determining the resilient modulus and Poisson's ratio. In this study, 30,000 cycles were used. The ballast may be tested either saturated, dry or moist, but if saturated, then drainage should be provided to prevent build-up of pore pressure caused by volume change during cycling. A density state representative of field conditions should be established by appropriate sample preparation procedures.

The test results can be used to establish the coefficients for stress-state-dependent modulus relationships as in Eqs. 1 or 2, or any other appropriate relationships. Although Eq. 1 was used for the granite ballast in section 18B, the test results showed that the resilient modulus, E_r (psi), could be fit at least as well to bulk stress, θ (psi), by

$$E_r = K_5 + K_6 \theta \quad (13)$$

in which K_5 was 10,000 to 23,000 psi and K_6 was 350 to 480, depending on the number of cycles and compaction state.

After the stress paths have been determined from the GEOTRACK analysis, a series of static and cyclic tests are needed to determine the cumulative permanent strain behavior for track settlement prediction. The static tests provided the conventional strength parameters, which are cohesion (c) and angle of internal friction (ϕ). For the granite ballast, these were:

	c (psi)	c (kPa)	ϕ (deg)
Uncompacted	4.8	33	37.8
Compacted	2.8	19	44.4

Permanent strain resulting from the first load-unload cycle can be obtained from both the static tests and the cyclic tests. The results for the granite ballast for a range of confining stresses from 5 to 20 psi (34 to 138 kPa) are given in Fig. 12, where Δq is the cyclic shear stress and q_f is the failure shear stress at the confining pressure σ_3 .

For a typical drained cyclic triaxial test, the elastic strain decreases each cycle and hence the resilient modulus increases. This is at least partly a result of the densification from the cumulative volumetric strain. The cumulative plastic strain also increases each cycle, approximately in proportion to the log of the cycle number.

For tests carried out to 100,000 cycles, the accumulated permanent vertical strain, ϵ_N , after N cycles was found to be related to the first cycle permanent strain, ϵ_1 , by approximately

$$\epsilon_N = \epsilon_1 (1 + 0.19 \log N) \quad (14)$$

which is similar to Eq. 4. However, a more precise fit to the data is given by

$$\epsilon_N = (0.85 + 0.38 \log N) \epsilon_1 + (0.05 - 0.09 \log N) \epsilon_1^2 \quad (15)$$

These equations are independent of ballast density state. Thus the effects of ballast density are

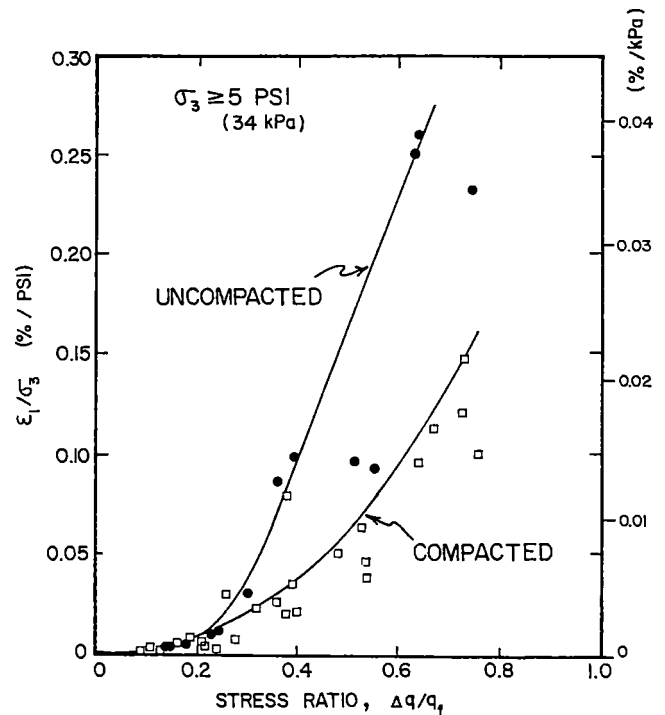


Fig. 12. Normalized Vertical Permanent Strain as a Function of Stress Ratio for Uncompacted and Compacted Samples after One Cycle

accounted for by ϵ_1 .

Contours of equal first cycle permanent strain ϵ_1 for compacted granite ballast are shown in Fig. 13. The failure envelope (K_f line) and constant confining pressure stress paths (diagonal lines) are

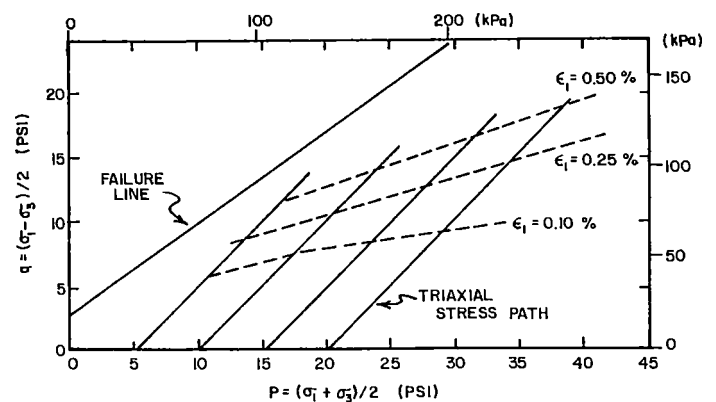


Fig. 13. Contours of Equal Strain after the First Cycle for Compacted Samples of Granite Ballast

also shown. Below about 5 psi (34 kPa), the strain contours converge to the origin. Thus the relationship of Fig. 12 for $\sigma_3 = 5$ psi (34 kPa) is used for the prediction of ϵ_1 below 5 psi (34 kPa). This relationship is given in Fig. 14, using values from Fig. 12 with σ_3 set at 5 psi (34 kPa).

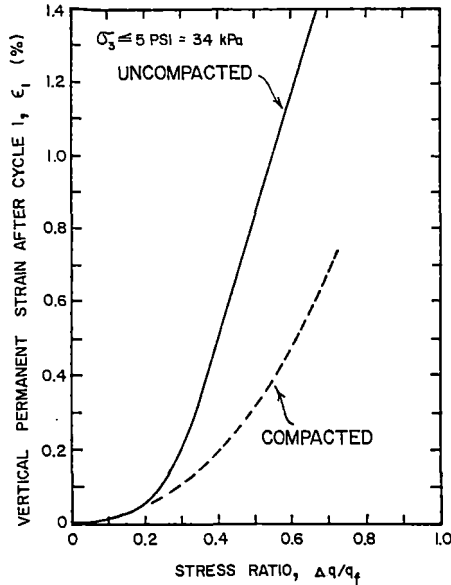


Fig. 14. Vertical Permanent Strain after the First Cycle as a Function of Stress Ratio and Degree of Compaction for Low Confining Pressures

PERMANENT STRAIN PREDICTION

For FAST Section 18B, the stress states in the middle of the ballast layer for paths CB and DE (Fig. 11) are given in Table 2. For each stress path and compaction state in Table 2, values of the $\Delta q/q_f$ ratio were calculated by the following relationship:

$$\frac{\Delta q}{q_f} = \frac{(\sigma_1 - \sigma_3)}{(\sigma_1 - \sigma_3)_f} = \frac{(\sigma_1 - \sigma_3)}{\left[\frac{2c \cos\phi + 2\sigma_3 \sin\phi}{1 - \sin\phi} \right]}, \quad (16)$$

From σ_3 and $\Delta q/q_f$, the values of the vertical permanent deformation after the first cycle, ϵ_1 , can be determined. For stress path CB, the values of ϵ_1 are given by Fig. 12, since $\sigma_3 > 5$ psi (34 kPa). For stress path DE, the values of ϵ_1 are given by Fig. 14, since $\sigma_3 < 5$ psi (34 kPa). The results are listed in Table 2. Similar values were obtained using the static triaxial test data. As expected, the stress path DE develops more permanent strain after the first cycle than stress path CB. Also, the

Table 2. Permanent Strain Prediction Calculations

Path	State	σ_3 (psi)	$\sigma_1 - \sigma_3$ (psi)	$\Delta q/q_f$	ϵ_1 (%)	ϵ at $N = 10^6$ (%)
CB	Uncompacted	6.3	16.7	0.42	0.57	1.63
	Compacted	6.3	16.7	0.39	0.18	0.55
DE	Uncompacted	3.5	16.7	0.54	0.96	2.55
	Compacted	3.5	16.7	0.56	0.40	1.17

NOTE: psi x 6.89 = kPa.

uncompacted ballast state produces larger permanent strains after the first cycle than the compacted state.

The values of permanent strain after the application of N cycles (ϵ_N) are predicted based on the values of ϵ_1 and N , using Eqs. 14 or 15. The values of ϵ_N for 1,000,000 cycles are also listed in Table 2, based on Eq. 15.

The measured values have been taken in the field as a function of million gross tons (MGT) of accumulated traffic. A conversion from MGT values to equivalent number of cycles of load application is necessary in order to compare the predicted results with the field measurements. According to the dynamic strain records available (Ref. 40), each axle pair in a truck acts nearly as a single ballast load cycle. Thus only two cycles of load would be imposed by each car of a train. Since the average static weight of a FAST car was 131.6 tons (119.5×10^3 kg), each cycle of load represents 65.8 tons (59.7×10^3 kg).

The predicted values of permanent strain for both stress paths and both compaction states are compared in Fig. 15 with the field measurements. The

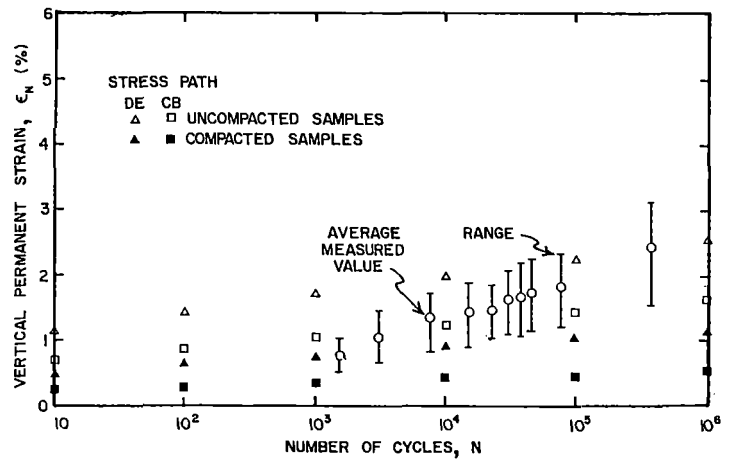


Fig. 15. Comparison of Predicted and Measured Values of Ballast Permanent Strain for FAST Section 18B

uncompacted lab results agree better with the field results after 10,000 cycles. Considering Fig. 15 and similar predictions for other track sections, the stress path DE also appears to be better than stress path CB for the middle of the ballast layer.

The numerical examples given were directed to the prediction of ballast strains. The prediction of the subballast strains and subgrade deformations is likely to be more straight-forward, because the stress paths imposed on these layers by the passing trains are close to those produced in the repeated load triaxial testing. This is not the case for the ballast layer, where truly three-dimensional conditions exist and large variations of stresses within the layer are developed. The problem is further complicated because the model employed predicts tension zones at the bottom of the ballast layer that are impossible to simulate in the triaxial test, and in fact cannot actually occur in the ballast. Thus differences between measured and predicted results are expected.

Some of the factors that could contribute to the disagreement of the predicted and measured values of the ballast permanent strain are:

1. There is a high variability in the field data of the measured response of the ballast.
2. The computer model predicts a tension zone at the bottom of the ballast layer. Since the ballast material cannot take tension, failure states are predicted for the equivalent triaxial stress paths. The computer model does not incorporate a failure criteria that can deal with this problem and hence may not be representing the stress states correctly.
3. The three-dimensional state of stress in the ballast layer is converted to an axisymmetrical state with variable confining pressure. However, the triaxial tests were carried out with an assumed equivalent constant confining pressure.
4. The representative point in the ballast layer is assumed to be the middepth. However, the predicted permanent strain is sensitive to the selected point because of the tension zone.
5. The cyclic laboratory testing used sinusoidal loading with full unloading each cycle to simulate the conditions imposed by the passing trains. Partial unloading was not taken into consideration.
6. The actual in-situ ballast density was not simulated, but a range of uncompacted and compacted ballast samples were tested.
7. The laboratory testing was limited to a small number of load applications, i.e., up to 100,000 cycles. In track, the loadings for a typical maintenance cycle are generally 10 to 100 times larger.

The methodology validation needs to be extended to the subballast and subgrade as well as the ballast.

SUMMARY

The objective of this study was to develop a methodology to predict the elastic and cumulative inelastic behavior of the railroad track structures under traffic loading as a basis for maintenance life determination.

Field observations performed at the U.S. DOT Facility for Accelerated Service Testing (FAST) in Pueblo, Colorado showed that the roadbed strains in the track structure caused by train loads were essentially elastic within each cycle, although the moduli of the materials were dependent on the stress level. After considering available computer models for representing the elastic response of the track structure, a new model, GEOTRACK, was developed because it was economical to use and contained the essential features of the track system. The model was shown to be in reasonable agreement with field results.

With the accumulation of traffic, the railroad track will behave inelastically, developing permanent

deformation. The inelastic behavior was predicted with the stress state from the elastic behavior and laboratory property tests. Available field permanent deformation data were used to validate the predictions obtained with the proposed methodology. The predicted results were in approximate agreement with the field results.

The methodology provides a rational approach for prediction of elastic and permanent deformation behavior of railroad track systems. The method can take into account the main factors influencing the deformation behavior, including axle load and number of cycles, rail and tie characteristics, and properties and thickness of the ballast and underlying layers.

ACKNOWLEDGMENT

The financial support for this research was provided by the United States Department of Transportation through contract number DOT-OS-70058. A substantial contribution to the computer model development, laboratory tests and field data reduction was provided by Harry E. Stewart. Assistance with the laboratory tests was also provided by Thomas J. Siller.

REFERENCES

1. Seed, H.B., Chang, C.K. and Monismith, C.L., "Effects of Repeated Loading on the Strength and Deformation of Compacted Clay," Proceedings, Highway Research Record No. 34, 1955, pp. 541-558.
2. Hargis, L.L., "A Study of Strain Characteristics in a Limestone Gravel Subjected to Repetitive Load," M.S. Thesis, Texas A & M University, College Station, Texas, 1963.
3. Barksdale, R.D., "Repeated Load Test Evaluation of Base Course Materials," Georgia Institute of Technology, Atlanta, Ga., May, 1972.
4. Haynes, J.H. and Yoder, E.J., "Effects of Repeated Loading on Gravel and Crushed Stone Base Course Materials Used in the AASHTO Road Test," Highway Research Record No. 39, 1963, pp. 82-96.
5. Hicks, R.G., "Factors Influencing the Resilient Properties of Granular Materials," Ph.D. Dissertation, University of California at Berkeley, 1970.
6. Allen, J.J., "The Effects of Non-Constant Lateral Pressures on the Resilient Properties of Granular Materials," Ph.D. Dissertation, University of Illinois at Urbana-Champaign, 1973.
7. Morgan, J.R., "The Response of Granular Materials to Repeated Loading," Proceedings, Third Conference of the Australian Road Research Board, Sydney, Australia, 1966, pp. 1178-1192.
8. Shackel, B., "Repeated Loading of Soils - A Review," Australian Road Research Record No. 5 (3), 1973, pp. 22-49.
9. Brown, S.F., "Repeated Load Testing of a Granular Material," Journal of the Geotechnical Engineering Division, ASCE, Vol. 100, No. GT7, July, 1974, pp. 825-841.
10. Robnett, Q.L., Thompson, M.R., Knutson, R.M. and Tayabji, S.D., "Development of a Structural Model and Materials Evaluation Procedures," Ballast and Foundation Materials Research Program, University of Illinois at Urbana-Champaign, Report No. FRA-OR&D-76-255, July, 1976.
11. Thompson, M.R., "FAST Ballast and Subgrade Materials Evaluation," Ballast and Fdn. Materials Res. Program, Univ. of Ill. at Urbana-Champaign, Report No. FRA/ORD-77/32, December, 1977.

12. Brown, S.F. and Hyde, A.F.L., "Significance of Cyclic Confining Stress in Repeated-Load Triaxial Testing of Granular Material," Transportation Research Board Record No. 537, 1975, pp. 49-57.
13. Knutson, R.M., "Factors Influencing the Repeated Load Behavior of Railway Ballast," Ph.D. Dissertation, University of Illinois at Urbana-Champaign, 1976.
14. Allen, J.J. and Thompson, M.R., "Significance of Variable Confined Triaxial Testing," Transportation Engineering Journal, ASCE, No. TE4, November, 1974, pp. 827-843.
15. Kalcheff, I.V. and Hicks, R.G., "A Test Procedure for Determining the Resilient Properties of Granular Materials," Journal of Testing and Evaluation, ASTM, Vol. 1, No. 6, November, 1973, pp. 472-479.
16. Boyce, J.R., Brown, S.F. and Pell, P.S., "The Resilient Behavior of a Granular Material Under Repeated Loading," Proceedings, Australian Road Research Board, Vol. 8, 1976, pp. 8-19.
17. Hicks, R.G. and Monismith, C.L., "Factors Influencing the Resilient Response of Granular Materials," Highway Research Board Record No. 345, 1971, pp. 15-31.
18. Olowokere, D.O., "Strength and Deformation of Railway Ballast Subject to Triaxial Loading," M.S. Thesis, Department of Civil Engineering, Queen's University at Kingston, Ontario, Canada, 1975.
19. Office for Research and Experiments, International Union of Railways, "Stresses in the Rails, the Ballast and the Formation Resulting from Traffic Loads," Question D71, Report No. 10, Vols. 1 and 2, Utrecht, Holland, 1970.
20. Shenton, M.J., "Deformation of Railway Ballast Under Repeated Loading Triaxial Tests," Soil Mechanics Section, British Railways Research Department, 1974.
21. Selig, E.T., Yoo, T.S., Adegoke, C.W. and Stewart, H.E., "Status Report - Ballast Experiments, Intermediate (175 MGT) Substructure Stress and Strain Data," Interim Report, FRA/TTC/Dr-10 (IR), Prepared for FAST Program, Transportation Test Center, Pueblo, Colorado, September, 1979.
22. Adegoke, C.W., "Elastic and Inelastic Deformation Response of Track Structures Under Train Loads," Ph.D. Dissertation, Dept. of Civil Engrg., State University of New York at Buffalo, December, 1978.
23. Raymond, G.P. and Williams, D.R., "Repeated Load Triaxial Tests on a Dolomite Ballast," Journal of the Geotechnical Engineering Division, ASCE, No. GT7, July, 1978, pp. 1013-1029.
24. Hyde, A.K.L., "Repeated Load Triaxial Testing of Soils," Ph.D. Dissertation, University of Nottingham, England, 1974.
25. Monismith, C.L. and Finn, F.N., "Flexible Pavement Design: State-of-the-Art 1975," Journal of the Transportation Engineering Division, ASCE, No. TE1, January, 1977, pp. 1-53.
26. Van deLoo, P.J., "Practical Approach to the Prediction of Rutting in Asphalt Pavements - The Shell Method," Transportation Research Board Record No. 616, 1976, pp. 15-21.
27. Barksdale, R.D., "Laboratory Evaluation of Rutting in Base Course Materials," Proceedings, Third International Conference on the Structural Design of Asphalt Pavements, University of Michigan at Ann Arbor, Vol. 1, 1972, pp. 161-174.
28. Duncan, J.M. and Chang, C.Y., "Nonlinear Analysis of Stress and Strain in Soils," Journal of the Soil Mechanics and Foundations Division, ASCE, Vol. 96, No. SM5, September, 1970, pp. 1629-1653.
29. Romain, J.E., "Rut Depth Prediction in Asphalt Pavements," Proceedings, Third International Conference on the Structural Design of Asphalt Pavements, Vol. 1, University of Michigan at Ann Arbor, 1972, pp. 705-710.
30. Morris, J., Haas, R.C.G., Reilly, P. and Hignell, E.T., "Permanent Deformation in Asphalt Pavements Can be Predicted," Proceedings, The Association of Asphalt Paving Technologists, Vol. 43, Minneapolis, Minn., 1974, pp. 41-76.
31. McLean, D.B. and Monismith, C.L., "Estimation of Permanent Deformation in Asphalt Concrete Layers due to Repeated Traffic Loading," Transportation Research Board Record No. 510, 1975, pp. 14-30.
32. Brown, S.F., Lashine, A.K.F. and Hyde, A.F.L., "Repeated Load Triaxial Testing of a Silty Clay," Geotechnique, Vol. 25, No. 1, 1975, pp. 95-114.
33. Monismith, C.L., Ogawa, N. and Freeme, C.R., "Permanent Deformation Characteristics of Subgrade Soils in Repeated Loading," Transportation Research Board Record No. 537, 1975, pp. 1-17.
34. Chou, Y.T., "Analysis of Permanent Deformations of Flexible Airport Pavements," U.S. Army Corps of Engineers, Waterways Experiment Station, Vicksburg, Miss., Final Report, 1977.
35. Brown, S.F. and Bell, C.A., "The Validity of Design Procedures for the Permanent Deformation of Asphalt Pavements," Proceedings, Fourth International Conference on Structural Design of Asphalt Pavements, University of Michigan at Ann Arbor, 1977.
36. Chang, C.S., Adegoke, C.W. and Selig, E.T., "GEO-TRACK Model for Railroad Track Performance," Journal of the Geotechnical Engineering Division, ASCE, Vol. 106, No. GT11, November, 1980, pp. 1201-1218.
37. Selig, E.T., Chang, C.S., Adegoke, C.W. and Alva-Hurtado, J.E., "A Theory for Track Maintenance Life Prediction," Final Report on First Year of Study, U.S. DOT, Office of University Research, Report No. DOT-RSPA-DPB-50-79-22, Dept. of Civil Engrg. Report No. OUR79-226F, University of Massachusetts at Amherst, December, 1979.
38. Selig, E.T., Chang, C.S., Alva-Hurtado, J.E. and Adegoke, C.W., "A Theory for Track Maintenance Life Prediction," Final Report on 2nd Year of Study, U.S. DOT, Office of University Research, Report No. DOT/RSPA/DPB-50/81/25, Dept. of Civil Engrg. Report No. OUR81-237F, University of Massachusetts at Amherst, June, 1981.
39. Alva-Hurtado, J.E., "A Methodology to Predict the Elastic and Inelastic Behavior of Railroad Ballast," Ph.D. Dissertation, Department of Civil Engineering, University of Massachusetts at Amherst, May, 1980.
40. Yoo, T.S. and Selig, E.T., "Field Observations of Ballast and Subgrade Deformations in Track," Transportation Research Board Record No. 733, 1979.

Cost/Performance of Geotextiles in Maintenance of Way

D. Bertel

Assistant Chief Engineer
MOW
Missouri Pacific Railroad

W. Puffer

Applications Engineering
Manager
Hoechst Fibers Industries

Cost/performance criteria for utilizing a properly designed geotextile in maintenance of way (MOW) practices is presented. A concept of comparing MOW expenditures as related to various MOW practices with and without geotextile is shown. The deciding criteria for incorporating geotextiles into the MOW practices is then illustrated.

NOMENCLATURE

C-P	Cost-Performance Factor
M.O.W.	Maintenance of Way
M.G.T.	Millions of Gross Tons
TAMOWE	True Annual Maintenance of Way Expenditures
T.S.I.	Track Serviceability Index

INTRODUCTION

The single most difficult decision with regard to the use of engineering fabric in open track rehabilitation is determining to what extent fabric should be incorporated in open track rehabilitation, based upon a cost versus anticipated performance basis.

Criteria for utilizing an engineering fabric or geotextile in the maintenance of way of railroads has been rather subjective oriented. Engineering fabric has become an accepted integral part of the rehabilitation of grade crossings, diamonds, turnouts, and other high impact areas on the more progressive railroads. In addition to such high impact areas, engineering fabric has been incorporated into open track Maintenance of Way (M.O.W.). Fabric use is generally restricted to the very worst locations which are being undercut or plowed, for example.

The decision making process for using fabric in open track is similar to the use of fabric as a part of grade crossing or turnout rehabilitation. Several

railroads have established criteria for fabric utilization. For certain railroads, the criteria may involve regional variations and restrictions such as use on certain mainline track.

Unfortunately, the current approach to determining extent of use of engineering fabric in open track rehabilitation has several shortcomings. The shortcomings include the lack of rationale for comparing open track rehabilitation with and without the use of a fabric based upon cost and performance criteria.

Therefore, a cost/performance concept is presented to compare various open track rehabilitation techniques which will also include the use of fabric.

CONCEPT

The cost/performance concept recognizes that level of service or performance of a particular section of track or the track network is dynamic and is forever changing. The secret to good track performance at reasonable M.O.W. expenditures rests in part with the recognition that the track performance today has been significantly influenced by the pattern of previous years M.O.W. expenditures. Additionally, the future track performance is significantly influenced by the continuity of the M.O.W. expenditures, changes in traffic patterns, and car design.

It is estimated and many top Railroad Maintenance Engineers agree, that rail has approximately 1.6 more life under conventional 80-ton loads of traffic than under 100-ton loads. The use of unit trains of 100-ton capacity further reduces rail life over the 80-ton conventional loads. Geotextiles maintain better surface, consequently prolong rail life.

Tie life is about 1.4 times greater when under 80-ton loads vs. 100-ton loads. Geotextile application will prolong tie life by elimination of water, muddy conditions, as well as better stability. It is hard to put these savings into facts and figures.

Ballast and surfacing have about 1.4 times more life under 80-ton cars mixed traffic than 100-ton unit train traffic. The accelerated trend for use of 100-ton unit trains continues to plague the Track Maintenance Engineer and geotextiles will play a more important role in the future.

The track performance over time can best be illustrated utilizing an indexing technique. For instance, let's define track serviceability index (TSI) as a direct measure of the track's performance. The TSI therefore reflects the track performance at any point in time and can be utilized to determine changes of track performance over time. A high TSI reflects trackage that has good line and surface and is properly maintained.

Figure (1) illustrates the concept of track serviceability index, which is shown as a function of millions of gross tons (MGT). The specific track being evaluated has X MGT/yr. The annual MGT therefore can be related to the change of track serviceability.

The track serviceability on January 1, 1981, is represented by point 1. The anticipated track serviceability for January 1, 1983, is represented by point 2.

The change over time of track serviceability is then represented by subtracting TSI_2 from TSI_1 . Thus, TSI_1 minus TSI_2 equals the change in TSI between January 1, 1981, and January 1, 1983. The

M.O.W. expenditure between January, 1981, and January, 1983, was assumed to have not included any out-of-face activity that would change the general decline of the track performance or serviceability as a result of the track traffic (MGT).

By examining Figure 1 still further, one ultimately would conclude that track serviceability would decline to an unacceptable level, causing some specific M.O.W. procedure to be required to raise the TSI above that unacceptable level.

Figure 2 illustrates the change of the TSI to a specific M.O.W. track rehabilitation project. Rehabilitation could include plowing, undercutting, surfacing, or renewal of rail or ties. For each particular rehabilitation technique, however, the resulting raise in TSI illustrated on line B-1 would be different. Referring to Figure 2, let's discuss two track rehabilitation programs. The first program consists of plowing out 8 inches of existing ballast, renewal of 600-800 cross ties per mile, installation of a properly designed geotextile application, new ballast as needed, followed by two 2 inch resurfacings. The second or alternative to plowing might be a series of 2 inch resurfacings (B-7, 8-9, 10-11, 12-13, 14-15, and 16-17).

By expending a certain amount of maintenance of way dollars, rehabilitation B-1 has temporarily raised the TSI of the track under evaluation. However, as expected, the TSI would begin to decline. The rate of decline is dependent on several factors which include the track section, subgrade type, available drainage, annual and type MGTs, and speed, etc. For simplicity, the typical annual MGT has been held constant for this particular section of track. Changes in typical annual MGTs can be considered using this concept. To simplify the concept presentation

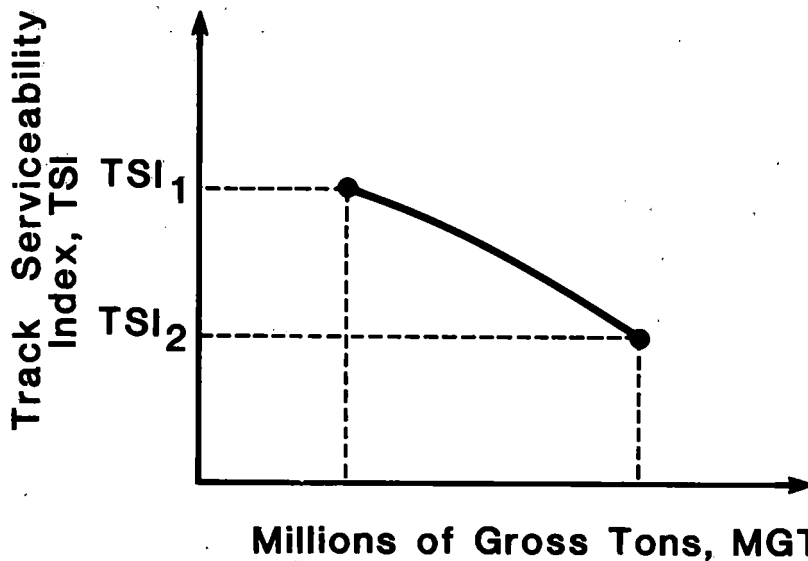


Fig.: 1 Track Serviceability Index, T.S.I.

somewhat, again a specific section of track is being considered with no immediate change in annual MGTs being anticipated.

For simplification, let us further assume that tie renewal, rail replacement requirements, etc., are equal for both plowing and resurfacing. Thus, the only variable we are examining is the TSI overtime, and at a known cost for resurfacing, plowing, and geotextile application.

Referring to Table 1, comparison of two different M.O.W. programs can be made. The costs per mile of the two different programs are \$46,000 and \$48,000 based upon assumed costs, recognizing that costs vary throughout the industry. On the basis of annual cash flow, one might be inclined to choose Alternate 2 -- six resurfacings. When one determines the average TSI index for plowing and subsequent resurfacing, and then considers the True Annual M.O.W. Expenditures per year, a different conclusion would be reached.

$$\begin{aligned} \text{Defining Track Serviceability Index, T.S.I. as:} \\ \frac{50,000}{\text{True Annual M.O.W. Expenditure/mi.}} \\ \text{or} \\ \frac{31,056}{\text{True Annual M.O.W. Expenditure/km.}} \end{aligned} \quad (1)$$

and calculating the average TSI for each alternate between 1981 and 1996 (assuming either it is 1996 or we can clearly look into the future), we can determine the True Annual M.O.W. expenditure/mi. for the two alternates, assuming 30 MGTs per year.

The True Annual M.O.W. Expenditure represents the total expenditures necessary to offset the mechanical wear and deterioration of all track components. Sadly to say, available M.O.W. dollars are far less than necessary to offset such wear and deterioration.

TABLE 1 -- 15 YEAR M.O.W. EXPENDITURE

	Alternate 1	Alternate 2
Plowing (with use of geotextile)	\$30,000	--
Resurfacings	\$16,000	\$48,000
Total per mi.	\$46,000	\$48,000
(per km)	\$28,571	\$29,814

TABLE 2 -- ALTERNATE COMPARISON -- 1 vs. 2

	Alternate 1 - Plowing with Geotex. Surfac.	Alternate 2 - Multiple Resurfacing
Area ¹	1,650	1,200
Avg. TSI ²	3.67	2.67
CP Factor ³	$\frac{750}{46,000} = .016$	$\frac{300}{48,000} = .006$
True Annual M.O.W \$/Yr.	\$ 13,624/mi. \$ 8,462/km.	\$ 18,727/mi. \$ 11,632/km.
Total True Annual M.O.W Expenditure (15 years)	\$204,360/mi. \$126,932/km.	\$280,905/mi. \$174,475/km.

- ¹Area determined from Figure 2 using 30 MGT/yr.
²Avg. TSI determined from Figure 2.
³C.P. Factor = Cost/Performance Factor.

The average TSI for Alternates 1 and 2 is 3.67 avg. TSI and 2.67 avg. TSI respectively. This, although informative, is not directly meaningful.

Utilizing the definition of TSI, the True Annual M.O.W. Expenditure per mile equals 50,000 divided by the T.S.I. This True Annual M.O.W. expenditure represents the total expenditures to include the mechanical wear and deterioration of all track components.

Thus, the True Annual M.O.W. Expenditures for Alternate 1 and 2 is \$13,624 versus \$18,727, respectively, as shown in Table 2. When one considers expenditures to offset the mechanical wear and deterioration of all track components over a 15 year period, the respective Total True M.O.W. dollars become \$204,360 and \$280,905. To compare each track maintenance of way program, the concept of the cost-performance factor (C-P factor) is introduced. The C-P factor is defined by the following expression:

$$C \cdot P = \frac{\left(\sum_0^{N_{Year}} TSI_T \cdot MGT_T \right) - \left(TSI_{MIN} \cdot \sum_0^{N_{Year}} MGT \right)}{\sum_0^{N_{Year}} MOW \ EXP} \quad (2)$$

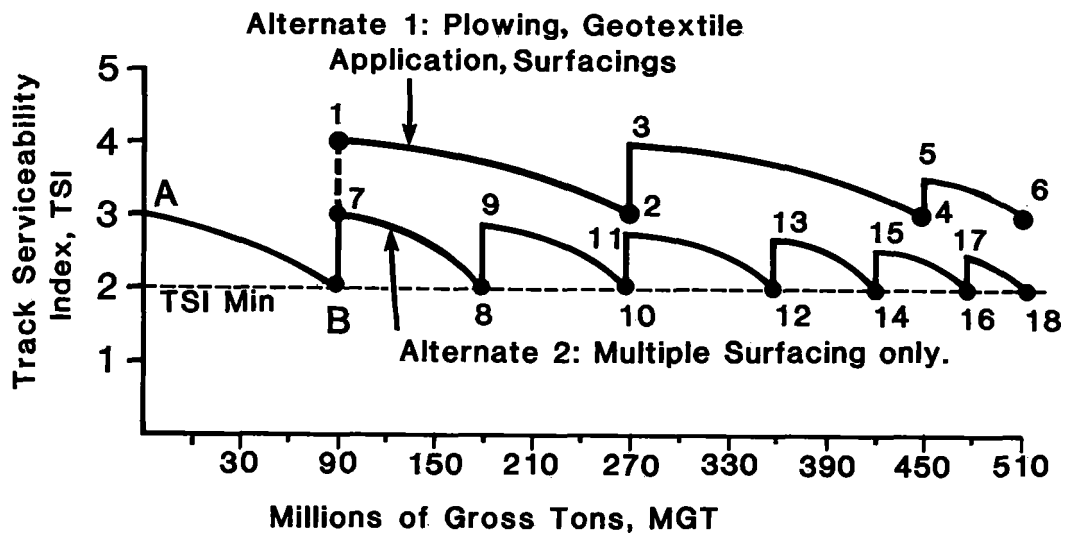


Fig.: 2 Comparison of Alternate 1&2

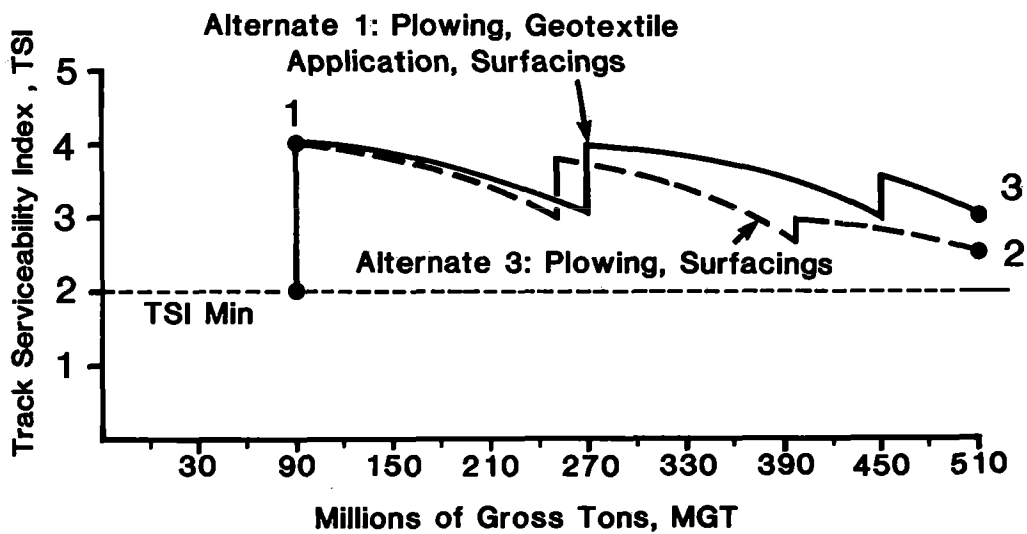


Fig.: 3 Comparison of Alternates 1 & 3

The cost-performance factor thus reflects the track's cost-performance based upon the average track serviceability as related to the MGTs and the maintenance of way expenditures.

The C-P factors for the example being considered can then be calculated. The C-P factor for the Alternates Plowing and Resurfacing are .016 and .006 respectively, as seen in Table 1.

The interpretation given to what the C-P factors reflect is given by the following. One can set minimum cost performance standards on any new product or MOW practice. Any new product or procedure should produce a higher resultant C-P factor if that product or procedure is truly beneficial on a cost-performance basis. Minimum C-P factors can be established as a basis of comparison.

Thus, the concept of cost-performance is a method of utilizing current accounting procedures to determine the cost-performance of various MOW practices. Similarly, the cost-performance of a geotextile can be evaluated by utilizing the C-P concept as presented.

Criteria

C-P criteria for utilizing a properly designed geotextile in MOW practices should include the items shown in Table 3, the criteria for the use of geotextiles.

TABLE 3

C-P Criteria for Geotextiles

Location To Location	Criteria	Remarks
	Ties Cost Site life Failure Mechanisms Change Out Procedure M.O.W. Expenditures	Establish the cost for tie average life life without the use of engineering fabric.
	Ballast Costs Thickness Condition Ballast Failure Mechanisms Rehabilitation Procedure Rehabilitation Cost (Resurfacing, Plowing, etc.)	Establish ballast costs without engineering fabric.
	Subgrade Costs Type Failure Mechanisms Drainage Maintenance of Surface Cost Maintenance of Alignment Cost	Establish the cost for current rehabilitation.

Once the criteria has been established, historical M.O.W. expenditures for a particular section of track mile post "A" to mile post "B", and future annual M.O.W. expenditures can be plotted similar to Figure 2. The C-P factor can be determined and an evaluation made for the introduction of an engineering fabric.

Evaluation of Geotextiles by C-P Method

Evaluation of geotextiles by utilizing the cost-performance method can be accomplished by following the same procedure as was done to evaluate Alternates 1 and 2.

T.S.I. for plowing utilizing geotextiles and not using geotextiles is shown in Figure 3. Plowing utilizing a properly engineered geotextile followed by resurfacing is shown as Alternate 1. Plowing without utilizing a geotextile and subsequent resurfacing is shown as Alternate 3.

Note: Alternate 3 track degenerates at an accelerated rate as compared to Alternate 1.

The respective cost performance evaluation is shown in Table 4. The extent to which a geotextile has been beneficial based upon a cost performance evaluation can be determined by comparing the resulting TSI, C-P factor, and ultimately the projected True Annual M.O.W. Expenditure per year.

TABLE 4 -- ALTERNATE COMPARISON -- 1 vs. 3

	Alternate 1*	Alternate 3**
Total Maintenance of Way Expenditures (U.S. dollars) (15 year)	\$ 46,000/mi. \$ 28,857/km.	\$ 36,000/mi. \$ 22,360/km.
Area	1,650	1,300
Avg. Track Serviceability Index	3.67	2.89
Cost Performance Factor	.016	.011
True Annual Maintenance of Way Expenditure \$/Year	\$ 13,624/mi. \$ 8,462/km.	\$ 17,301/mi. \$ 10,746/km.
Total True Maintenance of Way \$ over 15 Year Period	\$204,360/mi. \$126,932/km.	\$259,516/mi. \$161,191/km.

* Plowing and application of geotextile followed by surfacing.

** Plowing and not using geotextile, then followed by surfacing.

After comparing the Cost Performance Factors of Alternate 1 and Alternate 3, as well as the average Track Serviceability Indices and Total True Maintenance of Way Expenditures (over a 15 year period), Alternate 1 clearly provides three advantages over Alternate 3. Those advantages are:

1. Higher Cost Performance Factor
2. Higher Track Serviceability Index
3. Lower True Annual M.O.W. Expenditures

Thus, the advantages of using a properly designed geotextile offset the initial cost of geotextile application.

CONCLUSION

The use of the cost performance technique to evaluate existing Maintenance of Way practices, geotextiles, concrete ties, continuous rail, etc. is feasible.

The cost performance technique, as presented, clearly demonstrates the advantages of utilizing a properly engineered geotextile.

Many railroads have not done "extensive" work in out of face applications of geotextiles in open track rehabilitation projects. The authors feel that using geotextiles in such projects helps maintain better line and surface, eliminates some surfacing recycle work, and develops indeterminate savings in reducing slow orders, damage to equipment, improved train handling, etc.

Adjustment of Transition Curve Length for Heavy-Haul Railroad Lines

Henryk Baluch

Deputy Director
Railway Research Institute
Polish State Railways
Poland

Andrew Siuz

Staff Research Engineer
Transportation Systems
Center
U.S. Department
of Transportation

Increases in superelevation of track are sometimes necessary to accommodate desired increases in train speed or axle load. Changes in superelevation require appropriate modifications in curve transition geometry. Such modifications can be costly due to the large displacements of the new track locations from the existing location. This paper presents a method of designing longer transition curves with linear superelevation ramps which minimize track displacement. Two spirals are used ahead of the transition spiral which allow an increase in curve superelevation with no increase in the superelevation ramp gradient and with little or no additional earthwork. Apart from the geometrical parameters, the criteria governing this design are the acceptable unbalanced centrifugal acceleration and the rate of its variation. A program designed for the programming use of a hand-held programmable calculator and several examples are presented.

NOMENCLATURE

		x, y	coordinate system for existing alinement
		x', y'	coordinate system for proposed alinement
a	unbalanced lateral acceleration	z	displacement of displacement spirals from existing alinement
a_{all}	allowable unbalanced lateral acceleration	z_{max}	maximum displacement of proposed spirals from existing alinement
Δe	amount the circular curve is displaced	Δe	displacement of proposed geometry from existing circular curve
Δe_{all}	allowable displacement of circular curve	ψ	rate of change of acceleration, jerk
h	amount of superelevation		
l_{AD}	length of track to be relocated		
l_d	length of existing spiral		
l_o	length of displacement spiral to be introduced		
l_{omin}	minimum length of displacement spiral		
l_{oz}	corrected length of displacement spiral		
l_p	desired length of superelevation transition spiral		
Δn	displacement of circular curve if displacement spirals are not used		
R	curve radius		
R_o	end radius of displacement spiral		
v	train velocity		

1. INTRODUCTION

Poland has the most heavily-laden, standard gage lines in Europe.¹ Increased track durability is being achieved by:

- 1) Overall strengthening of the track structure by such means as: use of heavier rails, higher strength steels, decreased tie spacing, elastic fasteners (instead of cut spikes), more abrasion resistant ballast, etc.
- 2) Supplementing existing track components with new elements, e.g., rail lubricators and/or restraining rail in curves, and filter fabrics laid on the subgrade.
- 3) Improving the quality of track maintenance work, by more exact track installation and replacement, better ballast compaction, and

¹Total annual tonnage on PKP lines is greater than the combined tonnage on the French and West German railroads. The combined length of railroad lines for these two countries is 2-1/2 times the length of lines on the PKP.

repair of localized track defects -- especially in the initial period of service.

- 4) Adjusting the track's geometry to the new level of service.

Use of these methods is based on research carried out in Poland and by international organizations. The practical result of these remedial measures can be identified by comparing the average track durability on the PKP in the late sixties, which was 250 Tg (227 MGT), to the current expected track life of 450 Tg (409 MGT). This 80% increase in track life has been obtained mainly by replacing S49 (98 lb/yd) rail with UIC 60 (120 lb/yd) rail. Experience garnered over 12 years use of UIC-60 rail has shown that rail replacement must be accompanied by other complementary trackwork in order to achieve maximum benefit from the use of the heavier rail section.

It is particularly important when improving overall track durability to adjust curve superelevation to the level of service of the track. This adjustment is particularly necessary if the line is to service higher speed traffic, but can have benefits in increased rail life under heavier axle loads. This paper will concentrate on the adjustment of transition curve length for curves where it is desirable to increase superelevation rate.

Normal design procedures for increasing transition curve length result in a realignment of the track with a displacement of the circular curve, Δn (see Figure 1). Often the amount of curve offset is unacceptable due to right-of-way restrictions or due to natural obstacles. Realignment of the tangent leading into the transition curve can cause lateral accelerations and

jerk that may be particularly undesirable for heavy-haul traffic.

This paper presents a method for determining a new track layout that takes into account the allowable amount of circular curve displacement, Δe_{all} , the maximum allowable realignment of the existing tangent, Z_{max} , and the allowable amount of centrifugal acceleration, a_{all} , and jerk, ψ_{all} . Two displacement spirals are introduced ahead of the spiral to be lengthened. These displacement curves allow optimization of alignment from the tangent with circular curve displacements.

2. THE SHAPE AND LENGTH OF TRANSITION CURVES FOR HEAVY HAUL TRACK

Proper adjustment of superelevation to level of service can lead to a decrease in lateral rail wear. Reference [2] presents algorithms and programs for adjusting superelevation for freight and passenger car speeds. This adjustment is particularly valuable on recently upgraded lines if it becomes necessary to increase train speeds. On lines with predominantly passenger traffic, i.e., cars with low center-of-gravity and softer torsional stiffness, it may be possible to achieve the increase in superelevation by:

- 1) Increasing curve superelevation without changing the length or shape of the existing spiral. The superelevation ramp remains linear but with an increased (or decreased) profile gradient.

Numbers in brackets represent references listed in the Bibliography.

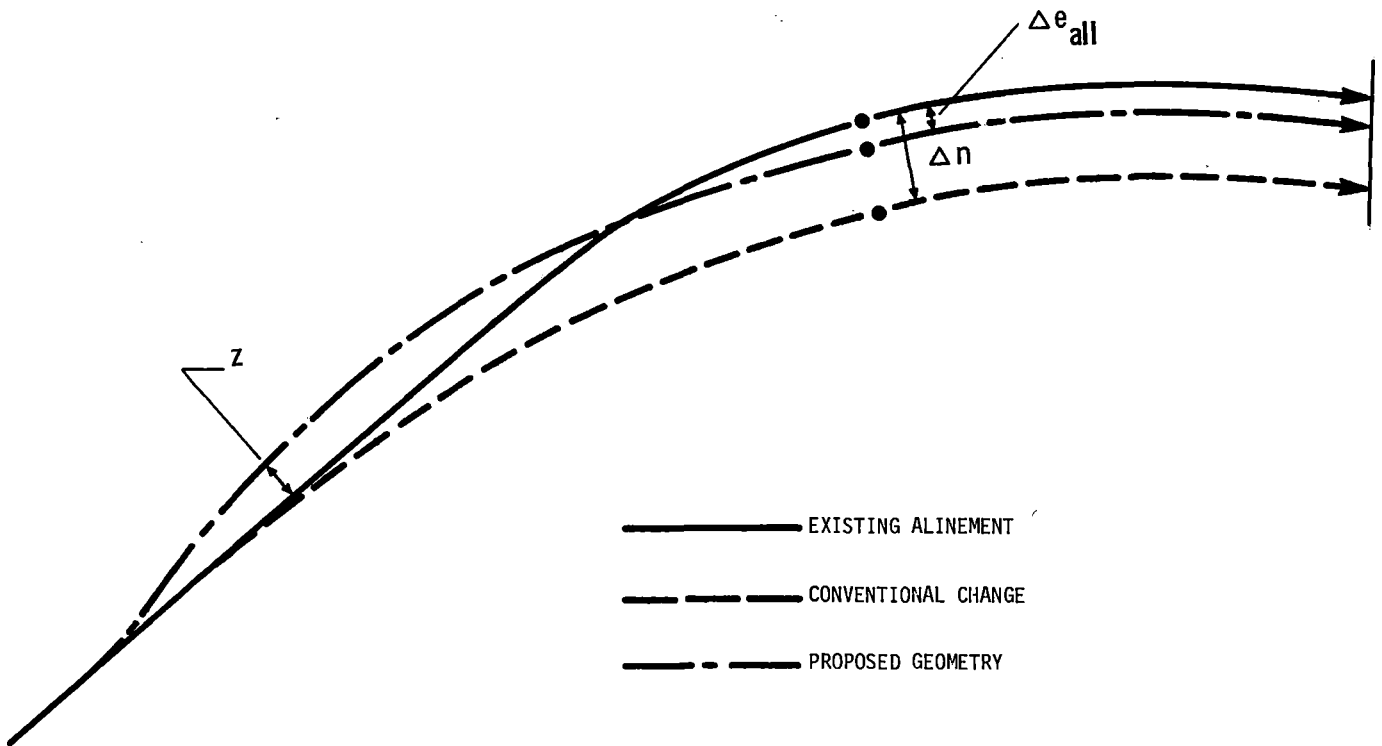


FIGURE 1. IMPACT OF NORMAL DESIGN PROCEDURES AND PROPOSED DESIGN PROGRAM ON TRACK ALINEMENT

2) Elongating the spiral and changing its shape. In this way, lengthening the spiral does not necessitate offsetting the existing circular curve by large amounts. For example, a third order spiral expressed by Equation (2) below can be replaced with a cosine curve with planar coordinates calculated by:

$$y = \frac{1}{2R} \left[\frac{x^2}{2} + \frac{l^2}{\pi^2} \left(\cos \pi \frac{x}{l} - 1 \right) \right]$$

The superelevation buildup along any point on the ramp can be computed from:

$$h_x = \frac{h}{2} \left(1 - \cos \pi \frac{x}{l} \right)$$

Similarly other elementary curves, e.g., sinusoidal curves or fourth order parabolis, can be employed.

3) Leaving the spiral shape unchanged but increasing its length. The circular curve is then offset a distance, Δn , calculated from Equation (1), if a third order spiral (Equation (2)) has been employed.

4) Leaving the spiral without change but continuing the runoff into the circular curve.

The above approaches can have significant disadvantages if the line carries dense, heavily-laden, freight traffic. Increasing the runoff gradient, for instance, increases track twist which is very dangerous for cars having high turning stiffnesses, e.g., tank cars.

The introduction of a nonlinear superelevation ramp increases track twist in the middle section of the ramp and, in addition, brings on difficulties in track maintenance. In addition, approaches 2 and 4 run contrary to the "Recommended Standards for Track Maintenance" [5] adopted by the Association of American Railroads (AAR), which specify that "Each elevation transition shall be made at a uniform rate of change with full elevation at the point of full curvature." Offsetting the circular curve a distance sufficient to require widening of the embankment can be expensive and lead to future maintenance problems with track subsidence. According to Titov [7], any change in track alignment or profile exceeding 20 to 30 cm (8 to 11 inches) requires a rebuilding of the subgrade. Failure to rebuild the subgrade could cause maintenance problems in the future.

3. PROPOSED MODEL FOR TRANSITION CURVE ELONGATION FOR HEAVY-HAUL TRACK

Having pointed out the disadvantages of the above means of dealing with the transition curves and superelevation runoff for increased application of superelevation; the authors propose an elongation geometry which employs two simple curves that shift the tangent ahead of the spiral to allow for a longer spiral length. The proposed geometry is illustrated in Figure 2. Compared to other proposals, e.g., references [6] and [8], the proposal in Figure 2 uses two curves, AB and BC, leading into the new spiral CD, as a means

of lengthening the transition curve instead of using one circular curve which may cause a sudden increment in acceleration.

The algorithm developed for this proposal ensures that:

- 1) The displacement of the circular curve, Δe , is held to an allowable value, $\Delta e < \Delta e_{all} \cdot 3$
- 2) The maximum displacement of the new line from the existing tangent, Z_{max} , is no greater than the determined allowable displacement, Z_{all} .
- 3) There is a minimum length of track displacement, l_{AD} .
- 4) The unbalanced acceleration, a , and its time increment (or jerk), ψ , are maintained within their assumed tolerances, or:

$$a \leq a_{all} \quad \text{and} \quad \psi \leq \psi_{all}$$

The above requirements are equivalent to keeping dynamic vehicle/track interactions within the limits accepted for a given line while simultaneously minimizing track relocation to avoid additional earthwork.

These criteria are European and not in standard use in the U.S. In the U.S., to use the recommendations and remain within the AAR recommendations [5], it would be necessary to determine the minimum length of transition curve (1 below) from the desirable rate of change in superelevation transition (Table 1) or, as an absolute minimum, the equation:

$$L = 1.22 E_u V$$

where:

- L = minimum desired length of spiral
- E = underbalanced elevation in inches
- V^u = maximum authorized train speed in miles per hour.

The value of L chosen can then be used to substitute for l_{min} in the following program development.

TABLE 1. UNIFORM RATES OF CHANGE DESIRABLE IN ELEVATION TRANSITIONS (after [5])

Class of Track [Train Speed (MPH)]	Rate of Change (inches/foot)
A (61-80)	0.012
B (46-60)	0.016
C (31-45)	0.020
D (16-30)	0.024
E (0-15)	NA

$$\text{desirable length of transition curve (feet)} = \frac{\text{actual superelevation (inches)}}{\text{rate of change (above table)}}$$

³Very often, it is desirable not to displace the circular curve so that: $\Delta e = \Delta e_{all} = 0$. A variation with $\Delta e > 0$ is shown in Figure 3.

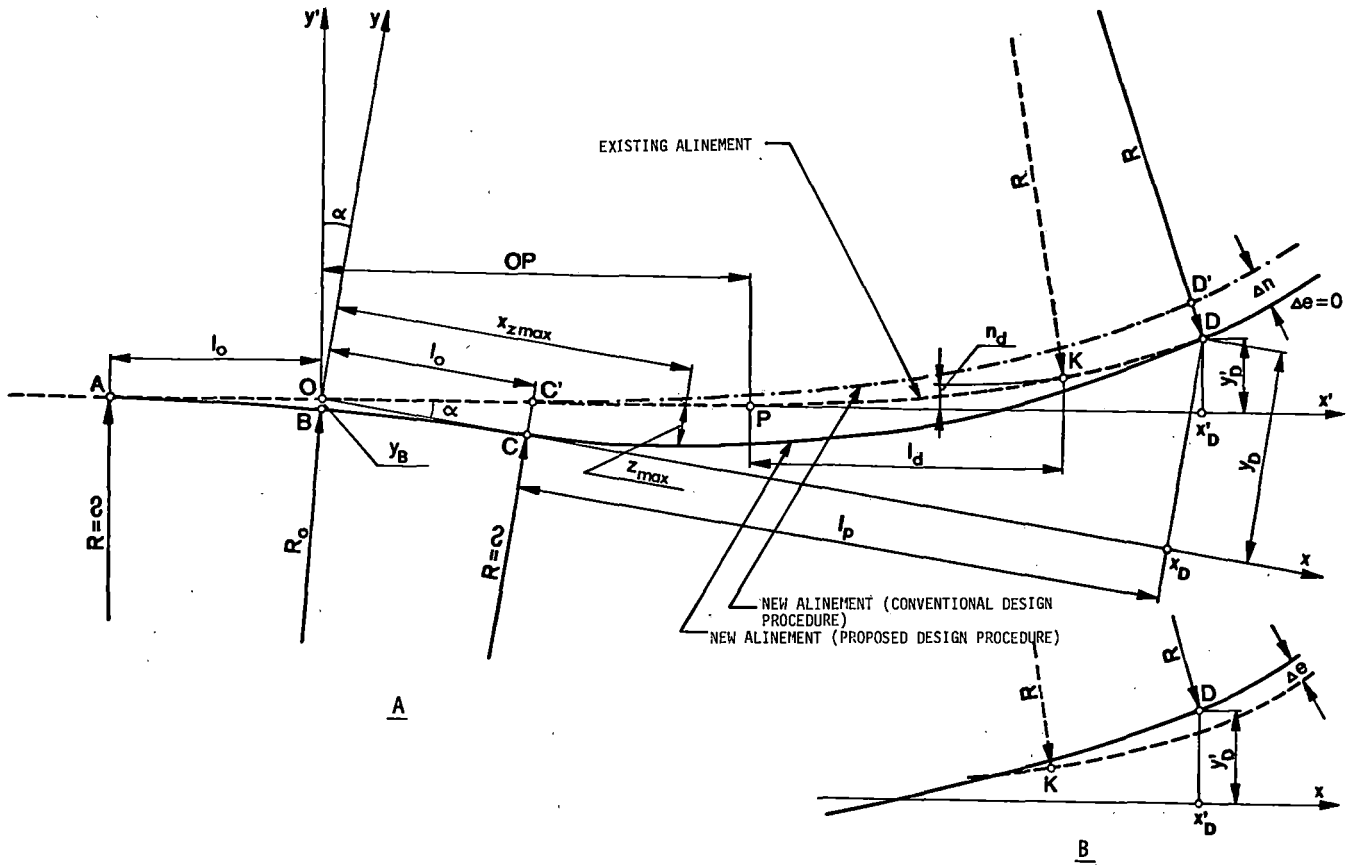


FIGURE 2. DETAILED GEOMETRY OF PROPOSED METHOD OF TRANSITION CURVE ELONGATION, (a) $\Delta e=0$, (b) $\Delta e>0$

Replacing the existing spiral PK of length l_d (shown in Figure 2 with a dashed line) with the design spiral CD (solid line) of length l allows the elimination of the track relocation $P \Delta n$, that would normally be associated with the introduction of a longer transition curve C'D' (dash/dotted line) with normal design procedures.

This displacement, Δn , can be expressed by:

$$\Delta n = \frac{\kappa_p l_p^2 - \kappa_d l_d^2}{6R} + R (\cos \xi_p - \cos \xi_d) \quad (1)$$

for a spiral based on a third order curve with equation:

$$y = \kappa \frac{x^3}{6Rl} \quad (2)$$

where: $\frac{4}{\kappa}$

$$\kappa = \frac{1}{\cos \xi} \quad ; \quad \xi = \arcsin \frac{l}{2R}$$

The displacement curves, AB and BC, are designed without superelevation and therefore their minimum length can be computed from:

⁴For short spiral lengths and long curved radii, it can be assumed that $\kappa = 1$.

$$l_{omin} = \frac{a_{all} \cdot V}{3.6 \psi_{all}} \quad (3)$$

where V is the design speed.

Looking more closely at curves ABC, Figure 3, one can write:

$$\alpha = 2\beta$$

From the derivative of the equation of the curve, Equation (2), one gets for $K = 1$:

$$\tan \beta = \frac{l_0}{2R_0} \quad (4)$$

The curvature radius R_0 at point B should be governed by:

$$R_0 > \frac{v^2}{a_{all}} \quad (5)$$

From equations (3), (4), and (5):

$$\tan \alpha_{max} = \frac{a_{all}^2}{\psi_{all} \cdot V} \quad (6)$$

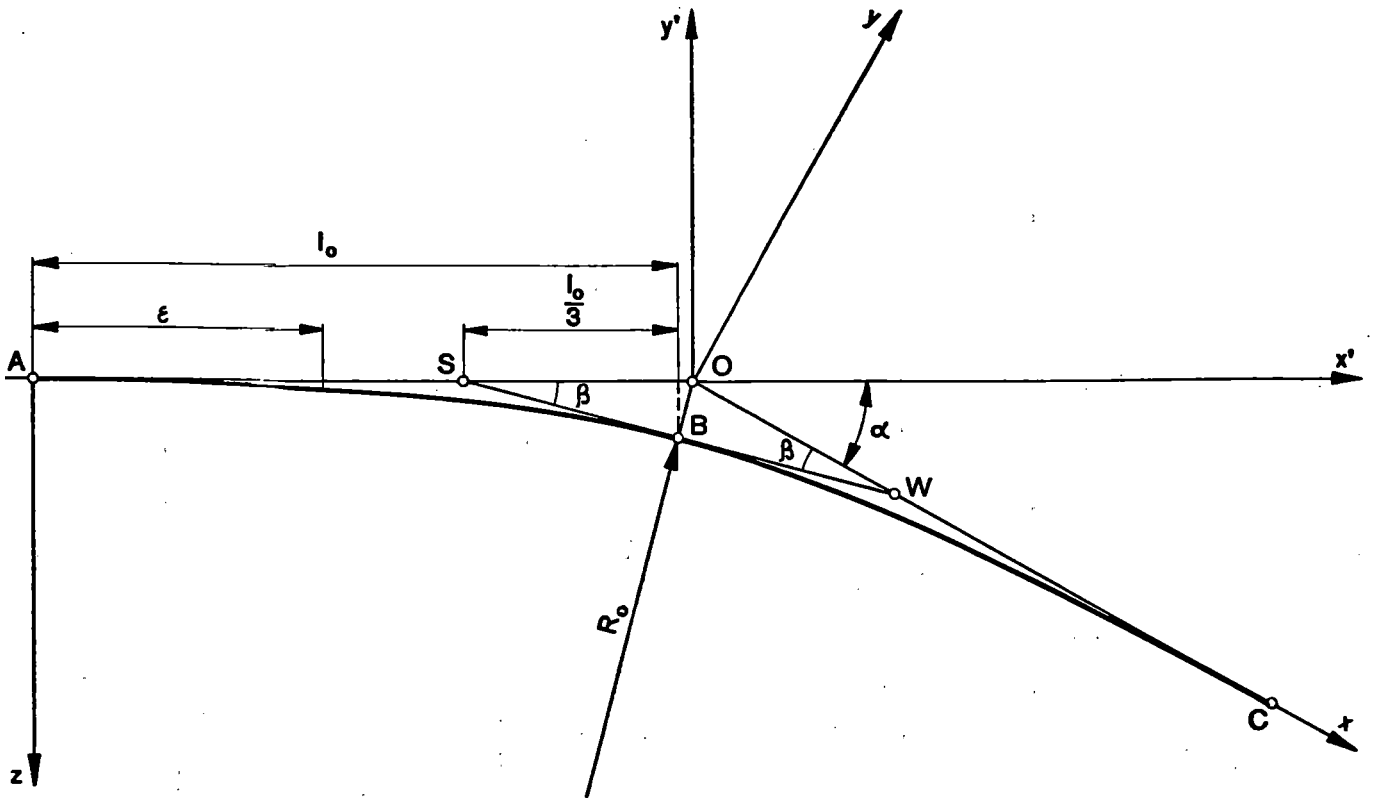


FIGURE 3. DETAIL OF THE TWO DISPLACEMENT SPIRALS

The angle α_{\max} given by Equation (6) is the maximum permissible angle associated with a_{all} and ψ_{all} . When α is less than α_{all} , then it follows that the value of $l_{o \min}$ could be decreased.

Tan α may be expressed as [3]:

$$\tan \alpha = \frac{\sqrt{\left(l_o + \frac{l_p}{2}\right)^2 + 2R(\Delta n - \Delta e) - \left(l_o + \frac{l_p}{2}\right)}}{R} \quad (7)$$

A very important parameter of the design configuration is the value of the largest displacement between the designed spirals and the existing alignment, Z_{\max} . The value of Z_{\max} determines the amount of earthwork that will need to be performed during realignment. One can calculate the value of displacement, Z , at any point, x , along the curve from:

$$Z = x \tan \alpha - \frac{\kappa_p (x - l_o)^3}{6R l_p} \quad (8)$$

Differentiating Equation (8), setting it equal to zero, and solving the resultant second order equation, one obtains:

$$x_{z\max} = l_o + \sqrt{2R l_p \tan \alpha} \quad (9)$$

Substituting back into Equation (8), one obtains:

$$Z_{\max} = \left(l_o + \sqrt{2R l_p \tan \alpha}\right) \tan \alpha - \left(\frac{\sqrt{2R l_p \tan \alpha}}{6 R l_p}\right)^3 \quad (10)$$

Some of the simplifications assumed for the purpose of this analysis result in a small discrepancy (a few millimeters for a few meters length) between the calculated coordinates for the end point of the configuration and the existing end point. This error of closure, ΔZ , can be compensated for by reducing the length of the initial displacement curves, AB and BC, to l_{oz} without changing angle α :

$$l_{oz} = l_o - \frac{\Delta Z}{\tan \alpha} \quad (11)$$

4. PROGRAMMING THE ALGORITHM

Design algorithms such as the ones presented above are ideally suited for a portable, programmable calculator such as the TI-59 which can be carried into the field. Figure 4 shows the block diagram for solution of the presented problem, including equations not presented in this paper (to save time and simplify the explanation).

⁵ A program for this configuration, including the detailed data, necessary to stake the curves in the field is presented in Reference [3].

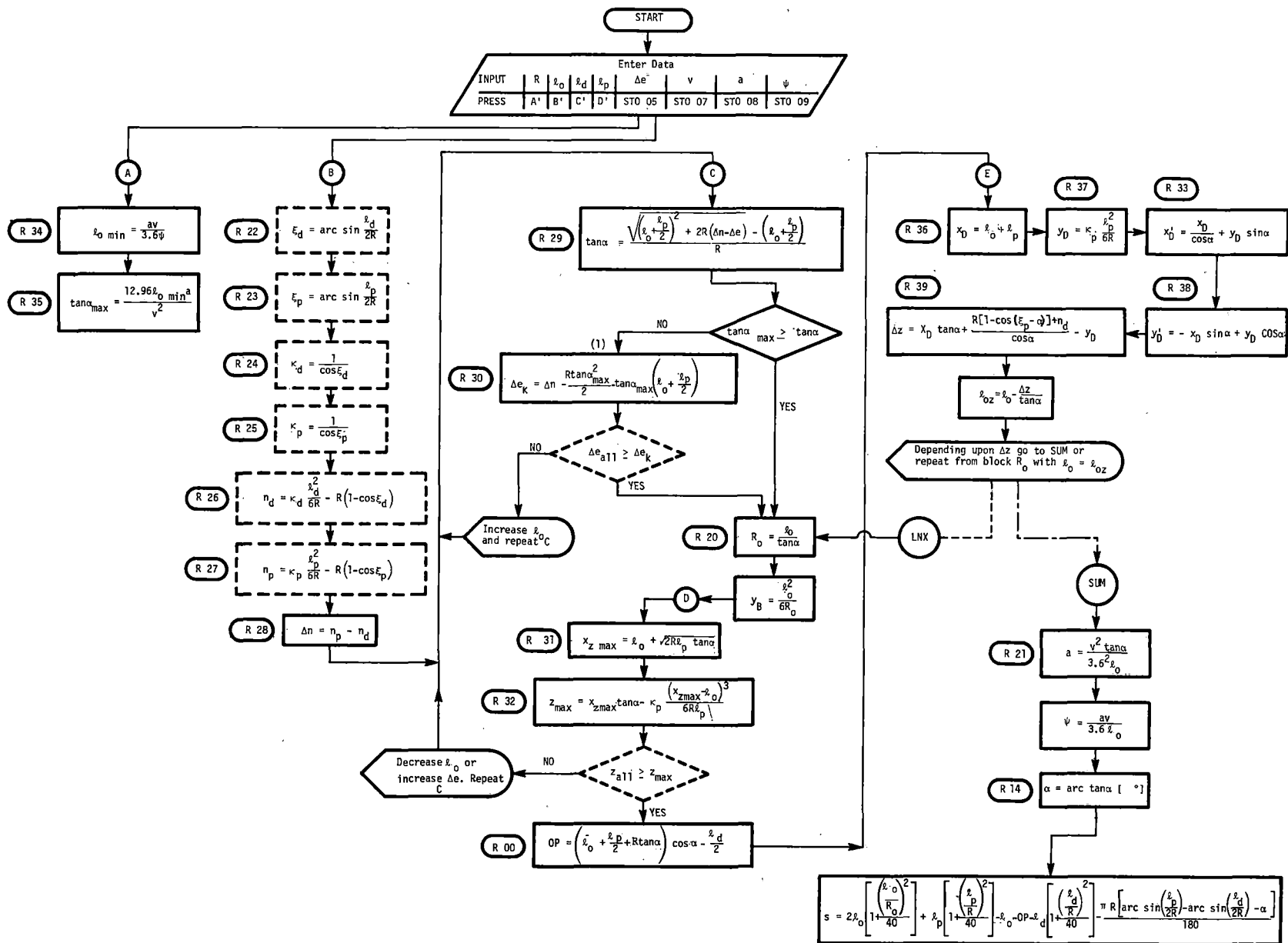


FIGURE 4. BLOCK DIAGRAM OF PROPOSED PROGRAM

In the input data block, under each value, a symbol of the calculator's key used to enter the data has been shown. The detailed program has been written for the TI-59 calculator. The values shown in dashed blocks are not displayed; but, if necessary, their values can be obtained. One can, for example, obtain the curve displacement value, n , in blockset B, by pressing the key RCL27. The letter R followed by a number means that the value in the adjacent block is stored in the register with given number. The capital letter above a blockset indicates that the key marked with that letter must be depressed to start the calculations in a given block. Continued progress of the calculations in a given block set is obtained by pressing the R/S key.

Calculations start in blockset A and proceed to blockset B. These calculations are performed only once, unless the input data is changed. Having obtained l_{omin} and $\tan \alpha$, l_o is assumed to be approximately l_{omin} . Depressing key C displays the value $\tan \alpha$. If $\tan \alpha > \tan \alpha_{max}$, the calculator blinks the number "1" and then displays the amount the circular curve must be displaced, Δe , in order to fulfill all assumptions. The designer must check that Δe does not exceed Δe_{all} . If Δe is excessive, then one may try the approach of increasing the initial spiral length l_o , but this is not usually an efficient solution.

Z_{max} is calculated in blockset D. Each solution will result in a condition where Z_{max} is less than allowable; but this does not mean that an optimum solution has been obtained. It is recommended that after Z_{max} is found, a new l_o be chosen, and the process repeated starting again at blockset C.

There are factors which could affect the final result and lead to variations without possible solutions. These factors are:

- 1) A minimum length of the initial displacement spiral, l_o , that leads to a curve that is difficult to distinguish from the existing tangent. Such a condition could make the new configuration difficult to maintain. This can be evaluated by checking the value y_p (see Figure 1) which should not be less than 0.04 to 0.05 meters.
- 2) Exceeding the value Δe_{all} , which is possible after repeating runs through blockset C.
- 3) Exceeding physical parameters a_{all} and ψ_{all} , which can occur in the block set SUM.6

The coordinates of the end point D for both coordinate systems is computed in blockset E. Also, the error of closure, ΔZ , is computed. The spiral length, l_o , should be replaced with the corrected value, l_{oz} , if ΔZ exceeds 2 to 3 X 10⁻³ meters. The calculation should then be repeated from the block where R_o is computed. This can be done by depressing in succession keys GTO, LNX, AND R/S.

The final blockset SUM computes the physical parameters associated with the computed geometry of the initial transition curves, AB and BC, as well as the

⁶Comprehensive analyses of permissible values of non-compensated accelerations and their time increments are presented by Yershkov et al in references [1] and [4].

angle α , in degrees, and the difference in length, s , between the designed and existing configuration.

Table 2 shows the detailed program developed for the TI-59 calculator, Table 3 contains the user instructions, and Tables 4 and 5 present two numerical examples. In the second example, $\tan \alpha$ exceeds $\tan \alpha_{max}$ which therefore requires that the circular curve be offset by a $\Delta e = 0.048m$. This displacement can be avoided if one accepts values for the physical parameters α and ψ exceeding their allowable values. In this example, the largest offset, Z_{max} , exceeded its allowable value which also led to the requirement of a slight displacement of the curve.

5. CONCLUSIONS

The paper presents a heuristic-algorithmic model for calculating field parameters resulting from a change in curve superelevation for heavy haul track using a programmable calculator. These parameters are of great interest to the designer. To remain consistent with American design practices, the minimum transition curve length should be determined as shown or by the practices of the user railroad. It should also be necessary to check that the two introductory spiral curves meet the user road's design standards, particularly with respect to the lack of superelevation.

Calculation of one design, including several iterations, can lead to an optimal solution in approximately 10 minutes. The solution algorithms and program presented take into account all the requirements for displacing the original alignment to derive a longer transition curve. At the same time, its goal is to minimize the extent of modernization work.

REFERENCES

1. Aleksandrov, K.K., O.P. Erskov, and M.N. Mescerskiy, "Evaluation of Permissible Speed in Correlation with Track Alinement", bulletin OSZD, Nr.z, 1976.
2. Baluch, H., "Use of Findings from Rail Wear Measurements in Curved Track for Railroad Track Diagnostics", Proceedings, International Conference on Wheel/Rail Load and Displacement Measurement Techniques, January 19-20, 1981, Cambridge, MA, September 1981.
3. Baluch, H., "Optimization of Track Geometry Changes for Elongation of Transition Curves", Prace COB:RTK, Nr. 77, 1980.
4. Erskov, O.P., A.A. Lvov, and V.J. Kareev, "Permissible Values of Noncompensated Accelerations and Their Time Increments on High Speed Railway Sections", Rail International, Nr. 1, 1978.
5. "Recommended Standards for Track Maintenance," Association of American Railroads, Engineering Division, adopted September 25, 1970.
6. Schramm, G., "Verlangern von Ubergangsbogen mit Kleinsten Seiten verschlebbunnen, "(Lengthening Transition Curves with Least Impact on the Track Layout), Eisenbahrengenieur, Nr. 7-8, 1977.
7. Titov, V.P., "Strengthening the Subgrade on Railroad Lines in Service", "Strojzdat", Moscow, 1980.
8. Manual for Railroad Personnel, "Put'i Putevoe Choziastvo", Moscow 1955.

TABLE 2. TI-59 PROGRAM DEVELOPED BY HENRYK BALUCH

LOC	KEYS	LOC	KEYS	LOC	KEYS	LOC	KEYS	LOC	KEYS	LOC	KEYS	LOC	KEYS	LOC	KEYS	LOC	KEYS
000	LBL	065	03	130	01	195	RCL	260	+	325	00	390	R/S	455	STO	520	x
001	A	066	+	131	x	196	35	261	RCL	326	R/S	391	(456	21	521	(
002	STO	067	2	132	(197	GE	262	02	327	LBL	392	RCL	457	R/S	522	+
003	01	068	+	133	1	198	LNx	263	=	328	F	393	23	458	RCL	523	1
004	R/S	069	RCL	134	-	199	1	264	STO	329	RCL	394	-	459	07	524	(
005	LBL	070	01	135	RCL	200	PAU	265	31	330	02	395	RCL	460	x	525	RCL
006	B	071	=	136	23	201	RCL	266	R/S	331	+	396	14	461	RCL	526	03
007	STO	072	INV	137	COS	202	28	267	RCL	332	RCL	397)	462	21	527	÷
008	02	073	SIN	138)	203	-	268	31	333	04	398	COS	463	+	528	÷ RCL
009	R/S	074	STO	139	=	204	RCL	269	-	334	=	399	+/-	464	3	529	01
010	LBL	075	22	140	STO	205	01	270	RCL	335	STO	400	+	465	.	530)
011	C	076	COS	141	27	206	x	271	02	336	36	401	1	466	0	531	x ²
012	STO	077	1/X	142	-	207	RCL	272	31	337	R/S	402	=	467	+	532	÷
013	03	078	STO	143	RCL	208	35	273	=	338	RCL	403	x	468	RCL	533	4
014	R/S	079	24	144	26	209	x ²	274	3	339	04	404	RCL	469	02	534	0
015	LBL	080	x	145	=	210	÷	275	=	340	x ²	405	01	470	=	535	-
016	D	081	RCL	146	STO	211	2	276	x	341	÷	406	+	471	R/S	536)
017	STO	082	03	147	28	212	-	277	RCL	342	6	407	RCL	472	RCL	537	RCL
018	04	083	x ²	148	R/S	213	RCL	278	25	343	÷	408	26	473	14	538	02
019	R/S	084	+	149	LBL	214	35	279	÷	344	RCL	409	+	474	INV	539	-
020	LBL	085	6	150	C	215	x	280	6	345	01	410	RCL	475	DMS	540	RCL
021	A	086	+	151	FIX	216	RCL	281	÷	346	x	411	05	476	FIX	541	00
022	FIX	087	RCL	152	5	217	13	282	RCL	347	RCL	412	=	477	5	542	-
023	3	088	01	153	RCL	218	=	283	1	348	25	413	+	478	R/S	543	π
024	RCL	089	-	154	02	219	STO	284	÷	349	=	414	COS	479	(544	x
025	08	090	RCL	155	+	220	30	285	RCL	350	STO	415	+	480	RCL	545	RCL
026	x	091	01	156	RCL	221	R/S	286	04	351	37	416	+	481	02	546	01
027	RCL	092	x	157	04	222	GTO	287	+/-	352	R/S	417	36	482	÷	547	x
028	07	093	(158	÷	223	LNx	288	+	353	RCL	418	x	483	RCL	548	(
029	÷	094	1	159	2	224	LBL	289	RCL	354	36	419	RCL	484	20	549	(
030	3	095	-	160	=	225	LNx	290	31	355	÷	420	29	485)	550	RCL
031	.	096	RCL	161	STO	226	RCL	291	x	356	RCL	421	-	486	x ²	551	04
032	6	097	22	162	13	227	02	292	RCL	357	29	422	RCL	487	÷	552	÷
033	+	098	COS	163	x ²	228	+	293	29	358	INV	423	37	488	4	553	RCL
034	RCL	099)	164	+	229	RCL	294	=	359	TAN	424	=	489	0	554	01
035	09	100	=	165	2	230	29	295	STO	360	STO	425	STO	490	+	555	÷
036	=	101	STO	166	x	231	=	296	32	361	14	426	39	491	1	556	2
037	STO	102	26	167	RCL	232	STO	297	R/S	362	COS	427	R/S	492	=	557)
038	34	103	RCL	168	01	233	20	298	RCL	363	+	428	RCL	493	x	558	INV
039	R/S	104	04	169	x	234	R/S	299	02	364	RCL	429	02	494	2	559	SIN
040	FIX	105	÷	170	(235	RCL	300	+	365	37	430	-	495	x	560	-
041	5	106	2	171	RCL	236	02	301	RCL	366	x	431	RCL	496	RCL	561	(
042	3	107	+	172	28	237	x ²	302	04	367	RCL	432	39	497	02	562	RCL
043	.	108	RCL	173	-	238	÷	303	+	368	14	433	+	498	+	563	03
044	6	109	01	174	RCL	239	6	304	2	369	SIN	434	RCL	499	RCL	564	÷
045	x ²	110	=	175	05	240	+	305	+	370	=	435	29	500	04	565	RCL
046	x	111	INV	176)	241	RCL	306	RCL	371	STO	436	=	501	x	566	01
047	RCL	112	SIN	177	=	242	20	307	01	372	33	437	R/S	502	(567	÷
048	34	113	STO	178	√x	243	=	308	x	373	R/S	438	LBL	503	1	568	2
049	x	114	23	179	-	244	+/-	309	RCL	374	RCL	439	SUM	504	+	569)
050	RCL	115	COS	180	RCL	245	R/S	310	29	375	37	440	RCL	505	(570	INV
051	08	116	1/X	181	13	246	LBL	311	=	376	x	441	07	506	RCL	571	SIN
052	÷	117	STO	182	=	247	D	312	x	377	RCL	442	x ²	507	04	572	-
053	RCL	118	25	183	÷	248	RCL	313	RCL	378	14	443	x	508	+	573	RCL
054	07	119	x	184	RCL	249	01	314	29	379	COS	444	RCL	509	RCL	574	14
055	x ²	120	RCL	185	01	250	x	315	INV	380	-	445	29	510	01	575)
056	=	121	04	186	=	251	RCL	316	TAN	381	RCL	446	÷	511)	576	÷
057	STO	122	x ²	187	STO	252	04	317	COS	382	36	447	3	512	x ²	577	1
058	35	123	÷	188	29	253	x	318	-	383	x	448	.	513	+	578	8
059	R/S	124	6	189	R/S	254	RCL	319	RCL	384	RCL	449	6	514	4	579	0
060	LBL	125	÷	190	FIX	255	29	320	03	385	14	450	x ²	515	0	580	=
061	B	126	RCL	191	3	256	x	321	÷	386	SIN	451	÷	516)	581	FIX
062	FIX	127	01	192	RCL	257	2	322	2	387	=	452	RCL	517	-	582	3
063	3	128	-	193	29	258	=	323	=	388	STO	453	02	518	RCL	583	RTN
064	RCL	129	RCL	194	x ≥ T	259	√x	324	STO	389	38	454	=	519	03		

TABLE 3. USER INSTRUCTIONS (See Figure 1)

Step	Procedure	Enter	Press	Output/ Mode
1	Repartition program memory	4	Op 17	639.39
2	Enter program			
3	Enter curve radius	R	A'	
4	Enter existing curve length	l_d	C'	
5	Enter proposed curve length	l_p	D'	
6	Enter curve displacement	Δe	STO 05	
7	Enter train speed	V	STO 07	
8	Enter allowable acceleration	a_{all}	STO 08	
9	Enter all. rate of change of acc.	ψ_{all}	STO 09	
10	Compute length l_{omin}		A	l_{omin}
11	Compute $\tan \alpha_{max}$		R/S	$\tan \alpha_{max}$
12	Set $l_o \sim l_{omin}$	l_o	B'	
13	Compute difference in displacement		B	Δn
14	Compute $\tan \sigma$		C	$\tan \alpha$
15 w*	Compute required curve displacement (Only if $\tan \alpha > \tan \alpha_{max}$)		R/S	(1), Δe_k
16 w	Increasing l_o and repeating computations from step 14 to allow for increasing Δe	Δe	STO 05	
17	Computing the radius at the end of the two initial transition curves		R/S	R_o
18	Compute the ordinate of the end point of the displacement curves		R/S	Y_B
19	Compute abscissa for the largest magnitude of curve displacement		D	X_{zmax}
20	Computation of the magnitude of greatest curve displacement		R/S	Z_{max}
21 w	Decrease l_o or increase Δe and repeat computations from step 14		R/S	$\tan \alpha$
22	Definition of section OP		R/S	OP
23	Computation of the abscissa of the curve end point in x-y coordinate system		E	X_D
24	Computation of the ordinate of pt. D		R/S	Y_D
25	Conversion of the abscissa of D into the x'-y' coordinate system		R/S	X'_D
26	Computation of Y'_D		R/S	Y'_D
27	Define the error of closure		R/S	ΔZ
28	Compute the corrected length of the displacement curve		R/S	l_{oz}
29 w	Redefinition of the displacement curve length	l_{oz}	B'	
30 w	Repeat of computation from step 17		GTO, LNX, R/S	
31	Calculation of the acceleration on the displacement curve		R/S	a
32	Calculation of the jerk		R/S	ψ
33	Definition of the angle of deviation from the existing tangent		R/S	$\alpha [^\circ]$
34	Computation of the difference in length between the new and existing alinements		R/S	S

Codes:

(n) displayed briefly, e.g. (0.5 S)

*The letter "w" signifies a conditional step.

TABLE 4. EXAMPLE NO. 1

Compute the characteristic parameters for elongating the transition curve for the following conditions: $R = 600$ m, $l_d = 50$ m, $l_p = 110$ m
 $\Delta e_{all} = 0.15$ m, $V = 90$ km/hr, $a_{all} = 0.5$ m/sec², $\psi_{all} = 0.4$ m/s³,
 $z_{all} = 0.35$ m

Enter	Press	Display	Comments
4	O _p 17	639.39	The calculator has 640 programming steps and 40 memory registers
<u>Program</u>			
600	A'	600.	Enter curve radius
50	C'	50.	Enter existing curve length
110	D'	110.	Enter new curve length
90	STO 07	90.	Enter train speed
0.5	STO 08	0.500	Enter allowable acceleration
0.4	STO 09	0.400	Enter allowable jerk
	A	31.250	Minimum length of displacement curve, $l_{omin} = 31.250$ m
	R/S	0.02500	$\tan \alpha_{max} = 0.02500$
35	B'	35.00000	Define $l_o = 35$ m
	B	0.675	Curve offset $\Delta n = 0.675$ m
	C	0.00732	$\tan \alpha = 0.00732$, i.e. displacement of the existing curve is unnecessary
	R/S	4779.293	$R_o = 4779.293$ m
	R/S	-0.043	$Y_B = -0.043$ m
	D	66.091	$X_{zmax} = 66.091$
	R/S	0.408	$Z_{max} = 0.408$ m > $Z_{all} = 0.35$ m
.1	STO 05	0.100	Introducing curve displacement $\Delta e = 0.100$ m
	C	0.00626	$\tan \alpha = 0.00626$
	R/S	5590.805	$R_o = 5590.805$ m
	R/S	-0.037	$Y_B = -0.037$ m
	D	63.746	$X_{zmax} = 63.746$ m
	R/S	0.339	$Z_{max} = 0.339 < Z_{all} = 3.5$ m
	R/S	68.754	OP = 68.754 m
	E	145.000	$X_D = 145.000$ m
	R/S	3.375	$Y_D = 3.375$ m
	R/S	145.018	$X_D^1 = 145.018$ m
	R/S	2.468	$Y_D^1 = 2.468$ m
	R/S	0.002	$\Delta Z = 0.002$ (Insignificant)
	R/S	34.641	$l_{oz} = 34.641$ m ($l_o \equiv 35$ m, difference insignificant)
	R/S	0.112	$a = 0.112$ m/s ²
	R/S	0.080	$\psi = 0.08$ m/s ³
	R/S	0.21324	$\alpha = 0^\circ 21' 32.4''$
	R/S	0.016	$s = 0.016$ m

} Iteration arriving at suboptimal solution

TABLE 5. EXAMPLE NO. 2

$R = 1500$ m, $l_d = 45$ m, $l_p = 200$ m, $\Delta e_{all} = 0.20$ m, $V = 160$ km/h, $a_{all} = 0.3$ m/s², $\psi_{all} = 0.3$ m/s³, $Z_{all} = 0.50$ m

Enter	Press	Display	Comments
4	O P	639.39	
<u>Program</u>			
1500	A'	1500.000	Enter radius of curve
45	C'	45.000	Enter length of existing transition curve
200	D'	200.000	Enter length of new transition curve
160	STO Ø7	160.000	Enter train speed
0.3	STO Ø8	0.300	Enter allowable acceleration
0.3	STO Ø9	0.300	Enter allowable jerk
	A	44.444	Minimum length of displacement curve $l_{omin} = 44.444$ m
	R/S	0.00675	$\tan \alpha_{max} = 0.00675$
45	B'	45.00000	Enter $l_o = 45$ m
	B	1.061	Curve offset $\Delta n = 1.061$ m
	C	0.00706	$\tan \alpha = 0.00706$
	R/S	(1), 0.048	$\tan \alpha > \tan \alpha_{max}$, \therefore the curve must be displaced $\Delta e = 0.48$ m. The final value of Δe will be a result of iteration.
	R/S	6374.169	$R_o = 6374.169$ m
	R/S	-0.053	$Y_B = -0.053$ m
	D	110.083	$X_{zmax} = 110.083$ m
	R/S	0.624	$Z_{max} = 0.624$ m $>$ $Z_{all} = 0.500$ m
0.18	STO Ø5	0.180	Enter curve displacement $\Delta e = 0.18$ m
	C	0.00590	$\tan \alpha = 0.00590$
	R/S	7631.866	$R_c = 7631.866$ m
	R/S	-0.044	$Y_B = 0.044$ m
	D	104.479	$X_{zmax} = 104.479$ m
	R/S	0.499	$Z_{max} = 0.499$ m
	R/S	131.342	$OP = 131.342$ m
	E	245.000	$X_D = 245.000$ m
	R/S	4.454	$Y_D = 4.454$ m
	R/S	245.022	$X_D^i = 245.022$ m
	R/S	3.010	$Y_D^i = 3.010$ m
	R/S	0.004	Error $\Delta Z = 0.004$ m requires correction
	R/S	44.303	$l_{oz} = 44.303$ m
	B'	44.303	Entering corrected deviation curve length
	GTO, LNX,		
	R/S	7513.686	$R_o = 7513.686$ m
	R/S	-0.044	$Y_B = -0.044$ m
	D	103.783	$X_{zmax} = 103.783$ m
	R/S	0.495	$Z_{max} = 0.495$ m
	R/S	130.645	$OP = 130.645$ m
	E	244.303	$X_D = 244.303$ m
	R/S	4.454	$Y_D = 4.454$ m
	R/S	244.325	$X_D^i = 244.325$ m
	R/S	3.014	$Y_D^i = 3.014$ m
	R/S	0.000	$Z = 0.000$
	R/S	44.303	$l_{oz} = 44.303$ m
	R/S	0.263	$a = 0.263$ m/s ²
	R/S	0.264	$\psi = 0.264$ m/s ³
	R/S	0.20168	$\alpha = 0^\circ 20' 16.8''$
	R/S	0.017	$s = 0.017$ m

Iteration resulting in suboptimal solution.

Corrected values
Corrected coordinates of end point D

Efforts of the European Railways to Meet Increasing Passenger and Freight Traffic Demand

J.P. Blank

Chairman
Office for Research
& Experiments
International Union of
Railways
Utrecht
The Neatherlands

Although European Railways operate under high density traffic conditions, there are many differences between the European and American railroad systems. In view of this it is important to define the differences and the resultant policy decisions of the European Railways in regard to equipment and track structure designs. This paper, while it recognizes the different philosophies of various countries, reviews the relationships of equipment design, train speeds and track design for existing and new lines in Europe.

INTRODUCTION

To obtain a clear idea of current development trends in Europe -- to some extent related to the theme of the present Conference "Meeting the challenge of increasing tonnage" -- I feel that mention should be made at the outset of some basic differences in Railway operation in Europe and in the USA.

Taking the objectives of the Railways in Europe as a starting point, there are a variety of operating objectives for coping with increasing passenger and freight traffic demands (Figure 1). These differ in ratio and intensity from one country to another. Generally speaking, the West-European Railways, faced with severe competition from other modes of transport, are actively striving above all to increase both the speed and quality of their passenger traffic, and to offer a freight service fully competitive with that offered by road transport and waterways. In the countries of Eastern Europe, priority is often given by national policy to freight traffic on the Railways. The essential aim here is to achieve optimum efficiency in the distribution of transport demands by using the existing railway transport infrastructure within a unified transport system, without a highly developed arterial road network.

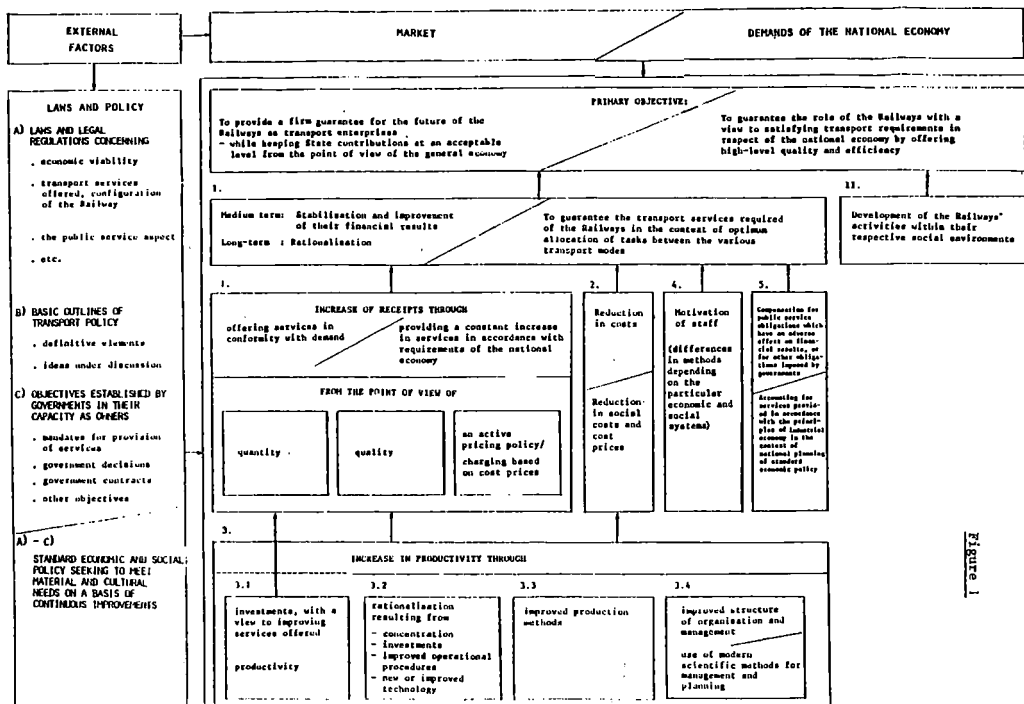
In this context, the following are typical operating conditions which dictate European Railway technology:

- Mixed traffic (i.e., combined passenger and freight traffic on the same lines) with high-speed passenger trains running at 140 to 160 km/h, sometimes even 200 km/h, and a relatively low volume of freight traffic of the order of 10 million gross ton/year.
- Mixed traffic, with heavy freight traffic of 50 million gross ton/year or more, and low passenger train speeds in the region of 100 to 140 km/h.

Though not a typical or widespread feature of the European Railways, we should not lose sight of very high-speed passenger traffic at 260 to 300 km/h, which is considered in Europe to be one of the most important stimuli for applying advanced technology in the construction of new lines and trains.

Comparing these well-known features of European Railway operation with the predominantly heavy freight traffic operating on the USA railroads, it is apparent that the technological and economical parameters of

STRUCTURE OF THE RAILWAYS' OBJECTIVES
(for the Railways of the States of Western Europe and (1) the Eastern European (CMEA Member countries and Yugoslavia))



both systems will differ substantially, which in turn will obviously affect the strategy adopted in constructing and maintaining track and rolling stock.

I would now like briefly to outline, within the scope of the presented papers, the basic philosophy behind the construction and maintenance of the European infrastructure.

BASIC CONCEPT OF THE CONSTRUCTION AND MAINTENANCE OF ROLLING STOCK

The essential differences between the American and the European Railway systems are the choice of axleload and the loading gauge. The axleload is 30 t in America whereas on most European Railways it is 20 t (Figure 2). The structure gauge of the European Railways is smaller than the American one, particularly the height; it does not permit the transport of lorries and road trailers on normal goods wagons.

The choice of axleload and the loading gauge represent the chief features of the vehicles. While 30 t axleloads are unfavourable for the track, they are favourable as regards the loaded weight of the goods wagon and permit the design of high-capacity diesel locomotives.

An American four-axled wagon for instance has a load capacity of 150 m³ and transports payloads of 91 t for a total weight of 120 t. A comparable type of wagon of the European Railways has a capacity of only 100 m³ and is designed for a payload of 58 t with a total weight of 80 t.

Figure 2

WORLD RAILWAY SYSTEMS

Chief features of:
- European
- North American
type of railway

Features	Railway	
	European	North American
Axleload	20/22 t	30 t
VEHICLES		
Wheel	Q(c)/D(m) ratio	15
	Carbon content of steel	0.7%
	Number of breakages per thousand million vehicle kilometres	A few
Diesel traction		
	High-speed engine	Low-speed or two-stroke engine
Electric traction		
	2/3 of total traffic	Negligible
	Driving axle power	-
Coupling		
	Screw coupling (automatic coupler by year 2000?)	Automatic coupler
Modern four-axled wagons		
	Total weight	120 t
	Payload	91 t
	Capacity	150 m ³
TRACK		
Rail		
	UIC 60 kg/m	70 to 77 kg/m
	Elastic rail fastening	Rail spike
	Transverse fastening	Yes, bolted
	Vertical fastening	Yes, guide
	Yes	No
Sleepers		
	Timber or concrete	Timber, concrete on the way in
Permissible geometrical deviations (normal maximum track defects)		
	(For a track carrying traffic at 140 km/h and with a base-length of 20 m)	
	Transverse profile	5 mm
	Vertical profile	7.5 mm

On the other hand, with the same wheel diameter the American system gives a higher specific pressure between wheel and rail than with the European system and consequently results in greater wear of the wheelsets.

High axleloads and a fairly large loading gauge permits the use of heavy twostroke diesel engines on locomotives and facilitates the adoption of simple and robust locomotive designs. The requirements due to the vehicle gauge and the axleload are, on the other hand, much stricter for the designer of diesel locomotives for the European Railways. They have necessarily led to the construction of locomotives which are more complex and more costly to maintain. A comparison of the specific weights shows that on these railways diesel traction plays a supplementary role to electric traction, whereas in America it is the major form of traction.

Finally the vehicles of the American Railways are without exception fitted with automatic couplers which make it possible to transmit higher tractive forces than the manual screw couplings still used in Europe. The European Railways have developed an automatic coupler to the point of readiness for introduction into service; it is based on the WILLISON system. However, for financial reasons its general introduction is unlikely before the year 2000.

Goods wagons

As characteristic examples of UIC standardised wagons, which since 1965 have all been built to accommodate the automatic coupler at a later stage, I should like to mention:

- Flat bogie wagons, without sides, Types 1 and 2, with a length between buffers of 19.9 m and/or 14 m. (R(e)s/R(e) mms) for the transport of long and heavy iron and steel products.
- Open bogie wagons (Eaos) of 71.3 m³ capacity, with fixed end walls, two double doors in the side walls and wooden or steel floors. (Further development of the 2-axled open wagon).
- Covered bogie wagon (Gabss) with ventilation louvres and 2 x 2 double doors with a 50 m² loading area, suitable for all goods (palletes) other than animals and bulk grain.

and

- High-capacity wagon, with sliding side walls (Habiss) and patented load-protection equipment, constructed entirely of metal and providing completely accessible loading space.

In order to keep up with the times the range of conventional wagons has been extended, in the course of the last 10 years, by a number of special purpose wagons, in order to cater for the individual requirements of the merchandise and of the freight handling facilities of the customer. The wagons in question are:

- Multi-purpose wagon with sliding roof that can be opened to its full extent, (Taems), especially suitable for food-dry products affected by the elements.
- Bogie wagon, with low level, high-speed gravity unloading from both sides, without roof (Fals).
- 60' container wagon for block train traffic (Sgss).
- 60' container wagon with damping equipment (Sgjss).
- 80' container wagon with 3 bogies (Saggs), articulated over the central bogie.
- Recess wagons for piggy-back traffic (for the transport of semi-trailers, swap-bodies and containers) (Sdkmss).

and

- Bogie wagons for the carriage of steel sheet coils affected by wet (coil transport wagons with sliding hoods) available in 4 and 6-axled versions (Shimms/Sahimms).

Besides these standardised wagons there are also components, sub-assemblies and containers which have been standardised or made sufficiently uniform to be interchangeable. This applies to all wagon components which are needed in large quantities and must be replaced frequently in service e.g., triangular brake beam, parts of the mechanical braking equipment, end step, mounting step, gangway, wheelsets, stanchions and flaps for flat wagons, stacking pins for container wagons, bogie (Y 25) for 100 and 120 km/h and 20 t axleloads, welded or cast, with the without integral brakes.

Measures were also taken to attain greater reliability for the wagons and components, to reduce building and maintenance costs. Improvements were made to the braking systems, wheelsets, bogies and other essential wagon components.

We can be proud of the standards so far attained in Europe, and shall continue with the standardisation of wagons. In future, however, we shall concentrate less on the standardisation of whole wagons and focus more on the uniformity of certain functional components which are important to the user and also on those parts of the wagon which are subject to wear and tear.

Although largely influenced by the requirements of safety and strength, the service life of wagons must always be adapted to the needs of the transport market. Depending on the way in which a wagon is used, its life may vary. Wagons will be designed in such a way that they can be adapted to accommodate other types of freight with only a few modifications. New materials and technologies will be used e.g., high-capacity springs (parabolic) and bogies, and cast-iron brake blocks with high phosphorus content. Running gear will be

developed which will provide for radial alignment of the wheelset in the track, thus reducing wear and tear of wheel flanges and rails. More robust buffing and drawgear as well as means of protecting the freight will contribute towards reducing breakdowns in service and minimising damage to freight and wagon during shunting.

Passenger coaches

Before the fifties all countries built their own types of coaches. As international passenger traffic gradually increased, the need for standardising the coaches used in international service was felt. At that time, the usual layout of coaches was a side-corridor and compartments, each for 6 or 8 persons. The passengers were seated opposite each other.

The UIC undertook this standardisation, which was essentially confined to fixing of the main dimensions. In view of the variation from one country to another of the length of platforms in stations, and the length of maintenance equipment in the workshops, it appeared impossible to standardise on one type of coach only, and hence two basic types, X and Y, for speeds up to 160 km/h, were accepted by the UIC.

Type X has a length over buffers of 26.4 m, with 12 second-class compartments each with 6 seats. The first-class coach has 10 compartments, each with 6 seats.

Type Y has a length over buffers of 24.5 m, with 10 second-class compartments each with 8 seats. The first-class coach has 9 compartments each with 6 seats.

European international passenger trains still consist mainly of these types of coaches.

Sleeping cars, couchette coaches, restaurant cars, mail vans, luggage vans and motor-car-carriers have also been standardised.

Based on the type X, air-conditioned coaches with high standards of comfort were developed, around 1970, for TEE^(*) and Inter-City traffic.

As competition with the ever increasing number of automobiles became more severe, some railroads desired to increase comfort. In 1975, six railroads decided to build a fully-standardised, air-conditioned coach (type Z), the so-called Eurofima coach, suitable for running at speeds up to 200 km/h.

This coach was a synthesis of the types X and Y, the advantageous features of which were retained, and the disadvantages eliminated. This means that it has the same length as the type X coach, with the more spacious compartments of the Y coach and with six seats in both first and second-class. The coach is fitted with modern, low-maintenance bogies and modern plug doors. The Eurofima coach, of which 500 have been built, is still a coach with side-

corridor and compartments. The high level of comfort and the generous dimensioning of the compartments resulted in a relatively low number of seats per coach.

However, the deteriorating economic situation compelled the railroads to increase the number of seats per coach. They found a solution by positioning the seats in successive rows, as in busses and airplanes, in open saloon coaches. In this way, it was possible to increase the number of seats in a second-class coach to 80.

Recently, the trend towards saloon coaches has spread over the whole of Europe, not only for international traffic, but also for domestic use. The coaches are fitted with modern bogies of high riding quality and low maintenance costs. The doors are of the modern plug type. The air-conditioned Corail coach VTU, developed for speeds up to 200 km/h, and a coach of similar design, the Bpmz 291/292, are well-known examples.

Recent developments are towards a greater length of coach, i.e., 27.5 m, and, as passenger demand is still for coaches with side-corridor and compartments, several railroads are preparing new designs of this type of coach.

Locomotives

The requirements to be met by locomotives, on account of the mixed operating system, are reflected in the traction programme of the German Federal Railway which typifies European conditions. It is envisaged that with a line resistance of 5N/kN the following trains can be hauled:

- 700 t passenger trains at 160 km/h or 200 km/h,
- 1,500 t high-speed goods trains at 100 km/h, and
- 2,200 t slow goods trains or 2,700 t block trains at 80 km/h.

To meet such requirements it is necessary to have different classes of locomotive. As part of the restructuring plan, steam locomotives have been replaced in the last 15 years by diesel locomotives. Parallel with this the main lines have been electrified.

The result of this development is that in Europe, at the moment, a large proportion of the traffic is carried on a small part of the network with electric traction. Diesel traction supplements electric traction, particularly on the less heavily loaded parts of the network and in shunting operations. The boundary between diesel and electric traction varies on the different railways according to the density of traffic and the extent of the passenger traffic; it is also affected by the changes in the price of oil. Transmission and braking of both diesel and electric locomotives have reached a high degree of perfection. By using components subject to little or no wear, and introducing large replacement assemblies, it has

been possible, particularly in the case of electric locomotives, considerably to increase mileage and hence reduce maintenance costs. Since the restructuring programme involved reducing both the number and variety of locomotives, it was possible to make appreciable savings in workshop services.

Since electric traction was introduced on the European Railways at about the turn of the century, four main electric traction operating systems have been used:

- two d.c. systems at 1,500 V and 3,000 V
- two a.c. systems at 16-2/3 Hz, 15 kV and 50 Hz, 25 kV.

For historical reasons the systems initially were used d.c. and 16-2/3 Hz a.c., which are more or less equally divided. Since the mid-fifties it has been possible, as a result of progress made with power electronics, for railways who were just beginning to electrify (e.g., the Yugoslavian and Portuguese railways) or which did not wish to extend their existing d.c. network any further (e.g., SNCF, CSD) to obtain power from the 50 Hz national grid.

The variety of current systems makes it difficult to use locomotives freely over all the different railways. This problem is resolved to a certain extent by using dual or multi-system locomotives.

A decisive change in locomotive power equipment has become possible in recent years with the use of thyristors. It is used in d.c. locomotives as a chopper and makes possible motor control with little power loss or wear. Used in the form of a controllable rectifier in a.c. locomotives it is superseding the conventional tap-changer. On the low-frequency a.c. system, it has facilitated the use of ripple-current motors which are considerably more economic and efficient than the a.c. motors previously used. By using power electronics it was possible to achieve the same specific weight with diesel-electric power transmission as with diesel-hydraulic power transmission.

The development of locomotives has taken a new turn in recent years after the perfecting of inverter and control techniques has made it possible to efficiently use the three-phase induction motor (involving little wear and maintenance) for traction purposes. This arrangement has an almost ideal traction performance for all purposes thus crowning the efforts of railway engineers with a universal locomotive. The first operating experience has been gained both with diesel locomotives and electric locomotives. The development of locomotive technology has also been much affected by efforts to increase the operating speed of the wheel/rail system. These efforts involved reduction of axleloads and of the unsprung mass of the running gear. Since the increasing driving and braking forces involved when running at high speeds entail the use of additional driving axles, electric multiple units have been specifi-

cally developed for this type of traffic, thus reducing axleloads by having an all-driving-axle system. For non-electrified tracks diesel trains have been developed with a power car at each end. It has been possible to obtain a favourable power-to-weight ratio by adopting lightweight construction techniques.

For economic reasons, however, locomotive hauled trains are also used for high-speed traffic. For this purpose six-axle high-speed electric locomotives have been developed.

BASIC PHILOSOPHY WITH RESPECT TO THE CONSTRUCTION AND MAINTENANCE OF TRACK STRUCTURES

As is known, a direct relationship exists between the track structure and its maintenance. Higher initial costs should result in reduced track maintenance. In this respect, the European Railways endeavour to optimize track design parameters and track maintenance procedure so as to minimize the overall expenditure to ensure the required quantity and quality of the railway traffic.

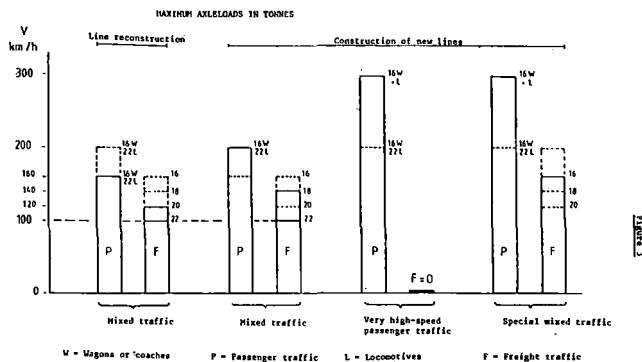
One of the most important and decisive factors here is the axleloads, which differ greatly between the European and American railway systems and which govern the optimum ratio of construction to maintenance costs, for a given pattern of railway traffic. This, for instance, is why the UIC 60 kg/m rail seems to present an adequate solution for the mixed European traffic with axleloads of up to 20 t, and why substantially heavier rails of 70 to 77 kg/m are required for USA Railroads operating with axleloads of 30 t and higher (Figure 2).

Further differences in rail fastening system, in design of track support and subgrade, along with permissible tolerances in track geometry, are thus merely a natural outcome of this approach for a given specific railway pattern.

As regards track maintenance, it might reasonably be expected that heavier axleloads will accelerate track deterioration under the same traffic pattern (speed, density, type and composition of trains). If track maintenance expenditure is to be in harmony with initial construction costs, i.e., to ensure the minimum overall expenditure, an optimum relationship must exist between axleload, speed, type and composition of trains. For the European Railway infrastructure this relationship is assumed to be met in the following respects (Figure 3):

- For existing lines with mixed traffic, maximum permissible axleloads for goods trains up to 20 t at speeds up to 90/100 km/h, and maximum permissible axleloads up to 16 t at speeds of 140 to 160 km/h for passenger trains.

EUROPEAN RAILWAY INFRASTRUCTURE



- For existing lines after reconstruction, and new lines designed for mixed traffic, the limiting value should be as follows:
 - a) goods trains, axleloads of 22.5 t for speeds up to 100 km/h and 18 t for speeds up to 120 km/h;
 - b) passenger trains at speeds up to 200 km with axleloads not exceeding 16 t.
- For new lines designed solely for passenger high-speed traffic, speeds up to 300 km/h with axleloads of 16 t, an exception here being special freight trains running at 160 km/h with 16 t axleload.

Present permanent way structures used on lines with heavy mixed traffic

The European Railway network at present comprises 250,000 km of lines of very different categories. Most of these were built during the last century. This has now created a heavy burden for the Railway of today. In many instances, obsolete structures are no longer suitable for current requirements. Some Railways possessing large numbers of secondary lines carrying low volumes of traffic, whilst being inadequately equipped on vital mainline routes where traffic is becoming increasingly dense, could no longer satisfy demands for increased speeds, capacity and quality of transport without first taking appropriate steps for the technological development of the railway structure. This development has resulted in an increased strength and reliability of the track as an essential prerequisite for coping with these demands.

On the occasion of track renewal, lines were progressively strengthened using heavier types of track structure. This involved the use of heavier rails, of improved design and better quality steel. Continuously welded rail and concrete sleepers have been used extensively. New techniques for increasing lateral track resistance, vertical

ballast strength and bearing capacity have been applied, and the quality of track subgrade has been improved.

Notwithstanding the different stages of development achieved as a result of national economic policies and transport requirements, there are nevertheless some common features in present track structure designs. The focusing of effort by the European Railways to unify the variety of track structure components with respect to well-defined traffic conditions, has resulted in the standardisation of the UIC 54 and UIC 60 rails. The UIC 60 kg rails, manufactured from grade "A" or "B" steel with a tensile strength of 900 M/mm² and a carbon content of 0.5 to 0.7%, are considered to be satisfactory for heavy mixed traffic.

However, under the extremely dense goods traffic conditions existing in Eastern Europe, exceeding 50 million gross ton/year and even reaching as much as 100 million gross ton/year on some sections of line, rails weighing 65 kg/m, and even 75 kg/m in the U.S.S.R., are used. High carbon content and heat treatment or surface hardening may be employed.

It has also been found that the rail inclination adopted, in conjunction with the wheel tyre profile, could substantially influence rail wear and thus the effective service life of the rail. It has therefore been recommended that rails should be laid with 1 in 40 inclination instead of the traditional 1 in 20 when the ORE S 1002 wheel tyre profile is used for the rolling stock.

Numerous rail fastening systems exist ranging from the widely used K-fastening system used on the DB network, and also on the Eastern European Railways with slight modifications, Nabla system used by the SNCF, Pandrol in the UK and many other countries, to a variety of different types of elastic fastening system applied with a view to reducing the high stiffness of concrete sleeper and slab or block-supported track. Although the efficient functioning of these fastening systems has been proved in service, there still remain some outstanding questions concerning the change of effective clamping force which is of vital importance for continued rail-sleeper contact, with the desired elasticity, and holding track gauge tolerances for maintenance-free service.

Due to both the shortage of high quality timbers for sleepers and efforts to lengthen the service life of sleepers exposed to heavy traffic and adverse weather, reinforced concrete sleepers have been used widely on the European Railways. Here again a variety of sleeper designs exists due to characteristic national features. For instance, the SNCF and NS have taken advantage of the twin-block sleeper, of comparable price to that of the wooden sleeper. On BR and DB, and also on many Eastern European Railways, the mono-block concrete sleeper is considered to constitute a more satisfactory solution. Apart from reduced maintenance costs and longer service life, they are now cheaper (on DB) than timber.

Concrete sleepers with 55 to 60 cm spacing are now laid on the majority of main lines and even with a spacing of 50 cm (i.e., 2,000 sleeper per km) on lines with heavy goods traffic. We may reasonably expect the service life of a concrete sleeper to be of the order of 40 to 50 years, provided that the detrimental effects of rail-wheel dynamic forces, usually higher than for wooden sleepers in spite of the use of elastic fastening systems, do not require frequent tamping, as this often results in damage to the upper part of the sleepers and thus reduces the bearing surface of the sleepers in the contact area with the ballast, when the track has settled under traffic.

In order to increase the bearing capacity of the track by a better distribution of compressive forces from sleeper to formation, the depth of ballast is being increased to 35 cm below the sleeper and the width of the ballast formation of 3.40 to 3.60 m, giving a minimum of 50 cm on both sides of the sleeper in order to increase the lateral resistance of the track. In addition, heavy types of ballast such as crushed stone and graded gravel are used here.

Attempts to use continuous slab track and track panel supports did not prove very successful on account of the very high initial costs. However, these track designs have found application in some special cases, such as in tunnels, on bridges, elevated structures, etc.

In the construction of point and crossing work manganese steel or surface hardening treatment are applied. Crossings with movable noses, producing an uninterrupted running surface, reduce the dynamic forces and thus extend the service life of switches and crossings.

Time considerations do not permit me to develop this account to embrace other structures such as bridges and tunnels. It should nevertheless be mentioned here that bridges occur very frequently in many European countries (on an average, at least 1 per km of track). This represents a limit on future increase in axleloads to increase track capacity.

Remarks concerning the execution of maintenance work on tracks with heavy mixed traffic

Increasing operating demands entailing maximum capacity of lines with heavy mixed traffic, raises special problems for track maintenance. A well known conflict exists here between the need for more frequent track possessions for maintenance work, as a result of the more rapid deterioration of the track under heavy mixed traffic, and the operating requirements; any longer track occupation by track maintenance machines represents serious disturbance to traffic.

In order to limit track occupation and to reduce maintenance operations the European Railways focus their attention on:

- Eliminating local small scale supervision and maintenance by concentrating partial operations into a single complex working process, carried out by a train of high capacity machines, involving a high degree of automation.
- Improving methods for assessing the condition of the track, using coaches with electronic measurement and data processing equipment, enabling a uniform evaluation of track geometry to be made.
- Developing diagnostic methods for assessing the quality and reliability of track components and for predicting track deterioration, as a basis for more sophisticated planning of track maintenance work according to technical necessity, rather than traditional rotational maintenance with prescribed types and cycles of maintenance work, now considered to be insufficient and economically unjustified.
- Seeking new methods for artificial stabilisation of the track which would in turn reduce the periods during which speed restrictions have to be imposed on the traffic as a result of maintenance work.
- Exercising greater care in constructing new tracks and achieving a higher quality of maintenance work by applying the above principles, which should contribute towards further reducing systematic maintenance operations and their frequency.

Please allow me at this juncture to show you, with the help of the following figures, how severe our maintenance problems are on heavy mixed traffic lines. On some sections of lines on the Eastern European Railways with heavy coal transport, annual traffic loads reach ninety million gross ton/year i.e., 250,000 ton/day. Taking an average freight train weight of about 2,000 tons, this figure represents 125 freight trains per day in each direction, i.e., an average of one train every ten minutes. If passenger trains with higher speeds are to be incorporated into the working time table, it is quite apparent that there is virtually no room left to provide for track possession for maintenance work without severely disrupting normal operation. On the other hand, it is also quite clear that this very dense traffic adversely affects the track resulting in rapid track deterioration which, together with track pollution, requires more frequent cleaning and tamping of the track, for which a track possession could hardly be provided.

In some track sections these works have to be repeated at short intervals of 6 to 12 months, so that the track structure is never consolidated by the traffic. This in turn results either in speed restrictions and thus further operational disturbances or in rapid track deterioration, which eventually

results in shortening of the effective service life of the track structure. It is obvious that existing line capacity is exhausted here and that appropriate remedial measures would have to be taken in order to satisfy these severe transport requirements.

POSSIBILITIES FOR INCREASING THE CAPACITY OF EUROPEAN RAILWAY NETWORKS AND THE IMPACT ON RAILWAY TECHNOLOGY

Of the various possible ways of increasing track capacity, the following are a subject of European interest:

- raising of axleloads,
- increase in the load of freight trains,
- increase of freight train speed,
- application of modern control and signalling techniques,
- electrification,
- construction of new lines.

Raising of axleloads

In addition to the need to increase axleloads as a means of increasing the capacity of lines operating close to their limit, there are also commercial reasons for raising the axleloads as a result of the severe competition from road transport and waterways.

One of the simplest ways of meeting these demands would be by raising the axleload from 20 to 22.5 t.

As far as rolling stock is concerned, recent ORE investigations have shown that the increase of axleloads up to 22.5 t would not raise any particular problem. The strengthening of suspension systems of bogies as well as slight improvements in Y 25C welded bogies appeared to be all that was necessary to adapt the present wagons for 22.5 t axleload.

The effect of the increased axleloads on track structure is still being investigated. The analyses of the tests on the Velim circuit, where experimental trains with 20 and 22.5 t axleloads have been running and have applied a tonnage of 150,000 t, should be completed very shortly.

Similar, though large-scale investigations with 21, 23, and 25 t were carried out in the U.S.S.R. over a period of more than 10 years, and it was on the basis of these investigations that the increase of axleload from 20 to 23 t was recommended. The results of these investigations showed that the introduction of 23 t axleloads on the main lines will require, for example, additional annual expenditure for track maintenance, including renewals, of about 40 million roubles, and an additional 580 km of heavy rails -- R 65 and R 75 -- per year.

On the other hand, this would enable about another 100-140 million gross tons of goods per year to be transported.

Taking into account that heavy liner trains with axleloads of 25 and 22.5 t are already being operated (albeit at low frequency, i.e., one or two trains daily) on BR and DB respectively, it could be reasonably expected that the 22.5 t axleload will be introduced on the European Railway network in spite of a possible increase in the volume of track maintenance.

Increase in the load of freight trains in freight transport

The length of the storage tracks in station installations and of passing loops on the open line varies on the European Railways around 700 to 750 m. The mean load of slow goods trains of such a length is 2,000 tonnes gross; a maximum of 2,600 t can be reached.

In the case of complete trains made up of large-capacity wagons a much greater load is possible. The decisive factor in the maximum load of a train is in this case not the length of the train but the strength of the screw coupling normally used in Europe. This limits the maximum transmissible tractive effort to 450 kN. Consequently the maximum gross train load that can be obtained is 4,000 t.

The maximum train length of about 700 m governed by the length of the fixed installations can be fully utilised only if the automatic coupler developed by the UIC is used, this being capable of tensile loads of up to 850 kN. A train made up in this way, for instance, consisting of 58 mineral wagons each 12 m long and with a gross weight of 80 t, would give a total train load of 4,600 t.

Such heavier trains are of paramount importance for maximising track capacity. They make it possible to increase the capacity of the network and have been successfully operated on certain routes with higher axleloads.

The DB, for instance, have developed a special 6-axle goods wagon for transporting ore, whose load capacity, length and coupling equipment (automatic coupler) are so designed that locomotives and track installations can be used to their full capacity.

Trains made up of such wagons have a gross load of up to 5,400 t with a 4,000 t payload. They are hauled by two 6-axled electric locomotives in tandem, and can also be hauled by three diesel locomotives.

Increase in speed of goods trains to 90/100 km/h

With a view to increasing the transport capacity of the UIC Railways and taking into account the fact that the top speed of passenger trains has been constantly increasing since 1960, studies were initiated within the UIC concerning an increase in the speeds of goods trains. In addition to making better use of the available infrastructure and vehicles, increased competition also plays a decisive role in the economic situation on

the various railways. This requires an improvement in the transport service effort, i.e., among other things a reduction of the transport time, as this is a very important criterion in the selection of the form of transport used by the customer. Thus, in the first analysis the railway services are compared with the transport time guaranteed by road transport.

Since 1966 all goods wagons used in international traffic have had to be suitable for a maximum speed of 80 km/h; wagons built since 1979 have had to be suitable for operating at 100 km/h.

In spite of these running requirements for wagons, the majority of all trains, the slow goods trains, still at a top speed of only 80 km/h. This is due to problems connected with the braking of long non-homogeneous trains, i.e., trains consisting of both empty and loaded wagons, with the normally existing braking distance of 1,000 m. On the one hand, the brake effect diminishes with increasing train length because the brakes of the wagons on the rear part of the train respond later, and on the other hand this retarded response results in surging in the train, with unacceptably high longitudinal forces.

The most recent studies have shown that an increase in the top speed of goods trains, in normal operation, to 90 km/h is possible in the short term by implementing suitable suspension and braking measures on the vehicles. It is intended that by 1990 goods wagons used in international traffic will be adapted in this way. A number of railways are attempting, by means of bilateral agreements, to implement this measure by 1986/87.

A further increase in the top speed of goods trains to 100 km/h, which is considered desirable, would mean, assuming a permissible braking distance of 1,000 m, the general adoption of brake system P, though such a changeover would not, in itself, be sufficient in every case.

High longitudinal forces may develop in the train, particularly when braking with the P system, and it will be necessary, when implementing this measure, for reasons of running safety of vehicles, to ensure that there is no deterioration in the longitudinal force level currently obtained. Relevant studies along these lines have been initiated.

An increase in the top speed of goods trains leads basically to an increase in track maintenance costs. This is estimated as being 0.6% to 2% for an increase in speed up to 90 km/h and about 1.2% to 4% for an increase up to 100 km/h. These figures are to be considered maximum values, valid for track sections on which a high proportion of goods wagons are run at increased speed. On a track carrying mixed traffic the increase in track maintenance costs will be less pronounced.

Increasing capacity through signalling and control

Developments in signalling, telecommunications and control strategies have made significant contributions towards improving the utilisation of the potential capacity of a railway network.

While the scope of this contribution does not lend itself to a detailed presentation of this vast and complex subject, I would like to mention some of the key developments in the European railways:

Despite a number of national variants, modern European railway signalling on all high traffic lines is based on the use of colour light signals and relay interlocking. In most countries these are complemented by safety devices (AWS, Crocodile, Indusi) that automatically apply the train's emergency brake if the driver fails to take the appropriate action at restrictive signal aspects.

Modern signalling systems also include electrically driven switches and, in the non-safety field, train describers, which provide essential information for traffic regulation.

As it is well known, capacity is largely defined by the spacing between signals and the number of aspects that can be displayed to the train driver as well as by the (worst case) train braking characteristics.

Nevertheless, this capacity is seldom achieved in practice due to the unavoidable, finite reliability of all sub-systems.

Current developments in the field of electronic interlockings, in most cases based on micro-processors, should increase this reliability and thus raise the capacity closer to the theoretical value -- without forgetting that many of the field components, switches, track circuits, axle counters, etc., remain a sensitive and not-as-reliable-as-wished link in the chain.

In theory at least, track to train communications combined with the automation of the driving function should permit an increase in capacity -- such as would be the case in moving block operation. Several urban railways in Europe have demonstrated this satisfactorily, but not in passenger service. In the busy urban situation, factors limiting capacity were found to be fluctuations in station stopping times and the propagation of disturbances through the network -- a much more complex problem than the simple simulation of a circular line without functions or stations!

Nevertheless, track to train communications make a useful contribution to track capacity:

- By providing the train driver (or an automatic driving module) information more finely quantised than a signalling system based on colour lights;

- By providing verbal communications between driver and signaller thus allowing for a faster recovery from disturbances.

The control of train traffic has evolved considerably in recent years to large, centralised, computer supported signal boxes/control centres.

The availability of train describers capable of accessing a stored timetable, an accurate and detailed overview of traffic over a large area and the early detection of possible conflicting movements have had a major impact on the design of timetables and on the punctuality of both passenger and freight services.

Many experiments have been carried out on simulation and on line optimisation systems in order to optimise the traffic flow in complex rail networks. While most of these experiments have been considered successful, no general solution has been found so far.

Current developments in traction and braking characteristics of trains, radio communications with moving trains and traffic control strategies now in progress within most European Railways indicate that further increases in real network capacity can still be achieved with higher cost-effectiveness than doubling a section of line or remodelling a complex junction -- but in many cases the capacity increase required does demand drastic measures.

Electrification and its effect on increasing line capacity

Electrification can increase line capacity by making it possible to provide a higher level of power than can be provided economically by diesel traction. This higher power level makes possible higher speeds, heavier trains, and greater acceleration. The last point is significant only in urban and suburban traffic; the others are relevant to all types of service, and particularly to single-track lines where the only other way of increasing the capacity would be track doubling.

For most main line operations it is possible to provide the same power level with diesel traction, but the operating costs, and first cost of locomotives, will be much greater. If line capacity is a problem, it is likely that the traffic density will be sufficient for the savings in operating costs to justify electrification. For very high speeds (> 200 km/h) and for intensive urban and suburban operation, the necessary power/weight ratio cannot be achieved at all with diesel traction.

A further point is that electric traction equipment (other than semi-conductors) has a longer thermal time constant than a diesel engine, and hence a much greater short-term overload capacity, which is particularly important for urban and suburban operations.

It will be obvious from the above that adequate power supply system capacity is important. In general, a higher power level will require the spacing of feeder or substations to be reduced, as well as an increase in their capacity; reduced spacing may entail an extended feeder network. Higher power levels are most expensive to provide on d.c. systems, especially third-rail, where the sub-stations are expensive (though the train equipment is cheaper) and there is usually a railway-owned high voltage network. For this reason such systems are usually designed with little spare capacity and any significant increase in service level requires reinforcement. High voltage a.c. overhead systems usually have some spare capacity initially, and additional capacity can often be provided by making alternative supplies available at all feeding points.

Many European networks are now electrified to the economic limit, e.g., Switzerland, Netherlands. Even on some with a lower proportion of electrified track most of the traffic is electrically hauled, e.g., DB with 80% of traffic on the electrified 55% of the network. In these cases electrification can contribute little more to increasing capacity.

Construction of new lines

Among the variety of further stated objectives, the construction of new lines represents one of the last steps in increasing network capacity. The European Infrastructure Master Plan, conceived by the UIC, makes provision for approximately 6 000 km of new lines of high technical quality (Figure 4). 1,600 km of these lines are under construction and, in some cases, partially open:

- in Poland, the Silesia-Baltic trunk route,
- in Italy, the Rome-Florence "Direttissima,"
- in France, the Paris-Lyons high-speed line,
- in the Federal Republic of Germany, the Hannover-Wurzburg and Mannheim-Stuttgart lines designed to boost transport capacity between the North and South of the country.

The construction of these lines is based on a similar concept to that of motorways with relatively straight track and, usually, through routes. However, the existence of mixed traffic will have a considerable influence here in the selection of principal design parameters.

I would like to illustrate this briefly in comparing the remarkable technical features to be found in the design of the Paris-Lyons line, intended solely for high-speed passenger traffic, and the Rome-Florence line to be operated with mixed traffic, including high-speed passenger trains.

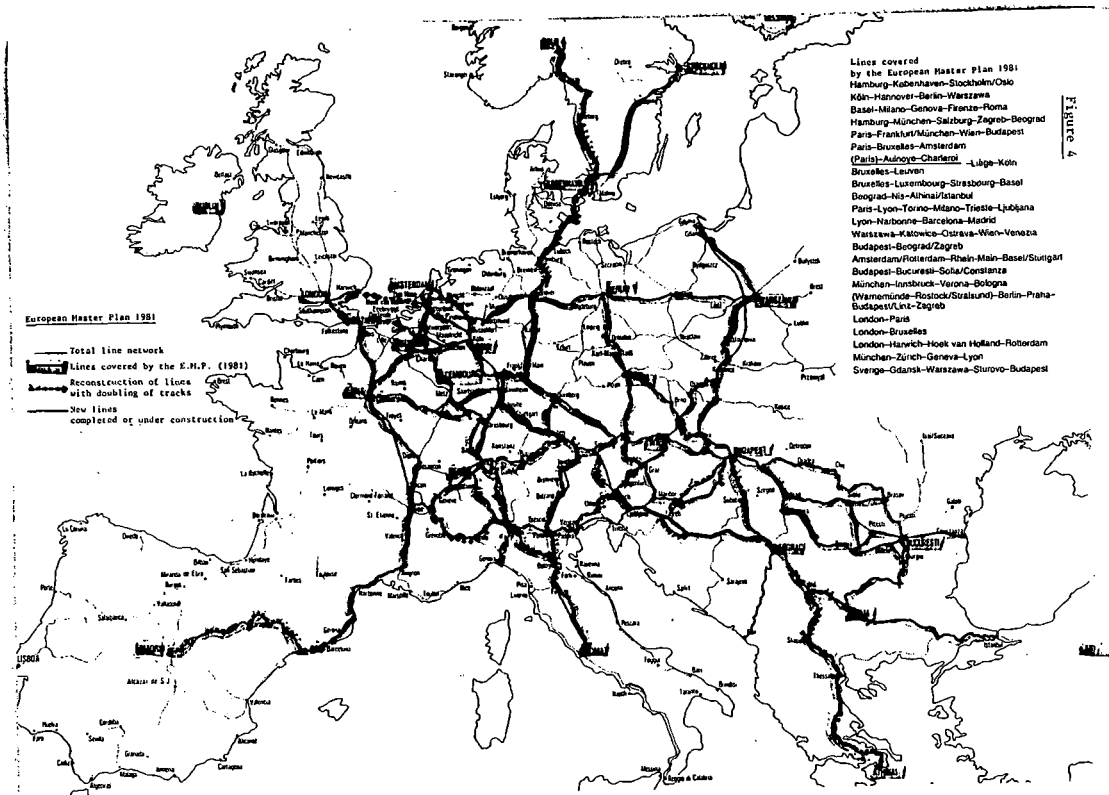


Figure 4

The main difference is in the ruling gradients. Technological progress in motive power design has made it possible to run light, high-speed passenger trains on tracks with gradients of up to 35°/100, as used in the Paris to Lyons line. This has had a considerable impact on the geometric configuration of the track in the vertical direction and hence on construction costs. The line could be laid out in such a way that it closely matched the surrounding terrain, and the number of bridges, tunnels and elevated structures was substantially reduced. This solution, whereby the passenger traffic is transferred to the new high-speed line, will obviously contribute towards increasing the potential capacity of the old line, which was virtually exhausted as regards freight traffic.

In the case of mixed traffic, it would probably not be possible, from the technological/economical point of view, to design gradients steeper than about 9°/100, as applied on the Rome-Florence line. Combined with the difficulties of line location in mountainous areas, this has resulted in the line being constructed with many bridges, tunnels and elevated structures.

A further impressive feature, common to both lines, is the construction of track bed formations consisting of several well-compacted sub-layers, with fairly impermeable upper layers. The costlier construction of such earthworks will certainly be offset by savings in maintenance, by ensuring gradual and even settlement of the track and thus long-term durability of track level.

Concluding with these illustrations of the latest European achievements in the construction of both the new Paris to Lyons and Rome to Florence lines, I would like to express my conviction that both our railway systems will continue to keep pace with technological developments and thus continue to meet future challenges as regards both quality and quantity of transportation on the railways.

Improving the Measurement, Evaluation and Control of Track Irregularities

Luo Lin

Research Engineer
Head of Track Measurement
Technique Group
China Academy of Railway
Sciences
Beijing
People's Republic of
China

The waveforms of track irregularities are quite random in nature. Track irregularities having different wave characteristics can produce quite different effects upon the wheel/rail interactions. It is not adequate to only evaluate the track irregularities and pinpoint the locations to be maintained by using offset values obtained from measuring the chord length. The author deems it necessary to improve the measurement, evaluation and control of track irregularities so as to discover and eliminate significant irregularities; this will reduce the induced dynamic load, ease the intensity of wheel/rail interactions and thereby extend the service life of the installations as well as better ensure the safe running of trains. Based on theoretical analyses and test results, it is recommended to adopt the "inertial reference technique" in place of the "chord offset method" as a more accurate way of providing the waveforms of track irregularities. The random nature of irregularities, together with the amplitude, wavelength, mean rate of change and resonant waveform, bear great influence on the safe running of trains, the vibrational effects upon locomotives and rolling stock and on the wheel/rail interactions. Therefore, it is recommended that mean square values, standard deviations and PSD be used for the statistical evaluation of the smoothness of a certain track section in determining the track maintenance requirements; and to use the amplitudes, mean rates of change and resonant waveforms for the evaluation of the local characteristics of the irregularities in determining the locations requiring spot or urgent maintenance.

INTRODUCTION

Track irregularities exert great influence on train safety, riding quality, wheel/rail interactions, service life of track components and rolling stock as well as the deterioration of track structures, etc. The track will not perform properly when the smoothness of the track is seriously affected, even if the stress and the elastic deformation are within the allowable tolerance. Therefore, measurements have to be made now and then so as to find out timely those track sections with excess irregularities and to repair them accordingly. This is an important aspect where the track structure is quite different from other engineering structures. In solving the problems arising from increasing traffic loads imposed on the track, greater attention must be paid to the track conditions as regards its irregularities, besides improving and strengthening the track structure.

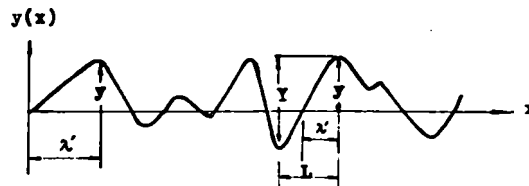
This paper is intended to deal with the measurement and evaluation of track irregularities and the identification of critical conditions. Proposals are also put forward for the improvements of the methods for measurement, evaluation and control of track irregularities.

WAVEFORM CHARACTERISTICS OF TRACK IRREGULARITIES AND THEIR EFFECTS

The waveforms of track irregularities are quite random in respect of their amplitudes and wavelengths. Track irregularities such as the profile and the crosslevel often possess a wide

range of wavelengths of 1 to several tens of meters as can be seen from their PSD diagram, longer waves having larger amplitudes while shorter ones smaller amplitudes. Track irregularities due to uneven wear have still shorter wavelengths at rail ends and switch areas. The wavelengths of corrugations on our heavy duty track often fall within the range of 0.2 - 0.5 m and those of the dipping wear at rail ends are mostly from 0.3 - 1.0 m. The amplitudes of shorter wave irregularities at rail top are generally not more than a few millimeters, while those of longer wave irregularities may reach several tens of millimeters.

The waveform characteristics of track irregularities at a point can be expressed by the amplitude, the wavelength, the mean rate of change and the resonant waveform. The mean rate of change roughly indicates the parameters of wavelength and amplitude, and may be expressed by $\frac{y}{\lambda'}$ (the ratio of half-peak value y to $1/4$ wavelength λ'), generally referred to as the mean rate of change of quarter wavelength. Otherwise it can be indicated by $\frac{Y}{L}$ (the ratio of peak-peak value Y to the distance L between the positive and negative peak values) referred to as the mean rate of change of peak-peak value (Fig 1). The latter indication is more expedient in interpreting the recorded



Half-peak value: y
Peak-peak value: Y
Mean rate of change for $1/4$ wavelength: $\frac{y}{\lambda'}$
Mean rate of change from peak to peak: $\frac{Y}{L}$
Wavelength: $\lambda = 4\lambda'$

Fig 1. Amplitude wavelength and mean rate of change of track irregularities

waveforms. The resonant waveforms refer to those continuous cyclic waveforms of track irregularities which tend to cause resonance of the carbody (Fig 4 and 11 d).

Track irregularities having different waveform characteristics generate very different effects on train/track interactions.

From the calculated results shown in Table 1, it can be seen that irregularities having a wavelength of 1 m produce 100 times as much acceleration as those having a wavelength of 10 m do. Obviously, irregularities with the same amplitude but different wavelengths can have entirely different effects and the acceleration caused thereby (without being damped) is inversely proportional to the square of the wavelengths.

Table 1

Speed V (km/h)	Wave length λ (m)									
	0.1		0.5		1.0		10		30	
	f (HZ)	a (g)	f (HZ)	a (g)	f (HZ)	a (g)	f (HZ)	a (g)	f (HZ)	a (g)
30	83.3	27.95	16.7	1.12	8.3	0.28	0.83	0.0028	0.278	0.00031
60	166	111.8	33.3	4.47	16.6	1.12	1.66	0.0112	0.555	0.00124
90	250	251.8	50.0	10.07	25	2.52	2.5	0.0252	0.833	0.0028
120	333	447.5	66.7	17.9	33.3	4.48	3.33	0.0448	1.11	0.0050
160	444	796	88.9	31.8	44.4	7.96	4.44	0.0796	1.48	0.0088

$a = \ddot{y}_{max} = 4\pi^2 (\frac{V}{\lambda})^2 y$	f — frequency (HZ)
$= 4\pi^2 (\frac{V}{\lambda})^2 / 9800 (g)$	a — acceleration (g)
y — Amplitude (mm)	g = 9800 mm/sec ²

Frequency (f) and acceleration (a) caused by sine form irregularities of different wave lengths with 1 mm peak value under various speeds

According to the formulas of some countries such as the Soviet Union, the inertia force of the unsprung mass caused by track irregularities is inversely proportional to the wavelengths.

Measured data show that irregularities with short wavelengths and high mean rate of change (such as the irregularities at rail ends and switch areas, poor rail welds, corrugations, etc) cause violent impact to be produced between wheel and rail as well as great unsprung accelerations and wheel/rail interactions, resulting in damages of track components and vehicles, intensified accumulation of ballast residual deformation and furtherance of track irregularities (Fig 2).

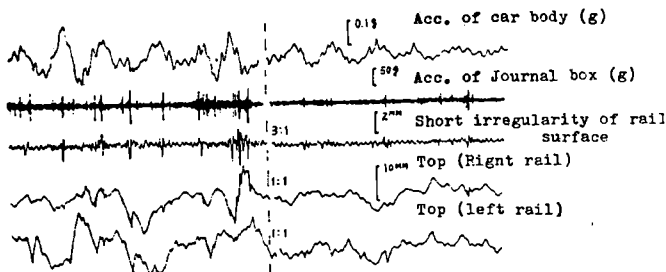


Fig 2. Effects of short irregularities on vertical acceleration of journal box and accumulation of ballast residual deformation

The significant effects from the wavelength have been proved by a group of on-track tests where the rail surface was ground to form irregularities of different wavelengths. With track geometry measuring vehicles running at uniform speeds, the journal box acceleration and the rail bending stress are measured and found to be roughly proportional to the amplitudes and inversely proportional to the wavelengths. The accumulation of track residual deformation also has apparent relations with the wavelength, i.e., when the amplitudes of rail surface irregularities are identical, the accumulation of the track residual deformation becomes more precipitous and more uneven with the decrease of the wavelength.

On the other hand, irregularities with longer wavelengths mainly affect the carbody in vibration. Track irregularities with both large amplitudes and corresponding large mean rates of change cause violent vibration of the carbody (Point A in Fig 3), while those with large amplitudes but smaller mean rates of change cause only mild carbody acceleration (Point B in Fig 3).

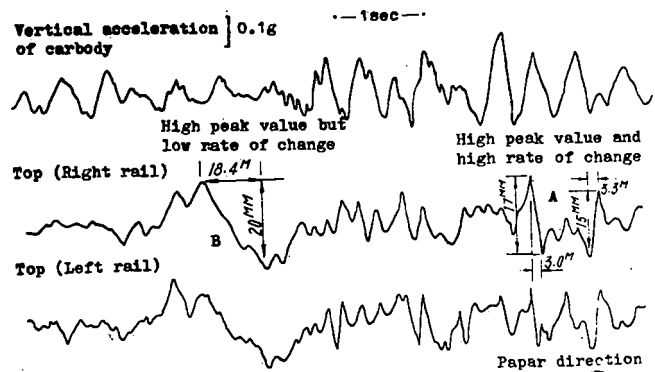


Fig 3. Influence of mean rate of change on carbody vibration (test record)

The frequency of the forced vibration caused by the profile irregularities of 1 - 28 m wavelengths, under a speed of 20 - 120 km/h, is close to the natural frequency of the vertical vibration of Chinese locomotives and cars. If such profile irregularities are cyclic, even though the amplitudes may be small, they tend to cause carbody resonance and herewith significant increase of the vertical acceleration of carbody vibration (Fig 4). This results not only in deterioration of the riding quality but also in great fluctuation of the wheel loading. When a large horizontal force is exerted on some wheel which has a decreased load, derailment may take place to seriously jeopardize the safe running of trains. If the decrease of load happen to take place on the driving wheel, the adhesion tractive effort will be impaired as well. The 1 - 28 m wavelengths are the resonant wavelengths of profile irregularities in our country. The waveforms of continuous cyclic irregularities within this range of resonant wavelengths are designated as resonant waveforms.

According to the test results of Japan, the cyclic waveforms of alignment and crosslevel irregularities have more serious influence on the safety of train operation.

TRANSFER RATIO OF CHORD OFFSET METHOD FOR MEASURING SINE FORM IRREGULARITY Table 2

Chord length wave length (l/λ)	$\cos \pi(\frac{l}{\lambda})$	Transfer ratio $H(\lambda) = N(x)/r(x) = 1 - \cos \pi(\frac{l}{\lambda})$	Example $(H(\lambda) = N(x)/r(x) = b\delta/\delta_0^2)$
$2, 4, 6, 8, \dots$	$+1$	0	
$1, 3, 5, 7, \dots$	0	1	
$1, 3, 5, 7, \dots$	-1	2	

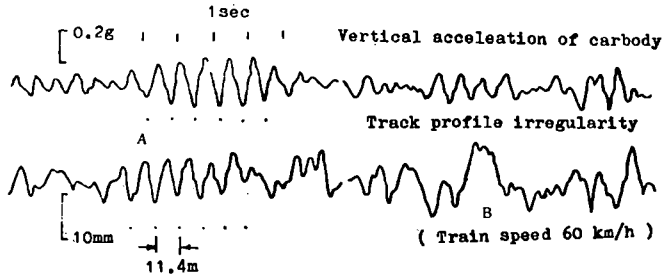


Fig 4. Carbody resonance caused by profile irregularity with resonant wave form at A

It is obvious, then, that it is far from enough to use only the amplitudes of the track irregularities or the chord offset of a certain chord length for evaluation of the smoothness of track and for the spotting of the sections requiring repair or maintenance. Factors such as the wavelength, mean rate of change, resonant waveform, etc. must be given due attention.

IMPROVING METHODS FOR MEASURING PROFILE AND ALIGNMENT IRREGULARITIES

Since amplitude and other waveform characteristics of track irregularities have non-negligible effects on train/track interactions, the actual waveforms of such irregularities as having influential wavelengths must be measured so as to find out and get rid of those hazardous track irregularities. The range of influential wavelengths are what requires investigation and measurement. Its upper limit is set by the max. value of resonant wavelengths, while the lower limit be such as to cover the short wavelengths as of track irregularities like the uneven wear on rail tops. Under our present conditions that the highest speed is 120 km/h, the natural frequency of carbody vibration is no lower than 1.2 Hz, and the short wavelengths of rail top irregularities are no less than 0.1 m, the wavelengths to be measured for profile irregularities should cover the range of 0.1 to 28 m. Of course the range should be extended accordingly if the running speed would be higher and the natural frequency of carbody vibration would be lower.

However, the "chord offset method" which has long been used in our country as well as in many other countries can not satisfy the measurement requirements for actual waveforms of track irregularities as described above. Neither can the value of chord offset give a proper indication of the wavelengths.

It is well known that the transfer ratio $H(\lambda)$ in the "chord offset method" measurement of sine-wave track irregularities varies within the range of $0 \sim 2$ with the ratio of the chord length l to the wavelength λ of track irregularities ($H(\lambda) = \text{measured value}/\text{actual value} = 1 - \cos \pi \frac{l}{\lambda}$). It can be seen from Table 2 that only when l/λ is equal to $1/2, 3/2, 5/2, 7/2, \dots$, can the transfer ratio be unity. In other words, only in limited cases as when the wavelength is $2, 2/3, 2/5, 2/7, \dots$, times of the chord, can the chord offset method give a correct representation of the magnitudes of the sine-wave track irregularities. When l/λ is an even

number such as 2, 4, 6, 8,, the transfer ratio of the chord offset method will become zero. In such cases, all the measured values would be zero (i.e., beyond measurement), no matter how big the track irregularities are, and when l/λ is an odd number such as 1, 3, 5, 7,, the measured values would be twice as much as the actual values.

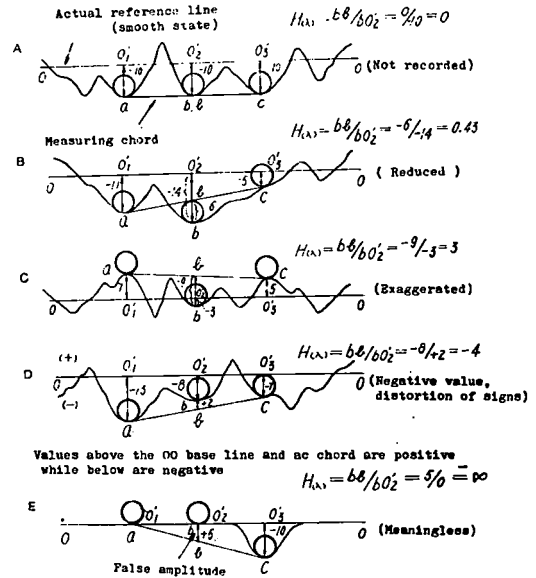
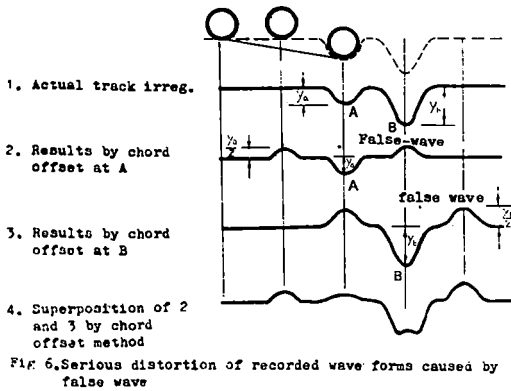


Fig 5. Graphic analysis of transfer ratio when chord offset method is used to measure non-sinusoidal irregularities

Further graphic analysis (Fig 5) shows that the transfer ratio $H(\lambda)$ in measuring the actual non-sine wave track irregularities by the chord offset method does not vary within the range of 0 - 2, but rather it may possibly go beyond 2. In this case, the positive and negative signs of the irregularities might get mixed. In the graphic recordings from the chord offset method, for each individual track irregularity (with amplitude y), there are two flanking "false waves" (with amplitude $-\frac{y}{2}$) which are non-existent and have opposite signs to the individual wave. Here $H(\lambda)$ is meaningless, for $H(\lambda) = -\frac{y}{2} / 0 = \infty$. Obviously, false waves, by superposition, can cause serious distortions in the recorded waveforms (Fig 6).

When calculation of the PSD of track irregularities is based on the chord offset method, it is not only onerous to making modifications and corrections for transfer ratios corresponding to the



wavelengths of each sine components from point to point, but also is helpless before the influence due to the zero transfer ratio and the false wave in the chord offset method. Still a true PSD of the track irregularities could not be obtained.

The test results from "check track", the irregularities of which are found out in advance, have proved the correctness of the foregoing graphic analyses. In Fig 7 and Fig 8, comparisons are made between the measured results obtained by the chord offset and the inertia methods and the actual waveforms of the track irregularities. As observed in the figures, the chord offset method gives distinctly distorted graphs marked with exaggeration, reduction, reversed positive and negative signs as well as false waveforms. The waveforms, amplitude and other waveform characteristics obtained by the chord offset method are all different from the actual waveforms of the track irregularities.

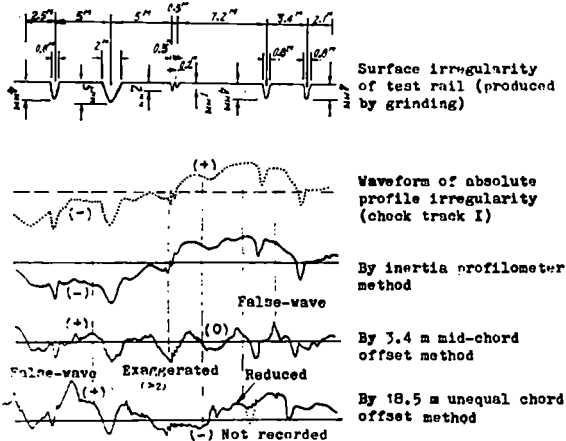


Fig 7. Records by chord method and inertia method checked against "Check track I" for track profile irregularities (Speed of 80 km/h)

It is observed too that the waveforms obtained by the inertia method (with CP-3 system) can compare closely to the actual waveforms of the track irregularities. The principle of the inertia method is shown in Fig 9. So far as the wheels are in contact with the rails, the locus of the vertical movement of the journal box will be the profile irregularities of the track. The vertical movement y of the journal box is equal to the sum of the vertical movement Z of the mass block M in the mass-spring

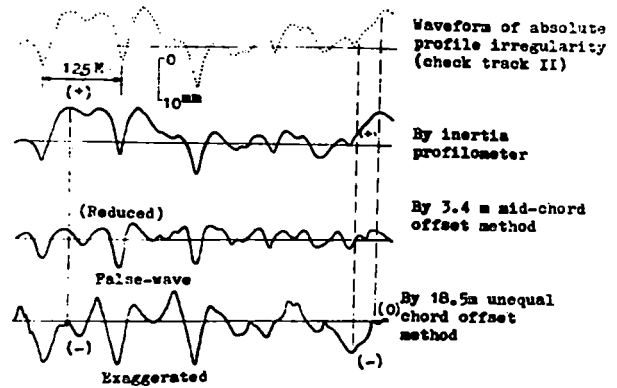


Fig 8. Records by chord method and inertia method checked against "check track II" for track profile irregularities (speed of 80 km/h)

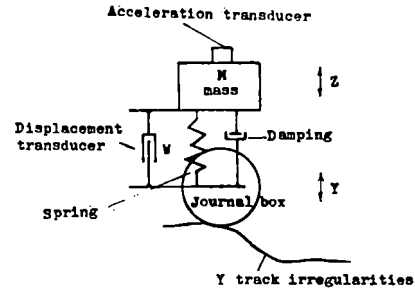


Fig 9. Schematic diagram of inertia profilometer

system and the relative displacement W of the mass block with respect to the journal box:

$$y = Z + W = \iint \ddot{Z} dt dt + W \quad (1)$$

The absolute displacement Z of the mass block M with respect to the inertia reference line can be obtained through double integration of the measured acceleration \ddot{Z} of the mass block, while the relative displacement of the mass block to the journal box can be obtained through direct measurement by displacement transducers. The absolute waveforms of profile irregularities within the desired range of wavelengths can thus be obtained by adding up Z and W and filtering the result through high pass filters to bar out the long waves (with wavelengths exceeding a certain value). For the measurement of alignment irregularities, the same principle applies, only the system must be rotated 90° to a horizontal position, as shown in Fig 9, and installed perpendicular to the track. To the measured loci of the transverse movement of the journal box, must be added the changing values of the play between the wheel flange and the gauge side of the rail head.

The measurable wavelength range by the inertia method may be easily controlled by regulating the cut-off frequency of high pass or low pass filters. The inertia technique provides very good transfer characteristics (Fig 10) and the transfer ratio is not so intangible as with the chord offset method. Thus it meets the requirements for the measurement

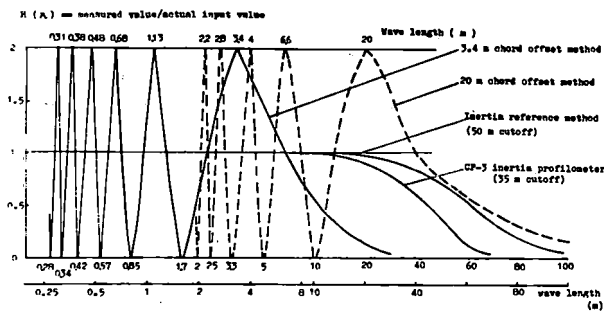


Fig 10. Transfer ratio for chord offset method and inertia method used to measure sine wave track profile irregularities

of the actual waveforms of track irregularities which lie within the range of influential wavelengths. Furthermore, the inertia reference measurement system provides many such other advantages as being capable of installation on locomotives, freight and passenger cars of different axle loads for the purpose of making measurements, requiring nothing special of the construction of the track geometry cars, offering readiness of calibration, etc. Hence, the inertia technique is recommended in place of the chord offset method which does not give true representation of the actual track irregularities.

The inertia technique and the inertia system have been successfully developed in the United States, Canada, Britain, China and some other countries, and have been put into application. The inertia system developed in Japan employing the method of integration of the journal box acceleration has also come nigh on practical use for the measurement of track irregularities of short wavelengths.

IMPROVEMENT OF THE METHOD OF EVALUATION AND CONTROL OF TRACK IRREGULARITIES

In order to prevent possible derailment, to reduce dynamic load so as to ease wheel/rail interactions and extend the service life of track and vehicles, and to better utilize the track capability, it is of great importance to scientifically evaluate the track irregularities and correctly identify the defective locations with a view to improving the roughness of the track by eliminating in time all hazardous irregularities.

It is inadequate to use only the recorded wave amplitudes of track irregularities for the evaluation of track smoothness and the locating of faulty places as is done at present. Take the waveforms of irregularities of four track sections (A, B, C and D) as shown in Fig 11 as an example. If the "over-limit" situation of the amplitude is taken to be the sole criterion for evaluation, we find that sections A, B and C have three over-limit places each and that there is none in section D. Consequently, it would be considered that only section D is in good condition while the other three sections are in identical conditions. But as a matter of fact, the four sections differ markedly from each other as regards irregularities. Their wavelength constructions, the mean rates of change at the over-limit places, the periodicity of waveform, the statistical value of their amplitudes, etc. are all different. Obviously, their respective effects on the locomotives and rolling stock would

differ as well.

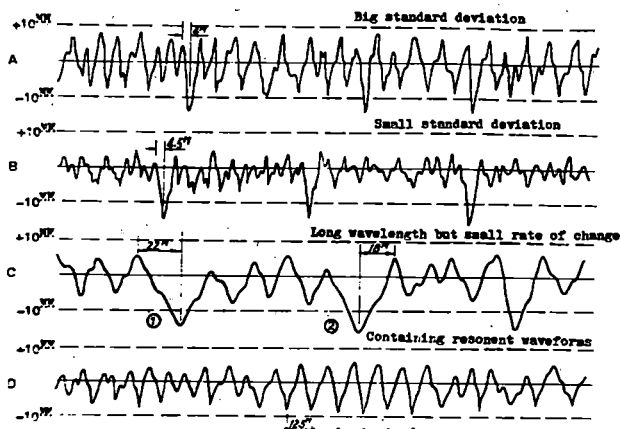


Fig 11. Different waveforms of profile irregularities for 4 measured sections

Therefore, it is necessary to improve the methods of evaluation of track state and of identification of hazardous irregularities. All the waveform characteristics and the statistical characteristics need be taken into account. We propose:

1 To use the three waveform characteristics (amplitude, mean rate of change, and resonant waveform) in evaluating the particular condition of track irregularities with a view to determining such places as require maintenance or urgent repair.

In evaluating a particular section of track irregularities in order to pick out the hazardous ones and to locate isolated "over-limit" places, due attention should be paid to the influence of wavelength. In this connection, in addition to the "over-limit" amplitudes, the corresponding mean rate of change, which reflects approximately the effect of wavelength, should also be taken into account at the same time. Those irregularities having large amplitudes and also having long wavelength and gentle inclination (of small mean rate of change) need not be counted as "over-limits", because they are less influential (see Fig 11C ① and ②). Only those irregularities which have both large amplitudes and large mean rates of change should be regarded as "over-limits" or extra "over-limits". And such locations are where maintenance or urgent repair is required (Fig 11 A and B).

In regard to periodic irregularities, which fall into the category of resonant waveforms, with their wavelengths within the range of resonant wavelengths, we should regard them as hazardous irregularities even though their amplitudes do not exceed the prevailing allowable tolerance (Fig 11 D). They need maintenance or urgent repair so that resonant vibration might be absolutely prevented. The maintenance of way divisions should take note of the actual values of resonant wavelengths, which may be obtained from Fig 12 making use of the natural frequencies and the running speed of the locomotives and vehicles operating in their respective districts.

2 To use the standard deviation σ_y and the PSD in evaluating, on a statistical basis, the general situation of the track irregularities, and then to proceed locate the track sections requiring maintenance.

Since track irregularities vary in a random

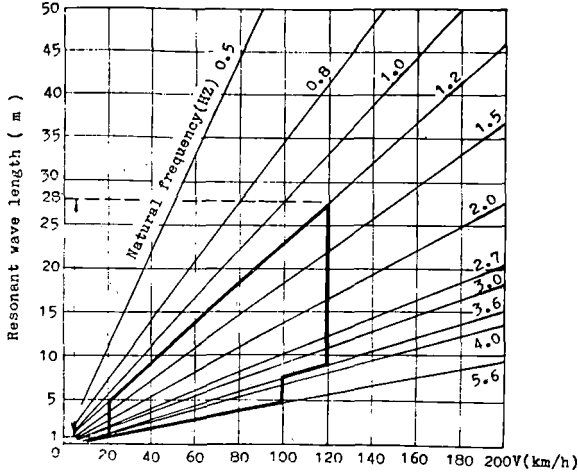


Fig 12. Relationship of resonant wave lengths with natural frequency and speed of vehicles

Note : Heavy lines indicate range of natural frequency and speed of China's rolling stock

fashion with the distance travelled over a track section and their waveforms are random sinusoidal ones composed of varied amplitudes, wavelengths, and phase angles, the characteristics of an isolated waveform at a particular place can not represent the general condition of a track section. Hence, it is necessary to rely on such statistical characteristics as the mean square value, standard deviation and PSD of the track irregularities to achieve an all-rounded evaluation of the amplitudes and the wavelength construction of the track irregularities within a certain length of track section.

The roughness (the average statistical condition of the amplitudes) of a certain track section can be interpreted by the mean square values and the standard deviations. The mean square value $\hat{\psi}_y^2$ of the track irregularities $y(x)$ of a certain track section, with kilometerage x as abscissa, can be expressed by:

$$\hat{\psi}_y^2 = \frac{1}{X} \int_a^x y^2(x) dx \quad (2)$$

The variance σ_y^2 :

$$\sigma_y^2 = \frac{1}{X} \int_0^x (y(x) - \mu_y)^2 dx$$

that is $\sigma_y^2 = \hat{\psi}_y^2 - \mu_y^2 \quad (3)$

As indicated in (3), the mean square values of track irregularities is composed of the mean value μ_y (statical component) and the variance σ_y^2 (dynamic component). If the mean value of track irregularities is equal to zero, then the mean square value equals the variance.

Owing to the fact that the variance of track irregularities of a certain section reflects the deviation of the random amplitude from the mean value, high variance indicates great scatter and fluctuation of the amplitudes and more intensive roughness of the track. Therefore, it will be well to use the variance to express the roughness. In practice, it is more convenient to use the positive root square value of the variance, i.e., the

standard deviation σ_y , to evaluate the roughness of various track sections. Standard deviation has been applied on the BR and some other railways to evaluate the quality state of track maintenance.

Taking into account the big difference in the track irregularities often encountered over a long section of track, we may take a 100 m track section as a basic section for quality evaluation and maintenance control for the sake of accurately identifying such sections as requiring maintenance, and of emphasizing the statistical characteristics of very rough track sections (also taking into account the need for stationary check). For any type of irregularity, the evaluation of its quality level is then to be based on 250 sampling standard deviations in 100 m of such track. (The sampling interval should be closer when measuring short wave irregularities on rail tops.) Any 100 m segment is to be repaired whenever the standard deviation σ_y is found to have gone beyond the allowable limit, no matter how the individual "overlimits" may appear. Then the standard deviation of various types of irregularities are calculated for every 1 km of track for use as basic data in the evaluation of track maintenance quality. Thus, the disadvantage of evaluating track irregularities only by some individual "over-limits" without considering the statistical characteristics of amplitudes can be overcome. For example, their standard deviations of the two sections A and B as shown in Fig 11, are similar in their level of individual "over-limits", but we find that the smoothness of section A is worse than section B if we make statistical comparisons between them.

The wavelength construction of track irregularities may be represented by the PSD. The estimated $\hat{G}_y(f)$ of the PSD for the stationary sampling record of track irregularities $y(x)$ of a certain track section is equal to the mean square value $\hat{\psi}_y^2(f, \Delta f)$ of $y(x)$ within the infinitesimal bandwidth Δf from f to $f + \Delta f$ divided by the bandwidth Δf :

$$\hat{G}_y(f) = \hat{\psi}_y^2(f, \Delta f) / \Delta f \quad (4)$$

where f is the spatial frequency, which is $f = \frac{1}{\lambda}$, the reciprocal of the wavelength.

When the PSD is obtained through FFT, it may be expressed:

$$\hat{G}_y(f) = \frac{2}{X} \left| \int_0^X y(x) e^{-i2\pi fx} dx \right|^2 \quad (5)$$

Fig 13 demonstrates the relation between the PSD $\hat{G}_y(f)$ and the frequency f . It shows clearly the wavelength components which form the random waveforms of track irregularities. The area included under the PSD is equal to the mean square value:

$$\hat{\psi}_y^2(f_i, f_n) = \int_{f_i}^{f_n} \hat{G}_y(f) df \quad (6)$$

If there is any local stationary situation in some non-stationary sample records of track irregularities, then the "single-sided" time varying PSD serves to express the spectral structure:

$$\hat{G}_y(f, x) = \hat{\psi}_y^2(x) \hat{G}_y(f),$$

$$\int_0^\infty \hat{G}_y(f) df = 1 \quad (7)$$

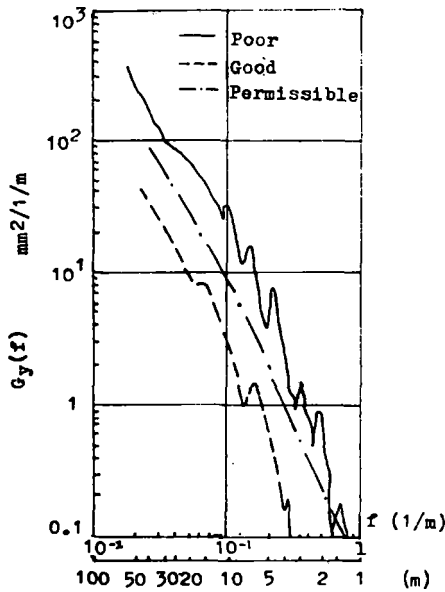


Fig 13. PSD of track profile irregularity

where $\hat{\Psi}_y^2(x)$ is the series formed of averages over short-distance segments
 $\hat{G}_y(f)$ is obtained by averaging over the entire recorded length as is the stationary sample records

The recorded field measurements of track profile irregularities show that sample records of the same are not always stationary. However, for the same kind of track structure, the records obtained are nearly stationary (except in the switch area and the breathing area of CWR), or at least locally stationary, and are generally stationary within a short distance in most cases. In the light of the above mentioned conditions, and in order not to reduce the statistical accuracy and the resolution, the track may be divided into several 1 km sections. Computers of real time preprocessors accompanied with FFT hardware are employed to calculate the PSD of track profile and alignment irregularities for each kilometer. (the sampling interval is 0.488 m and 2048 sample records are taken from each kilometer.) At the same time, the mean square values of irregularities of the ten 100 m segments in the kilometer under consideration is subjected to run test so as to ascertain the stationarity of the sample records of track irregularities in the kilometer. In case the assumption of stationarity should not be suitable, the expression (7) may be used for approximate calculation of the "single-sided" time varying PSD values which is related to the mean square values obtained over the ten 100 m segments. Then the measured PSD is compared with the allowable limit of the PSD, which varies with wavelength. (Allowable value is higher for long wave PSD and smaller for short wave PSD, see Fig 13.) The "over-limit" values of PSD corresponding to different wavelengths, along with the isolated "over-limits" and the standard deviations for that kilometer of track are based upon to calculate the number of kilometers of excellent, good and defective track under the respective jurisdiction of different

levels of maintenance of way units, from the track gang up to the railway administrations. The insufficiencies in evaluating track roughness of a random nature only in terms of the magnitude of irregularity, amplitudes without duly making account of the wavelength situation, the resonance-producing factors and the statistical characteristics are overcome in the foregoing manner. A substantial improvement of track quality may be expected.

REFERENCES

- 1 罗林 轨道随机干扰函数 中国铁道科学 第三卷 第一期 1981年
- 2 专题研究小组 惯性基准法轨道高低检测装置的研究 中国铁道科学 第一卷第一期 1979年
- 3 (日)佐藤裕 轨道力学 中国铁道出版社 1981年
- 4 池守昌幸 轨道狂いの波形の整備に関する研究 铁道技术研究報告 No.1038 1977年3月
- 5 北岡寛太郎 轨道狂いに関する研究について 铁道线路 第14卷10号 昭和41年10月
- 6 阿部俊一 轨道狂い測定法についての原理的考察 铁道技术研究資料 VQ117 No11 1960年
- 7 佐藤吉彦, 相沢泰治 轨道狂い絶対形状の測定装置(第一報) 铁道技术研究報告 No.381 1963年11月
- 8 佐藤吉彦, 竹下邦夫, 石井太一 961-高速轨道检测装置(HISTIM)の構想とその设计 铁道技术研究資料 No.32-4 1975年4月
- 9 沼田実 轨道狂い量の統計評価 铁道業務研究資料 第10卷8号 昭和28年4月
- 10 座談会 轨道狂いの管理をめぐる 铁道线路 第28卷 第7号 昭和55年7月
- 11 佐藤吉彦 諸外国における轨道整備限度と轨道检测方式 铁道线路 第28卷 第7期 昭和55年9月
- 12 宮本俊光, 渡辺備年 线路-轨道の设计管理-山海堂 昭和55年9月
- 13 E.M. Бромберг, М.Ф. Вериге, В.Н. Данилов, М.А. Фришман, Взаимдействие пути и подвижного состава ГТЖИ 1956
- 14 В.Ф. Парабошик, Неровности на рельсе-источник деформаций в балласте путь и путевое хозяйство 1965. 12
- 15 Otmar Weishaupt, Probleme beim genauen Ertaessen der Gleisunebenheiten mit Schienenfahrzeugen DET 1-73.
- 16 P.N. Bhaskaran Nair, Track Measurement System -- Concepts and Techniques, Rail International, No 3 March 1972.
- 17 Ta-Lun Yang, Edward D. Howarter, Richard L. Inman, Inertial and Inductive Measurement Techniques for Track Geometry *, 1981.1.
- 18 Luo Lin, Measurement of Track Profile Irregularities *, 1981.1.
- 19 R.B. Lewis, W.L. Cook and R.J. Forsyth, The High Speed Track Recording Coach, Railway Technical Center, Derby, BR, Nov. 1976.
- 20 O. Kretteck, Die Registrierung und Analyse Von Gleisunregelmäßigkeiten, ZEV-Glas Ann, 99, 1975 No 11.
- 21 O. Esveld, Das Messen und Korrigieren der Gleisgeometrie, ETR, 1980. 29. No 5.

- 22 Communications of ORE, Power Spectral Density of Track Irregularities, Rail International No 12, December , 1972.
 - 23 J.S. Bendat and A.G. Piersol, Random Data: Analysis and Measurement Procedures, Wiley-Interscience, 1971.
- * Preprint - Presented at the International Conference on Wheel/Rail Load and Displacement Measurement Technique, January 19 - 20, 1981, At the Transportation System Center, Cambridge, Massachusetts, USA.

B.H. Price

Senior Development
Engineer
Bessemer & Lake Erie
Railroad
Greenville
Pennsylvania

Use of Force Level Data for Policing Track Quality

There is a definite relation between the vertical and lateral forces recorded at the wheel to rail interface and the geometry of the track. The Bessemer and Lake Erie Railroad is successfully using force data collected by their A-333 system to locate geometric defects and monitor the geometric quality of the track.

Properly designed and maintained equipment operating on well designed and maintained track would not be expected to develop undesirable dynamic forces at the wheel to rail interface when speeds are below fifty miles per hour. When such forces do occur, they are often the result of the vertical or lateral accelerations of the wheel as it attempts to follow the imperfections in the steel rail guideway. Such accelerations of the wheel act through the suspension system to produce accelerations in the car body. These, in turn, can produce additional forces which must eventually be constrained at the wheel to rail interface. Limiting the magnitude of the track irregularities which can excite such undesirably high dynamic forces is necessary to the continued safe and efficient operation of trains.

Safety in train operations is the ultimate goal of the Federal Track Safety Standards. These standards were developed from operator experience and judgment. They are expressed geometrically so that the track inspector, or other Maintenance of Way person, can readily understand them and monitor them in the field. Dimensionally defined as they are, exceptions can be communicated orally, or in a written form, in a generally universal Maintenance of Way language.

The Track Safety Standards are a measure of track quality, but often in a negative sense. Many times they indicate short length, or spot, exceptions

to a desired level of maintenance and not specifically the overall quality level for longer sections of railroad. Their underlying purpose is to limit dynamic forces which, up until recently, could not be measured with ease or accuracy.

The A-333 system was developed by the Bessemer and Lake Erie Railroad and others as a practical tool for measuring the forces at the wheel to rail interface while the train is in motion. The A-333 itself is simply a data recording vehicle. It is a converted steel caboose which has been equipped with amplifiers and recorders for the collection of data. It is also furnished with heat, air conditioning, and sanitary facilities for the comfort and convenience of the operators and observers.

The instrumentation for measuring those quantities needed to calculate the desired forces is mounted on one truck of a standard open top, four-pocket Bessemer hopper. This is a 100-ton capacity car which was built in 1975 and which is equipped with D-5 springs, ride control, and 36-inch wheels. The load in the car is unchanged from year to year so that the gross weight on rail is constant, except as it is affected by moisture content. Because of the nature of the lading, moisture can produce a maximum weight change of only a few percent, either plus or minus. The hopper is always operated next to the recording car and the instrumented truck is always run as the lead truck of the car when force data is being collected.

An adapter pad, modified as a load cell, is mounted between the side frame and the journal on each of the four corners of the instrumented truck. This load cell is comprised of matched strain gages mounted in the horizontal plane on the bearing face

of the adapter pad in the configuration of a bridge. An input voltage is supplied through shielded leads from the A-333. Shielded leads also return the load cell data to the recorder.

Strain gages are also mounted at known points inside the wheels on each end of each of the two axles of the truck. These gages are paired and are 180 degrees apart on the circumference of the axle. They measure the bending of the axle as it rotates. Leads from these gages come out through slip rings on one end of each axle. While both axles are instrumented, force data for track quality purposes is normally collected from the lead axle only.

Figure 1 shows a free body diagram of an instrumented axle.

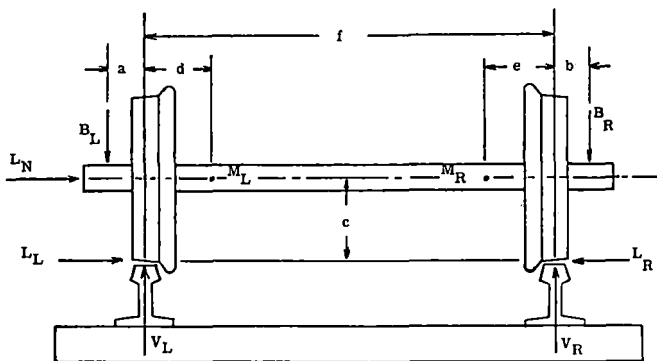


Figure 1

Four particular equations of equilibrium can be derived from it. Equation 1 and Equation 2 state the condition of equilibrium about the left hand instrumented point of the axle with one equation referenced to the left hand forces and the other referenced to the right hand forces.

$$1. M_L = L_L c + B_L (a+d) - V_L d$$

$$2. M_L = L_R c + B_R (b+(f-d)) - V_R (f-d)$$

Equation 3 and equation 4 similarly give the condition of equilibrium about the right hand instrumented axle point.

$$3. M_R = L_L c + B_L (a+(f-e)) - V_L (f-e)$$

$$4. M_R = L_R c + B_R (b+a) - V_R e$$

In these equations the values of "a", "b", "c", "d", "e" and "f" are known physical dimensions which were established when the axle was instrumented. The values of "M_L", "M_R", "B_L" and "B_R" are the measured quantities from the instrumentation. If equation 1 and equation 3 are solved

as a simultaneous pair to eliminate the unknown left lateral value (L_L), the resulting equation 5 gives the left vertical force (V_L) in terms of known or measured quantities.

$$5. V_L = \frac{M_L - M_R}{f - d - e} + B_L$$

If the same two equations are solved to eliminate the unknown left vertical force (V_L), the resulting equation 6 gives the left lateral force in known terms.

$$6. L_L = \frac{M_L - M_R}{f - d - e} \left(\frac{f-e}{c} \right) + \frac{M_R}{c} - B_L \left(\frac{a}{c} \right)$$

Using the same logic, equation 7 and equation 8 can be derived from equation 2 and equation 4 as expressions of the right vertical force (V_R) and the right lateral force (L_R).

$$7. V_R = \frac{M_R - M_L}{f - d - e} + B_R$$

$$8. L_R = \frac{M_R - M_L}{f - d - e} \left(\frac{f-d}{c} \right) + \frac{M_L}{c} - B_R \left(\frac{b}{c} \right)$$

Since the wheel set system is in equilibrium in Figure 1, equation 9 and equation 10 can also be written.

$$9. L_N = L_R - L_L$$

$$10. V_L + V_R = B_L + B_R$$

This analysis ignores the weight of the wheel set which is quite small compared to the static values of "B_L" and "B_R".

While the bending moments and load cell values are recorded on magnetic tape in real time on the A-333, the lateral and vertical forces are not computed on the car. This work is done on another computer after the measurement run is completed. Normally, some 16 hours are required to process approximately 250 miles of data. The final processed information is presented in strip charts to a scale of about 20 inches per mile. The left rail lateral force and the right rail lateral force are shown as independent data traces. The left rail vertical force and the right rail vertical force are also shown, but they are shown as dynamic values. The static load on each rail has been subtracted out in the computer. A corresponding L/V ratio is calculated during the processing of the data and is produced on the strip chart. Mile posts and other events which were manually input to the data recorder during the measurement run are also shown on the brush chart.

It was stated previously that the A-333 system is a practical tool for measuring the forces at the wheel to rail interface while the train is in motion. As with any tool, it has limitations and conditions of use. These must be recognized by the user.

On theoretically perfect track the only significant velocity is in the longitudinal direction. This is the speed of the train. Lateral or vertical velocities and accelerations are zero. As the wheel enters a geometric defect in the track, it must begin to move laterally, vertically, or both in following the guide of the rail. In so doing it will gain a temporary velocity in other than the longitudinal direction. The greater the longitudinal velocity of the wheel, the faster it must adjust to the configuration of a given defect.

Acceleration is defined as the rate of change of velocity with respect to time. The larger the velocity which is developed in following a given defect in a unit of time, the larger the associated accelerations.

Force is a function of mass times the acceleration of that mass. Therefore, as the vertical and lateral accelerations of the wheel, or the car, increase when adjusting for a track defect, the resulting vertical and lateral force levels increase. Conversely, for a given rate of acceleration a change in mass produces a change in force levels.

The outputs of the A-333 system are therefore highly sensitive to the speed of the train. Forces developed at 25 miles per hour will be significantly different than forces recorded at 35 miles per hour. In order to produce force level data that can be meaningfully compared from one measurement run to another, it is necessary to maintain a relatively constant train speed during all data collection runs. The Bessemer has arbitrarily set this speed at 35 miles per hour.

For the same reason it is necessary to maintain the weight of the instrumented car within small percentage limits between force data collection runs. It is also necessary to maintain the distribution of that weight within similarly close tolerances.

Because the car body and lading are a sprung mass, the condition of the spring nest is important and requires periodic inspection. The forces generated by the car body accelerations, and transferred to the wheels through the spring nests, are governed by the equations of harmonic motion. These equations include a term of the spring constant. With differing constants, identical anomalies on each rail will not give identical force results.

It should also be recognized that geometric defects in the track are seldom symmetrical. As a result, bi-directional repeatability of force levels is questionable. The vertical and lateral accelerations experienced by the system will differ, dependent upon the direction of train movement. While force levels of relative magnitude can be expected from the same defect when the direction of motion is reversed, the actual magnitudes can be significantly different. Force levels for track quality

comparison purposes should always be taken in the same direction of travel. Bi-directional force level comparison or analysis should be avoided.

The final force level data for the 250 miles of a measurement run requires some 400 feet of brush chart. Normally, two man days of office work are required to review these strip charts and identify the anomalies which are found in terms of locations on the track. High lateral or vertical force spikes, or high L/V ratios, are significant, as are abrupt changes in the magnitude of any of the force levels. Areas of significantly elevated forces are located and recorded. Generally, vertical forces exceeding 17,500 pounds, or lateral forces exceeding 18,000 pounds, are indicative of geometric defects which may violate Class 3 Track Safety Standards. It is very seldom that L/V ratios in excess of 0.50 are found.

Working with these strip charts, the engineer can often tell the general type of defect which produced the force levels. High vertical forces usually relate to profile, or track surface, defects. High lateral force spikes indicate crosslevel or alignment irregularities. A uniform elevation of lateral force levels usually occurs in a curve, although a smooth curve with balanced elevation may show little change from tangent track. Abrupt spikes in an elevated portion of the lateral traces also suggest misalignment or a crosslevel change in the curve. A sudden change in the lateral forces at the end of a curve indication is probably the result of a defective spiral.

Each of the anomalies located on the strip chart must still be analyzed in the field. The Roadmaster, or Track Supervisor, will inspect the location to determine exactly what the defect is and how it may best be corrected. The Bessemer is having considerable success with this program. It is being used to determine where and when portions of the track begin to exceed the geometric limits of most parameters of the Track Safety Standards. While force levels cannot accurately tell the exact magnitude of a geometric defect, or the nature of defects if more than one is present at a location, high force levels do indicate imperfections which should be called to the attention of the track maintenance forces. Field supervision is now anxious for the defect location report following each measurement run. They are prompt to analyze and correct the more serious deficiencies.

The A-333 system is usually run some five times a year over our entire Main Line. The first measurement run is scheduled for late April, after the frost has left the ground. Subsequent measurement runs are made every six to eight weeks until early November. The system is not operated during the winter months, primarily because of the frozen condition of the ballast and subgrade.

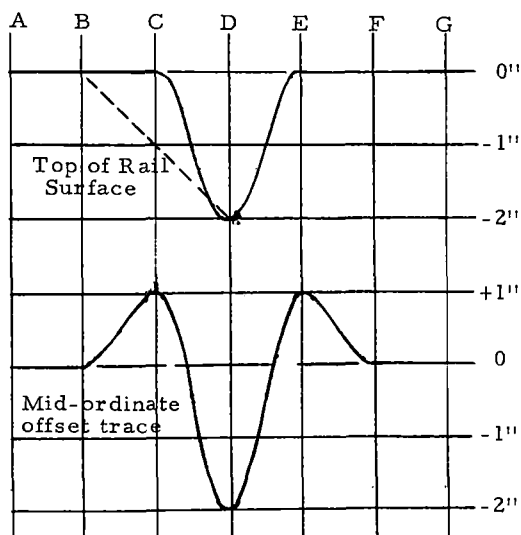
In addition to the practical success which the Bessemer has had in using this system to monitor

track conditions, distinct relationships have been found between recorded geometric track data and corresponding force data. The A-333 system and a track geometry measurement car have been run together in the same consist and the outputs of the two have been compared. Much of the remainder of this paper will discuss these comparisons.

An attempt to relate track geometry measurement system data with force level data should recognize that the geometry traces are not necessarily an accurate picture of the track in the field. This is particularly true of the profile parameter, but it can also apply to any parameter where the significant defect value is expressed as the mid-ordinate of a chord of stated length. Profile traces are the plots of the vertical offset of the top of rail from the midpoint of a moving chord. The ends of the chord are assumed to be resting on the top of the rail.

The chord method is the simplest, practical means of determining profile in the field. The concept is in general use throughout the railroad industry and is specified by the FRA Track Safety Standards. But, when the calculated mid-ordinate offset values of a moving chord are plotted as a continuous trace, the chord method can give false readings. Artificial high spots are created. Low spots are often understated. At times a genuine low spot in the track can be lost.

The upper line in the following trace represents a profile defect in the surface of one rail. The defect is 62 feet long and two inches deep at its center. It is also symmetrical. Stations "A" thru "G" are each 31 feet apart. The lower line is the continuous mid-ordinate offset trace determined by a moving chord of 62 feet in length. Since points "A", "B", and "C" are in the same plane, when one end of the chord is at "A", and the other end is at "C", the offset at "B" is zero. The reading on the chord trace at "B" is then zero.

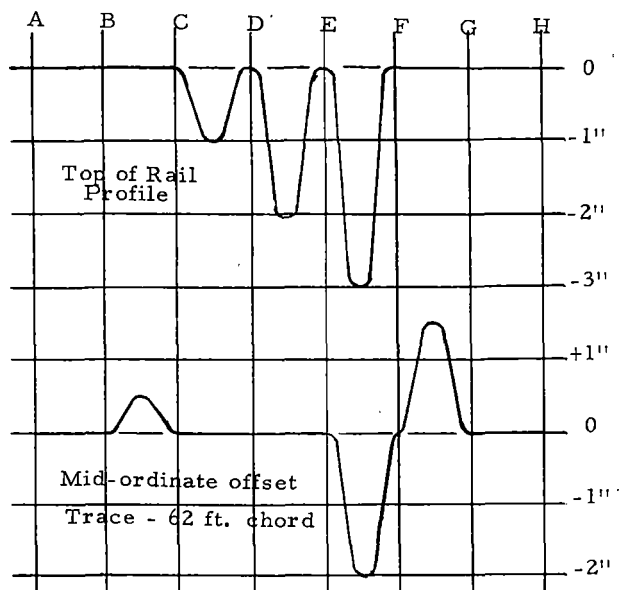


As the chord moves to the right along the defect, the right end begins to drop until at "D" it is two inches below the supposed top of rail. The left end of the chord is now at "B", as shown by the broken line in the surface trace. The true elevation of the center of the chord, which is at "C", is the average of the actual elevations of the two ends, or one inch low. Since the top of rail elevation at "C" is actually zero, the vertical offset measured at "C" is plus one inch. The chord trace shows a false high spot of that magnitude at "C".

As the chord continues to move to the right, the right end begins to rise out of the defect until at "E" it is at zero elevation again. The left end is now at "C" where the top of rail elevation is also zero. The elevation of the midpoint of the chord, which is now at "D", is therefore zero. But the actual elevation of the top of rail at "D" is minus two inches. Thus, the vertical offset of the mid-point of the chord is minus 2 inches, or 2 inches low.

As the chord continues to move to the right, this process is repeated until the mid-ordinate offset trace is complete. The resultant trace is symmetrical, but has two false high spots. In this example, the low point of the top of rail profile defect is accurately recorded in terms of location and magnitude.

In the next trace the top of rail surface shows three consecutive low spots. Each is 31 feet long and each is symmetrical. From left to right they are one inch, two inches, and three inches low respectively. The mid-ordinate plot of the moving 62 foot chord shows the three inch low spot to be two inches low, but completely masks the first two spots. Because of the configuration of the defects in respect to the length of the chord, the chord sees the first two defects as perfect track.



The preceding traces are special cases, selected to demonstrate the potential deficiencies in the chord method. They show that the pictured top of rail profile in the following exhibits is not necessarily the top of rail profile as it exists in the field. However, the forces shown in the exhibits are the actual forces generated at the wheel to rail interface as the reaction to the stimulus of the track configuration encountered.

Typical vertical force traces are shown in Exhibit I. Even on very good track there is a constant cycle of force which results from vertical movements of the car body. Normally, these force level peaks are only 5,000 pounds to 7,000 pounds above static loading. When more noticeable deviations in the rail profile occur, the magnitude of the vertical force oscillations increases on both rails and can reach peaks of as much as 25,000 pounds above static. Once a force cycle has been generated the excitation will continue for some five to twenty cycles before it dies out. In the comparison study, it was found that short chord profile irregularities generate forces of higher magnitude than long chord irregularities. There appears to be several explanations for this. The 14-1/2 foot

chord is so short that it cannot span most significant defects. Therefore, while the magnitude may be understated, the defect will be shown. On the other hand, the 62 foot chord will more than span most perturbations and therefore may distort or mask them.

If the sine wave is used as the idealized configuration for a profile irregularity, the maximum vertical acceleration will occur at the quarter points, since this is where the slope of the curve is the greatest. A defect which is 62 feet long will require a magnitude of more than two inches to produce the same maximum slope of the curve as a defect which is 14-1/2 feet long with a magnitude of one half of an inch. At the same time, the distance between the quarter point and the mid-point of such an idealized 62 foot irregularity is more than four times the distance for a 14-1/2 foot defect. This is the area of deceleration. At constant train speeds the wheel will require more than four times as long to traverse this area.

Geometry measurement car runs on the Bessemer will seldom find a half dozen Class 4 profile defects - that is, two inches low as the mid-ordinate of the 62 foot chord. It is possible that the lack of correlation between long chord irregularities and high dynamic vertical forces is also due in part to a lack of serious defects of this nature.

Typically, the magnitude of the dynamic vertical force level on one rail is approximated by the dynamic vertical force level on the opposite rail. Even though the profile imperfection is only in one rail, the action of the wheel set in following the change in the cross-level plane will cause a vertical reaction of the car body. The force of this reaction is transferred by the body bolster to the truck bolster which in turn transmits it through each of the side frames to the wheels.

From the foregoing it can be seen how "poor" track becomes "bad" track, or how a profile irregularity can propagate into "rough" track. Once a cycle of high vertical force has been generated, additional cycles of high force will be applied to both rails until the oscillation dies out. Similar cars, with similar lading, at similar speeds (as with unit trains) will generate almost identical force patterns at the location. When the ballast, or sub-grade can no longer constrain these repeated loadings, the track surface will progressively deteriorate.

In Exhibit II the dynamic vertical forces reach a maximum which exceeds 20,000 pounds. Yet, these forces do not relate to any sizable profile irregularities. Instead, they are caused by a series of five short chord imperfections any one of which, by itself, would not cause a serious increase in the force levels. The longitudinal distance between each of these spots is approximately the same. Each spot on the east rail has a deviation opposite

Exhibit I

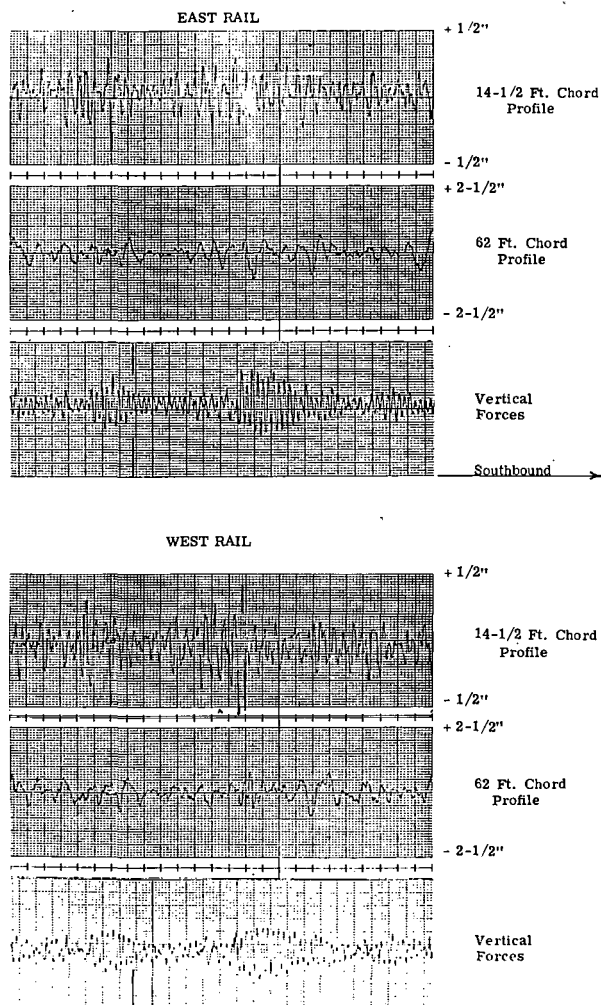
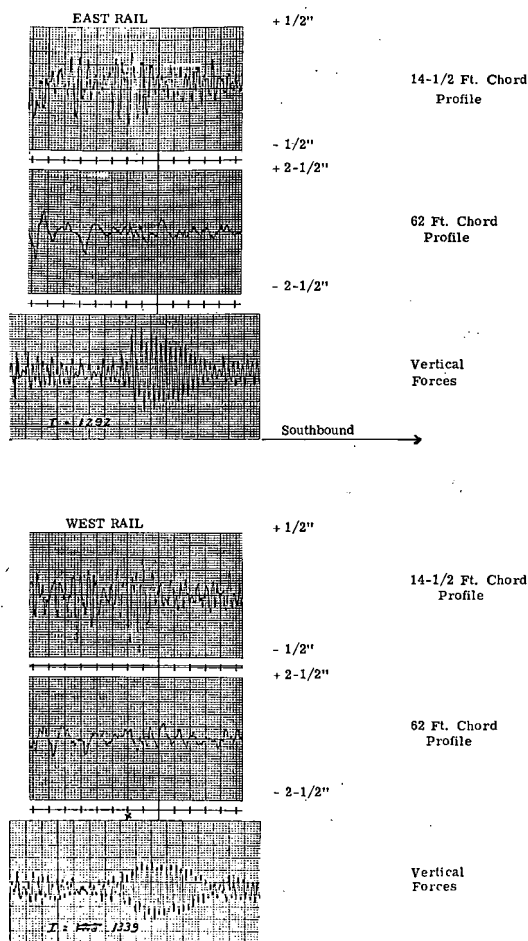


EXHIBIT II



it on the west rail. The track is laid with continuous welded rail. Acting together, the series of spots set up a harmonic oscillation in the car body. Each cycle reinforces the previous cycle. Surface deterioration will progress until corrective action is taken.

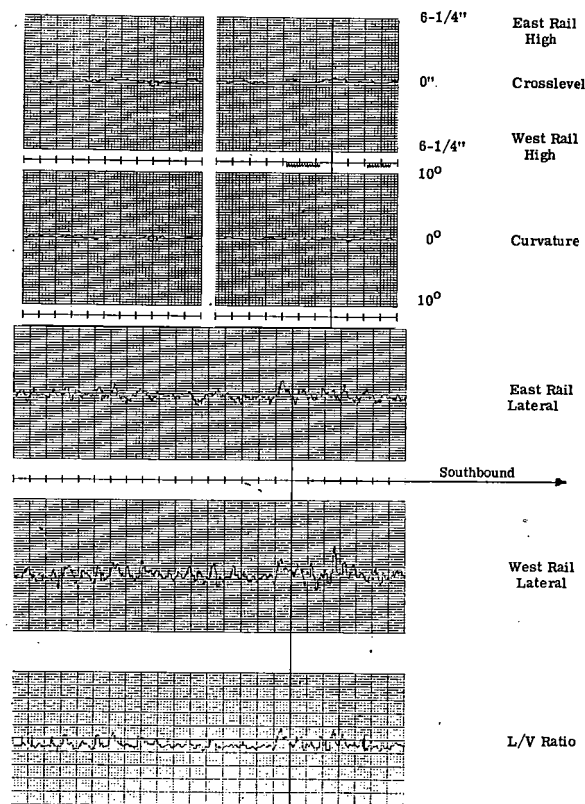
In these two exhibits the vertical force level patterns on the two rails are in phase. That is, their maximums occur simultaneously on both rails, as do their minimums. This in-phase condition indicates that the car body is in a bounce or pitch mode. As stated before, the train speed is 35 miles per hour. At speeds of ten miles per hour to twenty miles per hour the car body would be in a rocking mode and the opposite rail vertical traces would be out of phase. The Bessemer has used the A-333 system to determine the critical rock and roll speeds and the resulting vertical forces for various designs of our cars. This work has been done on both tangent and curved track.

Lateral forces of undesirable magnitude are most generally produced by irregularities in the crosslevel and alignment parameters. Exhibit III

represents a stretch of tangent track with good alignment and crosslevel. The resulting lateral forces and associated L/V ratios are low. But, relatively minor changes in crosslevel can produce significantly high lateral forces.

When one rail drops in relation to the opposite rail, and thereby suddenly induces a super-elevation effect in the track, a rotational acceleration is induced in the car body as the wheels follow the guiding of the rail. This rotational acceleration has a sizable lateral component directed toward the lower rail.

EXHIBIT III



In Exhibit IV the alignment is as uniform as in Exhibit III. However, the crosslevel is more irregular with two locations which show anomalies at the limit of Class 4 track. There is a lateral force peak associated with each of these and the peaks approach 20,000 pounds. It is interesting to note that there are no severely elevated L/V ratios related to these lateral force peaks. The rotation of the car body also has a vertical component on the low rail which tends to keep the ratio of the lateral and vertical forces low.

When an object moves in a circular path, it develops a radial acceleration which is a direct function of the square of its lineal velocity and an inverse function of the radius of the circle. The greater the speed or the sharper the curve (shorter the radius) the greater this radial acceleration. The larger the radial acceleration of a railroad car as it negotiates a curve, the greater the lateral

force produced by the wheels against the outer rail of the curve. This lateral force can be reduced, or even eliminated, by elevating the outer rail of the curve so that the resultant of the lateral and vertical forces of the car is normal to the plane of the top of the two rails. Thus, a car moving around a uniform curve with proper, or balanced, super-elevation will produce no significant dynamic lateral forces on either rail.

not enough to produce significant lateral forces. By FRA Track Safety Standards the curve is elevated for a maximum speed of 55 miles per hour.

EXHIBIT V

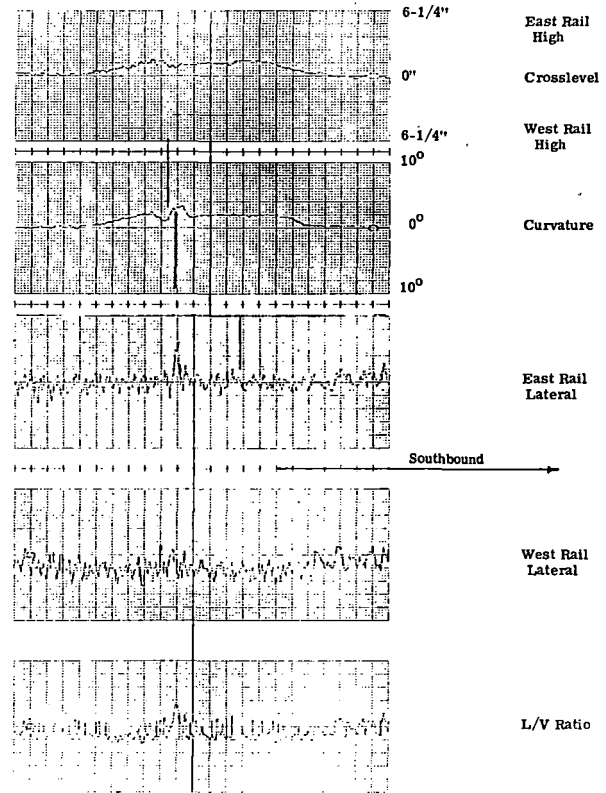


EXHIBIT IV

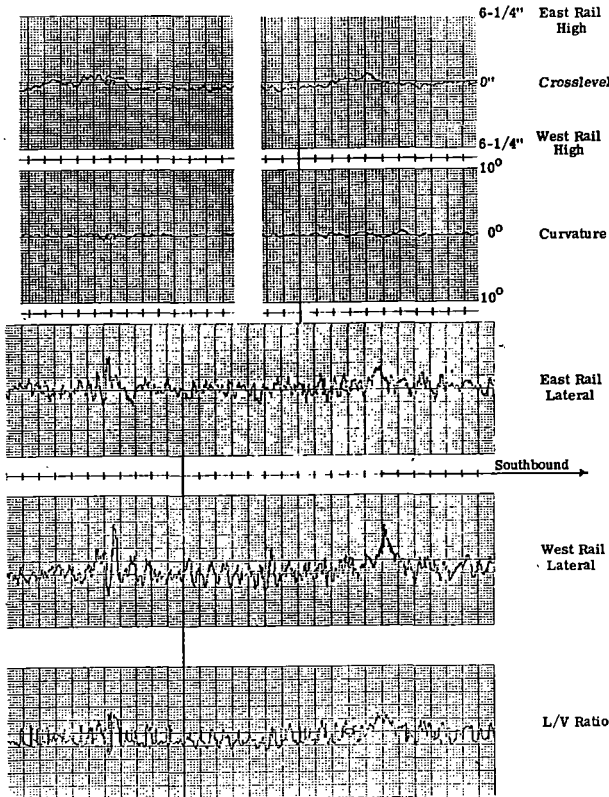


Exhibit V is an example of this. It shows a two degree curve to the west. For the most part the curve is uniform and the easement spirals are quite acceptable. However, near the north third point there is a misalignment, which changes as much as 1.8 degrees in less than 31 feet. It is a defect which violates Class 3 Track Safety Standards and permits a speed of no more than 25 miles per hour.

The lateral force traces are generally low and indicate well lined track with good crosslevel and super-elevation. The east lateral trace, however, shows a peak exceeding 15,000 pounds, 2-1/2 to 3 times the other laterals, associated with the misalignment. This change in lateral forces would be expected since there is no compensatory adjustment of super-elevation. The L/V ratio also elevates at this location.

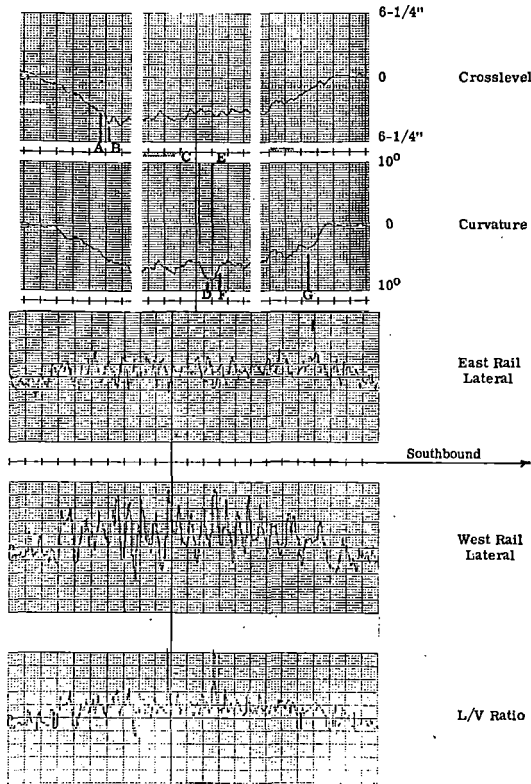
At point "A" the curvature is 1.2 degrees. The corresponding radius of curve is 4,800 feet. At point "B" the curvature has increased to 3.0 degrees with a corresponding radius of 1,900 feet. The change in radius alone should increase the unadjusted lateral forces by about 2-1/2 times.

Balanced elevation can be maintained for one specific train speed only. Had the A-333 system been traveling at 45 miles per hour, an elevation of nearly three inches would have been required for balance. With an unbalance elevation of at least 1-1/2 inches, the system would have measured elevated lateral forces on the outer rail.

Crosslevel throughout the curve is generally smooth and averages about 1-1/4 inches. Balanced elevation in a 2-degree curve for a 35 mile per hour train speed would be approximately 1-3/4 inches. Therefore, the curve is slightly under-elevated, but

Unacceptable track shows up dramatically in the A-333 force traces. The six-degree curve in Exhibit VI is poorly lined and badly elevated. Lateral forces in excess of 25,000 pounds and L/V ratios exceeding unity result. At point "A" the super-elevation is 3-1/4 inches while at point "B" it is 4-1/2 inches. This is a change of 1-1/4 inches of super-elevation in 31 feet in the spiral. The spot is at the limit of Class 3 track standards.

EXHIBIT VI



At point "C" the curvature is 5.6 degrees while at point "D" it is eight degrees. This change more than exceeds the intent of Class 3 Track Standards and maximum speeds should be reduced to 25 miles per hour. The radius of curvature at point "D" is 1,025 feet while at point "D" it is reduced to 715 feet, a factor of 1.4 effect on the radial acceleration. Actual elevation at point "C" is 3-1/4 inches while balanced elevation for 35 miles per hour would be 4-3/4 inches. Super-elevation is 1-1/2 inches unbalanced entering the alignment defect but it is within the three inches unbalance allowed by the Track Standards. At point "D" the actual elevation is also 3-1/4 inches while balanced elevation should be 6-7/8 inches and exceeds the allowable unbalance of the Track Standards.

At point "E" the curvature is 8.4 degrees while at point "F" it is 6 degrees. Again, the change more than exceeds the intent of Class 3 Track Standards. Actual elevation of the high rail at point "E" is 3-1/4 inches. Balanced elevation for 35 miles per hour would be 7-1/4 inches. The curve at point "E" has four inches of unbalanced elevation. At point "F" the elevation is only 1-3/4 inches and thus falls within the allowable unbalance of three inches. One of the two L/V ratio peaks is associated with the defect area between points "C" and "F". This peak approaches 1.25 and is serious cause for concern.

At point "G" the mismatch of crosslevel and curvature, in part due to the poor spiral alignment, produces 1-3/4 inches of unbalanced elevation.

While this condition does not exceed the allowable three inches of unbalanced elevation, it is great enough to produce a significant lateral force. Just to the right of point "G" the curvature changes by at least 2-1/2 degrees in 31 feet and violates the intent of Class 3 Track Standards.

There is also a particular condition of profile which can affect the dynamic lateral forces measured in a curve even though the curvature is excellent and the super-elevation is smooth and balanced. If there is a profile defect on each rail, such that the cross-level (or super-elevation) is not affected, the profile defect will cause a change in dynamic vertical forces. The change in the vertical forces alone will change the direction of the lateral-vertical force resultant so that it is no longer normal to the plane of the rails. As a result, a change in the lateral force will be generated and recorded.

Unfortunately, there is one parameter of track geometry which cannot be monitored by the A-333 system. Gage widening may, or may not, be detected. On tangent track the wheel will tend to follow a relatively straight line even though the gage is one inch wide. In such a case there would be little or no lateral acceleration of the wheel to produce lateral forces. Wide gage in a tangent might aggravate truck hunting and the lateral accelerations that result. However, significant hunting is seldom found at the speeds allowed on the Bessemer. Bolted rail on the high side of a curve may develop gage widening at the joints. If the spot is short enough and the gage widening is great enough, the wheel will sense it as an alignment defect. Significant lateral forces may result. However, when the track is laid with continuous welded rail, the weak spots represented by the joints are absent. Gage widening, if it occurs, will be of greater length and less magnitude. The resulting lateral forces could well be insignificant. An area where the gage measures as much as 58 inches in an otherwise well lined and elevated curve would probably not generate lateral forces of sufficient magnitude to alert the operator. This is particularly true if the area of gage widening is more than 10 or 20 feet long.

In addition to monitoring the quality of Main Line track and studying the ride stability of cars, the Bessemer has used the A-333 system to investigate derailments where car body motion was a possible cause. On several occasions the system has been used to determine the effectiveness of the radial, or self-steering truck, in reducing the lateral force of the wheel on the rail.

In summary, the force level data obtained from the A-333 system can provide a good indication of the general geometric condition of the track. It can provide a valid means for quality control of geometry related track maintenance. It can furnish a useable method for monitoring the ride quality of track. Because geometric irregularities are the chief source of excitation of high dynamic forces, use of

the A-333 system has enabled the Bessemer to reasonably eliminate major geometric defects.

The force level data obtained from the A-333 system cannot be used to determine the exact nature or magnitude of geometric track defects. It cannot be used to guarantee the absence of geometric violations of the FRA Track Safety Standards.

Ideally, it should be used as a program to reduce dynamic force levels. The measurement system would be operated on a scheduled basis and the location of the highest vertical, lateral, and L/V readings would be reported to the Track Department for corrective maintenance work. In this way the magnitude of the higher recorded forces would be gradually reduced and developing imperfections are identified. The overall geometry of the track is improved. The ride quality becomes better.

It is also possible to analyze the output data statistically to provide quality rating values for discreet lengths of track in much the same fashion that statistical values have been applied to track geometry data. These quality rating values provide good measures of the deterioration of the track with time and traffic; or measures of the improvement in the track as a result of maintenance work.

The speed sensitivity of the force measurement system must be recognized if the program is to be a success. A standard measurement train speed of 35 miles per hour would appear best suited to Bessemer requirements. This is the maximum allowable speed for Main Line Trains and can be maintained over most of the railroad.

Dynamic force levels recorded on the instrumented hopper car will not represent the actual force levels produced by every other car. High force levels on the instrumented car should equate to relatively high force levels on other types of cars.

Track & Vehicle Maintenance Management on the Mt. Newman Mining Railroad

Dr. J.H. Brown

Superintendent
Technical Dept., Railroad
Mt. Newman Mining Co.
Western Australia

M.G. Baggott

Superintendent
Permanent Way Dept.
Railroad
Mt. Newman Mining Co.
Western Australia

The Mt. Newman Mining Railroad has now carried some 600 million gross tonnes on its single line track. Comprehensive studies of defect occurrence and wear rates of the rail have led to the use of optimised rail grinding and rerailing practices. A computer based track history system has allowed automated gathering and collation of track component performance. Head hardened rail will be used to rerail curved and tangent track and steel sleepers have been chosen to replace the timber sleepers. A locomotive and ore car condition monitoring system known as TRAINDATA involving axle load, bearing condition, draft gear condition, wheel profile, automatic car identification and loco logging is in development. These improvements have allowed an increase in operating axle load from 30 tonnes to 32.5 tonnes with planned trials of 35 tonnes.

INTRODUCTION

The Mt Newman Mining Company carries about 50 million gross tonnes (MGT) of traffic annually over its 420km railroad with 30 tonnes axle loads, 10 trains per day and single line operation (Appendix 1).

The current operating budget for Track Maintenance amounts to about \$25,000,000 annually, of which 30% is for maintenance of rail, 15% is for sleepers and 5% is for the ballast and formation. The budget for Rolling Stock Maintenance is about \$40,000,000 annually, of which 60% is for wheels, 12% is for draft gear and 11% is for bearings. The total cost of transporting the ore is about \$2.00 per tonne.

The track was originally built with 66kg rail, non-treated timber sleepers spaced at 533mm, dog spike fastenings with double shouldered AREA base plates at 1 in 30 cant. Early problems of splitting and general deterioration of the sleepers due to environmental attack and termites led to the need to use sleepers treated with creosote and furnace oil. During a period of extensive rail transposition the AREA plates in curves and 1 in 4 in tangent track were replaced with Pandrol plates.

THE FORMATION AND BALLAST

Relatively little routine maintenance has been required on the formation because the original design was conservative and construction work was performed to a high standard. Figure 1 shows a typical track cross section. In the past the

ballast type has been granitic rock whereas basaltic rock is now being used.

The track is subject to flood damage and in some parts the surrounding country-side is so flat that there is no definable water course. The water may run parallel to the track and scour the toe and shoulder. Wave action in some parts has eroded the formation.

The ballast also has received relatively little maintenance except that at about 250MGT a general lift of 50mm was performed increasing the ballast depth to 300mm. The tamping cycle appears to be about 150MGT with the quality of trial geometry being closely monitored using an EM80 Track Recording Car. Geometry degradation rates are calculated for about 900 track segments over the 470km length.

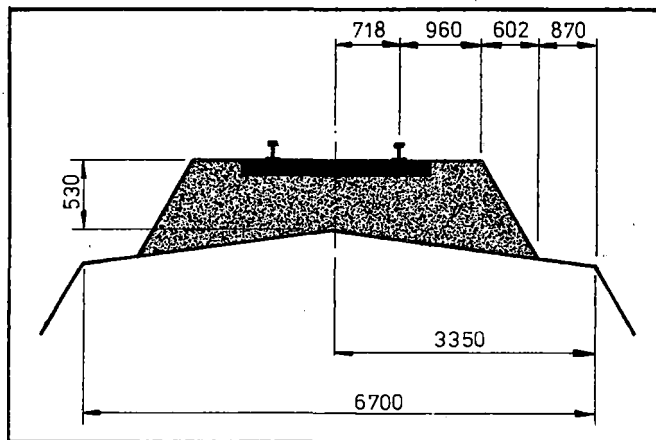


Fig. 1 Typical Track Cross Section

A survey of ballast bed conditions is underway at selected locations, using four methods, namely,

- (a) the track supervisors assessment
- (b) conventional sieve analysis
- (c) deflection measurements using a Laser system
- (d) ballast density

The performance will be correlated against track maintenance costs and the definition of economically poor ballast will be used in monitoring ballast degradation. Economical time for changeouts will then be determined.

SLEEPERS

It became clear early in the life of the railroad that the untreated timber sleepers had very short lives, typically between 3 years and 8 years. A study was undertaken to evaluate alternative sleepers and preference was given to the manufactured sleepers such as steel and concrete, in which uniformity of product from one sleeper to another is assured.

The cost of timber sleepers track per kilometer was determined to be \$108,000 excluding jewellery (which was to be reused from the existing sleepers), concrete sleepers track was \$110,000 and steel sleepers track was \$105,000. The technical considerations included steel sleeper mass, which is about the same as an equivalent timber sleeper and

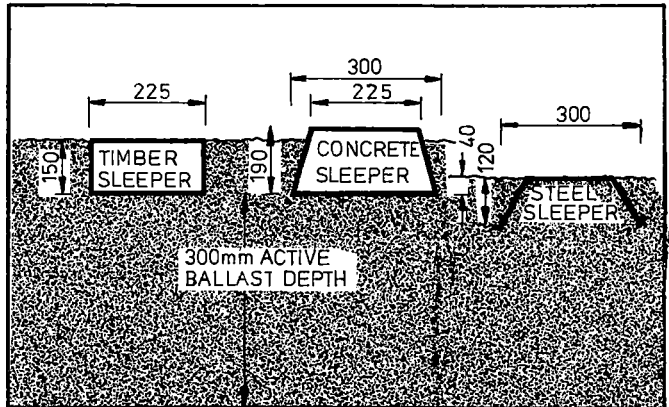


Fig. 2 Cross Sections of Typical Track Structure

about 1/3 that of an equivalent concrete sleeper. The steel sleeper track is considerably more stable than timber sleepers track because the shape of the sleeper beds into the ballast, as shown in Figure 2.

Historically the major problems with steel sleepers have been the fastener and electrical insulation. In choosing the fastener, fatigue life, inspection practices, ease of application and cost were considered. The Omark Trak-Lok II fastener was chosen. In addition, considerable work was done on the insulation pad, and the type finally chosen wraps around the rail foot as shown in Figure 3.

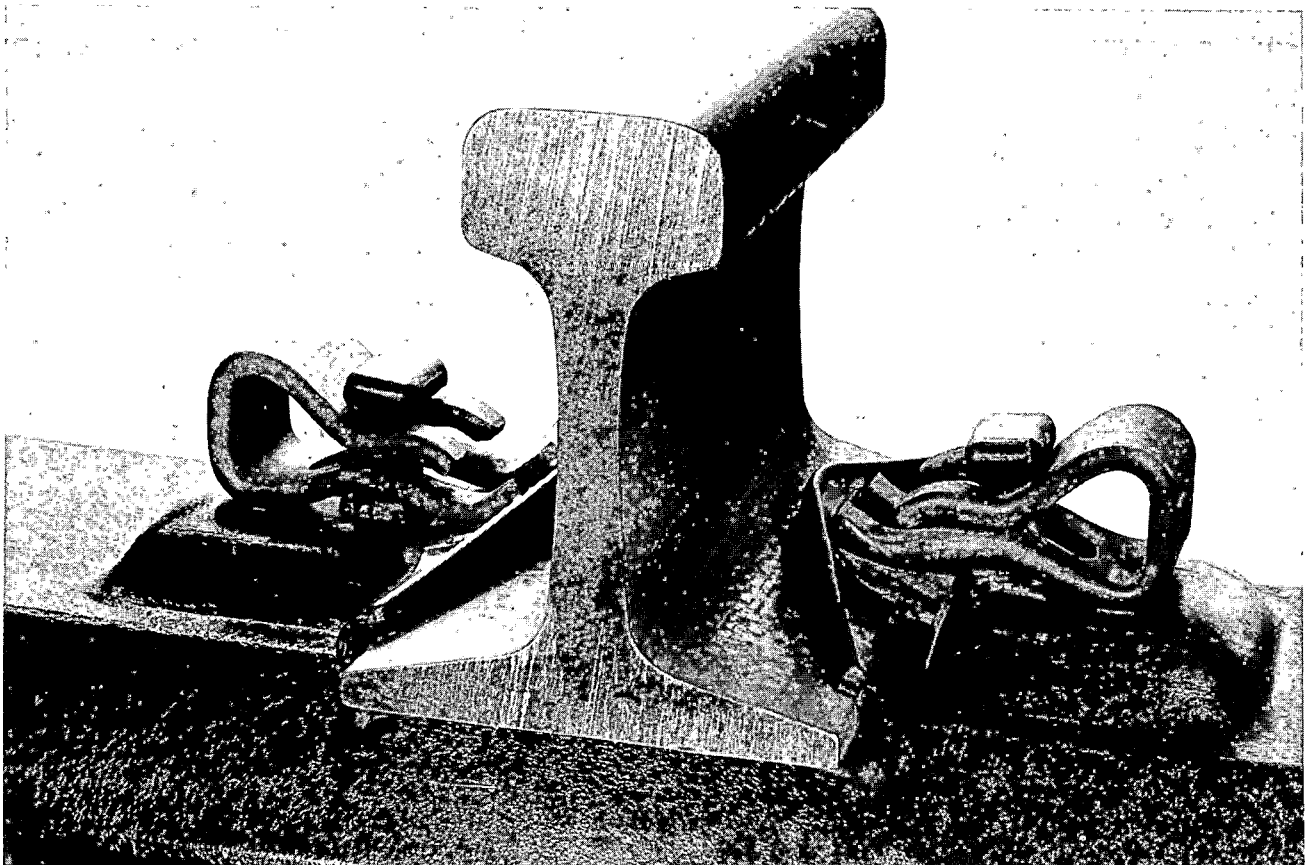


Fig. 3 The Heavy Haul Steel Sleeper with Traklok Fastener and Pad

Tamping of the sleepers was carried out with standard machines. It was shown that the ballast "pod" was formed after one insertion of two squeezes, see Figure 4. No additional ballast was necessary in laying these sleepers. In the case of steel sleepers the active ballast depth is approximately 40mm greater than for the original timber sleepers because the hollow shape of the sleeper allows ballast all the way up to near the top surface, as shown previously in Figure 2.

The resleeping method is essentially manual and is described schematically in Figure 5. The relatively light weight of the steel sleeper makes manual handling easy. In addition to the mass resleeping, track gangs without machines insert the steel sleepers in bad locations such as tight curves where lateral stability has been a problem with timber sleepers.

The steel sleepers were proved in the laboratory at Melbourne Research Laboratory of the Broken Hill Proprietary Co Ltd., and in track over three years of 180 MGT of traffic. The trial section has been described extensively in previous papers (eg Brown, 1980) and included Pandrol and Trak-Lok fasteners, 660mm and 600mm spacing, tangent and curved track and two different sleeper thicknesses. It was shown that the sleeper life will be at least 40 years. There has been very little change in track geometry over the 180MGT and surfacing is expected to be required after 250MGT. A spacing of 660mm has been chosen for all future installations.

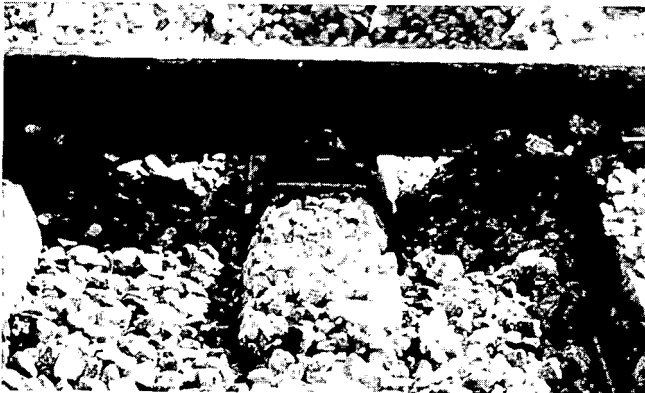


Fig. 4 Ballast Under Sleeper After One Tamp

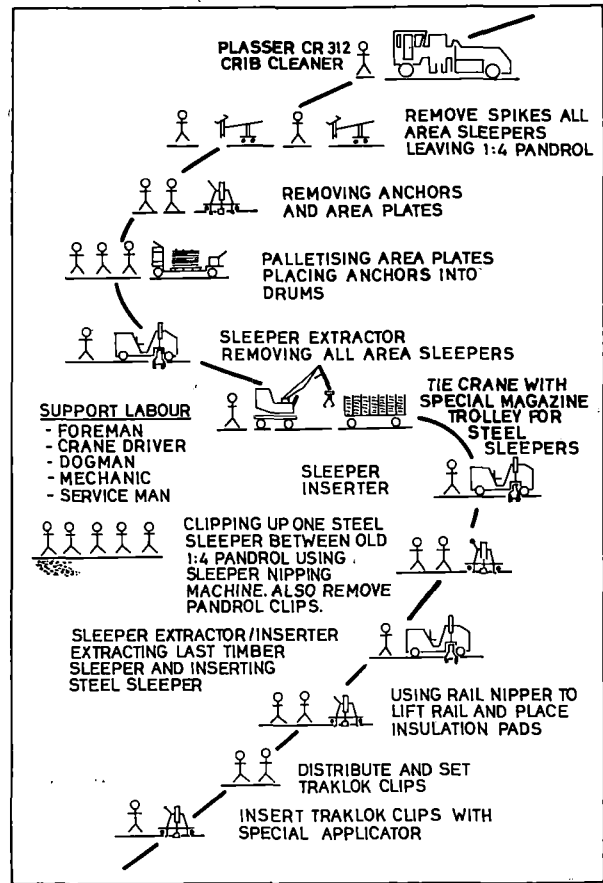


Fig. 5 Resleeping Method

To locate failed pads a device known as PADSEEK was developed which may be towed behind a Hi-rail vehicle at 20 kph over the suspected section of track. Pad life was expected to be more than 10 years.

Mt Newman Mining ordered 190,000 steel sleepers for delivery in Ore Years 13 (which commenced April 1, 1981), 14, 15 and 16.

Steel sleepered turnouts are also being used. The only equipment required to fabricate the turnouts are, a saw to cut the sleeper bar to length, a drill to make holes of approximately 30mm diameter for the fastener and a jig for pressing the ends to the spaded shape.

THE RAIL

The life obtained to date from standard carbon rail of 600 MGT is amongst the longest achieved anywhere. The principle track management tools used to achieve this have been transposition and rail grinding (e.g. Townend and Marich, 1978). Profile grinding of the rail is in use to provide better vehicle tracking, particularly around curves. A rail planer is being considered to supplement the grinding machines.

Grinding is also beneficial in controlling defect growth, however, because the bulk of the Mt Newman Mining Rail is semi-killed standard carbon steel,

the occurrence of transverse defects is prolific. It is essential that defects are located and cut out before they grow to catastrophic proportions and accordingly, ultrasonic rail inspections are made every three weeks.

A rail management model has been developed in conjunction with MRL (Roney, 1980). The model allows the track to be divided into various sections, (eg. all curved track of a specified radius or discrete lengths.) This has permitted reliable categorization of defect occurrences as shown in Figure 6. The analysis provides a prediction of occurrence of defects and thus an economic case can be made for continuation of defect repair or rerailing.

In addition a study showed that the cost optimum plug length for rail renewal was 400 metres. Combining this data with the optimum rail renewal times led to ranking of the entire track in discrete 'modules'. The priorities will be updated on a continual basis when more defect data become available and as costs change.

MRL work (Curcio, 1979) has shown clearly that head hardened rail is cost effective in curved track where the wear life is increased by factor of 2, and the cost is increased by a factor of 30%, in comparison to standard carbon rail. However, as vehicle curving is improved by more effective grinding, the amount of wear on rails and curves will become less and rail life will be controlled more and more by fatigue rather than wear.

An economic study was undertaken to evaluate the cost benefit of using fully-killed head hardened rail in tangent track. The study covered such factors as fatigue defect occurrence, reduced grinding, reduced inspection requirements, etc, and it was shown that the fatigue defect occurrence aspect was a controlling factor. An additional benefit is obtained with the head hardening in that the yield strength and fracture toughness are high. Results of the economic analysis are given in Table 1 where it is shown that head hardened rail is cheaper in tangent track than standard rail.

RAIL CHARACTERISTICS	STANDARD CARBON RAIL	HEAD HARDENED RAIL
YEILD STRESS (MPa)	490	850
HARDNESS (HB)	260	340
PURCHASE COST	63.0	80.0
FATIGUE DEFECT COSTS	24.0	2.4
TRACK INSPECTION COSTS	4.0	3.0
GRINDING COST	12.0	7.8
TRACK MAINT. COST DUE TO RAIL DETERIORATION	3.0	1.8
TOTAL COST	106.0	95.0

Table 1. Rail Costs per Track Kilometer (\$1000) (Assumed 15 Year life @ DCF ROR of 15%)

Rail Maintenance Management

A Track History System has been developed for job reporting. An inspector reports the job type,

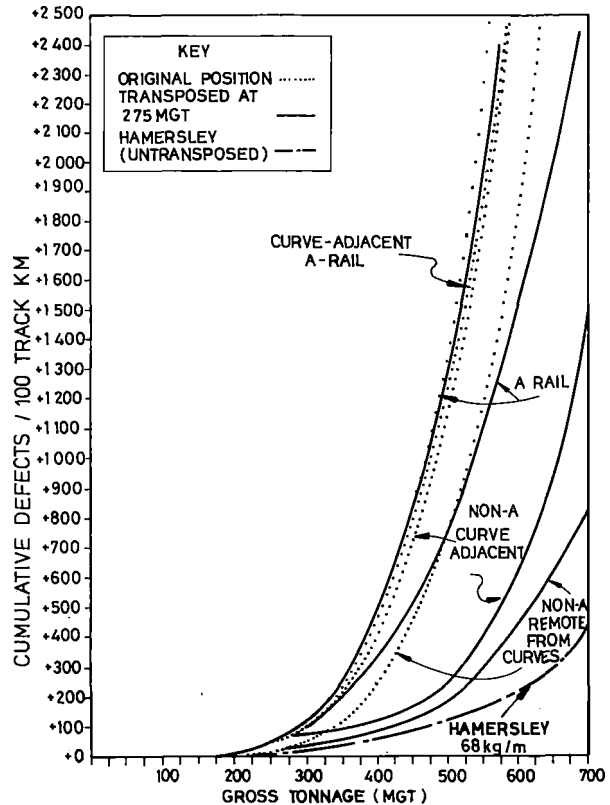


Fig. 6 Defect Occurrence in Various Rail Categories

location, severity of defect, priority, man hours required to do the job, the material required and the latest date the job is to be done on an Inspection Sheet shown in Figure 7.

As well as recording the jobs actually required other parameters are also stored. These include track geometry index, internal rail flaws, ballast modulus measurements, tonnage carried, rail wear, 'rerailing, resleeping, rail grinding, track machine work and costing information.

Each of the jobs recorded has attached to it a standard costing rate and so over a period of time it is possible to ascertain which parts of the track are costing more to maintain. This information is invaluable in assessing the economics of capital upgrades such as ballast changeout/cleaning, better quality rail or turnout component upgrade. It is also necessary for assessment of work which is to be included in longer term plans.

The general thrust of the system is to give those who plan the work and make policy decisions more knowledge and a better understanding of the track. This applies from the foreman who plans his gang's work up to the Superintendent who must determine where the highest priorities lie for the whole system.

The greater understanding achieved through the use of the system allows for a better decision to be made. If rail wear rates are accurately known proper planning can be done for rerailing using

SECTION: HEMAND		PERMANENT WAY TRACK INSPECTION SHEET		DATE COMPLETED: / /		TYPE: 15			
LOCATION: 1131.61		TRACK: 014	DATE REQUIRED: 12/03/81	SEVERITY: S 3	PRIORITY: 6	HISTORY REQUIRED: Y	JOB NUMBER: 30781		
DESCRIPTION OF WORK REQUIRED (40 characters recorded)									
DEFECT CODE	DEFECT NUMBER	JOB CODE							
D.3.1.0		CHANGE CLOSURE RAIL AND ONE INSUL INT ON GOLDSMORTHY SPUR.							
				ESTIMATED/STANDARD					
				NUMBER ON TRACK OF MEN	HOURS	TOTAL MAN HRS.			
				0,5	1,0	5,0			
SPECIAL EQUIPMENT REQUIRED				HOURS					
				EST.	ACTUAL				
DATE LOCATED 26 02 81 BY									
MATERIAL REQUIRED TO DO THE JOB									
MATERIAL CODE	DESCRIPTION	EST. QTY.	ACTUAL QTY.	N/S	MATERIAL CODE	DESCRIPTION	EST. QTY.	ACTUAL QTY.	N/S
M001	Anchor Rail 132 lb.				M351	Insulated Joint Portec Comp			
M011	Base-Plates Area				M391	Dog Spike			
M013	Base-Plates Pandrol 1-14				M396	Lock Spikes - Type LB			
M014	Base-Plates Pandrol 1-20				M397	Insulating Pads			
M015	Base-Plates Pandrol 1-30				M453	Rail Standard - 56 KG/M			
M020	Ballast Crushed Rock				M466	Rail Nippon Improved M/H-68 KG/M			
M021	Ballast Quarry Fines				M467	Rail Nippon Kolan M/H-68 KG/M			
M037	Bolt Head (1 1/2" x 1 1/8")				M532	Screws Coach			
M130	Clips Harpin				M581	Sleepers Area			
M131	Clips Pandrol RH				M582	Sleepers Pand Drilled 2 Ends			
M132	Clips Pandrol LH				M583	Sleepers Pandrol 1-14			
M133	Trak Lok				M584	Sleepers Pandrol 1-20			
M220	Fish Bolt - Ordinary Joint				M585	Sleepers Pandrol 1-30			
M221	Fish Bolt - Insulated Joint				M586	Sleepers Composite 1-20			
M222	Fish Plate - Insulated				M587	Sleepers Composite 1-30			
M240	Frog No. 10				M590	Sleepers Steel			
M241	Frog No. 15				M621	Switch Blades LH 1-10			
M242	Frog No. 20				M622	Switch Blades LH 1-15			
M280	Guard Rail 1-10				M625	Switch Blades RH 1-10			
M281	Guard Rail 1-15				M626	Switch Blades RH 1-15			
					M801	Grease (Kilograms)			
					M802	Oil (Litres)			

Fig. 7 Inspection Sheet

greater knowledge which allows one to make less conservative decisions with confidence. In some instances this will allow a deferment of expenditure. On the other hand the valuable information will assist in the justification for funds when they are really necessary.

The cost of the entire project was about \$250,000 and this expenditure was probably saved in the first year.

ROLLING STOCK MAINTENANCE

While unit trains are simple to operate, they present a special hazard in terms of epidemic failures because a large number of components such as couplers may reach a critical point in terms of fatigue life simultaneously.

Maintenance by repair of defects as they are identified makes it difficult to plan work straight into the workshop. As availability improves, less cars are in the queue and planning becomes more essential. To make preventive maintenance work, it is necessary to have a tracking system for the major components in the ore cars. With 2,000 cars, 16,000 wheels and 16,000 bearings, manipulating such numbers is only possible with a computer. A system known as The Component Tracking System was established for this purpose.

In addition a planning group was formed to look at the shop loading, spare parts required, layouts and improved working methods. A daily meeting is held

by the maintenance planner with the section foremen, at which the shop plan for the next four days is established based on ore cars waiting in the workshop queue.

It was decided to use the One-Spot facility in a flexible way, mainly as a rewheeling facility. A reconditioned set of bogies is fitted to every car that goes through it, and light running repairs are done to the equipment on the body. A rewheeling and light repair track was built around the One-Spot with provision of a heavy repair track with relocated rip jacks and 20 tonne crane bay. This improved the productivity of the workshop and the resulting ore car availability is shown in Figure 8 (Walker, 1980).

This redesigned layout is not ideal and it is planned to close one of the two underfloor lathes and set up a production line using a one-spot and a portal lathe as the two critical pieces of equipment.

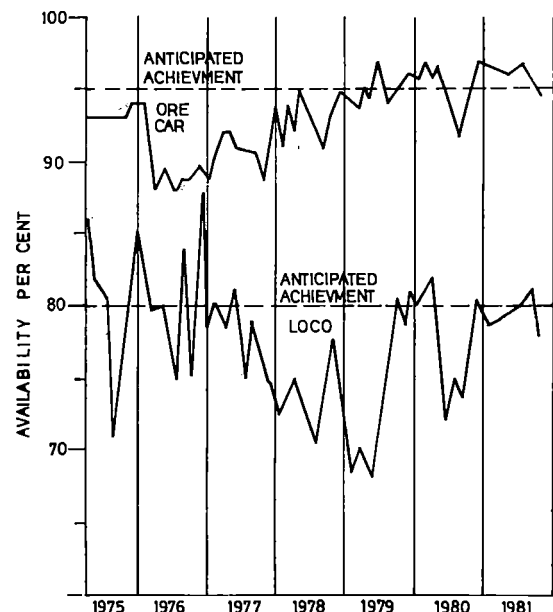


Fig. 8 Ore Car and Locomotive Availability

Rolling Stock Condition Monitoring

Railroad vehicle maintenance practice is usually based on condition monitoring by spot checks and maintenance by distance travelled or time in service. A system, TRAINDATA, is under development for locomotive and ore car condition monitoring using automatic measurement of condition and data collation on an HP1000 host computer. Automatic reports will be produced for exceptional conditions and a performance history will be established for long term maintenance. TRAINDATA comprises six items (see Figure 9), namely:

Axle Load

A weighbridge has been established using strain gauged rails to automatically measure all wheel loads. A statistical analysis of wheel, axle, bogie, car and train loads is produced. This data

is used to optimize car loading and also in the other TRAINDATA items.

Valuable data has been obtained describing the offset of load in the cars which has allowed adjustment of the 13 chutes in the load out tunnel. The mean payload has been increased from 96 tonnes to 100 tonnes with a standard deviation of 3.5 tonnes. Variation of payload has been statistically correlated with Fe grade, stockpile height, proportions of lump ore, beneficiation plant material and Marra Mamba ore.

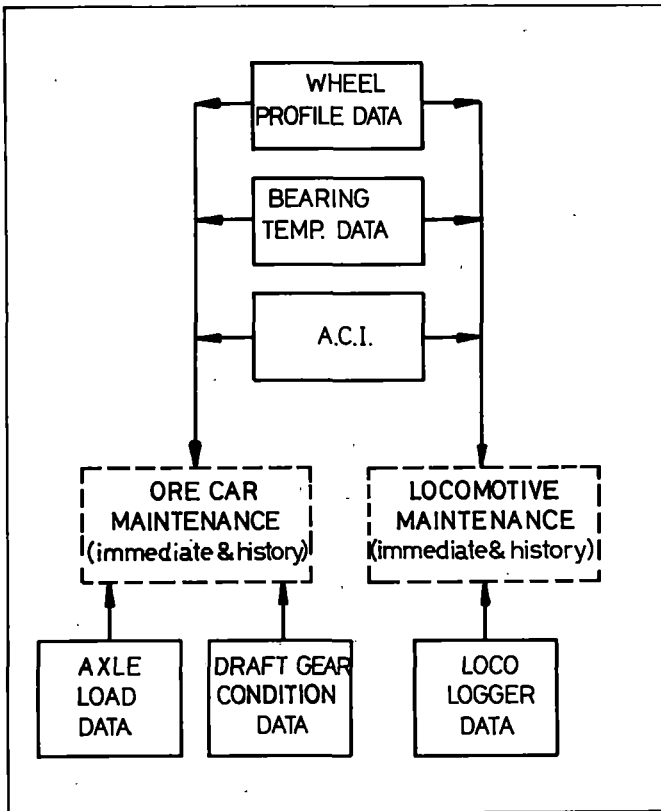


Fig. 9 TRAINDATA

Hot Box Detector Monitoring

The network of six hot box detectors will be monitored and examined for consistent or unusual changes of bearing temperatures, in addition to the present alarm only situation. Comparison will be made of temperatures between train trips and between different hot boxes during one trip.

Individual microprocessors will be attached to the Hot Box Detector inputs and a host minicomputer will control the data collection and manipulation. A condition index for all 16000 bearings will be computed and bearings will be given a priority for maintenance.

Draft Gear Evaluation

Draft gears will be monitored by measuring the extension of the gears under a known load during normal operation. The motor driven index arm on the car dumper provides a measurable force. Several

methods of automatically measuring the deflection of the draft gear are under study. These include measurement of the relative displacement between adjacent cars using line scan cameras or a radar device.

The measured load deflection curves will be compared with acceptable limits and a condition index will be established and regularly updated for each draft gear.

Wheel Profile Monitoring

A feasibility study has been completed using a laser based system to illuminate and measure the profiles of all wheels as trains pass. The observed profiles will be compared with acceptable limits and a condition index would be established for each wheel.

A study is underway on a prototype system presently in use measuring the profile of steel rod during production in a steel mill.

Automatic Car Identification (ACI)

To facilitate collation of data from the above four areas, ACI is necessary to allow axle load, bearing, draft gear and wheel condition to be collated for each car. The Siemens Sicarid system is under trial on locomotives and, if appropriate, will be extended to the entire fleet. The system uses passive (wave guide) transponders attached to the underside of the vehicles and a reader positioned between the rails on the track. The reader emits a varying frequency microwave beam and receives an attenuated version returning from the transponder.

Locomotive Performance Monitoring

A prototype LOCO LOGGER is under test on a locomotive. It monitors 16 parameters including 3 engine temperatures, 2 pressures, engine speed, alternator voltage and current etc. It is planned to install loggers on all locomotives. The LOCO LOGGER was developed as a low cost system at \$5000 to \$10,000 (depending on configuration) rather than a comprehensive individual logging device.

Data tapes will be replaced regularly on the locomotives and examined on the host computer. A performance history will be established for each locomotive for nominating long term maintenance requirements. Also immediate exception reports will be produced.

OPERATIONAL STUDIES

A feasibility study of Electrification of the Railroad has been produced. The consultants recommended that the catenary voltage should be 50 KV AC. This arrangement would require 6 sub stations between Hedland and Newman, with track sections of approximately 80 kilometers. (25 KV AC electrification would require double this number). It was shown using conservative assumptions that electrification was marginally viable.

Expansion of the railroad capacity could be achieved by track duplication, regrading of the ruling grade section through the Chichester Range and use of Locotrol. These scenarios are described by Brown (1982).

Studies have been made to reduce the cost per tonne of transporting ore. Axle load has been increased recently from 30 tonnes to 32.5 tonnes and if this

change continues to be successful, it will be increased possibly to 35 tonnes. The major disadvantages of increasing axle load is that transverse defect occurrence in the rail increases and life of bearing on the cars decreases. There has been no measurable increase in defect occurrence over the last 6 month period that 32.5 tonne axle loads have been in use but of course the fatigue process is a long term phenomenon and it is expected there will be a reduction in rail life for the benefit of the operation as a whole.

A train driving simulator, TRAINMASTER was used to develop the philosophy of free-wheeling whereby train drivers allowed the train speed to run to approximately 75 kilometers per hour, on downhill areas (10 kilometers per hour over the nominal speed limit), and also to fall back to about 55 kilometers per hour in other areas. This approach reduced fuel consumption by about 2% (\$300,000 per annum) and reduces the number of brake applications and the consequent brake and wheel wear.

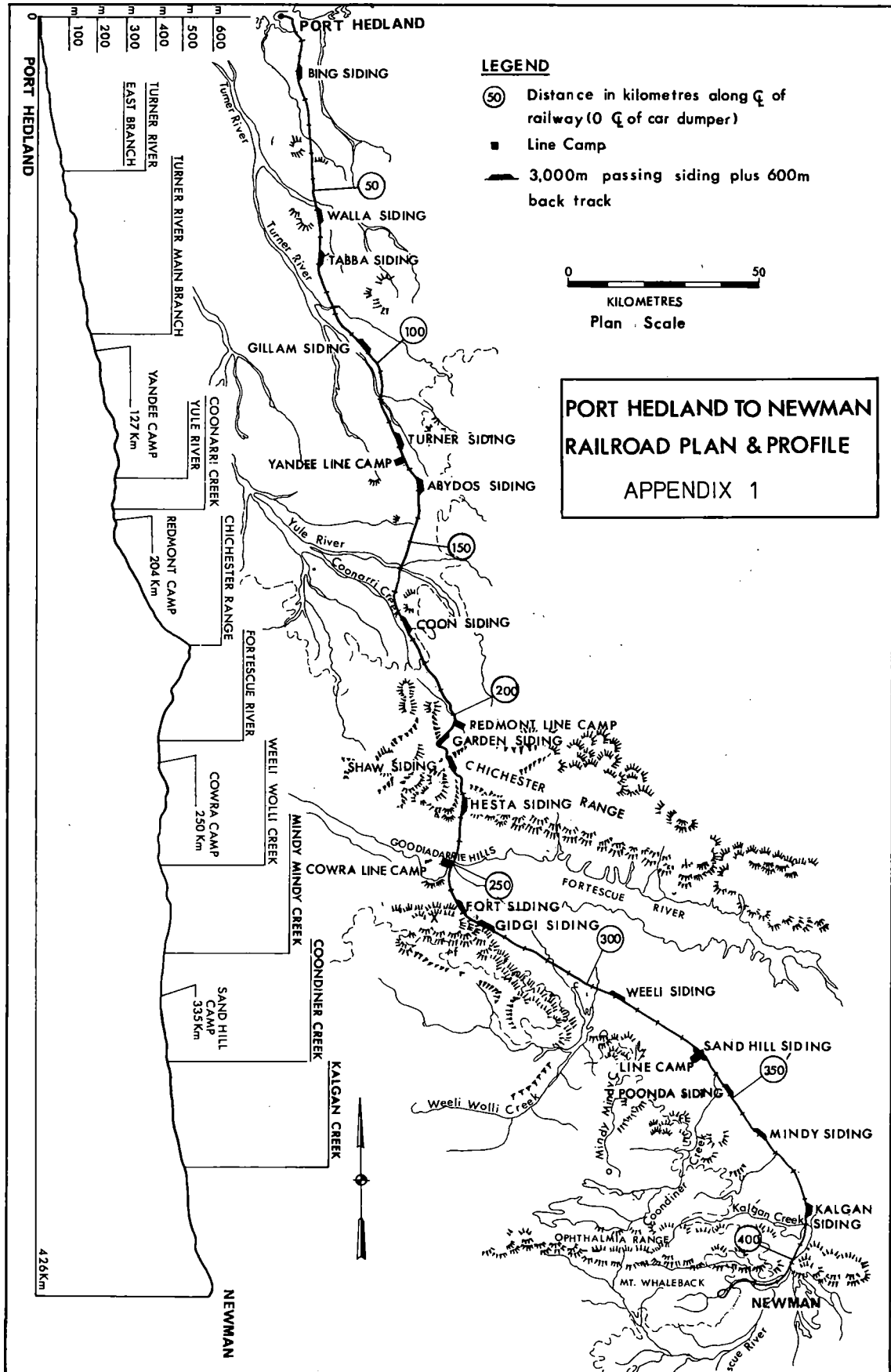
SUMMARY

A concerted research effort has lead to the solution of a number of railway problems. Rail grinding has lead to an increase in rail life and wheel life of significant proportions. The use of steel sleepers will provide a reduction in sleeper maintenance costs and the use of head hardened rail in track will allow a significant reduction in rail maintenance costs. TRAINDATA, is under development for automatic logging and collation of ore car load, bearing, draft gear and wheel condition and locomotive engine condition.

Appendix 1. Overleaf

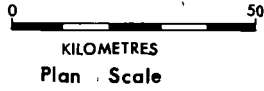
REFERENCES

- 1 Brown J.H., "Design Refinements make the Steel Sleeper Viable", Railway Gazette, Int. October 1979.
- 2 Brown J.H., "The Cost to the Company of a Cancelled Train", Mt Newman Mining Co. Report, MNM/RR/80/81/015, 1981.
- 3 Brown D.N., "Optimising Operational Modes on the Mt Newman Mining Co. Railroad", Proceedings of Heavy Haul Conference, Colorado, 1982.
- 4 Curcio P., Marich S., "In Track Assessment of Trial Sections at Mt Newman (April 1979)", B.H.P. Melbourne Research Laboratories Report, MRL/CA23/79/004, August 1979.
- 5 O'Rourke M., "Ballast Specifications Grading", Internal Correspondence Melbourne Research Laboratories to Mt Newman Mining Co., June 1980.
- 6 Roney M., "Probability Analysis of Defects in Mt Newman Mining and Hamersley Iron Tangent Track", BHP Melbourne Research Laboratories Report, BHP/MNM/HI/RPC/80/1, Nov 1980.
- 7 Towend P., and Marich S., "Life of Rail in Tangent and Curved Track on the Mt Newman Mining Co. Railroad", BHP Melbourne Research Laboratories Report, MRL/C77/78/023(3), May 1978.
- 8 Walker W., "Unit Train Operations Demand Preventative Maintenance of Wagons", Railway Gazette Int., Sept. 1980.



LEGEND

- (50) Distance in kilometres along C of railway (0 C of car dumper)
- Line Camp
- 3,000m passing siding plus 600m back track



**PORT HEDLAND TO NEWMAN
RAILROAD PLAN & PROFILE**
 APPENDIX 1

Management of Track Maintenance : A Systems Approach

E. Joubert

Pr.Eng., B.Sc.(Eng)(Rand)
Inspecting Engineer
Chief Civil Engineer's
Department
South African Transport
Services
Johannesburg
South Africa

Like any other activity of any business organization, track maintenance management should be practised to yield maximum return on investment for the organization. The process of track maintenance management is analysed showing that the design and execution of an integrated strategic plan is a prerequisite for producing track in the right condition for use by the trains operating department. Single parameters to describe the operating department's needs and track conditions respectively are defined and a forward planning model on which to base a short and long term strategic plan is produced.

NOMENCLATURE

A	effective bearing area of sleeper, cm^2
B	ballast stress ratio
d	sleeper spacing, cm
F	various factors defined by subscript
I	rail moment of inertia, cm^4
PO_2	number of standard 22,4 tonne axle loads
V	speed, km/h
W	load, tonne
\emptyset	track condition, workplaces/km

SUBSCRIPTS

o	reference value
a	axle load factor
b	load balance in truck, factor
c	speed and track condition factor
e	effective load (EL)
g	gross static load (GSL)
p	traffic pattern factor
s	track structure factor
w	wheel condition factor

INTRODUCTION

Maintenance of the track is not normally included in the detail or even broad planning of a new railway line. It is also ignored when the operating department takes decisions with respect to scheduling of trains and the speed at which trains should pass over the track. Traditionally the track maintenance engineer will contrive to live with whatever is presented to him to the best of his ability. Such an ad-hoc approach may very well lead to a situation where the profitability of the railway organisation is adversely affected. The lack of a systems approach to the management of track maintenance on the S.A.R. resulted in an increase in the percentage of total train running costs spent on track maintenance from 1976 to 1979. A total amount of some R20 million per annum was involved. This "loss" could possibly have been avoided by integrated planning of all maintenance work on the track and its ancillary structures and equipment as a function of the short and long term requirements of the trains operating department, relative to the amount of money available for such work.

THE PROCESS OF TRACK MAINTENANCE MANAGEMENT

The Principle Of Indivisibility Of Track Maintenance

In order to promote the systems approach to management of track maintenance, it is essential that track maintenance be considered indivisible especially with respect to the various engineering disciplines that are involved. It is pointless for the civil engineer to optimise the "civil" maintenance work on the track, only to discover that the work performed some time ago must be repeated because the work of the signals department was not considered during the planning stage. In this text, therefore, track maintenance must be read to mean all the work on the track for= mation and structure and not tamping, rerailing, track= welding, work on track circuits, or electrical bonding etc. as individual items. The track structure as a whole is considered to be operationally ready or other= wise and not individual parts thereof.

Subsystems Involved In The Management Process Of Track Maintenance

The following subsystems can be identified as being involved in the management process of track maintenance :

- Trains operating department
- Stores department
- Staff department
- Financial department
- Civil engineering department
- Electrical engineering department
- Signalling department
- Mechanical engineering department

The involvement of each sub-system is diagrammatically illustrated in figure 1. It must be obvious that optimisation of the track maintenance effort is a complicated process and ad-hoc decisions by any of the managers involved will inevitably lead to non-achievement of the goal of the railway organisation. The design and execution of the integrated work plan to ensure both maximum return on investment and the desired operational readiness of the track is the job of the track maintenance engineer. This paper will attempt to show how this can be done.

FORWARD PLANNING OF TRACK MAINTENANCE

Prediction Of Traffic Volumes And Track Condition

In order to plan track maintenance for maximum return on investment it is essential that long term strategy be decided upon. To do so it is necessary to predict future volumes of traffic flow as well as future track condition. The following prediction model has been evolved for the track maintenance section of the Chief Civil Engineer's department of the S.A.R. It was first used for planning the civil engineering track maintenance work of the Orange Free State System for the years 1982 to 1991 with promising results. In this paper the model was applied to predict the civil engineering track maintenance effort required for the rebuilt coal line between Vryheid and Richards Bay from 1986 to 1995 (both inclusive), for three alternative maximum axle loadings viz. 18,5 tonne, 20 tonne and 26 tonne. In addition the model was applied for three alternative configurations of single and double line sections for each maximum axle loading. These alternative configurations were :

Alternative Configuration 1

59,6 km of single line section plus 140,4 km of double line section with loaded coal traffic using the down line (Vryheid - Richards Bay) and the empty coal trains returning on the up line.

Alternative Configuration 2

200 km of twinned single line sections with 50% of all the traffic being carried on each single line section.

Alternative Configuration 3

59,6 km of single line section plus 140,4 km of twinned single line section with 50% of all traffic being carried on each single line of the twinned sections.

The model has thus far only been used for civil engineering purposes and the integrated track maintenance plan is not a reality as yet. In the description of the model it will be indicated how the model can be adapted in order not to violate the principle of indivisibility of track maintenance.

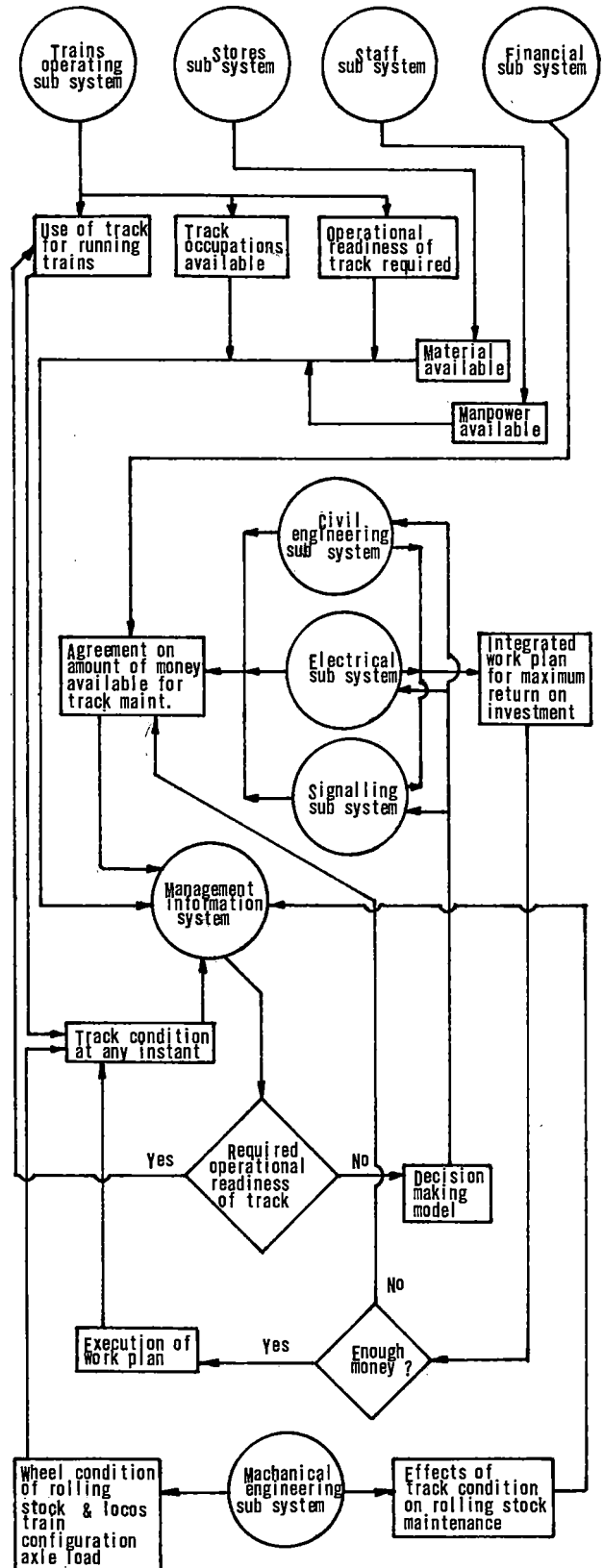


Fig.1 Flow diagram of track maintenance management.

With regard to the prediction of future traffic volumes, the Planning Department of the S.A.R. already provides this data with acceptable accuracy for use in the model.

The prediction model is only a small but essential part of the general decision-making model that is shown as an output of the management information system in figure 1. The alternative solutions with respect to maximum axle loading and single/double line configurations will each lead to a different 10 year maintenance plan having different influences on the return on investment. Before agreement can be reached as to funds available for track maintenance these alternatives must be evaluated and a decision taken. The decision has been taken by the S.A.R. without this analysis and the matter will not be discussed in the paper. The paper attempts to show that such an analysis is possible and desirable.

Operational Readiness Of The Track

Definition of the operational readiness of the track required by the trains operating department is a matter of agreement between all the sub-systems involved and will not be dealt with at length. As far as the civil engineering department is concerned it can be stated that the operating department's needs should be defined in terms of a single parameter reflecting the fact that a certain annual load must be able to pass over the track at a certain speed, the total annual load being applied in portions not exceeding the maximum axle load. The single parameter that will encompass all factors from a civil engineering point of view is the product of effective annual load and speed with effective annual load being suitably defined in terms of the gross static annual load. Denoting this parameter as track momentum, the trains operating department can be said to require such a track condition that will enable it to generate a specific number of units of track momentum annually. The unit of measurement is known in the civil engineering department of the S.A.R. as the Hill in honour of its incumbent Chief Civil Engineer. One Hill of track momentum is generated when one million tonnes of traffic passes over one kilometre of track at 1 kilometre per hour.

The track can be described as 100% operationally ready when the trains operating department is able to generate the planned number of Hill per annum. Once the desired operational readiness required is known for each particular track section that makes up the total railway network of a company, the total amount of money available for track maintenance can be apportioned for each section in accordance with the number of Hill required to be generated. In this process fixed and variable costs must naturally be separated. The so-called coal line of the S.A.R. will then receive its fair share of money for track maintenance and the planning process shown in figure 1 may commence. Track condition will dictate, in the end, the amount of money needed for its maintenance. The art of managing track maintenance for maximum return on investment lies in the maintenance engineer's ability to balance track condition demands with availability of funds.

PREDICTION OF FUTURE TRACK CONDITION

A Single Parameter Describing Track Condition

The planning process cannot be attempted without a proper definition of track condition. A single parameter to describe track condition is necessary and has been accepted by the civil engineering department of the S.A.R. as the number of workplaces per kilometre in a track section. A workplace is defined as a section of track of 50 metres in length in which one or more defects occur which is worse than the reference standard. The reference standard is defined as the minimum acceptable standard, below which remedial work on the track becomes mandatory.

It is easy to see that this parameter can be used by all engineering disciplines concerned in track maintenance, each discipline setting its own reference standard. Whenever any defect occurs in a particular 50 metre section, the section is known as a workplace. Dividing the entire track network up into 50 metre sections, it becomes possible to describe the condition of any sub-section of track as the number of workplaces per kilometre that exist at any instant. The civil engineering department of the S.A.R. has chosen 10 kilometres as the standard length of a sub-section.

Monitoring Track Condition

While the definition of the track condition parameter is relatively easy, the practical determination of the track condition is not an easy matter and each engineering discipline will have to design its own methods. Track geometry is comparatively inexpensively measured with respect to 7 geometric parameters on the S.A.R. at a cost in 1980/81 of approximately R19 per kilometre. Statistical methods of evaluating condition of the materials that make up the track structure have been designed. Regular visual inspection by means of inspection cars (trolleys) or from the footplate or on foot forms part of the monitoring system in use on the S.A.R. The formalised reporting relative to fixed 50 metre worklengths of track is being promoted on the S.A.R. at present and a formal management information system has been established by the civil engineering department early in 1981.

Relationship : Track Condition And Load

Definition : Effective Load (EL)

The effective load on the track structure is that proportion of the gross static load to which the track structure is subjected when the gross static load (GSL) passes over the track.

The estimated EL can be expressed as

$$W_e = W_g \cdot F_a \cdot F_c \cdot F_w \cdot F_p \cdot F_b$$

F_w , F_p and F_b are unknowns at present and will be assumed to equal one for the purpose of this exercise. The engineer may however take these factors into account and estimate its effect because of his knowledge of local conditions. For instance, because the occurrence of flat wheels is known to be frequent on a particular section the engineer may decide to make allowance for this fact by equating F_w to 1,1.

Axle Load Factor

The Lombard (1) formula was used :

$$F_a = 0,0224 \cdot (PO_2)$$

The so-called (PO_2) factor used by the S.A.R. is the number of standard axle loads of 22,4 tonne per million tonnes of GSL that will do the same damage to the track as the particular mixture of axle loads to which the track is actually subjected.

The value of (PO_2) is readily obtainable for all track sections on the S.A.R. from the Traffic Density Statistics.

Speed And Track Condition Factor

The value of F_c may be derived from the formula

$$F_c = 1 + qst'$$

The formula was produced by Lombard (2) based on the Eisenmann (3) proposal.

Eisenmann's valuation of q is also adopted viz.

$q = 0,1$ for running top in excellent condition
 $q = 0,2$ for running top in good condition
 $q = 0,3$ for running top in bad condition.

$$s = 1 + (V-60)/140 \quad (V \geq 60 \text{ km/h})$$

$t' = 1$ for statistical upper confidence of 84,1%
 $t' = 2$ for statistical upper confidence of 97,7%
 $t' = 3$ for statistical upper confidence of 99,9%

Important Reference Track Conditions

These reference track conditions can best be summarised in some basic axiomatic laws of track maintenance :

The Best Ever Condition (BE)

The BE condition of track, i.e. zero workplaces per km, occurs immediately after the so-called consolidation period after completion of construction or relaying.

The Best Possible Condition (BP)

The BP condition of track after use at any instant, is the condition that may be obtained by elimination of basic defects (EBD) and cannot be obtained by normal day to day maintenance. The BP condition is always worse than the BE condition.

The Best Possible Practical Condition (BPP)

The BPP condition of track is achieved by preventive maintenance by means of a heavy tamper and day to day maintenance.

The BE, BP and BPP track conditions are all functions of the cumulative effective load (CEL) to which the track has been subjected up to a particular point in time.

These laws are general and basic and can also be used by the other engineering disciplines as a basis to find common ground for integrated planning of track maintenance.

Track Condition (\emptyset) As A Function Of CEL

The nature of the function is not an easy matter to determine and as a starting point the statistics of the present coal line with respect to track geometry measurements, \emptyset and the GSL, over the period 1976 to 1980 were analysed.

The CEL of each sub-section of the Vryheid - Richards Bay section was calculated separately for the single line, and the up and down lines of the double line sections.

In the calculation of F_c the value of q was determined on the following basis.

For $\emptyset = 0$ to 1,0 ; $q = 0,1$
 For $\emptyset = 1,01$ to 6,5 ; $q = 0,2$
 For $\emptyset = 6,51$ to 20,0 ; $q = 0,3$

These values are based on experience ; from all the track measuring car results taken by the S.A.R. relative to the reference standard known as the B-standard, the boundary between good and bad track appears to be of the order of 6,5 workplaces per km. For the boundary between excellent and good track, the geometry measurements of several newly constructed track sections were found to be rarely less than 1,0 workplaces per km.

To ensure that the worst possible dynamic effect of the GSL is taken into account the value of the statistical factor t' was taken as 3.

The values of F_a for the coal line exercise was calculated for the various types of traffic that used the line from 1976 to 1980. These values are shown in Table 1.

Type Of Train	Axle Load (Tonne)	F_a
Loaded coal trains	18,5	0,69
Loaded coal trains	20,0	0,80
Loaded coal trains	26,0	1,35
Mixed goods trains	18,5 maximum	0,58
Empty coal trains	18,5 scheme	0,11
Empty coal trains	20,0 scheme	0,11
Empty coal trains	26,0 scheme	0,13

Table 1 Values of F_a for various types of train.

The speed, V used in the calculation of the CEL, is the probable speed of the train over the sub-section. This was obtained from the planned point to point running times determined by a simulation method used by the Planning Department of the S.A.R. The average speed was taken over a 10 km sub-section. Further development in this field includes the possibility that the simulation computer programme may be used in conjunction with the track geometry measuring car to produce the probable speed over individual 50 metre worklengths, if indeed such accuracy is considered desirable.

The values of W_g used were the actual GSL over the single line sections from statistical data and the apportionment of W_g for the up and down lines in the double line portions pro rata with the latest available track condition values \emptyset for each line.

Regression Analysis : \emptyset And CEL

The track condition values, \emptyset measured by means of track geometry measuring vehicles were examined in relation to the CEL calculated for each line in each sub-section. A direct plot produced no correlation whatever. The cause was thought to be that in a 10 km sub-section consisting of 200 50 metre worklengths, the trend can easily be masked by local variations and that an envelope of values of \emptyset against the CEL should rather be sought, than a single graph. Such an envelope of values would still be very useful to the engineer trying to predict future track condition.

Grouping all \emptyset values for 10 million effective tonne load intervals together, double sided confidence limits were calculated for \emptyset for each interval at the

95% confidence level using the T-distribution. This procedure yielded minimum and maximum expected ϕ values for each 10 million tonne group in the range 10 to 160 million tonnes of effective load. Regression analysis to fit the data to the following functions were carried out with the success obtained indicated by the coefficient of determination in brackets :

Linear

$$\phi = a + b.W_e \quad (0,58)$$

Exponential

$$\phi = a.exp(bW_e) \quad (0,70)$$

Logarithmic

$$\phi = a + b.lnW_e \quad (0,78)$$

Power

$$\phi = a.W_e^b \quad (0,82)$$

The power function produced the best, but by no means an exceptionally good fit. As a starting point this was regarded as being acceptable. Fitting power curves to the minimum and maximum values of ϕ for each 10 million tonne group the following values of the functions are obtained :

Minimum Value Of ϕ

$$\phi = 0,05825 W_e^{0,62729}$$

Maximum Value Of ϕ

$$\phi = 0,24581 W_e^{0,47749}$$

It must be noted that the functions so identified is for the particular track structure that exists in the present coal line between Vryheid and Richards Bay viz. 57 kg/m continuously welded rails on S.A.R. type F4 monolithic concrete sleepers spaced at 700 mm. It should also be noted that statistically the result is only valid between 0 and 160 million tonnes of CEL.

Plotting the graphs of these functions - figure 2 - it will be noticed that the rate of deterioration in track condition decreases with an increase in CEL. Experience with track tamping by means of heavy tamping machines confirms this tendency of rapid deterioration immediately after repair to a gradual stabilisation. At some point beyond the 160 million tonne mark it is felt however that the deterioration rate will increase as basic defects in the track structure begin to assert themselves.

Projecting the graphs beyond the statistical validity range though not normally acceptable, will serve as a valuable first approximation of the BP condition function of track deterioration with CEL. To obtain this condition, by definition, EBD must be performed so that another set of graphs for the BPP condition is required.

In the validity range 0 to 160 million tonnes it is thought that the BP and BPP track conditions will more or less coincide but that the deterioration rate will increase for the BPP condition relative to that of the BP condition.

Again from experience it is surmised that 100% of the track will need to be worked on after passage of some 2 000 tonnes of effective load if EBD is not performed at some stage; i.e. $\phi = 20$ and by definition ϕ cannot exceed 20 per kilometre.

Performing another regression analysis on the values of the BP minimum curve between 0 and 150 and the point (2000,20) the BPP (minimum) equation of

$$\phi = 0,02087 W_e^{0,87167}$$

is obtained.

The BPP minimum condition is the condition that can be obtained by day to day maintenance and tamping by heavy tamper and is the best possible that can be obtained without EBD, starting from some maximum BPP condition. Assuming that the difference between minimum and maximum values for a particular CEL value will be of the same order for both the BP and BPP conditions, the BPP maximum curve below can be produced, fitting a curve, again by regression analysis.

$$\phi = 0,06848 W_e^{0,74705}$$

It is realised that there is no real scientific proof that the functions determined above are valid. It is certain that any prediction and forward planning, is probably wrong. It must therefore be accepted that the above analysis is merely a starting point of some value. Gathering statistics meticulously and conscientiously in future in the form required, the above method of analysis will almost certainly yield valid results.

In the meantime using the theory experimentally for forward planning of civil track maintenance on the Orange Free State system in 1981, results were produced that were entirely acceptable from a practical point of view.

Variation In Track Structure

Some allowance had to be made for the difference in track structure between the present coal line and the rebuilt line that will come into existence in 1986. Track condition with respect to geometry depends largely on the ability of the ballast layer under the sleepers to transmit the load to the formation without serious change in density.

Lombard (2) produced the concept of the ballast stress ratio for different types of track structure. The track structure factor that may be applied to the BP and BPP minimum and maximum functions can reasonably be thought to be a constant which equals 1 for the 57/F₄ Structure of the present line.

Definition : Track Structure Factor

$$F_s = (B/B_e)^x$$

The value of x will at this stage be regarded as 1 due to lack of evidence to the contrary.

The value of B_e according to Lombard (2) equals 0,9.

The value of B can be calculated from

$$B = \left[(d/do)^3 . (Ao/A)^3 . (Io/I) \right]^{0,25}$$

For the rebuilt coal line structure consisting of 60 kg/m chrome manganese rails on FY type monolithic concrete sleepers spaced at 600 mm it is pre-

dicted that the track will deteriorate in accordance with the following functions

BPP maximum condition

$$\phi = 0,05326 W_e^{0,74705}$$

BPP minimum condition

$$\phi = 0,01623 W_e^{0,87167}$$

BP maximum condition

$$\phi = 0,1912 W_e^{0,47749}$$

BP minimum condition

$$\phi = 0,04531 W_e^{0,62729}$$

The graphs of these functions are shown in figure 3.

STRATEGIC PLANNING OF TRACK MAINTENANCE

The predicted theoretical track condition can be determined for as long a period as for which future traffic volumes can be predicted, using the above formulae. The track maintenance engineer can determine well ahead the strategy to be followed with day to day maintenance, and periodical re-investment in the railway line in the form of total relaying, re-railing or EBD. The prediction method leads to the inevitable conclusion that it is futile to pour funds into day to day maintenance methods with the aim of improving the track condition beyond the BPP minimum value of ϕ . This was proved beyond doubt with accurate daily track geometry measurements after tamping by heavy tamper. It also shows clearly that EBD will improve track condition to the BP minimum value of ϕ relative to the CEL, but no more. To improve the track condition to a ϕ -value of zero, complete track renewal including ballast will be required. Both these last statements coincide with experience gained in practice with EBD and complete relaying.

With regard to rerailing the position is not equally clear. Since rerailing must be performed for reasons of wear or fatigue, it must be assumed that the normally worn or fatigued rail will not contribute to the generation of workplaces. Neither will replacement of the rail eliminate existing workplaces. Abnormal rail conditions will contribute to the formation of workplaces and it must be regarded as day to day maintenance to eliminate these defects as they occur. If this reasoning is accepted rerailing will only be done for safety reasons and not for economic reasons.

A suitable computer programme has been designed that will yield the following output for each subsection of track for each year under consideration in a short time :

- CEL value
- Heavy tamper cycles.
- Minimum expected ϕ -value (BPP).
- Maximum expected ϕ -value (BPP).
- Total workplaces (minimum).
- Total workplaces (maximum).
- Minimum emergency workplaces.

Maximum emergency workplaces.

Day to day maintenance labour required (3 different approaches).

Labour requirements for emergency maintenance.

Means to determine the economically optimum time for EBD and relaying by the discounted cash flow method. The influence on the life of the track structure of different track maintenance strategies can be determined and the optimum strategy adopted.

Control graphs of predicted track condition with which to compare actual track condition as measured.

After such a computer run for the Vryheid - Richards Bay section of the rebuilt coal line, the influence of the decision taken as to maximum axle loading and line configuration on track maintenance is shown in the following graphs.

VRYHEID - RICHARDS BAY COAL LINE : RESULT OF FORWARD PLANNING EXERCISE FOR THE PERIOD 1986 - 1995.

In the graphs that follow the alternatives 1, 2 and 3 referred to are the alternative configurations 1, 2 and 3 described hereunder. The prediction levels of the aspect shown in each graph for each year are for the 26 tonne, 20 tonne and 18,5 tonne maximum axle loadings side by side, for ease of comparison.

Alternative Configuration 1

59,6 km of single line section plus 140,4 km of double line section with loaded coal traffic using the down line (Vryheid - Richards Bay) and the empty coal trains returning on the up line.




Alternative Configuration 2

200 km of twinned single line section with 50% of all the traffic being carried on each single line section.

Alternative Configuration 3

59,6 km of single line section plus 140,4 km of twinned single line section with 50% of all traffic being carried on each single line of the twinned sections.

Legend

- 26 Tonne Axle Load 
- 20 Tonne Axle Load 
- 18,5 Tonne Axle load 

Note

20^T and 18,5^T axle loads carried on present track structure. Fig. 2 applicable. 26^T axle load carried on new track structure. Fig. 3 applicable.

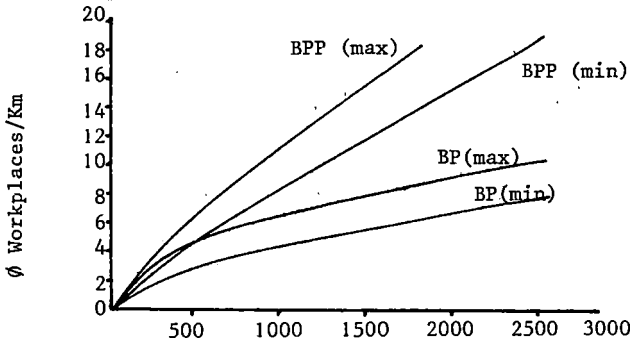


Fig.2 Existing Coal Line : Track Deterioration With CEL

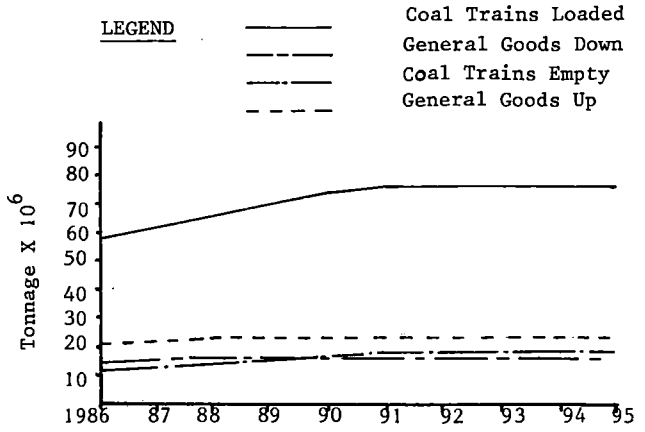


Fig.4 Predicted Traffic Volume

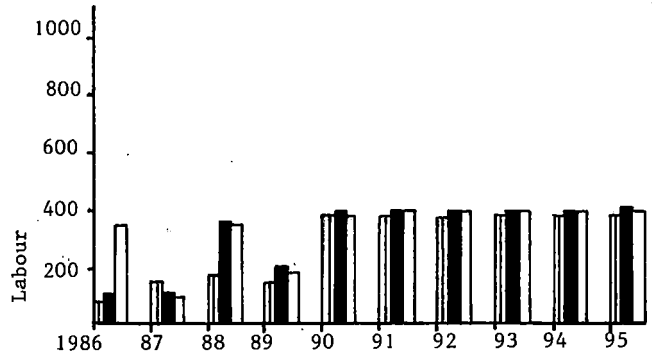


Fig.5 Total Labour Alternative 1

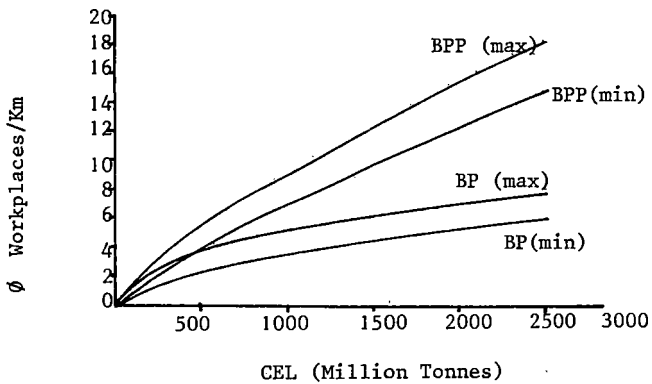


Fig.3 Rebuilt Coal Line : Track Deterioration With CEL

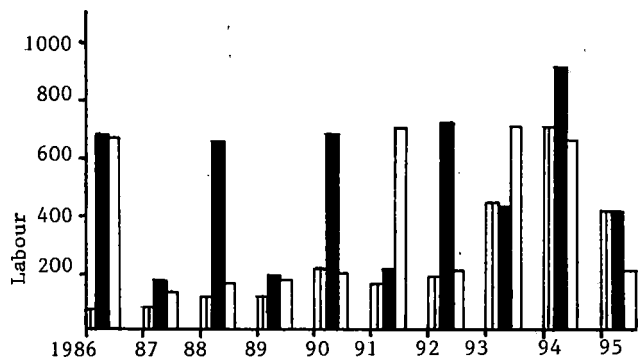


Fig.6 Total Labour Alternative 2

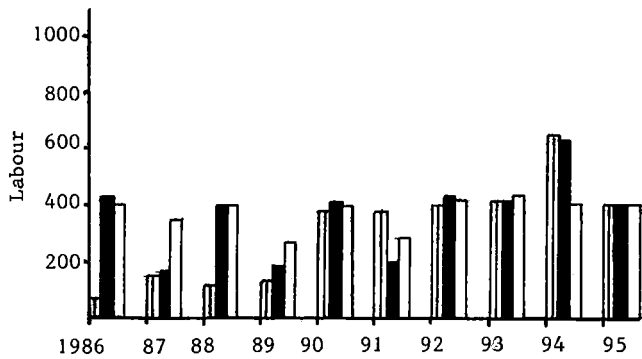


Fig.7 Total Labour Alternative 3.

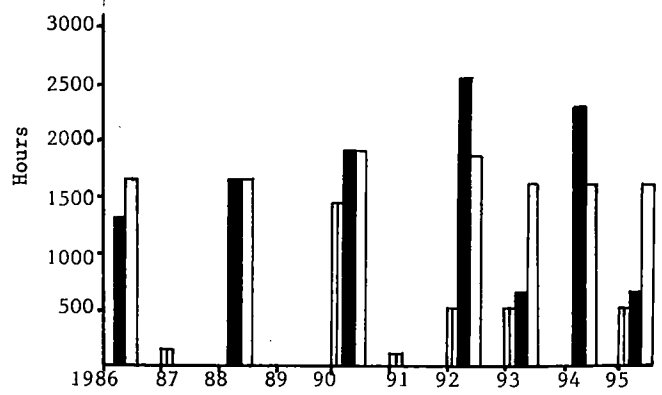


Fig.10 Nett Occupation Hours Required Alternative 3

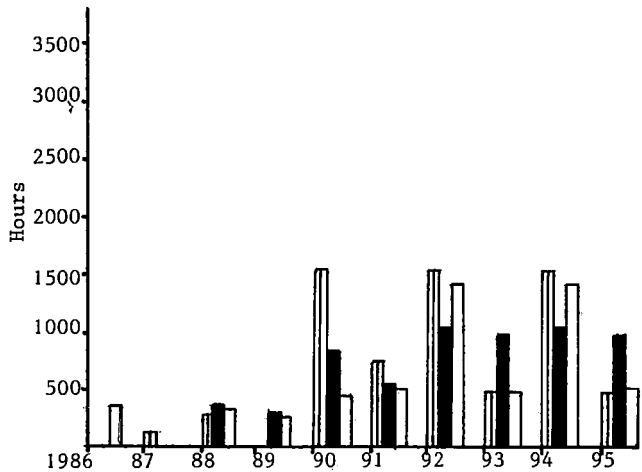


Fig.8 Nett Occupation Hours Required Alternative 1.

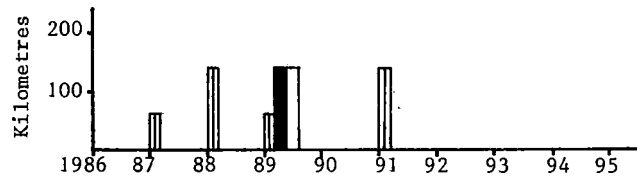


Fig.11 Rerailing Alternative 1

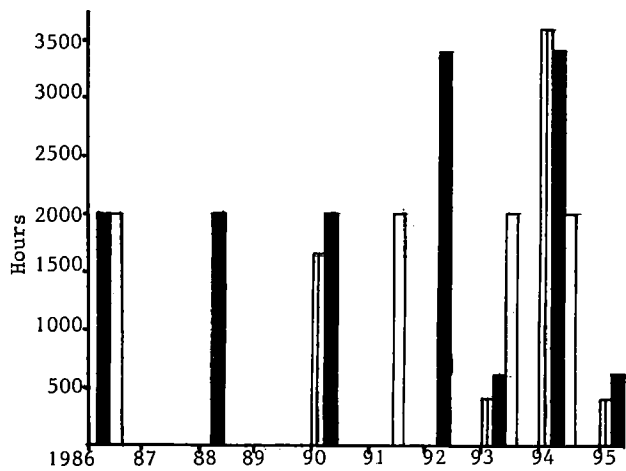


Fig.9 Nett Occupation Hours Required Alternative 2

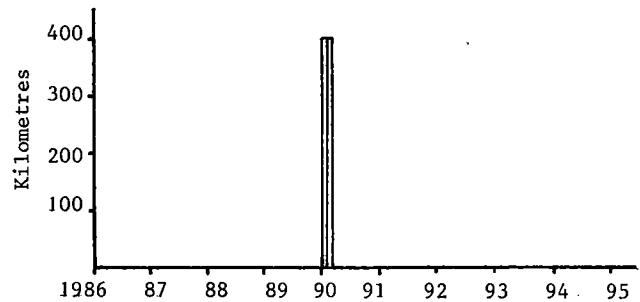


Fig.12 Rerailing Alternative 2

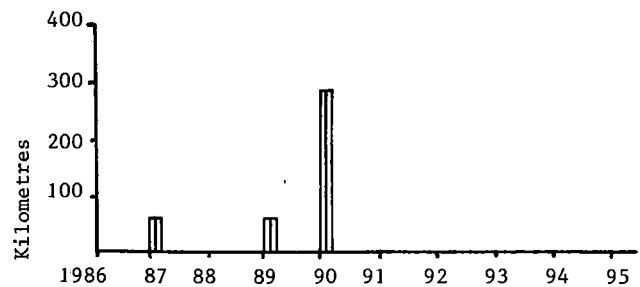


Fig.13 Rerailing Alternative 3.

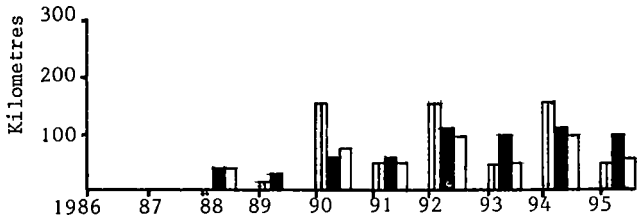


Fig.14 Elimination Of Basic Defects
Alternative 1

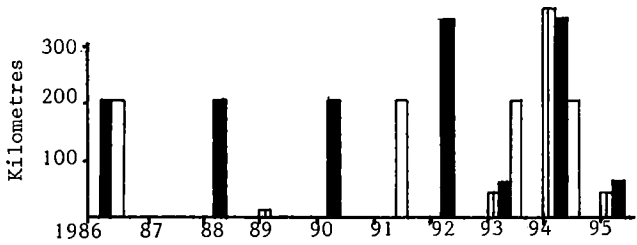


Fig.15 Elimination Of Basic Defects
Alternative 2

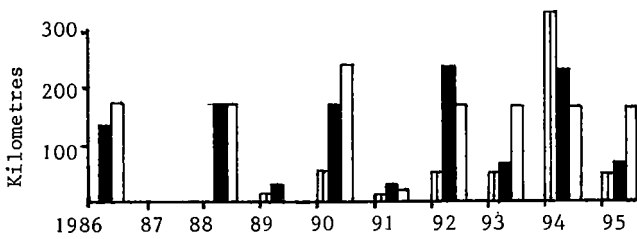


Fig.16 Elimination Of Basic Defects
Alternative 3

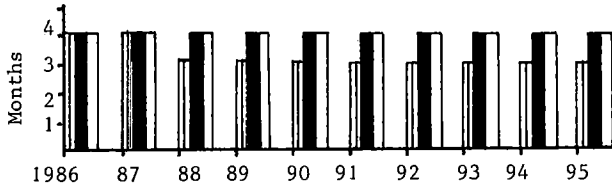


Fig.17 Tamping Cycle Alternative 1
Single Line

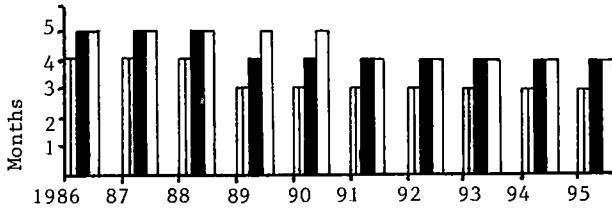


Fig.18 Tamping Cycle Alternative 1
Double Down Line.

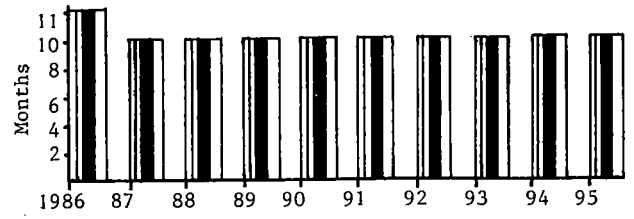


Fig.19 Tamping Cycle Alternative 1
Double Up Line.

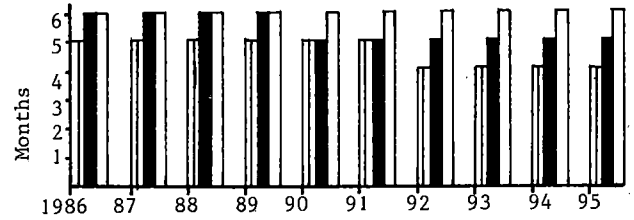


Fig.20 Tamping Cycle Alternative 2
Each Single Line.

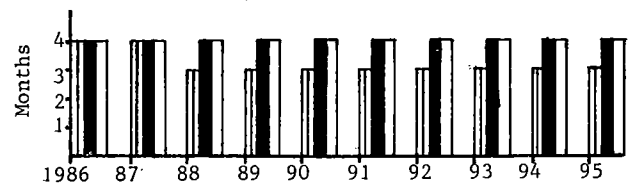


Fig.21 Tamping Cycle Alternative 3
Single Line.

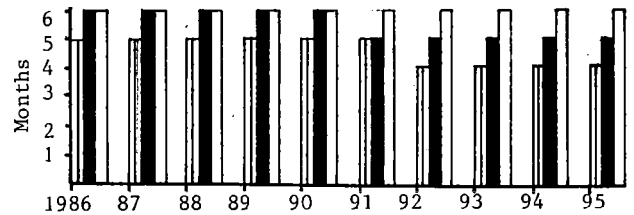


Fig.22 Tamping Cycle Alternative 3
Double Down Line.

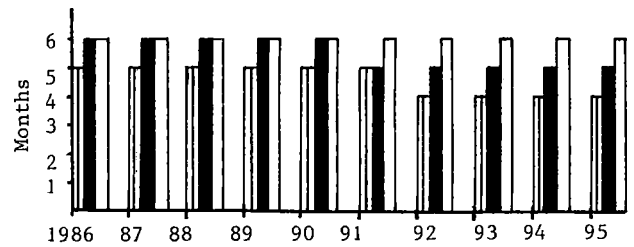


Fig.23 Tamping Cycle Alternative 3
Double Up Line.

CONCLUSION

Once a strategic plan for track maintenance has been accepted and its costs evaluated, the process outlined in figure 1 can take its course. There will then be at least some reason to believe that an attempt has been made to manage track maintenance in such a manner that the right work is performed at the right place on the track at the right time. This will contribute to the short and long term goals of the organisation as a whole.

Other departments are invited to join the civil engineering department of the S.A.R. in the effort to design an integrated track maintenance plan as proposed in the above process. The S.A.R. will soon be in a position to schedule the integrated maintenance plan properly with respect to time and place if present negotiations with British Rail to purchase the CAMPS and CROWS computer software packages prove successful. The joint effort of all engineering disciplines involved will then become a fact.

REFERENCES

1. Lombard, P.C., "Spoorbaanstructuur : Verband Tussen Structuurparameters, Verkeerslading en Onderhoud". Thesis (M.Sc Eng.) University of Pretoria, 1976, pp 71 - 81
2. Lombard, P.C., "Track Structure-Optimisation of Design" Proceedings Of The Heavy Haul Railway Conference, Perth, Western Australia, September 1978, Paper B5.
3. Eisermann, J., "Stress Distribution In The Permanent Way Due To Heavy Axle Loads And High Speeds". Area Bull. No. 622 Proc. Vol. 71. Sept - Oct. pp.24 - 59

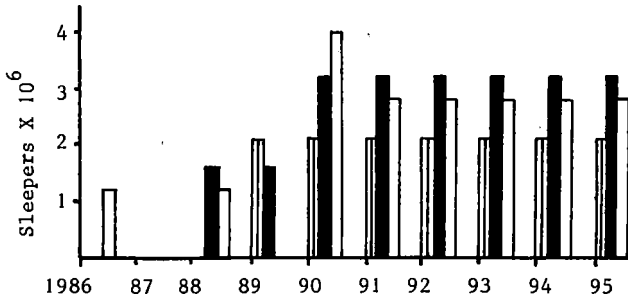


Fig.24 Sleepers To Be Tamped Alternative 1.

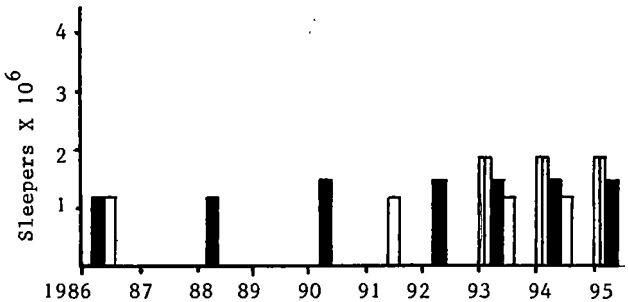


Fig.25 Sleepers To Be Tamped Alternative 2.

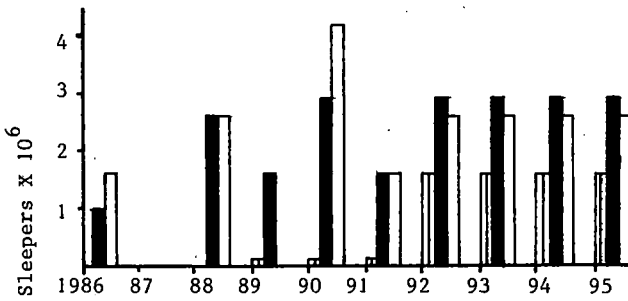


Fig.26 Sleepers To Be Tamped Alternative 3.

Low Dynamic Action 100 Ton Covered Hopper Development Program

Keith L. Hawthorne

Manager
Track/Train Dynamics
Association of American
Railroads

Based on a review of the performance of various freight car types in the North American fleet, the covered hopper car, specifically as configured for grain service, was selected as first candidate for development. Independent studies conducted by AAR and FRA identified the present 100-ton covered hopper car fleet as accounting for a disproportional number of derailments. This paper reviews the procedure for establishing design specifications for the new generation of 100-ton covered cars and the program for their development.

INTRODUCTION

On May 2, 1979, the Track Train Dynamics (TTD)* Steering Committee reviewed and approved a comprehensive plan for the program's third phase. In keeping with Phase III objectives set forth in the original TTD program plan issued on March 31, 1972 (Reference 1), this new plan called for encouraging the development and demonstration of advanced equipment utilizing design and analysis techniques developed during the intervening years.

Based on reviews of the performance of various freight car types in the North American fleet, the covered hopper car, specifically as configured for grain service, was selected as the first candidate for development. Independent studies conducted by the AAR and FRA identified the present 100-ton covered hopper car fleet as accounting for a disproportionate number of derailments. In addition, a considerable proportion of rail damage, both wear and fatigue, can be attributed to these cars. The results are costly to railroads and disturbing to shippers.

Further, it was felt that improvements to the covered hopper car; with its high center of gravity,

* The Track Train Dynamics program is a cooperative government-industry research program sponsored by the Association of American Railroads, the Federal Railroad Administration, the Railway Progress Institute, and the Transport Canada Development Centre.

inherently high torsional rigidity resulting from its closed structure, and truck centers near the length of jointed rail sections, would prove to be particularly challenging. Many potential improvements in the dynamic performance of covered hopper cars could also be seen as readily transferrable to other car types.

It should be noted that this program does not intend to develop or propose the development of a standard covered hopper car. The intent is to demonstrate that several alternative design approaches can satisfy a set of goals for improved performance.

This report summarizes progress made during the developmental stages of the High Performance/High Cube Covered Hopper Car Program. Much of the material presented has been excerpted from the Performance Guidelines (Reference 2) and the Economic Evaluation Methodology (Reference 3) which were developed as part of the program effort.

PROCEDURE

With the concurrence of the TTD Steering Committee, a six-stage program was established as follows:

1. Development of performance guidelines and economic evaluation methodology.
2. Solicitation and selection of participants.
3. Concept development and review.
4. Detailed design.
5. Prototype procurement and construction.
6. Test and Evaluation.

To lead in the development of performance guidelines, a twenty-three person ad hoc technical review committee was selected. This committee was chaired

by Mr. H. L. Scott, Jr., then General Manager Motive Power and Equipment of the Norfolk and Western Railway Company.

To assure a comprehensive view of industry needs and capabilities, the guidelines committee included representation from railroad mechanical and engineering departments, freight car and freight car truck suppliers, the Federal Railroad Administration, and the AAR Mechanical Division. In cooperation with AAR Research and Test Department staff, the committee established performance guidelines or "goals" which designers should attempt to meet with the next generation of covered hopper cars.

PERFORMANCE GUIDELINES

In the guidelines (Reference 2), dynamic forces are divided into three major categories: Stability (truck hunting and car body rocking), Ride Quality (vibrations and trackability), and Impact (yard handling and train action).

Stability

The designer shall attempt to meet the following stability goals:

1. Hunting. The car and its trucks shall be capable of operating in all lading conditions and on dry tangent track at speeds up to 80 mph without experiencing unstable hunting oscillations leading to loss of tread contact, or to flange contact loads exceeding those outlined below with wheels and other truck components having any stage of wear or deterioration not condemnable by current AAR standards.
2. Flange Climbing. The ratio of the instantaneous lateral guiding force (L) exerted by a single wheel on the rail to the instantaneous vertical load (V) sustained by that wheel shall not exceed 0.8 for more than 6 feet of track, when operating in all lading conditions on track with allowable irregularities under the FRA Track Safety Standards at allowable speeds for each class of track. Speeds on curves shall be that corresponding to 3 inch unbalanced superelevation.
3. Rail Overturning. The ratio of the sum of the instantaneous lateral guiding forces exerted on the rail by the wheels on one side of a truck to the sum of the instantaneous vertical loads sustained by those wheels shall not exceed 0.6 for more than 6 feet of track when operating in all lading conditions on tangent track at speeds up to 80 mph or in curves at speeds up to that corresponding to 3 inch unbalanced superelevation.
4. Track Displacement. The resultant lateral guiding force exerted on the track by the two wheels of any wheelset shall not be greater than the value given by:

$$H = 0.85 \times (2,200 + \frac{\text{Axle load-lbs.}}{3}) \text{ lbs for}$$

more than 6 feet of track when operating in all lading conditions on tangent track at speeds up to 80 mph or in curves at speeds up

to that corresponding to 3 inches unbalanced superelevation

5. Harmonic Roll. The car shall meet or exceed the harmonic roll performance of the base car under the test conditions specified in the AAR approval test for special devices to control stability of freight cars as indicated by roll angle, and by maximum and minimum wheel loads.
6. Angle of Attack. The angle of attack between the wheels and rail shall be such that the lateral load on the rail is the least possible within the cost constraints. This lateral load in steady state shall not exceed a value of one-half of H as calculated in item 4, above.
7. Vertical Wheel Loads. The car design shall aim at a goal of at least 25% reduction in dynamic vertical load over the present 100 ton reference car over all classes of track under the FRA Track Safety Standards up to the maximum permissible speeds below 80 mph. An example vertical load distribution curve for a 100 ton car is shown in Figure 1 by the solid

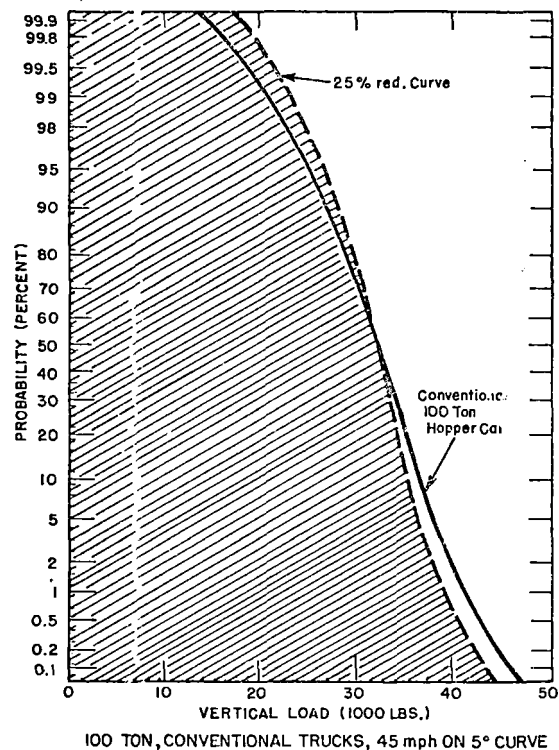
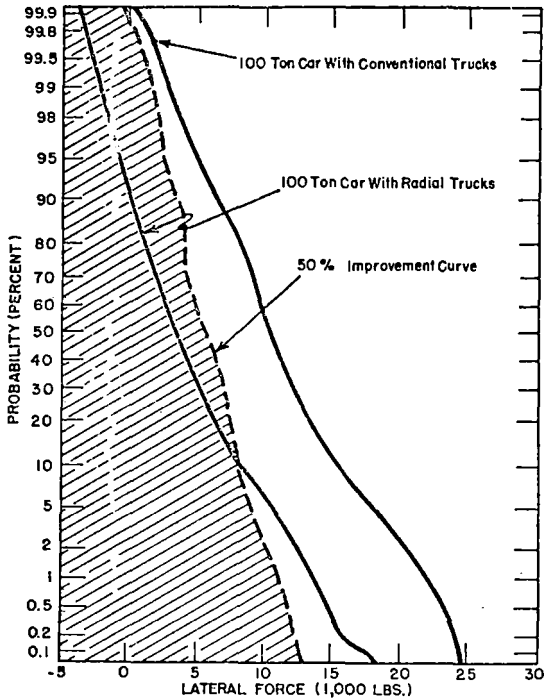


Figure 1

line. A 25% improved curve is indicated by the broken line. The data shown in this figure are for class 5 track at 45 mph on a 5 degree curve. It should be noted that the wheel load goal is achieved when the curve is anywhere within the shaded region; i.e., the goal could be achieved through reduction in static wheel load sufficient to produce a load distribution within the shaded area.

8. Lateral Wheel Loads. The lateral wheel load performance goal for this car is a 50% reduction over the present 100 ton reference car on curves up to 8 degrees over all classes of track to the maximum permissible speeds below 80 mph. An example cumulative distribution curve of lateral loads for a 100 ton car is shown in Figure 2 for a car



100 TON CAR WITH CONVENTIONAL TRUCKS AND RADIAL TRUCKS, 45mph ON 5° CURVE ON CLASS 5 TRACK.

Figure 2

with standard trucks and for one with radial or steerable trucks. These curves show what is currently achievable; hence, the lower bound is a goal for the new car design.

9. Load Equalization. To assure proper load equalization with the empty car on level track, raising or lowering any one wheel 2-1/2 in. vertically shall not cause any other wheel tread to lose contact with the rail and raising or lowering the wheels on one side of a truck 2-1/2 in. shall not reduce any wheel loads on the car more than 40%.

Ride Quality

The ride quality shall be such that no component of the car and car structure shall exceed the fatigue limit during the life of the car when operating under any track conditions at speeds allowable under the FRA Track Safety Standards. Frequency response functions of these various areas can be developed experimentally or analytically by performing a modal analysis. Particular attention should be paid to excitations occurring in the range of 0 to 25 Hz.

Impact

The car must meet the squeeze and impact requirements of the AAR specifications.

The car shall not induce any more free slack than the slack introduced with standard AAR components.

In addition to the dynamic performance requirements, the guidelines addressed issues of interchangeability, structural integrity, safety standards, and maintainability.

ECONOMICS EVALUATION

In parallel with the development of performance guidelines, the AAR Engineering Economics Division pursued two objectives: First, to develop an economic evaluation methodology to evaluate the net economic benefits resulting from the use of dynamically improved equipment in providing transportation service; second, to provide an evaluation of the system economics of a conservatively designed high performance car which minimally meets the specified performance goals in a range of operating scenarios.

The major emphasis of this study was on the comparison of a high performance/high cube covered hopper car to the current conventional 100 ton covered hopper car. A limited comparison with the lighter 80 ton car was conducted to indicate the relative economics of the three alternatives in the areas of rail, fuel, accident, and car maintenance.

The major components of system economics of utilizing freight cars in providing rail transportation service are shown in Figure 3. For the economic

DYNAMICALLY STABLE, BULK COMMODITY CAR

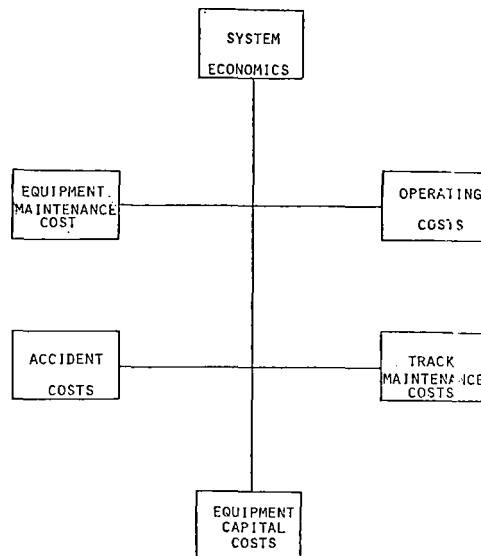


Figure 3

analysis of the high performance/high cube covered hopper, the optimum approach to modeling each of these components was identified and benefit estimates developed on a component-by-component basis. These benefits were aggregated to a net annual benefit associated with the provision of 2.5 million ton-miles of service per car per year (25,000 miles carrying 100 net tons with an equivalent empty back-haul). The incremental capital investment justified by these benefits was then computed.

The base case 100 ton covered hopper was assumed to have 263,000 pound gross weight with 63,000 pound tare weight and two two-axle conventional three-piece trucks with 36 inch wheels resulting in 33 kip static wheel load. The conventional light car alternative was assumed to have a gross weight of 220,000 pounds with a tare weight of 60,000 pounds resulting in a load capacity of 80 tons. The light car has two two-axle conventional three-piece trucks with 33 inch wheels resulting in a 28 kip static wheel load.

The high performance/high cube covered hopper was assumed to have a 263,000 pound gross weight with a 63,000 pound tare weight and 100 ton load capacity. It was assumed to have two two-axle radial trucks with 36 inch wheels and an improved suspension system resulting in a 33 kip static load and a 50% reduction in lateral and a 25% reduction in vertical dynamic loads. These assumptions provide a conservative representation of the high performance/high cube covered hopper car minimally meeting the goals set forth in the performance guidelines.

Economic benefits associated with improved car design depend on the service utilization rates and on the nature of service provided. Initial comparisons were based on a car providing 2.5 million ton-miles of service per year, or 25,000 loaded car miles with a 100 ton load. An equal amount of empty car mileage (back-haul) was assumed in each analysis. This level of utilization of 50,000 car miles per year is somewhat greater than the present covered hopper fleet average, but substantially below the utilization rate of equipment in unit train operation. This level of utilization is representative of a well-managed grain service pool.

Other important dimensions of the type of service provided include the typical speed of movement, the degree of curvature and gradient of the route, and the quality of the track. For the analyses, the typical operating speed was assumed to be 45 mph, which represents moderate speed main line freight service on many roads in grain territories.

Three alternate route specifications having variations of gradient and curvature were evaluated including the following:

- A tangent route consisting of 100% less than 1/2 degree curvature in level territory,
- A moderate route consisting of 85% less than 1/2 degree, 7.5% of 1/2 degree to 2 degrees, 5% of 2 degrees to 5 degrees, and 2.5% of greater than 5 degrees curvature in low gradient territory, and
- A severe route consisting of 61.5% less than 1/2 degree, 5.4% of 1/2 degree to 2 degrees, 21.1% of 2 degrees to 5 degrees, and 12.0% of greater than 5 degrees curvature with moderate gradients.

These routes were selected as representative of the operating environment of most bulk commodity movements in the U. S. rail system. The tangent and severe routes represent actual track segments of approximately 100 miles in length, while the moderate route, based on the opinion of industry people knowledgeable in the area of track, is a typical North American route.

To allow meaningful comparison among the alternative car specifications without conducting an extensive number of evaluations, certain parameters which effect component lives or maintenance cycles and the economic consequences of these variations were held constant in this study.

- A traffic density of 15 MGT per year involving 50% fully loaded movements and 50% empty returns with all traffic in cars of the specified design,
- Track constructed of 136 lb. per yard continuous welded rail (CWR) of standard carbon metallurgy on wood ties; and
- Track support characterized by a track modulus of 2,000 pounds per inch per inch representing moderate ballast and subgrade conditions.

To evaluate the potential impact of the alternative cars on track maintenance costs, an engineering model developed by the Canadian Institute for Guided Ground Transport (CIGGT) was utilized. This model was further enhanced to deal with non-rail portions of track maintenance cost and to incorporate fatigue considerations in predicting rail life.

The accident record of the high performance/cube covered hopper car cannot be determined from historic data, but given the dynamic performance goals, the assumption that it should be no worse than the average car in the existing rail fleet appears to be a conservative assumption and was used in the economic evaluation.

In analyzing potential benefits from reduced car maintenance cost, there appears to be no measurable difference per car mile between conventional 100 ton and conventional 80 ton covered hoppers; however, because of the greater number of 80 ton car miles required, a proportionate increase in cost could be anticipated.

For the high performance/high cube 100 ton car, potential maintenance savings in the area of wheel wear, primarily in the flange with a small amount of rim wear reduction, were identified. Although no specific modeling was done of the relationship between wheel flange and rim wear as a function of lateral and vertical dynamic forces, an approximation that the wheel wear differentials are proportional to the rail wear differentials was used to estimate equivalent annual benefits through improved dynamic behavior.

The use of high performance/high cube cars should produce fuel savings due to the improved curving behavior resulting in lowered train resistance in curves. The 80 ton car has an increased fuel requirement due to the increased number of car-miles required to provide the equivalent 2.5 million net ton-miles of service per year and the increased tare weight involved. The Train Operations Simulator (TOS) developed by the Track Train Dynamics program was utilized for the evaluation of the fuel requirements for

for operations over the specified routes.

Figures 4, 5, and 6 show the predicted annual

COST COMPARISONS WITH CURRENT 100-TON CAR
SEVERE CURVATURE - MODERATE GRADE ENVIRONMENT

COST CATEGORY	IMPROVED 100-TON CAR		CURRENT 80-TON CAR	
	ANNUAL SAVINGS ¹	WARRANTED ² INVESTMENT	ANNUAL SAVINGS ¹	WARRANTED ² INVESTMENT
TRACK	\$ 259	\$ 3,864	\$ 366	\$ 5,461
ACCIDENT	\$ 164	\$ 2,447	(\$ 84) ³	(\$ 1,253)
CAR MAINTENANCE	\$ 75	\$ 1,119	(\$ 258)	(\$ 3,849)
OPERATING (FUEL)	\$ 72	\$ 1,074	(\$ 170)	(\$ 2,536)
TOTAL	\$ 570	\$ 8,504	(\$ 146)	(\$ 2,177)

¹ IN AFTER-TAX DOLLARS ASSUMING A 48 PERCENT MARGINAL TAX RATE.

² IN BEFORE-TAX DOLLARS ASSUMING A 9 PERCENT DISCOUNT RATE, A 10 PERCENT INFLATION RATE, A 20 PERCENT HURDLE RATE, A 48 PERCENT MARGINAL TAX RATE, AND A .0 PERCENT INVESTMENT TAX CREDIT.

³ () INDICATES HIGHER COST THAN BASE (LOSSES).

Figure 4

COST COMPARISONS WITH CURRENT 100-TON CAR
MODERATE CURVATURE - LEVEL ENVIRONMENT

COST CATEGORY	IMPROVED 100-TON CAR		CURRENT 80-TON CAR	
	ANNUAL SAVINGS ¹	WARRANTED ² INVESTMENT	ANNUAL SAVINGS ¹	WARRANTED ² INVESTMENT
TRACK	\$ 130	\$ 1,940	\$ 317	\$ 4,730
ACCIDENT	\$ 164	\$ 2,447	(\$ 84) ³	(\$ 1,253)
CAR MAINTENANCE	\$ 25	\$ 373	(\$ 258)	(\$ 3,849)
OPERATING (FUEL)	\$ 13	\$ 194	(\$ 160)	(\$ 2,387)
TOTAL	\$ 332	\$ 4,954	(\$ 185)	(\$ 2,759)

¹ IN AFTER-TAX DOLLARS ASSUMING A 48 PERCENT MARGINAL TAX RATE.

² IN BEFORE-TAX DOLLARS ASSUMING A 9 PERCENT DISCOUNT RATE, A 10 PERCENT INFLATION RATE, A 20 PERCENT HURDLE RATE, A 48 PERCENT MARGINAL TAX RATE, AND A .0 PERCENT INVESTMENT TAX CREDIT.

³ () INDICATES HIGHER COST THAN BASE (LOSSES).

Figure 5

COST COMPARISONS WITH CURRENT 100-TON CAR
STRAIGHT, LEVEL TRACK ENVIRONMENT

COST CATEGORY	IMPROVED 100-TON CAR		CURRENT 80-TON CAR	
	ANNUAL SAVINGS ¹	WARRANTED ² INVESTMENT	ANNUAL SAVINGS ¹	WARRANTED ² INVESTMENT
TRACK	\$ 82	\$ 1,223	\$ 300	\$ 4,476
ACCIDENT	\$ 164	\$ 2,447	(\$ 84) ³	(\$ 1,253)
CAR MAINTENANCE	\$ 4	\$ 60	(\$ 258)	(\$ 3,849)
OPERATING (FUEL)	\$ 0	\$ 0	(\$ 138)	(\$ 2,059)
TOTAL	\$ 250	\$ 3,730	(\$ 180)	(\$ 2,685)

¹ IN AFTER-TAX DOLLARS ASSUMING A 48 PERCENT MARGINAL TAX RATE.

² IN BEFORE-TAX DOLLARS ASSUMING A 9 PERCENT DISCOUNT RATE, A 10 PERCENT INFLATION RATE, A 20 PERCENT HURDLE RATE, A 48 PERCENT MARGINAL TAX RATE, AND A 10 PERCENT INVESTMENT TAX CREDIT.

³ () INDICATES HIGHER COST THAN BASE (LOSSES).

Figure 6

savings for each selected operating environment. As may be noted, the potential increase in per car investment warranted by a high performance/high cube covered hopper car ranges conservatively from \$3730 to \$8504. Conversely, a conventional 80-ton car utilized in the same service would warrant a per car cost reduction of from \$2177 to \$2685. This latter case does not take into account additional handling costs (siding capacities, switching costs, etc.) which a larger fleet size would cause to be incurred.

It should again be noted that these economic evaluations were preliminary and comparative estimates should be considered accordingly. The Engineering Economics Division is continuing to enhance their evaluation techniques and will apply the latest methods in evaluating the potential impact of the high performance/high cube covered hoppers.

TEST PLAN

The basic rationale for the test program is to conduct comparative performance tests between a base car and each prototype car. The tests will cover each of the dynamic performance regimes, especially those that have a direct bearing on wheel/rail wear, track degradation and derailment potential. Emphasis will be on comparing parameters in the format defined by the performance guidelines. The dynamic characteristics are again considered under three separate major categories: Stability (including nine separate sub-categories), Ride Quality, and Impact (yard and train).

The plan envisages tests in the following dynamic performance regimes:

1. Curving, including curve entry/exit
2. Rock and Roll

3. Vertical Bounce
4. Hunting
5. Ride Quality

The base car will be a 100 ton, 4750 cubic foot covered hopper of conventional design. For the rock and roll, vertical bounce, and curving tests, the car will be tested in the empty condition only. A suitable lading will be obtained so that the car is filled to cubic capacity at gross rail load.

Dynamic Tests

Dynamic tests will be done at the Transportation Test Center, Pueblo, Colorado. The appropriate test tracks will be delineated as test zones covering the balloon loop, the LIM Track, the Railroad Test Track (RTT), and the Transit Test Track (TTT). Site selections are contingent upon an operations review to ascertain if the speed and other desired conditions are obtainable.

Curving

Curving tests will mainly be for the loaded condition. The curving regime is divided into curve entry/exit and steady state curving. Alternate wear indices will be developed for the base car and for each prototype car. These will require measurement of vertical and lateral forces for the wear critical wheel, along with the angle of attack and the L/V ratio. It is expected that the following curves will be identified as test zones: 0°50' (RTT), 1°30' (TTT), 3° (FAST, 17), 4° (FAST, 13), 5° (FAST), 5° reverse (FAST, 7) and 7½° (Balloon Loop). At-balance, under-balance and over-balance conditions will be run, with two above and two below the nominal balance speed. Curving data will be acquired without track lubrication. The spirals leading to the above curves will be used as curve entry/exit test zones.

Data output formats will consist of means, standard deviations, and probability distributions for the steady-state curving performance. For curve entry, time histories and minimum vertical wheel loads and maximum L/V ratios will be produced. For angle of attack data, mean values and standard deviations will be obtained for each test zone.

Harmonic Roll

Particular emphasis is to be placed on roll performance for both the empty and loaded conditions. Car body roll angle and wheel vertical unloading will be the primary criteria for comparison.

The first series of rock and roll tests will be run on tangent perturbed track. The perturbed track shall be configured to provide 20 rail lengths of perturbations. The resonance condition shall be determined, with 1 mph resolution for the empty and loaded car. At a minimum, the 3/4 inch low joint track condition will be the condition selected for the roll site. It is also anticipated that curve roll tests will be done on the 7½° balloon loop.

Vertical Bounce

A series of vertical bounce simulations with rectified sine bounce conditions will be done on the LIM. Parallel non-staggered track, with 19½ ft. joint

spacing and configured to a rectified sine profile representing 3/4 inch low joints will be used. Vertical car body acceleration at each body center plate and vertical wheel unloading shall be the primary criteria for evaluation. Truck transmissibility using vertical accelerations will also constitute an evaluation criteria.

Truck Hunting

Tests will be conducted to determine the hunting characteristics of each car. Critical speed at onset of wheelset hunting, full flange-to-flange hunting speed, and RMS lateral acceleration at each end of the test car will be monitored. Since these characteristics are wheel profile dependent, the tests will be run in three series: first, with an effective conicity of 0.3; second, with modified Heumann wheelsets, and lastly, with instrumented wheelsets with prevailing profiles. Matched wheelsets, with the same conicity on all wheel/rail interfaces will be used. The lateral loads on a wheelset during onset and flange-to-flange hunting conditions will be obtained using a pair of instrumented wheelsets for the last set of runs. The higher speed curving runs for empty cars may be combined with the truck hunting runs. All hunting tests will be for the empty car only.

Ride Quality

The objective here is to define the vertical load environment seen by the car body as it relates to the ride quality afforded the lading as well as the fatigue life expectancy of car body structural components.

To quantify this dynamic performance regime, it is necessary to have revenue service data covering a spectrum of operating conditions. It is also desirable to obtain direct comparisons between base cars and prototype cars during simultaneous operation.

To quantify ride quality performance, it is proposed to measure vertical car body accelerations at the center plate and bolster center plate loads and side bearing loads.

Static Tests

Each prototype covered hopper will be tested in accordance with the AAR Mechanical Division specifications. Car body squeeze tests and brake system tests will be conducted at the AAR Technical Center in Chicago. In addition, a modal analysis test will be conducted to ascertain the structural adequacy of each prototype.

Evaluation Reports

Detailed technical reports will be issued covering performance testing and economic evaluation of each prototype. In all cases, the prototype cars will be compared to the conventional base car. No comparisons among prototypes will be made.

STATUS

Three car builders are presently participating in the high performance/high cube covered hopper car program. Detailed designs have been completed by The Budd Company and the Thrall Car Manufacturing Company. Present schedules call for testing prototypes built to these designs in late 1982 and early 1983. ACF is

presently completing their detailed design, and the test program for this car is scheduled for mid-1983.

REFERENCES

1. Proposed National Research Program on Track-Train Dynamics, Prepared by Southern Pacific Transportation Company for the Association of American Railroads, March 31, 1972.

2. Manos, W. P., Johnstone, B. and Hawthorne, K. L., "Performance Guidelines High-Performance/High Cube Covered Hopper Car, 100 Tons or Greater," June 1980, Association of American Railroads.

3. Hargrove, M. B., "Economic Evaluation Methodology: High Performance/High Cube Covered Hopper Car," March 1980, Association of American Railroads

The Design of a 104-t Rotary Dump Gondola Coal Car for the Upgraded Richards Bay Coal Export Line

H.M. Tournay

B.Sc. Eng. (Mech.) (Rand)
Mechanical Engineer
(Structures)
Design Section
South African Railways
Pretoria
South Africa

Increased demand on the export of coal from South Africa necessitated upgrading the line to accommodate trains consisting of 200 rotary dump gondola coal cars of 104 tons each, head hauled by four locomotives against ruling grades of 1:160. The rationale behind the choice of train consistency is discussed together with the demands placed on the cars with respect to physical dimensions, axle load, load/tare ratio, draft, buff and braking forces. These requirements were met by a car of monocoque construction with a load/tare ratio of 4:2. The design philosophy behind the monocoque construction is discussed, including aspects such as overall strength, reduction of stress concentration and weld design detail. The results of a Finite Element Stress Analysis of the car is compared with strain gauge tests under static conditions.

1.0 INTRODUCTION

The Richards Bay coal line was originally constructed in 1976 for the export of 22×10^6 t per annum from the coal fields of the Eastern Transvaal through Richards Bay on the eastern seaboard of South Africa. On being loaded at the mines the coal is hauled over 3 kV d.c. lines with a ruling gradient of 1:100 (compensated) to a central marshalling yard at Ermelo and subsequently over a 25 kV a.c. single line with a ruling gradient of 1:66 (compensated) to Richards Bay. The maximum distance travelled from the mines to Ermelo is 165 km, the distance from Ermelo to the port is 405 km, the gauge is 1 065 mm and the minimum curve radius is 500 m.

Until 1979 train consists comprised 84 type CCR rotary dump gondola coal cars each with a loaded mass of 74 t (18,5 t axle load) and one caboose, head hauled by either five type 6E1 d.c. locomotives or four type 7E a.c. locomotives. In 1979 in order to increase line capacity and after tests on both rail and car a 20 t axle load service was successfully introduced using existing rolling stock. A prerequisite for this move was that all cars would be fitted with Scheffel radial axle trucks so as to minimise track and wheel damage. Details of existing rolling stock are listed in appendix A.

The demand for export coal is expected to reach 44×10^6 t per annum by 1986 and measures were sought to meet this demand under the following constraints:

1.1 Any measure to increase capacity should not affect the present increasing coal exports.

1.2 There is a limit of 26 t axle load for cars and 28 t for locomotives on existing bridges and structures on the Richards Bay line.

1.3 For practical and economic reasons a minimum limit of 1:160 (uncompensated) was placed on the ruling grade on the line between Ermelo and Richards Bay; downgrades for the loaded train would remain at 1:66. Grades would remain unaltered between the mines and Ermelo.

1.4 Consideration of train brake response times placed a maximum limit on train length at 2,4 km (i.e. 200 cars each of length 12 m).

The decision was taken to upgrade the line for 26 t axle load operation for cars and 28 t axle load for locomotives; the line would be regraded to the limits set in 1.3. In order to achieve an output of 44×10^6 t per annum train consists comprising 200 cars each with a load of 84 t of coal were required to operate over the single line between Ermelo and Richards Bay; between the mines and Ermelo train consists would comprise 100 cars each. These trains would be head hauled by either type 10E d.c. or type 11E a.c. locomotives; tenders are being called for the supply of these locomotives, basic specifications for which are given in appendix B. The option of doubling the line between Ermelo and Richards Bay was retained for future expansion to a proposed 80×10^6 t per annum.

This decision together with constraints 1.1 to 1.4 placed exacting demands on the design, supply and delivery of rolling stock and the future operation of train consists.

2.0 26 t AXLE LOAD OPERATION

The decision to upgrade the Richards Bay coal line to 26 t axle load operation should be seen in the light of the favourable experience gained with such operation on the Sishen - Saldanha export iron ore line. Since its inception in 1976, this line

has been operated under 26 t axle loads (for cars) on UIC 60 rail. All cars were fitted with Scheffel radial axle trucks and wheels with profiled treads. Initial problems were encountered with the formation of fatigue cracks on the subframe of the truck and with the formation of head checks on the rail [1]. An improved subframe design was introduced and has been in trouble-free operation for 4 years [1]. The problem of head check formation has been successfully stopped by the introduction of an improved wheel tread profile [2]. A greater understanding and experience of wheel/rail contact conditions has resulted in the design of a rail profile on the Richards Bay line which is better suited for 26 t axle load operation and which is designed to avoid the conditions favourable to the formation of head checks [2].

It was considered that the South African Railways (S.A.R.) had the capability of operating a line under 26 t axle loads with a truck of dynamic and structural integrity to keep rail and wheel damage to a minimum.

3.0 TRAIN FORCES ON THE UPGRADED RICHARDS BAY COAL LINE

The requirement for 200 car trains head hauled against the grade limitations set in 1.3 will increase longitudinal static train forces beyond limits presently experienced on the S.A.R. - affecting in particular the performance of proprietary drawgear components.

The highest continuous static coupler force presently experienced on the S.A.R. is 1 220 kN. Under these conditions no yoke failures have been experienced using yokes, at present the weakest link in existing drawgear, with a yield strength of 2 330 kN (grade C steel). This would imply that a maximum dynamic augment of 0,9 could occur under present train handling conditions (if the maximum dynamic augment is assumed to be the ratio of the yield strength to the static load). The maximum continuous coupler force on a train of 200 cars, each having a loaded mass of 104 t on a ruling grade of 1:160 is 1 500 kN. Hence the introduction of 200 car trains on the upgraded Richards Bay line implies a required maximum reduction in dynamic forces in the train to 0,6 - of the order of 30 %. It was considered that such a reduction could be achieved for the following reasons:-

3.1 Cars will be semi-permanently coupled in pairs by means of bar couplers, thus reducing free slack in the train.

3.2 A brake ratio of 16 % will be used on the 104 t cars as against a ratio of 27 % presently in use; thereby reducing force differentials between adjacent cars during the propagation of brake applications and releases.

3.3 It is planned to reduce adhesion demand by locomotives on ruling gradients from 26,1 % on the existing locomotives to 24 % on new locomotives for the upgraded line. This measure could reduce the dynamic loading on the train resulting from wheelslip or wheelslip correction, when high tractive efforts are exerted.

3.4 Until now no means of measurement of in-train forces at numerous points in the train has been available on the S.A.R. By the time 200 car trains are operative a train dynamics instrumentation vehicle will be in service. A knowledge of in-train forces and their propagation will enable problem areas in

train handling to be identified and analysed and remedial action taken.

3.5 A train dynamics simulator is available on the S.A.R. which will permit thorough driver training and thereby minimise dynamic forces which can be ascribed to poor handling techniques. The number of drivers operating trains on the Richards Bay line is small enough to permit individual training on the simulator.

Problems have been encountered on the Sishen - Saldanha line with knuckle failure. This phenomenon has been attributed to the generation of unwanted emergency brake applications due to faulty ABDW brake valve operation. Shorter, regular maintenance schedules have been introduced to reduce the occurrence of unwanted emergency applications and a system is presently being developed to enable the faulty valve to be detected under operating conditions and in turn reduce the incidence of knuckle failure.

A further problem area in train handling is envisaged when the loaded train stops at a signal on a 1:66 downgrade. Since the standard AAR quick release air brake system is envisaged the possibility exists that the train brakes require to be recharged whilst the train is held at the signal. Under these conditions the train could exert a compressive force of approximately 3 MN on the rear coupler of the rear locomotive in the consist. If conventional locomotive brakes were used the adhesion available at the locomotives would be exceeded. At the time of writing two alternative brake configurations are being assessed:

3.6 A second train pipe could be introduced to couple the locomotive brake air supply directly to the brake cylinders on a limited number of cars immediately adjacent to the locomotives. This connection could be effected by means of a double check valve placed as shown in figure 1. Thus the combined adhesion of the locomotives and certain cars in the train would hold the train on the downgrade whilst the train brakes were recharged. Consideration of locomotive brake air supply pressure, the time re-

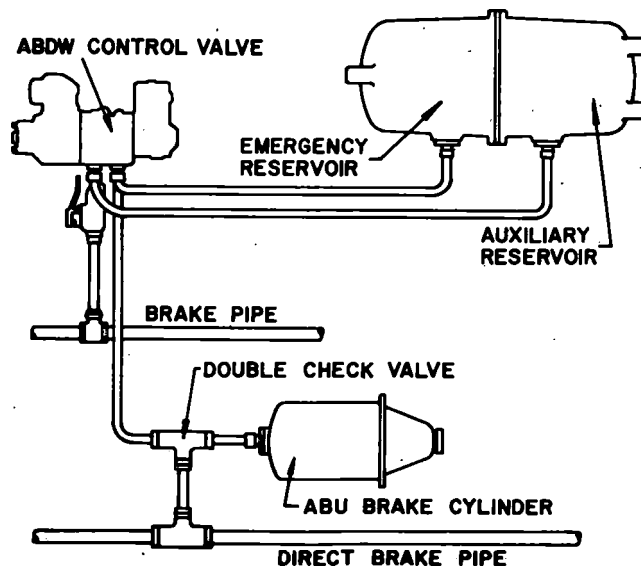


FIGURE 1: POSSIBLE TWO-PIPE BRAKE CONFIGURATION

quired to supply both the locomotives and cars with air, the air capacity available and the maximum compressive coupler force allowable in the train would determine the number of cars to be braked in this manner.

This system has the advantage that the train is held positively on the downgrade during recharging and that the normal operation of the train brakes is unaffected by the modification. It has the disadvantage that the complete car fleet would have to be fitted with the second pipe system to avoid problems in marshalling and that maintenance problems (leaks, burst pipes) are increased.

3.7 The use of retainers is being considered to throttle the release of air from the car brake cylinders on recharging the train brakes. With this system the time available to recharge the brake system must be less than the time taken to release the brakes under throttled conditions plus the time taken for the train to accelerate to operating speed down the grade. The advantage of this system is that it requires the minimum of hardware. The maximum static compressive force in the train will be approximately 2,2 MN - the adhesion available to the locomotives when braking. Under normal braking, response times will obviously be increased.

Tests are presently being conducted to assess the merits of both systems and the influence of reduced response time of arrangement 3.7 on normal train handling.

4.0 THE DESIGN OF A 104 t CAR DESIGNATED CCL-5

4.1 Capacity

The density of export grade coal through Richards Bay is a maximum of 958 kg/m^3 . In order to obviate the possibility of overloading at facilities where manual or volume based loading controls are installed the car was designed with sufficient capacity for the maximum coal density. A lower limit was placed on the tare mass of the car at 20 t; the heaped volume of the car was thus required to be $87,7 \text{ m}^3$.

The existing fleet of 20 t axle load CCR cars was inadequate to meet constraint 1.1 in the period up to 1986. Rather than build further CCR cars for the transition period, which would become obsolete for the line after 1986, it was decided that the 104 t car should be produced from 1982 and placed in operation together with existing 80 t cars on the line under a reduced axle load of 20 t. The 104 t cars thus had to be geometrically compatible with existing loading and dumping facilities and in turn with existing cars. In order to comply with this condition and condition 1.4 the length of the CCL-5 car requires to be identical to that of the CCR car - hence an additional 20 m^3 had to be found within the length of the existing car.

The means by which the additional volume was obtained is illustrated in figure 2. The 80 t car is of bathtub construction similar to cars at present in operation in the United States of America. It may be seen that within the existing car width additional volume has been obtained by placing stanchions on the inside of the car as opposed to the previous design. The bathtub has been broadened and lowered to follow the moving structure gauge; the clearance of the bathtub to the rail is such that in most derailments occurring at slow speeds in marshalling yards, the bathtub would not contact the rail and would thus remain undamaged. As a result of lowering the bathtub

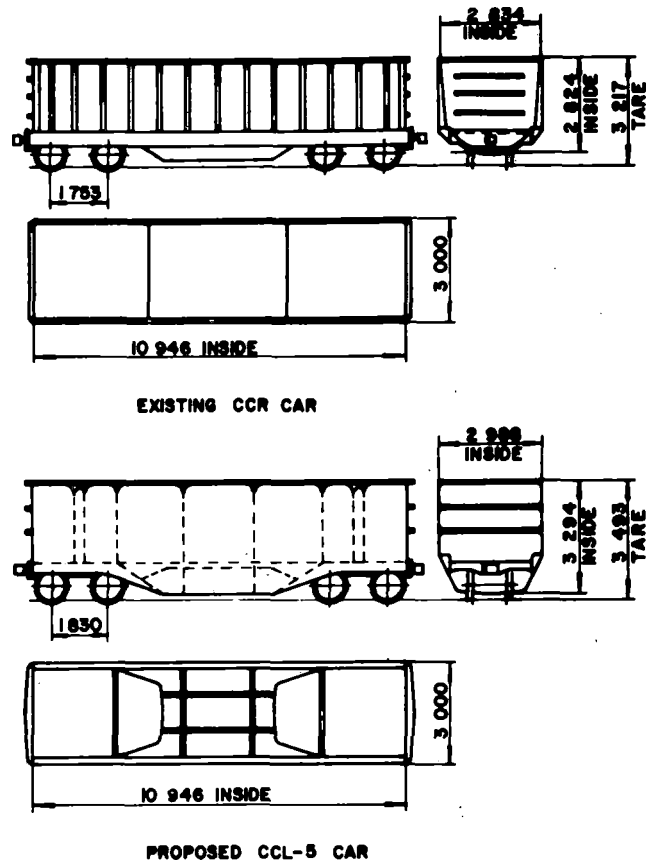


FIGURE 2: OVERALL DIMENSIONS OF CCR AND CCL-5 CARS

profile and since heavier 26 t axle load trucks are fitted, the overall height of the car could be increased without exceeding the present limitation of 1,83 m on the height of the centre of gravity. An increase in the height of the car implies minor alteration to the constraining booms on the cage of the rotary dump facility so as to accept both car heights.

4.2 Structural Requirements

Structural specifications for car design on the S.A.R. closely follow the A.A.R. equivalent with the exception of the minimum compressive end load which the car should withstand; in this instance the allowable minimum set by the S.A.R. is 3,56 MN against that of 4,45 MN presently set by A.A.R. Cars designed to the S.A.R. specifications in unit train operation in South Africa have proved to be structurally adequate. Since the tare mass of the car is largely influenced by this load condition it was decided to retain the present S.A.R. standard and rather extend efforts towards reducing dynamic train forces and limit static compressive train loads, this decision could influence the choice of holding brake configuration described in 3.6 and 3.7.

A deviation from present A.A.R. specifications and the identical S.A.R. equivalent has been effected in the required strength of the end wall of the car. It was argued that the present requirements were specified to enable the car to withstand forces imposed by the lading on the end wall during fly shunting

operations. Fly shunting operation is not permitted on the Richards Bay line; if it does occur en route to the line ex workshops or on being taken out of service for maintenance purposes the car is invariably empty. It was decided to reduce the strength requirements of the end wall by an arbitrary 30 % on existing coal cars. Limited tests and experience to date have not revealed any adverse effects. This aspect is being investigated further.

Indexing equipment (train pushers and train locks) at the loading and dumping facilities have been designed to engage between the cars in the manner indicated in figure 3. Forces of a maximum of 0,59 MN may be applied in this way to the side sills of the car.

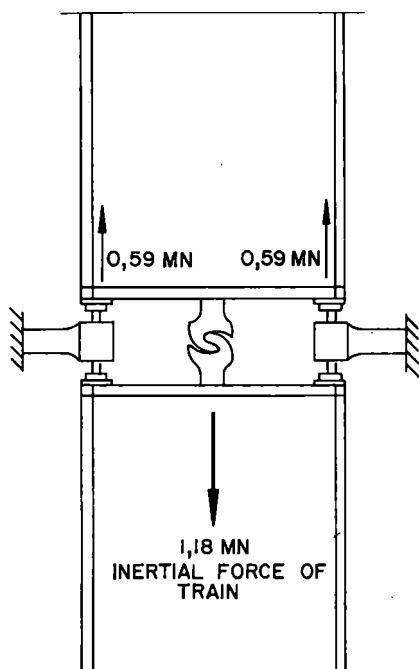


FIGURE 3: PLAN VIEW OF COAL CARS INDICATING THE ENGAGEMENT OF THE TRAIN INDEXING MECHANISM AND RESULTANT FORCES ON CAR

4.3 Structural Design

4.3.1 The Design Concept. Traditionally, car design on the S.A.R. has centred on steel construction methods similar to those used in America; an underframe is fabricated from rolled sections onto or integral with which is mounted a stiffened box structure to contain the lading. Initial investigation revealed that a car designed according to this method would not meet the capacity constraints of 4.1 and the maximum tare constraint of 20 t. Experience on the S.A.R. in the use of lightweight materials in car construction is at present limited; a single car of aluminium construction has been placed in service to gain more experience with this material. It was thus considered prudent at this stage to retain steel (in

this case Corten) as the construction material and exploit a monocoque design concept in order to meet capacity and tare demands.

Consideration of design for lightweight car construction leads the designer to the hypothesis that the optimum would be a car in which all the material in its structure would be equally stressed to the limit of its strength under all required load combinations. A corollary to this statement is that stress gradients through the structure should be zero - there should be no regions of stress concentration. Attempts to achieve this idealised structure are hampered by geometric constraints and the fact that intense concentrated loads are applied in the region of the drawgear pocket. It was however considered of prime importance in developing the design concept to approximate as closely as possible the idealised model.

In pursuing the design concept, it was concluded that the best means of approximating the idealised model and exploiting a monocoque design was to form the body into a shell of varying plate thickness integral with the underside of the drawgear pocket (figure 4). This shell would then be cut-away to allow clearance for the truck wheels and be strengthened by means of a floor plate integral with the top of the drawgear pocket and welded to the car side and bathtub floor; webs would be placed between the body shell and the floor to form stub sills, the body bolster, and side sills. The shell would then be stiffened against buckling and strengthened in areas of stress concentration by introducing internal ribbing in order to achieve a structure of uniform stiffness and with minimum stress gradients.

After finalising the design concept use was made of the Finite Element Method (F.E.M.) of stress analysis to examine the linear behaviour of the body shell. Since little experience was available to assess the non-linear plate buckling behaviour of the structure a design prototype car was built in order to assess the optimum placing of internal stiffening ribs; the integrity of the F.E.M. model was checked by means of strain gauges.

4.3.2 Structural Analysis and Tests. A linear, static three-dimensional analysis of the structure was made using the F.E.M. programme 'Stardyne' [3]. The body shell was modelled with quadrilateral and triangular plate elements overlaid with beam elements to simulate the stiffening ribs. A mesh was constructed of one quarter of the car using a total of 315 elements and 1 326 degrees of freedom and constrained as shown in figure 5; the loading conditions simulated are also shown.

A design prototype car was built in the Bloemfontein Mechanical Workshops of the S.A.R. in order to check the integrity of the F.E.M. model and the design detail and to assess the buckling stability of the body shell (see figure 6). In order to minimise tooling required for the design prototype and to allow freedom to reposition internal stanchions during test, the side panels of the body shell were not pressed. In other respects the prototype conformed to the design as initially modelled by means of the F.E.M. The car body was subjected to a compressive end load in both the empty and loaded condition (loaded with water). The end load was increased in seven discrete steps of approximately 0,5 MN to a maximum load 3,56 MN. Electric resistance strain gauges were used to record stress levels within the body in regions of high stress predicted by the F.E.M. model. In areas of the shell where the possibility of buckling instability was considered to be high, strain gauges were

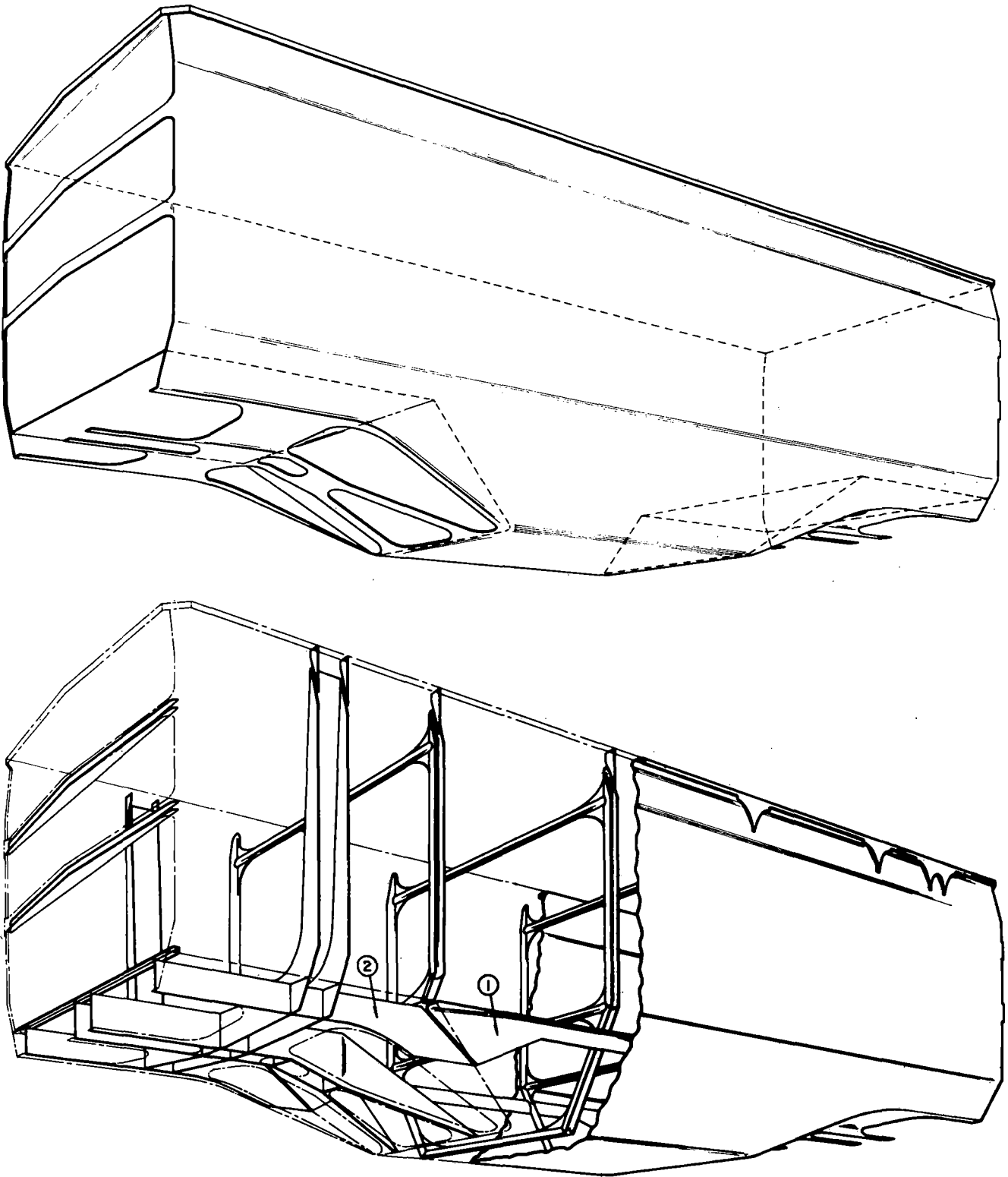
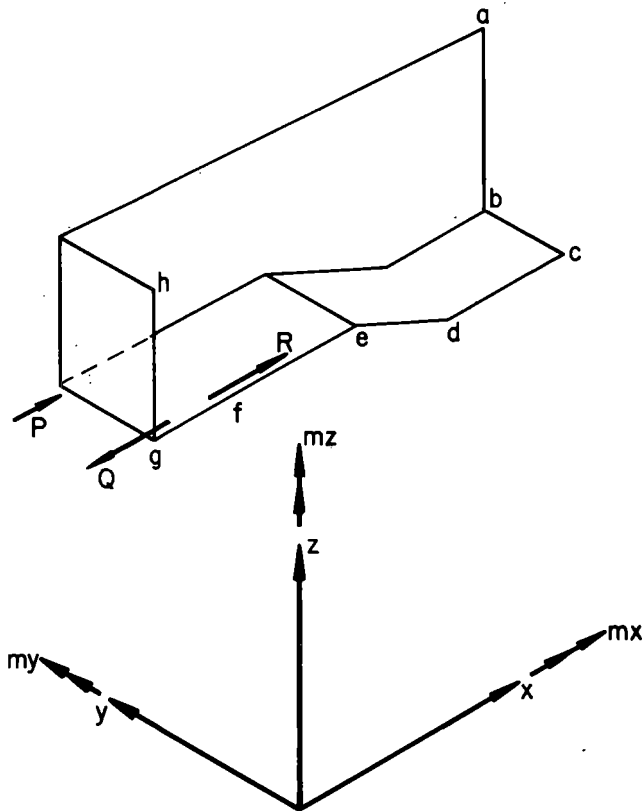


FIGURE 4: FORMATION OF SHELL AND STIFFENING MEMBERS



IMPLIES TRANSLATION (x, y, z)

IMPLIES ROTATION (m_x, m_y, m_z)

CONSTRAINT APPLIED TO: NODES ON:

EDGE AB: x, m_y, m_z

EDGE BC: x, m_y, m_z

POINT C: x, y, m_x, m_y, m_z

EDGE CDEG: y, m_x, m_z

POINT F (TRUCK CENTRE): y, z, m_x, m_z

EDGE GH: y, m_x, m_z

LOADS APPLIED:

LOAD R = $\frac{3,56 \text{ MN}}{2}$

LOAD Q = $\frac{1,56 \text{ MN}}{2}$

LOAD P = 0,59 MN

EACH OF THESE LOADS WAS APPLIED SEPARATELY,
OR IN COMBINATION WITH AN INTERNAL HYDRO-
STATIC LOAD

FIGURE 5 : APPLIED LOADS AND CONSTRAINTS ON F.E.M. MODEL

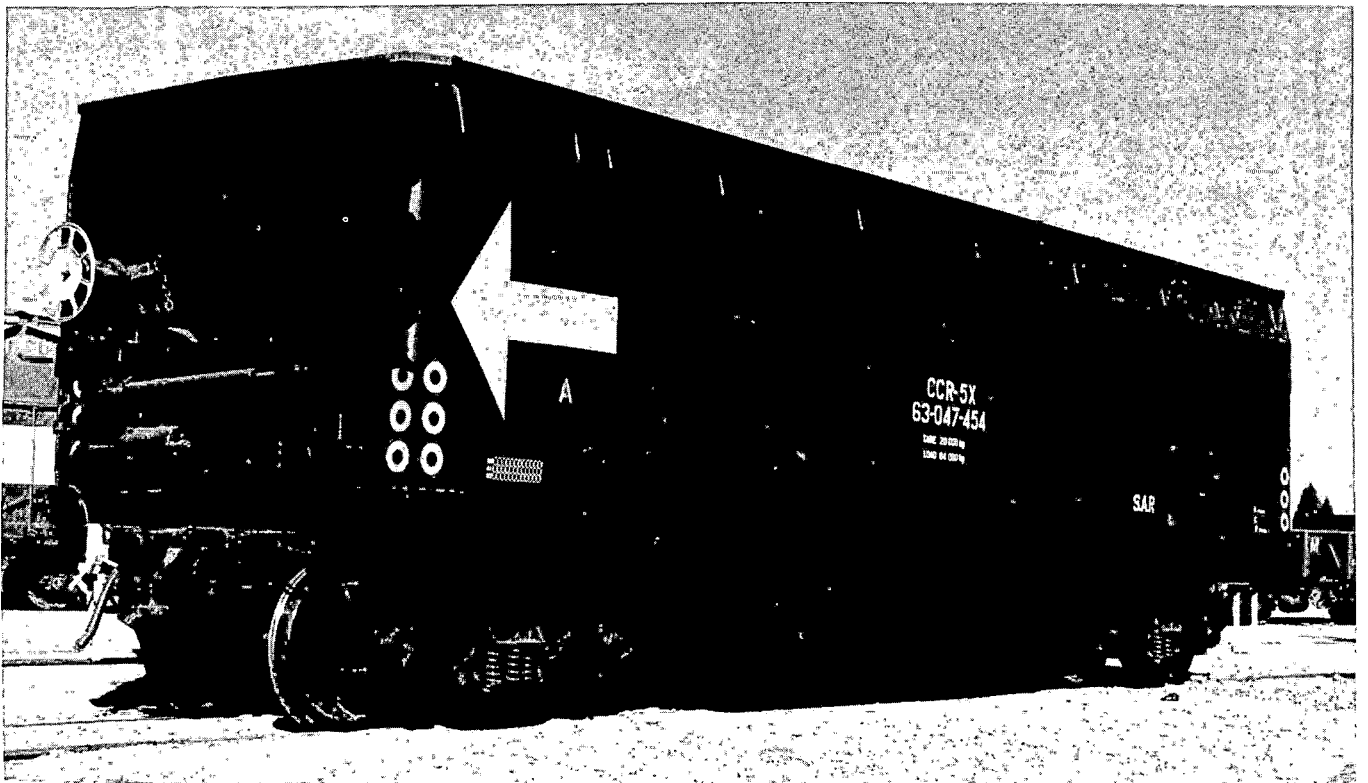


FIGURE 6 : DESIGN PROTOTYPE CAR

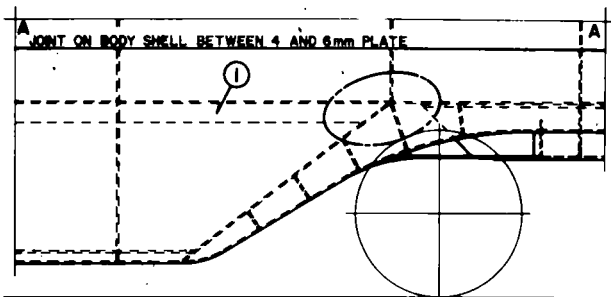
placed in complimentary positions on either side of the plate in order to detect out-of-plane bending as well as in-plane stresses.

The analysis showed that if the shell was constructed of 4 mm plate above line A-A in figure 7 and 6 mm plate below that line (the floor and the bathtub being 6 mm plate) that stresses were below the maximum permissible (Corten having a minimum yield of 345 MPa). However, the structure was by no means evenly stressed under the longitudinal compressive load of 3,56 MN .

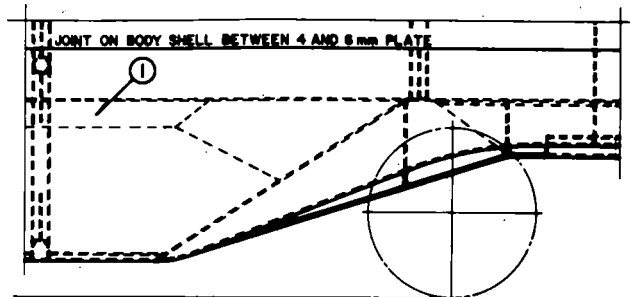
It was found that approximately 80 % of the end load was transmitted directly to the side walls of the shell via shear stresses through that part of the floor of the car over the truck (figure 9b). The remainder of the longitudinal force may be assumed to be transmitted through the stub sills behind the draw-gear pocket to the floor of the bathtub in a bending/compression mode. It is interesting to note that the shear stresses in the floor reach a maximum 'behind' the backstops where the load is applied. Review of the stress profile together with the magnitude of the stresses indicated in figure 10b shows that for this load condition the thickness of the floor plate could

be reduced in the region between the headstock and the body bolster; under the vertical and longitudinal tensile load conditions however, this section of the floor is stressed and hence the floor plate thickness cannot be reduced (see figure 11). It may be seen from figure 9a that the longitudinal compressive load, after being fed in shear through the floor plate to the side walls of the body shell results in a compressive stress in the side wall which peaks at the height of the coupler centre line; this peak is reduced by the influence of a longitudinal strengthening member attached to the side wall (item 1 in figures 4 and 7).

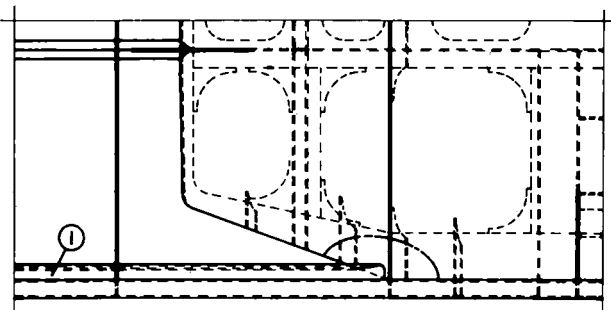
Under the first test load application local collapse due to buckling occurred in that part of the shell and floor indicated in figure 7 under a load of approximately 3 MN . This was due to the omission during construction of a web to box-in the shell/floor area (item 2 in figures 4 and 8). The longitudinal strengthening member (item 1 in figure 7) 'punched through' that part of the floor forming the bulkhead at the end of the bathtub. As a result item 2 was built-in and item 1 was modified so as to butt-up against item 2 through the bulkhead (see figure 8).



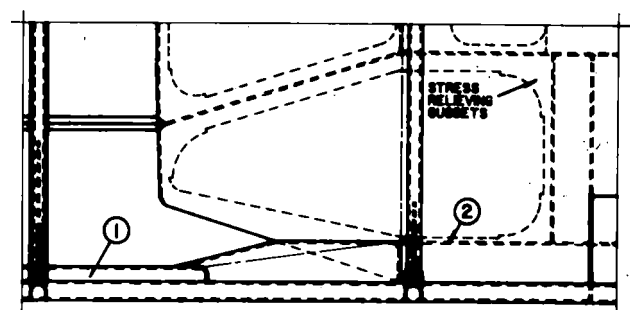
ELEVATION



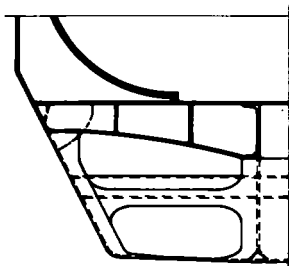
ELEVATION



PLAN VIEW

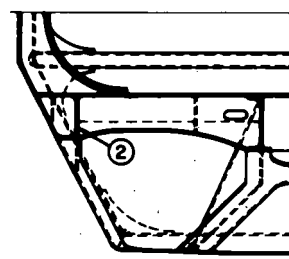


PLAN VIEW



END VIEW

--- INDICATES REGION IN WHICH LOCAL BUCKLING OCCURRED UNDER A LONGITUDINAL COMPRESSIVE LOAD OF APPROXIMATELY 3MN



END VIEW

FIGURE 7: ORIGINAL CONFIGURATION OF TRANSITION BETWEEN BATHTUB AND BODY SHELL OVER TRUCK

FIGURE 8: FINAL CONFIGURATION OF TRANSITION BETWEEN BATHTUB AND BODY SHELL OVER TRUCK

On subsequent loading this modification was found to be satisfactory and strain gauge recordings were taken. The stresses recorded followed closely those predicted by the F.E.M. model. It may be seen however from figure 9a that the test results showed a higher concentration of compressive stresses on the side wall at the height of the centre line of the drawgear. This was attributed to the buckling of the 4 mm plate on the side wall and subsequent loss of in-plane load carrying ability of this plate. Similarly, but to a lesser degree that region of 6 mm plate below the coupler centre line carried less load.

Tests confirmed the stress concentration in the side wall of the car above the trucks as indicated by the stress profile C-C in figure 9a.

It was concluded from the analysis and tests that the concentration of stresses in the floor and side wall would never be completely eliminated as these occurred along the most direct load carrying path through the car. Maximum shear stresses due to the high stress gradients are however within acceptable limits (see figure 10) but in pursuance of the idealised model of an evenly stressed skin the following design changes were introduced:-

**CONTOUR LEVELS
(MPa)**

A	3,5492
B	14,629
C	26,1098
D	37,369
E	48,669
F	59,949
G	71,229
H	82,509
I	93,792
J	105,066
K	116,349
L	127,633

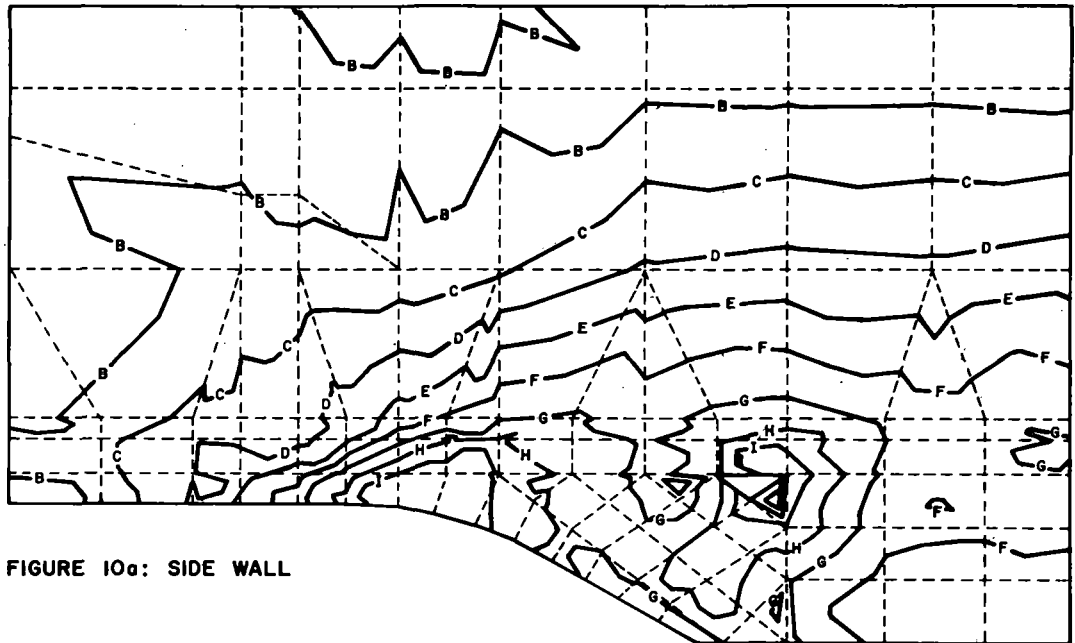


FIGURE 10a: SIDE WALL

**CONTOUR LEVELS
(MPa)**

A	10,85
B	40,978
C	71,107
D	101,239
E	131,36
F	161,491

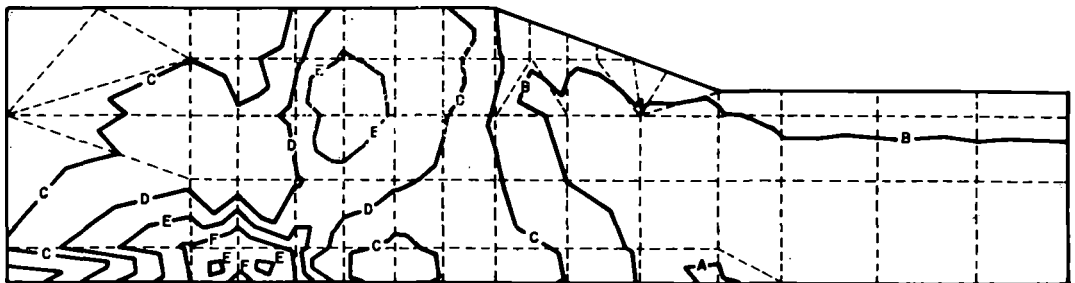


FIGURE 10b: FLOOR

FIGURE 10: PLOT OF MAXIMUM SHEAR STRESS IN THE SIDE AND FLOOR OF THE BODY SHELL UNDER A COMPRESSIVE LOAD OF 3,56 MN APPLIED AT THE BACKSTOPS

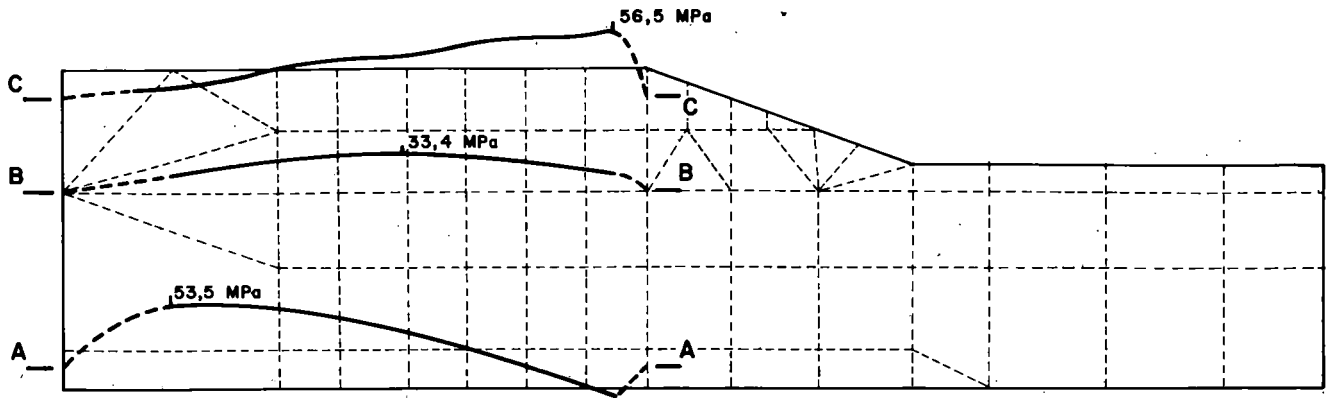


FIGURE 11: SHEAR STRESS IN FLOOR PLATE AS A RESULT OF A TENSILE FORCE OF 1,56 MN APPLIED TO FRONT STOPS

4.3.2.1 The stub sills behind the truck centre casting were altered to form a more direct and hence stiffer coupling between the drawgear backstops and the floor of the bathtub as shown in figure 8. They have been splayed laterally to form an A-frame in order to introduce the longitudinal force closer to the joint between the bathtub floor and the side wall - this being the longitudinally stiffer portion of the bathtub. It was argued that this measure would reduce the forces transmitted through the floor to the side wall and hence relieve the peak stresses in these components on the coupler centre line. In addition that part of the side wall close to the bathtub floor would be more highly stressed thus smoothing the stress profiles D-D, E-E and F-F in figure 9a.

4.3.2.2 The profile of the body bolster and the side wall of the car were altered as shown in figure 8 in order to supply more material in the area of high stresses indicated by profile C-C in figure 9a. It is estimated that this measure will

reduce the peak stress of 183 MPa in this region by 12 %. In addition it will reduce the transition between the bathtub and the body over the trucks and hence the resulting stress concentration.

4.3.2.3 The original embossed design for pressing the 4 mm thick side wall was altered to afford more stiffness against buckling in the region of high stresses near the joint line A-A. The original profile shown in figure 12a was designed to provide diagonal bracing across the side wall plates whilst allowing clean evacuation of the coal on rotary dumping. It is braced along its vertical edges by internal ribs and along the top edge by a 14° kink connecting to the top chord of the car. It has no bracing however along the joint line with the 6 mm plate. The modified pressing shown in figure 12b comprises a series of triangular indents - the base of the bottom indent being close to the weld line with the 6 mm plate. The profile of the indent in this region will provide a maximum slope of 14° to the vertical so as to allow

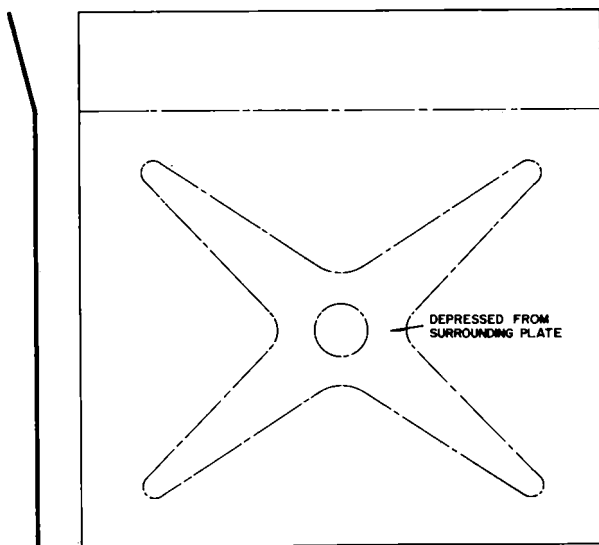


FIGURE 12a: ORIGINAL DESIGN OF PRESSING FOR 4mm SIDE WALL

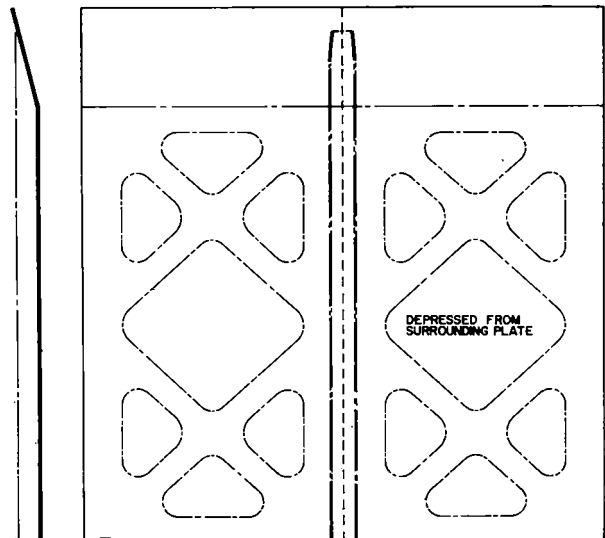


FIGURE 12b: IMPROVED DESIGN OF PRESSING FOR 4mm SIDE WALL

complete evacuation of the coal on dumping. Provision has been made in the pressing for the introduction of an additional stanchion to stabilise the shape of the 4 mm and 6 mm side wall above the height of the longitudinal stiffener, item 1, shown in figure 4.

A prototype car incorporating these design modifications will be built during November 1981 after which the expected gains in stress smoothing of the body shell will be assessed.

4.3.3 Design Details. In order to provide a body shell of light construction it is of importance to reduce forces acting out-of-plane to the shell to a minimum. A source of many of these forces are for example lap joints as shown in figure 13. In addition to causing out-of-plane motion which decreases buckling stability under compression, the joint increases forces on the weld and causes stress concentrations as a result of the geometric discontinuity. Emphasis was thus placed on the provision of butt-joints to form as continuous a shell as possible. Thus the bottom flange of the body bolster, for example, 'flows' into the side wall of the body shell 'wrapping around' the unavoidable butt-joint of the floor with the side wall as indicated in figure 4. A similar philosophy was used in the design of the end wall and end wall stiffeners. The butt-joints are pre-prepared for full weld penetration.

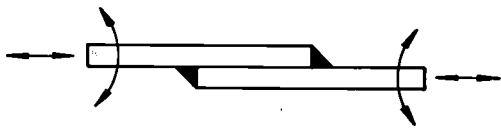


FIGURE 13: RESULTANT MOMENTS IN PLATE DUE TO LAP JOINT

It may be argued that this design procedure places unacceptable tolerance levels on the production of the car, however anticipation of this problem in the early design stage has avoided many problem areas leaving one unavoidable constraint: all plates require to be trimmed on at least three edges before being used in order to meet limits on squareness and hence maximum acceptable weld gaps for semi-automatic welding.

At critical weld joints in the car and in particular in the region of the body bolster and stub sills square corners have been gusseted in order to reduce the geometric discontinuity and lead peak stresses away from welds ending in the respective corners. This may be seen in figure 8.

A critical part of the design was considered to be the attachment of the stanchions to the body shell. On loading, the weld between the stanchion and the body shell is subject to tensile stresses due to the pressure of the lading normal to the body shell as well as local out-of-plane bending as shown in figure 14. Calculations reveal the stresses due to the normal load to be minimal (approximately 7 MPa). Stresses due to out-of-plane bending are a function of the out-of-plane stiffness of the shell and the moment of inertia of the weld root (if the weld were considered to be a hinge, zero tensile stresses due to bending would occur). On rotary dumping of the car, the body shell lies against a reaction plate which would 'straighten' any out-of-plane bending causing

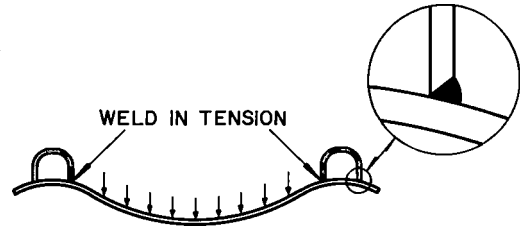


FIGURE 14: HORIZONTAL SECTION THROUGH CAR SHOWING FORCES AND DEFLECTIONS ON SIDE WALL

the weld to work in a fatigue mode. It was considered that this weld joint be pre-prepared in order to ensure full penetration in addition to a minimum moment of inertia. Tests on the design prototype with unpressed side plates and a water load reveal a maximum stress of 23 MPa across the weld; a minimum stress concentration factor of 11 would thus have to occur across the length of the strain gauge used in the test before failure occurred. The design was thus considered acceptable.

The vertical webs between the floor plate and the body shell which form the body bolster and longitudinal stub sills was coarsely modelled by means of the F.E.M. An example of the mesh of one of the body bolster webs is shown in figure 15. Little knowledge of the shear stress distribution across the webs was gained by means of the F.E.M. and predicted maximum tensile and compressive stresses in the body bolster under a water load of 85,5 t were 53,5 MPa and 58,4 MPa respectively in comparison to test results of 64 MPa and 69 MPa respectively. These stress values are within limits specified by A.A.R. however the design of the body bolster profile has been altered as described in 4.3.2.2 and provision has been made for air piping running through the webs of the body bolster. Stress concentrations due to these modifications will be measured on completion and test of the production prototype car.

Detail design in the region of the drawgear pocket has remained unaltered with respect to existing designs used on the S.A.R.: the stub sills are formed of channel sections, a fabricated composite box is lock-bolted to the stub sills and a proprietary cast headstock is slot-welded to these sills.

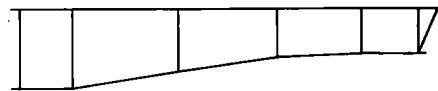


FIGURE 15: F.E.M. MESH OF BODY BOLSTER WEB

4.3.4 Assessment Of The Design And Analysis. Analysis and tests have revealed that there are regions of low in-plane stress within the car body shell in addition to the higher stressed regions mentioned. This is particularly true of the 4 mm body side panels and the bathtub floor. It may thus be concluded that an optimal lightweight steel design has not yet been achieved. However further gains in tare mass reduction should be weighed against cost increases in car production and unknown factors such as rates of corrosion

in the environment of the Richards Bay line and crashworthiness and resultant repair procedures. The target of a 20 t tare mass has been achieved and investigation will continue into further lightening the design with due consideration to gains achieved.

Investigation is at present under way into the use of stainless steel in order to produce thinner side plates and bathtub floor plates. The analysis and tests have shown however that this could imply the more extensive use of pressings to stabilise the plate structure against buckling. This move would exceed present press capacity on the S.A.R. The economics of increasing press capacity or buying pre-pressed plates would have to be considered against gains in tare mass reduction.

4.4 Brake Rigging

The physical dimensions of the CCL-5 car precludes the use of conventional brake rigging under-slung on the car body. Two alternative brake configurations are being considered:-

4.4.1 Body Mounted Brake Rigging. In order to fit body-mounted brake rigging it was found that a 178 mm (7 inch) ABU cylinder had to be mounted on each end of the car to brake each truck. Two 178 mm cylinders would then be supplied from each ABDW valve and auxiliary/emergency reservoir. This brake ar-

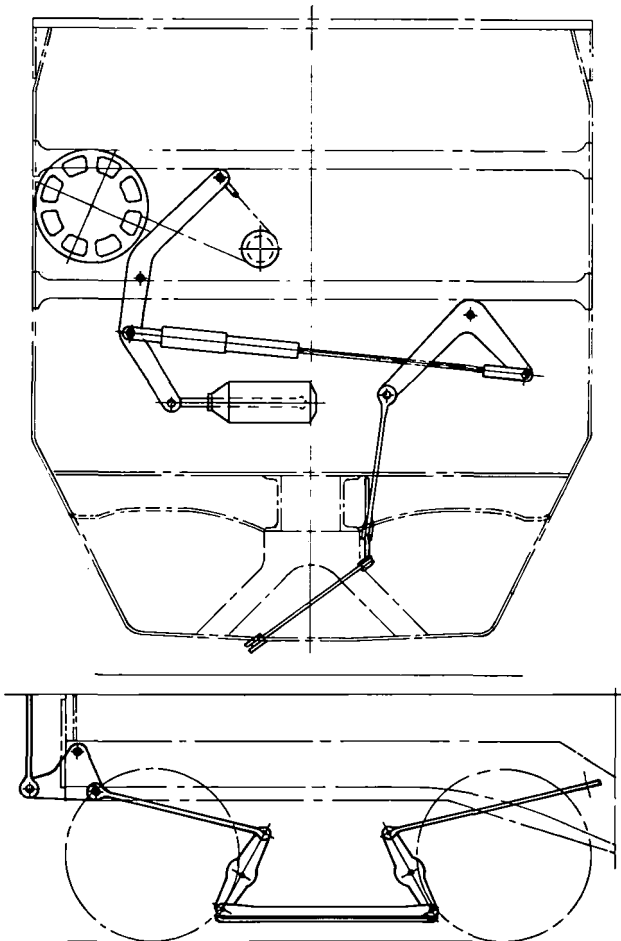


FIGURE 16: CAR-MOUNTED BRAKE CONFIGURATION

angement is illustrated in figure 16. Two slack adjusters are required per car and inclined vertical levers require to be fitted to the truck (as per American practice). The pullrods to the truck brake rigging are shorter than what is standard practice on S.A.R. Objections to this arrangement are that two slack adjusters and ABU cylinders are required increasing mass and cost and that the shortness of the pullrods increases the chances of the brakes binding as the truck yaws in negotiating curves.

4.4.2 Truck Mounted Air Cylinders. A truck mounted brake system would overcome the objections raised in 4.4.1. Unfortunately no experience has yet been gained with a pack-type brake system on the S.A.R. Tests are being conducted to determine air consumption rates, brake loading times and the mechanical efficiency of such a system in comparison with that mentioned in 4.4.1.

Since production of the CCL-5 car commences in September 1982 and insufficient experience has been gained to date with truck mounted brake systems it has been decided to fit the first 800 cars with the system described in 4.4.1. In anticipation of a possible change to system 4.4.2 a bolster has been designed for the Scheffel radial axle truck to accommodate truck mounted air cylinders; in addition a brake beam for 1 065 mm gauge to accept such cylinders has been designed.

5.0 CONCLUSIONS

A 104 t car of monocoque construction has been designed with a tare mass of 20 t and a length of 12,07 m. Analysis and tests on a design prototype car have shown that structurally the design concept could perform satisfactorily under the operating conditions prevailing on the upgraded Richards Bay coal export line. Modifications to the design detail have been made to stress the structure more evenly. A production prototype is to be built in November 1981 to prove the production method and detail design changes. Production of the first 800 cars will commence in September 1982.

6.0 ACKNOWLEDGEMENTS

The author wishes to thank the Director General of the South African Railways for permission to publish this article.

7.0 REFERENCES

- [1] Sheffel, H., "Experience Gained by South African Railways with Diagonally Stabilised (Cross-Anchor) Bogies Having Self-Steering Wheelsets", Proceedings of the Heavy Haul Railways Conference, Perth, Western Australia, 18-22 September 1978.
- [2] Scheffel, H. and Tournay, H.M. "The Development of an Optimum Wheel Profile for Self-Steering Trucks Under Heavy Axle Load Conditions", ASME, Winter Annual Meeting, November 16-21, 1980, Chicago, Illinois. Reference 80-WA/RT-5.
- [3] User's Information Manual, "Stardyne", for Scope 3.4 Operating System, 1978, Control Data Corporation, Publications and Graphics Division, Data Services Publications, Minneapolis, United States of America.

APPENDIX A : SPECIFICATIONS FOR EXISTING ROLLING STOCK ON THE RICHARDS BAY LINE

CCR, 18,5 t AXLE LOAD CARS :

Length over headstocks	- 11 044 mm
Length over pusher pads	- 11 094 mm
Length over coupler centre lines	- 12 070 mm
Width (outside)	- 3 000 mm
Width (inside)	- 2 834 mm
Height (tare)	- 3 217 mm
Capacity	- 67,5 m ³
Tare mass	- 21 200 kg
Load	- 52 800 kg
Truck type	- Three piece frame
Wheel diameter	- 864 mm
Coupler	- F-type interlock
Body Material	- Mild Steel/Corten

CCR, 20 t AXLE LOAD CARS :

Specifications as above with following exceptions:

Load	- 58 800 kg
Truck Type	- Scheffel radial axle

6E1 3 kV d.c. LOCOMOTIVE

Total Mass	- 88 904 kg
Maximum Permissible Axle Load	- 22 226 kg
Axle Configuration	- B0-B0
Starting Tractive Effort	- 311 kN
One Hour Rating	- 221 kN
Continuous Tractive Effort	- 193 kN
Power (1 hour rating)	- 2 492 kW
Power (Continuous)	- 2 252 kW

7E 25 kV a.c. LOCOMOTIVE

Total Mass	- 123 500 kg
Maximum Permissible Axle Load	- 21 000 kg
Axle Configuration	- CO-CO
Starting Tractive Effort	- 450 kN
One Hour Rating	- 319 kN
Continuous Tractive Effort	- 300 kN
Power (1 hour rating)	- 3 240 kW
Power (Continuous)	- 3 000 kW

APPENDIX B : SPECIFICATION FOR PROPOSED ROLLING STOCK FOR THE UPGRADED RICHARDS BAY LINE

CCL, 26 t AXLE LOAD CARS :

Length over headstocks	- 11 044 mm
Length over pusher pads	- 11 094 mm
Length over coupler centre lines	- 12 070 mm
Width (outside)	- 3 000 mm
Width (inside)	- 2 988 mm
Height (tare)	- 3 493 mm
Capacity	- 85,7 m ³
Tare Mass	- 20 000 kg
Load	- 84 000 kg
Truck Type	- Scheffel radial axle
Wheel Diameter	- 914 mm
Coupler	- F-type interlock
Body Material	- Corten

10E 3 kV d.c. LOCOMOTIVE

Total Mass	- 126 000 kg
Maximum Permissible Axle Load	- 21 000 kg
Starting Tractive Effort	- 450 kN
Continuous Rating (34 km/h)	- 310 kN
Continuous Rheostatic brake dissipation	- 2 200 kW

11E 25 kV a.c. LOCOMOTIVE

Total Mass	- 168 000 kg
Maximum Permissible Axle Load	- 28 000 kg
Starting Tractive Effort	- 580 kN
Continuous Rating (34 km/h)	- 400 kN
Continuous Rheostatic brake dissipation	- 4 500 kW

W.N. Caldwell

Senior Research Engineer
CN Rail Research Centre
Montreal, Quebec
Canada

G.W. Cope

Manager
Research & Development
Dresser Transportation
Equipment
Depew, New York, USA

H.A. List

President
Railway Engineering
Associates, Inc.
Bethlehem, Pennsylvania
USA

The Development and Testing of a Steering Type Freight Car Truck for Heavy Haul Service

The truck discussed in this paper is made by adding a DR-1 Cast Steel Steering Assembly to a conventional AAR roller bearing freight car truck. This paper summarizes the development process leading to this design, the service experience to date, and the latest data available on wear. The first production models of the subject truck entered service in 1979, and many have now accumulated over 200,000 miles (320,000 km). On CN Rail, wheel wear has been monitored for a test population of seven standard and fifteen DR-1 equipped carsets of trucks on 100-ton car unit train service operating in Western Canada. Parameters monitored include loss of wheel tread and flange cross-sectional area, loss of flange thickness, increase in flange height, and loss of rim thickness during reprofiling. Wheel wear measurements indicate a possible 2-5 fold increase in rail life in curves.

1. SUMMARY

This paper describes the development and initial operating experience with a steerable-axle freight car truck for 100-ton capacity freight cars in heavy haul service.

This truck is identified by the trade mark "DR-1 Steering Assembly." The term "steering assembly" is used because only the steering parts are new. The side frames, bolsters, brakes, and wheelsets are standard AAR parts.

Most of the DR-1 trucks now in service are the result of "retrofitting" existing conventional trucks. However, some have had the DR-1 Steering Assemblies applied during new car construction, but the side frames and bolsters are still standard.

Some of the DR-1 trucks are approaching 400,000 miles of service. Field measurements indicate large reductions in wheel wear and substantial reductions in rolling resistance in curved track. Car and truck maintenance are also expected to be significantly lower.

The development program included theoretical analysis, experiments with 1/8 size models, and experiments with full size trucks. The full scale experiments have included laboratory testing of components, performance testing of trucks, and revenue

service testing.

2. INTRODUCTION

The objectives of the development program were:

- (1) Reduce wheel and rail wear in curves.
- (2) Eliminate truck hunting at freight train operating speeds.
- (3) Reduce rolling resistance in curves.

In 1962 the third author modified the trucks of some 7-1/2 inch gauge garden railway cars to introduce axle steering. The purpose then was to reduce rolling resistance in curves and reduce track damage due to high lateral wheel/rail forces.

In the mid 1960's several European railway groups began publishing the results of theoretical studies applying modern control theory to railway vehicle guidance and stability. At the same time, the shortcomings of the conventional North American freight car truck were becoming apparent, particularly under high mileage cars having heavy axle loads. The time seemed right for a fresh look at rail car truck design.

It was already clear that additional basic information was needed on the forces acting within trucks when negotiating curves, rough track, and at high speed on straight track. There was some information in the literature regarding conventional trucks, but no experimental information was available on steering trucks.

In 1971, Railway Engineering Associates and CN initiated a joint truck development program. Basic designs had already been developed^[1] for both an "all new" truck and a "retrofit" arrangement. It was then decided to build the "all new" truck to confirm theoretical predictions on full scale performance and provide experimental data on design loads.

The "all new" truck shown in Figure No. 1 was built in 1973. Preliminary curving tests showed great promise. Early in 1974 it was run at 80 mph under an empty hopper car on a worn wheel profile without encountering truck hunting^[2] ^[3]. This truck met all the development objectives.

In late 1974 construction was started on the first "retrofit" steering type truck. The detailed design used information from the "all new" truck testing. The steering assemblies were fabricated from weldments.

During 1975 there was a series of tests and design refinements of the "retrofit" with the "all new" truck serving as the standard of performance for curving and stability. Also in 1975, both Dresser Transportation Equipment Division and Dofasco joined in the development effort.

By late 1976, the first cast DR-1 assemblies were produced. Figure No. 2 is a photograph of this assembly fitted to a set of standard side frames and bolsters to check clearances. Performance testing of the retrofit trucks was carried out at CN in 1977 with satisfactory results^[4].

3. SERVICE EXPERIENCE, DR-1 STEERING TRUCK

The first set of DR-1 castings were strain gauged and used to develop a service fatigue load spectrum for these components which were then subjected to laboratory fatigue tests^[5].

A preproduction run of about 30 carsets of steering parts was then made incorporating minor changes indicated by the fatigue tests on the first castings. Some of these DR-1 assemblies were applied to cars in revenue service: 10 carsets on CN Rail, 4 carsets on the Southern Railway, 2 carsets on the Santa Fe Railway and 1 carset in the TDOP wear test program. All of these cars are still running in high mileage unit train service. In all cases, wheel wear is being observed, and in the CN and Santa Fe tests, there are conventional cars being monitored for direct comparison of wheel wear.

One carset of these DR-1 trucks was tested for curving and stability by CP Rail and reported on^[6]. Three carsets are in the FAST truck test program, four carsets have been run by the Southern Pacific Railway and two carsets are in company service (ballast cars) on the Missouri Pacific Railway.

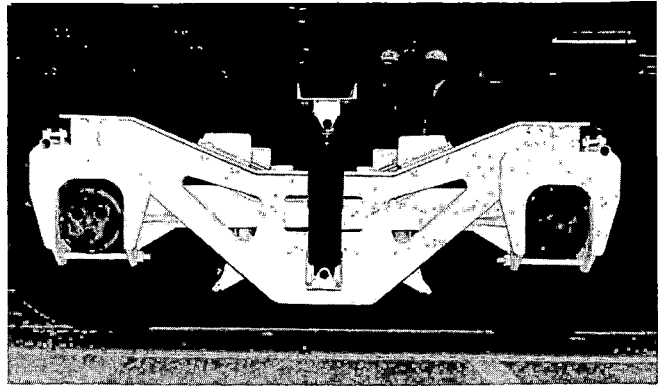


Fig. 1 Photograph of full scale "all new" steering truck

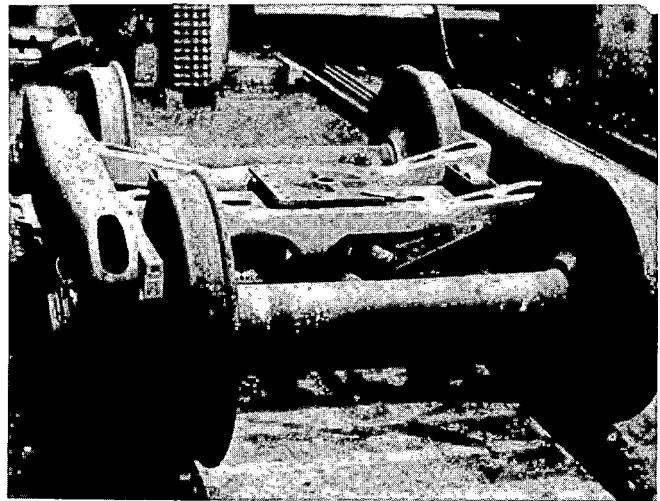


Fig. 2 First set of retrofitted production trucks

Most of the remaining castings from this first preproduction run were used in laboratory testing.

A second production run of castings was made including additional modifications based on service and testing experience with the first production run.

One hundred "retrofit" carsets were used to expand the CN Rail fleet of DR-1 equipped cars so that comparative drag tests could be run with a complete unit train of steering trucks under curving conditions with loaded cars and high speed return movement with empty cars. Forty carsets were also applied to new cars by the Southern Railway.

One carset is running in a P.P.&L. unit coal train on Conrail. In this application there is also a conventional car being monitored for wheel wear comparison.

In all service testing, substantial reductions in wheel flange wear have been measured for the DR-1 trucks. As well, in the TDOP tests[7], a 30% - 50% reduction of curve rolling resistance was measured for a single car in curvature to 6.2°.

There have been some development problems with the steering assembly parts, particularly in the early production components, but following corrective design changes on casting fatigue detail, defective bearing adaptor bolts, and improvements in rubber bushing bonding, our recent experience indicates that maintenance requirements for the DR-1 components should be low.

Brake shoe replacement is somewhat less convenient than with conventional trucks due to the presence of the steering casting approximately 2 inches (50 mm) above the brake head. A simple chain tool has been devised to overcome this problem and allow brake shoe key application and removal via an access hole in the steering casting. It has been difficult to ensure that the car inspector always has the tool with him when only a small percentage of the cars are involved. However, this problem seems to be growing less important as more cars are introduced. An alternative locking brake shoe key has also been devised which has the advantage that it is easier to apply with standard tools to all cars, but as yet there is no service experience with this key.

4. PERFORMANCE TESTS

A number of performance tests designed to provide information on

- (a) High speed dynamic stability under empty car/worn wheel conditions and lateral ride quality.
- (b) Wheel/rail angle of attack and lateral forces in curves.
- (c) Rolling resistance of loaded cars in curves.
- (d) Tracking capability on uneven track surface.
- (e) Structural stiffness and fatigue loading spectrum

have been carried out on the DR-1 steering system by independent investigators and their results have been reported in the literature [4-7 inclusive]. The results show a significant improvement for trucks of the steering type compared to the conventional three piece freight car truck.

It is also interesting to note that on CN Rail, five DR-1 equipped cars are known to have been involved in derailments, all caused by problems with other equipment. To date, the DR-1 steering assemblies have survived these derailments with no signifi-

cant damage or distortion and have been continued in service.

5. SERVICE WEAR TESTS

This section of the paper is based on wheel measurements made by CN. Similar tests are being carried out on the Santa Fe (2 DR-1 cars and 1 control) in the York Canyon coal train and comparable results are being obtained with up to 400,000 miles of service.

5.1 Test Population. In November and December 1978, CN introduced 10 carsets of DR-1 steering trucks retrofitted to rotary dump gondolas in 100-ton unit train coal service along with 2 conventional cars as a control population. All these cars were fitted with new CJ-36 class C two wear cast steel wheels with wide flange CN Heumann tread contour for purposes of monitoring wheel wear. One year later, a larger test program was undertaken to retrofit another 100 carsets of 100-ton gondolas. Five additional DR-1 equipped carsets and 5 additional conventional cars were introduced into the wear test population for a total wear test population of 15 DR-1 cars and 7 conventional control cars.

5.2 Test Route. The majority of cars are operated between Luscar, Alberta and Vancouver, BC on the CN Southline through the Rocky Mountains. This particular route is now carrying approximately 50 MGT of traffic per annum and the route alignment is shown in Table 1 along with the alignment for another CN Rail resource route and the Pueblo Fast Track for comparison. As is seen, approximately 37% of the 680-mile one-way route is curved track. In CN operations, the cars are turned for each round trip between the mine and the ocean terminal.

5.3 Measurement Methodology. Precision wheel contour measurements were taken using a profilometer system developed by CN for this work. The profilometer is registered to the wheel always at the same cross section. The profilometer is held against the rim back face and two dowels rest on the flange tip. A clamp screw with a semi-spherical end is then placed in a V-shaped reference mark drilled into the rim front face (3/8" [9.5 mm] diameter x .050" [1.2 mm] deep, 114° included angle). This instrument registration procedure provides initial profilometer alignment repeatability in application to the wheel. Figure No. 3 shows the instrument applied to a wheel.

An (x',y') data set is taken across the wheel contour as a group of 61 coordinate pairs. The x' axis of the instrument is tilted to approximately 15° to the axle centerline to improve accuracy of profile measurement in the flange face area. The x' coordinates are spaced .05" (1.2 mm) apart in the flange face and fillet area and 0.1" (2.4 mm) elsewhere.

In the field, the data set is encoded by a shaft encoder fitted to the dial gage

and recorded digitally on a cassette tape recorder along with wheel serial numbers. The data is subsequently processed by computer to yield wheel profile plots and wear parameter data described below. Wheel service mileage at each profile measurement is obtained from CN TRACS system car movement records.

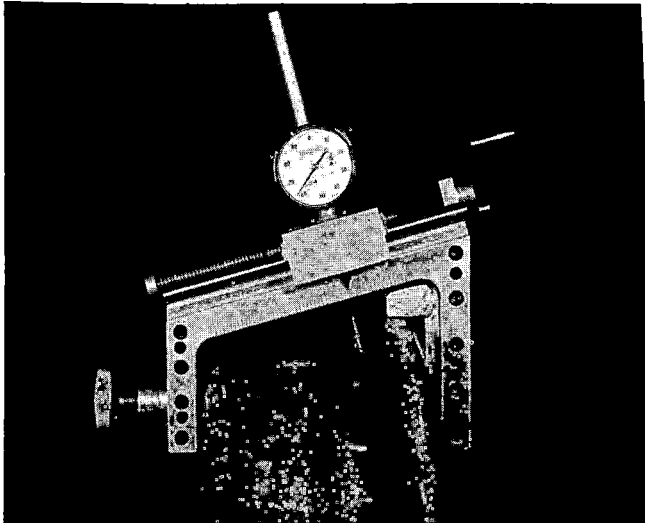


Fig. 3 CN precision wheel profilometer mounted on a wheel

5.4 Wear Parameters. Five wear parameters are being monitored by wheel profile measurements on both the DR-1 and control car populations to quantify the reductions in rail and wheel wear achieved under service conditions. These are:

1. Wheel flange cross-sectional area loss.
2. Wheel tread cross-sectional area loss.
3. Reduction in wheelset flange thickness.
4. Increase in wheelset flange height.
5. Reduction in wheelset rim thickness due to the wheel reprofiling operation
 - (a) to original WF (wide flange) contour or
 - (b) to AAR minimum requirements of NF (narrow flange) contour.

5.5 Rail Wear. The first two parameters (wheel flange and tread cross-sectional area loss) are a measure of the volume of wear metal lost from the wheel. Wheel metal loss is caused by brake shoe abrasion (primarily on the wheel tread) and wheel/rail interface contact (flange abrasion on gage face of rail and adhesive wear on the rail head due to wheel tread creepage).

Since both the control cars and the DR-1 cars have the same braking equipment, it is assumed that they would experience similar wheel wear due to brake shoes. Hence, any

reductions in wheel wear observed on the DR-1 cars are related to improved curving. It is further assumed that reductions in wheel wear would be accompanied by a proportional reduction in rail wear. However, since wheel tread wear is primarily due to brakes, the effect of reducing lateral wheel/rail creep in curves on rail head wear cannot be reliably observed and the observed wheel wear reduction is a conservative or lower bound estimate of the relative rail wear reduction effected by the DR-1 trucks. A direct measure of rail wear reduction was not possible because the DR-1 cars are a very small fraction of the cars using this route.

Figure Nos. 4 and 5 show the definition of wheel flange and tread cross-sectional area loss. The separation point between "flange" and "tread" has arbitrarily been taken as the 45° tangent point in the flange/tread fillet on the new WF CN Heumann contour (approximately 1.5" from the wheel back face). This angle has been adopted because there is no point on the gage face of rail whose slope is less than 45°.

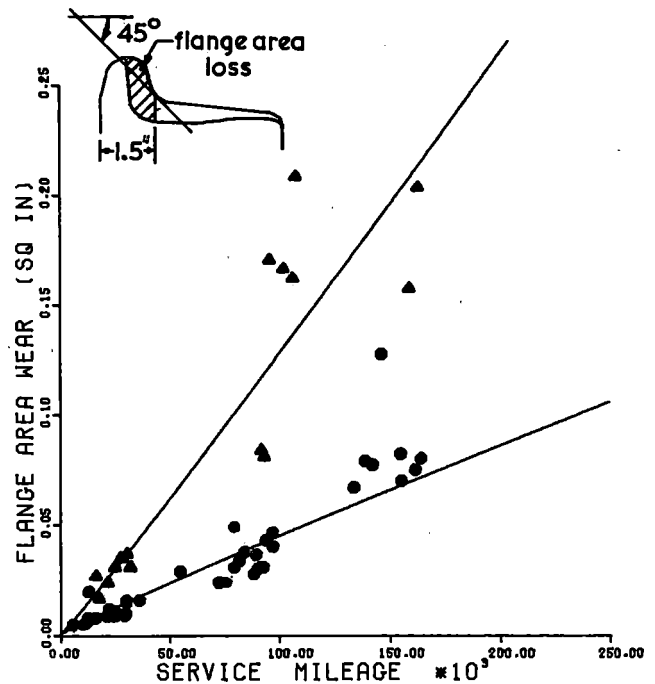


Fig. 4 Wheel flange cross-sectional area loss per wheel versus service mileage for DR-1 [●] and control cars [▲]. Wear area is averaged over all 8 wheels of car (1 in.² = 645.16 mm², 1 mi. = 1.609 km)

In Figure No. 4 flange area loss vs. service mileage is plotted for the two test populations. A least squares power function of the form $Y = ax^b$ is fitted to the data points in each population to produce a wear trend line for the DR-1 equipped cars and the control cars. In this trend line equation, Y is the wear parameter, X is the mileage, a and b are the regression coefficients.

At 160,000 miles (257,500 km) of service, the trend lines show that the flange cross-sectional area loss is reduced to approximately

30% of that developed on the control cars. It is assumed that rail gage face wear in curves would also be reduced by a factor of approximately 3 for DR-1 equipped cars. Figure No. 5 shows the tread cross-sectional area loss vs. service mileage for the DR-1 and control car populations. As can be seen, there is no significant difference in tread cross-sectional area loss between the DR-1 cars and the control cars. It appears that tread wear caused by braking predominates. The expected reduction in rail head adhesive wear for DR-1 trucks (account of lower lateral creep in curves) cannot be measured by evaluating wheel tread metal loss because observation of this wear is masked by the very much higher abrasive wear of the wheel treads by the composition brake shoes.

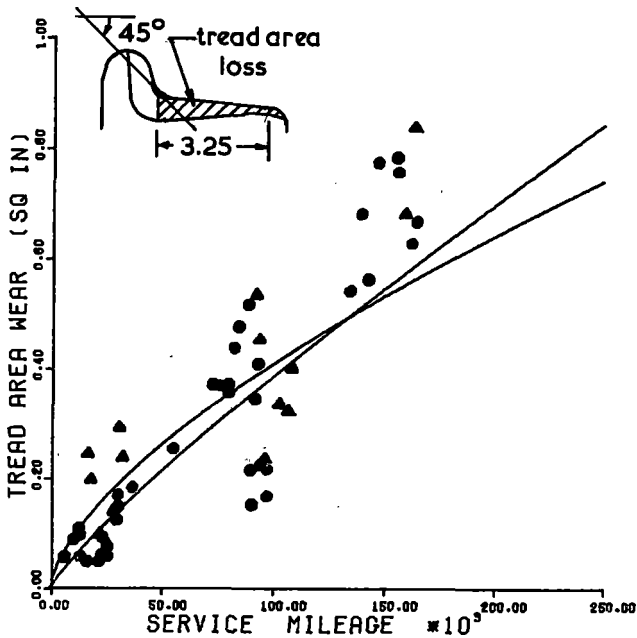


Fig. 5 Wheel tread cross-sectional area loss per wheel versus service mileage for DR-1 [●] and control cars [▲]. Wear area is averaged over all 8 wheels of car (1 in.² = 645.16 mm², 1 mi. = 1.609 km)

It is interesting to note the rather wide scatter of tread metal loss observed for the test population of both DR-1 and control cars. This is surprising in view of the fact that all cars are equipped with the same brake equipment and operate under the same train handling conditions. This scatter may be related to variations in individual car braking system operation (either or both the pneumatic system and the brake rigging), and variations in abrasive wear caused by different manufacturers' composition brake shoes. This effect is even more striking when it is noted that there are large variations even on the same car.

It should be noted that all 8 wheels of each test car are included in the grouped

car wear averages for flange and tread cross-sectional area loss, since all wheels cause rail wear.

5.6 Wheel Wear. The next three wear parameters (flange thickness, flange height, and rim thickness) are measures of wheel wear as it affects service life and wheelset removals because wear condemning dimensions have been reached. These condemning dimensions are defined by AAR Interchange Rules and special gages are used in the field for checking potentially condemnable wheels. A wheelset is changed if either wheel is condemnable. These same procedures are applied numerically to the test data to determine the wear of the test wheels.

In the case of wheel wear, however, only the wear measurement for the worst wheel of the wheelset is retained in forming the grouped car average since both wheels of the wheelset are removed and reprofiled if one wheel is condemned for wear limits.

Figure No. 6 shows a plot of the loss in flange thickness as a function of car mileage for the two test populations. As can be seen from the trend lines at 160,000 miles (257,500 km) the loss of wheelset flange thickness on the DR-1 cars is reduced to approximately 1/3 that of the control cars.

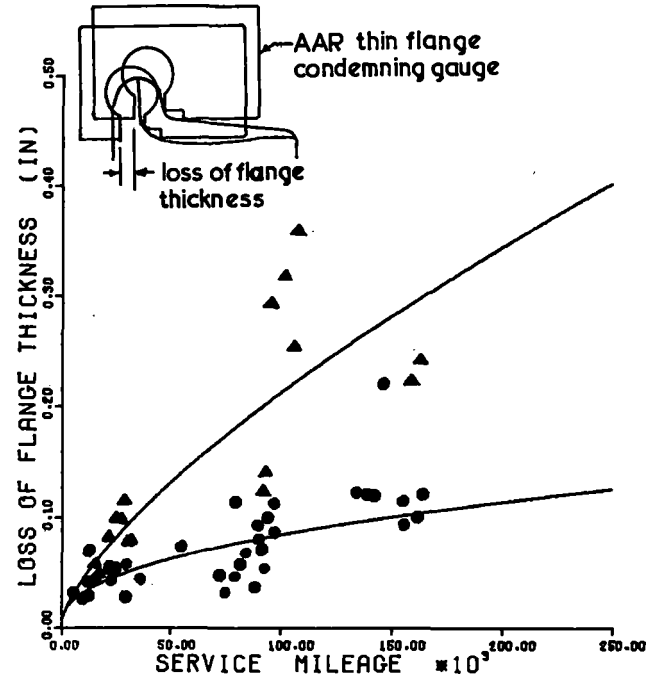


Fig. 6 Loss of flange thickness per wheel versus service mileage for DR-1 [●] and control cars [▲]. Flange thickness loss is average of 4 worst wheels of wheelsets (1 in. = 25.4 mm, 1 mi. = 1.609 km)

Figure No. 7 shows the plot of increase in flange height vs. mileage for the test populations. Again, no significant differences in tread wear can be ascribed to either test population as was previously discussed.

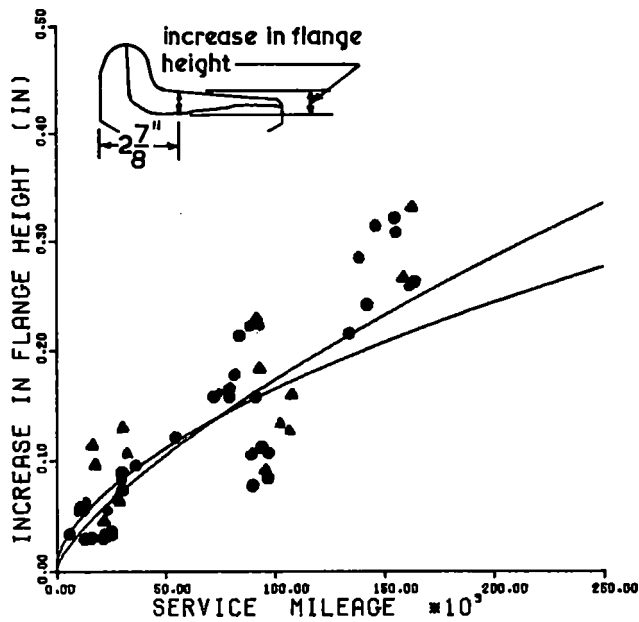


Fig. 7 Increase in flange height per wheel versus service mileage for DR-1 [●] and control cars [▲]. Flange height increase is average of 4 worst wheels of wheelsets (1 in. = 25.4 mm, 1 mi. = 1.609 km)

Figure No. 8 shows a plot of the rim thickness loss against service mileage for the test cars. In this case rim thickness loss refers to rim metal loss due to service wear plus the metal loss in the machining operation to reprofile the wheelset back to the original specifications of WF Heumann contour. At 160,000 miles of service, the trend lines show that the DR-1 cars would have only 55% of the rim thickness loss of the control cars. This arises primarily because of the lower flange wear on the DR-1 cars. It is in this area that the major improvement in wheel life is expected because thin rim condemning on a two wear wheel will be considerably reduced.

Rim thickness loss in reprofiling to NF (narrow flange) Heumann contour (current wheel shop reprofiling practice) is also being monitored but is not shown here because to date (160,000 miles [257,500 km]) the grouped car average of flange thickness has not gone below that of a narrow flange wheel (i.e. loss of flange thickness must exceed 0.25" (6.4 mm) before the flange is thinner than a new narrow flange.

This wear data shows that DR-1 wheelset removals for wear condemning limits will essentially be caused by increase in flange height (i.e. tread wear) whereas the control cars will be removed either for thin flange or for high flange with substantial flange wear--a condition which will substantially increase rim metal loss in wheel reprofiling operations and shorten wheel life.

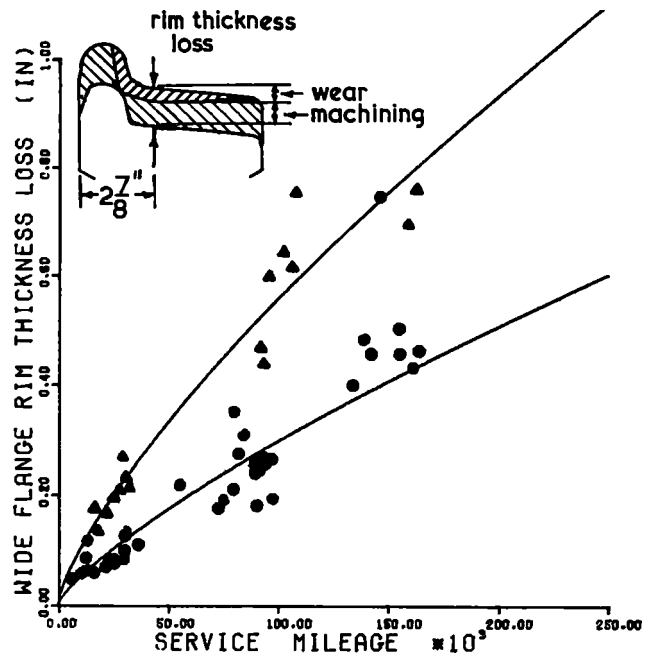


Fig. 8 Wide flange contour rim thickness loss versus service mileage for DR-1 [●] and control cars [▲]. Rim thickness loss includes rim metal loss due to service wear plus machining loss to reprofile the wheel to original WF Heumann contour (1 in. = 25.4 mm, 1 mi. = 1.609 km)

6. CONTINUING DEVELOPMENT ACTIVITIES

The first cost of the DR-1 can be justified for certain applications on the basis of the estimated benefits including savings in rail wear, wheel wear and fuel. However, only the wheel wear savings have been well documented to date.

Wheel wear measurements are continuing. Additional measurement of reduced rolling resistance are being made. It is anticipated that within a few years we will be able to observe rail wear reductions directly by having enough cars in service to dominate the wear picture for certain sections of track. The design of the DR-1 is continually being reviewed for potential cost reductions.

The measurement of reduced rolling resistance is made difficult by the fact that the total rolling resistance is already small compared with the kinetic and potential energy levels of train operation. The planned improvements in these measurements include the measure of drawbar horsepower hours for relatively long time periods for both DR-1 cars and conventional cars over the same piece of railroad in the same train to minimize effects of variations in train handling and ambient conditions as well as drag resistance reduction on empty return moves where hunting is eliminated.

The principal cost reduction strategies being explored for the DR-1 are:

1. Increased use of jigs, fixtures and automated machinery to produce the parts.
2. Minor revisions to the side frame castings for new car applications to minimize the total amount of work in assembling the truck.
3. Casting the bearing adaptors integral with the steering arms.
4. Alternative locations for the connections between the steering arms to accommodate using existing shallow bolsters and truck mounted brake equipment.

The DR-1 steering arm is already designed for machine welding of three castings into a single rigid frame. Quantities to date have not justified setting up special machines for the other manufacturing operations. The use of such machines will lower unit costs.

The bearing adaptors used in the existing DR-1 trucks have been machined to obtain some additional longitudinal clearance at the side frame pedestal opening. This machine work can be eliminated by minor revisions to the side frame pedestal opening. Similarly, the work now done to provide additional longitudinal clearance between the roller bearing and the pedestal can be eliminated. When these side frame revisions are made, a pocket can be provided for the resilient pads. This will eliminate the need for a separate pad stop that is now welded on, and the contribution of the pad thickness to coupler height can be eliminated. At present, this additional height tends to raise the new car coupler height 1" above the normal upper limit.

Casting the bearing adaptor integral with the steering arm may offer additional cost savings. Moving the inter-axle connection out of the bolster will improve access for servicing and inspection, provide room for truck mounted brakes, and permit retrofitting of cars with shallow bolsters. However, it should be noted that it will take time to verify the structural integrity of the modifications in service.

7. CONCLUSIONS

- The DR-1 is providing substantial wheel wear reduction in heavy haul service.
- Preliminary measurements indicate a potential reduction in locomotive fuel consumption.
- It seems reasonable to assume that the rail wear is also being reduced on a per-car basis, but the DR-1 cars are still a small portion of the traffic over any given piece of rail and a direct observation is not possible.
- The service experience to date suggests that the DR-1 itself will require very little maintenance and that the maintenance of other truck and car components will be reduced.

8. ACKNOWLEDGMENTS

The authors wish to thank Dominion Foundries and Steel Ltd. and Dresser Transportation Equipment Division for their co-operation and support in producing the test trucks. Financial assistance was also provided by Transport Canada, Research and Development Centre. The authors are very grateful to colleagues and research personnel at CN Rail for their valuable support in all phases of this project.

9. REFERENCES

- 1 List, H.A., "An Evaluation of Recent Developments in Rail Car Truck Design," ASTM 71-RR-1.
- 2 List, H.A., "Design System Approach to Problem Solving," Technical Proceedings, 12th Annual Railroad Engineering Conference, Pueblo, Colo., 1975, Report No. FRA OR&D 76-243.
- 3 List, H.A., Caldwell, W.N., and Marcotte, P.P., "Proposed Solutions to the Freight Car Truck Problems of Flange Wear and Truck Hunting," ASME 75-WA/RT-8.
- 4 Marcotte, P.P., Caldwell, W.N., List, H.A., "Performance Analysis and Testing of a Conventional Three-Piece Freight Car Truck Retrofitted to Provide Axle Steering," ASME Transactions, Journal of Dynamic Systems, Measurement and Control, Vol. 104, No. 1, Mar. 1982, pp.93-99.
- 5 Caldwell, W.N., Dibble, D.W., "Development and Testing of DR-1 Self-Steering Freight Car Truck," Proceedings of the 5th Symposium on Engineering Application of Mechanics, Canadian National Research Council, Ottawa, June 1981, pp.277-282.
- 6 Ghonem, H., Gonsalves, R., and Bartley, G., "Comparative Performance of Type II and Premium Trucks," ASTM 80-RT-8.
- 7 Bakken, G., Ramachandran, P.V., and Glaser, R., Truck Design Optimization Project, Phase II. Final Project Review Report. Wyle Laboratories. Apr. 2, 1981. DOT-FR-742-4277.

TABLE NO. 1

TRACK ALIGNMENT (1) COMPARISON FOR CN-LUSCAR
AND CN-ALBERTA RESOURCES (ARR) ROUTES WITH
FAST-PUEBLO TEST TRACK

(Expressed as Percentage of Total Route
Mileage)

Route Alignment	CN-Luscar(2) (680 miles)	CN-ARR(2) (674 miles)	IFAST-Pueblo (4.77 miles)
Tangent	63.38%	62.57%	45.91%
0 - 1°	5.08	4.19	2.38 (3)
1 - 2°	7.64	7.61	0
2 - 3°	5.77	6.00	0
3 - 4°	6.61	7.11	13.21
4 - 5°	2.49	2.88	7.64
5 - 6°	4.67	6.32	30.86
6 - 7°	.95	.94	0
7 - 8°	2.66	2.31	0
8 - 9°	.18	.009	0
9 - 10°	.31	.055	0
10 - 11°	.05	0	0
11 - 12°	.19	.004	0
12 - 13°	.008	.007	0
13 - 14°	.003	.003	0
14 - 15°	.003	.003	0

- Notes: (1) Curved track length includes spirals plus circular arc.
 (2) Data from analysis by K.J. Arrey, December, 1970.
 (3) Represents two - 300-foot long spirals of unspecified curvature.

Truck and Suspension Systems— Premium Designs and Performance Improvements

P.V. RamaChandran

Manager
Transportation Engineering
Wyle Laboratories
Colorado Springs
Colorado

M.M. ElMadany

Senior Research Engineer
Wyle Laboratories
Colorado Springs
Colorado

During the Federal Railroad Administration (FRA) sponsored Truck Design Optimization Project/Phase II, extensive field test and analytic investigations were carried out to characterize and compare the engineering performances of the standard, three-piece freight car trucks and the premium freight car trucks featuring a number of innovative design features. This paper presents some of the salient engineering performance comparisons between these two classes of trucks and assesses their implications for heavy haul railroads in terms not only of improved rolling stock performance, but also of track related considerations.

INTRODUCTION

The standard, three-piece freight car truck has served the railroad industry for a long time as a reliable work horse on a cost effective basis. However, changing times have brought increasing demands on today's rail transportation systems. Gross rail weight of freight cars have increased, resulting in higher wheel loads and accelerated deterioration of the track, and higher centers of gravity have increased the risk of derailment. The demands of the market place have resulted in a number of new freight car configurations giving rise to a variety of operational and maintenance problems. Recent advances in freight-car truck design have tried to address these problems through a number of innovations, as manifested in the various types of premium trucks available in the market today, such as rigid and radial trucks, among others.

While a number of premium truck designs have attempted to improve performance in one or more specific areas, whether a significant improvement in overall performance has been achieved is a question that remains to be answered. Furthermore, an identification of the added cost associated with such improvements also needs to be made.

The Federal Railroad Administration sponsored Truck Design Optimization Project Phase II is an attempt at providing some answers to these points (1, 2)*. The engineering objectives of the project, which

*Numbers in parentheses denote References at end of paper.

form the subject of this paper, are: (a) to define the performance of both standard and premium freight car trucks in quantitative terms, represented by performance indices economically related to railroad operations; (b) to establish a quantitative basis for evaluating the economic benefits to be derived from premium design freight car trucks; and, (c) to provide a set of guideline performance specifications for freight car trucks. Engineering investigations have been carried out in four distinct and non-overlapping performance regimes (lateral stability, ride quality, curve negotiation, and trackability). Data from extensive field tests conducted during the project have been reduced and analyzed during the process. Through a comparative study of the resulting quantitative characterizations of performance of the standard and the premium freight car trucks, an attempt have been made to identify the potential benefits from the premium designs which will be useful in a cost/benefit analysis.

FREIGHT CAR TRUCK PERFORMANCE

The standard three-piece freight car truck is characterized by several advantages. It is relatively inexpensive to produce in large quantities by casting. Its loose construction, i.e., the bolster-side frame and adapter-pedestal connections, makes it tolerant of vertical track imperfections. In other words, it provides an excellent load equalization. However, increasing demands on the rail transportation system, in the form of heavier car weight, higher center of gravity, and increasing speed, coupled with increasing requirements for maintenance of equipment and track, have brought into focus two major problems of such truck design.

The first performance problem arises from the fact that the vehicle system experiences lateral instability (hunting) in the operating speed range (60 to 65 mph), as shown in Fig. 1. This self-induced lateral, yaw, and roll oscillation is economically important because of the damage it causes to lading, vehicle and track components. Deterioration in the form of wear

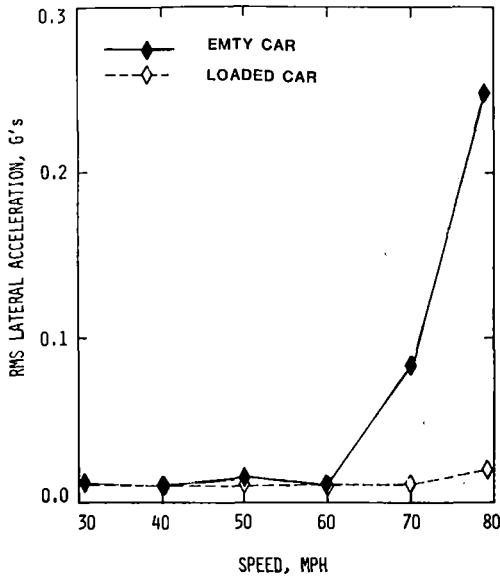


Fig. 1 RMS lateral acceleration versus speed - Type I truck

occurs not only at the wheel treads and brake shoes but also at the snubber, center plate, bolster gibs and side frame columns, as well as at this rail. The high lateral wheel loads and the high ratio of the lateral-to-vertical wheel loads at the wheel/rail contact points, Fig. 2, may result in gauge widening, track wear, wheel climb, and rail rollover.

The other major problem is that the standard truck depends on flange guidance force, and exhibits large angle of attack of the wheels with respect to the rail, during curve negotiation. The lateral wheel loads in curves cause high wear in both wheels and rail, particularly when accompanied by a large angle of attack. This inadequate curving performance of the truck can lead to excessive wheel and rail wear, increased maintenance and renewal, gage widening, derailment, and increased fuel consumption.

PREMIUM TRUCKS AND THEIR PERFORMANCE

Truck Design Improvements

In response to the railroad industry's requirement for improved suspension systems, the supply industry has developed a variety of add-on devices and retrofit packages for the Type I trucks, as well as completely new suspension systems incorporating innovative design features in the form of Type II trucks. The goals of the new suspension design premium trucks are to provide higher safe operating speed, greater load-carrying capacity, improved ride quality, reduced damage and deterioration to vehicle components, reduced wheel and rail wear, and improved rolling and curving resistance and consequent reduction in fuel consumption. Each premium truck attempts to achieve these goals, through certain improved design features. Among these features that reduce or prevent truck hunting susceptibility are increased tramping stiffness by various wheelset or side frame interconnections, and the use of soft lateral suspension stiffness. The unique characteristics of the premium trucks that are intended to

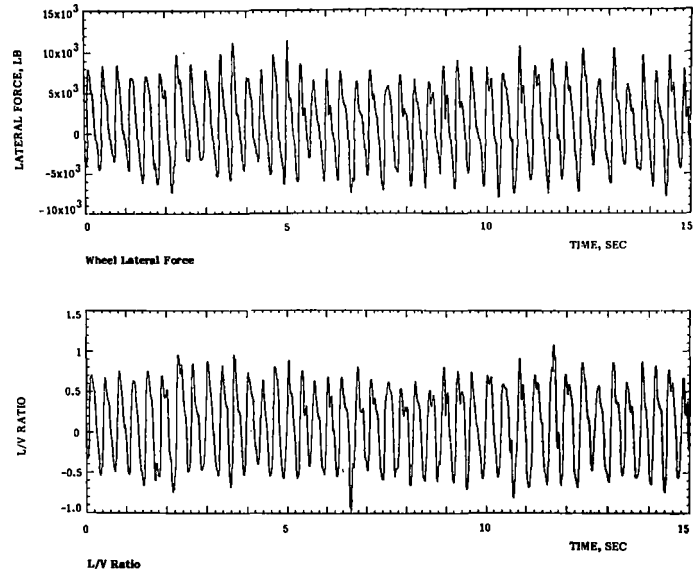


Fig. 2 Wheel/Rail lateral forces and L/V ratios generated during sustained oscillation

reduce flanging in curves are featured in allowing both wheelsets to align themselves radially in the curve, either passively, through the effect of longitudinal creep forces at the wheel/rail interface, or actively, by special linkages. The suspension of some of the premium trucks are designed with a view towards combining stiffness in tram with the freedom of the side frames to pitch, so as to improve lateral stability and load equalization. The use of primary suspension in the design of the truck aims at providing smooth ride condition to the lading and reducing vertical dynamic loads.

However, the design features of a truck that fulfills the requirements of good curve negotiability, high critical speed, and improved load equalization are, to some extent, incompatible. The loose bolster-side frame connection allows relative rotation in yaw. This reduces the kinematic wavelength of the truck and lowers the critical speed at which body hunting begins. A second effect of yaw rotation is the parallelogramming of the truck in curves, which increases the angle of attack of the leading wheels with respect to the rails and thus promotes wear of both. On the other hand, holding the truck in tram has the advantage of providing good lateral stability and reduced angle of attack, but at the same time promoting the generation of lateral forces while rounding a curve, and providing less adequate load equalization. The regime of flange-free curving can be extended to curves of smaller radii by providing some longitudinal flexibility at the axle boxes, which allows the wheelsets to approach a radial position. However, a compromise is required between good curving ability and lateral stability: a truck with too soft a wheelset yaw restraint has a low critical speed. Therefore, the trucks that have special design features to allow them to take near-radial alignment while curving, require suitable elastic longitudinal restraints at the axle boxes, in the form of elastomeric springs, to assure lateral stability.

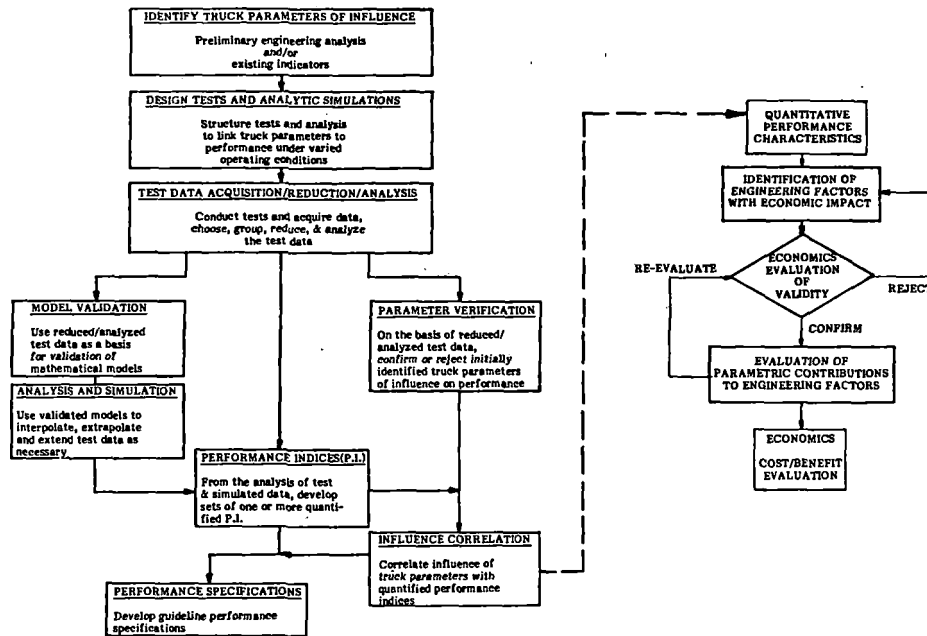


Fig. 3 Methodology for truck evaluation

In the following sections a framework for truck evaluation through which freight car trucks can be studied and the relationship between performance improvements and increased costs can be analyzed, is discussed; the field testing of freight car trucks under revenue service operating conditions is described; and the analysis of test data and the resulting performance characteristics are presented.

Truck Evaluation Methodology

The major elements comprising the methodology for truck evaluation are:

- o Field testing of several Type I and Type II trucks to obtain performance test data and the reduction and analysis of the field test data leading up to quantitative definition of performance.
- o Mathematical modeling of freight car trucks to augment and complement results from field test data.
- o Determination of wear and degradation of freight car trucks under revenue service conditions through a structured program of periodic measurements of various truck components.
- o Collection of economic data on truck maintenance and operation, and correlation of such data with information on truck performance.
- o Engineering interpretation including effect on performance of eventual wear and deterioration of truck components.

- o Correlation of the costs and benefits associated with incremental changes in the levels of performance as obtained from the results of the engineering evaluation of the trucks.

A block diagram indicating the flow of elements in the methodological scheme is shown in Fig. 3.

Field Test Program

Over-the-road testing was conducted in order to obtain performance data on Type I and on several Type II freight car trucks in the four performance regimes of lateral stability, ride quality, steady state curve negotiation, and trackability.

In addition to transducers installed to measure truck and carbody relative motion and rigid body car motion new instrumentation was developed during TDOP Phase II to obtain measurements required to calculate the forces at the wheel/rail interface, and the wheel/rail angle of attack.

Wheel/Rail Position Measurements. The forces at the wheel/rail interface provide the key parameters in the characterization of truck performance during curve negotiation. After an extensive review of available techniques for measuring these forces, the axle-bending method was chosen. To improve accuracy, additional terms were included in the equations to calculate the lateral and vertical forces. Furthermore, measurements of the point of application of the vertical loads were implemented, (3). The approach to the measurement of wheel/rail vertical and lateral forces consisted of: (a) instrumentation of the axle with strain gages; and, (b) instrumented bearing adapters or displacement measurement across primary spring groups to determine vertical loads.

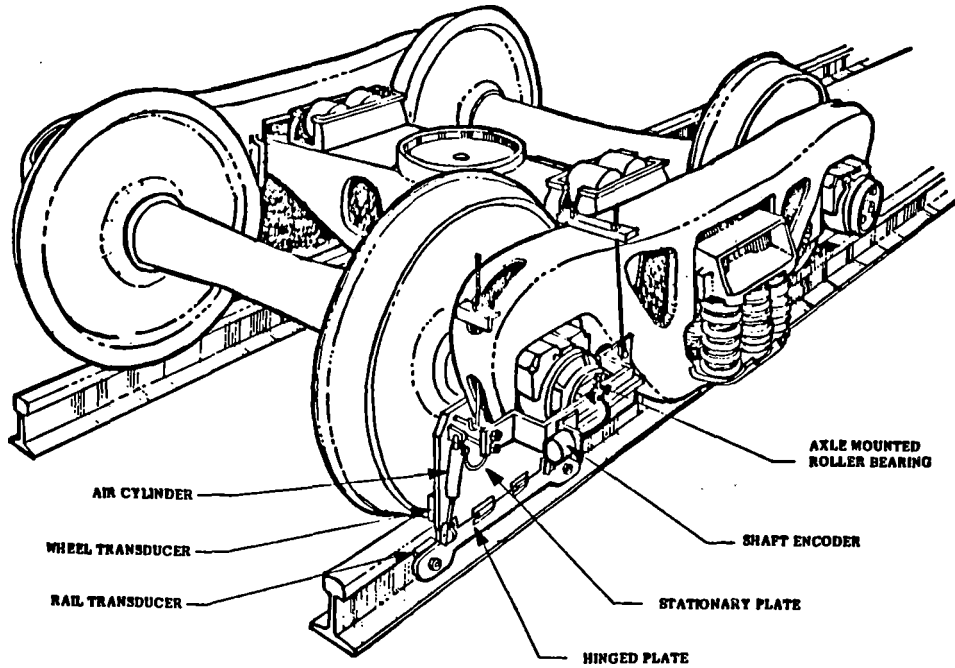
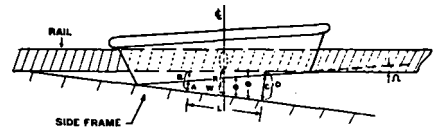


Fig. 4 Wheel to rail displacement measurement fixture shown in running position

Wheel/Rail Position Measurement. A state-of-the-art instrumentation system comprised of four eddy current transducers as developed and used at one end of each axle of the leading truck to measure the relative position and angle of attack of the wheel relative to the rail. This is the first known vehicle-borne instrumentation system for the continuous measurement of wheel/rail angle of attack. The concept is shown schematically in Figure 4. The transducers were mounted on a support system which was attached to the side frame. Two of the transducers measured the side frame position relative to the rail and two of the transducers measured the side frame position relative to the wheel (see Figure 5). The difference between the corresponding two transducers gives the relative angle; the difference between the side frame to wheel and the side frame to rail angles results in the angle of attack.

Truck and Carbody Measurements. Displacement and acceleration measurements were made on the truck to measure relative motion between truck components and acceleration on the axles. The carbody was instrumented with accelerometers at the sill and roof levels to measure the longitudinal, vertical, and lateral accelerations at different locations on the carbody. Fig. 6 illustrates typical locations of these accelerometers.



$$\begin{aligned} \phi &= \text{RAIL TO SIDEFRAME} \approx \frac{C-B}{L} \text{ RADIANS} = \frac{C-B}{L} (57.3) \text{ DEGREES} \\ \psi &= \text{WHEEL TO SIDEFRAME} \approx \frac{D-A}{L} \text{ RADIANS} = \frac{D-A}{L} (57.3) \text{ DEGREES} \\ \Omega &= \text{WHEEL TO RAIL} \leftarrow = \phi - \psi \\ R &= \text{SIDEFRAME TO RAIL DISTANCE} = \frac{B+C}{2} \\ W &= \text{SIDEFRAME TO WHEEL DISTANCE} = \frac{A+D}{2} \\ R/W &= \text{RAIL WHEEL POSITION} = R-W \end{aligned}$$

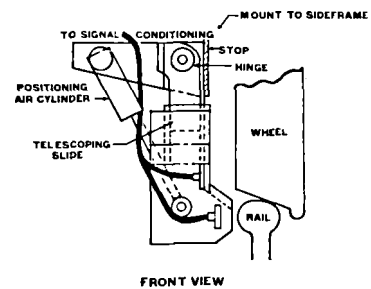


Fig. 5 Wheel/rail position measurement

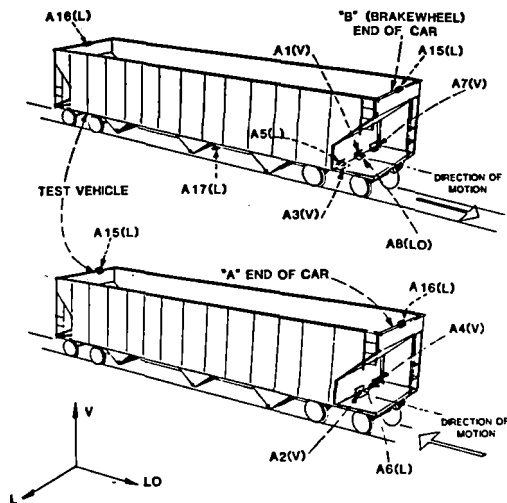


Fig. 6 Carbody instrumentation

Test Description

The Type I and Type II trucks (100-ton capacity) were tested under 100-ton open hopper cars. The 100-ton hopper cars were chosen because they are representative of the higher capacity cars being placed into service today. Furthermore, the rail wear problems can be largely attributed to 100-ton car loadings which cause high static and dynamic wheel/rail loads both vertically and laterally. Two carbodies from the same series were instrumented, one empty and one loaded. Type I truck used the new AAR Standard 1:20 taper wheel profiles. Type II trucks used new Canadian National (CN) wheel profiles which approximate the flange condition of worn wheels and have better steering characteristics than AAR 1:20 wheel profiles.

The test sites used for testing the freight car trucks to obtain performance data on the trucks, in order to characterize their operational behavior in the lateral stability, steady state curve negotiation, and trackability regimes, consisted of mainline and yard tracks of Union Pacific's south central district and California division. The first test zone consisted of mainline track with curves of 1 to 6 degrees. The second test zone provided a section of tangent track, made of bolted jointed rail (BJR) over which high speed (up to 79 mph) tests were conducted. The third test zone consisted of a section of yard track over which load equalization (trackability) tests were conducted.

A standard test train consisting of a locomotive, instrumentation car, buffer car, test car, buffer car, and a caboose was established for all test runs and maintained throughout the test program. The buffers were open hopper cars. Prior to the start of testing, each buffer car was loaded with gravel. To provide for easier interchange of test cars, the instrumented coupler was placed on the test car end of each buffer car.

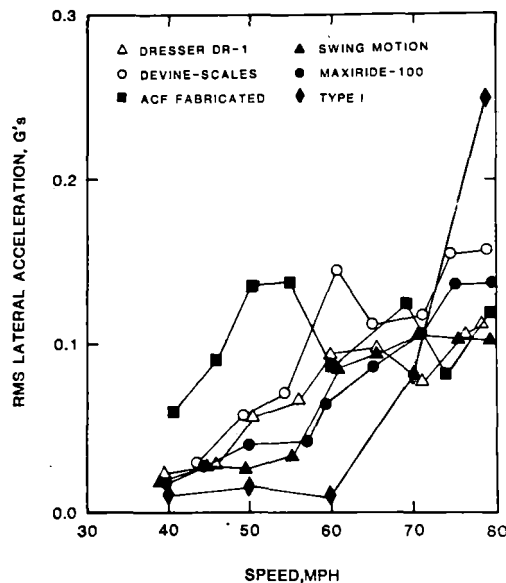


Fig. 7 RMS lateral accelerations versus speed - empty cars

Truck Performance Evaluation

Lateral Stability. Fig. 7 shows the rms lateral accelerations of the different Type II trucks plotted along with the rms value of the Type I truck. It should be mentioned here that the Type I truck was tested under a covered hopper car and equipped with AAR 1:20 wheel profiles (the lateral stability data for Type I truck were acquired earlier in Phase I of the project), while Type II trucks were tested under open hopper car and equipped with CN wheel profiles. As can be seen from the figure, the acceleration levels are well controlled compared to the Type I truck, and no severe hunting phenomenon is observed in these high speed runs. The control of the lateral motions in the performance of the different trucks is attributed to unique design features implemented in these premium design trucks. The Swing Motion truck contains a spring plank to rigidize the truck in tram, while the pendulum action of the spring nest and adapters softens the lateral spring rate; this tends to uncouple the carbody from the truck and raises the critical speed of hunting. Control of the building-up of the lateral oscillations using DR-1 is accomplished through the use of steering arms which have the capability of rigidizing the truck and thus reducing the parallelogramming action of the truck. The rigid truck with primary suspension, Maxiride-100, has the advantage of reducing the unsprung mass. The stiffness in tram (rigidity of the frame), with the variable spring rate, improves the lateral stability of such trucks and reduces the severity of the lateral oscillations of the carbody.

Hunting is attenuated in the ACF truck through the increase in truck swivel resistance (by supporting the car load on the side frames and the use of a rigid frame). In other words, the ACF truck's stability is due to both truck swivel energy dissipation and to warp rigidity; it also has very low lateral damping (known to be desirable in preventing hunting, as stated by the

Japanese) as well as some dual rate suspension characteristics that affect the hunting behavior of the empty car. However, it should be mentioned here that provision should be made to provide damping in both the vertical and lateral directions in the medium speed range. Mounting the hydraulic absorbers vertically only, as in the case of ACF trucks, may cause a resonant phenomenon in the medium speed range of 40 to 60 mph with very high lateral motion.

Steady State Curve Negotiation. The test data acquired on the curving zone enabled quantification of the effect of speed (superelevation deficiency) and track curvature on lateral and vertical forces as well as

L/V ratios and wheel unloading index. Typical results for Type I and Type II trucks are shown in Figs. 8 through 15. The results show differences in the curve negotiability of Type I, rigid and radial trucks.

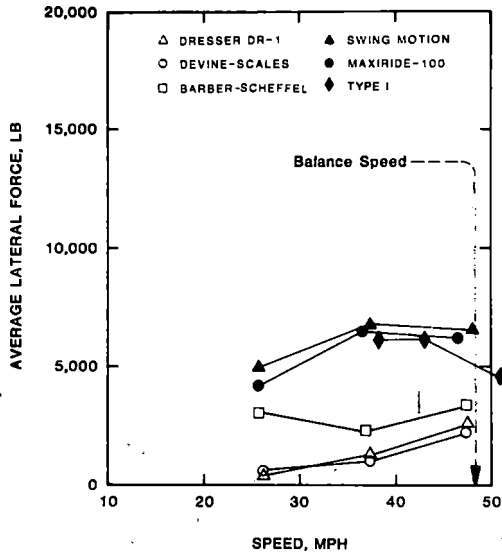


Fig. 8 Average lateral forces versus speed - loaded cars - 2.5° curve

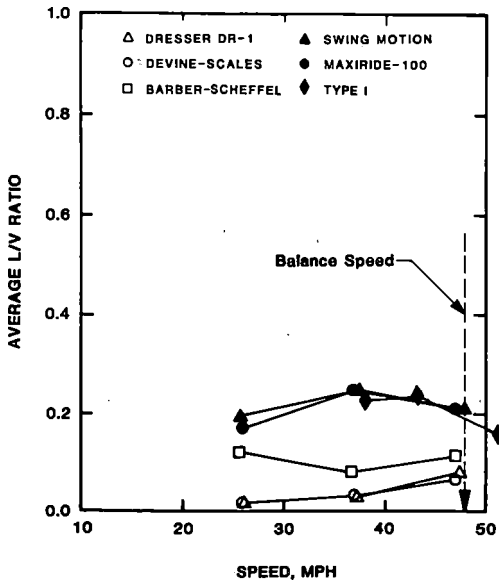


Fig. 9 Average L/V ratios versus speed - loaded cars - 2.5° curve

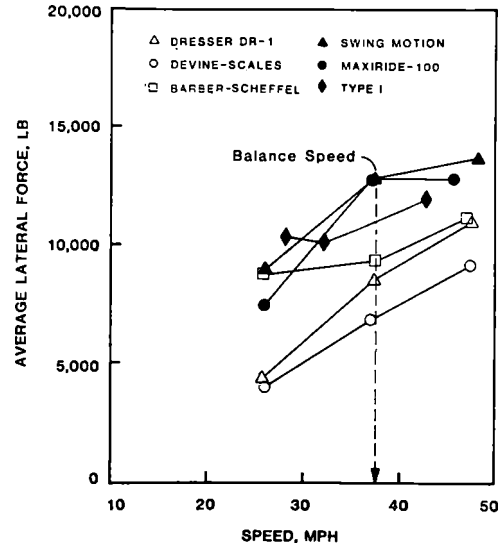


Fig. 10 Average lateral forces versus speed - loaded cars - 5.2° curve

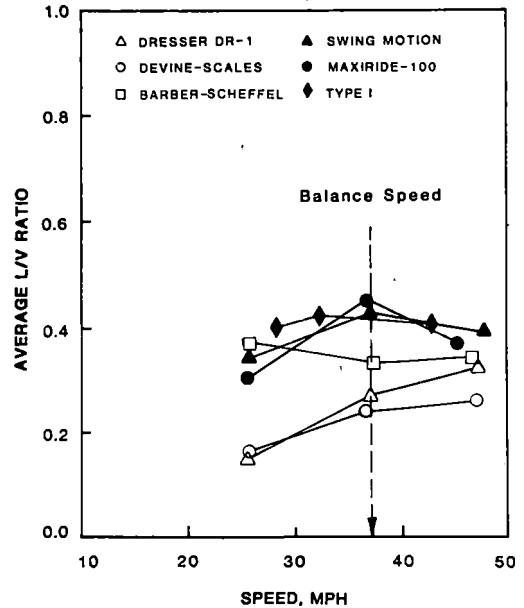


Fig. 11 Average L/V ratios versus speed - loaded cars - 5.2° curve

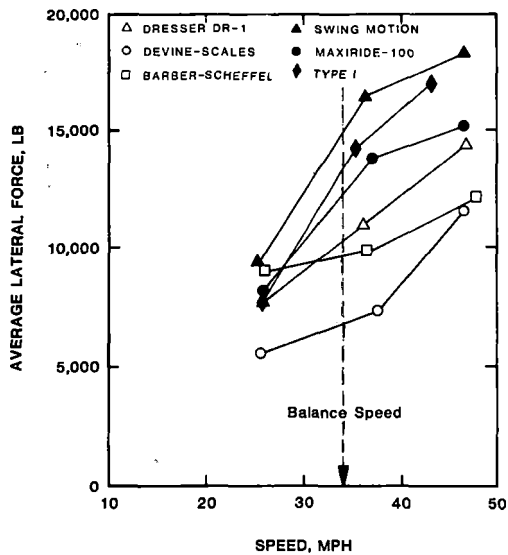


Fig. 12 Average lateral forces versus speed - loaded cars - 6.2° curve

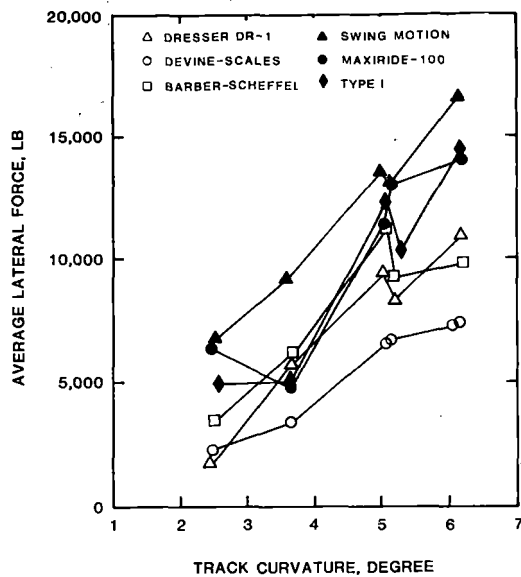


Fig. 14 Average lateral forces versus degree of curvature near balance speed - loaded cars

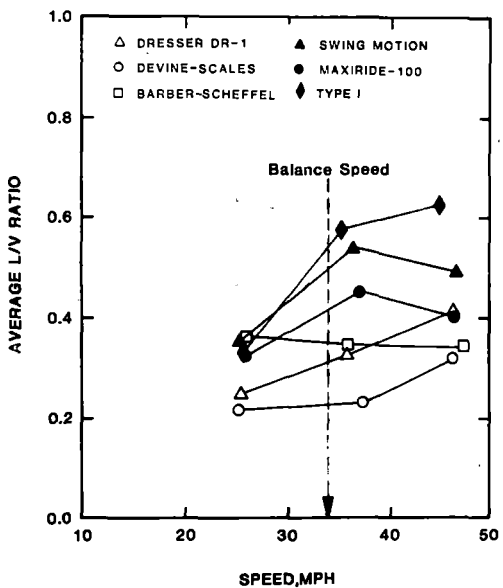


Fig. 13 Average L/V ratios versus speed - loaded cars - 6.2° curve

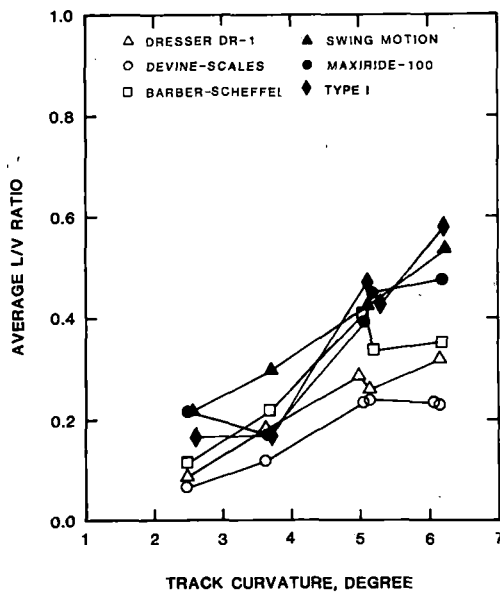


Fig. 15 Average L/V ratios versus degree of curvature near balance speed - loaded cars

For Type I trucks, the lateral forces and L/V ratios on the leading outer wheel increase with increasing vehicle speed and degree of curvature, and they tend to have the same characteristics. For moderate curves of 2.5° (2200 ft) and 3° (1910 ft), the lateral forces are comparable. However, these lateral forces show substantial increase in magnitude as the degree of curvature increases, reaching an approximate value of 14,000 lb at 6.2° curve (924 ft). This high rise in lateral forces is due to the ability of the wheelset to yaw and consequently attain higher angles of attack with the rail. These high angles of attack will result in greater lateral forces. The behavior of the truck on the sharp curves is manifested in high lateral forces on the leading outer wheels with the leading outer wheel being in flange contact with the rail at high speeds. High lateral forces are generated at the leading inner wheel to balance the flange force on the leading outer wheel.

The wheelsets of the rigid trucks (National Swing Motion and Maxiride-100) are unable to align themselves with the local normal to the curve, and that guidance depends on the flange forces guiding the truck around the curve. In other words, the leading outer wheel is in flange contact (free curving) while negotiating the test zone.

Flange-free curving is a goal for Type II trucks, but generally unachievable on sharp curves (curves of 5° or more). In the radial trucks studied (DR-1, Barber-Scheffel, and Devine-Scales), the test data indicate differences in curving characteristics on moderate and sharp curves. While the radial truck axles assume an approximate radial position in curves of small and moderate curvature (2.5 degrees -3.7 degree curves) resulting in truck guidance being supplied by the creep forces, the truck relies on flange contact in guidance during negotiation of sharp curves (5 degree -6.2 degree curves). In other words, the test on small and moderate curvature (2.5 degree -3.7 degree curves) have shown that the radial trucks have the ability to provide satisfactory curving performance in the sense that low levels of lateral forces are generated at wheel/rail interface. This is accomplished through various truck design features. The steering arms for the Dresser DR-1 allows the axles to align almost radially under the action of tread creep forces. The wheelsets of the Barber-Scheffel truck are interconnected by a light-weight anchor, thus, a yaw moment and a lateral force is transmitted between wheelsets. As the truck traverses a curve, the wheelsets will tend to align themselves radially to the curve and a reduction in the lateral forces is achieved during curve negotiation. In the active steering truck (carbody-steered truck), Devine-Scales, the attitude of the truck wheelbase on the curve is used to align the axle boxes. The steering capability of this truck greatly improves curve tracking characteristics and the truck provides satisfactory curving performance without excessive lateral forces on the rail. The wheelsets are steered in the curve without flanging and guidance is achieved by the creep forces.

From the analysis of the data for steady state curving negotiability, it may be stated that steering-arm and cross-anchor trucks cannot completely achieve an ideal radial position, particularly on sharp curves, but there is promise that the carbody-steered trucks will achieve this goal.

Trackability. Trackability is the ability of the truck to maintain sufficient loads on all wheels to allow the development of guidance forces which prevent derailment for all extremes of in-service track geometry. The trackability regime discussed in this paper includes as subsets the ability of the truck to accommodate: (a) track twist, and (b) curve entry and exit. This ability is important for successful negotiation of low sidings, extremely poor track in switch yards, and transition from the tangent to the curve track for a wide range of operating conditions and environmental factors. Typical results are presented in Table 1 and Figs. 16 and 17.

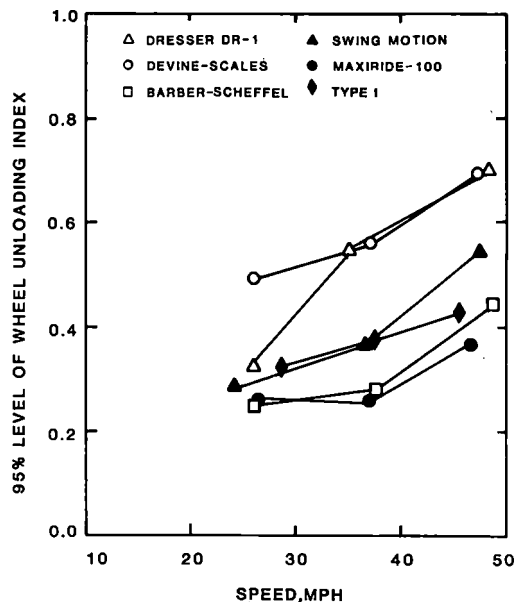


Fig. 16 95% level of wheel unloading index versus speed - empty cars

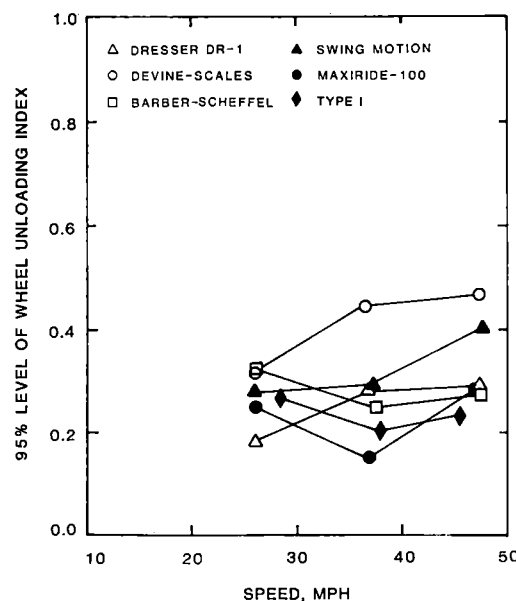


Fig. 17 95% level of wheel unloading index versus speed - loaded cars

Table 1 Wheel unloading index (WUI) levels (track twist)

TRUCK	EMPTY CAR WUI ₉₅	LOADED CAR WUI ₉₅
DRESSER DR-1	0.783	0.281
BARBER-SCHEFFEL	0.343	0.400
DEVINE-SCALES	0.744	0.512
SWING MOTION	0.553	0.368
MAXIRIDE-100	0.297	0.307
TYPE I	0.351	0.364

From examining the results in Table 1 and Figs. 16 and 17, it may be said that the use of low unsprung mass as manifested in the design of the primary suspension trucks, Maxiride-100, and the use of dual rate suspension characteristics result in reduction in the vertical dynamic forces. However, in general, the Type I truck has better performance in the trackability regime and in particular the track twist than many of Type II trucks.

TRACK RELATED IMPLICATIONS OF IMPROVED TRUCK PERFORMANCE

Apart from improving functional performance and endurance of rolling stock itself, improved performance characteristics of the premium trucks in specific performance regimes carry significant implications of heavy haul railroads affecting the operation, maintenance and refurbishment of trackwork. For example, considering some of the specific characteristics in individual performance regimes, a cursory delineation of some of the significant influences indicate the following:

- Reduced lateral force and angle of attack attainable through the use of self-steering (radial) trucks can reduce rail wear significantly.
- Reduced peak lateral forces during hunting (or the wide range of unstable oscillations occurring continuously or intermittently) indicate that the influence of trains to laterally batter the rails leading to gage widening could be mitigated, if not altogether eliminated.
- Reduced dynamic loads attainable through the use of primary suspension trucks could be translated possibly to an alleviation of track degradation and perhaps reduced maintenance on the track.

While these are but some examples of the implications, the engineering and economic evaluation methodologies developed during TDOP/Phase II could be advantageously utilized in casting them in more concrete terms for the conditions attendant upon a specific railroad operation.

ACKNOWLEDGEMENT

The work reported herein was sponsored by the Federal Railroad Administration (FRA). The authors would like to thank Mr. Phil Olekszyk, Dr. Thomas Tsai and Mr. Arne Bang of the Federal Railroad Administration for their support and encouragement. Thanks are due to our colleagues and staff at Wyle Laboratories for their continued contribution and guidance during the course of this work. Gratitude is expressed to the many outstanding members of the industry who contributed through their participation in the TDOP Consultant Group.

REFERENCES

- 1 RamaChandran, P. V., ElMadany, M. M., Glaser, R. J., and Bakken, G. B., "Truck Design Optimization Project Phase II - Final Report", Report No. FRA/ORD-81/48, September 1981.
- 2 RamaChandran, P. V., ElMadany, M. M., and Tsai, N.T., "Performance Characteristics of Conventional Freight Vehicle Systems", ASME, Paper No. 81-WA/RT-3, November 1981.
- 3 Bakken, G. B., Peacock, R. A., and Gibson, D. W., "Wheel/Rail Measurements from Concept to Utilization", International Conference on Wheel/Rail load and Displacement Measurement Techniques, Transportation System Centers, Cambridge, Massachusetts, January 19-20, 1981.

High Utilization Cars for Unit Coal and Ore Trains

Henry E. Keniston

Vice President
Ortner Freight Car Co.
Cincinnati, Ohio
Member ASME

Meeting the challenge of increasing tonnages in this nation's railroad system can be met in one of two ways; either a greater number of railcars and/or with greater capacities introduced into the system, or methods of train operation are improved to maximize individual car utilization. With the cost of car ownership increasing every day, shippers and carriers alike can no longer afford the extravagance of simply adding more cars to the system. It will be essential for shippers, carriers and suppliers to work in a coordinated effort to ensure a maximum use of labor and equipment. This maximum utilization of equipment will require a railcar of proper design and sufficiently investigated components selection to remain in service between scheduled preventative maintenance work as well as reduce deterioration of roadbed during operation. Only through a total system approach to bulk transportation will material be delivered at its lowest delivered cost per ton.

The United States is blessed with an abundance of energy in the form of coal, a fact that many are just beginning to give full recognition to since coal seemed to have fallen in disfavor after World War II. Many other nations similarly blessed are actively seeking means to develop mining, transporting and using techniques for their coal. Transportation is a major function in the success of any coal endeavor. It has been concluded that this coal must move in unit trains; more specifically, dedicated in one service and tailored to the parameters of the coal move to ensure the highest degree of train utilization. No single facet of the transport can be finalized without giving full recognition to the inter-relationship of the associated functions. Although coal will be emphasized, the same parameters basically apply to ore.

Accordingly, a review will be made of some of the technical aspects of unit trains and the logistics of moves that should come under consideration in the planning stages, with emphasis on railcars that can provide the high utilization necessary to actually carry the coal requirements through the year 2000. It has been expressed by many that the only real answer to avoiding costly errors in judgment is an honest appraisal of operating practices and cooperative engineering effort on the part of railroads, equipment suppliers, coal producers and users and their consulting engineering groups. No one group can selfishly try to impose his self serving ideas on all others.

First, let us dispel the thought that we hear all too often, namely, to obtain a greater carrying capacity all that is necessary is to "scale up" railcars. Theoretically, we can build cars of 100 (90.78), 125 (113.48), 150 (136.17) ton (tonnes) capacity by such scaling up or simply filling the envelope of the railroad's clearance diagram. But, there is a lot more involved if we are to prevent increasing car and track maintenance expenses and prevent bringing on operating restrictions. No doubt you are aware of cases of premature failure of railcar components, such as center plates and bolsters, the need for supplemental devices in the car truck area to keep certain unit train coal cars on the track and, very seriously, the rapid deterioration of roadbed with subsequent rail failures where some unit trains operate. These are, for the most part, due to the use of components that were satisfactory for general interchange cars but are inadequate for the high utilization, high capacity, unit train car. Equally as important has been the failure to accept some fundamental engineering facts involving centers of gravity, harmonics of train action and dynamic effects of loads imposed on rails.

A total systems approach must be made taking into consideration all aspects of the move, recognizing the impact variations that one component can have on all other parts of the system. A factor that is of paramount importance is the effect of car design on the roadbed over which the train is to move. Contrary to popular thought, it is not always the fully loaded car that imparts the most destructive conditions to the roadbed, nor is the loaded car condition always the one that creates the most deteriorating effects on the cars.

Railroads, historically, have attempted to purchase cars that have had the most universal appeal to all customers. The hopper car was usually acquired for general interchange service with the thought that it must serve the coal industry as well as sand, gravel and aggregate producers. Often such a car moves one commodity in one direction and another on the return move. Little economic value is placed on car days lost switching, yarding and seeking loads. A car designed for specific purpose can incorporate features that would not be economical on a general interchange car. In the case of coal, we must be careful that the car designer not let his experience with the design of general interchange cars limit his vision as to innovative benefits in car design that will bring a return on investment, either directly or by reducing expenses in some other part of the system creating an indirect savings. Here again, emphasis should be placed on the effect car design has on roadbed maintenance.

To put the picture of rail coal cars in its proper perspective, we should first delve into history to see where we have been. I think we also should point out how we have applied, or neglected to apply, what past experience should have taught us. Risking the repercussion that I would expect from making such a statement, I feel that if the medical profession had doubted the discoveries of its individual members and refused to accept them and go on from there as much as the railroad industry has refused to profit by the experience of individual railroads, we would still be in the dark ages as far as combating the major diseases of man. The interchange of information in the medical profession has virtually wiped out most of the killers of 50 years ago. An equal interchange of information in the railroad industry and acceptance of that information by those who may not have participated in the actual testing would have advanced our industry far beyond where it is today. Sometimes I think that through our individual preconceived ideas and inability to accept innovation, we are our own worst enemies.

We can safely start with the fact that coal carrying by rail has been with us a long time and obviously is going to be with us for a good while longer. Since coal was so often stored in bins it was only natural that the bin on wheels developed as the most usual vehicle of coal handling - this we came to call the hopper car. Doors were provided on the bottom of the hopper chutes of these cars to allow the coal to drop into a stationary bin or onto some transfer apparatus. We have had twin hopper cars, triple hopper cars and recently, quadruple hopper cars. As long as the value of time was of minor importance, this conventional hopper car served its purpose. But, with increasing consciousness of labor expenses and the value of time, the receivers of these cars began to worry about the cost of getting them unloaded, for they are usually not self-clearing.

This brought into being the car shaker and rotary car dumper, or tippler, as expedience to unloading, but still we kept the same general configuration of car. Except for the noise generated at the consignee's unloading site, the only person who really worried about the car shaker was the mechanical officer of the railroad owning the cars who suddenly found his car maintenance expense sky-rocketing due to car shaker damage. The rotary car dumper proved less destructive on the cars themselves, but still took its toll as far as car maintenance expense is concerned due to the unnatural loadings imposed on the conventional coal hopper car used in this service.

We are now about to the period of the late 1950's in time when all of us began to be pinched by the rising costs of labor and now all of us, not just the coal receiver, became interested in time required for unloading and labor costs to accomplish it. Such words as "equipment utilization", "bulk" and "train load" rates, "unit and integral trains" and "systems planning" came into our railroad vocabulary indicating new thought on the part of some railroads to combat these rising costs through innovations that today we categorize as marketing techniques. Time and labor had suddenly been recognized as valuable commodities.

As a result, railroads began looking at coal train moves in an entirely new light, that is, no longer was coal handled when nothing else was scheduled to move, but coal had attained its rightfully recognized position as a revenue producing commodity. The car designers could now come into the picture for this awakening industry became cognizant of the fact that only through new concepts in car equipment could the problems of the past be eliminated. Let's see what the car designers came up with and look at the relative merits of each.

There were two car types accepted for coal; the hopper car and the solid bottom gondola car. The latter must be rotary dumped, whereas the hopper car has the advantage that it can be either rotary dumped or bottom unloaded. However, a standard coal hopper car possesses very poor unloading characteristics inherent in its design. In unit coal train service the conventional hopper car, although still used by some, has given way to self-clearing, quick discharge cars that can be automatically or semi-automatically emptied in a matter of seconds. Figure 1 shows a self-clearing Rapid Discharge® Car of the type used where trains unload in motion. An example of a conventional flat bottom gondola car is shown in Figure 2 as well as the more recent lightweight design shown in Figure 3.

Historically, railcar designers either were with railroads or with carbuilders, but recently outside engineering groups addressed themselves to the subject of coal car design. The resultant car configurations have certainly taken into full account static structural integrity of the car body but appear to have ignored, at least to a degree, the effects of the dynamics of train action which are amplified

in high utilization unit train moves. Figure 2 shows a typical flat bottom gondola car for coal handling. From the static structural standpoint, I certainly have no argument with the fact that it is rugged enough but let's look at what happens to this car in actual train service coupled to as many as 100 identical cars to make up a unit train. This car must be rotary dumped for unloading. Accordingly, the cars are equipped at one end with a rotary coupler which is designed specifically for this

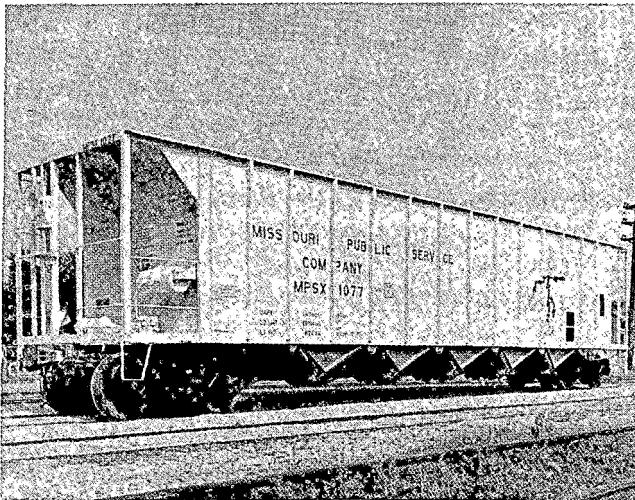


Fig. 1 Rapid Discharge® Car

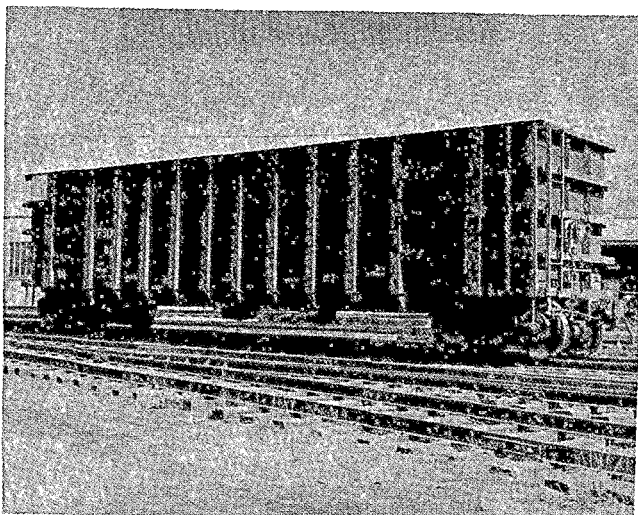


Fig. 2 Flat Bottom Standard Gondola

purpose. Here is a dilemma to the car engineer for the car must be capable of swivelling about the center line of this rotary coupler during unloading and the rest of the time this swivel coupler must be capable of transferring the full buff and draft forces between cars of a moving train. This can be quite a task for a

train of fully loaded cars and without question this swivelling coupler requirement generates maintenance expense and increases potential out of service time for a car.

If we move back from the coupler of this gondola car, we come to the main area of car weight support, the body bolster. Let's look at this area in detail. Dimensionally, we have only about 13 inches (330 mm) of height available to us as designers to insert as much strength as possible. In service experience is showing us that this height is insufficient, but we have only one recourse - - go into the coal carrying box to place support. Looking at the problem in a little more detail, the upper sketch of Figure 4 shows a loaded gondola car during a heavy train action or in the emergency brake application.

The lower sketch is an enlargement of one end to show the reactions on the bolster. Note that just as in your automobile when you apply the brakes the load surges forward and the car tends to nose down in the direction of braking loading the lead truck and unloading the trailing truck. With the solid bottom gondola, the vertical car end wall is out at the coupler. This end wall as the resisting element to the forces of sudden stopping, creates high stress in the bolster. At the same time, downward thrust of this load is transferred to the bolster ends by the sides (these side forces have been transferred into the sides from the floor crossbearer members). Note in the upper sketch of Figure 4, the tendency of this loading to want to "break the back" of the bolster across the center plate. The bolster center plate area of this design of car is subject to distress early in life, but we continue to build them. A more realistic approach would be as shown in Figure 3.

To understand why this is more realistic, let us look at how the hopper car design fares under the same forces imposed by the sudden stopping example just described. The upper sketch of Figure 5 shows such a car in cross section and the lower sketch is the enlargement of one end.

Note the completely different structural arrangement of this bolster, for with a hopper car, structural elements can be installed above what was the floor area in the gondola car. The end slope sheet is now the restraining element for the load, but look at the bracing we have that keeps all of the car parts in proper relationship, minimizing any destructive loading in the center plate area. The triangular plates between the floor sheets, bolster web and centersill are real support members. Look at the lower sketch of Figure 6 showing how the load of the sides is transferred to the center plate without breaking the "back" of the cars. Here is a real plus for the hopper car bolster design.

From the standpoint of dynamic tracking stability we will see forces coming into the car body from the track where in braking it was just the reverse. Referring to Figure 2, the outside view of our gondola car, we note that the side certainly looks as strong as a battleship and with the ends shown will stay square and rigid, but do we really want it to - no! A rail-

LIGHT WEIGHT.....46500 LBS.
 CUBIC CAPACITY LEVEL.....40500 CU FT
 CUBIC CAPACITY W/10' HEAP.....44700 CU FT

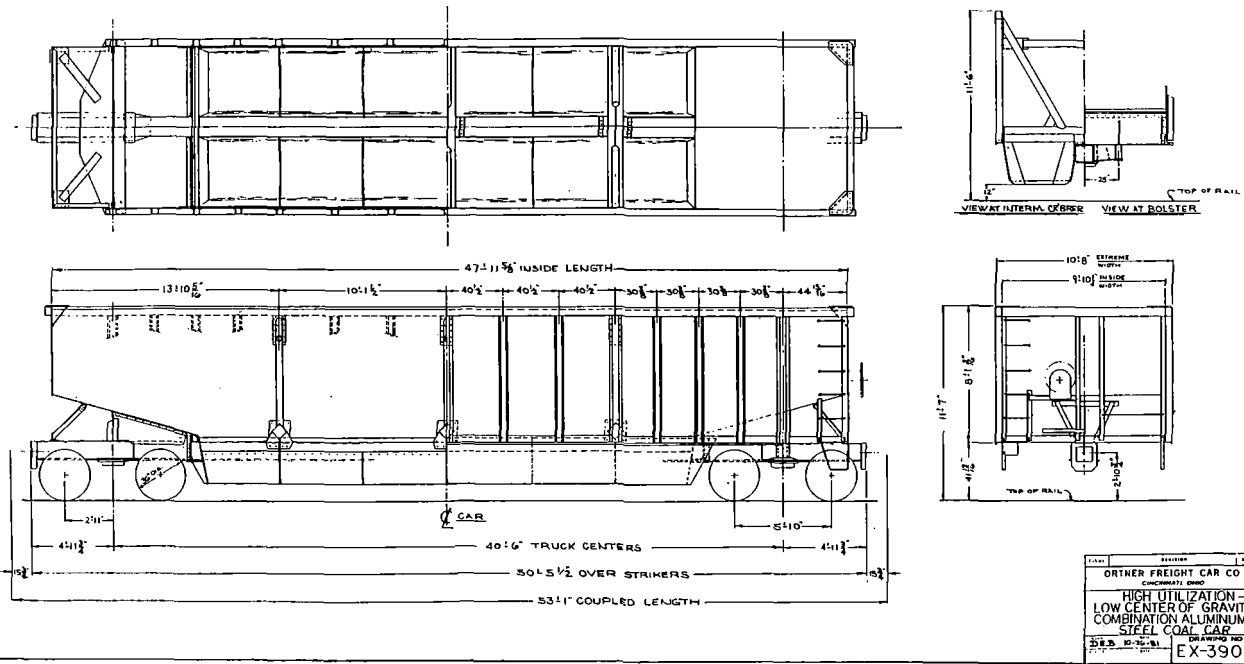


Fig. 3 Combination Aluminum Steel Lightweight Gondola Car

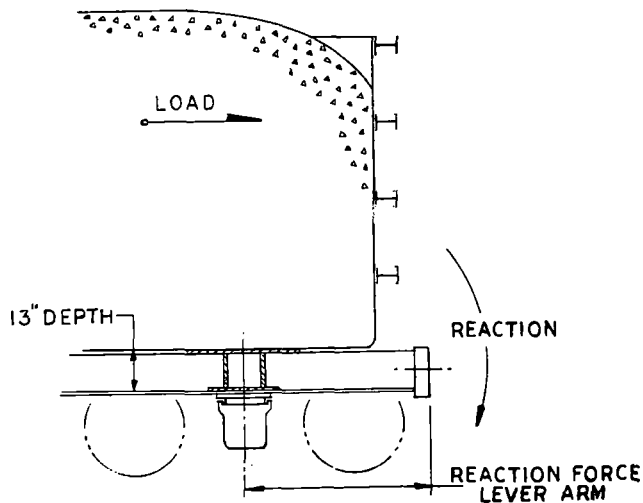
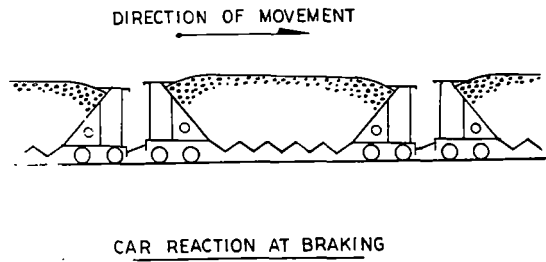
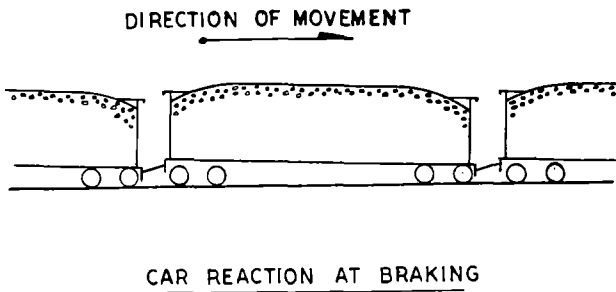


Fig. 4 Loaded Gondola during Emergency Braking

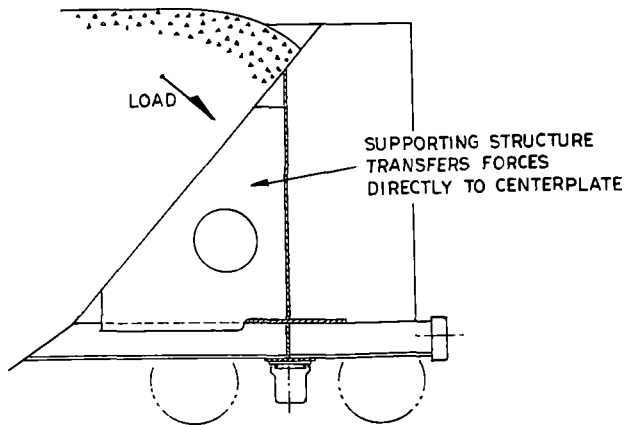


Fig. 5 Loaded Hopper Car During Emergency Braking

car should be a relatively flexible vehicle. We actually want it to be able to conform to normal track irregularities and return to neutral position without permanent detrimental effects on car body or track.

Looking at the hopper car design from this standpoint, the sides are purposely less rigid, but the bolster structures at each end of the car are fairly rigid elements. As slight irregularities are encountered in the track roadbed structure, they will be transferred through the trucks into the car body. These comparatively rigid hopper car bolster structures transfer track shocks from the trucks into the sides and center sill where in a properly designed car, they are absorbed and not transferred to the bolster at the other end of the car. This absorption with associated twisting capability is termed "racking" by railcar engineers. If the car responds by "racking", wheel lift tendencies are minimized. Note the long low profile of the hopper car of Figure 1 as compared to the short high profile exhibited by the gondola car of Figure 2. This twisting capability of the long low center of gravity hopper car interacting with long travel springs tend to dampen the forces of roll oscillation and vertical bounce, minimizing displacement between truck and body bolsters. The gondola car design shown in Figure 2 does not have this available because of the stiff side and end construction that forces the individual shallow bolster to either absorb track irregularities within itself, or transfer an undesired amount to the other end of the car causing wheel lift or springs going solid.

For several years these problems were further aggravated by the designing and building of 125 ton (113.48 tonnes) (315,000 pound (142.86 tonnes) gross weight on railcars on four axles) gondola coal cars. Now, even the economics of the 100-ton car are being questioned (Mr. R. Ahlf, Illinois Central Gulf Railroad, "Modern Railroads" - February 1980). It is Mr. Ahlf's hypothesis that under certain conditions with respect to Maintenance of Way costs, car utilization, fuel costs and car costs, the "80" ton (72.62 tonnes) (220,000 pound (99.77 tonnes) gross weight on rail) car makes better economic sense than the "100" ton (90.78 tonnes) (263,000 pounds (119.27 tonnes) gross weight on rail) car. This is subject to debate, but proves that all aspects of a move should receive equal attention before a piece of equipment is settled upon.

What factors govern some of the design considerations that result in such a difference of design opinion? Three major factors are volume of car, size of car and car weight.

Designing cars for a specific service gives us certain flexibility, as well as constraints, in engineering an envelope to handle the type lading involved.

As an example, coal can range in weight from 45 pounds (.72 tpcm) per cubic foot to 55 pounds (.88 tpcm) per cubic foot, therefore, we consider lading density. Unrestricted by the "universal commodity requirement" coal cars may vary 400 cu. ft. (11.33 cu. meter) in volumetric

capacity, as an example, for service in the Eastern Kentucky area as compared to movements out of the Powder River Basin in Wyoming.

Train dynamics should also be an important consideration in today's coal car design. Unlike the general service car of the past that might handle 2 loads a month, today's unit trains typically accumulate well over 100,000 miles annually and encounter accelerated wear in running gear, as well as heavier stress through the draft area. Geographical location of routing will affect car service requirements. Also, will the car operate over welded or jointed rail? Truck centers corresponding to rail joint lengths can create serious dynamic problems at what have been deemed critical speeds. By extending truck centers to approximately 45 ft., it has been found that a reasonably stable vehicle results for either type of rail.

The tare or lightweight of a car has become the subject of much debate. Without going into the philosophy involved but following the design criteria established in the years of unit coal train experience, the car in Figure 3 is offered. An all steel version for 263,000 pounds (119.27 tonnes) gross weight on rail would weigh approximately 55,500 pounds (25.17 tonnes), however in a combination aluminum-steel design the lightweight would be approximately 46,500 pounds (21.09 tonnes). Note adherence to the concept of a hopper car type of bolster and a through center sill. The latter will provide a "backbone" for the car assisting in absorption of buff and draft forces thus eliminating critical stress concentration points where such forces must transfer from shear plates to sides in center sill-less cars.

SERVICE PERFORMANCE

There are some ideas that must be altered if we are to attain maximum car in service time at minimum car and track maintenance cost. Foremost is the idea that a railcar is a railcar, irrespective of its service. I think that we will shortly come to realize that we may really need two sets of standards as far as railcars are concerned. First, would be a set of standards pertaining to general interchange car equipment, and secondly, more stringent standards pertaining to high mileage, heavy duty service cars such as those used in unit coal train operations. I think all of us recognize that the unit coal train is either fully loaded or fully empty, while the general service interchange car is seldom loaded to its full capacity and usually operates in trains mixed with both loaded and empty cars.

What might be involved with the idea of two sets of standards for car design? At the present time all U.S. carbuilders, when offering cars to prospective domestic customers, offer them as meeting the standards of the Association of American Railroads as well as the requirements of the Federal Railway Administration, Department of Transportation. These standards were established by the member railroads to assure that general interchange cars meet an acceptable minimum level of uniform strength. There are two major documents involved: one is entitled "The Design, Fabrication and Construction of Freight

Cars" which spells out the forces that are involved in general interchange cars and minimum strength requirements of car components to meet these forces. The second document is the "AAR Manual of Accepted Practice", which coupled with the AAR Rules for the Interchange of Traffic, lists approved car components. To attain such AAR acceptance for approval, a manufacturer of a car component must only demonstrate to the AAR that his item meets the minimum standards set forth. These standards do not differentiate between service requirements to which a car is to be used. As a general rule, the average interchange rail-car will accumulate no more than 15,000 miles in any one year. On the other hand, many coal unit trains are scheduled to accumulate nearly ten times such mileage in a year's time. Yet, as matters stand today, car components may be offered to identical standards. Is it any wonder then that cars so equipped do not always stand up in severe service?

You, the user of these cars, have within your power the ability to correct this situation. It is solely up to you, for if you buy on competitive bid where you have merely indicated the capacity of car required, you will get the minimum car with resultant maximum maintenance expense and excessive out of service time. If, on the other hand, you ask for a heavy duty car and properly evaluate the car offered, you will get value for your dollar. I would suggest that you have the features that mean longevity spelled out to you in a proposal along with the cost differential, then you can see that you are getting full value for the price paid. What is an extra thousand dollars per car initial price spread over a 15 to 20 year period, when you consider that this extra thousand dollars will result in the car remaining in service, in lieu of repeatedly being cut-out for repair. Missed trips are irrecoverable from your standpoint and have to be very costly.

Mr. J. A. Johnson, Director of Customer Service Engineering, Southern Railway, in paper delivered at Kansas City at the Coal Handling Seminar, June 11 of last year, stated Southern's philosophy after a study of the growing investment in freight car equipment, and the declining revenue productivity of the capital employed. He stated that "In these twenty plus years of unit train experience, the Southern has developed a design philosophy which differs markedly from many railroads and private car owners. We recognize that many of the design specifications insisted upon by the Southern, increase the initial cost and the lightweight of the car but now know that they result in a longer life without shopping for car body repairs". He went on to cite various examples including the use of a through center sill, heavy body bolster construction, high capacity car components and special braking arrangements.

UNIT UNLOADING EFFICIENCY

Thus far, we have presented a few of the considerations in car design, which we as carbuilders and many of you as car owners, must keep in mind when designing or purchasing cars to operate in the dedicated unit train of today.

Another potential increase in car utilization and reduction in system costs can be obtained through the separation of the transportation function and materials handling function at the receiving facilities. Train handling costs for a facility handling millions of tons of coal a year and multiple unit trains daily can become very significant. Consider an increase of just 5¢ a ton at a facility handling 10 million tons (9 million tonnes) of coal per year.

There are several coal unloading systems that have been tried, all with varying degree of success. In planning a system, the obvious approach, and the one least subject to criticism, is to copy an existing system that has been in service for several years. However, there is generally very little information available as to the problems that have been encountered with the system being copied, for human beings seldom publicize their mistakes. Furthermore, seldom do the factors that give rise to the particular design being copied remain constant long enough to render full comparison to another operation, yet we continue to see system after system duplicating what twelve to fifteen years ago was a technological advance, but is now superseded by more modern technology.

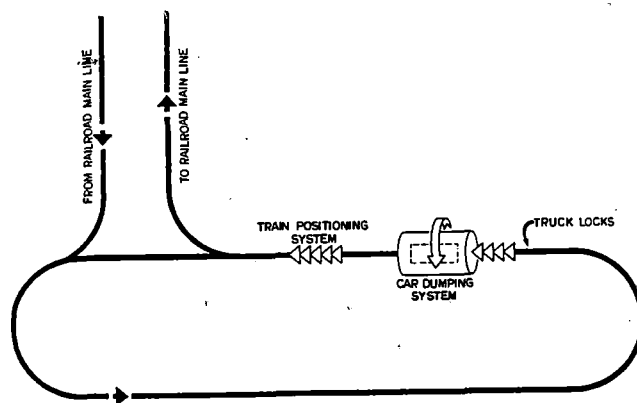


Fig. 6 Dumper System

The current design of the car dumper system usually includes a train positioner. A fully loaded train arrives on a loop track; road locomotives do initial car spotting, then positioner takes over. Control and movement of the entire train are handled automatically by the positioning system. Cars are successively indexed on dumper platen. After each car is spotted, train is locked in position for dumping sequence by truck restraints. The car dumper performs integrated sequence: clamps car on platen rails, rotates up to 180°, dumps, returns to original position, releases clamping force gradually; all without uncoupling. The hopper under the dumper directs material onto conveyor. The positioning/dumping sequence continues until train is empty. Equipment suppliers cite typical times of two minutes per car, four hours per train. This system is shown diagrammatically in Figure 6.

Citing again, Mr. Johnson of the Southern Railway - "In the early 1970's, it was evident the size of the coal fueled electric generating plants was increasing. Georgia Power announced plans for the construction of Plant Wansley near Carrollton, Georgia with four units capable of generating 3.5 million kilowatts annually and consuming approximately 10 million tons (9 million tonnes) of coal each year. It was obvious that with such volume involved, and without the rapid unloading of trains, the queueing of trains while awaiting unloading would defeat our primary objective of maximum utilization of equipment. This, in turn, would increase drastically the cost of transporting the coal. Rapid unloading of an entire train was essential.

The Southern had been involved in testing under rather severe conditions, several experimental cars equipped with doors which were air activated for opening and closing and easily rigged for automatic operation. Georgia Power Company, working with others, developed a car meeting these demands for rapid unloading, and had proven its practicability at their Plant Bowen, served by the Family Lines. We realize this was the only feasible means of handling the large volume of coal to be used at these large coal consuming power plants."

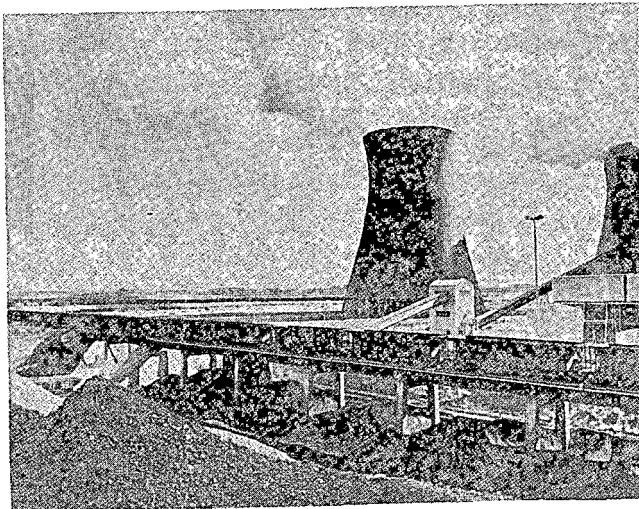


Fig. 7 Trestle System

The most recent installations of bottom dump systems use the self-clearing design of car equipped with a door activating system that permits unloading while train is in motion. Cars empty into either undertrack hoppers or the space under a trestle. In the latter case, the space beneath the trestle doubles as live storage reducing coal handling requirements. Figure 7 shows one of these installations.

Trestle length depends upon amount of live storage desired. For efficiency the area should hold a full train of coal as a minimum. Usually several train loads can be accommodated. This provides train unloading capability even if the belt system is inoperative. Train queueing as a result of unloading system bottleneck is thus avoided.

Where undertrack hoppers are used for unloading trains in motion, questions arise as to hopper length. Using the Ortnor Rapid Discharge® car as an example, it is recognized that a car will unload in from 15 to 20 seconds after the doors are opened. Figure 8 shows the length required to unload a car at varying speeds of train movement. At first thought, one would think that a few seconds one way or the other would be insignificant, but since locomotives pulling the trains are under control of a human being, seconds become important. This is a definite advantage for the trestle unloading system as compared to the undertrack hopper of the type shown in Figure 9.

Another advantage of the trestle that has come to attention after seeing them in service is the reduction in overall coal dust problem. With a live storage beneath the trestle serving directly to the plant, the only time coal is exposed to the environment to where it could be blown about is when it comes out of the cars. It is relatively simple to create a spray system for a trestle when one considers that the coal does not drop the full height of the trestle freely. As coal is being unloaded from a train in motion, cars are progressively unloaded so that coal rolls down the face of the pile and at unloading this suddenness of clearing of the Rapid Discharge® car confines each particles within columns of coal from each set of doors.

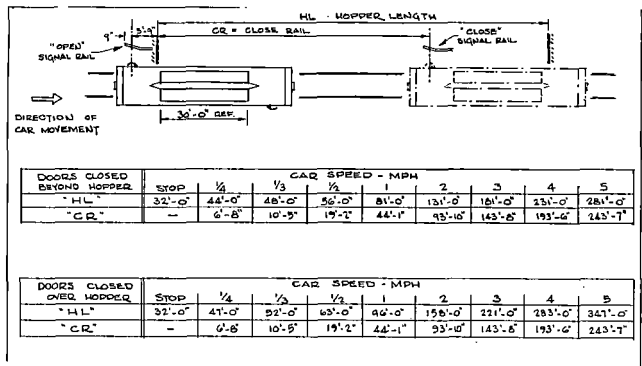


Fig. 8 Length to Unload Cars at Varying Speeds

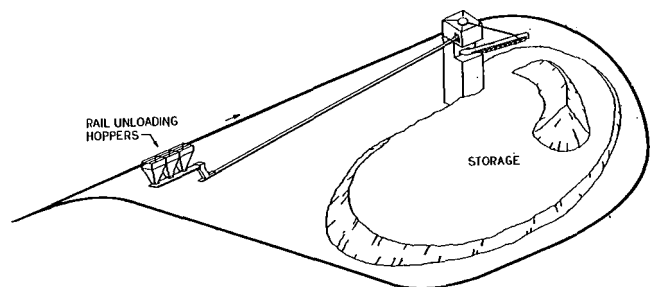


Fig. 9 Undertrack Hopper

If track maintenance costs are to be kept within reasonable bounds, railcar design must be looked at carefully. The allied industries supplying components to rail carbuilders and Maintenance of Way departments alike, must make technological advances, giving full consideration to service intended. We cannot take the easy way out and simply do it the way we did yesterday.

In the railroad industry, this technological innovation will provide utilization of cars, locomotives and rights of ways, as described herein, to meet the demands of growth. All of this must be accomplished within an economic climate that will provide incentive for the investment community to finance the growth. Engineering is thus charged with the responsibility of providing the essential research time to assure that every advantage of technological development is utilized to its fullest. Many engineers in the railroad and allied industries are accepting this responsibility, recognizing that all must seek new ways to increase productivity per dollar invested.

Survey of Railroad Rail and Wheel Contour Studies

G. M. Magee

Assistant Vice President
(Retired)
Research Department
Association of American
Railroads
Railway Engineering
Consultant

This report is a review of the research and tests that have been conducted in the United States and Canada, relative to the effects of rail and wheel contours on rail and wheel wear. Data reviewed include the views of A.M. Wellington, research by the AAR's Engineering Division Research Staff, on the Black Mesa and Lake Powell Railroad, by the Quebec, North Shore and Labrador Railway, by the Griffin Wheel Company on the Burlington Northern, by the Canadian National Railways, by the Canadian Pacific and at the FAST Test Track. The review indicates there are several factors that influence wheel life other than wheel contour. However, for 100-ton cars in unit train service, it appears that some economy in wheel life may be attained by using the Heamann-type wheel profile, providing the speed of empty cars is limited to 40 mph. No change in the present A.R.E.A. rail designs is indicated at this time.

INTRODUCTION

The optimum design for new rail and wheel contours has been a subject of great interest to railway track and rolling stock engineers for many years. In 1887, A.M. Wellington [1]* expressed some views on the design of rail and wheel contours, relative to fundamental considerations. His primary concern was the relationship between the radius of the gage corner of the rail and the radius of the throat between the wheel tread and flange. Wellington stated [2] the following:

"Only a very small percentage of wheels ever get sharp flanges, and there are never two sharp flanges on an axle; showing that some mechanical defect of wheel or truck (usually the latter) is the chief cause of sharp flanges, and not some general cause acting on all wheels alike."

"Except in the one case of the outside rail on curves, rails invariably wear to a much smaller corner radius."

"In the one case of the outside rail on curves, the rails do wear away until the side of the rail takes almost an exact form of the flange, but there is then much more friction, more rapid wear, and more danger of derailment than when the wheels are new."

"Imagine a heavy sphere rolling down a plank. It has a very small bearing surface, yet any additional bearing surface which might be gained by turning the plank into a trough 'exactly fitting' the sphere would plainly produce more friction and more wear rather than less."

"What sound practice would seem to require, therefore, is:

- (1) The tread of the wheel should have a fillet radius of at least 3/4 in.
- (2) The original corner radius of the rail should be little, if any, greater than 1/4 or 5/16 in.

In this way we shall postpone as long as possible the evil day when the rail and wheel will not simply roll upon, but grind into each other."

Figure 1 illustrates Wellington's concept of the ideal new wheel and rail contours [3].

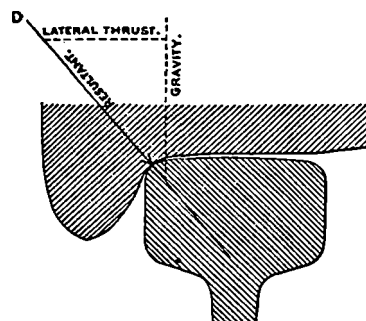


Figure 1. Wellington's Recommended Rail and Wheel Contours.

This theory was no doubt sound for that time, but it does not take into account the plastic flow of the gage corner of the rail, resulting from today's heavy wheel loads and lateral forces.

A.R.E.A. - A.A.R.'S ENGINEERING DIVISION RESEARCH

Worn Rail Head Contours

In 1933, the American Railway Engineering Association (AREA) adopted as a recommended standard the 131-RE rail section [4] (Figure 2), in lieu of the old 130-RE section. Although the primary objective in

*The numbers in square brackets [] refer to the references, listed at the end of this paper.

this design was to give more stiffness to the rail, a greater fishing height and, therefore, a stronger joint bar, the 131-RE section also had a different top-of-rail contour. A 24-in. radius formed the central part of the head, and the corners were formed by a combination of a 1-in. radius near the corners with a $\frac{1}{2}$ -in. radius right at the corners.

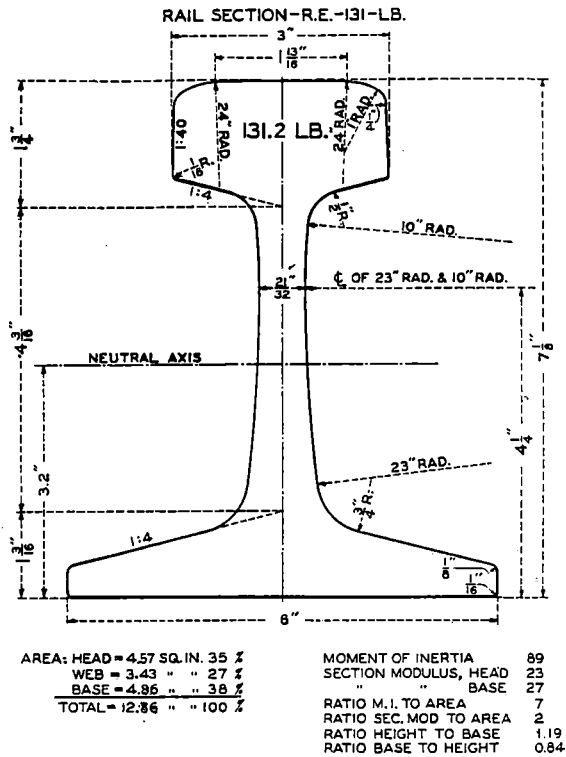


Figure 2. Original AREA 131-RE Rail Section (U.S. Steel #13125).

Shortly thereafter, the 110-RE rail section was revised to the 112-RE rail [5] (Figure 3) for the same reasons, and the top of the rail for this new design was patterned after that of the 131-RE.

After only a few months of service with these two sections, it was found that a substantial bead had formed on the gage corner of the rail on tangent track [6], more than had been experienced with the old 110-RE and 130-RE rail sections. Accordingly, after considerable study, including taking worn top-of-rail contours and worn wheel contours, a revision was adopted in 1937 by the AREA [6] to change the design of the top of rail of the 112-RE section to a 14-in. radius over the center portion of the rail head, with a combination of 1-in. radius near the head corners and $\frac{3}{8}$ in. radius right at the corners (Figure 4).

In 1938 the AREA adopted a corresponding change for the 131-RE section [7] (Figure 5). In neither case did the change in rail section require a compromise joint, since the revised 112-RE was interchangeable with the original 112-RE and the revised 131-RE was interchangeable with the original 131-RE. The rail mills gave them different designations, however; for U.S. Steel the original 112-RE and 131-RE were given the section numbers of 11225 and 13125, respectively. Also, the revised 112-RE and 131-RE were given the section numbers of 11228 and 13128, respectively.

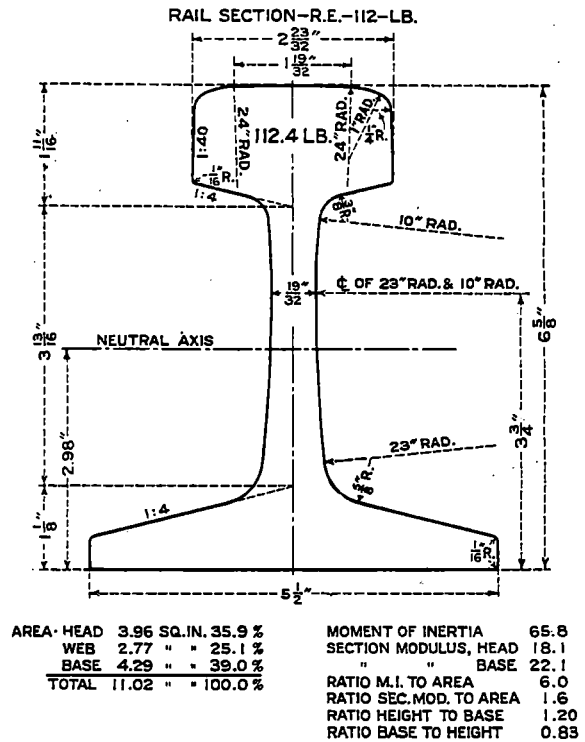


Figure 3. Original AREA 112-RE Rail Section (U.S. Steel #11225).

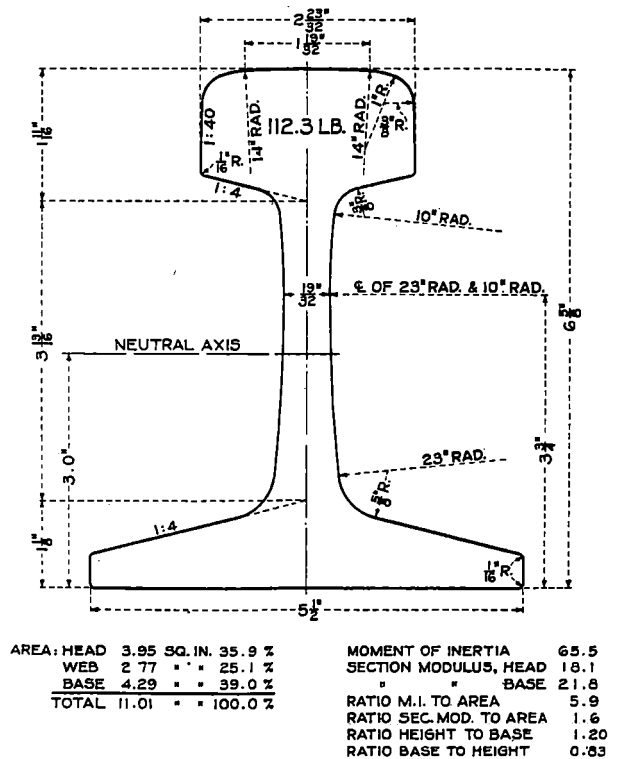


Figure 4. Modified AREA 112-RE Rail Section (U.S. Steel #11228).

131 LB. R.E. RAIL.

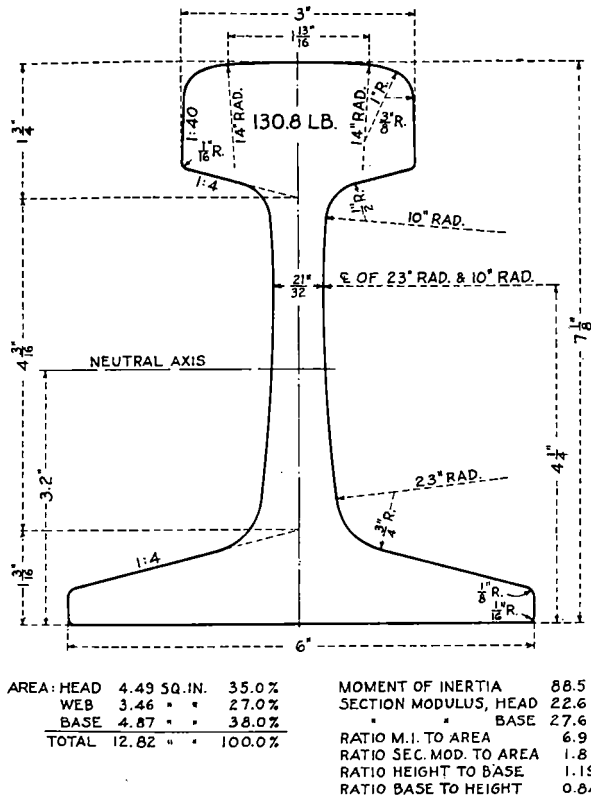


Figure 5. Modified AREA 131-RE Rail Section (U.S. Steel #13128).

In a search for solutions to the shelly rail problem, the AAR's Engineering Division Research Staff in June, 1942 took some 40 rail contours on the Santa Fe main line tracks in Illinois [8], in order to study the progressive change in the shape of the top of rail effected by traffic wear. These contours were made with a rail contour machine on tangent track and curves of 1 and 2 degrees. The rail sections contoured were 11025, laid in 1927 and 1932; 11225, laid in 1934 and 1936; and 11228, laid in 1937.

In October, 1942, the Research Staff measured rail and hopper car wheel contours on the Norfolk and Western and the Chesapeake and Ohio [8,9]. The contours of some 80 worn rails in track were taken at locations where shelly, head checking and flaking spots had occurred, and were taken on tangents, light curves, moderate curves and curves up to 12 degrees. The contours of some 200 car wheels on 70-ton and 50-ton coal cars that regularly ran over these tracks were made with a wheel contour machine. A straight edge was placed on the heads of the two rails of the track, in such a manner that a straight line was drawn on each rail contour card, so that the rail contour that was drawn could be oriented with respect to the cross level of the track. Similarly, a straight edge was placed on the flanges of the two wheels of an axle, in such a manner that a straight line parallel to the center of the axle was drawn on each wheel contour card. Thus, the wheel profiles could be superimposed and oriented to the rail profiles to study the bearing conditions of the worn wheels on the worn rails.

In the case of tangent track, it was found that the worn, top-of-rail contour could be well approximated by a compound curve having three different lengths of radii, as shown in Figure 6.

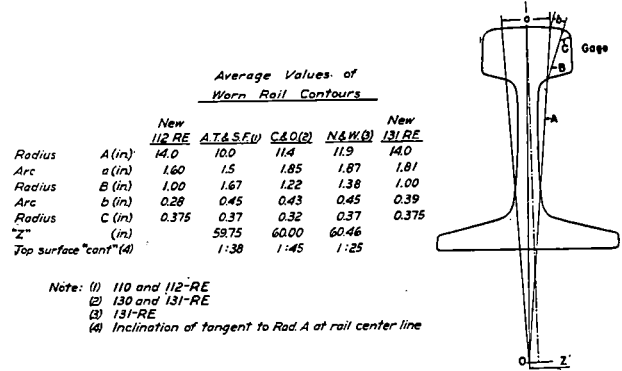


Figure 6. Comparison of Rail Head Contours on Tangent Track.

Accompanying the illustration is a tabulation showing the average length of radii and length of arc, as determined from the rail contour cards taken on tangent track on the Santa Fe, Norfolk and Western and Chesapeake and Ohio. The individual head contours taken at different locations did not vary much from the average contour for each railway, as given in the tabulation. It was evident that new rail soon wears to the common contour. The radius that fits the central part of the worn heads is quite definite as to length and as to the position of the center, 0.

A comparison of the worn contours, as obtained in these measurements, with the design contours for rail of the same section shows a surprisingly good agreement. If the top surface of the new rail head should be laid out, in accordance with the combination of compound curves of the three radii A, B, & C, as shown in Figure 6 for the worn 131-RE rail (modified or 13128 section), the difference is, however, surprisingly small and does not anywhere exceed 1/32 inch. Some tendency for the early wear on the rail to be somewhat greater at the gage side was evident from this comparison.

The top surface "cant" of the worn rails, as shown in Figure 6, was determined in the following manner. The distance between the center line of the rail heads for the 112-lb. RE section placed to standard gage is 59.22 inches. Subtracting this from the 59.75-in. value of Z gives 0.53 inch, which, if divided equally between the two rails, places the center point, 0, 0.265 inch outside of a vertical line through the center line of the rail head. Therefore, the rail, if canted 0.265 in. in 10 inches or 1:38 would have its center line through the center point, 0. For both the Santa Fe and C. & O. conditions, a rail cant of 1:40 should give uniform wear over the width of the rail head on tangent track. For the N. & W., the tie plates in general use cant the rail inwardly 1:20, and, according to the rail contours, this cant should give uniform wear over the width of the rail head.

Worn Wheel Tread Contours

Figure 7 shows the average measured multiple and two-wear wrought steel wheel contours obtained on the N. & W. and C. & O. cars [9].

It is interesting to note how closely the average contour of the worn wheels for the two roads correspond. It is also interesting to note that the amount

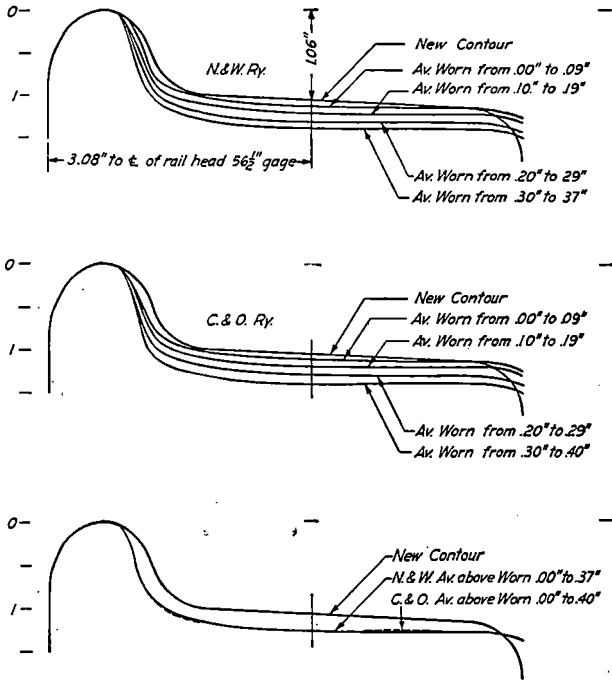


Figure 7.

Measured Average Multiple and Two-Wear Wrought Steel Wheel Contours on N. & W. and C. & O. Hopper Cars. (Only those wheels with a gage between 53 1/4 and 53-3/8 inches were included in the average contours).

of average wear is reasonably uniform across the entire wheel tread. All of the wheels showed a considerable overflow at the outer edge of the rim.

Figure 8 shows the worn contours on matching wheels of an axle in the R₁-L₁ and R₄-L₄ positions on five N. & W. 70-ton hopper cars. These wheels were the only wheels readily accessible for measurement with the wheel contour instrument. In four of the ten wheelsets, the amount of flange wear was about the same on both mating wheels. On the other six sets, the flange wear was different by varying amounts, with one wheelset having a badly worn flange on one wheel, with very little flange wear on the mating wheel.

It was also found that for all wheels on one railroad the central portion of the tread hollowed by wear to the same radius, and the distance between the center points "O" of the two radii for mating wheels was closely the same. This is shown in Figure 9, and it will be noted that the radius of the hollow-worn tread was 17.5 inches for the N. & W. cars and 15 inches for the C. & O. cars. The effective "cant" of the worn hollow portion on the 131-lb RE rail at standard gage was 1:26 for the N. & W. wheels and 1:27 for the C. & O. wheels.

Wheel/Rail Bearing Contact Conditions

From those rail and wheel contours that could be oriented together properly, it was possible to make some significant observations of wheel-rail bearing contact conditions. Studies were made of new and worn wheels, bearing on new and worn rail, on both tangent and curves. Figure 10 is of interest because it shows the possible bearing conditions of considerably worn wheels on moderately worn rail, on the outer and inner rails of an 8 degree, 06 minute curve.

The normal tracking position of a four-wheel truck on a curve is for the wheel of the leading axle

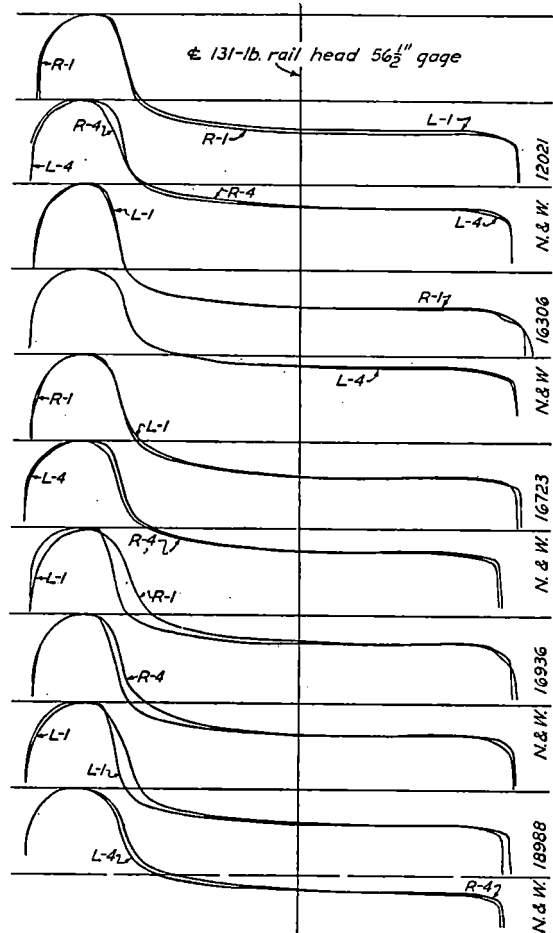


Figure 8.

Matched Wheelset Contours for N. & W. 70-Ton Hopper Cars With Multiple or Two-Wear Wrought Steel Wheels.

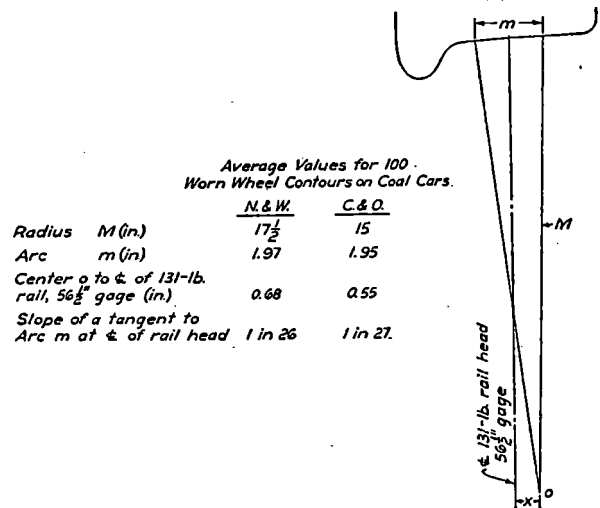


Figure 9.

Comparison of Average Values of Worn Wheel Contours From N. & W. and C. & O. Hopper Cars.

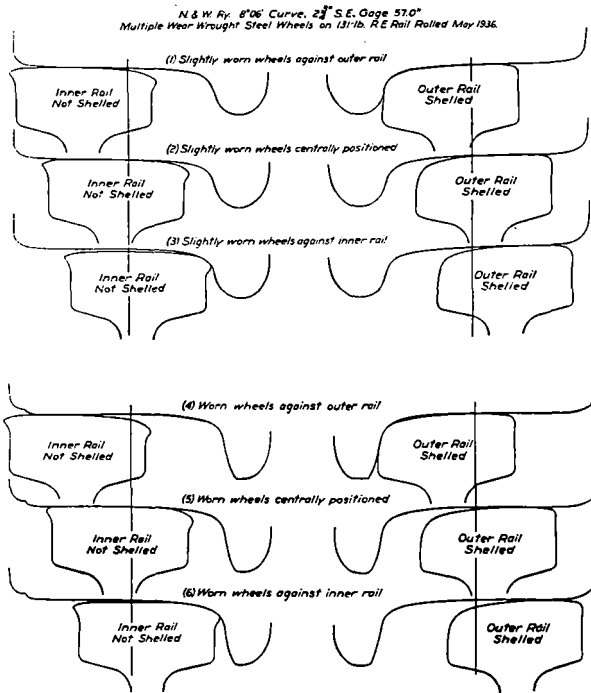


Figure 10.

Study of Wheel/Rail Bearing Contact Conditions, in an Eight Degree Curve on the N. & W.

to bear against the outer rail, whereas its mating wheel will be as far away from the inner rail as the relative rail and wheel gages permit (including any gage spreading that may occur). The trailing axle will tend to assume a radial position in the curve, if clearance permits. It is evident from Figure 10 that there is a close fit between the flange of the outer leading wheel and the worn rail contour on the top and gage side of the rail. It is also evident that some

wheels are contacting the top of the inner rail on the field side, as evidenced by the amount of rail flow on the field side. Some wheels must be bearing on top of the inner rail on the gage side to have produced the measured gage corner flow. It should be realized that a truck on a curve wants to roll in a straight line or climb the outer rail. The pressure of the flange of the lead wheel against the rail keeps it from climbing. Its mating wheel also wants to roll in a straight line and tends to drop off the low or inner rail onto the track. To prevent this, the flange pressure against the outer rail must slip the inner wheel towards the center point of the curve; or the field side of the inner rail. Thus, the two wheels of a leading axle exert a force outward from the centerline of the track on the outer rail and also on the inner rail. This also tends to produce flow on top of the inner rail.

Figure 11a shows the wheel bearing condition on the rails of tangent track, for new wheels and new rail on 1:40 cant tie plates. When the wheel flange is towards the gage side of one rail, as might occur in a hunting condition, the fit of wheel and rail at the gage corner is almost perfect. However, as the wheels become hollowed by wear, there is more contact on top of the gage corner. Therefore, to accommodate the average worn wheel contour, without producing plastic flow and high residual stress in the gage corner of the rail, until the rail contour becomes worn to fit the average worn wheel contour, as explained in more detail in [10], the modification of the top-of-head contour for the 131-lb. RE rail, as shown in Figure 12 [11], and for the 112-lb. RE rail, as shown in Figure 13 [11], were recommended for the 132-lb. RE and 115-lb. RE rail sections, respectively [12]. These recommended rail sections were adopted by the AREA in 1947.

Possibly the most significant finding from this research is that, since only a small percentage of the total number of car wheels are going to be renewed or recontoured each year in common carrier service, what-

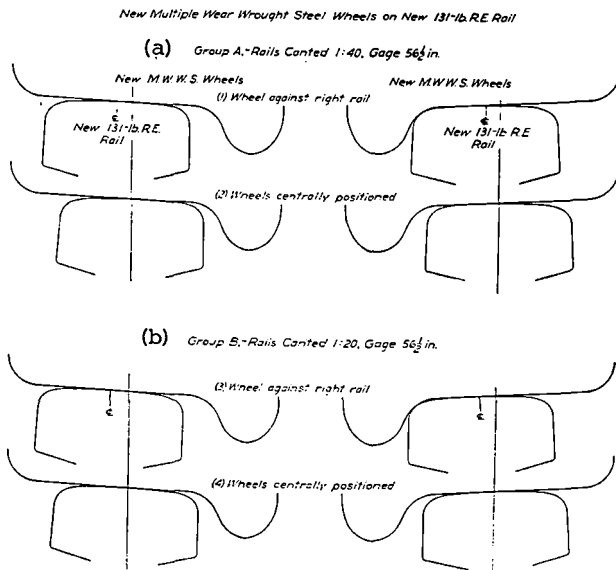


Figure 11.

Study of Wheel/Rail Bearing Contact Conditions, for New Wrought Steel Wheels on New 131-RE Rail.

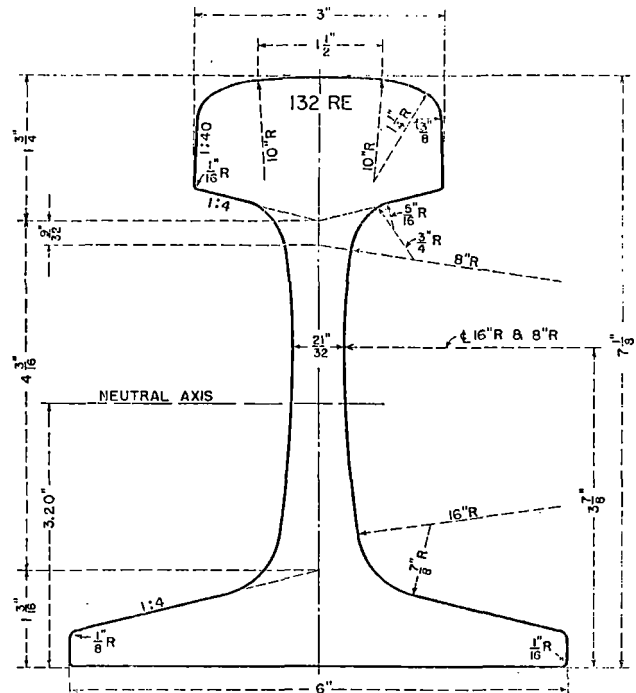


Figure 12.

AREA 132-RE Rail Section, Adopted in 1947.

BLACK MESA AND LAKE POWELL RAILROAD EXPERIENCE

At the request of the Black Mesa and Lake Powell Railroad, a rail study was made in June of 1976, after an estimated tonnage of 15.8 million gross tons of traffic, including loaded and empty coal cars, and locomotives [14]. An unusual condition noted was the formation of a bead on the gage corner of the rail on tangent track. At the time the railroad started operation, all rail, car wheels and locomotive wheels were new. Figure 14 shows a comparison of the gage corner contour of the 119-C.F. & I. rail section used with the 115-RE rail section. It should be noted that the 119-C.F. & I. section is about 1/32 in. higher than the 115-RE near the gage corner.

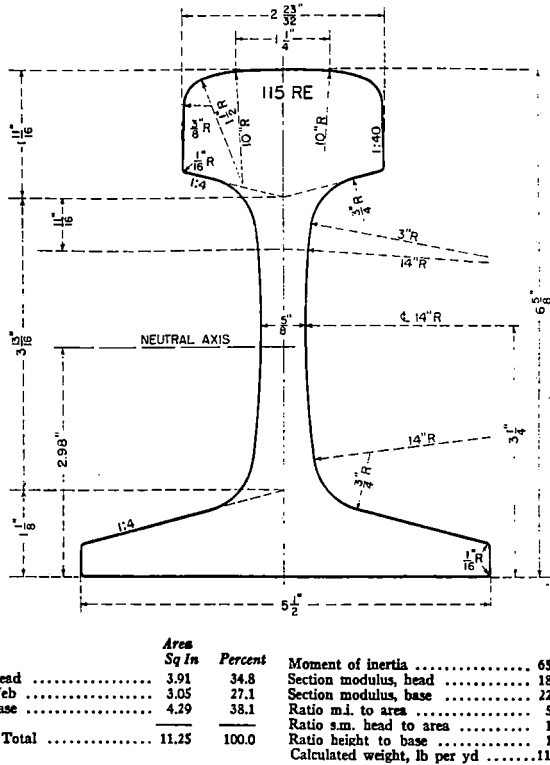


Figure 13. AREA 115-RE Rail Section, Adopted in 1947.

ever new rail contour is used will soon assume the average worn rail contour from the large number of average worn wheels passing over it; also, whatever new wheel contour is used will soon assume the average worn wheel contour, because of passing over the many miles of rail with the average worn rail contour. What is important is that during this relatively short transition period the rail and wheel metal shall not be subjected to excessive plastic flow, with resulting high residual stresses being developed.

Wheel/Rail Bearing Contact Pressures

To illustrate the beneficial effect that hollowing of the wheel tread by wear has on the normal contact pressures between wheel and rail, calculations have been made by Thomas [13] for a new 36-in. diameter wheel, bearing on new 132-RE rail, for the full wheel load of a 100-ton car or 32,875 lb. For this wheel-rail contact condition, the maximum calculated bearing pressure in the elliptical contact area is 213,620 psi. However, for the same conditions, except with the wheel tread hollowed by wear to a 15-in. radius, the calculated maximum bearing pressure in the elliptical contact area is only 146,150 psi., or 32 per cent less. The calculated maximum shearing stress for the new wheel on the rail is 71,000 psi., at a depth of 0.12 in. below the surface, and for the worn hollow wheel is 48,000 psi., at a depth of 0.15 in. below the surface, again a 32 per cent decrease. These calculations were made to illustrate the principle of the beneficial lowering of the wheel-rail contact stresses, due to wear hollowing of the wheel tread. The example given applies to the condition that would normally exist on tangent track, when the wheel tread is bearing on or near the center of the rail head.

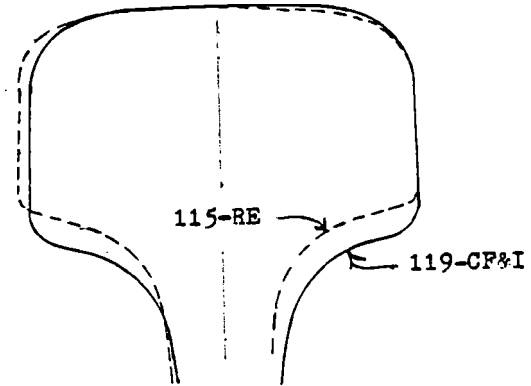


Figure 14. Comparison of Gage Corner Contours of 119-RE (C.F. & I.) and 115-RE Rail Sections.

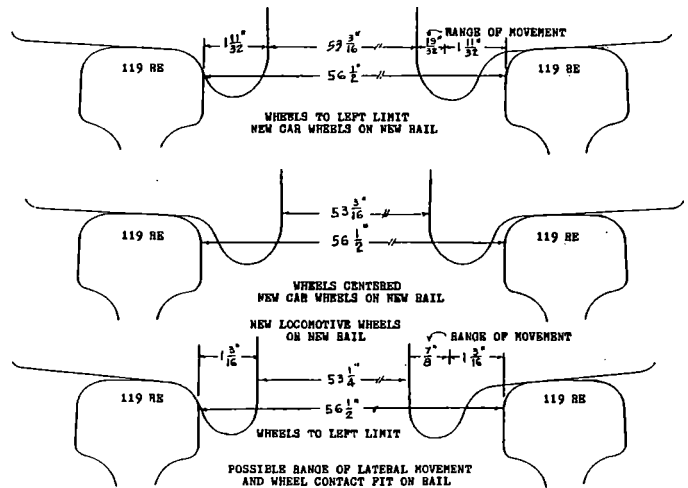
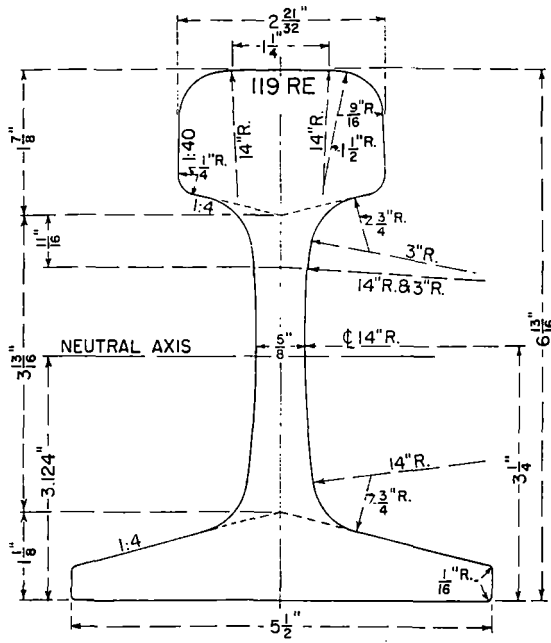


Figure 15. Study of New Car and Locomotive Wheel/Rail Bearing Contact Conditions, on New 119-RE (C.F. & I.) Rails on the B.M. & L.P. Railroad.

Figure 15 shows the bearing condition of new car and locomotive wheels on the 119-C.F. & I. section. The C.F. & I. section has a combination of 1-1/2 in. radius, but mostly a 9/16 in. gage corner radius (Figure 16) [11].

The AAR standard wheel contour has a 11/16 in. throat radius. The bearing contact condition looks good for new wheels on new rail (Figure 15).

Figure 17 shows the possible bearing positions of



	Area	Sq In	Percent	Moment of inertia	
Head	4.32	37.1		19.4	Section modulus, head
Web	3.04	28.1		22.9	Section modulus, base
Base	4.29	36.8		6.13	Ratio m.i. to area
				1.70	Ratio s.m. head to area
				1.24	Ratio height to base
Total	11.65	100.0		118.8	Calculated weight, lb per yd

Figure 16. 119-RE (C.F. & I.) Rail Section.

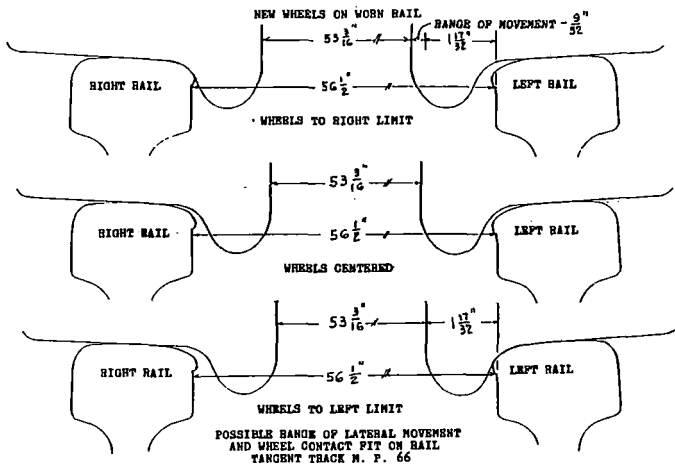


Figure 17. Study of New Car Wheel/Worn 119-RE (C.F. & I.) Rail Bearing Contact Conditions; Tangent Track.

new car wheels on typically flowed and worn rail on tangent track after 15.8 million gross tons of traffic. Note the bead formed on the gage side of both rails.

Figure 18 shows the probable bearing conditions of worn wheels on a 2-deg., 30-min. curve.

There are three possible factors causing the flow on the gage corner of the tangent rail. One is the 1/32 inch increased height of the 119-C.F. & I. rail section near the gage corner, as compared to the 115-RE. This is probably the most important factor when one considers the small change made between the 11225 and 11228 sections (and the 13125 and 13128 sections),

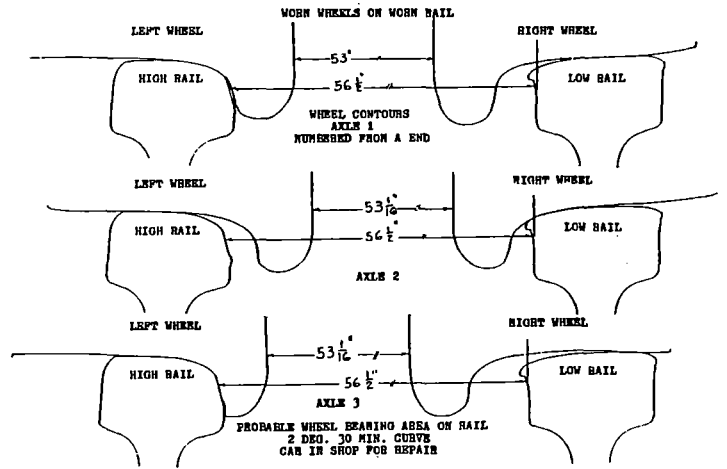


Figure 18.

Study of Worn Car Wheel/Worn 119-RE (C.F. & I.) Rail Bearing Contact Conditions; 2 Degree, 30 Minute Curve.

which eliminated the bead problem on these sections. Another possible factor is the 40,000-lb. wheel load on 38-in. diameter wheels with the 125-ton cars fully loaded. A third is that it was found that the return movement of the empty cars at 55 mph resulted in excessive truck hunting. Reducing this speed to 40 mph eliminated this hunting. For several years, the operating practice was to operate both empty and loaded cars at 55 mph, wherever possible. Present practice is to operate loaded cars at a maximum speed of 50 mph, and empty cars at 40 mph. Besides eliminating the hunting, this still permitted a turn to be made in 8 hours, and also effected a substantial reduction in electric power costs for the electric-powered locomotives.

In repeating the rail study during 1980, a condition was noted that so far as is known has not been found before. On a few of the 2-deg., 30-min. curves and at a few locations, a crack had formed on the field side of the low rail. This crack formed at the juncture of the flowed metal and the field side of the rail head, about 1/4 in. down. The appearance of the crack suggests that it is a shelly crack, such as sometimes forms on the gage side of the outer rail on curves, and that it is a result of the bearing of the tread of worn wheels of loaded cars on the field side of the inner rail. This is, however, only a speculative explanation at this time.

QUEBEC, NORTH SHORE AND LABRADOR RAILWAY'S EXPERIENCE

About 1960, observations of the wear condition of new or reprofiled wheels on this railway showed that, with the standard AAR wheel for 36-in. diameter multiple-wear wheels, metal from the gage side of the flange was being literally displaced and packed into the tread throat. This did not seem to be a desirable condition, and a study and tests were started by H. A. Tyler, Mechanical Engineer of that railway. Mr. Tyler subsequently prepared an ASME Paper on the subject [15] and the following is taken from the Appendix:

"Examination of the geometry of contact between a newly profiled wheel having AAR standard contour and the high rail (132-lb. RE) in a curve, indicates that wheel-to-rail bearing occurs at two points; namely, on the conical tread portion and at the flange. Figure 19 is a recorded contour which illustrates

that an area of the flange throat has not established contact with the rail, although the wheel has run 4500 miles. Full contact condition is attained after running approximately 10,000 miles."

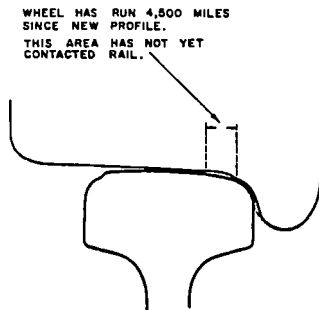


Figure 19.

Bearing Contact Conditions for a Standard AAR Narrow Flange Profile Wheel on New 132-RE Rail, With a 1:40 Cant.

In order to establish a full bearing condition with newly turned wheels, the author suggested a modified form of the AAR standard profile, in which the flange throat portion conformed to the head profile of the 132-lb. RE rail, but keeping the flange thickness and height at the respective gaging points the same; Figure 20 illustrates this profile bearing on the high rail of a curve. Mr. Tyler refers to this as the Modified AAR Contour.

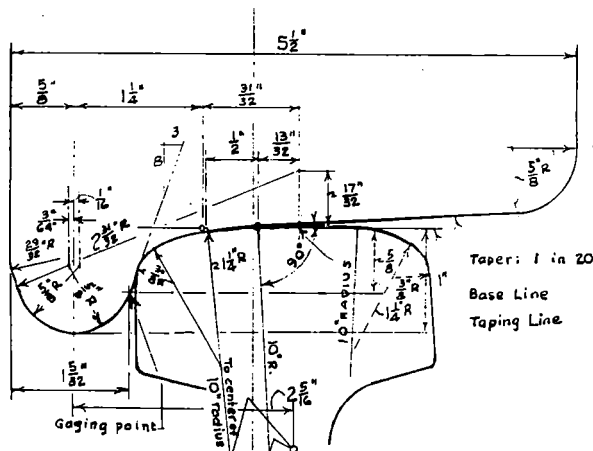


Figure 20.

Study of Modified AAR Narrow Flange Profile Wheel/ 132-RE Rail Bearing Contact Conditions on the Q.N.S. & L. Railway. Rail Cant is 1:40.

In a report in the railway files, dated July 5, 1966 [16], Mr. Tyler gives the following data on wheels with AAR standard contour:

"The 50 per cent removal level for the first turning was reached at a mileage of 300,000. This is the value of average mileage on the original tread for E-36, Class 'CR' wheels in ore car service, under current operating conditions on this railway."

"For purposes of comparison, the mileage at 50 per cent turned for the first time for

Class 'CR' wheels under the four series of ore cars are:

1st series, into service 1954...115,000 miles

2nd series, into service 1955...175,000 miles

3rd series, into service 1956...300,000 miles

4th series, into service 1957...300,000 miles

"It is quite evident that a considerable improvement in performance has taken place on the 3rd and 4th series reported herein; this is attributable to the stabilization of roadbed and improvement in the number and location of rail lubricators."

To study the comparative wear of the AAR Standard versus the Modified AAR profile, 13 ore cars were equipped with complete sets of new turned wheels having the Modified AAR contour. Beginning in June, 1962, this contour was applied to all wheels turned in the Seven Island's shop. In addition, two ore cars were equipped with the AAR Standard wide flange contour on one truck and the Modified AAR wide flange contour on the other truck. For one of these cars, the Modified AAR profile had 15 per cent more wear, while on the other car the Modified AAR profile had 45 per cent less wear.

Mr. Tyler concluded:

"Notwithstanding the fact that in direct comparison of profiles, one car showed less flange wear with the Modified AAR profile, it still has the same degree of unpredictability in its wear properties as the AAR Standard profile; this is further borne out (in the tests with the 13 ore cars with the Modified AAR narrow flange profile) where the modified profile has not effected any significant reduction in the tendency for flange cutting to occur. The contact condition between wheel and rail has improved, as it is observed that the complete flange throat area has taken bearing on the rail from the commencement of running."

Mr. Tyler then developed the Q.N.S. & L. narrow flange profile. He states:

"This was developed in the Railway Mechanical Engineering Office, from information gathered from an article by J. L. Koffman [17], from correspondence between Mr. J. L. Koffman and Mr. M. S. Riegel, Consulting Engineer, Technical Committee on Railroad Materials, American Iron and Steel Institute, Chicago; and from a discussion with Mr. J. L. Koffman, during a visit to that gentleman's office in England."

"It should be mentioned that the concept of this principle was originally advocated by Prof. Heumann, Engineer, German Federal Railways. The basis of this profile is that it conforms to a worn wheel flange throat configuration, and thereby it will maintain a one-point contact with the high rail when negotiating curves, thus effecting an improvement on the wheel set dynamics."

"In order to establish the worn flange throat configuration, contours were obtained from those wheelsets which displayed uniform tread diameter and wear pattern on both wheels of the set, and which had run mileages exceeding 150,000 since last reprofiling. These contours were enlarged four times by an optical projector and recorded. This served as the basis for establishing the various throat radii."

The Q.N.S. & L. profile so developed is shown in Figure 21, as it would fit on the 132-lb. RE new rail section.

Mr. Tyler then arranged for tests to be conducted

with the new Q.N.S. & L. profile. He states:
 "Two ore cars were equipped with this profile as follows: each car has one truck of AAR Standard narrow flange profile wheels and the other truck has Q.N.S. & L. profile wheels. Early results of this test are that on both cars the AAR Standard profile has worn at the flange, while the Q.N.S. & L. profile displays imperceptible wear."

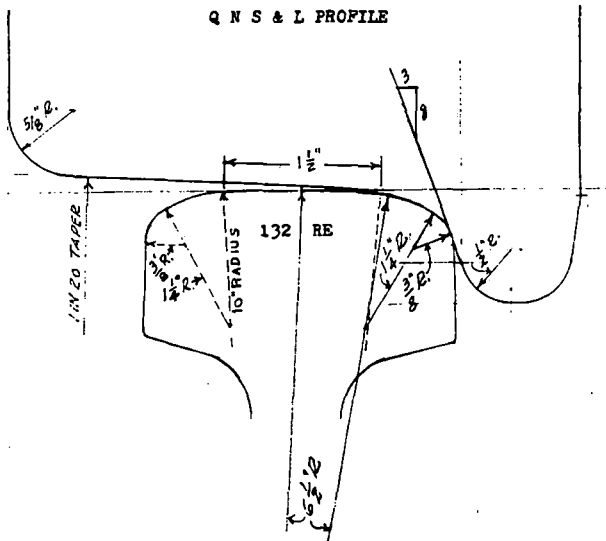


Figure 21.
 Fit of the Q.N.S. & L. Railway's Narrow Flange Wheel Profile on New 132-RE Rail, With a 1:40 Cant.

The Q.N.S. & L. profile was then adopted as standard for reprofiling wheels, but it is not known whether it was possible for the railway to purchase new wheels with this profile.

A letter from Mr. B. Carrier, Superintendent-Car and Locomotive Maintenance, dated April 4, 1980, states:

"Our wheels are now supplied with the Heumann profiles, and these are purchased 50-50 from C.S.W. (Canada Steel Wheel of Hawker Siddely, Canada) and Griffin Steel."

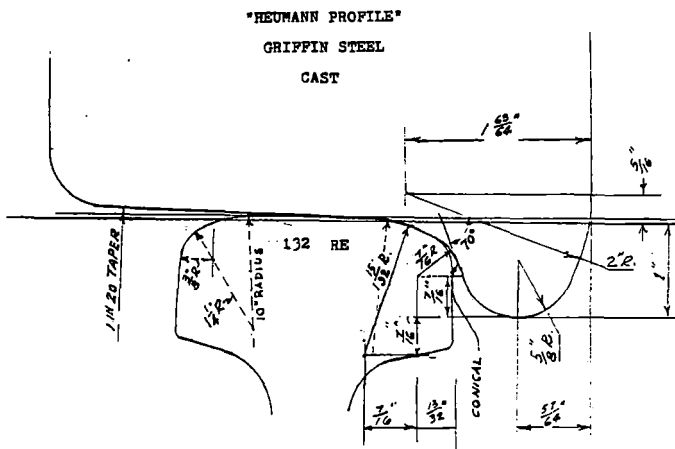


Figure 22.
 Fit of the Griffin Wheel Company's Heumann Profile on New 132-RE Rail, With a 1:40 Cant.

Figure 22 shows the fit of the "Heumann Profile," as furnished by Griffin Steel, on new 132-lb. RE rail. This profile and that furnished by C.S.W. are almost identical in fit. Both Figures 21 and 22 show that when the wheel flange becomes located near the gage corner of the rail, the wheel load bearing is at or near the gage corner. This raises the question of whether these wheel profiles would result in flow of the rail head to form a bead at the gage corner of the rail on tangent track. This could best be determined by observation of new rail put in track, where there would be a movement of new wheels with these profiles on heavy cars.

In a telephone conversation on March 12, 1980, Mr. Carrier advised that their 90-ton ore cars had been modified to carry 100 long tons, giving a wheel loading of 35,000 lbs. These cars were equipped with two-wear 36-in. diameter wheels with the Heumann profile. 70 per cent of these wheels were changed out because of shelling and their average life was 280,000 miles. The rim thickness allowed was 1-1/4 in., minimum.

Later advice from Mr. Carrier's office on February 9, 1981, was to the effect that:

"We do reprofile 'Profile A,' which is between the Heumann profile and the Q.N.S. & L. profile."

GRIFFIN WHEEL COMPANY TESTS ON THE BURLINGTON NORTHERN

In late September and early October, 1970, a Griffin Wheel Company Test Team conducted road tests on 20 miles of BN track, using a freight car with one truck "rigidized" and equipped for successive tests, both fully loaded and empty, with six different designs of wheel contour. An article [18] describes the tests in more detail. A later article [19] gives some of the results from the tests. Bernard J. Eck, Director, Product Engineering, Griffin Wheel Company, furnished a copy of their final report on these tests, which he co-authored with N. A. Berg, and the following information is taken from this report [20]:

"Griffin tested five different wheel contours in the Fall of 1970. The first contour is the AAR Standard wide flange contour, with a 1-3/8 in. flange thickness and 1:20 taper. The second design is the same AAR Standard wide flange contour, with the exception of a 1:10 dropoff taper, beginning 1-3/4 in. from the outside rim face. The third type of wheel tested had an AAR cylindrical tread with a 1-3/8 in. flange and 1:20 dropoff taper, beginning about 1-5/8 in. from the outside rim face. Our next type was a set of worn unbalanced wheels, which are shown in Figures 23, 24, 25, and 26. We later balanced these wheels and repeated the tests.

"The fifth and final type of contour we tested was the modified Heumann contour, shown in Figures 27 and 28. The Heumann contour was developed in the 1930's by Dr. Heumann, a German engineer. He designed this contour, such that only a single contact point existed between rail and wheel. The modified Heumann contour used in the tests is this design, modified to U.S. rail conditions."

"The test consist used was a locomotive followed by an observation car (which held the basic instrumentation and doubled as a buffer car), the test car (which had a capacity of 180,000 lbs. and a light weight of 84,000 lbs.) and another instrument car (which held the television-monitoring equipment, as well as our observers)."

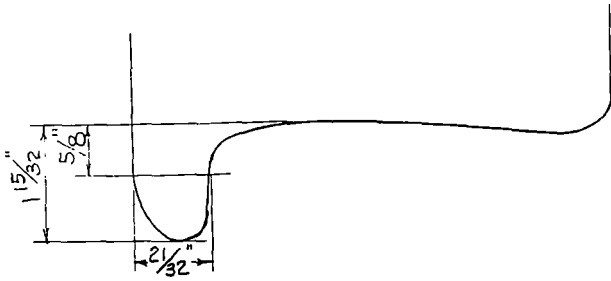


Figure 23.
Profile of Worn Wheel No. 456, Used at Location 1A in the Griffin Wheel Company's Road Tests on the Burlington Northern.

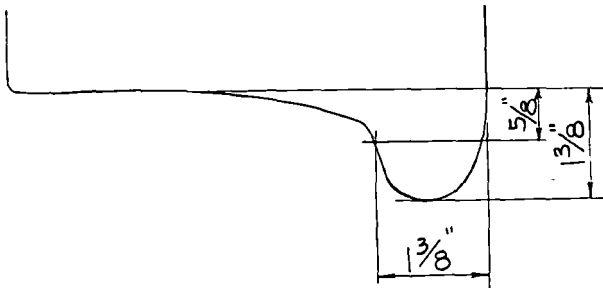


Figure 24.
Profile of Worn Wheel No. 598, Used at Location 1B in the Griffin Wheel Company's Road Tests on the Burlington Northern.

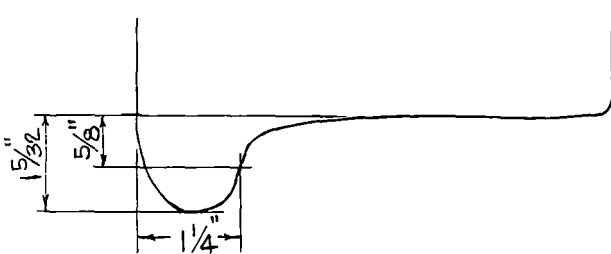


Figure 25.
Profile of Worn Wheel No. 89586, Used at Location 2A in the Griffin Wheel Company's Road Tests on the Burlington Northern.

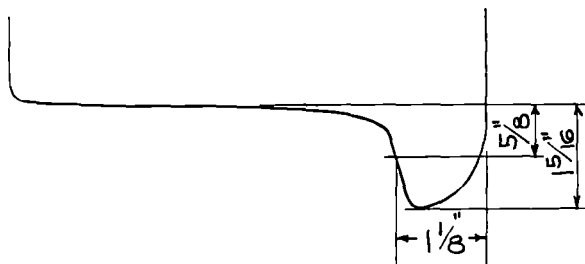


Figure 26.
Profile of Worn Wheel No. 87461, Used at Location 2B in the Griffin Wheel Company's Road Tests on the Burlington Northern.

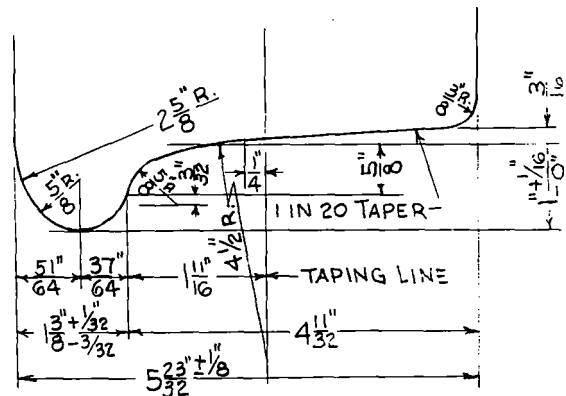


Figure 27.
Modified Heumann Profile Wheel, Used in the Griffin Wheel Company's Road Tests on the Burlington Northern.

"The test car's trucks were standard American Steel Foundries Ride Control Trucks. Although the trailing truck was not altered, the lead truck was outfitted with a device which would allow it to be rigidized. Rigidizing, in this instance, means that the side frames were held parallel and square to each other. Rigidizing was used to eliminate the variables which would produce extraneous movements within the truck configuration."

"The test car was instrumented to record bolster rotations and lateral forces at the roller-bearing adapter wedges. A 16mm movie camera and TV cameras were positioned to include truck and wheel motion."

"An oscillograph was used to record lateral and vertical forces by the truck and car body. An automatic electronic tabulator was used to tally the amount of lateral accelerations exceeding 0.15g, 0.30g, 0.45g and 0.60g."

"Rather than give our results in terms of fractional 'g' forces, we simplified our findings by using a Lading Damage Index, as it is a standard way to express these fractional figures in a single number. This is the formula we used:

$$LDI = N_{0.15g} + 4N_{0.30g} + 9N_{0.45g} + 16N_{0.60g}$$

where N is the number of lateral accelerations of that magnitude recorded during a test run. In another effort to simplify, we are using only

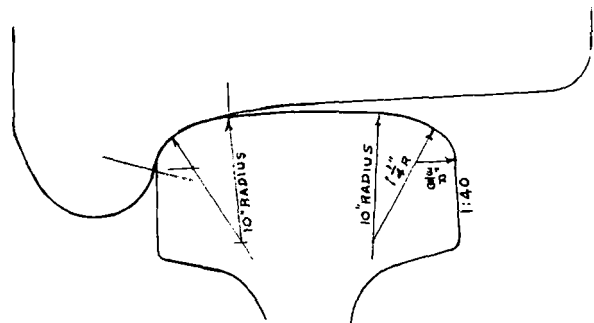


Figure 28.
Fit of the Modified Heumann Profile Wheel on New 132-RE Rail, With a 1:40 Cant.

that data received from the platen inside the test car. While we received a great amount of data from the sensors at the roller-bearing sensor plates, this only substantiated our data received on the inside of the car."

"The test route that was selected was on the Burlington Northern Railroad, from their North St. Louis Yards at MP7 north to MP29, about nine miles north of West Alton, Missouri. Four separate sections of track picked along this distance presented track conditions, such as curve left, curve right, turnouts and switches. Each section had identification markers at the beginning and end by which we could trigger our test instruments. Mileposts 26 to 29 was tangent track and it was here that we did the bulk of our testing. This three mile section was negotiated by each wheel contour at speeds of 40, 60 and 79 mph."

The rail section in the test track was not given in the report, although it did state that the rail was on 1:40 cant tie plates. The report did include a composite gage corner contour obtained from plaster-of-paris casts taken at various places on the test track. The report did not show a gage corner contour of the rail for the test track on tangent. It is stated that "railhead profiles of the types of rail found in this country" were taken and a "composite" of these is compared with the new 132-RE rail contour. Because of the considerable difference found between the new 132-RE rail gage corner and that shown in the report for the "composite" rail gage corner, an attempt was made to determine whether this "composite" contour was obtained from tangent track or curved track, or a combination thereof. The only advice received was that plaster-of-paris casts were made of rails at several locations and the contours were obtained from them. In the author's opinion, it does not appear that as thorough a job was made, to obtain this "composite" contour, as was made by the AAR's Engineering Division Research Staff, in the work previously described, to design the top of the 132-RE contour to fit the average worn car wheel.

The Griffin Report [20] continues:

"Finally, the conclusions we have been able to draw from our test results are:

1. The variations in lateral lading damage, due to wheel design, were significant only at high speeds.
2. Standard and cylindrical tread designs produced similar lateral lading damage indices, while the worn wheels produced much higher indices.
3. Balanced worn wheels produced slightly lower damage indices than did unbalanced.
4. Wheels with a modified Heumann design produced a higher lading damage index than all other designs, although single point contact was achieved."

The effect of speed on the lateral lading damage index, as obtained in the Griffin Road Test, is shown in Figure 29. Figure 30 shows the relative lateral damage index for the empty test car at 79 mph with the five wheel conditions.

It would seem that two very significant comparisons can be made from these test data:

1. The lateral lading damage index at 79 mph is on the order of seven times greater for the empty car than for the loaded car. This is not significant, insofar as lading damage is concerned, because an empty car would have no lading to damage. It is significant relative

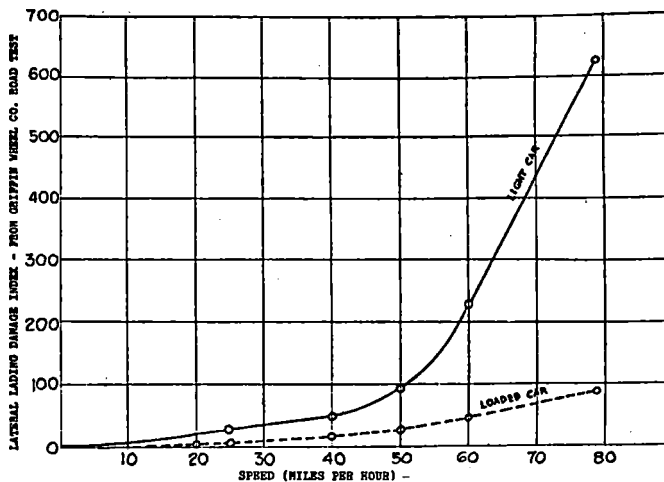


Figure 29.

Lateral Lading Damage Index vs. Speed, For Light and Loaded Cars With Standard Contour Wheels and Rigid Trucks. Griffin Wheel Company's Road Tests on the Burlington Northern.

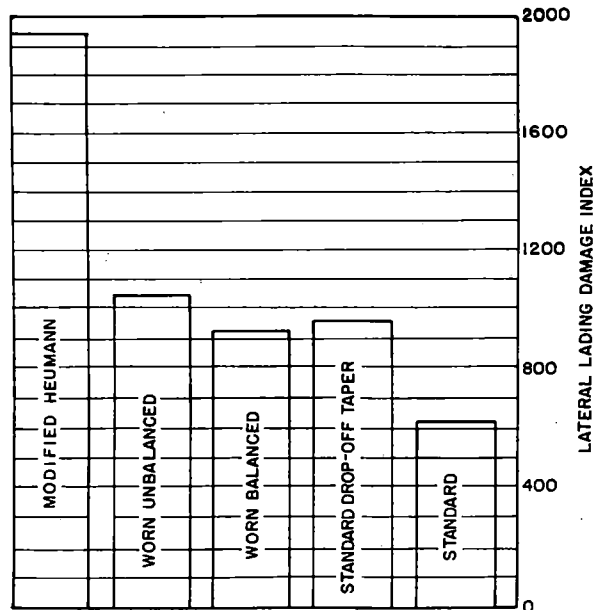


Figure 30.

Lateral Lading Damage Indices From a Light Car (84,200 Lb. Rail Load) With a Rigidized Truck at 79 MPH on Tangent Track. Griffin Wheel Company's Road Tests on the Burlington Northern.

to the possibility of derailment, wear of equipment and lading damage in a lightly loaded car.

2. The lateral lading damage index at 79 mph with an empty car is almost twice as much with the modified Heumann wheels as with the worn wheels, and three times as much as with the new AAR standard tread wheels.

CANADIAN NATIONAL RAILWAYS' RESEARCH AND EXPERIENCE

The Canadian National Rail Research Centre has

been conducting research since 1973 on the design of wheel contours for freight cars. Dr. W. N. Caldwell, Senior Research Engineer, has furnished a copy of all research reports relating to this subject that have been prepared at the Research Centre.

The report [21] contains in the Introduction: "A report entitled 'Service Tests of Heumann Wheel Profile on Locomotives' issued by the Chief of Motive Power and Car equipment in January, 1973, showed that substantial increase in wheel life should be expected with the use of Heumann type profiles on locomotives. The report does not recommend the use of the Heumann profile on freight car trucks because:

- (1) Freight car trucks are often lightly loaded and subject to hunting, which was found to be severe on a service test of this profile.
- (2) It is felt that the single point contact characteristic of the Heumann profile would impose higher stresses in the rail and probably increase the occurrence of shelling.
- (3) The freight car truck brake rigging can impose a non-symmetrical wear pattern on the wheels and the advantages of a specially designed profile would be lost."

This report then examines the above statements, using a "new computer method" to develop a "flange wear index" on curved track; presents a formula to calculate the rolling resistance on curves, in order to predict the effect of wheel profile; examines truck hunting test results with respect to unit train operating conditions; makes theoretical calculations of wheel-rail contact stresses; presents a theory which shows that a different initial wheel profile could improve accelerated wheel wear arising from unsymmetrical truck characteristics; and makes a study of the characteristics of two possible designs of profiled wheels.

In the conclusions, the report states:

"It is believed that with traffic, including a large number of heavy cars, such as today's unit train operation, some effort must be devoted to improving the service performance of freight trucks."

"The introduction of profiled wheels to existing trucks will definitely not produce the best curving trucks."

"In present unit train operation, where a large percentage of the route is on curved track and where speeds are restricted, an experiment with profiled wheels is certainly justifiable."

A second report [22] gives the results of a series of tests carried out on a 5-deg. curve in Montreal Yard, equipped with three special dynamometer base plates to compare the curving forces of trucks with four different wheel profiles, as follows:

- Standard AAR - service worn. . . 1220 lbs.
- Modified Heumann profile . . . 1330 lbs.
- Profile A 1900 lbs.
- Standard AAR - new 2940-3840 lbs.

(2 tests)

Figures 31, 32 and 33 show the profiles of the new wheels included in these tests and their fit on the 132-RE new rail section.

The report recommends a comparative service test on the Luscar unit train coal service with 25 carsets on Profile A wheels and 25 carsets on standard AAR profile wheels. Other recommendations are made with

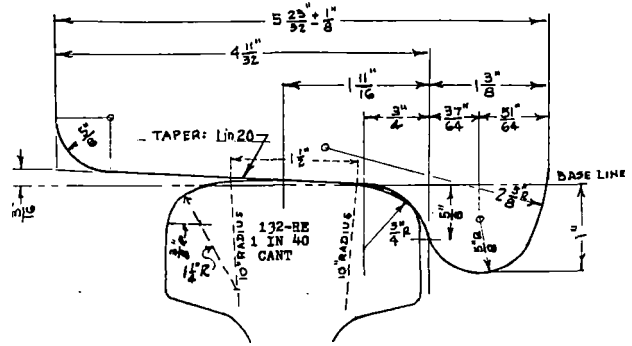


Figure 31.

Fit of a Wide Flange Contour Wheel With the AAR's Standard Tread Profile on New 132-RE Rail, With a 1:40 Cant.

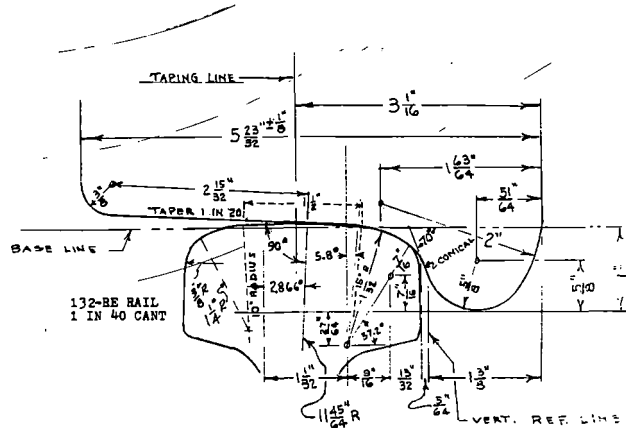


Figure 32.

Fit of a Wide Flange Contour Wheel With the Heumann Profile on New 132-RE Rail, With a 1:40 Cant.

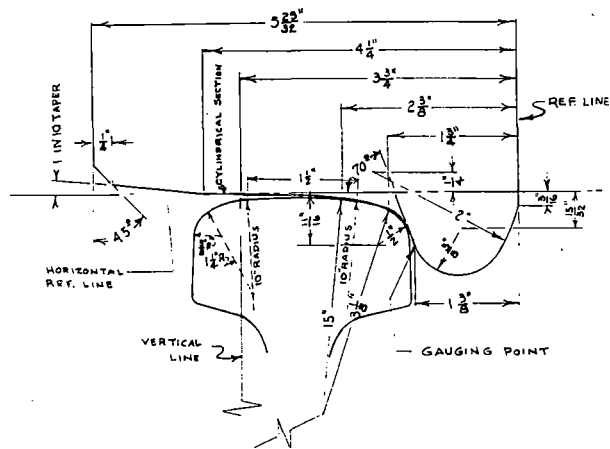


Figure 33.

Fit of a Wide Flange Contour Wheel With Profile A on New 132-RE Rail, With a 1:40 Cant.

respect to brake rigging; axle bearing adapters and manufacturing tolerances in wheel set/truck frame assemblies; and validation tests of computer programs.

to simulate the steady-state behavior of railway trucks on curves.

Another report [23] states that a comparative wheel wear test including 25 cars with standard AAR wheel profiles and 25 cars with Profile A wheel profiles was started in October-November, 1975. The first car for each series had the wheels specially equipped with witness grooves on both sides of the wheel rims, in order to use a precision wheel profilometer which was developed to accurately reproduce the wheel profiles. Profiles were taken with the wheels newly machined, at 1500 miles, at 4800 miles (one loaded trip) and at 9300 miles (4 loaded trips). During this period the AAR profile showed considerably more flange wear (total cross sectional area loss); the Profile A wheels gave considerably more tread area loss; and the total wheel wear after 9300 miles was slightly more on the Profile A wheels.

The Second Progress Report [24] gives the results after a total service mileage of 17,000, which included 10 loaded movements from Luscar to Neptune Terminal for a total of 6900 loaded miles. Important conclusions are:

- (2) Profile A tends to wear generally parallel to its original profile.
- (3) Flange wear on Profile A is approximately 50 per cent lower than on the AAR profile.
- (4) The cumulative tread wear is now higher on the AAR profile than on Profile A.

Appendix A of this report presents a discussion on "The Selection of a Performance Index for Wheel Wear," taking into account tread loss in recontouring and remaining serviceability of the recontoured wheel.

The Third Progress Report [25] gives the results after 39,500 service miles on the two control cars, with wheels prepared for use of the precise profilometer. This feature of the test was subsequently interrupted, due to premature removal of the AAR standard profile test wheels of that car because of brake-related defects. The service life to condemning limits was, however, projected from the data obtained during the 39,500 miles, as follows:

Standard AAR profile - 193,000 miles average

Experimental Profile A - 345,000 miles average

This projection seems to be relatively disproportionate, because it is stated:

"It appears that this average AAR profile shape after 39,500 miles (R2 and R4 not included) is approaching the average Profile A shape. . . ."

It would be expected that the increased wheel life for Profile A would be on the order of only 40,000 to 50,000 miles.

Dr. Caldwell advised in a telephone conversation on March 14, 1980, that after 270,000 miles, 61% of the Profile A and only 47% of the AAR profile wheels were still in service. Not having any data available on wheel life probability, the author assumed that wheel life probability would follow the same general pattern as tie life probability. On the basis of tie life probability curves [26], the projected average wheel life for Profile A wheels removed after 270,000 miles would be $28/24 \times 270,000 = 315,000$ miles. For AAR profile wheels, with 53 per cent removed after 270,000 miles, the average wheel life would be $28/27.2 \times 270,000 = 278,000$ miles a difference of 37,000 miles.

The report points out several factors that influence wheel life. One is that, since it is much cheaper to reprofile a wheel set, the wheel set will normally be reprofiled when one wheel has reached the condemning limit for flange height or flange thickness. Also, the placement of brake shoes on the

wheel tread may have a considerable influence upon when one wheel of the wheel set reaches the condemning limit.

It is stated that the common AAR steel wheel gauge offers a means of monitoring wheel wear without the need for profile measurement. A flange height conversion table with gauge readings from 0 to 6 is given. A flange thickness conversion table for gauge readings from 0 to 11 is also given.

The report [27] is of particular interest, because of the results obtained in the Griffin tests. Four empty gondola cars were equipped with wheel sets, having the (1) new AAR standard-wide flange profile, (2) Profile A-wide flange version, (3) Profile A-narrow flange version and (4) AAR standard-service worn. The report states:

"The main objective of this test was to determine the critical speed of lateral truck hunting instability for the cars equipped with Profile A contour wheels, and to compare it with the critical speed which presently exists on empty coal gondolas with AAR service worn wheels."

Profile measurements of each wheel on the four test cars were taken prior to testing, following 1300 miles of empty movement from the test wheel application to the test site. Tests were conducted on a 9.3 mile section of track, laid with 132-lb. CWR in June 1975 over a ballast bed which had previously supported 39-ft. jointed rail. (A comparison made by overlaying the measured profiles over the design profiles shows the following during this 1300 mile empty movement: Wide flange AAR wheels showed a slight flange wear, with the metal displaced to the throat; narrow flange Profile A showed no perceptible change; wide flange Profile A showed a slight amount of flange wear in the throat and a slight hollowing of the tread near the throat).

In the test runs, Profile A-wide flange wheels and AAR service worn wheels showed some hunting oscillations at 41 mph. At 45 mph, Profile A-wide flange wheels showed sustained hunting oscillations, whereas the AAR service-worn wheels showed only a burst of unstable hunting. The car equipped with Profile A-narrow flange wheels began to develop hunting oscillations at 55 mph. At 55 mph, all of the cars showed sustained hunting, except the car equipped with the new AAR Standard wide flange wheels. Tests were not made at speeds above 55 mph. From the results of the hunting tests, it was concluded that the dynamic tracking properties of the Profile A-wide flange contour are similar to those now obtained with AAR service worn contours. Hunting was determined during the tests from records from lateral accelerometers, placed at each end of each test car. Typical records are reproduced, as well as the measured profile of each wheel just before making the test runs.

An excellent review of these extensive Canadian National studies and tests was published in 1980 [28]. Although not discussed here, the reader is urged to carefully read Items 5; "Potential Benefits and Implementation," and 6: "Conclusions," since they are very informative.

Probably the most significant part of this research will be the final results from the service tests of 25 cars, equipped with AAR standard wide flange contours, and 25 cars, equipped with Profile A wide flange contours, in regular unit coal train service. The results from technical research were obtained from tests and measurements of one car of the 25 with an AAR contour and one car of the 25 with a Profile A contour, supplemented with curve negotiation and hunting test data. This technical research

resulted in sufficient scientific evidence to indicate that a longer service life would be obtained with the Profile A wheels, when the 50-car service test has been completed.

The information previously given on the car wheel service test, after 270,000 miles of service, was said to have been obtained on March 14, 1980. Mr. R. W. Radford, Chief Mechanical and Electrical Engineer, CNR, was contacted by telephone on June 10, 1980 to see if later information was available. He stated that, due to bridge and other problems, there had not been much additional service mileage on the 50 test cars. He also advised that it would not be possible to determine the service life of the two-wear wheels from new to scrap, because when the wheels were reprofiled they went into the general wheel pool and could no longer be followed. In response to an inquiry on the relative amounts of metal removed from the AAR and Profile A wheels during reprofiling, he stated that they were not able to take profiles of the AAR and Profile A wheels when they were removed from the cars, but had to rely on a series of profiles taken on specific wheels during the test. They expect, however, to get good measurements of the relative amounts of metal removed during the reprofiling process. Theoretically, the Profile A wheels should lose less metal on reprofiling, and he felt sure this would be verified by the data to be obtained.

The Canadian National's research has been thoroughly and scientifically conducted, using the latest techniques in a well considered manner. It has established the fundamentals of the relative performances of the various wheel contours. It will be very valuable in understanding the results from the large scale service test of 50 cars over a long period of time, and most importantly will create more confidence in the accuracy of the results so obtained.

In a letter dated March 12, 1981 Mr. Radford sent a copy of the joint CN/CP drawing, showing the Heumann contour obtained by CN Rail for J-36 or CJ-36 two-wear wheels for 100-ton cars. Figure 34 shows this Heumann tread and flange contour and Figure 35 shows the fit of this contour on new 132-RE rail with a 1:40 cant.

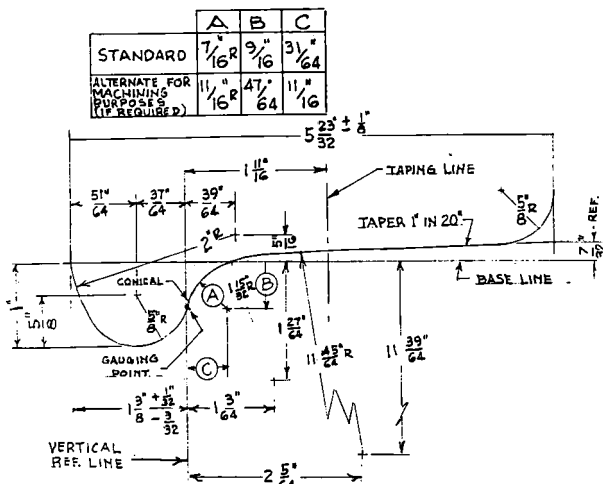


Figure 34.
Joint Canadian National-Canadian Pacific's Heumann Wheel Tread and Flange Contour.

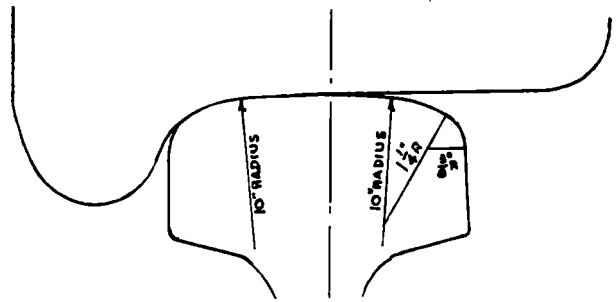


Figure 35.
Fit of the C.N.-C.P.'s Heumann Wheel Tread Contour on New 132-RE Rail, With a 1:40 Cant.

CANADIAN PACIFIC LTD.'S RESEARCH AND EXPERIENCE

At the suggestion of Dr. Caldwell, Mr. A. E. Bethune, Director of Technical and Operations Research of the Canadian Pacific, was contacted and asked if he would furnish data on the tests they were conducting on the effect of wheel profile on wheel wear [29] for inclusion in this report. In response to this request, a copy of an Interim Report was received from Mr. Walter Pak, Engineering Analyst, CP Department of Research.

The following information was taken from that report:

A comparative wheel profile test was undertaken by the Canadian Pacific's Research Department, in order to evaluate the relative wheel wear of 100-ton coal cars in unit train service. Four cars were used in the test, using the standard AAR profile and CN's profile with the following variations:

- Car 1 - A profile; brakes operational
- Car 2 - A profile; no brakes
- Car 3 - AAR profile; brakes operational
- Car 4 - A profile; brakes operational; C-PEP side bearings

All of the cars have two-wear, 36-in. diameter, Class C wrought wheels, designated J-36. Each car is fitted with a Wabcopac brake assembly and 4-in. H.F. composition brake shoes. Profile measurements were taken of the wheels when new, and after accumulated mileages of 1,720, 2,180, 8,750, 44,470, and 67,000 miles, respectively. All of the field measurements were taken in Revelstoke, B.C., within the period from September, 1979 to May, 1980. The present report discusses the results up to 44,470 miles. The data from the last measurements are still being analyzed.

A precision wheel profilometer was designed. It is an electro-mechanical device, using a 2-in. potentiometer and DC voltage to trace the profile. The output signal is digitized and stored on digital magnetic tape. A precision calibration block was used before and after the profile measurements, in order to orient the measurements relative to the backface of the wheel rim and periodically, during the tests, to verify the accuracy of the potentiometer.

Initial profile measurements were taken in the shop at six equi-distant locations on each wheel. In subsequent field measurements, only one accessible location was measured per wheel.

The most significant data on flange and tread wear are shown in Table 1. The average maximum flange wear and average tread wear (measured 2-7/8 in. from the wheel backface) for the leading and trailing axles of each car, after 8,750 miles and 44,470 miles, respectively, are shown in centimeters (cm). The

TABLE 1

Wheel Flange and Tread Wear Measurements on Four Canadian Pacific 100-Ton Unit Train Coal Cars.

Car No.	Test Condition	Average Maximum Flange Wear (cm.)		Average Tread Wear (cm.)*	
		8,750 Miles	44,470 Miles	8,750 Miles	44,470 Miles
<u>Leading axles</u>					
1	- A profile, brake	0.149	0.340	0.021	0.046
2	- A profile, no brake	0.183	0.355	0.018	0.078
3	- AAR profile, brake	0.258	0.468	0.039	0.111
# 3A	- AAR profile, brake	0.222	0.367	0.016	0.062
4	- A profile, brake, C-PEP	0.198	0.373	0.024	0.083
<u>Trailing axles</u>					
1	- A profile, brake	0.106	0.157	0.015	0.044
2	- A profile, no brake	0.112	0.185	0.018	0.078
3	- AAR profile, brake	0.143	0.262	0.039	0.066
# 3A	- AAR profile, brake	0.142	0.222		
4	- A profile, brake, C-PEP	0.079	0.148	0.015	0.065
Notes: * Measured 2-7/8 in. from the backface of the wheel.					
# Excluding mismatched wheels.					
Author's Note: The values in this table were scaled from the measured profiles in order to conserve space, and are not indicative of the original accuracy. They will, however, serve as relative wear measurements.					

measured wear increased rapidly from the start of the test and was not greatly different for the four cars in the readings at 1,720 miles and 3,180 miles.

It will be noted from Table 1 that there is a large difference in flange wear between the leading and trailing axles for all four cars. This is because the coal train is only turned every six months, and during this test period the leading axles remained leading axles throughout.

By matching worn wheel profiles from the two mating wheels on one axle, a non-symmetrical wear pattern was noted for some axles. For example, for the No. 3 axle of car No. 2, a tread hollowing on the left hand wheel was accompanied by a large flange and tread wear on the right hand wheel. A small diameter mismatch is suspected, although the tape size and measured difference between axles were initially identical. Accelerated flange and tread wear were also observed on a pair of diagonally opposite wheels in the trailing truck of the No. 3 car with AAR wheels. Furthermore, heavy shelling occurred on all four wheels in the leading truck of the same car, between 44,470 and 67,000 miles. The exact cause of these phenomena is not clear at the present moment and is still under investigation.

By matching the final worn wheel profiles of different cars against each other, it was observed that

both the AAR and Profile A wheels are developing into exactly the same profile, up to 80 mm from the backface of the wheel.

Comparing the average worn profiles obtained in the CN and CP tests, a very close match was observed in the flange-throat area, up to 75 mm from the backface. The tread section of the CP test wheels is generally canted more downwards, and departs from the more cylindrical tread on the CN's worn profile. This difference may be due to the 1:20 rail cant on CP tracks versus the 1:40 rail cant on CN tracks.

The contact geometries of a new AAR profile, Profile A and a Heumann profile relative to a worn rail gage profile are shown in Figure 36 [29]. From these contact configurations, the wheel-rail conformity is better with both the A profile and Heumann profile wheels than with the AAR profile wheels. However, some initial wear must occur for both the A and Heumann profile wheels, in order to achieve complete profile stabilization. For the A profile wheels, profile stabilization generally occurred before 10,000 miles. The AAR profile wheels did not complete the stabilization process even at 44,470 miles.

From the measured profiles, a study was made of the change in flange angle. With the flange angle stabilized, it was found to be 75 to 76 degrees for both the AAR and A profile wheels, similar to that re-

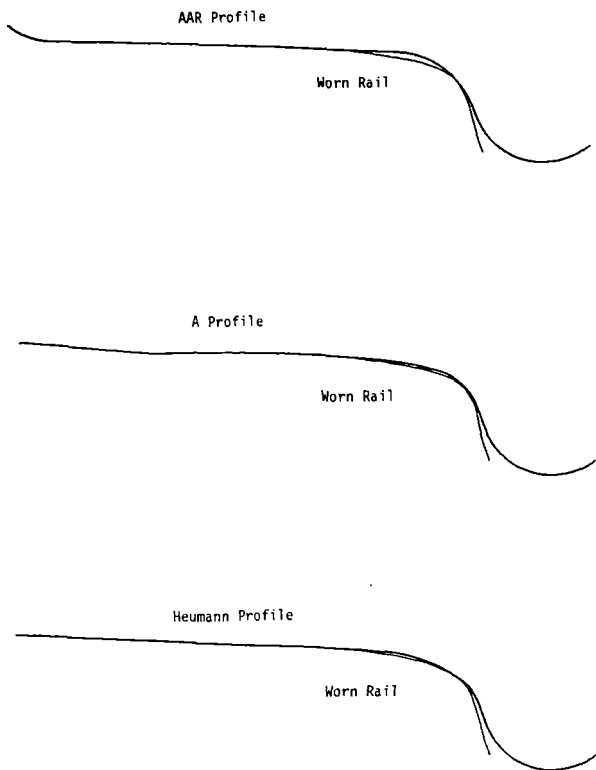


Figure 36.
Contact Geometries of New AAR, Profile A and Heumann Profile Wheels at the Gage Corner of a Worn Rail.

ported by CN. These results indicated a rapid wear-in period, for both leading and trailing A profile wheels, within the first 3,000 to 4,000 miles, after which the flange angle is more or less constant. The flange angle for the leading AAR wheels stabilized in about the same mileage, but the trailing wheels had not stabilized after 44,470 miles.

Tread wear, as shown in Table 1, was measured 2-7/8 in. from the wheel backface. However, it was noted that the tread wear patterns are quite dissimilar for wheels with and without brakes. To clarify this point, the maximum tread wear after 44,470 miles for wheels with and without brakes were also compared. This maximum tread wear is usually observed at a point farther away from the backface than 2-7/8 in., and does not differ appreciably between braked and non-braked wheels. Braking tends to retain the original cylindrical portion of the tread longer, whereas wheels with no brakes develop tread hollowing faster.

The C. P. report [29] concludes:

"From the standpoint of wheel-rail conformity, the recent replacement of the AAR profile by modified Heumann profile wheels (Figure 34) as standard in CP operation will improve both wheel and rail wear and lower contact stresses during curving. However, initial wear-in is still required at the flange root, and the 1:20 conicity of new Heumann profile wheels induces high contact stresses in the wheel tread region until it becomes hollowed by wear."

WHEEL EXPERIMENTS ON THE FAST TRACK AT PUEBLO, COLORADO

Preliminary results from the FAST wheel experi-

ments were published in 1979 [30]. A comparison of wheel performance of the CN Heumann profile wheels (Figure 34) and AAR Standard profile wheels was included in the test described in this report. The following two paragraphs in the Executive Summary give the essential results:

"Finally, an analytical model was developed, based on a regression of the logarithm of the flange thickness with the logarithm of the mileage weighted by a combination of dummy variables representing the wheel variable states. This model was used to analyze the relative contributions of the test variables on flange life. The model indicated that heat treatment extended the flange life significantly, on the order of two and one-third times. In addition, the model indicated that cast wheels, CN profiles, 14-in. center plates and Type 1 trucks seemed to improve performance slightly. There was no significant difference in flange wear between 1-wear and 2-wear wheels."

"The large difference in the observed wear of supposedly identical components indicates the presence of unidentified sources of variation, other than the planned experimental factors introduced into the first wheel experiment. The findings of the regression analysis must be conditioned by the fact that approximately 50 per cent of the variation in observed wear is attributed to unidentified sources. A second wheel test embodying an improved experimental plan was begun in the summer of 1978 and is still in progress."

DISCUSSION

Rail and Wheel Contours

- (1) A wheel contour that will give point contact on the rail, as advocated by Wellington and Heumann, reduces the initial rate of wheel wear, but increases the contact stresses in both rail and wheel, and with today's heavy wheel loads, produces excessive plastic flow of the gage corner of the rail.
- (2) Since only about 2 per cent of main line track miles are relaid with new rail each year, it is evident that the original contour of new rail will be worn to the average worn contour of existing rail in track within a short time. It seems most important that the new rail contour not be subjected to excessive plastic flow during this period. An attempt to achieve this goal was made when the 115-RE and 132-RE rail sections were adopted by the American Railway Engineering Association in 1947.
- (3) In common carrier service, there is more tangent track than curved track, and the rail has a longer life on tangent track than on curved track. Therefore, it is believed that rail should be designed to conform to the average worn contour of rail on tangent track. Also, the top-of-rail contour should be symmetrical about its centerline. The use of an asymmetrical top-of-rail contour presents many practical problems in welding and laying CWR, and it is believed that this would not be met with favor by railroad chief engineers. The 11523 rail section was an asymmetrical section, was used by only a few roads and is no longer rolled.

- (4) Only a relatively small percentage of new or reprofiled wheels are placed in service each year. It is evident that the contour of new (or reprofiled) wheels will soon wear to conform to the average worn contour of the remaining wheels. It is also important that this occur without excessive plastic flow of the new contour metal. There is evidence that such excessive plastic flow is occurring with the AAR standard wheel profile; metal is being displaced from the flange, and, in some instances, packed into the flange throat where there is initially no rail-wheel contact. This is especially noticeable with 100-ton cars in unit train service on lines with a considerable amount of sharp curvature.
- (5) The Canadian National has done an excellent research job on the subject of wheel profile design. The CN Profile A contour will undoubtedly give somewhat longer wheel life than the standard AAR contour. It does offer some problem with truck hunting of empty cars at high speed, but the same problem exists with the operation of empty cars with service-worn standard AAR contours. To the author's knowledge, one railroad has restricted the operation of empty 100-ton car unit trains to 45 mph, because of derailments at higher speeds. Another road has restricted the operation of empty 100-ton and 125-ton cars in unit train service to 40 mph, because of excessive hunting at higher speeds.

Rail and Wheel Metallurgy

- (1) Regarding the improved metallurgy of rails and wheels and the best economic solution to the rail-wheel metallurgy problem, extensive research has been conducted on rail metallurgy for years and is still underway [31]. Present rail metallurgy is adequate for tangent track, and the only possible economic improvement would be the development of a manufacturing process to produce an absolutely clean steel of pearlitic structure, at a cost substantially the same as for present processes in use. The cost of an alloy or heat-treated steel is not economically justified on tangent track.
- (2) Extensive research has been conducted for many years in collaboration with rail manufacturers, procedures for providing a heat-treated steel rail and suitable chemical compositions for alloy steel rail are available, and research for further improvement is continuing. The author assumes that the same is true for wheel manufacture.
- (3) As for the ideal combination for rail-wheel metallurgy, the ideal is the rail that will give the most economical service life and the wheel that will do the same. The relative hardness of rail and wheel steel is of no practical significance. Contact pressures and the associated internal stresses are the most important consideration; the modulus of elasticity of all types of steel are substantially the same, but the harder steels have higher yield and fatigue strengths.

Railway track engineers have been concerned for years with the increasing contact pressures between rail and wheel, resulting from the increase from 70-ton to 90-ton, to 100-ton and to 125-ton cars on four-wheel trucks. The AAR did prohibit wheel loads heavier than those for 100-ton cars from general interchange service, but this was because many miles of track and many bridges were not strong enough to support the heavier loads. Available information indicates that the use of six-wheel trucks is uneconomical and impractical. The overall economics of the operation of 70-ton, 90-ton, 100-ton and 125-ton cars for railway transportation would make a very interesting, but complicated, study.

The AAR Track-Train Dynamics program includes an evaluation of a high performance/high cube 100-ton covered hopper car, and comparisons of 80 and 100-ton hopper cars of current design.

CONCLUSIONS

- (1) There are several factors that influence the rate of wheel wear other than its profile. These include the relative diameters of mating wheels, parallelism of axles in the truck, truck design, brake system design and wheel metallurgy. It is probable that the Heumann-type profile can be used on 100-ton cars in unit train service, with some economy in wheel life, if the speed of empty cars is limited to 40 mph. In common carrier service, however, where speeds of up to 70 mph may be attained with empty cars, the use of the Heumann-type profile does not seem to be advisable with trucks of current design.
- (2) The AAR Track-Train Dynamics Research Program should result in the development of freight car trucks and braking systems that will prevent truck hunting at speeds up to 70 mph, regardless of wheel profile, and reduce the variability of wheel wear that is now found to occur in service.
- (3) No changes should be made in the present A.R.E.A. rail designs at this time.
- (4) Improvements can be expected from current research on rail and wheel metallurgies and improved heat treatment processes.

REFERENCES

1. Wellington, A.M., The Economic Theory of the Location of Railways, John Wiley and Sons, New York, New York, Revised Edition, 1887, p. 307.
2. Ibid, p. 308.
3. Ibid, Figure 59, p. 309.
4. Faries, R., "The Design of a Rail Section," A.R.E.A. Proceedings, Chicago, Illinois, Volume 34, 1933, pp. 640-643.
5. Harris, G.W. (Subcommittee Chairman), et al., "Appendix J - Redesign Rail Sections Heavier Than 100 Lbs. per Yard so as to Obtain the Most Economical Distribution of Metal With the Maximum Strength of Section," Proceedings of the American Railway Engineering Association (A.R.E.A.), Chicago, Illinois, Volume 35, 1934, pp. 872-876.
6. Scholes, R.T. (Subcommittee Chairman), et al., "Appendix K - Effect of Contour of the Head of Rail Sections on the Wear," Proceedings of the A.R.E.A., Chicago, Illinois, Volume 38, 1937, pp. 249-251 and 639-641.

7. Johns, C.W. (Subcommittee Chairman), et al., "Appendix K - Effect of Contour of the Head of Rail Sections on Wear," Proceedings of the A.R.E.A., Chicago, Illinois, Volume 39, 1938, pp. 396-397 and 806.
8. Hewes, F.S. (Subcommittee Chairman), et al., "Report on Assignment 11 - Investigate Causes of Shelly Spots and Head Checks in Rail Surfaces for the Purpose of Developing Measures for Their Prevention," Proceedings of the A.R.E.A., Chicago, Illinois, Volume 44, 1943, pp. 597-601.
9. Hewes, F.S. (Subcommittee Chairman), et al., "Report on Assignment 11 - Investigate Causes of Shelly Spots and Head Checks in Rail Surfaces for the Purpose of Developing Measures for Their Prevention. Appendix A, Field Investigation by Engineering Division Research Staff," Proceedings of the A.R.E.A., Chicago, Illinois, Volume 45, 1944, pp. 446-462.
10. Hewes, F.S. (Subcommittee Chairman), et al., "Report on Assignment 11 - Investigate Causes of Shelly Spots and Head Checks in Rail Surfaces for the Purpose of Developing Measures for Their Prevention. Appendix 11-a: Field Investigation by Engineering Division Research Staff," Proceedings of the A.R.E.A., Chicago, Illinois, Volume 46, 1945, pp. 643-648.
11. American Railway Engineering Association, Manual for Railway Engineering, Chicago, Illinois, March 28, 1979.
12. Nuckols, L.T. (Subcommittee Chairman), et al., "Report on Assignment 1 - Revision of Manual," Proceedings of the A.R.E.A., Chicago, Illinois, Volume 48, 1947, pp. 655-673 and 908.
13. Thomas, H.R., "Appendix A - Formulas and Diagrams for Computing Shearing Stresses in Rail Head Which are Due to Direct Action of the Wheel Load," Proceedings of the A.R.E.A., Chicago, Illinois, Volume 39, 1938, pp. 835-842.
14. Magee, G.M., "Report on Rail Study on Black Mesa and Lake Powell Railroad, June-July, 1976," Central Technology, Inc., now Parsons Brinckerhoff CENTEC, Inc., McLean, Virginia, Unpublished Report, pp. 1-11.
15. Tyler, H.A., "Wheel Mileage Performance on Ore Cars Operating Over the Quebec, North Shore and Labrador Railway," ASME Paper No. 64-WA/RR-6, 1964, pp. 1-12.
16. Tyler, H.A., "Report of Test on Two Wheel Tread and Flange Profiles," Mechanical Department - Engineering Office, Quebec, North Shore and Labrador Railway, Sept Isles, Quebec, Canada, Internal Document, July 9, 1966, pp. 1-8.
17. Koffman, J.L., "Tire Profile Test on British Railways," Railway Gazette, London, England, April 2, 1965.
18. "Where Treads Meet the Track," Railway Locomotive and Cars, Simmons-Boardman Publishing Corp., New York, New York, November, 1970, pp. 13-15.
19. "AAR Wheel Outperforms Others," Railway Locomotive and Cars, Simmons-Boardman Publishing Corp., New York, New York, November, 1971, pp. 10-15.
20. Eck, B.J., and Berg, N.A., "Looking for Tomorrow's Wheel Contour," Griffin Wheel Company, Chicago, Illinois, Unpublished Report, pp. 1-7 plus 14 Drawings.
21. Marcotte, P.P., "Theoretical Study Concerning the Use of Profiled Wheels on Freight Car Trucks," Technical Research Centre, Research and Development, Canadian National Railways, St. Laurent, Quebec, Canada, CN Rail Research Internal Report No. 115, August 2, 1973, 59 Pages.
22. Marcotte, P.P., "Test Report on the Comparative Curving Performance of Freight Car Trucks on Special Wheel Profiles," Technical Research Centre, Research and Development, Canadian National Railways, St. Laurent, Quebec, Canada, CN Rail Research Report No. 122, March, 1975, 74 Pages.
23. Marcotte, P.P., and Mathewson, K.J.R., "Wheel Profile Test - Luscar Coal Service Gondolas," Technical Research Centre, Research and Development, Canadian National Railways, St. Laurent, Quebec, Canada, Progress Report No. 1, CN Rail Research Memorandum Report No. 125, March 18, 1976, 30 Pages.
24. Marcotte, P.P., and Mathewson, K.J.R., "Wheel Profile Test - Luscar Coal Service Gondolas," Technical Research Centre, Research and Development, Canadian National Railways, St. Laurent, Quebec, Canada, Progress Report No. 2, CN Rail Research Memorandum Report No. 128, June 14, 1976, 34 Pages.
25. Marcotte, P.P., and Mathewson, K.J.R., "Wheel Profile Test - Luscar Coal Service Gondolas," Technical Research Centre, Research and Development, Canadian National Railways, St. Laurent, Quebec, Canada, Progress Report No. 3, CN Rail Research Memorandum Report No. 182, January, 1977, 37 Pages.
26. Golta, W.F., "What is the Average Life of Ties?," Railway Age, Simmons-Boardman Publishing Corp., New York, New York, Volume 79, Number 7, August 15, 1925, pp. 311-315.
27. Caldwell, W.N., and Bousquet, J.L., "Wheel Profile Test on Luscar CN 199000 Series Coal Gondolas - Hunting Tests," Technical Research Centre, Research and Development, Canadian National Railways, St. Laurent, Quebec, Canada, CN Rail Research Memorandum Report No. 126, April, 1976, 37 Pages.
28. Marcotte, P.P., Mathewson, K.J.R., and Caldwell, W.N., "Improved Wheel Tread Profiles for Heavy Freight Vehicles," American Society of Mechanical Engineers, New York, New York, Paper No. 80-RT-3, April, 1980.
29. Izbinsky, G., and Pak, W., "Experimental and AAR Wheel Profile Measurements on a C.P. Unit Coal Train," Department of Research, Canadian Pacific, Windsor Station, Montreal, Quebec, Canada H3C 3E4, Interim Report, July, 1980.
30. Larsen, K.W., "Analysis of Data From the First Wheel Experiment at the Facility for Accelerated Service Testing," Interim Report No. FRA-TTC-79-01, July, 1979, 29 Pages. Available as Publication No. PB-299433/A5 from the National Technical Information Service, Springfield, Virginia - 22161.
31. Chapin, W.E., King, R.D., Pestel, H.C., and Breslen, R.H., "Research Report - A Bibliography on Rail Technology," Battelle - Columbus Laboratories, Columbus, Ohio. Final Report for the U.S. Department of Transportation, Federal Railroad Administration, Office of Research and Development, Washington, D.C. - 20590, March, 1976, 531 Pages.

Wheel Flange Wear Test Results in Heavy Haul Service

T.J. Devine

Senior Engineer
Griffin Wheel Company

R.H. Alber

Manager
Field Engineering
Griffin Wheel Company

A proposed means of reducing thermal cracks in railroad wheels is to reduce the carbon content. The tests described herein were designed to examine the possible consequences in terms of wear of this change. To provide insight into wear behavior, material characterizations were conducted. Results indicate a positive dependence of flange wear upon carbon content. A similar effect, although less dramatic, was seen in the influence of hardness on flange wear. Differences in operating environments between service tests were also documented, and used to explain wear rate variations. The magnitude of flange wear rates and the overall ranking of different material types are affected by the service environment including rail lubrication, percentage of curves, and speed.

INTRODUCTION

The objective of the work described is to develop a relationship between wheel wear and carbon content and wheel hardness. The test work was undertaken with the cooperation of the Wheels, Axles, Bearings and Lubrication (WABL) Committee of the Association of American Railroads (AAR). Their concern stems from the dramatic increases in wheel removals because of observed thermal cracks and overheating since 1978.

A proposed means of reducing thermal cracks in railroad wheels is to reduce the carbon content. With respect to current specifications, this means lowering the carbon content in untreated class U wheels and to use class B in lieu of class C for heat treated wheels. As a performance trade off the consequences of this change may be to increase wheel wear and increase susceptibility of the wheels to shelling. These factors must be fully understood before any chemistry changes are implemented.

The following sequence of topics will be discussed in this report:

- Material Characterization
- Car Components and Test Description
- Test Operating Environment
- Measurement Techniques

- Measurement Frequency
- Analysis Technique
- Results and Discussion
- Conclusion

GENERAL DESCRIPTION OF TEST GROUPS

All test wheels were manufactured by the Griffin pressure pouring technique¹. The geometric design used was the CH36 with a standard AAR 1:20 tread profile.

Two general categories of wheels were tested: normalized wheels, and normalized and quenched wheels. These groups being commonly referred to within the industry as nonheat treated and heat treated wheels respectively. By category the group designation as well as a general description follows:

Normalized (nonheat treated)

Group U_{LC}: Low carbon material cast with 0.63-0.65% carbon content. This level is outside the 0.65-0.77% carbon range as specified by AAR Specification M-208 for class U steel. Resulting hardness values range from 235 to 255 BHN.

Group U_{HC}: High carbon material cast with 0.74-0.77% carbon content. Hardness values range from 262 to 285 BHN.

Normalized and Rim Quenched (heat treated)

Group B: Normal class B steel cast to 0.61-0.63% carbon, this being the middle of the AAR specified range of 0.57-0.67%

carbon. After quenching the hardness ranged from 302-341 BHN.

Group B_{HH}: High hardness class B steel cast to 0.64-0.66% carbon. A more severe water quench resulted in hardnesses of from 341 to 363 BHN. The specified range for class B material is 277-341 BHN.

Group C: Normal class C steel cast with a restricted carbon range of 0.70-0.74% carbon. The full AAR range for class C material is 0.67-0.77% carbon. After rim quenching the hardness ranged from 321 to 363 BHN, this also being the AAR specified range for this material.

The complete description for the AAR specification can be found in "Wheels, Cast Carbon Steel", Specification M-208-80 of the AAR Manual of Standards and Recommended Practices.

In addition, to the above restricted carbon ranges, residual chemistry variations were minimized by obtaining test wheels for each group from a maximum of two cast heats.

MATERIAL CHARACTERIZATION

Introduction

Wheel wear is understood to be a function of the particular material used. In light of this, understanding wear behavior requires knowledge of a particular materials' microstructure and mechanical properties, as determined by chemistry and cooling. While these wear tests deal with pearlitic microstructures they actually compare steels with varying degrees of pearlite "fineness", a steel phase that promotes wear resistance², as well as differing amounts of a soft, relatively tough, ferrite phase. In manufacturing, the presence of either of these phases is controlled by the chemistry (carbon content primarily) and also by the cooling rate from the critical temperature. In this section of the paper, the relationship between chemical content, microstructure, and mechanical properties will be analyzed. Later, the discussion of wear rates will refer to certain of these features to help understand the wear processes.

Chemical Analysis

Test wheels were cast with the nominal chemistries listed in Table I. One wheel per heat was sectioned to verify heat analysis. Carbon content was determined using a Leco Carbon Determinator; manganese, silicon, phosphorous, and sulfur were determined using a Perkin-Elmer Atomic Absorption Spectrophotometer. The FAST results shown in Table I are averages determined by the same techniques but run on drillings from the front rim face of all test wheels.

Microstructural Characterization

Samples were taken from the rim of one wheel per test group for metallurgical examination. Representative microstructures are shown in Figures 1-5.

Table I Chemical Analysis by Test Group Weight Percent

Test Group	Service	C	Mn	Si	S	P
U _{LC}	Coal	0.61	0.71	0.41	0.029	0.014
	FAST	0.66	0.68	0.43	0.028	0.008
U _{HC}	Coal	0.76	0.73	0.43	0.026	0.010
	FAST	0.78	0.68	0.41	0.027	0.013
B	Coal	0.65	0.67	0.43	0.031	0.012
	FAST	0.66	0.68	0.38	0.027	0.010
B _{HH}	Coal	0.65	0.75	0.43	0.027	0.014
C	Coal	0.74	0.69	0.35	0.027	0.014
	FAST	0.75	0.71	0.42	0.030	0.013

The consequence of slower cooling rates is evident in the two nonquenched test groups, Figures 1 and 2, in the form of visibly coarser pearlitic structures, as well as in an increased amount of proeutectoid ferrite. Assuming consistent cooling rates, the difference in volume fraction of proeutectoid ferrite, as effected by carbon content, can be seen in comparisons between the (nonquenched) normalized samples, U_{LC} and U_{HC}, Figures 1 and 2, and between the quenched samples, B and C, Figures 3 and 5.

The formation of the pearlite phase is a rate dependent diffusion process, consequently highly effected by cooling rate through the critical temperature and also by the carbon content. It was shown with the tested materials that cooling rate and carbon content both have significant impacts on how fine the pearlite was after formation. Using the Gensamer³ technique the average pearlite interlamellar spacings were determined where possible, and are listed in Table II. Past researchers have noted a pronounced effect of pearlite spacing on hardness⁴ and on subsequent wear resistance⁵.

Table II Microstructural Examination of Five Wheel Types

Test Group	Treatment	Nominal Carbon	Prior Austenitic Grain Size No.	Pearlite Spacing (Angstroms)	Volume Fraction Pearlite
U _{LC}	Unquenched	0.61	7.4	4110	.87
U _{HC}	"	0.76	6.7	2080	.98
B	Quenched	0.65	6.9	<1500 ^a	.96
B _{HH}	"	0.65	8.7	"	.97
C	"	0.74	7.0	"	.97

^abelow limits of analysis

The prior austenitic grain size is determined primarily by heat treatment, in particular the time above the austenitizing temperature. Additional influence can be seen through alloy addition or prior heat treatments. While the effect of grain size on wear resistance is not clearly understood, it does have a dramatic effect on fracture toughness as will be discussed in the next section.

The prior austenitic grain size was determined

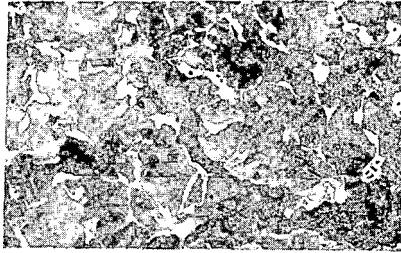


Figure 1 Photomicrograph of Type U_{LC}, .61C, Normalized. Nital Etch

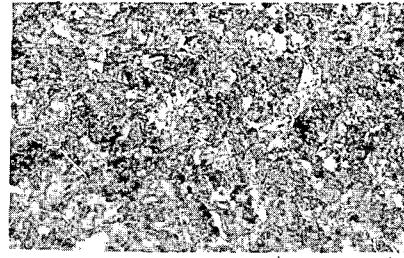


Figure 3 Photomicrograph of Type B, .65C, Normalized and Quenched. Nital Etch

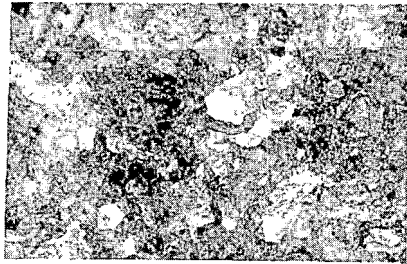


Figure 2 Photomicrograph of Type U_{HC}, .76C, Normalized. Nital Etch

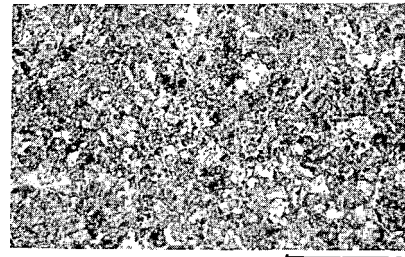


Figure 4 Photomicrograph of Type B_{HH}, .65C, Normalized and Quenched. Nital Etch

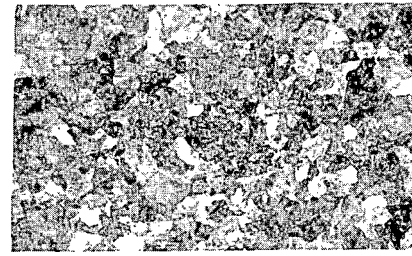


Figure 5 Photomicrograph of Type C, .74C, Normalized and Quenched. Nital Etch

for each test group with ASTM E112 as a guideline. These values are listed in Table III. Since these materials all experienced the same time above the critical, the results are consistent in that a relatively constant grain size is achieved. The exception is the B_{HH} group which, besides receiving a more severe quench, did have it's grain size controlled.

Table III Summary of Mechanical Properties^a
(SI conversion of this table is given in appendix)

Group	BHN	Yield Stress ksi	Tensile Stress ksi	K _Q /K _{max} ksi/in	Valid K _{1C} ?
U _{LC}	240	55.9	111.9	49.9/56.2	No
U _{HC}	272	70.5	135.2	38.0/47.8	No
B	318	103.0	149.7	40.2/43.9 ^b	Yes
B _{HH}	347	116.7	168.2	54.2/55.6	Yes
C	338	111.1	178.7	44.8/44.8 ^b	Yes

^a Values presented for BHN, Yield and Tensile Strengths are averages. Range for BHN was ± 10 BHN, for Yield and Tensile, ± 10 ksi.

^b Values for the B and C materials were obtained from wheels similar to those reported on here. The values for the other test groups were obtained from the actual unit coal service test heats.

Total pearlitic volume was determined through stereology and is shown in Table III. The effect of carbon is seen with the nearly 100% pearlite in the class C and U_{HC} samples, Figures 2 and 5. In addition, the ability of quenching to suppress the equilibrium proeutectoid ferrite reaction in the B sample, Figure 3, is evident in comparison with the U_{LC} sample, Figure 1, both of which have nearly the same carbon level but exhibit differing amounts of pearlite.

Mechanical Properties

Brinell hardness measurements were taken on the front rim face of each test wheel using the method defined in AAR Specification M-208. These values were summarized and are presented in Table III in the form of mean hardnesses for each test group. In addition, a standard ASTM A370 monotonic tensile test was run on .505 inch (12.7mm) diameter bars machined from the rim of one wheel from each test heat. These samples were oriented axially and cut immediately be-

low the tread. Mean yield and tensile stresses are also reported in Table III.

The room temperature fracture toughnesses of the five test materials were determined using compact tension specimens (ASTM E399). Using the test validity requirements, constraints on the maximum sample size obtainable did not allow conditional K_{I0} values to be considered valid plane-strain fracture toughness, K_{IC} for all materials. For this reason, K_{I0} and the maximum stress intensity factor, K_{max} are listed in Table III with the valid K_{IC} values noted.

CAR COMPONENTS AND TEST DESCRIPTION

Unit Coal Service Test

Twenty cars, built between 1968 and 1977, from a fleet of 450 open top high side gondolas were used. All have 100 ton (90.7 tons) capacity with a fully loaded gross weight on rail of approximately 260,000 pounds (117936 kg). It is assumed that half the mileage experienced by these cars is in the loaded condition. All of the test cars were equipped with truck mounted brakes with ABD brake valves and 1.5 inch (3.8 cm) composition shoes. No constant contact side bearings or other snubbing device exists between the car body and the truck nor within the truck itself.

The test cars were divided into two groups of eight and twelve cars respectively. Test wheels within these cars were located systematically to minimize a bias due to axle location.

The first group of eight cars was dedicated to the comparison of the normalized (nonquenched) wheels. On four of these, the U_{HC} were placed in the 1 and 3 axle positions and the U_{LC} in the 2 and 4 positions. The reverse scheme was adopted on the remaining four cars. Three of the eight cars have 16 inch (41 cm) centerplates and constant column loading, two have 14 inch (36 cm) centerplates with constant column loading and three cars have 16 inch (41 cm) centerplates with variable column loading.

The second group of twelve cars contained the B, B_{HH} , and C test groups. The wheels were positioned such that each group was applied a total of four times at each axle position and each truck had no more than one pair of the same type wheels. Two of these test cars had 14 inch (36 cm) centerplates and constant column loading while the remaining ten cars have 16 inch (41 cm) centerplates with variable column loading.

FAST Tests

The Wheels II⁶ experiment at FAST incorporated 16 hopper cars which were loaded to a gross weight of 263,000 pounds (119297 kg) and were assumed to be sufficiently similar so as not to bias the test. Each car was equipped with high friction composition shoes, roller bearings and double roller side bearings. The majority of the cars were equipped with standard D-5 springs. Brake equipment was mixed truck and body mounted. Two different centerplate sizes, 14 inch (36 cm) and 16 inch (41 cm) were included.

Sixty Griffin wheels were supplied for the Wheels

II test, 26 class C and 34 class U wheels. The wheels were taken at random from normal production. Consequently, chemical content and hardnesses other than the AAR M-208 specification were not controlled. The wheels were placed under the test cars as follows:

Class C		Class U	
Axle #1	Axle #2	Axle #1	Axle #2
24	2	18	16

The Wheels IV FAST⁷ experiment incorporated 24 cars and was designed specifically to develop an understanding of wheel wear as it is affected by hardness and carbon content. All the test cars were fully loaded, 263,000 pounds (119297 kg), and were equipped with 16 inch (41 cm) centerplates and trucks with variable column loading. Test wheels were identical to the four test groups, excluding the B_{HH} group, as described earlier. Wheel distribution among the test cars was patterned after the Unit Coal Service Test, i.e. systematically distributed to minimize the effect of axle and truck location.

TEST OPERATING ENVIRONMENT

FAST

The 4.8 mile (7.7 km) FAST loop contains 2.2 miles (3.5 km) of tangent track, 0.4 mile (0.6 km) of 3° curve, 0.3 mile (0.5 km) of 4° curve and 1.1 miles (1.8 km) of 5° curve; the remaining 0.8 mile (1.3 km) is in transitional spirals. Curves amount to 54% of the total track and grades vary from 0 to 2%. The consist is run at an average speed of 45 miles/hr (72 km/hr) in nominal 3 inch (8 cm) unbalance conditions. On tread braking is kept to a minimum.

Unit Coal Service

Introduction. Unlike FAST, the operational environment of the Unit Coal Service Test cars is difficult to describe. The cars operate in unit coal train service with a specific origin and a specific destination and, although railroads have well defined track profiles which describe this route, alternate routes exist over which the cars occasionally travel. Even more difficult to define, is the way the train is handled on this profile. Railroads teach their engineers how a specific train is to be handled over a particular profile, however, each engineer does things slightly different than the next. In addition, each trip that the train makes has its own little idiosyncrasies such as train meets, speed restrictions, available power and dynamics, and rail lubrication.

Mine-site. The mine-site is a loop track arrangement with a combination of curves varying from 2° to 9°. The train is pulled light thru these curves at speeds of about 5 miles/hr (8 km/hr). None of the curves are lubricated. The train then enters tangent track and is tipple loaded at speed of 0.35 to 1.50 miles/hr (0.56 to 2.41 km/hr).

After loading, the train heads east for a 1200 mile (1931 km) journey with five units of power all dynamically equipped. The train is neither broken or turned prior to or after the loading operation.

Description of terrain and train handling. For the first 50 miles (80 km) of the loaded east bound

movement, the train traverses .5 to .8% grades three to seven miles long, both ascending and descending. Train speed is 50 miles/hr (80 km/hr) and 9% of the distance is curves or less than 2°.

For the next 26 miles (42 km), the train travels over generally level track at speeds up to 50 miles/hr (80 km/hr) with 2% of the distance in curves less than 2°. At this point, the east bound train takes one of two routes:

The first route is a 25 mile (40 km) ascent at .8% grade with 13% of the distance in curves, 8% between 2° and 4°, 5% below 2°. This is followed by a 30 mile (48 km) descent with an average grade of 1.2% at a maximum speed of 35 miles/hr (56 km/hr). Eleven percent (11%) of the distance is curves with 7% between 2° and 4° and 4% less than 2°. The grade is handled with dynamics and 8 to 10 psi (0.055 to 0.069 Mpa) brake pipe reductions from a 90 psi (0.62 Mpa) brake pipe pressure, cycled on and off as needed. The second route is an 18 mile (29 km) ascent at 1.6% to 2.1% grade with 33% of the distance in curves less than 2°. This is followed by a 39 mile (63 km) descent at a nearly constant .8% grade with a maximum speed of 40 miles/hr (64 km/hr). Fifty percent (50%) of the distance is curves less than 2½°, and the curves are super-elevated for 60 miles/hr (97 km/hr) passenger service. The grade is handled with dynamics and 8 to 10 psi (0.55 to 0.069 Mpa) brake pipe reductions as needed.

For the next 500 miles (805 km) the train is descending on an average grade of .2% while traversing 21 miles (34 km) of curves (4%), 3% of which are less than 2°. Train speed is 50 miles/hr (80 km/hr) maximum, attained with two locomotives. Undulations in track profile and the grade itself are handled primarily with dynamic braking and minor use of power braking.

At this point the train is passed to another handling line which places three locomotives on the head end. These locomotives may or may not be equipped with dynamic brakes or, because its use is optional, it may not be used even if available. Over the next 470 miles (756 km), the train will negotiate 57 miles (92 km) of curves less than 2° and 16 miles (26 km) of curves between 2° and 4°. Speed is reduced to 40 miles/hr (64 km/hr) maximum although 30 to 40 miles/hr (48 to 64 km/hr) is far more typical. Three hundred and ninety of the 470 miles (627 of 756 km) are undulated profile requiring, at times, heavy power braking with 15 psi (0.1 Mpa) brake pipe reductions from a 90 psi (0.62 Mpa) brake pipe pressure while under 75% to 100% full power. These undulations translate to 54 miles (87 km) of ascending and descending grade .6% or greater (.9% max.).

For the last 80 miles (129 km) to the Power Plant, head-end power is reduced to two locomotives with maximum speed of about 30 miles/hr (48 km/hr). Dynamic braking is not regularly practiced and power braking continues to be heavy at times because of continuing profile undulations. Grades are now .5% or less and curves account for 11 miles (17 km) or 13% at less than 2°.

Power Plant. At the Power Plant, the loaded train is split into three sections, each of which is pulled through two 7° curves off the mainline onto

three 6° curved ladder tracks. Speeds during this operation are 5 to 10 miles/hr (8 to 16 km/hr). Each section is then pulled thru a rotary dumper which is on a 7° curve, at speeds of 1 to 5 miles/hr (2 to 8 km/hr). The dumper track does have one rail lubrication point at the start of the 7° track. When empty, the three sections of train are recoupled from the rear, effectively turning the train for each round trip.

Summarizing the 1200 miles (1931 km) loaded trip:

- 95 miles (153 km) descending grade at .6% or greater
- 65 miles (105 km) of ascending grade at .6% or greater
- Curves totalling 10% of the distance travelled, 8% of which were less than 2°.
- Maximum speed is 50 miles/hr (80 km/hr)

Return trip empty. Virtually the same profiles are encountered with the empty unit coal train on its return trip to the mine-site. Train speeds are held to a maximum of 50 miles/hr (80 km/hr) with 40 miles/hr (64 km/hr) more typical of the first 550 miles (885 km) and the last 150 miles (241 km) because of severe grades. Round trip time under ideal operating conditions is 5 days with an average yearly mileage accumulation of about 90,000 miles (144800 km).

MEASUREMENT TECHNIQUES

For the Wheels II experiment and Unit Coal Test wheel flange thickness and height and wheel rim thickness were measured with an AAR Standard Steel Wheel Gage, as shown in Figure 6. The flange thickness measurement was taken by rotating the movable finger to the flange, removing the gage and then, measuring

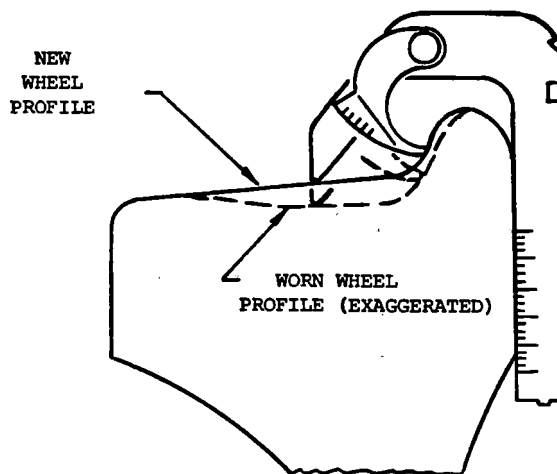


FIGURE 6 WHEEL PROFILE ILLUSTRATION WITH AAR STANDARD STEEL WHEEL GAGE

the distance between the end of the movable finger to the leg of the gage with a graduated scale. All wheel measurements were taken on each test wheel at two locations, 180° apart.

The Wheels IV test utilized a dial indicator device called the Snap Gage to take the same three measurements.

A comparison of the repeatability of the two methods was carried out by FAST⁸ and a comparison of the standard deviation using the two methods is as follows:

Measurement	Standard Deviation			
	Finger Gage		Snap Gage	
	in.	cm	in.	cm
Flange Thickness	0.016	(0.041)	0.005	(0.013)
Flange Height	0.025	(0.063)	0.006	(0.015)
Rim Thickness	0.030	(0.076)	0.023	(0.058)

Regardless of the shortcomings described above, the AAR Standard Steel Wheel Gage was used to measure flange thickness, flange height, and rim thickness on Unit Coal Test wheels. The primary reasons for not using the FAST Snap Gage were the time and location constraints of measuring wheels in service.

To improve accuracy, however, the AAR Standard Steel Wheel Gage was modified to measure flange thickness in decimals. This was accomplished by the application of a decal (developed by Standard Car Truck) on the flange finger. This then allowed reading flange thickness to an accuracy of .025 inches (0.063 cm).

A problem in the data that must be realized when using the AAR Standard Wheel Gage (or the Snap Gage) is that the reference point on the tread changes as the tread wears (see Figure 6). The result is that the flange thickness reading is taken at constantly lower points on the flange as the tread wears. Because of the slope of the flange, if rim wear is significant it is possible to actually register an increase in flange thickness.

MEASUREMENT FREQUENCY

Frequency of wheel measurements at FAST vary with the experiment conducted. In Wheels II, with lubrication as a variable, the test consist was operated in a manner to equalize component wear at all locations on the test cars and involved a four day cycle. In addition to direction changes every other test day, two groups of eight cars were shifted from one end of the consist to the other and each test day four cars were removed from the consist for measurements while four previous cars were reinserted. This procedure ensured that each test car was cycled through the consist and received measurements at least once every 22 days or 11,000 miles (17706 km).

In Wheels IV, track lubrication was eliminated by design during the first 7,000 miles (11265 km) of test and reinstated for the next 14,000 miles (22530 km). The non-lubricated portion of the test resulted in rapid wear, requiring the frequency of measurement to be increased to once every 1,000 miles

(1609 km). During the lubricated portion of the test, wheel measurements were taken at the start or 7,000 miles (11265 km) and at the end of the test or 21,000 miles (33795 km).

It has been shown⁹, that the wheel wearing process with a standard AAR profile involves rapid metal loss due to high contact stresses and slip at the two points of contact with service worn rails. This rate of wear differs from, and is higher than, that which occurs after the wheel has worn to the rail profile. In unit coal service of this type this wear rate change occurs typically between 15,000 and 25,000 miles (24140 and 40232 km). In order to define this wear transition, wheel measurements were taken for the first 125,000 miles (201125 km) as follows for the coal service test:

Miles	Kilometers	Miles	Kilometers
0	(0)	50,000	(80465)
7,000	(11265)	65,000	(104605)
14,000	(22536)	85,000	(136790)
20,000	(32186)	105,000	(168976)
35,000	(56325)	125,000	(201162)

ANALYSIS TECHNIQUE

Unit Coal Service Test

Figure 7 shows a plot of the change of flange thickness versus mileage. Wheel data shown are from one low carbon nonquenched wheel. Within the initial 20,000 miles (32186 km) the flange displays the typical rapid wear as described in the section on measurement schedule. Subsequently, much lower changes in dimension with mileage are seen. To describe this pattern quantitatively, the data was fit to two straight lines by simple regression (least squares estimation) techniques. The first line contains the initial readings and extends to 22,000 miles (35405 km). The second projects from 18,000 miles (28967 km) to the current mileage. Results of these analyses yield linear intercepts and wear coefficients for each wheel, these values were then sorted by test group. The mean of the wear coefficients for each group was determined and used in the comparisons made in the Results section.

The 18,000 to 22,000 mile interval (28962 to 35405 km) was determined to contain the wear "transition" by comparing alternate delineations for a limited sample of wheels. It should be noted however that sufficient condition variability exists such that some wheels encountered a transition above or below of this interval. In addition, the previously defined measurement schedule, which was based upon earlier tests, may also have influenced this determination.

FAST - Wheels II

Wheels II results were determined in a similar manner as those for the Coal Service Test. This investigation considered only Griffin wheels.

The highly lubricated environment of the Wheels

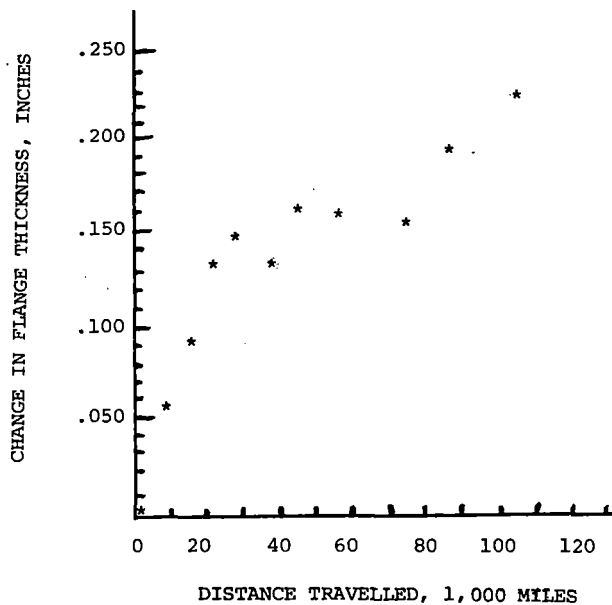


Figure 7 Example of flange wear-in and bilinear definition of curve.

II experiment resulted in a flange wear-in during the first 5,000 miles (8047 km) of running.

FAST - Wheels IV

Individual measurement datum from each of the test wheels were sorted to create separate files by group. Considering each measurement point as an independent sample, the SPSS SCATTERGRAM¹⁰ program was utilized to develop the wear regression coefficients for each file. Statistically, the difference between results from this analysis technique and the second level technique described above are expected to be minimal. In the Wheels IV test with no rail lubrication, the wear-in occurred within 2,000 miles (3218 km).

RESULTS & DISCUSSION

Group Comparisons

Table IV presents the results to date for the Unit Coal Service Test. The slopes of the wear lines are for all the wheels within a test group for each distance interval. These values, along with the standard deviation for the group, are listed.

There are a number of interesting observations that can be made concerning the initial, 0 to 22,000 miles (0 to 35405 km) interval. The mean rate in this interval is approximately ten times the rate experienced in the subsequent distance interval. In group to group comparisons, the range of wear rates is less than 20% versus the over 200% in the later distance interval. As a conclusion then, we can assume that the wear in the initial interval is more dependent on other factors such as those described earlier (profile change, for instance) rather than purely on material characteristics. Future phases of this test will involve new and worn profile characterization which may shed more light on this observation.

Table IV Mean Flange Wear Rates in Unit Coal Service by Test Group. Wear Rates Shown are Inches per 10⁶ Miles. (SI conversion of this table is given in Appendix)

Group	Distance Interval, Miles				
	0-22,000 All Wheels	18,000 & Up All Wheels	Ratio ^a	18,000 & Up Worst Whls ^b	Ratio
U _{LC}	4.76	0.618	3.09	0.893	1.87
U _{HC}	4.91	0.386	1.93	0.620	1.30
B	5.59	0.598	2.99	0.957	2.00
B _{HH}	5.51	0.447	2.23	0.773	1.62
C	5.27	0.200	1.00	0.478	1.00

^aRatio is with respect to the best wearing group in the "steady state" distance interval beyond 18,000 miles.

^bAverage is of worst wearing wheel per axle for a test group.

Results from beyond 18,000 miles (28967 km) lead to quite different conclusions. The mean flange wear rates are related to material type. When comparing carbon levels with equivalent heat treatment, the non-quenched wheels exhibit about a 100% increased wear rate with a 0.15 decrease in carbon. For the quenched wheels (Groups B and C) a 0.09% decrease in carbon results in a 200% increase in wear rate. Comparisons by cooling rate, the B group develops a 3% lower wear rate than the slower cooling U_{LC} group of approximately the same carbon. Furthermore, the B_{HH} group developed a 25% lower rate than the B group. Similarly, the C group develops a wear rate about 50% of the U_{HC} group rate.

Worst Wheel Analysis

Also listed in Table IV are analyses including only the worst wheel per axle. In some ways this type analysis is more useful to the wheel user since the rapid wear of one wheel will result in the removal of both wheels from service. It is unlikely that this variation in side to side wear is caused by wheel material variations. Rather it is a result of variations in the load environment created by other car component variations and operating conditions. It is however reasonable to expect that a better wearing material overall will be better able to minimize the effect of these other variations. As shown, the worst wheel analysis provides two outcomes. Generally much higher wear rates are listed for all test groups. The second result is the tightening of the spread in wear rates from the best wearing group to the worst.

Test to Test Comparisons

Table V is a presentation of steady state flange wear rates for the three wheel tests described earlier. The Wheels IV data are divided into wear rates derived under unlubricated and lubricated running. The last four columns, entitled "Ratios", are ratios of each group within a test to the best performing group.

Table V Comparison of Flange Wear Rates and Ratios in Coal Service Test and FAST Wheel Tests^a (SI conversions of this table is given in Appendix)

Group	Wear Rates				Ratios			
	Coal	Wheels IV ^b	Wheels IV ^c	Wheels II ^d	Coal	Wheels IV ^b	Wheels IV ^c	Wheels II ^d
U _{LC}	0.618	20.0	2.3	1.59	3.09	3.33	3.29	1.43
U _{HC}	0.386	18.0	0.9	---	1.93	2.25	1.29	---
B	0.598	14.0	0.8	---	2.99	1.75	1.14	---
B _{HH}	0.447	---	---	---	2.23	---	---	---
C	0.200	8.00	0.7	1.11	1.00	1.00	1.00	1.00

^aInches per 10⁶ miles in steady state

^bTo 7,000 miles unlubricated running

^c7,000 to 21,000 miles lubricated running

^dGriffin wheels only, from 5,000 to approximately 100,000 miles. Test wheels were of nominal class U and C chemistry, which did not necessarily coincide with other test groups.

The FAST data comparison highlights the effect of rail lubrication. On the order of ten to one, the lubrication effect on wheels appears similar in magnitude to its reported effect on rails at FAST¹¹.

As a general statement, the tendency towards greater flange wear resistance with greater carbon and hardness is evident in each test. However, inconsistencies arise between the different services that make a more definitive comparison difficult. The FAST data, for instance, generally indicate overall higher wear rates. Also, the apparent difference in metallurgies, as far as flange wear rate, shows the B performing near the C. The Coal Service Test, on the other hand, ranks the B as performing near to the class U_{LC} group.

Analysis of Other Variables

After an analysis of data by truck type, wheels under trucks with constant column pressure did show a lower wear rate when compared to those under the variable column pressure trucks. The confidence is less than 80% that a real difference exists. A similar analysis of 14 inch (36 cm) versus 16 inch (41 cm) resulted in less than 50% confidence that a difference in wheel wear rates is influenced significantly by this variable.

Data Variability

The standard deviations of the wear rates within a test group were nearly as large as the mean wear rates themselves. Statistically this makes the above stated generalizations tenuous. Table VI shows results of hypothesis testing using the Student's *t* Test. After statistically comparing the group wear

Table VI Group Comparisons and Hypothesis Testing, Coal Service Test. Wear Rate Beyond 18,000 Miles, Inches per 10⁶ Miles

Group	Wear Rate	Group	Wear Rate	95% Confidence Interval	Statistically Discernable?
C	0.200	B	0.598	0.398±0.309	Yes
C	0.200	B _{HH}	0.447	0.247±0.266	No
B _{HH}	0.477	B	0.598	0.151±0.286	No
U _{HC}	0.386	U _{LC}	0.618	0.232±0.230	Yes
B	0.598	U _{LC}	0.618	0.020±0.289	No
C	0.200	U _{HC}	0.386	0.186±0.255	No

rates listed, a 'Yes' result indicates that, with 95% confidence, there is some actual difference in the true wear rates. It does not prove that these ratios determined experimentally are representative of true wear rates. Using the first analysis for example, group C versus group B, the true difference in wear rates falls within the interval of 0.089 to 0.707 inches per 10⁶ miles (0.14 to 1.12 cm per 10⁶ km). In other words the class C group actually performs from 44% better to 335% better than the class B group. As a result of this large variability the user of these data must exercise caution when trying to relate experimentally determined wear rates to other quantitative economic analyses.

As discussed earlier, the measurement technique

itself distorts the wear results. The location on the flange at which this measurement is taken is determined by the tread point on the gage. Therefore, as the rim wears or deforms the flange gaging point will move radially inward. Due to the flange face angle, approximately at 70°, a thicker portion of the flange will be measured.

Table VII lists the change in flange height for the five groups in the Unit Coal Service Test. In the absence of severe metal flow at the flange apex this measure describes the change in rim thickness more accurately than the conventional rim thickness measurement. As evident, the softer/lower carbon materials show large increases in flange height (i.e. decreases in rim thickness). The result of this is an understatement of the 'true', i.e. constant location, flange wear rates for the softer materials. It is expected that after the tread materials work-harden this advantage may diminish in effect.

Table VII Mean Change in Flange Height after 100,000 Miles (1,609,000 km) - Unit Coal Service

Group	Initial BHN	Flange Height Change ^a , In. (cm)	Ratio of Flange Wear in Steady State ^b
U _{LC}	240	0.138(0.350)	2.14
U _{HC}	272	0.104(0.264)	1.20
B	318	0.075(0.190)	2.02
B _{HH}	347	0.070(0.178)	1.48
C	338	0.081(0.206)	1.00

^aInitial flange height, determined from sample of 128 new wheels, equal to 1.024 inches (2.600 cm), with standard deviation of 0.016 inches (0.039 cm)

^bAs determined in Table IV

As brought out earlier, distinguishing between material types is difficult because of the large variations in wear rates within a test group. It became apparent in the analysis of FAST data that, overall more consistent wear rates were obtained within any test group in that test. This result can be attributed to a number of factors; FAST's consistent operating speeds, absence of appreciable on-tread braking and lubrication control all which work to lower the variability in the load magnitudes and environment characteristics that the wheel sees.

This is not to imply, however, that FAST is necessarily better suited to run wheel tests. The greater degree of control provides better statistical validity of results, but it does not necessarily indicate adequate simulation of the wear mechanisms operative in revenue service. The higher wear rates themselves, as discussed earlier, could be indicative of wear mechanism not present in revenue service. It should be apparent by now that in order to adequately characterize a material with regard to wear, results

from controlled environments such as at FAST must be coupled with results from the range of conditions found in service.

To further confound any conclusions from this information, characterization is made of these materials by only one parameter, i.e. flange wear. Decisions on the use of any material must include, beside flange wear resistance, resistance of the surface fatigue (as an indication of shelling resistance), and thermal crack resistance.

Operating Environment

Differences in the wear rates, differences in the material ranking, as well as possible differences in wear mechanisms can be attributed to aspects of the operating environments of the described tests.

Isolating some obvious differences between FAST and the Unit Coal Service:

(1) Lubrication, or in FAST's case, the controlled absence of lubrication, has a very pronounced effect upon flange wear rates. Revenue service can be expected to have a range of lubrication levels.

(2) Since FAST has a high percentage of curves, over 50% and runs 3 inches (8 cm) unbalance, which implies constant flange contact in curves, it can expect higher wear rates. Revenue service has a range of operating conditions as well as a far lower percentage of curves.

(3) FAST cars are fully loaded all the time. In contrast in the Unit Coal Service, cars are only loaded half the time.

(4) The last two differences, the effect of alloy rail and consistency of rail profile, will effect wear, although at this point, to an unknown extent. To date there has only been limited service data and little consistent lab data to indicate the effect of rail metallurgy on wheel wear.

The above differences hold not only for comparisons of FAST to other services, but also between any separate services in general.

Material Behavior

As discussed earlier the results to date are very consistent with earlier concepts of wear resistance. The higher carbon and higher hardness materials performing, in general, better than the lower carbon and lower hardness materials.

A case which deserves special mention here is the performance of the B_{HH} group in the Unit Coal Service Test. Of the same nominal carbon level as the class B group its overall Brinell hardness was only slightly higher, about 30 BHN. (This higher hardness being attributed to the more rapid cooling rate, combined with the finer austenitic grain size, probably producing a reduction in pearlitic spacing). Flange wear rates were, on average, 25% lower in the B_{HH} group than the B group. The role of material toughness however may be significant in inhibiting the flow/ductile fracture mechanism of flange wear. The B_{HH} group exhibiting a much improved, K_{IC} of 54.2 versus 40.2 ksi/in (191. versus 142. kg-mm^{-3/2})

for the B group. This was an obvious result of its finer austenitic grain size and was not too adversely effected by the lower pearlite spacings.

Wear Mechanisms

Microstructural examination of wheels removed from the FAST test give indications of the wear mechanism involved. As shown in Figure 8, the area

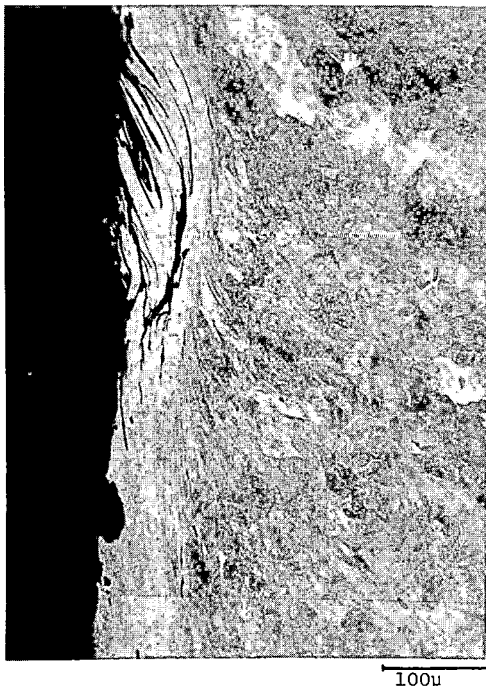
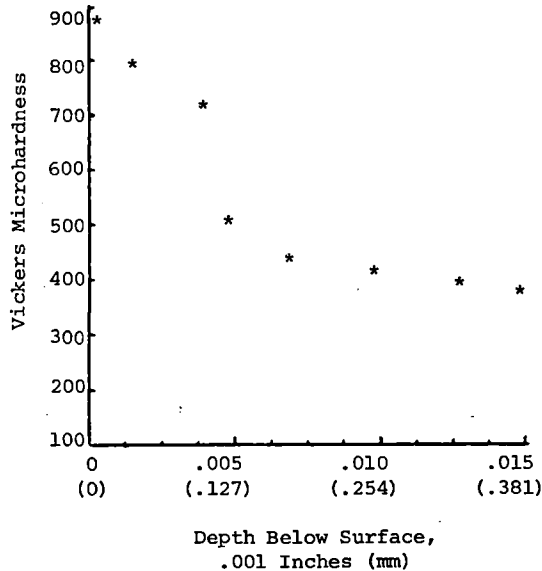


Figure 8 Bottom photomicrograph is of worn flange surface (Nital Etch). Top curve shows Vickers microhardness change with depth.

near the surface of the flange exhibits a great degree of metal flow and deformation. The shallow depth and directional flow of this region reveals the high tangential forces operative. The top portion of Figure 8 demonstrates the extreme but shallow hardening in the wear region. A transition of from 900 to 450 BHN through the heavily flowed region is shown. Also evident in the photomicrograph is the degree of microcracking associated with the loss of material. While it's difficult to determine in two dimensions, the cracks appear to be of surface or of near surface origin.

The magnitude of the coefficient of friction which results in the severe surface flow, has a dramatic effect upon the appearance of the flange, Figure 9. The top view of a well lubricated flange does not show the signs of the severe metal flow, and subsequent metal removal, as indicated in the bottom view of the same wheel in an unlubricated environment. In this case it maybe possible that the flow/fracture mechanism is supplanted by a sub-surface delamination mechanism similar to that proposed by Suh¹². Under these conditions, this mechanism would result in necessarily milder wear rates which is supported by the varying wear rates in the Wheels IV experiment at FAST.



Figure 9 Appearance of flange surface after lubricated (top) and unlubricated (bottom) running at FAST.

CONCLUSIONS

- Results from the Unit Coal Service Test indicate a strong positive dependence of flange wear rate upon carbon content. A similar although less dramatic effect was the influence of hardness on flange wear.

- Indications are that material fracture toughness has a significant impact on reducing the susceptibility to flange wear mechanisms.

- The magnitudes of flange wear rates and the overall ranking of different material types are affected by the service environment of the wheel such as rail lubrication, percentage of curves, and speed.

- Large variations exist in flange wear rates for wheels within a given test group indicating that appreciable variability exists in the service environment. Besides confounding wheel service tests, the implication is that this variability may overshadow the effect of material type.

REFERENCES

- 1 Railroad Wheels, Simmons-Boardman Publishing Company, Omaha, Nebraska, 1978.
- 2 Moore, M. A., "A Review of Two-Body Abrasive Wear," Source Book on Wear Control Technology, American Society for Metals, Metals Park, Ohio, 1978.
- 3 Gensamer, M., Pearsall, E. B., Pellini, W. S., Low, Jr., J. R., Transactions of the ASM, 30, 1942, p. 983.
- 4 Brick, R. M., Gordon, R. B., Philips, A., Structure and Properties of Alloys, p. 273, McGraw-Hill Company, 1965.
- 5 Stone, D. H. and Steele, R. K., "The Effect of Mechanical Properties Upon the Performance of Railroad Rails" Rail Steels - Developments, Processing, and Use, ASTM STP644, 1978.
- 6 Gray, Donald E., "Major Variables That Affect Wheel Wear," Proceedings of the 1981 FAST Engineering Conference, 1982.
- 7 Kahle, V. E., Leary, J. F., "Wear Rates of Freight Car Wheels as a Function of Chemistry," Proceedings of the 1981 FAST Engineering Conference, 1982.
- 8 Allen, R. A., Jollay, J. P., "Radial Truck Experiment-Preliminary Observations Prior to Restart," FAST/TTC/TN-81/02.
- 9 Marcotte, P. P., Mathewson, K. J. R., Caldwell, W. N., "Improved Wheel Tread Profiles for Heavy Freight Vehicles," ASME 80-RT-3.
- 10 Statistical Package for the Social Sciences, is a system of computer programs developed by McGraw-Hill Book Company, New York.
- 11 Steele, R. K., "Observations of In-Service Wear of Railroad Wheels, and Rails Under Conditions of Widely Varying Lubrication," Transportation Test Center, Pueblo, CO, 1981.
- 12 Suh, N. P., "An Overview of the Delamination

Theory of Wear," Wear, 44 (1977).

APPENDIX

SI Conversions of Tables

Table IIIA Summary of Mechanical Properties^a

Group	BHN	Yield Stress Mpa	Tensile Stress Mpa	K_Q/K_{max} $Kg-mm^{3/2}$	Valid K_{Ic} ?
U _{LC}	240	385.	771.	176.6/198.9	No
U _{HC}	272	486.	932.	134.5/169.2	No
B	318	710.	1032.	142.3/155.4 ^b	Yes
B _{HH}	347	805.	1159.	191.8/196.8	Yes
C	338	766.	1232.	158.6/158.6 ^b	Yes

^aValues presented for BHN, Yield and Tensile Strengths are averages. Range for BHN was ± 10 BHN, for Yield and Tensile, ± 69 Mpa.

^bValues for the B and C materials were obtained from wheels similar to those reported on here. The values for the other test groups were obtained from the actual unit coal service test heats.

Table IVA Mean Flange Wear Rates in Unit Coal Service by Test Group. Wear Rates shown are cm per 10⁶ km.

Group	0-35398 All Whls	28962 & Up All Wheels	Ratio ^a	28962 & Up Worst Whls ^b	Ratio
U _{LC}	7.51	0.975	3.09	1.409	1.87
U _{HC}	7.74	0.609	1.93	0.978	1.30
B	8.82	0.944	2.99	1.510	2.00
B _{HH}	8.69	0.705	2.23	1.219	1.62
C	8.31	0.316	1.00	0.754	1.00

^aRatio is with respect to the best wearing group in the "steady state" distance interval beyond 28962 miles.

^bAverage is of worst wearing wheel per axle for a test group.

Table VA Comparison of Flange Wear Rates and Ratios in Coal Service Test and FAST Wheel Tests^a

Group	Wear Rates				Ratios			
	Coal	Wheels IV ^b	Wheels IV ^c	Wheels II ^d	Coal	Wheels IV ^b	Wheels IV ^c	Wheels II ^d
U _{LC}	0.975	31.5	3.6	2.51	3.09	3.33	3.29	1.43
U _{HC}	0.609	28.4	1.4		1.93	2.25	1.29	
B	0.944	22.0	1.2	---	2.99	1.75	1.14	---
B _{HH}	0.705	---	---	---	2.23	---	---	---
C	0.316	12.6	1.1	1.75	1.00	1.00	1.00	1.00

^aCentimeters per 10⁶ kilometers in steady state

^bTo 11263 km unlubricated running

^c11263 to 33789 km lubricated running

^dGriffin wheels only, from 8045 to approximately 160900 km. Test wheels were of nominal class U and C chemistry, which did not necessarily coincide with other test groups.

Kenji Hirakawa

Central Research Labs.
Sumitomo Metal Industries

Kazuo Toyama

Central Research Labs.
Sumitomo Metal Industries

Sigeru Suzuki

Head Office
Sumitomo Metal Industries

Atsushi Hamazaki

Osaka Steel Works
Sumitomo Metal Industries
Amagasaki
Japan

Effects of Chemical Composition and Microstructure on Wear Properties of Steels for Railroad Wheel

To develop wear resistant wheel steels for heavy duty use, the rolling sliding contact tests have been conducted. The results show that a high wear resistance is achieved by a fine spacing and a large volume fraction of pearlite, and that an austenite grain size has no influence on the wear properties, and that in plain carbon steels a wear resistant martensite is inferior to that of ferrite pearlite at the same hardness level. In contrast, with an alloy steel such a difference does not exist and a single weight loss versus hardness curve is drawn regardless of microstructure. Based on the results of the present study, the improved wear resistant wheel steel whose fracture toughness is also improved by grain refinement has been developed and manufactured.

1 INTRODUCTION

The recent trend in railway industry toward increased axle load and operating speeds causes wheel to meet with two major problems. One is the wheel fracture which leads to the serious traffic accident and the another is the excessive wear. Particularly, introduction of 100 ton cars put forward these problems economically(1). The performance against fracture is determined from the wheel configuration(2) as well as the material properties of wheel steels where low susceptibility to thermal cracking and high fracture toughness are strongly demanded.

Many studies have been conducted on the mechanisms of thermal crack initiation(3)(4) and on the development of wheel steels which have the lower susceptibility to thermal cracking(5)-(9) and the higher fracture toughness(10)(11). Many of these studies have indicated that low carbon content and quenched and tempered heat treatment are desirable for the above properties.

While, wear resistance is thought to be achieved by higher hardness. P. Clayton(12) has obtained that wear behavior of pearlite steel strongly depends on its carbon content. M.A. Babb and M.J. Lee(13) have found that wear resistance of martensite is inferior to that of ferrite-pearlite at the same hardness levels. The similar results are reported by F. Hergenbarth(14). From these studies, carbon content increased to get a high wear resistance. It should be noted that the improvement of wear resistance by increasing hardness or carbon content inevitably decreases the fracture toughness as well as the performance against thermal cracking.

On the contrary, M. Kraus and J. Scholten(15)

have shown that the wear resistance of wheel steels depend not only on the nature of the material itself but also on the kind of mated rail steel. Moreover, W.E. Jamison (16) pointed that these behaviors are significantly affected by atmosphere. These results indicate that a further research about wear behavior of wheel steels is necessary to obtain more detail informations.

On the other hand, a great effort has been made to develop the new rail steels which have the higher fracture toughness(17)(18) and higher wear resistance (19)(20). These studies on rail steel can contribute to the development of wheel steel.

The purpose of the present study is to clarify the effect of chemical compositions, hardness and microstructures on the wheel steel wear from the point of practical application.

2 EXPERIMENTAL MATERIALS AND PROCEDURE

2-1 Materials

The standard AAR class B and U wheel steels and modified AAR class B, C and U wheel steels were investigated. The chemical composition of these steels are listed in Table 1. In this table, #1 and #2 steels are the standard ones, and #3 to #11 except #7 steels are the grain refined ones to get a higher fracture toughness by adding aluminum, niobium and vanadium elements. Furthermore, #7 to #11 steels are micro-alloyed for good hardenability and solid solution strengthening, so that these steels are expected to have a higher hardness. #12 is the alloy steel to compare the wear behavior of alloy steel with these of the carbon steels. #13 is a rail steel used for the mated test piece.

2-2 Test piece

Test pieces are machined as shown in Fig. 1 from block of about 100 mm in section and 200 mm in length which is taken from a rim of wheels. To know the effect of hardness on wear of wheel steel with the same chemical composition, some blocks are additionally heat treated of a different cooling rate or tempering

temperature as shown in Table 2.

All test pieces except #4-H and #12-H have a ferrite pearlite structure. While, test pieces of #4-H and #12-H have been heat treated after machining to obtain a martensite structure.

Table 1 Chemical compositions (wt %)

No.	C	Si	Mn	P	S	Cr	Remarks
1	0.63	0.24	0.66	0.029	0.022	—	—
2	0.67	0.32	0.73	0.022	0.015	—	—
3	0.60	0.28	0.76	0.023	0.021	—	Grain Refined
4	0.66	0.33	0.65	0.009	0.010	—	"
5	0.69	0.28	0.76	0.026	0.024	—	"
6	0.70	0.28	0.75	0.036	0.026	—	"
7	0.64	0.53	0.76	0.014	0.012	0.43	—
8	0.73	0.52	0.84	0.013	0.007	0.50	Grain Refined
9	0.70	0.63	0.78	0.009	0.005	0.19	"
10	0.74	0.63	0.80	0.008	0.004	0.20	"
11	0.72	0.60	0.83	0.015	0.004	0.64	"
12	0.45	0.31	0.73	0.014	0.015	1.0	Mo; 0.31
13	0.71	0.26	0.67	0.035	0.021	—	—

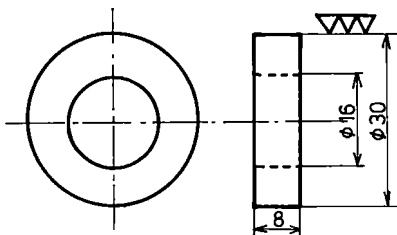


Fig. 1 Test piece

Table 2 Heat treatment and hardness

No.*	Heat treatment	Hardness (HB)	No.	Heat treatment	Hardness (HB)
1	850°C → R.Q 490°C → AC	284	6-L1	As Roll	269
2	As Roll	308	6-L2	"	260
			6-H	"	331
3-L	850°C → OQ 500°C → AC	293	7-H	850°C → OQ 500°C → AC	357
3-H	" 400°C → AC	321	8-L	" 500°C → AC	337
4-L1	850°C → F.C	219	8-H	" 450°C → AC	371
4-L2	850°C → AC	256			
4-H1	850°C → OQ 650°C → AC	246	9	As Roll	326
4-H2	" 600°C → AC	271	10	"	320
			11-L1	"	319
4-H3	" 500°C → AC	339	11-L2	"	292
			11-H	"	352
4-H4	" 400°C → AC	399	12-L	850°C → FC	212
5-L	" 520°C → AC	321	12-H1	850°C → WQ 670°C → AC	256
			12-H2	" 550°C → AC	367
5-H	" 450°C → AC	340			

* L,H indicates the lower hardness and the higher hardness, respectively.

2-3 Test apparatus

All the test was made by an Amsler type wear testing machine at a rotating speed of 400 rpm in laboratory air under rolling-sliding contact of two rollers which simulate the wheel/rail contact system. The slip ratio between two rollers is 3% and some tests are additionally made at 10% slip. Tests were continued up to 5×10^5 revolutions at a contact load of 780 N. The weight loss was measured intermittently during the test.

3 RESULTS AND DISCUSSION

3-1 Effect of hardness

The weight loss of the wheel rollers after 5×10^5 rev. is listed in Table 3 and is plotted in Fig. 2. It is shown that a wear resistance seems to increase with the hardness but its correlation is not so satisfactory. Therefore, another factor is expected to have an influence on the results. The results of #3, #5, #7 and #8 indicate that the higher hardness obtained by lower tempering temperature does not improve wear resistance of ferrite pearlite structure of the same chemical compositions. Whereas, in martensite structure, as it will be described later, tempering temperature affects a wear behavior.

On the contrary, the wear resistance of the higher hardness steel obtained by a higher cooling rate (#4-L2) is much greater than the lower hardness steel (#4-L1).

Table 3 Weight loss of wheel rollers after 5×10^5 revolutions

No.	Weight loss (g)	No.	Weight loss (g)
1	1.39	8-L	0.40
2	1.13	8-H	0.46
3-L	1.54	9	0.31
3-H	3.75	10	0.43
4-L1	1.32	11-L1	0.42
4-L2	0.62	11-L2	0.42
5-L	0.69	11-H	0.37
5-H	0.93	1*	1.81
6-L1	0.96	2*	1.09
6-L2	0.33	4-L1*	3.55
6-H	0.83	4-L2*	1.82
7-L	0.50	7-L*	1.36
7-H	0.63	7-H*	1.33

* test under 10% slip ratio

3-2 Effect of carbon content

The weight loss is also plotted against carbon content in Fig. 3. The correlation between them is similar to the below Fig. 2, and #7 to #11 steels are recognized to have a higher wear resistance than these of the other steels having the same carbon content. It is also shown that the grain refined steels (#3 to #6) have nearly the same wear resistance as the standard wheel steels. Accordingly an austenite grain size seems to have no influence on the wear properties. The reason why a certain tendency in the relationship between wear resistance and carbon con-

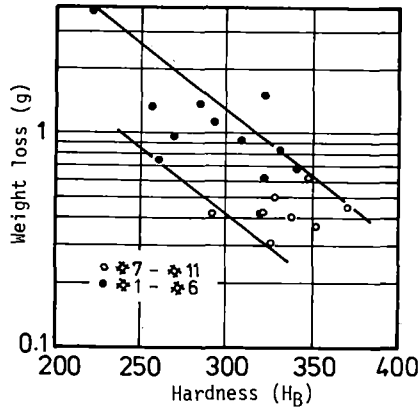


Fig. 2 Relationship between weight loss and hardness

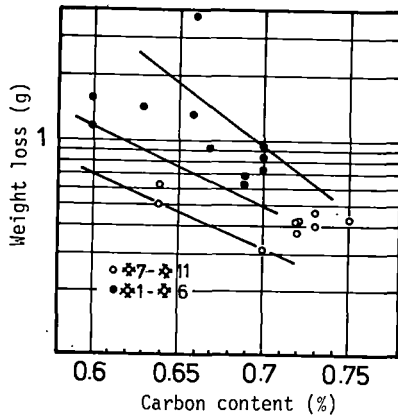


Fig. 3 Relationship between weight loss and carbon content

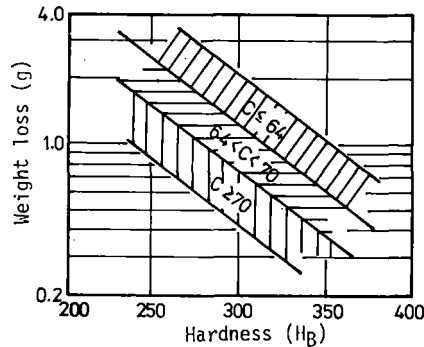


Fig. 4 Effect of hardness and carbon content on weight loss

tent regardless of the hardness levels is because the all microstructure used are ferrite pearlite so that the carbon content represents the mechanical properties to some extent.

From Figs. 2 and 3, the weight loss can be estimated by the hardness and carbon content. The result is shown in Fig. 5. This means that a pearlite lameller spacing and a pearlite volume fraction play a significant role in wear behaviors because a volume fraction of pearlite and a lameller spacing are determined from carbon content and cooling rate. Therefore, these effect will be examined quantitatively.

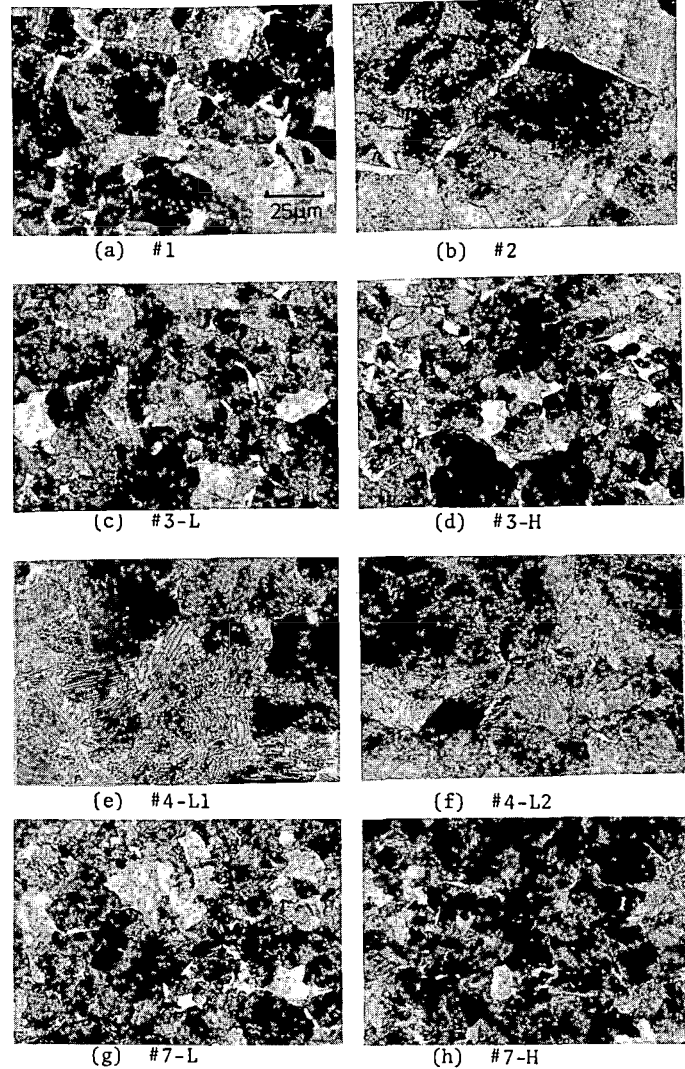


Fig. 5 Examples of optical micrographies

Examples of the microstructure obtained by an optical and a two stage replica electron microscopes are shown in Figs. 5 and 6. A lameller spacing and a volume fraction are measured from these photographs. The effect of a lameller spacing on the weight loss is represented in Fig. 7. In this figure, the points encircled by a dotted line are the results of test pieces taken from as rolled wheels (class U). It can be shown that a wear resistance strongly depends on a pearlite lameller spacing (Recall that a vertical axis is the normal scale in Fig. 7 and is the logarithmic in Figs. 2 and 3) and this dependency is slightly different in as rolled wheel steels. Not enough information has yet been obtained to explain the cause of this difference but it can be noted that the microstructure of as rolled steels have a coarser pearlite colony than that of other heat treated steels as shown in Fig. 6-(b).

A possible source of the fact that an additional hardness by lowering a tempering temperature does not contribute to a wear resistance is that a pearlite lameller spacing is independent upon a tempering temperature as illustrated in Fig. 6(C)(D) and (G)(H). Whereas a cooling rate has a significant influence on a spacing as shown in Fig. 6(E)(F). Therefore, high wear resistance can be achieved by increased a cooling

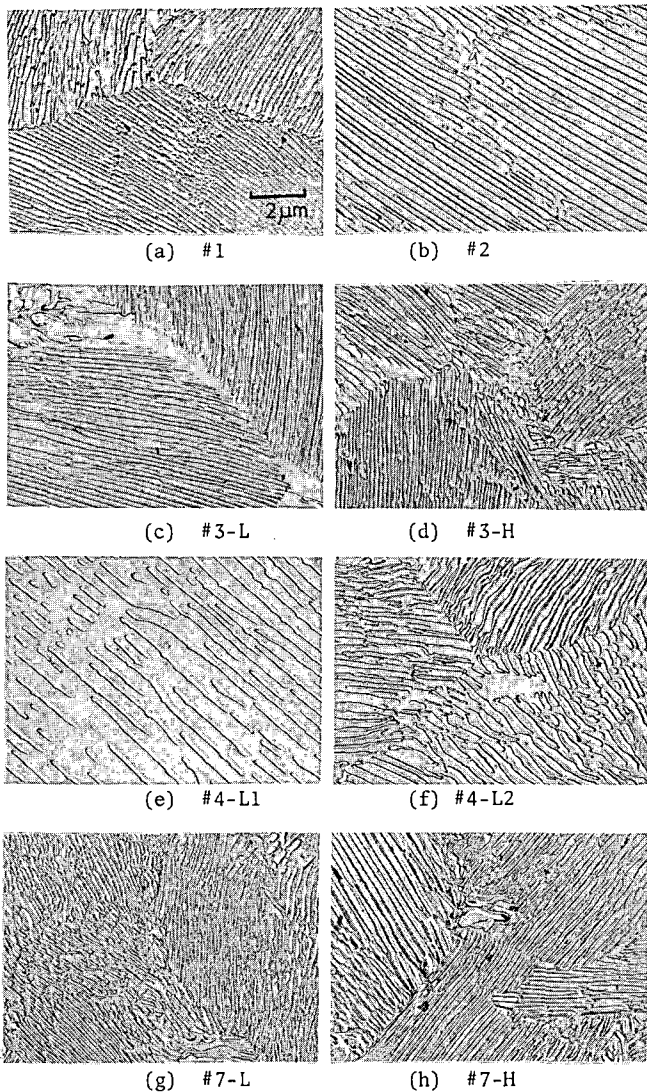


Fig. 6 Examples of two stage replica electron microphotographies

rate.

The weight loss is plotted in relation to a pearlite volume fraction in Fig. 8. It is shown that a small volume of ferrite decreases a wear resistance and the relationship is slightly different between the group of #7 to #11 wheel steels and #1 to #6 ones. The former group shows higher wear resistance than the later group at the same volume of ferrite. The reason may be that #7 to #11 wheel steels are added silicon and chromium elements so that the fine pearlite are precipitated under the same cooling rate and that ferrite is strengthened by solid solution.

When a hardenability becomes too high, a small bainite phase is formed and hardness becomes very high. But the mixed structure of ferrite, pearlite and a little bainite, for example #7, #8, #6-H and #11-H steels, is not so improved in spite of its high hardness. Ichinose et al. (19) shows that a wear resistance of bainite is inferior to that of other structure in alloy steels for rail. In the present study, however, bainite phase is very limited in volume, accordingly it is not clear whether the bainite is favorable or harmful to wear.

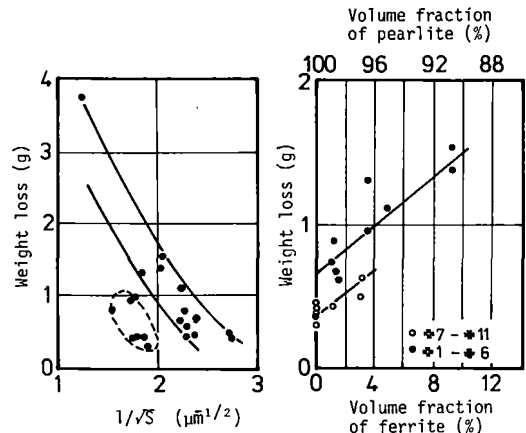


Fig. 7 Effect of a pearlite lameller spacing (S) on weight loss

Fig. 8 Effect of a pearlite volume fraction on weight loss

3-3 Effect of slip ratio

The ratio of the weight loss under 3% slip to 10% slip is plotted versus hardness in Fig. 9. In this figure, two dotted lines indicate the ratio ($W_{10\%}/W_{3\%}$) of 1 and 10/3 respectively. The former means that no effect of slip ratio exists and the later is followed by the Holm-Archard equation. It can be seen that little effect of slip ratio is recognized where hardness is less than 220 H_B and that it becomes remarkable with the increase of hardness. These behavior may be depend on the experimental condition i.e. whether the Hertzian stress is higher than the yield strength of wheel steel or not. This means that when an applied axle load is too high, the expected wear resistance of the high hardness wheel may not be obtained under a large slippage such as on a small curvature track line. Therefore, the results must be carefully interpreted taking the condition of an actual wheel/rail system into consideration.

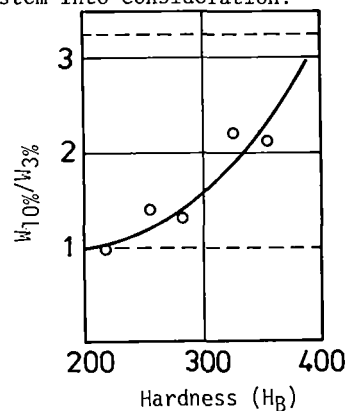


Fig. 9 Effect of slip ratio on wear behavior of wheel steels

3-4 Effect of microstructure

The weight loss of #4-H and #12-H steels whose structures are martensite is plotted versus hardness in Fig. 10. In martensite, hardness is changed by tempering temperature which determines a dislocation density and a carbide morphology. Replica images of these microstructure are illustrated in Fig. 11. Large and spherical carbide are formed by increasing of tempering temperature. The following results can be noted from Fig. 10. Firstly, in case of plain

carbon steel (#4), ferrite pearlite structure has superior wear resistance of about 3 times as that of martensite, regardless of the hardness because hardness versus the weight loss curves of these structures are parallel each other in the wide range of hardness. Secondly, in case of alloy steel (#12), wear behavior does not affected with microstructure but with hardness only. Therefore, a single curve of the weight loss versus hardness could be fitted for

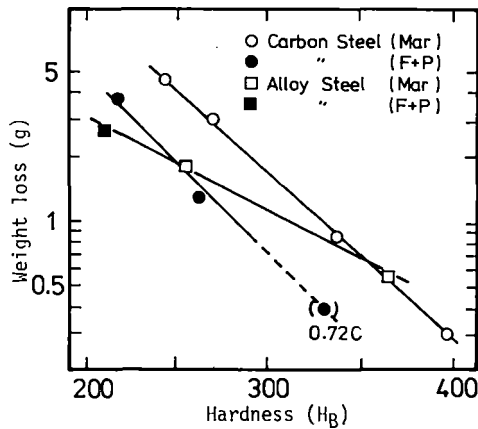


Fig. 10 Effect of microstructure on wear behavior of alloy and carbon steels

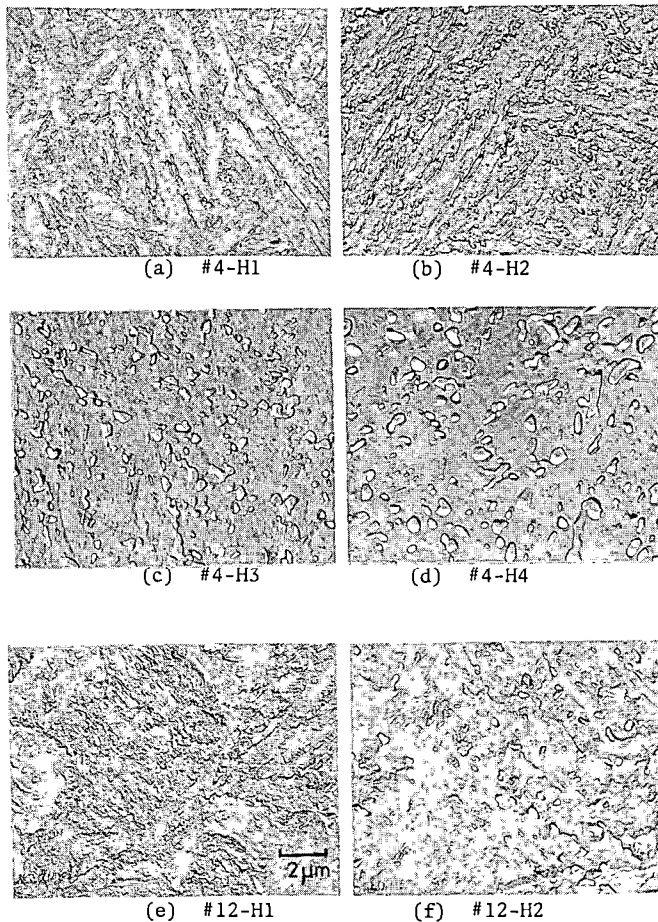


Fig. 11 Two stage replica electronmicrographs of martensite used

both structure. Thirdly, gradient of these three curves are not the same. The gradient of the alloy steel is smaller than that of the plain carbon steel. As a result, the curve of the alloy steel intersects ones of the carbon steel at two points. This points are 375H_B in ferrite pearlite's curve and 270H_B in martensite's one. In the hardness range lower than this point, the wear resistance of the alloy steel is superior to that of high carbon steel. These behavior may depend on chemical composition of an alloy steel. Namely, it is prospective to find out the suitable chemical composition for wheel steel whose wear resistance in higher over a wide range of hardness than that of high carbon steels currently used.

4 CONCLUDING REMARKS

To develop wear resistant wheel steels, the rolling-sliding contact tests have been conducted. The following conclusions are obtained.

- (1) Carbon contents is an important factor for the improvement of wear resistance in ferrite pearlite wheel steel and silicon and chromium elements have also a favorable influence. But aluminum, niobium and vanadium elements as a grain refinement element have little effect on wear behavior of these steels tested.
- (2) A wear resistance of wheel steels is improved by hardness. But the higher hardness obtained by lower tempering temperature does not contribute to wear resistance on ferrite pearlite wheel steels.
- (3) Taking into account of hardness and carbon content simultaneously, the exact prediction of wear can be made. This means that a pearlite lameller spacing and a volume fraction of pearlite has a great influence on a wear resistance. A high wear resistance is achieved by a fine spacing and a large fraction of pearlite.
- (4) In a plain carbon steel, a wear resistance of martensite is inferior to that of ferrite pearlite at the same hardness levels. While in an alloy steel, such a difference does not exist and a single curve of weight loss vs hardness can be drawn regardless of microstructure.
- (5) The hardness dependence of wear resistance in an alloy steel is weaker than in a carbon steel. As a result, an alloy steel has higher wear resistance in the low hardness range than a carbon steel.

Based on the results of the present study, the improved wear resistance wheel steel whose fracture toughness is also improved by grain refinement has been developed and manufactured. Furthermore, to achieve the marked improvement of fracture toughness and thermal crack, an alloy steel for railroad use may be developed in the near future.

ACKNOWLEDGEMENT

The authors gratefully acknowledge Dr. Kunio Nishioka and Dr. Yoshiaki Masuko for their support and encouragement.

Reference

- (1) J. Kalousek and A.E. Benthune; "Rail Wear under Heavy Traffic Conditions" ASTM STP 644 (1978) .63
- (2) K. Hirakawa, H. Sakamoto; "Effect of Design Variation on Railroad Wheel Fracture" ASME 81-WA/RT-4 (1981)
- (3) J.L. van Swaaij; "The Mechansim of Thermal Cracking in Railway Wheels" 3rd Int. Wheelset Congress paper No. 11 (1969) Sheffield
- (4) J.L. van Swaaij; "Thermal Damage to Railways Wheels" Int. Conf. on Railway Braking C176/79 (1979) IME

- (5) G.C. Hewitt and C. Musiol; "The Search for Improved Wheel Materials" *ibid* C176/79 (1979) IME
- (6) P. Brozzo, L. Callegari, L. Brazzoduro, R.De. Martini and C. Bianchi; "Development of Quenched and Tempered Solid Wheel and its Evaluation by means of Drag and Stop Tests" 5th Int. Wheelset Congress vol. 1 paper 10 (1975) Tokyo
- (7) L. Brazzoduro, P. Brozzo, R. Domartini and T. Venturelli; "Final Results of the Research Work on a New Solid Wheel apt to the Most severe Operative Condition" vol. 1 paper 4, 6th Int. Wheelset Congress (1978) Colorad
- (8) A.S. Babb, D.S. Hoddinott and D.J. Naylor; "Wheelset Research and Development in British Steel Corporation" 5th Int. Wheelset Congress vol. 1 paper 2 (1975) Tokyo
- (9) K. Forsh; "Developing and Testing of New Wheel Steels with Improved Wear and Thermal-Shock Behavior" *ibid* vol. 2 paper 1 (1975) Tokyo
- (10) T. Kigawa, R. Isomura, Y. Tanaka and K. Tokimasa; "High-Toughness Steel for Railroad Solid Wheel" *ibid* vol. 1 paper 11 (1975) Tokyo
- (11) K. Nishioka, K. Hirakawa, H. Sakamoto, K. Toyama, S. Suzuki and A. Hamasaki; "Development of Improved Railroad Wheels" 7th Int. Wheelset Congress session A paper 6 (1981) Vienna
- (12) P. Clayton; "The Relationship between Wear Behavior and Basic Material Properties for Pearlite Steels" *Wear* 60 (1980) 75
- (13) M.A. Babb and M.J. Lee; "The Laboratory Wear testing of Tyre and Wheel Steels" 4th Int. Wheelset Congress vol. 2 paper 16 (1972) Paris
- (14) F. Hergenbarth; "Operational Tests with Different Wheel Tire" Steels 3rd Int. Wheelset Congress (1966) 179 Munch
- (15) H. Krause and J. Scholten; "Factors Influencing the Frictional and Wear Behavior of the Wheel/Rail-System" 5th Int. Wheelset Congress vol. 1 paper 6 (1975) Tokyo
- (16) W.E. Jamison; "The Wear of Railroad Freight Car Wheels and Rail" *J. of ASLE* July (1980) 401
- (17) S. Marich and P. Curio; "Development of High-Strength Alloyed Rail Steels Suitable for Heavy Duty Applications ASTM STP 644 (1978) 167
- (18) G.K. Bouse, I.M. Bernstein and D.H. Stone; "Role of Alloying and Microstructure on the Strength and Toughness of Experimental Rail Steels" *ibid* (1978) 145
- (19) H. Ichinose, J. Takehara, N. Iwasaki and M. Ueda; "An Investigation on Contact Fatigue and Wear Resistance Behavior in Rail Steels" 1st Int. Heavy Haul Railway Conf. session 307 paper I.3 (1978) Perth
- (20) J.D. Young and W.H. Hodgson; "The Development and Manufacture of High Tensile Wear Resistance 1% Chromium Rails for Heavy Duty Applications" *ibid* session 217 paper H.4 (1978) Perth

The Wear Mechanism of the Railroad Wheel Steel in the Free Rolling and Braking Conditions

V. Aronov

Assistant Professor
Dept. of Mechanics
Mechanical & Aerospace
Engineering, Illinois
Institute of Technology
Chicago, Illinois

M. Pons

Engineer
Dept. of Mechanics
Mechanical & Aerospace
Engineering, Illinois
Institute of Technology
Chicago, Illinois

The experimental investigation of the wear mechanisms of the railroad wheel steel is carried out in the free rolling and braking conditions. The SEM analysis of the friction track, x-ray analysis of the wear particles, statistical analysis of the wear particles and amount of material lost have shown that plastic deformation with subsequent fatigue, oxidation (mild wear) and adhesion (severe wear) mechanisms are responsible for the wear particle formation. The occurrence of this mechanism and transition from one mechanism to another is discussed. An attempt is made to relate wear to the mechanics of rolling contact.

NOMENCLATURE

A_i	constant
A_0	adhesion area
A_c	contact area
A_s	microslip area
A_{sr}	microslip real contact area
A_r	real area of contact
A_{or}	real contact area
A'_{or}	adhesion real contact area
a	constant
a_0	contact area major semi-axis
a_0'	adhesion area major semi-axis
b_0	contact area minor semi-axis
b_0'	adhesion area minor semi-axis
K	constant
K'	constant
n	constant
s	standard error
R	regression coefficient
Var	variance
w	wear
\bar{X}_L	average length
\bar{X}_w	average width
α	a_0/a_0'
β	μ/μ_m
γ	A_s/A_0
μ	coefficient of friction
μ_m	limited coefficient of friction
σ	standard deviation

INTRODUCTION

The proper selection and development of a new railroad wheel and rail materials in order to reduce the rate of material removal (wear) from the contacting surfaces are presently restricted by the lack of theoretical and experimental data related to the nature of the mechanisms responsible for wear particles formation.

The principal wear mechanisms reported up to date (1-3) are abrasion, adhesion and tribochemical reactions. The individual proportion of these mechanisms are dependent on creep. In the range of creep of up to 1%, the wear always begins as pure tribo-oxidation. The tangential force causes increase in the surface chemical activity that leads to compact oxide formation. The shear stresses and oxide volume increase during the growing process breaks up the oxide layer to form wear particles contained 70-80% $\alpha\text{Fe}_2\text{O}_3$. After the rolling conditions have been stabilized, "the wear particles consists of approximately half each of $\alpha\text{Fe}_2\text{O}_3$ and αFe ; as, together with the tribo-oxidation, adhesive and abrasive wear components are also acting" (3).

Beagley (4) indicated transition from mild (oxidative) wear to severe (adhesive) wear for B11 rail steel. This transition can be brought about by increasing the creep rate between 0 and 3% or by increasing the contact stress. He related this transition to the shake down limit, using Johnson's (5) approach. Jamison (6) found that wear proceeds by one or two mechanisms; smearing wear or flow-fatigue wear, which differ in metal loss rates by factors of ten to one hundred. The low rate flow-fatigue type of wear occurs when the normal forces between the wheel and rail produce subsurface shear stresses which exceed 2.32 times the yield stress of the material. Smearing wear occurs when a tractive force is superimposed on the normal force such that the subsurface plastic flow boundary is brought to the surface.

All investigators used approximately the same experimental technique in which the microslip (creep)

and normal force were controlled. This paper represents data of the wear mechanisms study in the free rolling and braking conditions. The wear measurement, statistical analysis of the wear particles, x-ray examination of the wear particles and SEM analysis of the friction track allowed to gain more insight into the nature of wear particles formation. An attempt is made to relate wear to the mechanics of the rolling contact area development.

EXPERIMENTAL PROCEDURE

The Test Machine

Test Machine consists of lower cylindrical (76.2 dia.) and upper toroidal (63.5 mm) wheels pressed against each other by the dead weight. Toroidal shape of the sample was chosen because it was felt that point contact rather than line contact is a better simulation of the field condition. Dead weight and toroidal radius were kept constant to insure 1448.3 MPa contact pressure that corresponds to 100T railroad car. Lower cylindrical wheel was driven by D.C. electric motor with approximately 600 rpm. The air operated brake was mounted on the axle of the upper toroidal wheel that allowed changing the coefficient of friction from 0 to 0.4. The friction force was measured by strain gages mounted on the arm connecting brake with machine foundation. Two electro-magnetic impulse gages connected to the differential impulse counter were used to measure the ratio of the rotational speeds of both axes. Special electro-magnet was designed to collect wear particles. Wear particles were collected using D.C. current. After required amount of wear particles was collected, the alternating cycles were used to demagnetize them.

Both samples of 20RHN were manufactured from the same U class wheel material contained about .7% carbon. Two experimental series were conducted. First series comprises "free" rolling mode, i.e., rolling without application of the braking torque. In this condition, the friction force was almost zero. After each 10^5 cycles both wheels were removed from the machine. The sample (cylindrical wheel) was subjected to the following analysis: weight lost measurement (accuracy 10^{-4} g), scanning electron microscope examination of the tread surface, measurement of the track profile by means of Talysurf -10 profilometer, shape and size distribution analysis of the wear particles, wear particles x-ray examination. At the same time, the bottom (toroidal) wheel was resurfaced that allowed to keep contact stresses almost constant during experiment.

In the second series, the braking torque was applied to the cylindrical wheel. Torque was applied by steps so that coefficient of friction was increased from .04 to .22 by increments of .04. Wheels were run 5×10^4 cycles and sample was subjected to the same analysis as in the first series.

RESULTS

The friction track profiles for free rolling conditions are shown in Fig. 1. Removal and mounting of the wheel after each 10^5 cycles led to lateral and angular misalignments that affected formation of the track. The lateral misalignment causes material to be replaced toward on particular side of the track. Considering growth of the track depth (Fig. 2), it becomes apparent that angular misalignment causes much larger plastic deformation that it is only due to "pure" rolling action. The rate of track depth growth is order of magnitude larger after 5 and

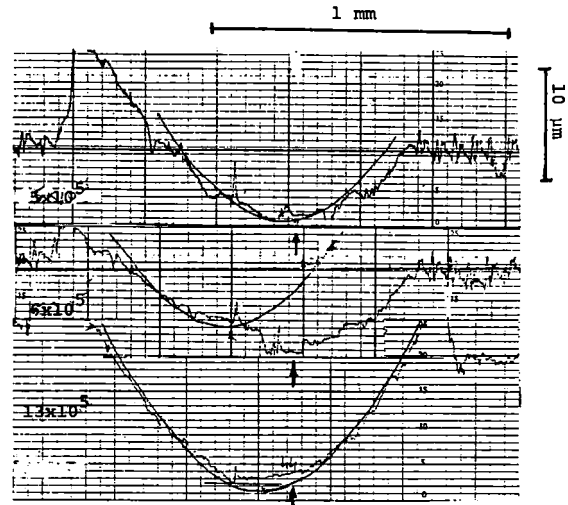


Fig. 1. Talysurf Cross Section Track Profiles made in the Free Rolling Experiment after 5×10^5 , 6×10^5 and 13×10^5 cycles. Arrow shows starting position of the wheels.

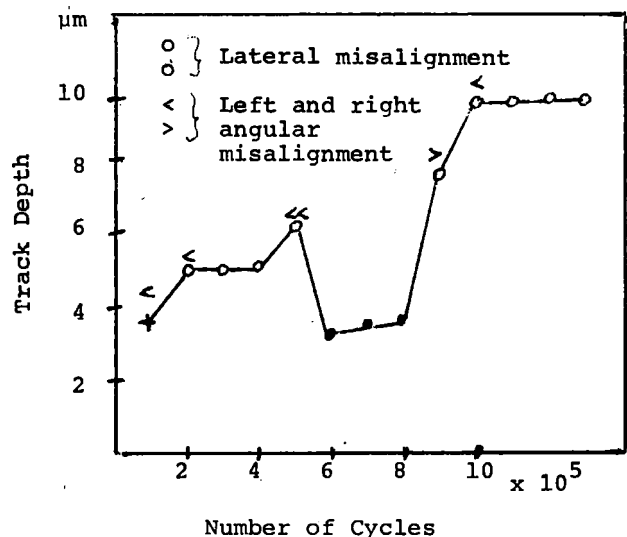


Fig. 2. The Track Depth Development in the Free Rolling Condition.

10×10^5 cycles (Fig. 2) when angular misalignment was occurred.

During the braking mode alignment of the wheels was much better and data represented track depth growth (Fig. 3) are much more consistent. The angular misalignment that occurred at .12 coefficient of friction causes deviation of this point from the smooth curve drawn. Despite that alignment in this case was better the rate of depth growth is much higher and increases with coefficient of friction. It indicates that upper layer of the material are subjected to the intensive plastic deformation.

SEM observation of the free rolling track reveals formation of the ripples directed toward sides of the track (Fig. 4a). Orientation of the ripples toward right or left side of the track depends on

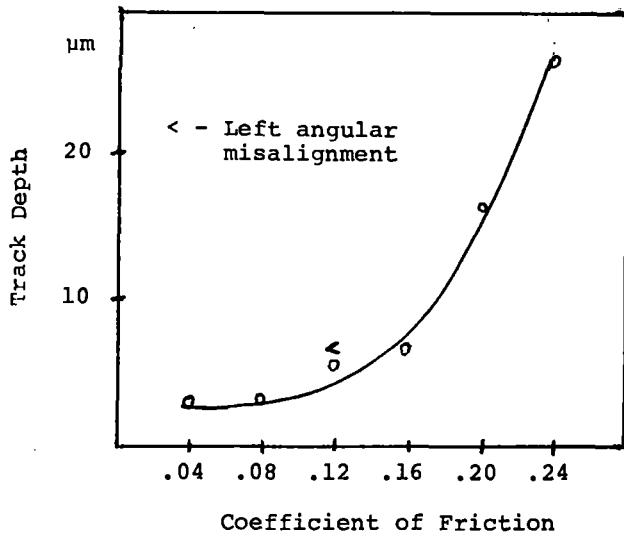


Fig. 3. The Track Depth Development in the Braking Rolling Condition.



Fig. 4b. SEM Photo of the Track in the Braking Condition (x 300 .12 coefficient of friction)

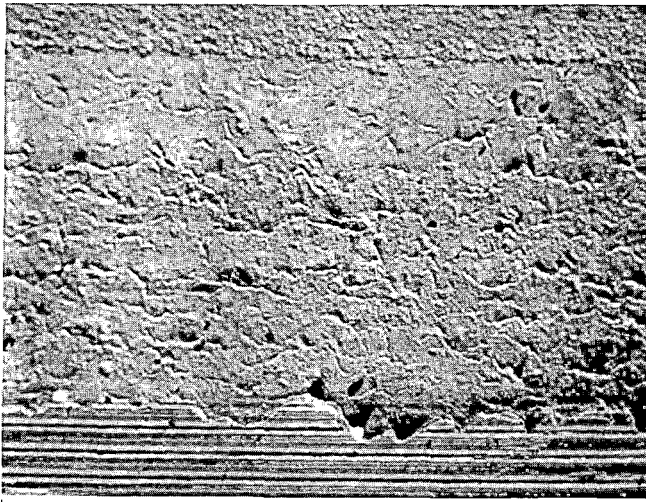


Fig. 4a SEM Photos of the Track in the Free Rolling Condition (x 100, 5×10^5 cycles)

the right or left angular misalignment. But even in the cases when angular misalignment is zero, ripples are directed perpendicular to the track indicating that direction of plastic flow in the free rolling condition is perpendicular to the rolling direction.

The braking torque causes formation of the ripples at some angle to the rolling direction. This angle depends on the friction force. The larger the friction force the better alignment of the ripples orientation with rolling direction. Figure 4b is a SEM microphotograph of the track after 2×10^5

loading cycles in the braking mode. During this time, the coefficient of friction was increased from .02 to .12. It is clearly seen that two systems of ripples are formed. One is oriented perpendicularly to the track and the other is at some (large) angle. Both systems interact with each other.

Wear behavior (material removal) in free rolling and braking conditions is quite different. No significant wear was detected during first 6×10^5 cycles in the free rolling mode (Fig. 5). The material

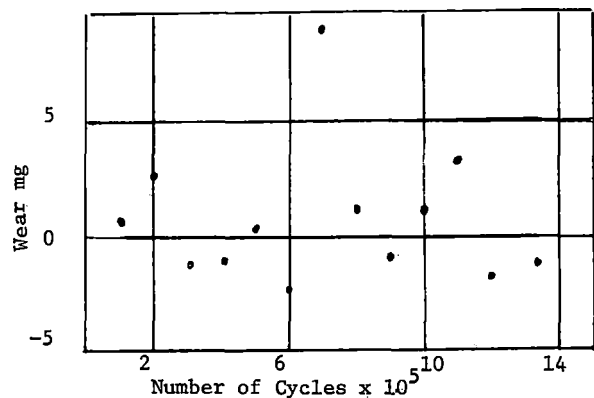


Fig. 5. Wear vs. Number of Cycles in the Free Rolling Condition.

transfer from one wheel to another very often caused the gain in the wheel weight. During the loading from 6 to 7×10^5 cycles the sudden loss of material occurred. This sudden wear was not associated with any particular misalignment. No particular change of track appearance was observed. Thus, it seems that

this sudden loss of material is associated with fatigue mechanisms. The misalignments of the wheels during preceding loading caused displacement of the material in the opposite directions finally resulting in the removal of material from the surface due to fatigue. After this happened the wear rate was reduced to approximately the same level as it was before. The rate of wear in the braking mode increases with accelerated rate with increase in the coefficient of friction (Fig. 6).

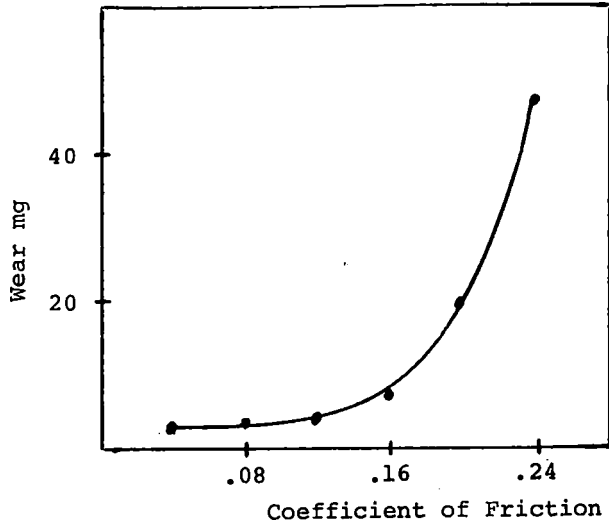


Fig. 6. Wear vs. Number of Cycles in the Braking Rolling Condition.

Due to the very small rate of wear in the free rolling mode, the amount of the wear particles collected during the first 5×10^5 cycles was not enough even to make a statistical analysis. Also the amount of the wear particles collected after 5×10^5 cycles was sufficient for statistical analysis, it was not enough for x-ray examination.

Statistical analysis of the wear particles shows (Fig. 7) that average size tends to decrease with number of cycles. Scatter of the data points for average length and average width and their standard deviations and variances depends on the lateral and angular misalignment of the wheels. The better alignment of the wheels, the wear particles formed are of the smaller length and width and have smaller distribution of their dimensions. The aspect ratio, calculated as ratio of average length and average width, changes from 1.5 to 2.4 being smaller for better alignment of the wheels.

The statistical analysis of the wear particles collected in the braking mode shows (Fig. 8) that average length, average width, standard deviations and variances increase with coefficient of friction. The deviation of the point at .12 coefficient of friction is caused by wheels angular misalignment. The aspect ratio variation is much smaller than for free rolling and is close to 2.

In this testing mode the amount of wear particles collected was not enough for statistical analysis and x-ray examination only after coefficient of friction was increased to .08 and .12 correspondingly.

The x-ray examination of the wear particles (Fig. 9) shows that intensities ratio of the Fe_2O_3 lines to the Fe lines are sharply decreased with increase in the friction coefficient.

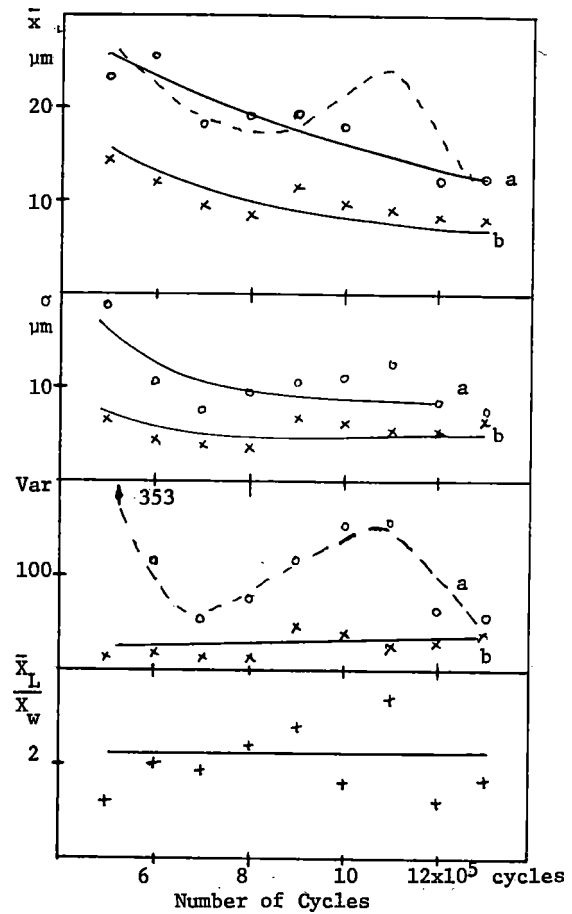


Fig. 7. The Average (\bar{x}) Dimensions, Standard Deviations (σ) and Variances (Var) of the Wear Particles Length (a) and width (b) and their Aspect Ratio ($\frac{\bar{x}_L}{\bar{x}_W}$) Variation in the Free Rolling Condition.

DISCUSSION

Before discussing the experimental results described in the previous section, let us consider the contact area between two wheels subjected to the normal and tangential forces.

In the general case this area is an ellipse and comprises the adhesion (stick) and microslip zones. The microslip (or creep) occurs on the areas where the ratio of the applied tangential stresses to the normal stresses becomes larger than the coefficient of friction. This area is adjoint to the leading edge of the contact (6) and is assumed to be of the elliptical shape. The relation between the coefficient of friction and the dimensions of the adhesive zone for the case of elastic bodies is given by (7):

$$\beta = \frac{\mu}{\mu_m} = 1 - \frac{3}{2} [\sqrt{2\alpha - \alpha^2} (1 - \frac{2}{3}\alpha + \frac{1}{2}\alpha^2) - (1 - \alpha)\sin^{-1}\sqrt{2\alpha - \alpha^2}] \quad (1)$$

For the elliptical shapes of the contact area and adhesion area, their ratio is:

$$\gamma = \frac{A'_0}{A_0} = \frac{\pi a'_0 b'_0}{\pi a_0 b_0} = \alpha \sqrt{2\alpha - \alpha^2} \quad (2)$$

$$b'_o = b_o \sqrt{2\alpha - \alpha^2}$$

Substituting for microslip area eq. (2) becomes

$$\gamma = \frac{A_s}{A_o} = 1 - \alpha \sqrt{2\alpha - \alpha^2} \quad (3)$$

All three parameters α , β and γ range from 0 to 1. Using eq. 1 and 2, it is possible to find relation between γ and β .

The best fit is a linear function:

$$\gamma = .014 + 1.13 \beta \quad (4)$$

with regression coefficient $R=.97$ and standard error $s(yx)=.06$.

The first and second coefficients of eq. (4) should equal 0 and 1 correspondingly to give:

$$\frac{A_s}{A_o} = \frac{\mu}{\mu_m} \quad (5)$$

for the ideally elastic contact and assumption that energy dissipation takes place only in the microslip area. In the case of non-perfect elastic contact, let us assume that:

$$A_s/A_o = a \left(\frac{\mu}{\mu_m}\right)^n \quad (6)$$

where coefficients a and n are functions of the material properties and environment.

In general, the rate of wear is proportional to the real contact area:

$$\omega = K' A_r \quad (7)$$

If the normal load is constant the average pressure on the adhesion and microslip zones are equal so that

$$A'_{or} + A_{sr} = A_{or} \quad (8)$$

Assuming that wear particles are formed only on the microslip zone:

$$\omega = K' A_{sr} = K A_s \quad (9)$$

Substituting eq. (9) into (6) and solving for ω :

$$\omega = a K A_o \left(\frac{\mu}{\mu_m}\right)^n \quad (10)$$

Or in a more convenient form:

$$\log \omega = \log \frac{a K A_o}{\mu_m^n} + n \log \mu = A + n \log \mu \quad (11)$$

The last equation means that ω versus μ plot in the log-log coordinate system should be a straight line. Such a plot is shown in Fig. 10 for the data of Fig. 6. As can be seen, the data points are quite well

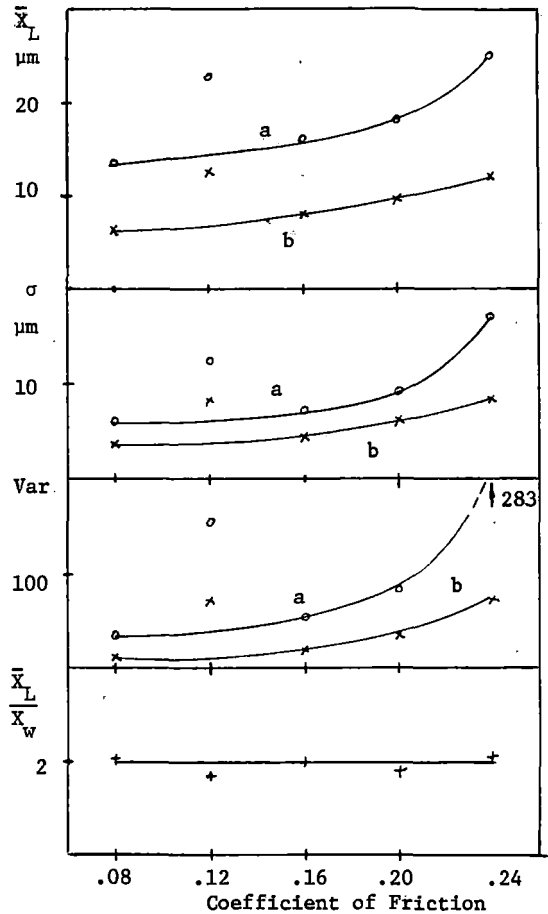


Fig. 8. The Average (\bar{X}) Dimensions, Standard Deviations (σ) and Variances (Var) of the Wear Particles Length (a) and Width (b) and their Aspect Ratio (X_L/X_w) Variation in the Braking Mode.

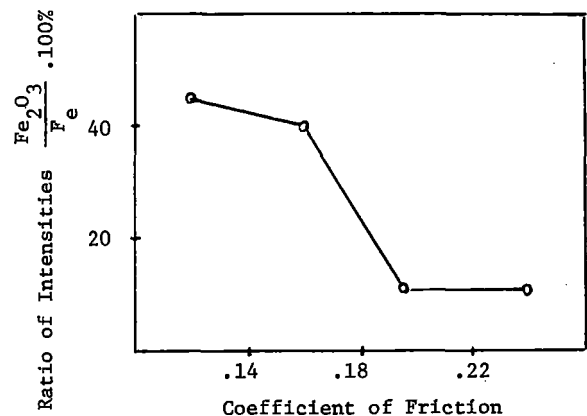


Fig. 9. Ratio of Intensities of Fe_2O_3 Lines to the Fe Lines vs. Coefficient of Friction.

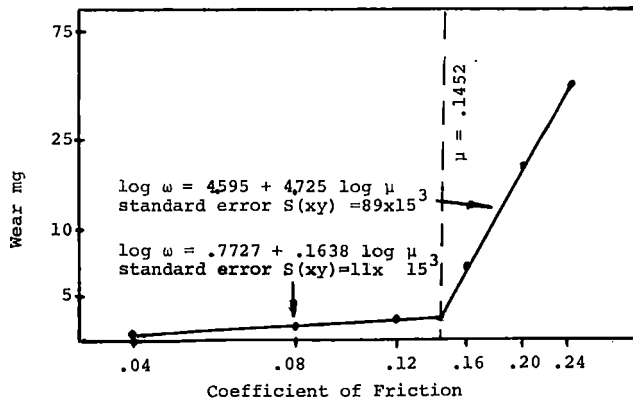


Fig. 10. Wear Rate vs. Coefficient of Friction in the Braking Mode.

represented by straight lines in this coordinate system. The discontinuity of the straight line at about .14 coefficient of friction indicates the transition from one wear mechanism to another. In the range of mild wear the coefficient n is very small. That indicates its independence on the material properties and that wear is governed by another mechanism. Examination of the x-ray analysis data (Fig. 9) and SEM analysis of the track (Fig. 11 and Fig. 5) reveals that discontinuity of the line on Fig. 10 is associated with the transition from oxidative to adhesive wear mechanisms. Thus, in the range of mild wear, the rate of wear is controlled by kinetics of oxide film formation and break down processes (8).



Fig. 11. SEM Photo (x 300) (the same as in Fig. 6 spot of the track) after running at .16 coefficient of friction.

In the case of free rolling when absence of the tangential force and alignment of the wheels are assured, the wear is practically zero. Also, some removal of materials takes place by transferring to the opposing surface. Even slight misalignment causes large plastic deformation of the materials and following wear by fatigue mechanism.

The mild oxidative wear is characterized by the smallest particles formed (Fig. 8). The variation of the standard deviation and variance (Figs. 7 and 8) show that increase in braking torque or misalignment cause formation of the larger wear particles. In the range of oxidative wear in the braking rolling mode, the maximum average length and width of the wear particles formed are about $18\mu\text{m}$ and $7\mu\text{m}$ correspondingly. Comparison of this data with data on Fig. 7 shows that oxidative wear prevailed only during 12 and 13×10^5 loading cycles when wheels were perfectly aligned. Microphoto of Fig. 12 clearly shows formation of the flakelike oxide wear particle during 11 to 12×10^5 loading cycles. This observation indicates that even slight misalignment of the wheels was

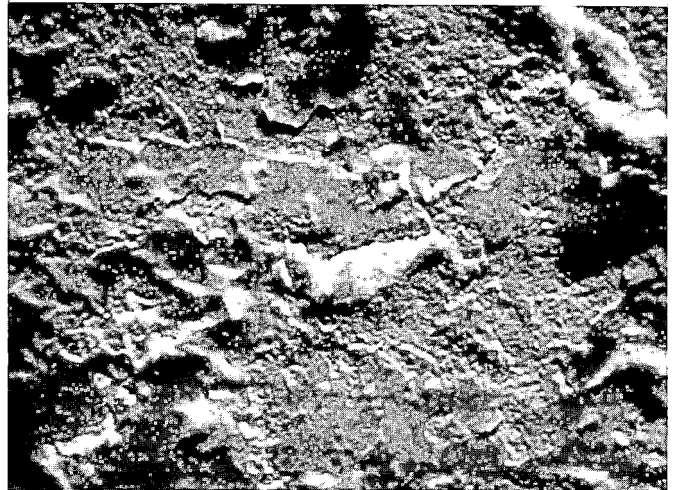


Fig. 12. SEM Photo (x 700) of the Track in the Free Rolling Condition after 12×10^5 Cycles.

enough to cause transition from mild to severe wear.

ACKNOWLEDGEMENT

The authors wish to thank the sponsors of the work, the Griffin Wheel Company.

REFERENCES

1. Krause, H. and Scholten, J., "Wear of Titanium and Titanium Alloys under Conditions of Rolling Stress" Proceedings of the International Conference on Wear of Materials, 1977, St. Louis, MO., USA.
2. Krause, H. and Scholten, J., "Factors Influencing the Frictional and Wear Behavior of the Wheel/Rail

- System", International Wheelset Congress, Tokyo, Japan, 1975.
3. Krause, H., "Tribiochemical Reactions in the Friction and Wearing Processes of Iron", Wear, 18 (1971), 403-412.
 4. Beagley, T.M., "Severe Wear of Rolling/Sliding Contacts", Wear, 36 (1976), 317-335.
 5. Johnson, K.L. and Jeffries, J.A., "Plastic Flow and Residual Stresses in Rolling and Sliding Contact", Symp. on Fatigue in Rolling Contact, Inst. Mech. Eng., London, 1963.
 6. Poritsky, H., "Stresses and Deflections of Cylindrical Bodies in Contact with Application to Contact of Gears and of Locomotive Wheels", J. Appl. Mech., Trans. Amer. Soc. Mech. Engrs., 1950, 72, 191.
 7. Haines, D.J., Ph.D. Thesis, University of Nottingham, 1964, Nottingham.
 8. Aronov, V., "Formation and Destruction Kinetics of Transformed Structures of Metals in Friction", Wear, 38 (2) (1976) 305-

Railroad Wheel Back Rim Face Failures: Data and Analysis

A.J. Opinsky

Association of American
Railroads
Chicago, Illinois

Back rim face failures occur in significant numbers (11-15% of the total) and are worthy of further study. Wheel designs possessing straight plates and Class B and Class C wheels appear to be disproportionately more prone to these failures. Initiation occurred at a rim stamping 43% of the time; at the bottom corner, 10% of the time; and the remainder of the time at approximately the intersection of the extrapolation of the tread line to the back rim face. Of the cracks that could be measured, there was no difference in the crack propagation of failures initiating at rim stamp or high on the back rim face. The average crack was about 0.75 in (19 mm) deep when catastrophic failure occurred. Calculations indicate that it may take on the order of a million cycles to reach this size.

NOMENCLATURE

a	Crack Depth, in
a/c	Aspect Ratio, Corner Crack
a/2c	Aspect Ratio, Surface Crack
AAR	Association of American Railroads
BRFF	Back Rim Face Failures
c	Semixaxis of Crack on the Back Rim Surface, in
da/dN	Crack Propagation Rate, in/cycle
Frisco	Saint Louis-San Francisco Railway (Now Burlington Northern Railroad)
HI	Failures Initiated High on the Back Rim Face
K	Stress Intensity Factor, ksi $\sqrt{\text{in}}$
K _{IC}	Fracture Toughness, ksi $\sqrt{\text{in}}$
LL	Failures Initiated at the Lower Corner
Q	Shape Factor
RS	Failures Initiated at a Rim Stamping
UP	Union Pacific Railroad
ΔK	Range of Stress Intensity Factor, ksi $\sqrt{\text{in}}$

Φ Complete Elliptic Integral of the Second Kind

σ Stress, ksi

σ_y Yield Strength, ksi

INTRODUCTION

Failures originating on the rim can initiate on the front (outside) face, the tread, the flange, or the back (inside) face. In this paper, the data of two railroads will be examined to establish a firm foundation for analysis and possible solution of the back rim face failure problem. In addition to failures initiated at identification marks stamped on the rim (RS), there are other failures that are initiated on the back rim face, even in rim-stamped wheels. Some have called them retarder failures; since such a designation infers causation, it will not be used here. Rather, it will be shown that these latter failures classify naturally into those initiating near the extrapolation of the tread line to the back rim face, Fig. 1, to be called HI (for high initiation), and those initiating at the bottom corner of the back rim face, Fig. 2, to be called LL (for lower limit). The inclusive term, BRFF (for back rim face failures), thus has subsets RS, HI and LL. Only verifiable failures are tabulated; if the failure did not occur at a rim stamping and no photograph was available, it is included in HI. Thus the LL totals may be slightly lower and the HI totals may be slightly higher than the actual situation.

The failure reports of two railroads have been examined, as follows: the Saint Louis-San Francisco (to be called the Frisco, even though they are now part of Burlington Northern) and the Union Pacific (UP). Much of the data were available in Chicago, but both Springfield, Mo. (Frisco) and Omaha, Neb. (UP) were visited to assure completeness of the data.



Fig. 1 Broken rim section, 33" wrought steel wheel, Car UP 491168 (1)

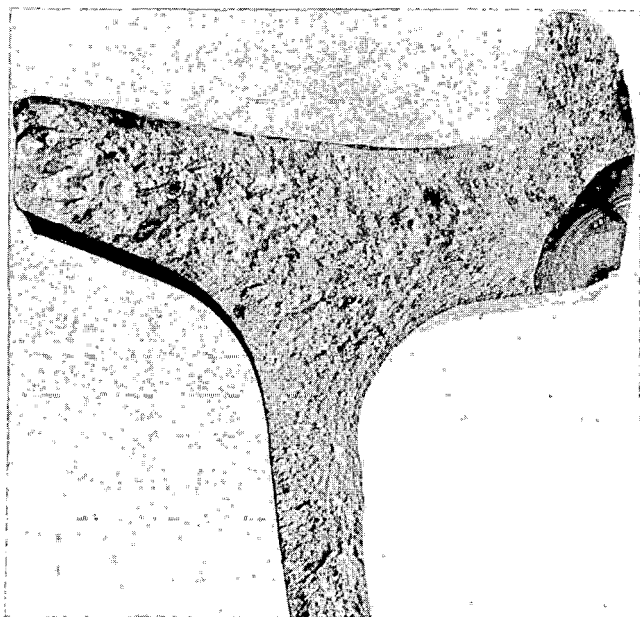


Fig. 2 Broken rim section, 28" wrought steel wheel, Car RTTX 501488 (1)

Two time periods were investigated. All failures occurring after 1 January 1977 and reported by March 1981 (Frisco) or May 1981 (UP) were collected and analyzed, mainly to provide an idea of the magnitude of the BRFF problem. Only BRFF occurring between 1 January 1973 and 31 December 1976 were collected, in order to permit an assessment of whether the problem is increasing or decreasing in frequency of occurrence.

The U-1 wheel has been excluded from the data. There may, however, be some U-1 wheels inadvertently included in the data, if they were not properly identified; i.e., identified as U rather than U-1.

RESULTS OF ANALYSIS OF THE RAILROAD DATA

The first task was to establish the severity of the problem, at least as far as the Frisco and UP were concerned. There are really two components of severity: the relative rate of occurrence, compared with other failures, and the relative risk of derailment. The data for the 1977-1981 period were more numerous from the UP, so it was useful to analyze them more closely (Table 1). On the UP, there were 61 BRFF out of 573; on the Frisco, 25 out of 169. Thus BRFF accounted for 11-15% of the failures.

TABLE 1. AAR-Reported Wheel Failures From January 1, 1977 To March 1981 (Frisco) or May 1981 (UP)

<u>Location of Failure</u>	<u>Total</u>	<u>Associated Derailments</u>
Union Pacific		
RS	30	19
HI*	23	19
LL*	8	5
Subtotal	61	43
Outer Tread	295	25
Center Tread	4	3
Flange	89	63
Shattered Rim	51	5
Thin Rim	7	1
Other	66	26
Total Union Pacific	573	166
Frisco		
RS	10	8
HI*	15	15
LL*	0	0
Subtotal	25	23
Other	144	19
Total Frisco	169	42

*If not shown in a photograph at the lower corner of the back rim face, the failure is automatically classified HI.

The other component of severity is how often the failure led to a derailment. On the UP, at least 43 of the 61 failures led to a derailment, while on the Frisco, at least 23 of the 25. If the data are combined, 66 out of 86, or close to 80%, of the failures led to derailments.

Only one other type of failure approached BRFF in severity. As shown in Table 1, the flange failure comes in second, with about 70% of the failures resulting in derailments. There were more flange failures (89) than BRFF (61).

Thus the data establish that BRFF are very serious, and hence worthy of further study. Is the problem getting better or worse? According to Table 2, that might depend on the railroad. Rim stamp failures seem to have increased on the UP, whereas HI failures seem to have increased on the Frisco. The problem is definitely not disappearing.

All in all, 143 BRFF have been tabulated. It can be shown(1) that 106 of these failures occurred in wheels that possessed rim stampings, but only 62 of the failures initiated at the rim stamping. Hence the presence of the rim stamping led to initiation there

TABLE 2. BRFF and Associated Derailments

Data Source	RS		HI*		LL*	
	Total	Derailments	Total	Derailments	Total	Derailments
1973-1976 UP	11	9	23	16	4	4
1977 on	30	19	23	19	8	5
Total UP	41	28	46	35	12	9
1973-1976 Frisco	11	5	6	4	2	1
1977 on	10	8	15	15	0	0
Total Frisco	21	13	21	19	2	1
Grand Total	62	41	67	54	14	10

*If not shown in a photograph at the lower corner of the back rim face, the failure is automatically classified as HI.

only about 60% of the time. Furthermore, 137 of the wheels possessed a straight plate(1). This latter is an extremely significant consideration.

Further conclusions can be drawn from Table 3, which segregates the failures according to wheel size, wheel type, and failure type. Note that 25 or 26 wheels were Class U; thus only about 20% of the failures were in Class U wheels. However, it is known that the proportion in the fleet is as lopsided the other way--that at least 80% of the fleet runs on Class U wheels. This is another extremely significant consideration.

Four significant trouble spots are found in Table 3. Rim stamp failures are significant in Class B and C 1-W 28 in (711 mm) diameter wheels and Class C 1-W 36 in (914 mm) diameter wheels. HI failures are especially significant in Class B 2-W 33 in (838 mm) diameter wheels, while there is another area of HI and LL failures in Class U 1-W 33 in diameter wheels. Note, in Table 3, that six of the 14 LL initiations occurred in Class U wheels, accounting for 25% of the Class U wheel failures. A theoretical analysis of the Class U LL failures will

be published elsewhere. The number of failures associated with the first three seems to be disproportionate to the actual fleet population. It is probable that the reasons will not be clear until a mechanism for these failures is postulated and the effect of rim quenching (common to the three) can be explained by that mechanism.

Twenty-four of the HI failures were shown in photographs such that a quantitative estimate could be made of the location of initiation. Eleven were within 1/4 in (6 mm) of the extrapolation of the tread to the back rim face; of the remaining, six were located between 1/4 and 1/2 in (6-13 mm) above, and five were located between 1/2 and 3/4 in below. The remaining two were located 3/4 to 1 1/4 in (19-31 mm) above the extrapolation. Of the twenty-four measured HI wheels, only one was a Class U (and that initiation was right on the extrapolation). Of the thirteen rim stamping failures that were measured, only two were Class U. It appears that the HI location of initiation is as much a manifestation of the rim quenched wheel as the LL may be associated with the Class U wheel. Unfortunately, these measurements were made on only fifty-one wheels out of 143.

TABLE 3. BRFF by Wheel Size, Wheel Type, and Failure Type

TYPE	CLS	Wheel Size										SUB	TOT		
		28 in (711 mm)			33 in (838 mm)			36 in (914 mm)			38 in (965 mm)			40 in (1016 mm)	
		RS	HI	LL	RS	HI	LL	RS	HI	LL	RS			LL	RS
1-W	B	12	5	0	2	0	0	0	0	0				19	
	C	4	1	1	3	6	0	14	5	2				36	
	U	0	0	1	4	6	4	2	0	0				17	
2-W	B				1	18	2	4	5	1	4	2		37	
	C				0	5	0	1	5	0	0	0		11	
	U				0	2	1	0	1	0	0	0		4	
M-W	B				4	4						3		11	
	C				0	0								0	
	U				1	0								1	
?	B	0			1	2								3	
	C	0			0	0								0	
	U	2			0	1								3	
	?	0			0	1								1	
SUBTOTALS:															
	RS	18			16			21			4		3	62	
	HI		6			45			16					67	
	LL			2		7			3		2			14	
	TOTALS:			26		68			40		6		3	143	

In (1), other attempts to analyze the historical data were not fruitful. There was almost a seasonal pattern, but it was disturbed by low occurrences in February and high occurrences in July. There was some indication that several geographical locations accounted for more failure sites than others, but it is not known whether any significance can be attached to these findings. Multiple failures (more than one failure on a given car or locomotive) occurred in only three instances.

It is believed that the main conclusions reached here--the preponderance of heat treated wheels and of straight plate wheels, and HI and LL correlations with heat treated and Class U wheels, respectively, would not be altered by taking a larger sample. It is also evident that the failure rate is significant and worthy of further study.

FRACTURE MECHANICS CALCULATIONS

One avenue of study is analyses of the crack sizes before the wheels failed catastrophically. Reasonably accurate measurements were available for 82 of the failures. The data (RS, HI, LL) were extracted from the data base and then subjected to a computer program that calculated the aspect ratio (depth of the crack divided by its length, which for a corner crack means a/c, or for a surface crack means a/2c) of the elliptical crack and also a tensile stress at the time of catastrophic failure, under the assumption of a uniform tensile stress field. The equations and fracture mechanics data of Carter and Caton(2) were used in the investigation, and the resulting statistical data are given in Table 4.

The dependence of aspect ratio on a, the crack depth, is shown in Figs. 3 and 4. The RS data are very similar to those of HI, which are shown in Fig. 4, as can be seen in Table 4. On the log-log basis, the equations relating a/2c to a are almost

identical for HI and RS failures. The average crack before catastrophic failure is about 3/4 in (19 mm) deep, and it is almost penny-shaped. While the site of initiation differs between these two classes of failures, it would appear that crack propagation does not. In other words, the same mechanism apparently controls both types of failure.

The average crack depth is a little smaller for HI failures, and consequently the average stress is a little higher; see Table 4. The calculated stresses fall within the range of the five calculated by Carter and Caton(2).

Note that the slopes of the lines in Figs. 3 and 4 are different. It is tempting to speculate that the aspect ratio decreases for the LL failures as the crack grows, because the hoop tensile residual stresses induced by excessive drag braking decrease more rapidly in the a direction (along the fillet) than in the c direction (along the back rim face)(3).

Finally, an estimate has been made of how many cycles are required to obtain a crack similar to that shown in Fig. 1. For this purpose, the crack growth equation of Opinsky for Class B rim steel(4) was used and modified for simplicity to:

$$\frac{da}{dN} = 2 \times 10^{-10} \Delta K^3 \quad (1)$$

K will be defined by the Tiffany-Masters equation(5):

$$K = 1.1 \sigma \sqrt{\pi a / Q} \quad (2)$$

where $Q = \phi^2 - 0.212(\sigma/\sigma_y)^2$, and σ is the stress, σ_y the yield strength, and ϕ is the complete elliptic integral of the second kind.

If it is now assumed that the cycle goes from 0 to K, K in the Tiffany-Masters equation becomes ΔK , and

TABLE 4. Statistical Data Derived from Fracture Mechanics Calculations

No. of Data Points	Type of Failure		
	RS 31	HI 41	LL 10
Average a (log basis)	0.74 in (19 mm)	0.67 in (17 mm)	0.75 in (19 mm)
Range of a	0.50-1.50 in (13-38 mm)	0.38-1.25 in (10-32 mm)	0.50-1.19 in (13-30 mm)
Average Aspect Ratio (log basis)	0.51 (a/2c)	0.50 (a/2c)	0.82 (a/c)
Equation	$a/2c = 0.57a^{0.42}$	$a/2c = 0.59a^{0.42}$	$a/c = 0.70a^{-0.51}$
Correlation Coefficient	0.50	0.46	-0.68
Average Stress	31.3 ksi (216 MPa)	33.4 ksi (230 MPa)	27.6 ksi (190 MPa)
Stress Range	20.1-40.4 ksi (139-279 MPa)	24.6-42.3 ksi (170-292 MPa)	18.6-37.7 ksi (128-260 MPa)
Data Assumed (2) To Get Stress:			
Yield Strength	Class B 87 ksi (600 MPa)	Class C 95 ksi (655 MPa)	Class U 55 ksi (379 MPa)
Fracture Toughness	38 ksi/in (42 MPa√m)	35 ksi/in (38 MPa√m)	35 ksi/in (38 MPa√m)

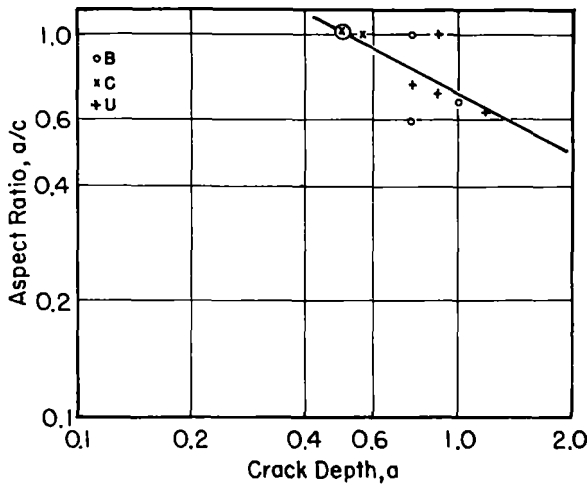


Fig. 3 Aspect ratio as a function of crack depth prior to fast fracture--failures initiated at the lower limit of the back rim face

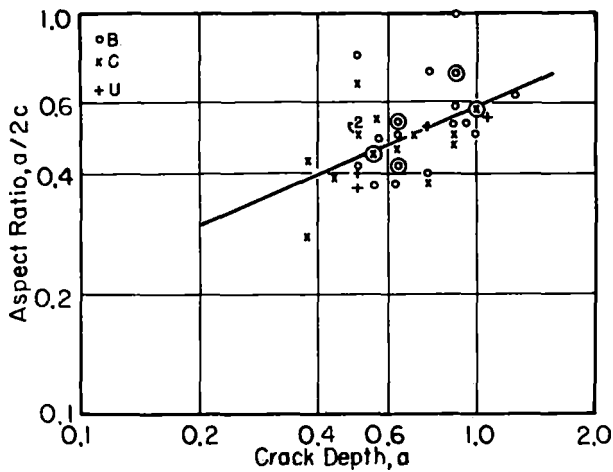


Fig. 4 Aspect ratio as a function of crack depth prior to fast fracture--HI failures

$$\frac{da}{dN} = 2 \times 10^{-10} [1.1 \sigma \sqrt{(\pi a/Q)}]^3 \quad (3),$$

or

$$dN = \text{const} [\phi^2/a - (0.212/a) \times (\sigma/\sigma_y)^2]^{3/2} da \quad (4).$$

If ϕ^2 is assumed to be a constant, the right hand term becomes $da/a^{3/2}$, which can be integrated in closed form. If ϕ is assumed to vary during the integration, an approximation of $\phi^2 = \phi^2(a/2c)$ can be further related to a by $a/2c=f(a)$ from Table 4 to yield an equation that can be integrated numerically.

Integrations were performed at constant $a/2c=0.5, 0.25$ and 0.15 from the smallest crack that would grow (which can be calculated if a threshold stress intensity factor is assumed) to a crack size of 0.666 in

(16.9 mm). Another integration using ϕ^2 in terms of $a/2c$ and the equation $a/2c=0.59 a^{0.42}$ was done by twenty-term Gaussian quadrature. For details, see (6). If a threshold of 5 ksi/in (5.5 MPa \sqrt{m}) is assumed, it is calculated that $0.6-1.1 \times 10^6$ cycles are needed; if the threshold is 10 ksi/in (11 MPa \sqrt{m}), $0.33-0.43 \times 10^6$ cycles. While these calculations are approximate, they seem to indicate that the final failure of the wheel need not necessarily occur soon after initiation of the crack.

CONCLUSIONS

1. The BRFF rate is significant and worthy of further study.
2. Straight-plate wheels appear to be more susceptible to BRFF.
3. BRFF occur mainly in heat treated wheels.
4. Failures not initiating at rim stampings tend to initiate either at the intersection of the extrapolation of the tread to the back rim face (Class B and C wheels) or at the lower limit of the back rim face (mainly Class U wheels).
5. Mechanistically, the data show no difference between crack propagation in failures initiating at a rim stamp or high on the back rim face.
6. Crack growth calculations show that it might take on the order of a million cycles to propagate a crack from initiation to the approximate $3/4$ in (19 mm) it attains before catastrophic failure.

ACKNOWLEDGMENTS

The author wishes to acknowledge the editorial assistance of R. F. Breese. F. D. Bruner, Assistant CMO, Research and Development, Union Pacific Railroad Company, and J. A. Gombold, Engineer of Tests, Burlington Northern, are thanked for permission to use Figs. 1 and 2, respectively.

REFERENCES

1. Opinsky, A. J., "Railroad Wheel Back Rim Face Failures I. Experience of Two Railroads Over the Period 1973-1981," R-503, November 1981, AAR, Chicago, Ill.
2. Carter, C. S. and Caton, R. G., "Fracture Resistance of Railroad Wheels," D6-41586, April 1974, Boeing Commercial Airplane Company, Seattle, Wash.
3. Johnson, M. R., Welch, R. E. and Yeung, K. S., "Analysis of Thermal Stress and Residual Stress Changes in Railroad Wheels Caused by Severe Drag Braking," ASME Preprint 75-WA/RT-3.
4. Opinsky, A. J., "Fracture Mechanics Data for Three Classes of Railroad Wheel Steels," Sixth International Wheelset Congress, Colorado Springs, Colo., October 1978, pp. S-1 to S-14.
5. Tiffany, C. F. and Masters, J. N., "Applied Fracture Mechanics," American Society for Testing and Materials Special Technical Publication 381, Philadelphia, Penn., 1965, pp. 249-278.

6. Opinsky, A. J., "Railroad Wheel Back Rim
Face Failures II. Fracture Mechanics Calculations
Based on Measured Crack Sizes," R-507, February 1982,
AAR, Chicago, Ill.

Design Features for Operational Acoustic Signature Inspection of Railroad Wheels

R.D. Finch

Professor
Dept. of Mechanical
Engineering, Univ. of
Houston, Houston, Texas
Member, ASME

W.E. Thomford

P.E., Manager
Research & Tests
Southern Pacific
Transportation Co.
San Francisco
California
Member, ASME

Research and development of systems for finding defective wheels using the acoustic signature method are reviewed. Pertinent test results are summarized, and the necessary improvements to hardware and data processing are discussed in terms of the ability to detect various wheel conditions and defects while minimizing false alarms. The requirements for an operating system are discussed and the main features of a design to meet these requirements are considered.

NOMENCLATURE

Z _{1k} , (Z _{2k})	Voltage level in frequency Channel k, obtained from signal from wheel 1(2)
SD	$\sum_k Z_{1k} - Z_{2k} $, except for channels with common resonances and one channel above and below common resonances
NC	Number of channels with common resonances
DI	$C_1 SD - C_2 NC + \text{constant}$ where C_1 and C_2 are constants (Difference Index).
%	Symbol used to indicate that a given variable has been normalized with respect to the complete spectrum.
$N_g(x)$	Number of good wheelsets having DI = x
N_{gT}	Total number of good wheelsets
m_g	Median DI value for good wheelsets
σ_g	Standard deviation of DI values for good wheelset population
$N_B(x)$	Number of cracked wheels having DI = x
N_{BT}	Total number of cracked wheels
m_B	Median DI value of cracked wheels
σ_B	Standard deviation of DI values for cracked wheels

INTRODUCTION

The purpose of this paper is to present the design considerations for an operational system for finding defective wheels using acoustic signature inspection (ASI). The requirement is to inspect wheels on moving trains from a convenient wayside location, automatically and continuously, and with minimal interference to normal operations. In particular, the number of false alarms should be kept to a minimum. The main failure categories which need to be found (based on 1979 costs) are broken plates, broken rims, broken flanges and loose wheels.

The concept of using acoustic signals for wheel inspection was the subject of an earlier feasibility study carried out at the University of Houston (U.H.) (1). A system consisting of an automatic hammer, a microphone, a real-time spectral analyzer (R.T.A.) and a computer was tested in the laboratory and defective wheels could be distinguished from good ones. An important conclusion was that the best detection method consisted of a comparison of sounds from the paired members of a given wheelset. The acoustic signature is dependent on the wheel type, size, load, wear and surface condition, but since wheels are mounted and changed in pairs they should have the same signature; thus a significant difference in the signatures from members of a wheelset should indicate the presence of a defect or an unusual condition in one of the wheels. In order to characterize these differences in sound, a quantity termed the difference index (DI) was computed. When the DI value was greater than a certain discrimination level an alarm was declared. The study was concluded with some preliminary field tests in which cracked wheels were detected on short consists. These demonstrations were encouraging but the question arose as to how well the system could work with a larger statistical sample. Arrangements were made for a six-week period of testing in the Englewood Switching Yard of the Southern Pacific in Houston (2). The system was operated in real-time and tape recordings were made to serve as a data base

for finding an algorithm which could adequately distinguish wheelsets with a defective member. No dangerously defective wheels were found during the testing period and so, for comparison purposes, some defective wheels were tested in the laboratory. One of the most interesting results was the finding that the preponderance of wheelsets with high DI values observed in the yard showed a characteristic shifting of resonance frequency values. It was postulated that this was probably due to differential wheel wear.

Following the Englewood Yard test, the FRA funded a testing and evaluation project as part of their program for the Wayside Detection Facility, at the Transportation Test Center (T.T.C.) at Pueblo, Colorado. The results of these tests have some important implications for the design of an operating system, so it is appropriate to review the highlights here. Further details may be found in reference (3).

2. T.T.C. TESTS

A consist was assembled, including six standard freight cars, a locomotive, and a specially modified truck for plate cracked wheels. This consist is illustrated in Fig. 1; more detailed information on the wheel conditions is given in reference (4). The only wheels with real cracks were those with plate cracks (axles 31 and 32). The other defects were saw cuts, which differ from real cracks both in mechanical damping and local stress distribution. Thermal cracks usually occur in profusion on a wheel, but the defects were simulated by one saw cut per wheel.

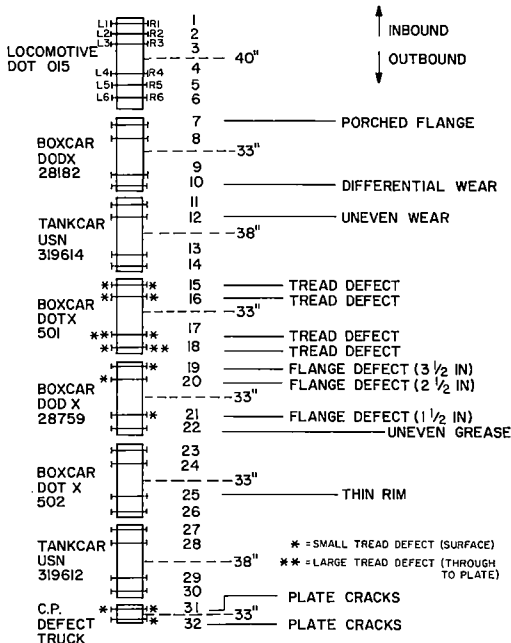


Fig. 1: T.T.C. test consist

Certain improvements were made to the system to facilitate performance of the tests. Of particular note was the replacement of the ACI wheel presence indicators with Honeywell wheel presence indicators, whose sensitivity was easier to adjust thus avoiding the problem of missed trigger pulses which could lead to erroneous wheel counting. Reconfiguration of the system was carried out to prevent cross-talk between the microphones. The final configuration is shown in Fig. 2 including a new timing and audio switching circuit designed to ensure that if a wheel presence pulse was missed, it would not cause incorrect wheel counting. The RTA operated in a "free-running" mode i.e., it was not synchronized with the acquired signal and this was recognized as a significant source of data uncertainty. An auxiliary timing circuit was built to attempt to correct this, but there was still an uncertainty of up to 50 m/sec in the start of the sampling time.

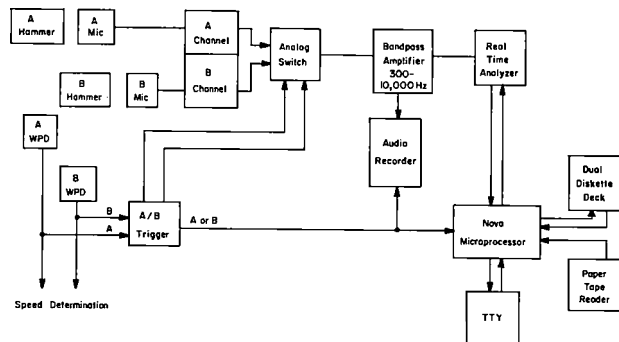


Fig. 2: Block diagram of ASI system for T.T.C. tests

A problem with the speed of data storage to diskette was also encountered; it was believed to lie in the software and was not a fundamental limitation to the system. Another speed limitation of the system arose from the action of the hammer, which was activated when a wheel flange depressed a plunger linked mechanically to the impacting arm. Consequently, the impact force depended on the train speed. In turn this caused the sound pressure level generated at the microphone to depend on the train speed. In order to keep the received signal within the dynamic range of the RTA, the settings of the instrumentation had to be changed when the speed of the consist was changed. A series of calibration runs was made to determine the optimum values of these settings. The slow speed of the teletypewriter used for input and output made data processing a tedious task.

3. ANALYSIS OF T.T.C. DATA USING DIFFERENCE INDEX

The DI algorithm used in the U.H. program having been used to collect data from in-service wheels (2), it was decided to investigate first how this algorithm performed against the T.T.C. consist. A major feature of the DI algorithm is in recognition of "common" resonance peaks, i.e., the number of resonances occurring at the same frequency in both wheels. However, because of the finite frequency bandwidth of the

RTA, some peaks are not always counted in the same frequency channel. The FRA project staff therefore expanded the definition of "common" resonances to allow for shifts of two channels.

The performance of a detection algorithm depends on the sample of wheels available. The T.T.C. Consist was not a statistical representation of wheels encountered in service. Since the only available data sample with in-service wheels was that obtained during the Englewood Yard test (2) it was decided to re-run the diskette recorded data from the Englewood test through the revised computer program for DI. The resulting histogram of DI values is shown in Fig. 3 and median values for the Test Consist are shown in comparison. Four wheels from the Englewood sample would have been flagged by the new program, if the discrimination level had been set at zero. Since a detailed examination of the wheels sampled during the Englewood test was not possible, there was no information on the actual condition of these wheels, but the probability was that none of them were dangerously defective. It should be noted that the four wheelsets on the Test Consist with the highest DI values were axle 31, with a place cracked wheel, axles 17 and 18 with "calamity" tread defects and axle 20 with a 2½ in. flange cut. All of these wheels had DI values well above the highest value in the Englewood sample.

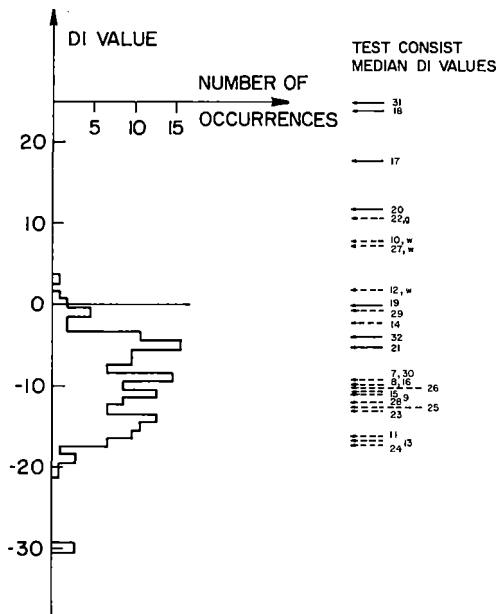


Fig. 3: Histogram of DI values from Englewood Yard Data using improved program, compared with median DI values for test consist using improved program. Solid arrow indicates crack or broken flange.

g = greasy, w = differential wear

4. ESTIMATE OF FALSE ALARM RATES WITH DI ALGORITHM

If, for the T.T.C. sample, the discrimination level were set at DI = 11.5, axles 31, 18, 17 and 20 would be declared bad, with a zero false alarm rate. However, if the discrimination level were reduced to DI = 0, only one more wheel, on axle 19 would be

found and false alarms would result from axles 22, 10, 27, 12. The false alarm rate (FAR) would then be 4/9, for the T.T.C. consist. Finally, if the discrimination level were reduced to DI = -5, defective axles 32 and 21 would also be detected, so that all defective wheels would alarm, but with additional false alarms on 29 and 14, to give FAR = 6/13 for the T.T.C. Consist. However, it is clear that DI = -5 is well into the population of good wheels, as represented by the histogram, so that the FAR would then be much greater for in-service wheels.

In order to estimate how well the algorithm would perform in the field the two wheel populations must be normalized. Assume that the populations of good wheels can be represented by Gaussian distributions:

$$N(x) = \frac{N_T \exp \left[-\frac{(x-m)^2}{2\sigma^2} \right]}{\sigma\sqrt{2\pi}} \quad (1)$$

In order to fit numerical values to these distributions information on the number of cracked wheels has to be obtained. Most cracked wheels are presently found by visual inspection, although some still elude inspectors and cause derailments. In order to determine the number of cracked wheels found by inspection an inquiry was made of the AAR's Car Maintenance Cost (CMC) Data Base (4). For the railroads participating in the CMC Data Base, wheel caused derailments are available from the FRA Accident Data Base. These statistics, for 1980, covered 19.8% of the U.S. car fleet, representing approximately 1,347,000 wheelsets.

Using these statistics:

N_{BT} = total of wheel failures (Why Made Code Numbers 66, 68, 71 and 83)

+ total broken wheel caused accidents
= 853 + 24 = 877

N_{GT} = (total number of wheelsets in fleet) - (number of wheelsets with a cracked member)
= 1,347,000 - 877
= 1,346,123

Means and standard deviations for the two populations are estimated from the numbers in Fig. 3:

$m = 10.1$

$m_B^g =$ median DI for wheelsets 31, 18, 17, 20, 19, 32, 21
= 10

$\sigma = 5.55$

$\sigma_B^g = 12.01$

Fig. 4 shows hypothetical Gaussian distributions fitted to these parameters. By integrating the area under the two curves it can be shown that for a discrimination level of DI = 4.5 the false alarm rate would be 0.91 and the detection rate 0.672. If the wheels missed by the inspectors are uniformly distributed among the types of cracked wheels, this would represent a savings of 0.672 of the accident costs. Increasing the discrimination level to DI = 10 would lower the false alarm rate to 0.31 and the detection rate to 0.50. On the other hand, decreasing the discrimination level would increase the false alarm rate to unacceptably high values without significantly improving the detection rate.

It is clear that one way to improve the performance of the system would be to reduce the false alarm rate. The false alarms are caused by wheel conditions other than cracks causing the members of a wheelset to sound different. Two such wheel conditions are: 1) differing amounts of grease on the two wheels, and 2) different degrees of wear. Algorithms to recognize these two conditions are discussed in the next section. Another way to improve the performance of the system would be to increase the sepa-

ration of the means of the good and defective populations. Evidence is presented in a subsequent section that this might be done by including a "time domain" term in the DI algorithm.

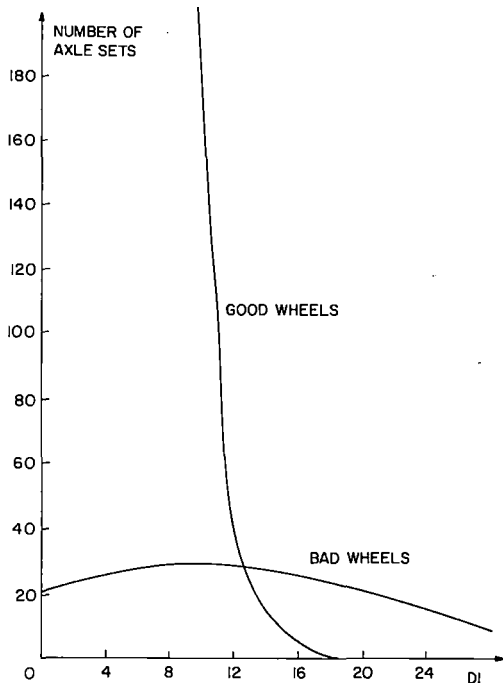


Fig. 4: Gaussian fits of good and bad axle sets to DI values

5. WHEEL CONDITION ALGORITHMS

Again referring to Fig. 3, the fifth highest DI value on the Test Consist was obtained from axle 22, which had one very greasy wheel. This condition was deliberately created by cleaning the mate wheel and is thus rather unlikely to be encountered in service. Although greasy wheels are usually indicative of a leaking journal bearing, which is an undesirable situation, the wheel itself should not be classified as defective. A new algorithm was therefore written to recognize greasy wheels, based on the fact that grease causes heavy damping at high frequencies. This discriminant was termed GI and is computed from the difference of energy in the highest and lowest quartiles of the frequency range. Details of the testing of the algorithm are given in reference (3) and it was concluded that a greasy wheel could be recognized as such by this algorithm to a highly reliable degree.

Referring once more to Fig. 3 it may be seen that the wheelsets with the next highest DI values, after the greasy wheel, are on axles 10 and 27. Both of these wheelsets show considerable differential wear. Following the S. P. Englewood Yard study, it was predicted that this condition could be recognized by using the finding that the prominent resonance lines in the spectrum are very close to the theoretical values for flexural modes of a ring (2). An algorithm was devised to search for a resonance in the vicinity of the predicted value.

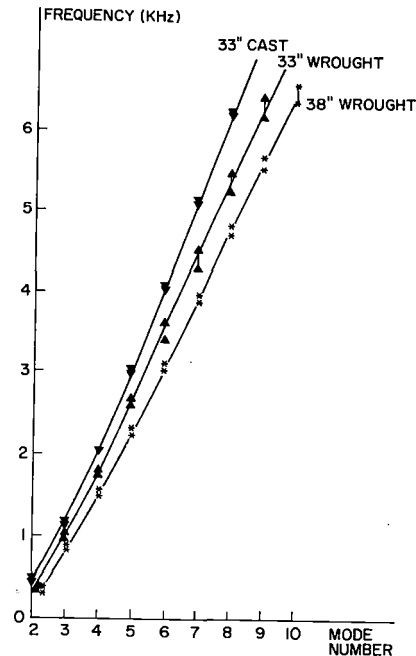


Fig. 5: ASI-Mode Search: modal frequency vs. modal number for different wheel types

Fig. 5 shows the resonance frequency values found by the search routine as a function of mode number. It can be seen that different wheel types fall on different curves, as might be expected. Once the software has been extended to characterize each of these curves with a single parameter, wheel type and differential wear could be added as a system output. Large differences in such a ring mode parameter among members of a wheelset might be used as an additional indicator of defects.

6. TIME DOMAIN ANALYSIS

All the forms of data analysis mentioned in the preceding sections involve processing of frequency domain data. Since this data is obtained by sampling over a short time period, much information from the sound signal is, in effect, discarded. Early studies (1) showed that the decay of the sound with time is increased by the presence of a crack. Fig. 6 is an oscillograph trace of a signal in the time domain. A beating effect is observed, and this is a common phenomenon. It is because of this beating that the previously mentioned 50 ms variability in the start of sampling by the R.T.A. causes a considerable variation in the amplitude of the sample. Furthermore, different resonances appear to beat differently. This in turn results in lack of repeatability in the product of analysis. The physical cause of the beating phenomenon is not completely understood.

Since the U.H. system had no A/D conversion capability the only way to get an idea of the prospects for incorporating time domain terms was by "paper and pencil" studies. Oscillograph traces of the signals from all the wheels obtained in two runs were taken and two measurements made to characterize the sound from each

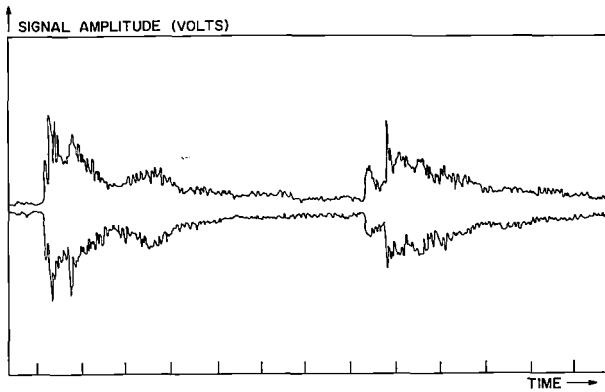


Fig. 6: Oscillograph trace of time domain signal showing beating (axle 7) (signal envelope), Time intervals: $\frac{1}{10}$ second.

impact:

- An exponential envelope fit by finding the closest match among a series of curves drawn on a template; and
- measurements of the "area" under each curve, using a digitizing pad and verified by checking with a planimeter.

Two indicators were then formed:

- DR, the difference in the decay rates of each wheel pair; and
- DA, the difference in the "areas" under each curve.

Correlations between DA and DR, and between DA, DR and various frequency domain indicators were investigated. It appeared that the best result was obtained from a plot of NC% and DA (see Fig. 7). A discriminating line separates the "good" wheels from all the cracked wheels, except for axle 21, which has a flange defect. Axle 22 is a false alarm, but would be flagged by the new GI indicator. The conclusion was that the incorporation of A/D conversion in the system either in series or in parallel with frequency analysis, could considerably improve the decision making reliability.

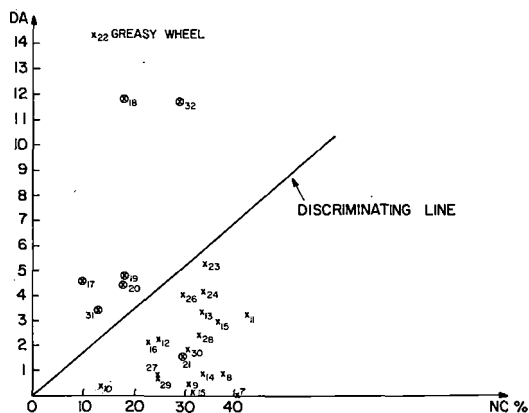


Fig. 7: Recognition by combining time domain term (DA) with frequency domain term (NC%)
 O Indicates wheel with crack or flange cut
 Numbers refer to axles

7. LOCATION AND OPERATING SPEED REQUIREMENTS

In order to decide on the optimum locations for inspection stations it is important to predicate the number of stations needed. A large number of defects are probably initiated by drag braking on steep grades (5). If this were the sole cause of defects then the required number of inspection station would be relatively small. However, if defects do not become dangerous until the residual stress in the rim becomes tensile, or if crack growth is due to repeated load cycling then wheels may not become dangerous until long after crack initiation (6). Furthermore, some defects may be caused by faulty brakes which do not release or possibly retarders (7) anywhere in the U.S. If wheels can become dangerous anywhere, then the required number of stations, I, will be given by:

$$I = \frac{M}{D} \quad (2)$$

where D is the average distance to failure after initiation of a defect, and M is the total railroad mileage or 183,055 miles (8). An estimate of D was made by Carter and Caton (9), at 350,000 cycles to failure, under a typical load, for a 0.15 inch length thermal crack in a class U or C wheel. This corresponds to:

$$D = 573 \text{ miles, for average car mileage, and}$$

$$I = 319 \text{ stations.}$$

This is equivalent to every wheel being inspected every 9.67 days. There are some important reservations on this estimate, and it should be regarded only as an illustration of a methodology in system design at this time.

It appears that the best location from an operational standpoint would be on the approach to a normal inspection point, such as the entrance to a yard with repair facilities to permit switching to a bad-order track with minimum inconvenience. The number of such yards in the U.S. is comparable to the predicted need for about 300 inspection points, and it is therefore assumed that systems will be designed for yard location. Location at or near a yard has the additional advantage of ready access to electric power, communication lines and track circuits. Train speed at the approach to a yard is about 15-20 mph and an interval of several minutes after passing the inspection point can be allowed before wheel condition reports would be needed. Another possible location is on the hump lead where speed is about 3-5 mph. However, wheel condition reports would then be due in 10-20 secs, after passing the inspection point. If this cannot be done and defective equipment has to be retrieved after reclassification the cost and time involved in switching may increase by an order of magnitude. The attainment of a 20 mph operational speed for the inspection system appears to be necessary. This has important design implications.

The shortest distance between wheel sets is taken to be 5'. Hence the shortest time interval between passage of successive axles is 170 ms at 120 mph. To achieve the best results processing should include parameters from both the frequency and time domains. For the T.T.C. tests, for recordings made at 5 mph the time-domain signal amplitude was evaluated over a 500ms interval. This interval could probably be reduced to one third without serious prejudice.

When frequency domain processing using a Fast Fourier Transform (FFT) is contemplated, the sample length required may be calculated as follows: Since the required Frequency Range is 0-7200 Hz, using the

Nyquist Criterion, the sampling rate should be twice the maximum required frequency, i.e., 15,400 Hz. Hence, the sampling period should be 0.065ms. All Fourier analysis to date has been in 40 Hz wide bands, i.e., $\frac{7200}{40} = 180$ frequency channels were computed.

It is assumed that the same number of frequency bands will be adequate in performing the FFT. The same number of samples will be required in the time-domain as values in the frequency domain, i.e., 180. Hence the minimum Fourier window will be $180 \times 0.065 = 11.7\text{ms}$. To improve reproducibility the signal could be averaged say 5 times, for a Fourier window of about 60ms. The conclusion is that for adequate sampling in the time and frequency domains, a signal duration of 170ms should be sufficient.

The basic criterion for operation up to a certain speed is that the signal from one wheel should have declined to below the noise level before the start of the signal from the next wheel. This means that for the operating system, the signal duration should not exceed 170 ms. But the signal duration from a stationary wheel using a non-directional microphone can be as long as several hundred milliseconds. It is therefore concluded that the microphone must either have a directivity or, if non-directional be located so that its response will be below the noise level before the arrival of sound from a following wheel. Another important design implication is that the hammer cycle must be completed in less than 170 ms. It should also be noted that the background noise from a moving train increases with speed and thus the impact force from the hammer might have to be greater than that used in the T.T.C. tests. There does not appear to be any fundamental reason why these design changes could not be accomplished and thus permit the higher speed operation.

8. COMPUTATIONAL REQUIREMENTS

It is concluded from the foregoing sections that an operational system will differ from the one assembled by the University of Houston in the following major ways:

- 1) data acquisition must be possible up to 20 mph, with normal operation at 15 mph, (5 mph in the U.H. system),
- 2) the false alarm rate should be reduced, with improvements in the software and
- 3) the data processing time for a 100 car train should not exceed 10 minutes.

The design requirement of a higher operating speed and its consequences were explained in the preceding section. But the necessary software improvements also require hardware changes. The U.H./T.T.C. program computed the difference in the Fourier transforms of the sound from members of a wheel pair obtained from a real time analyzer. However, as pointed out in Section 6, the inclusion of a measure of the decay of the signal in time should improve the discrimination of defective wheels. It was not possible to compute such terms in the U.H. system because the signal itself was not retained in memory. It is therefore proposed that in an operating system A/D conversion of the signal be made and that this digitized record of the signal be retained to permit time domain analysis. The second recommended improvement in the software is the use of a "cascaded" decision logic to filter out good wheelsets which give rise to high DI values and thus might cause false alarms. For example, greasy

wheels and wheelsets with differential wear have been identified as causes of false alarms. Algorithms to recognize these conditions should be incorporated in the software of an operating system.

The third major design change is due to the need for a short processing time. Even with the limited software of the U.H./T.T.C. system, calculation of the DI value for a wheelset took about 30 seconds using BASIC on a NOVA 1200 computer, which would take 3 hours to compute the results for a 100 car train. Clearly a much faster language and computer are necessary. To obtain an indication of the possible improvement in computing speed a test program was run on a NOVA 1200 and a Data General Eclipse. It was concluded that the old U.H./T.T.C. program could be run in less than 2 minutes on the Eclipse for a 100 car train. Although the additional inclusion of time domain terms and cascaded decision logic will increase the processing time, it is still reasonable to expect all processing to be completed within a 10 minute period. Some additional time saving would result from data acquisition, with a foreground program, and simultaneous data processing, with a background program. A computer such as the Eclipse is not suitable for a wayside location, and thus the system is conceived as shown in Fig. 8, with the wayside hardware located at a convenient point and data and control signals handled through a communications link to a computer center.

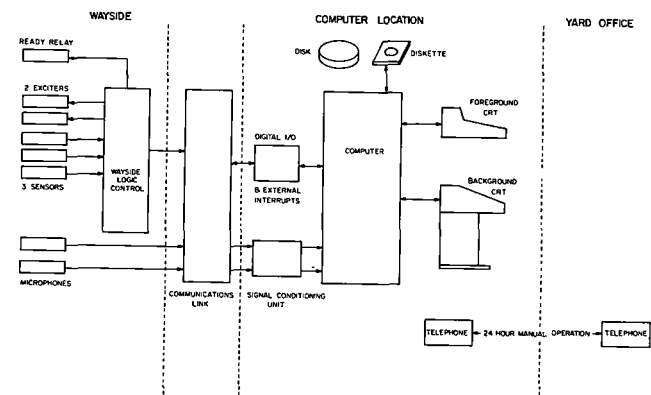


Fig. 8: Schematic of Operational ASI System

At a sampling rate of 15,400 Hz and signal duration of 170 ms there will be $0.170 \times 15,400 = 2618$ samples or "words" to be stored per wheel. Although 12 bit precision (1 part in 4096) will be adequate, disk and CPU memory is usually arranged for 16 bit words. Hence the memory requirement per wheel would be $2618 \times 16 = 41,888$ bits. The storage of the information must be accomplished before the arrival of the data from the next wheel on the same side, or within a time period of 170 ms. This corresponds to a data acquisition rate of 246,400 bits/sec. The memory required for a 200 car train with 8 wheels/car is then calculated to be 8.4 megabytes. It is possible that data processing could begin before completion of train passage, in which case these memory requirements could be reduced. Data acquisition and processing would then need to be independent functions. As mentioned earlier, the desire to include time

domain analysis leads to the idea of storing the signals, but the most compelling argument for total signal storage is that it does not constrain the use of improved signal processing techniques which may result from later research.

9. DISCUSSION

The Southern Pacific Transportation Company and the Association of American Railroads have entered into a contract with CRC-Bethany International and the University of Houston to design and install a prototype ASI system. This system should be operational by the time of the Heavy Haul Conference and a report on its performance will then be made.

It is planned to evaluate the system for a trial period by gathering data from wheels in service and from cracked wheels on a test consist. The key parameters from a cost/benefit standpoint are the fraction of grossly defective wheel detected and the associated false alarm rate. Sufficient information will be gathered to predict how these numbers would be affected by changes in discrimination levels. In addition, information on the causes of false alarms will be gathered with a view to recommending additional sensors and/or improvements to the software.

REFERENCES

- (1) Nagy, K., Dousis, D.A., and Finch, R.D., "Detection of Flaws in Railway Wheels using Acoustic Signatures," J. Engrg. for Ind., Trans. ASME 100, No. 4, 1978, 459-467.
- (2) Dousis, D.A., and Finch, R.D., "A Yard Test of Acoustic Signature Inspection of Railroad Wheels," ASME Paper No. 80-WA/RT-2.
- (3) Finch, R.D., "Cracked Plate Detector Tests," Report to the Aerospace Corporation, 1980, with programmatic and technical commentary from F.D. Bruner and R.M. Vandenberg, Union Pacific Railroad Company, G.W. Brock and M. Dembosky, Ensco Inc., and E.L. Feigenbaum and G.J. McPherson, Aerospace Corporation.
- (4) Guins, T.S., Association of American Railroads, Communication to the authors.
- (5) Thomas, T.J., Garg, V.K., and Stone, D., "Thermal fatigue Analysis of a Railroad Wheel under Drag Braking," ASME Paper No. 80-WA/DE-4.
- (6) Park, Y.J. and Stone, D.H., "Cyclic Behavior of Class U Wheel Steel," ASME Paper No. 80-WA/RT-9.
- (7) Opinsky, A.J., "Railroad Wheel Back Rim Face Failures I. Experience of Two Railroads over the Period 1973-1981," AAR Report No. R-503, November 1981.
- (8) AAR Yearbook of Railroad Facts, 1979.
- (9) Carter, C.S. and Caton, R.G., "Fracture Resistance of Railroad Wheels," DOT Interim Report No. FRA-ORD&D-75-12, September 1974.

ACKNOWLEDGEMENTS

The authors wish to acknowledge the help and support of the following:

The Southern Pacific Transportation Company and the Association of American Railroads for their commitment to design, install and test an operating ASI system,

The Federal Railroad Administration for testing at the Transportation Test Center and continued help with the operational system,

The Union Pacific Railroad Company for help with research and testing,

CRC-Bethany International for undertaking the installation contract,

and the numerous individuals who have contributed to the research, development and ongoing design of the operating system.

Ring Growth in Case Hardened Railway Journal Roller Bearings

A.P. Voskamp

SKF Engineering & Research
Centre B.V.
Netherlands

B. Schalk

SKF Engineering & Research
Centre B.V.
Netherlands

Overhaul statistics from many US railroads demonstrate that the inner rings of case-hardened railway journal roller bearings may grow during service. During overhaul, it is the major cause for bearing replacement. Inner ring growth accelerates fretting corrosion which leads to the loosening of end cap bolts and potentially to failure of the bearing. Dimensional changes of inner rings were analyzed after long term laboratory tests. Material parameters and operating conditions were considered in the evaluation of the inner ring bore growth. The results of the study show a correlation between the amount of austenite phase present in the case micro-structure and the observed growth rate. The growth rates are, however, also significantly affected by the bearing operating temperature and the running-in conditions. Medium austenite contents in the case microstructure together with a well designed, cool running bearing can reduce inner ring growth in case-hardened bearing to acceptable levels.

INTRODUCTION

During the service life of a railway axle bearing, large variations in the operational speed, load and temperature levels, are experienced; therefore it is difficult to draw straightforward conclusions about phenomena such as inner ring bore growth from overhaul statistics. In spite of this McCrew et al. (1) concluded that a time-dependent parameter was involved. It is believed that the inner ring bore growth is related to changes in specific volume due to metallurgical phase transformations and/or accumulation of cyclic microplastic deformation (2). Both processes take place during service and are preferentially induced in the highest loaded bearing section. The current trend towards higher axle loads and increased operational speeds together with a strong requirement for high reliability of railway journal bearings over extended service intervals has defined the need for a more detailed analysis of the ring growth phenomenon.

This paper reports on experience with complete bearing units in the laboratory under simulated service conditions. The evaluation of ring growth data together with quantitative data on structural phase changes and residual stress levels is discussed.

CAUSE OF RING GROWTH

Dimensional instability of quenched and tempered steels is affected by three different mechanisms: Phase transformations, cyclic microplastic deformation and relaxation or creep (3,4,5).

Phase Transformations

Decomposition of a metastable phase or the precipitation of a new phase in the material microstructure can result in a volume change.

These phase transformations can occur during service as a result of temperature increase and/or cyclic stressing. Especially the amount of the austenite phase present in the microstructure is of importance, since decomposition of this phase results in a volume increase of 3% relative to the phase volume present.

Cyclic Micro-plastic Deformation

Cyclic stressing due to overrolling, as in roller bearings, can result in a gradual build-up of residual stresses in regions beneath the raceway. This is a direct result of the accumulation of microplastic deformations caused by the load induced stress cycles. These residual stresses present in a small sub-surface zone, which are compressive in the circumferential direction, result in an elastic strain in the bulk of the ring giving a diameter increase.

Relaxation or Creep

Primary creep under stress at moderate temperature levels can occur by which some of the circumferential induced elastic strain will be transformed into bulk plastic strain resulting in an increase of the inner ring bore diameter. The strain induced by the interference fit and/or the cyclic induced strains from the Hertzian contact load during each overrolling can contribute to this phenomenon.

These three principle mechanisms, which may cause ring growth, are affected by the operating conditions of the bearings and the material characteristics. The number of parameters which may influence the dimensional instability is shown in Fig. 1 on a qualitative basis.

The major operating conditions are load, speed and temperature. These are interrelated to some extent and influenced by bearing geometry and interference fit.

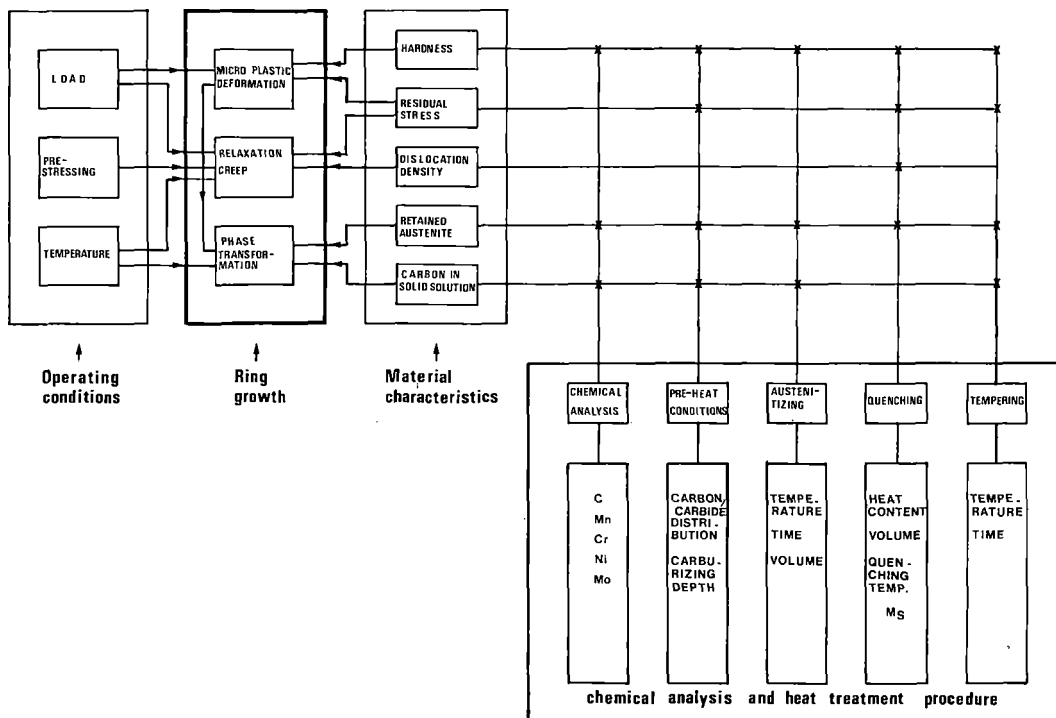


Fig. 1 Parameters affecting dimensional instability

The material characteristics are determined by the heat treatment procedure and steel composition.

Although in most practical applications only a few of the variables shown will be dominant, it is clear that many parameters are potentially present. It becomes, however, very complicated if more than one mechanism is involved at the same time. For instance, thermally activated phase transformation in pre-stressed material results in preferential growth (6). This can occur when an excessively tight interference fit is applied to bearings which operate at relatively high temperatures.

To evaluate these observations properly, information is needed on the kinetics of the phase transformations, the related volume change, the stress conditions and the material properties. Progress of the phase transformations is mainly determined by the bearing temperature, whilst relaxation depends, in addition, on the applied load, bearing geometry and relaxation behaviour of the material. Full size bearing tests under simulated field conditions should therefore be used in studying the relaxation phenomenon.

TESTING PROGRAMMES

All test bearings were of SAE 4320 carburizing steel, the composition of which is given in Table 1. The applied heat treatment cycles for the NU 226 test programme (A) are given in Table 2, and the testing

conditions for this programme are given in Table 3. Railway bearing units have been tested on modified endurance test rigs as shown in Fig.2. Testing conditions for this programme (B) are given in Table 4

TEST STRATEGY

Ring growth tests were performed within the framework of two programmes. Programme (A) was designed to analyse the effect of heat treatment parameters and Programme (B) to evaluate the performance of the railway bearing units under various realistic testing conditions. A cylindrical roller bearing, type NU 226, was selected for Programme (A) to reduce the complex grinding operation required for tapered rings. In the programme (B), parameters such as applied radial bearing load, operating temperature and test duration were varied.

DIMENSIONAL MEASUREMENTS

Dimensional measurements were carried out on all inner rings before and after testing. The inner bore diameters were measured at three equidistant positions with respect to the ring width.

For each position, the minimum and maximum bore diameters were recorded. Average values for each position before and after testing were used for the growth calculation.

The measuring accuracy was within $1 \mu\text{m}$.

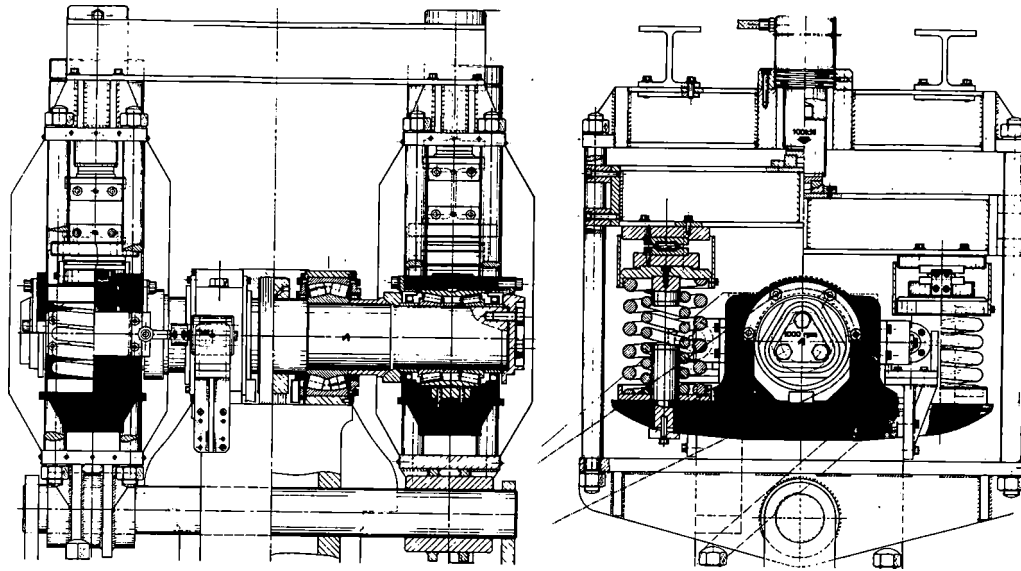


Fig. 2 Cross sections over the main shaft and adaptor of the modified test rig in the loaded and unloaded position.

C	Si	Mn	Cr	Ni	Mo
0.18	0.25	0.50	0.40	1.70	0.3

Table 1 Composition of the SAE 4320 material used (wt%)

Material 4320 (Batch)	A	B	C	D
Carburizing temp. (°C)	940	940	940	940
Carbon potential (%)	1.05	1.05	0.95	0.95
Case depth HV=525 (mm)	2.5	2.5	2.0	2.0
Diff. temp. (°C)	870	870	870	870
Quenching medium	oil	oil	oil	oil
Quenching temp. (°C)	50	50	50	50
Sub crit. temp. (°C)	590	590	590	590
Sub crit. time (hrs)	4	4	4	4
Austenitizing temp. (°C)	835	835	835	835
Austenitizing time (min)	45	45	45	45
Quenching medium	oil	oil	oil	oil
Tempering temp. (°C)	220	170	220	170
Tempering time (hrs)	4	1.5	4	1.5

Table 2 Heat treatment parameters for the NU 226 test programme (A).

Test bearing	: Cylindrical Roller Bearing type NU226
Test rig	: Standard SKF R3
Radial bearing load	: 50 (kN)
Maximum contact stress	: 1500 (MPa)
C/P	: 5.1
Operational speed	: 1000 (rpm)
Test duration	: 60 (days)
Equivalent distance	: 200.000 (km)
Lubricant	: circulating oil VITREA 68
Oil inlet temperature	: 45 (°C)
Outer ring temperature	: 70 (°C) \pm 1 (°C)

Table 3 Test conditions for the NU 226 programme (A)

Test bearing	: Railway Journal Roller Bearing 6" x 11"
Test rig	: Modified SKF R3
Radial bearing load	: 150 (kN)
C/P	: 3.7
Maximum contact stress	: 1500 (MPa)
Operational speed	: 1000 (rpm)
Test duration	: 60 (days)
Equivalent distance	: 200.000 (km)
Lubricant	: Various charges of grease ranging from 150 to 500 (gramme)
Outer ring temperature	: Aiming for 70°C
Cooling	: Forced air

Table 4 Test conditions for the Railway Journal Roller Bearing test programme (B).

X-RAY DIFFRACTION MEASUREMENTS

X-ray diffractometry techniques were used for quantitative phase analysis, residual stress analysis and for the determination of relative changes in second order stresses. These analyses were performed at and below the surface of specimens taken from both tested and untested inner rings. A number of specimens from each ring were prepared at three circumferential positions with different depths. The surfaces of all specimens were electro-polished before analysis.

Quantitative Phase Analysis

Quantitative phase analysis was used to determine the retained austenite percentage. The retained austenite content was calculated from the net intensities of two martensite and two austenite reflections using $\text{Mo K}\alpha_{1,2}$ radiation and the intensity correction factors for quantitative phase analysis given by Faninger and Hartmann (7). The accuracy was within $\pm 1\%$.

Residual Stress Analysis

Residual stresses were determined in the circumferential direction and were based upon $\alpha(211)$ line shift measurements using $\text{Cr K}\alpha_{1,2}$ radiation and the X-ray elastic constants given by Hartmann (4).

The accuracy of each determination under the selected experimental conditions was found to be about ± 50 MPa for the residual stress measurements.

Line-Broadening Measurements

Line-broadening measurements were determined on two reflections from the martensite phase and two from the austenite phase using $\text{Mo K}\alpha_{1,2}$ radiation and computer monochromatization. This type of analysis was applied in order to detect relative changes in second order stresses and/or coherence length in the atomic arrangements of both phases.

RESULTS

Programme (A)

Average data on austenite percentage and residual stress level below the raceway surfaces before and after testing are presented in Fig. 3. These data, shown as depth profiles, are typical for carburized steel and do not indicate any significant difference between the two conditions. This can be explained in the following way: either the material response under the applied load-induced stresses is entirely elastic over the given number of stress cycles or only small differences have been induced. These small differences, if present, could be obscured by relatively large scatter in the collected data. This scatter, is mainly caused by differences in microstructure and inherent to carburized materials.

However, data on the growth, obtained from these rings, show significant differences and indicate a correlation between growth, case depth and initial austenite content present in the case microstructure. This is shown in Fig. 4 where the average retained austenite level within a surface zone of 0.05 to 0.4 mm is plotted against the observed growth.

This effect of case depth and austenite level on ring growth was further investigated to determine the effect of time and microstructure.

From each of the four batches, four rings were taken for an additional second testing period under the same tightly controlled running conditions. The results shown in Fig. 5 clearly indicate that in all four cases, a considerably smaller amount of growth had been added to the growth than that obtained after the first test period.

That these trends and differences could be detected is due only to the tight control of the operating temperature ($\pm 1,0^\circ\text{C}$). The temperature level of 70°C was maintained by a controlled oil flow through the bearings.

Programme (B)

Using grease lubrication, the operating temperature is much more difficult to control. This was the experience with the railway bearing unit test programme. Differences in grease charge and seal configuration significantly affect the operating temperatures. Average temperature levels during this test programme ranged from 59 to 78°C depending upon the friction losses inside the bearing units. The growth observed in this test programme showed a greater spread in values than that observed with the NU 226 programme (A), and it was found that the extent of growth increases significantly with higher operating temperatures.

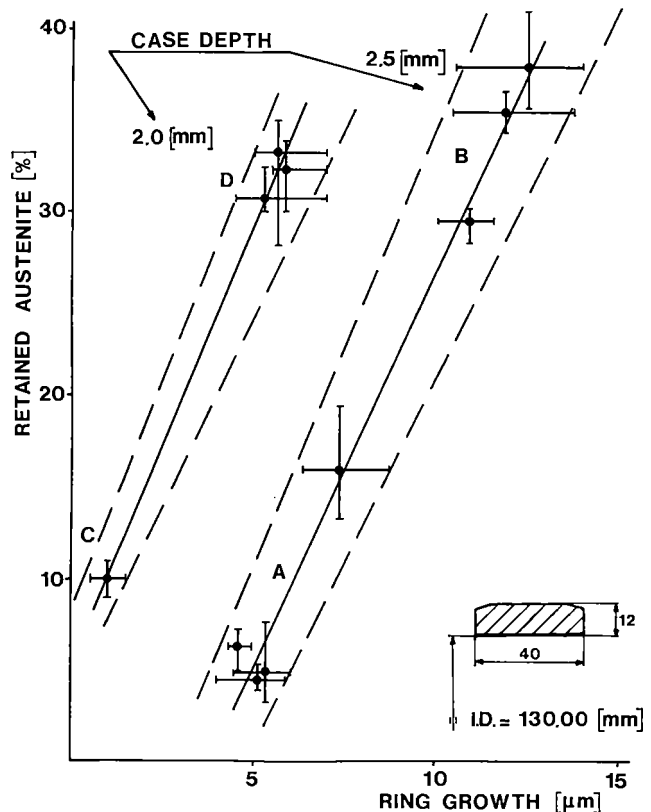


Fig. 4 The relationship between the average retained austenite level in a surface zone of 0.4 mm thickness and the growth observed after 200.000 km testing.

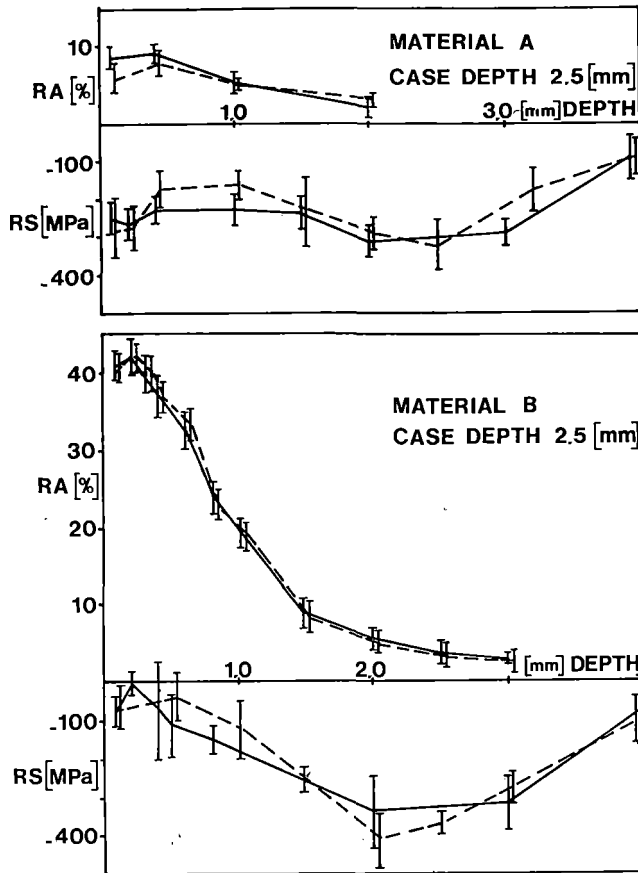


Fig. 3a The retained austenite and residual stress distribution below the raceway surfaces (—) tested (-----) unrun.

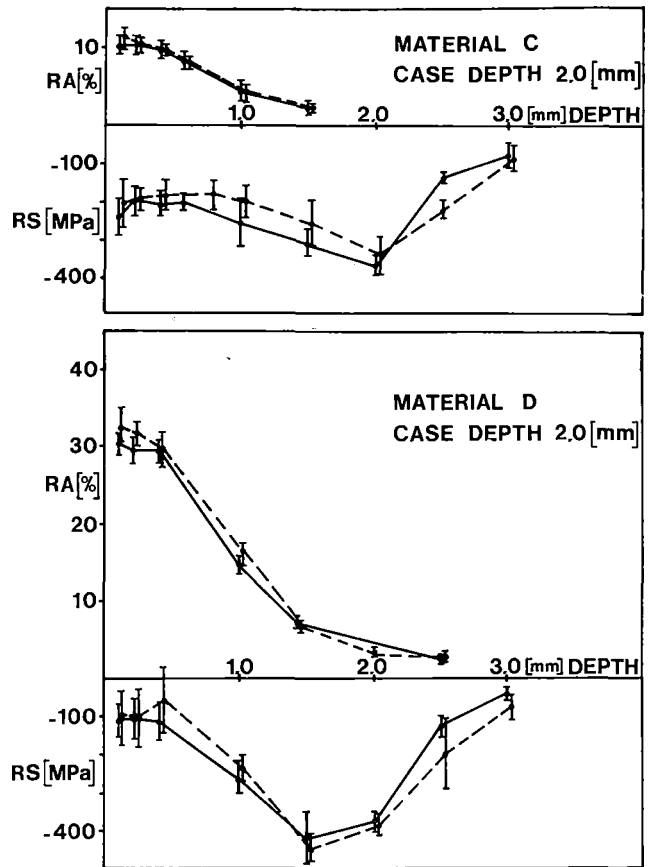


Fig. 3b The retained austenite and residual stress distribution below the raceway surfaces (—) tested (-----) unrun.

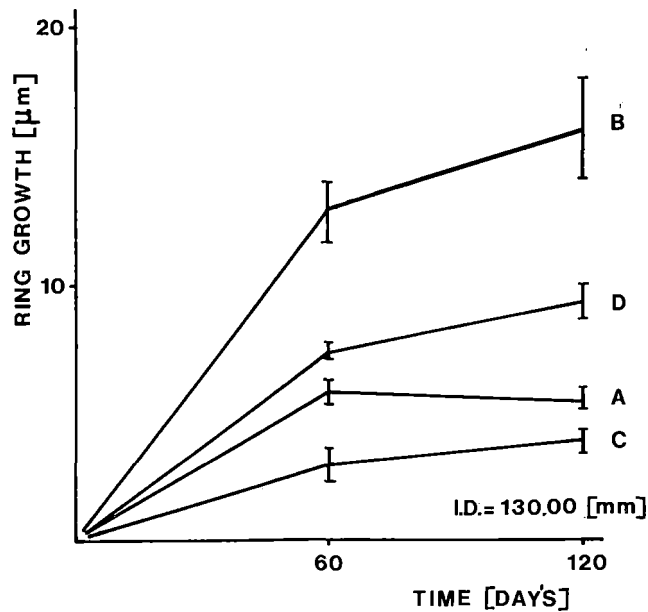


Fig. 5 The effect of test duration on the extent of ring growth.

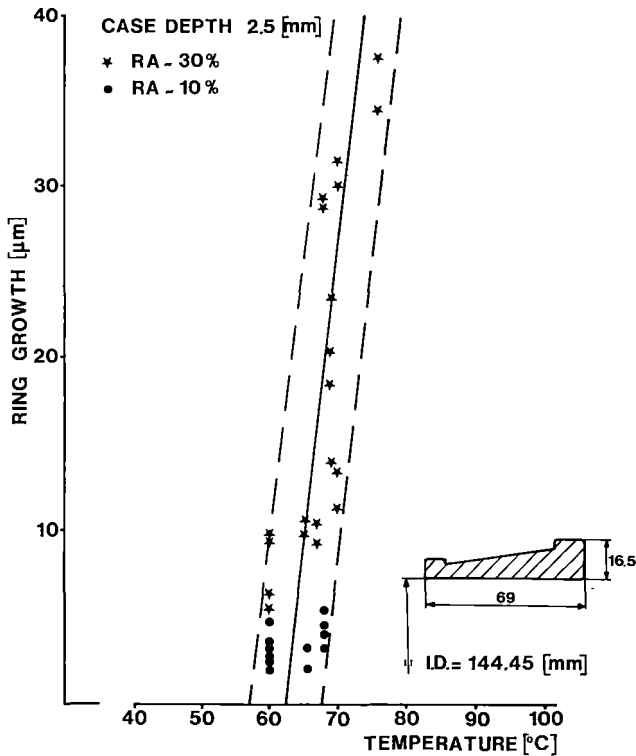


Fig. 6 The effect of the mean temperature, as measured at the outer ring of the Journal Roller Bearing, on growth observed after 200.000 km testing.

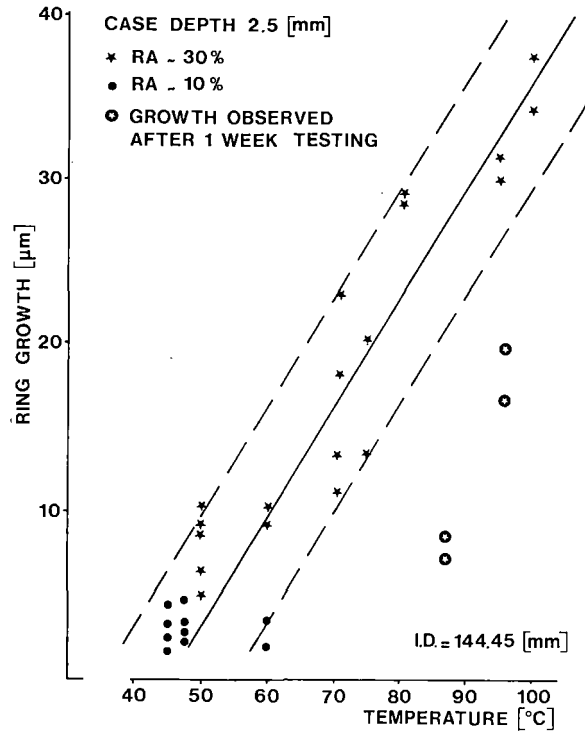


Fig. 7 The effect of the "running-in" temperature in the first week of the test on the growth as observed after 200.000 km testing.

This effect is shown in Fig. 6. and indicate that, for the load and speed conditions involved, almost zero growth can be obtained if the operating temperature level, as measured on the outer ring, is kept below 60°C.

The growth data in this figure still reveal a rather large scatter for a given average outer ring temperature. Part of this can be explained by differences in austenite level in the microstructure. However, a remarkable correlation between growth and average "running-in" temperature was found, which also revealed less scatter as shown in Fig. 7. These data indicate that a considerable part of the observed growth appears to occur during the first week of the bearing service life. Short "running-in" tests with new rings confirmed these findings. These results are also indicated in Fig. 7, and it can be concluded from these that 50% of the total growth can occur during this running-in period and depends upon maximum temperature level reached. It should be noted that temperatures in excess of 140°C have been found at various positions on the rotating inner ring flange when the outer ring peak temperature during "running-in" was 90°C. These figures were recorded with "Temp-plate" stickers and indicate that, in particular during the "running-in" period, substantially higher temperatures are reached by the inner ring than those measured on the outer ring.

A number of inner rings from these tested journal roller bearings were further examined with X-ray diffraction techniques for austenite content and residual stress level at and below the raceway surface. Particular attention was given to these rings with high growth figures. Fig. 8 shows typical diffractograms for run and unrun conditions taken from specimens 200 μm below the raceway.

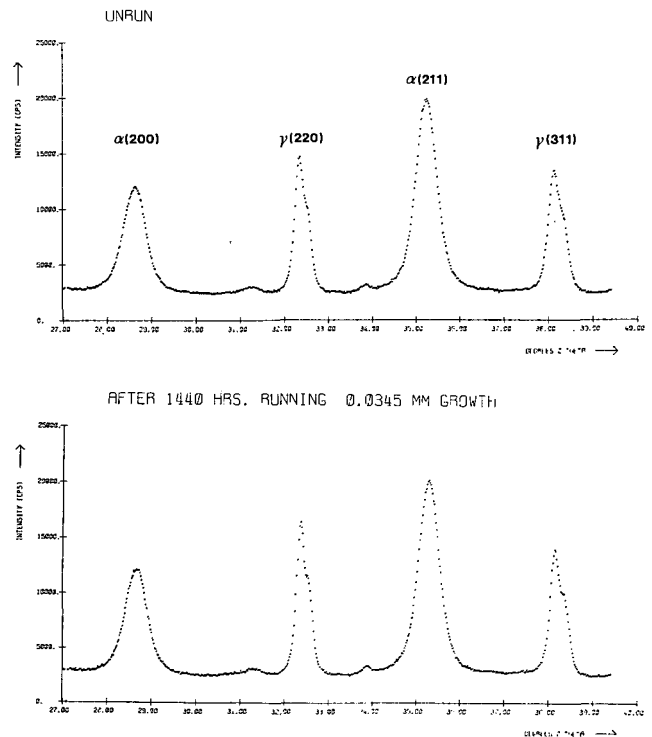


Fig. 8 Part of the X-ray diffractograms, showing the line shapes of the two austenite and two martensite reflections as observed on samples taken from both tested and untested rings at 200 μm below the raceway.

The tested rings showed a growth of 34,5 μm after testing. The specimens were also examined for relative changes in second order stresses by means of line broadening measurements. None of the data in Table 5 show any significant change due to 200.000 km endurance. The average austenite levels in the surface zone plotted against the observed growth for all tested inner rings, shown in Fig. 9 however, qualitatively confirms the trend as observed with the NU 226 inner rings: the higher the austenite level present in the case, the higher the growth level.

Test duration (hrs)	Depth (μm)	R.S. (MPa)	R.A. (%)	F.W.H.M. (degrees 2θ MoK α)			
				α (200)	γ (220)	α (211)	γ (311)
Unrun	- 50	-145	33	0.53	0.22	0.49	0.27
	-200	- 15	34	0.54	0.23	0.48	0.28
	-400	-115	32	0.52	0.23	0.47	0.28
	-600	- 90	24	0.53	0.24	0.46	0.29
1440 (60 days)	- 50	-185	34	0.54	0.22	0.48	0.26
	-200	- 85	35	0.53	0.21	0.46	0.25
	-400	-115	32	0.52	0.21	0.47	0.27
	-600	-135	24	0.53	0.25	0.44	0.30

R.S. is the Residual Stress as measured in the circumferential direction.
 R.A. is the amount of Retained Austenite in the material microstructure.
 F.W.H.M. is the Full Width at Half of the Maximum intensity of the recorded line profile.
 α (200) and α (211) are two crystallographic planes of the martensite phase
 γ (220) and γ (311) are two crystallographic planes of the austenite phase

Table 5 X-ray diffraction data obtained from several analyzed inner rings with 30 to 40 μm growth.

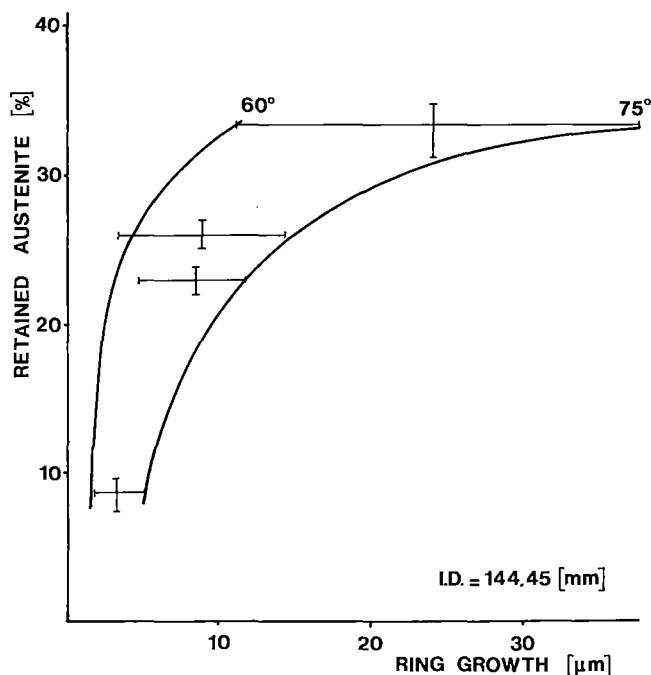


Fig. 9 The relationship between the average retained austenite level in a surface zone of 0.4 mm thickness and the growth as observed after 200.000 km testing.

DISCUSSION

It is clear from all presented data that the magnitude of ring growth is affected by both the material microstructure and the operating temperature. A relationship has been found between the austenite content in the case and the inner ring bore growth for rings tested at a fixed and constant operating temperature. Increasing the operating temperature shows an increase in the growth figures. Ring growth appears to occur in two stages: the first during the "running-in" period, during which the growth amplitude depends on the highest temperature level experienced during that period, the second takes place during steady state testing, but at a much smaller rate.

There is no indication that austenite decomposition occurs due to long term testing, nor is there evidence of a build-up in residual stresses due to accumulated microplastic deformation in the highest loaded sub-surface material volume.

The scatter in the data might have masked minor changes; but, even the microstructure of inner rings with 30 to 40 μm growth, did not show any detectable change in austenite level or in residual stress. This indicates that, for the applied loading conditions, the material resistance to cyclic stressing is sufficiently high to avoid microplastic deformation and/or decomposition of austenite.

These results therefore do not support a model for ring growth based upon volume changes induced by austenite decomposition or shape changes resulting from overrolling induced residual stresses. It is clearly shown that growth increases with an increase in operating temperature especially if a high austenite level is present in the case microstructure. Such high austenite levels present are normally coupled with relatively high levels of dissolved carbon in the martensite and austenite phase. Although an initial tempering treatment activates carbon migration and carbide precipitation in the form of Fe_2C carbides (the first stage of tempering) not all of the carbon is rejected from the martensitic phase. Results previous obtained (9) have shown that this process is not completed by a tempering treatment at 150°C for 1 or 2 hours; but, that it continues even during the austenite transformation in the second stage of tempering. Carbon rejection, however, is coupled with volume reduction, and the presence of a stress field is required to produce a size increase by this mechanism if the austenite does not decompose.

The results discussed clearly indicate a creep or relaxation phenomenon, by which the resistance of the material is lowered particularly if high austenite contents are present in the case microstructure. The main trends found in this study are qualitatively in agreement with a creep phenomenon; increased growth rate with higher austenite volume fractions, with higher case depths and with higher operational temperatures. Further studies will be needed to quantify these trends.

A direct practical solution to the ring growth problem of case-carburized rings appears to be to maintain a low austenite level in the case microstructure.

It is not recommended, however, to aim for an austenite-free case in carburized bearing rings. A certain amount of austenite in the microstructure of the direct raceway surface enhances the resistance to contact fatigue damage (10). This relatively soft phase allows for local peak stress relaxation in the immediate vicinity of microdefects, and lowers the probability of surface crack initiation.

Furthermore, it should be noted that the lowering of the austenite level through too high a tempering treatment gives rise to cementite formation (M_3C) in the microstructure (start of third stage of tempering) which reduces the local ductility and consequently the mechanical properties.

The optimized design with SAE 4320 steel should therefore have a specified retained austenite level in the case (15 to 20%) and a well-selected case depth. Further optimization must come from the bearing design and from carefully selected grease charges to reduce the internal friction losses and maintain the lowest operating temperature.

REFERENCES

1. McCrew, Jr. J.M., Krauter, A.M., and Moyer, G.J., "Reliability of Railroad Roller Bearings," ASME Journal of Lubrication Technology, Vol. , 1977, pp. 30-40.
2. ibid reference 1 discussion STEEL, R.K. page 39.
3. Kurdjumov, G.V., "Phenomena Occurring in the Quenching and Tempering of Steel," Journal of the Iron and Steel Institute, Vol. 5, 1960, pp. 26-48.
4. Lement, B.S., "Distortion in Tool Steels," Transactions of ASM Metals Park Novelty Ohio 1959.
5. Lement, B.S. Averbach, B.L., and Cohen, M., "Microstructural Changes on Tempering Iron-Carbon Alloys," Transactions of ASM, Vol. 46, 1954, pp. 851-881.
6. Lucas, G., Nützel, H., "Gefüge- und Massänderungen von Wälzlagerteilen bei erhöhten Betriebstemperaturen," Wälzlagertechnische Sonderschriften, no. 99, SKF Schweinfurt, Dd 5379.1.69, Rep. 41715.
7. Faninger, G., and Hartmann, U., "Physikalische Grundlagen der quantitativen röntgenographischen Phasenanalyse," HTM 27, November, 1972, pp. 233-244.
8. Hartmann, U., PhD thesis, University of Karlsruhe 1973.
9. Voskamp, A.P., "Einfluss der Kohlenstoffausscheidung und der Restaustenitumwandlung auf die Massänderung von gehärtetem Wälzlagerstahl 100 Cr6." Fachausschuss Spannungszustand und Werkstoffverhalten, Beitrage am 30-4-1977, unpublished.
10. Sheehan, J.P., and Howes, M.A.H., "The Effect of Case Carbon Content and Heat Treatment on the Pitting Fatigue of 8620 Steel", Soc. of Automotive Engineers, Autom.Eng.Conference Congress, Jan. 10-14, 1972, no. 720268.

Researches on the Dynamics of Bo-Bo Electric Locomotives

T. Ionescu

Senior Scientific Researcher, The Institute of Technological Research & Design in Transports Bucharest, Romania

A. Lie

Head to the Locomotive Research Department, The Institute of Technological Research & Design in Transports, Bucharest, Romania

A programme of theoretical and experimental research has been established for the four-axle electric locomotive, aiming at achieving a better dynamic behaviour of the locomotive, higher reliability of the rolling equipment as well as the least possible negative effect upon the track. Along with the theoretical efforts for considering the analytical models and mathematical representations of the locomotive and track, and the vehicle-track interaction phenomena, the research has also been focused on the experimental aspects of evaluating and measuring the functional dynamic characteristics of the locomotive in keeping with track parameters. The results, which can be considered technically and economically, characterise the dynamic behavior of the vehicle, the quality and state of the track as well as their complex correlations.

NOMENCLATURE

A	constant describing rail roughness, $m^2 \text{cycle/m}$
c	damping coefficient, KNs/m
D	damping ratio
f	spatial frequency, cycle/m
H	relative displacement transmissibility
J	pitch moment of inertia, Kgm^2
k	stiffness constant, KN/m
m	mass, Kg
Q	suspension quality factor
s	Laplace transform variable
S_i	vibration amplitude of i order
S_z	power spectral density for rail vertical profile, $m^2/\text{cycle/m}$
T	period of vibration, s
u	vertical track input, mm
x	longitudinal displacement, mm
z	vertical displacement, mm
δ	logarithmic decrement
θ	pitch displacement, rad
ϕ	roll displacement, rad
ω	angular frequency, rad/s

SUBSCRIPTS

o	total or reference value
a	for the wheel-axle set
B	for the carbody
cr	critical value
d	refers to damped motion
t	for the truck
x	refers to longitudinal direction
z	refers to vertical direction

SUPERSCRIPTS

.	first-order derivative
..	second-order derivative
-	vector

INTRODUCTION

A comprehensive theoretical and experimental research is being developed for the 3,400 Kw four-axle electric locomotive, aiming at achieving its better dynamic behaviour, the higher reliability of the elements of the rolling equipment and the least possible negative effect upon the track.

The present stage of the research consists in the constructive and functional analysis of the locomotive regarding its dynamic behaviour, the performances of its suspending and damping systems as well as the resistance and working life of the rolling parts.

The paper goes into the dynamics of the locomotive in simulated conditions on the test rig as well as in actual exploitation.

The results of this analysis could be useful in reconsidering and redesigning some mechanical parts of the locomotive and even in building a new, improved locomotive.

THEORETICAL ANALYSIS

The analysis refers to the dynamics of the locomotive and the vehicle-rail interaction, pointing out the vertical response phenomena of the locomotive to the track irregularities and disturbances.

Mechanical Model of the Locomotive

The functional-constructive diagram of the four-axle locomotive is presented in Fig. 1 (1).

parameters; the superposition principle for inputs and outputs is applied and the frequency analysis is valid;

- b) the locomotive carbody and trucks are considered absolutely rigid;
- c) the suspension and damping elements are considered linear;
- d) the angular displacements have small amplitudes;
- e) the wheelsets are in continuous contact with the rails, acting essentially as one; the excitations of the vehicle may be considered motion inputs arising from roadbed disturbances and acting through the rail elements;
- f) the locomotive construction is symmetrical against a vertical plane passing through its geometric centreline.

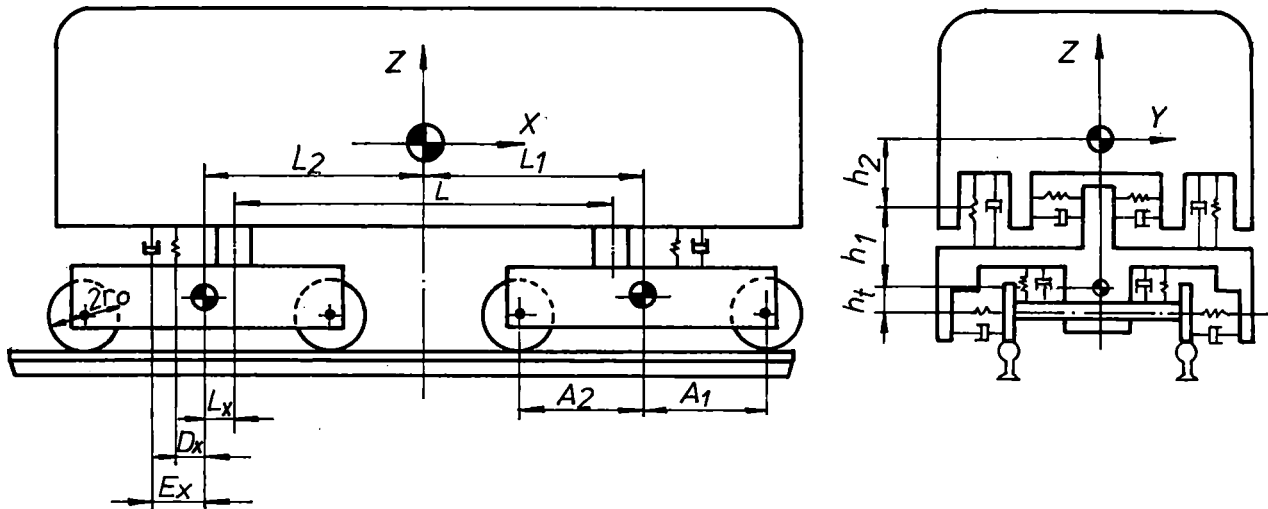


Fig. 1 Functional diagram of the 4-axle locomotive

- (A₁) Distance between Wheelset 1 and gravity centre of the truck
- (A₂) Distance between Wheelset 2 and gravity centre of the truck
- (D_x) Distance between gravity centre of the truck and the vertical axis of secondary suspension
- (E_x) Distance between gravity centre of the truck and the vertical axis of secondary dampers
- (h₁) Vertical distance between gravity centre of the truck and secondary suspension
- (h₂) Vertical distance between gravity centre of the carbody and secondary suspension
- (h_t) Vertical distance between gravity centre of the truck and the axis of the wheelset
- (L) Distance between the bolsters of Truck 1 and Truck 2
- (L₁) Distance between gravity centre of the carbody and gravity centre of Truck 1
- (L₂) Distance between gravity centre of the carbody and gravity centre of Truck 2
- (L_x) Distance between gravity centre of the truck and the axis of the bolster
- (r₀) Wheel tread radius

Fig. 2 shows the vertical mechanical model. It is made up of the unsuspended masses of the wheelsets, the suspended masses of the trucks and the carbody and the primary and secondary suspending and damping vertical systems (2, 3).

We have to note the following about the mechanical model:

- a) the model is linear, with lumped

The assumptions of linearity and symmetry make it possible to consider vertical motions and lateral and roll motions independently.

Track Representation

Considering its effects upon rail vehicles, a homogeneous segment of track may be defined by three basic processes (4):

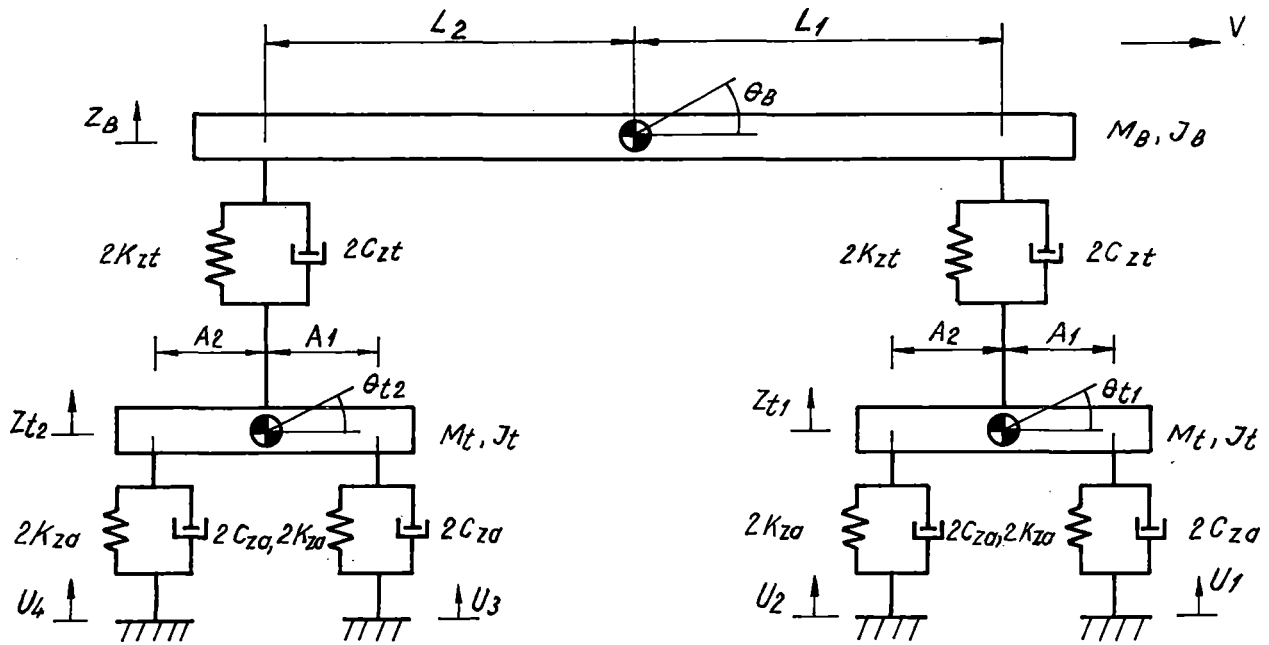


Fig.2 Mechanical model of the locomotive on a vertical plane

- (c_{za}) vertical damping coefficient of primary suspension, for an axle box
- (c_{zt}) vertical damping coefficient of secondary suspension, for half of the truck
- (k_{za}) vertical stiffness constant of primary suspension, for an axle box
- (k_{zt}) vertical stiffness constant of secondary suspension, for half of the truck
- (V) locomotive forward speed

a) a periodic deterministic process represented by the rectified sine wave of u_0 amplitude and wave length corresponding to the distance between joints (Fig. 3); this is valid for welded rails, too, due to the "ballast memory" phenomenon; it is expressed

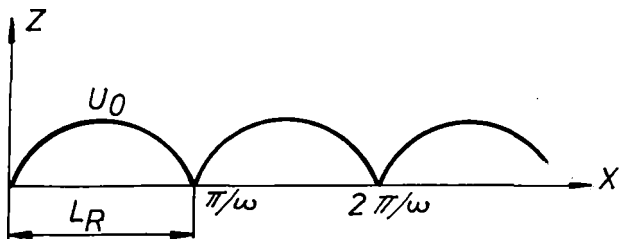


Fig.3 Periodic deterministic rail vertical irregularity

by:

$$u(t) = u_0 |\sin(\omega t)| \quad (1)$$

b) a stationary random process considered with the help of the associated power spectral density (PSD) of the vertical profile, expressed by:

$$S_z(f) = \frac{A}{f^2} \quad (2)$$

c) a modulated periodic deterministic process. The modulation of the periodic process is expressed by reshaping the associated

narrow spectral lines and results in broadening spectral lines and developing sidebands, etc.

Assuming that all periodic processes are independent of the random process, their PSDs become additive. In this way, the PSD, representing rail irregularities and considered in theoretical studies, is a combination of the contributions of the three basic processes (Fig. 4).

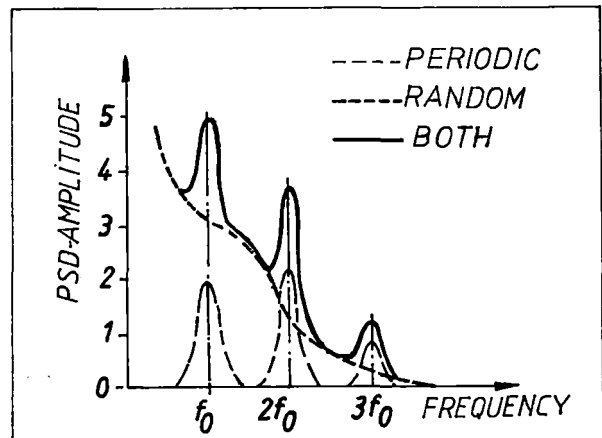


Fig.4 All-round view of rail irregularities

Vertical Plane Equations of Motion

Vertical plane movements of the locomotive may be described function of the mechanical model with six degrees of freedom, shown in Fig. 2. The six degrees of freedom are the vertical displacement (bounce) and pitch displacement of the trucks and carbody ($z_{t1}, \theta_{t1}, z_{t2}, \theta_{t2}, z_B, \theta_B$).

The six second-order differential equations of motion are:

a) carbody equations:

$$m_B \ddot{z}_B + 2c_{zt} [(\dot{z}_B - \dot{z}_{t1} + L_1 \dot{\theta}_B) + (\dot{z}_B - \dot{z}_{t2} - L_2 \dot{\theta}_B)] + 2k_{zt} [(z_B - z_{t1} + L_1 \theta_B) + (z_B - z_{t2} - L_2 \theta_B)] = 0 \quad (3)$$

$$J_B \ddot{\theta}_B + 2c_{zt} [(\dot{z}_B - \dot{z}_{t1} + L_1 \dot{\theta}_B)L_1 - (\dot{z}_B - \dot{z}_{t2} - L_2 \dot{\theta}_B)L_2] + 2k_{zt} [(z_B - z_{t1} + L_1 \theta_B)L_1 - (z_B - z_{t2} - L_2 \theta_B)L_2] = 0 \quad (4)$$

b) truck 1 (front) equations:

$$m_t \ddot{z}_{t1} + 2c_{za} [(\dot{z}_{t1} - \dot{u}_1 + A_1 \dot{\theta}_{t1}) + (\dot{z}_{t1} - \dot{u}_2 - A_2 \dot{\theta}_{t1})] - 2c_{zt} (\dot{z}_B - \dot{z}_{t1} + L_1 \dot{\theta}_B) + 2k_{za} [(z_{t1} - u_1 + A_1 \theta_{t1}) + (z_{t1} - u_2 - A_2 \theta_{t1})] - 2k_{zt} (z_B - z_{t1} + L_1 \theta_B) = 0 \quad (5)$$

$$J_t \ddot{\theta}_{t1} + 2c_{za} [(\dot{z}_{t1} - \dot{u}_1 + A_1 \dot{\theta}_{t1})A_1 - (\dot{z}_{t1} - \dot{u}_2 - A_2 \dot{\theta}_{t1})A_2] + 2k_{za} [(z_{t1} - u_1 + A_1 \theta_{t1})A_1 - (z_{t1} - u_2 - A_2 \theta_{t1})A_2] = 0 \quad (6)$$

c) truck 2 (rear) equations:

$$m_t \ddot{z}_{t2} + 2c_{za} [(\dot{z}_{t2} - \dot{u}_3 + A_1 \dot{\theta}_{t2}) + (\dot{z}_{t2} - \dot{u}_4 - A_2 \dot{\theta}_{t2})] - 2c_{zt} (\dot{z}_B - \dot{z}_{t2} - L_2 \dot{\theta}_B) + 2k_{za} [(z_{t2} - u_3 + A_1 \theta_{t2}) + (z_{t2} - u_4 - A_2 \theta_{t2})] - 2k_{zt} (z_B - z_{t2} - L_2 \theta_B) = 0 \quad (7)$$

$$J_t \ddot{\theta}_{t2} + 2c_{za} [(\dot{z}_{t2} - \dot{u}_3 + A_1 \dot{\theta}_{t2})A_1 - (\dot{z}_{t2} - \dot{u}_4 - A_2 \dot{\theta}_{t2})A_2] + 2k_{za} [(z_{t2} - u_3 + A_1 \theta_{t2})A_1 - (z_{t2} - u_4 - A_2 \theta_{t2})A_2] = 0 \quad (8)$$

The equations may be solved either in the time or in the frequency domain. In the time domain, the time history of the solutions is ascertained. Using state variable techniques, when the bounce, bounce rate, pitch, pitch rate of the trucks and carbody are the state variables, we come to twelve first-order differential equations, which can be solved through numerical integration. Numerical integration procedures, such as Wilson- θ or Newmark methods, may be used alternatively.

Using the Laplace transform, the original second-order differential equations

result in a set of linear algebraic equations which can be considered under the form:

$$\{[A]s^2 + [B]s + [C]\} z(s) = \{\bar{b}(s)s + \bar{c}(s)\} u(s) \quad (9)$$

where the square brackets designate a square matrix.

In the frequency domain, the substitution variable $s = j\omega$ is employed and the complex linear nonhomogeneous set of equations is solved for discrete values of frequency. Both cases require the use of digital computers and applied calculus algorithms.

EXPERIMENTAL ANALYSIS

After the theoretical approach for achieving proper analytical models of the locomotive and the track and their mathematical consideration, the analysis has been focussed on the experimental aspects of evaluating and measuring the actual functional dynamic characteristics of the locomotive, in keeping with the track parameters.

Measuring Methodology and Test Programme

After an elaborated analysis, we decided to perform the following measurements with the locomotive (6, 11):

a) vertical relative displacement between axle box and truck frame, on the left and right, at the leading wheelset of the locomotive (two measurement points);

b) vertical relative displacement between truck frame and carbody, at the leading truck, aligned with the secondary suspension, on the left and right (two measurement points);

c) vertical relative displacement between truck frame and carbody, at the leading truck, in the middle of the frontal beam (one measurement point);

d) vertical and horizontal accelerations, on one of the axle boxes of the leading wheelset (two measurement points);

e) vertical and horizontal accelerations in truck frame, above the leading wheelset, on the same side as d) measurement (two measurement points);

f) vertical acceleration in truck frame under its geometric centre (one measurement point);

g) vertical acceleration in carbody, aligned with the centre of the leading truck, on the same side as d) and e) measurements (one measurement point);

h) vertical acceleration in carbody, under its geometric centre (one measurement point);

i) vertical and horizontal accelerations in the locomotive driving cab, at the floor level (two measurement points). In this way the performances of the suspending-damping systems are measured and evaluated through dynamic vibratory responses in displacement and acceleration.

The disposal of the measurement points is schematically shown in Fig. 5 and details about mounting transducers are presented in Fig. 6 and Fig. 7.

The measuring methodology and programme try to point out the behaviour of the sus-

pending-damping systems and the dynamic response of the locomotive to the track vibration and shock inputs developed in tangent track and curves. The overall response is

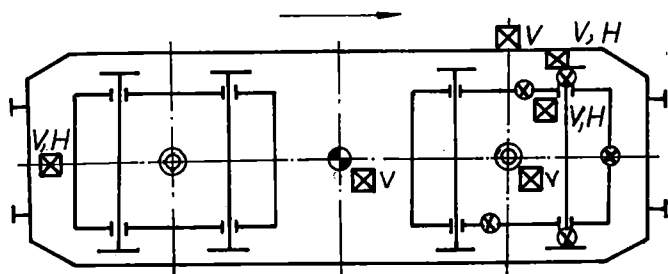


Fig.5 Lay-out of transducers within the locomotive

- ⊗ Vertical displacement transducers
- ⊠ V,H Vertical and horizontal acceleration transducers

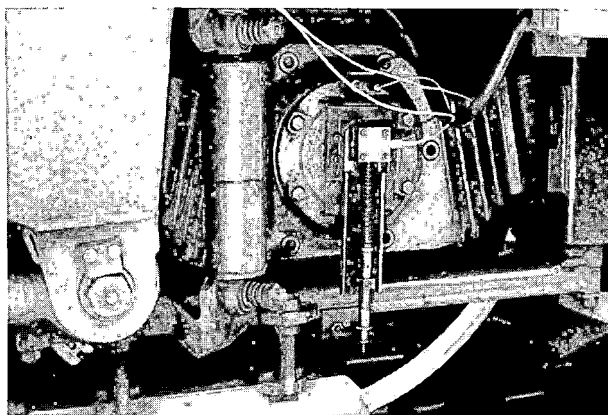


Fig.6 Displacement and vibration transducers within the axle box

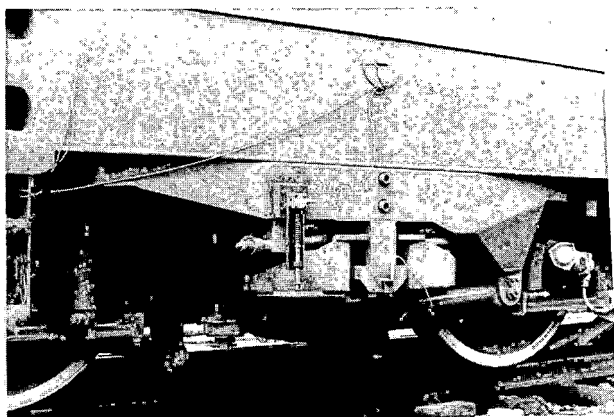


Fig.7 Displacement and vibration transducers within the carbody

determined by the input-output relations, transmissibilities and frequency transfer functions.

At the time of the experiments, the locomotive had run about 1,000 km since the

latest tread reshaping into a normal 1/20 tapered wheel profile.

The track disturbances were considered to have identical effects for all the four axles and to be delayed function of the speed and the distances between the axles.

We used displacement transducers of + 50mm maximal value and acceleration transducers of 200 m/s² and 1,000 m/s² nominal values, both of Hottinger-Baldwin construction. The measuring, controlling and recording equipment consisting of two 6-channel amplifying bridges (Hottinger-Baldwin), a specialized tape-recorder (Philips) and an oscilloscope were placed in a measurement car next to the locomotive. Their connection is schematically shown in Fig. 8. All chosen

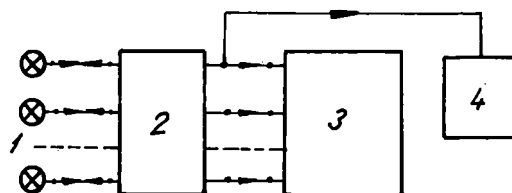


Fig.8 Block diagram of the measuring apparatus

- (1) Transducer
- (2) Measuring amplifying bridge
- (3) Tape-recorder
- (4) Oscilloscope

points were measured and recorded simultaneously. The experiments, carried out in a progressive manner at speed intervals of 10 km/h up to 120 km/h, observed running safety at all times.

Besides dynamic measurements, strain gauge measurements were accomplished, too. They aimed at determining the distribution and level of strains in the rolling equipment under static and normal exploitation conditions and establishing the regions characterized by extreme mechanical efforts. This was achieved by mounting simple and special sets of strain gauges and measuring and recording the stress components of interest. Processing the recorded experimental data, using a digital computer, made it possible to evaluate and establish the fatigue behaviour and lifetime of the elements of the rolling equipment (7).

Test Rig Experiments

The experiments were carried out in simulated conditions on the test rig and in normal conditions of exploitation within traffic sections.

The test rig, schematically presented in Fig. 9, was provided with tangent track and curve sectors for speeds up to 140 km/h as well as with sectors characterized by specially built rail defects of different types, nominal values and successions. The disposal of the specially arranged track sectors I, II, III, IV is shown in Fig. 10 and their characteristics are presented in Fig. 11.

To reveal the dynamic behaviour of the locomotive at shock excitements, one hillock

was arranged at the same place on the two rails, with a vertical maximum permitted deviation, followed by a sector of good track (at 10.900 km).

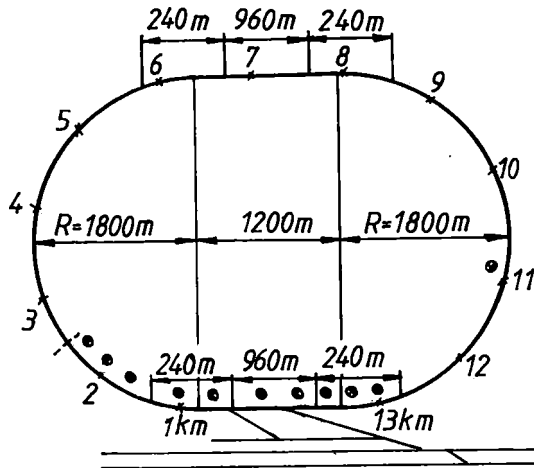


Fig.9 Diagram of the test rig

- ⊗ track prepared with irregularities
- 960 m tangent track
- 240 m connecting curve

At the end of the experiments, the test rig track was measured and its characteristics recorded with a track geometry car confirming the specially built irregu-

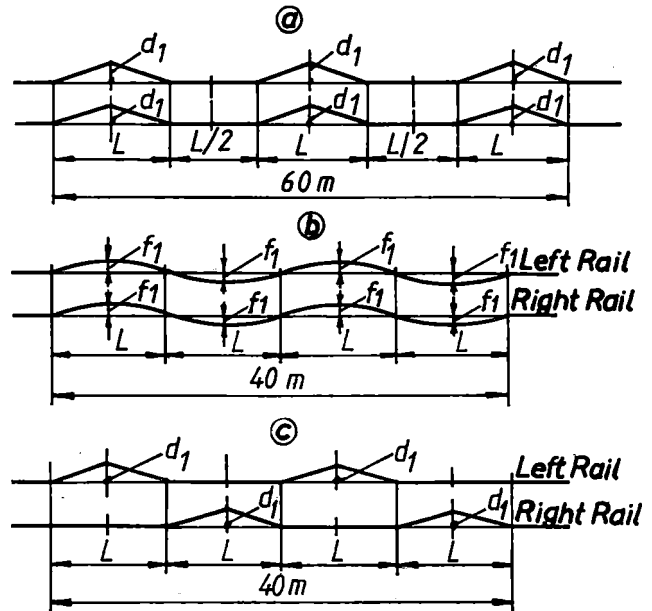


Fig.11 Rail irregularities characteristic of the four arranged sectors

- (a) irregularities in sectors I&IV
- (b,c) irregularities in sectors II&III
- $d_1 = 10 \text{ mm}$; $1/500$ gradient
- $f_1 = 10 \text{ mm}$

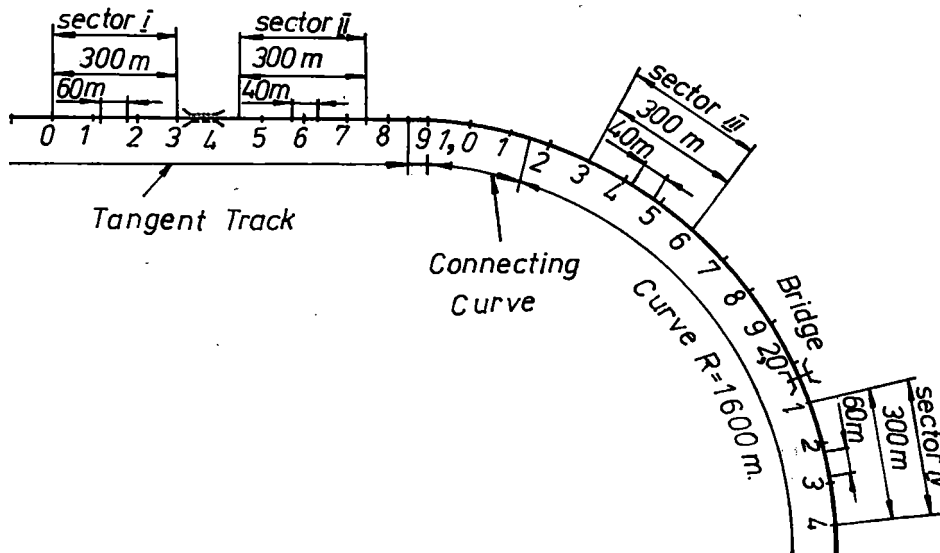


Fig.10 The disposal of measurement track sectors with irregularities

- Sector I vertical profile rail irregularities in tangent track
- Sector II horizontal profile rail irregularities combined with twists in tangent track
- Sector III horizontal profile rail irregularities combined with twists in curve
- Sector IV vertical profile rail irregularities in curve

larities qualitatively and quantitatively (Fig. 12). The vertical irregularities of the left rail, about 10.900 km, are partly presented for exemplification in the appendix.

THE ANALYSIS OF EXPERIMENTAL DATA

The experimental data of the relative displacements are processed and analysed as shown in the block-diagram of Fig. 13. The

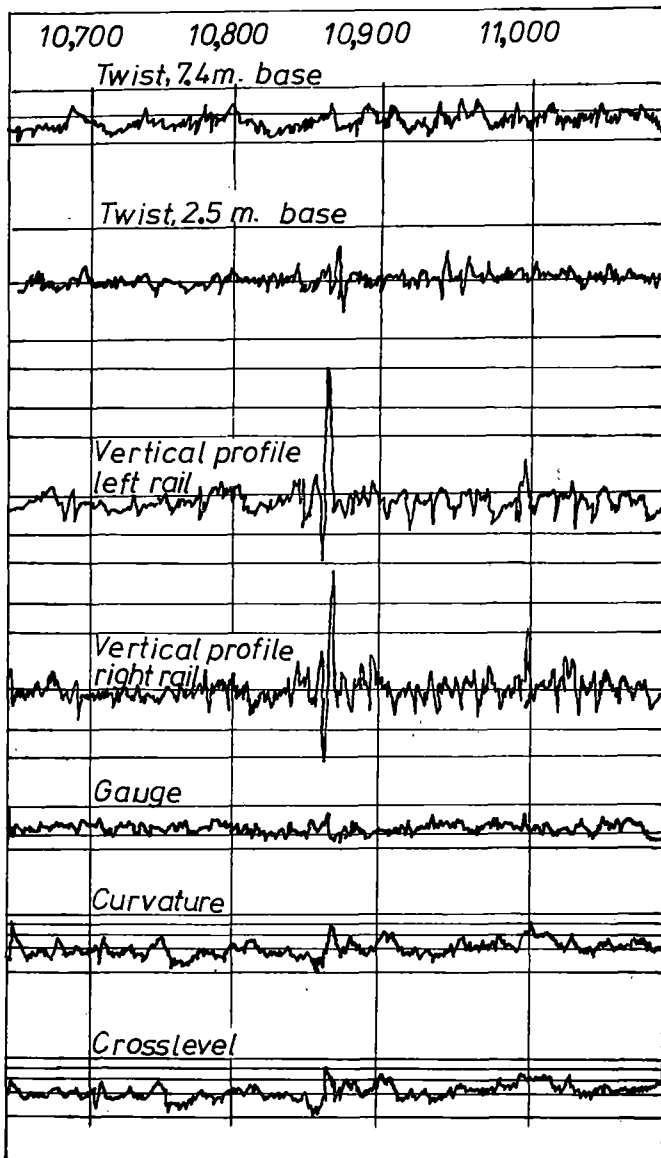


Fig.12 A record of the track geometry car including the unique extreme irregularity

analogously recorded data on magnetic tape are transferred onto ultra-violet oscillograph tape and then converted by digitization. The subsequent analysis is ensured by a desktop computer (6).

The analysis of the data defining the constructive characteristics of the test rig track follows the same routine with the recording tape of the track geometry car as the primary source (6).

During the analysis of the experimental data regarding the absolute accelerations of locomotive parts, correlated with track measurements, we found that the working volume exceeded our predictions. We are going to complete this analysis in order to have a general view of the problem. The analysis is partly based on a programme, which, starting from the discrete Fourier transform (DFT)

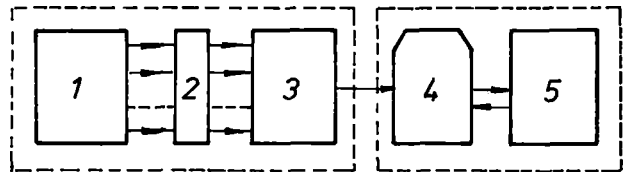


Fig.13 Block diagram of the apparatus used in experimental data analysis

- (1) Tape recorder (Philips, Analog 14)
- (2) Electrical adjustments
- (3) Oscillograph (ABEM, Ultralette 5681)
- (4) Digitizer (Hewlett-Packard 9874A)
- (5) Desktop computer (Hewlett-Packard 9835A)

by using the fast calculus algorithm (FFT), leads to determining the correlation functions, power spectral densities of the input and output signals and eventually the track-locomotive transfer functions (8, 9, 10). We are also going to get features of the riding quality of this locomotive.

Fig. 14 presents a sequence characterizing the vibratory response in displacement of the locomotive to the extreme track irregularity at a running speed of 110 km/h.

The singular track irregularity proved to be very efficient in characterizing the dynamic response of the locomotive to vertical shocks and in evaluating the suspending-damping systems. We were able to materialize and measure the primary and secondary vibration logarithmic decrements without appealing to extensive techniques, such as the Random-Decrement, etc (12).

The dynamic functional characteristics of the Bo-Bo electric locomotive, revealed by experiments and retained for analysis, function of the locomotive speed, are (6):

- 1 relative displacement amplitude (rda) between axle box and truck frame (primary);
- 2,3 rda between truck frame and carbody, lateral left and right (secondary);
- 4 rda between truck frame and carbody, mid frontal (secondary);
- 5 relative position of truck frame and carbody, along the longitudinal central line, at secondary suspension abscissa;
- 6 component of pitch displacement between truck frame and carbody;
- 7 relative pitch angle of truck frame and carbody $|\theta_B - \theta_{t1}|$;
- 8 component of roll displacement between truck frame and carbody;
- 9 relative roll angle of truck frame and carbody $|\phi_B - \phi_{t1}|$;
- 10;11&12 primary relative displacement transmissibility (rdt) ; lateral and mid frontal secondary rdt;
- 13;14 ratio of lateral secondary rdt to primary rdt; ratio of mid frontal secondary rdt to primary rdt;
- 15;16&17 stabilization time of the primary vibratory response (pvr); stabilization time of the secondary lateral and mid frontal

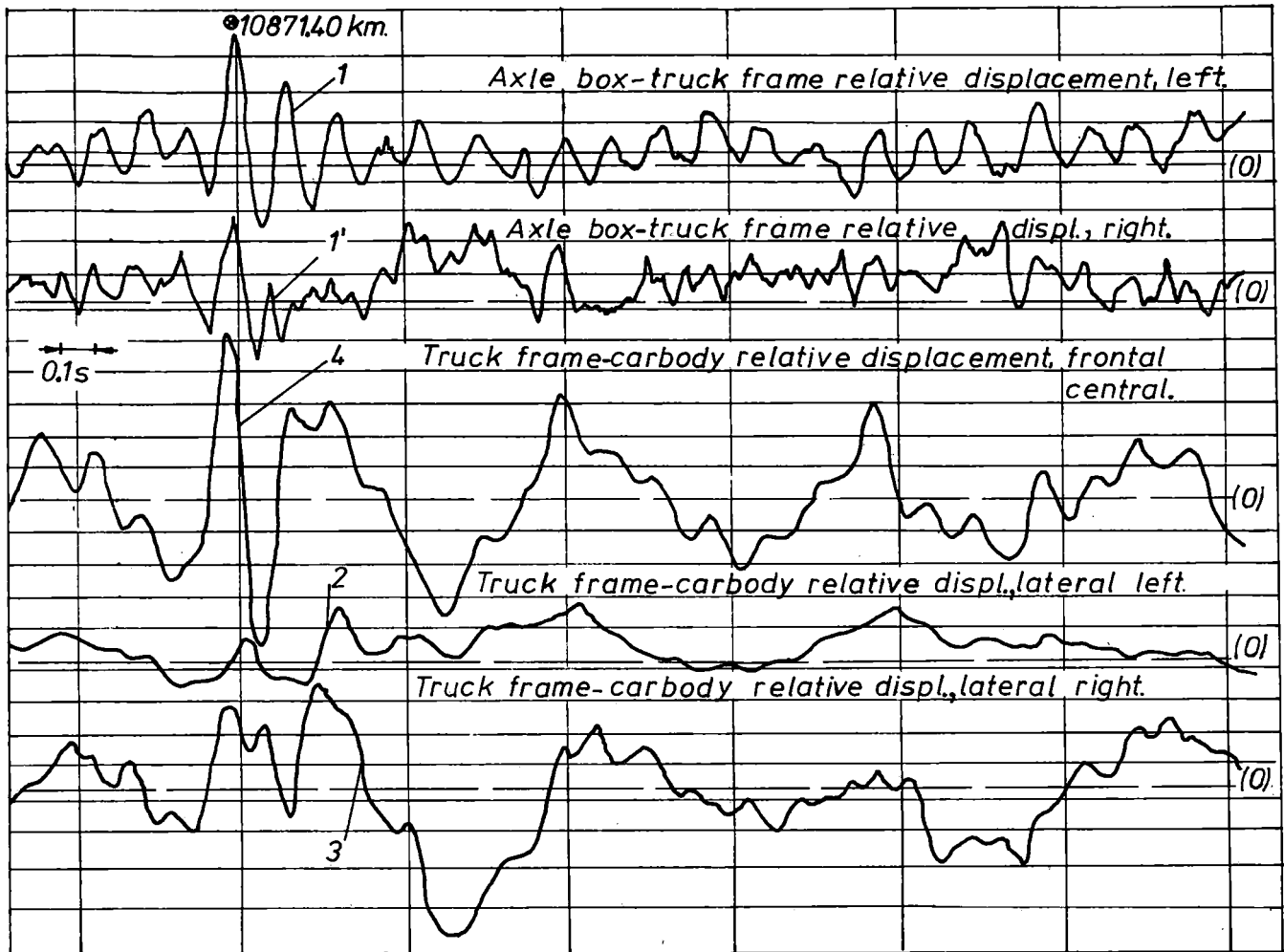


Fig.14 Elements of the dynamic response of the locomotive to the unique extreme irregularity, at 110 km/h

vibratory response (svr);

18&19 time delay of lateral and mid-frontal svr to pvr;

20;21&22 primary maximum relative speed; lateral and mid frontal maximum secondary relative speed;

23;24&25 natural period of the pvr; natural period of the lateral and mid frontal svr;

26;27&28 natural angular frequency of the pvr; natural angular frequency of the lateral and mid frontal svr;

29;30&31 natural frequency of the pvr; natural frequency of the lateral and mid frontal svr;

32;33&34 logarithmic decrement of the pvr; logarithmic decrement of the lateral and mid frontal svr;

35;36&37 damping ratio of the pvr; damping ratio of the lateral and mid frontal svr;

38&39 proportion of the lateral and mid frontal svr damping ratio to pvr damping ratio;

40;41&42 quality factor of the primary suspension; quality factor of the lateral and mid frontal secondary suspension;

43;44&45 normalized primary damping coefficient; normalized lateral and mid frontal secondary damping coefficient;

46;47&48 normalized primary stiffness constant; normalized lateral and mid frontal secondary stiffness constant;

49 ratio of normalized primary damping coefficient to normalized primary stiffness constant;

50&51 ratio of normalized lateral and mid frontal secondary damping coefficient to normalized lateral and mid frontal secondary stiffness constant. Some of these characteristics are presented in Table 1 as average informative values.

The determination of these characteristics is based on the following relations:

$$H = \frac{\text{parameter } 1(2,3,4)}{\text{rail irreg. amplit.}} \quad (10)$$

for the relative displacement transmissibilities;

$$\delta = \ln \frac{S_i}{S_{i+1}} \approx \frac{S_i - S_{i+1}}{S_i} \quad (11)$$

for the logarithmic decrement of the response

Table 1 Functional dynamic characteristics of the Bo-Bo 3,400 Kw electric locomotive

No.	Functional dynamic characteristic	Primary suspension and damping system	Secondary suspension and damping system	
			bounce	bounce & pitch
1	Vertical displacement amplitude, mm	13.40	24.40	54.65
2	Truck-carbody pitch angle, half-amplitude, degrees			0°35'50"
3	Relative displacement transmissibility	0.54	1.14	2.19
4	Relative maximum speed, cm/s	19.10	18.90	31.40
5	Stabilization time, s	0.64	3.42	3.02
6	Natural angular frequency, rad/s	45.32	7.75	8.06
7	Logarithmic decrement of the displacement oscillation	0.62	0.49	0.57
8	Damping ratio	0.098	0.078	0.091
9	Quality factor	5.30	6.38	5.49
10	Normalized stiffness constant, KN/mKg	2155	63.85	68.88
11	Normalized damping coefficient, KNs/mKg	8.67	1.16	1.30

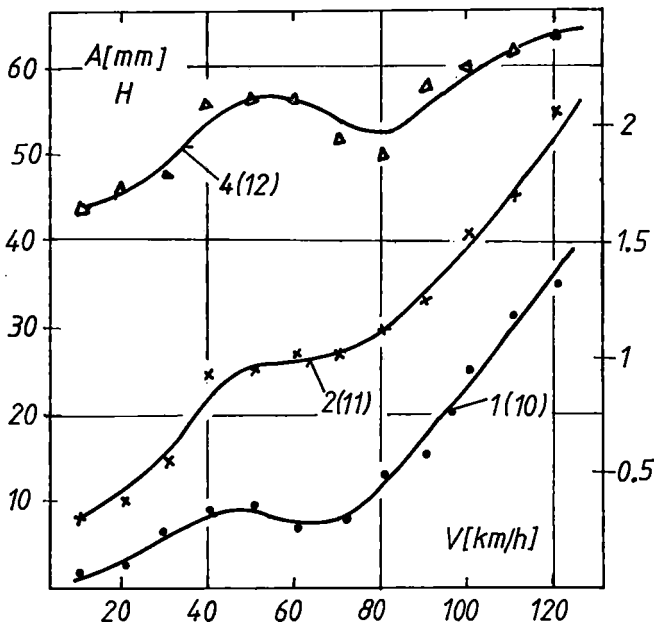


Fig.15 Variation of the relative displacement amplitudes and of the relative transmissibilities

oscillations;

$$\frac{2\pi D}{\sqrt{1-D^2}} = \ln \frac{S_i}{S_{i+1}} \quad (12)$$

or, approximately, for $\delta < 0.2$

$$D = \frac{c}{c_{cr}} \approx \frac{1}{2\pi} \ln \frac{S_i}{S_{i+1}} \quad (13)$$

for the damping ratio;

$$Q = \frac{1}{2D} \quad (14)$$

for the suspension quality factor (for $D < 0.1$);

$$\frac{c}{m} = \frac{\omega_d}{\pi} \delta = 2 \frac{\delta}{T} \quad (15)$$

for the normalized damping coefficient;

$$\frac{c}{k} = 4D^2 \cdot \frac{m}{c} \quad (16)$$

for the ratio between normalized damping coefficient and normalized stiffness constant;

as the ratio $\frac{k}{m}$ of the two previous parameters.

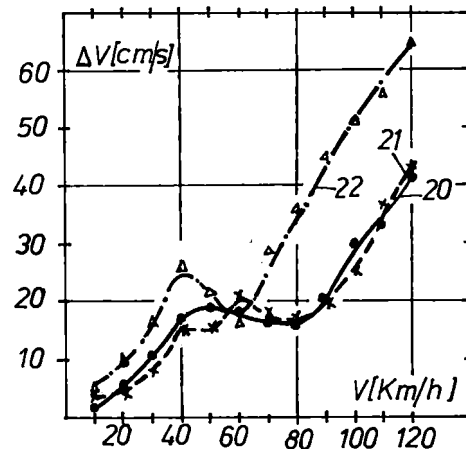


Fig.16 Variation of relative velocities on a vertical plane

Fig. 15 shows the variation of the amplitude of axle-truck-carbody relative displacement (parameters 1, 2, 4) as well as of the relative displacement transmissibilities (parameters 10, 11, 12) function of the speed of the locomotive.

Fig. 16 shows the variation of extreme maximum values of primary and secondary relative speeds on a vertical plane (parameters 20, 21, 22) function of the locomotive speed. The measuring and processing methodology makes it possible to determine the total dis-

tribution of vertical relative speeds of axle box-truck frame-carbody. These values are essential for defining the working regimes of the primary and secondary damping systems, as well as for their reconsidering and redesigning.

In the previous two figures, one can notice the evolution of the dynamic characteristics of the locomotive: they increase at 10-40 km/h, they are relatively stationary at 40-80 km/h and grow abruptly at 80-120 km/h.

Fig. 17 shows the evolution of the logarithmic decrements of the primary and secondary vibratory responses (parameters 32, 33, 34) function of the locomotive speed.

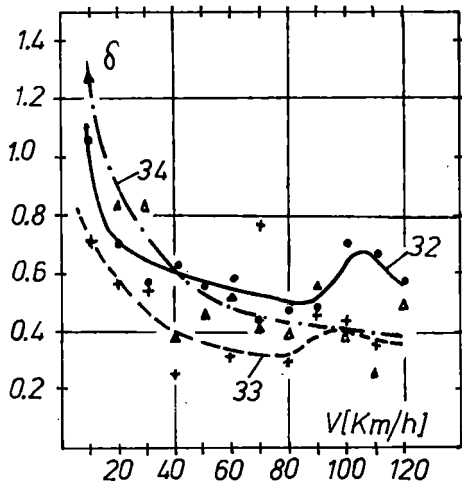


Fig.17 Logarithmic decrements of the response oscillations function of the locomotive speed

A more accurate determination of the stabilization times of the response forced oscillations would be possible on a specialized test stand, capable of simulating the locomotive running speed. Although we suitably adapted the analysis technique, our determinations suffer from the fact that it was practically impossible to achieve and maintain a sector of perfectly smooth track after the unique extreme irregularity, as can be seen in the appendix. We consider our results fair approximations of the actual values. Further conclusion upon the variation of the stabilization times with the locomotive running speed will be drawn in the future.

Finally, the validation of the mechanical and mathematical calculus model requires the comparison and correlation of the theoretical and experimental results. This can be done as the last stage of the analysis, which will eventually lead to an accurate and efficient theoretical model for the considered problems. The accuracy of the model is function of its complexity and the latter determines the volume of necessary work and the utilization of associated technical equipment. We think that, at the linear analysis level, and with frequency domain developments, a simpler model, as

considered in the present paper, may prove adequate, furnishing qualitative and limited quantitative indications. A more detailed theoretic research must be further developed on quasilinear and nonlinear bases. This requires advanced mathematical methods as well as costly calculus programmes. However, when great expenses are incurred, the alternative of extensive experimental analysis is preferable.

CONCLUSIONS

The mechanical and mathematical model considered for the locomotive vertical dynamics and vehicle-rail interaction have answered our objectives. The measuring methodology and programme have successfully met the expectations concerning the experimental analysis in simulated conditions on the test rig as well as in exploitation. The results obtained by processing the experimental data facilitate the knowledge of the functional dynamic characteristics and reliability of the Bo-Bo electric locomotive. The results are important technically and economically for the constructive qualities of the locomotive, quality and condition of the track and their intercorrelation. We are currently completing a study on acceleration responses, which will be corroborated with our gains in displacements. On the basis of the already obtained results, a few constructive modifications have been designed as to the suspending-damping vertical system and the rolling equipment. After making the improvements suggested and properly equipping a prototype locomotive, this vehicle will undergo further analyses to be carried out under identical conditions. The final conclusions will state the efficiency of the improvements and will decide upon the necessity of further altering the stiffness-damping parameters or rolling equipment.

REFERENCES

- 1 Chang, E.H., Garg, V.K., Hartmann, P.W., "Locomotive Response Model," Report AAR-R-295, Chicago, 1978.
- 2 Fallon, W.J., Cooperrider, N.K., Law, E.H., "An Investigation of Techniques for Validation of Railcar Dynamic Analyses," Report DOT-FRA OR&D-78/19, Washington, 1978.
- 3 Klinger, D.L., Cooperrider, N.K., Hedrick, J.K., "Guideway-Vehicle Cost Reduction," Report DOT-TST-76/95, Washington, 1976.
- 4 Corbin, J.C., Kaufman, W.M., "Classifying Track by Power Spectral Density," Mechanics of Transportation Suspension Systems, ADM-Vol.15, 1975.
- 5 Ionescu, T., Hedrick, J.K., Law, E.H., "Linear Steady-State Curving Analysis of 21 Degrees of Freedom Locomotive," Report VDL-1978-7, Cambridge, M.I.T., 1978.
- 6 Ionescu, T., Lie, A., et al., "Optimization of the Functional Dynamic Characteristics of the Bo-Bo Electric Locomotive," Report ITRDT, 1981.
- 7 Serban, V., Rogoz, T., et al., "Experimental Analysis of the Mechanical

Stresses in the Rolling Equipment of the Bo-Bo Electric Locomotive," Report ITRDT, 1980.

8 Harris, C.W., Crede, F.C., Shock and Vibration Handbook, Vol. 1, 2, 3, McGraw-Hill Book Co., 1961.

9 Broch, J.T., Mechanical Vibration and Shock Measurement, Brüel & Kjaer, 1976.

10 Anon., "A Comparison of Theoretical and Experimental Vehicle Behaviour Using a 2

Axled Vehicle," Report ORE No.2/G116, Utrecht, 1972.

11 Ionescu, T., Lie, A., "Experimental Analysis of the Elastic Correlation between Axle and Bogie," The 6th International Wheel-set Congress, 6-4, Colorado Springs, 1978.

12 Fries, R.H., Cooperrider, N.K., Law, E.H., "Railway Freight Car Field Tests," ASME, 80-WA/DSC-7, 1980.

APPENDIX

VALUES OF EXPERIMENTAL MEASURED DATA

Xn-Space(m) Yn-Rail Vertical Irregularity(mm)
 Yn(+) Hill;(-) Valley ; K-Measurement Amplifying Factor
 Table 2

No	Xa (mm)	Kx	Xn (m)	Ya (mm)	Ky	Yn (mm)	V (Km/h)
1	2	3	4	5	6	7	8
PARAMETER Yn-Rail Vertical Irregularity PVCs							
1	35.35	4.00	10841.40	-1.80	1.20	-2.16	60
2	36.93	4.00	10847.70	3.85	1.20	4.62	60
3	37.85	4.00	10851.40	-0.48	1.20	-0.57	60
4	38.55	4.00	10854.20	3.33	1.20	3.99	60
5	39.28	4.00	10857.10	-4.33	1.20	-5.19	60
6	40.53	4.00	10862.10	3.85	1.20	4.62	60
7	41.65	4.00	10866.60	-12.10	1.20	-14.52	60
8	42.85	4.00	10871.40	21.45	1.20	25.74	60
9	43.88	4.00	10875.50	-2.93	1.20	-3.51	60
10	44.88	4.00	10879.50	-0.13	1.20	-0.15	60
11	45.83	4.00	10883.30	-3.98	1.20	-4.77	60
12	46.90	4.00	10887.60	1.03	1.20	1.23	60
13	47.78	4.00	10891.10	-2.58	1.20	-3.09	60
14	48.33	4.00	10893.30	1.50	1.20	1.80	60
15	49.65	4.00	10898.60	-3.33	1.20	-3.99	60
16	50.38	4.00	10901.50	2.23	1.20	2.67	60
17	53.23	4.00	10912.90	-4.73	1.20	-5.67	60
18	55.40	4.00	10921.60	0.88	1.20	1.05	60
19	56.83	4.00	10927.30	-6.80	1.20	-8.16	60
20	57.85	4.00	10931.40	0.30	1.20	0.36	60
21	58.78	4.00	10935.10	-1.73	1.20	-2.07	60
22	60.23	4.00	10940.90	-0.40	1.20	-0.48	60
23	61.40	4.00	10945.60	-4.75	1.20	-5.70	60
24	62.38	4.00	10949.50	1.13	1.20	1.35	60
25	65.30	4.00	10961.20	-3.98	1.20	-4.77	60
26	66.33	4.00	10965.30	1.20	1.20	1.44	60
27	68.70	4.00	10974.80	-3.55	1.20	-4.26	60
28	69.28	4.00	10977.10	1.30	1.20	1.56	60
29	70.28	4.00	10981.10	-0.43	1.20	-0.51	60
30	71.10	4.00	10984.40	1.33	1.20	1.59	60
31	73.15	4.00	10992.60	-3.85	1.20	-4.62	60
32	75.60	4.00	11002.40	0.10	1.20	0.12	60
33	77.08	4.00	11008.30	-4.18	1.20	-5.01	60
Mean Natural Period, T=10.431 m Angular Frequency, w=0.602rad/m Frequency, Fv=0.096 1/m							

DITAO2//HP 9835A/9874A/2631A/TI/

Table 2 presents a sequence of the left rail before and after the unique extreme irregularity and some of the track

characteristics.

Wheel Wear on High Adhesion Locomotives

C.A. Swenson

Supervisor
Truck Design
Electro-Motive Division
General Motors Corp.
LaGrange, Illinois

This paper presents the results of an 8-year field study of wheel wear on locomotives which use a new wheel creep control system to develop 33% higher adhesion levels. This system allows the wheels to creep at a higher rate with respect to the rails, and it uses sand only as a last resort on very poor rail adhesion conditions. The wear study results show that wheel tread and wheel flange wear rates are equivalent or lower than on locomotives which have conventional wheel slip systems and much lower adhesion capabilities. The reduction in wheel wear is attributed to reduced sand usage.

INTRODUCTION

The low rolling resistance of the steel wheel on the steel rail makes rail transportation inherently energy efficient. However, the wheels wear and the rails wear, as illustrated in Fig. 1. Wheels and rails must be maintained, and eventually they must be replaced.

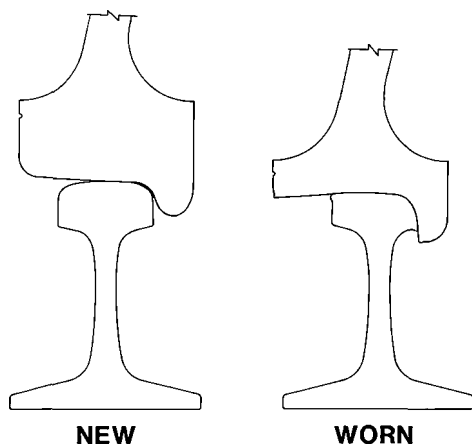


Fig. 1 New and worn wheel and rail profiles

The unpowered wheels of freight cars and passenger cars experience wear not only from rolling on the track but also from the wheel-rail interaction caused by curve negotiation, track irregularities, vehicle dynamics, and braking. Powered locomotive wheels are subjected to all of these influences plus the requirement of developing tractive effort at the wheel-rail interface. This additional demand results in increased wear of the locomotive wheels and the rails.

In the USA, locomotives usually use multi-wear wheels, and most major railroads have wheel truing facilities that allow machining of wheels back to a new profile without removing the wheelsets from the locomotive. While the use of multi-wear wheels and wheel truing machines greatly extend wheel life, the maintenance and replacement of locomotive wheels represent a significant cost to the railroads.

The maintenance and replacement of rails due to wear, some of which is caused by powered locomotive wheels, is one of the major costs to railroads. Accordingly, the influence of locomotive design on wheel wear and rail wear should be of vital concern to the railroad industry.

There have been many papers published on the subject of locomotive wheel-rail loading, and some of these papers address locomotive wheel wear due to curving loads. There appears to be very little published, however, on the influence of adhesion levels and wheel slip systems on locomotive wheel wear. This paper attempts to fill some of this void by reviewing locomotive wheel wear data from previous studies and reporting the results of an extensive study of wheel wear on a new generation of high adhesion locomotives developed by Electro-Motive Division (EMD).

HIGHER HORSEPOWER AND ADHESION

The history of locomotive development in the USA has been one of incremental increases in horsepower ratings. As shown in Fig. 2, the traction horsepower of EMD 4-axle, diesel-electric locomotives has increased from 338 hp/axle to 875 hp/axle over the past

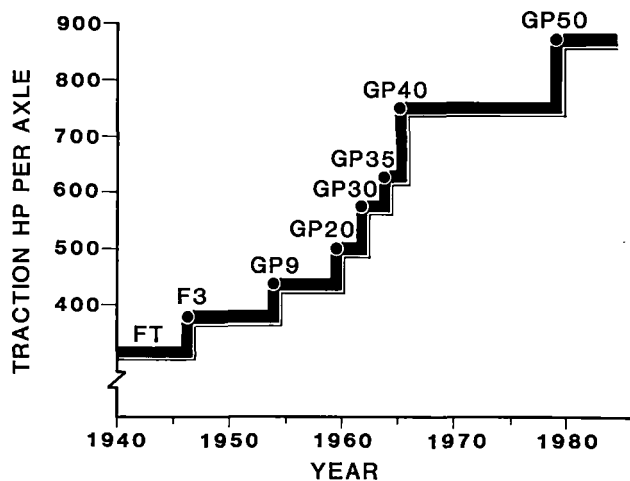


Fig. 2 Horsepower per axle for EMD 4-axle locomotives

40 years. In most cases, the locomotive horsepower increases were accompanied by increases in axle load and tractive effort capabilities.

The EMD 40 Series 4-axle locomotive introduced in 1965 develops 750 hp/axle. Typically, USA railroads dispatch these locomotives, and lower horsepower locomotives as well, to require a maximum adhesion demand of 18% of the locomotive weight. Some USA railroads utilize a slightly higher adhesion demand.

The EMD 50 Series 4-axle locomotive introduced in 1980 develops 875 hp/axle. Through use of a new wheel creep control system called Super Series, these locomotives can be dispatched at 33% higher adhesion than locomotives with the previous type wheel slip system. This means that railroads previously dispatching locomotives at 18% adhesion can dispatch these locomotives at 24% adhesion.

As EMD began to develop the 50 Series locomotives with more horsepower and dramatically higher adhesion capabilities, one concern was the effect of the higher adhesion demand on wheel wear. It was recognized that the wheel-rail contact would be subjected to higher loads and potentially higher wear rates. This concern was also supported by the experience of the mid-1960s when EMD 35 and 40 Series locomotives were put into service and numerous railroads reported that these higher horsepower locomotives had shorter wheel life than older, lower horsepower locomotives.

As a result, a program was initiated to develop a locomotive design which would minimize wheel wear at high adhesion levels. A study of locomotive wheel wear was an integral part of this development program.

MEASURING WHEEL WEAR

In order to make thousands of wheel wear measurements on different railroads, a simple and reliable measurement technique was needed. The AAR standard steel wheel gage illustrated in Fig. 3 was used for this purpose. The advantages of this gage are that it is readily available, easy to transport, and can be used quickly so locomotives are not delayed for special, time-consuming measurements. Unlike some wheel measuring instruments, this simple gage can be used without removing the wheelsets from the locomotive.

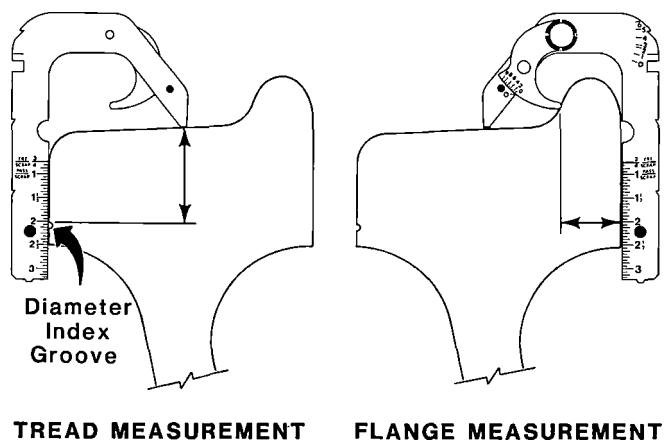


Fig. 3 Wheel tread and flange wear measurements

This gage is not a precision, laboratory instrument. If it is used carefully, however, tread and flange measurements can be made to an accuracy of $\pm 1/64$ in. Using successive measurements to establish flange and tread wear data, this technique typically has a measurement accuracy in the range of 5 to 15%.

Each of the wheels used in the recent studies had a wheel diameter index groove machined on the front side of the wheel rim. This was used as the reference for tread wear readings.

For both tread and flange measurements, more than one reading was usually taken to verify that there was a consistent wear pattern around the wheel and that the readings were not affected by local deviations of the wheel.

Regarding flange wear readings, it is important to recognize that as the wheel tread wears, the gage moves closer to the wheel center and the flange thickness reading is taken across a different part of the flange. Therefore, the flange wear rate may appear to be very small or even negative if there is excessive tread wear compared to flange wear.

A comprehensive wheel wear study of the kind undertaken here requires not only many man-hours of tracking down locomotives and making wheel measurements, but it also requires meticulous searching and record keeping of all information which may affect the wear data. This includes wheel truing, which are often done on only one or two wheelsets of a locomotive, and unscheduled traction motor changeouts which may result in replacement of the wheelset. It is also necessary to carefully interpret the causes of wheel truing, since some truing are for reasons not related to normal wear - such as flat spots on the wheels caused by abnormal braking.

PREVIOUS WEAR STUDIES

In 1968, the Locomotive Maintenance Officers Association (LMOA) sponsored a major survey of locomotive wheel wear on USA railroads. Data from 28 railroads was obtained, and this data was provided to EMD for processing and analysis. The findings of this survey, which were published by the LMOA [1], indicated that a number of variables had an effect on locomotive wheel life.

The data showed that locomotive horsepower per trailing ton had a definite effect. It was shown that railroads using a low hp/ton ratio had generally experienced proportionately shorter locomotive wheel life.

The survey also showed that locomotives in lower speed operations had shorter wheel life. It was recognized, however, that lower speed was generally a result of lower hp/ton operation.

Another variable studied in the LMOA survey was locomotive horsepower per axle. Many railroads reported a reduction in locomotive wheel life as hp/axle increased. However, the data from some railroads indicated no significant change in wheel life for different hp/axle ratios.

In the late 1960s, EMD was actively involved in conducting a number of locomotive wheel wear tests. Tests were conducted on five different railroads and involved various wheel design parameters. Tests of wrought vs. cast steel wheels indicated that both types of wheels had approximately the same wear rate. Tests of AAR Class B and C wheels indicated that the softer B wheels used by most USA railroads had a slightly higher wear rate.

The data developed in these tests, together with the information obtained in the LMOA survey, provided an overall picture of locomotive wheel life on USA railroads. This combined data showed that mainline diesel-electric locomotives using 40-inch diameter, multi-wear wheels experienced total wheel life in a wide range of 35,000 to 450,000 miles. The locomotives getting only 35,000 miles of wheel life were used in heavy pusher service on track with nearly continuous curvature. The locomotives getting wheel life of 450,000 miles were running in high hp/ton operation on relatively straight track.

Using the wheel wear information obtained in these studies, together with additional studies made in the 1970s, it was possible to develop approximate tread and flange wear rates for locomotives with conventional wheel slip systems operating in the USA. The range of wear rates represented by this data may not be completely applicable to current conditions since there have been operational changes in recent years such as a trend towards lower hp/ton operation to conserve fuel. However, this data can be used as a reference, and since this information has not previously been published, it will be summarized here.

TREAD WEAR

Table 1 summarizes wheel tread wear rates developed in the late 1960s and the 1970s for EMD 35 and 40 Series locomotives with an axle load range of

	Tread Wear Rate to First Truing (in./1000 mi.)	REFERENCE - Total Wheel Life (mi.) Based on 1.5 in. Tread Wear
Minimum	0.0024	625,000
Normal Range:		
Low	0.0030	500,000
Medium	0.0060	250,000
High	0.0080	190,000
Maximum (Heavy Pusher Service)	0.0160	95,000

Table 1 Wheel tread wear rates on 35 and 40 Series locomotives

60,000 - 65,000 lbs. This data applies to 40-inch diameter wheels to the first wheel truing.

The normal range of tread wear rates on these locomotives was found to be 0.0030 to 0.0080 in. (on the radius) per 1000 mi. The lowest tread wear rate found was 0.0024 in./1000 mi. for locomotives in high hp/ton service on relatively straight track. The highest tread wear rate was 0.0160 in./1000 mi. in heavy pusher service.

For reference, Table 1 also shows the approximate total wheel life that could be expected at these wear rates, assuming that the wheels have 1.5 in. of available radial tread wear. In many cases, the actual wheel life is less than shown in this table when the wheels are trued because of flange wear ("thin flanges") instead of tread wear ("high flanges").

When analyzing wheel tread wear readings, it is important to recognize that actual wear rates may differ significantly from average wear rates. As illustrated in Fig. 4, wear depth measurements generally indicate a relatively high wear rate at the beginning of service and a lower wear rate as the mileage increases.

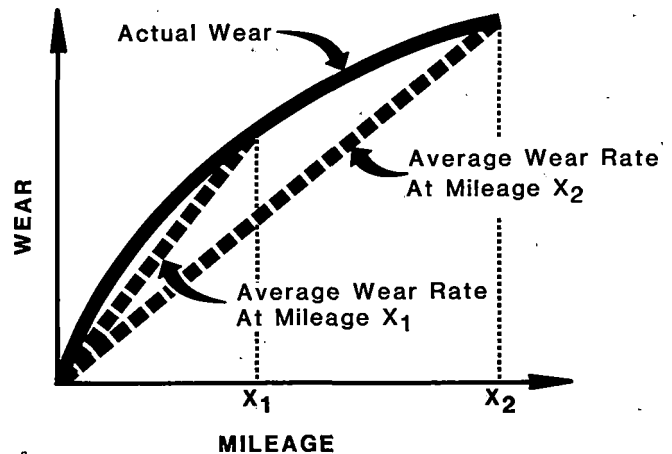


Fig. 4 Average vs. actual wheel wear rates

The main reason for this is that new wheels with a conical tread profile roll on a curved rail surface and the first increment of wear occurs relatively quickly. As the wheel continues to wear and conform more closely to the rail profile, each increment of wheel wear depth is associated with a larger wear volume and the wear rate is reduced. In some cases, it has been observed that the wear rate begins to accelerate again prior to wheel truing.

When wheels are trued, the process starts over again of accelerated wear followed by slower wear. However, wheel truing records usually show that less mileage is obtained between each successive wheel truing. This is generally felt to be the result of a smaller wheel diameter and reduced wheel hardness below the original tread surface.

FLANGE WEAR

Table 2 summarizes wheel flange wear rates developed on the 35 and 40 Series locomotives. The available flange wear data was not as comprehensive as the tread wear data, but where both types of data were available for the same locomotives, the flange

	Flange Wear Rate (in./1000 mi.)	REFERENCE-Wheel Mileage Between Truings (mi.)	
		Based on 1/4 in. Flange Wear	Based on 3/8 in. Flange Wear
Minimum	0.0014	180,000	
Normal Range:			
Low	0.0020	125,000	190,000
Medium	0.0050	50,000	75,000
High	0.0070	35,000	55,000
Maximum (Heavy Pusher Service)			
	0.0120	20,000	

Table 2 Wheel flange wear rates on 35 and 40 Series locomotives

wear rate was generally slightly lower than the tread wear rate. Accordingly, the normal range of flange wear rates was considered to be 0.0020 to 0.0070 in./1000 mi. for these locomotives.

On one railroad, it was reported that the wheels went 180,000 mi. to the first truing, indicating that the average flange wear rate was not more than about 0.0014 in./1000 mi. At the other extreme, standard narrow flange wheels had reached the condemning flange width in only 20,000 miles on locomotives used in heavy pusher service. This corresponds to an average flange wear rate of about 0.0120 in./1000 mi. During periods when the locomotives were operated exclusively in pusher service, flange wear rates as high as 0.0300 in./1000 mi. were measured.

In order to improve wheel life where heavy flange wear was involved, EMD designed the Unipoint wheel profile in the late 1960s. This profile is similar to the Heumann profile but has a wide flange. Field tests showed that this wheel design provided a 35 - 60% increase in mileage to the first wheel truing compared to the standard AAR 1:20 taper narrow flange wheel.

A number of USA railroads have adopted the Unipoint wide flange wheel profile for locomotives operating in freight service. This profile is particularly effective when a significant amount of curving is involved and the dominant wear is flange wear. Under these conditions, the Unipoint profile provides extended mileage to the first truing, at which time wheel material removal is minimized by truing the wheels to the standard narrow flange profile.

Accelerated flange wear on one wheel of a wheelset is sometimes found. Where this situation has been studied closely, it has usually been found that the wheel diameters were not matched properly, either at initial wheel application or when the wheelset was re-profiled on a wheel truing machine. To minimize uneven flange wear, EMD applies new wheels on a mainline locomotive wheelset to within 1/2 tape (0.020 in. on the diameter).

HIGH ADHESION LOCOMOTIVE DEVELOPMENT

In the 1970s, EMD conducted an extensive research program in the field to determine available adhesion levels with different rail conditions such as dry, dry-sand, water, water-sand, oil, and oil-sand. The results of this research program, which have been documented by C.F. Logston and G.S. Itami

[2], statistically established the relationship between wheel-rail friction and creep for creep levels up to 30%.

This fundamental friction-creep data was used as the basis for developing the EMD Super Series wheel creep control system, which has been described by B.R. Meyer and A.P. deBuhr [3]. The criteria used in developing this system included provision for operation in the macro-creep range (greater than 2% creep) to maximize adhesion and restricted use of sand to minimize wheel and rail wear. The friction-creep research program had showed that sand should not have to be used under dry rail conditions and normally would not be needed under wet rail conditions. It was recognized that automatic sanding would be required under very poor adhesion conditions caused by oil or combinations of oil and water.

Table 3 shows the levels of control provided by the Super Series system to provide high adhesion while minimizing sand usage. Under good rail conditions, the wheels are allowed to creep as needed up to a pre-set creep limit. The maximum creep is nominally 5%, which is significantly more creep than allowed by the previous wheel slip system. Wheel creep, without sand, cleans the rails and improves the available adhesion for trailing wheels.

- | |
|---|
| <ul style="list-style-type: none"> ● Good Rail Adhesion Conditions - Wheels can creep as needed up to pre-set creep limit.
No sand used ● Poor Rail Adhesion Conditions- Horsepower is reduced as needed to maintain creep limit.
No sand used ● Very Poor Rail Adhesion Conditions- Automatic sand is used if power drops below 90% normal horsepower. |
|---|

Table 3 Levels of Super Series wheel creep control

When rail conditions are poor, the Super Series system reduces horsepower to each traction motor as needed to maintain the creep limit. Automatic sanding is called for only if the power drops below 90% normal horsepower. The automatic sanding is stopped as soon as 95% horsepower is reached. In addition, automatic sanding cannot occur unless the locomotive is operating above throttle position 2 (of 8 positions).

As a result of past experience, locomotive operators often use manual sanding continuously during periods of high adhesion demand in an attempt to minimize wheel slip. With Super Series, manual sanding is not needed in power except under certain very low speed conditions. Therefore, the control system prevents manual sanding in power above 5 mph.

From the standpoint of wheel and rail wear, the most significant feature of the Super Series system is that it uses less sand, and therefore, reduces the abrasive wear due to sand at the wheel-rail interface. However, without full-scale field tests, it was not known if the reduction in sand would offset the effect of higher creep levels.

Wheel wear tests with the Super Series wheel creep system were conducted in the field in three phases as shown in Table 4.

PHASE I _____ **1975-1976**
Wheel Wear Study on
Pre-Prototype Locomotives

PHASE II _____ **1978-1980**
Wheel Wear Study on
40X Series Prototype Locomotives

PHASE III _____ **1980-1981**
Wheel Wear Study on
50 Series Production Locomotives

wheel gage. However, the wheels of the baseline locomotives were trued for flange wear while the wheels of the modified locomotives were trued at about the same time for tread wear.

Instrumentation was used to monitor sanding time on the baseline and modified locomotives. In spite of the significant increase in adhesion demand, the modified locomotives with the Super Series system reduced sanding time an average of about 70% during pusher locomotive operation and about 40% in the overall locomotive duty cycle. On individual runs, sand usage varied depending on rail conditions and manual sanding practices.

Table 4 Wheel wear study on high adhesion locomotives

PROTOTYPE LOCOMOTIVE TESTS

PRE-PROTOTYPE LOCOMOTIVE TESTS

The Phase I wheel wear tests were conducted in 1975 - 1976 on pre-prototype locomotives modified to have a Super Series wheel creep control system. These tests were conducted on 6-axle, 3600-traction horsepower locomotives operating in heavy coal train service. Two locomotives were used as baseline units at 600 hp/axle, and two locomotives were modified to make two of the six axles unpowered and have four driver axles at 900 hp/axle. The baseline and modified locomotives were assigned to the same tonnage service.

The six powered axles of the baseline locomotives exhibited average tread wear of 0.0042 in./1000 mi. At 50% higher hp/axle, the four powered axles of the modified locomotives had average tread wear of 0.0069 in./1000 mi. These Phase I tests used a control system that allowed wheel creep up to about 15%. Later testing showed that the creep limit could be reduced significantly while still obtaining high adhesion levels, and this development suggested that wheel wear could be reduced.

The measured wheel flange wear rate on the modified locomotives averaged only 0.0018 in./1000 mi. compared to 0.0037 in./1000 mi. on the baseline locomotives. It was recognized that the actual flange wear improvement on the modified locomotives was not as great as indicated because of the effect of tread wear on flange thickness measurements with the AAR

The Phase II wheel wear tests were started in 1978 when EMD delivered twenty-three 4-axle GP40X prototype locomotives to USA railroads for testing and evaluation. In 1979, four 6-axle SD40X prototype locomotives were also put into service. The primary concern was to evaluate wheel tread wear, and this was done on three different railroads.

Table 5 provides information regarding axle load, wheel diameter, and other data on these locomotives. Average tread wear rates are shown in the far right column.

The four GP40X locomotives on Railroad 'A' generally operated in high speed freight service and accumulated an average mileage in excess of 300,000 miles during the study. This group of locomotives experienced numerous wheel truing as a result of flat spots associated with braking practices, and the available data between truing showed an average tread wear rate of 0.0019 in./1000 mi.

On Railroad 'B', the GP40X locomotives were followed to the first wheel truing and averaged tread wear of 0.0031 in./1000 miles. These locomotives were used in a combination of low speed, heavy drag service and high speed service.

The 6-axle SD40X locomotives on Railroad 'C' were used in low speed, heavy drag service but showed an average tread wear of only 0.0016 in./1000 mi. to the first wheel truing, which were at mileages in excess of 100,000 mi.

The tread wear rates in the range of 0.0016 to 0.0031 in./1000 mi. for these prototype locomotives

Railroad	Loco. Model	Traction HP	Axle Load (1000 lbs)	Wheel Diameter (in.)	Wheel Type	Wheel Profile	Brake System	No. of Locomotives in Study	Ave. Tread Wear Rate (in./1000 mi.)
"A"	GP40X 4-Axle	3500	68.0	42	Wrought Class B	Std. AAR 1:20 Taper	Single Shoe Composition	4	0.0019
"B"	GP40X 4-Axle	3500	69.1	42	Wrought Class B	EMD Unipoint	Single Shoe Composition	3	0.0031
"C"	SD40X 6-Axle	3500	64.5	40	Wrought Class B	EMD Unipoint	Single Shoe Composition	3	0.0016

Table 5 40X Series prototype locomotive wheel wear summary

compared very favorably to the tread wear rates developed earlier for lower horsepower locomotives with conventional wheel slip systems (reference Table 1). These tests showed that a wheel creep control system could be designed to achieve significantly higher adhesion without producing excessive wheel wear on 4-axle and 6-axle locomotives. In addition, this data indicated that it should be possible to achieve high adhesion levels and actually reduce wheel wear with an optimum combination of wheel creep and sand usage.

PRODUCTION LOCOMOTIVE TESTS

Production of the 50 Series locomotives began in 1980. Wheel tread and flange wear was closely monitored on two railroads where EMD Engineering Representatives on special assignment were available to make the many wheel measurements that are necessary for a good wear study.

As shown in Table 6, Railroads 'D' and 'E' had 4-axle GP50 locomotives delivered with 40-in. diameter wheels and Unipoint wheel profiles. Railroad 'D' had Class B wrought steel wheels, and Railroad 'E' had Class B cast steel wheels. All of the locomotives in the study used a single shoe brake system with high friction composition brake shoes.

A number of locomotives were selected at random for wheel wear measurements, and these locomotives were followed for the duration of the study. Locomotive mileages were obtained from railroad computer records.

On Railroad 'D', comprehensive data was obtained to the first wheel truing on eight locomotives. As shown in Table 6, the tread wear averaged 0.0037 in./1000 mi. and the flange wear averaged 0.0031 in./1000 mi. The average test mileage used to establish the tread and flange wear rates was in excess of 50,000 mi.

The data obtained on this railroad established an average mileage to the first wheel truing of just over 80,000 mi. for the GP50 locomotives. This mileage with 875 hp/axle and Super Series wheel creep control was comparable or better than current mileages reported by the railroad for older EMD locomotives with 500 hp/axle and conventional wheel slip systems.

On this railroad, the 33% higher adhesion rating of the GP50 locomotives was utilized by assigning these 4-axle locomotives to essentially the same tonnage service as older 6-axle locomotives with the same axle load.

On Railroad 'E', wheel wear data was obtained on twenty-two GP50 locomotives. As shown in Table 6, the tread wear averaged only 0.0018 in./1000 mi. and the flange wear averaged only 0.0012 in./1000 mi.

The average test mileage on this railroad was 115,000 mi. When this paper was submitted in January 1982, only a few of the wheels had been re-profiled and a number of these locomotives had exceeded 150,000 mi. without requiring the first wheel truing.

The tread and flange wear rates on Railroad 'D' were found to be 2 to 2-1/2 times as great as on Railroad 'E'. One reason for this difference was felt to be the more severe track curvature on Railroad 'D'.

Another reason for the difference in wear rates appeared to be a lower hp/ton operation on Railroad 'D'. On Railroad 'D', the GP50s were assigned to service ranging from less than 1 hp/ton to over 3 hp/ton. In general, the service averaged about 1.3 hp/ton. On Railroad 'E', the GP50s were assigned to service in the 1.2 to 2.4 hp/ton range, with the average being about 1.8 hp/ton. It should also be noted that the GP50s on Railroad 'D' used dynamic braking whereas the GP50s on Railroad 'E' did not.

The wheel tread wear rates established for the production GP50 locomotives (Table 6) are consistent with the wear rates developed earlier for the prototype 4-axle and 6-axle locomotives (Table 5).

A comparison of this data (Tables 5 and 6) to the historical wear data (Tables 1 and 2) shows that the 50 Series locomotives have achieved equivalent or lower tread and flange wear rates than locomotives with conventional wheel slip systems and much lower adhesion capabilities.

A wheel wear survey on the 50 Series locomotives is continuing so that wheel wear rates beyond the first wheel truing can also be studied.

WHEEL LIFE

The impact of the favorable wheel wear rates on total wheel life will be influenced by a number of factors.

If wheels are normally trued for tread wear, the tread wear rates measured on the 50 Series locomotives can be expected to maintain or improve total wheel life.

If wheels are normally trued for flange wear, reductions in tread wear do not necessarily improve total wheel life. The data developed to date indicates, however, that flange wear is actually reduced in some cases with the Super Series wheel creep control system.

The amount of metal removed in reprofiling wheels is very dependent on the thickness of the worn flange, and if the predominant cause for truing shifts from flange wear to tread wear, it is generally an advantage because less metal is removed in the truing operation.

Railroad	Loco. Model	Traction HP	Axle Load (1000 lbs)	Wheel Diameter (in.)	Wheel Type	Wheel Profile	Brake System	No. of Locomotives in Study	Ave. Wear Rate (in./1000 mi.)	
									Tread	Flange
"D"	GP50 4-Axle	3500	67.4	40	Wrought Class B	EMD Unipoint	Single Shoe Composition	8	0.0037	0.0031
"E"	GP50 4-Axle	3500	68.1	40	Cast Class B	EMD Unipoint	Single Shoe Composition	22	0.0018	0.0012

Table 6 50 Series production locomotive wheel wear summary

Total wheel life is also affected by railroad wheel truing practices. In addition to closely matching wheel diameters to minimize uneven flange wear, it is important to determine the optimum truing time in order to maximize total wheel life.

In some cases, it may be best to reprofile individual wheelsets only as needed as condemning limits are reached. However, in some cases of flange wear, it may be better to reprofile before reaching the flange thickness condemning limit in order to prevent removal of excessive metal in the truing operation. Therefore, wheel wear patterns need to be studied closely in order to establish a good wheel truing strategy.

LABORATORY WEAR TESTS

The field wheel wear program has been supplemented by wear tests conducted on a scale model wheel-rail test facility at the Railroad Engineering Laboratory of the Illinois Institute of Technology in Chicago. Tests co-sponsored by the Federal Railroad Administration and EMD have included a preliminary evaluation of the effect of sand on wheel and rail wear. S. Kumar has reported that under laboratory conditions, the introduction of sand in the wheel-rail contact region increases the wear by two to three orders of magnitude¹ [4].

This observation shows that when sand is used, wheel and rail wear increases very dramatically. This indicates that even though it may be applied during only a portion of the locomotive duty cycle, sand can be a major factor in wheel and rail wear.

SUMMARY

For many years, it has been recognized that sand can be used at the wheel-rail interface to significantly increase locomotive adhesion levels. In some countries, including the USA, locomotives have depended on sand to help prevent wheel slip when operating under poor rail adhesion conditions. However, sand produces abrasive wear of the wheel and rail, and laboratory tests have shown that sand increases wear rates very dramatically.

Fundamental research in the field has demonstrated that adhesion levels can be significantly increased without sand by allowing the wheels to creep with respect to the rails. With a controlled wheel creep system, sand is needed only under the worst rail adhesion conditions.

A new generation of locomotives has been developed to provide 33% higher adhesion capability while using significantly less sand. An extensive field study of these locomotives has shown that they exhibit equivalent or lower wheel tread and wheel flange wear rates than locomotives which have conventional wheel slip systems and much lower adhesion capabilities.

It appears that in the overall locomotive duty cycle, the increase in wheel wear due to higher wheel creep has been more than offset by the reduction in wheel wear due to reduced sand usage.

It can be expected that the reduced sand usage will also reduce abrasive wear of the rails. This should be most noticeable on heavy grade operations where excessive sand is normally used.

In addition to accelerating wheel and rail wear, sand contributes to fouling of the track ballast. Therefore, a locomotive wheel creep control system that reduces sand usage should have a favorable effect on track maintenance costs.

FUTURE RESEARCH

Future research work needs to be directed at developing a more complete understanding of wheel and rail wear with high adhesion locomotives.

Regarding wheel tread wear, an effort could be directed at developing a locomotive wheel wear index that would quantify the trade-off between wheel creep level and sand usage for various adhesion levels.

Further work is needed to more fully explain the apparent reduction seen in wheel flange wear. There appears to be a double benefit from reducing the use of sand. Not only is abrasive wear reduced, but lateral wheel-rail loads are reduced in curves (as demonstrated in field tests conducted by EMD and others). Also, theoretical considerations suggest that with the wheels creeping in the longitudinal direction to develop high adhesion, lateral wheel-rail curving loads may be further reduced because of a reduction in the available lateral friction.

Finally, the dramatic effect of sand seen in laboratory wear tests suggests that future research could include precision measurements of rail wear in the field to compare the effect of wheel creep to the effect of sand with high adhesion locomotives.

ACKNOWLEDGEMENTS

A number of people at EMD were instrumental in putting together the wheel wear data presented in this paper. H.A. Marta, K.D. Mels, R.T. Yoshino, and G.S. Itami developed the 35 and 40 Series locomotive data. S.P. Novak developed the 40X and 50 Series data. A number of Engineering Representatives made many of the wear measurements in the field.

A special thanks is due to the railroads who supported this work.

CONVERSION TO SI UNITS

1 in.	= 25.40 mm
1 mi.	= 1.609 km
1 lb.	= 0.4535 kg

REFERENCES

- 1 "Locomotive Wheel Wear Study," LMOA 30th Annual Meeting Proceedings, 1968.
- 2 Logston, C.F., Jr. and Itami, G.S., "Locomotive Friction-Creep Studies," ASME Paper No. 80-R1-1, April 1980.
- 3 Meyer, B.R. and deBuhr, A.P., "Super Series Wheel Creep Control System," ASME Paper No. 80-WA/RT-3, November 1980.
- 4 Kumar, S., "Small Scale Investigation of Improved Rail Wheels - Phase I," Illinois Institute of Technology Report No. IIT-TRANS-79-1 submitted to Federal Railroad Administration under Contract No. DOT-FR-766-4301, December 1978.

¹ 2 to 3 orders of magnitude = 100 to 1000 times

Electrification Applied to Heavy Haul Operation in the Republic of South Africa

R.S. Mann

B.Sc. Eng. (Elect.)
Member S.A.I.E.E.
Electrical Engineer
South African Transport
Services
South Africa

The two lines in the Republic of South Africa which are classed as heavy haul have both been electrified since 1978. The 860 km line between Sishen and Saldanha Bay is electrified at 50 kV AC and is utilised for the exclusive transport of iron ore for export through Saldanha Bay. The 540 km line between Broodsniersplaas and Richards Bay is electrified in two sections using 3 kV DC and 25 kV AC and is utilised primarily for the transport of coal for export through Richards Bay. The South African Railways (now known as the South African Transport Services) has proven that the decision to electrify was the right one and the paper describes the electrical installations on both lines with some of the problems encountered and achievements obtained. Of particular interest is the system introduced on the 50 kV line to reduce electricity costs.

NOMENCLATURE

AAC	All Aluminium conductor
AC	Alternating current
ACSR	Aluminium conductor steel reinforced
DC	Direct current
ESCOM	Electricity Supply Commission
SAR	South African Railways

1.0 INTRODUCTION

There are two railway lines in the Republic of South Africa built specially for heavy haul operation. Both are electrified using industrial frequency, 50 Hz supplies to the railway but there the similarity ends. This paper will cover the pertinent details of the electrical installations on both lines with some detail of operating experience to date.

1.1 Sishen - Saldanha Railway Line

This 860 km line was electrified in 1978 using 50 kV supply voltage to the railway. The line is used for the transport of iron ore for export through Saldanha Bay and has a ruling gradient of 4 per mil (compensated) against loaded trains and 10 per mil (compensated) against returning empties. 210 wagon trains, 21 840 tons gross are hauled by 3 class 9E, 3 670 kW AC locomotives with a total continuous demand capability of 16,14 MVA from the power supply system. The line presently handles 3 of these trains per direction per day giving a capacity of 18 million tons nett per annum.

1.2 Broodsniersplaas - Ermelo - Richards Bay Line

This 540 km line was electrified in two sections.

The 90 km section from Broodsniersplaas to Ermelo was electrified in 1978 using 3 kV DC which was the standard for electrification in the country. The 450 km section from Ermelo to Richards Bay was also to be electrified at 3 kV DC. This portion of the line passes through some of the most difficult terrain in the country from a civil and electrical engineering viewpoint and after initial studies highlighted severe limitations of the 3 kV system over this route the line was finally electrified in 1978 using 25 kV AC. The line is used primarily for the transport of coal for export through Richards Bay and has a ruling gradient of 15,15 per mil in both directions.

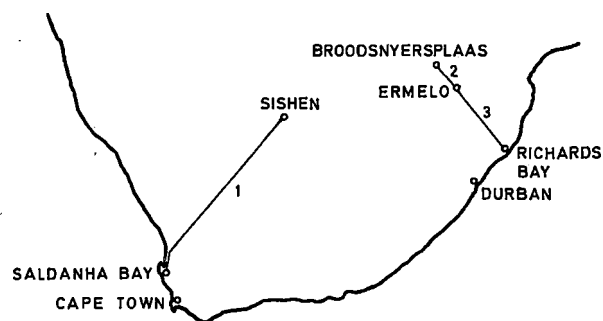


Fig. 1 Heavy haul lines in the Republic of South Africa.

- 1 - 50 kV AC Iron ore line
- 2 - 3 kV DC Coal line
- 3 - 25 kV AC Coal line

On the 3 kV DC section of the line 84 wagon trains, 6 720 tons gross, are loaded at the mines along the route and hauled by 5 class 6E, 3 kV DC locomotives to Ermelo. Ermelo station was designed to permit the energising of the overhead wires at either 3 kV DC

or 25 kV AC for the purpose of changeover of locomotives. Four class 7E, 2 920 kW 25 kV AC locomotives then haul the train over the most difficult route from Ermelo to Richards Bay. This train can demand up to 16 MVA continuously from the power supply system.

At present 26 million tons nett is being transported per annum over this line in 18 trains per day in each direction. This is to be increased to 44 million tons per annum by 1985, necessitating strengthening of the power supply system. Further increases in capacity to 80 million tons per annum beyond 1985 have been authorised but full details are not available at this stage.

Figure 1 is a map showing the geographic arrangement of the two heavy haul lines.

2.0 POWER SUPPLY SYSTEM

In the Republic of South Africa the generation and distribution of electricity over a national grid is governed by the Electricity Supply Commission (ESCOM).

2.1 Sishen - Saldanha 50 kV line

Electrification of this line was decided upon by the then owners and builders of the line, the South African Iron and Steel Corporation (ISCOR). The line was taken over by the South African Railways (SAR) shortly before the completion of electrification. Initial studies indicated that electrification at 25 kV would be far more costly than at 50 kV due to the larger number of substations required for 25 kV and the cost of getting supplies to these substations. The line was being built through uninhabited and undeveloped country remote from major electricity supply lines. It was also possible to plan for adequate electrical clearances required by the higher voltage, which often rules out electrification of existing lines at 50 kV.

Further comparative studies were then confined to diesel electric versus 50 kV electrification. The studies were carried out in a period of uncertainty regarding the future availability and cost of crude oil. The projected increase in cost of oil compared with the comparatively cheap production of electricity swung the balance narrowly in favour of electrification. The present costs of electricity and diesel fuel completely justify the decision to electrify the line. At the present level of export the cost of electricity is less than half the cost of the equivalent amount of diesel fuel which would be required. Also the operation is now only reliant on locally available resources i.e. electricity from coal.

2.1.1 Electrical Feeding Arrangements

Figure 2 shows the power supply arrangements to feed the 50 kV traction system.

Six substations were built by Escom to supply power at 50 kV to the track feeder stations next to the railway line. Four substations take supplies at 400 kV, two taking supplies at 275 kV. Escom also built the 50 kV transmission lines between the substations and the track feeder stations, the length of line varying from 0 to 28 km.

The track feeder stations are part of the railway

system and were positioned approximately 160 km apart in such a way that only one train can draw current from any one feeder section, except under emergency conditions.

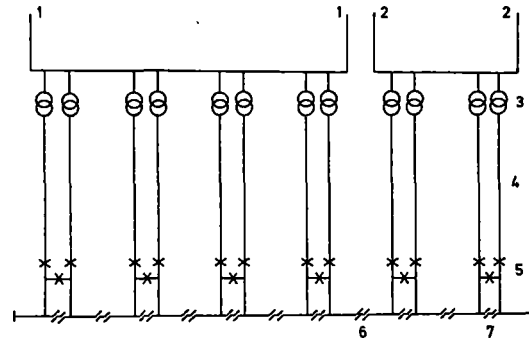


Fig. 2 Power supplies to Sishen - Saldanha 50 kV line.

- 1 - 3 Phase transmission line, 400 kV
- 2 - 3 Phase transmission line, 275 kV
- 3 - Escom substation transformers, 40 MVA, 400/275/50 kV single phase
- 4 - Single phase transmission lines, 50 kV
- 5 - SAR track feeder stations
- 6,7 - Intermediate and substation neutral sections

2.2 Ermelo - Richards Bay 25 kV Line

The initial decision to electrify this line using the 3 kV DC system, was based on an annual tonnage of 10 million tons nett. As the restrictions on further growth by adoption of this system became apparent the decision was amended to adoption of the 25 kV AC system with its larger capacity and potential for growth. This decision has been proved over and again to be the right one as the line is now handling 26 million tons per annum and with relatively simple improvements, electrically, is being strengthened to cater for the transport of 44 million tons per annum. Electrification at 50 kV was ruled out primarily on the basis of inadequate electrical clearances through existing tunnels of which there are 23 on the line.

2.2.1 Electrical Feeding Arrangements

Figure 3 shows the power supply arrangements to feed the 25 kV traction system.

Fourteen substations at approximately 30 km intervals are positioned next to the railway line. These substations are owned by the SAR. Supplies to thirteen substations are obtained from an 88 kV three phase transmission line owned and built by Escom especially to supply the traction network, and dedicated to this purpose. One substation has a supply at 132 kV. The 88 kV line is connected at approximately 100 km intervals to a 400 kV line which is a part of the main grid supplying the Richards Bay Industrial area.

3.0 SUBSTATIONS

Figures 4 and 5 show the basic substation feeding arrangements to the railway overhead equipment on both lines.

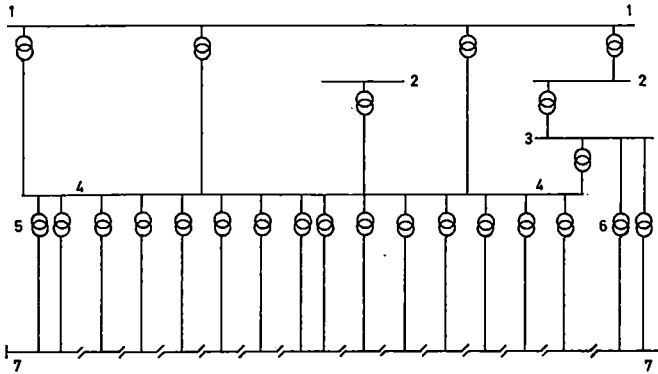


Fig. 3 Power supplies to Ermelo - Richards Bay 25 kV line.

- 1 - 3 Phase transmission line, 400 kV
- 2 - System busbar, 275 kV
- 3 - System busbar, 132 kV
- 4 - 3 Phase transmission line, 88 kV
- 5 - Single phase trackside substations, 88/25 kV
- 6 - Single phase trackside substation, 132/25 kV
- 7 - Railway overhead track equipment, 25 kV

3.1 Sishen - Saldanha 50 kV Line

Each substation is equipped with two 40 MVA single phase transformers. Normally each transformer feeds one section of line through the track feeder station but the rating is sufficient to enable one transformer to feed both sections of line. The transformers are naturally cooled and have an off-load tap changing facility. The short circuit reactance is 14 %.

The track feeder stations have small oil volume circuit breakers with a continuous rating of 1 250 A and a breaking capacity of 16,5 kA, which are in excess of actual requirements.

The overhead track equipment is protected in the track feeder stations by instantaneous over current and impedance-distance relays. Fault currents vary from 5 500 A at the track feeder station to 1 100 A at the end of the longest section and no difficulty is experienced in discriminating with the load current as the maximum current of one train is 320 A.

Telecontrol of the track feeder station circuit breakers is provided over a microwave link between the control centre at Saldanha and each track feeder station.

3.2 Ermelo - Richards Bay 25 kV line

Each substation feeds a section of approximately 30 km of line from the mid point i.e. 15 km each side of the substation. Eleven substations were initially equipped with single 20 MVA transformers, with the substations at each end and in the middle of the line being equipped with two 20 MVA transformers each for security rather than reasons of loading.

At the junction of two adjacent substation sections is situated a track sectioning station (TSS) for emergency switching purposes.

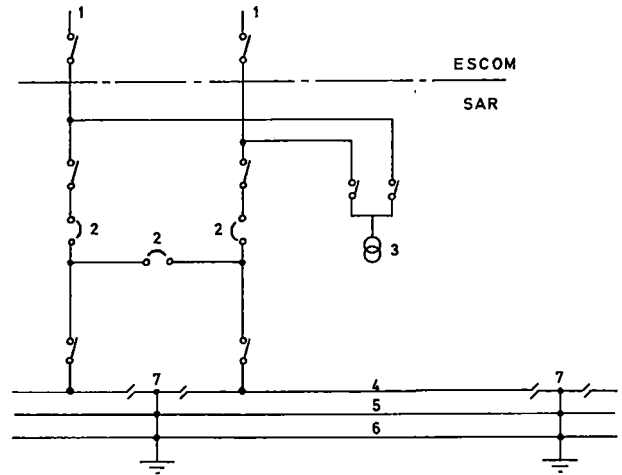


Fig. 4 50 kV Substation schematic diagram and feeding arrangements to track.

- 1 - Single phase transmission lines, 50 kV
- 2 - Small oil volume circuit breakers
- 3 - Auxiliary supplies transformer, 50/0,22 kV
- 4 - Contact and catenary wires, 50 kV
- 5 - Return conductor, earthed
- 6 - Traction rails, earthed
- 7 - Neutral section

The transformers are naturally cooled and can deliver up to twice their rated output for two minutes. Short circuit reactance is 11 %. An offload tap changer is provided on the secondary winding giving a voltage range of 25 kV plus 15 % minus 0 % in 6 equal steps. No-load voltage is set normally at 27,5 kV.

Connection of the transformers to the supply line is through two pole oil circuit breakers. On the secondary side of the transformer one leg of the winding is connected by overhead conductors to the traction return circuit (earthed). The other leg of the winding feeds through a single pole vacuum circuit breaker onto a busbar from which vacuum circuit breakers feed the sections of track. The vacuum circuit breakers are housed in individual steel cubicles assembled into a modular building with an annexe at one end to house telecontrol equipment, batteries and charger unit, selector telephone etc.

Above each circuit breaker associated protection relays are mounted in a relay panel. Track feeder circuits are provided with impedance distance relays for protection against earth faults and thermal relays for protection against sustained overloads. The impedance relay is of the 3 zone type with instantaneous tripping for faults within the first zone and adjustable time delayed tripping for more distant faults in zones 2 and 3. Some problems were experienced with the settings of this relay, as an arcing fault in zone 2 for example was not being cleared fast enough with consequent burning through and parting of overhead conductors. This problem was overcome by reducing the operating times on zones 2 and 3 to their minimum. The resultant loss in discrimination between parallel feeding circuit breakers was of secondary importance. Total fault clearance time is now less than 80 ms.

Fault currents vary from 6 000 A at the substation to 2 500 A at the end of a 15 km section. Again no problems are experienced in distinguishing between fault and load currents.

Insulation levels for substation equipment were chosen on the basis of an equivalent 3 phase 44 kV system. Lightning impulse withstand level is 250 kV peak with power frequency withstand of 90 kV rms . Earth clearances for substations are 540 mm outdoors and 320 mm indoors.

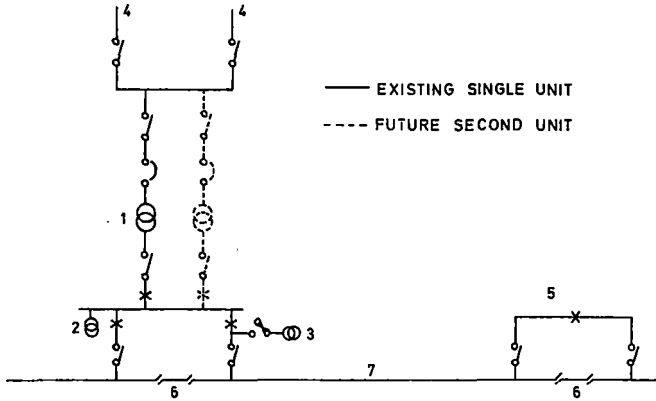


Fig. 5 25 kV Substation schematic diagram and feeding arrangements to track.

- 1 - Traction transformer, 20 MVA
- 2 - Voltage transformer, 26,4/0,11 kV
- 3 - Auxiliary transformer, 25/0,22 kV
- 4 - Three phase supply lines, 88 kV
- 5 - Track sectioning station
- 6 - Neutral section
- 7 - Contact and catenary wires, 25 kV

3.3 Unbalanced Loading Of Single Phase Substations

Single phase loads on a 3 phase network create negative sequence voltages which can be harmful to other equipment supplied from the 3 phase system. The design of the power supply system was based on the following restrictions on the generation of such voltages :-

The negative sequence voltage caused by continuously varying single phase loads connected to alternate pairs of phases shall not exceed 2 % of the positive sequence voltage, at the point of common coupling with other consumers.

Scott connected and other similar transformer connections were rejected as means of balancing the loads on the 3 phase system as balance is only effected for equal loads on the two output windings. With the proposed size and spacing of trains this was not a realistic situation and the simplicity of the pure single phase transformer was preferred.

3.3.1 Ermelo - Richards Bay 25 kV line

Alternate transformers are connected to alternate phase pairs of the 3 phase supply line in rotation to achieve a degree of balance over the system as a whole. It was assumed that the worst out of balance over the whole line would be equivalent to the rated load of one transformer i.e. 20 MVA, requiring a fault level of 1 000 MVA at the point of common coupling with other consumers. This condition moves the point of common coupling to the primary (400 kV) side of the Escom transformers feeding the 88 kV, 3

phase transmission line which feeds the traction substations, and results in this line being dedicated to railway usage. This of course gives rise to a significant factor in the cost of electricity in that the entire cost of provision of this line must be borne by the Railways through the electricity tariff.

3.3.2 Sishen - Saldanha 50 kV Line

Single phase transformers are connected to alternate phase pairs in rotation to balance the load as far as possible. To meet the negative sequence requirement 4 substations are fed from a 400 kV line with fault levels sufficiently high so as not to require any further measures. Two substations however could not be fed from this 400 kV line but from an existing 275 kV line only. Under normal conditions the fault levels are adequate to ensure compliance with negative sequence limits, however under certain line outage conditions these limits would be exceeded. To cater for this eventuality a compensator has been installed by Escom to compensate automatically for unbalanced voltages. This device uses static switching techniques to vary the amount of capacitive and inductive reactance connected between phases necessary to compensate for the unbalanced load.

4.0 OVERHEAD TRACK EQUIPMENT

Table 1 lists the main characteristics of the overhead track equipment on both heavy haul lines. Following the initial decision to electrify the line from Ermelo to Richards Bay with 3 kV DC a large amount of construction work had already been done between Vryheid and Richards Bay before the decision was made to use 25 kV AC . This included the provision of an 11 kV 3 phase transmission line on the same structures as the traction wires for supplies to signalling and telecommunication installations. As much use as possible was therefore made of the work already done and the 3 kV DC design was modified and adapted to suit the 25 kV AC electrification. The design and installation on this portion of the line were carried out by the SAR.

Both heavy haul lines utilise a simple catenary construction. Balance weight tensioning of both contact and catenary wires is used on the 50 kV line and the Ermelo - Vryheid portion of the 25 kV line. On the section converted from 3 kV DC to 25 kV AC balance weight tensioning of the contact wire is used while the catenary wire is fixed tensioned except through tunnels where balance weights are used.

On both lines an uninsulated return conductor is carried on and connected to the steel masts. The rails carrying traction return current are connected to the steel masts at regular intervals, generally every 5 to 6 spans.

A difficulty arose on the 50 kV line as to the method of making electrical connections to the rails. When the usual exothermic welding process is applied to the chrome-manganese rails used on this line it leads to excessive Martensite formation and an increased risk of rail fracture. To overcome this problem a friction welding technique was developed to weld aluminium studs to the rail web at much lower heat, onto which a lug is bolted to form the electrical connection.

TABLE 1 Characteristics of overhead track equipment.

	Ermelo - Vryheid	Vryheid - Richards Bay	Sishen - Saldanha
Contact wire	107 mm ² HD Cu	161 mm ² HD Cu	107 mm ² HD Cu
Catenary wire	65 mm ² HD Cu	80 mm ² HD Cu	70 mm ² HD Cu (coastal)
Return conductor (earth wire)	150 mm ² AAC	250 mm ² AAC	130 mm ² ACSR (inland) 70 mm ² HD Cu (coastal) 130 mm ² ACSR (inland)
25 kV feeder wire	150 mm ² AAC	-	-
Span length	71 m	67 m	70 m
Contact wire height - normal	5,15 m	5,20 m	5,00 m
- minimum	4,50 m	4,50 m	4,50 m
- maximum	6,00 m	6,00 m	6,20 m
Tension length	1 610 m	1 830 m	2 500 m
Wire tension - contact wire	11 kN	14,5 kN	10,0 kN
- catenary wire	11 kN	7,8 kN	12,8 kN (inland)
Normal static clearance	300 mm	300 mm	616 mm
Minimum passing clearance	190 mm	190 mm	406 mm
Impedance (ohms/km)	0,169 + j0,369	0,135 + j0,321	0,171 + j0,403
Current rating - continuous	740 A	806 A	-
- 5 min.	835 A	980 A	-
- 1 min.	1 510 A	1 775 A	-

Steel masts are used exclusively on both lines. The 50 kV line runs along the coastline for 90 km, subjecting the line to extreme pollution and corrosion attack. The masts in this area were galvanised and given additional protection in the form of epoxy undercoating and vinyl painting. Even this proved insufficient in certain areas, requiring regular maintenance.

On the Ermelo - Vryheid section of the 25 kV line galvanised steel and 'Corten' masts were used in core type foundations. On the section converted from 3 kV DC, steel masts bolted to the foundations were used with the insulation normally provided between mast and foundation for DC electrification omitted.

Both lines end at coastal ports requiring special attention to insulator pollution. Composite insulators have been employed on both lines in areas subject to salt spray pollution. No problems have been experienced with these insulators on the 25 kV line, while failures have resulted on the 50 kV line. These failures are described later in the paper. In the inland regions of both lines both solid core and disc type insulators have been used.

The use of tension lengths of 2,5 km on the 50 kV line resulted in initial problems being experienced with excessive creep of the contact wire. This was apparently due to the purity of the South African copper used. This necessitated readjustment of equipment and lifting of weights.

A feature of the equipment on the 25 kV line is the positioning of the return conductor above the catenary wire. This provides lightning coverage for the equipment, reduces the system impedance and improves the screening of trackside circuits. On the 25 kV line only one rail is available for traction return current on single line sections and the return conductor supplements the return circuit, and is adequately rated to carry the return current in the event of a broken traction rail.

Post Office telecommunication routes in the vicinity of the railway lines were generally converted to a carrier system immune to interference from the traction system. Only in areas of high concentration of telecommunication circuits were booster transformers used in the overhead equipment for the

suppression of interference.

It was found after energising of the 50 kV line that return currents of up to 28 amps were flowing in steel fences alongside the track. Alarming sparking occurred when gates in the fence were opened. The solution adopted was to ensure continuity of the fence via underground connections bridging the gap between gateposts. This problem was not experienced on the 25 kV line as the fences were constructed with steel uprights providing adequate earthing, whereas the fences on the 50 kV line used wooden uprights over long distances.

4.1 Current Rating of Equipment

On the 50 kV line the lower currents resulting from the use of the higher voltage do not present a problem regarding the size of overhead conductors. The accepted minimum conductor sizes from mechanical strength considerations are more than adequate for the current to be carried.

On the 25 kV line the design of the equipment was based on the running of 76 wagons of 74 tons gross hauled by 3 x 7E locomotives having a normal full load current of 480 A. Allowance was made for the crossing of a loaded and an empty train in a feeder section and in certain potentially heavily loaded areas a back-up feeder was provided to increase the continuous rating of the equipment to 1 100 A. Very soon after the start of electric operation the train size was increased to 84 wagons of 80 tons gross hauled by 4 x 7E locomotives.

5.0 LOCOMOTIVES

Brief details of the class 9E 50 kV locomotive and class 7E 25 kV locomotive are described below. Table 2 lists the main performance characteristics as they affect the power supply system and railway operation.

The restriction of one train per feeding section on the Sishen - Saldanha line ensures that the voltage at the train never falls below 35 kV under normal operations. Under abnormal conditions with two trains in a section the voltage can drop to 25 kV and the locomotives are designed accordingly.

Table 2 Locomotive Characteristics

	Class 9E	Class 7E
Wheel arrangement	Co-Co	Co-Co
Mass	168 ton	124 ton
Gauge	1 065 mm	1 065 mm
Continuous tractive effort	383 kN	300 kN
Speed at continuous tractive effort	34,5 km/h	35,0 km/h
Continuous output	3 670 kW	2 920 kW
Supply voltage range	55 kV/ 25 kV	28,75 kV/ 17,5 kV
Power factor at full load	0,88	0,93
Full load input to locomotive	5 380 kVA	4 000 kVA
Locomotives in multiple per train	3	4
Full load input to train	16,14 MVA	16,00 MVA
Current drawoff of train	323 A	640 A

On the Ermelo - Richards Bay line the system caters for one loaded and one empty train each at full power in one feeding section. As the empty train uses only the power of 3 locomotives out of the consist of 4 the total current demand for the section is 1 120 A, with a minimum voltage in the section of 21 kV . As one transformer feeds two sections of track, trains in the adjacent section may cause the voltage to fall to 19 kV or less under abnormal conditions. The locomotives can deliver rated output down to 19 kV and reduced output down to 17,5 kV .

6.0 ELECTRICITY COSTS AND UTILISATION

The tariff applied by Escom to the electricity consumed for traction purposes is the same as that applied to all large power users in the country. The actual method of application however is not favourable to users of electricity for traction purposes.

6.1 Standard Tariff

The standard tariff has two parts in which separate charges are levied for the monthly maximum demand and for the energy consumed. In addition a monthly charge is levied to cover the actual cost of the extensions to the system required to provide the connections to the consumer.

6.1.1 Demand Charge

The demand charge is related to Escom's costs in respect of capital expenditure, operating costs, maintenance etc. of generating plant and transmission equipment.

Escom's policy with regard to single phase traction systems is to split the traction system into sections for demand purposes, each section comprising a number of traction substations. These are referred to as metering sections.

In each metering section the half hour average load of each substation is summed every half hour to get the simultaneous half hour demand for that section. At the end of each month the highest of the simultaneous half hour demands recorded is used to levy the demand charge for that metering section for the month.

The measured unit of demand is the kVA .

6.1.2 Energy Charge (Unit Charge)

This charge is related simply to the cost of fuel to generate the electricity and the consumer is levied on the energy he consumes.

The measured unit of energy is the kWh.

6.1.3 Extension Charge

This charge is related to the extensions to the system provided by Escom to connect the consumer to the system. In the case of single phase traction systems the policy of building dedicated transmission lines to feed the traction substations, as demanded by the negative sequence voltage criteria, means that these costs are extremely high and cannot be shared with other consumers.

6.2 Actual Electricity Tariffs

Table 3 gives the latest tariffs applicable to the heavy haul operations together with typical figures for a months operation. All figures have been converted to U.S. \$ which at the present exchange rate are equal to 0,76 S.A. Rand.

Table 3 Electricity Tariffs and Consumptions *

	Sishen - Saldanha	Ermelo - Vryheid
Energy charge ¢/kWh	1,37	1,21
Demand charge \$/kVA	7,16	6,17
Nett tonnage	1 418 100	2 240 475
Energy consumed kWh	14 534 300	39 180 000
Total demand kVA	64 320	164 350
Energy cost	\$ 198 684	\$ 472 201
Demand cost	\$ 460 228	\$1 014 656
Extension charge	\$ 539 734	\$ 498 894
Total electricity cost	\$1 198 646	\$1 985 751
Cost per net. ton hauled	84,5 ¢	88,6 ¢

* As at end of July 1981

6.3 Utilisation Of Electricity

6.3.1 Energy charge.

In a traction system the energy consumed and thus the energy charge is directly related to the gross tonnage transported. While savings in energy consumption are possible by improved efficiency of locomotives, reduced losses in supply systems etc., these measures can only affect the total energy consumption by a relatively small percentage.

Significant energy savings are possible as train size increases, by the optimum utilisation of momentum of heavier trains by locomotive drivers in progression from steep down grades to short up grades. On the 25 kV line savings of up to 12 % have been predicted by computer simulation and verified by test for train size increasing from 84 wagons of 80 tons gross to 164 wagons of 80 tons gross.

The use of regenerative braking on locomotives to save energy was considered. On the 25 kV line it was calculated that even if a 25 % reduction of energy consumption could be achieved this would not affect the demand or extension charges, and result in only a 5 % saving in total electricity costs. This saving could be offset by about 2 % by extra locomotive equipment costs.

6.3.2 Extension Charge

The extension charge is not affected by the actual railway operation and would be payable even if trains did not run.

6.3.3 Demand Charge

The measured demand is created by a combination of the demands of individual trains. As the demand paid for amounts to more than double the bill for energy consumed, savings in this area can have a significant effect on the total electricity bill. One measure adopted on the 25 kV line was to improve the power factor of the locomotives by the use of forced commutation or switched capacitors, to 0,93 at full load. This was calculated to reduce demand by 10 % and overall electricity costs by 4 % .

The demand charge is also extremely sensitive to the manner of operation of the train service. This is especially so on the two lines under discussion where the power demand of individual trains is so high.

Consider the situation where for a whole month the train service operates in a regular fashion resulting in a half hour demand in a particular section of X units. In accordance with the train timetable not more than Y number of trains should be operating in that metering section at any one time. Just before the end of the month a broken rail is found and while repairs are in progress trains are delayed and build up in the metering section. When the break is repaired there are now 2Y number of trains in the section and in the process of reducing the accumulated backlog the half hour demand is doubled to 2X units. For the sake of one half hour in the month the demand charge payable is double what it would otherwise be.

6.4 Monitoring And Control Of Demand

In order to avoid unnecessary peaks in demand caused by bunching of trains in a metering section the following requirements should be met :-

- (1) A demand monitoring facility should be provided which must be able to predict the progress of demand and provide an early warning when demand is likely to exceed a set level unless corrective action is taken.
- (2) It should be possible to control the demand to avoid exceeding the set level at the end of each half hour period.

The second condition is the most important and often the most difficult to achieve. On both heavy haul operations locomotives are equipped with radios. The train controller is therefore in continuous radio contact with the driver of each train throughout its journey. Effective control of demand can be exercised by requesting drivers of certain trains to slow down and so reduce their contribution to the demand. As empty trains travel at higher speeds than the loaded trains it is much easier for empty trains to make a significant reduction in demand on request and this action has been limited to empty trains.

The monitoring of demand requires a means of continuously measuring the traction load at each substation in a metering section. This is also possible on both lines by using the telecontrol

system installed for remote control of substation equipment to relay desired quantities to a central processing point.

In the control centre the individual substation loads in a metering section are summated and then integrated to produce the total energy consumption since the start of the particular half hour metering period. The set half hour average demand determines the maximum allowable energy consumption for the half hour. A comparison is then made of the actual energy consumed and the total energy consumption allowed, and using the rate of energy consumption a prediction can be made of the expected energy consumption at the end of the half hour. If this is above the figure allowed an alarm is initiated for further action to be taken by the train controller.

6.4.1 Sishen - Saldanha 50 kV Line

Escom has broken this line into 3 metering sections of 2 substations each.

A system along the lines of that described above has been developed by SAR engineers and has proved extremely successful in aiding the train controller in the scheduling of trains to avoid unnecessary peak demands. On occasion when the system has not been properly utilised the effect has been immediately evident costing thousands of rands in excessive demand charges.

Figure 6 shows the total of the highest half hour demands measured by Escom over the 3 metering sections, compared with the total energy consumption over the line for the month.

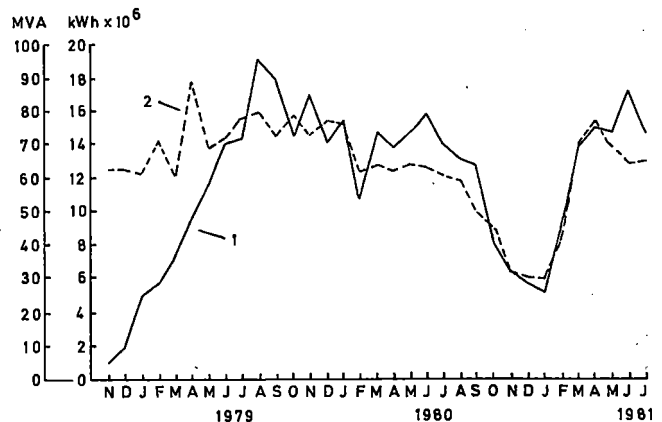


Fig. 6 50 kV line - Monthly demand and energy consumptions

- 1 - Energy consumption per month
- 2 - Monthly maximum demand

Reductions of up to 13 % in the monthly demand paid for have been achieved since introduction of the monitoring and control system on the basis of similar tonnages transported and energy consumed per month. This represents a saving of 10 000 kVA per month, or more than \$70 000 per month.

6.4.2 Ermelo - Richards Bay 25 kV Line

Escom has broken this line into 5 metering sections containing 4,3,3,3 and 1 substations respectively. Based on the success of the monitoring and control system introduced on the 50 kV line a similar system

has been purchased for installation on the 25 kV line early in 1982.

Figure 7 shows the demand and energy consumption figures for this line without any attempt at control of demand.

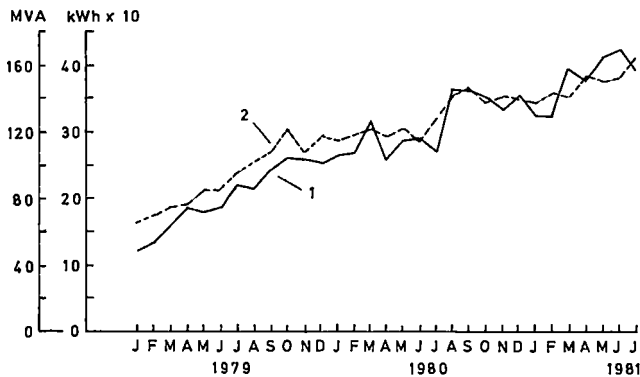


Fig. 7 25 kV line - Monthly demand and energy consumptions

- 1 - Energy consumption per month
- 2 - Monthly maximum demand

7.0 INDUCTIVE INTERFERENCE AND HARMONICS

Together with the generation of negative sequence voltages the generation of harmonics and the inductive coupling of the traction system with adjacent circuits constitute the major disadvantages of AC traction systems.

7.1 Harmonics

It is a requirement that at the point of common coupling with other consumers harmonics caused by an individual consumer shall not exceed the following limits :

- (1) individual harmonics; less than 1 % of V_1 ,
- (2) r.m.s. total; less than 3 % of V_1 ,

where V_1 is the positive sequence fundamental frequency voltage at the point of common coupling.

Measurements have been carried out by the SAR at the point of connection of a traction substation to the 88 kV supply line at Normandie between Ermelo and Vryheid. This point was the closest that the SAR could come to a point of common coupling.

The only known problem resulting from generation of harmonics occurred at Vryheid on the Ermelo - Richards Bay line. It was suspected that harmonics were affecting a ripple control system installed by the local authority for the remote control of equipment such as hot water geysers. The problem was overcome by the installation of suitable filters by the local authority.

7.2 Induction Into Trackside Circuits

The problems resulting from induction into trackside signalling and communications circuits are being dealt with in a separate paper.

On the power supply side the high transformer impedance, 11 % on the 25 kV line, 14 % on the 50 kV

line, is a deliberate measure to reduce the fault current levels on the track to assist in immunisation of signalling and telecommunication circuits. This also introduces into the power supply system a self regulating feature in that attempts to demand excessive load current by too many trains in a section results in reduced voltage and therefore reduced power demand from individual trains.

In the design of the overhead equipment every endeavour is made to reduce the screening factor as much as possible. Computer programs have been written to compute screening factor and induced voltages in trackside cables for any configuration of overhead wires. Computations have generally shown good correlation with measured results.

On the 25 kV line the present use of single rail track circuits leaves only one rail available for traction return current purposes. This of course increases the screening factor compared with the availability of two rails for traction current. These track circuits are going to be replaced with a form of signalling allowing use of both rails for traction current return.

For the line between Ermelo and Vryheid the screening factor of the basic equipment (i.e. without back-up feeder) on single track is 0,25. Between Vryheid and Richards Bay the presence of two additional earth wires above the 3 phase 11 kV transmission line on the track structures improves the screening factor to 0,20.

8.0 IN-SERVICE EXPERIENCE

Both heavy haul lines have been operating with electric traction since 1978, giving 3 years experience on each line. The SAR is satisfied with the performance of the electric systems on both lines with the exception of certain problems. Some of these will be described below as well as the achievements to date.

8.1 Sishen - Saldanha 50 kV Line

A number of failures of composite insulators occurred after the line had been energised for about one year. The failures took the form of holes through the insulator sheds which were about 1 mm in diameter and looked as though they had been deliberately made with a hot needle. The failures were attributed to partial discharges occurring in gas pockets trapped between adjacent shed interfaces. The gas discharge activity resulted in the oxidation of the polymer to an acid and lead to final puncture. Non uniform voltage distribution as a result of pollution on the insulator surfaces increases partial discharge activity and the likelihood of failure.

As a result the insulators are now being coated with silicone grease at 6 monthly intervals to reduce the failure rate. A number of replacement composite insulators have been supplied for in-service evaluation and these are being installed in the normal manner.

Problems were experienced at an early stage with power circuit thyristor and diode failures on the 9E locomotives. The failures were traced to overvoltages on the overhead supply system. As a consequence of the long feeding sections, 90 km from

feeder station to end of feeder section, the natural resonant frequency of the system is reduced to the range of significant harmonic currents generated by the locomotives. Injection of such harmonic currents into the system with corresponding high harmonic impedance results in distortion of line voltage waveform and hence high overvoltages.

Peak voltages of up to 144 kV were measured at the locomotive pantograph during test runs. This value is 85 % higher than the initial design allowance for overvoltage and resulted in devices being stressed to within 20 % of their peak withstand voltage. Subsequent computer analysis predicted the possibility of peak voltages exceeding the measured value.

Thorough computer studies indicated that the resonance and associated overvoltages could be reduced by either line-side filters permanently connected at the end of each feeding section or on-board filters mounted in each locomotive. An on-board filter was chosen as the solution to be adopted and these filters are presently being installed in the locomotives. During tests with these filters a maximum peak voltage of 96 kV was recorded. This was considered acceptable.

Some malfunctioning of electronic equipment occurred due to high ambient temperatures within the locomotives. This was solved by the installation of additional cooling fans.

Due to a recent reduced export demand the line has not been operating at full capacity. Over the 12 month period to August 1981 12,766 million tons of ore have been transported at an average specific energy consumption over this period of 8,04 Wh/ton-km (gross, excluding locomotive mass).

8.2 Ermelo - Richards Bay 25 kV Line

Some problems have been experienced with pollution of insulators in tunnels resulting from the operation of diesel locomotives on the line. Insulators in tunnels and near the coast are now coated with silicone grease which has to be removed and replaced at 6 monthly intervals.

Problems have also been experienced with the first series of locomotives purchased. The body structure requires strengthening to reduce flexing in operation and gear assemblies must be modified to eliminate vibration induced problems in the traction motors. Especially encouraging is the reliability of the electronic equipment in service.

It is now considered that the technical superiority of the 25 kV AC system over the 3 kV DC system has been satisfactorily proven in respect of the following features :-

- (a) Elimination of power control and switching problems in electric locomotives.
- (b) Adequate power for heavy trains with little restriction.
- (c) Greater reliability and reduced maintenance of locomotives, substation equipment and overhead equipment.
- (d) Improved control of locomotive wheel slip resulting in higher adhesion levels in practical service with multiple consists of

about 24 %, and reduced rail surface damage.

- (e) Virtual elimination of lightning failures and other transient overvoltage problems.
- (f) Virtual elimination of wear on contact wire due to use of carbon pantograph strips.

Table 4 shows the actual costs in service on the 25 kV line of electrical energy and capital and maintenance costs of electrification for the financial year 1979/80. For comparison approximate costs of the original diesel service are shown corrected to a 1979/80 basis.

The figures are expressed in U.S. cents per 1000 gross ton km which includes wagon mass but excludes locomotive mass.

Table 4 In-service Operational Costs

<u>Energy and Power Supply</u>	<u>Electric</u>	<u>Diesel Electric</u>
Electricity or fuel	88	267
Lubrication	-	12
Interest on fixed equipment	36	-
Maintenance of fixed equipment	<u>11</u>	<u>-</u>
Subtotal	135	279
<u>Locomotives</u>		
Interest on capital	87	87
Maintenance *	<u>25</u>	<u>57</u>
Subtotal	<u>112</u>	<u>144</u>
Grand total	<u>247</u>	<u>423</u>
Cost per ton of coal hauled	<u>165</u>	<u>202</u>

* Maintenance costs of electric locomotives are not firm until their first major overhaul has been completed after 7 years or about 1,4 million kilometres. The above figures are based on the average maintenance cost in service with 3 kV DC locomotives of 24 ¢/km and for diesel electrics of 34¢/km. Experience to date with 25 kV AC locomotives indicates that these will be more economical to maintain. The same interest on capital costs of electric and diesel electric locomotives are shown since their cost per kWh of output power is of the same order.

8.3 Change-over Stations

The 25 kV line from Ermelo to Richards Bay has links with the 3 kV DC traction network at 3 places, viz. Ermelo and Empangeni (Richards Bay) at the two ends of the line and Vryheid in the middle of the line.

As the locomotives ordered to haul the trains on the 25 kV line from Ermelo to Richards Bay were required for a special purpose duty it was not considered advisable to compromise their design by making them suitable for dual voltage operation. It was therefore necessary to provide a change-over facility at each interconnection of the 3 kV DC and 25 kV AC systems whereby locomotives of different types could be exchanged.

The system adopted was one whereby the overhead wires in a change-over station are broken up into individual electrical circuits each fed by two switches, one supplying 3 kV DC and one 25 kV AC to the equipment. Furthermore the electrical sections correspond with signalling sections defined by block

joints in the rails. The electrical switches feeding power to the overhead wires are motor driven and operation is controlled automatically by the signalling system.

As the switches feeding the overhead wires are normally open, and close whenever a train is to enter the particular section, these switches are required to perform up to 2 000 operations per month. Reliability was of utmost importance and after various possibilities were explored the only suitable switch which could be used was a normal 25 kV AC sectioning switch.

More than 200 of these switches were installed at the 3 change-over stations and after three years are still operating satisfactorily with a minimum of maintenance.

The switches are driven by 24 V DC motors. Minor problems were experienced with dirty contacts and malfunction of relays at this voltage. These have been overcome but future systems will employ 110 V DC drives to eliminate these problems at the outset.

In any operation of this nature accidental contact between the 25 kV AC and 3 kV DC systems is inevitable. A protection device was developed along the lines of a device described in an article published in Rail International and used in Russia. The SAR device was simpler using fewer and cheaper components and has been tested and proven to protect equipment connected to the 3 kV DC system from damage resulting from contact with the 25 kV AC system. Figure 8 is a schematic diagram of the device developed by the SAR.

It is considered that the SAR is unique in the extent and flexibility of the change-over stations built to interface its 3 kV DC system with the 25 kV AC system, for without this facility further expansion of the 25 kV AC system would not be feasible.

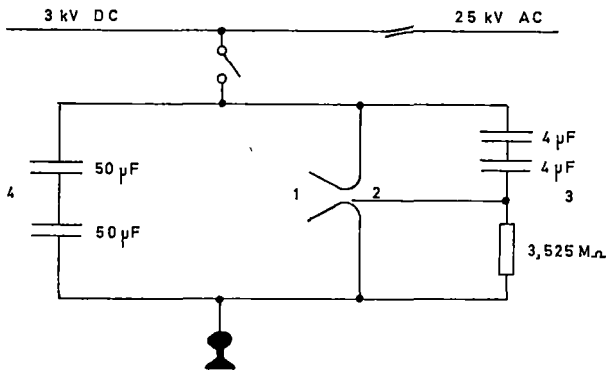


Fig. 8 AC/DC Protection Device

- 1 - Spark gap/arcing horns
- 2 - Ignition electrode
- 3 - RC potential divider
- 4 - Line capacitors

9.0 PLANNING FOR INCREASED CAPACITY

The capacity of the Ermelo - Richards Bay line is to be increased from the present 26 million tons of coal per annum to 44 million tons per annum by the

end of 1985. The train size is to be increased to 20 800 tons, 200 wagons hauled by a consist of 4 locomotives of a new class designated 11E. To enable the locomotive to haul from the front of the train the ruling grade sections in the direction of the loaded train will be regraded to 6,25 per mil uncompensated.

The consist of 4 class 11E locomotives will have an output of 3 900 kW each and a total demand capability of 22 MVA; with empty trains using 3 locomotives only under power having a demand of 16,5 MVA. The total demand of a loaded and empty train crossing in a substation section could thus reach 38,5 MVA.

To cater for the increased demands on the power supply system, second 20 MVA transformers are being installed at each substation. To further improve the voltage conditions at the trains the feeding arrangements to the tracks are being changed as shown in fig. 9. 30 km of track will then be fed from each end through transformers at adjacent substations connected in parallel. The ratings of the overhead equipment will also be increased by the provision of back-up feeders throughout on all single line sections.

To make the optimum use of the available power in the locomotives within the constraints of maximum allowable adhesion the locomotive axle loading will be increased to 28 tons per axle. This is higher than the limit of 26 tons per axle set for the wagons but will be permitted because of the comparatively small number of axles at this load per train.

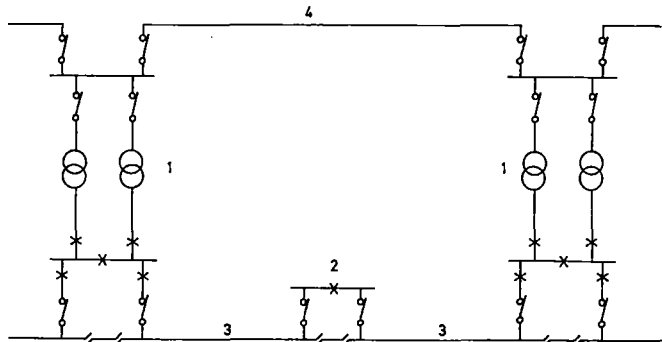


Fig. 9 Proposed parallel feeding between substations

- 1 - Double unit substation, 2 x 20 MVA
- 2 - TSS circuit breaker, normally closed
- 3 - 25 kV overhead equipment
- 4 - Transmission lines, 88 kV

10.0 CONCLUSION

The rate of increase in traffic over the Ermelo - Richards Bay line has resulted in the full capacity of the line and the power supply system being reached within two years of the introduction of electrification. Astute thinking at the initial planning of the power supply system resulted in adequate allowance for future expansion being made. As a result the capacity of the original power supply system will be doubled with a minimum amount

of work and disruption to the existing service.

The experience gained from the operation of two heavy haul lines using AC electrification has confirmed the soundness of the choices and the superiority over other forms of traction.

11.0 ACKNOWLEDGEMENTS

The author wishes to thank the Director General of the South African Railways and Harbours for permission to publish this paper, and to thank his colleagues for their valued assistance and comment.

12.0 REFERENCES

- 1 Norman, H.B., "Utility Problems in Providing Supplies to Electric Transport System," Proceedings of the Symposium on Electric Transport, South African Institute of Electrical Engineers, 1979.
- 2 Rees, M.T., "This Sishen - Saldanha 50 kV Electrification Project," Proceedings of the Symposium on Electric Transport, South African Institute of Electrical Engineers, 1979.
- 3 Quail, J.B., "Economics of the use of Electric Traction by the South African Railways for the transport of coal on the Richards Bay line," Paper presented to the Transportation Research Board of the National Research Council, January 1981.
- 4 Lapin, V.B., "Equipment for the contact points between different electric traction systems on the Soviet Railways," Rail International, September 1979.

Design of Electrification for Heavy-Haul Railroads : Its Contribution to Increased Tonnages

A. Daniels

Chief Engineer, Railroad & Electrification Div., International Engineering Co., Inc., San Francisco California

W.D. Weiss

Chief, Economics & Operations, Railroad & Electrification Div., International Engineering Co., Inc., San Francisco California

Many heavy-haul railroads, both dedicated mining railroads and mainlines with unit train operations, are electrifying to reduce operating costs and increase line capacity. This paper discusses ways in which electrification can achieve these objectives and examines electrification design aspects that require special attention on such lines. Typical characteristics of heavy-haul railroads requiring special design considerations are: heavy train loadings; weak and/or remote power supply; severe climatic conditions; and strict reliability requirements. Design approaches appropriate to heavy-haul railroad electrification are presented for electric locomotive selection; traction power system design, including treatment of voltage unbalance and reduction of system power demand; mitigation of harmonics; and overhead contact system design. Examples are given from the Black Mesa and Lake Powell Railroad, the Sishen-Saldanha Railway, and others.

INTRODUCTION

Many heavy-haul railroads are turning to electric traction in order to remain competitive in their respective markets and to eliminate reliance on an unstable supply of diesel fuel. In the process of electrifying, they are gaining advantages in operating cost savings, improved operations, and with these, greater capacity for hauling increased tonnages.

In order to obtain the maximum benefit from electric traction, the design of the electrification system for heavy-haul railroads, both dedicated mining railroads and mainlines with unit train operations, must take into account the unique operating conditions characteristic of such railroads and the physical environment that is often typical of such lines. Frequently, these design parameters are much different from those applicable to mixed freight or passenger service, and therefore dictate appropriate design approaches. Characteristics commonly requiring special treatment include the following:

- Heavy trains running relatively infrequently
- Weak and/or remote primary electrical supply systems
- Severe climatic and soil conditions
- Remote location of the railroad
- Strict reliability requirements

This paper discusses the various ways in which electrification can enhance line capacity and

facilitate increased throughput, and examines the principal aspects of railroad electrification system design that require special attention for heavy-haul lines. Specific design approaches are discussed, with particular reference to actual applications on a number of recent electrification projects, some of them already constructed and some still in preparatory stages.

Two recently completed projects that are discussed in particular are the 125-km Black Mesa and Lake Powell (BM&LP) Railroad in Arizona, USA (see Figure 1), and the 860-km Sishen-Saldanha Railway in South Africa (see Figure 2). Both are heavy mineral-haul railroads, and both use 50-kV

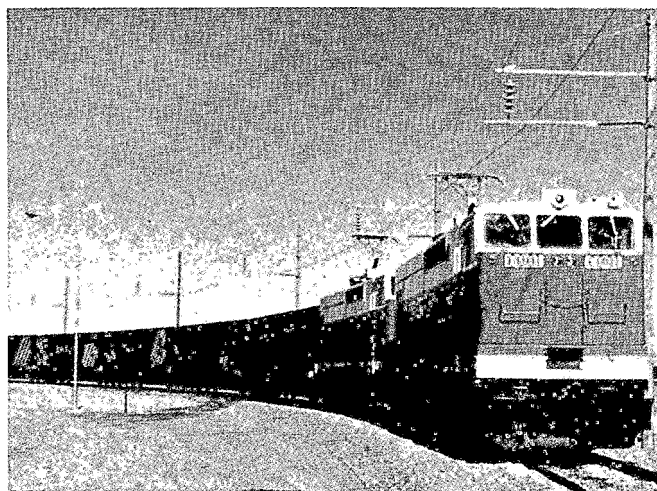


Fig. 1 The 125-km Black Mesa and Lake Powell Railroad, energized at 50 kV ac, has been operating since 1973.

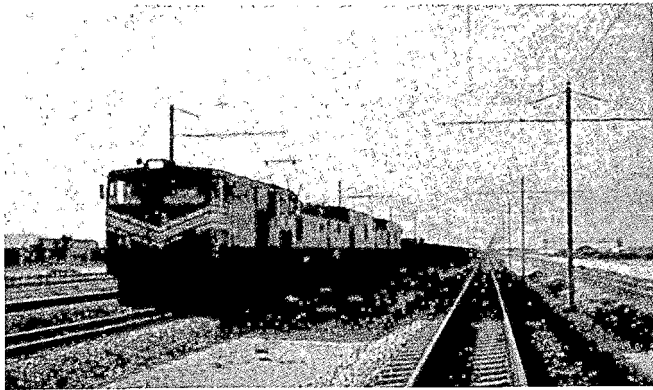


Fig. 2 The 860-km Sishen-Saldanha 50-kV electrification in South Africa was completed in 1978.

traction voltage, the only two operational railroads in the world electrified at that voltage level to date.

References are also made to electrification projects currently in the study or design stages, including the 56-km Deserado-Bonanza Western Railway (DBWR) in Colorado, USA; the 400-km Hamersley Iron Railway and the 420-km Mt. Newman Railway in Australia; the 550-km Vitoria-Minas Railroad (EFVM) in Brazil; and others. The majority of these are coal or iron ore lines designed for heavy tonnages, and most are in remote areas with harsh climatic conditions, typical of many such railroads now considering electrification. Many of the same design problems and solutions adopted for these lines are equally applicable to mainline railroads with heavy freight service, especially those with extensive unit train operations.

In order to derive the maximum benefit from electrification, in terms of increased capacity, improved operating efficiency and cost-effectiveness, the design must be prepared on a system-wide basis. This involves a complex optimization process among the various elements related to electrification, including locomotive and car fleet sizes, operating schedules and procedures, signaling and communications systems, traction power systems, overhead contact systems, and the primary electrical supply.

The operational advantages of electrification over diesel traction derive from several sources: faster turnaround times, lower locomotive maintenance requirements, greater in-service reliability, and resulting improvements in locomotive utilization and availability. With proper system operation established at the design stages, these advantages can be employed to enhance tonnage capacity with the same car fleet, or maintain present levels with a smaller fleet and more efficient operations. In either case, fewer locomotives are required, for reasons discussed below.

LOCOMOTIVE SELECTION

Central to the design of an electrified operation which will allow increased tonnages is selection of the appropriate electric locomotive, optimizing the application of its special performance characteristics. The principal design parameters affecting the selection of electric locomotives for a heavy-haul railroad stem from the common practice of using large trains operating at low speeds.

A modern electric locomotive has considerably more power available for traction than the equivalent diesel-electric, especially on an axle-for-axle basis. For example, common six-axle electric locomotives are rated at 6,000 hp (diesel equivalent), and some reach as high as 10,000 hp, whereas the largest six-axle diesel-electric in common use is around 3,600 hp. For illustration, Figure 3 shows power at the rail vs. speed for two common locomotives: The SD40-2 diesel-electric, manufactured by General Motors EMD, and the E60C electric, manufactured by General Electric.

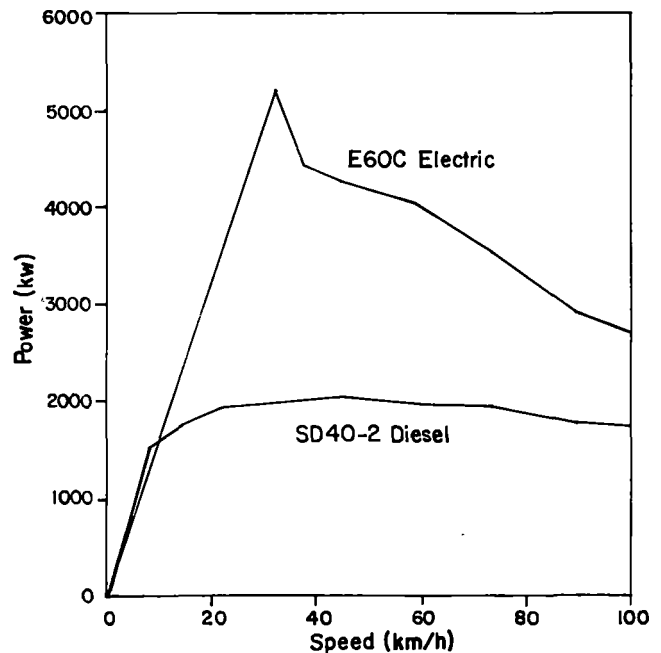


Fig. 3 Comparative power at rail vs. speed curves for typical electric and diesel-electric locomotives.

In all railroad operations, however, tractive effort is of key concern in selecting the locomotive. The electric locomotive can develop greater tractive effort over a wider speed range than an equivalent diesel-electric because of its increased power and improved adhesion characteristics. The availability of greater power in the electric locomotive, as noted in Figure 3, is particularly important at the vital speeds between 20 and 40 km/h. The resulting superior tractive effort developed over this speed range is shown in Figure 4, which again compares the SD40-2 diesel-electric with the E60C electric.

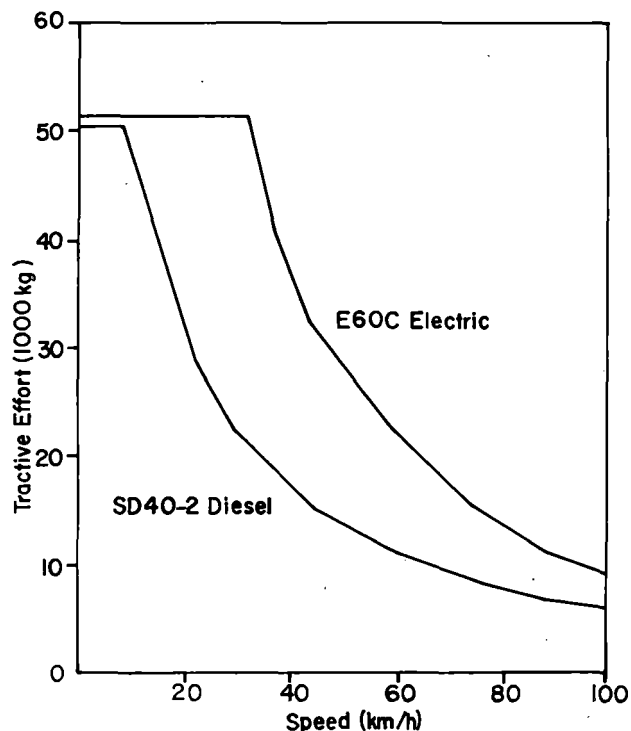


Fig. 4 Comparative tractive effort vs. speed curves for typical electric and diesel-electric locomotives.

A further advantage is that power can be called upon instantaneously, as the electric locomotive does not have the in-built inertial restraints of the diesel engine. The electric is also capable of short-time power ratings of at least double the continuous rating, by exploiting the thermal capacity of the electrical equipment.

Using this additional power and tractive effort effectively is contingent upon optimizing the levels of adhesion. The modern electric locomotive, with stepless control of tractive effort, sensitive wheel-slip equipment, and mechanical/electrical compensation of weight transfer, achieves this aim. Adhesion values between 26 and 27 percent up to speeds of 30 km/h are not uncommon, with starting adhesion much higher.

The resulting capabilities, particularly the ability to climb relatively steep gradients without severe loss of speed, are important assets, especially on single-track, heavy-haul railroads operating near line capacity. Given these performance advantages, electrified railroads require fewer locomotives per train, and hence a smaller overall fleet size. This reduction in fleet size not only impacts on initial capital costs, but also results in subsequent savings in maintenance and improvement in labor productivity.

To assess the motive power requirements for any given railroad, the electrification system designer normally employs a computerized Train Performance Calculator (TPC), which mathematically

simulates movement of the train over the railroad alignment. For this analysis the train size anticipated for future use must be specified. Locomotive consists of various power and tractive effort values can then be tested to determine the optimum set of traction characteristics for the given train size, and thereby select the most suitable locomotive available. The final selection should be that which provides satisfactory performance and minimizes the combined value of the following costs:

- Locomotive purchase cost
- Locomotive maintenance cost
- Electrical energy cost (including charges for power demand)

Regarding electrical energy costs, the use of more powerful locomotives will, of course, result in higher peak loading on the electrical supply system with correspondingly higher demand charges deriving from the normally higher cost of installed power generation and transmission capability.

An example of the design approach described above is a recent electrification study for an existing iron ore railroad in Australia. For this line two common electric locomotive sizes were examined: 4,000 kW (approximately 6,000 diesel hp equivalent) and 7,000 kW (10,000 hp), both 6-axle units. The loaded train was 180 cars long, having a trailing weight of 20,700 tonnes, but consideration was given to expanding the train size to 240 cars, weighing 27,600 tonnes.

The two locomotives were compared for the full range of train sizes. The results favored the smaller 4,000-kW unit for most of the range, since the same number of units per train was required for either size locomotive. However, of additional importance in overall economic comparison, the larger 7,000-kW locomotives were found to impose significantly higher power demands on the electrical system in all cases, thus placing a severe cost penalty on the requirements for power generation and transmission. The study therefore concluded that for the range of train sizes considered, the 4,000-kW unit provided the lowest combination of all costs, without adversely affecting the throughput of the line.

The choice of locomotive will theoretically be unique for any given railroad, yet the 4,000-kW size has been selected for a number of similar heavy-haul lines, as shown in Table 1. In each case the combination of train weight and ruling grade has led to selection of this size locomotive.

Table 1. Electric Locomotive Sizes on Various Railroads

Railroad	Locomotive Power Rating (kW)	No. Axles	No. Units/Train	Loaded Train Weight (T)	Maximum Grade in Loaded Dir. (%)
BM&LP, USA	4,200	6	3	13,000	0.8
Sishen-Saldanha, S. Africa	3,780	6	3	21,800	0.4
DBWR, USA	4,000	6	4	8,200	2.0
EFVM, Brazil	4,000	6	2	14,480	0.3

In the study of the Australia iron ore railroad discussed above, two 4,000-kw electric locomotives were found capable of replacing three existing diesel-electrics on each train, resulting in an appreciable reduction in locomotive fleet size. In addition, the train round-trip times were determined to be approximately 3-1/2 hours less than the present 19-1/2 hours using diesel traction, without increasing maximum speed limits at any point. This reduction in cycle time has an important side effect, apart from reducing the locomotive fleet size: it will result in a reduction in the ore car fleet as well, thus generating savings in capital costs with corresponding reductions in car maintenance costs. Alternatively, this type of car fleet savings can be employed for increasing total throughput over the same time period without adding to the fleet.

TRACTION POWER SYSTEM

Although the locomotive is central to the design of any electrified railroad, of critical importance to its final successful operation, in terms of reliability and economics, is the traction power system. The design of the traction power system for a heavy-haul railroad must take into account not only the large, infrequent loads imposed by the trains, as discussed above, but also the possibility that the primary power supply may be remote and relatively weak. This is often the situation in the case of mining railroads, which are themselves normally located in remote regions. Thus, design efforts must be made to reduce the amount of installed electrical capacity required, as well as the energy consumption during operation, while ensuring a reliable and economical source of supply.

Traction Voltage Selection

With heavy-haul railroads normally located in remote areas, or covering large distances such as in the western USA, the choice of 50-kV traction voltage, rather than the more common 25 kV, often results in appreciably lower costs. At 50 kV, using similar conductor sizes, catenary feeding lengths can be normally at least twice as long as for 25 kV, resulting in fewer than half the number of traction substations. This in turn reduces the length of high-voltage transmission lines and the number of line taps, resulting in substantial overall capital cost savings, especially where the primary supply is some distance from the railroad.

These considerations led to the choice of 50 kV for both the Black Mesa and Lake Powell Railroad in Arizona and the Sishen-Saldanha Railway in South Africa. For the same reasons, 50 kV has been chosen for electrification of the Deserado-Bonanza Western Railway in Colorado, due to be constructed by 1984, and has been selected at the conceptual design level for the Hamersley Iron Railway in Australia.

To illustrate the order of savings, the numbers of substations required on several selected railroads for the two alternative voltage levels are summarized in Table 2, based on individual design studies performed on each line.

Table 2. Number of Substations Required for 25-kV and 50-kV Traction Voltage

Route	Length (km)	No. of Substations Required	
		25 kV	50 kV
BM&LP, USA	125	3-4	1
Sishen-Saldanha, S. Africa	860	21	6
Hamersley, Australia	400	10-12	5
DBWR, USA	56	2	1
EFVM, Brazil	550	29	11
Cerrejon, Colombia	160	3	1-2

One factor sometimes opposing 50-kV traction voltage is the need to modify overhead structures to accommodate the larger electrical clearances required. However, on many heavy-haul railroads the number of structures is small and the additional cost is not significant. This was the case on the majority of the lines discussed above.

Power Demand Reduction

One of the most striking advantages of electrification, in terms of energy savings and cost to railroad management, is the ability to control the energy required for operation. Utility tariff systems normally take into account a power demand charge as well as a charge for energy consumption. The demand charge is based on the peak level of power required by the system over a specified time interval during each billing period, compared to the total consumption in that interval. This charge by the utilities is derived from the capital cost of their fixed facilities, such as generating plant and transmission lines, which must have a capacity sufficient to meet consumer peak load requirements. The energy consumption charge is based on the cost of producing the actual total energy used by the consumer.

Therefore, under this type of tariff system the total cost per kWh consumed varies considerably, depending on how uniformly the power is utilized. Any measures which will increase the load factor (ratio of average load to maximum demand) will, therefore, reduce the overall cost of energy to the railroad. A number of measures are available for minimizing the power demands of an electrified railroad, in both systems design and operational procedures.

An important factor in selection of traction voltage is that 50 kV normally provides superior load factors on individual substations, compared to 25 kV. The advantage stems from the greater spacing of the 50-kV substations, which results in more trains operating in each substation section at any one time. This has the effect of "evening out" the load profile on each substation, or reducing its load factor. Where power is metered at each substation by the serving utility, this appreciably reduces total power demand charges.

Further savings in energy costs can be achieved through close cooperation with the utilities. For example, it is important that the number

of electricity metering points be kept to a minimum. This is due to the fact that maximum demand usually occurs at different times at different substations and is usually caused by heavy localized train operations. Over the line as a whole, these operations even out, and a more uniform demand is drawn from the whole system. Thus, if metering at each individual substation took place (say every 30 to 80 km), it could mean extremely low load factors at each meter with the consequent heavy maximum demand penalties. However, using three-phase metering on the system as a whole, much better system load factors can be achieved with consequent increased savings. This improvement is illustrated in Figure 5.

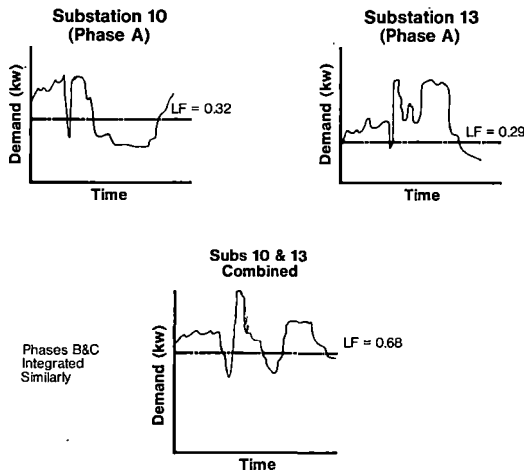


Fig. 5 Substation (single-phase) metering vs. integrated (three-phase) metering.

Where power metering is done on a system-wide basis, or where the railroad itself is concerned with the cost of installing primary system capacity, the design should be aimed at minimizing peak system loads, rather than individual substation loads.

Several measures are available for achieving this reduction. Load flow simulations can be used to identify train movements which impose high power demands, and minor speed reductions or rescheduling can then be implemented so as to avoid the coincidence of trains drawing high levels of power.

An example is a recent electrification design for mineral railroad in which extensive studies were performed to achieve reductions in peak system demands by nominal revisions in the train schedule. The base schedule developed for electrified operation is shown in Figure 6, which reflects a round-trip run time of 14.3 hours for trains serving Mine A, and 9.4 hours for Mine B. The system load profile for this dispatch schedule is shown in Figure 7, indicating a peak system demand of approximately 53 MW. Minor adjustments to this schedule were then tested, comprising primarily the following:

- Power restrictions on some downgrades
- Speed limits just prior to some stops
- Delayed departures for selected trains until others reach lower demands

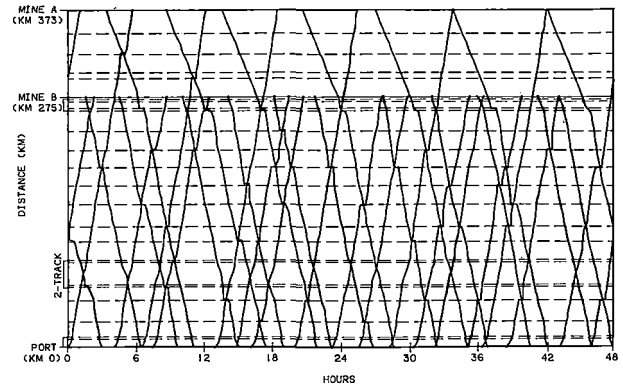


Fig. 6 Graphical timetable for a mining railroad operating an average of nine trains per day.

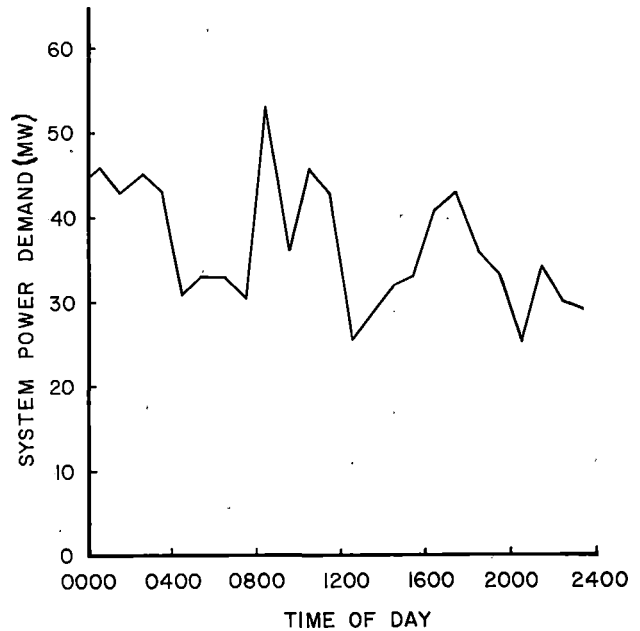


Fig. 7 Electrical load profile for the train schedule shown in Figure 6.

The combined effects of the scheduling adjustments reduced the peak system demand from 53 MW to 42 MW, while increasing average round-trip run time by only 1.3%. The modifications had a negligible effect on total throughput or fleet size, yet reduced significantly the required additional generation and transmission capacity, an important factor given the weak existing supply in that remote area.

During actual operation, additional load control can be exercised on a properly-designed electrified system. All modern electric railroads have a continuous monitoring system to measure energy used. This means that specific consumption

requirements per train, particularly on freight movement, can be accurately measured and predicted. Given this information, and by having available continuous access by radio-telephone to the locomotive engineer, the dispatching, speed and general control of each train, and hence its energy demand, can be closely monitored such that the agreed maximum demand on the system is not exceeded, provided always that the overall railway scheduling is not adversely affected. Good examples of this type of control can be found on the Black Mesa and Lake Powell Railroad in Arizona and the Richards Bay line in South Africa, where optimization of energy demand control has been brought to a fine point.

Another means of reducing peak demands that is often suggested is the use of smaller trains running more frequently. While this will obviously reduce power demands, the economics on a remote railway are usually questionable because of increased train crew requirements. Most heavy-haul railroads pay a high premium on any labor and must constantly strive to minimize the total number of employees.

Voltage Unbalance

In order to achieve the full contribution of electrification in railroad operations, some inherent problems in the traction power system must be overcome. One of these is the voltage unbalance caused in the primary supply system by the single-phase traction load. While this phenomenon has in the past created particular obstacles, correct design approaches can be applied to overcome these difficulties and still achieve the benefits of electrification. The nature of voltage unbalance is explained below, along with descriptions of various common measures to overcome the problem.

Three-phase voltages of the utility network are normally balanced. However, when a single-phase load of significant size is connected to two of the three phases, as is normally the case with electrified railways, the voltages become unsymmetrical and a negative sequence voltage is generated. Negative sequence voltage, if excessive, is undesirable because of the negative sequence current it causes to flow in the utility network. Besides the additional energy losses, this current can cause overheating and consequent damage to generating units and polyphase motors.

Voltage unbalance is defined as the ratio between the negative and the positive sequence voltage, and for convenience can also be expressed as

$$V_{unb} = \frac{MVA_L}{MVA_{SC}}$$

where

MVA_L = single-phase load, comprising traction load and the MVA losses in the feeding transformer and overhead contact system.

MVA_{SC} = short circuit capacity of utility network

It can be seen from this equation that the voltage unbalance generated by a single-phase load

depends upon the "stiffness" of the utility system. As previously stated, heavy-haul railroads are usually located in remote areas where the possibility of a weak power supply network can be high. Consequently, the problem of voltage unbalance has to be considered at the initial design stage if these railroads are to be electrified.

Voltage unbalance limits are normally established by each serving utility, or in some cases by the national electrical supply agency. Applying the appropriate criteria, several measures may be considered to reduce voltage unbalance, such as the following:

Connection of Traction Substations to Higher-Voltage Supply Lines. Traction substations should be fed from locations in the high-voltage network where the available short-circuit capacity is as high as possible. The economics of installing high-voltage transmission lines should, of course, always be assessed against other methods of reducing voltage unbalance. In addition, successive traction substations should be fed from alternate phases of the three-phase system. With this type of arrangement an inherently balanced system could result when coupled with a properly coordinated train schedule.

Adjustments in Train Operations. The use of shorter trains with higher frequency can be considered to reduce the single-phase load caused by individual trains. Such adjustments, of course, must be balanced against increased locomotive fleet and crew sizes, as discussed previously.

Three-to-Two Phase Transformers - In this scheme, power is transformed from three-phase to two-phase by means of two transformers. With essentially equal loads in the two phases this would result in a balanced three-phase load. There are several methods to achieve this, the most popular of which is the Scott-connection, as shown in Figure 8.

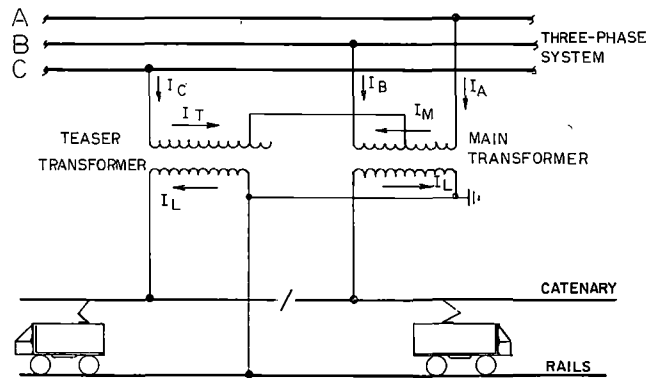


Fig. 8 Three-phase to two-phase transformation by Scott connection.

Power from the substation using Scott-connected transformers is fed to adjacent sides of the phase break. The main transformer is connected across two phases of the three-phase system while the 86.6 percent tap of the teaser transformer is connected to the 50 percent tap (midpoint) of the main transformer, and the other terminal of the

teaser transformer is connected to the third phase of the three-phase system.

The use of Scott-connected transformers to minimize voltage unbalance is desirable where simultaneous loading of the two phases is essentially equal. However, if the phases are unequally loaded, such as can occur with the large single-point loads in a heavy-haul railroad, the voltage unbalance would be the same as when using single-phase transformers. Its use must therefore be carefully assessed for a heavy-haul electrified railroad.

Three-Phase Transformers - The use of three-phase transformers is widely accepted in the Soviet Union as a means of reducing voltage unbalance caused by a single-phase load. Some of the types of transformer connections used include Y-Y, Y-Y with compensating winding, and V or open. As with the Scott-connected transformers, these types of connections effectively reduce voltage unbalance only when the two phases of the three-phase system are relatively equally loaded. For this reason, again, their use is limited for heavy-haul operation.

Reactive Compensation. In this method, reactive loads are used to balance the effect of a

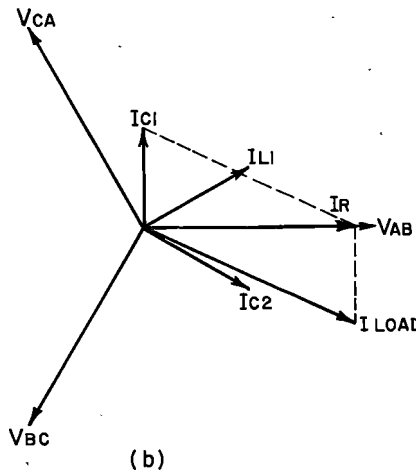
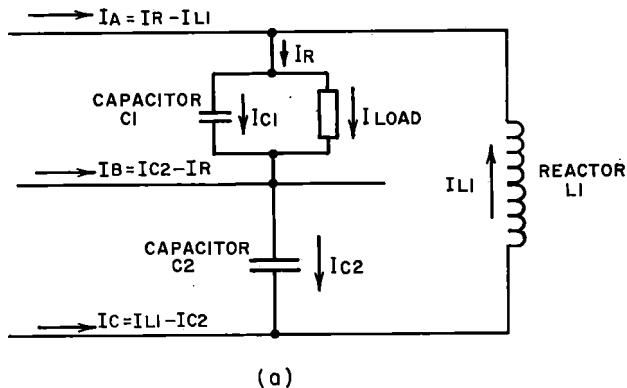


Fig. 9 Reactive compensation of a single-phase load in a three-phase system.

single-phase load in a three-phase system. To illustrate, consider a single-phase load such as a traction load to be connected to two phases of the three-phase system, as shown in Figure 9. To mitigate the phase unbalance, reactive elements are used and connected as shown in Figure 9a. Traction loads normally have lagging power factor, and capacitor C1 is used to compensate for the reactive part of the traction current. The corresponding vector diagram for this system would be as shown in Figure 9b.

If the impedances of capacitor C2 and L1 are made equal, and furthermore, if these impedances are made equal to 3 times the effective parallel impedance of the single-phase load and capacitor C1, then

$$I_{C2} = I_{L1} = \frac{1}{3} I_R$$

The resultant line currents are shown in the vector diagram in Figure 10. It should be noted that the line currents and hence the line voltages will be equal and 120° apart.

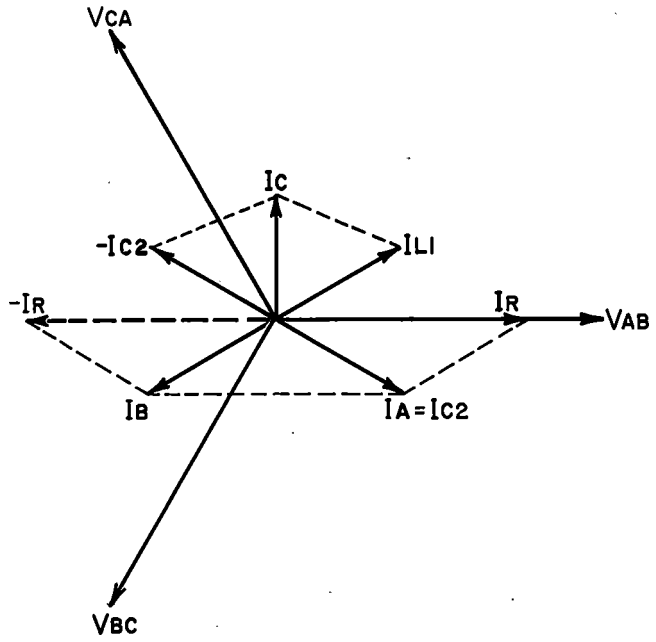


Fig. 10 Vector diagram showing the effect of load balancing using reactive compensation.

The same approach would be applicable if another single-phase load were connected to the three-phase system. Under this condition, rather than providing individual reactive compensation for each single-phase load, combined three-phase load balancing equipment could be used and connected at a suitable electrical junction (critical bus). This is typically the case on electrified railroads, where several single-phase traction substations may be supplied by a dedicated transmission line. Load balancing under this condition may be required only at the point where the dedicated transmission line is connected to the utility

system, or at any point from which other consumers might be served.

An example of this arrangement is the reactive compensation equipment installed at the Ferrum substation supplying traction power to the 50-kV Sishen-Saldanha Railroad in South Africa. At this station, voltage unbalance is caused mainly by the traction loads at Sishen and Gariep substations. This type of arrangement is shown in Figure 11.

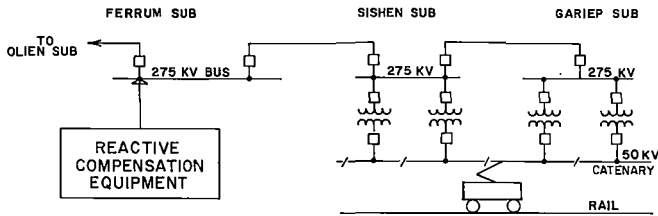


Fig. 11 Location of reactive compensation equipment relative to single-phase load on the Sishen-Saldanha Railroad.

The single-phase electric traction load is constantly varying, and a means of controlling the reactive elements in each phase must be provided. At Ferrum Substation this is achieved by means of thyristor or static controllers. The amount of reactive power required in each phase is determined by a voltage regulator which compares each measured phase-to-ground voltage with a reference VAR voltage. The single-line diagram of the static VAR system (SVS) at Ferrum Substation is shown in Figure 12.

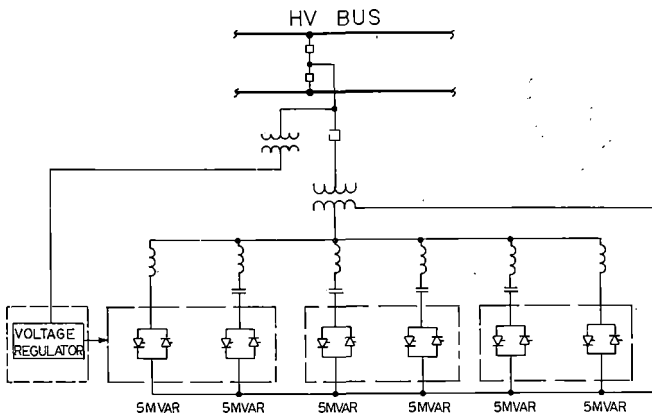


Fig. 12 Single-line diagram of the static VAR system at Ferrum substation on the Sishen-Saldanha Railroad.

The SVS is connected to the high-voltage system through a 20-MVA transformer. The reactive elements consist of four 5-MVAR thyristor-switched capacitor banks and two 5-MVAR thyristor-controlled reactors, thus providing a continuous regulation range from 10 MVAR lagging to 20 MVAR leading. The thyristors are used either to switch discrete amounts of capacitance into or out of the circuit, or to vary the current through the reactors by changing the point on the voltage wave at which the thyristors fire. A small reactor is provided in

series with each capacitor block to limit inrush current in the event of a thyristor misfire, and it can be tuned with the capacitance to form either a harmonic filter or to avoid resonance with the utility system reactance.

Because of the success in the use of the static VAR system to mitigate the problem of voltage unbalance, additional units are being considered for the remaining substations supplying power to the Sishen-Saldanha Railroad. This scheme is also being considered in the conceptual design for the electrification of the Hamersley Iron Railway in Australia.

HARMONICS

Although the modern thyristor-controlled locomotive has proven to be a benefit to the electric railroad industry in terms of performance, it has presented some electrical system problems stemming from the nature of the electronic equipment. Of particular concern are the harmonic currents generated by the locomotive, which can cause a number of detrimental effects in the traction power system.

Harmonic currents are produced at frequencies which are multiples of the power frequency and are inherently generated by any rectifier load. The thyristor-controlled locomotive, being in essence a rectifier load, is therefore a source of harmonic currents. The mere injection of harmonics into the electrical environment need not be considered dangerous or damaging to the subsystems. Much depends on the magnitude, the order, and the persistence of the harmonics pervading the particular system, as well as the overall power system parameters themselves.

In the case of a moving harmonics source, such as an electric locomotive, the magnitude and the order depend on: the locomotive characteristics; the particular mode of operation; its speed and distance from the traction substation; the number of locomotives in the section; the characteristics of the overhead contact system; and whether unloaded lines fed from the same ac feeder are switched in or not at any given instant.

Following is a brief description of the more readily defined detrimental effects of harmonics and the preventive or remedial measures available to counteract them.

Overvoltages Due to Resonance

The overhead contact system behaves characteristically as a transmission line which is generally not subject to resonant conditions at commercial power frequencies of 50 or 60 Hz. But when harmonic currents are present, resonance can occur. Depending on the location of the locomotive from the substation, the capacitive and inductive characteristics of the supply system could appear favorable to resonant excitation from one or more harmonic frequencies emanating from the locomotive, possibly producing overvoltages which could superimpose on an already existing standing wave on the line. When this occurs, consequent overvoltages may damage power components, such as diodes, thyristors, insulators and surge arrestors.

The prospect of overhead contact system resonance occurring increases with increasing catenary section lengths, as in a 50-kV system, since the frequency of resonance of the system is reduced. In general, the lower the harmonic frequency the greater the current magnitude.

For solutions, one has to either modify the thyristor circuitry to reduce harmonic current levels, or overrate power components such as diodes, thyristors, insulators and surge arrestors to withstand high overvoltages. These solutions, however, need to be economically feasible and practicable, since control of harmonics is warranted only when their magnitude can be a source of trouble. In general, available solutions fall into two categories: correction at the source of harmonics, e.g. on board the locomotive, or mitigation at the point where the effects are sensed, e.g. alongside the tracks.

On-board correction. Filters applied on the locomotive are L-C tank circuits tuned to control the frequency or frequencies of interest. Since in the harmonics spectrum the lower-order odd harmonics are generally predominant, e.g. 3rd, 5th, 7th, 9th and 11th, each of these is filtered out through individual filters while the higher-order frequencies are filtered through a single high-pass filter as needed.

The principal advantage of on-board filters is that the harmonics are controlled directly at the source and that low isolation voltages are available when the equipment is located on the transformer secondary. However, it also entails installing such equipment in the entire locomotive fleet. As space and rating requirements may be more than a locomotive can accommodate without affecting its performance, normally only one or two dominant frequencies are suppressed through on-board filtering. A case where this technique has been successfully applied is the Sishen-Saldanha Railway, electrified at 50 kV, 50 Hz, single-phase.

Wayside Correction. Unlike on-board filters, the use of wayside filter banks does not suffer from physical size limitation. Therefore, system resonance and consequent overvoltages can be entirely removed, if required, while power losses and no-load voltage rise can be kept within acceptable limits.

Figure 13 shows one application of a wayside filter bank, that employed on the Black Mesa and Lake Powell 50-kV line. In this case the need for additional system capacity and control of harmonics was indicated. A solution was realized by increasing the size of the existing capacitor bank at the substation and installing an additional series capacitor and a 3rd and 5th harmonic filter bank at about the midpoint of the line. This application has demonstrated how series compensation and harmonic filters were effectively employed to permit long catenary sections.

Wayside filter banks are designed on the assumption that the system impedance will not change radically. This assumption can prove to be

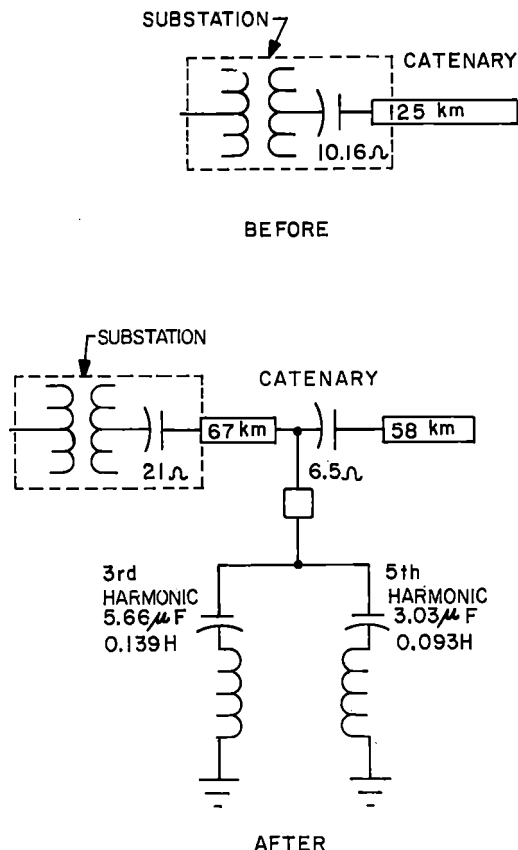


Fig. 13 Wayside filter application on the Black Mesa and Lake Powell Railroad.

an unacceptable restriction on the expansion and operational capabilities of either the power utility or the railway authority. It is important, therefore, that each system be judged on its own merits.

Interference in Communication and Signalling Circuits

With the common practice of carrying railway telephone and telecommunications circuits alongside the tracks, railroads can be faced with the problem of voltages electromagnetically induced into these lines by normal ac load activity. Harmonics from thyristor locomotive operations can compound these problems. Unsuppressed, the harmonics can cause unacceptable induced voltages in cables running parallel to the overhead contact system. This situation, however, is by no means unique to heavy-haul railroads, and mitigation measures are commonly available.

The degradation of the quality of speech and data transmission by these harmonics has been given wide coverage in the traction industry literature and recommendations and techniques have been established to mitigate the harmful effects. Several techniques for on-board correction are suggested to mitigate noise voltages. Some consist of adjusting the inductance of the circuit, others of varying the arrangements of the transformer

secondary winding. The basic objective of all these techniques is to reduce the steep rate of rise or the peak value of the commutated current. In addition to on-board correction, shielding of the affected circuits is virtually universally used. Some of the commonly used techniques for this purpose are:

- Twisting of the pair of wires of the circuit. This reduces the mutual inductance of the circuit and consequently the offending electromagnetic energy. This method is particularly important in attenuating cross-talk and transverse noise voltages in bundled circuit pairs.
- Providing the pair or bundle with a conducting sheath to reduce the transverse and longitudinal noise voltages.
- Using coaxial conductors.
- Use of booster transformers or autotransformers.

A related area which is also susceptible to the harmful effects of harmonics is the railroad signalling system. In simplified form, when ac track circuits are employed to operate railroad signalling systems, a signal current of a specific frequency is passed through the running rails, energizing a holding relay. Any vehicle present on the circuited tracks shorts the rails, de-energizing the relay and operating the signal. Significant harmonic currents of the same frequency as the signal current, if allowed to flow into the track circuit, will cause the signal system to malfunction.

Though attenuation of harmonics can be achieved to a significant degree by using filter circuits on board the locomotive, it is found that these means may not be sufficient to limit disturbances in the signalling circuits to an acceptable level. As a result, standard practice has been to adopt a signal frequency outside the harmonic spectrum range, e.g. for a supply frequency of 60 Hz, a signal frequency of 100 Hz, and for a 50-Hz supply, an 83 1/3-Hz signal. There are other methods too, such as frequency shift modulation, and application of filter circuits at the signal control devices, but these are less commonly employed.

Voltage Distortion

Nonsinusoidal current, rich in harmonics, drawn by thyristor locomotives while accelerating or pulling on an intermediate notch brings about catenary voltage distortion even when the harmonics are not amplified through resonance. Depending on the severity of the distortion, its effects can be felt in both the traction system and the high-voltage (HV) system.

Voltage distortions reflected into the HV system are appreciably attenuated, as the primary side network appears as a low system impedance with respect to the source locomotive. Furthermore, the traction substation transformer and the overhead supply system also tend to attenuate some of the higher order harmonics. As a consequence, no harmful effects of harmonic voltage distortion on consumer systems have yet been experienced, but care should be taken to consider such system components as capacitors and filter banks, which may appear as a low impedance to the offending

harmonic current, resulting in capacitor overloading. Whether harmonic voltage distortion in the HV system will be of concern will depend primarily on the "stiffness" of the system.

Harmonic distortion can also affect the locomotive performance itself, in that it can compound the system voltage deterioration. However, this distortion is low and normally not of concern in the overall performance of the system.

OVERHEAD CONTACT SYSTEM

The harsh environment associated with many heavy-haul railroads, especially those in remote mining areas, can impose unusual design conditions, often requiring a significant departure from the normal catenary design. As examples, temperatures in the Pilbara region of Australia reach 50°C, with coastal winds up to 240 km/h in cyclones, whereas temperatures in coal mining areas of Colorado drop to -38°C. These conditions must be accounted for in conductor and pole sizing, pole spacing, insulator design and other design aspects.

On the other hand, heavy-haul railroads often offer an opportunity for economical designs not possible on more conventional railroads. For example, on isolated lines an economic advantage can sometimes be realized by using locomotive pantographs wider than the normal 2.0 m, thus permitting longer catenary spans. For speeds below 110 km/h, pantograph width is basically limited only by lateral clearance constraints such as tunnels and through-truss bridges, and these obstructions do not exist on many heavy-haul railroads. With a pantograph width of 2.6 m, for example, catenary spans of 80 to 100 m can be used, rather than the normal 70 m. Although pole costs may not decrease, since longer spans require taller and heavier poles, the number of crossarms will be reduced, resulting in savings in both their installation and subsequent maintenance costs. This approach was incorporated in the design for the Deserado-Bonanza Western Railway, with a 2.6 m pantograph width permitting a maximum pole spacing of 84 m.

Of frequent concern in remote areas are the construction logistics required to install the electrification system efficiently and rapidly. Recent construction of the overhead contact system for the Sishen-Saldanha Railroad in South Africa is a case in point.

Typical electrification projects will normally employ 100 to 200 men, and this 860-km line, involving 940 track-km of catenary, was no exception. Recruitment required widespread advertising in order to attract staff to the relative desolation of the Kalahari desert. The remoteness of the work prompted the adoption of a 20-day continuous work period followed by a 6-day shut-down. This permitted staff to make trips home which could often take up to two days in travel.

Construction camps were located 150 km apart. Three were normally in use at any one time, and were dismantled and "leap-frogged" as construction moved up the line. A static base camp accommodated staff working in the main construction stores and maintenance area.

The 90-km spacing between passing sidings made the use of work trains for construction unfeasible, so self-propelled vehicles with off-tracking capability were used. This arrangement was not conducive to handling such materials as sand, aggregate and cement in bulk, and prompted the design of a concrete sleeve into which a plain steel pole could be inserted and grouted.

In spite of these and other special considerations, the overhead contact system for the Sishen-Saldanha Railroad was designed and constructed in less than 2 1/2 years, without disruption to normal levels of ore delivery, thus demonstrating what can be achieved even in such remote areas.

CONCLUSIONS

This paper has described some of the more significant advantages of modern high-voltage ac electrification for heavy-haul railroads, and aspects of the design that require special attention. While some of these special design considerations stem from the environment of such railroads and their severe climatic conditions, many are simply inherent in the complex nature of the electrical and mechanical subsystems that make up the total electrification system.

In either case, proven design techniques carefully applied can overcome these difficulties, and have been demonstrated on a number of recent electrification projects on heavy-haul lines. The results of these design applications are evidenced by a marked improvement in rail operations over the alternative diesel traction mode. These improvements are enabling heavy-haul operators to increase line capacity with the same or reduced rolling stock fleet, reduce train turnaround time, increase operating reliability, and significantly reduce locomotive maintenance costs. The combined results have contributed substantially to the overall objective of increased tonnage throughput, while at the same time generating improved operating economies.

ACKNOWLEDGEMENTS

The authors wish to express their appreciation to staff of the Railroad and Electrification Division of International Engineering Company who have contributed to this paper and assisted in its review, particularly Tomas B. Tolentino and Bismark DaCosta.

REFERENCES

1 Adam, C.P. and Nutter, J.L., "Power Supplies for Railway Electrification and General Use in a Remote Area", Electrical Energy Conference, Brisbane, May 1979.

2 Baldwin, D., "Total System Concepts for AC Traction", in "Developments in Electric Traction", GEC Traction Symposium, March 1976.

3 Burke, J.J., et al, "Increasing the Power System Capacity of the 50-kV Black Mesa and Lake Powell Railroad Through Harmonic Filtering and

Series Compensation", Transaction on Power Apparatus and Systems, Institute of Electrical and Electronics Engineers, Vol. 98, No. 4, July/Aug. 1979.

4 "Cape Northern Region, Ferrum Substation, Static Compensator", Electricity Supply Commission, Johannesburg, undated.

5 Daniels, A., "Electrifying Isolated Lines in Desert Regions", Railway Gazette International, February 1982.

6 Daniels, A., "Mainline Electrification - A Sound Return on Investment", presented at 20th Annual Convention of Railway Supply Association and Annual Meetings of Coordinated Mechanical Associations, Chicago, September 1981.

7 Jäger, A., et al, "Measures for Improving the Grid Response of Thyristor-Controlled Traction Vehicles", Brown Boveri Corporation Publication CH-B 0180 E.

8 Rees, M.W.T., "The Sishen-Saldanha 50-kV Electrification Project", Symposium on Electric Transport, South African Institute of Electrical Engineers, Pretoria, April 1979.

9 "The Static VAR System in Ferrum - A Proof of Flexibility", ASEA (internal report), Vasteras, Sweden, Nov. 1980.

10 Torseng, S., "Shunt-Connected Reactors and Capacitors Controlled by Thyristors", Proceedings, Institution of Electrical Engineers, Vol. 128, Pt. C, No. 6, Nov. 1981.

11 Yacamini, R., et al, "Modelling of Traction Load Distortion in Electricity Supply Systems", Proceedings, Institution of Electrical Engineers, Vol. 128, Pt. B, No. 3, May 1981.

Research on the Reduction of the Wear of Locomotive Tires

Traian Taran

Doctor of Engineering
Senior Scientific
Researcher, The Institute
of Technological Research
& Design in Transports
Bucharest, Romania

Aurel Lie

Dipl. Engineering
Head to the Locomotive
Research Department, The
Institute of Technological
Research & Design in
Transports, Bucharest,
Romania

This research work has as its main objectives the establishment of the causes producing abnormal wear of the tires of diesel and electrical locomotives of Romanian Railways (CFR) driving stock and the working out of constructive, technological and operating measures for reducing the wearing dynamics of tires. The research findings on the deformation through wear of the wheel tread of the locomotives, in the existing operational conditions of CFR, as well as the findings of laboratory and operational trials for optimizing the mechanical characteristics of tires, are shown.

RESEARCH ON THE REDUCTION OF THE WEAR

AT LOCOMOTIVE-TYRES

Introduction

In railway operation, the wear of locomotive tyres represents a very important indicator, both through the volume of the expenses related to repairs and metal consumption and through the implications upon the traffic safety.

For the time being, the locomotive construction firms and especially the railway administration, conduct intensive research for reducing the wear of rolling stock wheels. The research includes a large area of aspects, i.e.: material quality, manufacturing technology, relation between mechanical and chemical characteristics of the wheel and rail materials, profile of the wheel tread, operation of vehicle on track etc.

In order to reduce to minimum the expenses related to restoring the running profile of locomotive wheels, it exists the trend of reducing the dynamics of wheel wearing, so as the re-turning be made at intervals of 350-400 covered-thousands kms, on the occasion of repairs with lifting from the wheel sets.

Research main objectives that represent the subject of this research, are, on one hand, the establishment of the cause that

produce the abnormal wear of tyres of diesel and electrical locomotives belonging to the driving stock of the Romanian Railways (CFR) and the working out of measures for reducing this wear, and, on the other hand, the working out of constructive, technological and operational measures for reducing the dynamics of tyre wearing, in general. To carry out these objectives, the research has focused on the following solving ways:

- statistical research of the dynamics of tyre wearing at diesel and electrical locomotives of the driving stock of CFR
- research of deformation through wear of the running profile of locomotive wheels in the existing operation conditions at CFR
- laboratory and operation trials for optimization of mechanical characteristics of tyres

Statistical research of tyre wear dynamics

This research has been made on the basis of the findings of tyres measurements in the last 2-3 years, conducted periodically in depôts and specified in special registers. Although the accuracy of the measurements made by devices existing in the depôts is relatively low, owing to the fact that a large number of measurements is statistically analysed, the accuracy of research findings is highly enough.

Thus, a number of 470 locomotives of the main depôts of country were selected. The variety of the driving stock and the operation conditions of CFR network have been considered when the depôts and the types of locomotives have been chosen.

Analysis of data obtained in the above-mentioned way has shown:

- at all types of diesel locomotives and at

Bo-Bo electrical locomotives of 3400kW the preponderent wear is on the tread of the tyres. Almost all of re-turnings are executed due to the reaching of wear limit on the tyre tread

- at Co-Co electrical locomotives of 5100 kW, which are operated on mountains areas, the wear of wheel flange at 1 and 6 wheel-sets is higher than the wear on tread. Inverting the leading wheel-sets by the intermediate ones, the locomotives are returned almost totally at the limit of wear on the tread

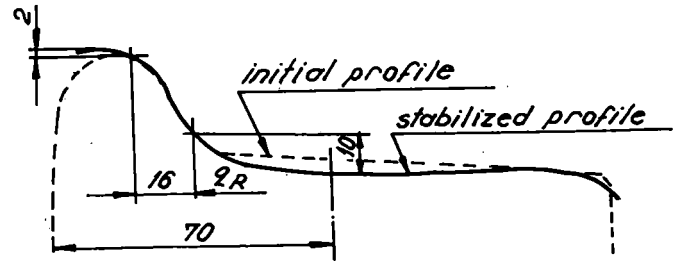
- average covered distances on 1 mm wear are generally low; practically, all locomotives execute a re-turning between the repairs with lifting from the wheel sets - the type of locomotive service influences very much the dynamics of tyre wear; thus, e.g. the locomotives which operate all the time to haul freight trains have a wear speed of 2-3 times higher than the locomotives operating only to haul passenger trains

Deformation through wear of the tyre-tread

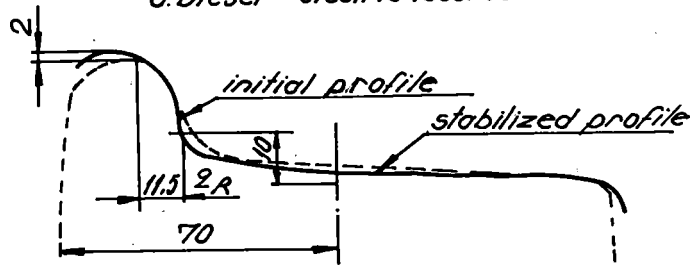
It is known that the wearing speed, depending

on the covered distance at the newly-profiled tyres is faster at the beginning, varying after an exponential function, after which decreases, varying then, after a linear function. After turning, the tyre-tread has some roughness, and the surface layer has a certain hardness. As the wheel begins to run on the track, owing to the interaction forces between wheel and rail, a hardening appears on the tread, having as result both the profile deformation and the increase of surface layer hardness up to a certain stabilized value.

When the newly-profiled wheels run on track, the contact surface between wheel and rail as well as the whole surface of the tyre on which the contact is made, is smaller, depending on the compatibility rate of tyre profile and of rail wear rate. As the wear is increasing the initial tyre profile is getting a deformation so that the contact surface of the tyre with the rail increases and the wear is lower. After a covered distance of 30-40 thousands kms, the profile shape becomes relatively stabilized, its modification afterwards being very slow. The stabilized shape of the profile depends on the normal profile of the rail, on the rail wear rate, on the shape of tyre initial profile, on the frequency of small-radius curves and on the constructive parameters of locomotive running equipment. Certainly, it results that in order to work out a tyre profile as appropriate as possible to the Romanian Railways operating conditions, the most accurate knowledge of the stabilized profile shape of the tyres at all types of locomotives and in characteristic operating conditions is required.



a. Diesel - electric locomotives



b. Electric locomotives

Fig. 1

Fig. 1 shows comparatively with the initial profile the characteristic stabilized profiles found at most of diesel and electrical locomotives. After analysing them, it results that, at the electrical locomotives the profile deformation is produced both on the tyre-tread and at the outer side of flange while at the diesel-electrical locomotives the preponderent wear, respectively the profile deformation, is produced on the tyre tread.

On the basis of this research, a new running profile for locomotive has been worked out, more suitable to the Romanian Railways operating conditions.

Optimization of tyres mechanical characteristics

The wear of tyres depends, to an important extent, on the values of hardness on the contact surface of tyre and rail and of their values ratio. By increasing the hardness on tyre tread and the ratio of the surface hardness of tyre and rail, an important reduction of tyre wear can be obtained. Excessive increase of tyre hardness could result in their sensitiveness to thermal crackings and shellings. The optimum mechanical characteristics of tyres, which ensure a satisfactory wearing dynamics, without the danger of tyre breaking or of shellings in operation, have to be established on the basis of haulings, taking into account the actual operating conditions at the Romanian Railways.

The tyres for Romanian Railways' locomotives are made of the so-called "L D steel" that has a chemical composition similar to that of BV 2 steel, standardized at ISO and UIC.

They are provided in normalized state, and the mechanical characteristics are the following: tensile strength is 800-930 N/mm², hardness: 230-270 HB and the resilience is KCU 30/2, minimum 20 J/cm².

To improve the resistance to wear of locomotives tyres, according also to the mechanical characteristics of the rails existing on Romanian Railway network, the research has been oriented towards the increase of tyre hardness by quenching and tempering, by keeping the same chemical composition. At this aim, a batch of tyres of normal production, in normalized state, was subjected to a quenching and tempering treatment, consisting of hardening in oil, followed by tempering in water. The mechanical characteristics obtained at the quenched and tempered tyres are: tensile strength 863-980 N/mm², hardness 260-300 HB, resilience KCU 30/2, minimum 29 J/cm². The quenched and tempered tyres have been mounted in 4 locomotives which work under normal operating conditions. Up to now, the first 2 locomotives have already covered over 100,000 km. The wearing speed at the improved tyres, in comparison with the wearing speed of normalized tyres, at the same locomotives and in the same operating

appeared on the tyre tread at these locomotives.

To check the behaviour under thermal shocks, two quenched and tempered tyres have been subjected to an intensive program of stand trials.

Fig. 2 shows a general view of the stand on which these trials were conducted. Trials program included stopping brake from the speed of 140 km/h and brakings for keeping the speed of 60 km/h for 10' and 20' at a power of 22 kW, followed by intensive cooling of the tyre. The temperatures in tyre mass, in the plan of tread circle at depths of 5, 35 and 65 mm from tyre tread and in the wheel rim at a depth of 5 mm from the contact surface between tyre and wheel centre, were recorded. The initial temperature in tyre mass, at every trial, was of 30-40°C. Top temperatures have been recorded at brakings of 20', reading frequently 330°C near the tyre tread and 250°C in tyre mass.

Stand trials have shown a good behaviour under thermal shocks of "LD steel" tyres with quenching and tempering treatment. At metallographic examination made at the end of trials program, micro-cracks in the superficial layer and in tyre depths were not discovered.

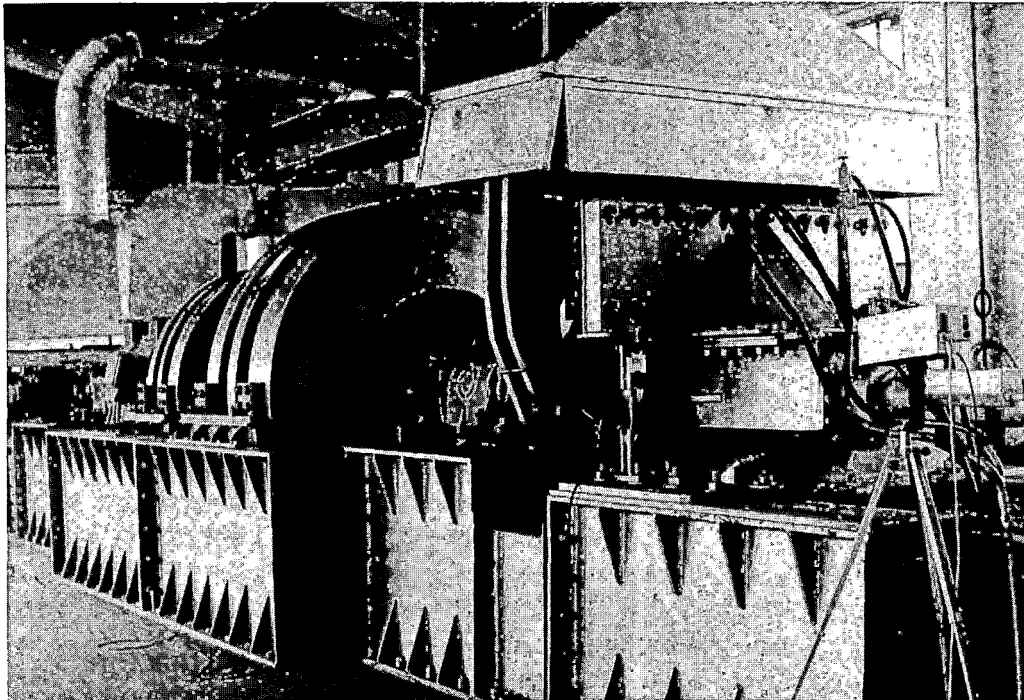


Fig. 2

conditions is, on the average, lower with 28,5%. Also, thermal cracks or shelling have not

Conclusions

The research has shown that the dynamics of

the locomotive tyre wearing and the stabilized shape of the running profile, depends both on the construction of locomotive running equipments and on their operating conditions.

The main means of reducing the dynamics of tyre wearing are the improvement of mechanical characteristics of the tyres and the adaption of a running profile suitable to the actual operating conditions.

Metamorphosis of Railroad Service at the Port of Conneaut, Ohio

John W. Read

General Manager
Bessemer & Lake Erie
Railroad Company
Greenville
Pennsylvania

The port of Conneaut, Ohio, has undergone a metamorphosis in the last twenty years, from a conventional rail-to-vessel-to-rail operation to what is probably the most complex ore and coal storage facility on earth. In that time, the cost of providing rail service has been drastically reduced. This paper explains the changes that have been made in rail operations, the elements that must be combined to assure the best coal dumping and boat loading rates possible, and outlines some of the things that have been learned in the process.

METAMORPHOSIS OF A PORT

During most of the nineteenth century, the port of Conneaut, Ohio, served only the limited needs of the agricultural community of northeastern Ohio, but in 1892 it became an important element in the nation's industrial scheme when iron ore was brought into Conneaut for transshipment to the steel mills of the Ohio and Mahoning valley. In later years, facilities were added for transferring coal from cars to Lake vessels. While this movement of coal did not assume great proportions, it helped to balance the traffic for the Bessemer and Lake Erie Railroad, which is the only railroad to serve the port. The coal and ore operations were geared to the transfer of commodity directly from boat to car or vice versa. The Bessemer and Lake Erie Railroad owns the coal facilities, and the Pittsburgh and Conneaut Dock Company owns and operates the ore facility, and operates the coal facility for the railroad with P&C employees.

During the early 1960's, however, a radically different concept was adopted, and since that time a metamorphosis has occurred which has almost completely divorced the railroad and shipping operations. The previous method required that large quantities of freight cars be available at all times to accommodate the incoming vessels during the nine-month navigation season, and these cars were, of course, superfluous during the time the lake was closed. The same seasonal utilization existed for the cars involved in the movement of coal, and there was the additional burden of accumulating all the cars for a coal cargo before the boat could be loaded.

It was decided to construct a storage facility for coal so that the cars could be dumped upon arrival,

greatly reducing the number of car days involved and allowing movement of coal to proceed throughout the whole twelve months.

A series of expansions of the coal facility followed, and movement of coal through the port has increased from 600,000 tons in 1960 to better than ten million tons in 1979. A similar development ensued for the ore side of the operation, and in the early 1970's an ore storage facility was constructed in such a way that all ore is put on the ground at the time it is unloaded from the boats and only loaded into cars as it is needed to satisfy current mill consumption. Both sides of the port can now handle cars on a year-round basis with almost complete independence between the railroad and vessel operation. During the process, some interesting things have come to light, and it is the purpose of this paper to deal with those things as they have had an effect on railroad operations.

Car Requirements

In 1960, the Bessemer and Lake Erie Railroad owned 8,900 open-top hopper cars. With these, it handled 300,000 revenue loads. In 1981, the road owns 6,000 hopper cars and will handle approximately the same number of loads. This reduction in ownership is, in large part, due to the changes that have been made in the port of Conneaut. At a price of \$45,000 a car, this represents \$135 million in cost avoidance.

Yard Crews

Under the old method of operation, five crews per turn were generally used. Present operations are performed with one crew a turn. This crew is able to do all the yard work necessary to handle the substantially increased number of cars handled into and out of Conneaut. This improvement was accomplished by changing the whole concept of handling cars.

On the coal side, cars were previously put on a coal hill by an assigned coal yard crew, cut individually, allowed to run through a kickback and were then shoved by a barney into the dumper, thence they ran into an empty yard. In the section of the new system which was built first, the cars are yarded into the

coal load yard by a road crew and then bottom-dumped on a track pit in coupled cuts of 50 cars. They are moved over the pit by a radio-controlled locomotive operated by the same Dock Company employee who controls the conveyors and shakers. When the cut of cars is empty, it is immediately available for reloading with ore or for movement to interchange if it is a cut of foreign cars.

On the ore side, the ore empties were placed for loading by a railroad crew in short cuts on five different tracks. Then a Dock Company sidarm pusher would move the cars under the five Hulett ore machines for loading. Ore was weighed on the Hulett. Another railroad crew would then gather these loads up, assemble them in a cut to make room for more loads, and turn them over to a third crew for marshalling in the load yard. An additional yard crew was on duty to prepare the empties for loading and for miscellaneous switching.

Under the present setup, the single yard crew shoves the coal empties onto one of two ore loading tracks where another radio-controlled locomotive operated by a Dock Company employee handles the complete cut of 35 cars. Weighing is done as the cars are loaded, and the cars are returned to the track on which they were spotted as empties. When the loading operation is completed, the same yard crew pulls the loads to the departure yard. Since there are two loadout tracks, and since it takes an appreciable amount of time to load a full track of ore, the crew has time to do all the miscellaneous work in the yard.

Separation Of Operations

With the advent of radio-controlled operation of locomotives by nonrailroad employees, it became necessary to ensure that there could be no conflict at the interface between the Railroad and Dock Company operations. This required attention to two aspects of the situation. First, there had to be protection against a runaway by the radio-controlled locomotive. This was provided by installing a set of ramps at the operating limits of the radio power. If the unmanned locomotive gets to that limit, a switch on the truck is contacted by the ramp and power is shut off and the brakes are applied. Second, there had to be a provision to assure that the railroad crews do not enter a radio-controlled locomotive's territory while that locomotive is in operation. This is accomplished by a series of interlocked derails, switches, and signals, and the railroad crew proceeds into this territory only after receiving a signal indication to do so. No unpleasant incidents have occurred in the seventeen years of this operation.

Road Crews

Road crews work in short turnaround service to Conneaut, and start out of the major crew terminal of Albion, Pa., fifteen miles away. They make two round trips per call, and deliver the loaded coal cars directly onto the track serving the coal facility. The line between Albion and Conneaut is single track, and operations are conducted by means of a staff system. The staff is simply a stick painted with the words "Conneaut Branch Staff", and if the crew has this in their possession they own the railroad.

Because of the large volume of traffic over this single track, it is important that the crews move expeditiously; and they do so, because they know that their tour of duty is over upon completion of two trips. The usual time is five and a half hours for the two trips. It becomes possible then to get eight round trips over this piece of railroad in a 24-hour period. In former times, the crews were called to

make three round trips, and their pace was such that they consumed something over 11 hours in making these trips. At that rate, the branch had a capacity of only six trains each way per day. The former method required continual operating supervision to keep crews on the move. The present method, at substantially the same crew cost, moves the cars faster; provides better locomotive utilization; and postpones the day when more expensive operating mechanisms or double-tracking will be required.

Track Pit And Car Dumper

The initial coal facility was constructed with a track pit for bottom-dumping three cars at a time. This was necessary because of room restrictions, and was the only way in which cars could be kept coupled together during the unloading operation. It has performed splendidly, and at no time in the more than 17 years of operation has it been out of service for unscheduled reasons for more than 48 hours. It does present problems in freezing weather, which will be discussed later.

In 1978, a second coal facility was completed after the first facility had undergone several expansions. Increased throughput required additional dumping and storage facilities. These were constructed in an entirely new location about a mile or so east of the then-existing facility. At that time, it was decided to build a car dumper because of the increasing incidence of badly frozen coal which was coming from greater distances. This required construction of an entirely new lead track, empty and load yard, and a dumper which was designed so that it could ultimately reach a rate of a car a minute. Experience so far indicates that, while the dumper has a greater capability to produce while it is working, it is subject to more frequent service interruption on account of mechanical failures. It will probably also require extended periods for rejuvenation as major components wear out.

An interesting aspect of this operation takes place in the empty yard. As is common in dumper operations, the cars run into a series of empty tracks by gravity. Automatic devices control the speed, and the cars are supposed to couple up. They don't! Initially a switchman was stationed in the yard to adjust couplers. The tracks had to be shoved together by either the road crew or a yard crew, a time-consuming operation, before the air test could be made, further delaying the crew. As it should be in all yards, room had been left between every second track for a roadway. To prevent this delay, the railroad purchased a rubber-tired, four-wheel drive "Unimog" and equipped it with a pushing arm. The switchman who adjusts the couplers also operates this vehicle. The tracks are now coupled and air-tested before the arrival of the crew.

Freezing And Thawing

The climate at Conneaut is severe. Below-freezing temperatures prevail for weeks at a time, and Conneaut is located in the Lake Erie snow belt so that snow accumulations are frequent from the middle of November through the middle of March.

The coal that arrives during the winter is a mixed bag, with some of it having been loaded less than 24 hours before arrival and some of it loaded as much as ten days before. Some of it is sized coal, some run-of-mine, and some the dry byproduct of washing plants. None of it will come out of a hopper car, either through the bottom or through the top, without thawing. Both the old and new facilities are equipped with 9-car thaw sheds, using electrical under car, side car, and top of car heat. A satisfactory, albeit dimin-

ished rate of production can be achieved in the most bitter weather if the coal is loaded in a reasonably dry condition. However, this is not always the case and some coal does arrive in bad condition. No amount of thawing alone can possibly make all coal amenable to bottom dumping.

When the track pit was the only facility available, numerous methods were tried to make it possible to accelerate dumping of this frozen coal. Microwaves were totally ineffective; dynamite bulged the pockets of the cars; and gasoline poured down the slope sheets would not ignite, which was probably a good thing. The most successful device was an Airdox machine which used many thousand pounds of air pressure in a rechargeable cylinder to blast the frozen chunks. This will do the job, but the varying slope configurations and the length of the cars made it impracticable to design a device that could handle a whole car at a time. The production rate was too slow.

Another reasonably effective device was the use of a very high pressure water jet which can be used to cut the lumps of frozen coal as they are blocking the hopper chute. These jets are so strong that they can cut a 2x4 in half, but, of course, they can only be used when the ambient is high enough to prevent the accumulation of new ice. As a last resort, coal can be transferred by clamshell to another car. This breaks up the lumps and leaves a thawable residue in the bottom of the parent car. A production rate of 25 to 30 cars per turn is achievable, but it is expensive.

In expanding the car dumping facility, advantage was taken of the experience with the track pit and it was designed with winter particularly in mind. The 9-car thaw shed is sufficient to assure the fact that all of the coal will dump out of the car at an acceptable production rate. The lumps that fall from the car drop onto a grate and are then broken up by a device, equipped with rotating hammers, that moves back and forth over the entire grate. Some lumps are too large for this to handle, and there are two remotely controlled air-operated jack hammers that can be brought to bear on any large lumps that remain. This takes time, but since it has to be applied to a very small percentage of cars dumped, it does assure an ability to dump any kind of car in any weather. With this setup, it has been possible to stockpile promptly all the coal that has been received.

Both the track pit and the car dumper have been equipped with heating elements on the receiving hoppers to prevent buildup which would interfere with the free flow of coal onto the conveyor. This is absolutely essential.

All of the under-track electrical heaters in both facilities are being replaced with gas-fired units. Conneaut is located in the northeastern Ohio gas field, and the railroad has drilled four wells which should provide an adequate supply of gas. The heaters are of a unique design. The conventional hotdogs require a great deal of maintenance and are continually plugging up with material dropping off the cars. The new heaters utilize a conventional gas furnace blowing its products of combustion into a boxlike steel plenum. These gases are then exhausted through slots in the top of the plenum, assuring a uniform application of heat to the car. Since there is no open flame and no intense heat, the usual problem of burnt air hoses is minimized.

Car Configuration

At the time of the inception of the storage facility at Conneaut, the Bessemer owned a large fleet of 100-ton hopper cars with 30-degree slope sheets and triple pockets. These are absolutely the worst

cars possible for bottom dumping, but there was no alternative but to go on using them. They require considerable shaking in the summer, and two or even three shakers per car are used on the track-pit to empty them in the wintertime. As they came due for rebuild, they were modified to a 42-degree upper slope and a 30-degree lower slope, and this minor modification cut the time to unload the cars approximately in half.

In 1970 and 1971, Bessemer acquired 1,000 "quick-drop" hoppers. These cars were built with a minimum slope angle of 52-degrees, and have longitudinal doors which open in such a way that the coal can drop out through practically the entire bottom area. The doors are pneumatically operated and electrically controlled. The car will empty 95 tons of coal in nine seconds. These "quick-drops" are restricted to specialized service because they require a device to open the doors, and recent purchases have been of conventional hoppers with four pockets and 45-degree slope sheets. These last require little or no shaking under normal conditions, and can be used in general service when they are not needed in the ore-coal turnaround.

Bathtub-type cars would be ideal for the dumper operation, but since the loaded ore cars are usually bottom-dumped on the steel mill trestles, they are not feasible for Conneaut.

Boat Loading

The Bessemer and Lake Erie Railroad owns the coal facility, and, since it is imperative that the best service possible be rendered to the arriving boats, it has been important to maximize the rate at which boats can be loaded. The key to this operation is to provide sufficient capacity to load the boat at a rate exceeding the ballast pumping capability of the boat and then to build in enough flexibility so that when something goes wrong with some machinery the boat loading can be continued from other sources. To this end, most coals are stored in at least two separate piles available for reclaiming by different methods, and there are many alternate ways that coal can be furnished to a boat though no more than three or four of these can be brought to bear on any one boat at any one time. At any one time there are 30 to 40 piles of coal in storage.

There are two separate shiploaders, and either of them is capable of loading a boat by itself. These are backed up by two 6,000-ton silos which can accumulate coal ahead of the boat arrival. There are two reclaim pits which are used to service a large volume customer, and a third which is used as a general purpose silo without walls.

On the older coal facility there is a caterpillar mounted, medium capacity, electrically-operated reclaim wheel and three smaller diesel reclaim wheels which can be used in conjunction with a stacker-reclaimer. These last have reached the end of their service life and are being replaced by a heavy duty rail-mounted wheel. The newer coal facility has one high capacity rail-mounted reclaimer. These machines, in addition to the fact that the track pit and car dumper can both dump direct to the boat, assure an ability to load boats under almost any condition.

The initial coal facility was designed with two belts - one for stocking and one for reclaiming. This would not be significant if only one or two kinds of coal were handled, but it assumes major importance with the multiplicity of consignments handled at Conneaut. Boat loading takes from five to twelve hours, and with a single belt facility and several boats per day this could mean that no coal could be dumped over long periods of time. This difficulty has been experienced with the newer facility, which is frequently unable to dump coal while a boat is loading because it only

has a single belt. Efficient operation is still possible because of the availability of the second, older facility.

Ore Loading

Ore is now unloaded from vessels by the five Hulett machines which have been modified to dump onto a conveyor which takes all ore to a multimillion-ton stocking area. Self-unloading Lake boats can unload through a hopper onto the same conveyor. Other conveyors are arranged so that two boats can be unloaded simultaneously into lower and upper ore storage areas.

Two reclaim wheels, an ore bridge, and two separate ore loadouts assure a flexibility comparable to that in the coal facility, and ore is loaded as the mills require it for blast furnace operations. A modest amount of ore is stored at the mills to cover any unexpected problem.

CAPACITIES

In considering the subject of capacity, it is essential to stipulate the conditions for which the capacity figures are valid. This is particularly true at Conneaut, for conditions vary drastically from season to season and substantially from day to day.

Car Dumping Factors

Some of the factors which affect the operations on the coal side (capacity does not usually come into play on the ore side) are as follows.

Room Left On Pile. Shippers are allocated a certain number of feet of belt for storage of their coal. When the piles are relatively low, the stacker can stack without obstruction into the designated areas, but as the piles grow higher, the material has to be moved out of the way of the stacker by a bulldozer. Eventually the rate at which the bulldozer operates becomes the limiting factor in the ability to stock coal on the specific pile. At that point, the stacker must be moved to a different location. This results in additional switching and stacker movement due to the smaller size of cuts.

Number Of Cars In Each Cut. Since the stackers have to be moved between each cut of cars, it is important that the size of the cuts be maximized, and judgments have to be made continually to decide whether to hold cars pending arrival of additional cars of the same consignment or to go ahead and dump them anyway. It is a matter of continually weighing the increased per diem against the increased dumping productivity that would be obtained by waiting for the larger cut to materialize.

Physical Characteristics Of Coal To Be Dumped. Most of the coal can be handled through the system as designed without unusual problems, but a minor amount of coal is received which is the dried fine product of coal mine washers. This gives trouble when passing through the transfer points. It also has a proclivity for blowing away under dumping and storage conditions, and it cannot be put through silos.

Temperature. There is a line of demarcation at 20°F. which is a breakpoint in the characteristic of coal unloadability. Production with daytime temperatures above that level is unimpeded; below that level additional thawing time slows down the operation.

Wind Conditions. Large rail-mounted, moveable machinery such as stackers and reclaimers are unstable in wind velocities over 35 miles per hour, and they must be tied down to prevent them from being blown

along the track. This minimizes, or inhibits entirely, the opportunity to dump coal for periods of time which are not of long duration but which can cause dumping and shiploading delays.

Backlog Size. It is a continual struggle to decide what backlog should be maintained. The size of the backlog, of course, is adjusted by working overtime or putting on additional turns, and that has to be weighed against the per diem cost. Since the Bessemer is a relatively short railroad, backlog is considered to be all of the coal on line, and an attempt is made to keep the backlog at about two days supply. If the incoming coal is in a relatively small number of consignments, this can be reduced to one and a half days. Under the most favorable conditions, an attempt is made to dump during the next 24 hours all the cars that are on hand at 7 a.m.

Boat Loading Factors

The rate at which a boat is loaded is extremely significant in the lake boat trade since the vessels make a large number of trips during the course of a season, and a substantial part of the time is consumed in loading and unloading. This is in contrast to ocean-going vessels where a reduction of a few hours in boat loading time is inconsequential. Every effort is made to minimize the amount of time it takes from tie-up to cast-off.

Size Of Boat. The size of the boat has a direct relationship to the tons per hour that can be loaded into it. Bigger boats have larger capacity per hold, and since either the boat or the shiploader has to be moved between holds, the number of tons that can be loaded between moves is increased as the size of the vessel grows larger. An interesting sidelight on this is that on the Great Lakes coal has traditionally been loaded with a fixed shiploader and the boat is moved to gain access to the next hold. Ocean-going ships are not usually equipped with winches to facilitate the longitudinal movement of the vessel, and these vessels take longer to load than a Great Lakes boat of the same capacity.

Some Boats Load Multiple Consignments. The interruption that occurs in changing consignments can increase the loading time of the vessel. Reclaim devices must be moved — delaying loading by as much as an hour per additional consignment.

Skill Of The Boat's Mate. The mate is responsible for seeing that the vessel is loaded in such a way that the boat remains in trim at all times. A well-qualified mate will get his boat loaded in half the time that would be required with a green overseer.

Pumps. Vessels come in with water ballast which has to be pumped out as the vessel is loaded. The ability of the boat to pump this ballast in tons per hour determines the rate at which the boat can be loaded, and there is a great deal of variance between the rates that are attained.

Size Of Pile. Reclaim wheels and reclaim pits can operate at a much greater loading rate when the pile is at or near its ultimate capacity. The ratio may vary as much as 3-1 between a reclaim rate from a full pile and that from a nearly empty one.

Number Of Sources Available To Load Boats. This is the most important element in boat loading, as it has a direct relationship to the rate at which vessels

can be filled. The rate varies almost directly with the number of sources available.

Interval Between Boats. If boats come in one behind the other, there is no opportunity to load the silos in the short interval between casting off and docking, and the rate at which the second boat is loaded suffers drastically. This is one of the important reasons why 100 percent dock occupancy is undesirable.

NUMERICAL CAPACITIES

With these things influencing production then the capacities at Conneaut are:

	<u>Ultimate Existing Capacity</u>	<u>Best Experienced Conditions</u>	<u>Usual Conditions</u>
Storage (Million Tons)	6.0	3.5	3.0
Dumper (Cars/Turn)			
Above 20° F.	300	240	150
Below 20° F. (Worst available coal)	-	-	100
Track Pit (Cars/Turn)			
Above 20° F.	250	220	140
Below 20° F. (Best available coal)	-	-	90
Boat Loading			
Very High Volume Customer (25,000 ton boat)	11,000	7,600	5,000
Other Customer (25,000 ton boat)	11,000	3,000	1,400
Other Customer (10-15,000 ton boat)	11,000	2,700	2,000
Annual Throughput (Million Tons)	13.6	10.2	10.0

At this point in the development of the port, the limiting capacity factor is in the shiploading. There is dumping capacity for 18 to 20 million tons, but at a throughput over 13.6 million tons, congestion at the dock would result in an unacceptable degree of boat queuing.

SUMMARY

The metamorphosis that has occurred at the port of Conneaut has resulted in benefits to all concerned. The Railroad can operate with fewer cars and with a reduced but stable and efficient labor force. The Dock Company operates at lower cost and provides employment for their people on a year-round basis. Boat owners are certain that their vessels will load and unload promptly. The ore and coal shippers are relieved of their former feast-or-famine way of doing business. The coal mines are able to work full-out all year around. The ultimate consumer of both coal and ore is in a position to receive the commodity at the lowest possible price, at a rate which best serves his purpose, and with the certainty of the availability of a steady supply of the commodity.

Effect of Brake Equipment Upon Capacity and Rolling Stock for Heavy Haul Routes

D.G. Blaine

Senior Marketing
Representative
Westinghouse Air Brake
Division, American
Standard, Inc.
Chicago, Illinois
Fellow, ASME

Heavy haul railway operations transport very large tonnages of coal, ore, grain, petroleum or chemicals in unit trains between specific origins and destinations. Heavy haul trains may be added on existing routes or new lines built for the purpose. Practical train size and average speed determine the number of heavy haul trains needed. Type of brake equipment, stopping and grade handling ability affect train length; speed and train spacing, AAR and UIC brake systems and styles of train operation are compared. Methods are displayed for determining braking level, train speeds within block distances, rolling stock required and brake system maintenance costs.

NOMENCLATURE

25.4 mm	= 1 inch (in)	BP	= Brake Pipe
1 meter (m)	= 3.28 feet (ft)	SAP	= Straight Air Pipe
1 kilometer (km)	= 3280 ft	MR	= Main Reservoir
1.61 km	= 5280 ft (1 mile)	BC	= Brake Cylinder
1 kilometer/hour (kmh)	= .62 mph	BCP	= Brake Cylinder Pressure
1 bar	= 14.5 psi	AR	= Auxiliary Reservoir
1 kg/cm ²	= 14.2 psi	ER	= Emergency Reservoir
1 liter (l)	= 61.3 in ³	NBR	= Net Braking Ratio
1 kilogram (kg)	= 2.2 lb		($\frac{\text{Actual Braking Force on Shoes}}{\text{(Vehicle Weight)}}$)
1 short Ton (T)	= 2000 lb	TOB	= Tons Per Operative Brake
1 metric ton (Mt)	= 2205 lb	NA	= North American associated and connecting continental railroads including USA, Canada, and Mexico.
1 US horsepower (HP)	= .746 KW	UIC	= Union International Chemin de Fer (European equivalent of AAR)
1 Tractive HP	= THP	AAR	= Association of American Railroads
Dynamic or Rheostatic Brake	= DYN	FRA	= Federal Railroad Administration (US)
Regenerative Brake	= RGN		
1 Braking Horsepower	= BHP		
1 Kilowatt	= 1.34 HP		

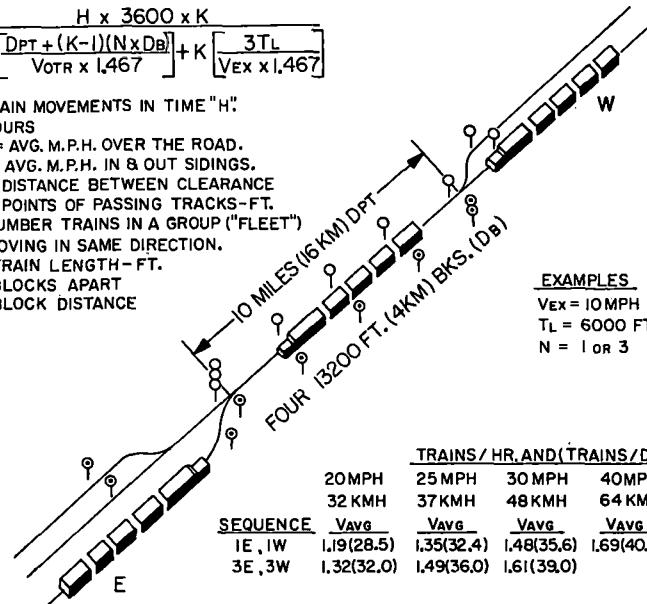
Two distinct types of heavy haul operations have emerged. First is a dedicated route and rolling stock handling only the heavy haul traffic. The second is addition of large heavy haul volume on a general traffic line. The choice of AAR or UIC brake equipment has major effect on practical train length and throughput per train movement and total number of trains required.

Braking level and stopping ability control the running speeds for signal block distances, thus affecting average speeds. This then determines train spacing and thus the total number of trains per unit of time (hour, day, month, year). Net loading per car, train length, and average speed are prime factors in throughput.

Fundamental decisions must be made whether the heavy haul throughput will require single, double or multiple track routes and where siding facilities must be located. Heavy haul train length is usually the major factor. This paper is offered as a practical guide for choices of brake equipment type and braking levels for heavy haul operations.

$$C = \frac{H \times 3600 \times K}{\left[\frac{DPT + (K-1)(N \times DB)}{VOTR \times 1,467} \right] + K} + \frac{3TL}{VEX \times 1,467}$$

C = TRAIN MOVEMENTS IN TIME "H"
H = HOURS
VOTR = AVG. M.P.H. OVER THE ROAD.
VEX = AVG. M.P.H. IN & OUT SIDINGS.
DPT = DISTANCE BETWEEN CLEARANCE POINTS OF PASSING TRACKS-FT.
K = NUMBER TRAINS IN A GROUP ("FLEET") MOVING IN SAME DIRECTION.
TL = TRAIN LENGTH-FT.
N = BLOCKS APART
DB = BLOCK DISTANCE



EXAMPLES
VEX = 10 MPH
TL = 6000 FT.
N = 1 OR 3

SEQUENCE	TRAINS / HR. AND (TRAINS / DAY)				
	Vavg	Vavg	Vavg	Vavg	Vavg
1E, 1W	1.19(28.5)	1.35(32.4)	1.48(35.6)	1.69(40.6)	1.97(47.3)
3E, 3W	1.32(32.0)	1.49(36.0)	1.61(39.0)		

Single Track Train Movement Capacity

Fig. 1

I. PRACTICAL TRAIN MOVEMENT CAPACITY

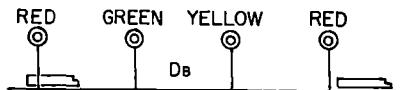
Figure 1 shows theoretical trains per hour for single direction operation on one track with 9000 and 13200 foot long blocks (2744 to 4025m). Figure 2 illustrates theoretical trains per hour and day for two direction operation on single track with passing facilities 10 miles (16 km) apart. Single track has about 1/4 the train movement capacity as double track @ 20 mph (32 kmh) overall average speed. Single track capacity can be doubled by adding a center passing track so opposing trains can meet without stopping either.

$$C = \frac{H \times 3600}{\left[\frac{DB \times N}{VOTR \times 1,467} \right]}$$

C = TRAIN MOVEMENT/UNIT TIME.
DB = BLOCK DISTANCE - FT.
N = NUMBER BLOCKS APART TRAINS NORMALLY OPERATE AT FULL TRACK SPEED.
VOTR = AVG. MPH OPERATING SPEED.

EXAMPLE: (N=3)

$$C = \frac{1 \times 3600}{\left[\frac{13200 \times 3}{60 \times 1,467} \right]} = 8 \text{ TRAINS/HOUR (EACH TRACK)}$$



VOTR		TRAINS/HOUR EACH TRACK	
MPH	KMH	9000 FT. BLOCKS	13200 FT. BLOCKS
20	32	3.9	2.7
30	48	5.6	4.0
60	96	11.7	8.0

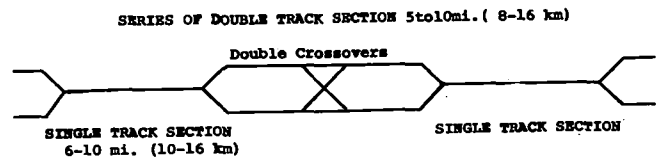
Train Movement Capacity - Single Direction Operation Each Track (Multiple Track)

Fig. 2

TABLE I - Average Trains/Day

Overall Average Speed	Single Track CTC	Hybrid Double Track	Double Track CTC Signaled for Two Direction Moves
20 mph 32 kmh	20-25	30-40	40-50
25 40	25-30	40-50	50-60
30 48	30-40	45-70	70-100
40 54	35-45	50-80	100-140

Table I shows the practical average train movements per day attainable over long periods of time on long distance North American routes. Higher values are only attainable with all trains carefully inspected; ample brake shoe material at each wheel; system leakage within practical limits; car components in good condition; and reliable motive power in all respects.



NOTE: ALL TRACKS SIGNALLED FOR BOTH DIRECTIONS

Figure 3 HYBRID DOUBLE TRACK

Figure 3 shows hybrid double track; a series of double track sections with high speed turnouts and crossovers connected by single track sections. All track is signaled for reverse running with CTC. This permits mixing general and heavy haul trains without severely hampering running speed capabilities of either. Construction costs are considerably less than full double track in hilly or mountainous terrain.

On double or multiple track passing facilities are necessary to accommodate mixed traffic. This allows faster trains to pass slower trains. The passing tracks may be outside tracks or sidings between main tracks. Sidings must have clearance length for longest trains.

II. COMPARISON OF AAR AND UIC BRAKES AND TRAIN OPERATION

Both AAR and UIC brake systems are automatic in that reduction in BP pressure causes all brakes to apply. Beyond this there significant differences because the AAR system is designed to suit the very long and heavy freight train. Adoption of the Quick Action Automatic Air Brake in 1889 recognized relatively long freight trains. Long distance routes in NA were and still are single track requiring long freight trains to meet throughput demands. UIC routes are basically double or multiple track to meet the needs for heavy dense passenger throughput.

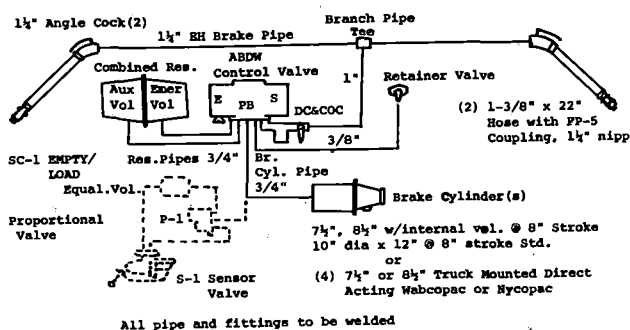


Figure 4 AAR FREIGHT CAR BRAKE EQUIPMENT

First the BP and reservoirs must be charged to a specific pressure, 70-110 psi (5-7.6 bar). Most UIC operations use 5 bar (71 psi). Both AAR and UIC systems will produce approx. 50 psi (3.5 bar) with a nominal 20 psi (1.4 bar) BP reduction. AAR and UIC brakes can be applied by several successive small BP reductions.

UIC control valves for both passenger and freight have a graduated release if BP is increased in several small steps of 2-3 psi (.14-.2) increments. MR release or filling positions are used in UIC locomotive brake valves to force BP air back quickly when using graduated release on short trains. The AAR freight brake control valve has only direct release because graduated release will not respond reliably or uniformly enough on long trains to prevent many stuck brakes, hot wheels and adverse slack action on trains with over 3000-4000 ft (1000-1200 m) brake pipe.

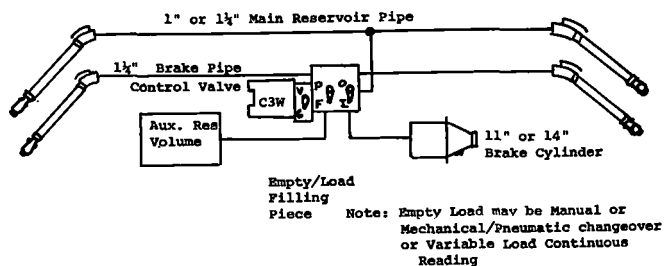


Figure 5 UIC FREIGHT CAR BRAKE EQUIPMENT

Another functional difference is the accelerated release in ABD and ABDW valves which can start release on the rear of a 7500 ft BP train in about 17 seconds. This permits running releases on very long trains at quite low speeds without very high run out forces which may pull the train apart.

Present standard AAR ABDW valves have an accelerated service application function which cuts the BC buildup time on the rear of 7500 ft (2290 m) BP length trains to about half that of ABD or AB valve trains. This function is arranged so it will not encroach on emergency sensitivity or cause apparently greater BP leakage on FRA initial terminal tests.

A fast quick action emergency propagation and higher emergency BCP has been standard for almost 100 years. Unique emergency BCP buildup to 15+% higher than full service controls train slack while optimizing stop distance. Car 150 on a 7500 ft BP train reaches within 5 psi (.35 bar) of maximum in about 18 sec. Emergency rate of BP reduction can be made by placing locomotive brake valve in emergency, opening wide the caboose valve, burst pipe or hose or uncoupling of hoses unintentionally. Table II shows service and emergency BCP.

TABLE II - AAR Equalization Pressures

BP Pressure System Charge		Full Service Brake Cylinder		Emergency Brake Cylinder	
psi	bar	psi	bar	psi	bar
70	4.83	50	3.45	60	4.14
75	5.17	53.5	3.69	64	4.41
80	5.52	57	3.93	68	4.69
85	5.86	60.5	4.17	72	4.87
90	6.21	64	4.41	76	5.24
100	6.90	71	4.89	84	5.79
110	7.59	78	5.39	92	6.34

Auxiliary - 2500 in³ ; Emergency - 3500 in³
 (41 liters) (57 liters)
 10" dia. (255 mm) Brake Cylinder, at 8"PT (203 mm)

Almost all UIC trains use 5 bar (71 psi) BP. Ample stopping ability is attained because most freight cars have empty-load or variable load brakes as a result of relatively short signal blocks. Most NA freight cars have single capacity brakes which need higher BP pressure giving higher BCP to obtain ample stopping ability with typically loaded trains, particularly in grade territories. Control of BP pressure in NA is with "pressure maintaining" which maintains service BP reductions against leakage up to AAR maximums. Service applications are held for an hour or more on long grades. BCP throughout the train is quite uniform. Release response is improved by eliminating continued BP reduction due to leakage. MR release or filling positions in UIC practice are not used in order to prevent overcharging head end cars of long trains. This may cause subsequent stuck brakes when the locomotive brake valve is returned to normal "running" position.

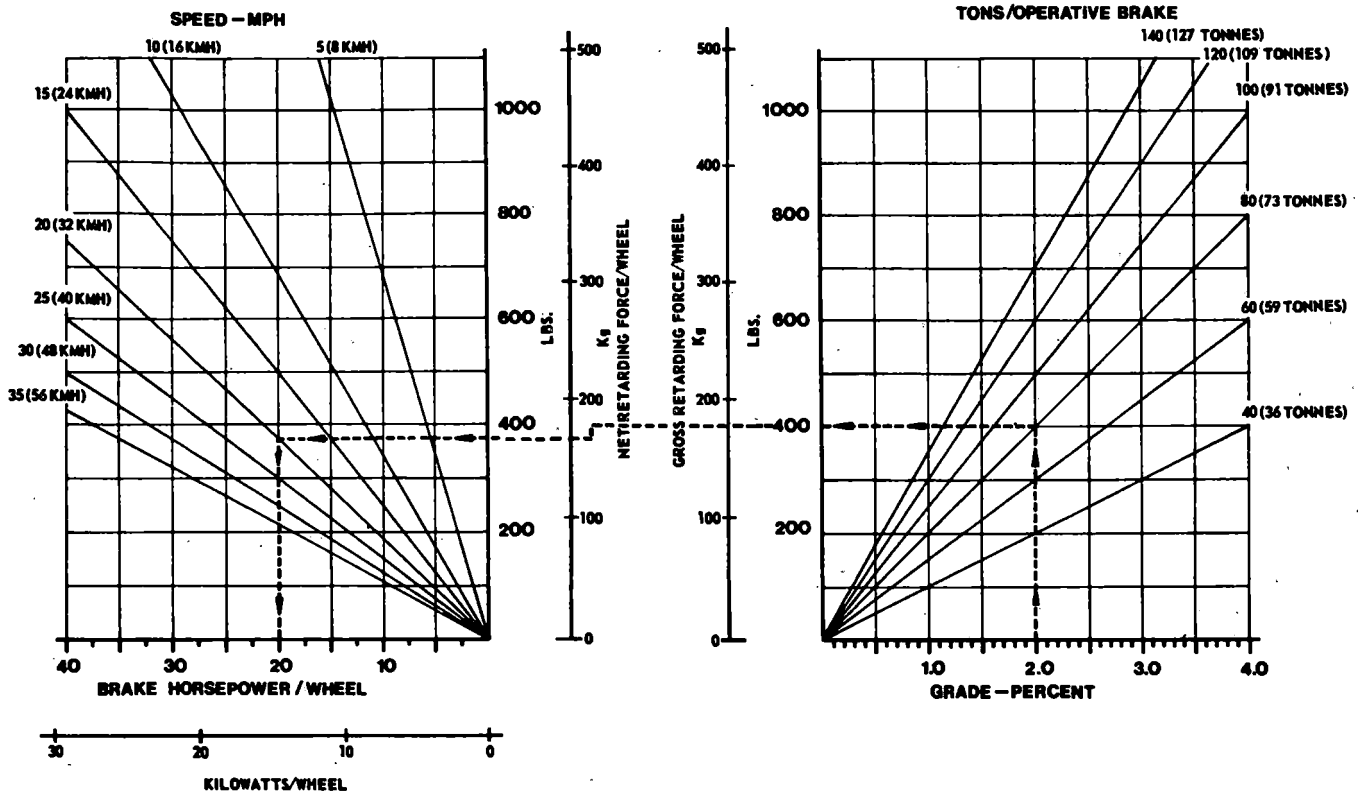


Fig. 6

Graphical Solution - weight, grade, resistance horsepower

III. GRADE BRAKING WITH AIR AND DYNAMIC BRAKES

Dynamic (DYN) or regenerative (RGN) brakes from locomotive traction motors are used in coordination with train air brakes on long and/or significant downgrades. Train air brakes are held steadily applied and DYN or RGN provides half to 2/3 the total retarding force on the heaviest part of the grade. Variations in resistance and small changes in gradient are accommodated by varying DYN or RGN.

Figure 6 shows a graphical method for determining retarding force and brake power (BHP or KW) per car wheel at various average weight (Tons per operative brake (TOB)) on grades up to 4% (1 in 25). TOB includes equivalent locomotive weight per car. Train resistance of 5 lb/Ton (2.06 kg/Mt) is typical in NA on light/moderate curves @ 20-30 mph (32-48 kmh).

If DYN or RGN is reliably available divide its total retarding force by the number of car wheels and add to train resistance for NET AIR BRAKE RETARDING FORCE PER WHEEL. Move left to train speed for BHP or KW friction brake per wheel. For continuous applications of an hour or more follow recommendations in Section X.

Fixed maximum HP (KW) capacity of DYN or RGN will cause retarding force to reduce with speed above some particular speed (18-25 mph generally or 30-40 kmh). This will require more air brake to balance the grade. Train speed may have to be promptly reduced if DYN or RGN is not properly effective. Operating rules must state these conditions and enginemen must understand and respond.

Welded pipe and fittings are recommended to help eliminate any undesired releases due to leakage in reservoir, BC or associated pipes and fittings during applications held for long periods.

Retainer valves are included with AAR direct release control valves to enable safe descent of grades with air brakes only. Retainers hold sufficient to control train speed if brake release and recharge is required. Ordinarily, the train would be stopped at the top and the bottom of the grade to manually set up or turn down retainers on each car.

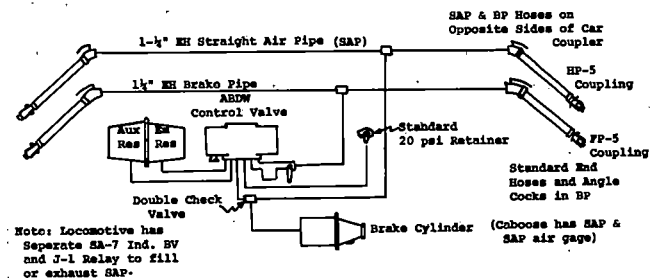


Figure 7 "ORINOCO" AUTOMATIC AND STRAIGHT AIR SYSTEM--VARIABLE RETAINED PRESSURE

Figures 7 and 8 show two methods used to avoid this time consuming process. Each requires a second train lined pipe. Figure 7 the so called "Orinoco" automatic and straight air system is used in a number of North and South American areas. The SAP is 1 1/2" size and is connected to each BC through a double check valve. The automatic brake is first applied to the normal degree required using this to get the application

quickly through the train. Then SAP is filled to approximately the BCP produced. When the caboose SAP gage has sufficient pressure the automatic brake is released and reservoirs recharged. BCP is thus maintained by the SAP which can be varied up or down to give steady grade balancing speed. SAP responds rather slowly because of pipe and BC volumes but this seems desirable in long heavy trains. Automatic full service and emergency are always available.

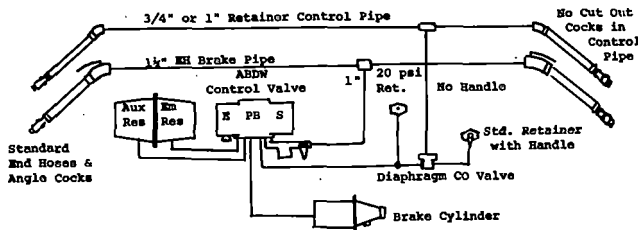


Figure 8 RETAINER CONTROL PIPE SYSTEM REMOTE ACTUATION OF RETAINERS

Figure 8 shows the "Retainer Control Pipe" system which uses a second retainer without handle permanently set for 20 psi. Filling the control pipe to over 8 psi (.55 bar) closes the diaphragm valve to the standard retainer and forces BC to exhaust through the second retainer. The engineman can "set up" or "turn down" retainers without stopping in 2-3 minutes by filling or exhausting the retainer control pipe. Obviously, locomotives and cars must be equipped properly for these systems to operate. They are used on some unit coal and ore trains.

Note in Figure 5 the basic UIC system uses a main reservoir pipe to continuously supply car reservoirs. This is effective on short trains to provide release and recharge flexibility. However, with 6000-10000 ft pipe lengths as in daily AAR practice, the volume of air and flow resistance at small pressure differentials to cause flow, have similar time restraints as on typical AAR single BP. Brake handling flexibility is not significantly improved with trainlined MRP and head end MR supply compared to the standard AAR system.

IV. EFFECT OF BRAKE EQUIPMENT ON RAILROAD CAPACITY

The generic type of brake equipment AAR or UIC will affect practical train length, stopping ability and signal spacing. Minimum distance between trains is controlled by signals and, at any given speed, controls the maximum number of train movements per unit of time. Thus the type of brake and the braking level can have far reaching economic effects. Table III shows the number of trains per day and tonnage which can be throughput per train to attain 30x10⁶ million metric tons in a 300 operating day year with both AAR and UIC style operations. Considering the 45-48 million gross tons of heavy haul traffic this should provide ample maintenance of way time plus other contingencies. Note the AAR style trains can reach 20000+ gross tons loaded.

North American AAR style operation can save from 700 to 1000 cars and up to 20 locomotive units. The 34 to 66 heavy haul trains/day with UIC style operation would require a double track route. However, AAR style long and heavy train operation could be accommodated on single track with passing sidings about 10 miles (16 km) apart. There would still be some room for other passenger or freight traffic on the single track route.

TABLE III ROLLING STOCK AND TRAINS REQUIRED FOR 30 MILLION NET Mt/YEAR
24 HOUR ROUND TRIP CYCLE PER TRAIN
FULL OPERATION - 300 DAYS/YEAR

	UIC Style Trains		AAR Style Trains			
	60 Mt (66 T)	80 Mt (88 T)	90.7 Mt (100 T)	150 cars	100 cars	150 cars
Nominal Car Capacity	60 Mt (66 T)	80 Mt (88 T)	90.7 Mt (100 T)	150 cars	100 cars	150 cars
Car Gross Rail Load	80 Mt (88 T)	100 Mt (110 T)	119.2 Mt (131.5 T)	13650 Mt	11340 Mt	17010 Mt
Wheel Load (8 Wheel Car)	10 Mt (22050-lb)	12.5Mt (27563-lb)	14.9 Mt (32875-lb)	14.9 Mt (32875-lb)	17.9 Mt (39376-lb)	17.9 Mt (39376-lb)
Train Length	50 cars	75 cars	100 cars	150 cars	100 cars	150 cars
Net Lading	3000 Mt	6000 Mt	9100 Mt	13650 Mt	11340 Mt	17010 Mt
Gross Tons Cars/Day	165000 Mt	153000 Mt	162294 Mt	154777 Mt	155088 Mt	152503 Mt
Gross Tons Cars/Train (Loaded Direction)	4000 Mt	7500 Mt	11927 Mt	17891 Mt	14286 Mt	21429 Mt
Loaded Trains/Day	33	17	11	7	9	6
Total Trains/Day	66	34	22	14	18	12
Locomotives Required* (3000-4000 THP/Unit)	66	68	44	42	54	48
Cars Required*	3300	2550	2200	2200	1800	1800

* Not including spares--No heavy ascending grades in loaded direction

Figure 9 is a graphical method for determining the number of trains and train sets of equipment required for any style operation per million net tons of lading, loaded one way and empty the other way.

Over the road running speeds are usually about twice the overall average speed required. 20-25 mph average (30-42 kmh) would require 40-50 mph (60-85 kmh) running capability. Overall average is affected by the number of times a train must slowdown to take siding and wait for opposing traffic or being passed by faster trains. Mixing of general and heavy haul traffic may require more THP on heavy haul trains to give better acceleration and maintain district average speeds or all traffic may suffer.

V. SIGNAL SPACING-TRAIN BRAKING ABILITY

Figures 10-15 show characteristic BC buildup time and stop distances on level grade for full service and emergency applications from 80 psi (5.5 bar) BP. These represent the best simulations of which we are aware for trains with 7500 ft (2286 m) BP and Cobra (R) high friction composition brake shoes. "Cobra" is the registered trade mark of Railroad Friction Products Corp.

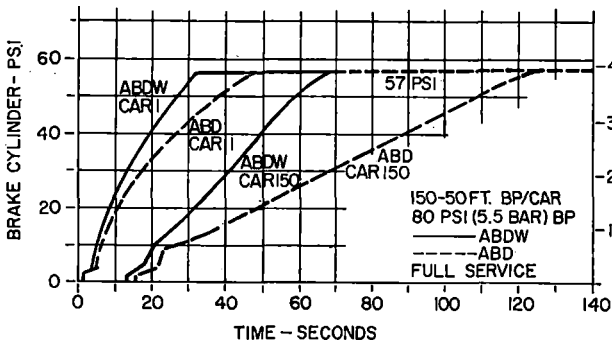
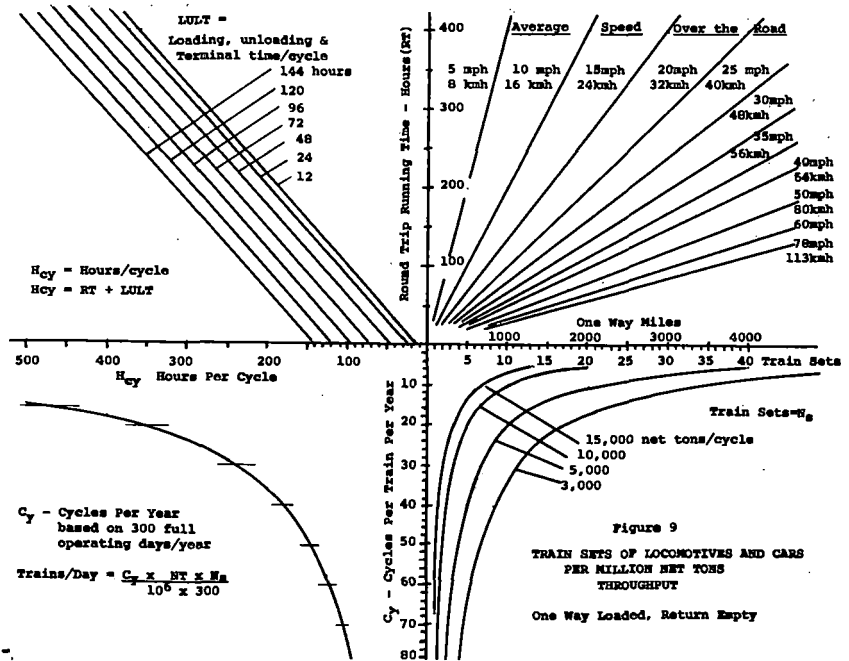


Fig. 10 Full Service Brake Cylinder Buildup

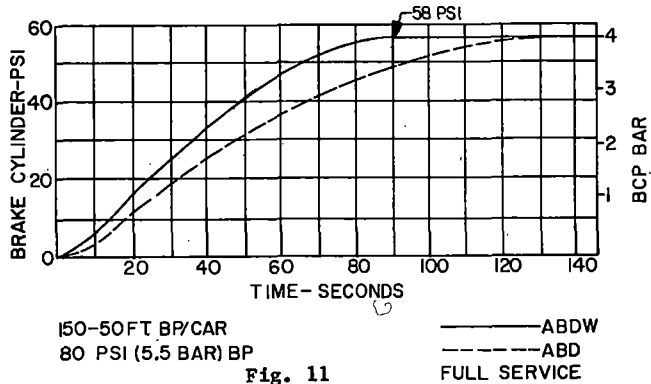


Fig. 11

Train Average Brake Cylinder Buildup

In NA practice any train must be able to stop from its maximum authorized speed within one signal block distance, with a full service application--NOT EMERGENCY. Three aspect signals require this. Common practice requires this stop in 75% or less

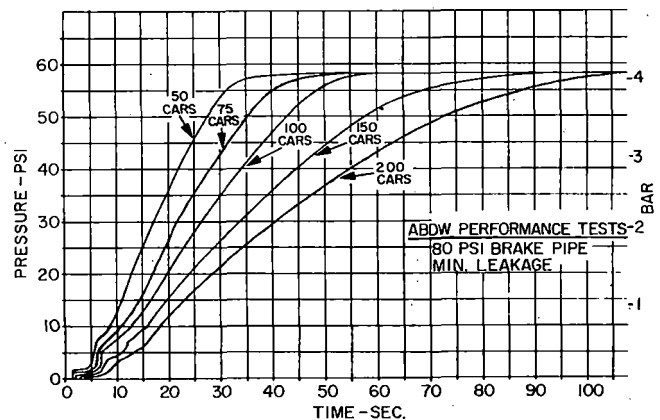


Fig. 12 Train Average Brake Cylinder Pressure

of block distance. Maximum speeds within given block distances can be determined from Figure 1. Net Braking Ratios (NBR) are stated at the NA standard comparison pressure of 50 psi (3.5 bar). NA block lengths are generally 9000-14000 ft (2700-4300 m), and average around 10000 ft (3000 m). Even though cab signals are used it is well to refer to clear sighting distances, usually 6000-8000 ft (1800-2500 m) with searchlight signals.

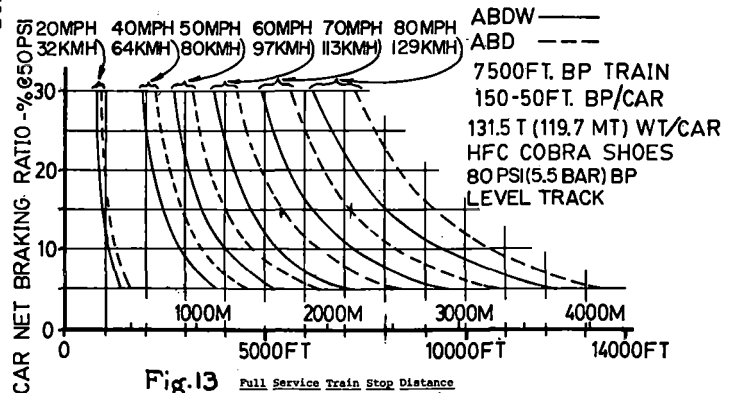


Fig. 13 Full Service Train Stop Distance

VI CHOICE OF CAR BRAKING LEVEL

50 mph (80 kmh) full service level stops from 80 psi BP with 6.5% NBR @50 psi (3.5 bar) BCP are in about 6000 ft (1800 m) range for 150 car 7500 ft (2286 m) BP trains. Loaded cars are 131.5T (119.7 Mt). Note that 60 mph (97 kmh) speed to stop in the same distance would need 7.5%-8% NBR on these same cars.

Net Braking Ratio is the actual braking force, measured with a calibrated brake shoe expressed as a % of vehicle weight.

TABLE IV - AAR Net Braking Ratios-Jan. 1981

Air Brake @ 50 psi (3.5 bar)	Max. Empty - 30%	Conventional Brake Rigging
	- 33%	Truck Mounted Direct Acting Wabcopac or Nycopac
Minimum @ GRL	- 6.5%	
Maximum @ GRL	-10.0%	
Handbrake @ AAR Std. Minimum @		
Horizontal GRL	-11.0%	
Chain Force		

80 mph (130 kmh) values are shown because most US signaled main line freight track does not have cab signal or train control. In this case the FRA limits train speed to 79 mph (127 kmh).

Higher BP pressures may be required to provide sufficient full service NBR to give ample margin for slowdowns or stops on descending grades. If gross to tare weight ratios exceed 4.62/1 empty-load equipment must be added in NA. Maximum AAR EMPTY CAR NBR @ 50 psi of 30% is a good practical value in order to avoid undue liability of wheel sliding when considering the higher BCP's which result from higher than 70 psi BP pressure. With a brake shoe friction of .4 to .5, 30% NBR requires wheel/rail adhesion of 12-15%. 90 psi BP emergency with 76 psi BCP would require 18-23% adhesion. Good NA practice tries to hold the handbrake NBR on the empty car to about 50% for similar reasons.

Empty-load can be a major benefit in brake shoe and wheel wear. Generally shoe wear varies with the square of the retarding force. With empty shoe force .6 of loaded and half the operation empty, the empty shoe wear would be expected to be 36% of that loaded assuming the same brake pipe reductions were made in each case. Overall shoe wear would be about 70% compared to single capacity. In NA the large majority of brake applications are to stabilize train slack and control speed on undulating profiles. The bulk of train brake applications are in the 7-10 psi BP reduction range(.5-.7 bar). Overall wheel wear benefits are in the 10% range for unit trains and upwards of 25% in mixed E/L and single capacity consists. Empty/load details add about 20% to cost of single capacity equipment. Around 35-50% of wheel removals are caused by brake use or misuse.

TABLE V - Minimum Empty Car Weights

NBR@ GRL	Max. G/T For 30% Empty	Single Capacity		Empty-60% Load	
		Min. Empty @263000-lb GRL	lb Mt	Min. Empty Wt. @263000-lb GRL	lb Mt
7%	4.29/1	61300	27.9	36800	16.7
8%	3.75/1	70130	31.9	42100	19.1
9%	3.33/1	78980	35.9	47300	21.5
10%	3.00/1	87670	39.8	52600	23.9

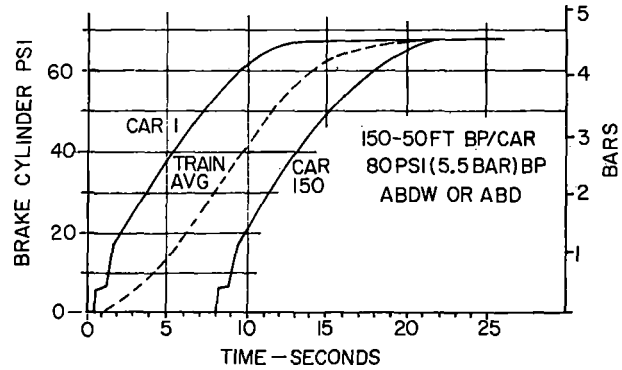


Fig. 14 Emergency Application-Brake Cylinder Buildup

Emergency application characteristics and stop distance on level track are shown to complete the general performance picture. Emergency performance is not used to determine basic train performance nor maximum speeds allowed within signal spacing. However, it is important to consider emergency braking level from the standpoint of available wheel rail adhesion and liability of wheel sliding. Net braking ratios in emergency will be about 20% higher than in full service. The product of NBR and brake shoe friction will indicate adhesion demand from the brakes. Good NA practice holds air brake NBR to around 40-45% max, and handbrake to about 50% max. The keeps adhesion demand in the 16-25% range.

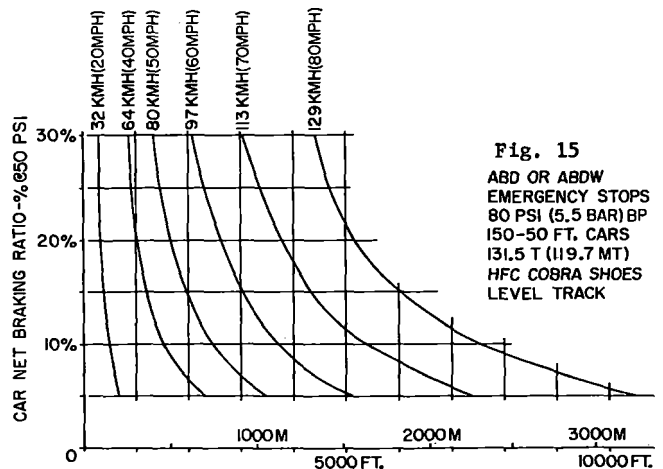


Fig. 15 ABD OR ABDW EMERGENCY STOPS 80 PSI (5.5 BAR) BP 150-50 FT. CARS 131.5 T (119.7 MT) HFC COBRA SHOES LEVEL TRACK

VII GRADE BRAKING CONSIDERATIONS

Over a century of heavy and significant down grade operations in NA strongly indicate best and safest operation does not use more than about half the full service brake to balance gravity, at the particular BP pressure employed. This gives reasonable slowdown or stopping ability anywhere on the grade. Train average retarding force for the NBR and friction material used should not exceed half that provided by full service. Table VI lists NBR required to give 2/1 margin on grades from 1% to 3% (1 in 100 to 1 in 33) grades.

TABLE VI - Net Braking Ratio - Down Grades

Grade	Train Resist		Net Grade Braking Force/Ton		Full Serv NBR		2xGr Bal	
	lb T	kg Mt	lb T	kg Mt	@ .33 f lb/T	kg/Mt	NA%	Met%
-1%	5	2.1	15	7.9	45	23.9	4.5	4.8
	10	4.1	10	5.9	30	17.9	3.0	3.6
	15	6.2	5	3.8	15	11.5	1.5	2.3
-2%	5	2.1	35	17.9	105	54.2	10.5	10.8
	10	4.1	30	15.9	90	48.1	9.0	9.6
	15	6.2	25	13.8	75	42.0	7.5	8.4
-3%	5	2.1	55	28.0	165	84.8	16.5	17.0
	10	4.1	50	26.0	150	78.7	15.0	15.7
	15	6.2	45	23.9	135	72.3	13.5	14.5

Note: Metric ton (2205-lb) requires 22.05-lb or appx. 10 kg gravity force/Mt/%Gr Train resistance kg/Mt same as specific lb/2000-lb Ton.

In any event, the grade must be able to be safely descended with air brakes only. Operating rules may require that train speed be reduced, if air and DYN or RGN are normally used, in order to follow recommendations in Section X for BHP/wheel.

NA experience shows maximum continuous DYN or RGN retarding force should not exceed 250,000 lb in any one locomotive consist (113,400 kg). Otherwise cars may be squeezed out of the train, rail may turnover or track may shift laterally. Some NA railways limit maximum DYN to 177,000 lb in any locomotive consist.

On light or moderate grades where max. DYN or RGN might hold the train against gravity it is much better practice to distribute the retarding force more evenly through the train. Using a minimum BP reduction and reducing the DYN or RGN will lead to improved rail, wheel and coupler/draft gear wear and service. Retarding force will be distributed along 5-7000 ft(1600-2200 m) of track rather than in 300 ft(100m) of rail under the locomotives.

Although there are improvements in train brake response with radio remote control, no operating property in North or South America has used this for other than maximizing tractive power per train. This is because the vital train speed control is the automatic air brake. Interlocks must be provided so that the electronic equipment will not compromise the integrity of the automatic air brake

in case radio continuity is lost or the electro pneumatic brake interface equipment malfunctions.

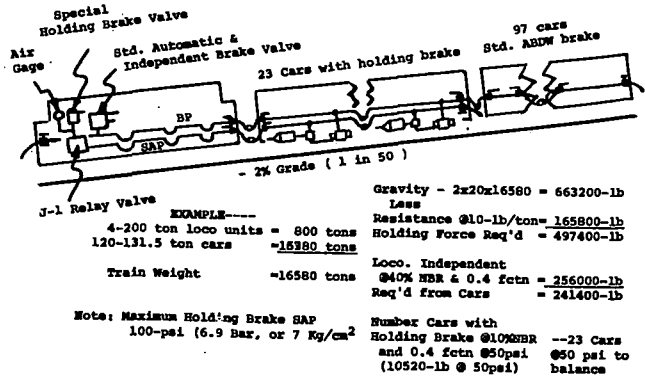


FIGURE 16

Locomotive independent brake should be able to hold the train stationary on the grade with all car brakes released so the train can be completely recharged if necessary after a stop. Otherwise handbrakes or other auxiliary brake must be employed. Such an auxiliary straight air holding brake is shown on Figure 16 where the loaded weight of 23 cars is needed to assist the locomotive.

VIII PUSHERS, HELPERS, AND RADIO REMOTE CONTROL

On heavy ascending grades in the loaded direction it is often necessary to use more total tractive effort than can practically be used in one locomotive consist. 15000-17000 T trains ascending 2-2.5% grades need 600000 to 800000 lb TE(273000 to 364000 kg). As many as 8-11 other locomotives are spaced back through the train, in up to two other consists. Pushing through the caboose or rear car is not recommended.

Many trains are handled with radio remote control of one other set of units, generally 40-66% of the way back in the train. On trains with 11000-14000 Mt of cars a third set of 4 or 5 locomotive units is placed about 80% the way back in the train. The second set of units is operated by manual control with voice radio contact between the lead and helper engineman. Experience has proven the lead engineman cannot successfully vary the controls on a second set of units which may be a mile or more away and on different curve and gradient conditions.

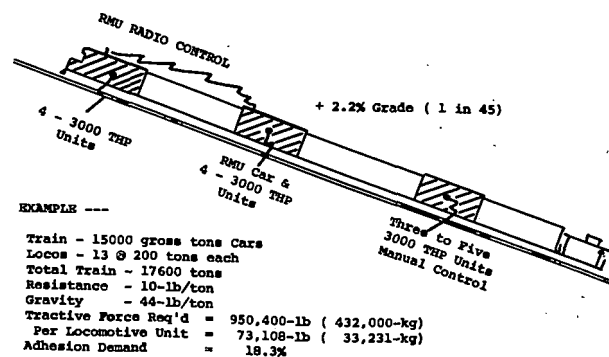


FIGURE 17- Radio Controlled Remote Locomotives and Helpers Heavy Ascending Grades

IX. ELECTRO PNEUMATIC ACTUATION FOR FREIGHT TRAINS

For over 90 years technology has existed to equip all freight cars with electric actuation of train brakes. Electro pneumatic brakes have been used in passenger and transit for about 80 years. Among many technical reasons why electric actuation has not been applied to long heavy freight trains are:

The ultimate or vital brake mode is the automatic air brake. Freight train mass is up to 10 or more times that of transit and passenger trains. Freight train lengths are in similar proportion. Partial EP response or failure of a significant part of the long freight train can create heavy excess in-train or train-track forces which will disrupt either the train or tack by squeeze out of cars, derailment, rail turnover, or track shift laterally.

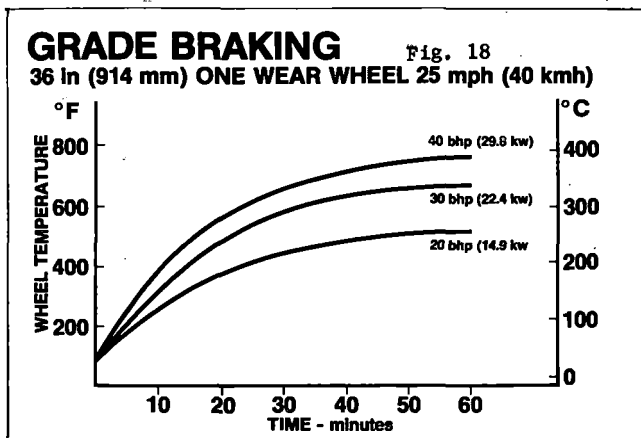
Electrically actuated brakes can be made "vital" by requiring some signal or energy level to be present or full brake is called for. Experience with long passenger trains indicates that 75-200 cars and required connectors would make it difficult to get trains out of the yards within present times and difficult to keep them moving reliably over the road.

Circuits of 6000-10000 ft length with inductive receivers and transmitters at each car would require impractically large and stiff connector cables. Attenuation in connectors which have to be parted and made up quickly either manually or automatically becomes serious. The rather sharp bends in conduit make use of VHF somewhat limited.

Wireless transmission of control signals and response checking information for vital data is subject to local transient loss of continuity, blank out or capture by powerful local transmission extraneous sources. While some temporary loss of continuity can be accommodated with traction power by using overrides, power must still shut down if a pneumatic brake pipe reduction is made during the LOC. In any event the electric or electronic components must not interfere with the automatic air brake integrity whether electric components are in use or not. Mobile train voice radio is quite different than dealing with vital data.

X. ENERGY ABSORPTION AND DISSIPATION

Car wheels are the primary heat sinks and radiators for absorbing and dissipating kinetic and potential energy converted to heat during braking.



On long and/or heavy grades it is important not to exceed the practical thermal capacity of wheels. Brake may be continuously and steadily applied for an hour or more. NA experience indicates train average wheel tread temperature should not exceed appx. 600 deg. F (315 deg. C) which is about half the grain change temperature in typical wheel steels. BHP generated on the wheel tread of AAR wheel designs for one hour steady applications and holding appx. 600 deg. F are in Table VII.

TABLE VII - Friction BHP Various Wheel Sizes

Dia.	AAR Type	Car Type	BHP/Wheel	Formulae
28" (710mm)	1-W	Special Low Level	20	$BHP = \frac{F_r \times Vel.}{K}$
33" (840mm)	1-W	50&70T Capacity	25	$BHP = \frac{lb \times mph}{375}$
36" (915mm)	1-W	100T Capacity	30	$BHP = \frac{kg \times kmh}{106}$
38" (965mm)	1-W	125T Capacity	35	
40" (1015mm)	MW	Locos 35000-lb Whl. Load	40	

Figure 18 shows temperature rise vs. time for dynamometer simulations of 36" (915 mm) AAR 1-W wheels at various BHP's. Best operations engineering uses somewhat less than in Table VII, i.e. 20 instead of 25, etc. Otherwise, if DYN or RGN is only partially effective, the train must be stopped immediately, secured while recharging the brake system fully, and then proceed at lower speed to avoid overheating shoes and wheels.

XI. BRAKE SHOE WEAR RATE CONSIDERATIONS

Generally brake shoe wear varies with the first power of time applied and the square of retarding force as long as wheel tread temperatures do not exceed appx. 600 deg. F (315 deg. C). Higher temperatures cause much more rapid wear varying with the cube or even greater powers of retarding force.

Train braking duty, or time applied vs. running time, ranges up to about 5% maximum in level territory (grades not over $\pm .5\%$). On general undulating territory (grades not over appx. $\pm 1.3\%$) typical braking duty rises to about 10-20% of the running time. Heavy grade territory usually always has some general undulating and flat sections. Typical braking duty may range from 25-50% of running time. Heavy grades are considered when grades run from $\pm 1.3\%$ to $\pm 3\%$ or more.

In NA undulating profiles cover about 2/3 the main and branch lines. Around 75% of braking work seen by a typical car is on undulating profiles with many light to moderate applications made to control speed and to stabilize train slack. Only about 5% of total braking duty is generated on so called "flat" territory, making the occasional slowdown or stop from any significant speed.

It is unlikely that full disc brakes or even disc assist brakes will be used on North American design freight cars. Coupler height and heavy center sill structure preclude adequate space for axle hub or inside wheel hub mounting, particularly on 150 ft radius curves. Outside wheel hub mounting would require inside truck frames which would have similar curve restrictions. Deeply dished and semi parabolic wheel plates of NA designs make cheek style discs on both sides of the wheel impractical.

XII. BRAKE SYSTEM OPERATING COST PER CAR PER YEAR

Overall car maintenance in the 2¢-3¢/mile range would be expected depending upon the relative maturity of the heavy haul car fleet. Brake system operating and maintenance costs can be estimated in a general way based on AAR general car repair billing and the experience of a number of long distance unit train owners and operators.

Assumptions are 100,000 car miles/year (160,000 km); 50,000 avg. miles/shoe change; air compressed by two stage machine direct driven from diesel crankshaft with main engine fuel oil at \$1/US gallon and cost per BHPHR prorated with engine operating cost; AAR Job Code Labor and Material Dec. 1981.

1. Brake shoes @ \$15/change
(100/50 x 8 x \$15) = \$ 240/yr
Shoe wear will vary with
braking duty and terrain!
2. Compressed air @ \$3/10⁴ ft³
appx. 50,000 ft³/car/yr = \$ 15/yr
3. Single Car Test, one/yr
one man hour @ \$ 40 = \$ 40/yr
4. Clean, Oil, Test compt.
ABDW & Empty Load plus
in date cleaning of a few items
at appx. 4% overall rate and
total of \$700 = \$ 28/yr
5. Brake rigging, pipes and
fittings, repair and replace
damaged air brake devices at
twice overall general service
AAR CRB rates and experience
 - a. Replace damaged portions
and parts---- \$14/car/yr
 - b. Pipe, fitting repairs plus
BP cocks and hoses
---- \$44/car/yr
 - c. Levers, rods, pins, carriers
and brake beams--- \$32/car/yr.
 - d. Hand Brakes and Auto. Slack
Adjusters---- \$16/car/yr = \$ 106/yr

Total \$429/yr/car

REFERENCES

1. Blaine, D. G., "Determining Practical Ton-
age Limits and Speeds in Grade Operations"
ASME 69WA/RR-6
2. Cabbie, G. M. "Effect of Wheel Diameter on
Tread Temperature in Grade Operations"
ASME 72WA/RT-10
3. Wilson, R. L. "Perspective of Freight Car
Braking Ratios" Air Brake Association
1977 Proceedings
4. Blaine, D. G. "Operational Environment
for North American Freight
Train Service and Effects
Kahr, J. C. Brake Equipment, Brake
Shoes and Wheels" 1978
International Wheel Set
Congress Proceedings
5. Blaine, D. G. "Train Brake and Capacity
Hengel, M. F. Requirements for the 80's"
Peterson, J.H. ASME 81 RT/ 11
6. Parker, C. W. "Development of Remote
Multiple Control of
Locomotives", Chapt. 6 in
"A Century of Progress in
Car and Locomotive Design"
ASME 1979

Meeting the Challenge of Increasing Tonnage : Signalling Implications of Increasing Tonnage

D.P. Marais

Pr.Eng., MSAIEE
Signal & Telecommunication
Engineer, Research &
Development Section
Office of the Chief
Engineer (Signals &
Telecommunications)
South African Railways
Johannesburg
South Africa

This paper outlines some of the main implications of increased tonnage on signalling equipment and philosophies, as experienced by the South African Railways. The provision of multi-aspect signalling as an aid in train-handling is discussed, as well as aspects such as increases in equipment complexity and cost. As a prelude to considering immunisation against 50Hz interference in signalling and telecommunication systems, the induction effects of AC electrification are examined. The necessity for on-train radio to facilitate the authorisation of moving trains is outlined, as well as details of systems in use. Finally the problem of train detection on heavy-haul lines is examined, and miscellaneous aspects such as:

- control of electric traction maximum demand,
 - radio interrogation of train-end brake pressure,
 - dragging equipment alarm systems,
 - maximising the availability of CTC equipment, and
 - maintenance considerations,
- are briefly covered.

INTRODUCTION

The two main examples of heavy haul railway lines to be found in the Republic of South Africa, are the Richards Bay coal line and the Sishen - Saldanha iron-ore line.

The former extends from Broodsniersplaas (near Johannesburg) over approximately 540 km of rather mountainous and uninhabited country, to Richards Bay on the east coast. Ruling gradients on this line are 1 in 66 (1,5 percent), and it conveys mainly coal to Richards Bay harbour in specially designed dedicated coal-trains. A certain amount of general purpose traffic also operates on the line.

The Sishen - Saldanha line is approximately 860 km long, running from Sishen in the north, over terrain somewhat less undulating than, but similarly uninhabited to that encountered on the coal line, to Saldanha Bay on the south-western coast. Ruling gradients are of the order of 1 in 250 (0,4 percent), and this line is a dedicated heavy-haul line. By far the main commodity being transported over it, is iron-ore, which is conveyed in custom designed ore trains.

The main effects of heavy haulage on the signalling and telecommunication equipment on these two lines will be discussed in the following sections.

SIGNALLING REQUIREMENTS

Philosophy

In the past, so-called 3-aspect colour-light signalling catered fairly adequately for the requirements of the South African Railways.

This version provides the aspects red, yellow, and green, with or without a route-indicator in the case of the proceed aspects yellow and green.

The aspect - meanings are : red - stop; yellow - proceed with caution; and green - line speed, with the route indicator (where applicable) to indicate whether the route ahead is straight, or one of a number of left-hand or right-hand possibilities.

Probably the main problem with the 3-aspect system however, is that of the non-singular meaning of the yellow aspect. The vague message "proceed with caution" arises from the fact that a yellow signal indicates for example, that the following signal is "at danger" (red), OR that the next signal is "at proceed" (yellow), but with the route beyond it over points set for the turn-out.

Quite naturally, with the tendency to run ever longer and heavier trains, the handling of these trains became a problem of increasing complexity.

It is not surprising therefore, that a strong need was felt to supplement the road-knowledge of the driver with additional train-handling information.

The requirements were therefore set that signals, as far as possible, be spaced at braking-distance, and that the driver be given adequate advance warning of -

- (i) turn-out routes over points ahead;
- (ii) signals ahead at danger, when signal spacings of less than braking-distance are involved (coal line only).

(Braking-distance is the distance required for a fully-laden train, travelling at line speed, to come to a standstill on the portion of line concerned.)

The spacing of signals at braking-distance has the advantage that sighting-distance is of little or no importance, and together with the advance warning of conditions ahead, results in the requirement that signal-aspects have only to be acted on when the driver is at the signal concerned.

Coal Line

Aspects Over Turn-outs : On this line, it was decided that all main-line points, including those which could be traversed in the turn-out direction by through-running trains, should have their turn-outs confined to 1 in 20. All other points, such as those providing access to a yard, have turn-outs of 1 in 12.

When a train is about to negotiate a 1 in 20 (medium speed) turn-out, the driver is given a pre-warning at the signal preceding the one reading over the points. This pre-warning is in the form of a green-over-yellow aspect, which tells the driver that -

- (a) the signal ahead is at proceed, and
- (b) at least one medium-speed (1 in 20) turn-out has to be negotiated after the next signal.

The driver only has to react to the aspect when he is at this preceding signal, as it is normally positioned at more than handling distance from the signal at the (first) turn-out. Handling distance is the distance required for a fully-laden train to reduce its speed from line speed to that required to safely negotiate the turn-out concerned. It therefore follows that handling distance is always less than braking distance, and is a function of -

- (a) train characteristics (mass, braking capabilities, etc.);
- (b) gradients, in the direction of travel, between the signals concerned;
- (c) governing line speed, and
- (d) type of turn-out to be negotiated.

Should the preceding signal however, be at less than handling distance from the turn-out, then the pre-warning aspect is transferred back one more signal.

In addition to the above pre-warning(s), the signal at the (first) turn-out will, in addition to a 3-lamp turn-out indicator (which indicates point of turn-out, as well as either a left-hand or right-hand turn-out), also display a green-over-yellow aspect, thus confirming that a medium speed turn-out is to be negotiated, and also that the following signal is at proceed.

Should the following signal not be proceed, then the signal at points will display a single yellow aspect.

When a signal reading over points displays a green-yellow (double) aspect, this could also (additionally) represent a pre-warning of a turn-out after the next signal. For this reason, it is of importance that an advance-starter or section - entry signal should exist after the last points when leaving a station, so that this signal may act as a speed de-restriction for trains departing over a turn-out route, by displaying a green aspect.

If any of the aforementioned turn-out routes over points contain one or more 1 in 12 (low speed) turn-outs, then the corresponding green-over-yellow aspects are replaced by yellow-over-yellow (double yellow) aspects.

Aspects With Braking Restrictions : Signals are generally spaced at a minimum of braking-distance.

However, when due to geographic or other considerations, two signals are positioned at less than braking distance apart (with an absolute minimum limit of 275 m), then the signal preceding these two is provided with a white aspect, which is situated next to the other aspects, on the side away from the track.

This white aspect is additionally displayed when the following signal is at yellow-only, with the one thereafter at danger (red), thus informing the driver that the signal-after-next is at danger, and that there is less than braking distance between it and the preceding one.

It should therefore be apparent that various aspect combinations are possible (e.g. yellow-white, double-yellow-white or green-yellow-white) depending on the status of the route(s) ahead.

Furthermore, the achievement of an unambiguous meaning for the single yellow aspect has been realised. It now clearly conveys the message "next signal at danger" with the only cause for exception being signalling faults (e.g. lamp failure).

Equipment Complexity and Cost Considerations : The practical implementation of signalling systems complying with the foregoing requirements has clearly demonstrated that the provision of the "multi-aspect" signalling under discussion does not result in an unexpected or unacceptable increase in equipment complexity.

It is however, a difficult and complicated task to quantify any statements in this regard.

Fortunately, equipment cost generally bears a fairly direct relation to equipment complexity. Cost comparisons have been made, and it has been found that the overall cost of a "multi-aspect" signalling installation, as described, is no more than 3 to 5% more expensive than a comparable conventional 3-aspect installation.

However, to convert an existing 3-aspect installation to "multi-aspect" would cost considerably more - probably of the order of 20 to 30% of the overall cost of the 3-aspect installation.

Sishen - Saldanha Line

As indicated earlier, gradients on the Sishen - Saldanha line are considerably less severe than on the coal line. Furthermore, all signals are spaced at braking-distance.

However, due to train-lengths and tonnages, the need for advance turn-out information still exists, and thus an additional aspect was provided on the intermediate - home signals (i.e. the signals preceding those reading over the facing points).

This additional aspect merely entails the provision of a white light (low speed pre-route indicator) on the the intermediate home signals. The purpose of the white light is to give pre-warning of the low-speed (1 in 12) turn-out after the following signal, and is thus only illuminated when the next signal is at proceed, and the route beyond is set for the turn-out. (All points have 1 in 12 turn-outs.)

Similarly, white lights are provided on the signals at the points (home signals) to either indicate point and direction of turn-out, in the case of a turn-out route, or a straight route.

Other than the above, the signalling is very similar to conventional 3-aspect, and together with the on-train radio provides a satisfactory medium for the control of the 2 1/4 km, 210-wagon trains of some 21 800 tons gross, which run on the Sishen - Saldanha line.

TRACTION EFFECTS

Theoretical Aspects

When a conductor is situated in the vicinity of a varying magnetic field, an electro-motive-force (EMF) is induced in the conductor, and this EMF is amongst others, a function of the strength of the field, the length of the conductor, its distance from the field and the degree of parallelism to the line.

In the case of alternating current (AC) traction systems, the traction currents give rise to a varying magnetic field which causes an EMF to be induced in any conductors in the vicinity of the track, and not running perpendicular to it.

For conductors running parallel to the line, this induced voltage v (in volts) can be shown to be given by :

$$v = M \cdot F_s \cdot i \cdot \ell \quad (V)$$

where M is a constant which is a function of soil resistivity ρ (Ohm.metre) and the separation d (metre) between the catenary and the conductor under consideration;

F_s is the screening factor which depends on (i) the type of cable concerned; (ii) constructional details of the

overhead traction system (e.g. return conductors reduce F_s); (iii) the number of railway tracks in the vicinity, and (iv) the distance from the substation.

i is the traction current in the catenary (A);

ℓ is the length of the conductor (km).

Practical Implications

To cater for the increased power requirements of heavy haulage, higher traction voltages must be resorted to, in order to keep traction currents down to acceptable levels. And since it is expensive and impractical to go beyond the traditional 3 kV DC traction voltage, an AC traction voltage is the only remaining electric alternative.

For reasons outside the scope of this discussion, the voltage employed on the Sishen - Saldanha line is 50 kV, whereas the traction voltage on the coal line and all subsequent projects, is 25 kV .

However, as was shown in the preceding section, the traction voltage has no direct effect on induced EMF levels. Indirectly though, higher voltages imply lower currents (for the same power output) which result in lower induction levels. (An electrostatic voltage, which is proportional to the traction-voltage, is also induced in track-side conductors, but this presents a relatively small problem.)

But whatever the traction voltage, the end result is that with traction current levels of hundreds of amperes, and cable conductor lengths of a few kilometres, induced longitudinal EMF's attain levels of many volts, and during traction fault conditions, these levels rise to hundreds of volts.

Now although these induced voltages in themselves do not present serious problems, they give rise to the following :

- (i) Differences between induced voltages in the two legs of conductor pairs, result in transverse voltages which create noise in communication circuits.
- (ii) Should the one end of a conductor become earthed, and thereafter the other end (be connected to earth) via a person or a piece of equipment, the full induced voltage is applied to the person or equipment.

Whilst the effects of (i) are highly undesirable, those of (ii) could be dangerous (as result of equipment maloperation or damage) or even lethal (in the case of a person).

Solutions To Induction Problems

Little or no control at all is possible over variables such as soil resistivity, cable separation, number of tracks, or even traction current. One is therefore more or less limited to traction system constructional details, cable characteristics, and cable lengths.

Space does not permit detailed discussion of the relative merits involved. Suffice to say that

the use of return conductors, booster- and auto transformers in the traction system, screened telecommunication cables with isolating transformers, and judicious limiting of cable lengths, all have worthwhile contributions to make in maintaining the induced voltages at acceptable levels.

The question as to what acceptable levels are, immediately arises, of course.

The South African Railways has fully adopted the CCITT recommendations in this regard. These basically limit rail-to-rail voltages to 60 V, cable voltages to 110 V (since qualified personnel only should work on cables), and, under traction short-circuit conditions, all induced voltages to 430 V for less than ½ second.

All signalling and telecommunication equipment which may be subjected to these voltages, must therefore be designed so as not to be damaged by such voltages. And under no circumstances may any unsafe maloperation ("wrong-side failure") of signalling equipment due to the above voltage levels, be permitted.

Needless to say, the provision of "AC immune" S&T equipment results in considerable cost increases, albeit that AC-electrification brings overall savings for the railway.

ON-TRAIN RADIO

The combination of gradients and initially planned train loads on the coal line resulted in the situation that a fully laden train could not start up from rest without problems (such as broken couplers) at certain points along the line. The unavoidable placing of signals at certain such points caused these signals to become known as "critical signals".

These signals in turn gave rise to the requirement of on-train radio, to enable the driver, without stopping, to be authorised to pass critical signals at danger, during signalling fault- or other conditions.

A sophisticated radio system was thus installed, providing radio communication between CTC operators, locomotive drivers, guards and maintenance personnel.

Communication takes place over 3 "systems" :

- (i) System I - Control Channel - is a reliable UHF duplex channel for the exchange of secret messages between CTC controller and driver of the selected train.
- (ii) System II - Utility channel - is a UHF duplex channel allowing communication between controller, drivers, guards, maintenance personnel and telephone exchange, in various combinations.
- (iii) System III - Driver/guard channel - is a

VHF two-channel system for communication between driver and guard of a train.

To obtain adequate coverage over the terrain involved, some 57 track-side repeater stations (i.e. approximately one every 10 km) which are linked over the telecommunication cable, either via physical circuits or carrier channels, had to be erected.

The control-centre equipment includes common data-processing equipment for data transmission, recording of data messages, the control of logic functions, the VDU's, the teleprinter, and control desk indications.

On the Sishen - Saldanha line, quite different considerations gave rise to on-train radio. Due to the considerable distances between crossing-loops (80 - 90 km), the cost of cabling the sections was prohibitive. Microwave links were thus selected, and radio communication with the trains was a logical consequence. On-train radio alleviates the problem of line capacity limitations as result of excessive running times, for it permits the authorisation of successive trains (or maintenance vehicles) into a section, simultaneously.

The radio network provides 4 "channels" of communication :

- (i) Between traffic controller and driver.
- (ii) Between driver and guard.
- (iii) Between control office and traction maintenance staff.
- (iv) Between control office and other maintenance staff.

Radio coverage is achieved by means of 26 microwave repeaters, 21 of which are spaced at intervals of approximately 40 km. Each repeater is linked via radio to at least one adjacent one, thus resulting in a radio link along the entire line, over which signalling interlocking information between adjacent stations, as well as Dragging Equipment Detector alarms to the control office, is conveyed.

The on-train radio has proved invaluable as an aid in train control, when used for authorisation during normal and fault conditions, as well as for the diagnosis and rectification of minor locomotive faults, whilst the train is on the move.

And the value of good radio communication with civil, electrical and S&T maintenance personnel can almost not be over-stated, due to the considerable reduction in fault-clearance times it delivers.

TRAIN DETECTION

In order to safely control rail traffic, it is of paramount importance to ascertain the position of the trains at regular intervals, preferably near-continuously.

Over many years, the track-circuit has proved

to be a safe, reliable, but expensive means of train detection. Other, possibly cheaper, methods are possible (axle-counters or radio), but each has its own unique disadvantages.

Most track-circuits to date have necessitated electrical isolation of sections of rail by means of block joints, which involves cutting the rail. Needless to say, block joints have to be extremely strong to withstand the tremendous forces encountered in the rails. And the problem is aggravated on heavy haul lines, due to increased axle loads.

It is not surprising, therefore, that considerable effort has been, and still is being, directed at obtaining a so-called (block-) "jointless" track-circuit.

The signalling section of the SAR has recently tested and approved a jointless track-circuit for use in either AC or DC electrified traction areas. However, it remains an expensive solution: over a 10 km section, for example, such a jointless track-circuit is of the order of ten times more expensive than an acceptable axle-counter. And even if an inexpensive, acceptable jointless track-circuit is found, the unpleasant problem of attaching or connecting signalling equipment to the rails, still remains. Signalling equipment or connections on the rails always have been, and always will be highly susceptible to damage, whether by maintenance staff or by trains. On heavy haul lines the problem is compounded by the use of special-alloy rails, on which drilling or conventional welding is not permissible.

Because of the extremely high future tonnages on the coal line, strong consideration is being given to the provision of axle-counters in place of the existing track-circuits, for purposes of train detection. The previously mentioned problem of rail-connections of the alternative - the jointless track-circuit - now reaches the stage where it becomes unacceptable: Due to the increased tonnage, the frequency of rerailing which necessitates disconnection and subsequent reconnection of the track-circuit to the rails, increases to the point where it poses a serious maintenance problem.

Axle-counters on the other hand, although providing no facility for broken rail detection, offer substantial advantages in cost, ease of rerailing, and unconditionally provide both rails for traction - current return.

On the Sishen - Saldanha line, because it is not track-circuited throughout between stations, use is made of so-called last vehicle detectors (LVDs), to check whether a train is complete when it enters or leaves a section.

The equipment employs a coil within a housing, which is attached to and hangs from, the coupler of the last wagon, and an inductively operated detector between the rails, in the vicinity of each section - entry signal. Thus when the last vehicle of a train (from any direction) passes over the detector, the inductance of the detector is increased, thus enabling its associated tuned oscillator, and positive proof of the vehicle's

presence is obtained.

(The mechanical design of the attachment of the coil assembly is such that it can only be attached to the coupler of the last vehicle - i.e., a free coupler.)

The LVD equipment is interlocked with the signalling, to prevent the associated signals from "clearing" (displaying a proceed aspect) until a complete train is detected on completion of the previous train-movement.

MISCELLANEOUS ASPECTS

Control of Electric Traction Maximum Demand

The electricity costs are determined by a tariff with three components: energy charge, demand charge, and extension charge.

The demand charge, which on the lines under consideration, presently accounts for the major portion of electricity costs (more than double the actual energy costs), is determined by highest half hour average consumption (in kVA) for a particular month. (Metering of the maximum half hour demand is on a "fixed window" basis, i.e. the (½ hour) metering periods are fixed in time.)

It should therefore be apparent that the electricity costs for a month could be dramatically increased merely by one half hour interval, and therefore control of traction maximum demand is an obvious necessity.

On the Sishen - Saldanha line, S&T personnel developed a system to aid in the control of maximum demand. During each half hour interval, the average consumption since the start of the half hour is displayed on a VDU, and when it approaches a predetermined maximum level, an alarm is given, thus enabling the controller to timeously contact the driver(s) of train(s) concerned.

This system has proved most successful, and has resulted in savings equal to many thousands of dollars per month.

As a result of the success on the Sishen - Saldanha line, a micro-computer based system for demand control is being purchased for installation on the coal line.

This equipment employs a "moving window" principle, in that a "30-minute wide" bar chart of the energy consumed for a particular metering section, is displayed on a colour VDU. This display always shows the preceding period of 30 minutes, and is updated every minute. It indicates by means of a colour, whenever the consumption during a particular minute exceeds the maximum demand level.

It is therefore logical that if the average energy consumption measured within this moving window is always within the set maximum demand limit, then it will be within limits during the metering half hour.

Other information is also displayed on the VDU; for example :

- (i) An active histogram indicating in which operational section of track, the greatest consumption is taking place.
- (ii) An active histogram showing the proportion of allowable maximum demand which was consumed in the previous 30 minutes, against the portion not used.
- (iii) A horizontal green/red bar against a time scale, such that if the trend of consumption suggests that the maximum demand figure will be exceeded within the next 30 minutes, then the remaining "safe" time duration remains coloured green, whilst the indication of later time is changed to red.
- (iv) Messages of actual consumption for the previous minute, time duration before maximum demand level is exceeded, etc.

There is therefore little reason to doubt that the provision of this information will, without placing an additional burden on the operator, facilitate considerable savings in electricity costs. Almost certainly the equipment will pay for itself in less than one month.

Radio Interrogation of Train-End Brake Pressure

On the coal line, the requirement exists for the driver to be aware of the brake pressure level in the last wagon.

Although this pressure could be monitored by the guard, the problem of conveying the information to the driver still exists.

In an attempt to overcome the problem, experimental automatic radio-telemetry equipment was installed in the last wagon, as well as in the driver's locomotive.

When the driver wishes to check his train-end brake pressure, he merely depresses a button. The equipment in his locomotive interrogates the train-end equipment, which transmits the pressure reading in coded form, and the locomotive equipment receives, decodes and digitally displays the reading to the driver.

It is essential that the pressure-readings are encoded for transmission, in order to ensure that the driver is not presented with a pressure-reading from another train.

Although still in the experimental stage, the equipment is proving to be quite successful, and the possibility of installing it on all air-brake trains, is being investigated.

Dragging Equipment Detectors (D.E.D.'s)

On the Sishen - Saldanha line, the driver of a train (which is 2 1/4 km long) simply does not become aware of it when one of the wagons of his train derails. Furthermore, since crossing-loops are 80 to 90 km apart, a derailed truck or any dragging object could cause extremely costly damage to the track before it is detected.

D.E.D. equipment was initially installed on the outskirts of each crossing-loop, but after 3 very expensive derailments, it was decided to

install such equipment at 10 km intervals.

This D.E.D. equipment consists firstly of vertical metal plates mounted on either side of each rail on a horizontal torsion bar. When these plates are deflected out of the vertical position, a contact at the end of the torsion bar is opened, thus causing an alarm to be transmitted from the associated track-side radio equipment of the D.E.D., via the microwave repeaters, to the control office. The track-side equipment is operated from batteries, which are charged by a panel of solar cells, and proper functioning of all the equipment is constantly and automatically checked.

If the controller does not react within 15 seconds to the D.E.D. alarm, a simulated voice message is automatically transmitted to the driver of the train concerned.

These additional D.E.D.'s have proved to be a great success, and have paid for themselves many times over, as result of early notification and even prevention of derailed trucks - so much so, that it is the intention to have D.E.D.'s installed on the coal line as well.

Maximising of Availability of CTC Equipment

On heavy haul lines, because of the very high income per train, any and all train delays should be avoided as far as possible.

Because of traffic densities on the coal line, and since the CTC system represents the main controlling nerve of this line, much consideration has been given to providing alternate circuits for the CTC equipment of the coal line, in order to minimise the effects of a break in the main telecommunication cable.

For although buried, a cable is considerably more vulnerable to damage by the forces of nature (or humans) than, for example, a microwave link.

A microwave link as alternate circuit for the coal line, is therefore a strong possibility.

Maintenance Considerations

The opinion is held that broadly speaking, the maintenance load of S&T equipment on heavy haul lines does not differ significantly from that on other lines.

It does however, have one main consideration in common with other lines - a consideration of great importance to the Signal and Telecommunication Department :

As the striving for greater efficiency and manpower savings brings about the commissioning of more and more (sophisticated) S&T equipment (in order to achieve stated objectives), a greater load is placed upon the Signal and Telecommunication Department, in terms of equipment requiring maintenance by highly skilled personnel.

And these personnel are generally harder to come by than the staff saved by the new equipment.

CONCLUSION

Although these two heavy haul lines have been

in operation for a relatively short period, it can safely be said that to date the Signal and Telecommunication Department has provided the facilities required of it.

Judging from activities planned for the future, it is alarmingly clear that the South African Railways is on the brink of experiencing heavy haul traffic densities and -tonnages as have never yet been seen in this country.

One interesting solution to the problem of the inevitable increase in traction currents and consequently higher induction levels, is the use of fail-safe data transmission over optical-fibres : a solution which, from the induction point-of-view is as "clean" as it is futuristic. Understandably, the investigation of this solution is presently enjoying the status of a major project.

The future looks exciting, albeit a little frightening, but doubtlessly the Signal and Telecommunication Department will do its utmost to meet the challenges of increasing tonnage.

ACKNOWLEDGEMENTS

I wish to express my sincere thanks to those colleagues and superiors who found the time to scrutinise the draft paper, for the constructive and helpful comments they made.

The Second International Heavy Haul Railway
Conference: Pre-Conference Proceedings:
Colorado Springs, Colorado, USA: September
25-September 30, 1982, 1982
AAR, FRA, RPI, AREA, ASME

PROPERTY OF EPA
RESEARCH & DEVELOPMENT
LIBRARY